Microscopic and dynamical description of the fission process including intrinsic excitations

Paul Carpentier

université PARIS-SACLAY

Microscopic and dynamical description of the fission process including intrinsic excitations

Description microscopique et dynamique du processus de fission incluant des excitations intrinsèques

Thèse de doctorat de l'université Paris-Saclay

École doctorale n°576 : particules, hadrons, énergie et noyau : instrumentation, imagerie, cosmos et simulation (PHENIICS)
Spécialité de doctorat : Physique nucléaire
Graduate School : Physique. Référent : Faculté des sciences d'Orsay

Thèse préparée dans l'unité de recherche **Laboratoire Matière en Conditions Extrêmes** (Université Paris-Saclay, CEA), sous la direction de **Nathalie PILLET**, directrice de recherche HDR et le co-encadrement de **Rémi BERNARD**, ingénieur de recherche

Thèse soutenue à Paris-Saclay, le 27 septembre 2024, par

Paul CARPENTIER

Composition du Jury

Membres du jury avec voix délibérative

Denis LACROIX Directeur de recherche, IJCLab, Université Paris-Saclay	Président
Jacek DOBACZEWSKI Professeur, Université de York	Rapporteur & Examinateur
Dario VRETENAR Professeur, Université de Zagreb	Rapporteur & Examinateur
Mikael FROSINI Ingénieur de recherche, CEA Cadarache	Examinateur
Guillaume SCAMPS Professeur junior, L21IT, Université Toulouse III	Examinateur
Nicolas SCHUNCK Chercheur, Lawrence Livermore National Laboratory	Examinateur

THESE DE DOCTORAT

NNT : 2024UPASP093

université PARIS-SACLAY

ÉCOLE DOCTORALE
Particules, hadrons, énergie et noyau : instrumentation, imagerie, cosmos et simulation (PHENIICS)

Titre : Description microscopique et dynamique du processus de fission incluant des excitations intrinsèques

Mots clés : Fission Nucléaire - Excitations intrinsèques - Dynamique

Résumé : L'étude de la déformation du noyau composé jusqu'à la scission est fondamentale. Elle permet en effet l'évaluation des rendements primaires en masse et en charge, ainsi que l'établissement du bilan énergétique à la scission. À l'aide de ces deux informations, il est possible de décrire la décroissance des fragments primaires et de prédire des observables telles que la multiplicité neutronique, l'énergie gamma totale et les rendements de produits de fission.

Lors de la déformation du noyau composé jusqu'à la scission, deux types de phénomènes prévalent. En effet, lorsque le noyau composé se déforme dans son ensemble (on parle de phénomènes collectifs) des excitations intrinsèques apparaissent (on parle de phénomènes dissipatifs). Cette distinction se retrouve dans la séparation qui s'opère entre les deux grands types d'approches théoriques microscopiques visant à décrire la déformation du noyau composé jusqu'à la scission. D'une part, les modèles de type Time Dependent Hartree-Fock (TDHF) incluent les phénomènes dissipatifs, aboutissant à de bons bilans énergétiques, mais leur manque de collectivité conduit à des rendements peu fiables. À l'opposé, les approches type Time Dependent Generator Coordinate Method (TDGCM) ont été construites pour décrire les phénomènes collectifs, mais elles peinent à inclure de la dissipation. Ces dernières conduisent donc à de bons rendements mais à des bilans énergétiques irréalistes.

Sans surprise, de nombreuses tentatives ont été proposées pour aboutir à un modèle microscopique permettant l'obtention de bilans énergétiques et de rendements fiables dans un cadre unifié cohérent. Le Schrödinger Collective Intrinsic Model (SCIM) compte parmi ces différentes tentatives. Se présentant comme une méthode de type TDGCM incluant des excitations intrinsèques, il a tout d'abord été proposé en 2011 par R. Bernard *et al*. Toutefois, du fait de nombreux verrous à la fois techniques et théoriques, aucune application n'avait été proposée à l'époque. L'objectif de ce travail de thèse a été la levée de ces différents verrous de manière à aboutir à une première application réaliste du SCIM. Cette dernière à été réalisée dans le cas du Plutonium-240, en considérant une dimension en déformation.

La mise en œuvre du SCIM a en particulier nécessité la création et l'implémentation numérique de nouvelles méthodes appartenant au champ de la théorie Hartree-Fock-Bogoliubov sous contraintes. Ces méthodes sont toutes basées sur la même idée de contraindre les recouvrements entre différents états. Deux d'entre elles "Link" et "Drop" permettent d'aboutir à des surfaces d'énergies potentielles (PES) 1D adiabatiques continues et régulières, incluant la scission ainsi que la relaxation des fragments. La méthode "Continuous Deflation", quant à elle, rend possible la création de nouveaux états excités variationnels, continus et réguliers, au-dessus d'une PES adiabatique.

université PARIS-SACLAY

ÉCOLE DOCTORALE
Particules, hadrons, énergie et noyau : instrumentation, imagerie, cosmos et simulation (PHENIICS)

Title : Microscopic and dynamical description of the fission process including intrinsic excitations

Keywords : Nuclear fission - Intrinsic excitation - Dynamics

Abstract : The study of the deformation of the compound nucleus up to scission is fundamental. It leads both to the evaluation of the primary yields in mass and charge and to the energy balance at scission. Using these data, it is possible to describe the decay of primary fragments and predict observables such as neutron multiplicity, total gamma energy and fission product yields.

During the deformation of the compound nucleus up to scission, two types of phenomena prevail. When the compound nucleus deforms as a whole (referred to as collective phenomena), intrinsic excitations appear (referred to as dissipative phenomena). This distinction is reflected in the separation between the two main types of microscopic theoretical approach aimed at describing the deformation of the compound nucleus up to scission. On the one hand, Time Dependent Hartree-Fock (TDHF) models include dissipative phenomena, resulting in good energy balances, but their lack of collectivity leads to unreliable yields. On the other hand, Time Dependent Generator Coordinate Method (TDGCM) approaches were designed to describe collective phenomena, but struggle to include dissipation. They therefore lead to good yields but unrealistic energy balances.

Unsurprisingly, numerous attempts have been made to develop a microscopic model that can provide both reliable energy balances and yields within a coherent framework. The Schrödinger Collective Intrinsic Model (SCIM) is one such attempt. This TDGCM-type method including intrinsic excitations was first proposed in 2011 by R. Bernard et al. However, due to numerous technical and theoretical hurdles, no application was proposed at the time. The aim of this thesis work was to overcome these various obstacles and produce the first realistic application of the SCIM. This application has been carried out in the case of the Plutonium 240 nucleus, considering one collective dimension.

The implementation of the SCIM required in particular the creation and numerical implementation of new methods belonging to the field of constrained Hartree-Fock-Bogoliubov theory. These methods are all based on the same idea of constraining overlaps between different states. Two of them, “Link” and “Drop”, lead to continuous and regular 1D adiabatic potential energy surfaces (PES), including scission and fragment relaxation. The “Continuous Deflation” method, on the other hand, enables the creation of new variational, continuous and regular excited states on top of an adiabatic PES.

Synthèse

L'étude de la déformation du noyau composé jusqu'à la scission est fondamentale. Elle permet en effet l'évaluation des rendements primaires en masse et en charge, ainsi que l'établissement du bilan énergétique à la scission. À l'aide de ces deux informations, il est possible de décrire la décroissance des fragments primaires et de prédire des observables telles que la multiplicité neutronique, l'énergie gamma totale et les rendements de produits de fission.

Lors de la déformation du noyau composé jusqu'à la scission, deux types de phénomènes prévalent. En effet, lorsque le noyau composé se déforme dans son ensemble (on parle de phénomènes collectifs) des excitations intrinsèques apparaissent (on parle de phénomènes dissipatifs). Cette distinction se retrouve dans la séparation qui s'opère entre les deux grands types d'approches théoriques microscopiques visant à décrire la déformation du noyau composé jusqu'à la scission. D'une part, les modèles de type Time Dependent Hartree-Fock (TDHF) incluent les phénomènes dissipatifs, aboutissant à de bons bilans énergétiques, mais leur manque de collectivité conduit à des rendements peu fiables. À l'opposé, les approches type Time Dependent Generator Coordinate Method (TDGCM) ont été construites pour décrire les phénomènes collectifs, mais elles peinent à inclure de la dissipation. Ces dernières conduisent donc à de bons rendements mais à des bilans énergétiques irréalistes.

Sans surprise, de nombreuses tentatives ont été proposées pour aboutir à un modèle microscopique permettant l'obtention de bilans énergétiques et de rendements fiables dans un cadre unifié cohérent. Le Schrödinger Collective Intrinsic Model (SCIM) compte parmi ces différentes tentatives. Se présentant comme une méthode de type TDGCM incluant des excitations intrinsèques, il a tout d'abord été proposé en 2011 par R. Bernard *et al.* [33,34]. Toutefois, du fait de nombreux verrous à la fois techniques et théoriques, aucune application n'avait été proposée à l'époque. L'objectif de ce travail de thèse a été la levée de ces différents verrous de manière à aboutir à une première application réaliste du SCIM. Cette dernière à été réalisée dans le cas du Plutonium-240, en considérant une dimension en déformation.

De manière générale, la plupart des méthodes TDGCM permettent l'obtention d'un hamiltonien décrivant localement (en déformation) la physique relative à la minimisation de l'énergie par rapport à une base d'états prédéfinis. Dans le cas du SCIM, cette base d'états comporte à la fois des états minimisant l'énergie à une déformation donnée (on parle d'états adiabatiques), mais aussi des états correspondant à des excitations intrinsèques au-dessus de ces derniers.
Une fois que l'hamiltonien SCIM est obtenu, on peut l'utiliser dans une équation de Schrödinger pour décrire la propagation d'un paquet d'onde dans le temps (cette partie est appelée la "dynamique").

En pratique, les méthodes utilisées dans le SCIM pour aboutir à l'hamiltonien SCIM impliquent des hypothèses assez contraignantes. Ces dernières peuvent être résumées par la nécessaire continuité et bonne régularité des états appartenant à une même strate d'excitation (la distance considérée étant la distance naturelle associée aux recouvrements entre états).

Dans ce travail de thèse, les états adiabatiques sont d'abord abordés, les états excités sont ensuite considérés, et la dynamique SCIM est enfin mise en place et ses résultats étudiés. Tous les calculs et résultats discutés ont été réalisés pour le Plutonium-240.

Au niveau adiabatique, conformément au travail réalisé en 2011, les états de type Hartree-Fock-Bogoliubov (HFB) sous contraintes préservant la symétrie axiale et étant pairs par renversement du sens du temps sont d'abord étudiées. Dans la pratique, ces états sont générés en utilisant l'interaction effective D1S et le solver HFB3.
Des calculs sous contraintes (utilisant le moment multipolaire Q20) sont réalisés de manière à obtenir une surface d'énergie potentielle (PES) décrivant l'élongation du noyau. Les états obtenus de la sorte peuvent parfois présenter des discontinuités. La plupart de ces discontinuités peuvent être facilement corrigées en contraignant davantage de moments multipolaires, Q30 et Q40 par exemple. Toutefois, la discontinuité présente à la scission est bien plus complexe : elle sépare des configurations ou le noyau composé est encore entier de configurations où apparaissent deux fragments séparés et aplatis correspondant davantage à la physique de la fusion (la PES constituée par les états de ce type est pour cela appelée "vallée de fusion"). Du reste, même dans les zones continues de la PES, les états adiabatiques ont tendance à être fortement irréguliers.
Pour résoudre ces problèmes, deux nouvelles méthodes utilisant les contraintes sur les recouvrements entre états sont proposées. La méthode "Link" est la première de ces deux méthodes, elle permet de générer un chemin continu et régulier d'états HFB entre un état HFB de départ et un état HFB d'arrivée. Cette méthode fonctionne très bien pour corriger les discontinuités autres que la discontinuité de la scission. En effet, pour cette dernière, comme aucune configuration d'arrivée pertinente n'est disponible, la méthode "Link" est inopérante. La seconde méthode "Drop" a été conçue spécifiquement pour passer continûment la scission. Elle ne requiert qu'un état HFB de départ à partir duquel elle génère un chemin continu et régulier d'états HFB en suivant une descente de gradient d'énergie. A l'aide de ces deux méthodes, une PES 1D (en déformation) complètement continue et présentant de bonnes propriétés de régularité peut être obtenue.
Les état adiabatiques générés par les méthodes "Link" et "Drop" sont ensuite analysés. La zone de scission est tout d'abord déterminée par l'étude conjointe des potentiels chimiques ainsi que du ratio local neutron/proton des états. La distribution sur le nombre de particules des fragments est ensuite étudiée, faisant notamment apparaître un effet pair-impair proton. Le bilan énergétique statique est réalisé en utilisant une version simplifiée de la méthode proposée par Younes et Gogny [35], ce bilan permet la détermination de l'énergie de déformation à la scission ainsi que de l'énergie cinétique de post-scission. Enfin, les potentiels et tenseurs d'inertie du

SCIM à la limite adiabatique sont comparés avec ceux obtenus dans le cas de l'approximation des recouvrements gaussiens (GOA). Cette comparaison révèle que le SCIM est d'une qualité comparable à la GOA exacte au niveau adiabatique.

En ce qui concerne les états excités, la formulation initiale du SCIM reposait sur l'utilisation d'états excités de type 2-quasiparticules au-dessus des états adiabatiques. Toutefois, ces états brisent le nombre moyen de particules et présentent également de forts problèmes de régularité. En pratique, ce sont ces derniers problèmes qui se montrent le plus handicapant allant jusqu'à rendre l'utilisation du SCIM impossible.
Cet état de fait conduit à la proposition de nouveaux états excités pour remplacer les états excités de type 2-quasiparticules. Les nouveaux états excités proposés sont des états excités variationnels créés en utilisant la nouvelle méthode "Continuous Deflation", également basée sur les contraintes sur les recouvrements. Cette méthode permet la création d'états excités naturellement continus et possédant de bonnes propriétés de régularité. Au total, dix excitations différentes ont été générées dans ce travail de thèse.
L'analyse de ces nouvelles excitations variationnelles montre que ces dernières peuvent être écrites la plupart du temps comme une somme d'états excités à 2 et 4-quasiparticules au-dessus de leurs états adiabatiques de référence. Par ailleurs, l'étude de la distribution sur le nombre de particules des fragments dans les états excités montre qu'ils incluent en général des phénomènes de brisure de paires, dont l'importance est connue dans la fission de basse énergie. Enfin, l'analyse des potentiels et tenseurs d'inerties SCIM correspondant aux différentes excitations (à la limité adiabatique-excitée) amènent à la formulation d'un scénario pour la dynamique dans lequel six excitations sont conservées.

La partie "dynamique" du SCIM est réalisée en résolvant numériquement l'équation de Schrödinger impliquant l'hamiltonien SCIM à l'aide de la méthode de Crank-Nicolson. Le paquet d'onde initial est construit à l'aide des états propres du puits de potentiel de l'état fondamental extrapolé et un potentiel complexe est ajouté au hamiltonien après la scission pour gérer l'absorption progressive du paquet d'onde.
Les flux de probabilité correspondant aux niveaux adiabatiques et excités sont alors extraits, ces flux permettent d'avoir accès à la probabilité d'obtenir tel ou tel état à la scission. En particulier, la relativement faible probabilité d'obtenir un état adiabatique à la scission (15.8%) confirme l'importance d'inclure des états excités dans la description de la scission.
La connaissance des probabilités associés aux différents états conduit naturellement aux observables à la scission. Tout d'abord, les distributions en charge et en masse qui pourraient être obtenues en utilisant le SCIM à 2D sont discutées au regard de la différence entre les distributions sur le nombre de particules des fragments dans le cas adiabatique et en incluant les excitations. Cette étude prospective montre la possibilité que l'inclusion des excitations élargisse les rendements en masse tout en tempérant les effets pair-impair associés à la distribution en charge. Enfin, un bilan énergétique complet à la scission est proposé. L'énergie d'excitation totale des fragments

est évaluée autour de 34 MeV. En comparaison, les données expérimentales indiquent un TXE d'environ 30 MeV, lequel correspond à l'émission de trois neutrons ainsi que de quelques rayonnements gamma. L'énergie cinétique totale des fragments évaluée est quant à elle proche de 178 MeV quand l'expérience prédit 181 MeV environ. Cette compatibilité entre évaluation et expérience souligne notamment l'importance de la prise en compte de l'énergie totale d'interaction (et non pas seulement de l'énergie coulombienne) dans l'évaluation de l'énergie cinétique de post-scission.

En conclusion, ce travail de thèse est parvenu à remplir son objectif premier : aboutir à une application du SCIM dans le cas réaliste du Plutonium-240. Cette première application a en particulier nécessité la création et l'implémentation numérique de nouvelles méthodes appartenant au champ de la théorie Hartree-Fock-Bogoliubov sous contraintes. Ces méthodes sont toutes basées sur la même idée de contraindre les recouvrements entre différents états. Deux d'entre elles "Link" et "Drop" permettent d'aboutir à des surfaces d'énergies potentielles (PES) 1D adiabatiques continues et régulières, incluant la scission ainsi que la relaxation des fragments. La méthode "Continuous Deflation", quant à elle, rend possible la création de nouveaux états excités variationnels, continus et réguliers, au-dessus d'une PES adiabatique.
Ce travail ouvre également de nombreuses perspectives. Les méthodes existantes utilisant des contraintes sur les recouvrements pourraient être améliorées et de nouvelles pourraient être proposées, notamment dans l'objectif d'obtenir des PES continues à 2D, lesquelles rendraient possible la mise en place du SCIM à 2D. La méthode Nuclear Paving (NP) est un premier pas en ce sens. Elle constitue une preuve de principe qu'il est possible, au moins localement, d'utiliser les prédictions de la GOA conjointement aux contraintes sur les recouvrements pour l'exploration des PES. Du reste, l'utilisation de contraintes sur les moments multipolaires en combinaison avec la méthode "Drop" ("Guided Drop") constitue également une direction prometteuse.
Aussi, il serait souhaitable de comparer la manière simplifiée avec laquelle le bilan énergétique statique a été réalisé dans ce travail avec la méthode complète proposée par Younes et Gogny [35].
Enfin, une étude plus étendue du SCIM à 1D serait du plus grand intérêt. En premier lieu, et parmi bien d'autres choses, la sensibilité des résultats au nombre d'excitations prises en compte devrait être étudiée.

À Thimothée,

Contents

Introduction

While some modern theories, such as string theory [1] or loop quantum gravity [2], are desperately chasing the phenomena required to verify their hypotheses, nuclear physics is a very pleasant playground for the theoretician. Indeed, the latter regularly deals with phenomena still awaiting the theory that might reveal their innermost nature. This is particularly true in the case of fission, which more than half a century has elucidated without exhausting all its mysteries. In this respect, we can of course cite certain fission observables, such as neutron multiplicity or fragment angular momenta, which theories struggle to reproduce with precision.

The history of theoretical fission actually began in 1939, when L. Meitner and O. Frisch proposed their interpretation [3] of the experiments carried out by O. Hahn and F. Strassmann [4, 5], based on the liquid drop model introduced by N. Bohr three years earlier [6]. A short time after this first qualitative interpretation, N. Bohr, along with A. Wheeler, proposed the first theoretical formulation of fission [7]. In this article, N. Bohr and A. Wheeler described fission as the process by which a compound nucleus deforms until it splits into two fragments. This phenomenon is explained by the balance between nuclear surface tension, which ensures the cohesion of the compound nucleus, and Coulomb repulsion, which inclines it towards separation. In addition, they put forward two fundamental concepts, still in use today. The first is the concept of "saddle point", the state of deformation at which the composite nucleus is fated to scission, with no return possible. The second is the "fissility", a concept based on the ratio between Coulomb repulsion and surface tension, to enable *a priori* evaluation of the propensity of nuclei to fission. Despite the indisputable qualities and pioneering nature of the model proposed by N. Bohr and A. Wheeler, this first approach suffers from not taking into account the fundamental degrees of freedom of the nucleus, *i.e.* the nucleons, and the quantum phenomena associated with them.
Following this early work, a shell model interpretation of the nucleus, inspired by the electronic one, saw the light of day in 1955 [8]. The integration of this point of view into the liquid drop model, known as the Strutinsky correction [9], significantly extended its qualities, enabling the theoretical description of fission isomers, for example. This first conclusive blend of shell model and theoretical fission signs the beginning of an increasingly important consideration of the fundamental degrees of freedom of the nucleus in fission studies.

The difference between the classical treatment of the nucleus as a whole and the explicit consideration of its components lies at the heart of the distinction usually made in theoretical nuclear physics between the so-called "macroscopic" and "microscopic" models. The macroscopic model by excellence is, of course, the one proposed by N. Bohr and A. Wheeler in 1939. On the other side of the spectrum, the most microscopic models used today in fission explicitly consider interacting nucleons, coupled to mean-field theories known as Energy Density Functional (EDF) [10]. The latter make it possible to significantly reduce the

complexity of the N-body quantum problem by considerably reducing the degrees of freedom explicitly taken into account, in particular in the case of heavy nuclei such as actinides. The nucleon-nucleon interactions used in theoretical fission are phonomenological effective interactions, *i.e.* their parameters have been obtained in such a way to reproduce some experimental data. These interactions form a large family whose best-known representatives are the Skyrme interactions [11–14] and the Gogny interactions [15–19]. In this PhD thesis, the latter ones that have been considered.

Within the various EDF-type theories applied to fission today, there is an important distinction. On the one hand, there are the dynamical models such as Time-Dependent Hartree Fock (TDHF) [20–22] methods, and more recently Time-Dependent Hartree Fock Bogoliubov (TDHFB) [23]. These models naturally take into account part of the dissipation during the fission process, but struggle to describe the variety of possible fragmentations that characterizes the fission phenomenon. As a result, they give predictions that are far from experiments in terms of charge and mass yields.
On the other hand, the Time-Dependent Generator Coordinate Model (TDGCM) theories [18, 24–26], historically the oldest, were designed to take into account the collective degrees of freedom in the fission phenomenon. These theories have shown their relevance in the evaluation of charge and mass yields [27, 28]. However, up to now, these theories neglect the intrinsic excitation phenomena in their description of fission (the so-called "adiabatic hypothesis") whereas experimental data show the importance of these phenomena, even in low-energy fission. In the work of F. Vives et al. [29], for instance, we observe very clearly low-energy pair-breaking phenomena manifested by a kink in the fragment kinetic energy. Similarly, the decrease of the odd-even effect visible in charge yields as a function of the incident neutron energy [30] testifies to the importance of the intrinsic pair-breaking phenomenon, even at low energy. Moreover, without the possibility of evaluating the energy of fission fragments, TDGCM-type approaches are unable to provide consistent predictions on fundamental observables such as neutron multiplicity.
Consequently, each of these two types of approach strives to fill the gaps. Within the framework of TDHF-type theories, for example, some recent works [31] have demonstrated the possibility of taking greater account of collective phenomena. With regard to the inclusion of intrinsic excitations in TDGCM-type theories, we can cite the recent work of [32], but also the work of R. Bernard et al. [33, 34], which led to the formulation of the Schrödinger Collective-Intrinsic Model (SCIM) in 2011. This model was conceived as an extension of the TDGCM, explicitly taking into account intrinsic excitation phenomena. By 2011, however, only the theoretical foundations of the model had been laid, and no applications had been proposed. The primary goal of this PhD thesis is to put the model into practice and to come up with a first application. As we will see in all the developments carried out, many theoretical and numerical difficulties had to be overcome.

The chapter 1 of this PhD thesis is intended to introduce the SCIM formalism, while recalling the fundamentals of the TDGCM-type formalisms from which it derives. Both the static and the dynamics part of these approaches are detailed.
Chapter 2 discusses all the problems we faced in the first attempts to implement the SCIM. Firstly, the difficulties associated with the two-quasiparticle excitations in the SCIM are reviewed and illustrated in the case of ^{240}Pu, in particular the impact of the average particle number breaking as well as the level repulsion issue. Secondly, we present the particle number projection method we have implemented to solve part of the problems generated by the two-quasiparticles excitations. We have discussed the improvements obtained and the remaining

issues. Finally, we discuss the lack of continuity and regularity of standard Potential Energy Surfaces (PES), both at the adiabatic level and with respect to intrinsic excitations.
In Chapter 3, we present the new methods based on overlap constraints that we have developed. They have proved to be very efficient in solving all the difficulties described in Chapter 2. The first method, known as the Link, enables the continuous connection of two Hartree Fock Bogoliubov (HFB) states of a PES. The second method, named the Drop, has been created to continuously cross the scission connecting to the Coulomb valley, which was not previously possible within the TDGCM-type approaches. Finally, the Continuous Deflation, which is the third method, has been designed to obtain continuous variational excitations above the adiabatic paths. In particular, we present detailed analyses of these methods in ^{16}O and ^{240}Pu nuclei. In practice, we will see how this set of new methods allows to determine both an adiabatic path and the associated continuous excited paths describing the asymmetric fission of ^{240}Pu.
Chapter 4 is dedicated to the study of the new results extracted from these adiabatic and excited continuous paths in the scission area. Firstly, we discuss in which extent the proton and neutron chemical potentials of the compound nucleus indicate the advent of scission for both the adiabatic and excited paths. Differences of the adiabatic results and excited ones are discussed. Secondly, we present a study of the neutron/proton assymmetry in the neck of the compound nucleus around the scission, for both the adiabatic and excited states. As we will see, this study reveals marked neutron necking phenomena in both adiabatic and excited states. Thirdly, we inspect the particle number distribution in the fragments, for both the adiabatic and the excited states. In particular, we study the proton odd-even staggering in adiabatic states, and evaluate the broadening of particle number distributions induced by intrinsic excitations. Finally, we look at the static energy balance at scission. Using a novel method called RC-separation, inspired by the pioneering work of [35], we study the respective binding energies of the fragments, as well as their interaction energies. Then, we propose an evaluation of the deformation and post-scission kinetic energies at the adiabatic level.
In chapter 5, we present the painstaking theoretical and numerical work required to calculate the overlap and Hamiltonian kernels. In particular, we introduce new formulas to more easily handle the case where different 2-center harmonic-oscillator representations are considered when evaluating the kernels. We also present the developments linked to the particle number projection formalism that has been useful in the search for the best intrinsic excitations for the SCIM. Finally, we discuss two important points associated with a non-trivial phasis problem linked to particle number breaking, and with the divergences observed in the Hamiltonian kernel evaluation between orthogonal states.
Chapter 6, which concludes this PhD thesis, deals with the implementation of the SCIM dynamics in the case of a ^{240}Pu asymmetric fission path. In particular, its implementation requires to obtain certain quantities, namely the SCIM potential, the dissipation tensor and the inertia tensor. We explain how these quantites have been calculated in practice. A detailed comparison is done with the equivalent quantities extracted from the Gaussian Overlap Approximation (GOA) approximation. Then, we explain the numerical implementations associated with the solution of the collective-intrinsic Shrödinger equation of the SCIM. Finally, we discuss the results obtained by realizing the dynamics. In particular, we evaluate the impact of the intrinsic excitations at scission on the charge and mass yields as well as on the energy balance.

Chapter 1

From the TDGCM to the SCIM

The TDGCM or Time-Dependent Generator Coordinate Method is a fully quantum mechanical method that consists in describing the time evolution of a TDGCM wave function built as a linear mixing of states of a given set [18, 24–26]. As far as we know, in the applications of the TDGCM, the sets chosen to build the TDGCM wave function were always made of deformed adiabatic states. This adiabatic approach demonstrated its relevance to describe fission yields in a satisfactory way. However, as it neglects the intrinsic degrees of freedom of the nucleus, the adiabatic TDGCM is unable to describe important observables such as the total excitation energy of the fragments or the neutron multiplicity. To tackle this issue, it has been proposed to enrich the TDGCM wave function with intrinsicly excited states. Although the idea may appear simple, it requires new theoretical developments on top of the TDGCM. The new theoretical framework we propose to use is called the SCIM or Schrödinger Collective-Intrinsic Model [33, 34].
In a first part, we describe the general concepts of the GCM and TDGCM approach. Then, we explain how the SCIM is formulated.

1.1 The GCM and the TDGCM

To understand the general concept of the TDGCM, it is first important to consider the GCM or Generator Coordinate Method, which is the static counterpart of the TDGCM. Indeed, the GCM is meant to answer the question "*How can we build a linear mixing of given states relevant to describe a nucleus ?*", when the natural continutation of the latter is addressed by the TDGCM: *"How do we make such a linear mixing evolves over time ?"*.
We moreover decided to present thoroughly here the GOA or Gaussian Overlap Approximation, as it is probably the most popular framework to solve the adiabatic TDGCM equations.

1.1.1 GCM

A GCM wave function is nothing but a linear mixing of the states of a given set, and can thus be very general (see for example [36]). However, we will restrict this presentation to the case of sets made of deformed time-reversal adiabatic HFB vacua, which are the ones that have been mostly used in fission studies. In this case, the GCM wave function reads:

$$|\Phi_{GCM}\rangle = \int dq f(q) |\Phi(q)\rangle \tag{1.1}$$

Here q is a collective coordinate that accounts for the deformation of the time-reversal HFB state $|\Phi(q)\rangle$ and the $f(q)$ are the coefficients of the linear mixing. These latter are determined through a variational principle applied to the total energy of the the system described by Eq.(1.1):

$$\delta(\langle\Phi_{GCM}|\hat{H} - E|\Phi_{GCM}\rangle) = 0 \tag{1.2}$$

The Hamiltonian $\hat{H}$ we consider is made of a kinetic part $\hat{T}$ and a two-body nucleon-nucleon interaction $\hat{V}$:

$$\hat{H} = \hat{T} + \hat{V} \tag{1.3}$$

The Eq.(1.2) is then developed using Eq.(1.1):

$$\delta(\int dq' \int dq f^*(q')\langle\Phi(q')|\hat{H} - E|\Phi(q)\rangle f(q)) = 0 \tag{1.4}$$

Performing the variations with respect to the $f^*(q')$, we get:

$$\forall q', \qquad \int dq\langle\Phi(q')|\hat{H}|\Phi(q)\rangle f(q)) = E\int dq\langle\Phi(q')|\Phi(q)\rangle f(q)) \tag{1.5}$$

This equation is called the Hill-Wheeler equation [24], it can be rephrased as follows:

$$\boxed{\mathcal{H}f = E\mathcal{N}f} \qquad \begin{cases}\mathcal{H}(q',q) = \langle\Phi(q')|\hat{H}|\Phi(q)\rangle \\ \mathcal{N}(q',q) = \langle\Phi(q')|\Phi(q)\rangle\end{cases} \tag{1.6}$$

In Eq.(1.6), $\mathcal{H}$ and $\mathcal{N}$ are called respectively the Hamiltonian kernel and the overlap kernel. The Hill-Wheeler equation is then transformed into an eigenvalue problem. To do so, different analytic approximations exist among which the already mentioned GOA is probably the most popular. It is also possible to do it exactly numerically.
For the time being, we will keep as much generality as possible and suppose that we know the inverse of the square root of $\mathcal{N}$. We can then write:

$$\boxed{\mathcal{H}_{col}g = Eg} \qquad \begin{cases}\mathcal{H}_{col} = \mathcal{N}^{-1/2}\mathcal{H}\mathcal{N}^{-1/2} \\ g = \mathcal{N}^{1/2}f\end{cases} \tag{1.7}$$

The problem to solve is now a hermitian eigenvalue problem, which is solvable. Although the wave function obtained with the GCM is already useful for nuclear structure purposes as it adds relevant correlations to the system, for fission, which is a dynamical process, we have to go further and add a time dependance on top of the GCM: this is the TDGCM.

1.1.2 TDGCM

The way the time is added on top of the GCM is pretty straightforward. Indeed, the TDGCM wave function reads:

$$|\Phi_{TDGCM}(t)\rangle = \int dq f(q,t)|\Phi(q)\rangle \tag{1.8}$$

The time dependence is fully absorbed into the $f(q,t)$ coefficients of the linear mixing. We don't want anymore to find the eigenfunctions of the collective Hamiltonian of Eq.(1.7), but we use it to make well-chosen initial coefficients evolve over time through the following Schrödinger equation:

$$\boxed{\mathcal{H}_{col}g(t) = i\hbar\frac{\partial}{\partial t}g(t)} \tag{1.9}$$

The Schrödinger equation is solved numerically and this part of the problem is called thereafter the "dynamics" (see Chapter. 4). Solving the "dynamics" gives access to some very important fission observables such as mass/charge yields.

1.1.3 GOA

As said earlier, the GOA is a very popular framework of approximations that enables to transform the Hill-Wheeler equation into an eigenvalue problem. As its name suggests, it first assumes that the overlap kernel has a gaussian shape in the sense that:

$$\mathcal{N}(q',q) = \langle\Phi(q')|\Phi(q)\rangle = e^{-\frac{1}{2}\gamma(\frac{q'+q}{2})(q-q')^2} \tag{1.10}$$

Here the γ function stands for the gaussian width. In practice, this γ function is considered to be constant in most of the calculations, which is *a priori* a strong approximation. However, it is possible to approach more properly this desired constant width at first order rescaling the collective coordinate q. To do so, we write:

$$\alpha(q) = \int^q \sqrt{\frac{\gamma(q')}{\gamma_0}}dq' \tag{1.11}$$

Here, γ_0 stands for the target width. At first order we find:

$$\gamma_0(\alpha(q)-\alpha(q'))^2 = \gamma_0(\frac{d}{dq}\alpha(\frac{q+q'}{2}))^2(q-q')^2 = \gamma(\frac{q'+q}{2})(q-q')^2 \tag{1.12}$$

The new α collective coordinate defined in Eq.(1.11) will be used in the rest of this part. With it, it is possible to write:

$$\mathcal{N}(\alpha',\alpha) = e^{-\frac{1}{2}\gamma_0(\alpha-\alpha')^2} \tag{1.13}$$

This operator has a trivial square root:

$$\mathcal{N}^{1/2}(\alpha', z) = (\frac{\pi}{2\gamma_0})^{1/4} e^{-\gamma_0(\alpha'-z)^2} \tag{1.14}$$

We'd like to express $\mathcal{H}$ as $\mathcal{N}^{1/2}\mathcal{H}_{col}\mathcal{N}^{1/2}$ to simplify the problem. We can start writing

$$\begin{cases} \mathcal{H}(\alpha', \alpha) = \int dz \mathcal{N}^{1/2}(\alpha', z) h(\alpha', \alpha) \mathcal{N}^{1/2}(z, \alpha) \\ h(\alpha', \alpha) = \frac{\mathcal{H}(\alpha', \alpha)}{\mathcal{N}(\alpha', \alpha)} \end{cases} \tag{1.15}$$

We then perform a Taylor expansion of h up to the second order. This is the second major approximation of the GOA:

$$\begin{aligned} h(\alpha', \alpha) = h(z, z) + (\alpha' - z) h^{(1,0)}(z, z) + (\alpha - z) h^{(0,1)}(z, z) \\ + (\alpha' - z)(\alpha - z) h^{(1,1)}(z, z) + \frac{1}{2}(\alpha' - z)^2 h^{(2,0)}(z, z) + \frac{1}{2}(\alpha - z)^2 h^{(0,2)}(z, z) \end{aligned} \tag{1.16}$$

We've used the shorthand notation $h^{(i,j)} = \frac{\partial^i}{\partial x^i} \frac{\partial^j}{\partial y^j} h(x, y)$. Due to time-reversal invariance, $h^{(1,0)}$ and $h^{(0,1)}$ vanishes. We end up with:

$$\begin{aligned} h(\alpha', \alpha) = h(z, z) + (\alpha' - z)(\alpha - z) h^{(1,1)}(z, z) \\ + \frac{1}{2}(\alpha' - z)^2 h^{(2,0)}(z, z) + \frac{1}{2}(\alpha - z)^2 h^{(0,2)}(z, z) \end{aligned} \tag{1.17}$$

Inserting Eq.(1.17) in Eq.(1.15), we get:

$$\begin{aligned} \mathcal{H}(\alpha', \alpha) = \int dz \mathcal{N}^{1/2}(\alpha', z) [h(z, z) + (\alpha' - z)(\alpha - z) h^{(1,1)}(z, z) \\ + \frac{1}{2}(\alpha' - z)^2 h^{(2,0)}(z, z) + \frac{1}{2}(\alpha - z)^2 h^{(0,2)}(z, z)] \mathcal{N}^{1/2}(z, \alpha) \end{aligned} \tag{1.18}$$

In addition, using Eq.(1.13) we remark that:

$$\begin{cases} (\alpha' - z) \mathcal{N}^{1/2}(\alpha', z) = \frac{1}{2\gamma_0} \frac{\partial}{\partial z} \mathcal{N}^{1/2}(\alpha', z) \\ (\alpha' - z)^2 \mathcal{N}^{1/2}(\alpha', z) = (\frac{1}{2\gamma_0} + \frac{1}{4\gamma_0^2} \frac{\partial^2}{\partial z^2}) \mathcal{N}^{1/2}(\alpha', z) \end{cases} \tag{1.19}$$

Using Eq.(1.19) and integration by parts, we obtain:

$$\begin{aligned} \mathcal{H}(\alpha', \alpha) = \int dz \mathcal{N}^{1/2}(\alpha', z) [h(z, z) + \frac{1}{4\gamma_0}(h^{(2,0)}(z, z) + h^{(0,2)}(z, z)) \\ - \frac{1}{4\gamma_0^2} \frac{\partial}{\partial z} h^{(1,1)}(z, z) \frac{\partial}{\partial z} + \frac{1}{8\gamma_0^2}(\frac{\partial}{\partial z^2} h^{(2,0)}(z, z) + h^{(0,2)}(z, z) \frac{\partial}{\partial z^2})] \mathcal{N}^{1/2}(z, \alpha) \end{aligned} \tag{1.20}$$

Here, we assumed that the various quantities and their derivatives are equal to zero at infinity. Moreover, due to the symmetry of the kernels, $h^{(2,0)}(z, z) = h^{(0,2)}(z, z)$. Commuting the derivative operators, we can write the collective Hamiltonian in its canonical form:

$$\boxed{\begin{aligned}\mathcal{H}_{col}(z) = h(z,z) + \frac{1}{2\gamma_0}h^{(2,0)}(z,z) + \frac{1}{8\gamma_0^2}\frac{\partial^2}{\partial z^2}[h^{(2,0)}(z,z)] \\ +\frac{1}{4\gamma_0^2}\frac{\partial}{\partial z}(h^{(2,0)}(z,z) - h^{(1,1)}(z,z))\frac{\partial}{\partial z}\end{aligned}} \tag{1.21}$$

From Eq.(1.21), we extract the collective potential V as well as the inertia tensor B and its corresponding mass M:

$$\boxed{\begin{cases} V(z) = h(z,z) + \frac{1}{2\gamma_0}h^{(2,0)}(z,z) + \frac{1}{8\gamma_0^2}\frac{\partial^2}{\partial z^2}[h^{(2,0)}(z,z)] \\ B(z) = \frac{1}{4\gamma_0^2}(h^{(2,0)}(z,z) - h^{(1,1)}(z,z)) \\ M(z) = -\frac{1}{2B(z)} \end{cases}} \tag{1.22}$$

In practice, the inertia tensor and the collective potential used in the TDGCM+GOA are not directly the ones derived in Eq.(1.22). Indeed, discontinuities between the generative states of the TDGCM (see Chapter 2) induce serious difficulties in the evaluation of the derivatives of h. To avoid these issues, the derivatives are handled using linear response theory and the Cranking approximation [37–39]. With these approximations, the collective potential, the inertia tensor, and the intertial mass read as:

$$\boxed{\begin{cases} \bar{V}(z) = h(z,z) + \mathrm{Tr}[M^{(1)-1}(z)M^{(2)}(z)M^{(1)-1}(z)\bar{B}(z)] \\ \bar{B}(z) = -\frac{1}{2\bar{M}(z)} \\ \bar{M}(z) = M^{(1)-1}(z)M^{(2)}(z)M^{(1)-1}(z)M^{(2)}(z)M^{(1)-1}(z) \end{cases}} \tag{1.23}$$

In Eq.(1.23), $M^{(k)}$ stands for :

$$M^{(k)}_{\alpha\beta} = \sum_{\mu<\nu} \frac{\langle\Phi|\hat{Q}_\alpha\xi^+_\mu\xi^+_\nu|\Phi\rangle\langle\Phi|\xi_\nu\xi_\mu\hat{Q}_\beta|\Phi\rangle}{(\epsilon_\mu+\epsilon_\nu)^k} \tag{1.24}$$

Note that α and β indices are related to the collective coordinates associated with the multipole moment operators $\hat{Q}$. The indices μ and ν span the quasiparticle basis, and ϵ_μ and ϵ_ν are the related quasiparticle energies.

To conclude, it is claimed that the latter quantities defined in Eq.(1.23) tremendously suffer from the lack of time-odd components [37]. Because of that, ATDHFB collective potential, inertia tensor, and inertial mass are often used instead of the TDGCM+GOA ones:

$$\boxed{\begin{cases} \tilde{V}(z) = h(z,z) + \mathrm{Tr}[M^{(1)-1}(z)M^{(2)}(z)M^{(1)-1}(z)\tilde{B}(z)] \\ \tilde{B}(z) = -\frac{1}{2\tilde{M}(z)} \\ \tilde{M}(z) = M^{(1)-1}(z)M^{(3)}(z)M^{(1)-1}(z) \end{cases}} \tag{1.25}$$

1.2 The SCIM

As for the TDGCM, the SCIM can be divided into two different parts. We first built a collective-intrinsic Hamiltonian. Then we use it to make the SCIM collective-intrinsic wave function evolves over time. These two parts are denoted respectively the "static part" and the "dynamics" of the SCIM thereafter. Although the SCIM has been developed to include any number of collective degrees of freedom, we've restricted the applications to the case of one collective degree of freedom in this PhD thesis. We therefore first give an overview of the static part of the SCIM in its full glory, then we thoroughly present the case when only one collective degree of freedom is considered. Finally, we give some hints about the dynamics, which is describe in great details in Chapter 6.

1.2.1 Static part

The SCIM wave function is a generalization of the GCM wave function Eq.(1.1):

$$\boxed{|\Phi_{SCIM}\rangle = \sum_i \int dq f_i(q) |\Phi^{(i)}(q)\rangle} \tag{1.26}$$

Indeed, in addition to the deformed adiabatic HFB states $|\Phi_0(q)\rangle$, the SCIM wave function expands on various intrinsicly excited states $|\Phi_i(q)\rangle$. Here, the collective coordinate $q \in \mathbb{R}^n$ spans n collective degrees of freedom and the $f_i(q)$ are the coefficients of the linear mixing we'd like to find. To determine those coefficients, a variational principle is applied to the total energy of the SCIM state. It reads:

$$\delta(\langle \Phi_{SCIM} | \hat{H} - E | \Phi_{SCIM} \rangle) = 0 \tag{1.27}$$

$$\delta(\sum_j \sum_i \int dq' \int dq f_j^*(q') \langle \Phi^{(j)}(q') | \hat{H} - E | \Phi^{(i)}(q) \rangle f_i(q)) = 0 \tag{1.28}$$

This expression is first transformed using the center of mass and relative coordinates:

$$\begin{cases} \bar{q} = \frac{q+q'}{2} \\ s = \frac{q-q'}{2} \end{cases} \tag{1.29}$$

We introduced the relative coordinate s with a factor 2 compared with [33], in order to make the derivations easier. We obtain:

$$\delta(\frac{1}{2^n} \sum_j \sum_i \int d\bar{q} \int ds f_j^*(\bar{q}-s) \langle \Phi^{(j)}(\bar{q}-s) | \hat{H} - E | \Phi^{(i)}(\bar{q}+s) \rangle f_i(\bar{q}+s)) = 0 \tag{1.30}$$

Using Taylor expansion to express the functions f_i at the point $\bar{q}$ leads to:

$$f_i(\bar{q}+s) = \sum_{\alpha_1=0}^{+\infty} ... \sum_{\alpha_n=0}^{+\infty} \frac{s_1^{\alpha_1} ... s_n^{\alpha_n}}{\alpha_1! ... \alpha_n!} \frac{\partial^{\alpha_1+...+\alpha_n}}{\partial q_1^{\alpha_1} ... \partial q_n^{\alpha_n}} f_i(\bar{q}) = e^{s \frac{\partial}{\partial q}} f_i(\bar{q}) \tag{1.31}$$

The quantities $(s\frac{\partial}{\partial q})^k = (s_1\frac{\partial}{\partial q_1} + ... + s_n\frac{\partial}{\partial q_n})^k$ are developed using the multinomial theorem:

$$(s\frac{\partial}{\partial q})^k = \sum_{\alpha_1+...+\alpha_n=k} \binom{k}{\alpha_1, ..., \alpha_n} s_1^{\alpha_1} \frac{\partial^{\alpha_1}}{\partial q_1^{\alpha_1}} ... \frac{\partial^{\alpha_n}}{\partial q_n^{\alpha_n}} \tag{1.32}$$

We can thus write the inner part of the Eq.(1.30) as follows:

$$\int d\bar{q} \int ds f_j^*(\bar{q}-s)\langle\Phi^{(j)}(\bar{q}-s)|\hat{H}-E|\Phi^{(i)}(\bar{q}+s)\rangle f_i(\bar{q}+s)) = \int d\bar{q} \sum_{k=0}^{+\infty} \frac{(-1)^k}{k!} \tag{1.33}$$
$$\sum_{\alpha_1+...+\alpha_n=k} \binom{k}{\alpha_1, ..., \alpha_n} s_1^{\alpha_1} \frac{\partial^{\alpha_1}}{\partial q_1^{\alpha_1}} ... \frac{\partial^{\alpha_n}}{\partial q_n^{\alpha_n}} [f_j^*(\bar{q})]\langle\Phi^{(j)}(\bar{q}-s)|\hat{H}-E|\Phi^{(i)}(\bar{q}+s)\rangle e^{s\frac{\partial}{\partial q}} f_i(\bar{q})$$

We transform this expression performing multiple integrations by parts and assuming that the various quantities implied and their derivatives are equal to zeros at infinity. We finally get:

$$\delta(\frac{1}{2^n}\sum_j\sum_i \int ds \int d\bar{q} f_j^*(\bar{q}) e^{s\frac{\partial}{\partial q}} \langle\Phi^{(j)}(\bar{q}-s)|\hat{H}-E|\Phi^{(i)}(\bar{q}+s)\rangle e^{s\frac{\partial}{\partial q}} f_i(\bar{q})) = 0 \tag{1.34}$$

Performing the variations with respect to the $f_j^*(\bar{q})$ we find:

$$\forall \bar{q},\ \forall j, \qquad \sum_i \int ds e^{s\frac{\partial}{\partial q}} \langle\Phi^{(j)}(\bar{q}-s)|\hat{H}-E|\Phi^{(i)}(\bar{q}+s)\rangle e^{s\frac{\partial}{\partial q}} f_i(\bar{q}) = 0 \tag{1.35}$$

We define the following shorthand notations for the kernels:

$$\begin{cases} \mathcal{H}_{ji}(\bar{q},s) = \langle\Phi^{(j)}(\bar{q}-s)|\hat{H}-E|\Phi^{(i)}(\bar{q}+s)\rangle \\ \mathcal{N}_{ji}(\bar{q},s) = \langle\Phi^{(j)}(\bar{q}-s)|\Phi^{(i)}(\bar{q}+s)\rangle \end{cases} \tag{1.36}$$

Now, we consider the effect of the exponentials on those kernels using the Symmetric Ordered Products of Operators (SOPO), detailed in Appendix A:

$$\begin{cases} e^{s\frac{\partial}{\partial q}}\mathcal{H}_{ji}(\bar{q},s)e^{s\frac{\partial}{\partial q}} = \sum_{k=0}^{+\infty} \frac{1}{k!}[\mathcal{H}_{ji}(\bar{q},s)(s\frac{\partial}{\partial q})]^{(k)} \\ e^{s\frac{\partial}{\partial q}}\mathcal{N}_{ji}(\bar{q},s)e^{s\frac{\partial}{\partial q}} = \sum_{k=0}^{+\infty} \frac{1}{k!}[\mathcal{N}_{ji}(\bar{q},s)(s\frac{\partial}{\partial q})]^{(k)} \end{cases} \tag{1.37}$$

As the dependence in s is totally included in the SOPOs, we can integrate inside them and write:

$$\begin{cases} \bar{\mathcal{H}}_{ji}(\bar{q}) = \int ds \sum_{k=0}^{+\infty} \frac{1}{k!}[\mathcal{H}_{ji}(\bar{q},s)(s\frac{\partial}{\partial q})]^{(k)} \\ \bar{\mathcal{N}}_{ji}(\bar{q}) = \int ds \sum_{k=0}^{+\infty} \frac{1}{k!}[\mathcal{N}_{ji}(\bar{q},s)(s\frac{\partial}{\partial q})]^{(k)} \end{cases} \tag{1.38}$$

Doing so, we can rewrite Eq.(1.35) as:

$$\forall \bar{q},\ \forall j, \qquad \sum_i \bar{\mathcal{H}}_{ji}(\bar{q}) f_i(\bar{q}) = E \sum_i \bar{\mathcal{N}}_{ji}(\bar{q}) \tag{1.39}$$

Or, in a more compact form:

$$\bar{\mathcal{H}} f = E \bar{\mathcal{N}} f \tag{1.40}$$

As for the GCM, we assume that we can get an expression of the inverse of the square root of $\bar{\mathcal{N}}$. This inversion process will be explicitly described in the case of one collective degree of freedom. With this inverse square root, it is finally possible to write the collective-intrinsic Hamiltonian:

$$\boxed{\begin{cases} \mathcal{H}_{SCIM} g = E g \\ \mathcal{H}_{SCIM} = \bar{\mathcal{N}}^{-1/2} \bar{\mathcal{H}} \bar{\mathcal{N}}^{-1/2} \\ g = \bar{\mathcal{N}}^{1/2} f \end{cases}} \tag{1.41}$$

1.2.2 SCIM Static part with one collective degree of freedom

Up to Eq.(1.38), the derivations are quite general. It is then possible to rewrite more explicitly the integrations inside the SOPOs, introducing the moments of order p of an operator:

$$\begin{cases} \mathcal{H}^{(p)}_{ji}(\bar{q}) = \int ds \mathcal{H}_{ji}(\bar{q}, s) s^p \\ \mathcal{N}^{(p)}_{ji}(\bar{q}) = \int ds \mathcal{N}_{ji}(\bar{q}, s) s^p \end{cases} \tag{1.42}$$

With these moments, we can rewrite Eq.(1.38) as follows:

$$\begin{cases} \int ds \sum_{k=0}^{+\infty} \frac{1}{k!} [\mathcal{H}_{ji}(\bar{q}, s)(s \frac{\partial}{\partial q})]^{(k)} = \sum_{k=0}^{+\infty} \frac{1}{k!} [\mathcal{H}^{(k)}_{ji}(\bar{q}) \frac{\partial}{\partial q}]^{(k)} \\ \int ds \sum_{k=0}^{+\infty} \frac{1}{k!} [\mathcal{N}_{ji}(\bar{q}, s)(s \frac{\partial}{\partial q})]^{(k)} = \sum_{k=0}^{+\infty} \frac{1}{k!} [\mathcal{N}^{(k)}_{ji}(\bar{q}) \frac{\partial}{\partial q}]^{(k)} \end{cases} \tag{1.43}$$

We choose to keep the SOPOs only up to order 2. This approximation follows what is usually done to tackle the Hill-Wheeler equation. As an example, h is expanded in Taylor series up to order 2 in the GOA Eq.(1.16). Indeed, the second order is often a good starting point. Note that this truncation implicitly implies a certain regularity of the functions f_i. Using the following shorthand notations:

$$\begin{cases} \bar{\mathcal{H}}_{ji}(\bar{q}) = \sum_{k=0}^{2} \frac{1}{k!} [\mathcal{H}^{(k)}_{ji}(\bar{q}) \frac{\partial}{\partial q}]^{(k)} \\ \bar{\mathcal{N}}_{ji}(\bar{q}) = \sum_{k=0}^{2} \frac{1}{k!} [\mathcal{N}^{(k)}_{ji}(\bar{q}) \frac{\partial}{\partial q}]^{(k)} \end{cases} \tag{1.44}$$

The full equation in its compact form reads as:

$$\forall \bar{q}, \qquad \bar{\mathcal{H}}(\bar{q}) f(\bar{q}) = E \bar{\mathcal{N}}(\bar{q}) f(\bar{q}) \tag{1.45}$$

The problem we are facing now is the inversion of the square root of the operator $\bar{\mathcal{N}}$. This inversion is not straightforward and we've followed what has been done in [33, 34]. We start writing $\bar{\mathcal{N}}$ more explicitly:

$$\boxed{\bar{\mathcal{N}}(\bar{q}) = \mathcal{N}^{(0)}(\bar{q}) + [\mathcal{N}^{(1)}(\bar{q})\frac{\partial}{\partial q}]^{(1)} + \frac{1}{2}[\mathcal{N}^{(2)}(\bar{q})\frac{\partial}{\partial q}]^{(2)}} \tag{1.46}$$

Note that the quantities $\mathcal{N}^{(p)}(\bar{q})$ are matrices whose coefficients are the $\mathcal{N}^{(p)}_{ji}(\bar{q})$:

$$\mathcal{N}^{(p)}(\bar{q}) = \begin{pmatrix} \mathcal{N}^{(p)}_{00}(\bar{q}) & \dots & \mathcal{N}^{(p)}_{0n}(\bar{q}) \\ \vdots & \ddots & \vdots \\ \mathcal{N}^{(p)}_{n0}(\bar{q}) & \dots & \mathcal{N}^{(p)}_{nn}(\bar{q}) \end{pmatrix} \tag{1.47}$$

The definition of the moments implies that the matrices $\mathcal{N}^{(p)}(\bar{q})$ are symmetric for even values of p and skew-symmetric for odd ones. As $\mathcal{N}^{(0)}(\bar{q})$ is a symmetric positive definite matrix for all $\bar{q}$, it is possible to define its square root:

$$\forall \bar{q}, \qquad \mathcal{N}^{(0)1/2}(\bar{q})\mathcal{N}^{(0)1/2}(\bar{q}) = \mathcal{N}^{(0)}(\bar{q}) \tag{1.48}$$

We factorize the full $\bar{\mathcal{N}}(\bar{q})$ operator with this square root. We also consider implicitly the $\bar{q}$ dependence to make notations clearer:

$$\bar{\mathcal{N}} = \mathcal{N}^{(0)1/2}(I + \mathcal{N}^{(0)-1/2}[\mathcal{N}^{(1)}\frac{\partial}{\partial q}]^{(1)}\mathcal{N}^{(0)-1/2} + \frac{1}{2}\mathcal{N}^{(0)-1/2}[\mathcal{N}^{(2)}\frac{\partial}{\partial q}]^{(2)}\mathcal{N}^{(0)-1/2})\mathcal{N}^{(0)1/2} \tag{1.49}$$

Using the product formula in Appendix A, we get:

$$\begin{aligned} \mathcal{N}^{(0)-1/2}[\mathcal{N}^{(1)}\frac{\partial}{\partial q}]^{(1)}\mathcal{N}^{(0)-1/2} &= \mathcal{N}^{(0)-1/2}\mathcal{N}^{(1)}(\mathcal{N}^{(0)-1/2})' \\ -(\mathcal{N}^{(0)-1/2})'\mathcal{N}^{(1)}\mathcal{N}^{(0)-1/2} &+ [\mathcal{N}^{(0)-1/2}\mathcal{N}^{(1)}\mathcal{N}^{(0)-1/2}\frac{\partial}{\partial q}]^{(1)} \end{aligned} \tag{1.50}$$

And:

$$\begin{aligned} \frac{1}{2}\mathcal{N}^{(0)-1/2}[\mathcal{N}^{(2)}\frac{\partial}{\partial q}]^{(2)}\mathcal{N}^{(0)-1/2} &= \frac{1}{2}((\mathcal{N}^{(0)-1/2})''\mathcal{N}^{(2)}\mathcal{N}^{(0)-1/2} \\ +\mathcal{N}^{(0)-1/2}\mathcal{N}^{(2)}(\mathcal{N}^{(0)-1/2})'' &- 2(\mathcal{N}^{(0)-1/2})'\mathcal{N}^{(2)}(\mathcal{N}^{(0)-1/2})') \\ +[(\mathcal{N}^{(0)-1/2}\mathcal{N}^{(2)}(\mathcal{N}^{(0)-1/2})' &- (\mathcal{N}^{(0)-1/2})'\mathcal{N}^{(2)}\mathcal{N}^{(0)-1/2})\frac{\partial}{\partial q}]^{(1)} \\ &+[\frac{1}{2}\mathcal{N}^{(0)-1/2}\mathcal{N}^{(2)}\mathcal{N}^{(0)-1/2}\frac{\partial}{\partial q}]^{(2)} \end{aligned} \tag{1.51}$$

Using the following shorthand notations:

$$\begin{aligned} \alpha_0 = \mathcal{N}^{(0)-1/2}\mathcal{N}^{(1)}(\mathcal{N}^{(0)-1/2})' - (\mathcal{N}^{(0)-1/2})'\mathcal{N}^{(1)}\mathcal{N}^{(0)-1/2} &+ \frac{1}{2}((\mathcal{N}^{(0)-1/2})''\mathcal{N}^{(2)}\mathcal{N}^{(0)-1/2} \\ +\mathcal{N}^{(0)-1/2}\mathcal{N}^{(2)}(\mathcal{N}^{(0)-1/2})'' &- 2(\mathcal{N}^{(0)-1/2})'\mathcal{N}^{(2)}(\mathcal{N}^{(0)-1/2})') \end{aligned} \tag{1.52}$$

And:

$$\mathcal{N}_{R_0}^{(1)} = \mathcal{N}^{(0)-1/2}\mathcal{N}^{(1)}\mathcal{N}^{(0)-1/2} + \mathcal{N}^{(0)-1/2}\mathcal{N}^{(2)}(\mathcal{N}^{(0)-1/2})' - (\mathcal{N}^{(0)-1/2})'\mathcal{N}^{(2)}\mathcal{N}^{(0)-1/2} \quad (1.53)$$

$$\mathcal{N}_{R_0}^{(2)} = \frac{1}{2}\mathcal{N}^{(0)-1/2}\mathcal{N}^{(2)}\mathcal{N}^{(0)-1/2} \quad (1.54)$$

Eq.(1.49) reads:

$$\bar{\mathcal{N}} = \mathcal{N}^{(0)1/2}(I + \alpha_0 + [\mathcal{N}_{R_0}^{(1)}\frac{\partial}{\partial q}]^{(1)} + [\mathcal{N}_{R_0}^{(2)}\frac{\partial}{\partial q}]^{(2)})\mathcal{N}^{(0)1/2} \quad (1.55)$$

Eq.(1.55) is the first iteration of an iterative process in which we assume that the Frobenius norm $||\alpha_0||$ is small and gets smaller as the factorization process is iterated. In practice, we stop at the i-th iteration when $||\alpha_i|| < 10^{-10}$. At the end of the process, we end up with the following expression:

$$\boxed{\bar{\mathcal{N}}(\bar{q}) = \mathcal{F}(\bar{q})(I + [\mathcal{N}_R^{(1)}(\bar{q})\frac{\partial}{\partial q}]^{(1)} + [\mathcal{N}_R^{(2)}(\bar{q})\frac{\partial}{\partial q}]^{(2)})\mathcal{F}^T(\bar{q})} \quad (1.56)$$

With:

$$\mathcal{F}(\bar{q}) = \mathcal{N}^{(0)1/2}(\bar{q})(I + \alpha_0(\bar{q}))^{1/2}...(I + \alpha_{i-1}(\bar{q}))^{1/2} \quad (1.57)$$

Defining $\mathcal{J}(\bar{q})$ as:

$$\boxed{\mathcal{J}(\bar{q}) = I + [\mathcal{N}_R^{(1)}(\bar{q})\frac{\partial}{\partial q}]^{(1)} + [\mathcal{N}_R^{(2)}(\bar{q})\frac{\partial}{\partial q}]^{(2)} = I + \mathcal{U}(\bar{q})} \quad (1.58)$$

We write the inverse of the square root of $\mathcal{J}$ as a series. The convergence of this series is probably the strongest approximation of the model as it implies for the derivatives of the overlap kernel's moments to tend towards zero very fast as derivation order increases:

$$\boxed{\mathcal{J}^{-1/2}(\bar{q}) = I + \sum_{k=1}^{+\infty}\frac{(-1/2)...(-1/2-k+1)}{k!}\mathcal{U}^k(\bar{q})} \quad (1.59)$$

Keeping this series only up to the second order in SOPO, we deduce the following expression for the inverse square root of $\bar{\mathcal{N}}$:

$$\boxed{\bar{\mathcal{N}}^{-1/2}(\bar{q}) = \mathcal{J}^{-1/2}(\bar{q})\mathcal{F}^{-1}(\bar{q})} \quad (1.60)$$

Using Eq.(1.60), the collective-intrinsic Hamiltonian reads:

$$\mathcal{H}_{SCIM}(\bar{q}) = \bar{\mathcal{N}}^{-1/2}\bar{\mathcal{H}}(\bar{q})(\bar{\mathcal{N}}^{-1/2})^T \quad (1.61)$$

Developing this expression only up to the second order in SOPO, the collective-intrinsic Hamiltonian eventually reads:

$$\boxed{\mathcal{H}_{SCIM}(\bar{q}) = V(\bar{q}) + [D(\bar{q})\frac{\partial}{\partial q}]^{(1)}] + [B(\bar{q})\frac{\partial}{\partial q}]^{(2)}} \tag{1.62}$$

The zero-order V and second-order part B of the collective-intrinsic Hamiltonian are comparable to the ones obtained in TDGCM. The first-order part D is totally new. The skew-symmetric matrix D called dissipation tensor accounts for dissipative dynamical correlations. Explicit formulas for V, D and B are given in Appendix M.

1.2.3 Dynamics

Once the collective-intrinsic Hamiltonian $\mathcal{H}_{SCIM}$ is found, it is possible to use it in the following Schrödinger equation to describe the "dynamics" of the nucleus including intrinsicly excited states:

$$\boxed{\mathcal{H}_{SCIM}g(t) = i\hbar\frac{\partial}{\partial t}g(t)} \tag{1.63}$$

Solving this equation gives access to lifetimes and yields corrected by the excitation process, but not only. Indeed, including these additional excitations, it is possible to give a more accurate description of energy balance at scission and thus evaluate the total kinetic energy and the neutron multiplicity, for example.

Chapter 2

SCIM static states: issues and challenges

The SCIM method relies on a set of static states $\{|\Phi_i(q)\rangle\}$. For each i spanning a specific intrinsic excitation ($i = 0$ standing for the adiabatic states), the set $\{|\Phi_i(q)\rangle\}$ is assumed to be continuous in the collective variable q. Moreover, the Hamiltonian and overlap kernels associated with this set are supposed to have a regular behaviour, *i.e* their derivatives tend towards zero quickly when the derivation order increases.
These continuity and regularity requirements are unfortunately far from being easy to fulfill, even for the adiabatic states. Indeed, performing HFB calculations with constraints on the multipole moments, we may find adjacent states with a very small overlap kernel [40]. This problem comes from the fact that the calculations with multipole moment constraints rely on some well-chosen degrees of freedom, letting free the others that may be discontinuous. Besides, even considering continous parts of the adiabatic set, we found that the Hamiltonian and overlap kernels were most of the time not regular enough. This lack of regularity is related to the choice of the collective coordinate which sometimes doesn't account faithfully for the evolution of the system.
When it comes to intrinsic excitations, the problems of the adiabatic states are still and get even worse. The non-self-consistent 2-quasiparticle excited states proposed by Bernard *et al.* [33, 34] were based on assumptions that turned out to be too optimistic. Indeed, these excited states break the average particle number in such a way that the regularity of the Hamiltonian kernels is never good enough for the SCIM to work. It is the case even when considering the "small" particle number variations (in the range $]-1, 1[$) assumed by Bernard *et al.* Moreover, the overlap kernels of the 2-quasiparticle excited states also present severe local irregularities when their quasiparticles are involved in level repulsions.

To tackle these issues we've tried different techniques. We have first implemented the particle number projection after variations method in order to correct the excited Hamiltonian kernels pathologies. The method worked well for this puprpose, but we unfortunately found out that the kernels regularity was still not good enough to perform SCIM calculations. Besides, the projected excited states were in general no more orthogonal to the projected adiabatic states.

2.1 HFB method for the adiabatic states

The HFB or Hartree-Fock-Bogoliubov method [41–45] is a pillar of the SCIM approach as it provides it with its static states. The HFB method consists in building a quasiparticle product wave function to describe a nucleus. This wave function reads:

$$|\Phi_{HFB}\rangle = \mathcal{N} \prod \xi_i |0\rangle \qquad \text{with} \qquad \forall i,\ \xi_i |\Phi_{HFB}\rangle = 0 \tag{2.1}$$

Here, $|0\rangle$ is the true vacuum of particle and the $\{\xi_i\}$ represent the quasiparticle annihilation operators. Moreover, $\mathcal{N}$ is the norm factor of the HFB wave function (its expression is explicitly given in Chapter 5). Eq.(2.1) clearly states that $|\Phi_{HFB}\rangle$ is a vacuum for those quasiparticle operators. The $\{\xi_i\}$ operators are defined as follows using an orthonormal basis associated with the creation and annihilation operators $\{c_k^+\}$ and $\{c_k\}$ respectively:

$$\xi_i = \sum_k U_{ki}^* c_k + V_{ki}^* c_k^+ \qquad \Leftrightarrow \qquad \begin{pmatrix} \xi \\ \xi^+ \end{pmatrix} = \begin{pmatrix} U^+ & V^+ \\ V^T & U^T \end{pmatrix} \begin{pmatrix} c \\ c^+ \end{pmatrix} \tag{2.2}$$

This transformation is the most general linear mixing of creation and annihilation operators. The matrix built up with the matrices U and V is called the Bogoliubov transformation matrix:

$$B = \begin{pmatrix} U^+ & V^+ \\ V^T & U^T \end{pmatrix} \tag{2.3}$$

For this transformation to be canonical, *i.e* to be invertible and preserve fermions anticommutation relations, the matrix B has to be unitary. This implies the following relations between the matrices U and V:

$$\begin{cases} U^+U + V^+V = I \\ UU^+ + V^*V^T = I \end{cases} \qquad \begin{cases} V^TU + U^TV = 0 \\ UV^+ + V^*U^T = 0 \end{cases} \tag{2.4}$$

In Eq.(2.1), the unknown quantities to determine are the elements of the U and V matrices under the conditions of Eq.(2.4). To do so, we use a variational principle on a functional that accounts for the energy of the system:

$$\boxed{\mathcal{E} = \frac{\langle \Phi_{HFB} | \hat{H} | \Phi_{HFB} \rangle}{\langle \Phi_{HFB} | \Phi_{HFB} \rangle}} \tag{2.5}$$

There exist different methods to guarantee the conditions Eq.(2.4). In [46] for instance, the one-body density ρ and the pairing tensor κ are defined:

$$\begin{cases} \rho_{\alpha\beta} = \langle \Phi_{HFB} | c_\beta^+ c_\alpha | \Phi_{HFB} \rangle = (V^*V^T)_{\alpha\beta} \\ \kappa_{\alpha\beta} = \langle \Phi_{HFB} | c_\alpha c_\beta | \Phi_{HFB} \rangle = (V^*U^T)_{\alpha\beta} \end{cases} \tag{2.6}$$

Then, a generalized density matrix R is built with these matrices:

$$R = \begin{pmatrix} \rho & \kappa \\ -\kappa^* & I - \rho^* \end{pmatrix} = B^+ \begin{pmatrix} 0 & 0 \\ 0 & I \end{pmatrix} B \tag{2.7}$$

The conditions stated in Eq.(2.4) are then equivalent to the simple condition $R^2 = R$, which is imposed in the derivations. In this work however, we've chosen to present the derivations based on the Thouless theorem [45]. They allow to present both the gradient and the diagonalization methods that will be useful in the following. The Thouless theorem (see Appendix B) is used to find variational parameters for which the conditions of Eq.(2.4) naturally hold. Indeed, let's suppose we already have a state $|\Phi_0\rangle$ that verifies Eq.(2.4). If we consider another state $|\Phi\rangle$ verifying Eq.(2.4) which is not orthogonal to the latter, we can write using the Thouless theorem:

$$\boxed{|\Phi(Z)\rangle = \langle\Phi_0|\Phi(Z)\rangle e^{\sum_{k<k'} Z_{kk'}\xi_k^+\xi_{k'}^+}|\Phi_0\rangle} \tag{2.8}$$

Here, Z is a skew-symmetric matrix. Conversely, each state built this way verifies Eq.(2.4). The matrix Z therefore gives a good parametrization of the functional $\mathcal{E}$ as it directly includes the conditions Eq.(2.4). We can write, considering any variation δZ of Z:

$$\delta\mathcal{E} = \sum_{ij} \frac{\partial\mathcal{E}}{\partial Z^*_{ij}}_{|Z=0} \delta Z^*_{ij} = 0 \qquad \forall\delta Z \tag{2.9}$$

Eq.(2.9) leads to:

$$\boxed{\forall i,j, \frac{\partial\mathcal{E}}{\partial Z^*_{ij}}_{|Z=0} = 0 \qquad \forall i,j} \tag{2.10}$$

To be consistent with the calculations we have made with the Gogny interaction, we assume that the Hamiltonian of the system contains an effective two-body nucleon-nucleon interaction with a density-dependent term in such a way that $\hat{H}$ depends on Z:

$$\hat{H}(Z) = \sum_{\alpha\beta} t_{\alpha\beta} c^+_\alpha c_\beta + \frac{1}{4}\sum_{\alpha\beta\gamma\delta} v^{(a)}_{\alpha\beta\gamma\delta}(Z) c^+_\alpha c^+_\beta c_\delta c_\gamma \tag{2.11}$$

Here $v^{(a)}$ is the antisymmetrized version of the nucleon-nucleon interaction v, *i.e*:

$$v^{(a)}_{\alpha\beta\gamma\delta} = v_{\alpha\beta\gamma\delta} - v_{\alpha\beta\delta\gamma} \tag{2.12}$$

When we state that the interaction has a density dependence, it means that the operator $\hat{H}(Z)$ depends on the state $|\Phi\rangle$ we consider through its one-body density. $\hat{H}$(Z) is thus a pseudo-operator in our case. It is useful to write $\hat{H}$(Z) in the quasiparticle representation [45]:

$$\hat{H}(Z) = H^0(Z) + \sum_{kk'} H^{11}_{kk'}(Z)\xi^+_k\xi_{k'} + \frac{1}{2}\sum_{kk'} H^{20}_{kk'}(Z)\xi^+_k\xi^+_{k'} + ... \tag{2.13}$$

We only keep the part of $\hat{H}(Z)$ that is relevant in the following. The different components read:

$$\begin{cases} H^0(Z) = \mathrm{Tr}(t\rho + \frac{1}{2}\Gamma(Z)\rho - \frac{1}{2}\Delta(Z)\kappa^*) \\ H^{11}(Z) = U^+h(Z)U - V^+h^T(Z)V + U^+\Delta(Z)V - V^+\Delta^*(Z)U \\ H^{20}(Z) = U^+h(Z)V^* - V^+h^T(Z)U^* + U^+\Delta(Z)U^* - V^+\Delta^*(Z)V^* \end{cases} \tag{2.14}$$

In Eq.(2.14), $\Gamma(Z)$ is called the mean field and $\Delta(Z)$ the pairing field. They read as follows:

$$\begin{cases} \Gamma_{\alpha\gamma}(Z) = \sum_{\beta\delta} v^{(a)}_{\alpha\beta\gamma\delta}(Z)\rho_{\delta\beta} \\ \Delta_{\alpha\beta}(Z) = \frac{1}{2}\sum_{\gamma\delta} v^{(a)}_{\alpha\beta\gamma\delta}(Z)\kappa_{\gamma\delta} \\ h(Z) = t + \Gamma(Z) \end{cases} \tag{2.15}$$

The matrices ρ and κ used in Eq.(2.14) are related to the state $|\Phi_0\rangle$, while the density $\rho(Z)$ used in the density-dependent term is the one of the state $|\Phi(Z)\rangle$:

$$\rho_{\alpha\beta} = \langle\Phi_0|c^+_\beta c_\alpha|\Phi_0\rangle \neq \rho_{\alpha\beta}(Z) = \langle\Phi(Z)|c^+_\beta c_\alpha|\Phi(Z)\rangle \tag{2.16}$$

Using Eq.(2.13) into Eq.(2.10), we write:

$$\frac{\partial\mathcal{E}}{\partial Z^*_{ij}}_{|Z=0} = \frac{\partial}{\partial Z^*_{ij}}\frac{\langle\Phi(Z)|\hat{H}(Z)|\Phi(Z)\rangle}{\langle\Phi(Z)|\Phi(Z)\rangle}|_{Z=0} = (\frac{\partial H^0}{\partial Z^*_{ij}} + H^{20}_{ij})_{|Z=0} \tag{2.17}$$

If we focus on the first term, we find:

$$\frac{\partial H^0}{\partial Z^*_{ij}}_{|Z=0} = \sum_{\alpha\beta}\frac{\partial H^0}{\partial\rho_{\alpha\beta}}\frac{\partial\rho_{\alpha\beta}}{\partial Z^*_{ij}}_{|Z=0} = \frac{\partial}{\partial Z^*_{ij}}\langle\Phi(Z)|\sum_{\alpha\beta}\frac{\partial H^0}{\partial\rho_{\alpha\beta}}c^+_\beta c_\alpha|\Phi(Z)\rangle_{|Z=0} \tag{2.18}$$

This result suggests that we could write the additional terms due to the density-dependent part of $\hat{H}(Z)$ as a one-body operator and preserve the behaviour of the equations. Doing so in quasiparticle representation, we get:

$$\hat{H} = H^0 + \sum_{kk'}\tilde{H}^{11}_{kk'}\xi^+_k\xi_{k'} + \frac{1}{2}\sum_{kk'}\tilde{H}^{20}_{kk'}\xi^+_k\xi^+_{k'} \tag{2.19}$$

This hamiltonian doesn't depend anymore on the state $|\Phi(Z)\rangle$, but is fully written with respect to $|\Phi_0\rangle$. Its components read:

$$\begin{cases} H^0 = \mathrm{Tr}(t\rho + \frac{1}{2}\Gamma\rho - \frac{1}{2}\Delta\kappa^*) \\ \tilde{H}^{11} = U^+\tilde{h}U - V^+\tilde{h}^TV + U^+\Delta V - V^+\Delta^*U \\ \tilde{H}^{20} = U^+\tilde{h}V^* - V^+\tilde{h}^TU^* + U^+\Delta U^* - V^+\Delta^*V^* \end{cases} \tag{2.20}$$

The fields now read:

$$\begin{cases} \Gamma = \Gamma|_{Z=0} \\ \Delta = \Delta|_{Z=0} \\ \tilde{h}_{\alpha\gamma} = t_{\alpha\gamma} + \Gamma_{\alpha\gamma} + \frac{1}{2}\sum_{ijkl} \frac{\partial v^{(a)}_{iljk}}{\partial \rho_{\gamma\alpha}} \rho_{kl}\rho_{ji} - \frac{1}{4}\sum_{ijkl} \frac{\partial v^{(a)}_{ijkl}}{\partial \rho_{\gamma\alpha}} \kappa_{kl}\kappa^*_{ji} \end{cases} \tag{2.21}$$

The new definition of $\hat{H}$ given in Eq.(2.19) leads to:

$$\boxed{\tilde{H}^{20}_{ij} = 0 \qquad \forall i,j} \tag{2.22}$$

The quasiparticles, and thus the U and V matrices, obtained from this equation are defined up to a unitary transformation. We can therefore choose the representation that diagonalizes $\tilde{H}^{11}$. In this representation, the Hamiltonian reads under the HFB approximation:

$$\hat{H} = H^{(0)} + \sum_k \tilde{H}^{11}_{kk}\xi^+_k\xi_k \tag{2.23}$$

Note that the HFB approximation consists in neglecting H^{40},H^{31} and H^{22}. We then have:

$$\hat{H}|\Phi_{HFB}\rangle = H^{(0)}|\Phi_{HFB}\rangle = E_{HFB}|\Phi_{HFB}\rangle \tag{2.24}$$

$$\hat{H}\xi^+_i|\Phi_{HFB}\rangle = (H^{(0)} + \tilde{H}^{11}_{ii})\xi^+_i|\Phi_{HFB}\rangle = (E_{HFB} + \epsilon_i)|\Phi_{HFB}\rangle \tag{2.25}$$

These equations clearly show why the quasiparticle representation that diagonalizes $\tilde{H}^{11}$ is chosen: it is the one in which the one-quasiparticle excited states are eigenstates of the Hamiltonian along with the HFB adiabatic state.

To conclude, we show how we obtain the usual formulation of the HFB equations. We first define the HFB Hamiltonian matrix $\mathcal{H}_{HFB}$:

$$\mathcal{H}_{HFB} = \begin{pmatrix} \tilde{h} & \Delta \\ -\Delta^* & -\tilde{h}^* \end{pmatrix} = B^+ \begin{pmatrix} \tilde{H}^{11} & \tilde{H}^{20} \\ -\tilde{H}^{20*} & -\tilde{H}^{11*} \end{pmatrix} B \tag{2.26}$$

The matrix B clearly diagonalizes $\mathcal{H}_{HFB}$:

$$\mathcal{H}_{HFB} \begin{pmatrix} U_i \\ V_i \end{pmatrix} = \epsilon_i \begin{pmatrix} U_i \\ V_i \end{pmatrix} \tag{2.27}$$

Since $\mathcal{H}_{HFB}$ and the generalized density matrix R defined in Eq.(2.7) are diagonal in the same representation, we finally get:

$$\boxed{[\mathcal{H}_{HFB}, R] = 0} \tag{2.28}$$

Eq.(2.22) is the starting point of the gradient descent method to solve the HFB problem while Eq.(2.28) naturally leads to an iterative diagonalization method. Both methods are presented later in this Chapter. We have derived the HFB equations in the most general case. In the following sections, we emphasize on the specificities of this PhD thesis work.

2.1.1 Symmetries

In the context of the methods based on the mean-field approximation, the more symmetries we break then restore, the better the description of the system. In practice, breaking symmetries and restoring them implies a non negligible numerical cost. This is the reason why breaking symmetries is a matter of compromise.
In the case of fission, the influence of pairing correlations is fundamental. A very convenient way to include them at the mean-field level is precisely to use the HFB approach. From Eq.(2.2), it is clear that the HFB wave function doesn't contain a definite particle number. By essence, it breaks the particle number symmetry. Even though we can impose the particle number to be conserved in average (see section on constraints), the fluctuations are far from being negligible.
Besides, on a good approximation, the fission process occurs along a symmetry axis (with the exception of the first barrier). This fact leads to the conservation of axial symmetry. It means that the states we consider have to be eigenstates of projection $\hat{J}_z$ of the total angular momentum operator, associated with the quantum number Ω.
In addition, the time-reversal symmetry (see Appendix O) is also preserved in our calculations. Even if it has the advantage to reduce a lot the complexity of the calculations, it also imposes to consider only even-even nuclei with $\Omega = 0$.
Finally, the experimental data show that the fission of a nucleus can lead to either a symmetric or an asymmetric fragmentation. In order to reflect this observation, the description has to allow the parity symmetry breaking.
In coherence with the symmetries chosen, we build quasiparticles with a specific Ω as a mix of creation and annihilation operators with the same Ω. Moreover, the $\{\xi_i\}$ are paired by the time-reversal operator $\hat{T}$, which means that the HFB wave function reads:

$$|\Phi_{HFB}\rangle = \mathcal{N} \prod_i \xi_i \bar{\xi}_i |0\rangle \qquad \bar{\xi}_i = \hat{T} \xi_i \hat{T}^{-1} \tag{2.29}$$

These conditions imply that the $\{\xi_i\}$ can be written as follows, U and V being real matrices:

$$\begin{cases} \xi_i^\Omega = \sum_{k \in \Omega} U_{ki} c_k + V_{\bar{k}i} \bar{c}_k^+ \\ \bar{\xi}_i^\Omega = \sum_{\bar{k} \in \Omega} U_{\bar{k}\bar{i}} \bar{c}_k + V_{k\bar{i}} c_k^+ \end{cases} \tag{2.30}$$

Applying explicitly the time-reversal operator, we find the following conditions:

$$\begin{cases} U_{ki} = U_{\bar{k}\bar{i}} \\ -V_{\bar{k}i} = V_{k\bar{i}} \end{cases} \qquad \forall k, i, \tag{2.31}$$

Then the full HFB transformation reduces to the simpler one:

$$\begin{pmatrix} \xi \\ \bar{\xi} \\ \xi^+ \\ \bar{\xi}^+ \end{pmatrix} = \begin{pmatrix} U^T & 0 & 0 & V^T \\ 0 & U^T & -V^T & 0 \\ 0 & V^T & U^T & 0 \\ -V^T & 0 & 0 & U^T \end{pmatrix} \begin{pmatrix} c \\ \bar{c} \\ c^+ \\ \bar{c}^+ \end{pmatrix} \Leftrightarrow \begin{pmatrix} \xi \\ \bar{\xi}^+ \end{pmatrix} = \begin{pmatrix} U^T & V^T \\ -V^T & U \end{pmatrix} \begin{pmatrix} c \\ \bar{c}^+ \end{pmatrix} \tag{2.32}$$

Note that U and V have also the Ω-block substructure:

$$U = \begin{pmatrix} U^{\Omega_0} & & 0 \\ & \ddots & \\ 0 & & U^{\Omega_n} \end{pmatrix} \qquad V = \begin{pmatrix} V^{\Omega_0} & & 0 \\ & \ddots & \\ 0 & & V^{\Omega_n} \end{pmatrix} \tag{2.33}$$

Since we do neglect proton-neutron pairing, we don't mix together the creation and annihilation operators with a different isospin, we can thus write the HFB wave function as a tensor product:

$$|\Phi_{HFB}\rangle = |\Phi_{HFB}^{\tau_n}\rangle \otimes |\Phi_{HFB}^{\tau_p}\rangle \tag{2.34}$$

Eq.(2.34) allows us to separate the U and V matrices with respect to the isospin. We can finally write the fully reduced U and V:

$$\begin{pmatrix} \xi^\tau \\ \bar{\xi}^{\tau+} \end{pmatrix} = \begin{pmatrix} U^{\tau T} & -V^{\tau T} \\ V^{\tau T} & U^{\tau T} \end{pmatrix} \begin{pmatrix} c^\tau \\ \bar{c}^{\tau+} \end{pmatrix} \; ; \qquad \begin{cases} U^\tau = \begin{pmatrix} U^{\tau\Omega_0} & & 0 \\ & \ddots & \\ 0 & & U^{\tau\Omega_n} \end{pmatrix} \\ V^\tau = \begin{pmatrix} V^{\tau\Omega_0} & & 0 \\ & \ddots & \\ 0 & & V^{\tau\Omega_n} \end{pmatrix} \end{cases} \tag{2.35}$$

Finally, each of the $U^{\tau\Omega}$ and $V^{\tau\Omega}$ block matrices defined in Eq.(2.35) exhibits a special internal structure described by the famous Bloch-Messiah theorem (see Appendix C):

$$\boxed{U^{\tau\Omega} = \bar{D}^{\tau\Omega}\bar{u}^{\tau\Omega}\bar{C}^{\tau\Omega}} \qquad \boxed{V^{\tau\Omega} = \bar{D}^{\tau\Omega}\bar{v}^{\tau\Omega}\bar{C}^{\tau\Omega}} \tag{2.36}$$

Here, $\bar{D}^{\tau\Omega}$ and $\bar{C}^{\tau\Omega}$ are orthogonal matrices and $\bar{u}^{\tau\Omega}$ and $\bar{v}^{\tau\Omega}$ read as follows:

$$\boxed{\bar{u}^{\tau\Omega} = \begin{pmatrix} u_1 & 0 & \dots & 0 \\ 0 & \ddots & 0 & \vdots \\ \vdots & 0 & \ddots & 0 \\ 0 & \dots & 0 & u_n \end{pmatrix} \quad \text{with } 1 \geq u_i \geq 0} \tag{2.37}$$

$$\boxed{\bar{v}^{\tau\Omega} = \begin{pmatrix} v_1 & 0 & \dots & 0 \\ 0 & \ddots & 0 & \vdots \\ \vdots & 0 & \ddots & 0 \\ 0 & \dots & 0 & v_n \end{pmatrix} \quad \text{with } 1 \geq v_i \geq -1} \tag{2.38}$$

2.1.2 The 2-center harmonic oscillator representation

As mentioned above, the HFB quasiparticles are a linear combination of the creation and annihilation operators associated with an orthonormal particle basis. It is standard to use

bases to build the quasiparticles that are either spherical, axial or triaxial harmonic oscillator bases [47]. Those bases are orthonormal, and are really convenient to evaluate interaction matrix elements and fields, in particular these associated with the Gogny interactions.
As they are all bases, there should be in principle no difference when using them. However, numerical limitations require to truncate the basis we use. In that case, we would like our truncated basis to fit at best the system it aims to describe. This is the reason why, for instance, spherical bases are used to describe nuclei close to sphericity when axial ones are more relevant when it comes to more deformed nuclei.
When trying to describe fission, we face heavily deformed nuclei that require to increase a lot the number of states we use in the truncated axial harmonic oscillator basis. These additional dimensions tend to significantly slow down the calculations. To avoid this drop in performance, the 2-center harmonic oscillator representation has been developed historically by J. F. Berger [47] and is still used in the new new HFB code employed for these PhD thesis applications, known as the HFB3 solver. Before going through this 2-center representation, we first start with the standard axial harmonic oscillator basis.
The functions of the axial basis are a product of two independent parts related to the z-axis and its perpendicular direction:

$$\boxed{\psi_{(m,n_\perp,n_z)}(\vec{r},b_r,b_z)=\phi_{(m,n_\perp)}(\vec{r}_\perp,b_r)\varphi_{n_z}(z,b_z)} \tag{2.39}$$

The first part is a cylindrical harmonic oscillator wave function and is characterized by the quantum numbers m and $n_\perp$ which account respectively for the angular momentum and the number of energy quanta in the perprendicular direction. The second one is a simple one-dimensional harmonic oscillator wave function and is labeled by the quantum number n_z which corresponds to the number of energy quanta in the z direction. Both wave functions are furthermore characterized by two oscillator lengths b_r and b_z, each combination (b_z,b_r) defining therefore a specific orthonormal basis. These functions explicitly read as follows:

$$\varphi_{n_z}(z,b_z)=\frac{1}{\sqrt{2^{n_z}b_z n_z!\sqrt{\pi}}}e^{-\frac{1}{2}(\frac{z}{b_z})^2}H_{n_z}(\frac{z}{b_z}) \tag{2.40}$$

$$\phi_{(m,n_\perp)}(\vec{r}_\perp,b_r)=\frac{1}{b_r\sqrt{\pi}}\sqrt{\frac{n_\perp!}{(n_\perp+|m|)!}}e^{im\phi}(\frac{r_\perp}{b_r})^{|m|}L_{n_\perp}^{|m|}[(\frac{r_\perp}{b_r})^2]e^{-\frac{1}{2}(\frac{r_\perp}{b_r})^2} \tag{2.41}$$

The H_{n_z} and $L_{n_\perp}^{|m|}$ are respectively the Hermite and the generalized Laguerre polynomials. As n_z is associated with the energy of φ_{n_z}, it characterizes the number of nodes of the latter function when b_z defines its spatial spreading. In Figure (2.1), we represented in the left side the effect of a variation of n_z, and in the right side we've highlighted the effect of the parameter b_z:

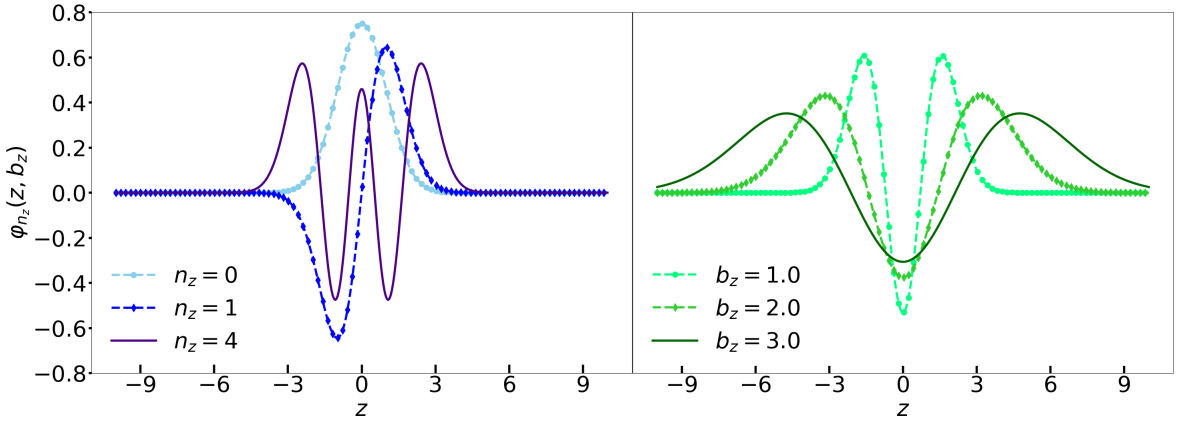

Figure 2.1: $\varphi_{(n_z)}(z, 1)$ with different n_z (left) and $\varphi_{(2)}(z, b_z)$ with different b_z (right).

Concerning the $\vec{r}_\perp$ part, $n_\perp$ defines the number of nodes of $\phi_{(m,n_\perp)}$ and b_r its spatial spreading. The effect of m is more complex and operates in both the spatial spreading and the oscillation frequency of the complex part of the wave function. In Figure (2.2), we represented the impact of a variation of $n_\perp$ in the left panel and the impact of a variation of b_r in the right panel:

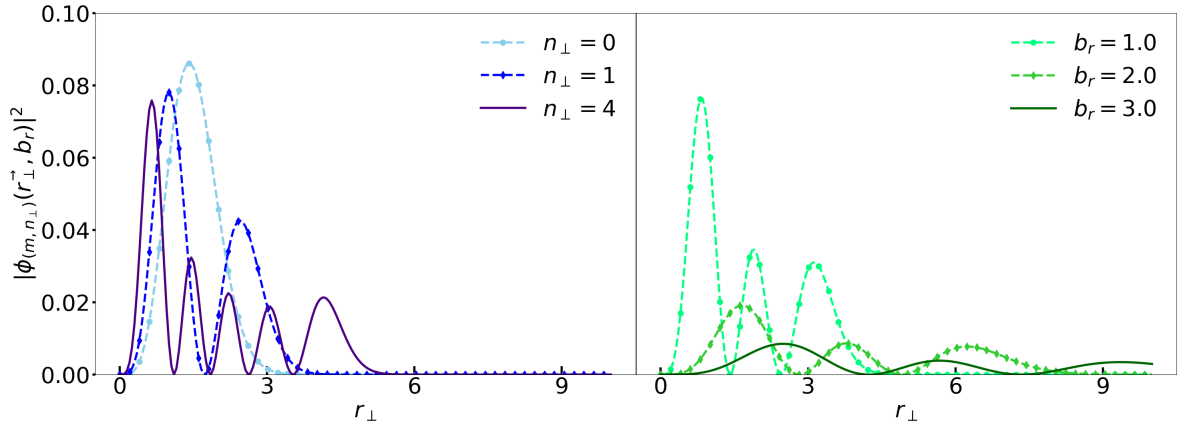

Figure 2.2: $|\phi_{(2,n_\perp)}(\vec{r}_\perp, 1)|^2$ with different $n_\perp$ (left) and $|\phi_{(2,2)}(\vec{r}_\perp, b_r)|^2$ with different b_r (right).

So far, we've only talked about the spatial parts of the orthonormal particle basis wave functions. However, to fully describe a nucleon state both spin and isospin have to be added in such a way that the underlying states of the orthonormal basis are written as:

$$|\Psi_i\rangle = |\Psi(m_i, n_{\perp_i}, n_{z_i})\rangle \otimes |s_i\rangle \otimes |\tau_i\rangle \tag{2.42}$$

Eq.(2.42) corresponds to the tensor product of the spatial, spin and isospin parts. To conclude this section, let's remark that the squared norm of the total harmonic oscillator wave functions often exhibit very aesthetic patterns. We show in Figure (2.3) the squared norm of the wave function $\psi_{(2,2,1)}(\vec{r}, 1, 1.5)$:

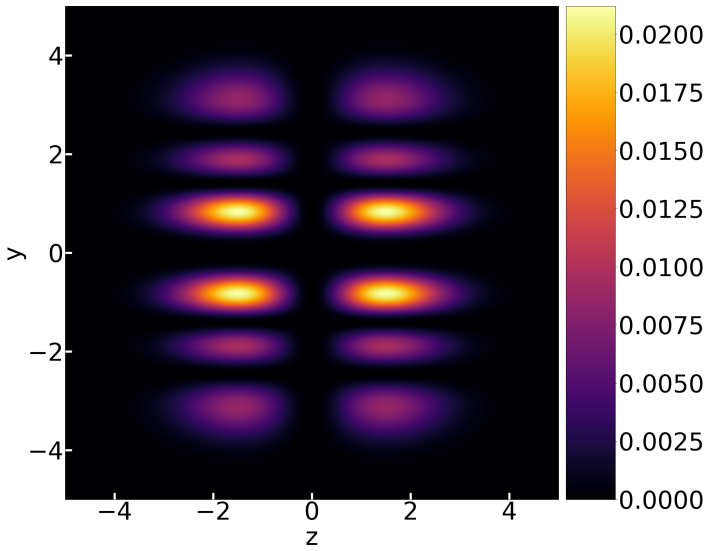

Figure 2.3: $|\psi_{(2,2,1)}(\vec{r}, 1, 1.5)|^2$.

Here, y is one of the Cartesian coordinates that stand for the perpendicular direction. If we consider a truncated harmonic oscillator basis $\{\psi_{(m,n_\perp,n_z)}(b_r, b_z)\}_{(m,n_\perp,n_z)}$, the associated 2-center harmonic oscillator representation is the space generated by the set of functions $\{\psi_{(m,n_\perp,n_z)}(b_r, b_z, d)\}_{(m,n_\perp,n_z)} \cup \{\psi_{(m,n_\perp,n_z)}(b_r, b_z, -d)\}_{(m,n_\perp,n_z)}$. Note that we choose to keep the same b_z and b_r for all the functions of the set. The new parameter d corresponds to a translation along the z-axis:

$$\boxed{\psi_{(m,n_\perp,n_z)}(\vec{r}, b_r, b_z, \pm d) = \phi_{(m,n_\perp)}(\vec{r}_\perp, b_r)\varphi_{n_z}(z \pm d, b_z)} \tag{2.43}$$

We illustrate it with the squared norm of the sum of two harmonic oscillator wave functions spanned by different $\pm d$ in Figure (2.4):

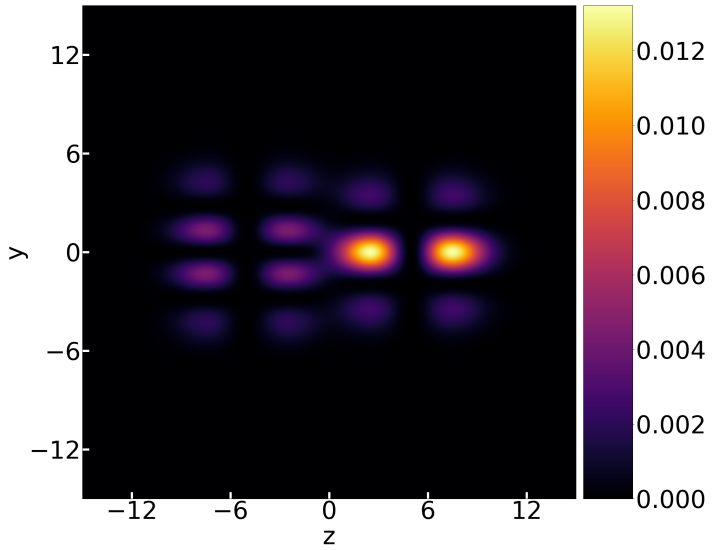

Figure 2.4: $|\psi_{(0,1,1)}(\vec{r}, 2, 2.5, 5) + \psi_{(1,1,1)}(\vec{r}, 2, 2.5, -5)|^2$.

The representation defined by the wave functions of Eq.(2.43) is not orthogonal in general. This is the reason why we talk about a 2-center representation and not a 2-center basis.

To use this representation in the HFB theory, the wave functions set has to be orthonormalized. In the HFB3 code, this is done by using the diagonalization technique. We first have to evaluate the overlap matrix O_{ij} between the wave functions of the set:

$$O_{ij} = \langle\psi_i|\psi_j\rangle = \delta_{s_i s_j}\delta_{\tau_i\tau_j}\int d\vec{r}\psi_i^*(\vec{r})\psi_j(\vec{r}) \tag{2.44}$$

These quantities have an analytical expression which is derived in great details in Appendix D. As $\mathcal{O}$ is a real symmetric matrix, it can be diagonalized with an orthogonal matrix Q:

$$Q^T\mathcal{O}Q = \mathrm{diag}(\lambda) \tag{2.45}$$

If we isolate one matrix element explicitly, we get:

$$\sum_i\sum_j Q_{ik}\mathcal{O}_{ij}Q_{jl} = (\sum_i\langle\psi_i|Q_{ik})(\sum_j Q_{jl}|\psi_j\rangle) = \delta_{kl}\lambda_k \tag{2.46}$$

If we consider only the eigenvalues λ_k greater than a small value $\epsilon > 0$, we can write:

$$(\sum_i\langle\psi_i|Q_{ik}\frac{1}{\sqrt{\lambda_k}})(\frac{1}{\sqrt{\lambda_l}}\sum_j Q_{jl}|\psi_j\rangle) = \delta_{kl} \tag{2.47}$$

From Eq.(2.47), we can extract an orthonormal set of states $\{|p_k\rangle\}$ such that:

$$\boxed{|p_k\rangle = \frac{1}{\sqrt{\lambda_k}}\sum_j Q_{jk}|\psi_j\rangle = \sum_j M_{jk}|\psi_j\rangle} \tag{2.48}$$

This equation defines the transition matrix M from the 2-center harmonic oscillator representation to its associated orthonormal basis. There is still one subtlety to understand in order to use correctly the 2-center representation. Let's suppose we want to write a one-body operator $\hat{A}$ in second quantization. Using the orthonormal basis $\{|p_k\rangle\}$, we deduce the following expression for $\hat{A}$:

$$\hat{A} = \sum_{kl}\langle p_k|\hat{A}|p_l\rangle p_k^+ p_l \tag{2.49}$$

If we want to express the matrix elements of the operator $\hat{A}$ in the 2-center representation, we end up with the following equation:

$$\hat{A} = \sum_{ij}\langle\psi_i|\hat{A}|\psi_j\rangle\sum_k M_{ik}p_k^+\sum_l M_{jk}p_l \tag{2.50}$$

If we call the $\{c_i^+\}$ the creation operators and the $\{c_i\}$ the annihilation operators associated with the 2-center representation, we have:

$$\sum_k M_{ik} p_k^+ \neq c_i^+ \tag{2.51}$$

Indeed, M^T is not the inverse of M since M is not orthogonal, but $M_{ij}^{-1} = \sqrt{\lambda_i} Q_{ij}$. Thus, Eq.(2.51) defines a new representation which is called the biorthogonal representation and whose associated creation and annihilation operators are denoted $\{\tilde{c}_i^+\}$ and $\{\tilde{c}_i\}$ respectively (and its wave functions $\{\tilde{\psi}_i\}$). The property standing for the biorthogonality reads:

$$\langle \tilde{\psi}_i | \psi_j \rangle = \sum_k \sum_l M_{ik} M_{lj}^{-1} \langle p_k | p_l \rangle = \delta_{ij} \tag{2.52}$$

The subtlety is therefore that an operator $\hat{A}$ whose matrix elements are evaluated in the 2-center representation comes with creation and annihilation operators in the biorthogonal representation :

$$\boxed{\hat{A} = \sum_{ij} \langle \psi_i | \hat{A} | \psi_j \rangle \tilde{c}_i^+ \tilde{c}_j} \tag{2.53}$$

In order to avoid really tedious notations and as it is clarified by the context, the differences between those three basis won't be specified unless necessary. All the creation and annihilation operators of those bases are thus denoted $\{c_i^+\}$ and $\{c_i\}$ in the following.

2.1.3 The effective interaction

In the work presented in this PhD thesis, we have used two variants of the Gogny interactions, the D1S original one [15–18] and the D2 interaction [19]. These interactions are local effective two-body nucleon-nucleon interactions. Some of the terms in these interactions are finite-range terms and some are contact ones. Note that, in a recent work, the DG interaction has been developed with only finite-range terms and includes a tensor term [48]. The D1S interaction reads:

$$\boxed{\begin{aligned} \hat{V} = \sum_{i=1}^{2} e^{-(|\vec{r}_1 - \vec{r}_2|)^2/\mu_i^2} (W_i + B_i P_\sigma - H_i P_\tau - M_i P_\sigma P_\tau) \\ + t_3 (1 + x_0 P_\sigma) \delta(\vec{r}_1 - \vec{r}_2) [\rho(\frac{\vec{r}_1 + \vec{r}_2}{2})]^\alpha \\ + i W_{LS} \overleftarrow{\nabla}_{12} \delta(\vec{r}_1 - \vec{r}_2) \wedge \overrightarrow{\nabla}_{12} . (\vec{\sigma}_1 + \vec{\sigma}_2) \\ + e^2 \frac{\delta_{\tau_p \tau_p'}}{|\vec{r}_1 - \vec{r}_2|} \end{aligned}} \tag{2.54}$$

The operators P_σ and P_τ stand respectively for the spin and isospin exchange operators. From the top to the bottom, the first term is called the central term, the second one the density-dependent term, the third one the spin-orbit term and the fourth one is the Coulomb term. Note that an additional term is often added which accounts for center of mass corrections $-\frac{1}{2MA}\vec{P}^2$. Moreover, the Coulomb term contribution to the energy is sometimes evaluated

using the Slater approximation [49] for the sake of numerical performances. In this PhD thesis, we have added the exact treatment of the exchange and pairing part of the Coulomb term in the HFB3 code. Thus, we have been able to perform calculations with and without the Slater approximation.
The difference between D1S and D2 is that the contact density-dependent term in D1S has been replaced by a finite-range one whose analytic expression is:

$$\boxed{\frac{1}{2(\mu_3\sqrt{\pi})^3}(W_3 + B_3P_\sigma - H_3P_\tau - M_3P_\sigma P_\tau)e^{-\frac{(\vec{r}_1-\vec{r}_2)^2}{\mu_3^2}}([\rho(\vec{r}_1)]^\alpha + [\rho(\vec{r}_2)]^\alpha)} \tag{2.55}$$

Note that D1S and D2 parameters have been fitted considering the Slater approximation for the Coulomb energy. It may be important to keep that in mind when interpreting calculations done with the exact treatment of the Coulomb term.

2.1.4 Constraints on particle number and multipole moments

In the previous presentation of the HFB equations, done in the beginning of the section 2.1, the constraints have been intentionally omitted. However, they are essential to perform HFB calculations. Indeed, in all the calculations, the average particle numbers associated with both isospins are constrained to the desired N or Z values. To do so, the particle number operator is added with a Lagrange multiplier λ_τ into the Hamiltonian:

$$\boxed{\hat{H}_c = \hat{H} + \sum_\tau \lambda_\tau \sum_i c_i^{\tau+} c_i^\tau} \tag{2.56}$$

The Lagrange multipliers λ_τ are adjusted throughout the gradient descent and the iterative diagonalization process in a way explained in the dedicated sections (section 2.1.5 and section 2.1.6 respectively).
To describe the deformations of the nucleus, constraints on the multipole moments are also imposed using the associated one-body operators $\hat{Q}^{(x0)}$ [45]. The latter are simply added to the Hamiltonian as in Eq.(2.56) such that the final Hamiltonian $\hat{H}_c$ reads:

$$\boxed{\hat{H}_c = \hat{H} + \sum_\tau \lambda_\tau \sum_i c_i^{\tau+} c_i^\tau + \sum_x \lambda_\alpha \sum_{ij} Q_{ij}^{(x0)} c_i^+ c_j} \tag{2.57}$$

Note that the mean value of $\hat{Q}^{(10)}$ is always constrained to zero in our calculations in order to avoid translations of the system. In the case of the gradient method, the one-body operators are easily written in the quasiparticle basis and added to the Hamiltonian. Constraining the different multipole moments allows to describe many shapes. In Figure (2.5), we represented three typical shapes we may find in potential energy surfaces. From left to right, in the first panel we recognize a spherical shape, in the second panel an axial quadrupole one, and in the last panel we eventually observe an axial asymmetric shape:

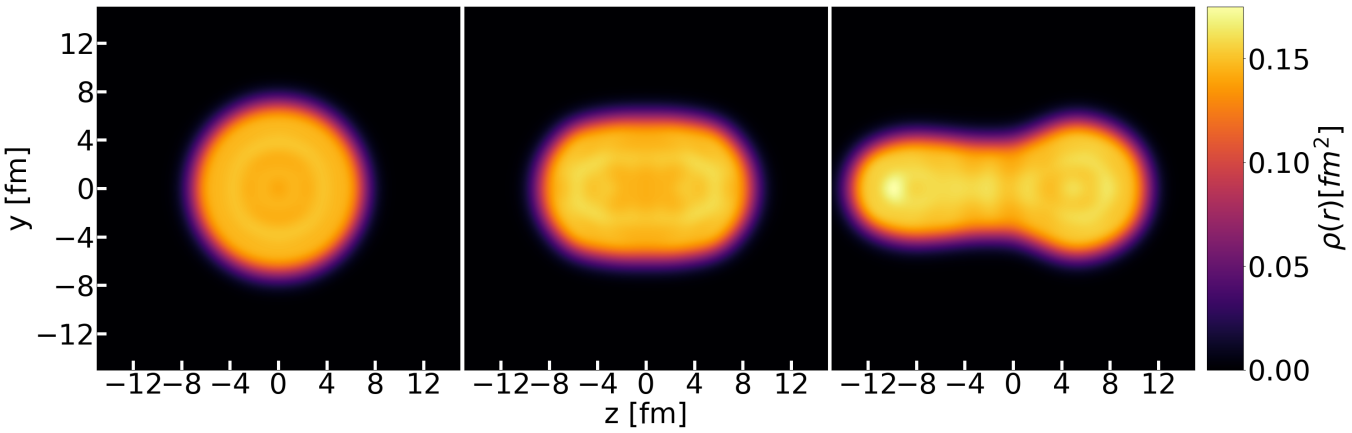

Figure 2.5: Local one-body density of ^{240}Pu for $(Q_{20}, Q_{30}) = (0,0), (1642,0), (5784,-19000)$.

It is important to know that the multipole moment operators are not univoquely defined in the literature. To help the reader find his way through these twists and turns, we've listed below the different conventions used in four HFB codes. All the results of this PhD thesis are displayed with respect to the HFB3 code definitions:

$$\underline{\textbf{HFB3 code:}} \quad \begin{cases} \hat{Q}^{(10)} = \frac{1}{2}\sqrt{\frac{3}{\pi}}z \\ \hat{Q}^{(20)} = \frac{1}{4}\sqrt{\frac{5}{\pi}}(2z^2 - r_\perp^2) \\ \hat{Q}^{(30)} = \frac{1}{4}\sqrt{\frac{7}{\pi}}(2z^3 - 3zr_\perp^2) \\ \hat{Q}^{(40)} = \frac{1}{16}\sqrt{\frac{9}{\pi}}(8z^4 - 24z^2r_\perp^2 + 3r_\perp^4) \end{cases} \tag{2.58}$$

$$\underline{\textbf{HFB2ct code:}} \quad \begin{cases} \hat{Q}^{(10)} = z \\ \hat{Q}^{(20)} = 2z^2 - r_\perp^2 \\ \hat{Q}^{(30)} = z^3 - \frac{3}{2}zr_\perp^2 \\ \hat{Q}^{(40)} = z^4 - 3z^2r_\perp^2 + \frac{3}{8}r_\perp^4) \end{cases} \tag{2.59}$$

$$\underline{\textbf{HFB axial code:}} \quad \begin{cases} \hat{Q}^{(10)} = z \\ \hat{Q}^{(20)} = z^2 - \frac{1}{2}r_\perp^2 \\ \hat{Q}^{(30)} = z^3 - \frac{3}{2}zr_\perp^2 \\ \hat{Q}^{(40)} = z^4 - 3z^2r_\perp^2 + \frac{3}{8}r_\perp^4) \end{cases} \tag{2.60}$$

$$\underline{\textbf{HFBTHO code:}} \quad \begin{cases} \hat{Q}^{(10)} = z \\ \hat{Q}^{(20)} = 2z^2 - r_\perp^2 \\ \hat{Q}^{(30)} = \frac{1}{4}\sqrt{\frac{7}{\pi}}(2z^3 - 3zr_\perp^2) \\ \hat{Q}^{(40)} = \frac{1}{16}\sqrt{\frac{9}{\pi}}(8z^4 - 24z^2r_\perp^2 + 3r_\perp^4) \end{cases} \tag{2.61}$$

2.1.5 The gradient descent method

The philosophy of the gradient descent is really straightforward [45, 50, 51] and is based on Eq.(2.22). We start from a state $|\Phi_0\rangle$ which verifies Eq.(2.4) and perform a little variation

on it which is parametrized by a Thouless matrix Z. Since the time-reversal invariance is preserved, Z is real and the new state reads:

$$|\Phi(Z)\rangle = \langle\Phi_0|\Phi(Z)\rangle e^{\sum_{0<k<k'} Z_{k\bar{k}'}\xi_k^+\bar{\xi}_{k'}^+}|\Phi_0\rangle \tag{2.62}$$

The little variation is performed in the direction that minimizes the energy. To ensure that, Z is chosen being parallel to the energy gradient:

$$\boxed{Z_{kk'} = -\eta\frac{\partial}{\partial Z_{kk'}}\frac{\langle\Phi(Z)|\hat{H}|\Phi(Z)\rangle}{\langle\Phi(Z)|\Phi(Z)\rangle}|_{Z=0} = -\eta\tilde{H}^{20}_{kk'}} \tag{2.63}$$

The norm η of Z defines the length of the step made in the direction given by Z. If η is small the convergence will be more stable but slower too. Different techniques exist to determine a "good" η (see [51] for a more complete disccusion).
Once Z is determined, the new U' and V' matrices related to the state $|\Phi(Z)\rangle$ are found thanks to the following formula:

$$\boxed{\begin{cases} U' = (U^{(0)} - V^{(0)}Z)(I - ZZ)^{-1/2} \\ V' = (V^{(0)} + U^{(0)}Z)(I - ZZ)^{-1/2} \end{cases}} \tag{2.64}$$

The process is iterated until the condition $||\tilde{H}^{20}|| < \epsilon$ is fulfilled, ϵ being a small quantity. Note that in the HFB3 code we chose $\epsilon = 5.10^{-4}$.
Constraints are treated throughout this process in a very simple way. Indeed we add the gradient of each constraint to the energy gradient such that:

$$\boxed{Z_{kk'} = -\eta\frac{\partial}{\partial Z_{kk'}}\frac{\langle\Phi(Z)|\hat{H}_c|\Phi(Z)\rangle}{\langle\Phi(Z)|\Phi(Z)\rangle}|_{Z=0} = -\eta(\tilde{H}^{20}_{kk'} + \sum_\alpha \lambda_\alpha C^{20}_\alpha)} \tag{2.65}$$

Here the $\{C^{20}_\alpha\}$ stand for the gradients of the general constraints $\hat{C}_\alpha$. The Lagrange multipliers λ_α are determined at each iteration in such a way that $|\Phi(Z)\rangle$ verifies the associated constraint to a linear order in Z. More explicitly, the following relation for each constraint $\hat{C}_\beta$ is used:

$$C_\beta - C^{(0)}_\beta = 2\mathrm{Tr}[ZC^{20}_\beta] = -2\eta(\mathrm{Tr}[\tilde{H}^{20}C^{20}_\beta] + \sum_\alpha \lambda_\alpha \mathrm{Tr}[C^{20}_\alpha C^{20}_\beta]) \tag{2.66}$$

Here C_β is the target value for the constraint $\hat{C}_\beta$ and $C^{(0)}_\beta$ is the expected value. Taking into account all the constraints, we end up with a linear system:

$$\boxed{M\Lambda = \Delta_C \qquad \text{with} \qquad \begin{cases} M_{\alpha\beta} = \mathrm{Tr}[C^{20}_\alpha C^{20}_\beta] \\ \Lambda_\alpha = \lambda_\alpha \\ (\Delta_C)_\beta = \frac{1}{2\eta}(C_\beta - C^{(0)}_\beta) + \mathrm{Tr}[\tilde{H}^{20}C^{20}_\beta] \end{cases}} \tag{2.67}$$

The convergence is achieved when $||\tilde{H}^{20} + \sum_\alpha \lambda_\alpha C_\alpha^{20}|| < \epsilon$. At this point, a last step remains. Indeed, we have to diagonalize $\tilde{H}^{11}$ in order to be in the desired HFB quasiparticle representation. The final U and V matrices are then deduced from the ones of the last iteration U_{last} and V_{last}:

$$\boxed{Q^T \tilde{H}^{11} Q = \text{diag}(\epsilon) \qquad \Rightarrow \qquad \begin{cases} U = U_{last} Q \\ V = V_{last} Q \end{cases}} \tag{2.68}$$

We introduced this part stating that the gradient algorithm starts from an HFB vacuum $|\Phi_0\rangle$. Practically, most of the time, we are performing calculations with different deformations. Thus we can use the result of some previous calculations as a seed for the new ones. However, sometimes no pre-defined initial state is available. In that case, a "random" state $|\Phi_0\rangle$ is created. For the convergence to work properly, it is important that $|\Phi_0\rangle$ approaches the good average particle numbers. Moreover, it has to verify the Bogoliubov equations Eq.(2.4). The way these requirements are fulfilled in the HFB3 code is inspired by the Bloch-Messiah theorem. Indeed, we first create two random matrices S_C and S_D and we create two skew-symmetric matrices out of them $\tilde{S}_C$ and $\tilde{S}_D$ such that:

$$\begin{cases} \tilde{S}_C = S_C - S_C^T \\ \tilde{S}_D = S_D - S_D^T \end{cases} \tag{2.69}$$

We then take the exponential of those matrices in order to end up with the unitary matrices $C^{(0)}$ and $D^{(0)}$:

$$\begin{cases} C^{(0)} = e^{\tilde{S}_C} \\ D^{(0)} = e^{\tilde{S}_D} \end{cases} \tag{2.70}$$

At this step, only $u^{(0)}$ and $v^{(0)}$ still need to be defined. As a good average particle number N is desired, we initialize the vector v_0 with N ones, the rest being set to zero. We then add to this vector v_0 a random pertubation whose elements are in the range $[-0.1, 0]$. This defines the vector v_1. Note that this random pertubation is added in order to start from a state already including pairing. The vector v_1 is then rescaled to preserve the good average particle number, the resulting vector being called v_2:

$$v_2 = v_1 \sqrt{\frac{N}{\sum_i (v_1)_i^2}} \tag{2.71}$$

The elements of v_2 can sometimes be slightly greater than 1. For this reason they are clamped. The resulting vector is the desired $v^{(0)}$. Because of the clamping, $v^{(0)}$ may not have exactly the good average particle number but the difference is so small in practice that it doesn't cause any numerical issue. The elements of $u^{(0)}$ are then defined using the ones of $v^{(0)}$:

$$u_i^{(0)} = \sqrt{1 - v_i^{(0)}} \qquad \forall i \tag{2.72}$$

We can eventually express the matrices $U^{(0)}$ and $V^{(0)}$ defining the starting state $|\Phi_0\rangle$ as:

$$\boxed{\begin{cases} U^{(0)} = C^{(0)} u^{(0)} D^{(0)} \\ V^{(0)} = C^{(0)} v^{(0)} D^{(0)} \end{cases}} \tag{2.73}$$

In this chapter we presented the plain theory of the gradient descent. It is however important to know that this theory only serves as a backbone for more sophisticated numerical approaches that enhance convergence speed and stability (see for example [50, 51]. In the HFB3 code, the so-called "heavy-ball" technique [52] is used and roughly consists in mixing the matrix $Z^{(i)}$ of an i-th iteration with the matrix $Z^{(i-1)}$ of the previous (i-1)-th iteration.

2.1.6 The iterative diagonalization method

The iterative diagonalization method comes from the Eq.(2.28). Let's assume we start with an HFB vacuum $|\Phi_0\rangle$, with the associated $U^{(0)}$ and $V^{(0)}$ defined previously. The matrix $\mathcal{H}^{(0)}_{HFB}$ defined in Eq.(2.26) is computed and diagonalized. The eigenvectors of $\mathcal{H}^{(0)}_{HFB}$ then stand for the new $U^{(1)}$ and $V^{(1)}$:

$$\mathcal{H}^{(0)}_{HFB} \begin{pmatrix} U^{(1)}_i \\ V^{(1)}_i \end{pmatrix} = \epsilon_i \begin{pmatrix} U^{(1)}_i \\ V^{(1)}_i \end{pmatrix} \tag{2.74}$$

The process is iterated until the i-th iteration for which the condition $||\rho^{(i)} - \rho^{(i-1)}|| < \epsilon'$ is fulfilled, ϵ' being a small quantity. This measure of the convergence is of course not the same as the one in the gradient descent, ϵ' is therefore different from ϵ. Note that, in the HFB3 code, we chose $\epsilon' = 10^{-6}$.
In the diagonalization method, the constraints are handled in a way slightly different to the one presented in the gradient method. The Lagrange multipliers are corrected pertubatively at first order at each iteration and ρ and κ are corrected accordingly (for more details see [47]).
It is important to know that the iterative diagonalization method can jump from a state $|\Phi_0\rangle$ to another very different state $|\Phi_1\rangle$, whereas the gradient implies to stay close to the starting point at each iteration. Because of that, the gradient tends to be more stable but also slower when the diagonalization method is faster but sometimes struggles to converge. In practice with the plain iterative diagonalization method it is most of the time not possible to converge without appropriate numerical techniques such as the Broyden mixing used in the HFB3 code.

2.1.7 The HFB3 and CHICON solvers

We conclude the presentation of the HFB method telling a few words about the HFB3 code we used during this PhD thesis [53]. This code is an HFB solver that can work with both one-center and two-center harmonic oscillator sets. For this reason, it is particularly well suited for fission.
Another peculiarity of the HFB3 code is that it is able to combine the advantages of both gradient and iterative diagonalization solvers in a new mixed solver. The gradient solver is indeed useful to perform the first iterations in a convergence process in order to reach a state close enough to the final solution for the iterative diagonalization solver to work properly. In that way, the convergences are both stable and fast.

Moreover, a particular attention has been paid during this PhD thesis to the implementation of the fields, which are most of the time the bottleneck in the numerical calculations. Thanks to the work done in the context of this PhD thesis, the HFB3 code demonstrates now very good performances using D1 type and D2 Gogny interactions. In Figure (2.6), we have plotted the convergence of the HFB wave function with respect to the time for different interactions and starting from random U and V matrices. These calculations have been done in the case of ^{240}Pu with a 2-center representation (2x11 shells). We clearly recognize the part associated with the gradient method and the one associated with the iterative diagonalization method. The curve associated with the interaction D1S with the Slater approximation shows a fast convergence (less than 80s). When an exact treatment of the Coulomb fields is added, only a factor 3 is added. Finally, we only observe a factor 2 between D1S and D2 calculations with the Slater approximation, which is an outstanding performance:

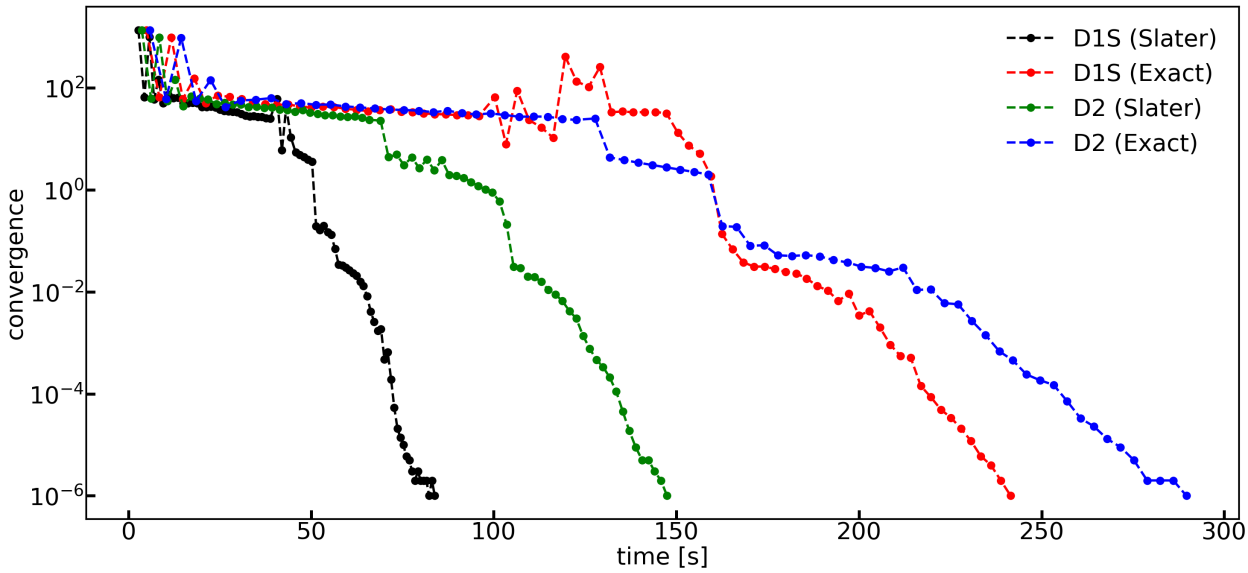

Figure 2.6: HFB3 performances on ^{240}Pu.

All the PES produced during this PhD thesis have been calculated using the combo HFB3+CHICON, in which CHICON is a driver of the HFB3 code adapted for HPC calculations on supercalculators. This driver contains a retro-propagation mechanism, avoiding at maximum local minima. Thanks to that combo, 1D and 2D PES are relatively easy and fast to produce on supercalculators. A 2D PES of ^{240}Pu is shown in Figure 2.7 as an exemple:

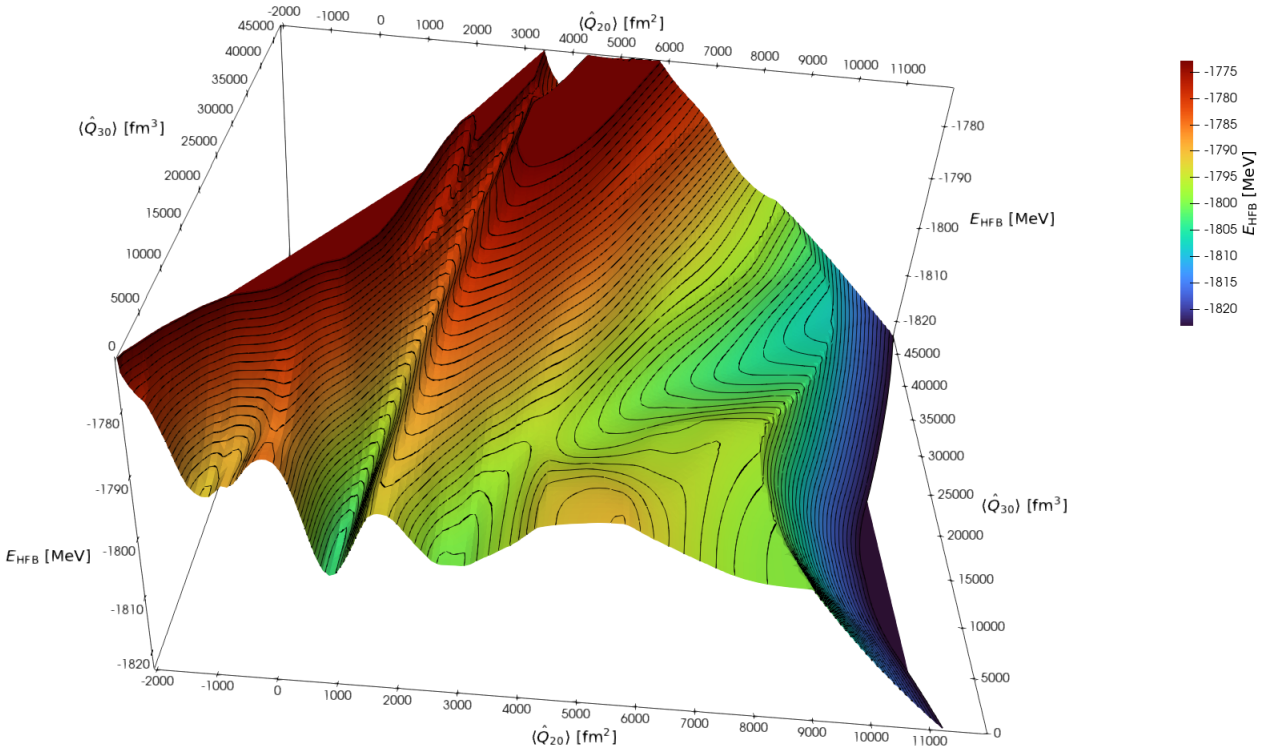

Figure 2.7: 2D potential energy surface of the ^{240}Pu made with the combo HFB3+CHICON.

2.2 The 2-quasiparticle excited states

In the first derivations of the SCIM [33], the excited states considered were non-self-consistent 2-quasiparticle excitations over the HFB adiabatic states. Indeed, the quasiparticle excitations are the elementary excitations of the system in the HFB theory and are convenient to use. Moreover, they allow us to describe the pair breaking phenomenon which is known to play a role in low-energy fission.
First, we recall how these excited states were to be constructed. Then, we discuss their major shortcomings.

2.2.1 Construction of time-even 2-quasiparticle excited states

To be consistent with the adiabatic approach, the time-even 2-quasiparticle excited states read as follows:

$$|\Phi_{ij}\rangle = \alpha_{ij}(\xi_i^+\bar{\xi}_j^+ + \xi_j^+\bar{\xi}_i^+)|\Phi\rangle \qquad \text{with} \qquad \alpha_{ij} = \frac{1}{\sqrt{2}}(1+\delta_{ij}(\frac{1}{\sqrt{2}}-1)) \tag{2.75}$$

The time-reversal invariance property can be easily checked:

$$\hat{T}|\Phi_{ij}\rangle = \alpha_{ij}(-\bar{\xi}_i^+\xi_j^+ - \bar{\xi}_j^+\xi_i^+)|\Phi\rangle = |\Phi_{ij}\rangle \tag{2.76}$$

Moreover, those states are properly normalized:

$$\langle\Phi_{ij}|\Phi_{ij}\rangle = \alpha_{ij}^2\langle\Phi|(\bar{\xi}_j\xi_i + \bar{\xi}_i\xi_j)(\xi_i^+\bar{\xi}_j^+ + \xi_j^+\bar{\xi}_i^+)|\Phi\rangle = 2\alpha_{ij}^2\langle\Phi|\bar{\xi}_j\xi_i\xi_i^+\bar{\xi}_j^+ + \bar{\xi}_j\xi_i\xi_j^+\bar{\xi}_i^+|\Phi\rangle \tag{2.77}$$

$$\langle \Phi_{ij} | \Phi_{ij} \rangle = 2\alpha_{ij}^2 (1 + \delta_{ij}) = 1 \tag{2.78}$$

In order to preserve the time-reversal symmetry, the quasiparticles are chosen in the same Ω-blocks. In addition, we don't mix different isospins.

2.2.2 2-quasiparticle excited states along a deformation path

As quasiparticles are not unequivocally defined by their quantum numbers Ω and τ, it is not straightforward to tell them apart. However, the SCIM formalism requires to clearly identify an excitation all along a deformation path. To do so, we define an excited state $|\Phi_{ij}(q + \delta q)\rangle$ at the deformation $q + \delta q$ thanks to its neighbouring state $|\Phi_{ij}(q)\rangle$ with the following requirement:

$$|\langle \Phi_{ij}(q) | \Phi_{ij}(q + \delta q) \rangle| = \max_{i'j'} |\langle \Phi_{ij}(q) | \Phi_{i'j'}(q + \delta q) \rangle| \tag{2.79}$$

The method to evaluate these overlaps is explained in great details in Chapter 5.

2.2.3 Average particle number of the 2-quasiparticle excited states

Unfortunately, a first drawback of the non-self-consistent 2-quasiparticle excited states is that they do not have a good average particle number. Moreover, this average particle number may strongly change with respect to the deformation, implying sudden discontinuities in the energy of the excited states:

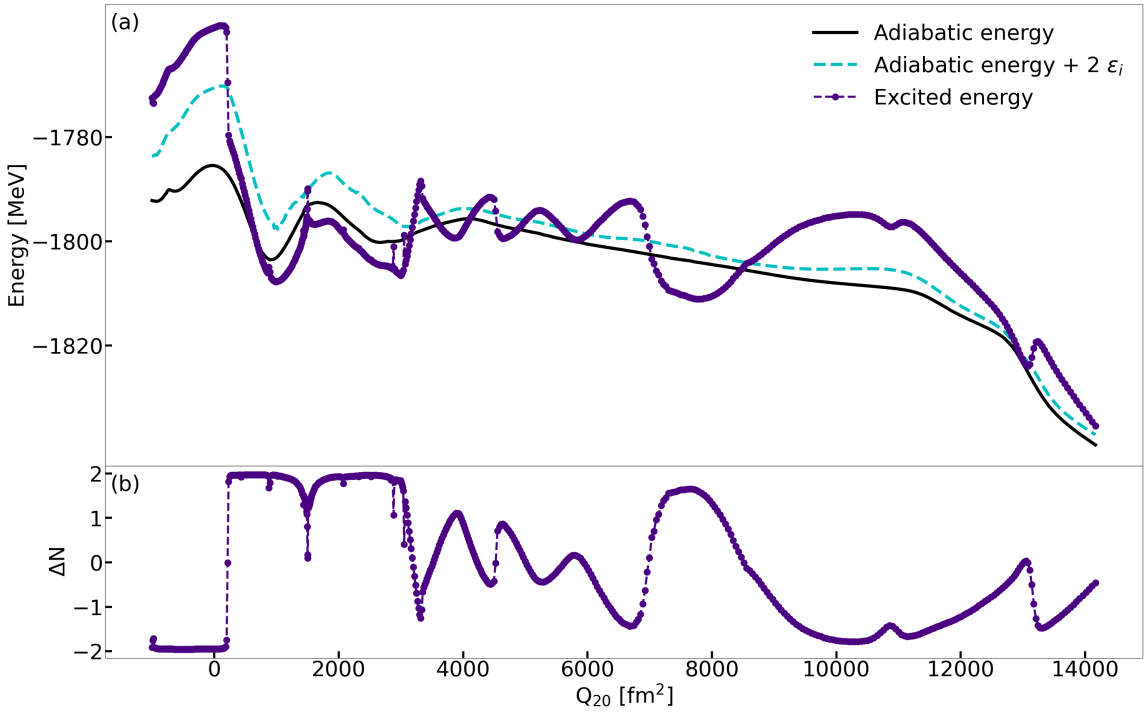

Figure 2.8: Illustration of the particle number issue in a 2-quasiparticle excited state with respect to the quadrupole deformation. Panel (a): comparison of the adiabatic PES with both 2-quasiparticle excited PES and with the HFB approximation of this excited energy. Panel (b): particle number difference between the adiabatic and the 2-quasiparticle excited state.

In panel (a) of Figure (2.8), we compare the 1D adiabatic PES of the ^{240}Pu with the PES of one of its 2-quasiparticle excited states (neutron with $\Omega = 1/2$ and of the type $\xi_i^+ \bar{\xi}_i^+ |\Phi\rangle$). We also represented in dashed blue the energy deduced from the HFB approximation. In panel (b) of Figure 2.8, we show the particle number difference ΔN between the excited state and the adiabatic state with respect to the deformation.
The effect of the particle number variation on the energy is stricking. The purple curve may indeed differ a lot from the blue one. When ΔN is close to zero, we find an energy close to the one deduced from the HFB approximation. In [33], this problem has been discussed and the solution pointed out was to choose 2-quasiparticle excited states that break particle number as less as possible. As shown in Figure (2.8), it is far from being possible all allong the deformation path. Moreover, even in the areas where ΔN belongs to $]-1,1[$, the spurious variations of the Hamiltonian kernel induced by the particle number variations may dramatically spoil the SCIM as it requires a high regularity of the kernels.

2.3 The projection after variation method applied to the particle number

Discovering the importance of the average particle number breaking in the 2-quasiparticle excited states, we immediately looked for a method to alleviate this issue. The most natural and straight way to proceed is the projection on particle number. Note that this possibility had already been discussed in the work of Bernard *et al*, but they didn't follow it up.
Both the Projection After Variations (PAV) and the Variations After Projection (VAP) [54] do exist. In the PAV case, an already existing HFB state is projected onto its subspace corresponding to the desired particle number. On the other hand, in the VAP method, the projection is already included in the HFB equations and therefore in the convergence process. The VAP is of course an ideal choice as it is self-consistent, but it also requires more numerical efforts. Therefore, to start with projections and evaluate the viability of our approach, we implemented the PAV method.

To understand how the PAV works, it is important to recall some properties of the time-even HFB wave functions. In the canonical basis (see Appendix C), the HFB wave functions read:

$$|\Phi_{HFB}\rangle = \prod_i (u_i + v_i a_i^+ \bar{a}_i^+)|0\rangle \tag{2.80}$$

Here, the $\{a_i^+\}$ are the particle creation operators in the canonical basis. In Eq.(2.80), we clearly see that the HFB wave function can be separated into components with only even particle numbers:

$$|\Phi_{HFB}\rangle = \sum_n c_{2n} |\Phi_{(2n)}\rangle \tag{2.81}$$

The c_{2n} are normalization coefficients such that each $|\Phi_{2n}\rangle$ is properly normalized. To evaluate the average particle number of a state, we first express the particle number operator $\hat{N}$:

$$\boxed{\hat{N} = \sum_i c_i^+ c_i} \tag{2.82}$$

Note that the creation and annihilation operators used in Eq.(2.82) have of course to be the ones of the orthonormal basis. Using the ones of the 2-center representation, for instance, may lead to some unpleasant surprises.
Thanks to the particle number operator $\hat{N}$, we define the projector $\hat{P}_{N_0}$. It is the projector on the subspace corresponding to the particle number N_0:

$$\boxed{\hat{P}_{N_0} = \frac{1}{2\pi}\int_0^{2\pi} d\varphi e^{-i\varphi(\hat{N}-N_0)}} \tag{2.83}$$

The effect of $\hat{P}_{N_0}$ on the HFB wave functions is straightforward:

$$\hat{P}_{N_0}|\Phi_{HFB}\rangle = \sum_n \frac{c_{2n}}{2\pi}\int_0^{2\pi} d\varphi e^{-i\varphi(\hat{N}-N_0)}|\Phi_{(2n)}\rangle = \sum_n \frac{c_{2n}}{2\pi}\int_0^{2\pi} d\varphi e^{-i\varphi(2n-N_0)}|\Phi_{(2n)}\rangle \tag{2.84}$$

Using, the following well-known result:

$$\frac{1}{2\pi}\int_0^{2\pi} d\varphi e^{i\varphi k} = \delta_{k0}, \qquad \forall k \in \mathbb{N} \tag{2.85}$$

Inserting Eq.(2.85) in Eq.(2.84), we finally find:

$$\hat{P}_{N_0}|\Phi_{HFB}\rangle = \sum_n \delta_{2nN_0} c_{2n}|\Phi_{(2n)}\rangle = c_{N_0}|\Phi_{(N_0)}\rangle \tag{2.86}$$

In practice, the integral is discretized in order to be evaluated numerically:

$$\boxed{\hat{P}_{N_0} = \frac{1}{n_\varphi}\sum_{\varphi=0}^{n_\varphi} e^{-i\frac{2\pi\varphi}{n_\varphi}(\hat{N}-N_0)}} \tag{2.87}$$

The convergence speed of this sum is really good. In this PhD thesis, we never had to use a value n_φ greater than 11. Besides, as the isospins are separated in the wave functions we consider, projections have to be performed on both isospin simultaneously:

$$\boxed{\hat{P}_{N_0} = \hat{P}^{\tau_n}_{N_0^{\tau_n}}\hat{P}^{\tau_p}_{N_0^{\tau_p}}} \tag{2.88}$$

Note that the final projected states $|\tilde{\Phi}_{HFB}\rangle$ have to be renormalized after projection. They read as follows:

$$\boxed{|\tilde{\Phi}_{HFB}\rangle = \frac{\hat{P}_{N_0}}{\sqrt{\langle\Phi_{HFB}|\hat{P}_{N_0}|\Phi_{HFB}\rangle}}|\Phi_{HFB}\rangle} \tag{2.89}$$

In Chapter 5, we discuss in great details how the different observables and kernels are evaluated with projected states.

2.3.1 Projected adiabatic states

The effect of the particle number projection on the HFB adiabatic states has been already widely discussed in literature [54]. Generally speaking, as long as the particle numbers of the HFB states are not exact, it increases their binding energy adding correlations to them. The more the particle number is spread, the more energy is added. Besides, as the pairing energy is directly related to the particle number spreading, the difference between the projected HFB energy and the HFB energy varies accordingly with the pairing energy. In Figure (2.9), we illustrated these general effects of the projection with respect to the quadrupole deformation in the ^{240}Pu. In panel (a), the difference between the projected adiabatic HFB energy and the adiabatic HFB energy is plotted. In panel (b), we've represented the evolution of the pairing energy. Finally, in panel (c), the standard deviation of the total particle number is displayed:

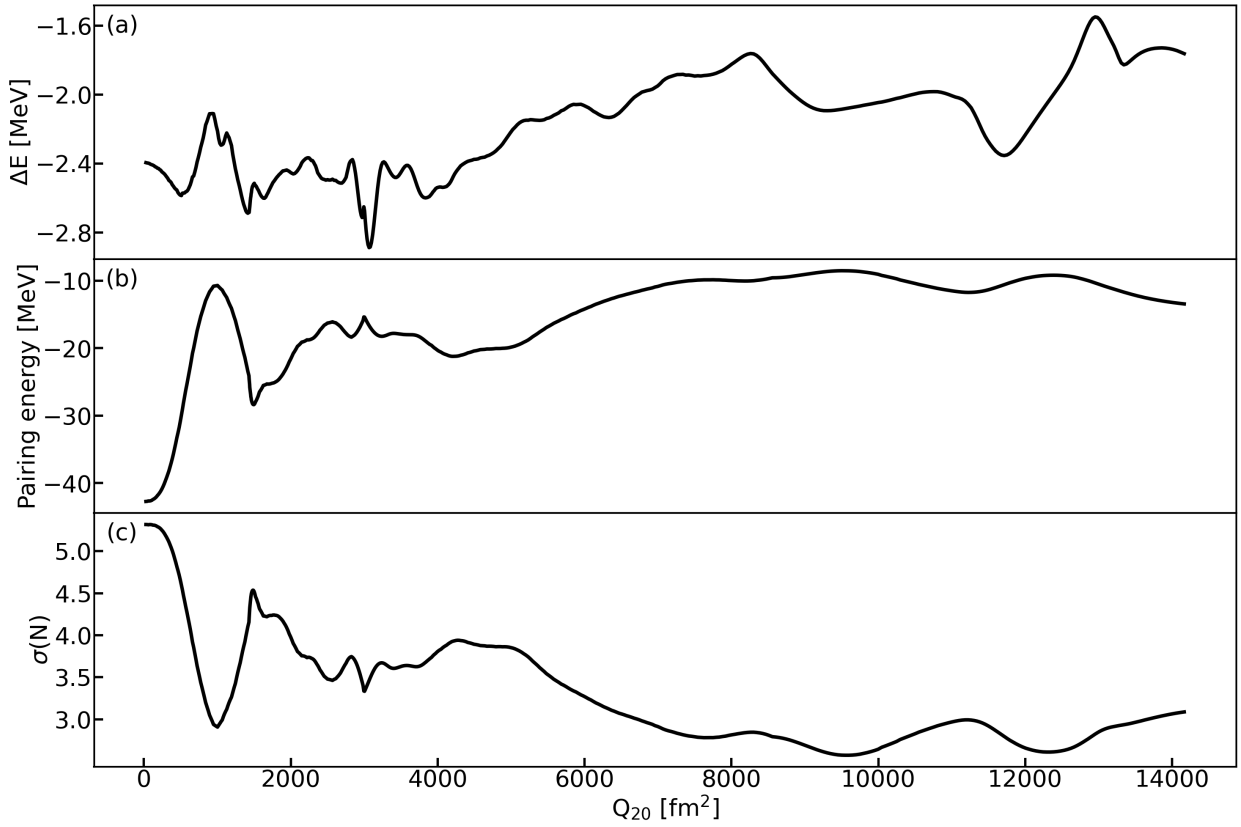

Figure 2.9: Illustration of the effects of particle number projection on ^{240}Pu with respect to the quadrupole deformation. Panel (a): difference between the projected HFB energy and the HFB energy. Panel (b): pairing energy of the adiabatic HFB states. Panel (c): standard deviation of the total particle number of the adiabatic HFB states.

Moreover, when an already continuous and regular set of HFB states (see section 3) is projected, the resulting set of projected states is still continuous and regular. In Figure (2.10), we represented this phenomenon in the ^{240}Pu with respect to the quadrupole deformation. The black curve represents the value of the overlap kernel between an adiabatic state and its neighbour on the right. The grey curve represents the same quantity for projected states. Even if the grey curve shows variations of high amplitude compared to the black curve, these fluctuations are in fact of the order of 10^{-3}. The projected states can therefore be considered fairly regular:

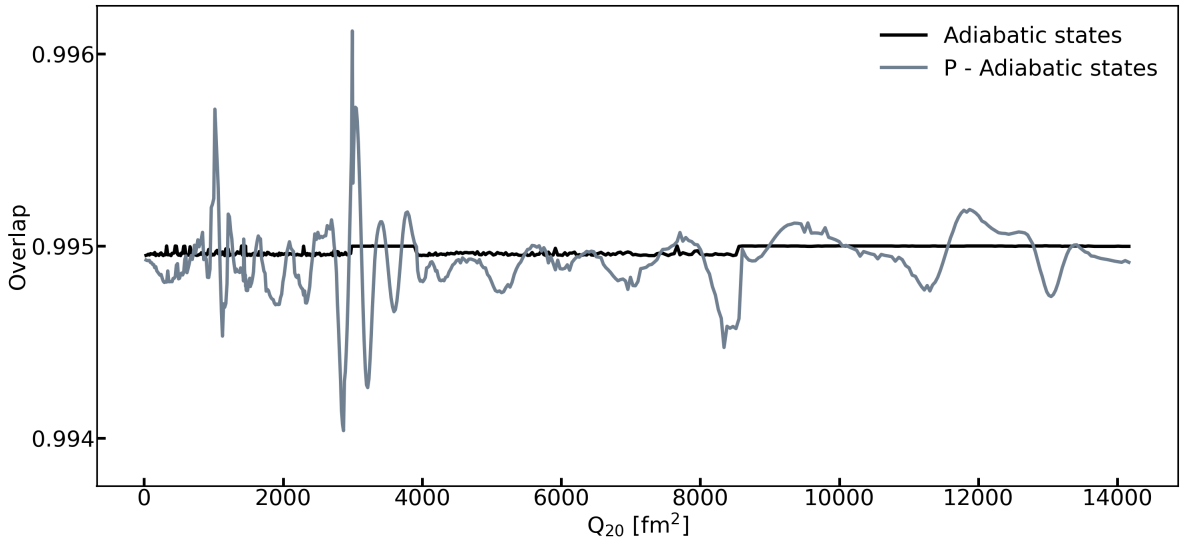

Figure 2.10: Overlap kernel of the adiabatic HFB states with their neighbour on the right compared to the overlap kernel of the projected adiabatic HFB states with their neighbour on the right with respect to quadrupole deformation.

This result is not surprising since a high continuity of the total wave function does imply the continuity of all of its components.

2.3.2 Projected 2-quasiparticle excited states

By analogy with the Eq.(2.89), the projected 2-quasiparticle excited states $|\tilde{\Phi}_{ij}\rangle$ read as follows:

$$\boxed{|\tilde{\Phi}_{ij}\rangle = \frac{\hat{P}_{N_0}}{\sqrt{\langle\Phi_{HFB}|(\bar{\xi}_i\bar{\xi}_j + \bar{\xi}_j\bar{\xi}_i)\hat{P}_{N_0}(\xi_i^+\bar{\xi}_j^+ + \xi_j^+\bar{\xi}_i^+)|\Phi_{HFB}\rangle}}(\xi_i^+\bar{\xi}_j^+ + \xi_j^+\bar{\xi}_i^+)|\Phi_{HFB}\rangle} \tag{2.90}$$

As expected, the energy of the 2-quasiparticle excited states behaves way better when they are projected onto the good particle number subspace.
In Figure (2.11), we represented the projected adiabatic PES (grey curve) along with the PES of a projected 2-quasiparticle excited state (neutron with $\Omega = 1/2$ and of the type $\xi_i^+\bar{\xi}_i^+|\Phi\rangle$) in the ^{240}Pu with respect to the quadrupole deformation. We observe that the energy of the projected 2-quasiparticle excited state behaves in line with the HFB approximation of the excited energy (blue dashed curve in Figure (2.8)):

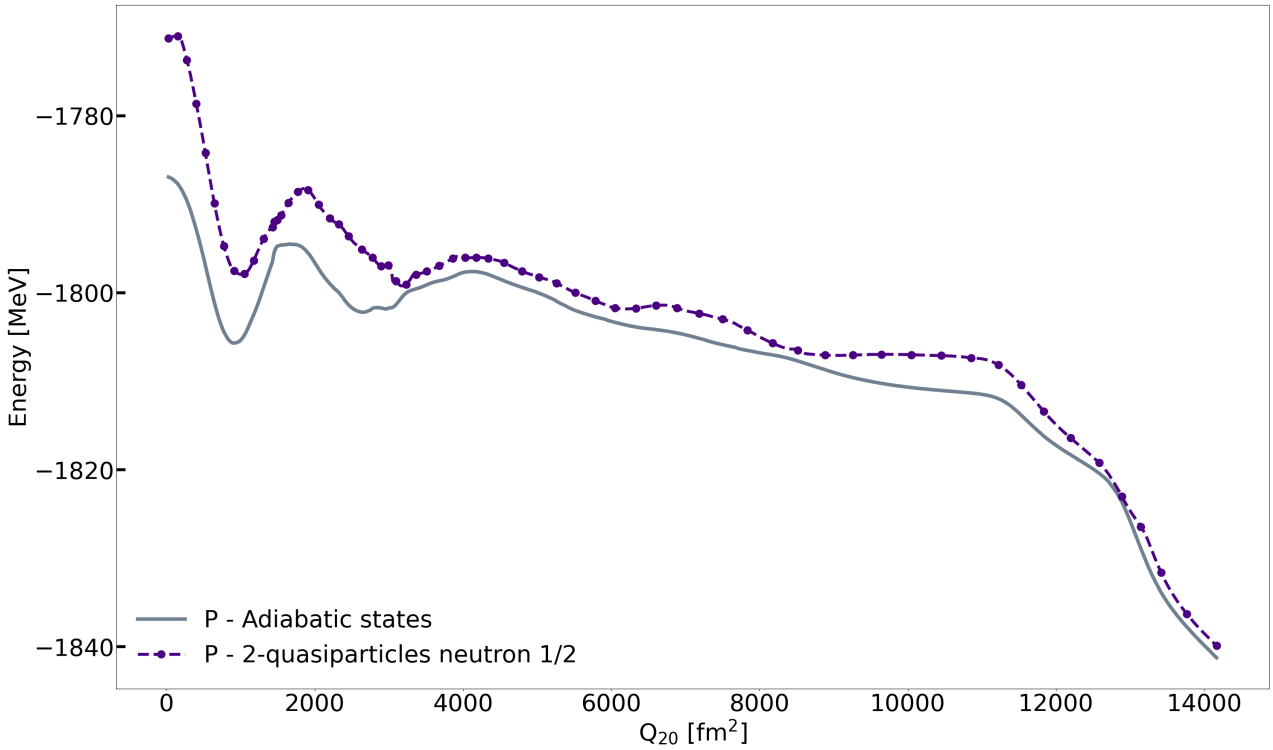

Figure 2.11: Projected adiabatic PES and projected 2-quasiparticle excited state PES in the ^{240}Pu with respect to quadrupole deformation.

Despite its success in correcting energies, the PAV method sill has some important shortcomings. The most straightforward one is the fact that the projected excited states are no more orthogonal to the projected adiabatic states. In Figure (2.12), we plotted the value of the overlap kernel between the projected adiabatic states and their associated projected 2-quasiparticle states with respect to quadrupole deformation in the ^{240}Pu. We observe significant variations with a maximum absolute overlap kernel value of 0.30 for $Q_{20} \approx 3000$ fm^2:

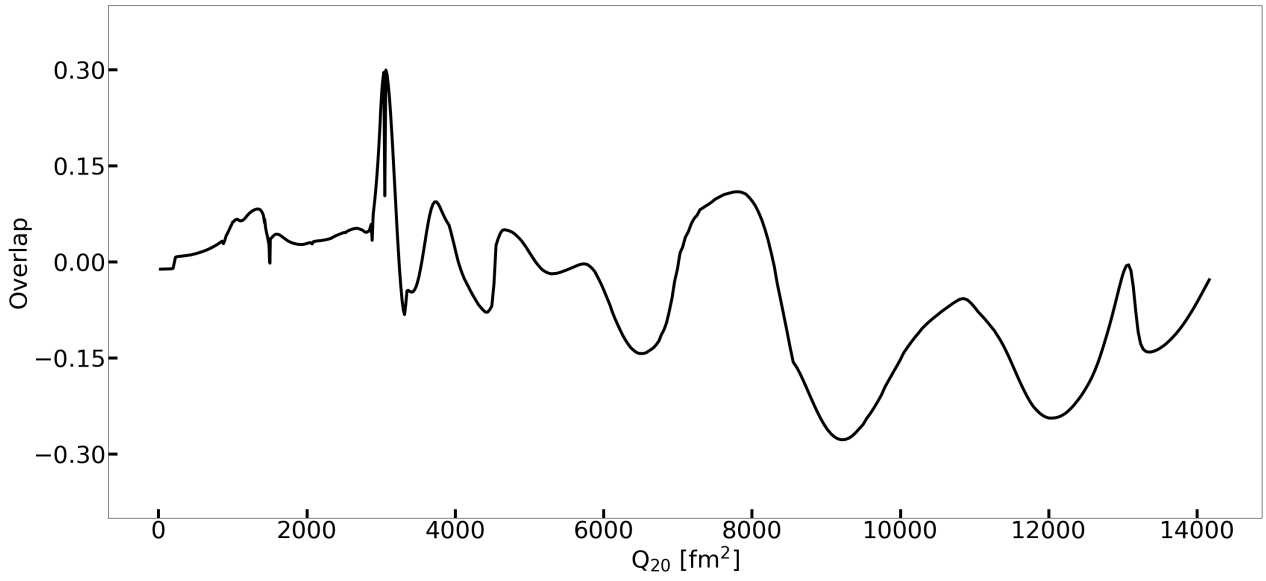

Figure 2.12: Overlap kernel between the projected adiabatic states and one of its projected 2-quasiparticle excited states with respect to quadrupole deformation in the ^{240}Pu.

For such non-orthogonal excitations, the physical interpretation of the SCIM results would be very ambiguous. Indeed, the high overlap kernel values show that the physics of the excitations is mixed with that of the adiabatic states.
Another drawback of the projected 2-quasiparticle excited states is a rather technical but important concern. Indeed, when the pairing energy drops to zero, the adiabatic HFB states have an exact particle number N_0. In that case, the 2-quasiparticle excited states also have an exact particle number, which can be equal to either N_0 or $N_0 \pm 2$. Unfortunately, if the exact particle number of an excited state equals $N_0 \pm 2$, it is no longer possible to project it onto the subspace associated with the particle number N_0 as this subspace simply does not exist.

2.4 Continuity and regularity

As stated in Chapter 1, both the continuity and the regularity of the kernels are important in the SCIM formalism. To specify these two concepts rigorously, we first need to define a distance in the HFB vacua Hilbert space. This assignement is rather straightforward as the customary overlap between states is the canonical Hermitian inner product of the HFB vacua Hilbert space. Because of that, the canonical norm simply reads:

$$|||\Phi\rangle|| = \sqrt{|\langle\Phi|\Phi\rangle|} \tag{2.91}$$

Once a norm is defined, it is easy to build a distance out of it:

$$\mathrm{d}_0(|\Phi_a\rangle, |\Phi_b\rangle) = ||\ |\Phi_a\rangle - |\Phi_b\rangle|| \tag{2.92}$$

As the HFB vacua are properly normalized, Eq.(2.92) can be rewritten as:

$$\mathrm{d}_0(|\Phi_a\rangle, |\Phi_b\rangle) = \sqrt{2}\sqrt{1 - \mathrm{Re}(\langle\Phi_a|\Phi_b\rangle)} \tag{2.93}$$

We rescale the distance d_0 into the final distance d:

$$\boxed{\mathrm{d}(|\Phi_a\rangle, |\Phi_b\rangle) = \sqrt{1 - \mathrm{Re}(\langle\Phi_a|\Phi_b\rangle)}} \tag{2.94}$$

The distance d goes from zero to $\sqrt{2}$, but two orthogonal states are characterized by d= 1 when the distance between a state and its negative counterpart reaches the maximum. In order to avoid this phases ambiguity, we could use the function d^* defined as follows:

$$\mathrm{d}^*(|\Phi_a\rangle, |\Phi_b\rangle) = \sqrt{1 - |\langle\Phi_a|\Phi_b\rangle)|} \tag{2.95}$$

However, d^* is not a distance anymore. Indeed, $|\Phi\rangle \neq -|\Phi\rangle$ but $\mathrm{d}^*(|\Phi\rangle, -|\Phi\rangle) = 0$. We therefore keep the distance d for the formal definitions in the following. In practice, the way we usually figure out the "distance" bewteen states is the plain absolute value of the overlap. It goes from 1 (when both states are equal up to a phase) to 0 (when both states are orthogonal). It is not a distance, but it is rather simple and convenient and avoid the phases issues. For these reasons, most of the figures in this section are displayed with respect to this absolute overlap value.

Besides, other ways exist in the literature to give a hint on the "distance" between states. For instance, the "Density distance" reads as follows [40]:

$$\boxed{\mathrm{d}_\rho(|\Phi_0\rangle, |\Phi_1\rangle) = \int d\vec{r} |\rho_0(\vec{r}) - \rho_1(\vec{r})|} \tag{2.96}$$

From Eq.(2.96), it is clear that d_ρ does not define a true distance. It's a rather classical way to evaluate the differences bewteen quantum states measuring a nucleon difference. It neglects both non-local effects and pairing effects. However, in practice, we found most of the time that the distance calculated with the overlap of Eq.(2.94) and the "Density distance" were in a good agreement. In Figure (2.13), we compared d_ρ (panel (a)) and d (panel (b)) evaluating them for each HFB state and its neighbour on the right with respect to the quadrupole deformation in a ^{240}Pu 1D adiabatic PES. We considered a PES made with the combo HFB3+CHICON in order to underline the behaviour of d_ρ and d with respect to discontinuities:

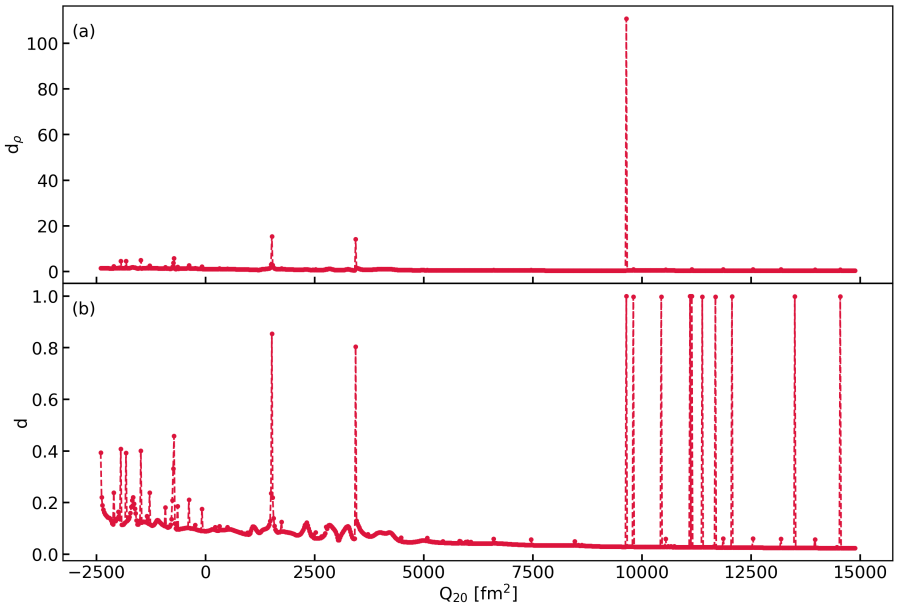

Figure 2.13: Comparison of d and d_ρ with respect to the quadrupole deformation in the ^{240}Pu. Panel (a): the "Density distance" d_ρ between each state and its neighbour on the right. Panel (b): the distance d between each state and its neighbour on the right.

Even if the behaviours of d_ρ and d are very similar, we observe two important phenomena. Firstly, they do not scale the same way. For this reason, d_ρ may be good to spot discontinuities but not to qualify their relative importance. Besides, we observe that in the fusion valley ($Q_{20} > 9500$ fm^2) the overlap distance d reveals discontinuities not raised by d_ρ. These discontinuities can be due to a number of factors, such as pairing or non-local effects. However, we didn't investigate further, as we were not interested in the physics of this part of the PES in this PhD work.

Definition of the continuity:

With the distance d, we have everything we need to define the continuity. If we consider a set of HFB states $\{|\Phi(q)\rangle\}$, q being a collective coordinate, the set $\{|\Phi(q)\rangle\}$ is said to be continuous in q, if the following property holds:

$$\boxed{\lim_{\delta q \to 0} \mathrm{d}(|\Phi(q+\delta q)\rangle, |\Phi(q)\rangle) = 0} \tag{2.97}$$

The explicit definition of the limit in Eq.(2.97) is more suitable for a numerical understanding of continuity:

$$\boxed{\forall \varepsilon > 0,\ \exists \eta > 0\ \ ;\ \ |\delta q| < \eta\ \Rightarrow\ \mathrm{d}(|\Phi(q+\delta q)\rangle, |\Phi(q)\rangle) < \varepsilon} \tag{2.98}$$

Indeed, from a practical point of view and in the context of this PhD thesis work, we always identify a set of HFB vacua with a given procedure. For instance, we consider the following procedure:

$\mathcal{P}_{20}$: "*HFB calculations constraining only the quadrupole moment* $Q_{20} \in [Q_{20}^{(i)}, Q_{20}^{(f)}]$."

$\mathcal{P}_{20}$ defines an infinite continuous set of HFB states $\{|\Phi(Q_{20})\rangle\}$. As we are not working numerically with infinite sets, we therefore have to give a discretized equivalent of Eq.(2.98). We first define a model for the discretized sets associated with $\{|\Phi(\mathrm{Q}_{20})\rangle\}$:

$$\{|\Phi(\mathrm{Q}_{20})\rangle\}_d = \cup_{k=1}^{n} \{|\Phi(Q_{20}^{(k)})\rangle\} \tag{2.99}$$

Here, the $Q_{20}^{(k)}$ stand for different values of Q_{20}. We assume in the following that the $Q_{20}^{(k)}$ are listed in ascending order. Moreover, we always impose $Q_{20}^{(1)} = Q_{20}^{(i)}$ and $Q_{20}^{(n)} = Q_{20}^{(f)}$. With these notations, we can give a discretized version of Eq.(2.98) for a full set:

$$\boxed{\forall \varepsilon > 0,\ \exists \{|\Phi(\mathrm{Q}_{20})\rangle\}_d,\ \ ;\ \ \forall |\Phi(Q_{20}^{(k)})\rangle \in \{|\Phi(\mathrm{Q}_{20})\rangle\}_d,\ \ \mathrm{d}(|\Phi(Q_{20}^{(k\pm1)})\rangle, |\Phi(Q_{20}^{(k)})\rangle) < \varepsilon} \tag{2.100}$$

In Eq.(2.100), the boundaries $1 \leq k \pm 1 \leq n$ are implicitly considered. Thanks to that definition, it is easy to characterize numerically the continuity of a set defined by a specific procedure. Note that it is straightforward to extend Eq.(2.100) in a case with more collective degrees of freedom.

Definition of the regularity:

In the context of this PhD thesis work, we only considered real bounded functions. Thus, we focus on the latter in the following. Let f be a real bounded function of the variable q. We define its infinity norm as follows:

$$||f||_\infty = \sup|f(q)| \tag{2.101}$$

In the literature, the concept of regularity can have several meanings. Most often, it's linked to the property of being differentiable up to a certain order. In the SCIM, this requirement is not sufficient though. Indeed, the SCIM requires that the derivatives of the functions considered tend towards zero when the derivation order increases. The concept of regularity needed is therefore defined as follows:

$$\boxed{\forall \varepsilon > 0,\ \exists N \in \mathbb{N}\ ;\ \forall n \geq N,\ \ ||\frac{\partial^n}{\partial q^n} f||_\infty < \varepsilon} \tag{2.102}$$

The quality of the regularity of a function f is thus given by the pairs $(\varepsilon, N_\varepsilon)$, where N_ε is the smallest integer such that the condition in Eq.(2.102) holds. Besides, we can extend the latter definition to any operator A such that we end up with the concept of $A-$regularity:

$$\boxed{\forall \varepsilon > 0,\ \exists N \in \mathbb{N}\ ;\ \forall n \geq N,\ \ ||A^n(f)||_\infty < \varepsilon} \tag{2.103}$$

This concept of A-regularity will be especially useful in Chapter 6. Indeed, the functions appearing in the SCIM formalism are in general not regular enough with respect to the customary discretized derivative operators. Because of that, special derivative operators have to be defined.
It is easy to consider Eq.(2.101), Eq.(2.102) and Eq.(2.103) from a numerical point of view. Indeed, the function $f : \mathbb{R} \to \mathbb{R}$ is just replaced by the function $\tilde{f} : D_{\tilde{f}} \to \mathbb{R}$ where $D_{\tilde{f}}$ is the discrete domain of $\tilde{f}$. Of course, $\forall q \in D_{\tilde{f}},\ \ \tilde{f}(q) = f(q)$. With these definitions, it is clear that the concept of A-regularity extends to the discrete case (which includes the customary discrete derivative operators).

2.4.1 Continuity issues

In practice, many procedures involving the usual constraints on multipole moments are associated with discontinuous sets of states. In Figure (2.14), we represented (panel (a)) the energy of two HFB adiabatic sets obtained with different procedures and three coloured circles highlighting discontinuities on the red PES. In panel (b), we displayed the overlap of these states with their neighbour on the right. All curves are presented with respect to the quadrupole deformation in the ^{240}Pu. The red dashed-dotted curve is obtained from the $\mathcal{P}_{20}$ prodecure and numerically evaluated using the CHICON code as a driver for the HFB3 code. The black curve corresponds to a more sophisticated procedure $\tilde{\mathcal{P}}_{20}$ and is numerically evaluated with the Link+Drop combo on top of the HFB3 code. Both the $\tilde{\mathcal{P}}_{20}$ procedure and the Link+Drop combo are detailed in the section 3 of this Chapter. We displayed both curves for the reader to have a reference point for comparing what is continuous and what it is not:

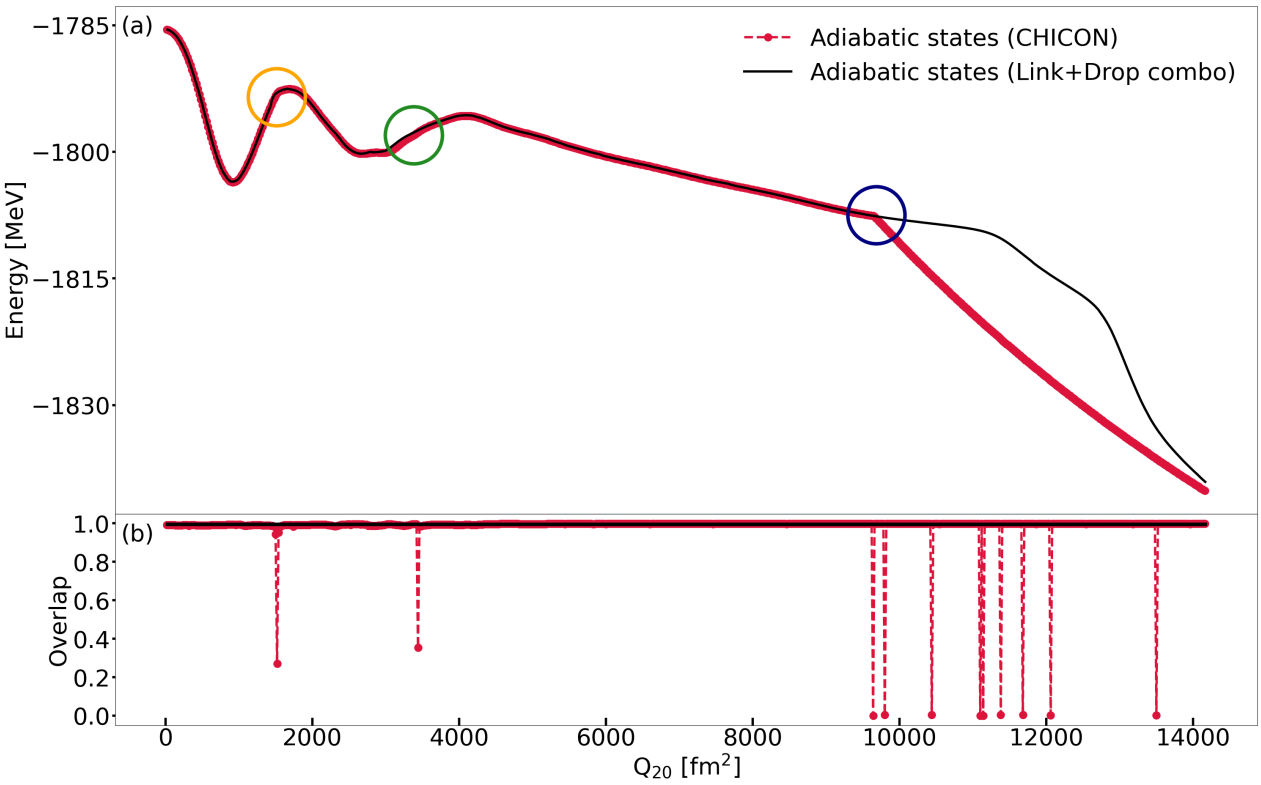

Figure 2.14: Illustration of the continuity of two different HFB adiabatic sets with respect to quadrupole deformation in the ^{240}Pu. Panel (a): PES associated with both sets with coloured circles highlighting discontinuities. Panel (b): Overlap between each state of the sets and their neighbour on the right.

The most obvious comment is that it is possible to be continuous in energy and discontinuous in overlap at the same time (red curve). Indeed, the procedure $\mathcal{P}_{20}$ guarantees that the energy of the states is continuous, as they are all built through an energy minimization process. On the other hand, as the only degree of freedom constrained is the quadrupole deformation, the nucleus is free to use the other unconstrained dimensions to minimize its energy. This process can introduce discontinuities.
Such a discontinuous rearrangement of the unconstrained degrees of freedom is more likely to happen in areas where a symmetry of the nucleus is broken. For instance, the green circle highlights the parity symmetry breaking and is related to the multipole moment Q_{30}.
The discontinuity identified by the golden circle is clearly associated with the multipole moment Q_{40}. Besides, we have good reasons to assume that it is related to the fact that the nucleus breaks the axial symmetry around this area if we let it free to do so. Indeed, we can guess that this peculiar spontaneous symmetry breaking may correlate with topological issues in the axial subspace. We've tested this hypothesis by performing triaxial calculations. In panel (a) of Figure (2.15), we've represented the HFB energy with respect to β_2 (accounting for the quadrupole moment Q_{20}) and γ (accounting for the triaxiality). In panel (b), we've displayed the quantity β_4 (accounting for the hexadecapole moment Q_{40}) with respect to β_2 and γ:

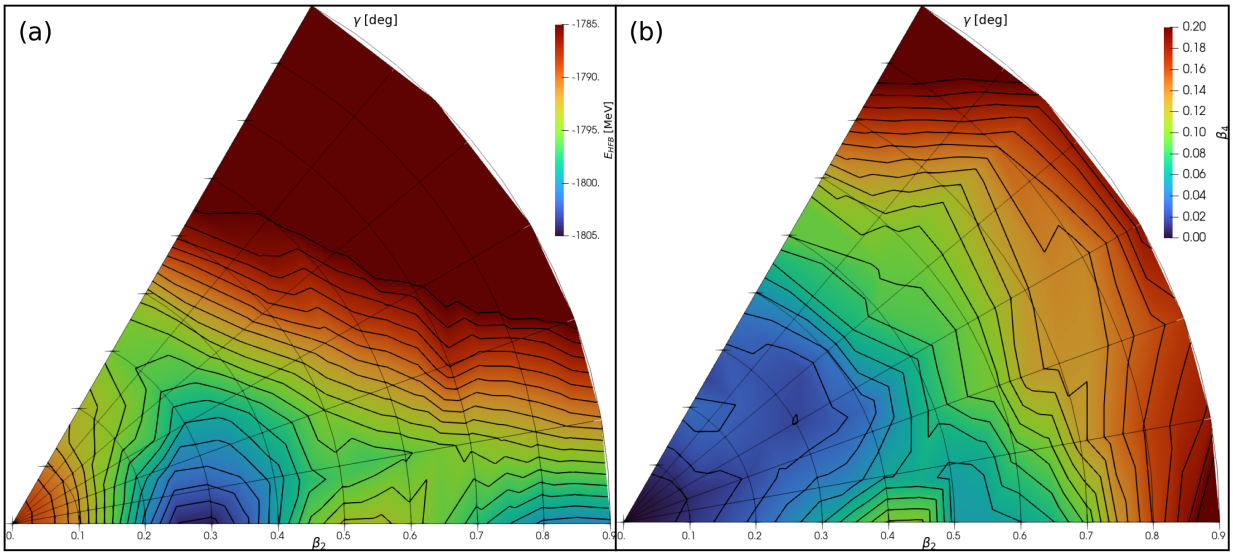

Figure 2.15: Study of the triaxility in the ^{240}Pu. Panel (a): HFB energy with respect to β_2 and γ. Panel (b): β_4 with respect to β_2 and γ.

In both panels, the discontinuity spotted by the golden circle corresponds to $\gamma = 0$ and $\beta_2 \approx 0.5$. In panel (b), along the axial path ($\gamma = 0$), we clearly observe the bump of β_4 between $\beta_2 = 0.4$ and $\beta_2 = 0.5$, which is associated with the Q_{40} discontinuity (see also Figure (2.16)). Besides, we remark that the triaxial path that minimizes the HFB energy also avoid this Q_{40} bump, displaying a way smoother behaviour with respect to β_4. Unfortunately, we were unable to measure the continuity of this triaxial path. If this path were found continuous, it would prove definitely that the usual discontinuity of the first barrier in the axial calculations and the spontaneous breaking of axial symmetry at the first barrier are one and the same phenomenon.
Back in Figure (2.14), the discontinuity circled in blue accounts for all the sudden changes encountered by the nucleus through the scission process and cannot be accurately described with just a few multipole moments. Finally, the remaining discontinuities testify to the complex structure of the fusion valley obtained with the $\mathcal{P}_{20}$ procedure.

In Figure (2.16), panel (a), we represented the evolution of the hexadecapole deformation with respect to the quadrupole deformation in the area of the golden cirlce in the ^{240}Pu for both the sets obtained with the $\mathcal{P}_{20}$ and the $\tilde{\mathcal{P}}_{20}$ procedure. In panel (b), we represented the evolution of the octupole deformation with respect to the quadrupole deformation in the area of the green circle for the same sets. Moreover, two local densities have been added in panel (a) and two others in panel (b) in order to highlight the modification in the shape of the nucleus:

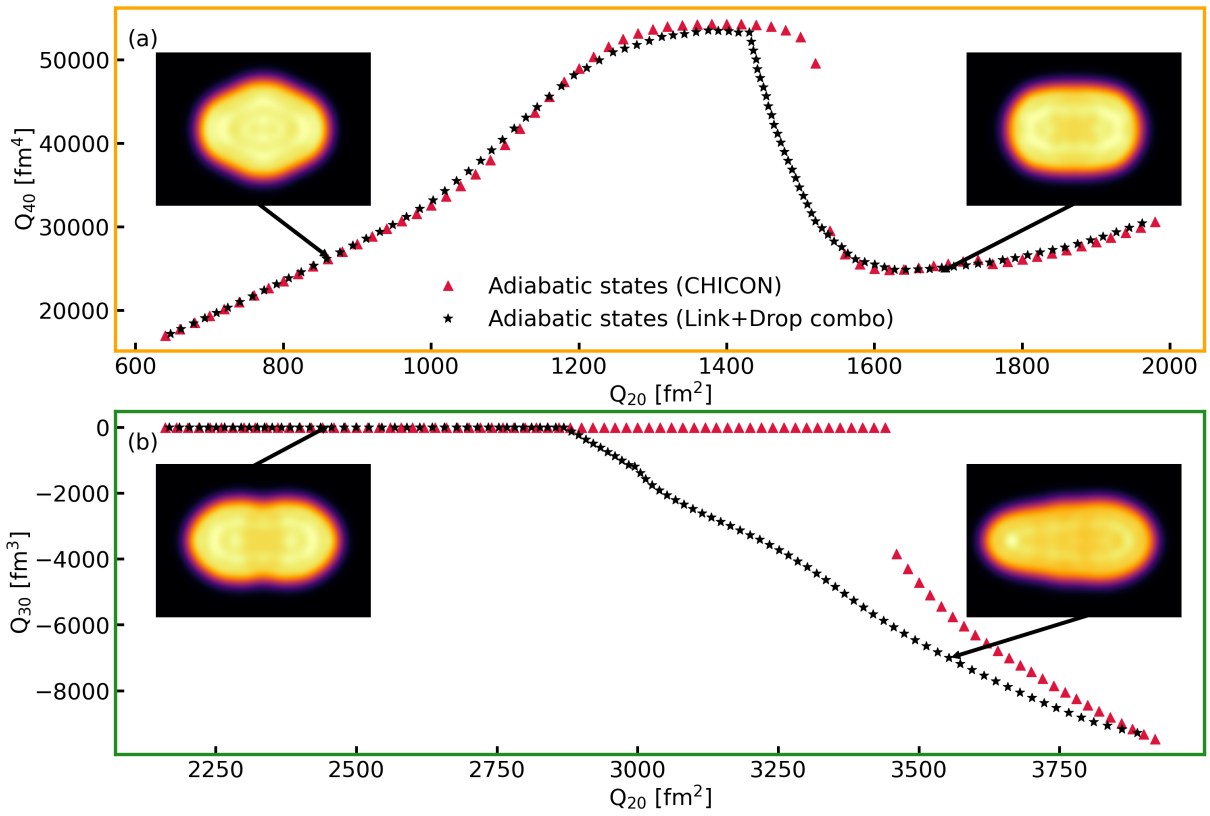

Figure 2.16: Illustration of the evolution of the hexadecapole and octupole moments in relevant areas in the ^{240}Pu sets obtained with $\mathcal{P}_{20}$ and $\tilde{\mathcal{P}}_{20}$. Panel (a): hexadecapole deformation with respect to the quadrupole deformation. Panel (b): octupole deformation with respect to the quadrupole deformation.

We observe that the black stars connect continuously the gap between the red dots. The reader may legitimately assume that smooting out discontinuities is just a matter of multipole moment interpolation, and he would be right. At least for these two specific cases.
Indeed, before ending up with the $\tilde{\mathcal{P}}_{20}$ procedure, we tried the most simple $\mathcal{P}^{(l)}_{20}$ one. If we consider a discontinuity in the set of the procedure $\mathcal{P}_{20}$ related to a multipole moment Q_{x0} with $(Q^{(d-1)}_{20}, Q^{(d-1)}_{x0})$ and $(Q^{(d+1)}_{20}, Q^{(d+1)}_{x0})$ labeling the moments before and after the discontinuity respectively, the associated procedure $\mathcal{P}^{(l)}_{20}$ reads as follows:

$$\mathcal{P}^{(l)}_{20}\text{: ``}\mathcal{P}_{20}\textit{ procedure for }\ Q_{20} \in [Q^{(i)}_{20}, Q^{(d-1)}_{20}] \cup [Q^{(d+1)}_{20}, Q^{(d-1)}_{20}]\textit{ and HFB calculations constraining both the quadrupole moment } Q_{20} \in [Q^{(d-1)}_{20}, Q^{(d+1)}_{20}]\textit{ and } Q_{x_0} = Q^{(d-1)}_{x_0} + (Q_{20} - Q^{(d-1)}_{20})\frac{Q^{(d+1)}_{x0} - Q^{(d-1)}_{x0}}{Q^{(d+1)}_{20} - Q^{(d-1)}_{20}}\text{.''}$$

$\mathcal{P}^{(l)}_{20}$ is nothing but a linear interpolation on the constraint related to the discontinuity. In practice, we have found it to be both efficient and convenient to use. However, as the linear interpolation is a rather naive interpolation scheme, one may argue that it probably doesn't provides us with the good adiabatic path. For this reason, a more sophisticated procedure has been proposed by W. Lau et al. [55], including explicitly the concern for the adiabaticity in the interpolation algorithm.
In the light of the last paragraphs, discontinuities appear to be rather simple problems to solve. Nevertheless, the situation is totally different when it comes to describe the scission

phenomenon. In Figure (2.17), we zoomed in on the blue circled discontinuity of Figure (2.14) and we illustrated it with different local densities:

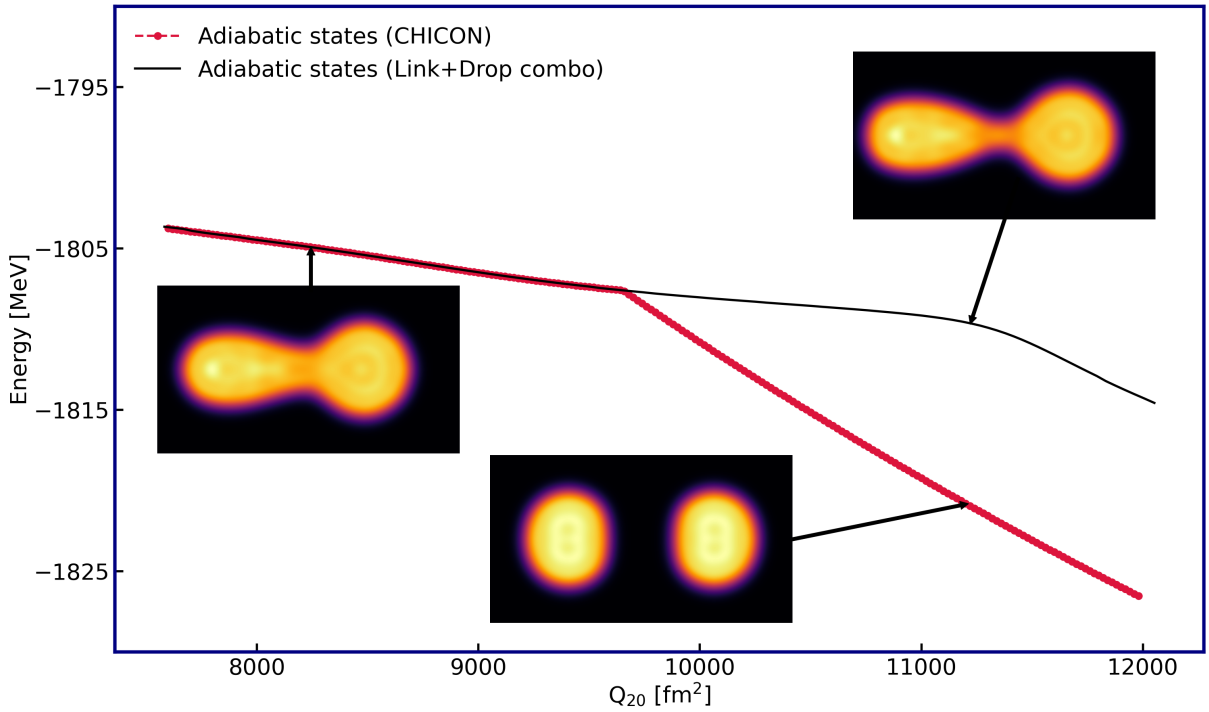

Figure 2.17: Illustration of the situation at scission zooming in on the blue circled discontinuity of Figure (2.14), in addition to relevant local densities.

The most stricking feature we observe in Figure (2.17) around $Q_{20} = 11300$ fm^2 is the fact that the local density associated with the black curve corresponds to a single highly-deformed nucleus, while the local density related to the red curve describes two already separated fragments with an oblate shape. This last case corresponds to the behaviour of two distant nuclei simply subjected to their Coulomb potential. This is the reason why the valley described by the red curve is usually called the "fusion valley". In a word, the customary procedure $\mathcal{P}_{20}$ is far from providing us with the expected physics at very large quadrupole deformations.
Besides, the geometry of this transition seems too complex to be described with few multipole moments. To circumvent this issue, a new geometric operator called Q_{neck} has been proposed by W. Younes and D. Gogny [56]. This operator is used to constrain the number of nucleons in an area between the two pre-fragments (the "neck"). The procedures involving Q_{neck} have shown some success in extending PES made originally with the procedure $\mathcal{P}_{20}$ [35, 57].
That being said, these procedures also suffer from certain limitations. First, they require at least to constrain both Q_{20} and Q_{neck} at the same time. As there is no easy way to guess how Q_{neck} should behave with respect to Q_{20}, two-dimensional calculations have to be made in order to extract an adiabatic one-dimensional set. Moreover, the numerical instabilities occuring around the scission area often impose to add some other multipole constraints for the convergences to work. Extracting an adiabatic path under these conditions can quickly become a tedious numerical challenge. Nor it is clear whether these procedures can achieve a reliable continuity of the order of that obtained in naturally continuous areas (with a standard step in Q_{20}, the overlap between adjacent states are in general greater than 0.99). To

conclude on this topic, the Q_{neck} operator is by definition restricted to the description of pre-fragments connected by a neck. As a result, it is dubious that it can describe properly the entire fragment separation process.

In this section, we have only discussed adiabatic results. The reason is quite simple: discontinuities at the adiabatic level always propagate to the 2-quasiparticle excited states. Dealing with these discontinuities is therefore of the utmost importance to make the SCIM work.

2.4.2 Regularity issues

The tests of the SCIM we were able to carry out on continuous areas showed us a need for more than just continuity. In fact, we have realized the vital importance of kernels regularity. First of all, we want to empasize a very important property of the kernels: the Hamiltonian kernel varies accordingly with the overlap kernel according to the following relation:

$$\boxed{\langle\Phi(q)|\hat{H}|\Phi(q')\rangle \approx \langle\Phi(q)|\Phi(q')\rangle E(\frac{q+q'}{2})} \tag{2.104}$$

Indeed, in Figure (2.18) we studied the absolute error on the hamiltonian kernel $\Delta\hat{H}(\bar{q}-s,\bar{q}+s)$ with respect to $\bar{q}$ and s:

$$\Delta\hat{H}(\bar{q}-s,\bar{q}+s) = 100\times|\frac{\langle\Phi(\bar{q}-s)|\hat{H}|\Phi(\bar{q}+s)\rangle - \langle\Phi(\bar{q}-s)|\Phi(\bar{q}+s)\rangle E(\bar{q})}{\langle\Phi(\bar{q}-s)|\hat{H}|\Phi(\bar{q}+s)\rangle}| \tag{2.105}$$

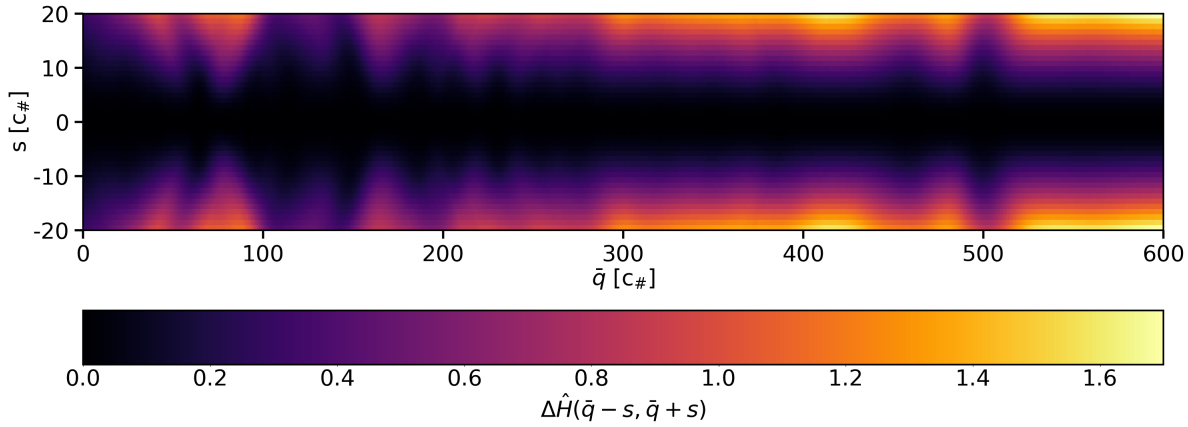

Figure 2.18: Absolute error on the Hamiltonian kernel with respect to $\bar{q}$ and s.

The quantities $\bar{q}$ and s used in Eq.(2.105) and Figure (2.18) are expressed in terms of the new collective coordinate $c_{\#}$, the construction of which is one the objectives of this section. To give an hint on this new collective coordinate, $c_{\#}=0$ is associated with $Q_{20}=28$ fm^2 and $c_{\#}=600$ is associated with $Q_{20}=18885$ fm^2. The results presented stand therefore for the entire adiabatic PES.
The closer we are from $s=0$, the better the approximation. Indeed in the range $s\in[-10,10]$, the absolute error peaks at 0.46% when in $[-5,5]$ the maximum of the absolute error is 0.15%. Moreover, as the value of the Hamiltonian kernel decreases quickly with respect to s, the part of the Hamiltonian kernel that the approximation describes the best is also the most relevant part for applications. For our purposes, this result is important because it shows that we can

focus on the regularity of the overlap kernel to get the regularity of both the Hamiltonian and the overlap kernels. Besides, this result fully justifies the well-known local approximation used, for example, in the GOA formalism [45].

We have also verified the relation displayed in Eq.(2.104) in the case of the PAV (with respect to particle number). In Figure (2.19), we've plotted the absolute error on the PAV Hamiltonian kernel $\Delta\hat{P}\hat{H}(\bar{q}-s,\bar{q}+s)$ with respect to $\bar{q}$ and s:

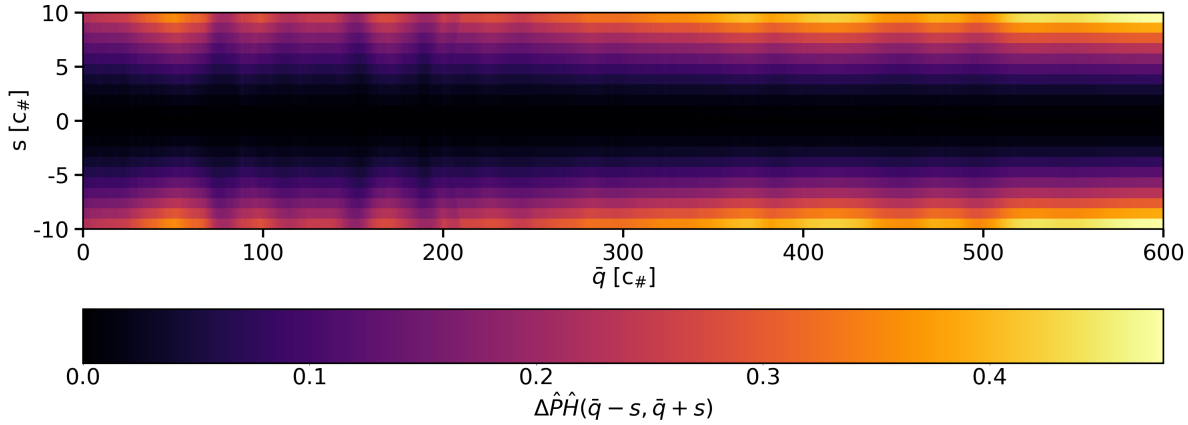

Figure 2.19: Absolute error on the projected Hamiltonian kernel with respect to $\bar{q}$ and s.

Here, we have limited ourselves to the values of s in the interval [-10,10] due to the numerical cost of the projected Hamiltonian kernels. Looking at Figure (2.19), it is clear that both the relation displayed in Eq.(2.104) and the local approximation still hold in the case of the PAV (with respect to particle number).

In the light of these results, we will only discuss the regularity of the overlap kernel in the following. This regularity depends on two different factors. The first one is extrinsic, as it is related to the choice of the collective coordinate. The second one is intrinsic and accounts for the inner regularity of the quantities described.

Extrinsic regularity:

A more detailed inspection of the overlap of a continuous zone of the PES obtained with the $\mathcal{P}_{20}$ procedure reveals a relatively high variability. In Figure (2.20), we considered the two usual adiabatic HFB sets obtained with the $\mathcal{P}_{20}$ and $\tilde{\mathcal{P}}_{20}$ procedures in the ^{240}Pu. In panel (a), for each of these sets, we displayed the overlap between each state and its neighbour on the right with respect to the quadrupole deformation. In panel (b), we zoomed in on a continuous area of the red curve:

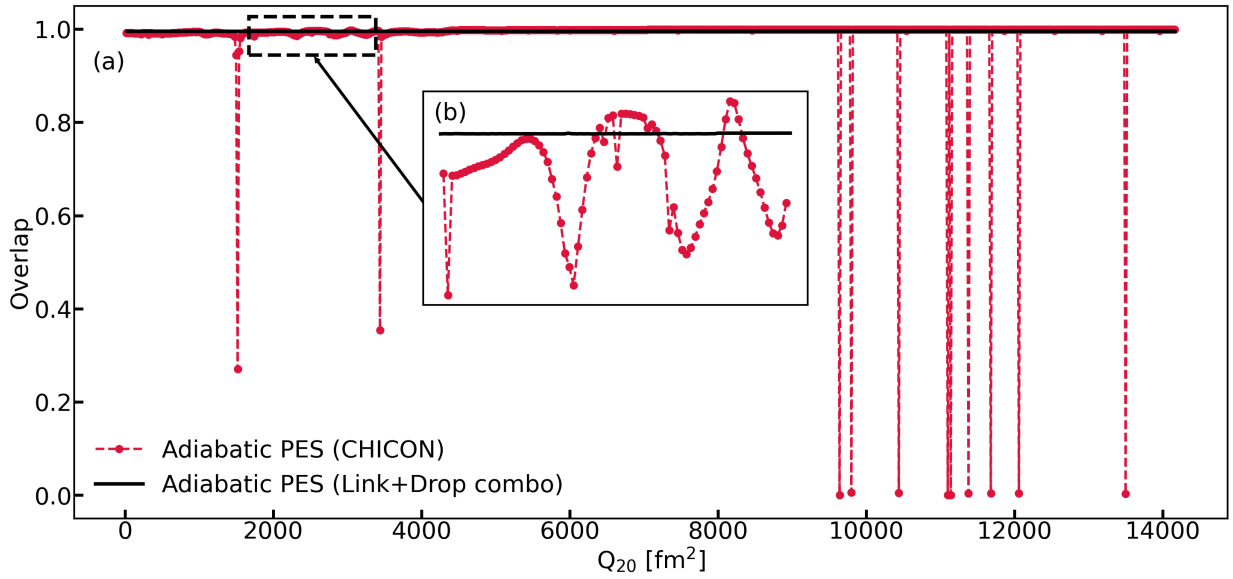

Figure 2.20: Illustration of the regularity issues in two adiabatic HFB sets obtained with the $\mathcal{P}_{20}$ and $\tilde{\mathcal{P}}_{20}$ procedures with respect to quadrupole deformation in the ^{240}Pu. Panel (a): overlap between each state of the sets and its neighbour on the right. Panel (b): zoom of a continuous part of the curves.

In the red curve, each state is separated from its neighbors by a fixed step in Q_{20}. What Figure (2.20) remarkably shows is that this fixed step in Q_{20} doesn't necessarily imply a fixed overlap distance between the states. In contrast, the states of the black curve constructed with the $\tilde{\mathcal{P}}_{20}$ procedure are all naturally separated by the same overlap distance. It is clear that the overlap kernel of the states belonging to the black curve and simply labeled by their position within their set will have a way better regularity than the overlap kernel evaluated for the states of the red curve labeled by Q_{20}. For this reason, the position of the states in the black set is a much better collective coordinate within the SCIM framework. As it is simply derived from the sequence of the states within their set, this new collective coordinate is denoted $c_{\#}$ thereafter.
It is interesting to compare both collective coordinates to characterize better the limitations of the collective coordinate Q_{20}. In Figure (2.21), we've represented the way Q_{20} scales with respect to $c_{\#}$ in the adiabatic set obtained with the $\tilde{\mathcal{P}}_{20}$ procedure in the ^{240}Pu:

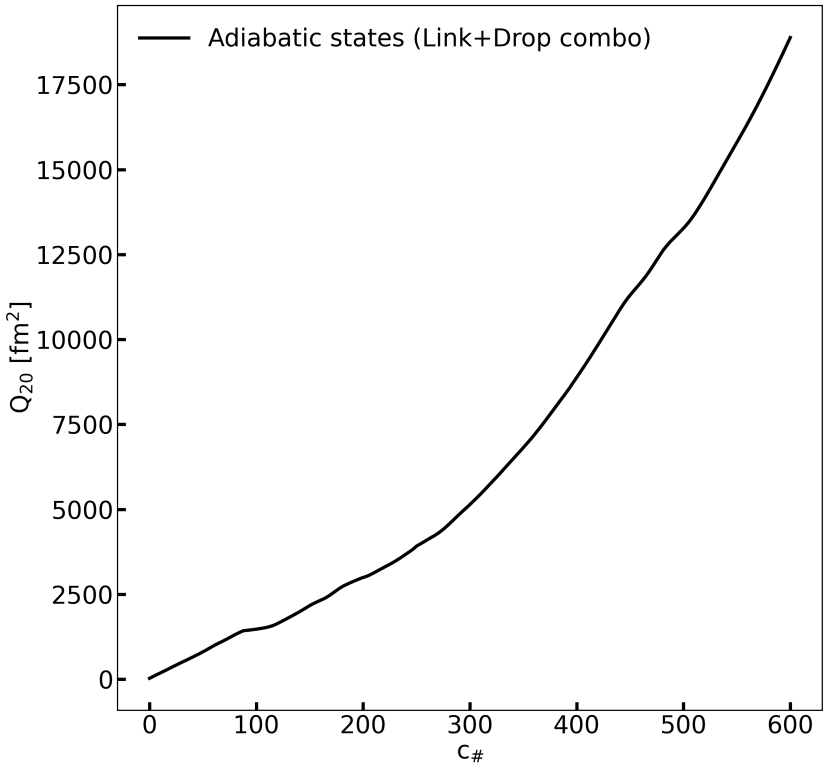

Figure 2.21: Scaling of the multipole moment Q_{20} with respect to the collective coordinate $c_{\#}$ in the ^{240}Pu.

If Q_{20} were an accurate collective coordinate, we would have expected linear behaviour with respect to $c_{\#}$. Figure (2.21) demonstrates that Q_{20} is not well-suited to describe the evolution of the nucleus globally.
It is important to understand that each of the Figures (2.20) and (2.21) highlights a different problem of the collective coordinate Q_{20}. Figure (2.20) shows that variability can be locally added to the kernels because of local mismatches between the overlap distance and a fixed step in Q_{20}. On the other hand, Figure (2.21) underlines that a spurious trend will appear in the evaluation of the kernels using the collective coordinate Q_{20}. Indeed, the behaviour described by the black curve in Figure (2.21) clearly implies that the kernels related to a high Q_{20} will be relatively overvalued compared to those with a lower Q_{20}.
The trend shown in Figure (2.21) is even more obvious comparing the same PES, but with respect to Q_{20} and $c_{\#}$. In panel (a) of Figure (2.22), we displayed the PES asscociated with the adiabatic set of states obtained with $\tilde{\mathcal{P}}_{20}$ in the ^{240}Pu with respect to the quadrupole deformation. In panel (b), we displayed these same PES, but with respect to the new collective coordinate $c_{\#}$. In both cases, black circles have been displayed every five calculated state:

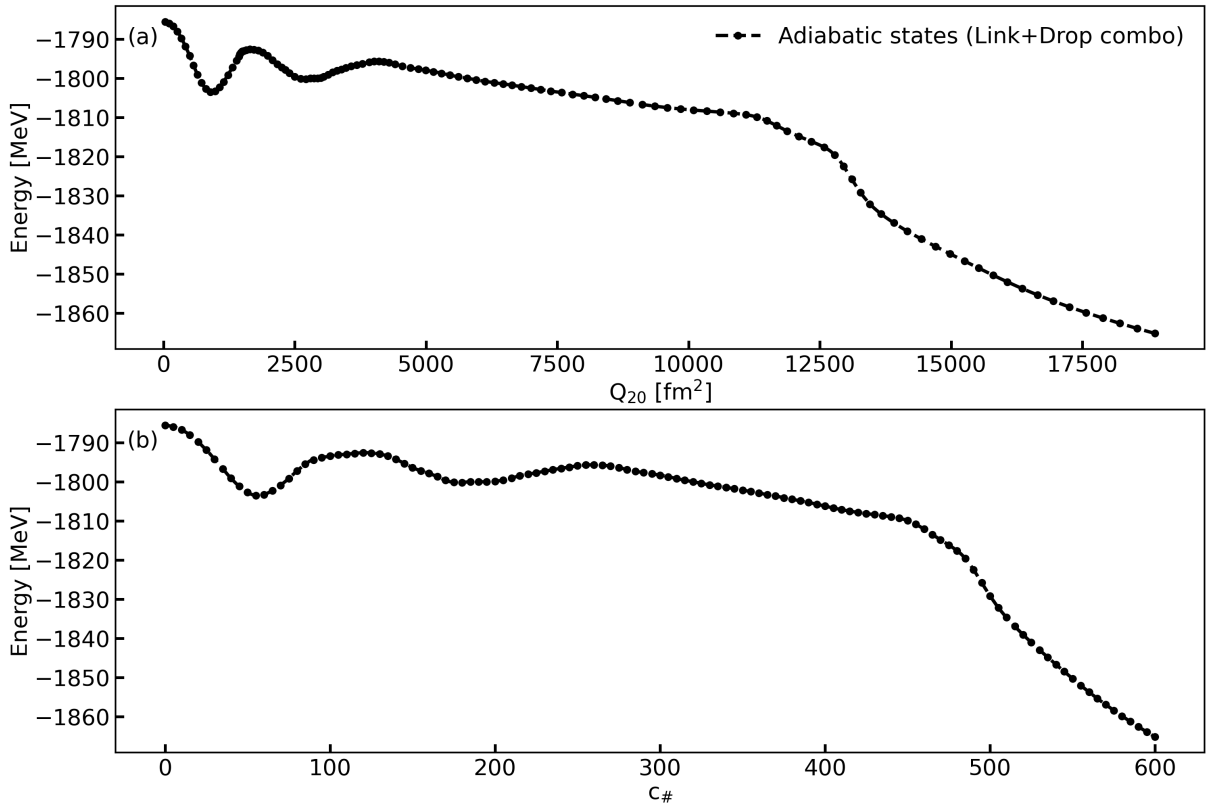

Figure 2.22: Comparison of the collective coordinates Q_{20} and $c_{\#}$ in a PES obtained from an adiabatic set related to the procedure $\tilde{\mathcal{P}}_{20}$ in the ^{240}Pu. Panel (a): PES with respect to the quadrupole deformation. Panel (b): PES with respect to $c_{\#}$.

We observe that the non-linear scaling of Q_{20} with respect to $c_{\#}$ implies significant differences in the topologies of the two PES. In particular, the width of the first barrier is greatly increased and the descent from the saddle point to scission is shorter and steeper in the $c_{\#}$ representation compared with the Q_{20} one. These two important changes surely imply important consequences in the dynamics that have been neglected until now.
The results of this section do not condemn the use of Q_{20} in absolute, but emphasize that if it is used, it must be done with an appropriate metric accounting for the phenomena described above. This is not a new statement at all. In fact, it's clearly linked to the change of variable made in the GOA to reduce to a constant the Gaussian width of the overlap kernel at first order.
In practice, using a metric in a set built with a fixed step in Q_{20} can often be tedious and even mismatch the formalism we want to use. In the SCIM for instance, the center of mass and relative coordinates we use in order to reduce the Hill-Wheeler equation clearly does not encourage us to use a metric. Indeed, in that case, all the kernels we have to evaluate are of the type $\langle\Phi(\bar{q}-s)|\Phi(\bar{q}+s)\rangle$ and $\langle\Phi(\bar{q}-s)|\hat{H}|\Phi(\bar{q}+s)\rangle$. In a numerical set built for the SCIM with a fixed Q_{20}, all the states $|\Phi(\bar{q}-s)\rangle$ are therefore paired with their $|\Phi(\bar{q}+s)\rangle$ counterpart, but if the collective coordinate changes due to a metric, the states are not paired anymore and the kernels cannot be calculated. Therefore, the numerical evaluation of a set for the SCIM must already include the concern for the metric. The most obvious way to do it with the customary $\mathcal{P}_{20}$ procedure is to determine the states sequentially. At each step, starting from a state with a quadrupole moment $Q_{20}^{(i)}$, the next state is found with a quadrupole moment $Q_{20}^{(i+1)}$ such that the overlap between the two states equals a fixed constant value x_0. This approach has however two clear drawbacks. Firstly, it includes sequential calculations

that cannot be parallelized. Then, finding the good Q_{20} at each step implies a rather time-consuming dichotomy.

After this discussion on the regularity of the adiabatic states, we can investigate how the 2-quasiparticle excited states behave in this respect. Especially, if we consider the most favorable case of a set constructed with the $\tilde{\mathcal{P}}_{20}$ procedure, where the states are evenly spaced with respect to the overlap distance, we legitimately expect the same regularity for the 2-quasiparticle excited states built on top of it. In Figure (2.23), we've considered an adiabatic set built with the $\tilde{\mathcal{P}}_{20}$ procedure in the ^{240}Pu along with one of its 2-quasiparticle excited states (neutron with $\Omega = 1/2$ and of the type $\xi_i^+ \bar{\xi}_i^+ |\Phi\rangle$). Panel (a) shows the overlap between each state of both sets with its neighbour on the right and panels (b) and (c) zoom in on specific areas of interest:

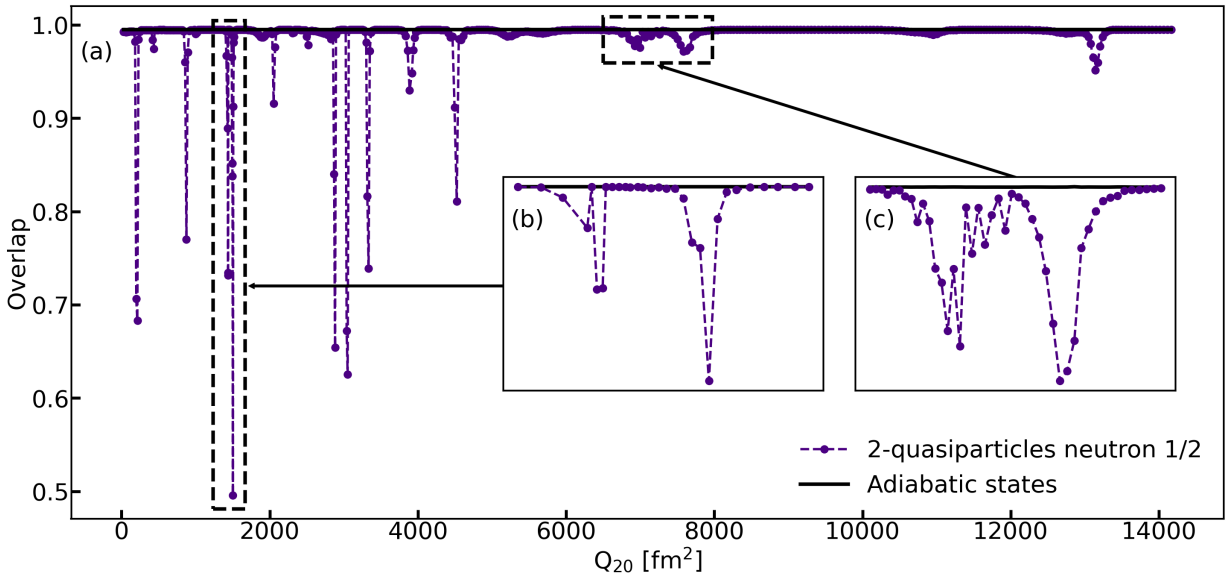

Figure 2.23: Illustration of the regularity of a 2-quasiparticle excited set built on top of an adiabatic set created thanks to the $\tilde{\mathcal{P}}_{20}$ procedure in the ^{240}Pu. Panel (a): overlap between each state of the sets and its neighbour on the right. Panel (b-c): zoom of relevant areas of the panel (a).

The peaks observed in Figure (2.23) are not discontinuities, but irregularities. Indeed, if we look at panels (b) and (c), we can see that the overlaps do not match with the scenario of two zones, each continuous, separated by a sudden and unique discontinituity. Instead, we are dealing with areas of "turbulence". These local turbulences are in fact related to level repulsions between quasiparticles. In Figure (2.24), we've highlighted the level repulsion that occurs in the first bump of the panel (c) of Figure (2.23). In panel (a), we've displayed the local projected PES associated with the two 2-quasiparticle excited states implied in the level repulsion. In panel (b), we've plotted the overlap kernel between the two excited states along with the overlap kernels between these excited states and the adiabatic ones:

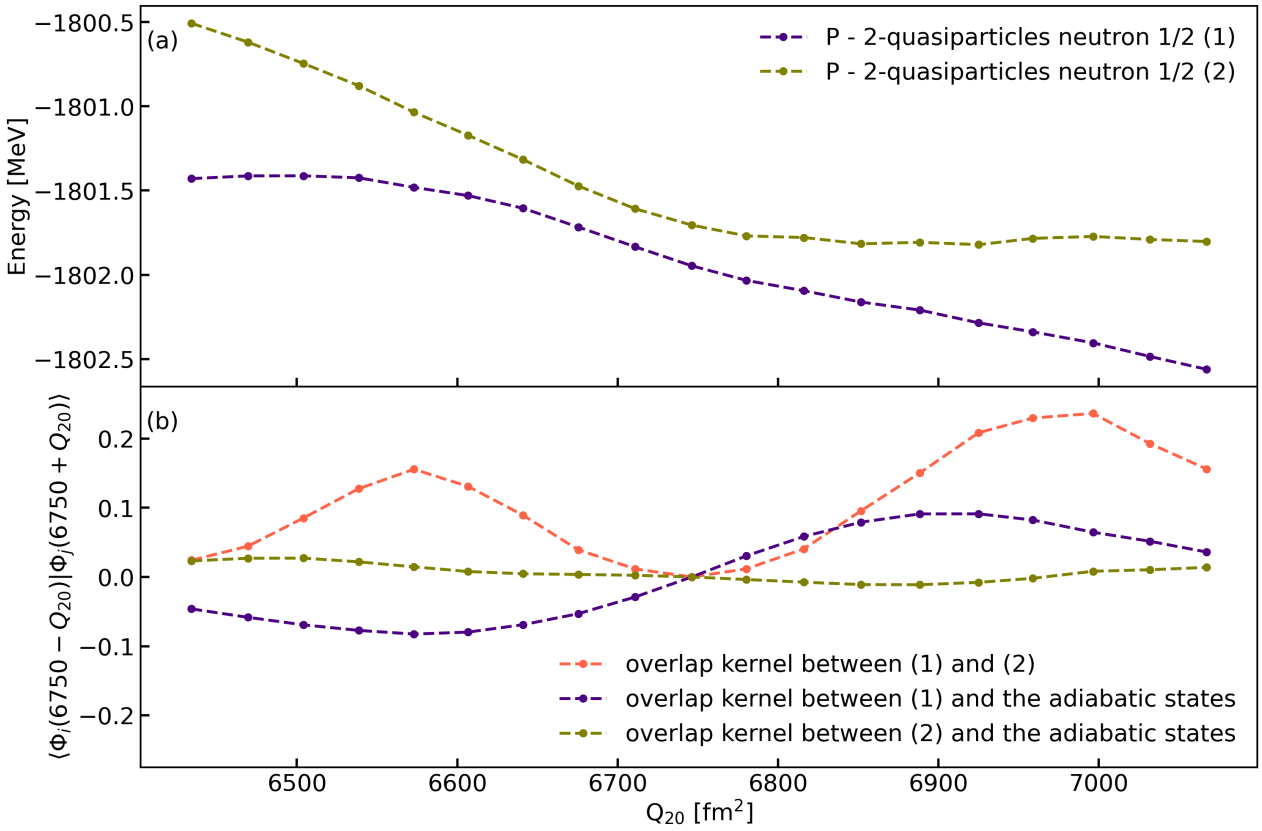

Figure 2.24: Illustration of different effects of level repulsions. Panel (a): projected PES of the 2-quasiparticle excited states involved in the level repulsion. Panel (b): overlap kernel between the two excited states and overlap kernels of these excited states with the adiabatic ones.

In panel (a), we clearly see that the trends of the curves suddenly change when the level repulsion occurs. It feels like these trends are exchanged through the level repulsion process. In panel (b), the overlap kernels tend to confirm this assumption of property exchange. Indeed, the red curve shows a larger amplitude than the two other ones. This feature implies that the two 2-quasiparticle excited states do have a lot in common with respect to a non-locality in Q_{20}. In fact, the phenomenon comes from the fact that the quasiparticles involved share common components at the particle level that repel each other according to the Pauli principle.
Due to these level repulsions, the 2-quasiparticle excited states sometimes vary at their own pace, which can be much faster than that of the adiabatic states. To take this phenomenon into account, we'd have to use a different collective coordinate for the adiabatic set and for each excited set. Unfortunately, the SCIM formalism requires to label all the sets with the same collective coordinate. So it seems that this type of 2-quasiparticle excited states are a dead end.

Intrinsic regularity:

Once we've done everything possible to deal with extrinsic irregularities, we face the intrinsic regularity of the kernels. We only consider here the intrinsic regularity of the adiabatic set obtained with the $\tilde{\mathcal{P}}_{20}$ procedure, as the extrinsic and intrinsic regularity of the 2-quasiparticle excited states cannot be disentangled for the moment (see Figure (2.23)).

A good way to measure the intrinsic regularity of the adiabatic set is simply to consider the zero-order moment of the overlap kernel $N_{00}^{(0)}$ which naturally appears in the SCIM formalism:

$$\boxed{N_{00}^{(0)}(\bar{q}) = \int ds \langle \Phi_0(\bar{q}-s)|\Phi_0(\bar{q}+s)\rangle} \tag{2.106}$$

In a perfect world, we would expect $N_{00}^{(0)}$ to be constant with respect to $\bar{q}$. For instance, under the GOA approximation, the fact that each of the adjacent states are evenly separated by an overlap of a given x_0 directly implies:

$$\boxed{N_{00_{GOA}}^{(0)} = \int ds e^{\ln(x_0)(2s)^2} = \frac{1}{2}\sqrt{\frac{\pi}{-\ln(x_0)}}} \tag{2.107}$$

In practice though, variations may occur. In panel (a) of Figure (2.25), we displayed $N_{00}^{(0)}(c_\#)$ and compared it with the constant value we would have obtained using the GOA (for $x_0 = 0.995$). In panels (b-c), we've shown respectively the kernels $\langle\Phi(201-s)|\Phi(201+s)\rangle$ and $\langle\Phi(330-s)|\Phi(330+s)\rangle$ with respect to s and compared it with the associated GOA curves:

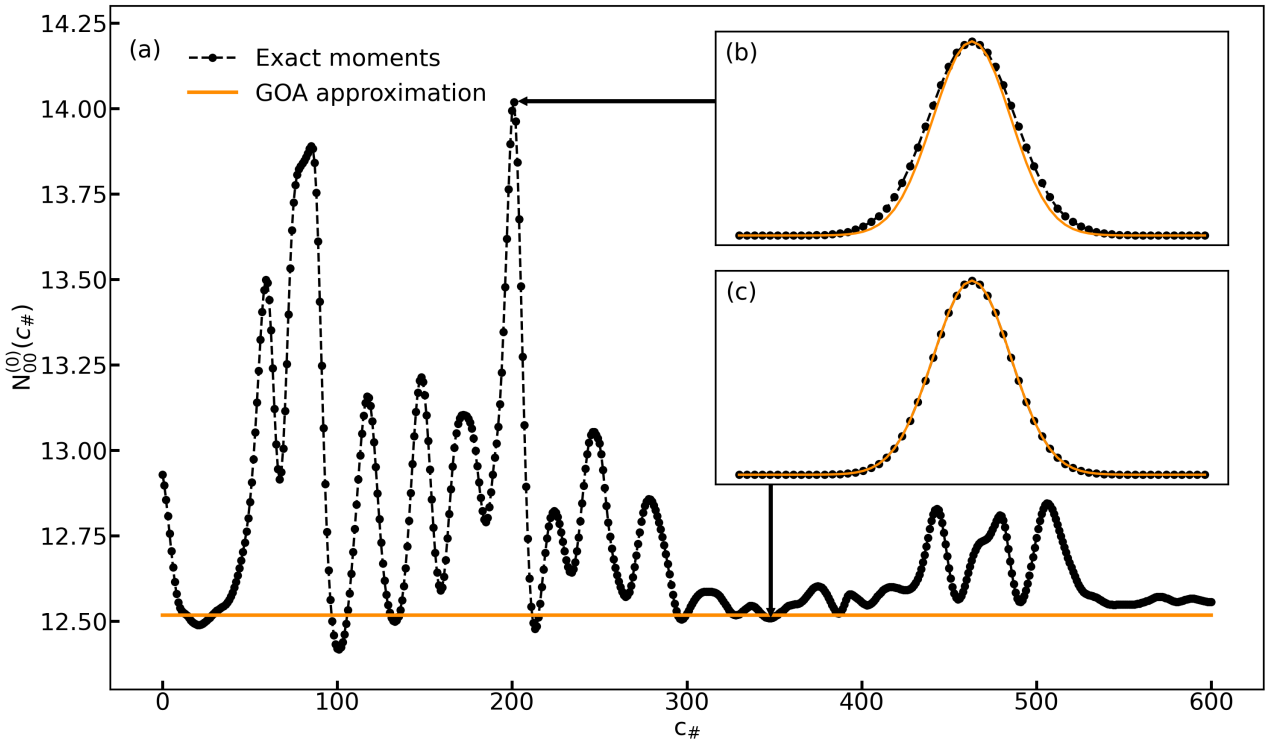

Figure 2.25: Illustration of the exact moment $N_{00}^{(0)}$, compared with the GOA approximation with two zooms of the kernels in relevant areas in the ^{240}Pu, with respect to $c_\#$. Panel (a): exact and GOA moment $N_{00}^{(0)}$ with respect to $c_\#$. Panel (b): exact kernels $\langle\Phi(\bar{q}-s)|\Phi(\bar{q}+s)\rangle$ for $\bar{q} = 201$, compared with the GOA kernels. Panel (c): exact kernels $\langle\Phi(\bar{q}-s)|\Phi(\bar{q}+s)\rangle$ for $\bar{q} = 330$, compared with the GOA kernels.

We see that in these conditions the GOA is overall a rather good approximation. Indeed, looking at the differences in the curves displayed in panel (b) and panel (c), we see how

close the kernels are from the GOA approximation, even in the worst case. In addition, it seems that the GOA tends to systematically underestimate the kernels.
Concerning the intrinsic regularity measured by the black curve, we observe first that the amplitude of the peaks seems reasonable. However, the oscillation frequency of the curve is worrying. It's not possible to say more at the moment. This topic will be discussed in great details in Chapter 5, which is dedicated to the dynamics.

Finally, in Figure (2.26), we have plotted the moments $N_{00}^{(0)}$ for both the adiabatic and projected adiabatic states. We observe that even if the grey curve is a little less regular than the black curve overall, the GOA still seems to be a reasonable approximation:

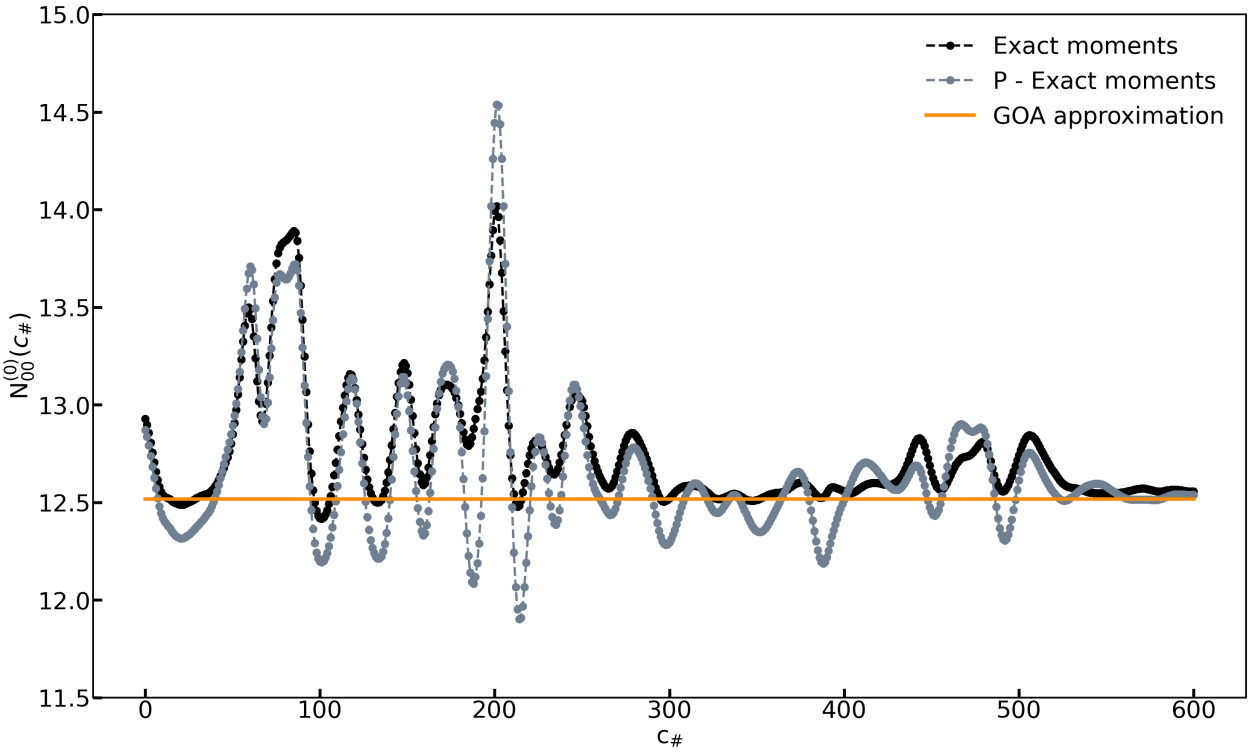

Figure 2.26: Illustration of the exact moment $N_{00}^{(0)}$ of the $\tilde{\mathcal{P}}_{20}$ adiabatic set along with the moment $N_{00}^{(0)}$ of the associated PAV set, compared with the GOA approximation in the ^{240}Pu with respect to $c_\#$.

Chapter 3

SCIM static states: new overlap constraints

In our first attempt to use the SCIM, we considered an adiabatic set of HFB states obtained through the $\mathcal{P}_{20}^{(l)}$ procedure defined in section 2.4.1. Linear corrections for the discontinuities were made so that the overlap between adjacent states was greater than 0.95. This first set stopped before the intersection between the fission and the fusion valley and the excited states considered were 2-quasiparticle excited states built on top of the adiabatic HFB states. Besides, all the kernels were evaluated projecting the states onto their good particle number subspaces.
We first tried to perform the dynamics on the adiabatic set only. We encountered great difficulties due to regularity problems discussed previously, which we were only able to solve by means of very strong approximations on the kernels. Indeed, we focused on the simplest case neglecting all the derivatives in the SCIM formalism. Doing so, we ended up with the following approximated collective potential and inertia tensor $V_{00}^{(ap)}$ and $B_{00}^{(ap)}$:

$$V_{00}^{(ap)}(\bar{q}) = \frac{H_{00}^{(0)}(\bar{q})}{N_{00}^{(0)}(\bar{q})} \qquad \text{and} \qquad B_{00}^{(ap)}(\bar{q}) = \frac{1}{2}\frac{H_{00}^{(2)}(\bar{q})}{N_{00}^{(0)}(\bar{q})} - \frac{1}{2}\frac{N_{00}^{(2)}(\bar{q})H_{00}^{(0)}(\bar{q})}{N_{00}^{(0)2}(\bar{q})} \tag{3.1}$$

We observed that $V_{00}^{(ap)}$ was very close to the GOA potential defined in Chapter 1, but $B_{00}^{(ap)}$ was much smaller than the GOA intertia tensor defined in Chapter 1. We attributed the good agreement between $V_{00}^{(ap)}$ and the GOA potential to the fact that the irregularities were smoothed out in the ratios of Eq.(3.1). Concerning the approximated intertia tensor, the result we found is easily explained by the approximation we discussed in Eq.(2.104). Indeed, under this approximation the second equation in Eq.(3.1) reads:

$$\frac{1}{2}\frac{H_{00}^{(2)}(\bar{q})}{N_{00}^{(0)}(\bar{q})} - \frac{1}{2}\frac{N_{00}^{(2)}(\bar{q})H_{00}^{(0)}(\bar{q})}{N_{00}^{(0)2}(\bar{q})} = \frac{E(\bar{q})}{2}\left(\frac{N_{00}^{(2)}(\bar{q})}{N_{00}^{(0)}(\bar{q})} - \frac{N_{00}^{(2)}(\bar{q})N_{00}^{(0)}(\bar{q})}{N_{00}^{(0)2}(\bar{q})}\right) = 0 \tag{3.2}$$

We deduced that the physics contained in the true inertia tensor B_{00} must come from the previously neglected derivatives. Note that it's probably the reason why the inertia tensor is such an unstable quantity in practice in the GOA formalism. Thus, we naturally decided to include higher order derivatives. However, we didn't want them to spoil the approximated $V_{00}^{(ap)}$ and $B_{00}^{(ap)}$ defined in Eq.(3.1). It may seem strange that we desired to preserve both $B_{00}^{(ap)}$ and $V_{00}^{(ap)}$, but we considered that the fact that B_{00} vanishes at the zero-order in derivatives (letting room for higher orders to express their physics) was as important as the fact that V_{00}

is already well approximated at the zero-order in derivatives. Therefore, we fitted $N_{00}^{(0)}$ with a second-degree polynomial and called the resulting quantity $f(N_{00}^{(0)})$. Then, we approximated the other moments implied in the adiabatic SCIM in order to preserve $V_{00}^{(ap)}$ and $B_{00}^{(ap)}$:

$$\begin{cases} f(H_{00}^{(0)})(\bar{q}) = \frac{H_{00}^{(0)}(\bar{q})}{N_{00}^{(0)}(\bar{q})} f(N_{00}^{(0)})(\bar{q}) \\ \\ f(H_{00}^{(2)})(\bar{q}) = \frac{H_{00}^{(2)}(\bar{q})}{N_{00}^{(0)}(\bar{q})} f(N_{00}^{(0)})(\bar{q}) \\ \\ f(N_{00}^{(2)})(\bar{q}) = \frac{N_{00}^{(2)}(\bar{q})}{N_{00}^{(0)}(\bar{q})} f(N_{00}^{(0)})(\bar{q}) \end{cases} \tag{3.3}$$

With the approximated quantities defined in Eq.(3.3), we found both potential and inertia tensor in line with the ones of the GOA and were able to run an adiabatic SCIM dynamics. Unfortunately, when we tried to extend this method to the excited states, we faced a wall. Indeed, the excited counterparts of $V_{00}^{(ap)}$ and $B_{00}^{(ap)}$ called $V_{ii}^{(ap)}$ and $B_{ii}^{(ap)}$ no longer had any good properties. The $V_{ii}^{(ap)}$ were oscillating at a high frequency with peaks more than 300 MeV away from the excited PES. Moreover, when we applied to the excited moments the approximations given in Eq.(3.3) in order to determine the final excited potential and excited inertia tensor, we ended up with an intertia tensor whose sign changed with respect to $\bar{q}$. This feature leading directly to very non-physical locally infinite masses. In addition to that, we didn't have any idea to handle the mixed moments of the type $N_{ij}^{(p)}$ and $H_{ij}^{(p)}$ that were also behaving very irregularly. Of course, the closer we were to a level repulsion area, the worse the problems.

In our search for solutions to improve the regularity of the excited states, we finally came across the work of Y. Beaujeault-Taudière and D. Lacroix [58]. In this work, they use a method from quantum chemistry called the "Deflation" [59] to create variational excited states they use for quantum computing purposes.
At first, the idea of variational excited states seemed a good one, as we thought it might improve the regularity in the level repulsion areas. Then, while implementing the "Deflation" within the HFB formalism, we realized that the overlap constraints at the heart of the method had a far greater potential than that. Indeed, by imposing an overlap constraint of zero with respect to a given state $|\Phi_\beta\rangle$ during an HFB convergence, we find a state orthogonal to $|\Phi_\beta\rangle$, which can often be interpreted as one of its excited states, but it is also possible to impose any overlap value between zero and one. That being said, it is possible to envisage plenty of new methods to deal with both the continuity and the regularity issues. In this PhD thesis work, we've created three new methods called the "Link", the "Drop" and the "Continuous Deflation". The first two are designed to precisely control the continuity and regularity of the adiabatic sets and the third one is devoted to the same goal but for variational excited states [60].

The way overlap constraints are included in the HFB formalism is rather simple. We add projectors onto the reference states associated with new Lagrange multipliers in the constrained Hamiltonian defined in Eq.(2.56) (section 2.1.4):

$$\boxed{\hat{H}_c = \hat{H} + \sum_\alpha \lambda_\alpha \hat{Q}_\alpha + \sum_\beta \gamma_\beta |\Phi_\beta\rangle\langle\Phi_\beta|} \tag{3.4}$$

Looking at Eq.(3.4), it is straightforward that the gradient method is perfectly suited to tackle these new constraints. Indeed, thanks to the Thouless theorem and in the case of time-reversal invariance, the gradient of those constraints simply reads as follows:

$$\boxed{\frac{\partial}{\partial Z_{kk'}}\gamma_\beta|\langle\Phi(Z)|\Phi_\beta\rangle|^2_{Z=0} = 2\sum_\beta \gamma_\beta\langle\Phi_\beta|\xi_i^+\bar{\xi}_j^+|\Phi\rangle\langle\Phi_\beta|\Phi\rangle} \tag{3.5}$$

The way to handle the quantities $\langle\Phi_\beta|\xi_i^+\bar{\xi}_j^+|\Phi\rangle$ that appear in Eq.(3.5) is explained in Chapter 5. Using Eq.(3.5), the overlap constraints are then treated as the other customary constraints.

In the following, we detail the new methods based on the overlap constraints developed during this PhD thesis.

3.1 The Link method

The "Link" method aims to connect two different HFB states $|A\rangle$ and $|B\rangle$ through a set of HFB states $\{|C_i\rangle\}$, such that the overlap between two adjacent states always equals a fixed value x_0 (with the exception of the overlap between $|B\rangle$ and the last state $|C_M\rangle$ for which we require to be greater than x_0). In Figure (3.1), we displayed a schematic view of the "Link" method:

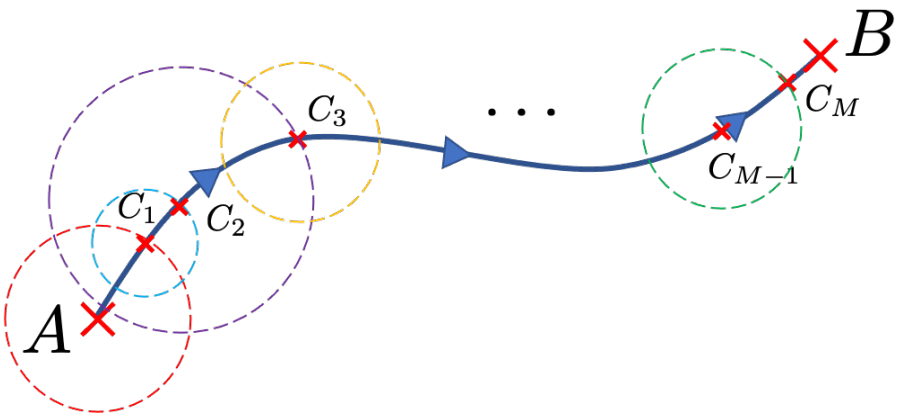

Figure 3.1: Schematic view of the Link method.

In practice, the "Link" method works as follows:

- We choose the value of the parameter x_0.
- We search for the state $|C_1\rangle$, such that its overlap with $|A\rangle$ is x_0, its overlap with $|B\rangle$ is maximum, and which minimizes the HFB energy.
- We iterate the previous process. At each iteration i, we search for the state $|C_i\rangle$, such that its overlap with $|C_{i-1}\rangle$ is x_0, its overlap with $|B\rangle$ is maximum, and which minimizes the HFB energy.
- We stop the iterative process as soon as we find a state $|C_M\rangle$ whose overlap with $|B\rangle$ is greater than x_0.

In the whole "Link" method described above, there is no other constraints than those on the overlaps, with the exception of the constraint on the average value of $\hat{Q}^{(10)}$ that avoids translations of the system, and the customary particle number constraints. Besides, it is way easier to impose an exact value for a constraint than to maximize it. Because of that, the requirements for maximizing the overlap with the state $|B\rangle$ are treated by dichotomy.
This method enables to cross continuously discontinuities. It is also very efficient to build a regular PES in terms of overlap. Indeed, using the "Link" method, we naturally switch from the customary collective coordinates associated with the multipole moments to the new collective coordinate $c_{\#}$ defined in section 2.4.
The "Link" method guarantees the perfect continuity of the path from the state $|A\rangle$ to the state $|B\rangle$. As the HFB energy is minimized at each step, we moreover assume that the paths created with the "Link" shouldn't be too far from the true adiabatic paths. It would be interesting to consider the latter statement in the light of an interpretation of the "Link" as the minimization of an action. However, we didn't have the time to do so during this PhD thesis work. Consequently, we evaluated the adiabaticity of the paths obtained by the "Link" method pragmatically by testing it.

3.1.1 Study in the ^{16}O

In Figure (3.2), we've displayed the results of calculations performed with the "Link" method in the ^{16}O. These calculations serve several purposes. Firstly, we can evaluate how close the paths obtained by the "Link" method are to the adiabatic one in a case where the latter is known. Then, we can study the impact of the parameter x_0. Finally, we investigate how paths built from $|A\rangle$ to $|B\rangle$ differ from the ones built from $|B\rangle$ to $|A\rangle$. In panel (a), we've represented different PES obtained with the "Link" for different values of x_0 along with the adiabatic PES of the ^{16}O with respect to the quadrupole deformation. The notation "$\rightarrow$" means that the paths are created starting from the adiabatic state associated with $Q_{20} = -8$ fm^2 with the adiabatic goal state labeled by $Q_{20} = 8$ fm^2. The notation "$\leftarrow$" stands for the inverse procedure. In panel (b), we've plotted the energy difference between the PES associated with the "Link" method and the adiabatic one (interpolated when necessary):

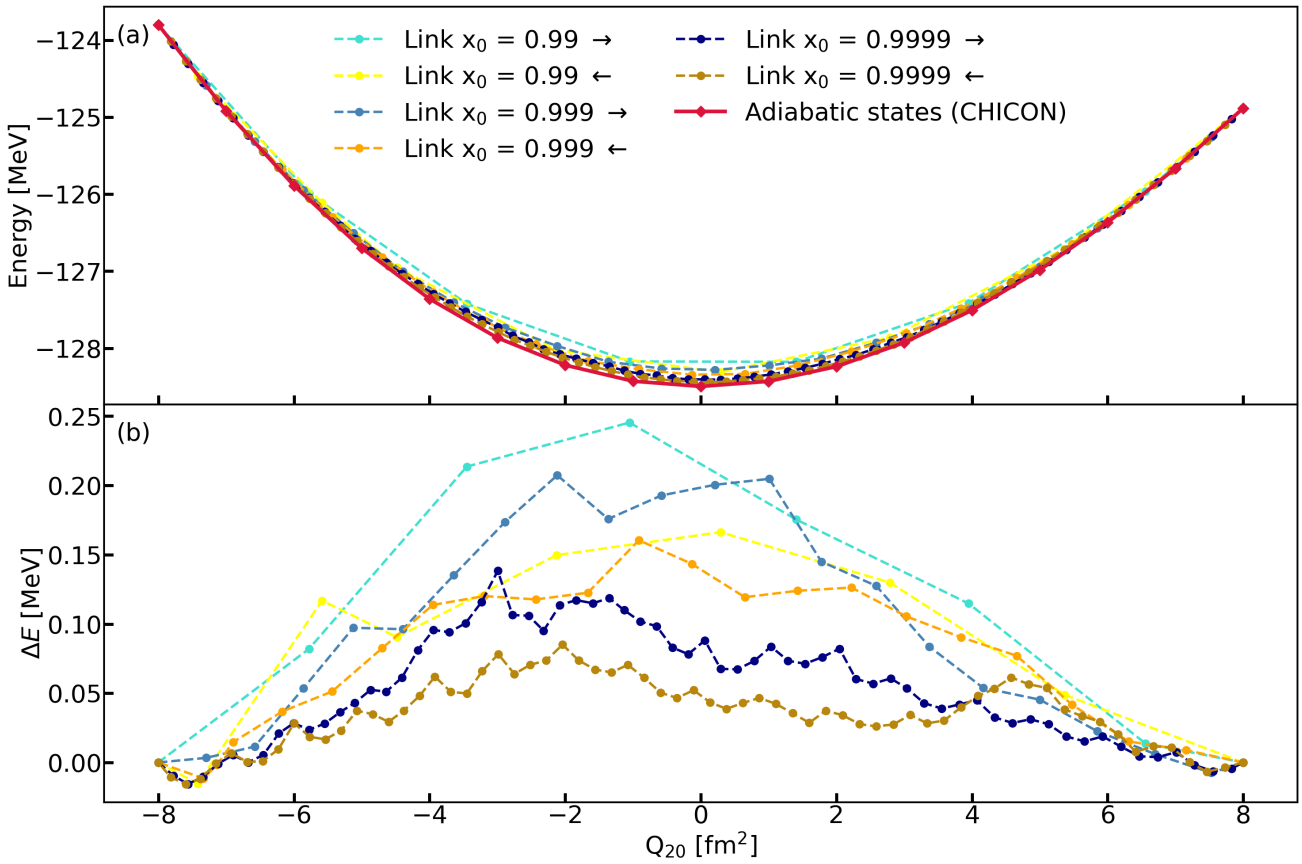

Figure 3.2: Illustration of the "Link" method in the ^{16}O. Panel (a): PES associated with paths obtained with the "Link" method using different parameters x_0 and different directions compared with the adiabatic PES with respect to the quadrupole deformation. Panel (b): energy differences between the different "Link" PES and the adiabatic PES with respect to the quadrupole deformation.

The most striking feature observed in Figure (3.2) is the fact that the closer x_0 is to one, the closer the "Link" PES are to the adiabatic one. With $x_0 = 0.9999$, the maximum energy difference between the "Link" PES and the adiabatic one is found to be 130 keV with respect to the direction $\rightarrow$ and 75 keV with respect to the direction $\leftarrow$. We believe that this level of precision is really satisfactory, as it represents less than 1 ‰ of the total binding energy of the nucleus.
When x_0 is closer to one, the "Link" method can explore more complex trajectories in the deformed ^{16}O HFB Hilbert space. We assume it is the reason why it minimizes better the energy overall. Concerning the directions, it would be tempting to state that the $\leftarrow$ direction leads to better results as the starting state has a lower energy. In practice, we found some counter-examples. Therefore, we think that the differences between the directions account for subtle topological properties of the deformed ^{16}O HFB Hilbert space, which are beyond the scope of this study.

Another interesting evidence that the "Link" method provides us with reliable states lies in the distance between the states created. As already discussed in section 2.4, the GOA is a rather good approximation to estimate the distance between states. More precisely, we assume that we know the overlap between the two states $|A\rangle$ and $|B\rangle$. If we consider a state $|C_i\rangle$ between $|A\rangle$ and $|B\rangle$, such as $\langle C_i|A\rangle = y$, the value of the overlap $\langle C_i|B\rangle$ is given by the GOA approximation:

$$\langle C_i|B\rangle = e^{\ln(\langle A|B\rangle)(1-\sqrt{\frac{\ln(\langle C_i|A\rangle)}{\ln(\langle A|B\rangle)}})^2} \tag{3.6}$$

In Figure (3.3), we've plotted the states obtained with the "Link" method with $x_0 = 0.99$ in the direction $\rightarrow$, the states obtained with the "Link" method with $x_0 = 0.9999$ in the direction $\leftarrow$, and the adiabatic states with respect to their overlap with the state $|B\rangle$ (adiabatic state labeled by $Q_{20} = 8$ fm^2) along the x-axis , and their overlap with the state $|A\rangle$ (adiabatic state labeled by $Q_{20} = -8$ fm^2) along the y-axis. Moreover, we represented with the black curve the results given by the GOA approximation:

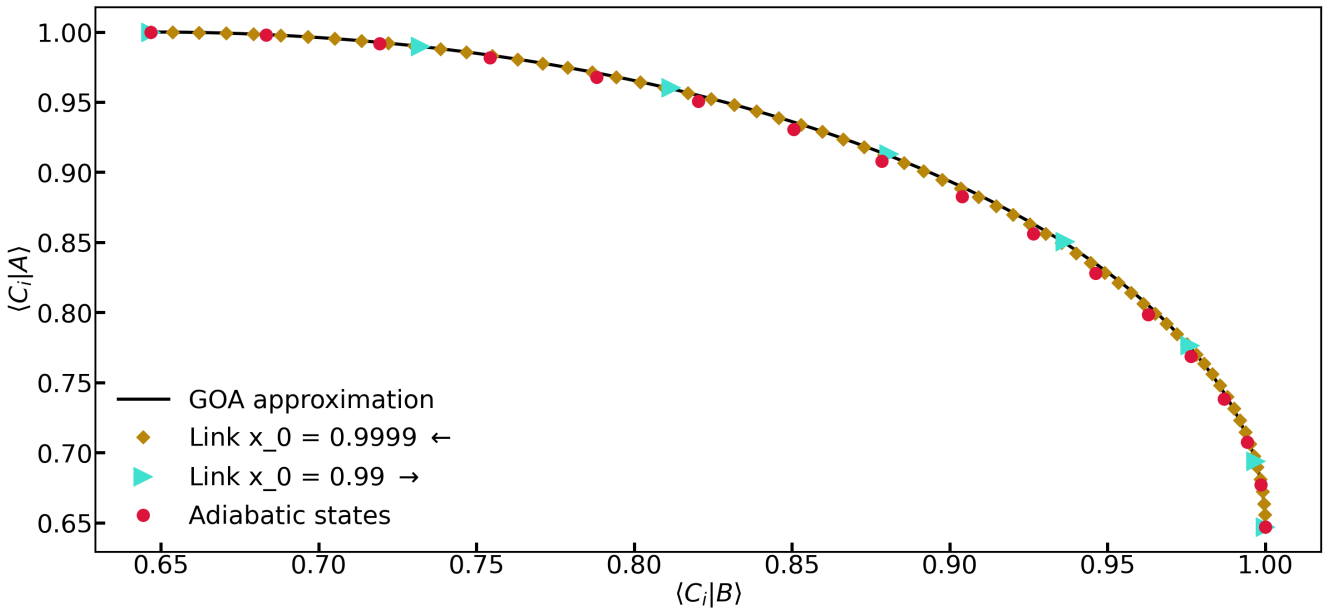

Figure 3.3: Comparison of the distance between the states obtained with the "Link" method, the adiabatic states, and the GOA approximation in the ^{16}O.

We observe that the states created with the "Link" method match very well with the GOA approximation. It reinforces the credibility of the states obtained with the "Link" method insofar as their mutual spacing approaches that found in customary adiabatic paths. Besides, it means that the requirement within the "Link" method, which imposes to maximize the overlap with the goal state at each step is relevant, and fits rather well the natural behaviour of the adiabatic states.
It is interesting to remark that the adiabatic states are slightly less close to the GOA approximation than the states obtained with the "Link". This provides an avenue of improvement for the "Link", which somehow "overfits" the GOA. Indeed, we could consider at each step of the "Link" a set of states whose overlap with $|B\rangle$ is close to the maximum and choose to keep only the state that minimizes the energy (or a ratio between the distance lost and the energy won).

3.1.2 Study in the ^{240}Pu

We now study the "Link" behavior in a case including a discontinuity. More precisely, we considered the discontinituity signed by the multipole moment Q_{40} which is found on the first barrier of the ^{240}Pu. This is the realistic case we treated in this PhD thesis to obtain

the $\tilde{\mathcal{P}}_{20}$ PES used for the dynamics. In Figure (3.4), we've represented in panel (a) the PES obtained with the "Link" method using different parameters x_0 and with respect to the direction $\rightarrow$, along with the PES associated with the adiabatic states obtained with CHICON (we separated this PES in two parts with respect to the discontinuity) with respect to the quadrupole deformation. In panel (b), we've displayed the related hexadecapole moments Q_{40} with respect to the quadrupole deformation:

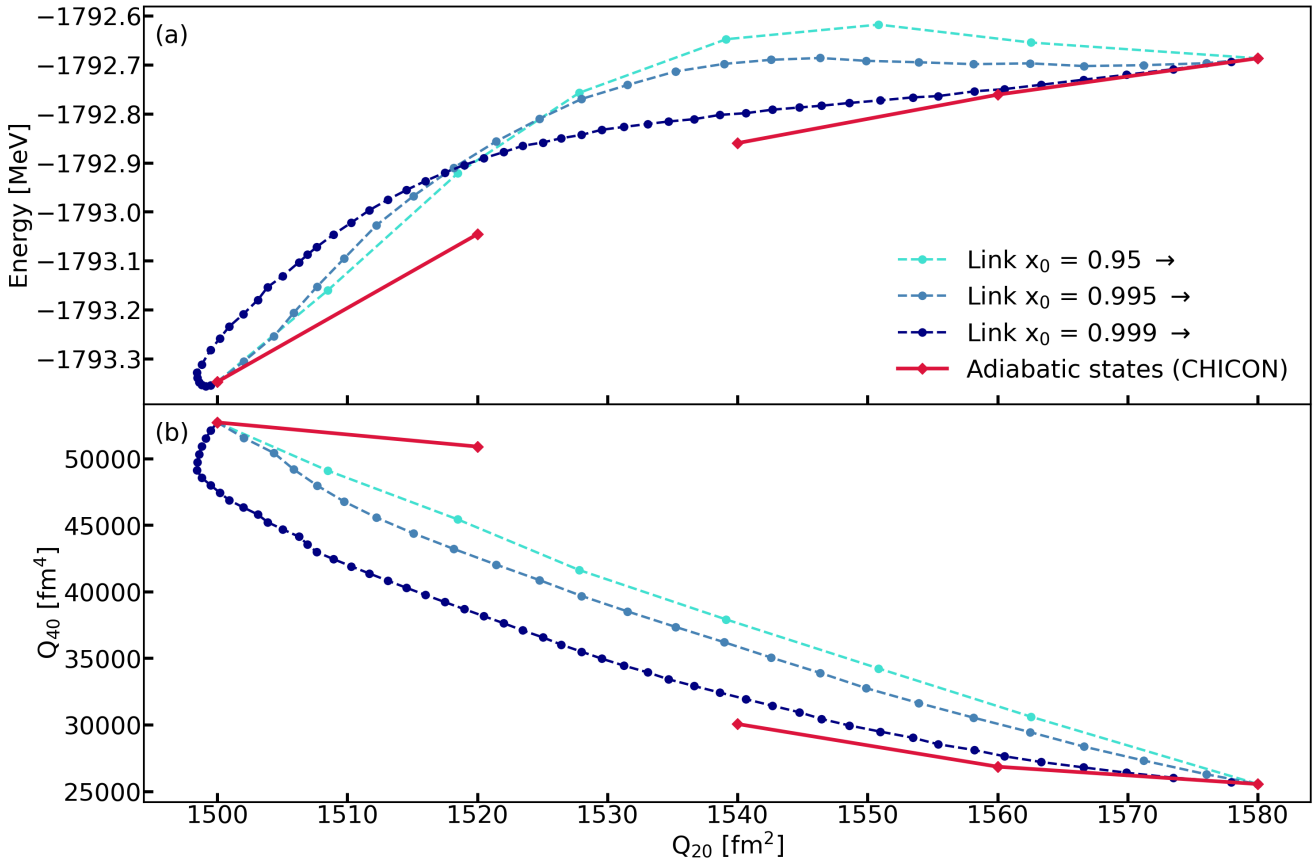

Figure 3.4: Illustration of the "Link" method at the Q_{40} discontinuity in the first barrier of the ^{240}Pu. Panel (a): PES associated with paths obtained with the "Link" method using different parameters x_0 compared with the adiabatic PES, with respect to the quadrupole deformation. Panel (b): hexadecapole deformation with respect to the quadrupole deformation.

First, we see in Figure (3.4) that the smoothing of the discontinuity doesn't make any hidden barrier appear. The energy difference between the existing adiabatic PES and the "Link" PES is never greater than 250 keV at a same Q_{20}. Besides, we observe that the path assosciated with $x_0 = 0.999$ follows a slightly different trajectory in both energy and Q_{40} compared to the other ones made with $x_0 = 0.995$ and $x_0 = 0.95$. In addition, the fact that the dark blue curve first goes backward with respect to Q_{20} indicates that it probably would have been beneficial to start the "Link" from a state associated with a lower Q_{20}.
It seems strange to observe in panel (a) that the dark blue PES not only displays a rather original behavior but is also above the other ones nearby $Q_{40} = 1500$ fm^4, while it is associated with a x_0 parameter closer to one. It looks like the dark blue "Link" misused the greater freedom it had to choose its trajectory. In reality, it is only a false impression due to the Q_{20} representation. In Figure (3.5) panel (a), we represented the same PES as in Figure (3.4), but with respect to the overlap with the state $|B\rangle$ (which is the adiabatic goal state of

the "Link" paths) instead of the quadrupole deformation. In panel (b), we represented the hexadecapole moment Q_{40}, also with respect to the overlap with the state $|B\rangle$:

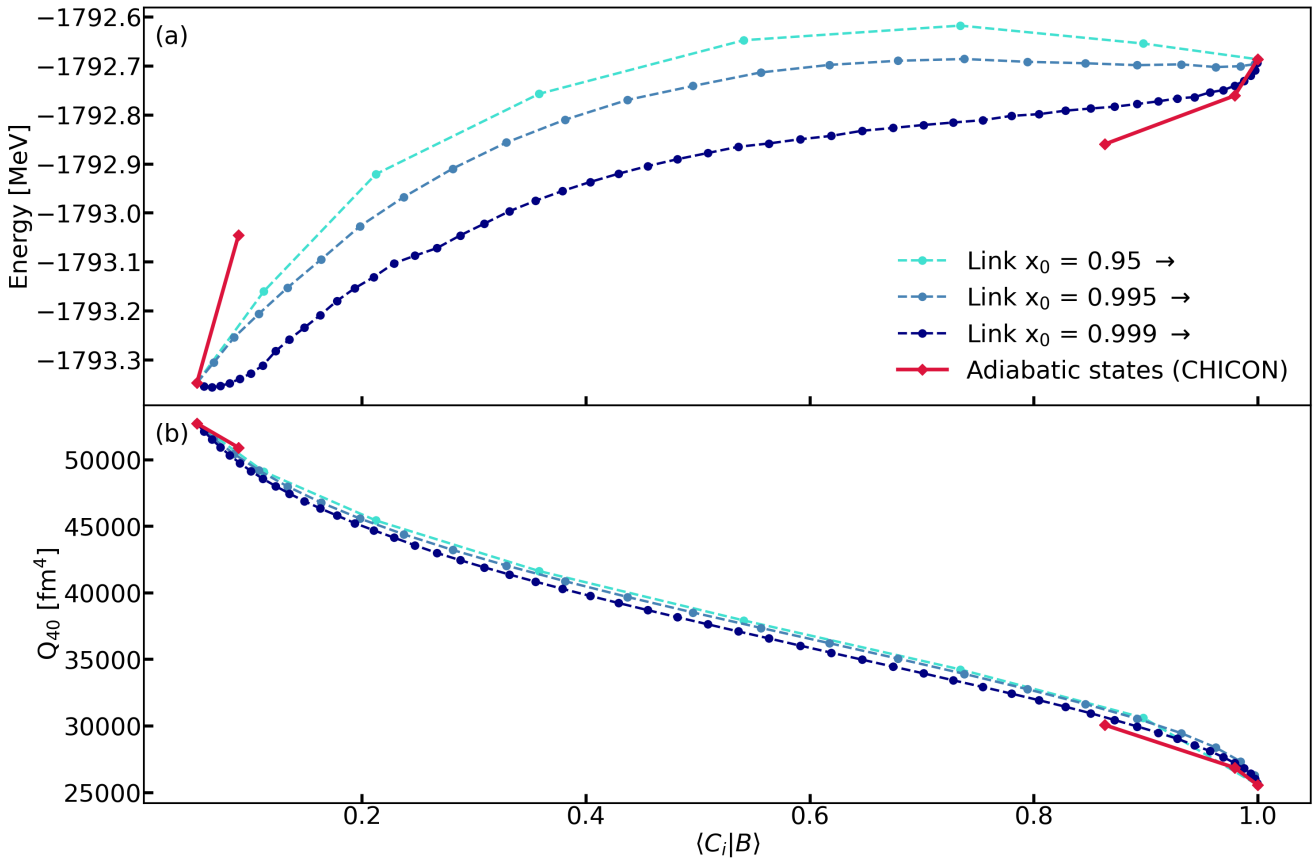

Figure 3.5: Illustration of the "Link" method at the Q_{40} discontinuity in the first barrier of the ^{240}Pu. Panel (a): PES associated with paths obtained with the "Link" method using different parameters x_0 compared with the adiabatic PES with respect to the overlap with $|B\rangle$. Panel (b): hexadecapole deformation with respect to the overlap with $|B\rangle$.

The choice of the overlap representation used in Figure (3.5) is very natural as it is the one related to the new collective coordinate $c_{\#}$, which is the relevant one within the dynamics. In this representation, we clearly see that the closer x_0 is to one, the lower the PES. In addition, the evolution of Q_{40} is way smoother.
To conclude, we investigated whether the good agreement between the "Link" and the GOA approximation observed in the ^{16}O were still valid in the case of the ^{240}Pu first barrier, which include a discontinuity. In Figure (3.6), we've plotted the states obtained with the "Link" method with $x_0 = 0.999$, with $x_0 = 0.95$, and the adiabatic states with respect to both their overlap with the state $|B\rangle$ (adiabatic state labeled by $Q_{20} = 1580$ fm^2) along the x-axis, and their overlap with the state $|A\rangle$ (adiabatic state labeled by $Q_{20} = 1500$ fm^2) along the y-axis. In addition, we represented by the black curve the results given by the GOA approximation:

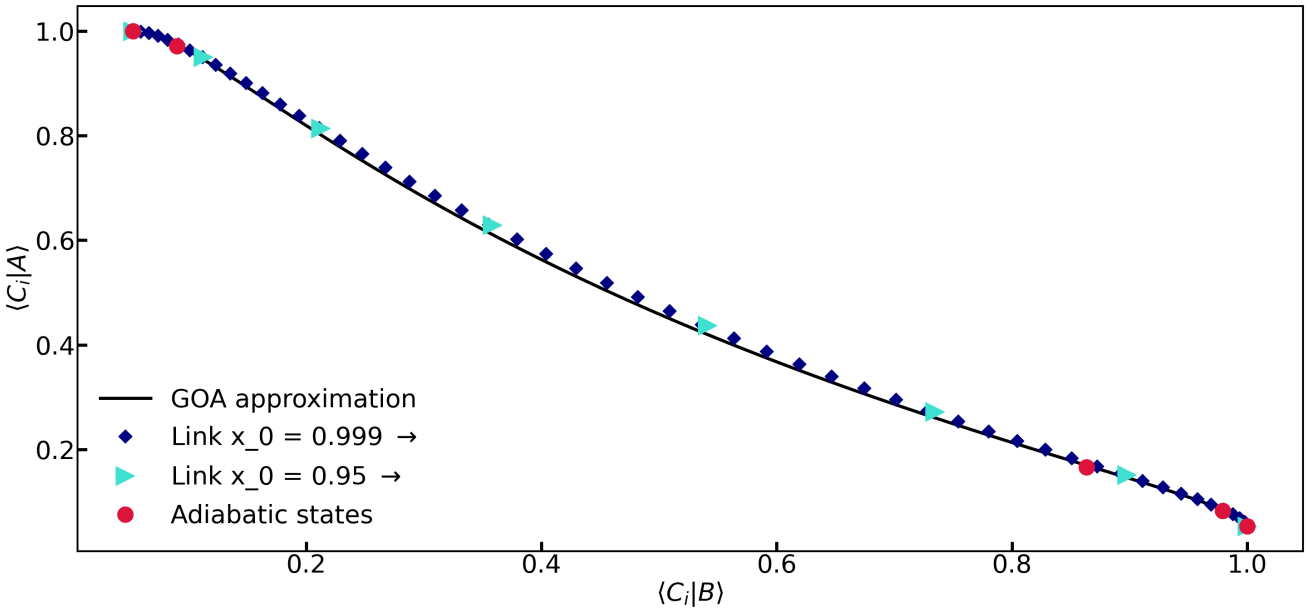

Figure 3.6: Comparison of the distance between the states obtained with the "Link" method, the adiabatic states, and the GOA approximation in the ^{240}Pu.

Looking at Figure (3.6), it is clear that the good agreement of the "Link" with respect to the GOA approximation still holds when a discontinuity is crossed. These results support the assumption that the paths obtained via the "Link" method are close to the adiabatic ones, even in the case of discontinuity smoothing.

3.1.3 The "Link" method within the $\tilde{\mathcal{P}}_{20}$ procedure

We conclude this section by explaining how the "Link" method takes place into the $\tilde{\mathcal{P}}_{20}$ procedure. The first step in the $\tilde{\mathcal{P}}_{20}$ procedure is to obtain an adiabatic set via the $\mathcal{P}_{20}$ procedure (using CHICON for instance). We truncate this first set, keeping only the states whose Q_{20} is lower than the Q_{20} of the saddle point plus 1000 fm^2. Doing so, we end up with a set of states $\{|\Phi_i\rangle\}$ ordered by increasing Q_{20}. Then, we consider the state $|\Phi_0\rangle$ and search for the first state $|\Phi_{i_0}\rangle$ such that $\langle\Phi_0|\Phi_{i_0}\rangle < 0.5$. We iterate the process searching for the first state $|\Phi_{i_1}\rangle$ (with $i_0 < i_1$) such that $\langle\Phi_{i_0}|\Phi_{i_1}\rangle < 0.5$. At the end of this process, we end up with a set $\{|\Phi_{i_j}\rangle\}$ which is called the set of the attractors.
Then, we perform a first "Link" starting from the state $|\Phi_0\rangle$ with the goal state $|\Phi_{i_0}\rangle$, and with a fixed parameter x_0 (we chose $x_0 = 0.995$ in this PhD thesis work). We stop the "Link" process when the overlap between the last state generated and $|\Phi_{i_0}\rangle$ is greater than 0.9. This operation provides us with a set of states $\{|L_0\rangle, ..., |L_{j_1}\rangle\}$, with $|\Phi_0\rangle = |L_0\rangle$. We iterate this process starting from the last state $|L_{j_{n-1}}\rangle$ obtained at iteration n, and using the attractor $|\Phi_{i_n}\rangle$ as the goal state. At the end of the whole process, we end up with a continuous set of states $\{|L_0\rangle, ..., |L_{j_1}\rangle, ..., |L_{j_f}\rangle\}$. This continuous set is the first part of the set associated with the $\tilde{\mathcal{P}}_{20}$ procedure. The way the second part is built is described just below in section 3.2, which is dedicated to the "Drop" method.
It took approximately a full day to perform the whole process described above in the case of the ^{240}Pu using 2x11 harmonic oscillator representations, with one processor.

3.2 The Drop method

Even if the "Link" method works well to connect two HFB vacua, the requirement for having both a starting and a target vacuum is no longer fulfilled when it comes to describe situations where final configurations are not known *a priori*, as in the scission process. The "Drop" method has been developed to partly tackle this issue. It creates an adiabatic and continuous set of states $\{|C_i\rangle\}$ from a starting state $|A\rangle$, only following an energy descent. The overlap between two adjacent states of the resulting set always equals a fixed parameter x_0. As this method is "goal-free", it enables us to describe efficiently processes such as the scission one. In Figure (3.7), we give a schematic view of the "Drop" method:

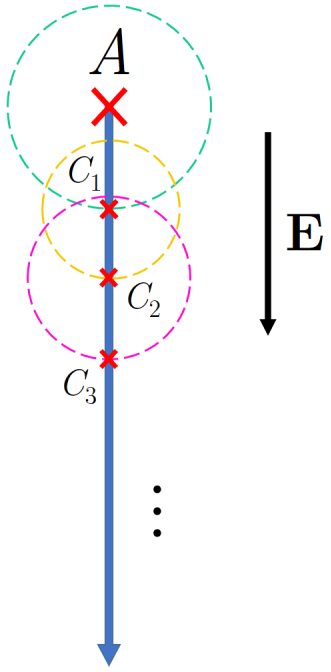

Figure 3.7: Schematic view of the Drop method.

In practice, the "Drop" method is very simple and can be described as follows:

- We define the overlap parameter x_0.
- We search for the state $|C_1\rangle$, such that its overlap with $|A\rangle$ is x_0, and which minimizes the HFB energy.
- We iterate the previous process. At each iteration i, we search for the state $|C_i\rangle$, such that its overlap with $|C_{i-1}\rangle$ is x_0, and which minimizes the HFB energy.
- The process stops after a given number of iterations or whenever the energy of a given point $|C_f\rangle$ is found to be greater than the one of the previous state $|C_{f-1}\rangle$.

As in the case of the "Link" method, the average value of $\hat{Q}^{(10)}$ and the average number of particles are constrained throughout the whole process. The other multipole moments can be left free, in which case we talk about a "free Drop", but they can also be constrained, in which case we talk about a "guided Drop".

3.2.1 The "free Drop"

As already stated, the "Drop" method works very well on the descent to scission. Indeed, the "Drop" not only allows to get closer to the scission (which other approaches using constrained multipole moments are already struggling to do) but provides us with a continuous description of the whole scission process including the relaxation of the fragments. This makes it possible to extract very interesting properties of the nucleus at scission, which were inaccessible before. In Figure (3.8), we've plotted the PES associated with the procedure $\tilde{\mathcal{P}}_{20}$ from the saddle point. In addition, local densities have been added to illustrate the different shapes taken by the nucleus on its way to scission, with respect to $c_{\#}$:

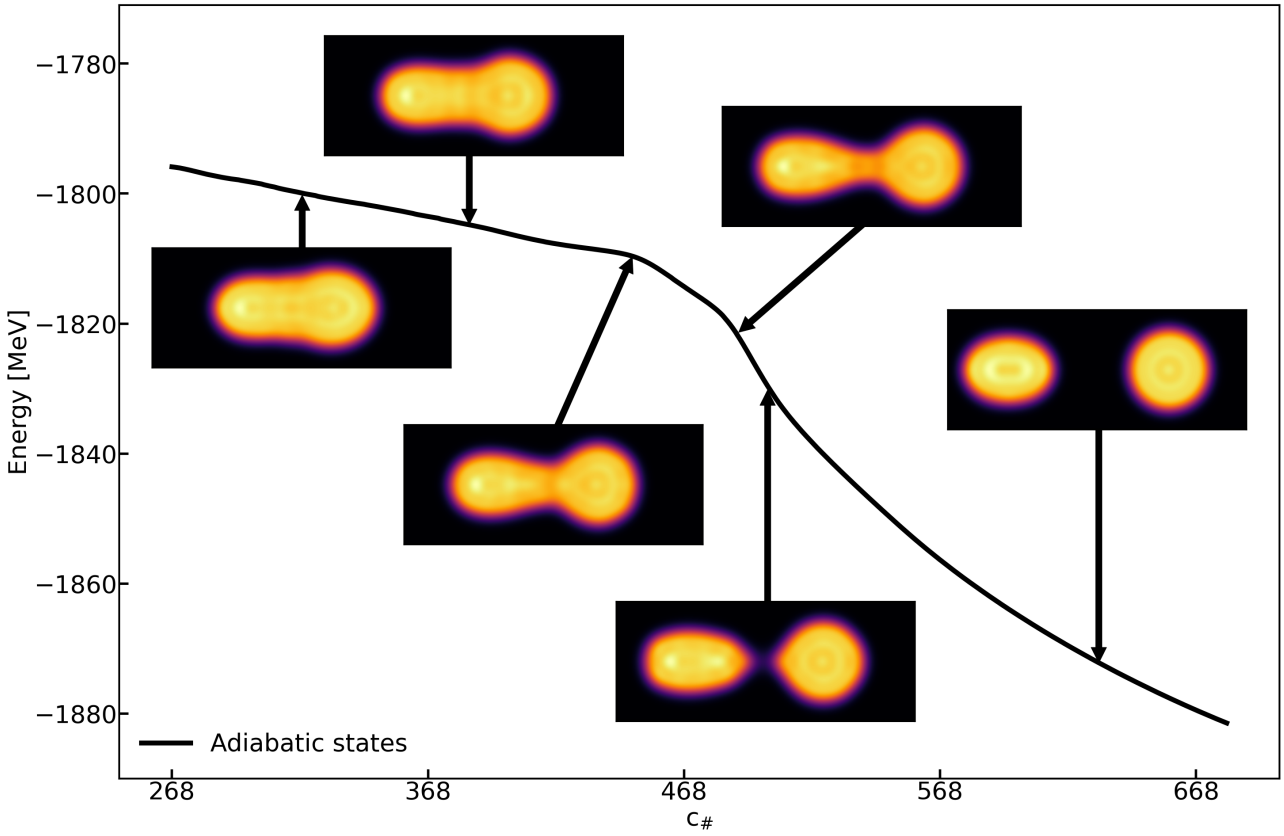

Figure 3.8: PES associated with the procedure $\tilde{\mathcal{P}}_{20}$ in the ^{240}Pu starting from the saddle point in addition to relevant local densities with respect to $c_{\#}$.

The prolate shapes observed close to the scission area are characteristic of the physics of the scission. Besides, we clearly see the fragments gradually relaxing into their ground states.
An important property of the "Drop" method is that the parameter x_0 doesn't change its trajectory. It is a big difference between the "Link" and the "Drop" methods. In figure (3.9), we've displayed the results of different drops from the saddle point of the ^{240}Pu for different x_0 values. The black curve is the PES obtained with the $\tilde{\mathcal{P}}_{20}$ procedure, which implies a drop from the saddle point with the parameter $x_0 = 0.995$. The red circles, the green triangles and the blue diamonds stand respectively for drops with the parameters $x_0 = 0.95$, $x_0 = 0.9$ and $x_0 = 0.8$, respectively:

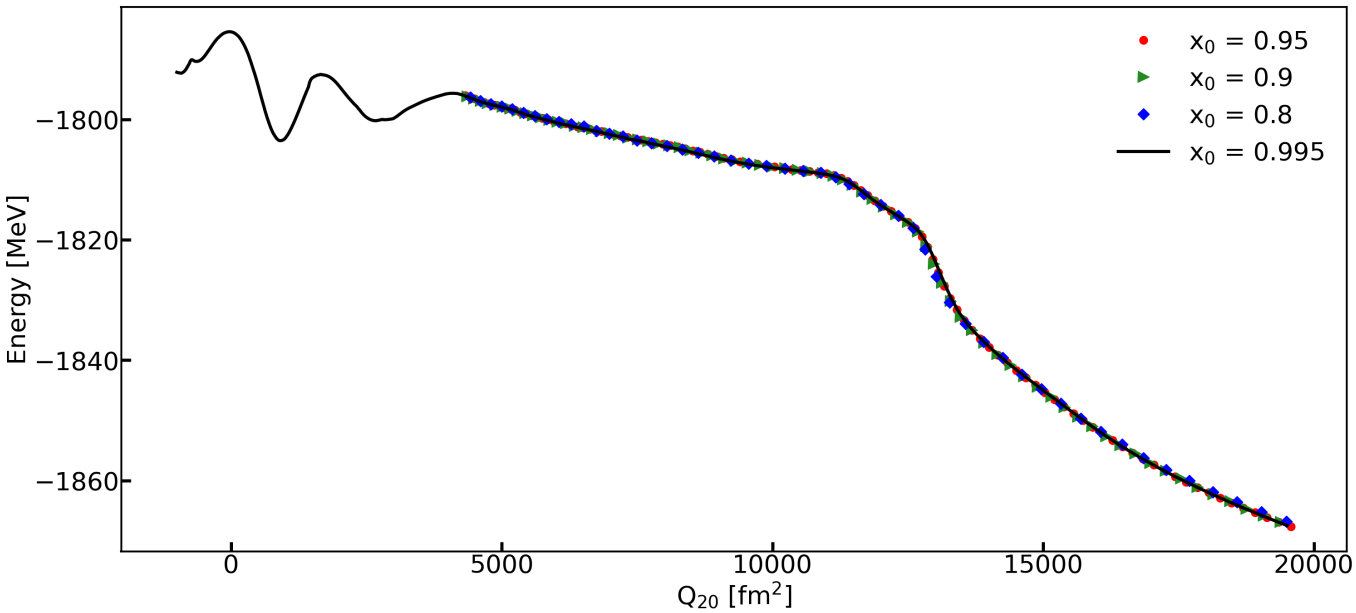

Figure 3.9: Illustration of the impact of the value of the parameter x_0 in the "Drop" method applied from the saddle point of the ^{240}Pu with respect to the quadrupole deformation.

This feature is very valuable, as it allows the "Drop" to be used in two different ways. First, it can be used in an exploratory way with a relatively small x_0. Doing so, it is possible to figure out the exact topology of a PES with just a few calculations. To give an idea, there are 51 blue diamonds, 74 green triangles and 107 red circles counting from the saddle point. In the case of the black curve, the same path is covered by 343 points. The second way of using the "Drop" is to make refined PES useful for both the precise extraction of static properties and to perform dynamics on them. The last-mentioned way of using the "Drop" is, of course, more time-consuming. With a proper basis optimization and 2x11 harmonic-oscillator representations, it took around 10 hours to create the set of states corresponding to the black curve starting from the saddle point.

3.2.2 The "guided Drop"

When we observe the "Drop" efficiency in generating a one-dimensional adiabatic path, we immediately wonder whether it could be extended to create multi-dimensional PES. The "guided Drop" has been designed to address this question.
In this PhD thesis work, we didn't have the time to use the "guided Drop" to build a full multi-dimensional PES. However, we have made an example of the "guided Drop" for a fixed given Q_{30} which stands as a proof of concept. More precisely, in Figure (3.10), we displayed the drop obtained starting from the state of the $\tilde{\mathcal{P}}_{20}$ PES labeled by $Q_{20} = 9870$ fm^2 and $Q_{30} = -38000$ fm^3 ($c_\# = 420$), along with the customary "free Drop". In panel (a), we have shown the resulting PES along with a relevant part of the $\tilde{\mathcal{P}}_{20}$ PES with respect to the quadrupole deformation. In panel (b), we've represented the associated Q_{30} with respect to the quadrupole deformation:

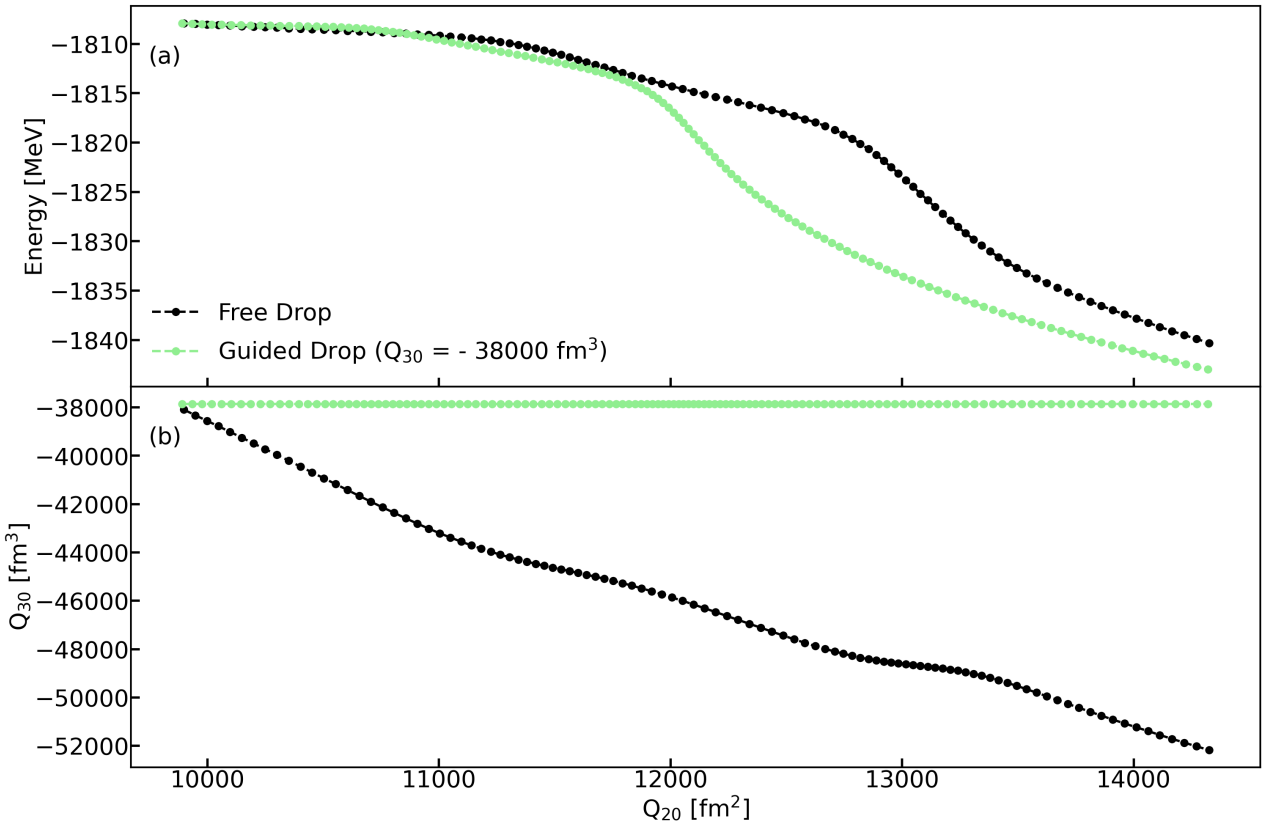

Figure 3.10: "Free Drop" and "guided Drop" with $Q_{30} = -38000$ fm^3 starting from the state $c_{\#} = 420$ of the $\tilde{\mathcal{P}}_{20}$ set. Panel (a): PES associated with the two drops with respect to the quadrupole deformation. Panel (b): octupole moments associated with the two drops with respect to the quadrupole deformation.

The "guided Drop" has been performed without encountering any particular difficulty. In the case of the green curve associated with the "guided Drop", we've found an average fragmentation (Z_l=43.2,Z_h=50.8) with respect to the charge and (A_l=107.7,A_h=132.3) with respect to the mass. Besides, we've found an average fragmentation (Z_l=42.4,Z_h=51.6) with respect to the charge and (A_l=106.1,A_h=133.9) with respect to the mass for the $\tilde{\mathcal{P}}_{20}$ PES. The fragmentations are all evaluated at the chemical potential peaks, (see section 4.1). To give a reference, the most probable fragmentation observed in the experiments at low-energy is characterized by $Z_l = 40$ and $N_l = 60$ [61].
The attentive reader will undoubtedly have noticed that the green PES is most of the time below the black PES in Figure (3.10). At first, it seems odd, as the black PES is supposed to be the 1D adiabatic path. In fact, this feature is once again a matter of representation. In Figure (3.11), we represented the same PES as in the Figure (3.10) panel (a), but with respect to their collective coordinate $c_{\#}$:

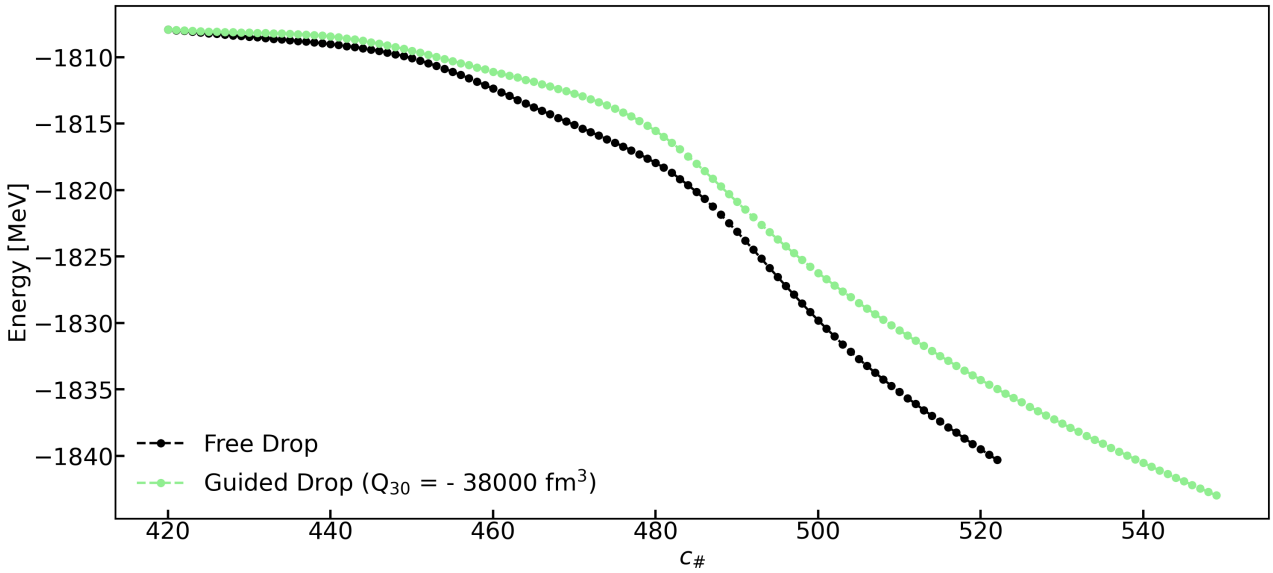

Figure 3.11: PES of the "free Drop" and the "guided Drop" with $Q_{30} = -38000$ fm^3 in the $c_\#$ representation.

The Figure (3.11) highlights the fact that the adiabatic path we consider is no more the continous path which is the lowest in energy with respect to Q_{20}, but the one which is the lowest in energy in terms of the collective coordinate $c_\#$ (which is the relevant one regarding the dynamics).

3.2.3 The "Drop" method with different interactions

We tried the "Drop" method with the D1S and D2 Gogny interactions including or not the exact treatment of the Coulomb exchange and pairing terms. In Figure (3.12), we displayed three different curves obtained from drops with different interactions in addition to the black PES related to the $\tilde{\mathcal{P}}_{20}$ procedure which is associated to the interaction D1S (Slater):

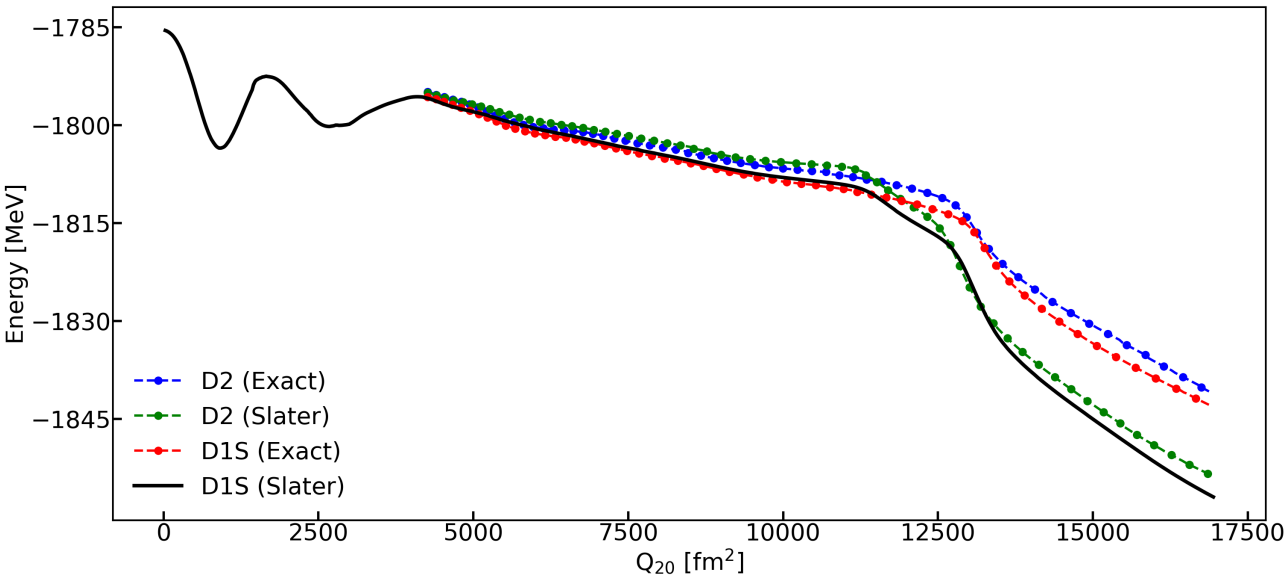

Figure 3.12: Comparison of the PES obtained using the "Drop" method with the D1S and D2 interactions considering both the exact and Slater treatments of the Coulomb exchange and pairing terms, with respect to the quadrupole deformation in the ^{240}Pu.

In Figure (3.12), we mainly observe that the PES are divided into two groups with respect to the treatment of the Coulomb term. Indeed, the red and blue curves are approximately 15 MeV above the black and green curves at $Q_{20} = 17000$ fm^2. To complement this observation, we represented in Figure (3.13) the multipole moments associated with the PES displayed in Figure (3.12). In panel (a), we've plotted the hexadecapole deformation with respect to the quadrupole deformation. In panel (b), we've displayed the octupole deformation with respect to the quadrupole deformation:

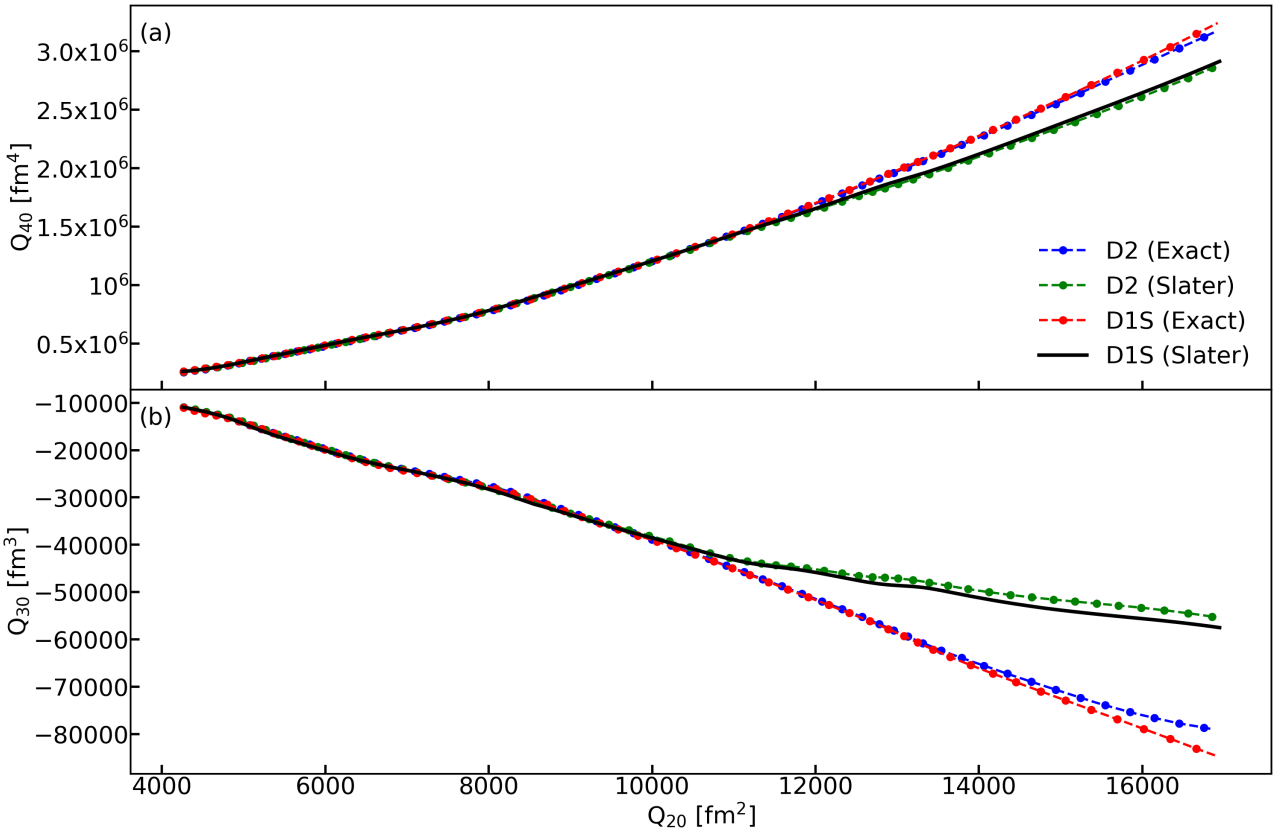

Figure 3.13: Comparison of the multipole moments of the sets obtained from drops with different interactions in the ^{240}Pu with respect to the quadrupole deformation. Panel (a): hexadecapole deformation with respect to the quadrupole deformation. Panel (b): octupole deformation with respect to the quadrupole deformation.

The results displayed in Figure (3.13) show that the treatment of the Coulomb term not only changes the energy of the adiabatic states but also their shape. The exact treatment tends to increase both Q_{30} and Q_{40} at high values of Q_{20} which correspond to the scission area. Regarding the differences between D1S and D2, we observe a global shift in energy in addition to a slight change in the shape of the PES nearby the scission area. More subtle differences are discussed in detail in the following (see Chapter 4).

3.2.4 The "Drop" method within the $\tilde{\mathcal{P}}_{20}$ procedure

We conclude this section by explaining how the "Drop" method takes place into the $\tilde{\mathcal{P}}_{20}$ procedure. We already discussed in the section concerning the "Link" method the first steps of the $\tilde{\mathcal{P}}_{20}$ procedure. After using the "Link" method on the adiabatic set obtained with the $\mathcal{P}_{20}$ procedure, we ended up with the continuous set $\{|L_0\rangle, ..., |L_{j_1}\rangle, ..., |L_{j_f}\rangle\}$. This set

has been built such as the state $|L_{j_f}\rangle$ is located after the saddle point (with respect to Q_{20}). Therefore, we simply perform a "free Drop" starting from the state $|L_{j_f}\rangle$ and imposing a x_0 value equals to the one used in the "Link" part of the $\tilde{\mathcal{P}}_{20}$ procedure. Doing so, we end up with the final set $\{|L_0\rangle, ..., |L_{j_1}\rangle, ..., |L_{j_f}\rangle, |D_1\rangle, ..., |D_f\rangle\}$ which is associated with the full $\tilde{\mathcal{P}}_{20}$ procedure.

3.3 The Deflation method

As previously discussed in the introduction of this section, the goal of the "Deflation" method is to create variational excited states imposing orthogonality conditions at the HFB level. Besides, the method can be iterated to explore the excitation spectrum of a nucleus. In Figure (3.14), we represented a schematic view of the iterated "Deflation" method:

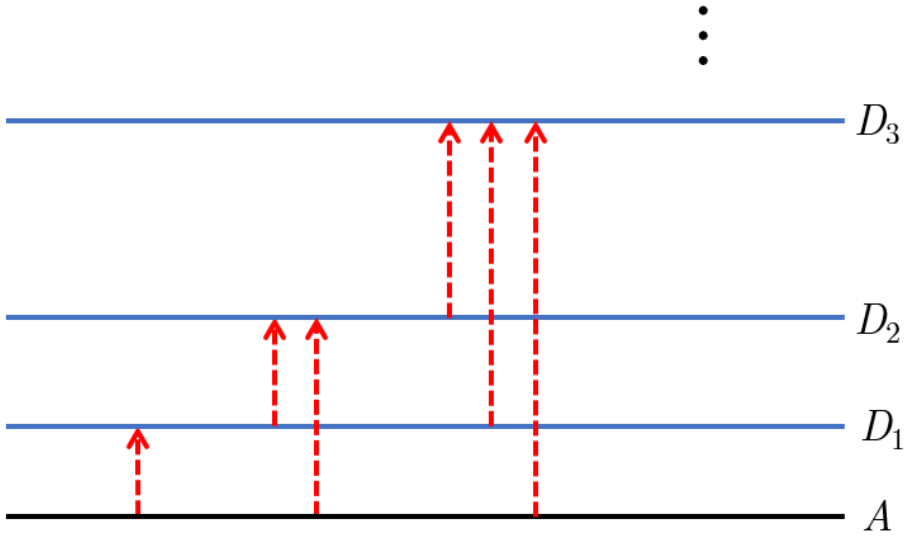

Figure 3.14: Schematic view of the iterated "Deflation" method.

In practice, orthogonality can be imposed in several ways. If we consider a reference HFB state $|\Phi_\beta\rangle$, the state $|\Phi\rangle$ can be forced to be orthogonal to the proton part of $|\Phi_\beta\rangle$:

$$\langle \Phi_\beta^{\tau_p} | \Phi^{\tau_p} \rangle = 0 \tag{3.7}$$

In this case, the neutron part rearranges itself freely. At the same time, we could also impose a fixed value d_n for the neutron overlap:

$$\begin{cases} \langle \Phi_\beta^{\tau_p} | \Phi^{\tau_p} \rangle = 0 \\ \langle \Phi_\beta^{\tau_n} | \Phi^{\tau_n} \rangle = d_n \end{cases} \tag{3.8}$$

As we preserve the quantum number Ω in our calculations, we can also impose overlap conditions with respect to a specific Ω. For instance, we could create an excited state imposing the following conditions to $|\Phi\rangle$:

$$\begin{cases} \langle \Phi_\beta^{\tau_p \Omega_{1/2}} | \Phi^{\tau_p \Omega_{1/2}} \rangle = 0 \\ \langle \Phi_\beta^{\tau_p \Omega_{5/2}} | \Phi^{\tau_p \Omega_{5/2}} \rangle = 0.5 \\ \langle \Phi_\beta^{\tau_n \Omega_{3/2}} | \Phi^{\tau_n \Omega_{3/2}} \rangle = 1 \end{cases} \tag{3.9}$$

Of course, it would also be possible to add some constraints on multipole moments on top of it. In short, the "Deflation" method is very versatile. As an illustration, in the "Continuous Deflation" method we discuss in section 3.4, we've used this versatility to our advantage in order to follow variational excitations all along a deformation path.
That being said, the general principle of the iterated "Deflation" method can be described as follows:

- We define the way we want to impose orthogonality as well as any other constraints.
- We search for the state $|D_1\rangle$, orthogonal to $|A\rangle$ and respecting the various other constraints imposed. Moreover, $|D_1\rangle$ minimizes the HFB energy.
- We search for the state $|D_2\rangle$, orthogonal to $|A\rangle$ and to $|D_1\rangle$ simultaneously and respecting the various other constraints imposed. Here again, $|D_2\rangle$ minimizes the HFB energy.
- We iterate the previous process. At each iteration i, we search for the state $|D_i\rangle$, orthogonal to $|A\rangle$ and to all the $|D_j\rangle$ with $1 \leq j < i$ simultaneously and respecting the various other constraints imposed, with $|D_i\rangle$ minimizing the HFB energy.

Note that the average value of $\hat{Q}^{(10)}$ as well as the particle numbers are always constrained. In Figure (3.15), we displayed an example of the iterated "Deflation" method in the ^{240}Pu. We have plotted the total binding energy of the ^{240}Pu ground state along with the energy of four variational excited states we built with the iterated "Deflation" method. For this study, we only imposed the orthogonality with respect to the neutron part of the states, letting everything else free:

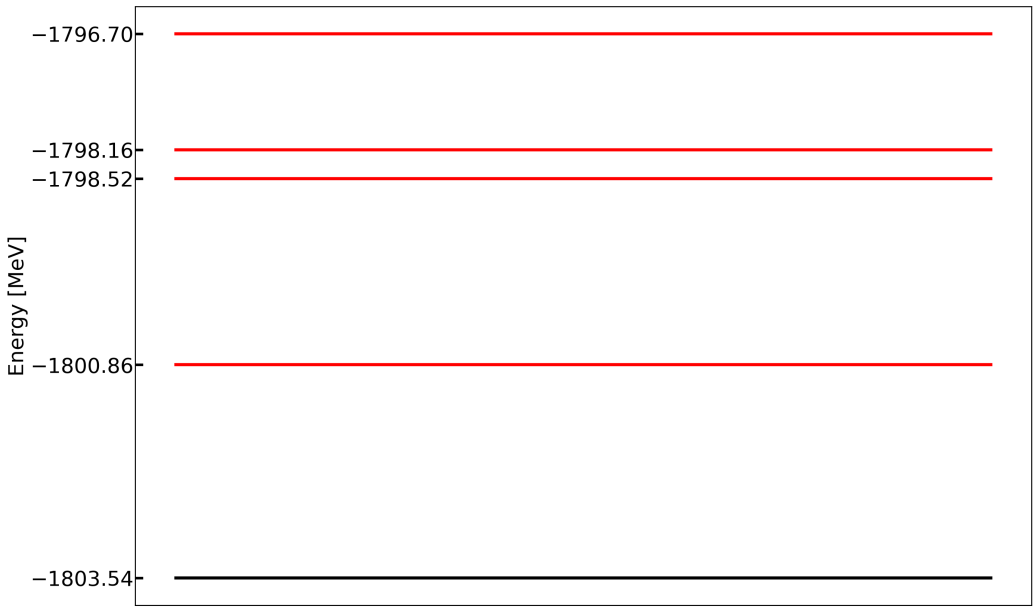

Figure 3.15: Energy of four variational excited states of the ^{240}Pu obtained with the iterated "Deflation" method, along with the ^{240}Pu ground state energy.

In addition, we give in Table (3.1) the values of the overlaps between the different states. $|A\rangle$ stands for the ground state, and $|D_1\rangle$, $|D_2\rangle$, $|D_3\rangle$ and $|D_4\rangle$ stand respectively for the first, second, third and fourth excited states:

	$\|A\rangle$	$\|D_1\rangle$	$\|D_2\rangle$	$\|D_3\rangle$	$\|D_4\rangle$
$\langle A\|$	1	4.1×10^{-4}	2.7×10^{-28}	8.0×10^{-21}	2.5×10^{-5}
$\langle D_1\|$	-	1	3.5×10^{-31}	7.7×10^{-23}	1.6×10^{-5}
$\langle D_2\|$	-	-	1	1.4×10^{-5}	7.9×10^{-27}
$\langle D_3\|$	-	-	-	1	9.4×10^{-19}
$\langle D_4\|$	-	-	-	-	1

Table 3.1: Overlaps between the states created with the iterated "Deflation" method in the ^{240}Pu.

The results shown in Figure (3.15) and Table (3.1) correspond to a specific type of excitations and cannot be interpreted as representative of the full low-lying spectrum in ^{240}Pu. However, they demonstrate the potential of the method for spectroscopy in a realistic case, as it is done in quantum chemistry.

It is now legitimate to question the nature of these variational excitations. First, we observed in the context of fission that they often include pair-breaking phenomena (see section 4.3), which are related to the physics of the 2-quasiparticle excited states. To introduce the other aspects of this concern, it is particularly interesting to study the deflation in the case of ^{16}O.

3.3.1 Study in the ^{16}O

It is well-known that in its ground state, the ^{16}O is spherical and doesn't manifest pairing phenomenon. In an HFB context, it implies that in the canonical representation, the occupation numbers v_i^2 are either zero or one. More precisely, we find three neutrons with $\Omega = 1/2$, one neutron with $\Omega = 3/2$, three protons with $\Omega = 1/2$ and one proton with $\Omega = 3/2$ (each of these particles being of course associated with its time-reversal counterpart).
We first performed a "Deflation" on the ^{16}O ground state, imposing orthogonality with respect to the neutron isospin only. In the canonical representation, the occupation numbers associated with the protons were practically the same, as for the canonical neutron particle states associated with $\Omega = 1/2$. On the contrary, the occupation numbers corresponding to the canonical neutron particle states with $\Omega = 3/2$ were changed. Indeed, we found only two non-zero v_i^2, both approximately equal to 0.5. Then, we did the same calculations with respect to protons, and found symmetric results, as expected. In both cases, the excitation energy of the states obtained with the "Deflation" approximately equals 15 MeV.
We have gone further in the analysis by considering the overlap with respect to both isospins and Ω. In the following, we call $|\Psi\rangle$ the ^{16}O ground state, $|\Psi_n^*\rangle$ the state obtained through the neutron "Deflation" and $|\Psi_p^*\rangle$ the state resulting from the proton "Deflation". We found:

$$\underline{\text{Neutron "Deflation":}} \qquad \begin{cases} \langle \Psi^{\tau_n \Omega_{1/2}} | \Psi_n^{*\tau_n \Omega_{1/2}} \rangle \approx 1 \\ \langle \Psi^{\tau_n \Omega_{3/2}} | \Psi_n^{*\tau_n \Omega_{3/2}} \rangle \approx 0 \\ \langle \Psi^{\tau_p} | \Psi_n^{*\tau_p} \rangle \approx 1 \end{cases} \tag{3.10}$$

$$\underline{\text{Proton "Deflation":}} \qquad \begin{cases} \langle \Psi^{\tau_n} | \Psi_p^{*\tau_n} \rangle \approx 1 \\ \langle \Psi^{\tau_p \Omega_{1/2}} | \Psi_p^{*\tau_p \Omega_{1/2}} \rangle \approx 1 \\ \langle \Psi^{\tau_p \Omega_{3/2}} | \Psi_p^{*\tau_p \Omega_{3/2}} \rangle \approx 0 \end{cases} \tag{3.11}$$

From Eq.(3.10) and Eq.(3.11), it is clear that we can restrict the analysis to the subspace $(\tau_n, \pm\Omega_{3/2})$ in the case of the neutron "Deflation" and to the subspace $(\tau_p, \pm\Omega_{3/2})$in the case of the proton one (the values in Eq.(3.10) and Eq.(3.11) are correct up to 10^{-3}). Besides, we can easily give the expression of $|\Psi^{\tau_n \pm \Omega_{3/2}}\rangle$ and $|\Psi^{\tau_p \pm \Omega_{3/2}}\rangle$ in the canonical representation:

$$\begin{cases} |\Psi^{\tau_n \pm \Omega_{3/2}}\rangle = a_n^+ \bar{a}_n^+ |0\rangle \\ |\Psi^{\tau_p \pm \Omega_{3/2}}\rangle = a_p^+ \bar{a}_p^+ |0\rangle \end{cases} \tag{3.12}$$

Here a_n^+ is the neutron particle creation operator in the canonical representation associated with $v_n^2 = 1$ and $\Omega = 3/2$, and a_p^+ is the proton particle creation operator in the canonical representation associated with $v_p^2 = 1$ and $\Omega = 3/2$. Then, we search for the expressions of $|\Psi_n^{*\tau_n \pm \Omega_{3/2}}\rangle$ and $|\Psi_p^{*\tau_p \pm \Omega_{3/2}}\rangle$ in the canonical representation of $|\Psi\rangle$. We call $D^{\tau\Omega}$ the transformation matrices from the harmonic oscillator representation to the canonical representation and $U_n^{*\tau_n \Omega_{3/2}}$, $V_n^{*\tau_n \Omega_{3/2}}$ and $U_p^{*\tau_p \Omega_{3/2}}$, $V_p^{*\tau_p \Omega_{3/2}}$ the Bogoliubov matrices of $|\Psi_n^{*\tau_n \pm \Omega_{3/2}}\rangle$ and $|\Psi_p^{*\tau_p \pm \Omega_{3/2}}\rangle$ respectively. It is clear that the expressions of these Bogoliubov matrices in the canonical representation of $|\Psi\rangle$ simply read as follows:

$$\begin{cases} \tilde{U}_n^{*\tau_n \Omega_{3/2}} = D^{\tau_n \Omega_{3/2} T} U_n^{*\tau_n \Omega_{3/2}} \\ \tilde{V}_n^{*\tau_n \Omega_{3/2}} = D^{\tau_n \Omega_{3/2} T} V_n^{*\tau_n \Omega_{3/2}} \end{cases} \tag{3.13}$$

$$\begin{cases} \tilde{U}_p^{*\tau_p \Omega_{3/2}} = D^{\tau_p \Omega_{3/2} T} U_n^{*\tau_p \Omega_{3/2}} \\ \tilde{V}_p^{*\tau_p \Omega_{3/2}} = D^{\tau_p \Omega_{3/2} T} V_n^{*\tau_p \Omega_{3/2}} \end{cases} \tag{3.14}$$

Using Eq.(3.13) and Eq.(3.14), we have extracted from the excited states the following structure (exact up to 10^{-3}):

$$\boxed{\begin{cases} |\Psi_n^{*\tau_n \pm \Omega_{3/2}}\rangle = \frac{1}{2}(-1 + a_{n*}^+ \bar{a}_n^+ + a_n^+ \bar{a}_{n*}^+ + a_{n*}^+ \bar{a}_{n*}^+ a_n^+ \bar{a}_n^+)|0\rangle \\ |\Psi_p^{*\tau_p \pm \Omega_{3/2}}\rangle = \frac{1}{2}(-1 + a_{p*}^+ \bar{a}_p^+ + a_p^+ \bar{a}_{p*}^+ + a_{p*}^+ \bar{a}_{p*}^+ a_p^+ \bar{a}_p^+)|0\rangle \end{cases}} \tag{3.15}$$

Here, the creation operators in the canonical particle basis a_{n*}^+ and a_{p*}^+ are associated with holes of the states $|\Psi^{\tau_n \Omega_{3/2}}\rangle$ and $|\Psi^{\tau_p \Omega_{3/2}}\rangle$, respectively. To make Eq.(3.15) easier to understand, we can make $|\Psi^{\tau_n \Omega_{3/2}}\rangle$ and $|\Psi^{\tau_p \Omega_{3/2}}\rangle$ appear:

$$\boxed{\begin{cases} |\Psi_n^{*\tau_n \pm \Omega_{3/2}}\rangle = \frac{1}{2}(a_n \bar{a}_n + a_{n^*}^+ a_n + \bar{a}_{n^*}^+ \bar{a}_n + a_{n*}^+ \bar{a}_{n*}^+)|\Psi^{\tau_n \Omega_{3/2}}\rangle \\ |\Psi_p^{*\tau_p \pm \Omega_{3/2}}\rangle = \frac{1}{2}(a_p \bar{a}_p + a_{p^*}^+ a_p + \bar{a}_{p^*}^+ \bar{a}_p + a_{p*}^+ \bar{a}_{p*}^+)|\Psi^{\tau_p \Omega_{3/2}}\rangle \end{cases}} \tag{3.16}$$

Both expressions in Eq(3.16) can be written with respect to the quasiparticles creation operators $\{\eta_k^+\}$ of the canonical representation, indeed:

$$\begin{cases} \eta_n^+ = \bar{a}_n \\ \eta_{n*}^+ = a_{n*}^+ \end{cases} \quad \text{and} \quad \begin{cases} \eta_p^+ = \bar{a}_p \\ \eta_{p*}^+ = a_{p*}^+ \end{cases} \tag{3.17}$$

Inserting Eq.(3.17) in Eq.(3.16), we get:

$$\boxed{\begin{cases} |\Psi_n^{*\tau_n \pm \Omega_{3/2}}\rangle = \frac{1}{2}(\eta_n^+\bar{\eta}_n^+ - \eta_{n*}^+\bar{\eta}_n^+ - \eta_n^+\bar{\eta}_{n*}^+ + \eta_{n*}^+\bar{\eta}_{n*}^+)|\Psi^{\tau_n\Omega_{3/2}}\rangle \\ |\Psi_p^{*\tau_p \pm \Omega_{3/2}}\rangle = \frac{1}{2}(\eta_p^+\bar{\eta}_p^+ - \eta_{p*}^+\bar{\eta}_p^+ - \eta_p^+\bar{\eta}_{p*}^+ + \eta_{p*}^+\bar{\eta}_{p*}^+)|\Psi^{\tau_p\Omega_{3/2}}\rangle \end{cases}} \tag{3.18}$$

Finally, we can use the matrices $C^{\tau\Omega}$ standing for the transition from the canonical quasiparticle representation to the original Bogoliubov quasiparticle representation:

$$\boxed{\begin{aligned} |\Psi_n^{*\tau_n \pm \Omega_{3/2}}\rangle = \frac{1}{2}\sum_{ij}(&C_{ni}^{\tau_n\Omega_{3/2}}C_{nj}^{\tau_n\Omega_{3/2}} - C_{n^*i}^{\tau_n\Omega_{3/2}}C_{nj}^{\tau_n\Omega_{3/2}} \\ &- C_{ni}^{\tau_n\Omega_{3/2}}C_{n^*j}^{\tau_n\Omega_{3/2}} + C_{n^*i}^{\tau_n\Omega_{3/2}}C_{n^*j}^{\tau_n\Omega_{3/2}})\xi_i^+\bar{\xi}_j^+|\Psi^{\tau_n\Omega_{3/2}}\rangle \end{aligned}} \tag{3.19}$$

$$\boxed{\begin{aligned} |\Psi_p^{*\tau_p \pm \Omega_{3/2}}\rangle = \frac{1}{2}\sum_{ij}(&C_{ni}^{\tau_p\Omega_{3/2}}C_{pj}^{\tau_p\Omega_{3/2}} - C_{p^*i}^{\tau_p\Omega_{3/2}}C_{pj}^{\tau_p\Omega_{3/2}} \\ &- C_{pi}^{\tau_n\Omega_{3/2}}C_{p^*j}^{\tau_p\Omega_{3/2}} + C_{p^*i}^{\tau_p\Omega_{3/2}}C_{p^*j}^{\tau_p\Omega_{3/2}})\xi_i^+\bar{\xi}_j^+|\Psi^{\tau_p\Omega_{3/2}}\rangle \end{aligned}} \tag{3.20}$$

We demonstrated that both the variational excited states can be written in that case as a sum of 2-quasiparticle excitations on top of their associated ground state. As we approximated values in the whole development, the conclusion is not totally exact though. However, it is easy to check the veracity of our statement evaluating numerically the following quantities:

$$\boxed{\begin{cases} \sigma_{n*}^{(2)} = \sum_{ij}|\langle\Psi_n^*|\xi_i^+\bar{\xi}_j^+|\Psi\rangle|^2 \\ \sigma_{p*}^{(2)} = \sum_{ij}|\langle\Psi_p^*|\xi_i^+\bar{\xi}_j^+|\Psi\rangle|^2 \end{cases}} \tag{3.21}$$

The two quantities defined in Eq.(3.21) measure the norm of the parts of the variational excited states that correspond to a sum of 2-quasiparticle excitations on top of $|\Psi\rangle$. In practice, we found $\sigma_{n*}^{(2)} = 0.993$ and $\sigma_{p*}^{(2)} = 0.993$. This precision is in line with the order of magnitude of the approximations we've done throughout the development. It means that more than 99% of the variational excited states we built can be described as a sum of 2-quasiparticle excitations on top of the ground state $|\Psi\rangle$.

3.3.2 Study in the ^{240}Pu

To check whether or not these results have any general significance, we evaluated the $\sigma^{(2)}$ quantity associated with the variational excited states we've created with respect to the ^{240}Pu ground state (see Figure (3.15)). We obtained:

$$\begin{cases} \sigma^{(2)}_{D_1} = 4 \times 10^{-3} \\ \sigma^{(2)}_{D_2} = 3 \times 10^{-52} \\ \sigma^{(2)}_{D_3} = 8 \times 10^{-38} \\ \sigma^{(2)}_{D_4} = 8 \times 10^{-4} \end{cases} \tag{3.22}$$

The results displayed in Eq.(3.22) are very different from the ones obtained in the ^{16}O. But they are not surprising. To interpret them, we propose to introduce three quantities. The first is called O^r. It represents the ratio of the full overlap between an excited state and its ground state and the lowest sub-overlap with respect to τ and Ω:

$$\boxed{O^r = \prod_{(\tau,\Omega)\neq(\tau^*,\Omega^*)} \langle \Phi^{*\tau\Omega} | \Phi^{\tau\Omega} \rangle} \tag{3.23}$$

It is clear that O^r qualifies the purity of an excitation. Or in other words, O^r describes the intensity of the global rearrangement implied by the orthogonality constraint imposed on a specific (τ,Ω) subspace.
Besides, we can deduce from Eq.(3.21) a very important relation linking O^r to the quantity $\sigma^{(2)}$. We start by writting the quantity $\sigma^{(2)}$ more explicitly:

$$\begin{aligned} \sigma^{(2)} = (O^r)^2 \sum_{ij} |\langle \Phi^{*\tau^*\Omega^*} | \xi_i^{\tau^*\Omega^*+} \bar{\xi}_j^{\tau^*\Omega^*+} | \Phi^{\tau^*\Omega^*} \rangle|^2 \\ + |\langle \Phi^{*\tau^*\Omega^*} | \Phi^{\tau^*\Omega^*} \rangle|^2 \sum_{(\tau,\Omega)\neq(\tau^*,\Omega^*)} \sum_{ij} |\langle \Phi^{*r} | \xi_i^{\tau\Omega+} \bar{\xi}_j^{\tau\Omega+} | \Phi^{r} \rangle|^2 \end{aligned} \tag{3.24}$$

In Eq.(3.24), we used the superscript r to refer to all the subspaces which are not related to (τ^*,Ω^*). As (τ^*,Ω^*) characterizes the orthogonal subspace, $|\langle \Phi^{*\tau^*\Omega^*} | \Phi^{\tau^*\Omega^*} \rangle|^2 \approx 0$. In addition, $\sum_{(\tau,\Omega)\neq(\tau^*,\Omega^*)} \sum_{ij} |\langle \Phi^{*r} | \xi_i^{\tau\Omega+} \bar{\xi}_j^{\tau\Omega+} | \Phi^{r} \rangle|^2 \leq 1$ and $\sum_{ij} |\langle \Phi^{*\tau^*\Omega^*} | \xi_i^{\tau^*\Omega^*+} \bar{\xi}_j^{\tau^*\Omega^*+} | \Phi^{\tau^*\Omega^*} \rangle|^2 \leq 1$. Inserting these three properties in Eq.(3.24) leads to the desired relation, which defines the boundary $b^{(2)}$:

$$\boxed{\sigma^{(2)} \leq (O^r)^2 = b^{(2)}} \tag{3.25}$$

This relation means that more than 2-quasiparticle excitations are required to describe an excited state when the variational excitation is not pure (O^r is not close to 1).
To characterize the variational excitations, another interesting quantity is the customary excitation energy $\Delta E^* = E^* - E$. As the 2-quasiparticle excitations are the elementary excitations of the HFB states when the time-reversal invariance is preserved, we assume that a lower ΔE^* favors greater values of $\sigma^{(2)}$. We evaluated the previously defined quantities O^r and ΔE^* associated with the states $|D_1\rangle$ to $|D_4\rangle$:

$$\begin{cases} b^{(2)}_{D_1} = 9 \times 10^{-3} \\ b^{(2)}_{D_2} = 5 \times 10^{-43} \\ b^{(2)}_{D_3} = 4 \times 10^{-32} \\ b^{(2)}_{D_4} = 0.314 \end{cases} \qquad \begin{cases} \Delta E^*_{D_1} = 2.67 \text{ MeV} \\ \Delta E^*_{D_2} = 5.01 \text{ MeV} \\ \Delta E^*_{D_3} = 5.37 \text{ MeV} \\ \Delta E^*_{D_4} = 6.84 \text{ MeV} \end{cases} \tag{3.26}$$

The results displayed in Eq.(3.26) are in line with our assumptions. The states $|D_1\rangle$, $|D_2\rangle$ and $|D_3\rangle$ illustrate the relation given in Eq.(3.25), stating that a very small O^r directly implies a very small $\sigma^{(2)}$. Besides, the variational excitation $|D_4\rangle$ is the purest, but has a relatively high ΔE^* in comparison with the other excited states. We assume that it is the reason why its associated $\sigma^{(2)}$ is relatively small. We know why the variational excited states $|D_1\rangle$ to $|D_4\rangle$ almost do not include 2-quasiparticle excitations, but we don't know yet what they are made of.

To try to answer this question, we first introduce the new quantity $\sigma^{(4)}$ that measures the norm of the parts of the variational excited states that can be described as a sum of 4-quasiparticle excitations on top of their reference states. The quantity $\sigma^{(4)}$ reads as follows:

$$\boxed{\begin{aligned}\sigma^{(4)} = \frac{1}{2}\sum_{\alpha\beta}\sum_{ij,\ (\Omega_{\alpha\beta},\tau_{\alpha\beta})\neq(\Omega_{ij},\tau_{ij})} |\langle\Phi^*|\xi^+_\alpha\bar{\xi}^+_\beta\xi^+_i\bar{\xi}^+_j|\Phi\rangle|^2 \\ +\frac{1}{4}\sum_{\alpha\beta}\sum_{ij,\ (\Omega_{\alpha\beta},\tau_{\alpha\beta})=(\Omega_{ij},\tau_{ij})} |\langle\Phi^*|\xi^+_\alpha\bar{\xi}^+_\beta\xi^+_i\bar{\xi}^+_j|\Phi\rangle|^2\end{aligned}} \tag{3.27}$$

Note that a special care must be taken when considering $\sigma^{(4)}$ as it may be numerically sensitive (see Chapter 5). By analogy with Eq.(3.25), we search for a relation linking O^r, $\sigma^{(2)}$, and $\sigma^{(4)}$. We start by writing explicitly the sum $\sigma^{(2)} + \sigma^{(4)}$:

$$\begin{aligned}\sigma^{(2)} + \sigma^{(4)} = (O^r)^2\Big(\frac{1}{4}\sum_{\alpha\beta}\sum_{ij}|\langle\Phi^{*\tau^*\Omega^*}|\xi^{+\tau^*\Omega^*}_\alpha\bar{\xi}^{+\tau^*\Omega^*}_\beta\xi^{+\tau^*\Omega^*}_i\bar{\xi}^{+\tau^*\Omega^*}_j|\Phi^{\tau^*\Omega^*}\rangle|^2 \\ +\sum_{ij}|\langle\Phi^{*\tau^*\Omega^*}|\xi^{+\tau^*\Omega^*}_i\bar{\xi}^{+\tau^*\Omega^*}_j|\Phi^{\tau^*\Omega^*}\rangle|^2\Big) \\ +\Big(\sum_{ij}|\langle\Phi^*|\xi^{+\tau^*\Omega^*}_i\bar{\xi}^{+\tau^*\Omega^*}_j|\Phi\rangle|^2\Big)\sum_{\alpha\beta,(\Omega_{\alpha\beta},\tau_{\alpha\beta})\neq(\Omega^*,\tau^*)}\frac{|\langle\Phi^{*r}|\xi^+_\alpha\bar{\xi}^+_\beta|\Phi^r\rangle|^2}{(O^r)^2}\end{aligned} \tag{3.28}$$

It is clear that Eq.(3.28) implies the following relation:

$$\sigma^{(4)} \leq (O^r)^2 + \sigma^{(2)}\Big(\frac{1-2(O^r)^2}{(O^r)^2}\Big) \leq 1-(O^r)^2 \tag{3.29}$$

The way $\sigma^{(4)}$ is bounded in Eq.(3.29) is often not precise enough to accurately interpret the results. Therefore, we have to consider more explicitly the (Ω,τ) subspaces. Doing so, we obtain a new inequality, which defines the boundary $b^{(4)}$:

$$\boxed{\sigma^{(4)} \leq (O^r)^2 + \sigma^{(2)}\Big(\sum_{(\Omega,\tau)\neq(\Omega^*,\tau^*)}\frac{1-|\langle\Phi^{*\tau\Omega}|\Phi^{\tau\Omega}\rangle|^2}{|\langle\Phi^{*\tau\Omega}|\Phi^{\tau\Omega}\rangle|^2} - 1\Big) = b^{(4)}} \tag{3.30}$$

In fact, the inequality in Eq.(3.30) is always better than the one in Eq.(3.29). Indeed, we can write:

$$\frac{1-(O^r)^2}{(O^r)^2} - \sum_{(\Omega,\tau)\neq(\Omega^*,\tau^*)}\frac{1-|\langle\Phi^{*\tau\Omega}|\Phi^{\tau\Omega}\rangle|^2}{|\langle\Phi^{*\tau\Omega}|\Phi^{\tau\Omega}\rangle|^2} = \frac{1+(n-1)(O^r)^2 - \sum_{(\Omega,\tau)\neq(\Omega^*,\tau^*)}\frac{(O^r)^2}{|\langle\Phi^{*\tau\Omega}|\Phi^{\tau\Omega}\rangle|^2}}{(O^r)^2} \tag{3.31}$$

Here, n is the number of non-orthogonal (Ω,τ) subspaces. To go further, we need to study the function f defined below:

$$f \; : \; \begin{cases} [0,1]^n \rightarrow \mathbb{R} \\ x = (x_1, ..., x_n) \rightarrow (n-1) \prod_i x_i - \sum_j \prod_{i \neq j} x_i \end{cases} \tag{3.32}$$

We can evaluate the partial derivatives of f:

$$\frac{\partial}{\partial x_\alpha} f(x) = (n-1) \prod_{i \neq \alpha} x_i - \sum_{j \neq \alpha} \prod_{i \neq j \neq \alpha} x_i \leq 0 \qquad \forall \alpha \tag{3.33}$$

From Eq.(3.33), it is clear that the function f reaches its minimum at $x = (1, ..., 1)$. Therefore:

$$f(x) \geq -1 \qquad \forall x \in [0,1]^n \tag{3.34}$$

We now rewrite the numerator at the right hand side of Eq.(3.31) using the function f:

$$1 + (n-1)(O^r)^2 - \sum_{(\Omega,\tau) \neq (\Omega^*,\tau^*)} \frac{(O^r)^2}{|\langle \Phi^{*\tau\Omega} | \Phi^{\tau\Omega} \rangle|^2} = 1 + \\ f(|\langle \Phi^{*(\tau,\Omega)_1} | \Phi^{(\tau,\Omega)_1} \rangle|^2, ..., |\langle \Phi^{*(\tau,\Omega)_n} | \Phi^{(\tau\Omega)_n} \rangle|^2) \tag{3.35}$$

Using Eq.(3.35), we finally find:

$$\boxed{\frac{1-(O^r)^2}{(O^r)^2} \geq \sum_{(\Omega,\tau) \neq (\Omega^*,\tau^*)} \frac{1 - |\langle \Phi^{*\tau\Omega} | \Phi^{\tau\Omega} \rangle|^2}{|\langle \Phi^{*\tau\Omega} | \Phi^{\tau\Omega} \rangle|^2}} \tag{3.36}$$

We evaluated the quantities $\sigma^{(4)}$ and $b^{(4)}$ associated with the states $|D_1\rangle$ to $|D_4\rangle$:

$$\begin{cases} \sigma^{(4)}_{D_1} = 0.026 \\ \sigma^{(4)}_{D_2} = 4 \times 10^{-49} \\ \sigma^{(4)}_{D_3} = 2 \times 10^{-35} \\ \sigma^{(4)}_{D_4} = 0.277 \end{cases} \qquad \begin{cases} b^{(4)}_{D_1} = 0.033 \\ b^{(4)}_{D_2} = 7 \times 10^{-43} \\ b^{(4)}_{D_3} = 5 \times 10^{-31} \\ b^{(4)}_{D_4} = 0.314 \end{cases} \tag{3.37}$$

The small values of $\sigma^{(4)}$ found for the states $|D_1\rangle$ to $|D_3\rangle$ are directly explained by the related small values of $b^{(4)}$. On the other hand, the quantity $\sigma^{(4)}_{D_4}$ is not negligible. We assume that the fact that $b^{(4)}_{D_4} \approx b^{(2)}_{D_4}$ while $\sigma^{(4)}_{D_4} >> \sigma^{(2)}_{D_4}$ is mostly explained by the fact that $\Delta E^*_{D_4}$ is relatively high.
We might want to try to explain a larger part of these variational excited states by calculating the other $\sigma^{(2p)}$ quantities. However, the higher the order, the more complex is to calculate these quantities, and the lower their numerical stability. In addition, the very low values of $O^r_{D_2}$ and $O^r_{D_3}$ suggest that a much larger p would have to be considered to achieve satisfactory results in this kind of excited states.

In order to study states whose structure can be explained by the lowest orders of p, we've decided to create other variational excitations on top of the ^{240}Pu ground state, but imposing conditions on O^r. We first created $|D'_1\rangle$, imposing orthogonality with respect to the neutron $\Omega = 1/2$ subspace and constraining the whole proton subspace to be the same as the one of the reference ground state. Then, we built $|D'_2\rangle$, imposing orthogonality with respect to the neutron $\Omega = 1/2$ subspace, and such that $O^r = 1$ (all the non-orthogonal subspaces are constrained to be the same as the ones of the ground state). Numerically speaking, the convergence leading to the state $|D'_1\rangle$ has been achieved without particular difficulties, but the condition $O^r = 1$ have been harder to impose in practice. Still, the results obtained with both states are really interesting:

$$\boxed{\begin{cases}\sigma^{(2)}_{D'_1} = 0.795 \\ \sigma^{(2)}_{D'_2} = 0.484\end{cases} \qquad \begin{cases}\sigma^{(4)}_{D'_1} = 0.187 \\ \sigma^{(4)}_{D'_2} = 0.460\end{cases}} \tag{3.38}$$

$$\boxed{\begin{cases}b^{(2)}_{D'_1} = 0.819 \\ b^{(2)}_{D'_2} = 0.998\end{cases} \qquad \begin{cases}b^{(4)}_{D'_1} = 0.189 \\ b^{(4)}_{D'_2} = 0.514\end{cases} \qquad \begin{cases}\Delta E^*_{D'_1} = 3.59 \text{ MeV} \\ \Delta E^*_{D'_2} = 6.55 \text{ MeV}\end{cases}} \tag{3.39}$$

Concerning the state $|D'_1\rangle$, $\sigma^{(2)}_{D'_1}$ and $\sigma^{(4)}_{D'_1}$ are found relatively close to their boundaries $b^{(2)}_{D'_1}$ and $b^{(4)}_{D'_1}$, while the excitation energy $\Delta E^*_{D'_1}$ is relatively low. On the other hand, $\sigma^{(2)}_{D'_2}$ is far from its boundary $b^{(2)}_{D'_2}$, $\sigma^{(4)}_{D'_2}$ is close from its boundary $b^{(4)}_{D'_2}$, while $\Delta E^*_{D'_2}$ is much higher than $\Delta E^*_{D'_1}$. These observations suggest that the lower the excitation energy, the closer the quantities $\sigma^{(2)}$ and $\sigma^{(4)}$ to their boundaries. Besides, the total norm explained by both the 2-and the 4-quasiparticle excitations equals 0.982 in the case of $|D'_1\rangle$ and 0.944 in the case of $|D'_2\rangle$.
In the case of $|D'_1\rangle$, the difference between $\sigma^{(2)}_{D'_1}$ and one is explained by $b^{(2)}$, which is related to the purity of the excitation. In the case of $|D'_2\rangle$, the difference between $\sigma^{(2)}_{D'_2}$ and one seems to be related to the excitation energy $\Delta E^*_{D'_2}$. Because of that, it is legitimate to think that the 4-quasiparticle excitations contributing to $\sigma^{(4)}_{D'_1}$ are of different nature to the one contributing to $\sigma^{(4)}_{D'_2}$. To clarify this assumption, we can separate the quantity $\sigma^{(4)}$ defined in Eq.(3.27) into two different contributions $\bar{\sigma}^{(4)}$ and $\tilde{\sigma}^{(4)}$:

$$\boxed{\bar{\sigma}^{(4)} = \frac{1}{4}\sum_{\alpha\beta}\sum_{ij,\,(\Omega_{\alpha\beta},\tau_{\alpha\beta})=(\Omega_{ij},\tau_{ij})} |\langle\Phi^*|\xi^+_\alpha\bar{\xi}^+_\beta\xi^+_i\bar{\xi}^+_j|\Phi\rangle|^2} \tag{3.40}$$

$$\boxed{\tilde{\sigma}^{(4)} = \frac{1}{2}\sum_{\alpha\beta}\sum_{ij,\,(\Omega_{\alpha\beta},\tau_{\alpha\beta})\neq(\Omega_{ij},\tau_{ij})} |\langle\Phi^*|\xi^+_\alpha\bar{\xi}^+_\beta\xi^+_i\bar{\xi}^+_j|\Phi\rangle|^2} \tag{3.41}$$

The quantity $\bar{\sigma}^{(4)}$ represents the part of $\sigma^{(4)}$ which is related to 4-quasiparticle diagonal in both spin and Ω when $\tilde{\sigma}^{(4)}$ describes the off-diagonal part of $\sigma^{(4)}$. Thanks to Eq.(3.28) and Eq.(3.30), it easy to find the boundaries $\bar{b}^{(4)}$ and $\tilde{b}^{(4)}$ standing respectively for $\bar{\sigma}^{(4)}$ and $\tilde{\sigma}^{(4)}$:

$$\boxed{\bar{\sigma}^{(4)} \leq b^{(2)} - \sigma^{(2)} = \bar{b}^{(4)}} \tag{3.42}$$

$$\boxed{\tilde{\sigma}^{(4)} \leq \sigma^{(2)} \sum_{(\Omega,\tau)\neq(\Omega^*,\tau^*)} \frac{1-|\langle\Phi^{*\tau\Omega}|\Phi^{\tau\Omega}\rangle|^2}{|\langle\Phi^{*\tau\Omega}|\Phi^{\tau\Omega}\rangle|^2} = b^{(4)} - \bar{b}^{(4)} = \tilde{b}^{(4)}} \tag{3.43}$$

Looking at Eq.(3.42), we observe that the quantity $\bar{\sigma}^{(4)}$ can possibly be high when $\sigma^{(2)}$ is far from its boundary, which we assume to be the case when ΔE^* is high. On the other hand, Eq.(3.43) highlights as expected that less pure excitations are beneficial for the quantity $\tilde{\sigma}^{(4)}$. Moreover, it is clear that $O^r \approx 1 \;\Rightarrow\; \tilde{b}^{(4)} \approx 0$.
We evaluated these four different quantities in the states $|D_1'\rangle$ and $|D_2'\rangle$:

$$\boxed{\begin{cases}\bar{\sigma}^{(4)}_{D_1'} = 0.024 \\ \bar{\sigma}^{(4)}_{D_2'} = 0.459\end{cases} \qquad \begin{cases}\tilde{\sigma}^{(4)}_{D_1'} = 0.163 \\ \tilde{\sigma}^{(4)}_{D_2'} = 0.001\end{cases}} \tag{3.44}$$

$$\boxed{\begin{cases}\bar{b}^{(4)}_{D_1'} = 0.024 \\ \bar{b}^{(4)}_{D_2'} = 0.513\end{cases} \qquad \begin{cases}\tilde{b}^{(4)}_{D_1'} = 0.165 \\ \tilde{b}^{(4)}_{D_2'} = 0.001\end{cases}} \tag{3.45}$$

The results presented in Eq.(3.44) and Eq.(3.45) are rather explicit. The 4-quasiparticle excitations structure of $|D_1'\rangle$ is related to simultaneously orthogonal subspaces of $|D_1'\rangle$ with respect to the ground state (we call this phenomenon "coupled 4-quasiparticle excitations"). On the contrary, the 4-quasiparticle excitations of $|D_2'\rangle$ seems to simply account for a higher excitation energy (we call these excitations "uncoupled 4-quasiparticle excitations").
In a nutshell, two factors appear to be decisive in understanding the structure of the variational excited states. The first factor is the purity of the variational excitations. It characterizes how the non-constrained (Ω,τ) subspaces of the variational excitations are impacted by the orthogonality constraints. The purity namely fixes the boundaries of the quantities $\sigma^{(2)}$ and $\sigma^{(4)}$. The second important factor observed is the excitation energy ΔE^*. We remarked that the higher the excitation energy, the closer the quantities $\sigma^{(2)}$ and $\sigma^{(4)}$ are to their boundaries.
We are aware that the data presented are still too limited for the moment to fully confirm the veracity of our hypotheses. In the following section, $\sigma^{(2)}$, $\sigma^{(4)}$, $b^{(2)}$, $b^{(4)}$ and ΔE^* are studied for numerous continuous variational excitations with respect to the collective coordinate $c_{\#}$.

3.3.3 Orthogonality and intrinsic excitations

To conclude this section on the "Deflation" method, it is important to remark that a state $|\Phi\rangle$ orthogonal to another state $|\Phi_\beta\rangle$ is not necessarily an intrinsically excited state of the latter. For instance, in the case of discontinuities associated with multipole moments, two states are found orthogonal but they are both adiabatic. As long as we perform "Deflation" with respect to the ground state, we can reasonably think that we avoid this problem. Indeed, starting from the ground state, we expect that the "Deflation" method won't investigate adiabatic deformed states nearby as the ratio between the binding energy lost and the decrease in overlap is clearly unfavorable in that case. On the contrary, if we perform a "Deflation" on an adiabatic state at the top of the first barrier, it is favorable both energetically and in terms of orthogonality to drop back towards the adiabatic ground state. These thoughts have led to the new "Continuous Deflation" method we've created in order to follow a variational excitation along a deformation path.

3.4 The Continuous Deflation method

The "Continuous Deflation" method aims to build a set of excited states $\{|D_i\rangle\}$ with respect to a continuous adiabatic set $\{|A_i\rangle\}$, such that $\forall i$, $\langle D_i|D_{i+1}\rangle = x_0$ and $\langle A_i|D_i\rangle = 0$. The parameter x_0 is the value of the overlap between two adjacent states of the given continuous adiabatic set $\{|A_i\rangle\}$. In Figure (3.16), we present a schematic view of the "Continuous Deflation" method:

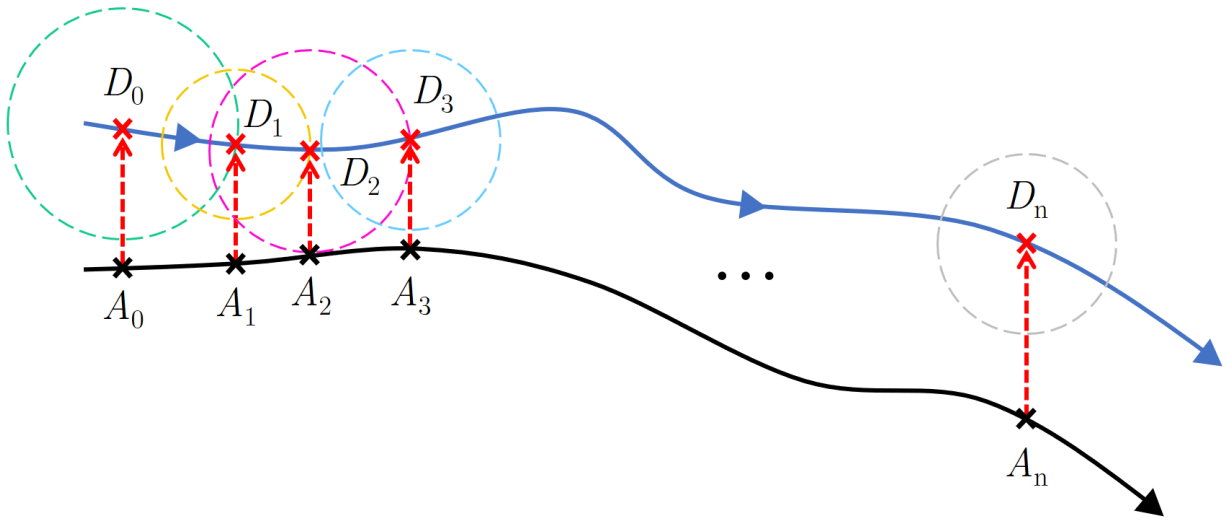

Figure 3.16: Schematic view of the "Continuous Deflation" method.

The first thing which is important to discuss, is the fact that this method has a starting point (or a seed). In Figure (3.16), this seed is the state $|D_0\rangle$ built on top of the adiabatic state $|A_0\rangle$. The seed can be chosen to be the variatonal excitation with the lowest energy on top of a given adiabatic state. However, to make this variational excited state evolve continuously in deformation, a continuity constraint is added. Because of this additional constraint, the new variational excited states obtained are not guaranteed to be the lowest in energy with respect to their associated adiabatic states. This feature is really essential, insofar as it implies that the seeds have to be chosen in the area where it matters to catch the physics of the low-lying excited states. In our case, we have experimental evidence of the importance of the low-lying excited states from the saddle point towards scission. Thus, we decided to build the excited seeds on top of the saddle point.
The second important topic concerns how we ensure that the orthogonal states we produce are indeed intrinsic excitations on top of their reference state. The most obvious way to do this is to impose to the excited states to have the same multipole moments as those of their related reference states. This method didn't work in practice in the calculations we have done. Imposing continuity, orthogonality and multipole moment constraints at the same time, the calculations are often "over-constrained". By "over-constrained" we mean that the constraints are not mutually compatible. To tackle this issue, we designed another way to constrain our calculations. Instead of the multipole moments, we decided to impose orthogonality with respect to a specific isospin while the overlap with respect to the other isospin is constrained to be one. The underlying assumption is that, doing so, we also constrain the shape of the variational state (but more softly), as the local neutron over proton ratio is found to be rather homogeneous in the nuclei. In practice, this method works very well and the multipole moments of the resulting variational states are found to evolve accordingly with the ones of the adiabatic states. In Figure (3.17), we displayed the

multipole moments of the adiabatic states obtained with the $\tilde{\mathcal{P}}_{20}$ procedure in the ^{240}Pu along with the multipole moments of a continuous neutron excitation built on top of them with the method described just above. In panel (a), panel (b) and panel (c) we plotted the quadrupole, octupole and hexadecapole moments respectively with respect to $c_{\#}$:

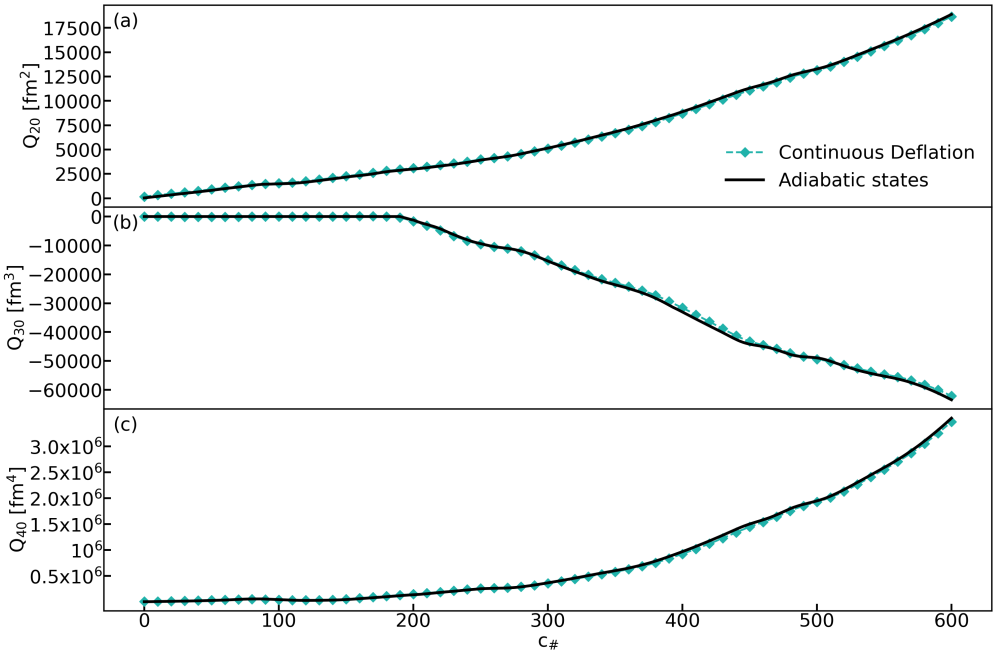

Figure 3.17: Comparison of the multipole moments of an adiabatic set obtained with the $\tilde{\mathcal{P}}_{20}$ procedure in the ^{240}Pu and the multipole moments of one of its continuous neutron variational excitation. Panel (a): quadrupole moment with respect to $c_{\#}$. Panel (b): octupole moment with respect to $c_{\#}$. Panel (c): hexadecapole moment with respect to $c_{\#}$.

An interesting by-product of this method is that a neutron variational excitation will naturally be orthogonal to a proton one. This is a very appealing feature, as it enables us to create several variational excitations without having to impose additional orthogonality constraints, as is the case with the customary iterated "Deflation".
In the light of this observation, we have tried to go one step further imposing the orthogonality in only one (Ω,τ) subspace, while everything else was constrained to one. Unfortunately, this approach proved disappointing. For the smaller Ω values, numerical convergences were much more difficult (leading to less precise orthogonality), and were sometimes impossible for larger Ω values. This phenomenon can be understood easily with the following example: suppose we have an adiabatic state $|\Phi\rangle$ with a subspace $|\Phi^{\tau\Omega}\rangle$ in which no particles are present. If we perform a convergence imposing $\langle\Phi^{*\tau\Omega}|\Phi^{\tau\Omega}\rangle = 0$, there is necessarily particles in the $|\Phi^{\tau\Omega}\rangle$ subspace. As we also constrain the average particle number, the increase in the average particle number due to $|\Phi^{*\tau\Omega}\rangle$ has to be offset elsewhere. Because of that, it is not possible to impose both $\langle\Phi^{*\tau\Omega}|\Phi^{\tau\Omega}\rangle = 0$ and $O^r = 1$ at the same time. All the cases are of course not that extreme, but this example clearly underlines the kind of interplays that may appear in practice.
The trade-off we've finally chosen in order to avoid these issues consists in imposing the orthogonality in only one subspace labeled by Ω^* and τ^* and to impose the overlap with respect to the whole subspace related to the other isospin $\bar{\tau}^*$ to be equal to one. If we call the reference state $|\Phi\rangle$ and its variational excited state $|\Phi^*\rangle$, these constraints read:

$$\begin{cases} \langle \Phi^{*\tau^*\Omega^*} | \Phi^{\tau^*\Omega^*} \rangle = 0 \\ \langle \Phi^{*\bar{\tau}^*} | \Phi^{\bar{\tau}^*} \rangle = 1 \end{cases} \tag{3.46}$$

Strictly speaking, the constraints displayed in Eq.(3.46) do not fully guarantee that two variational excited states associated with different Ω values but with the same isospin are orthogonal. However, in practice, among the ten variational excitations we've created we found that the maxium overlap between two variational excitations on top of the same adiabatic state was 0.033 (neutron excitations with $\Omega = 1/2$ and $\Omega = 3/2$). We assume that this good behaviour is due to the fact that a case of spontaneous orthogonality with respect to two subspaces when only one subspace is constrained is not energetically favored at all. Indeed, the configuration that minimizes the energy is the adiabatic one. If we constrain a subspace to be orthogonal, the mean field changes causing the other subspaces to rearrange themselves. This global rearrangement phenomenon can be important in some cases leading to small values of O^r. However, in these cases, the impact of the rearrangement is spread out, and does not concern only one other specific subspace. Therefore, at low energy, it is highly improbable to find two subspaces such that imposing orthogonality with respect to one of them necessarily implies the orthogonality with respect to the other and conversely. That being said, the "Continuous Deflation" method can be summarized as follows:

- We choose the isospin τ^* (the other isospin being $\bar{\tau}^*$) and the projection of the total angular momentum Ω^* characterizing the excitation.
- We search for the state $|D_0\rangle$, such that $\langle A_0^{\tau^*\Omega^*} | D_0^{\tau^*\Omega^*} \rangle = 0$ and $\langle A_0^{\bar{\tau}^*} | D_0^{\bar{\tau}^*} \rangle = 1$. Moreover, $|D_0\rangle$ minimizes the HFB energy. This state $|D_0\rangle$ is the seed of the excited set.
- We search for the state $|D_1\rangle$, such that $\langle A_1^{\tau^*\Omega^*} | D_1^{\tau^*\Omega^*} \rangle = 0$, $\langle A_1^{\bar{\tau}^*} | D_1^{\bar{\tau}^*} \rangle = 1$ and $\langle D_0 | D_1 \rangle = x_0$. Moreover $|D_1\rangle$ minimizes the HFB energy.
- We iterate the previous process. At each iteration i, we search for the state $|D_i\rangle$, such that $\langle A_i^{\tau^*\Omega^*} | D_i^{\tau^*\Omega^*} \rangle = 0$, $\langle A_i^{\bar{\tau}^*} | D_i^{\bar{\tau}^*} \rangle = 1$ and $\langle D_{i-1} | D_i \rangle = x_0$. Moreover, $|D_i\rangle$ minimizes the HFB energy.

An excited state $|D_i\rangle$ is always built using the orthonormal particle basis of the state $|A_i\rangle$. Doing so, there is no basis optimization in the "Continuous Deflation" method. Note that, when the bases of two adjacent states $|A_{i-1}\rangle$ and $|A_i\rangle$ are different, numerical complications are added. Regarding the performances of the method, around 10 hours were required to build one excited set of more than 700 states in the ^{240}Pu, using 2x11 harmonic oscillator representations. In the following, we refer to the procedure described above as the $\tilde{\mathcal{P}}^*_{20}$, when it is performed on top of an adiabatic set obtained with the $\tilde{\mathcal{P}}_{20}$ procedure.

During this PhD thesis work, we created up to ten variational excited sets using both isospins and imposing values of Ω ranging from 1/2 to 9/2. As already mentioned, the seeds of these excitations have been created on top of the saddle point ($Q_{20} = 4230$ fm^2). In Figure (3.18), we've displayed the PES of these ten excited sets along with the PES of their associated adiabatic set built with the $\tilde{\mathcal{P}}_{20}$ procedure in the ^{240}Pu with respect to quadrupole deformation Q_{20}:

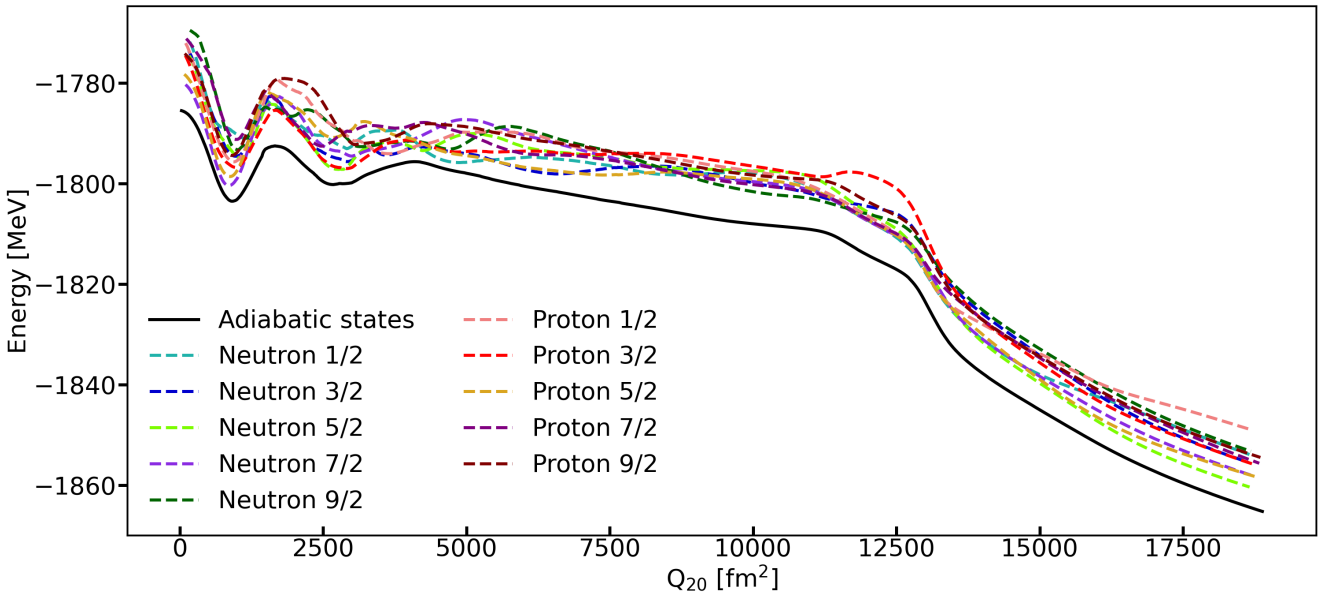

Figure 3.18: PES of ten variational excited sets built with the $\tilde{\mathcal{P}}^{*}_{20}$ procedure along with the PES of their associated adiabatic set built with the $\tilde{\mathcal{P}}_{20}$ procedure in the ^{240}Pu, with respect to quadrupole deformation.

Perhaps the most striking feature of Figure (3.18) is the fact that the colored curves get noticeably closer nearby the scission area ($Q_{20} \approx 13000$ fm^2) and separate again afterwards. This phenomenon could be the signature of a greater low-energy level-density close to the scission area.
In Figure (3.19), we've provided the reader with the equivalent of Figure (3.18) in the $c_{\#}$ representation (in this representation, the saddle point is found at $c_{\#} = 267$). It is important to keep in mind that the PES topologies which are relevant for the dynamics are the one obtained in the representation defined by $c_{\#}$:

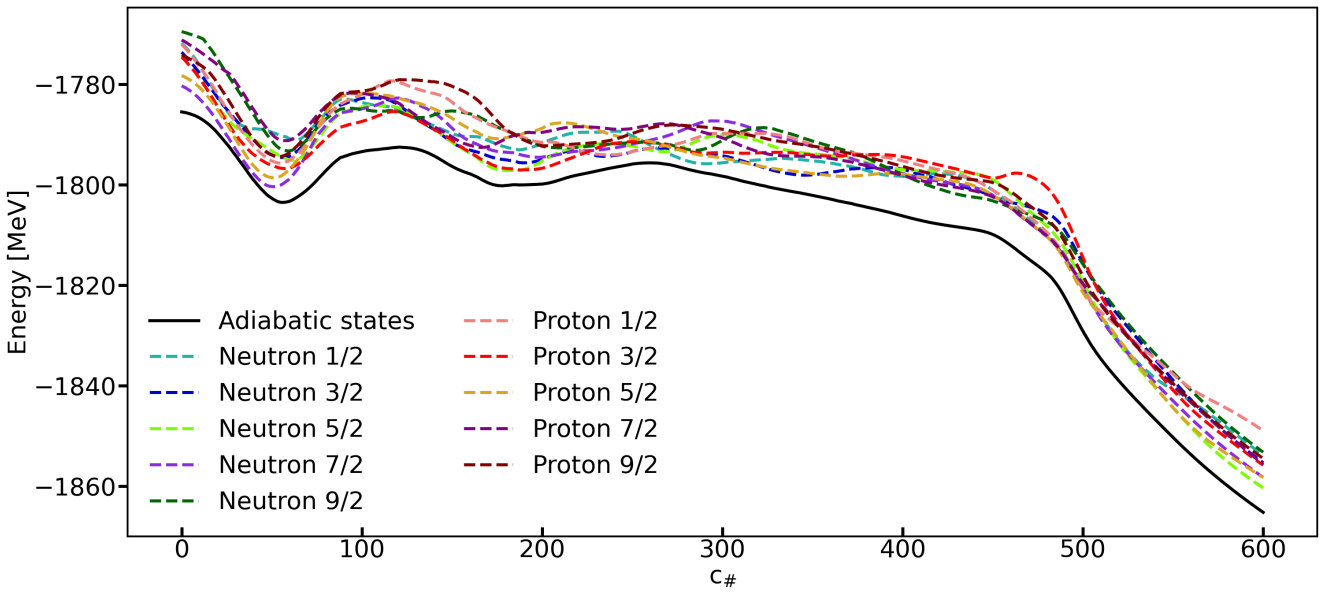

Figure 3.19: PES of ten excited sets built with the $\tilde{\mathcal{P}}^{*}_{20}$ procedure along with the PES of their associated adiabatic set built with the $\tilde{\mathcal{P}}_{20}$ procedure in the ^{240}Pu with respect to the new coordinate $c_{\#}$.

There are two main differences between Figures (3.18) and (3.19). First, in Figure (3.19), the first barrier of the PES are wider. Then, we observe a shorter and steeper descent from the saddle to scission in the case of Figure (3.19).

3.4.1 Study of the variational excitation content

The first thing we analyze is the content of the variational excitations we've created with the $\tilde{\mathcal{P}}^{*}_{20}$ procedure. We expect this study to allow to test the hypotheses formulated in the previous section 3.3. Namely, we want to characterize more precisely the impact of both the purity and the excitation energy of the variational excitations on their structure. In Figures (3.20-3.29), we've displayed the quantities O^r, ΔE^*, $\sigma^{(2)}$,$\bar{\sigma}^{(4)}$, $\tilde{\sigma}^{(4)}$ and $\sigma^{(4)}$ introduced in section 3.3 in addition to $\sigma^{tot} = \sigma^{(4)} + \sigma^{(2)}$ with respect to the collective coordinate $c_{\#}$ for all our variational excitations. For each Figure, we displayed in panel (a) the quantities $\sigma^{(2)}$,$\bar{\sigma}^{(4)}$, $\tilde{\sigma}^{(4)}$, $\sigma^{(4)}$ and σ^{tot} with respect to $c_{\#}$; in panel (b), we displayed O^r with respect to $c_{\#}$; in panel (c), we displayed ΔE^* with respect to $c_{\#}$:

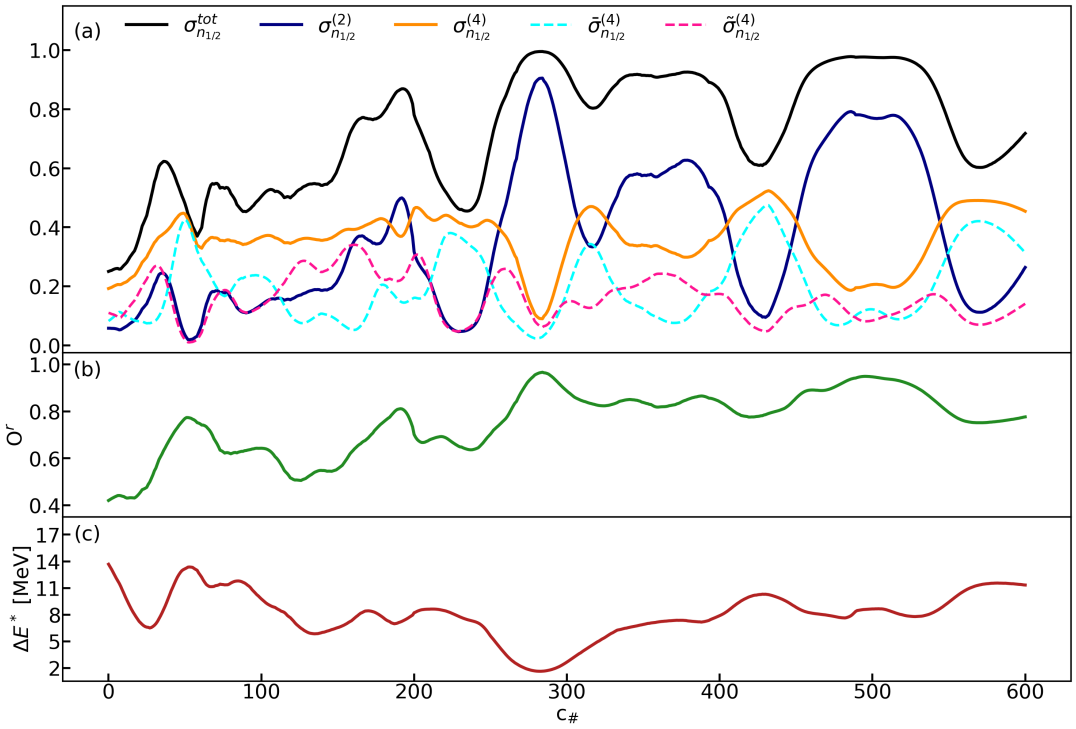

Figure 3.20: Behavior of the quantities ΔE^*, O^r, $\sigma^{(2)}$,$\bar{\sigma}^{(4)}$, $\tilde{\sigma}^{(4)}$, $\sigma^{(4)}$ and σ^{tot} with respect to $c_\#$ in the neutron variational excitation associated with $\Omega = 1/2$. Panel (a): $\sigma^{(2)}$,$\bar{\sigma}^{(4)}$, $\tilde{\sigma}^{(4)}$, $\sigma^{(4)}$ and σ^{tot} with respect to $c_\#$. Panel (b): O^r with respect to $c_\#$. Panel (c): ΔE^* with respect to $c_\#$.

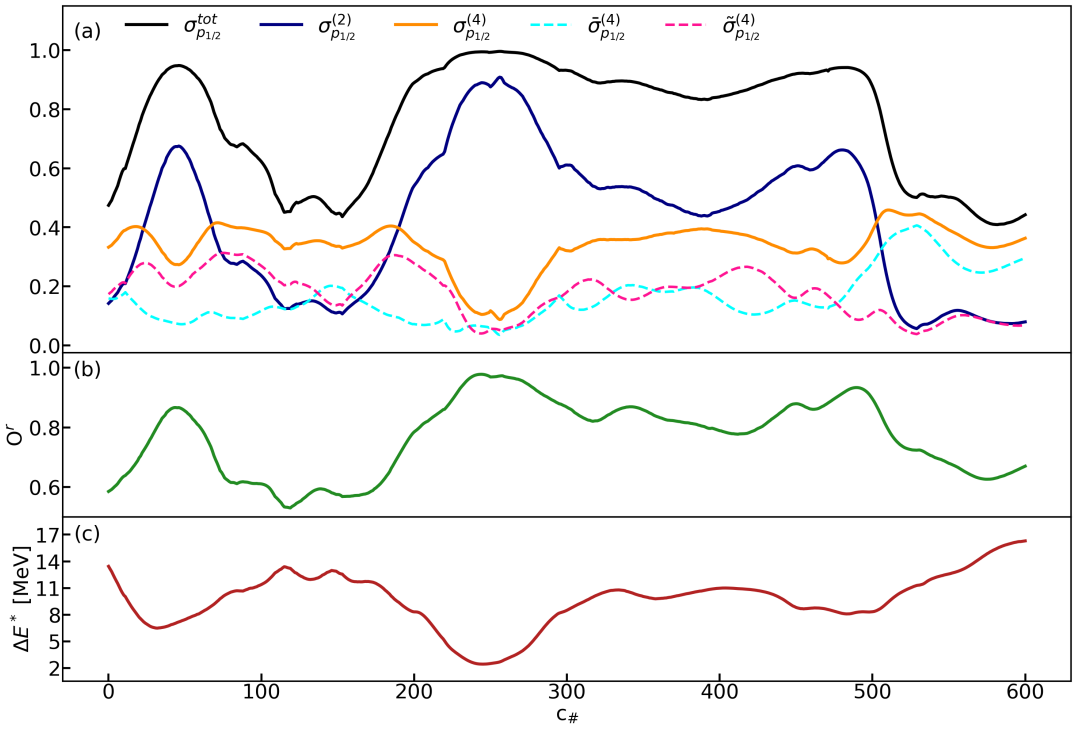

Figure 3.21: Behavior of the quantities ΔE^*, O^r, $\sigma^{(2)}$,$\bar{\sigma}^{(4)}$, $\tilde{\sigma}^{(4)}$, $\sigma^{(4)}$ and σ^{tot} with respect to $c_\#$ in the proton variational excitation associated with $\Omega = 1/2$. Panel (a): $\sigma^{(2)}$,$\bar{\sigma}^{(4)}$, $\tilde{\sigma}^{(4)}$, $\sigma^{(4)}$ and σ^{tot} with respect to $c_\#$. Panel (b): O^r with respect to $c_\#$. Panel (c): ΔE^* with respect to $c_\#$.

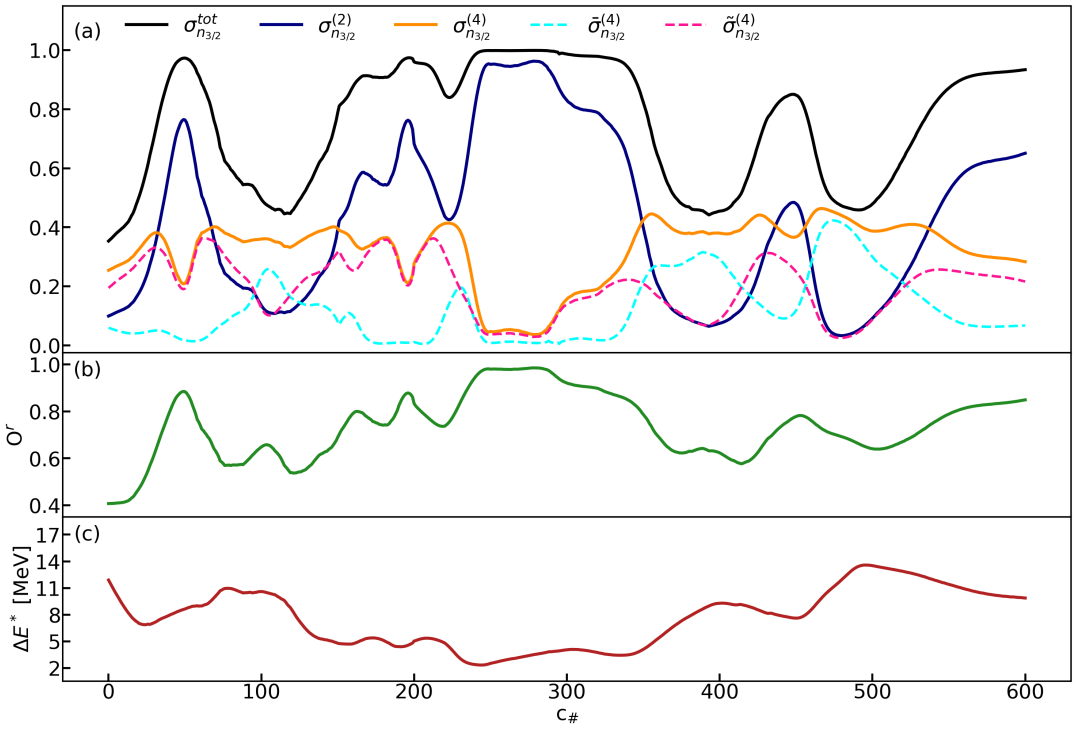

Figure 3.22: Behavior of the quantities ΔE^*, O^r, $\sigma^{(2)}$,$\bar{\sigma}^{(4)}$, $\tilde{\sigma}^{(4)}$, $\sigma^{(4)}$ and σ^{tot} with respect to $c_\#$ in the neutron variational excitation associated with $\Omega = 3/2$. Panel (a): $\sigma^{(2)}$,$\bar{\sigma}^{(4)}$, $\tilde{\sigma}^{(4)}$, $\sigma^{(4)}$ and σ^{tot} with respect to $c_\#$. Panel (b): O^r with respect to $c_\#$. Panel (c): ΔE^* with respect to $c_\#$.

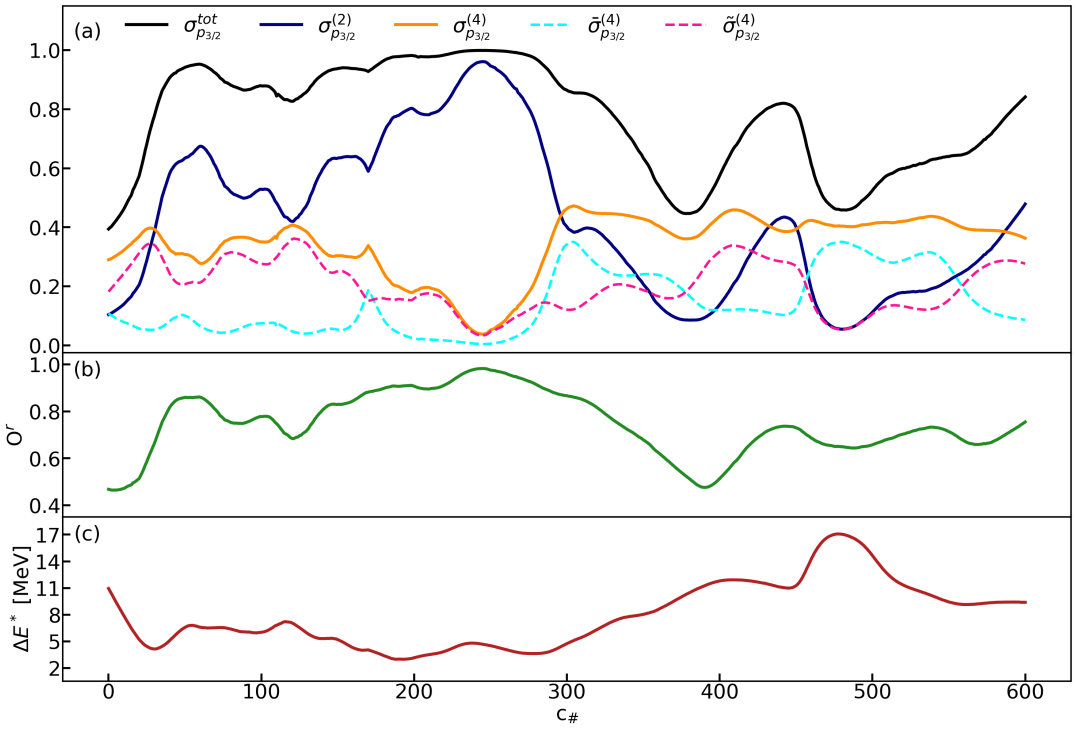

Figure 3.23: Behavior of the quantities ΔE^*, O^r, $\sigma^{(2)}$,$\bar{\sigma}^{(4)}$, $\tilde{\sigma}^{(4)}$, $\sigma^{(4)}$ and σ^{tot} with respect to $c_\#$ in the proton variational excitation associated with $\Omega = 3/2$. Panel (a): $\sigma^{(2)}$,$\bar{\sigma}^{(4)}$, $\tilde{\sigma}^{(4)}$, $\sigma^{(4)}$ and σ^{tot} with respect to $c_\#$. Panel (b): O^r with respect to $c_\#$. Panel (c): ΔE^* with respect to $c_\#$.

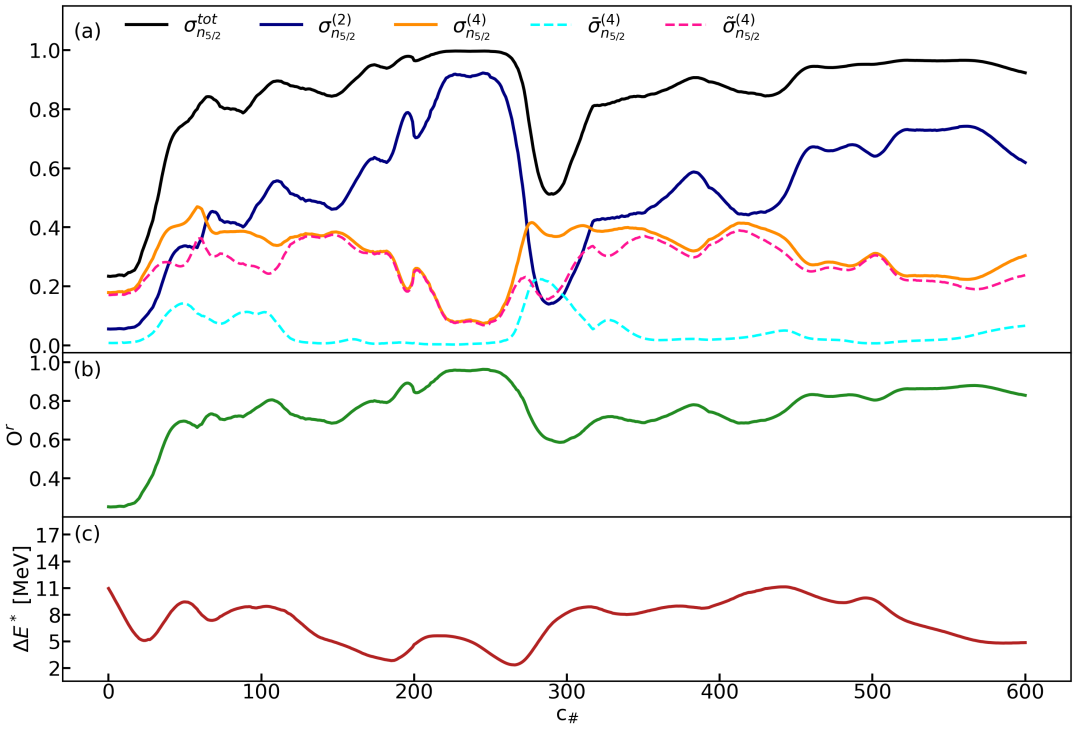

Figure 3.24: Behavior of the quantities ΔE^*, O^r, $\sigma^{(2)}$,$\bar{\sigma}^{(4)}$, $\tilde{\sigma}^{(4)}$, $\sigma^{(4)}$ and σ^{tot} with respect to $c_\#$ in the neutron variational excitation associated with $\Omega = 5/2$. Panel (a): $\sigma^{(2)}$,$\bar{\sigma}^{(4)}$, $\tilde{\sigma}^{(4)}$, $\sigma^{(4)}$ and σ^{tot} with respect to $c_\#$. Panel (b): O^r with respect to $c_\#$. Panel (c): ΔE^* with respect to $c_\#$.

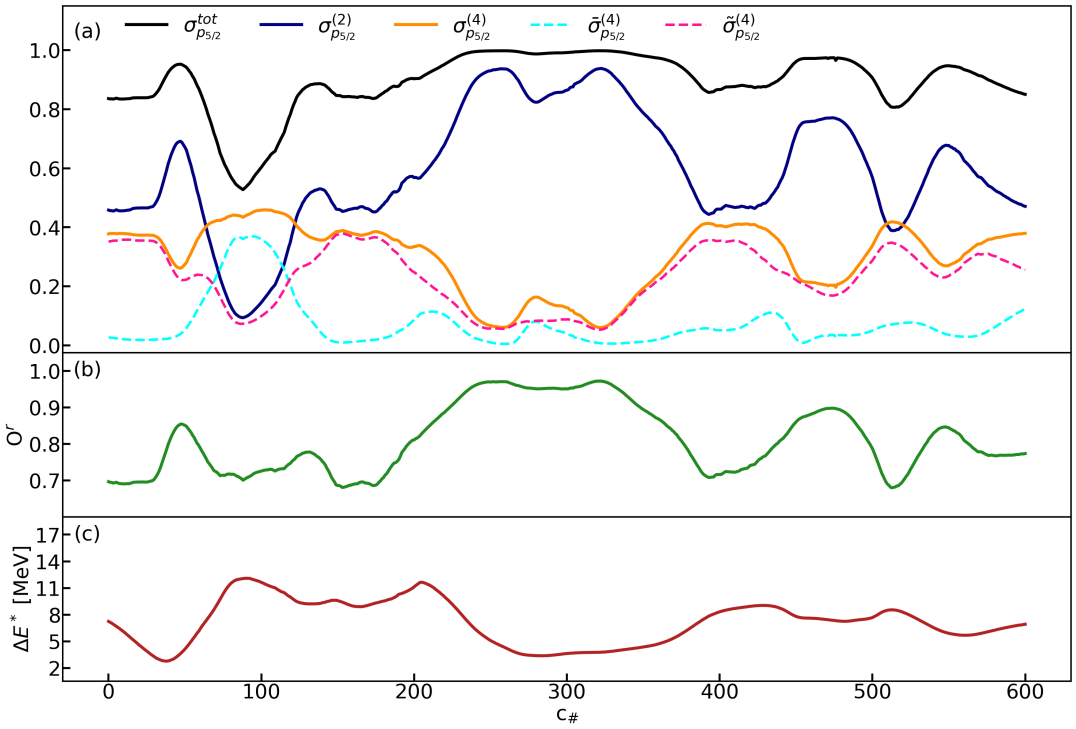

Figure 3.25: Behavior of the quantities ΔE^*, O^r, $\sigma^{(2)}$,$\bar{\sigma}^{(4)}$, $\tilde{\sigma}^{(4)}$, $\sigma^{(4)}$ and σ^{tot} with respect to $c_\#$ in the proton variational excitation associated with $\Omega = 5/2$. Panel (a): $\sigma^{(2)}$,$\bar{\sigma}^{(4)}$, $\tilde{\sigma}^{(4)}$, $\sigma^{(4)}$ and σ^{tot} with respect to $c_\#$. Panel (b): O^r with respect to $c_\#$. Panel (c): ΔE^* with respect to $c_\#$.

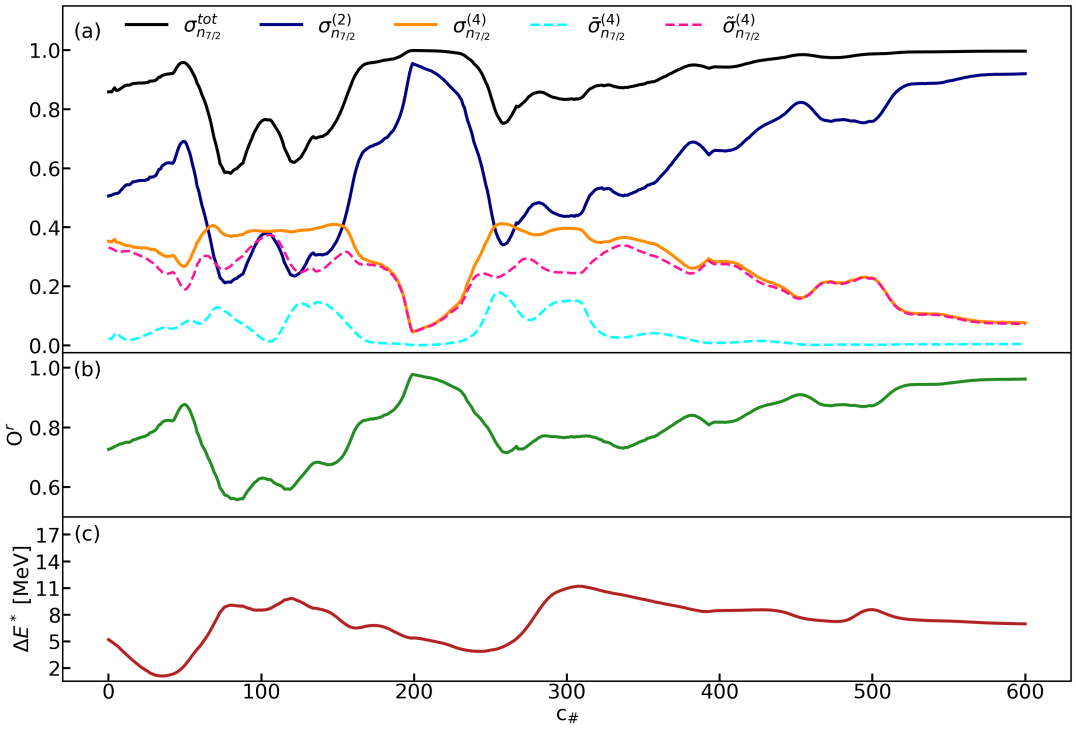

Figure 3.26: Behavior of the quantities ΔE^*, O^r, $\sigma^{(2)}$,$\bar{\sigma}^{(4)}$, $\tilde{\sigma}^{(4)}$, $\sigma^{(4)}$ and σ^{tot} with respect to $c_\#$ in the neutron variational excitation associated with $\Omega = 7/2$. Panel (a): $\sigma^{(2)}$,$\bar{\sigma}^{(4)}$, $\tilde{\sigma}^{(4)}$, $\sigma^{(4)}$ and σ^{tot} with respect to $c_\#$. Panel (b): O^r with respect to $c_\#$. Panel (c): ΔE^* with respect to $c_\#$.

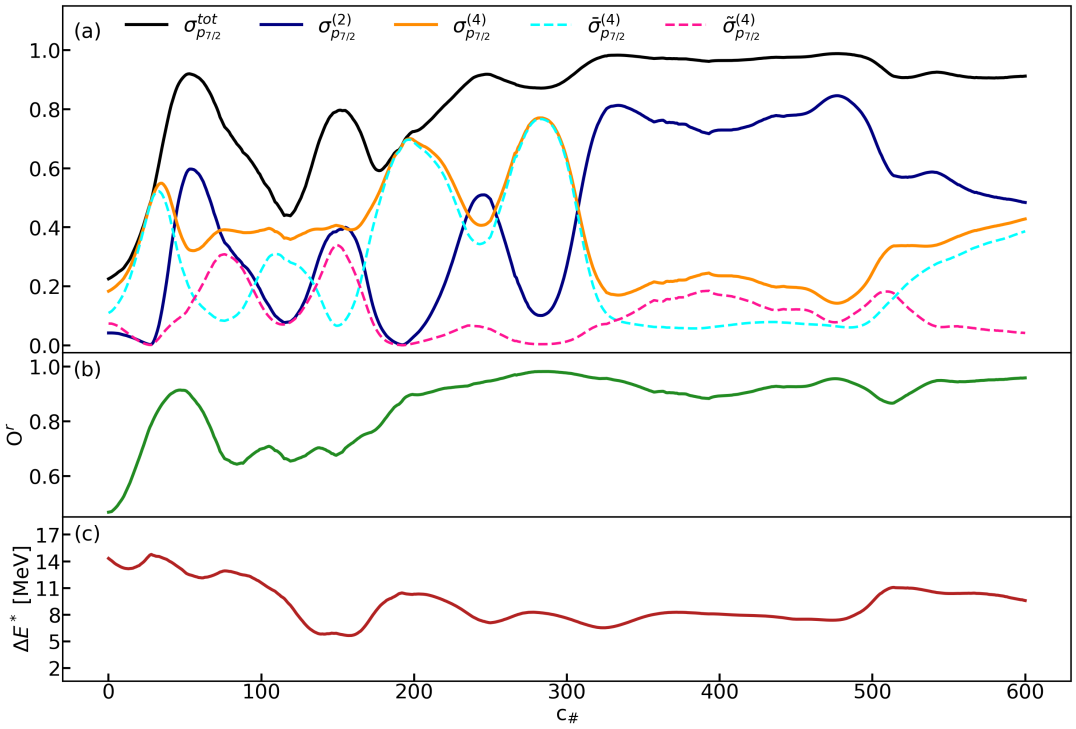

Figure 3.27: Behavior of the quantities ΔE^*, O^r, $\sigma^{(2)}$,$\bar{\sigma}^{(4)}$, $\tilde{\sigma}^{(4)}$, $\sigma^{(4)}$ and σ^{tot} with respect to $c_\#$ in the proton variational excitation associated with $\Omega = 7/2$. Panel (a): $\sigma^{(2)}$,$\bar{\sigma}^{(4)}$, $\tilde{\sigma}^{(4)}$, $\sigma^{(4)}$ and σ^{tot} with respect to $c_\#$. Panel (b): O^r with respect to $c_\#$. Panel (c): ΔE^* with respect to $c_\#$.

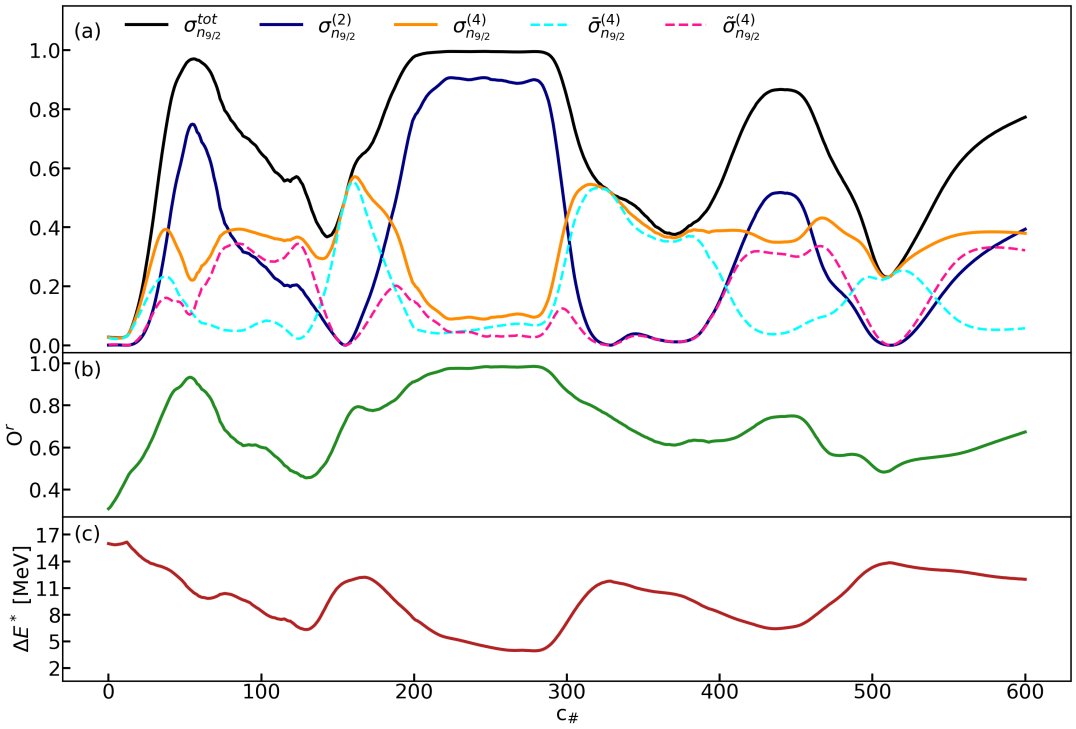

Figure 3.28: Behavior of the quantities ΔE^*, O^r, $\sigma^{(2)}$,$\bar{\sigma}^{(4)}$, $\tilde{\sigma}^{(4)}$, $\sigma^{(4)}$ and σ^{tot} with respect to $c_\#$ in the neutron variational excitation associated with $\Omega = 9/2$. Panel (a): $\sigma^{(2)}$,$\bar{\sigma}^{(4)}$, $\tilde{\sigma}^{(4)}$, $\sigma^{(4)}$ and σ^{tot} with respect to $c_\#$. Panel (b): O^r with respect to $c_\#$. Panel (c): ΔE^* with respect to $c_\#$.

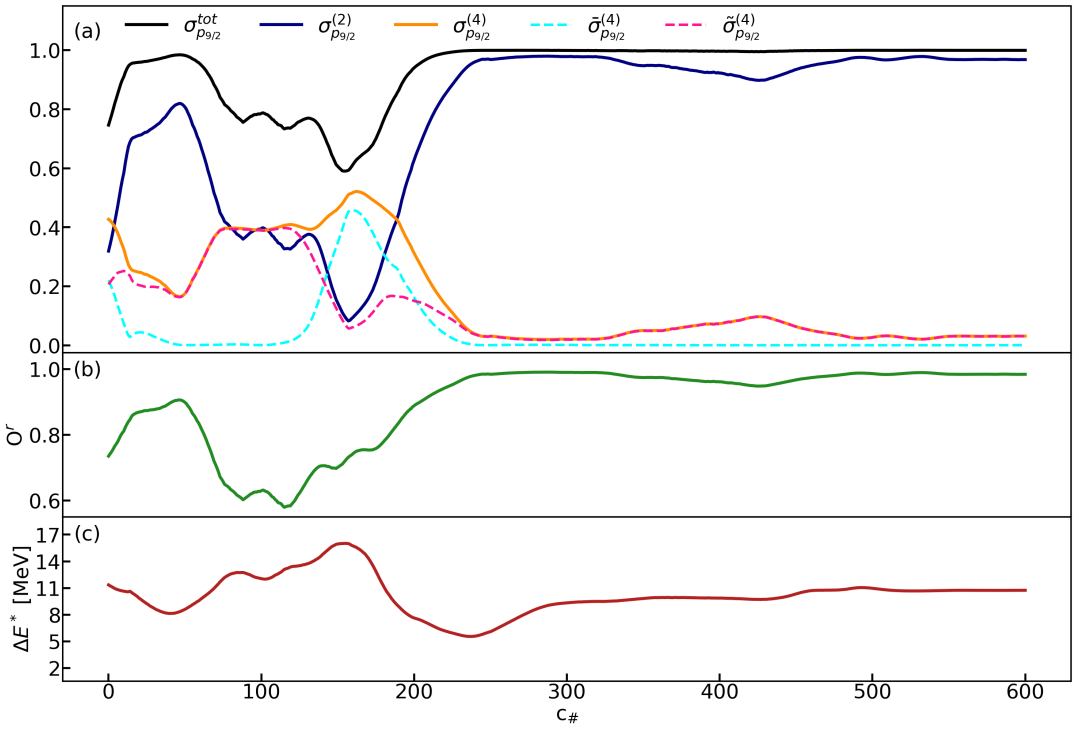

Figure 3.29: Behavior of the quantities ΔE^*, O^r, $\sigma^{(2)}$,$\bar{\sigma}^{(4)}$, $\tilde{\sigma}^{(4)}$, $\sigma^{(4)}$ and σ^{tot} with respect to $c_\#$ in the proton variational excitation associated with $\Omega = 9/2$. Panel (a): $\sigma^{(2)}$,$\bar{\sigma}^{(4)}$, $\tilde{\sigma}^{(4)}$, $\sigma^{(4)}$ and σ^{tot} with respect to $c_\#$. Panel (b): O^r with respect to $c_\#$. Panel (c): ΔE^* with respect to $c_\#$.

The first thing we notice in these figures is that the 2 and 4-quasiparticle decomposition is usually more than sufficient to describe a relatively large proportion of the variational excitations considered. Moreover, we can see that some excitations behave very stably as they pass through the scission (around $c_{\#} = 495$), as in Figures (3.24),(3.26),(3.27) and (3.29) while the composition of others are much less stable, as in Figures (3.20),(3.21),(3.22),(3.23) and (3.28).
This observation led us to formulate an hypothesis on the nature of variational excitations. We think that some of them tend to couple the two pre-fragments while others act almost independently on each pre-fragment. If this were the case, the structure of the excitations coupling the pre-fragments would be strongly linked to that of the compound nucleus. We therefore easily understand why the scission would lead to particularly violent structural changes for these variational excitations. In contrast, the variational excitations acting independently in each pre-fragment would naturally be less subject to structural changes upon scission. This hypothesis is discussed in more details in the following.

Regarding the other analyzes that can be made with the data presented in Figures (3.20-3.29), we judged that it is preferable to gather all the data in such a way as to underline more clearly the links between the various quantities studied. In panel (a) of Figure (3.30), we've represented the quantity $\sigma^{(2)}$ as a function of O^r for all the data collected. In panel (b), we've displayed the curve illustrating the relation linking these two quantities presented in Eq.(3.25):

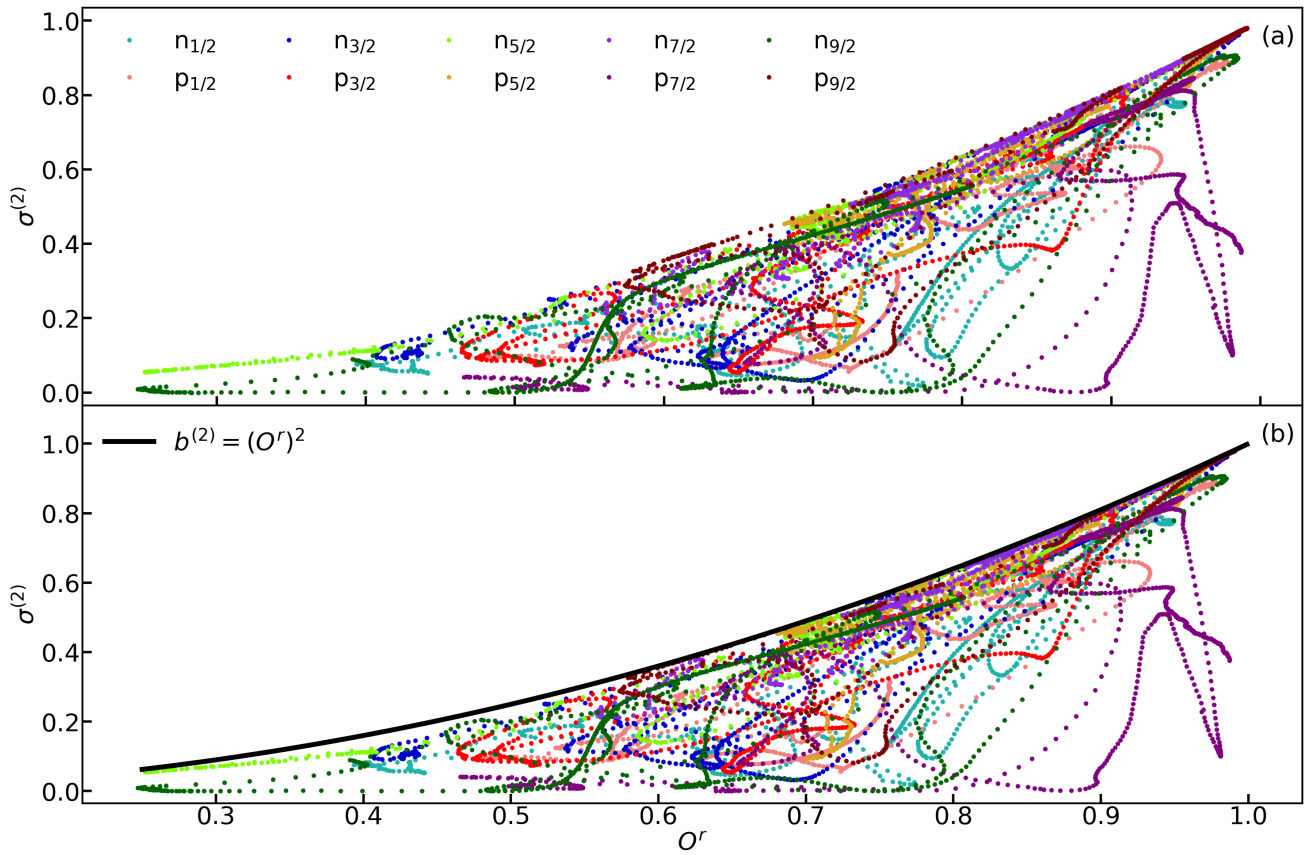

Figure 3.30: Panel (a): study of the relation between the quantities $\sigma^{(2)}$ and O^r. Panel (b): illustration of an important property linking these two quantities.

In panel (a), we clearly see that the larger O^r is, the larger $\sigma^{(2)}$ tends to be as well. Furthermore, we observe in panel (b) that the inequality given in Eq. (3.25) is perfectly verified. In section 3.3 we hypothesized that the differences between $\sigma^{(2)}$ and its boundary $b^{(2)}$ could be explained by the excitation energy ΔE^*. To check this assumption, we introduce the quantity $\delta^{(2)}$, defined as follows:

$$\boxed{\delta^{(2)} = \frac{b^{(2)} - \sigma^{(2)}}{b^{(2)}}} \tag{3.47}$$

This quantity measures the relative difference between $\sigma^{(2)}$ and its boundary $b^{(2)}$. In Figure (3.31), we plotted the excitation energy ΔE^* as a function of the quantity $\delta^{(2)}$ for all the data collected:

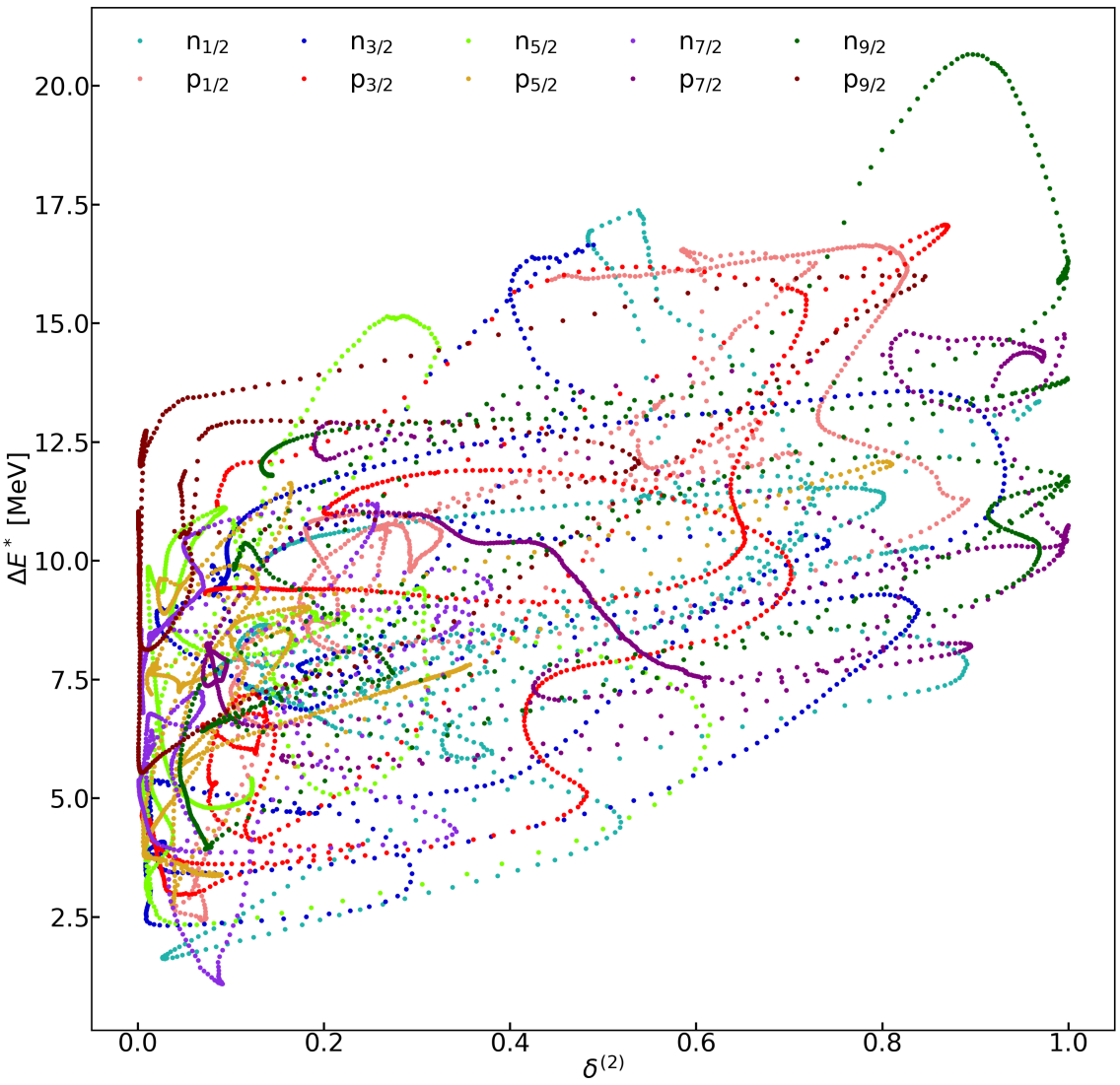

Figure 3.31: Evolution of the quantity ΔE^* with respect to $\delta^{(2)}$.

We clearly observe a correlation between the two quantities. In particular, we observe that larger values of $\delta^{(2)}$, associated with $\sigma^{(2)}$ values relatively far from their boundaries, are obtained only from a certain excitation energy threshold.

Besides, we could improve the quality of the description by working on the renormalization of the excitation energy. In Figure (3.31), we implicitly consider that the excitations energies are comparable at different deformations and for different Ω, which is not necessarily the case. Indeed, the excitation energy for which we consider that an excitation is a low-energy one is not the same at the scission and at the saddle point for example. The same goes for the different values of Ω.

In panel (a), Figure (3.32), we studied the link between the values of $\sigma^{(4)}$ and their boundaries $b^{(4)}$. Besides, we have illustrated the inequality given in Eq.(3.30). In panel (b), we displayed the excitation energy with respect to the relative difference $\delta^{(4)}$ between $\sigma^{(4)}$ and $b^{(4)}$. This relative difference reads as follows:

$$\boxed{\delta^{(4)} = \frac{b^{(4)} - \sigma^{(4)}}{b^{(4)}}} \tag{3.48}$$

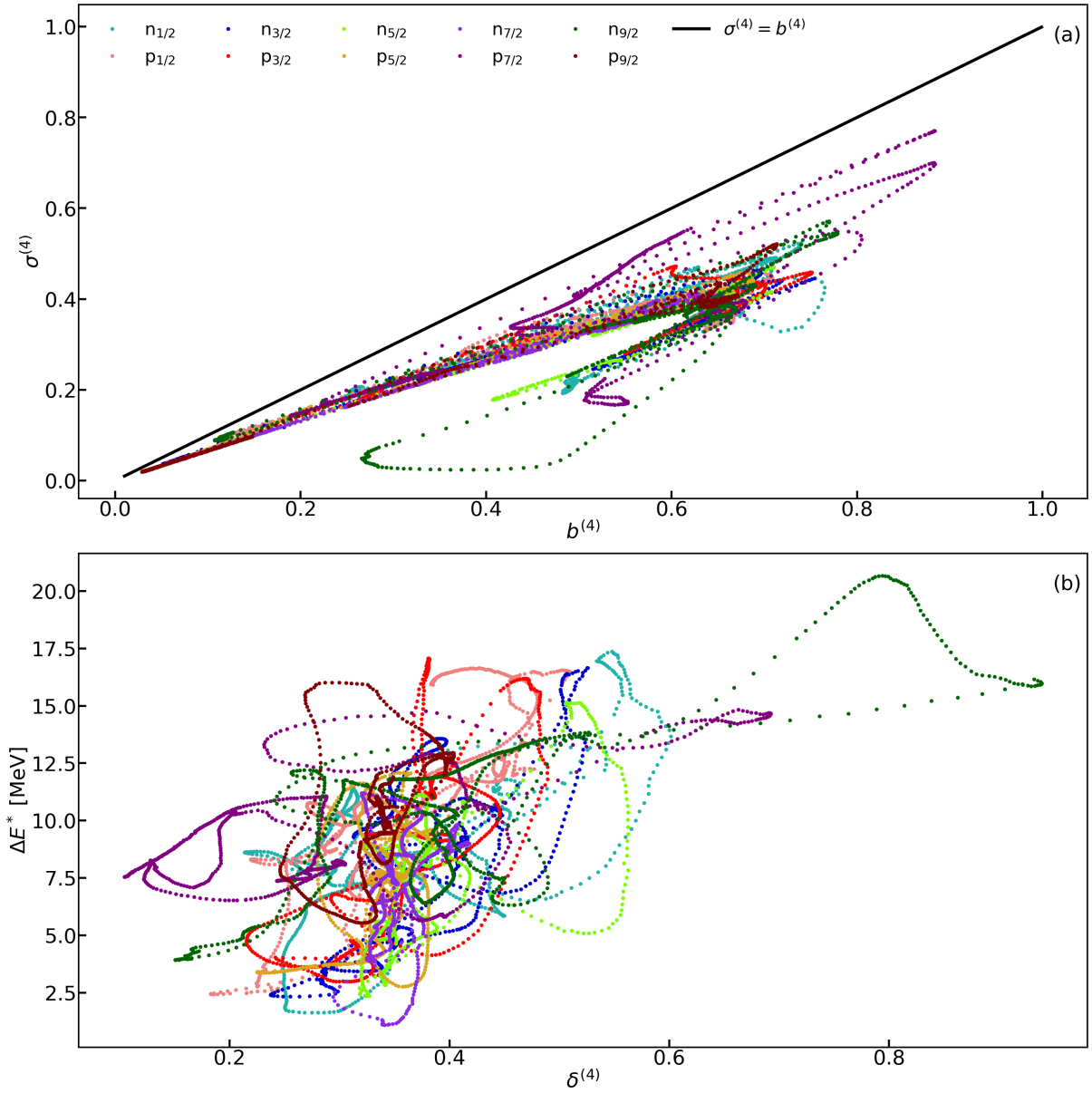

Figure 3.32: Panel (a): evolution of $\sigma^{(4)}$ with respect to $b^{(4)}$. Panel (b): evolution of the excitation energy ΔE^* with respect to the relative difference $\delta(4)$ between $\sigma^{(4)}$ and $b^{(4)}$

In panel (a), we clearly see that the values of $\sigma^{(4)}$ tend to be overall closer to their boundaries than the values of $\sigma^{(2)}$ were. We attribute this phenomenon to the fact that the excitation energy is probably often above the excitation energy threshold relevant for the 2-quasiparticle excitation but much less often above the 4-quasiparticle excitation energy threshold. For the rest, finer behaviors are observed in the study of $\bar{\sigma}^{(4)}$ and $\tilde{\sigma}^{(4)}$, which is carried out below.
In panel (b), we observe as expected a correlation between the relative difference between $\sigma^{(4)}$ and $b^{(4)}$ and the excitation energy ΔE^*. Overall, the higher the excitation energy, the bigger the relative difference $\delta^{(4)}$.

Figure (3.33) is dedicated to the study of $\bar{\sigma}^{(4)}$. This plot is perculiar insofar as we first study $\sigma^{(2)}$ with respect to $b^{(2)}$ in panel (a), then $\bar{\sigma}^{(4)}$ with respect to $b^{(2)}$ in panel (b) and finally the sum $\sigma^{(2)} + \bar{\sigma}^{(4)}$ in panel (c). The reason of this choice is connected to the form of the different $\bar{\sigma}^{(2n)}$ values, which stand for the fully diagonal 2n-quasiparticle content of the variational excitations. Indeed, $\bar{\sigma}^{(2n)}$ reads:

$$\boxed{\bar{\sigma}^{2n} = c_n (O^r)^2 \sum_{i_1 j_1} ... \sum_{i_n j_n} |\langle \Phi^{*\Omega^*} | \xi^{+\tau^*\Omega^*}_{i_1} \bar{\xi}^{+\tau^*\Omega^*}_{j_1} ... \xi^{+\tau^*\Omega^*}_{i_n} \bar{\xi}^{+\tau^*\Omega^*}_{j_n} | \Phi^{\tau^*\Omega^*} \rangle|^2} \tag{3.49}$$

Here, the coefficient c_n account for the double counting of the 2n-quasiparticle excitations. As a direct consequence of Eq.(3.49), the following relation holds:

$$\boxed{\sum_{n=1} \bar{\sigma}^{(2n)} \leq (O^r)^2 = b^{(2)}} \tag{3.50}$$

Here, of course, $\bar{\sigma}^{(2)} = \sigma^{(2)}$. In the light of Eq.(3.50), we thought that it could be interesting to see how close we can get from the boundary $(O^r)^2$, adding progressively new terms in the sum:

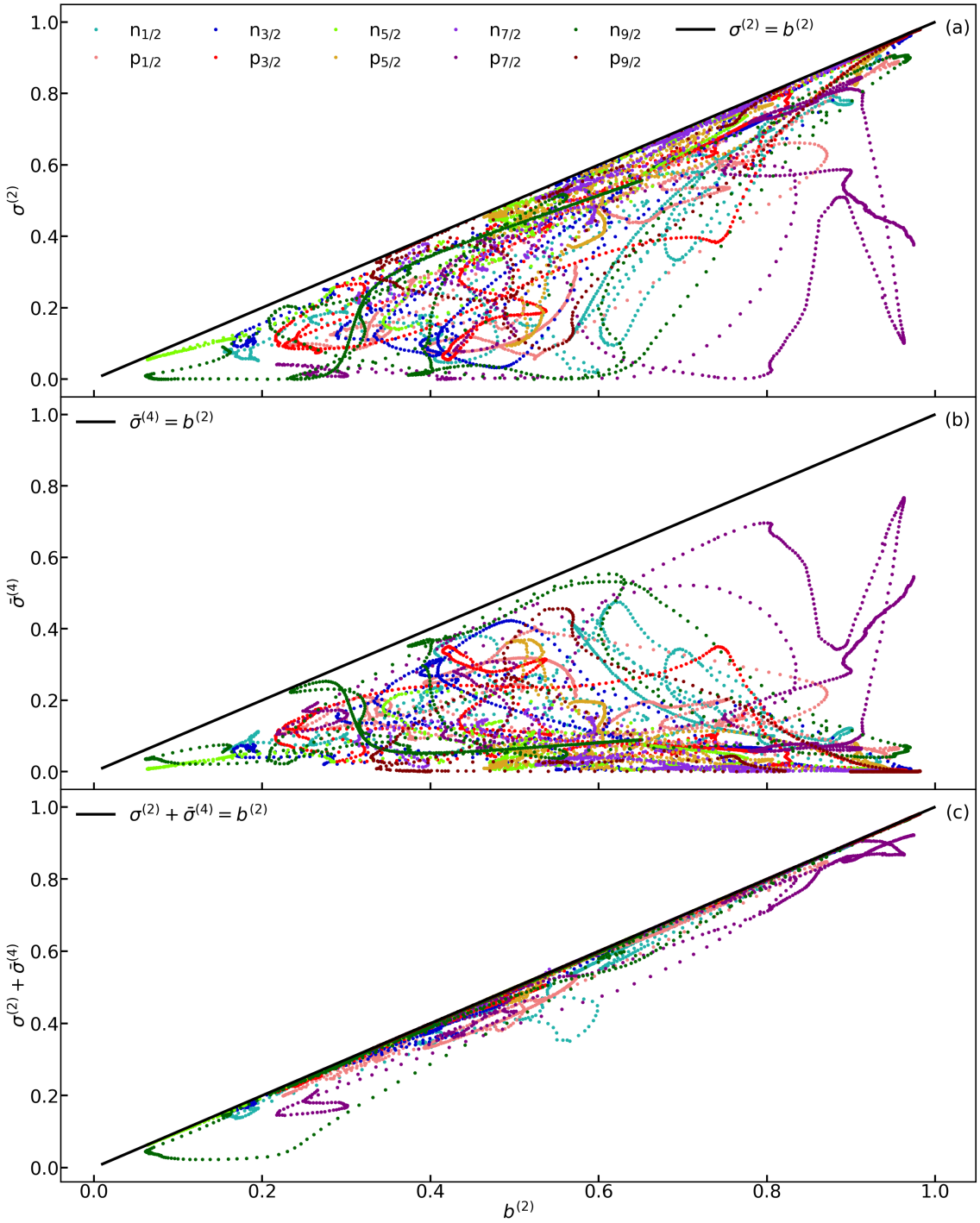

Figure 3.33: Study of the complementarity of $\sigma^{(2)}$ and $\bar{\sigma}^{(4)}$. Panel (a): $\sigma^{(2)}$ with respect to $b^{(2)}$. Panel (b): $\bar{\sigma}^{(4)}$ with respect to $b^{(2)}$. Panel (c): $\sigma^{(2)} + \bar{\sigma}^{(4)}$ with respect to $b^{(2)}$.

The results obtained in Figure (3.33) are striking. Indeed, as the full sum of the $\bar{\sigma}^{(2n)}$ is bounded by $b^{(2)}$, the vicinity of the colored points with the black curve in panel (c) directly means that most of the "diagonal" part of the variational excitation is accurately described by the 2- and 4-quasiparticle excitations. It signifies that the differences between σ^{tot} and 1 have mostly to be attributed to the "off-diagonal" part of the variational excitations, which is directly related to the purity of the latter. Thus, we can legitimately think that the 2n-quasiparticle structure of our variational excitations with $n > 2$ does not account for a too high excitation energy, but for their lack of purity. Consequently, these results suggest that the variational excitations created have most of the time an excitation energy which ranges

between the typical excitation energies of the 2-quasiparticle and 4-quasiparticle excitations. It reinforces the assumption that our variational excitations are relevant to describe the low-lying intrinsicly excited states of the nucleus.
Then, we wanted to quantify the excitation energy dependence of the quantities $\sigma^{(2)}$, $\bar{\sigma}^{(4)}$ and of the sum $\sigma^{(2)}+\bar{\sigma}^{(4)}$. To do so, we defined the relative differences $\bar{\delta}^{(4)}$ and $\bar{\delta}^{tot}$ as follows:

$$\boxed{\bar{\delta}^{(4)} = \frac{b^{(2)} - \bar{\sigma}^{(4)}}{b^{(2)}}} \qquad \boxed{\bar{\delta}^{tot} = \frac{b^{(2)} - (\sigma^{(2)} + \bar{\sigma}^{(4)})}{b^{(2)}}} \tag{3.51}$$

In Figure (3.34), we've studied the complementarity of $\sigma^{(2)}$ and $\bar{\sigma}^{(4)}$ with respect to the excitation energy ΔE^*. In panel (a), we have plotted the excitation energy ΔE^* with respect to the relative difference $\delta^{(2)}$. In panel (b), we have displayed the excitation energy ΔE^* with respect to the relative difference $\bar{\delta}^{(4)}$. Finally, in panel (c), we have represented the excitation energy ΔE^* with respect to the relative difference $\bar{\delta}^{tot}$.

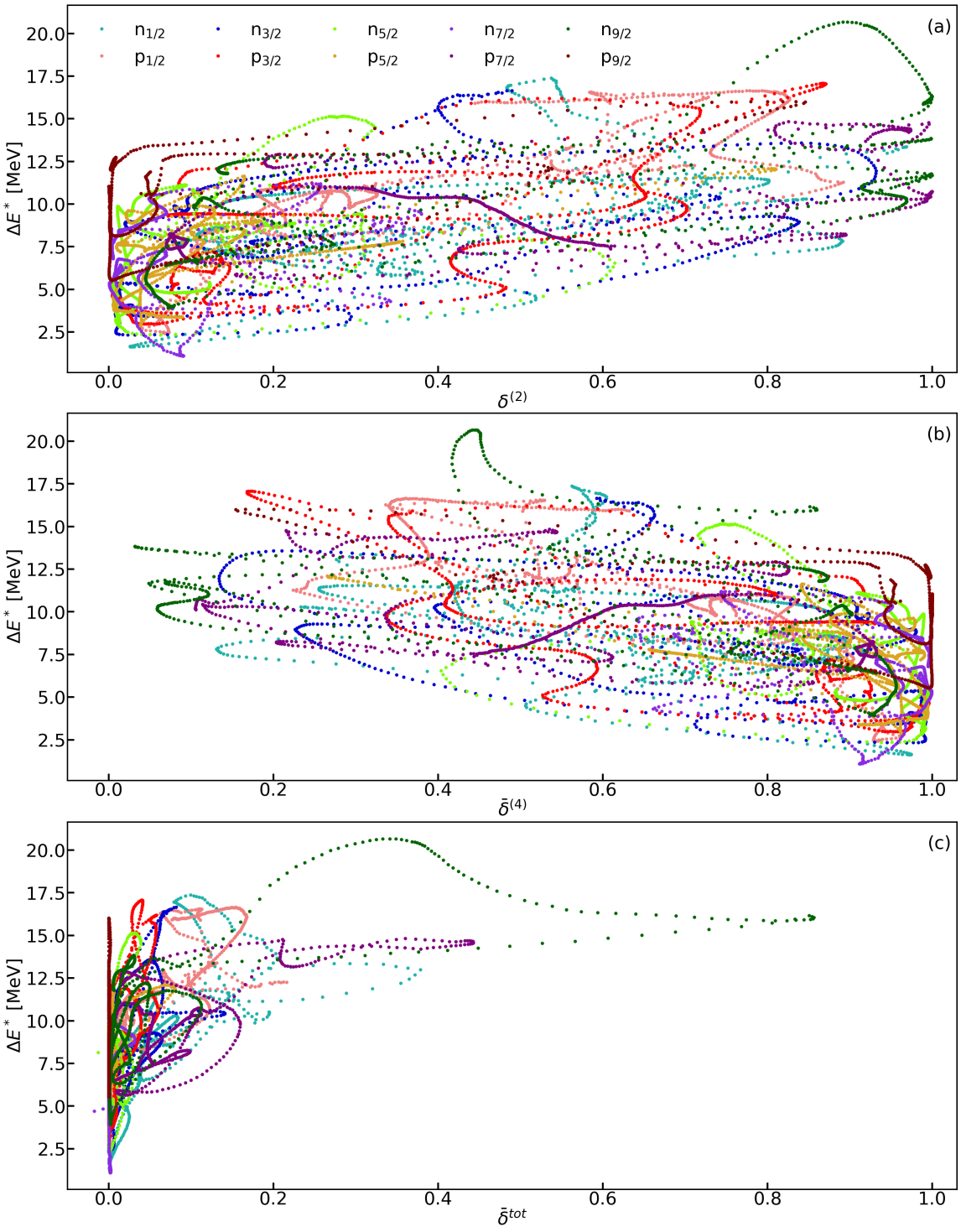

Figure 3.34: Study of the complementarity of $\sigma^{(2)}$ and $\bar{\sigma}^{(4)}$ with respect to the excitation energy ΔE^*. Panel (a): $\delta^{(2)}$ with respect to ΔE^*. Panel (b): $\bar{\delta}^{(4)}$ with respect to ΔE^*. Panel (c): $\bar{\delta}^{tot}$ with respect to ΔE^*.

The results displayed in Figure (3.34) tend to confirm the hypotheses made on the influence of the excitation energy on the content of the variational excitations. Indeed, we observe in panel (a) that a lower excitation energy tends to reduce the difference between $\sigma^{(2)}$ and $b^{(2)}$. On the contrary, in panel (b), we see the inverse situation where higher excitation energies favor a smaller difference between $\bar{\sigma}^{(4)}$ and $b^{(2)}$. To conclude, the results displayed in panel (c) show that the situations when the 2 and 4-quasiparticle excitations are not enough to describe the "diagonal" structure of the variational excitations are related to higher excita-

tions energies. In particular, we observe that the "diagonal" part of the variational excited states whose excitation energy is smaller than 10 MeV are composed of 2 and 4-quasiparticle excitations at 80% or more.

In the panel (a) of Figure (3.35), we've displayed the values of $\tilde{\sigma}^{(4)}$ with respect to their boundaries $\tilde{b}^{(4)}$, and we've illustrated the inequality given in Eq.(3.42). In panel (b), we've studied the relation between ΔE^* and the relative difference $\tilde{\delta}^{(4)}$ defined as follows:

$$\boxed{\tilde{\delta}^{(4)} = \frac{\tilde{b}^{(4)} - \tilde{\sigma}^{(4)}}{\tilde{b}^{(4)}}} \tag{3.52}$$

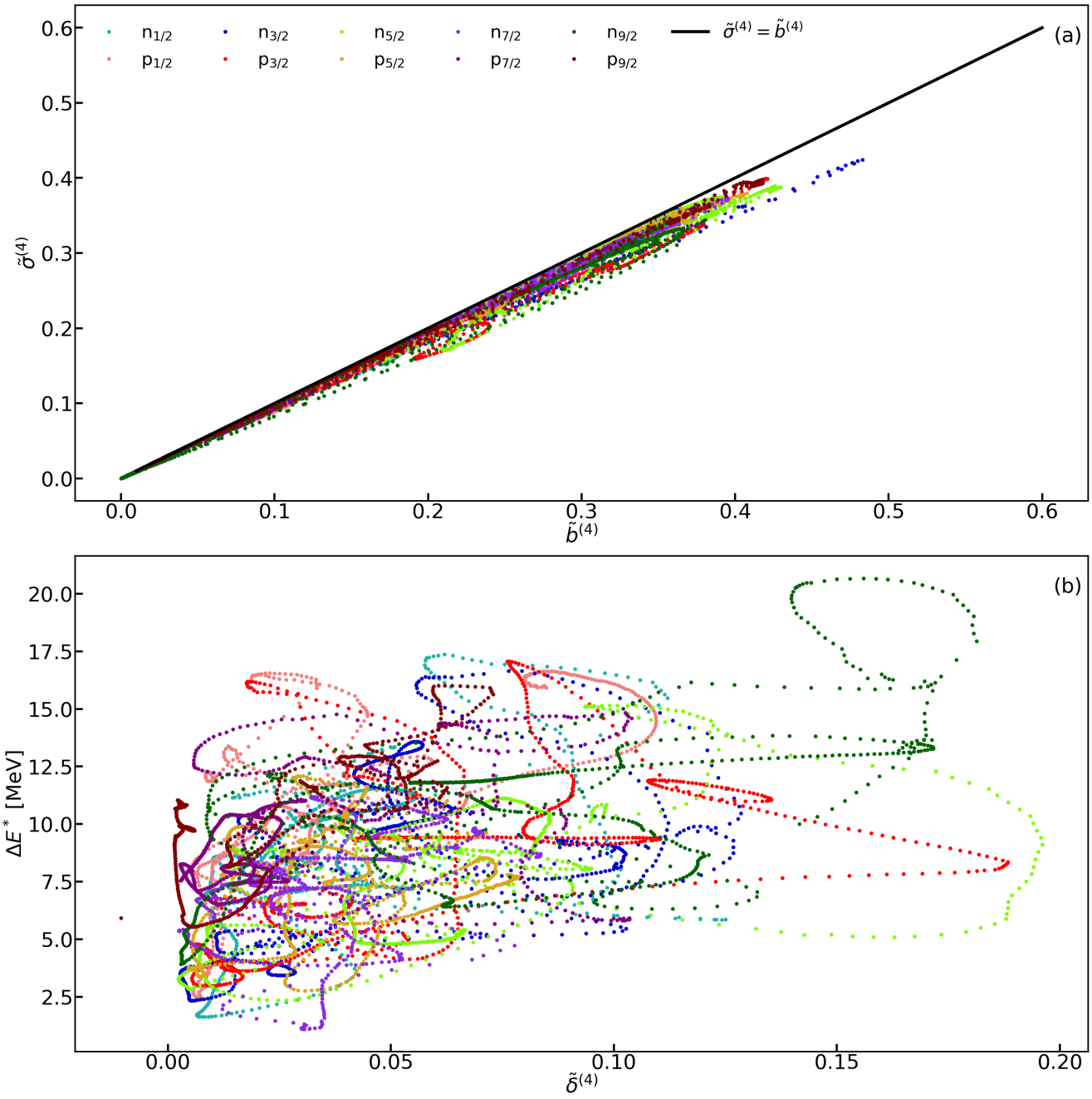

Figure 3.35: Panel (a): evolution of $\tilde{\sigma}^{(4)}$ with respect to $\tilde{b}^{(4)}$. Panel (b): evolution of the excitation energy ΔE^* with respect to the relative difference $\tilde{\delta}(4)$ between $\tilde{\sigma}^{(4)}$ and $\tilde{b}^{(4)}$

We observe in panel (a) that the values of $\tilde{\sigma}^{(4)}$ are most of the time very close to their boundaries $\tilde{b}^{(4)}$. This result suggests that the quantities $\tilde{b}^{(2n)}$ are probably very useful to estimate the additional content of the "non-diagonal" part of the variational excitations we could describe increasing the quasiparticles excitation order.
In panel (b), we globally remark that the values of $\tilde{\sigma}^{(4)}$ depend slightly less on the excitation energy than the ones of $\sigma^{(2)}$ (Figure (3.31)) and much more less than the ones of $\bar{\sigma}^{(4)}$ (Figure (3.34)). These observations are in line with the assumptions we made. Indeed, we assumed that the values of $\bar{\sigma}^{(4)}$ are mostly explained by the excitation energy ΔE^*, while the ones of $\tilde{\sigma}^{(4)}$ account mostly for the variational excitation purity.
To check the latter statement on the purity dependence of the values of the values $\tilde{\sigma}^{(4)}$, we displayed in Figure (3.36) the values of $\tilde{\sigma}^{(4)}$ with respect to O^r:

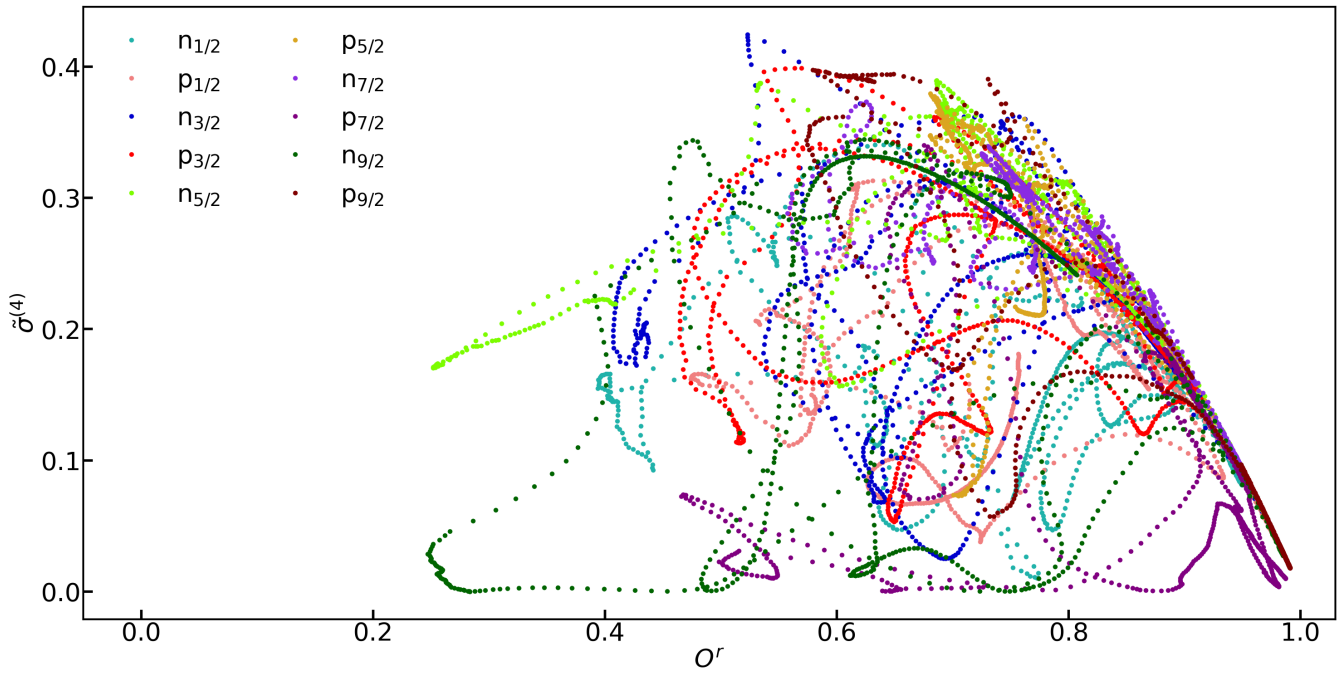

Figure 3.36: Illusation of the relation between $\tilde{\sigma}^{(4)}$ and O^r.

As expected, $\tilde{\sigma}^{(4)}$ tends to zero as the variational excitations get purer. Moreover, it is interesting to note that the larger values of $\tilde{\sigma}^{(4)}$ are found especially for values of O^r ranging between 0.5 and 0.9. The maxium value of $\tilde{\sigma}^{(4)}$ corresponds to $O^r = 0.575$.
This phenomenon is not difficult to explain. Indeed, $\tilde{\sigma}^{(4)}$ describes the orthogonality couplings between the constrained (Ω^*,τ^*) subspace and exactly one other unconstrained (Ω,τ) subspace. On the one hand, when O^r is close to one, these couplings do not exist. On the other hand, if O^r is too small, it means that probably more than one unconstrained (Ω^*,τ^*) subspaces are simultaneously strongly coupled. In that case, higher quasiparticles excitation orders would be more relevant to describe the "non-diagonal" part of the variational excitations.

In Figure (3.37), we've studied the quantity σ^{tot} while presenting a synthesis of certain of the most relevant observations made previously. In panel (a), we've displayed the values of $\sigma^{(2)}$ with respect to both the quantity O^r and the excitation energy ΔE^*. In panel (b), we've represented the values of $\sigma^{(4)}$ with respect to both the quantity O^r and the excitation energy ΔE^*. Finally, in panel (c), we've shown the values of σ^{tot} with respect to both the quantity O^r and the excitation energy ΔE^*:

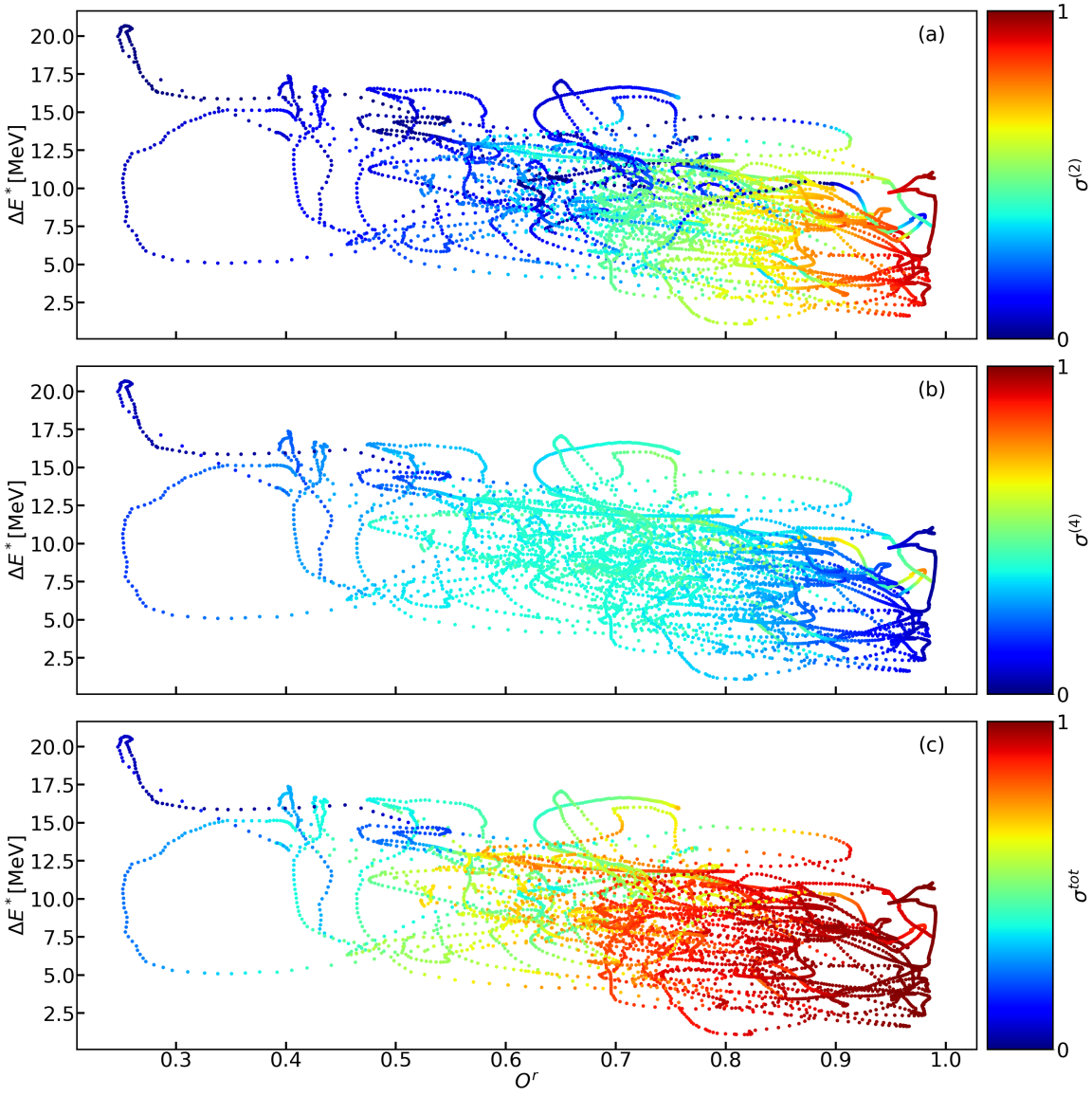

Figure 3.37: Study of σ^{tot} and synthesis of relevant properties concerning the variational excitations content. Panel (a): values of $\sigma^{(2)}$ with respect to both O^r and the excitation energy ΔE^*. Panel (b): values of $\sigma^{(4)}$ with respect to both O^r and the excitation energy ΔE^*. Panel (c): values of σ^{tot} with respect to both O^r and the excitation energy ΔE^*.

In panel (a), we observe that the higher values of $\sigma^{(2)}$ are found at relatively low excitation energies and for values of O^r close to one. It means that the 2-quasiparticle decomposition is particularly relevant when the variational excitations considered are very pure with a relatively low excitation energy.
In panel (b), we remark that the higher values of $\sigma^{(4)}$ are found at excitation energies greater than the ones relevant for $\sigma^{(2)}$. In addition, the values of $\sigma^{(4)}$ are higher when O^r ranges between 0.5 and 0.9 approximately. It means that the 4-quasiparticle decomposition is particularly relevant for variational excitations with both a rather mid-range excitation energy and purity.
In panel (c), we see the complementarity of $\sigma^{(2)}$ and $\sigma^{(4)}$. Indeed, the quantity $\sigma^{(4)}$ completes efficiently the relatively lower values of $\sigma^{(2)}$ found for both mid-range excitation energies and O^r values. In particular, we observe that for excitation energies up to 12.5 MeV and for values of O^r ranging between 0.7 and 1, the 2- and 4-quasiparticle excitations decomposition is very accurate to describe the variational excitations (σ^{tot} is globally greater than 0.8 in

this zone).

Finally, we investigated the link between the quantities $\sigma^{(2)}$ and $\sigma^{(4)}$. In figure (3.38), panel (a), we have displayed $\sigma^{(4)}$ as a function of $\sigma^{(2)}$. In panel (b), we've illustrated some relevant relations observed:

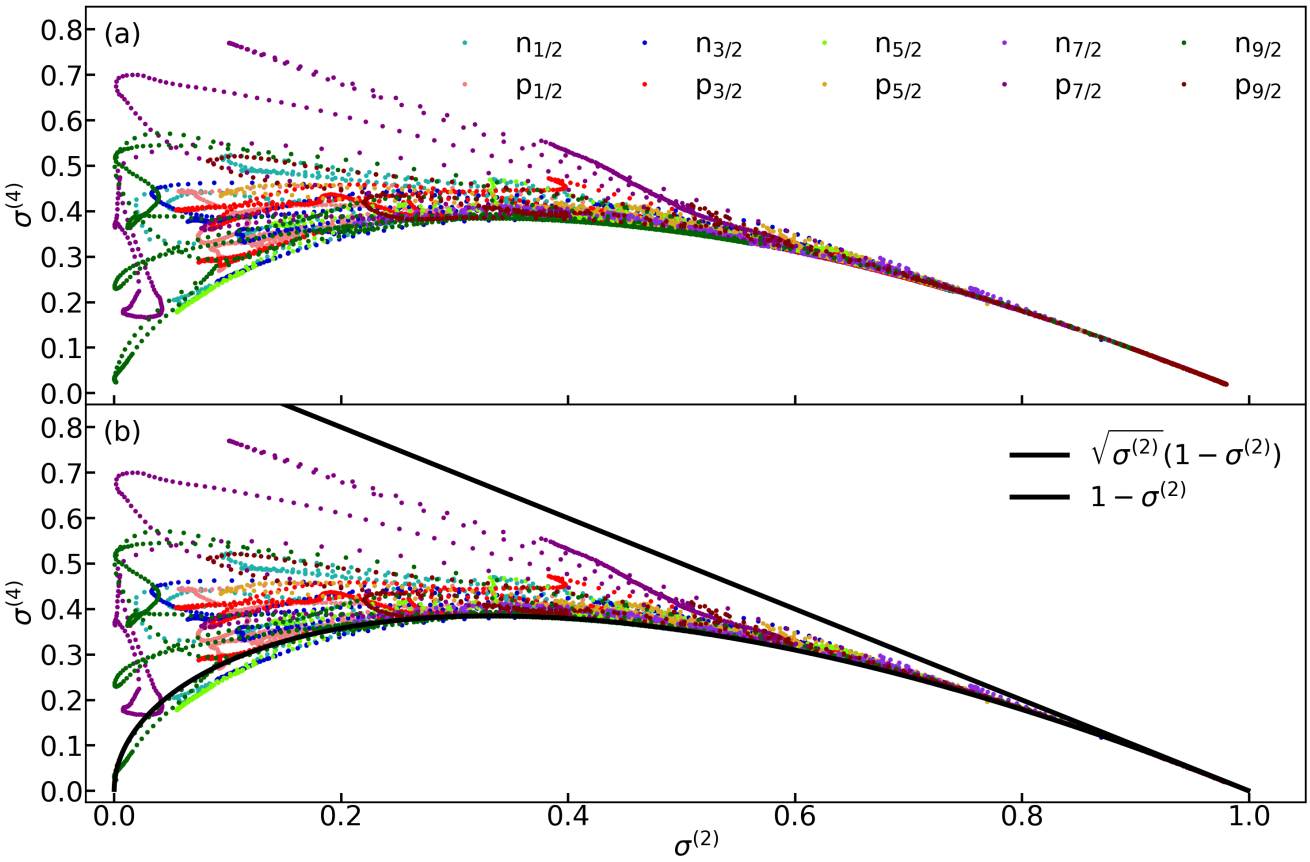

Figure 3.38: Illustration of the correlations between the quantities $\sigma^{(4)}$ and $\sigma^{(2)}$. Panel (a): the quantity $\sigma^{(4)}$ with respect to the quantity $\sigma^{(2)}$. Panel (b): two interesting relations linking both quantities.

While the first relation $\sigma^{(4)} \leq (1-\sigma^{(2)})$ is trivial, the second $\sigma^{(4)} \geq \sqrt{\sigma^{(2)}}(1-\sigma^{(2)})$ is far less so, and we don't yet know how to explain it exactly. This second relation emphasizes that a certain proportion of 2-quasiparticle excitations necessarily implies a certain proportion of 4-quasiparticle excitations. This could be due to the interplay between the energy minimization and the level density structure of the low-energy quasiparticles excitations. But it could also reflect a requirement for the conservation of the HFB structure when summing quasiparticles excitations.

3.4.2 Regularity of the variational excitations overlap kernels

In order to make the SCIM work, the most important concern about these variational excited states is undoubtedly their regularity properties. In figure (3.39), we've plotted the diagonal overlap kernel moments of order zero of all the variational excitations along with the one of their associated adiabatic set with respect to $c_{\#}$. In addition, we've given the related GOA

approximation of these moments. In panel (a), we focused on the neutron isospin. In panel (b), the proton isospin is considered:

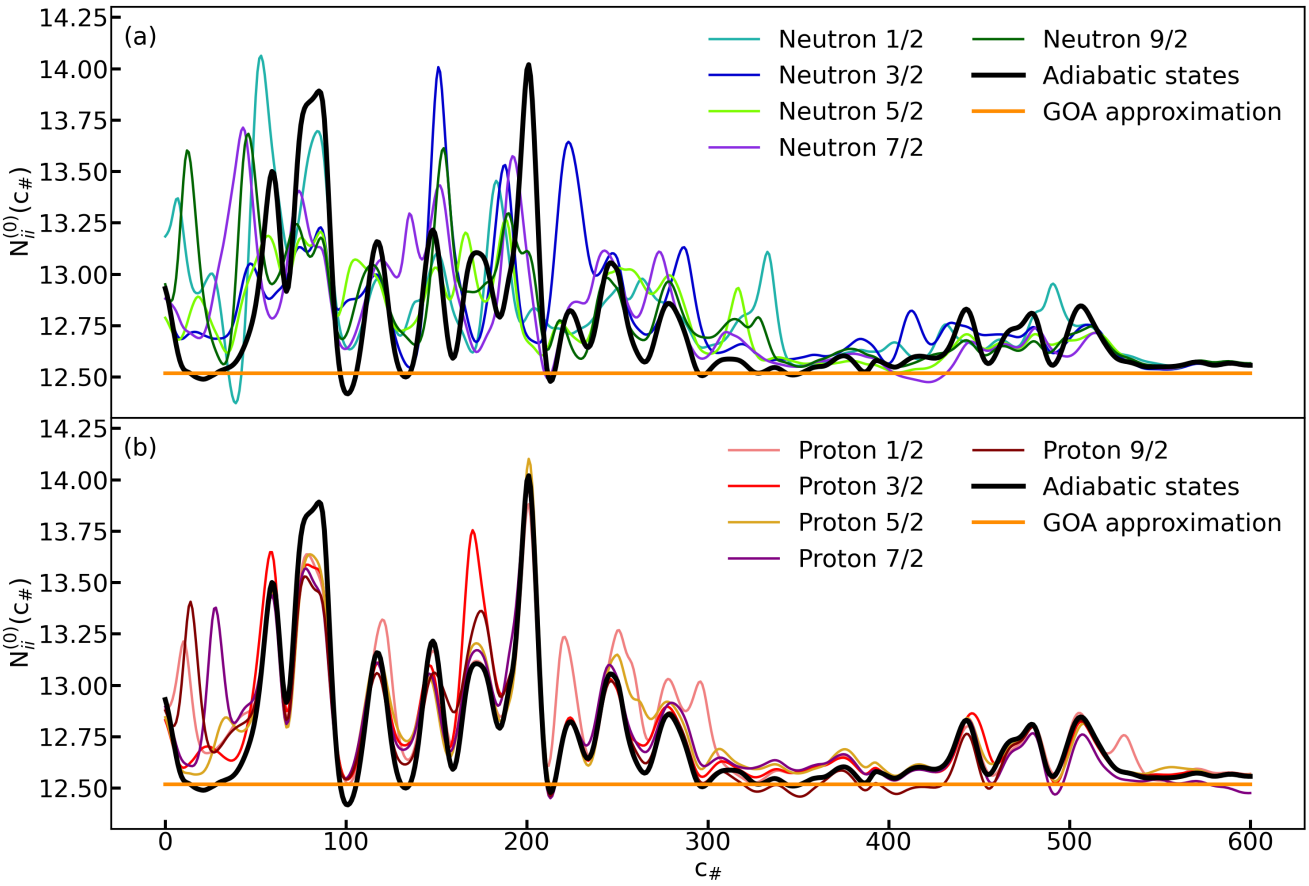

Figure 3.39: Diagonal overlap kernel moments of order zero of all the variational excitations along with the one of their associated adiabatic set and the related GOA approximation with respect to $c_\#$ in the ^{240}Pu. Panel (a): focus on the neutron isospin. Panel (b): focus on the proton isospin.

In Figure (3.39), we clearly observe that the regularity of the overlap kernels of the variational excitations is globally as good as the one of the adiabatic set. The question of whether this regularity is sufficient or not for the SCIM formalism is discussed in Chapter 6.
When it comes to the non-diagonal kernels, we have no reference to say whether their regularity is satisfactory or not. However, the moments of order 0 and 2 of the non-diagonal overlap kernels are in general from 1 to 4 order of magnitudes smaller than the diagonal ones. We therefore assume that their regularity is relatively less important. In practice, we never encountered problems in the dynamics associated with the non-diagonal quantities.

3.4.3 Regularity of the variational excitations Hamiltonian kernels

We have shown that the regularity of the overlap kernels of the variational excitations are as good as the one of the adiabatic set. However, we still have to prove that the same properties hold for the Hamiltonian ones. To do this, we investigated whether the approximation linking the Hamiltonian and overlap kernels at the adiabatic level displayed in Eq.(2.104) is still true for the variational excitations. Therefore, we considered the following quantities:

$$\Delta\hat{H}_{ii}(\bar{q}-s,\bar{q}+s) = 100 * |\frac{\langle\Phi_i(\bar{q}-s)|\hat{H}|\Phi_i(\bar{q}+s)\rangle - \langle\Phi_i(\bar{q}+s)|\Phi_i(\bar{q}+s)\rangle E_i(\bar{q})}{\langle\Phi_i(\bar{q}-s)|\hat{H}|\Phi_i(\bar{q}+s)\rangle}| \quad (3.53)$$

In Figure (3.40) we plotted $\Delta\hat{H}_{ii}$ for all the neutron variational excitations with respect to $\bar{q}$ and s:

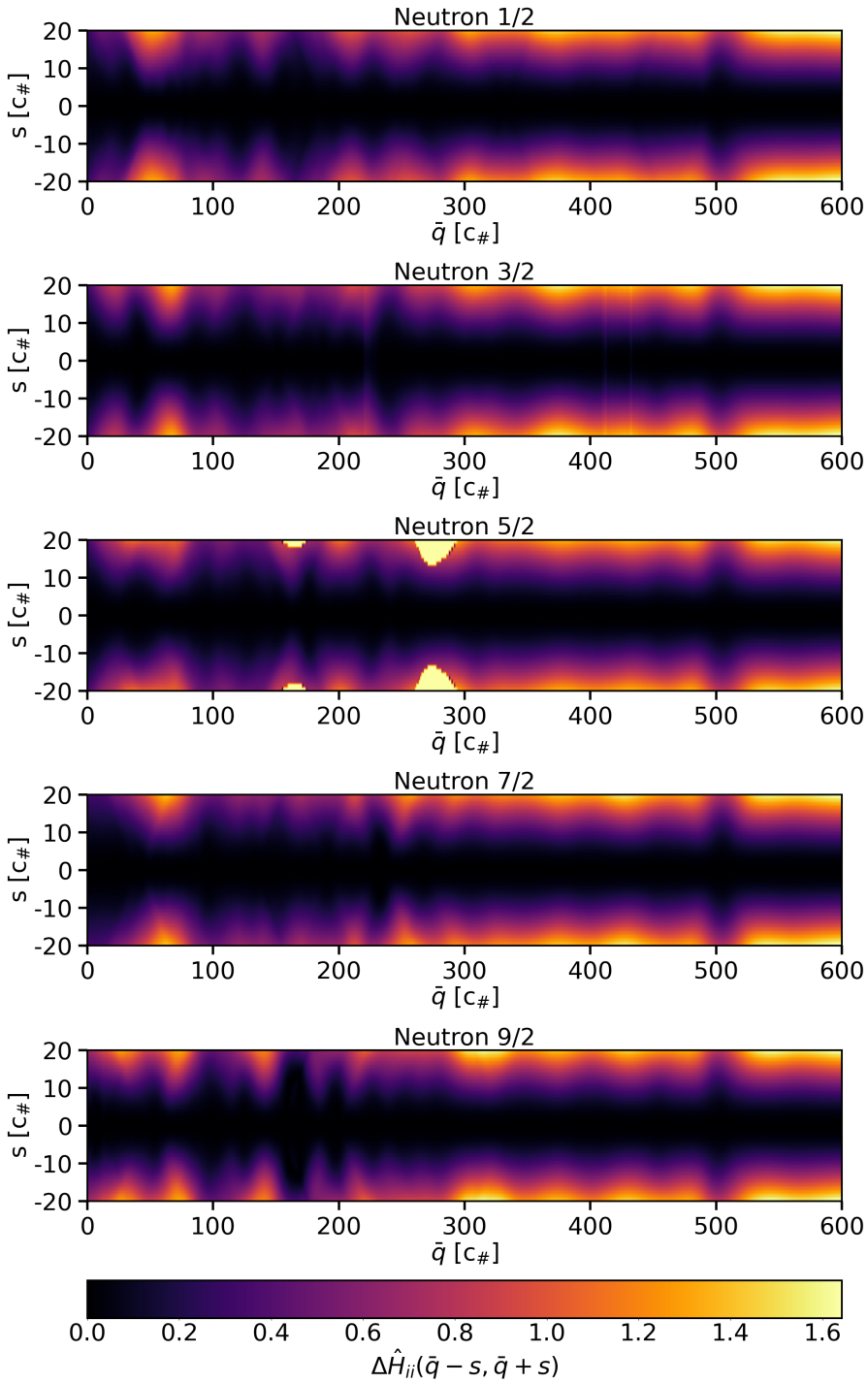

Figure 3.40: $\Delta\hat{H}_{ii}$ for all the neutron variational excitations with respect to $\bar{q}$ and s.

The overall behaviour is the same as in the adiabatic case. There is however one exception for the neutron variational excitation with $\Omega = 5/2$. Indeed, in that case, close to $\bar{q} = 270$

and for values of s such that $|s| > 13$, we found relatively huge differences of up to 77%. Given the large values taken by s, this phenomenon does not call into question the good regularity of the Hamiltonian kernels associated with this excitation. Nevertheless, we will see in Chapter 6 that this feature leads to consequences in the dynamics. In Figure (3.41) we plotted $\Delta\hat{H}_{ii}$ for all the proton variational excitations with respect to $\bar{q}$ and s:

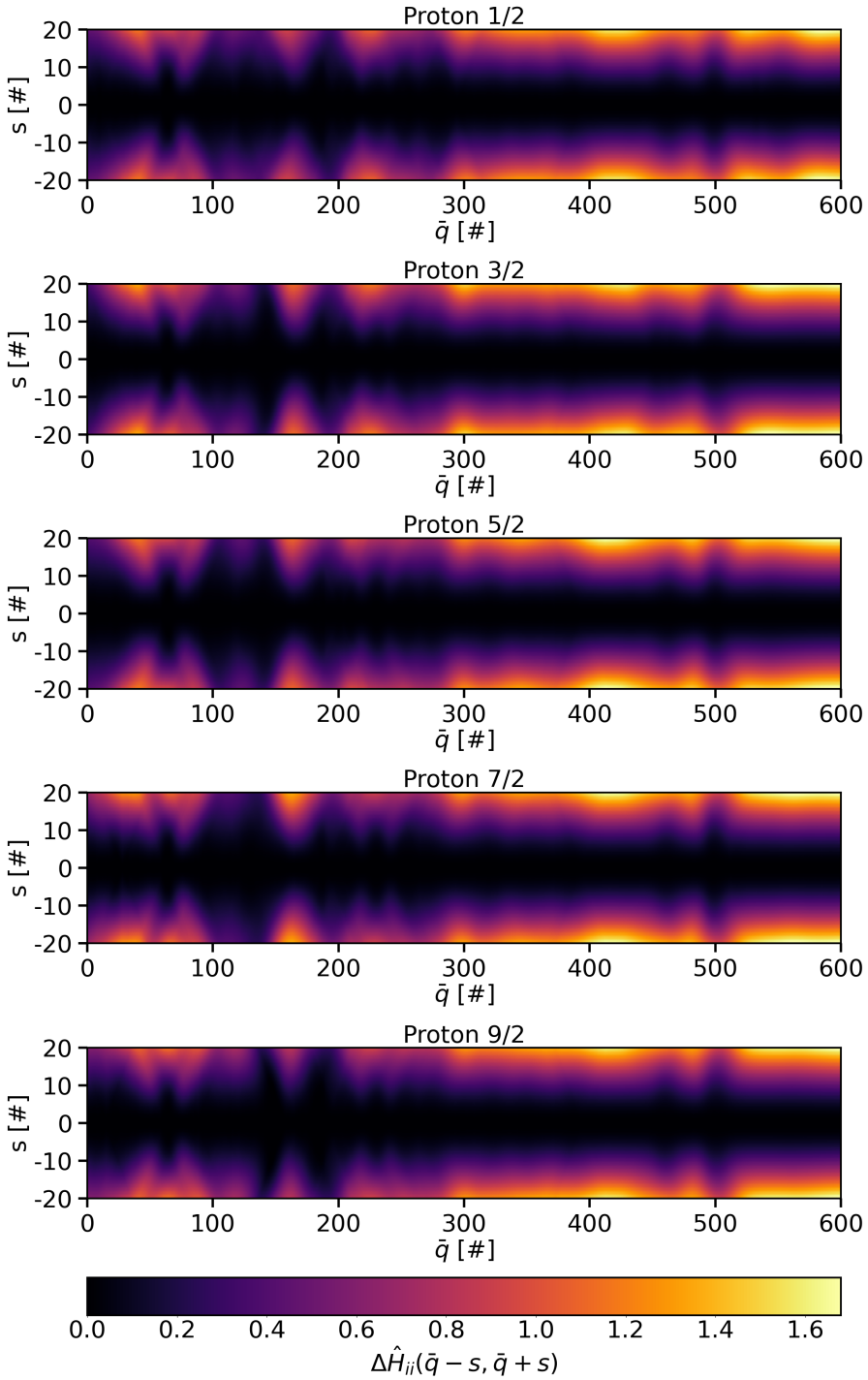

Figure 3.41: $\Delta\hat{H}_{ii}$ for all the proton variational excitations with respect to $\bar{q}$ and s.

The behaviour of $\Delta\hat{H}_{ii}$ is very satisfactory for the proton case. Moreover, in constrast to the neutron case, there is no exceptions.

The situation with the off-diagonal Hamiltonian kernels is the same as with the off-diagonal overlap ones. Indeed, we have no references to evaluate their regularity. Nevertheless, their relatively small order of magnitude compared to the diagonal Hamiltonian kernels suggests that their regularity doesn't matter that much. In practice, performing the dynamics we didn't find any problems coming from this side.
Besides, the numerical evaluation of the off-diagonal Hamiltonian kernels may be challenging when s equals zero. This question is discussed in great details in Chapter 5.

3.4.4 Orthogonality quality

We've already had occasion to discuss the orthogonality of variational excitations with respect to each other, but we haven't yet tackled the orthogonality of these same variational excitations with respect to their adiabatic set.
For the variational excitations associated with $\Omega = 1/2,\ 3/2$ and $5/2$, we have managed to always maintain an overlap smaller than 10^{-2}. For the rest, the maximum overlap is 0.03 and the average overlap is approximately 5×10^{-4}. In Figure (3.42), we displayed the overlap between each variational excited state and its related adiabatic state with respect to $c_{\#}$. In panel (a), we focused on the neutron variational excitations. In panel (b), we considered the proton variational excitations:

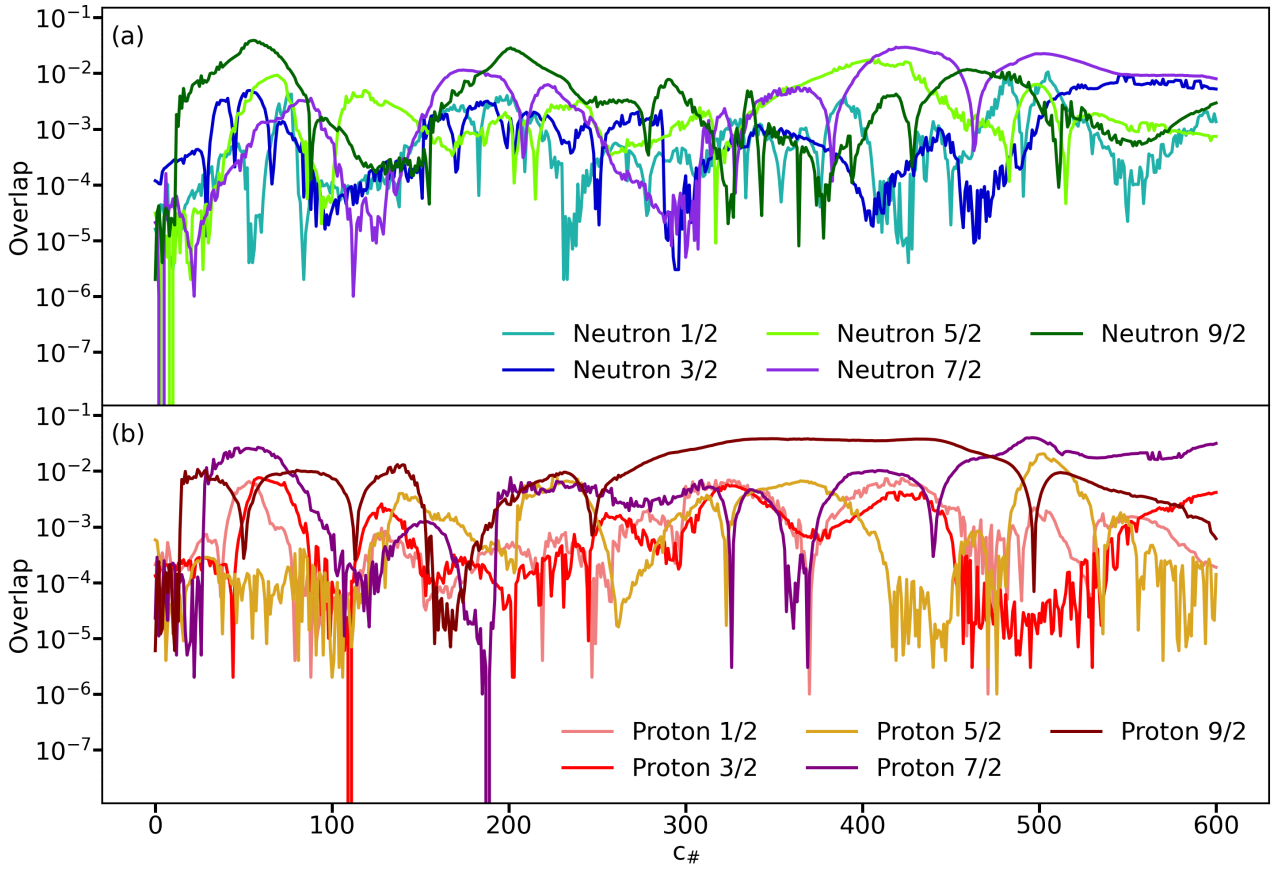

Figure 3.42: Overlap between each variational excited state and its related adiabatic state with respect to the collective variable $c_{\#}$. Panel (a): focus on the neutron variational excitations. Panel (b): focus on the proton variational excitations.

A priori, it's hard to say whether the orthogonality quality is satisfactory or not. Nevertheless, if such an overlap were to be found between two neighboring states in an adiabatic PES,

we wouldn't hestitate to call it a major discontinuity. Consequently, we believe it is legitimate to consider the overlaps obtained to be sufficiently close to zero to clearly dissociate the adiabatic set from the variational excitations and avoid double counting.
As for the reasons that prevented us from achieving greater orthogonality, we assume that they are of two kinds. On the one hand, there may sometimes be intrinsic incompatibilities between the various constraints we impose, aggravated by their complex interplay with the symmetries we preserve. On the other hand, the simultaneous consideration of numerous different constraints represent a numerical challenge. Thus, improvements can undoubtedly be made on the technical front.

Chapter 4

Static characterization of ^{240}Pu scission properties

Although the methods based on the overlap constraints have been initially developed for the SCIM, they have some really interesting by-products. For instance, as the "Drop" method allows to cross continuously the scission, it is now possible to extract fine properties of the static states in the scission area. We've notably observed proton odd-even staggering, a neutron excess in the neck at scission and striking chemical potential peaks.
To conclude, efforts have been made in order to determine the distribution of the energy between the fragments at scission. We have separated both fragments in the canonical basis and evaluated the different components of their energies.

4.1 Chemical potentials

As the chemical potentials of the compound nucleus give a qualitative hint on the separation energy of the nucleons, their study can provide us with a better understanding of the scission phenomenon. Besides, understanding neutron emission at scission is a key issue in predictive decay models such as FIFRELIN [62]. This is the reason that initially motivated this study. The chemical potentials characterize the energy variation implied by a particle number variation. For instance, if it is favorable for a neutron to separate from the two pre-fragments at scission, we assume that this must correlate with a relatively low neutron chemical potential nearby this area (reflecting a lower separation energy).
In the constrained HFB theory, we easily have access to the chemical potentials. They are the Lagrange multipliers associated with the constraints on the particle numbers. To understand this statement, we can explicitly write at first order the energy variation associated with a particle number variation. This particle number variation is expressed as a change from a density ρ to a density ρ':

$$E(\rho') = E(\rho) + \sum_{ij} (\rho'_{ij} - \rho_{ij}) \frac{\partial}{\partial \rho_{ij}} E(\rho) \tag{4.1}$$

As the density ρ is a self-consistent solution of an HFB convergence process associated with the state $|\Phi\rangle$, we can write in addition:

$$\sum_{ij} \frac{\partial}{\partial \rho_{ij}} E(\rho) = \sum_{ij} \frac{\partial}{\partial \rho_{ij}} \langle \Phi | \hat{H} | \Phi \rangle = - \sum_{\tau} \mu_\tau \sum_{ij} \frac{\partial}{\partial \rho_{ij}} \langle \Phi | \hat{N}_\tau | \Phi \rangle = - \sum_{\tau} \mu_\tau \sum_{ij} \delta_{ij} \tag{4.2}$$

Here, the μ_τ stand for Lagrange multipliers associated with the particle number constraints. Inserting Eq.(4.2) into Eq.(4.1) leads to:

$$E(\rho') = E(\rho) - \sum_\tau \mu_\tau \mathrm{Tr}(\rho'^\tau - \rho^\tau) \tag{4.3}$$

Calling $\Delta E = E(\rho') - E(\rho)$, we finally get:

$$\boxed{\Delta E = -\mu_{\tau_n} \mathrm{Tr}(\rho'^{\tau_n} - \rho^{\tau_n}) - \mu_{\tau_p} \mathrm{Tr}(\rho'^{\tau_p} - \rho^{\tau_p})} \tag{4.4}$$

In Eq.(4.4), the term $\mathrm{Tr}(\rho'^\tau - \rho^\tau)$ corresponds to the particle number variation associated with the isospin τ. Therefore, it is clear that μ_τ is a chemical potential.

4.1.1 Adiabatic states chemical potentials

In Figure (4.1), we displayed both the chemical potentials associated with the neutrons and the protons in the adiabatic set obtained with the $\tilde{\mathcal{P}}_{20}$ procedure in the ^{240}Pu with respect to the quadrupole deformation:

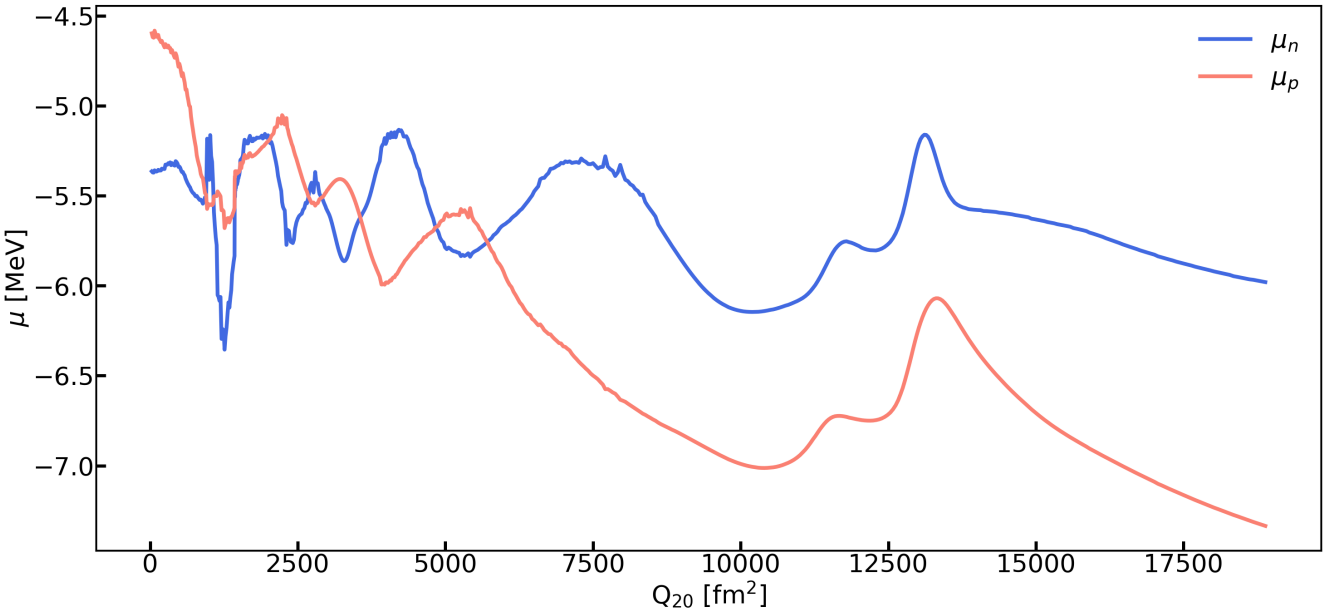

Figure 4.1: Chemical potentials associated with the neutrons and the protons in the adiabatic set obtained with the $\tilde{\mathcal{P}}_{20}$ procedure in the ^{240}Pu with respect to the quadrupole deformation.

In Figure (4.1), we clearly observe a decreasing trend in the red curve related to the proton chemical potentials. It signifies that the protons are more bound overall as the quadrupole deformation increases. In fact, this feature is due to the charge distribution inside the compound nucleus. The closer the protons are to each other, the stronger they repel because of the Coulomb interaction. Therefore, greater quadrupole deformation leads to a more spread-out charge distribution, which tends to stabilize the protons.
Some of the patterns observed in the curves can be directly linked to the PES topology at small deformations. The well around $Q_{20} = 1500$ fm^2 are related to the nucleus ground state whose stronger binding energy also implies a greater stability of the nucleons. On the

other hand, the barriers in the PES are associated with a relatively lower binding energy of the nucleus, which should imply smaller absolute values of the chemical potentials. This phenomenon is really clear for the neutron chemical potentials around $Q_{20} = 2300$ fm^2 (first barrier) and $Q_{20} = 4000$ fm^2 (second barrier). However, the proton curve is more difficult to interpret. We assume that it is due to the complex interplay between both the nuclear interaction (described by the effective Gogny interaction) and the Coulomb interaction when the deformation changes. In addition, even some neutron patterns cannot be explained by the PES topology. We suppose that they are associated with specific deformed shell effects related to the formation of the pre-fragments.
Finally, the most interesting phenomenon is that peaks appear around $Q_{20} = 13000$ fm^2 ($c_{\#} = 495$) in the chemical potentials associated with both isospins. These peaks signify that the related nucleons are locally relatively less bound. Moreover, the low nucleon density in the neck between the pre-fragments ($Q_{neck} = 0.38$ nucleons at $c_{\#} = 495$) and the suddenness of the peaks indicate that they probably sign the scission phenomenon. In the following, we simply call these peaks the "chemical potential peaks".

With regard to neutron emission, this study shows that there are indeed relatively favorable conditions at scission. This study gives only a qualitative analysis of the neutron emission during the scission process, and a more quantitative study would be of great interest.

4.1.2 Variational excitations chemical potentials

Following on from our first study carried out at the adiabatic level, we wanted to know the influence of the variational excitations on chemical potentials. In Figure (4.2), we've displayed the chemical potentials associated with the five neutron variational excitations created in addition to the adiabatic ones. In panel (a), we've represented the neutron chemical potentials. In panel (b), we've plotted the proton ones:

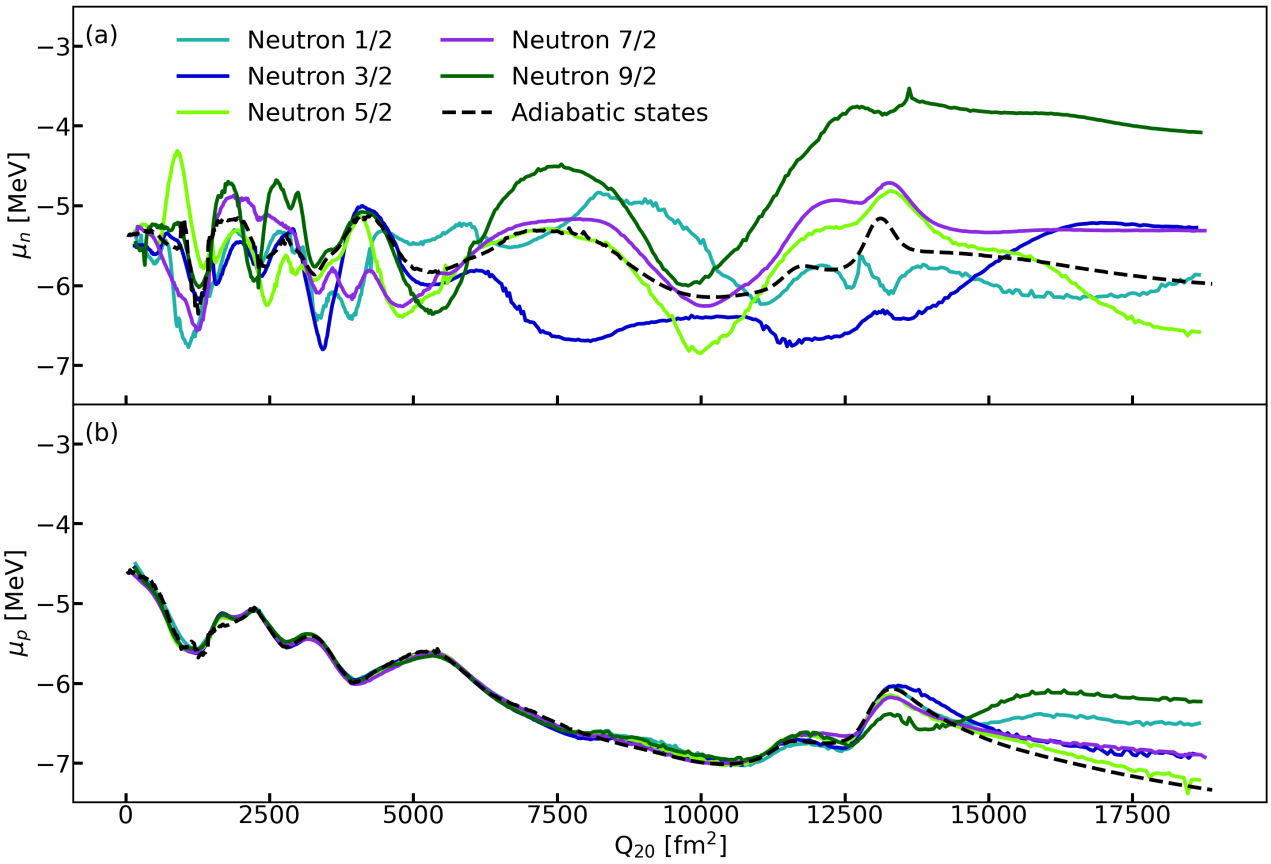

Figure 4.2: Chemical potentials associated with five neutron variational excitations built with the $\tilde{\mathcal{P}}^*_{20}$ procedure on top of an adiabatic set built with the $\tilde{\mathcal{P}}_{20}$ procedure in the ^{240}Pu with respect to quadrupole deformation. Panel (a): neutron chemical potentials. Panel (b): proton chemical potentials.

In panel (a), we observe first that each neutron variational excitation involves a specific behaviour of the neutron chemical potentials. In the curves associated with $\Omega = 5/2$ and $\Omega = 7/2$, the chemical potential peaks still exist but are wider. On the contrary, in the other curves, the chemical potential peaks have almost disappeared. We attribute this phenomenon to the different ways variational excitations operate on the compound nucleus. Indeed, we think that the orders of magnitude of the intrinsic effects on the neutron chemical potentials are sometimes much greater than the one of the purely collective phenomenon observed at the adiabatic level. We believe that the neutron chemical potential peaks are washed out precisely because of these differences of magnitude.
In panel (b), we clearly see that the proton chemical potentials of the variational excitations are almost the same as the adiabatic ones until the scission area. We assume that the spreading of the curves through the scission process and after accounts for both intrinsic and collective phenomena (we show in section 4.3 that the intrinsic excitations do change the particle number distributions of the pre-fragments) .

In Figure (4.3), we've displayed the chemical potentials associated with the five proton variational excitations created in addition to the adiabatic ones. In panel (a), we've represented the neutron chemical potentials. In panel (b), we've plotted the proton chemical potentials:

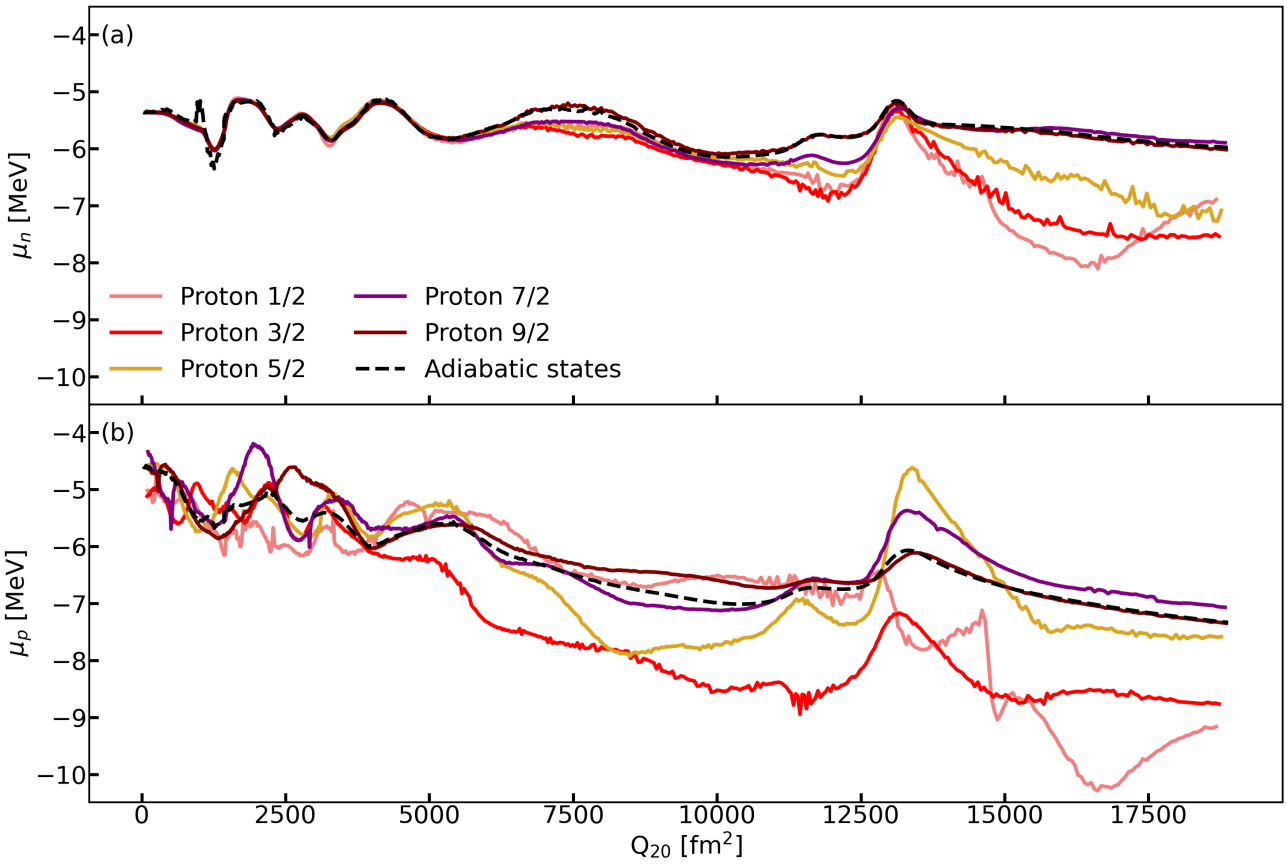

Figure 4.3: Chemical potentials associated with five proton variational excitations built with the $\tilde{\mathcal{P}}^*_{20}$ procedure on top of an adiabatic set built with the $\tilde{\mathcal{P}}_{20}$ procedure in the ^{240}Pu with respect to quadrupole deformation. Panel (a): neutron chemical potentials. Panel (b): proton chemical potentials.

In panel (a), we observe that the different curves separate earlier than in panel (b) of Figure (4.2). This feature may stand for the fact that variations of the same order of magnitude in the nucleus structure are relatively more impactful on the proton side, as there are fewer protons than neutrons. Here also, we suppose that the spreading of the curves accounts for both intrinsic and collective phenomena. Besides, the fact that the purple ($\Omega = 7/2$) and the black curves are superimposed while their proton particle number distributions are not the same at all underlines the importance of intrinsic phenomena.

In panel (b), we observe a situation similar to the one described in panel (a) of Figure (4.2). Indeed, the proton chemical potentials associated with each variational excitation have their own behaviour. Moreover, the proton chemical potential peaks appear in the curves associated with $\Omega = 3/2$, $\Omega = 5/2$, $\Omega = 7/2$ and $\Omega = 9/2$, but not in the one related to $\Omega = 1/2$. Unlike the results obtained in panel (a) og Figure (4.2), where the excited chemical potential peaks were all comparable in magnitude with the adiabatic one, we find here that some of the peaks have a greater magnitude than the adiabatic one. Here again, we assume that all these differences originate form different orders of magnitude between the collective and the intrinsic effects.

4.1.3 Chemical potentials associated with different Gogny interactions

We conclude this study of the chemical potentials by showing the impact of using different interactions (D1S and D2) with or without exact treatment of the Coulomb term. We consider the sets obtained with the drop method, starting from the saddle point already presented in section 3.2. In Figure (4.4), panel (a), we show the evolution of the neutron chemical potentials for the different sets considered, with respect to the quadrupole deformation. In panel (b), we displayed the evolution of the proton chemical potentials, with respect to the quadrupole deformation:

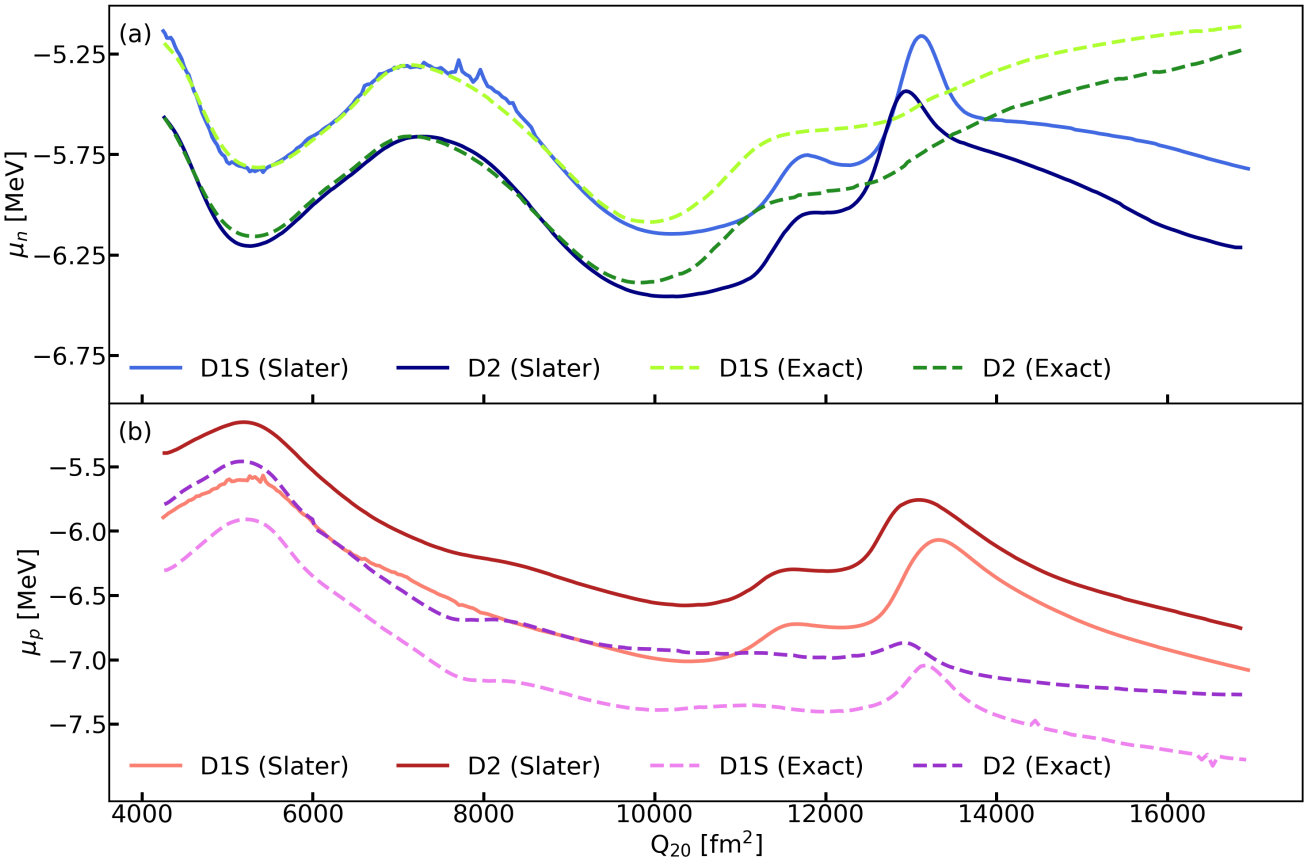

Figure 4.4: Evolution of the chemical potentials from the saddle point to scission for the D1S and D2 interactions with and without the exact treatment of the Coulomb term of the interaction, with respect to the quadrupole deformation. Panel (a): neutron chemical potentials. Panel (b): proton chemical potentials.

The Figure (4.4) confirms the observations previously made about the interactions stating that the exact treatment of the Coulomb term of the interaction has a predominant effect. It makes the neutron peaks disappear and strongly smoothes the proton peaks. It therefore seems that the sets obtained with the Coulomb interaction exact treatment miss some of the physics expected at scission. Insofar as the D1S and D2 parameters were obtained considering the Slater approximation, significant differences could be expected using the exact Coulomb treatment. Usually, however, mostly a global shift in binding energy is observed. The results presented here show a new important difference, which underlines the need to use the exact treatment of the Coulomb term with interactions fitted in coherence. It would be interesting

to repeat the same calculations with the DG interaction [48], whose parameters were obtained considering the exact treatment of the Coulomb interaction.
Finally, with regard to the differences between D1S and D2, we can see that the neutron chemical potentials are smaller in absolute value for D1S, whereas the opposite is true for the proton ones. We also note that the neutron peak occurs at a lower Q_{20} for the D2 interaction ($Q_{20} = 12943$ fm^2 for D2 and $Q_{20} = 13110$ fm^2 for D1S).

4.2 Neutron necking

Because of the repulsive Coulomb interaction, we expect the protons to be more inclined to separate rapidly at scission, with neutrons acting as the last glue between both pre-fragments. If this were the case, it's clear that it would be favorable for neutron emission at scission. To study this hypothesis, we defined the local neutron/proton ratio r_ρ as follows:

$$r_\rho(\vec{r}) = \begin{cases} \frac{\rho^{\tau_n}(\vec{r})}{\rho^{\tau_p}(\vec{r})} & \text{if } \rho(\vec{r}) > 5 \times 10^{-3} \\ 0 & \text{if } \rho(\vec{r}) \leq 5 \times 10^{-3} \end{cases} \tag{4.5}$$

4.2.1 Adiabatic states neutron necking properties

In panel (a) of Figure (4.5), we've displayed the neutron and proton chemical potentials associated with the adiabatic set obtained with the $\tilde{\mathcal{P}}_{20}$ procedure. We added three black crosses to identify the three states for which the ratio r_ρ is represented in panels (b-d). Panel (b) is related to the leftmost state, whose Q_{20} equals 12782 fm^2 ($c_\# = 485$). Panel (c) corresponds to the middle cross and is associated with $Q_{20} = 13110$ fm^2 ($c_\# = 495$). Finally, the local neutron/proton ratio represented in panel (d) is associated with a state at $Q_{20} = 13454$ fm^2 ($c_\# = 505$):

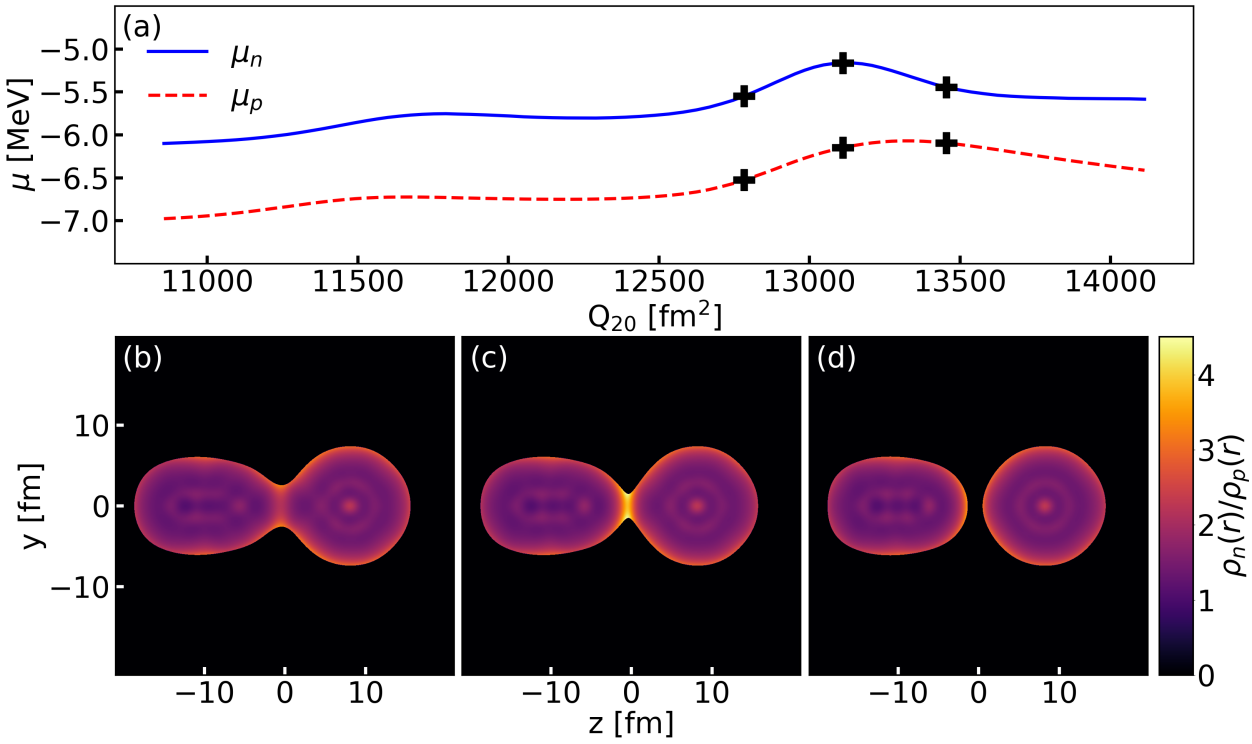

Figure 4.5: Study of the local neutron/proton ratio r_ρ in three states of the adiabatic set obtained with the $\tilde{\mathcal{P}}_{20}$ procedure in the ^{240}Pu. Panel (a): neutron and proton chemical potentials associated with the states of the adiabatic states with respect to the quadrupole moment. Panel (b): local neutron/proton ratio r_ρ for the adiabatic state labeled by $Q_{20} = 12782$ fm^2. Panel (c): local neutron/proton ratio r_ρ for the adiabatic state labeled by $Q_{20} = 13110$ fm^2. Panel (d): local neutron/proton ratio r_ρ for the adiabatic state labeled by $Q_{20} = 13454$ fm^2.

In panel (c), we clearly see an abnormally high local neutron/proton ratio between the pre-fragments. More precisely, this ratio reaches the value 4.505, when the average neutron/proton ratio in the ^{240}Pu equals 1.553. Moreover, this behaviour is not observe in panel (b) and panel (d), which suggests that this phenomenon is really sudden and brief within the whole scission process.
This results are fully in line with our hypothesis stating that it is the neutrons that hold the pre-fragments together in the final moments of the scission process in the ^{240}Pu.

4.2.2 Variational excitations neutron necking properties

In the previous section 4.1, we've seen how the chemical potentials associated with the variational excitations could differ greatly from those observed at the adiabatic level. This raises the legitimate question of whether the neutron necking observed at the adiabatic level is also present in the variational excitations.

In Figure (4.6), we've displayed the local ratios r_ρ associated with our five neutron variational excitations at three different deformations, corresponding to the three black crosses in Figure (4.5):

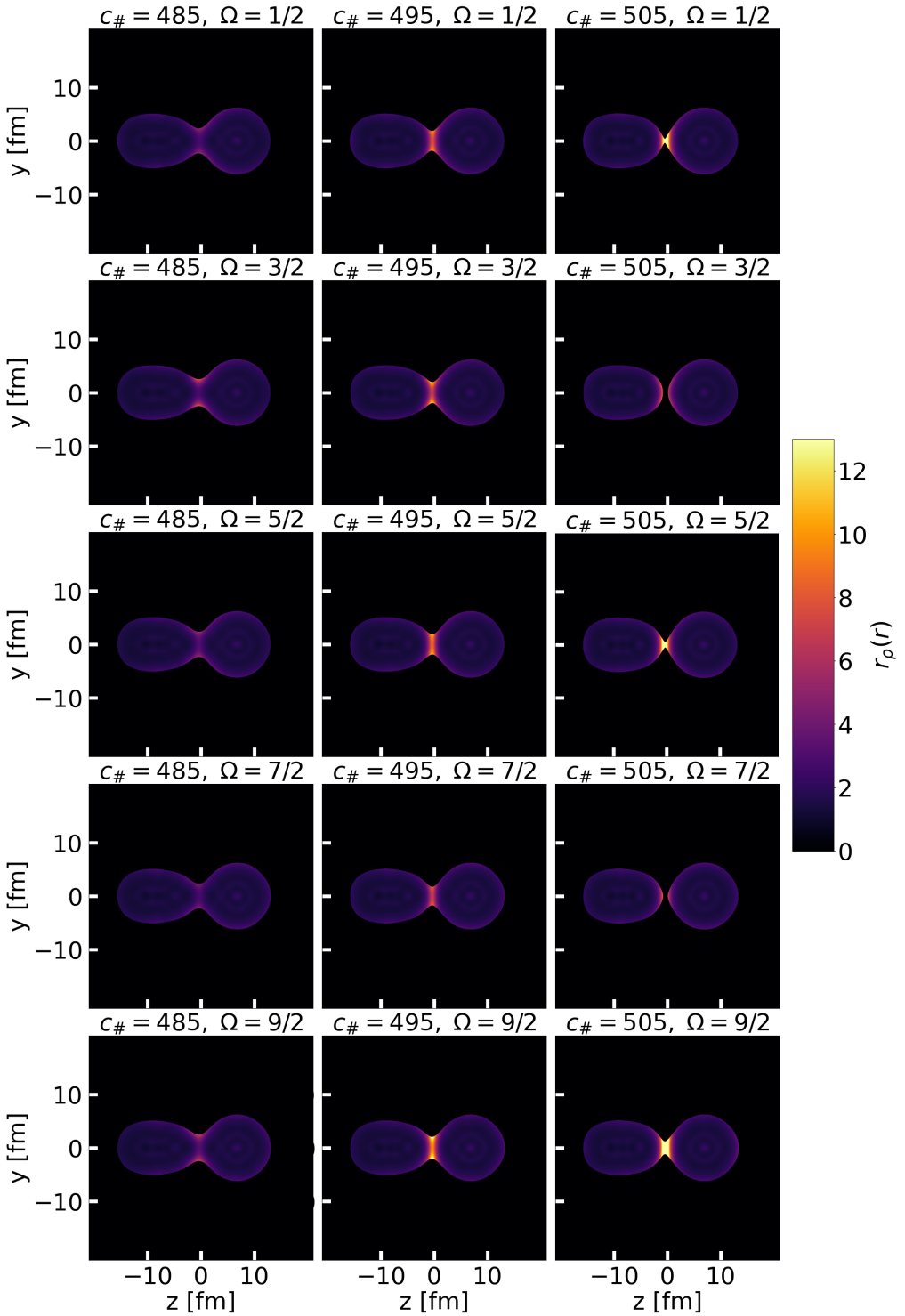

Figure 4.6: Illustration of the local neutron/proton ratio r_ρ for different neutron variational excited states whose Ω ranges from 1/2 to 9/2 and labeled by $c_\# = 485$, $c_\# = 495$ and $c_\# = 505$.

The phenomena observed for the neutron variational excited states are very different from the adiabatic level. Firstly, the local ratios r_ρ between the two pre-fragments, which were already abnormally high in the adiabatic case, are even higher this time. Moreover, there are important differences from one excited state to the other. Because of these differences and to preserve contrasts, the maxium values of r_ρ has been set to 13 in Figure (4.6). In Table (4.1), we've displayed the true local maximum values of r_ρ for each state considered:

	$n_{1/2}$	$n_{3/2}$	$n_{5/2}$	$n_{7/2}$	$n_{9/2}$
$c_{\#} = 485$	5.56	8.62	5.65	4.66	7.65
$c_{\#} = 495$	10.40	12.38	11.30	8.73	14.22
$c_{\#} = 505$	20.21	9.23	20.48	9.41	29.13

Table 4.1: Maximum values of the local ratio r_ρ for the states considered in Figure (4.6).

In addition, observing the states labeled by $c_{\#} = 505$ in Figure (4.6), we clearly see that some excited states are separated in two fragments, when others are not (with respect to the criteria $\rho(\vec{r}) > 5 \times 10^{-3}$). Furthermore, comparing Figure (4.6) and Table (4.1) we observe that these differences in separation are correlated with the maximum value of r_ρ. The greater the maximum of the r_ρ ratio, the later the separation. We will see in section 4.4 that the way in which the neutron variational excitations slow down the scission process implies significant consequences related to the TKE evaluation. It underlines the importance of including intrinsic excitations in the "dynamics".
These observations bring us back to the assumptions made earlier about the variational excitations nature and how they couple the pre-fragments. Indeed, it seems reasonable to assume that the more or less early separation of the fragments is a good indicator of the couplings intensity brought about by the variational excitations. It turns out that the excited state with the earliest separation $\Omega = 7/2$ also corresponds to the states whose neutron chemical potentials were closest to the adiabatic ones (Figure (4.2)). In addition, the quantities $\sigma^{(2)}$ and $\sigma^{(4)}$ associated with this excited state were also the most stable ones. On the contrary, the states $\Omega = 1/2$ and $\Omega = 9/2$ with later separations are associated with more exotic neutron chemical potential behaviors and less stable $\sigma^{(2)}$ and $\sigma^{(4)}$.
Finally, on the subject of neutron emission at scission, it can be broadly stated that taking neutron intrinsic excitations into account seems to be necessary to bring the description closer to the physics of the phenomenon. Indeed, in the case of neutron emission between the fragments, the ratio r_ρ should tend towards infinity, which is maybe what we begin to see in the case of the neutron variational excitations.

To address the above phenomena in a more quantitative way, we've studied the behaviour of Q_{neck} with respect to the collective coordinate $c_{\#}$. In panel (a) of Figure (4.7), we've plotted the evolution of the neutron Q_{neck} associated with our five neutron variational excitations in addition to the evolution of the adiabatic one with respect to $c_{\#}$. In panel (b), we've displayed the evolution of the total Q_{neck} associated with our five neutron variational excitations in addition to the evolution of the adiabatic one, with respect to $c_{\#}$. The red line in panel (b) corresponds to the value of Q_{neck}^{tot} found for the adiabatic set at the neutron chemical potential peak ($c_{\#} = 495$):

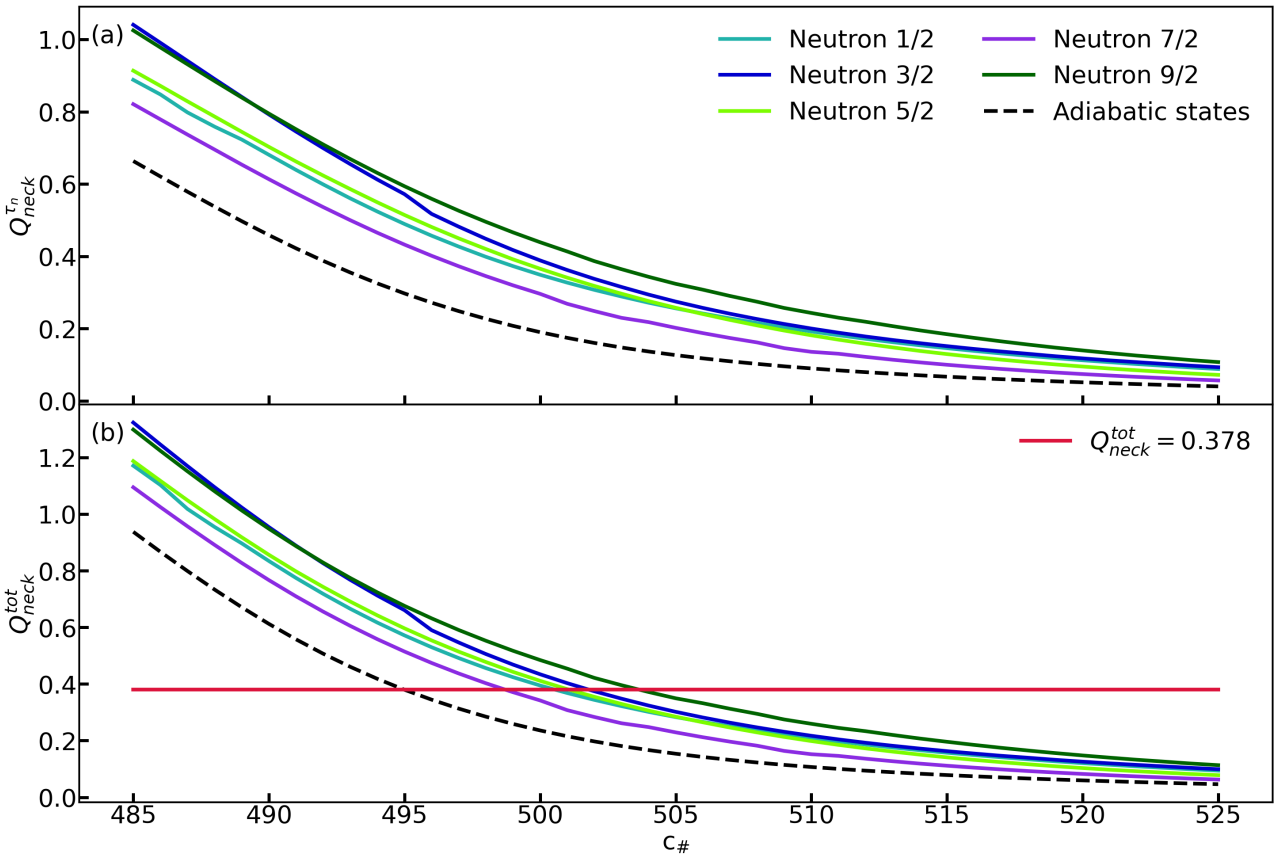

Figure 4.7: Study of the evolution of Q_{neck} for our five neutron variational excitations and for their related adiabatic states. Panel (a): evolution of the neutron Q_{neck} with respect to $c_\#$. Panel (b): evolution of the total Q_{neck} with respect to $c_\#$.

In panel (a) of Figure (4.7), we observe that the purple curve is the closest to the adiabatic one when the dark green curve is most of the time the farthest to it. These two observations match the ones made from Figure (4.6). Surprisingly, the dark blue curve is overall slightly above the light blue and light green ones, while we see in Figure (4.6) that the excited states associated with the dark blue curve are separated in two fragments earlier. As the operator $\hat{Q}_{neck}$ has a Gaussian range, these differences could testify of a peculiar geometry of the neutrons inside the fragments of the $\Omega = 3/2$ excited states. In addition, we remark a kink in the dark blue curve, which is absent from the others. These two features point to the limits of our hypotheses. A more specific study would be of great interest.
The points of intersection between the red line and the different curves are very different. More precisely the neutron variational excitations $\Omega = 1/2$, $\Omega = 3/2$, $\Omega = 5/2$, $\Omega = 7/2$ and $\Omega = 9/2$ are associated respectively with $c_\# = 501$, $c_\# = 502$, $c_\# = 501$, $c_\# = 499$, $c_\# = 504$. These results suggest that intrinsic excitations may contribute to holding the pre-fragments tohether in the scission area.

We've done the same study for the proton variational excitations. In Figure (4.8), we've displayed the local ratios r_ρ associated with our five proton variational excitations at three different deformations, corresponding to the three black crosses in Figure (4.5):

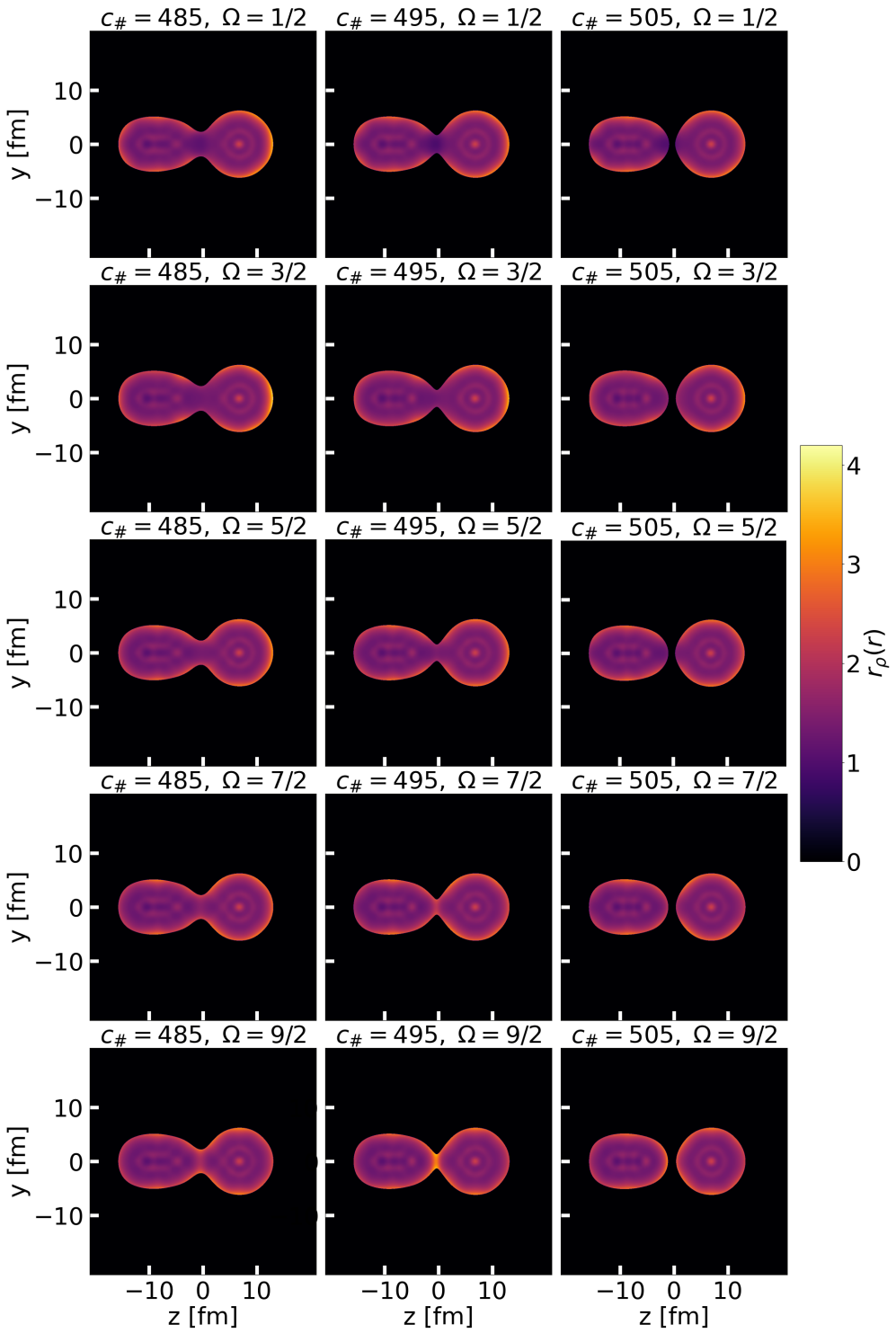

Figure 4.8: Illustration of the local neutron/proton ratio r_ρ for different proton variational excited states whose Ω ranges from 1/2 to 9/2 and labeled by $c_\# = 485$, $c_\# = 495$ and $c_\# = 505$.

In contrast to the neutron case, the local r_ρ ratios are quite similar overall to those obtained in the adiabatic case (we have not clamped any values). That said, we observe that the local neutron/proton ratio r_ρ is smaller between the pre-fragments than in the adiabatic case. We can still clearly identify a neutron neck in the $\Omega = 9/2$ variational excitation, and less clearly in the $\Omega = 7/2$ one, but we don't see any in the other variational excitations. Besides, in the variational excitation labeled by $\Omega = 1/2$, we see a slightly abnormally low r_ρ ratio between

the pre-fragments.
These results are in line with the ones found through the study of the chemical potentials (Figure (4.3)). Indeed, the variational excitation with the clearer neutron neck ($\Omega = 9/2$) is also the one whose proton chemical potentials are the closest to the adiabatic ones. The variational excitation labeled by $\Omega = 7/2$ still have a neutron neck and its proton chemical potentials are not that far from the adiabatic ones. The variational excitations labeled by $\Omega = 5/2$ and $\Omega = 3/2$ do not show any neutron neck and they display proton chemical potential peaks with an amplitude much greater than the adiabatic one. Finally, the variational excitation $\Omega = 1/2$, which is associated with a slightly abnormally low r_ρ between the pre-fragments, is the one whose proton chemical potentials show the strangest behaviour.
Now want to find the cause of this attenuation or disappearance of the neutron neck. There are two possibilities. Either there are fewer neutrons in the neck, either there are more protons. As the neutron part of the proton variational excitations has been constrained to be the same as the adiabatic one, the answer is quite straightforward. There are more protons in the neck.
In panel (a) of Figure (4.9), we quantified these additional protons in the neck, displaying the proton Q_{neck} for the proton variational excited states along with the proton Q_{neck} associated with the adiabatic states, with respect to $c_\#$. In panel (b), we've displayed the evolution of the total Q_{neck} associated with our five proton variational excitations in addition to the evolution of the adiabatic one, with respect to $c_\#$. The blue line in panel (b) corresponds to the value of Q^{tot}_{neck} found for the adiabatic set at the neutron chemical potential peak ($c_\# = 495$):

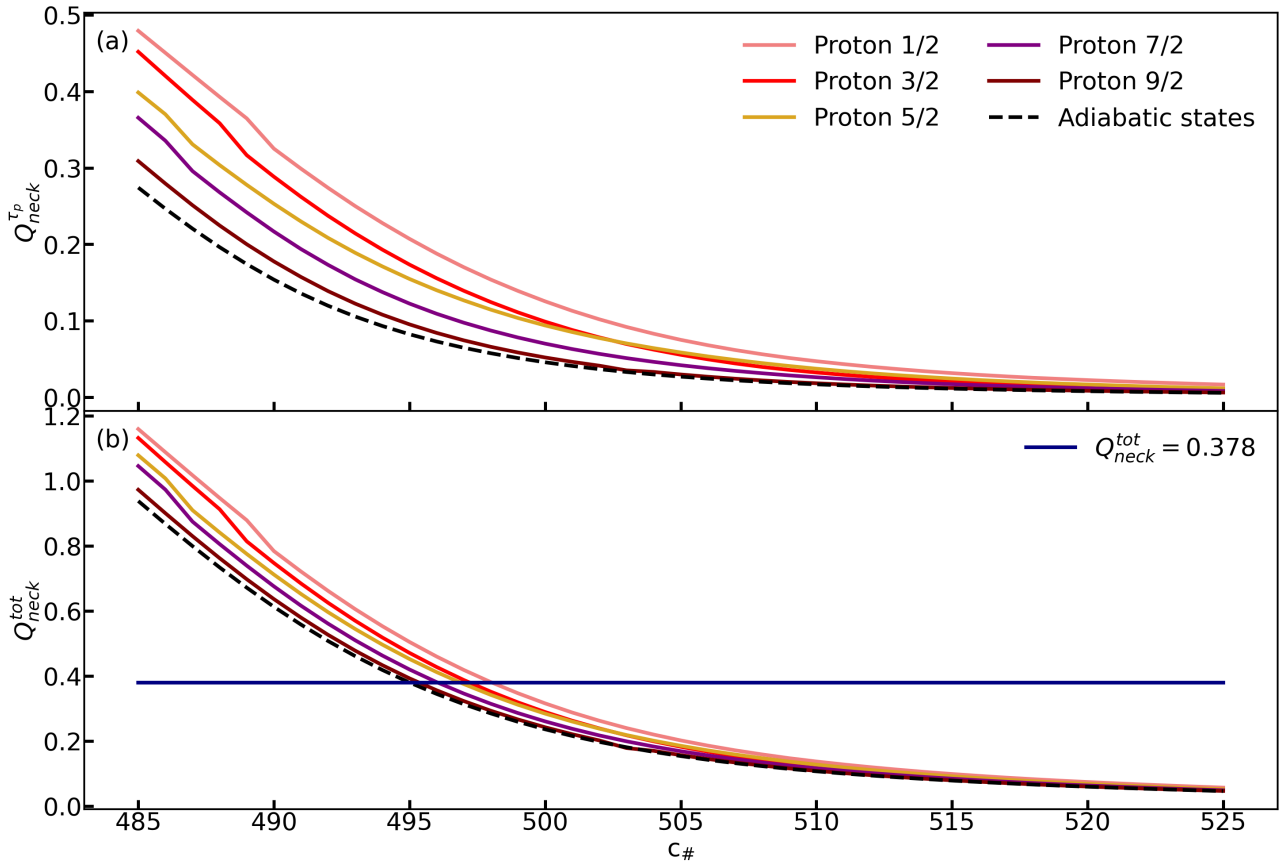

Figure 4.9: Study of the evolution of Q_{neck} for our five proton variational excitations and for their related adiabatic states. Panel (a): evolution of the proton Q_{neck} with respect to $c_{\#}$. Panel (b): evolution of the total Q_{neck} with respect to $c_{\#}$.

This time, in Figure (4.9), there doesn't seem to be any particular behaviour unmatching our assumptions. Indeed, the greater the Q_{neck}, the smaller the neutron necking phenomenon. Besides, these results also cofirm the assumptions about the variational excitations pre-fragments couplings. We observe that the earlier the separation, the closer the proton chemical potentials to the adiabatic ones and the more regular the associated $\sigma^{(2)}$ and $\sigma^{(4)}$ quantities.
Here also, we provide the reader with the different values of $c_{\#}$ corresponding to the intersection between the blue line and the curves. We found that the protons excitations labeled by $\Omega = 1/2$, $\Omega = 3/2$, $\Omega = 5/2$, $\Omega = 7/2$ and $\Omega = 9/2$ are associated respectively with $c_{\#} = 498$, $c_{\#} = 497$, $c_{\#} = 497$, $c_{\#} = 496$ and $c_{\#} = 495$. These values are closer to $c_{\#} = 495$ than in the neutron case. It signifies that the proton variational excitations probably contribute less to holding the pre-fragments together than the neutron ones.

4.2.3 Neutron necking properties using different Gogny interactions

To conclude this section, we investigate the impact of using different interactions (D1S and D2 with or without exact treatment of the Coulomb term of the interaction) on the neutron necking phenomenon. In Figure (4.10), we've displayed the local neutron/proton ratio r_ρ for two states associated with D1S (with the exact and Slater treatment of the Coulomb term of the interaction), and two states associated with D2 (with the exact and Slater treatment

of the Coulomb term of the interaction). We considered the states related to the chemical potential peaks displayed in Figure (4.4):

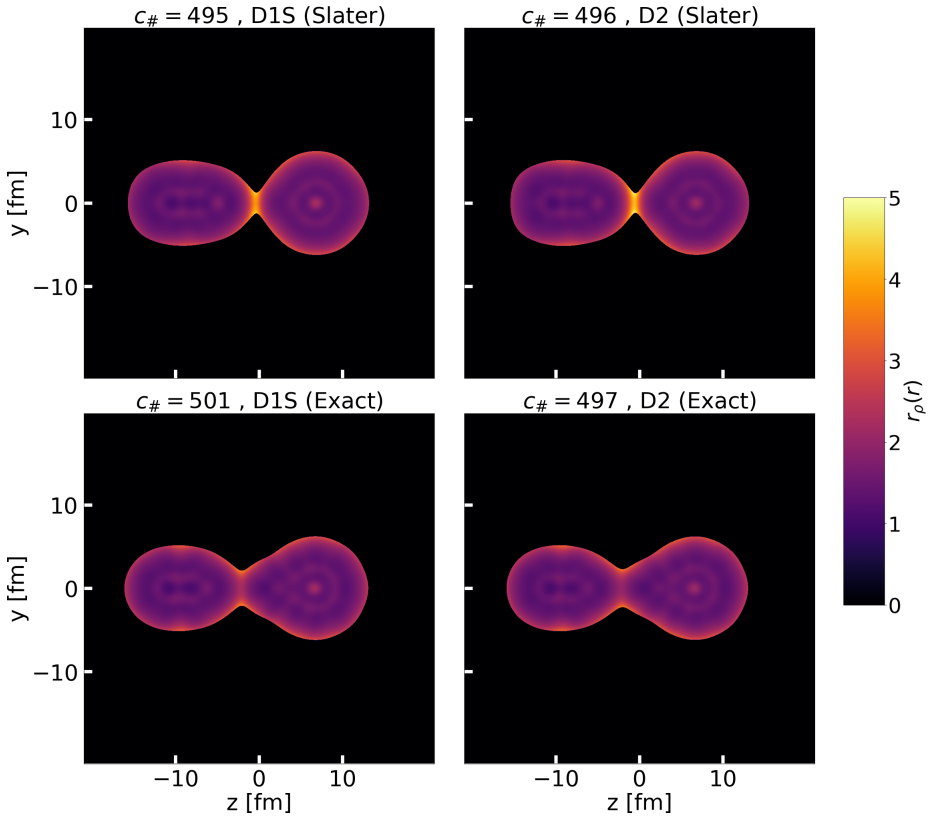

Figure 4.10: Study of the neutron necking at scission for the D1S and D2 interactions with and without the exact treatment of the Coulomb term.

Once again, we see that the D1S and D2 interactions give similar results, the main differences bewteen the plots being explained by the treatment of the Coulomb interaction.
Besides, we observe that neutron necks are almost non-existent when the exact treatment of the Coulomb term is used. The nucleus seems to be more spread in space with the exact treatment of the Coulomb interaction, which is consistent with the neutron chemical potentials observed in Figure (4.4), panel (a). Neutron are less and less bound as Q_{20} increases. Concerning the results obtained with the Slater approximation, the maximum value of the local ratio r_ρ, 4.82, is found for the state related to the D2 interaction, while the maximum value of r_ρ associated with the D1S state is 4.51.

4.3 Fragment particle numbers

Charge and mass yields are undoubtedly among the most important fission observables. To obtain these yields within TDGCM type approaches, we start by defining certain HFB states of the GCM basis as corresponding to possible events of the fission process. The "dynamics" then gives access to the probability associated with each of these events. We then multiply the probability of each event by the fragmentation of the associated state to get the fission yields. This section discuss how to access the fragmentation associated with a given HFB state.
In practice, it is common to determine the fragmentation associated with an HFB state from the local density $\rho(\vec{r})$, which is integrated with respect to the subspaces corresponding to

each fragment. While this method gives an account of the average fragmentation, it does away with many phenomena associated with the exact particle number distribution of the fragments, such as proton odd-even staggering observed in charge yields. For this reason, we have chosen in this work to focus on another method that gives access to the exact total particle number distribution of the fragments.
As well as enabling a better evaluation of the fission yields, the total particle number distribution of the fragments also allows a better understanding of the nature of the variational excitations.

4.3.1 The z-separation method

The method we've chosen to use comes from [63, 64]. We call it the z-separation method because it relies on separating in space the orthonormal particle basis wave functions $\{\varphi_k\}$. To operate this separation, we first define a z_{neck} abscissa that divides the space into two parts. In practice, there exist various methods for defining z_{neck}. For instance, we can choose the abscissa z that minimizes the local density $\rho(\vec{r})$ along the z-axis between both fragments. In this work, we've used the definition already implemented in the HFB3 code, which consists in choosing the z abscissa that minimizes Q_{neck}.
Once z_{neck} is defined, we can rewrite the φ_k wave functions as follows:

$$\varphi_k(\vec{r}) = \varphi_k(\vec{r})\delta_{(z<z_{neck})} + \varphi_k(\vec{r})\delta_{(z\geq z_{neck})} \tag{4.6}$$

We search for the squared norms of the functions appearing on the right hand side of Eq.(4.6):

$$\begin{cases} (c_k^{(l)})^2 = ||\varphi_k\delta_{(z<z_{neck})}||^2 = \int d\vec{r}_\perp \int_{-\infty}^{z_{neck}} \varphi_k^*(\vec{r})\varphi_k(\vec{r}) \\ (c_k^{(r)})^2 = ||\varphi_k\delta_{(z\geq z_{neck})}||^2 = \int d\vec{r}_\perp \int_{z_{neck}}^{+\infty} \varphi_k^*(\vec{r})\varphi_k(\vec{r}) \end{cases} \tag{4.7}$$

In practice, we evaluate both $(c_k^{(l)})^2$ and $(c_k^{(r)})^2$ numerically. Thanks to Eq.(4.7), we can define the left and right normalized wave functions $\varphi_k^{(l)}$ and $\varphi_k^{(r)}$ associated with φ_k:

$$\begin{cases} \varphi_k^{(l)}(\vec{r}) = \frac{1}{c_k^{(l)}}\varphi_k(\vec{r})\delta_{(z<z_{neck})} \\ \varphi_k^{(r)}(\vec{r}) = \frac{1}{c_k^{(r)}}\varphi_k(\vec{r})\delta_{(z\geq z_{neck})} \end{cases} \tag{4.8}$$

Using Eq.(4.8) in Eq.(4.6) leads to:

$$\boxed{\varphi_k(\vec{r}) = c_k^{(l)}\varphi_k^{(l)}(\vec{r}) + c_k^{(r)}\varphi_k^{(r)}(\vec{r})} \tag{4.9}$$

The left and right sets $\{\varphi_k^{(l)}\}$ and $\{\varphi_k^{(r)}\}$ associated with the left and right normalized wave functions are unfortunately not orthonormal. We orthonormalize these sets using the same method as for the 2-center representations presented in section 2.1.2.
After this orthonormalization process, we end up with two orthonormal bases $\{\tilde{\varphi}_i^{(l)}\}$ and $\{\tilde{\varphi}_j^{(r)}\}$. The total orthonormal basis $\{\tilde{\varphi}_\alpha^{(lr)}\}$, which is the direct sum of $\{\tilde{\varphi}_i^{(l)}\}$ and $\{\tilde{\varphi}_j^{(r)}\}$, allows to represent all the wave functions of the initial set $\{\varphi_k\}$. We call $\Theta^{(l)}$, $\Theta^{(r)}$ and $\Theta^{(lr)}$ the transformation matrices between these latter bases:

$$\boxed{\begin{cases}\Theta^{(l)}_{ki} = \int d\vec{r}\varphi^*_k(\vec{r})\tilde{\varphi}^{(l)}_i(\vec{r}) \\ \Theta^{(r)}_{kj} = \int d\vec{r}\varphi^*_k(\vec{r})\tilde{\varphi}^{(r)}_j(\vec{r})\end{cases}} \tag{4.10}$$

And:

$$\boxed{\Theta^{(lr)} = \begin{pmatrix}\Theta^{(l)} & 0 \\ 0 & \Theta^{(r)}\end{pmatrix}} \tag{4.11}$$

As the bases considered are orthonormal, we can associate to them particle creation and annihilation operators $\{a^{(l)+}_i\}$,$\{a^{(l)}_i\}$, $\{a^{(r)+}_j\}$, $\{a^{(r)}_j\}$, $\{a^{(lr)+}_\alpha\}$ and $\{a^{(lr)}_\alpha\}$. Our goal is to rewrite the HFB wave functions using these creation and annihilation operators.
In the code, we've chosen to use the canonical particle basis as the starting point of the method. We made this choice not only because it is more convenient to work with, but also because we can eliminate certain quasiparticle states associated with small v_k. In practice we keep only the quasiparticle annihilation operators η_k associated with $|v_k| > 10^{-4}$. These operators read:

$$\eta_k = u_k a_k + v_k \bar{a}^+_k \tag{4.12}$$

We transform Eq.(4.12) using the matrices defined in Eq.(4.10):

$$\boxed{\eta_k = u_k(\sum_i \Theta^{(l)}_{ki} a^{(l)}_i + \sum_j \Theta^{(r)}_{kj} a^{(r)}_i) + v_k(\sum_i \Theta^{(l)}_{ki} \bar{a}^{(l)+}_i + \sum_j \Theta^{(r)}_{kj} \bar{a}^{(r)+}_i)} \tag{4.13}$$

Using Eq.(4.11), we can put Eq.(4.13) into a more compact form:

$$\boxed{\begin{pmatrix}\eta \\ \bar{\eta}^+\end{pmatrix} = \begin{pmatrix}u & v \\ -v & u\end{pmatrix}\begin{pmatrix}\Theta^{(lr)} & 0 \\ 0 & \Theta^{(lr)}\end{pmatrix}\begin{pmatrix}a^{(lr)} \\ \bar{a}^{(lr)+}\end{pmatrix}} \tag{4.14}$$

We would like the transformation displayed in Eq.(4.14) to be an HFB transformation. However, in general, it is not the case as the matrix $\Theta^{(lr)}$ is rectangular. Therefore, we complete $\Theta^{(lr)}$ into a square matrix adding a basis of its null space to it. Calling k' the index spaning the additional space, we extend the diagonal matrices u and v setting $u_{k'} = 1$ and $v_{k'} = 0$. Doing so, we've created a new set of "ghost" quasiparticle annihilation operators $\{\eta_{k'}\}$ that do not change the content of the HFB wave function but enable us to consider Eq.(4.14) as an HFB transformation. In the following, we assume that this operation has been made, and we still call $\Theta^{(lr)}$, u, and v the completed matrices.

Now, we can project a given HFB wave function $|\Phi\rangle$ onto a specific fragmentation. As both isospins are treated independently, we neglect them in the following to simplify the derivations. We start by defining the left and right particle number operators $\hat{N}^{(l)}$ et $\hat{N}^{(r)}$:

$$\begin{cases}\hat{N}^{(l)} = \sum_i a^{(l)+}_i a^{(l)}_i \\ \hat{N}^{(r)} = \sum_j a^{(r)+}_j a^{(r)}_j\end{cases} \tag{4.15}$$

Thanks to the operators $\hat{N}^{(l)}$ and $\hat{N}^{(r)}$, we can define the left and right particle number projectors $\hat{P}^{(l)}$ and $\hat{P}^{(r)}$:

$$\begin{cases} \hat{P}^{(l)}_{N_0^{(l)}} = \frac{1}{2\pi}\int_0^{2\pi} e^{-i\varphi(\hat{N}^{(l)}-N_0^{(l)})}d\varphi \\ \hat{P}^{(r)}_{N_0^{(r)}} = \frac{1}{2\pi}\int_0^{2\pi} e^{-i\varphi(\hat{N}^{(r)}-N_0^{(r)})}d\varphi \end{cases} \tag{4.16}$$

The projector $\hat{P}^{(l)}_{N_0^{(l)}}$ projects the left part of the HFB wave function onto its subspace associated with the particle number $N_0^{(l)}$, and $\hat{P}^{(r)}_{N_0^{(r)}}$ projects the right part of the HFB wave function onto its subspace associated with the particle number $N_0^{(r)}$.
In the following, we assume that the true total particle number of the nucleus is N_0. We want to find the probabilities $Y(N_0^{(l)}, N_0^{(r)})$ associated with all the fragmentations such as $N_0^{(l)} + N_0^{(r)} = N_0$. Calling $\hat{P}_{N_0}$ the customary particle number projector, we can write:

$$\boxed{Y(N_0^{(l)}, N_0^{(r)}) = \left(\frac{\langle\Phi|\hat{P}^{(l)}_{N_0^{(l)}}\hat{P}^{(r)}_{N_0^{(r)}}|\Phi\rangle}{\langle\Phi|\hat{P}_{N_0}|\Phi\rangle}\right)^2} \tag{4.17}$$

After discretization, the numerator in Eq.(4.17) reads as follows:

$$\begin{aligned}\langle\Phi|\hat{P}^{(l)}_{N_0^{(l)}}\hat{P}^{(r)}_{N_0^{(r)}}|\Phi\rangle = \frac{1}{n_{\varphi_l}}\frac{1}{n_{\varphi_r}}\sum_{\varphi_l=1}^{n_{\varphi_l}}\sum_{\varphi_l=1}^{n_{\varphi_r}} & e^{2i\frac{(n_{\varphi_l}-\varphi_l)}{n_{\varphi_l}}\pi N_0^{(l)}} e^{2i\frac{(n_{\varphi_r}-\varphi_r)}{n_{\varphi_r}}\pi N_0^{(r)}} \\ & \langle\Phi|e^{-2i\frac{(n_{\varphi_l}-\varphi_l)}{n_{\varphi_l}}\pi\hat{N}^{(l)}} e^{-2i\frac{(n_{\varphi_r}-\varphi_r)}{n_{\varphi_r}}\pi\hat{N}^{(r)}}|\Phi\rangle\end{aligned} \tag{4.18}$$

It's clear that the difficult part in evaluating Eq.(4.18) is to treat the following quantities (factors in the exponentials have been intentionally omitted for simplification purposes):

$$\langle\Phi|\Phi(\varphi_l,\varphi_r)\rangle = \langle\Phi|e^{-i\varphi_l\hat{N}^{(l)}}e^{-i\varphi_r\hat{N}^{(r)}}|\Phi\rangle \tag{4.19}$$

Using Eq.(4.13), we can describe how the exponentials operate on the quasiparticle annihilation operators η_k:

$$\eta_k(\varphi_l,\varphi_r) = e^{-i\varphi_l\hat{N}^{(l)}}e^{-i\varphi_r\hat{N}^{(r)}}\eta_k e^{i\varphi_l\hat{N}^{(l)}}e^{i\varphi_r\hat{N}^{(r)}} \tag{4.20}$$

$$\boxed{\begin{aligned}\eta_k(\varphi_l,\varphi_r) = u_k\Big(\sum_\alpha \Theta^{(l)}_{ki}e^{i\varphi_l}a_i^{(l)} + \sum_\beta \Theta^{(r)}_{kj}e^{i\varphi_r}a_i^{(r)}\Big) \\ + v_k\Big(\sum_\alpha \Theta^{(l)}_{ki}e^{-i\varphi_l}\bar{a}_i^{(l)+} + \sum_\beta \Theta^{(r)}_{kj}e^{i\varphi_r}\bar{a}_i^{(r)+}\Big)\end{aligned}} \tag{4.21}$$

A detailed proof of Eq.(4.21) is given in Chapter 5. We can define the matrix $\Theta^{(lr)}$ as follows:

$$\Theta^{(lr)}(\varphi_l,\varphi_r) = \begin{pmatrix} \Theta^{(l)}e^{i\varphi_l} & 0 \\ 0 & \Theta^{(r)}e^{i\varphi_r} \\ \Theta^{(cl)}e^{i\varphi_l} & \Theta^{(cr)}e^{i\varphi_r} \end{pmatrix} \tag{4.22}$$

Here, $\Theta^{(cl)}$ and $\Theta^{(cr)}$ stand for the vectors introduced to complete $\Theta^{(lr)}$ into a square matrix. Thanks to Eq.(4.22), we can write the HFB transformation between the quasiparticle operators $\{\eta_k^+(\varphi_l,\varphi_r)\}$ and $\{\eta_k(\varphi_l,\varphi_r)\}$ and the particle operators $\{a_k^{+(lr)}\}$ and $\{a_k^{(lr)}\}$:

$$\boxed{\begin{pmatrix} \eta(\varphi_l,\varphi_r) \\ \bar{\eta}^+(\varphi_l,\varphi_r) \end{pmatrix} = \begin{pmatrix} u & v \\ -v & u \end{pmatrix} \begin{pmatrix} \Theta^{(lr)}(\varphi_l,\varphi_r) & 0 \\ 0 & \Theta^{(lr)}(\varphi_l,\varphi_r) \end{pmatrix} \begin{pmatrix} a^{(lr)} \\ \bar{a}^{(lr)+} \end{pmatrix}} \tag{4.23}$$

Using the formulas demonstrated in Chapter 5, we can finally write:

$$\boxed{\begin{aligned} \langle\Phi|\Phi(\varphi_l,\varphi_r)\rangle = \det(&u\Theta^{(lr)}(\Theta^{(lr)}(\varphi_l,\varphi_r))^T u(\Theta^{(lr)}(\varphi_l,\varphi_r))^* \\ &+v\Theta^{(lr)}(\Theta^{(lr)}(\varphi_l,\varphi_r))^+ v(\Theta^{(lr)}(\varphi_l,\varphi_r))^*) \end{aligned}} \tag{4.24}$$

With Eq.(4.24), it is straightforward to calculate the fragmentation probabilities $Y(N_0^{(l)}, N_0^{(r)})$ defined in Eq.(4.17).

4.3.2 Fragment particle numbers of the adiabatic and variational excited states

We've used the z-separation method to obtain the fragment particle number distributions associated with the adiabatic states and with all the variational excitations created.
In Figure (4.11), we've displayed the neutron particle number distributions associated with the light (which is also the left one) fragment of the adiabatic states and of the neutron variational excited states with respect to the collective coordinate $c_\#$:

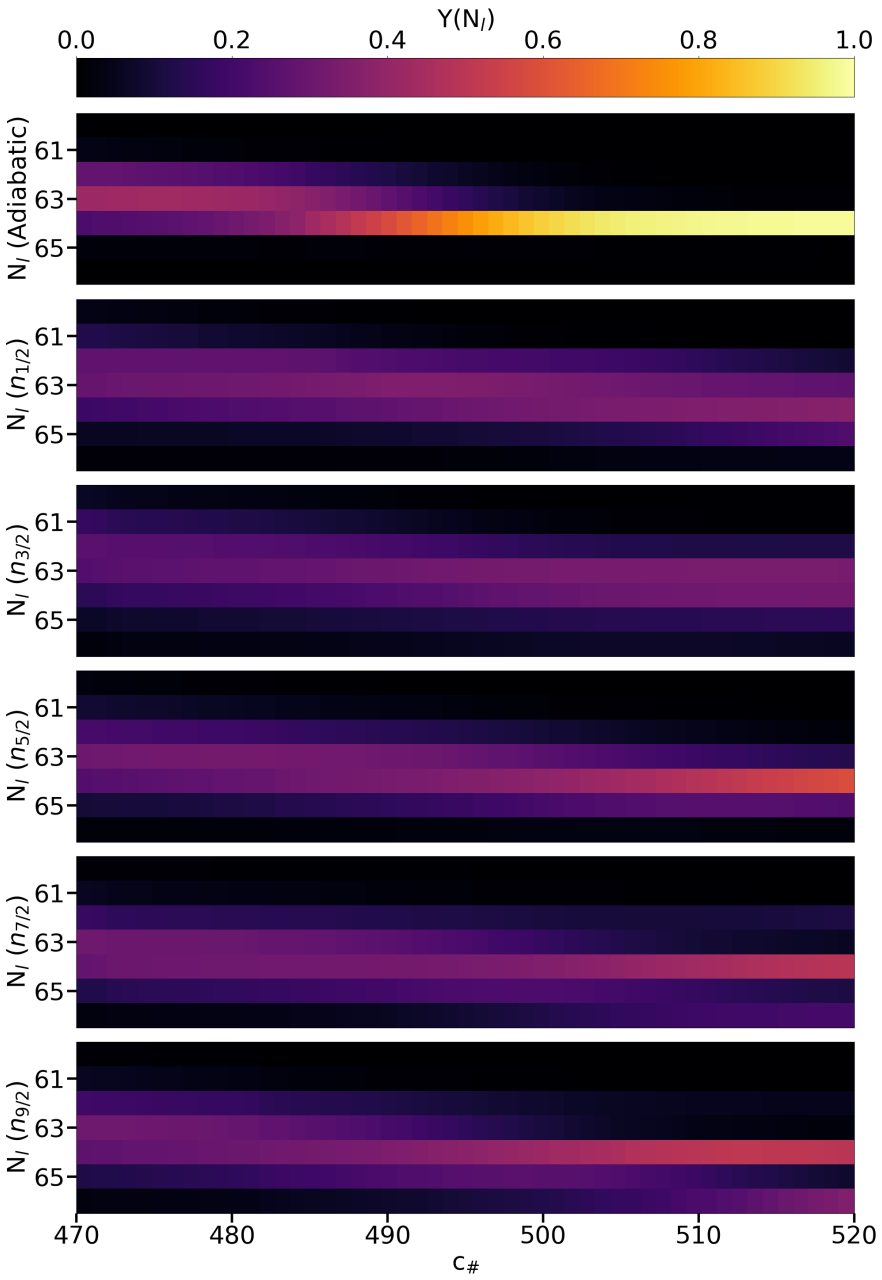

Figure 4.11: Study of the light fragment neutron particle number distributions of the adiabatic states and of the neutron variational excited states with respect to $c_{\#}$.

While the distribution related to the adiabatic states clearly peaks at N_l= 64 after $c_{\#} = 495$, the distributions associated with the neutron variational excited states are much broader. In addition, we remark non negligible odd components in the variational excited states distributions. The relative importance of these odd components is highlighted in Figure (4.12), where the total odd components squared norm c^2_{odd} is displayed with respect to $c_{\#}$:

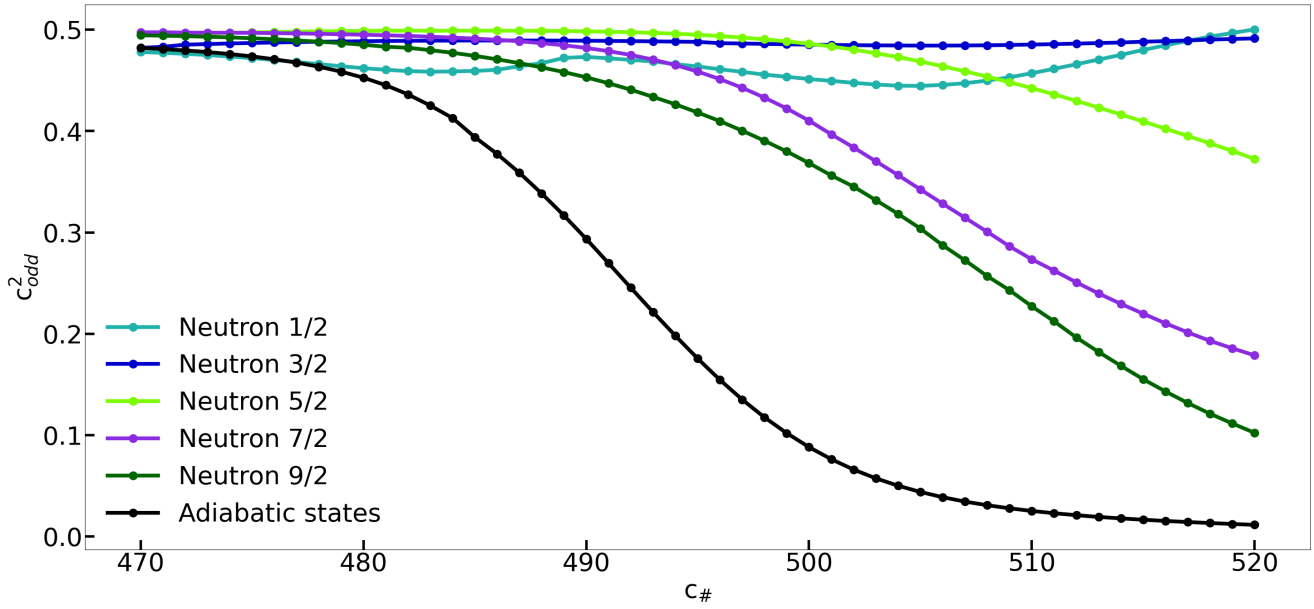

Figure 4.12: Study of the importance of the odd components in the light fragment neutron particle number distributions of the adiabatic states and of the neutron variational excited states with respect to $c_\#$.

First of all, it is clear that the variational excited states present more odd components than the adiabatic ones. In terms of couplings between the pre-fragments, we understand that if a variational excitation changes the particle number distribution in one of the two pre-fragments, it also necesarily changes the distribution related to the other. Because of that, we think that the curve displayed in Figure (2.1.5) provide us with a good hint on the intensity of the pre-fragments couplings.
That being said, the results shown in both Figure (4.11) and Figure (4.12) should be treated with caution. Both the particle number distributions and the average particle numbers of the fragments may vary with respect to $c_\#$, even after scission. Indeed, as the average particle number is only imposed globally, a system of communicating vessels can take place between both fragments. For this reason, the more relevant for the analysis is to consider the particle number near scission and not too far after.
In Figure (4.13), we've represented the neutron particle number distributions associated with the light fragment of the adiabatic state at scission and of the neutron variational excited states at scission ($c_\# = 495$):

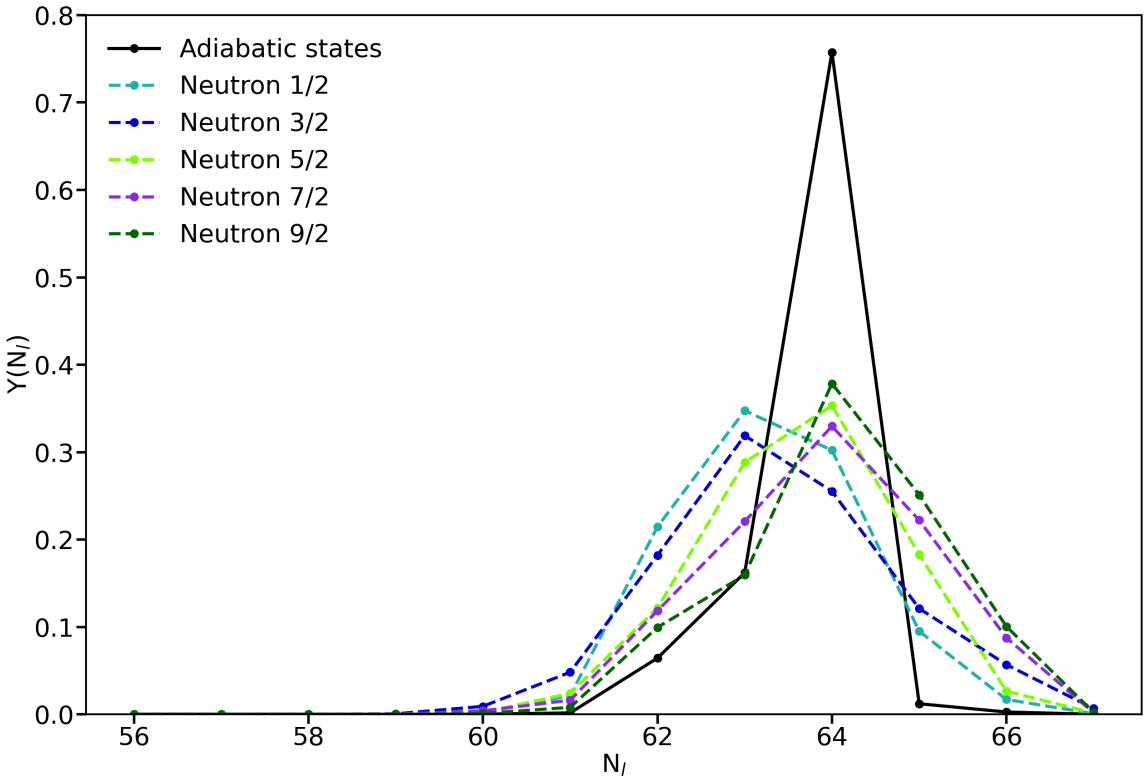

Figure 4.13: Light fragment neutron particle number distributions of the adiabatic state and of the neutron variational excited states at scission.

Figure (4.13) confirms the observations already made. The adiabatic distribution clearly peaks at N=64 when the other excited distributions are broader. As a comparison, the experimental neutron yields slightly peak at N = 60 for the light fragment [61]. Besides, the odd components are far from being negligible. For instance, the $\Omega = 3/2$ distribution associated with the dark blue curve has more odd components than even ones.
These results underlines two important things. The first one is that the neutron variational excitations created do include pair breaking phenomena, as they strongly increase the odd/even component ratio. Secondly, it's good to see that the particle number distributions associated with the variational neutron excited states are wider. Indeed, yields obtained with the adiabatic TDGCM are often criticized for being too narrow. Looking at Figure (4.13), we can see that the inclusion of neutron variational excited states will help address this problem.

In Figure (4.14), we've displayed the proton particle number distributions associated with the light fragment of the adiabatic states and of the proton variational excited states with respect to the collective coordinate $c_{\#}$:

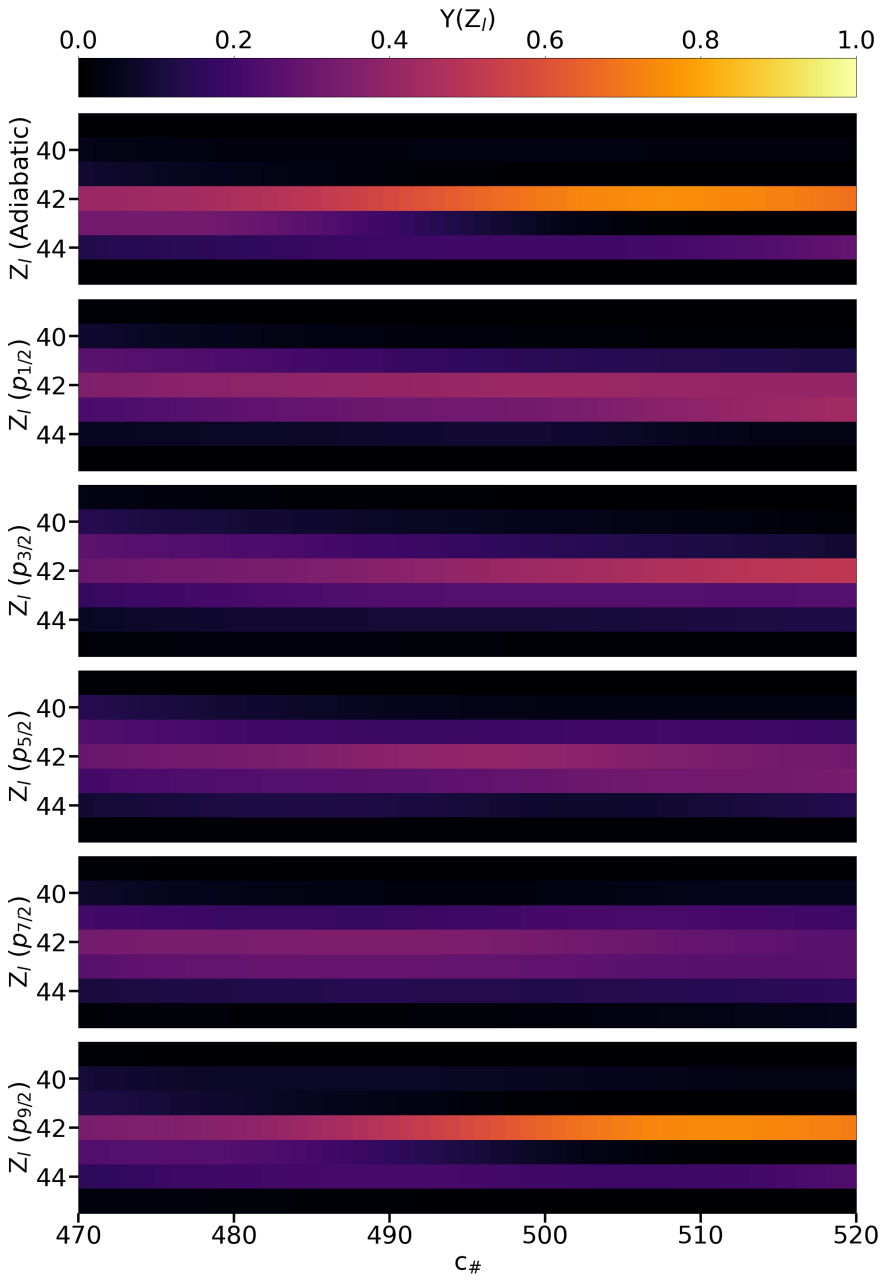

Figure 4.14: Study of the light fragment proton particle number distributions of the adiabatic states and of the proton variational excited states with respect to $c_{\#}$.

At the adiabatic level near scission, we observe not only a peak, but two main contributions for the even components $Z_l = 42$ and $Z_l = 44$. As a comparison, the experimental charge yields slightly peak at $Z_l = 40$ with a secondary peak at $Z_l = 42$ for the light fragment. In addition, the odd components are negligible. This phenomenon is called proton odd-even staggering and appears in the experimental results. It reflects the greater intensity of the proton pairing compared with the neutron pairing one. As far as we know, it is the first time that this phenomenon is observed for HFB states at scission in a realistic PES. Trials had already been made in the past [65], but they had not been conclusive as they could not get close enough to the scission with their method.
As far as proton variational excitations are concerned, we can see that most of them do not exhibit the odd-even staggering. This is of course linked to the fact that pairs are broken in the

excitation process. However, the proton variational excitation labeled by $\Omega = 9/2$ is different as its related distribution is very similar to the adiabatic one. This is not a coincidence, as this is also the variational excitation that has shown the most regular behaviour with respect to the quantities $\sigma^{(2)}$ and $\sigma^{(4)}$ ($\sigma^{(2)}+\sigma^{(4)} = 1$ near and after scission). In addition, its chemical potentials were the closest to the adiabatic ones and its neutron necking properties were also very close to the adiabatic ones. We therefore assume that this proton variational excitation is a typical example of a variational excitation that does not couple the pre-fragments. This statement is discussed in greater detail in the next section 4.4.
As in the neutron case, we've displayed in Figure (4.15) the evolution of c^2_{odd} for both the adiabatic states and the proton variational excited states, with respect to $c_{\#}$;

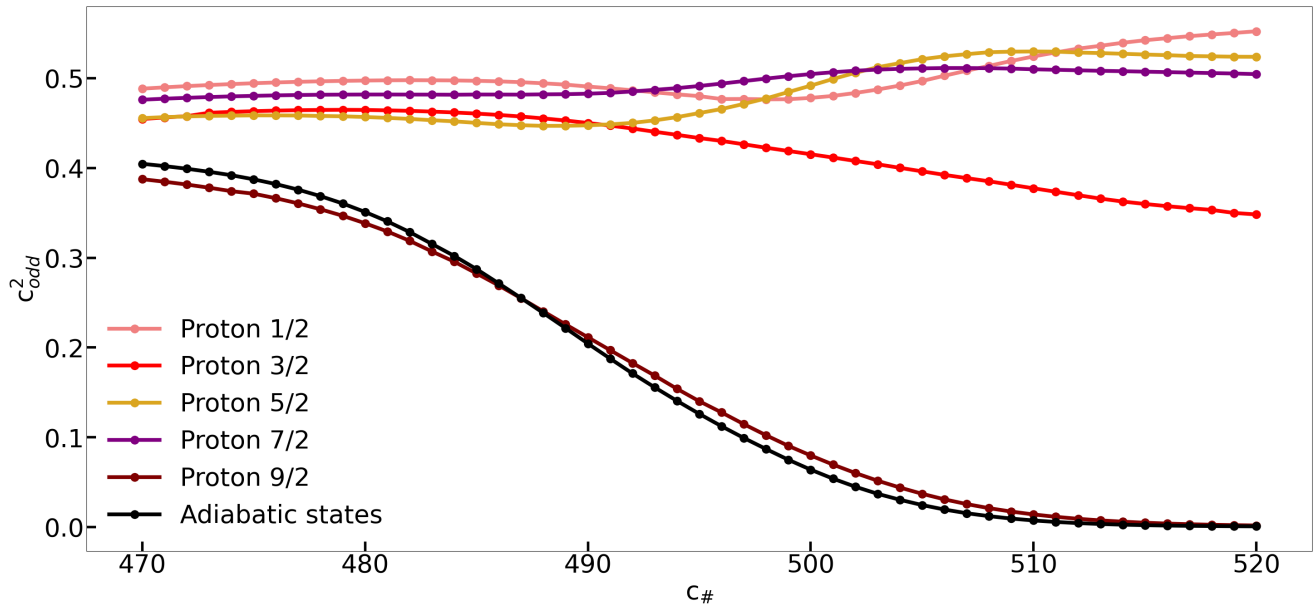

Figure 4.15: Study of the importance of the odd components in the light fragment proton particle number distributions of the adiabatic states and of the proton variational excited states with respect to $c_{\#}$.

Here also, we assume that the different c^2_{odd} values provide us with a good hint on the intesity of the pre-fragments couplings.
As in the case of neutrons, we've isolated the proton particle number distributions at scission. In Figure (4.16), we've represented the proton particle number distributions associated with the light fragment of the adiabatic state and of the proton variational excited states at scission ($c_{\#} = 495$):

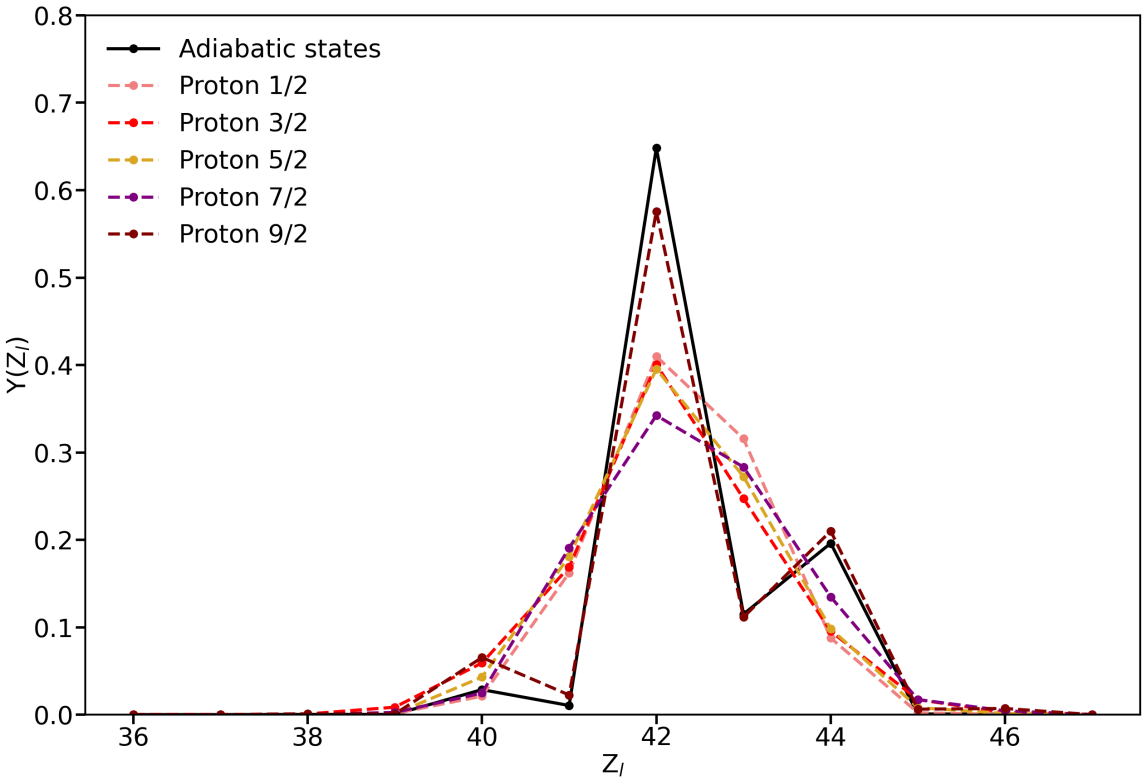

Figure 4.16: Light fragment proton particle number distributions of the adiabatic state and of the proton variational excited states at scission.

The Figure (4.16) shows more clearly the phenomena described above. We clearly see the proton odd-even staggering related to the adiabatic state along with the wider distributions associated with the variational excitations (with the exception of the $\Omega = 9/2$ one). In addition, we observe how close the adiabatic distribution and the $\Omega = 9/2$ distribution are. If all the states corresponding to a fission event showed proton odd-even staggering comparable to that of the adiabatic state displayed in Figure (4.16), then the sawtooth that would be obtained in the charge yields would be far greater than that observed in experiments. This again underlines the importance of including intrinsic excitations in the fission "dynamics". Not only will they broaden the yields, but they will also unable us to achieve a better description of the sawtooth in the charge yields by attenuating the strong proton odd-even staggering at the adiabatic level. This statement is illustrated in Chapter 6.

4.3.3 Fragment particle numbers using different Gogny interactions

We conclude this section by studying the impact of both the D1S and D2 interactions (with or without exact treatment of the Coulomb term of the interaction) on the fragment particle number distributions.
In Figure (4.17), we've displayed the neutron particle number distributions associated with the light fragment of the adiabatic states obtained with both D1S and D2 (with and without exact treatment of the Coulomb term of the interaction), with respect to the collective coordinate $c_{\#}$. In Figure (4.18), we've done the same work on the proton side:

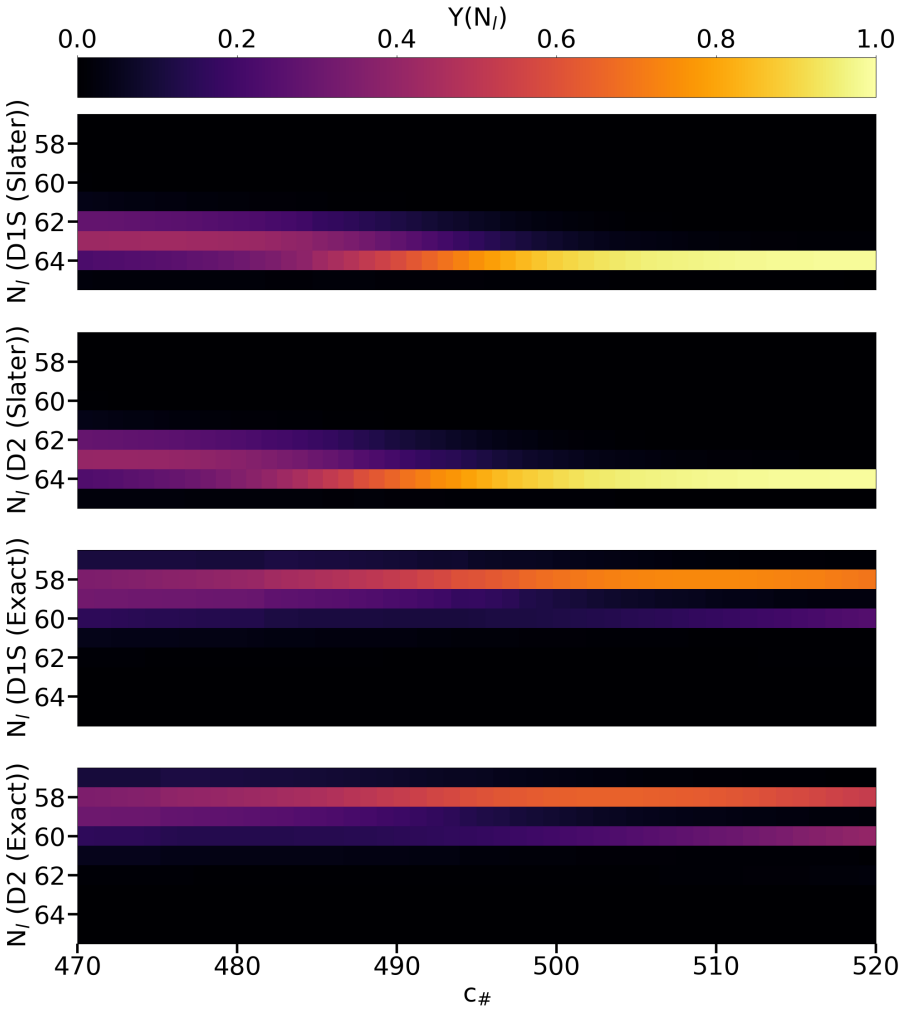

Figure 4.17: Study of the light fragment neutron particle number distributions of the adiabatic states obtained with both D1S and D2 (with and without exact treatment of the Coulomb term of the interaction), with respect to $c_{\#}$.

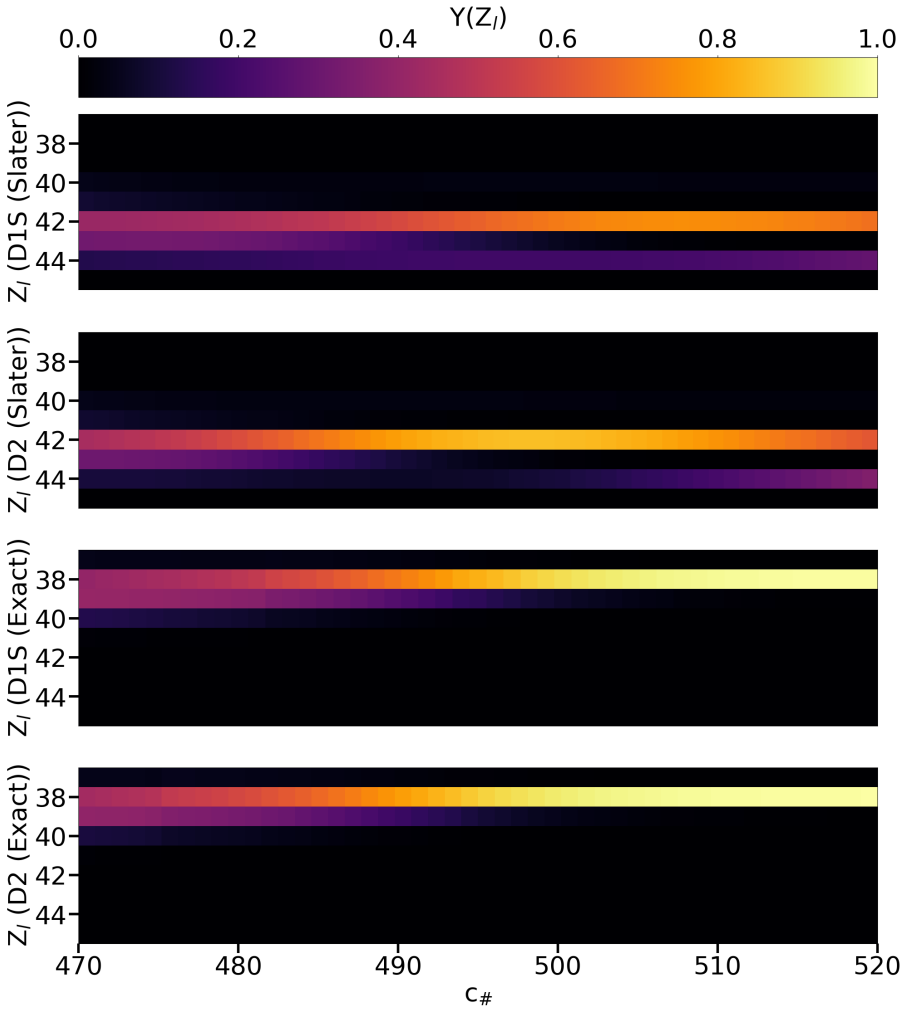

Figure 4.18: Study of the light fragment proton particle number distributions of the adiabatic states obtained with both D1S and D2 (with and without exact treatment of the Coulomb term of the interaction), with respect to $c_{\#}$.

The results presented in Figure (4.17) and Figure (4.18) show two important things. The first is that the D1S and D2 interactions have similar properties concerning the particle number distributions of the fragments. Secondly, it's clear that the pairing intensity is far from the desired physics when the exact treatment of the Coulomb term is used. Indeed, we observe neutron odd-even staggering instead of the proton one, and the major fragmentation is strongly modified, with a number of protons changed by four units.

4.4 Static energy balance at scission

In this section, we focus on the static state energy balance at scission. More specifically, we propose a method for separating the HFB states into left end right sub-states, and calculating the left and right binding energies, as well as the interaction energy between the left and right sub-states. This method is inspired by what has been proposed in [35], but we have adapted it, in particular using the canonical basis. For this reason, we call this variant the RC-separation method.
At the adiabatic level, this method gives access to the part of the TKE that comes from the Coulomb interaction potential at scission. It also makes it possible to determine the

deformation energy of the sub-states by looking at the evolution of their respective binding energies. As a by-product of the method, it is also interesting to observe how the various components of the interaction energy behave as the fragments move apart.
Applying this method to variational excited states is more difficult, and sometimes even impossible. The reasons are quite subtle and will be detailed further in this section. In some cases, however, the method is applicable. It is used, for example, to decide definitively on the nature of the proton variational excitation labeled by $\Omega = 9/2$. To conclude on variational excitations, the method enables us to give an interesting particle state interpretation of the neutron necking properties observed in the neutron $\Omega = 9/2$ variational excitation in section 4.2.
Finally, it is possible to couple this method to the particle number projection formalism to obtain the Projection Onto Fragmentation (POF) method. The POF method allows to evaluate fragmentation-projected energies. We didn't have the time to fully explore the possibilities offered by this method, but we propose an application in the determination of the standard-deviation of the Coulomb interaction energy associated with the particle number fluctuations.

4.4.1 The RC-separation method

Before developing the RC-method, we'd like to say a few words about the reason why the z-separation method is not used here. In fact, the latter is very efficient for obtaining reliable fragment particle number distributions, because it enables odd components to be evaluated. However, we don't have the means to calculate the energy associated with this type of state. Unlike the z-separation, the way HFB states are separated by the RC-separation allows only time-even sub-states. This is not a problem when the fragments particle number components of a state are naturally even, as is the case at the adiabatic level (see section 4.3). On the other hand, it implies serious problems in the case of the variational excited states, whose fragments particle number odd components are far from being negligible. We will come back to this issue later on in this section.

We start by presenting the separation method proposed in [35]. It aims to separate the quasiparticle annihilation operators of a given HFB state into left and right subsets noted $\{\xi_{\mu_l}\}$ and $\{\xi_{\mu_r}\}$. Indeed, doing so, it is possible to separate the matrices ρ and κ accordingly:

$$\boxed{\begin{cases} \rho_{\alpha\beta} = (VV^T)_{\alpha\beta} = \sum_\mu V_{\alpha\mu}V_{\beta\mu} = \sum_{\mu_l} V_{\alpha\mu_l}V_{\beta\mu_l} + \sum_{\mu_r} V_{\alpha\mu_r}V_{\beta\mu_r} = \rho^{(l)}_{\alpha\beta} + \rho^{(r)}_{\alpha\beta} \\ \kappa_{\alpha\beta} = (VU^T) = \sum_\mu V_{\alpha\mu}U_{\beta\mu} = \sum_{\mu_l} V_{\alpha\mu_l}U_{\beta\mu_l} + \sum_{\mu_r} V_{\alpha\mu_r}U_{\beta\mu_r} = \kappa^{(l)}_{\alpha\beta} + \kappa^{(r)}_{\alpha\beta} \end{cases}} \tag{4.25}$$

To determine which quasiparticle subset a given annihilation operator ξ_μ belongs to, we consider its contribution to the local density $\rho(\vec{r})$. Indeed, the latter reads (isospins are voluntarily omitted for simplicity purposes):

$$\rho(\vec{r}) = \sum_{\alpha\beta} \delta_{s_\alpha s_\beta}\psi^*_\alpha(\vec{r})\psi_\beta(\vec{r})\rho_{\beta\alpha} = \sum_\mu \sum_{\alpha\beta} \delta_{s_\alpha s_\beta}\psi^*_\alpha(\vec{r})\psi_\beta(\vec{r})\rho^\mu_{\beta\alpha} = \sum_\mu \rho^\mu(\vec{r}) \tag{4.26}$$

In Eq.(4.26), we naturally set $V_{\alpha\mu}V_{\beta\mu} = \rho^\mu_{\beta\alpha}$ and $\rho^\mu(\vec{r}) = \sum_{\alpha\beta} \delta_{s_\alpha s_\beta}\psi^*_\alpha(\vec{r})\psi_\beta(\vec{r})\rho^\mu_{\alpha\beta}$. Then, we introduce the two quantities $(v^{(l)}_\mu)^2$ and $(v^{(r)}_\mu)^2$:

$$\begin{cases} (v_\mu^{(l)})^2 = \int d\vec{r}_\perp \int_{-\infty}^{z_{neck}} \rho^\mu(\vec{r}) \\ (v_\mu^{(r)})^2 = \int d\vec{r}_\perp \int_{z_{neck}}^{+\infty} \rho^\mu(\vec{r}) \end{cases} \tag{4.27}$$

Here, the z_{neck} abscissa is the same as for the z-separation method. The quantities $(v_\mu^{(l)})^2$ and $(v_\mu^{(r)})^2$ evaluate the left and right contributions to the quasiparticle ξ_μ to the local density. Therefore, we consider that if $(v_\mu^{(l)})^2 > (v_\mu^{(r)})^2$, $\xi_\mu \in \{\xi_{\mu_l}\}$, while $(v_\mu^{(r)})^2 \geq (v_\mu^{(l)})^2$, $\xi_\mu \in \{\xi_{\mu_r}\}$. Then, it is natural to define the separation index s as follows:

$$\boxed{s = 2\sum_\mu \min((v_\mu^{(l)})^2, (v_\mu^{(r)})^2) = \sum_\mu s_\mu} \tag{4.28}$$

Here, the factor 2 stands for the time-reversal contributions. The separation index s corresponds to the total particle number spatially localized in one subspace while it has been attributed to the other by the method.
If we were to apply the method as it stands, we'd probably be disappointed with the results though. Indeed, the quasiparticle operators $\{\xi_\mu\}$ are defined up to a rotation, and there is no particular reason why they should spontaneously be found in the respresentation that minimizes s. In [35], this issue is tackled by performing rotations on relevant pairs of quasiparticles. A similar feature is also included in the RC-separation method and will be discussed later on.

We assume that the rotation that minimizes s has been found. We end up with the matrices $\rho^{(l)}$, $\rho^{(r)}$, $\kappa^{(l)}$, and $\kappa^{(r)}$. Thanks to them, we can rewrite the HFB energy:

$$\boxed{E = E^{(l)} + E^{(r)} + E_{int}} \tag{4.29}$$

With:

$$\boxed{\begin{cases} E^{(l)} = \sum_{\alpha\beta} t_{\alpha\beta}\rho^{(l)}_{\alpha\beta} + \frac{1}{2}\sum_{\alpha\beta\gamma\delta} v^{(a)}_{\alpha\beta\gamma\delta}\rho^{(l)}_{\gamma\alpha}\rho^{(l)}_{\delta\beta} + \frac{1}{4}\sum_{\alpha\beta\gamma\delta}(-1)^{s_\beta - s_\delta} v^{(a)}_{\alpha\beta\gamma\delta}\kappa^{(l)}_{\alpha\beta}\kappa^{(l)}_{\gamma\delta} \\ E^{(r)} = \sum_{\alpha\beta} t_{\alpha\beta}\rho^{(r)}_{\alpha\beta} + \frac{1}{2}\sum_{\alpha\beta\gamma\delta} v^{(a)}_{\alpha\beta\gamma\delta}\rho^{(r)}_{\gamma\alpha}\rho^{(r)}_{\delta\beta} + \frac{1}{4}\sum_{\alpha\beta\gamma\delta}(-1)^{s_\beta - s_\delta} v^{(a)}_{\alpha\beta\gamma\delta}\kappa^{(r)}_{\alpha\beta}\kappa^{(r)}_{\gamma\delta} \\ E_{int} = \sum_{\alpha\beta\gamma\delta} v^{(a)}_{\alpha\beta\gamma\delta}\rho^{(l)}_{\gamma\alpha}\rho^{(r)}_{\delta\beta} + \frac{1}{2}\sum_{\alpha\beta\gamma\delta}(-1)^{s_\beta - s_\delta} v^{(a)}_{\alpha\beta\gamma\delta}\kappa^{(l)}_{\alpha\beta}\kappa^{(r)}_{\gamma\delta} \end{cases}} \tag{4.30}$$

In Eq.(4.29), $E^{(l)}$ is the binding energy associated with the left sub-state, $E^{(r)}$ is the one associated with the right sub-state, and E_{int} is the interaction energy between both sub-states. To evaluate the contribution of the density-dependent term to $E^{(l)}$, $E^{(r)}$ and E_{int}, we have used the prescription given in [35]. This prescritpion involves using the one-body densities $\rho^{(l)}$ and $\rho^{(r)}$ to evaluate the binding energies $E^{(l)}$ and $E^{(r)}$ respectively. The interaction energy E_{int} is then deduced from the difference between the total binding energy E and the left and right binding energies $E^{(l)}$ and $E^{(r)}$.

The RC-separation differs from the method presented previously, as it assumes that the C

matrix of the Bloch-Messiah theorem (see Appendix C) is a relevant rotation for separating the quasiparticle operators. In other words, the RC-separation method consists in separating the quasiparticle operators $\{\eta_k\}$ associated with the so-called "canonical representation". The original intuition comes from the fact it simplifies naturally the quasiparticle operator structures. Therefore, we expect this representation to provide us with rather small values of the separation index s. In the following, we observe that the choice of the "canonical representation"is an ansatz really efficient in practice. Moreover, in the "canonical representation", the quasiparticle annihilation operators and the particle creation operators are labeled by the same index. Thanks to that, it is possible to give an interpretation of the RC-separation results in terms of single particle orbitals, which we find very interesting. Besides, it is this special feature that allows to couple the RC-separation with the projection formalism.
In the canonical representation, the sub-matrices ρ^k and κ^k labeled by the quasiparticle index read as follows:

$$\begin{cases} \rho^k_{\alpha\beta} = D_{\alpha k} D_{\beta k} v_k^2 \\ \kappa^k_{\alpha\beta} = D_{\alpha k} D_{\beta k} v_k u_k \end{cases} \tag{4.31}$$

To tell if a quasiparticle operator η_k belongs to the left subset $\{\eta_{k_l}\}$ or to the right one $\{\eta_{k_l}\}$, we still use their contribution $\rho^k(r)$ to the local density. The latter reads:

$$\rho^k(\vec{r}) = v_k^2 \sum_{\alpha\beta} \delta_{s_\alpha s_\beta} D_{\beta k} D_{\alpha k} \psi^*_\alpha(\vec{r}) \psi_\beta(\vec{r}) = v_k^2 |\varphi_k(\vec{r})|^2 \tag{4.32}$$

In Eq.(4.32), the wave functions φ_k are the wave functions associated with the canonical particle orthonormal basis. Using the notations introduced in Eq.(4.7) to characterize the squared norm of the left and right parts of the wave functions φ_k leads to:

$$\begin{cases} (v_k^{(l)})^2 = v_k^2 (c_k^{(l)})^2 \\ (v_k^{(r)})^2 = v_k^2 (c_k^{(r)})^2 \end{cases} \tag{4.33}$$

Thanks to Eq.(4.33), we can define the s index standing fot the RC-separation method:

$$\boxed{s = 2 \sum_k v_k^2 \min((c_k^{(l)})^2, (c_k^{(r)})^2)} = \sum_k s_k \tag{4.34}$$

In Figure (4.19), we've displayed the values of the s indexes associated with both isospins along with the values of the total s_t index found performing the method previously described in the adiabatic set, with respect to $c_\#$:

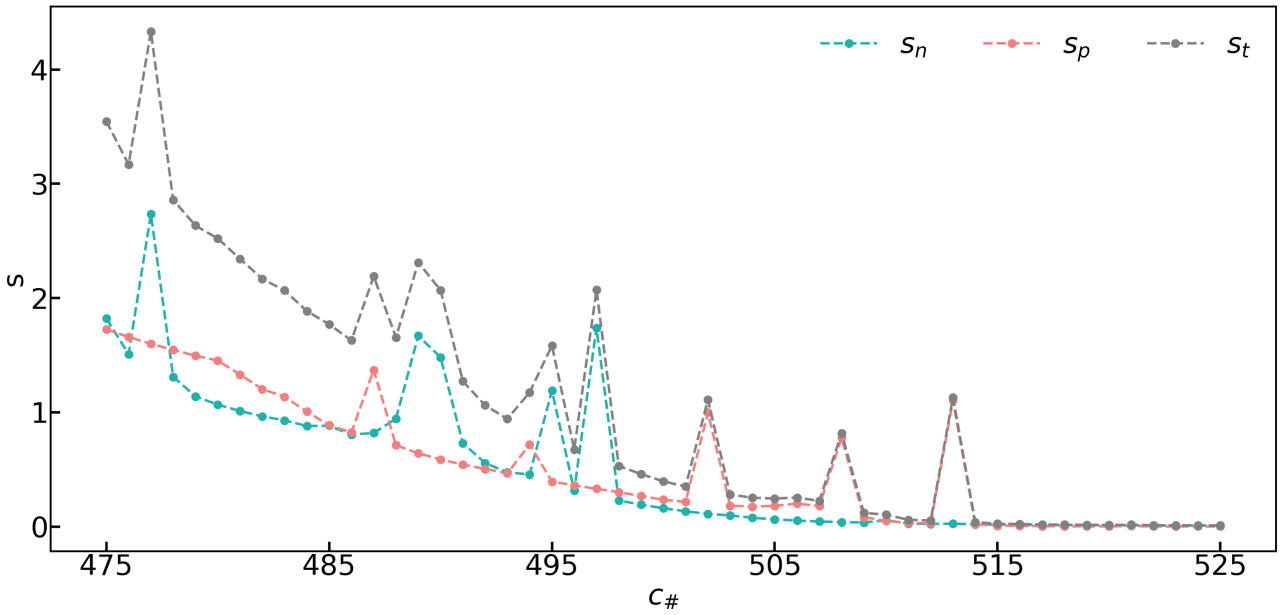

Figure 4.19: Study of the indexes s_n, s_p and s_t standing respectively for the neutron, proton and total separation indexes in the adiabatic set, with respect to $c_\#$.

The results in Figure (4.19) are really frustrating. Indeed, decreasing trends clearly appear, which corresponds to our expectations. However, some specific anomalies are spoiling these good trends. We searched for the cause of these anomalies by comparing two neighbouring states labeled by $c_\# = 486$ and $c_\# = 487$. The first one follows the trends, while the second one exhibits an abnormal behaviour. We found out that all the s_k values associated with both states were comparable, except for two specific ones, both associated with proton $\Omega = 1/2$ particle states (the realted s_k values were 0.307 and 0.306). In addition, the v_k^2 quantities associated with these two particle states were very close (we found an absolute difference of 2×10^{-6}).
This latter observation guided us towards the cause of the anomalies. Indeed, the Bloch-Messiah matrix D, is defined up to rotations with respect to the degenerated subspaces of both v_k and u_k, as long as only ρ and κ are considered. The latter are rotations among the particle states. Of course, to preserve the structure of the U and V matrices, the same rotation has to be added to the C matrix, which defines a rotation among the quasiparticle states. It's clear that the whole process preserves the properties of the canonical representation.
Calling the two particle state wave functions associated with the anomaly φ_1 and φ_2, the previous paragraph signifies that we can replace these wave functions by their rotated counterparts $\tilde{\varphi}_1(\theta)$ and $\varphi_2(\theta)$, preserving the "canonical representation" properties. These rotated wave functions read as follows:

$$\boxed{\begin{cases} \tilde{\varphi}_1(\theta) = \cos(\theta)\varphi_1 - \sin(\theta)\varphi_2 \\ \tilde{\varphi}_2(\theta) = \sin(\theta)\varphi_1 + \cos(\theta)\varphi_2 \end{cases}} \tag{4.35}$$

In the light of these observations, we've completed the RC-separation method with a rotation step, whose procedure is described above:

- We search for paired states φ_1 and φ_2 belonging to the same (Ω, τ) subspace, such that $s_1 + s_2 > 0.005$ and $|v_1^2 - v_2^2| < 10^{-4}$.

- We find the rotation angle $\theta \in [0, \pi]$ such that the value $d_{12} = \tilde{s}_1 + \tilde{s}_2$ is minimized.
- We add the resulting rotation characterized by the angle θ to the matrix D.

As v_1^2 and v_2^2 are not exactly equal, the additional rotations may induce a small change in the ρ and κ matrices. In practice, we've never found a distance between the initial and the rotated ρ and κ matrices whose order of magnitude was greater that 10^{-4} (with respect to the Frobenius norm).
In Figure (4.20), we've represented the squared modulus of the wave functions φ_1 and φ_2 associated with the anomaly in the state labeled by $c_{\#} = 487$ before and after rotation:

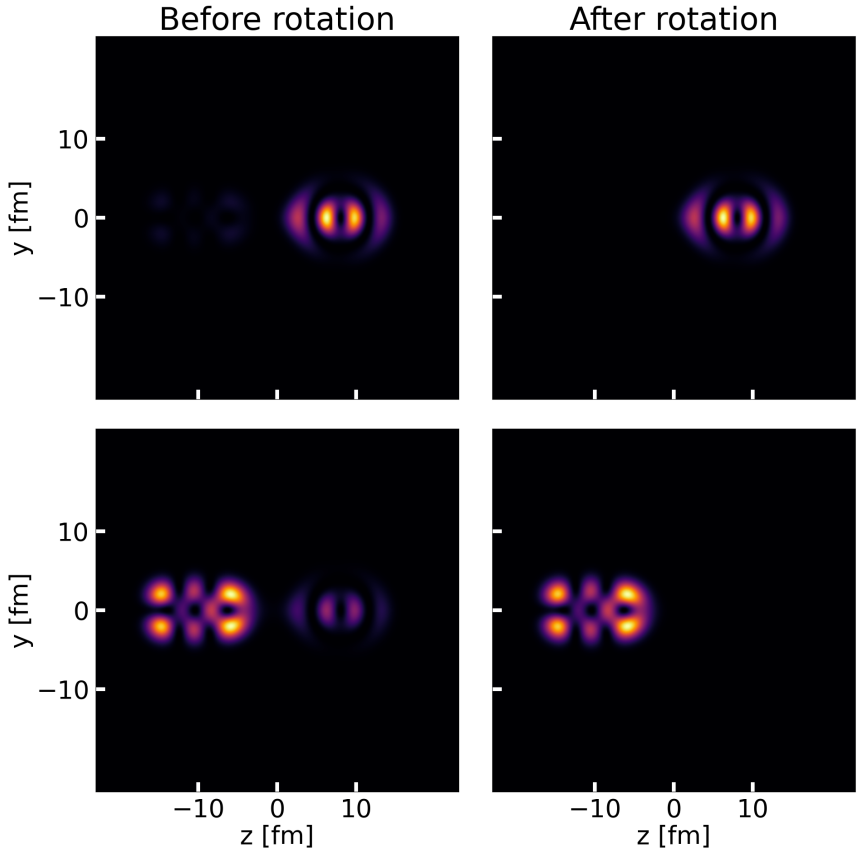

Figure 4.20: Effect of a rotation on the particle state φ_1 and φ_2 associated with the adiabatic HFB state labeled by $c_{\#} = 487$.

We observe in Figure (4.20) that the particle states before rotation clearly share a common structure. Each state is made up of a major component in addition to the "ghost reflect" of the major component associated with the other state. After rotation, both states are totally decoupled. In this case, we found $\theta = 0.41$ and $d_{12} = 0.002$.
In Figure (4.21), we've compared the values of the s and the rotated $\tilde{s}$ indexes associated with both isospins along with the values of the total indexes, with respect to $c_{\#}$.

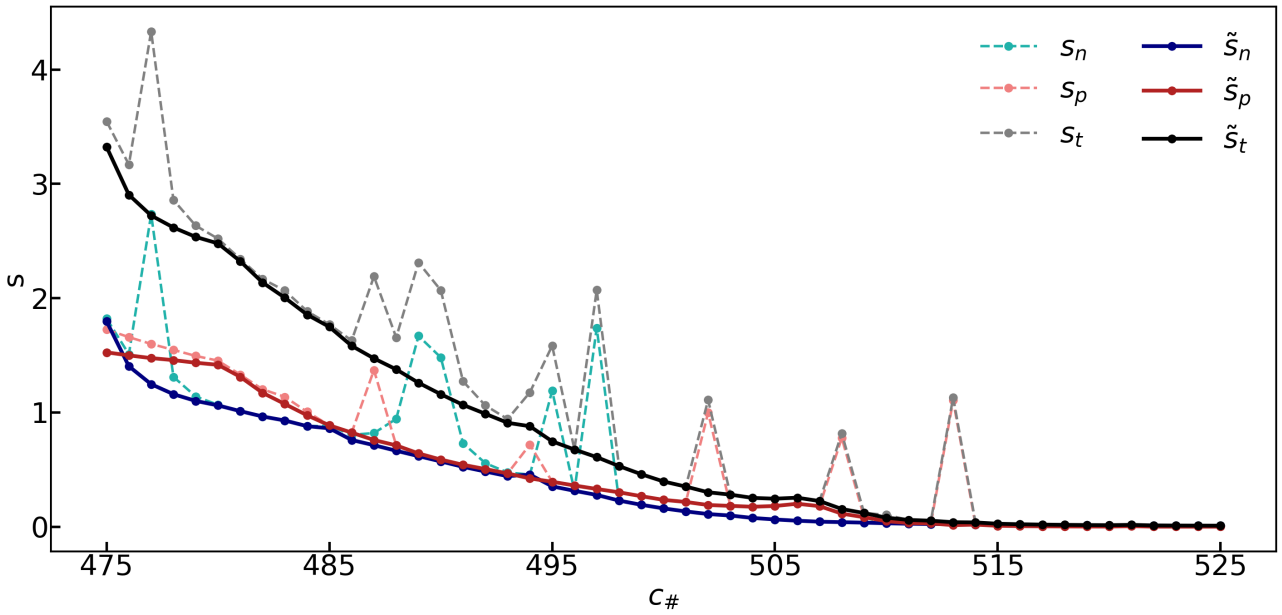

Figure 4.21: Study of the indexes s_n, $\tilde{s}_n$, s_p, $\tilde{s}_p$, s_t, and $\tilde{s}_t$ in the adiabatic set, with respect to $c_\#$.

We clearly observe that the RC-separation method works much better including rotations. All the major anomalies have been smoothed out. We still see some minor bumps along the curves. Future studies would be required to tell whether they have a physical or a technical origin.
At the scission point (localized at $c_\# = 495$), we find a total separation index value of 0.747. In fact, even with the better quasiparticle rotation (of the type proposed in [35]), it wouldn't be possible to find $s_t = 0$, as Figures (4.13) and (4.16) shows that the spatially separated wave functions do include odd particle number components. In the light of this statement, we do believe that our "canonical ansatz" is rather satisfactory overall. In the future, it would be very interesting to compare it with the results given by the method described in [35].
To conclude, we provide the reader with a more visual illustration of the RC-separation method. In Figure (4.22), we've displayed the local densities associated with the left, total, and right densities for five different adiabatic HFB states. This plot isn't just pretty, the fact that the fragment tails retract continuously also tends to prove the quality of the RC-separation method:

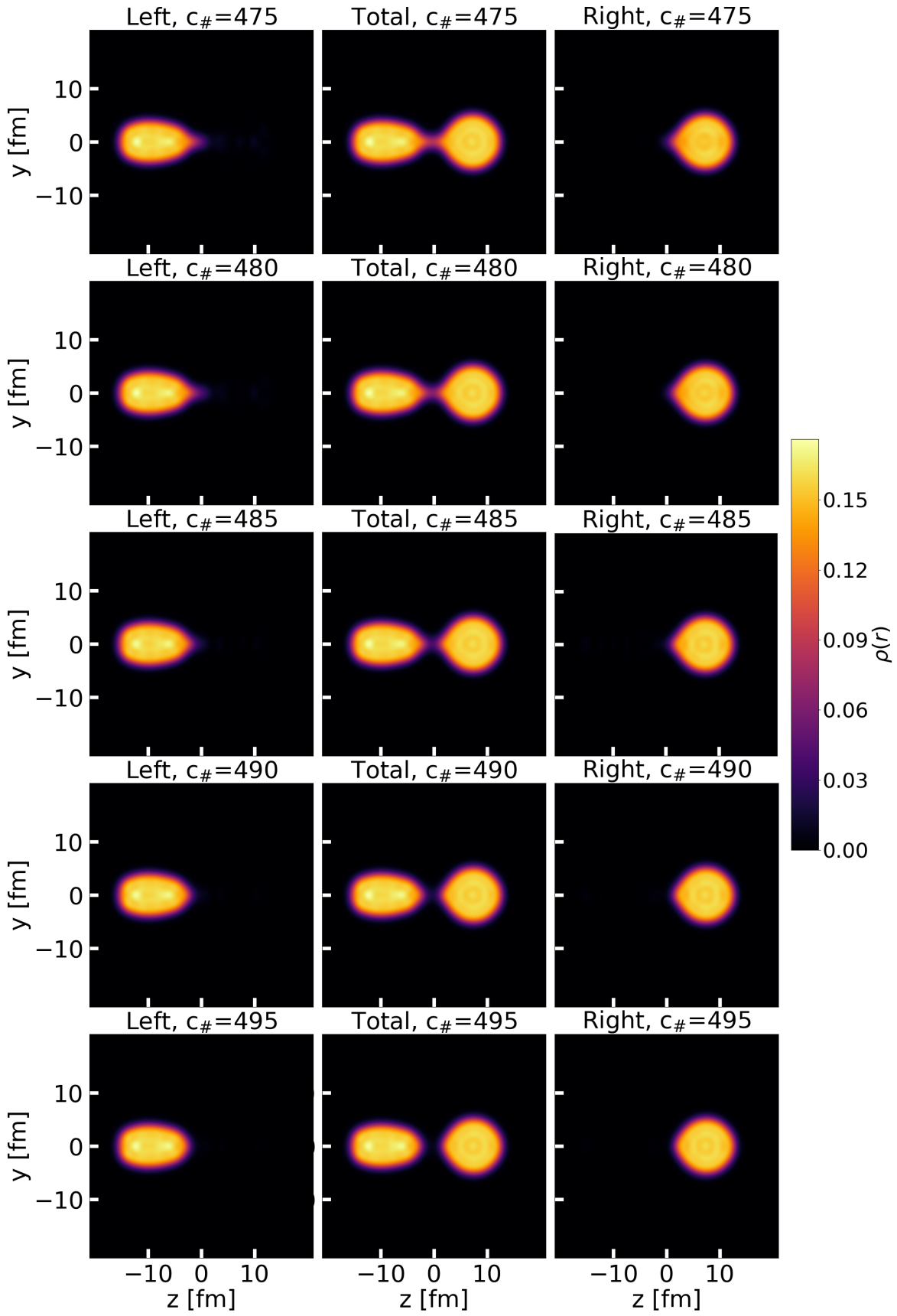

Figure 4.22: Local densities associated with the left, total, and right densities obtained with the RC-separation method for five different adiabatic HFB states.

4.4.2 Adiabatic state study

In Figure (4.23), we've displayed the Coulomb interaction energy found using the RC-separation method on the adiabatic states, with respect to $c_{\#}$. We've added a black line that stands for the Coulomb interaction energy at scission:

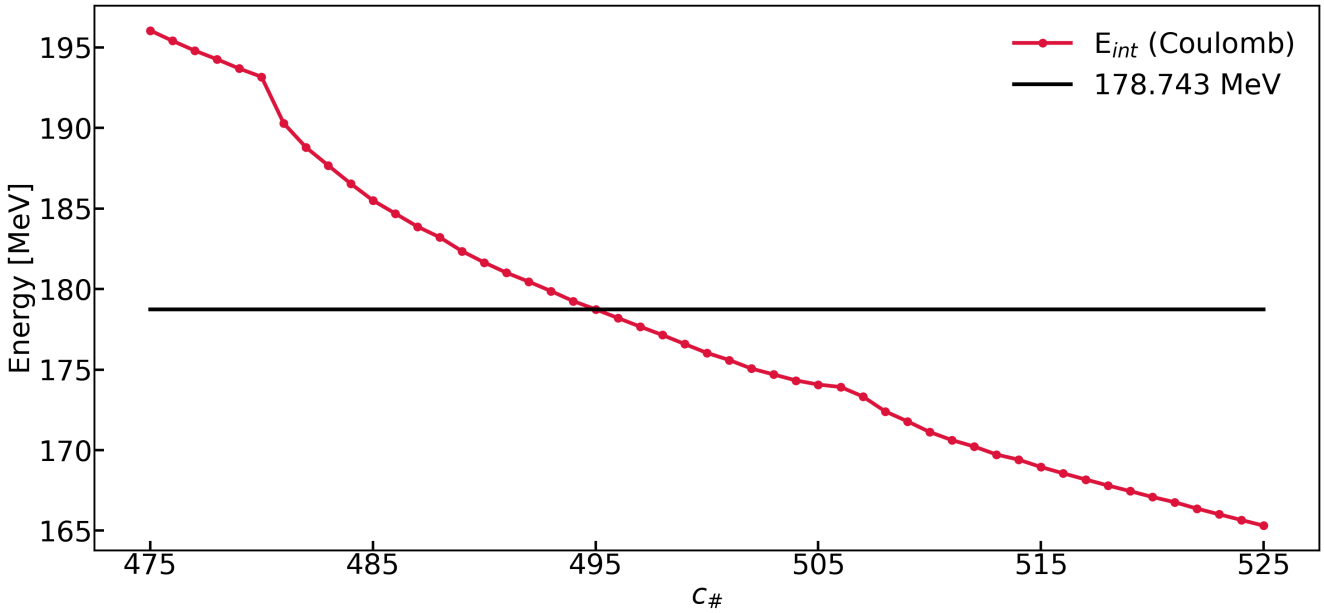

Figure 4.23: Coulomb interaction energy of the states of the adiabatic set obtained with the RC-separation method and displayed with respect to $c_{\#}$.

The Coulomb interaction energy does not directly give the full TKE. In fact, it gives only the part of the TKE which comes from the Coulomb repulsion of the fragments after scission. An other part of the TKE is the well-known pre-scission kinetic energy. It accounts for the kinetic energy accumulated by the pre-fragments through all their journey to scission. In addition, the remaining nuclear interaction energy probably also plays an important role with regard to the fragment kinetic energy. This point is discussed later on in this section. Finally, the agreement between the results presented in Figure (4.23) and the experiments are discussed in the light of the "dynamics" results in Chapter 6.

In panels (a-c) of Figure (4.24), we've plotted for the adiabatic states the binding energy of the left sub-state $E^{(l)}$, the binding energy of the right sub-state $E^{(r)}$, and the total $E^{(tot)} = E^{(l)} + E^{(r)}$, with respect to $c_{\#}$. In addition, we've added black arrows corresponding to the left, right and total deformation energies $\Delta E^{(l)}$, $\Delta E^{(r)}$ and $\Delta E^{(tot)}$ we've evaluated at scission:

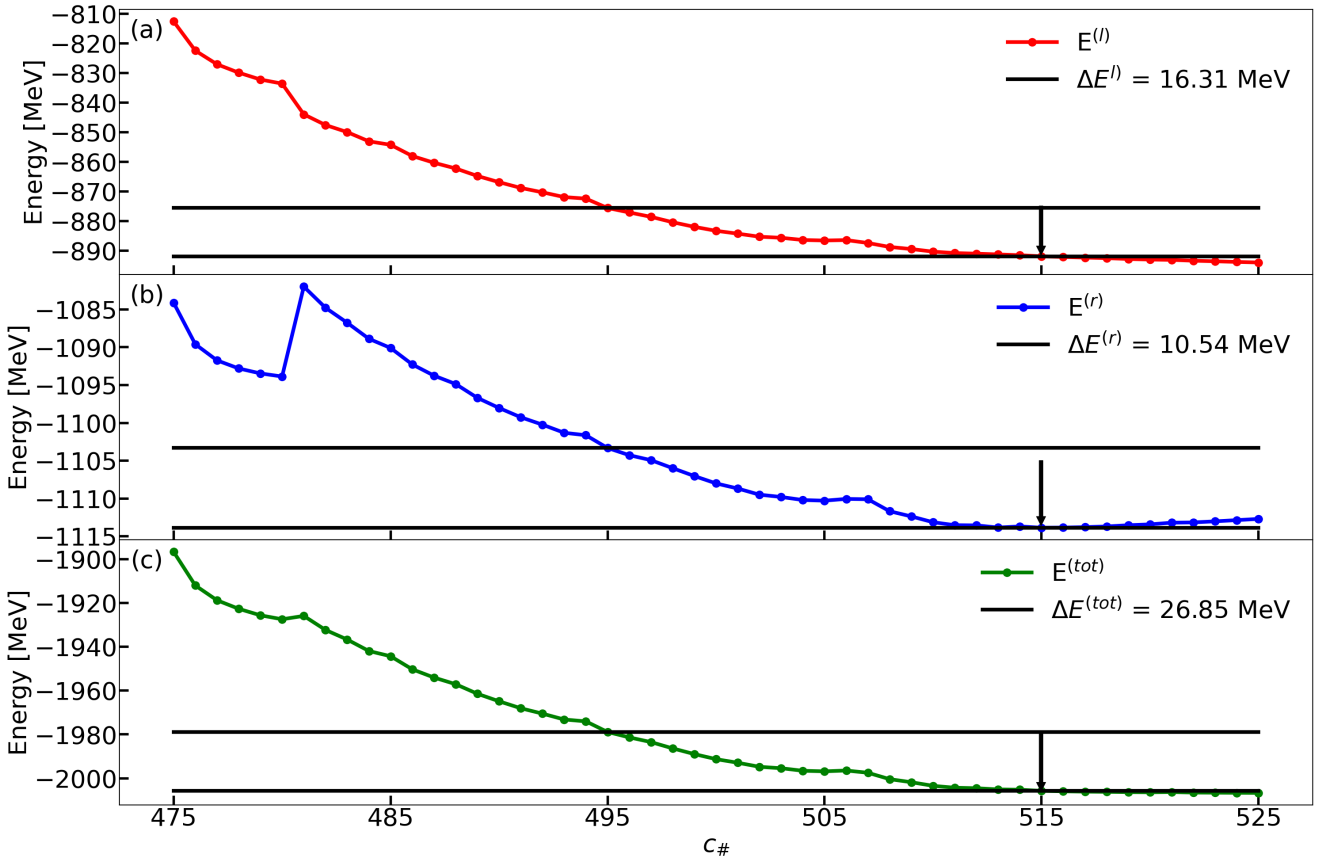

Figure 4.24: Study of the binding energies of the sub-states obtained with the RC-separation method applied on the adiabatic states. Panel (a): binding energy $E^{(l)}$ of the left sub-state with respect to $c_{\#}$. Panel (b): binding energy $E^{(r)}$ of the right sub-state with respect to $c_{\#}$. Panel (c): total energy $E^{(tot)} = E^{(l)} + E^{(r)}$ with respect to $c_{\#}$.

It is first puzzling to observe that the blue curve in panel (b) representing the binding energy $E^{(l)}$ associated with the right sub-state increases a little after $c_{\#} = 515$. Indeed, as the fragments relax their deformation into their ground state, we expect the binding energy to increase in absolute value. However, this strange behaviour of the right sub-state is not related to its deformation but to its particle number distribution that changes with respect to $c_{\#}$, even after scission. In fact, the decrease of the red curve associated with the left sub-state binding energy $E^{(l)}$ we observe in panel (a), is not related to the deformation of the left sub-state but to its particle number distribution. It is a communicating vessels phenomenon between the left and right parts, which is not visible in the sum. In addition to the particle number distributions discussed in section 4.3, the previous statements are proven by the fact that the total energy $E^{(tot)} = E^{(l)} + E^{(r)}$ displayed in panel (c) hardly changes after $c_{\#} = 515$. This discussion explains why we've considered the differences between the binding energies at $c_{\#} = 495$ and the ones at $c_{\#} = 515$ to evaluate the deformation energies $\Delta E^{(l)}$, $\Delta E^{(r)}$ and $\Delta E^{(tot)}$. A way to tackle this issue could be to use the POF formalism presented in the following to specifically extract the deformation energy related to each fragmentation. Unfortunately, we didn't have the time to do it in this PhD thesis. Still, it could be a very interesting study.

We are aware that the way we measure the deformation energies introduces uncertainties in the calculations. However, we believe that this level of uncertainty is acceptable and is in line with the overall precision of the whole formalism. For instance, if we had chosen to evaluate the deformation energies at $c_{\#} = 494$, we would have obtained $\Delta E^{(tot)} = 31.70$

MeV instead of 26.85 MeV. Similarily, if we had considered the deformation energies at $c_{\#} = 496$, we would have obtained $\Delta E^{(tot)} = 24.39$ MeV. The order of magnitude of the latter uncertainties related to the choice of the scission point, in addition to the fact that we miss the physics of the odd fragmentations, clearly underline that there's not point in being more picky than necessary evaluating the deformation energies.
The deformation energies are often evaluated in a very different way. First, the multipole moments $\{Q^{(l)}\}$ and $\{Q^{(r)}\}$ associated with both fragments are evaluated as well as the average particle numbers of the fragments $\{N^{(l)}\}$ and $\{N^{(r)}\}$ (in fact, the closest even integers are considered) . Then, the left and right deformation energies are obtained as the differences between the energies of the deformed HFB states built imposing the constraints $\{Q^{(l)}\}$, $\{N^{(l)}\}$ and $\{Q^{(r)}\}$, $\{N^{(r)}\}$ and their related ground states. This method has two major drawbacks. The most important is that it neglects the particle number distributions of the fragments. This problem could be avoided by applying the method for all the possible fragmentations. However, the latter proposition could be very tedious in practice as it would require many calculations, including odd fragmentations. In addition, it would require the evaluation of the projected multipole moments of the fragments. The second problem of the method, is that it only considers few multipole moments, while the description of the peculiar shapes of the fragments near scission propbably requires more.

To conclude this adiabatic study, we've considered separately all the components of the interaction energy.
In Figure (4.25), we've displayed both the central part and the zero-range density-dependent part of the interaction energy E_{int} with respect to $c_{\#}$:

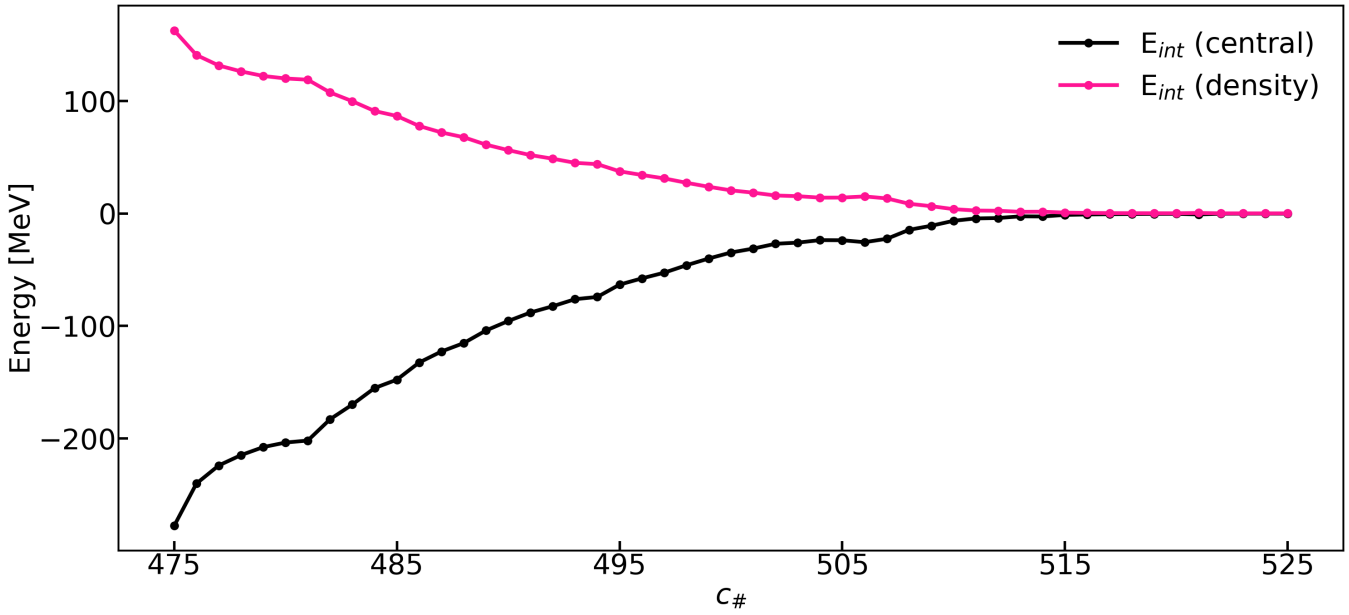

Figure 4.25: Evolution of the central and density components of the interaction energy E_{int} with respect to $c_{\#}$.

The first striking property we observe in Figure (4.25) is the fact that both curves vary accordingly, with opposite signs. The Central contribution is attractive, while the density-depdenent one is repulsive. Besides, we could have expected a much more irregular behaviour from the density-dependent interaction energy, as the density term is a zero-range one. However, the fact that the total density is still used within the density dependent term of the

Hamiltonian explains why the curve behaves smoothly.

In Figure (4.26), we've displayed both the two-body center of mass correction and the zero-range spin-orbit part of the interaction energy E_{int} with respect to $c_{\#}$:

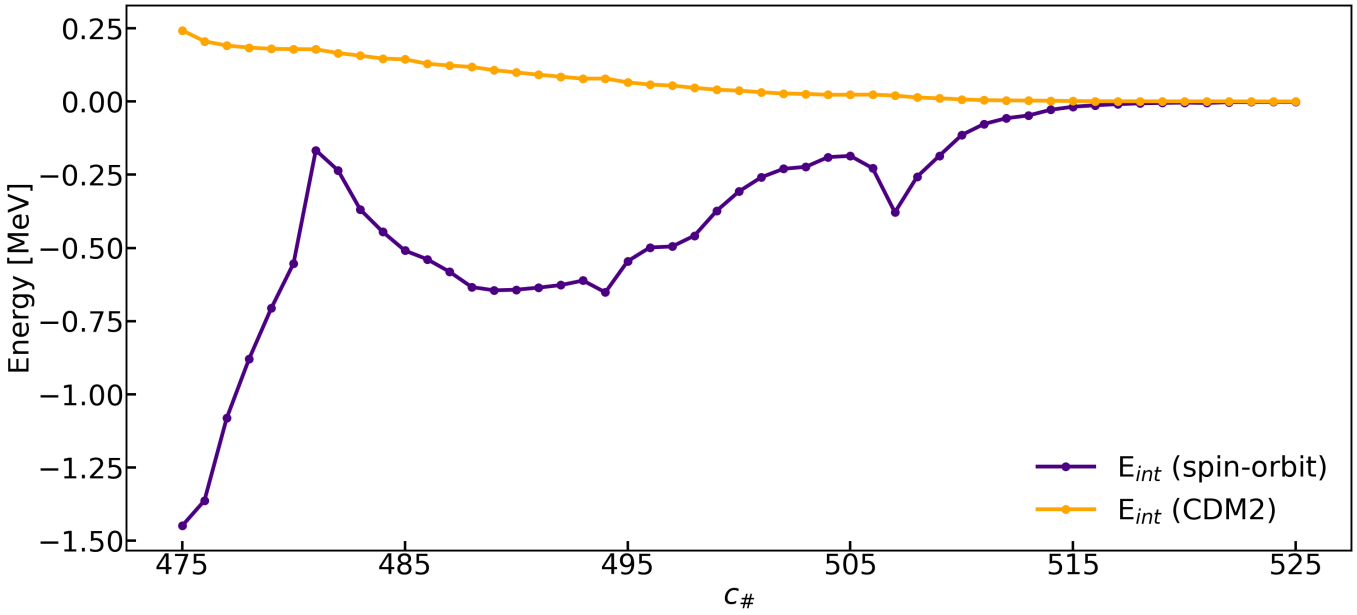

Figure 4.26: Evolution of the two-body center of mass correction and of the spin-orbit components of the interaction energy E_{int} with respect to $c_{\#}$.

First of all, we see that the spin-orbit and the two-body center of mass correction contributions are of a much lower order of magnitude than the central and density-dependent ones. While the two-body center of mass correction interaction energy exhibit a very smooth behaviour, the curve associated with the spin-orbit energy is very bumpy. We assume that, being a zero-range component, the spin-orbit interaction energy is much more sensitive to small variations induced by the RC-separation, which are not felt by the other interaction energy components.

Finally, we've considered the ratio between the total interaction energy and the Coulomb interaction energy r_c, naturally defined as follows:

$$\boxed{r_c = 100 \times |\frac{E_{int}}{E_{int}(Coulomb)}|} \tag{4.36}$$

This ratio characterizes the respective strengths of both the Coulomb interaction, which tends to separate the pre-fragments, and the nuclear interaction, which tends to bring them together. In figure (4.27), we've displayed the ratio r_c with respect to $c_{\#}$:

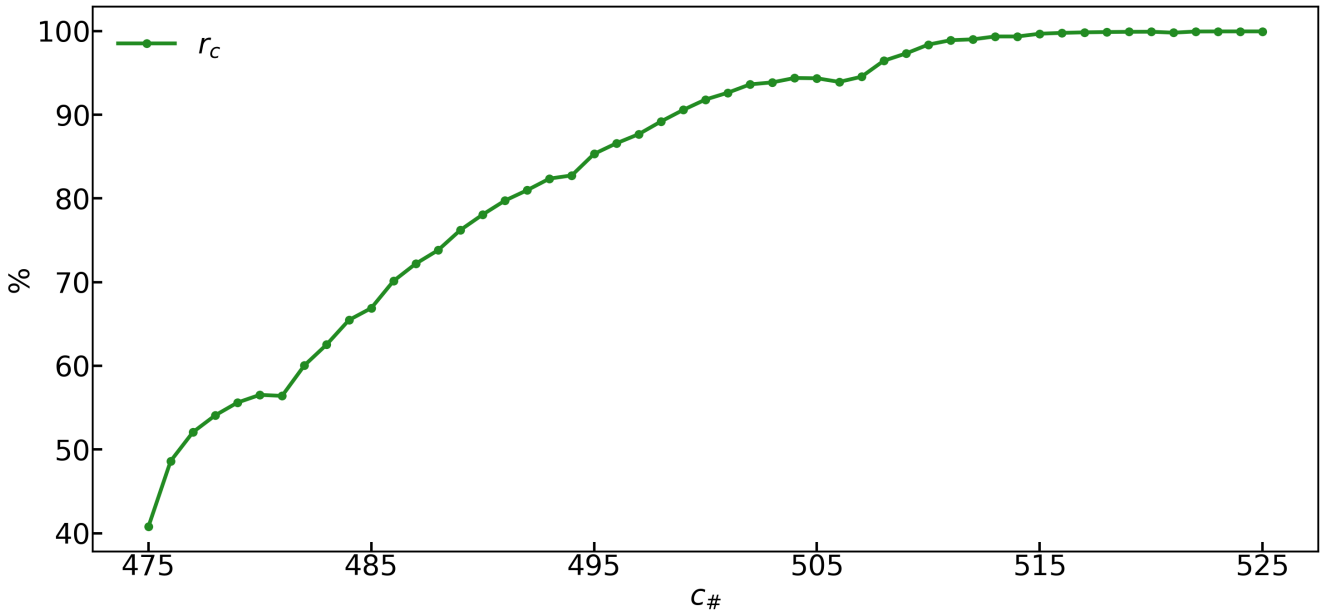

Figure 4.27: Study of the ratio r_c between the Coulomb interaction energy and the total interaction energy.

This curve is very interesting as it gives an idea of how the D1S interaction behaves when describing the nuclear interaction between two almost separated pre-fragments and between two separated, but close, fragments.
At scission ($c_\# = 495$), we've found that the total interaction energy equals 152.50 MeV, while the Coulomb interaction energy equals 178.74 MeV. This result clearly highlights that the nuclear interaction energy that glues the fragments is far from being negligible. Consequently, in Chapter 6, two hypotheses are considered to evaluate the post-scission kinetic energy. The first is the usual assumption that only includes the Coulomb interaction energy. The second consists in considering the whole interaction energy instead.

4.4.3 Variational excitations study

As evoked earlier, the fragments defined by the RC-separation cannot contain odd particle number components. Indeed, if a particle is associated with the left or right subspace, its time-reversal counterpart is automatically associated with the same subspace (they share the same squared modulus). Because of the non negligible odd components part of their fragments particle number distributions (see section 4.3), we expect that the RC-separation won't work well for most of the variational excitations.
In panel (a) of Figure (4.28), we've displayed the neutron separation indexes s_n associated with the adiabatic states and with the neutron variational excitations, with respect to $c_\#$. In panel (b), we've plotted the proton separation indexes s_p associated with the adiabatic states and with the proton variational excitations, with respect to $c_\#$:

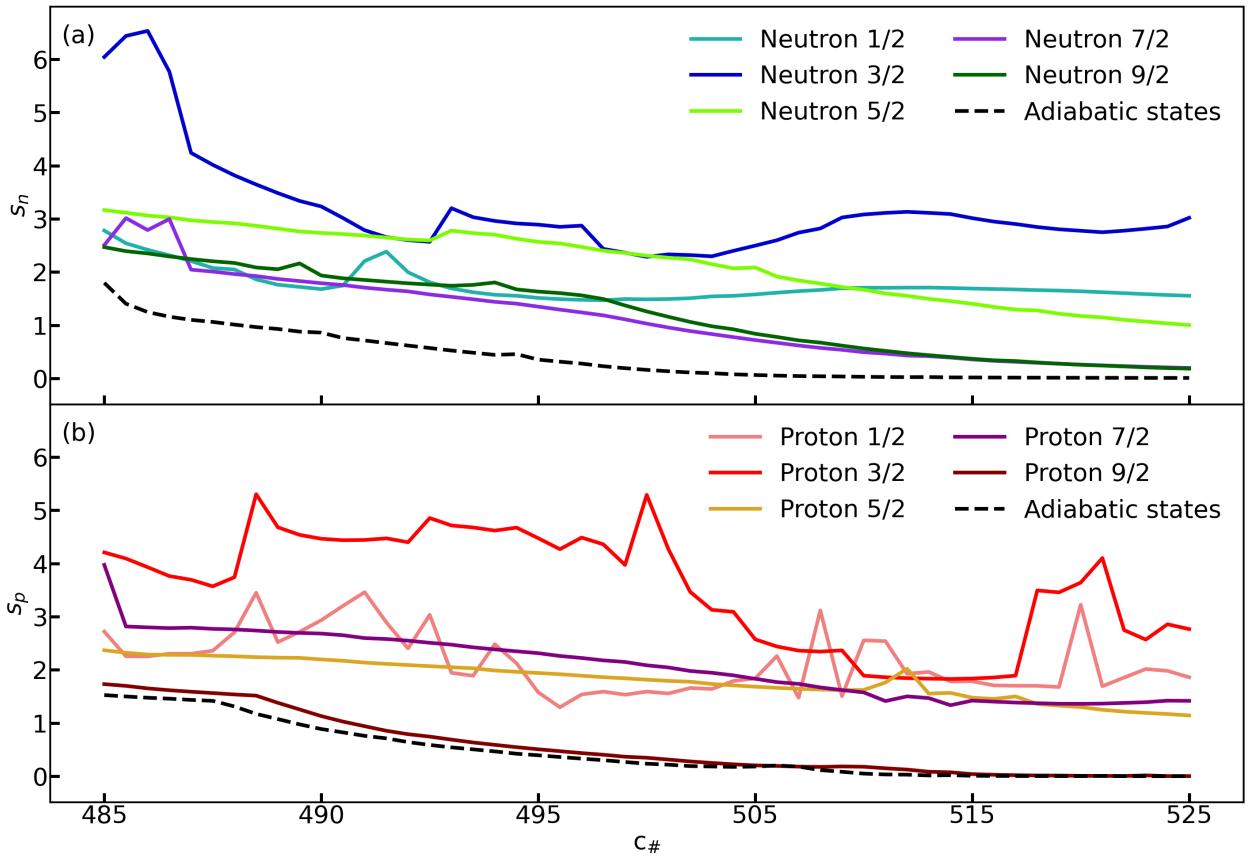

Figure 4.28: Study of the behaviour of the variational excitations with regard to the RC-separation method. Panel (a): neutron separation indexes s_n associated with the adiabatic states and with the neutron variational excitations, with respect to $c_\#$. Panel (b): proton separation indexes s_p associated with the adiabatic states and with the proton variational excitations, with respect to $c_\#$.

The numerous irregularities shown by the light blue and dark blue curves in panel (a) and by the red and pink ones in panel (b) underline the limitations of the RC-separation method when it comes to analyze fragmentations with non negligible odd particle number components.
In panel (b), the brown curve standing for the proton $\Omega = 9/2$ variational excitation exhibits a behaviour very similar to the adiabatic one. This result was expected as their fragments particle number distributions were comparable.
As it is not possible in general to estimate relevantly the deformation and interaction energies associated with the variational excitations using the RC-separation method, their adiabatic counterparts at $c_\# = 495$ are considered in Chapter 6 instead.

We've taken advantage of the good behaviour of the proton $\Omega = 9/2$ variational excitation with respect to the RC-separation method to study it in greater detail. The aim of this study is to determine whether it is possible or not to associate this variational excitation with a specific fragment. The idea is to compare the left and right binding energies and the interaction energy of the variational excitation with the ones of the adiabatic states. To do so, we define the three following quantities:

$$\begin{cases} \Delta E^{*(l)} = E^{*(l)} - E^{(l)} \\ \Delta E^{*(r)} = E^{*(r)} - E^{(r)} \\ \Delta E^{*}_{int} = E^{*}_{int} - E_{int} \end{cases} \tag{4.37}$$

In Figure (4.29), we've represented the energy differences $\Delta E^{*(l)}$, $\Delta E^{*(r)}$ and ΔE^{*}_{int} obtained considering both the proton $\Omega = 9/2$ variational excitation and the adiabatic states, with respect to $c_{\#}$:

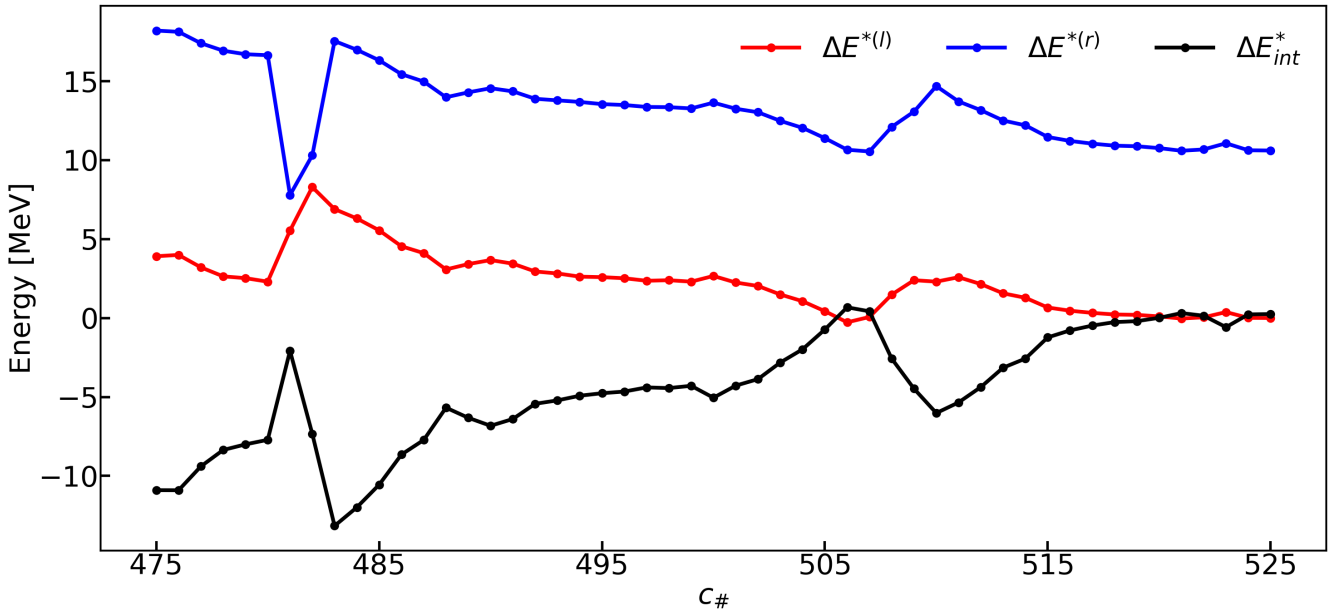

Figure 4.29: Evolution of the energy differences $\Delta E^{*(l)}$, $\Delta E^{*(r)}$ and ΔE^{*}_{int} between the proton $\Omega = 9/2$ variational excitation and the adiabatic states, with respect to $c_{\#}$.

In Figure (4.29), we observe two major variations in the curves, the first ones are centered around $c_{\#} = 482$ and the second ones at $c_{\#} = 510$. As the energy differences are very sensitive quantities, these bumps probably account for v_k and u_k degeneracies, which are not considered by the RC-separation algorithm as they have a small impact on the separation index. Note that these bumps may also originate from v_k and u_k degeneracies implying three particle states at the same time, which are not considered by the RC-separation method.
That said, the results displayed in Figure (4.29) meet our expectations. Firstly, we clearly see that the blue curve is well above the red one. More precisely, at scission ($c_{\#} = 495$), the left binding energy difference is five times lower than the right one. Secondly, after $c_{\#} = 517$ approximately, the left (light fragment) binding energy differences and the interaction energy differences are very close to 0 MeV when the right (heavy fragment) binding energy differences approximately equal 10.6 MeV, which corresponds to the total excitation energy ΔE^{*} of the variational excitation. Besides, if we do not take into account the bumps in the red and black curves centered in $c_{\#} = 510$, which probably have a technical origin, we can define the beginning of the energy differences convergence around $c_{\#} = 505$. All these observations lead us naturally to conclude that the proton $\Omega = 9/2$ variational excitation mostly operates on the right pre-fragment, which is also the heavy one, within the compound nucleus, and becomes entirely an intrinsic excitation of this fragment after scission.

The canonical basis associated with the RC-separation also allows to give an interpretation of certain phenomena in terms of particle orbitals. As an exemple, we've studied the single particle orbitals of the neutron $\Omega = 9/2$ variational excitation, whose neutron necking properties were the most remarkable (see Figure (4.8)).
In Figure (4.30), we have represented for different values of $c_{\#}$ the local modulus associated with the particle state that mostly accounts for the abnormal neutron necking properties of the neutron $\Omega = 9/2$ variational excitation. We've given in parentheses the quantities $2v_k^2$ associated with the orbital. These quantities account for the total number of particle related to the orbital and its time-reversal counterpart:

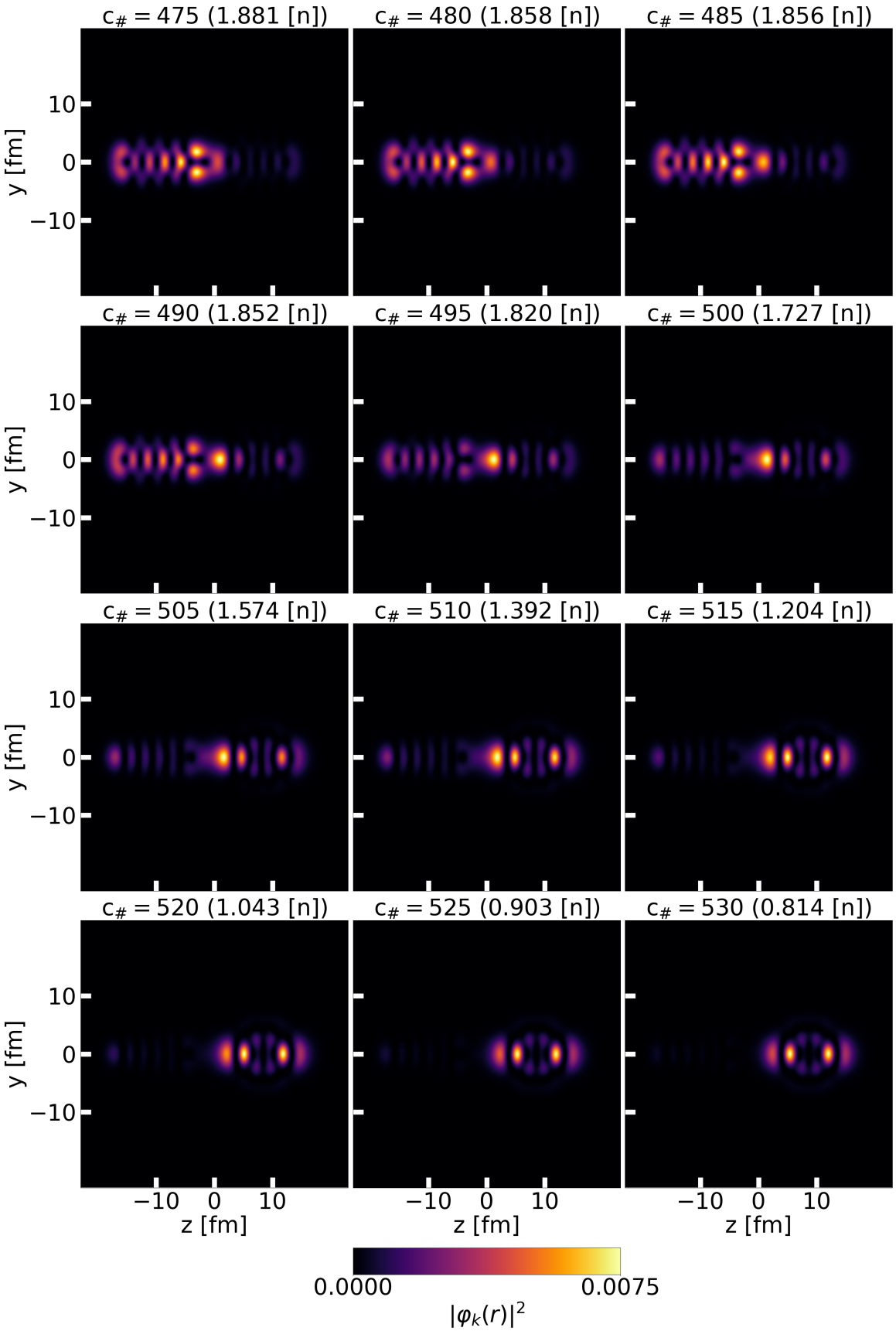

Figure 4.30: Study of the evolution of the squared modulus of the canonical particle wave function that we've attributed to the remarkable neutron necking properties of the neutron $\Omega = 9/2$ variational excitation, with respect to $c_{\#}$.

Before commenting on the results shown in Figure (4.30), we start by explaining how the orbital considered was chosen. We began by assuming that an orbital localized in the middle of the pre-fragments would naturally contribute a lot to the value of the separation index s_n. Thus, we've considered the state labeled by $c_\#$ which was associated with remarkable neutron necking properties, and we've observed the squared modulus associated with the particle state contributing to s_n the most. Then, we've followed continuously this state to obtain the whole results displayed in Figure (4.30).
For all the states labeled by a value of $c_\#$ greater than 490, the particle state considered is still the one that contributes to s_n the most. Before $c_\# = 490$ it is not the case anymore, as the pre-fragments are not separated yet. Then, calling s_{n_i} the part of the neutron separation index due to the particle orbital considered (and to its time-reversal counterpart), the following ratio r_{s_i} is very interesting to study:

$$\boxed{r_{s_i} = 100 \times |\frac{s_{n_i}}{s_t}|} \tag{4.38}$$

The ratio r_{s_i} is a good way to measure the relative importance of the orbital we've chosen in holding both pre-framents together. We found the values 37.7%, 50.6%, 52.8 %, 59.2 %, and 58.5% for $c_\# = 495$, $c_\# = 500$, $c_\# = 505$, $c_\# = 510$, and $c_\# = 515$ respectively. These values signify that the orbital we've isolated is very relevant within the scission process, as it mostly explains the last couplings between the pre-fragments.
An interesting information about this particle orbital is the fact that it is a neutron $\Omega = 1/2$ orbital, while the variational excitation is a neutron $\Omega = 9/2$ excitation. It means that most of both the neutron necking properties of the states and the additional couplings between the pre-fragments are in this case due to the rearragement induced by the constrained (τ^*, Ω^*) subspace and not by this (τ^*, Ω^*) subspace in itself. This is an important observation as it underlines the physical consequences of allowing rearrangements when creating variational excitations.
It is also important to observe in Figure (4.30) that the orbital is mostly related to the left pre-fragment at $c_\# = 475$ and totally included in the right fragment at $c_\# = 530$. This kind of phenomenon illustrates what we had in mind when we spoke of sudden and particular changes at scission in the structure of the variational excitations that couple the pre-fragments.
Regarding neutron emission at scission, the results presented in Figure (4.30) highlight again the importance of considering intrinsic excitations to catch the physics of the phenomenon. Indeed, it seems natural to assume that an orbital with a behaviour as peculiar as the one described in Figure (4.30) will be more likely to separate from the compound nucleus. This assumption is supported by the neutron chemical potentials near scission related to this neutron $\Omega = 9/2$ variational excitation that are much smaller than the other ones in absolute (see Figure (4.2)).

4.4.4 The Projection Onto a Fragmentation (POF) method

When we use the customary PAV formalism, the resulting projected states have a good particle number. However, nothing guarantees that it is also the case for the related fragments. We've created and implemented the POF method to tackle this issue. For the moment, the POF formalism is limited to the even fragmentations. To extend it to the odd ones, a new RC-separation method would be required as well as a time-odd HFB solver. As already states, this method works because the quasiparticles annihilation operators and the particles operators are indexed the same way in the canonical representation. Therefore, in general,

the POF method is not applicable within the context of the separation method presented in [35]. This point is a clear advantage of the RC-separation from this point of view.
We start the method presentation by introducing the left and rigth particle number operators $\hat{N}^{(l)}$ and $\hat{N}^{(c)}$:

$$\begin{cases} \hat{N}^{(l)} = \sum_{k_l} a^+_{k_l} a_{k_l} \\ \hat{N}^{(r)} = \sum_{k_r} a^+_{k_r} a_{k_r} \end{cases} \tag{4.39}$$

The expression given in Eq.(4.39) is formally the same as the one related to the z-separation and displayed in Eq.(4.15). However, the orthonormal particle bases considered are not the same ones. Then, we define the left and right particle number projectors $\hat{P}^{(l)}_{N_0^{(l)}}$ and $\hat{P}^{(r)}_{N_0^{(r)}}$:

$$\begin{cases} \hat{P}^{(l)}_{N_0^{(l)}} = \frac{1}{2\pi} \int_0^{2\pi} e^{-i\varphi(\hat{N}^{(l)} - N_0^{(l)})} \\ \hat{P}^{(r)}_{N_0^{(r)}} = \frac{1}{2\pi} \int_0^{2\pi} e^{-i\varphi(\hat{N}^{(r)} - N_0^{(r)})} \end{cases} \tag{4.40}$$

The projector $\hat{P}^{(l)}_{N_0^{(l)}}$ projects the left sub-state onto its subspace associated with the particle number $N_0^{(l)}$, and $\hat{P}^{(r)}_{N_0^{(r)}}$ projects the right sub-state onto its subspace associated with the particle number $N_0^{(r)}$. With these two operators, it is possible to evaluate the energy associated with a specific fragmentation $(N_0^{(l)}, N_0^{(r)})$. We call this energy the fragmentation-projected energy. It reads as follows:

$$\boxed{E(N_0^{(l)}, N_0^{(r)}) = \frac{\langle \Phi | \hat{P}^{(l)}_{N_0^{(l)}} \hat{P}^{(r)}_{N_0^{(r)}} \hat{H} \hat{P}^{(l)}_{N_0^{(l)}} \hat{P}^{(r)}_{N_0^{(r)}} | \Phi \rangle}{\langle \Phi | \hat{P}^{(l)}_{N_0^{(l)}} \hat{P}^{(r)}_{N_0^{(r)}} | \Phi \rangle}} \tag{4.41}$$

Besides, we've demonstrated in Chapter 5, that this projection method preserves the total energy decomposition in terms of $E^{(l)}$, $E^{(r)}$ and E_{int}, in such a way that the fragmentation-projected energy reads:

$$\boxed{E(N_0^{(l)}, N_0^{(r)}) = E^{(l)}(N_0^{(l)}, N_0^{(r)}) + E^{(r)}(N_0^{(l)}, N_0^{(r)}) + E_{int}(N_0^{(l)}, N_0^{(r)})} \tag{4.42}$$

More details regarding the evaluation of the quantities displayed in Eq.(4.42) are presented in Chapter 5.

Unfortunately, we didn't have enough time to exploit the full potential of the POF method. However, we propose a first application. This application consists in studying the standard deviation of the Coulomb potential part of the TKE that accounts for particle number fluctuations. In other words, we've evaluated all the fragmentation-projected Coulomb interaction energies $E^C_{int}(Z_0^{(l)}, Z_0^{(r)})$, such that $Z_0^{(l)} + Z_0^{(r)} = Z_{(0)}$ (here, $Z_{(0)} = 94$). Then, we've used the probabilties associated with each fragmentation to get the average value $\bar{E}^C_{int}$ and the standard deviation σ^C_{int} associated with this reduced Coulomb interaction energy distribution:

$$\boxed{\bar{E}^C_{int} = \sum_l Y(Z_0^{(l)}, Z_{(0)} - Z_0^{(l)}) E^C_{int}(Z_0^{(l)}, Z_{(0)} - Z_0^{(l)})} \tag{4.43}$$

And:

$$\boxed{\sigma_{int}^{C} = \sqrt{\sum_{l} Y(Z_0^{(l)}, Z_{(0)} - Z_0^{(l)})[E_{int}^{C}(Z_0^{(l)}, Z_{(0)} - Z_0^{(l)}) - (\bar{E}_{int}^{C}]^2}} \tag{4.44}$$

In Figure (4.31), we've represented the part of the Coulomb interaction energy $\bar{E}_{int}^{C}$ distribution associated with the particle number fluctuations. This study has been performed for the adiabatic state labeled by $c_{\#} = 495$ and obtained via the POF method. On the x-axis, we've indicated the charge of the related light fragments in parentheses:

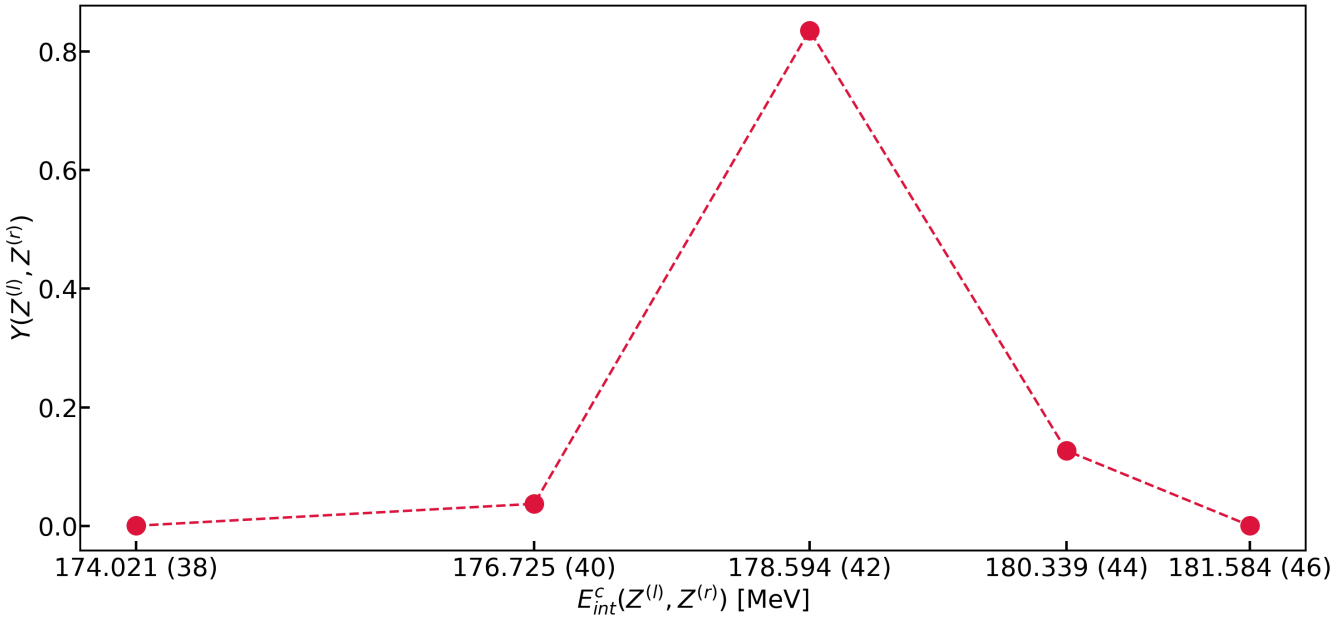

Figure 4.31: Particle number related Coulomb interaction energy distribution associated with the adiabatic state labeled by $c_{\#} = 495$ obtained via the POF method.

The average value $\bar{E}_{int}^{C}$ associated with the distribution displayed in Figure (4.31) is 178.45 MeV, and the standard deviation σ_{int}^{C} equals 0.729 MeV. In parallel, we've obtained the full standard deviation associated with the same state and evaluated thanks to the "Nucleoscope" code developed by A. Bernard and D. Regnier [66]. The "Nucleoscope" code uses the Monte Carlo method to evaluate observables distributions related to the relevant total particle number subspace of a given HFB state. The full standard deviation associated with the Coulomb interaction energy found equals 3.88 MeV (the average energy was found equal to 177.5 MeV with "Nucleoscope"). The important difference between this value and the value σ_{int}^{C} obtained with the POF method underlines that, in this case, the standard deviation associated with the Coulomb interaction energy mostly comes from the center of charge fluctuations related to both fragments and not from the particle number ones.

Chapter 5

Kernel calculations

One of the major difficulties of the SCIM approach is the evaluation of the overlap and Hamiltonian kernels. In this Chapter, we demonstrate all the formulas used in this PhD thesis work to tackle them.
The main challenge was probably to handle kernels between states built with different harmonic-oscillator representations. Sometimes, we've found solutions in the literature, other times we've demonstrated our own new formulas.
Insofar as the 2-quasiparticle excited states have led us to implement the PAV formalism (see Chapter 2), we always present kernel formulas along with their projected counterparts. Besides, some sections are dedicated to the ingredients required by the POF method developed in Chapter 3.
The reader may be frightened by the complexity involved in treating the 2-quasiparticle excited states in a Wick-based manner. However, we thought it would be more efficient numerically than transforming the U and V Bogoliubov matrices with respect to each 2-quasiparticle excitation (as proposed in [36] for instance). In addition, using the Wick theorem to evaluate 2-quasiparticle excited states kernels has the valuable advantage to avoid the divergences due to states orthogonality.

To conclude, the Hamiltonian kernel derivations would be useless without the associated fields derivations. We've displayed the latter in Appendix E-F.

5.1 Overlap kernels

This section is dedicated to the presentation of numerous results concerning the overlap kernels.
Firstly, we explain the evaluation of the overlap between two HFB states built with the same harmonic-oscillator representations. These derivations follow [67]. Then, we focus on the axial and time-reversal case. Finally, we show the link between the formulas found and the famous "Onishi-Yoshida" formula [68].
Secondly, we present the new formulas we've developed to tackle the overlap between two HFB states built with different harmonic-oscillator representations. This work has been inspired by [69]. Then, we focus on the axial and time-reversal case. Finally, we show the connection between our new formulas and the one obtained by L.M. Robledo [69] as well as the link between our formulas and the famous "Haider-Gogny" formulas [70].
We conclude this section treating the burning "V Phasis" issue we've discovered when calculating PES. We present both our analysis of the nature of this phenomenon and the solution

we've found to tackle it in practice.

To conclude, we assume in this whole section that all the $\{u_k\}$ associated with the Bogoliubov matrices U considered are different from zero. In practice, has always been the case.

5.1.1 HFB states normalization

We first give the expression of the normalization factor $\mathcal{N}$ of a given HFB state. This factor will be very important in the following. Let $|\Phi\rangle$ be an HFB state defined by the set of quasiparticle annihilation operators $\{\xi_i\}$:

$$|\Phi\rangle = \mathcal{N} \prod_i \xi_i |0\rangle \tag{5.1}$$

We transform the quasiparticle annihilation operators $\{\xi_i\}$ into the quasiparticle annihilation operators $\{\eta_k\}$ associated with the canonical representation of $|\Phi\rangle$ (see Appendix C):

$$|\Phi\rangle = \mathcal{N} \det(C^*) (\prod_{k>} \eta_k \bar{\eta}_k) |0\rangle \tag{5.2}$$

Then, we remark the following property:

$$\eta_k \bar{\eta}_k |0\rangle = (u_k a_k + v_k \bar{a}_k^+)(u_k \bar{a}_k - v_k a_k^+)|0\rangle = v_k (u_k + v_k a_k^+ \bar{a}_k^+)|0\rangle \tag{5.3}$$

Thanks to Eq.(5.3), we can write:

$$|\Phi\rangle = \mathcal{N} \det(C^*) \prod_{k'>} v_{k'} \prod_{k>} (u_k + v_k a_k^+ \bar{a}_k^+)|0\rangle \tag{5.4}$$

We evaluate the norm of the state $\prod_{k>}(u_k + v_k a_k^+ \bar{a}_k^+)|0\rangle$:

$$|\prod_{k>}(u_k + v_k a_k^+ \bar{a}_k^+)|0\rangle|^2 = \langle 0|(\prod_{k'>} u_{k'} + v_{k'} \bar{a}_{k'} a_{k'}) \prod_{k>}(u_k + v_k a_k^+ \bar{a}_k^+)|0\rangle \tag{5.5}$$

As all the pairs $\bar{a}_{k'} a_{k'}$ commute with the pairs $a_k^+ \bar{a}_k^+$ except when $k' = k$, we find:

$$|(\prod_{k>} u_k + v_k a_k \bar{a}_k^+)|0\rangle|^2 = \langle 0| \prod_{k>}(u_k + v_k \bar{a}_k a_k)(u_k + v_k a_k^+ \bar{a}_k^+)|0\rangle = \langle 0| \prod_{k>}(u_k^2 + v_k^2)|0\rangle = 1 \tag{5.6}$$

Inserting Eq.(5.6) in Eq.(5.4) leads to:

$$\langle \Phi|\Phi\rangle = \frac{|\mathcal{N}|^2}{\prod_{k>} u_k^2} = 1 \tag{5.7}$$

Among the different possibilites, we choose the following $\mathcal{N}$:

$$\boxed{\mathcal{N} = \det(C) \prod_{k>} u_k} \tag{5.8}$$

Indeed, this definition enables us to write the state $|\Phi\rangle$ in the canonical representation as follows:

$$\boxed{|\Phi\rangle = \prod_{k>} (u_k + v_k a_k^+ \bar{a}_k^+)|0\rangle} \tag{5.9}$$

5.1.2 Overlap between HFB states built with the same harmonic-oscillator representations

In this case, we consider two different HFB states $|\Phi_0\rangle$ and $|\Phi_1\rangle$ associated with the quasi-particle annihilation operators $\{\xi_{0,i}\}$ and $\{\xi_{1,i}\}$ respectively. Thanks to the Thouless theorem (see Appendix B) and calling $U^{(0)}$, $V^{(0)}$ and $U^{(1)}$, $V^{(1)}$ the Bogoliubov matrices associated with the states $|\Phi_0\rangle$ and $|\Phi_1\rangle$ respectively, we can write:

$$\langle\Phi_0|\Phi_1\rangle = \langle 0|\Phi_1\rangle\langle\Phi_0|0\rangle\langle 0|e^{\frac{1}{2}\sum_{kk'}(V^{(0)}U^{(0)-1})_{kk'}c_{k'}c_k} e^{\frac{1}{2}\sum_{kk'}(V^{(1)}U^{(1)-1})^*_{kk'}c_k^+ c_{k'}^+}|0\rangle \tag{5.10}$$

We set:

$$\begin{cases} M^{(0)} = (V^{(0)}U^{(0)-1})^* \\ M^{(1)} = (V^{(1)}U^{(1)-1})^* \end{cases} \tag{5.11}$$

Both $M^{(0)}$ and $M^{(1)}$ are skew-symmetric. We rewrite Eq.(5.10):

$$\langle\Phi_0|\Phi_1\rangle = \langle 0|\Phi_1\rangle\langle\Phi_0|0\rangle\langle 0|e^{\frac{1}{2}\sum_{kk'} M^{(0)*}_{kk'}c_{k'}c_k} e^{\frac{1}{2}\sum_{kk'} M^{(1)}_{kk'}c_k^+ c_{k'}^+}|0\rangle \tag{5.12}$$

Now, we use the fermionic coherent states built using Grassmann algebras (see Appendix L). We can introduce them into Eq.(5.12) thanks to their completness:

$$\int |z\rangle\langle z| \prod_{k=1}^{n} (dz_k^* dz_k) = \mathrm{id} \tag{5.13}$$

Eq.(5.13) does not corresponds to the one used by L. Robledo in [67]. This difference comes from a scaling in the super Hilbert space dot product. Inserting Eq.(5.13) into Eq.(5.12) leads to:

$$\langle\Phi_0|\Phi_1\rangle = \langle 0|\Phi_1\rangle\langle\Phi_0|0\rangle \int \langle 0|e^{\frac{1}{2}\sum_{kk'} M^{(0)*}_{kk'}c_{k'}c_k}|z\rangle\langle z|e^{\frac{1}{2}\sum_{kk'} M^{(1)}_{kk'}c_k^+ c_{k'}^+}|0\rangle \prod_{k=1}^{n}(dz_k^* dz_k) \tag{5.14}$$

The fermionic state $|z\rangle$ is an eigenvector of the particle annihilation operators:

$$\boxed{c_k|z\rangle = z_k|z\rangle} \qquad \boxed{\langle z|c_k^+ = \langle z|z_k^*} \tag{5.15}$$

Here, z_k et z_k^* are Grassmann numbers. We apply Eq.(5.15) into Eq.(5.14):

$$\langle\Phi_0|\Phi_1\rangle = \langle 0|\Phi_1\rangle\langle\Phi_0|0\rangle \int \langle 0|e^{\frac{1}{2}\sum_{kk'} M^{(0)*}_{kk'} z_{k'} z_k}|z\rangle\langle z|e^{\frac{1}{2}\sum_{kk'} M^{(1)}_{kk'} z_k^* z_{k'}^*}|0\rangle \prod_{k=1}^{n}(dz_k^* dz_k) \tag{5.16}$$

Then:

$$\langle\Phi_0|\Phi_1\rangle = \langle 0|\Phi_1\rangle\langle\Phi_0|0\rangle \int \langle 0|z\rangle\langle z|0\rangle e^{\frac{1}{2}\sum_{kk'} M^{(0)*}_{kk'} z_{k'} z_k} e^{\frac{1}{2}\sum_{kk'} M^{(1)}_{kk'} z_k^* z_{k'}^*} \prod_{k=1}^{n}(dz_k^* dz_k) \tag{5.17}$$

In Appendix L, we've demonstrated the following property:

$$\langle 0|z\rangle = e^{-z^*.z/2} \tag{5.18}$$

This property is also different from the one found in [67]. In fact, Eq.(5.18) precisely gives the scaling factor between both dot product definitions. Of course, the effects of the differences related to Eq.(5.13) and Eq.(5.18) cancel out in the equations. Inserting Eq.(5.18) into Eq.(5.17) leads to:

$$\langle\Phi_0|\Phi_1\rangle = \langle 0|\Phi_1\rangle\langle\Phi_0|0\rangle \int e^{-z^*.z} e^{\frac{1}{2}\sum_{kk'} M^{(0)*}_{kk'} z_{k'} z_k} e^{\frac{1}{2}\sum_{kk'} M^{(1)}_{kk'} z_k^* z_{k'}^*} \prod_{k=1}^{n}(dz_k^* dz_k) \tag{5.19}$$

We define the following notations:

$$z = \begin{pmatrix} z_1^* \\ . \\ z_n^* \\ z_1 \\ . \\ z_n \end{pmatrix} \qquad \text{and} \qquad M = \begin{pmatrix} M^{(1)} & -I \\ I & -M^{(0)*} \end{pmatrix} \tag{5.20}$$

It is clear that the matrix M is a $2n \times 2n$ skew-symmetric matrix. Thanks to these notations, we write:

$$\langle\Phi_0|\Phi_1\rangle = \langle 0|\Phi_1\rangle\langle\Phi_0|0\rangle \int e^{\frac{1}{2}z^T M z} \prod_{k=1}^{n}(dz_k^* dz_k) \tag{5.21}$$

To use the results concerning Gaussian integration on a Grassmann algebra, we need to reorder the volume elements in the right hand side of Eq.(5.21):

$$\langle\Phi_0|\Phi_1\rangle = (-1)^{\frac{n(n+1)}{2}} \langle 0|\Phi_1\rangle\langle\Phi_0|0\rangle \int e^{\frac{1}{2}z^T M z} dz_n ... dz_1 dz_n^* ... dz_1^* \tag{5.22}$$

Now, we can write:

$$\boxed{\langle\Phi_0|\Phi_1\rangle = (-1)^{\frac{n(n+1)}{2}}\langle 0|\Phi_1\rangle\langle\Phi_0|0\rangle \mathrm{pf}\begin{pmatrix} M^{(1)} & -I \\ I & -M^{(0)*}\end{pmatrix}} \tag{5.23}$$

In Eq.(5.23), the notation "pf" stands for the Pfaffian. It is possible to factorize the matrix M:

$$\begin{pmatrix} I & 0 \\ -M^{(1)-1} & I\end{pmatrix}\begin{pmatrix} M^{(1)} & -I \\ I & -M^{(0)*}\end{pmatrix}\begin{pmatrix} I & M^{(1)-1} \\ 0 & I\end{pmatrix} = \begin{pmatrix} M^{(1)} & 0 \\ 0 & -M^{(0)*}+M^{(1)-1}\end{pmatrix} \tag{5.24}$$

Using this factorization into Eq.(5.23) leads to:

$$\mathrm{pf}\begin{pmatrix} M^{(1)} & -I \\ I & -M^{(0)*}\end{pmatrix} = \mathrm{pf}(M^{(1)})\mathrm{pf}(-M^{(0)*}+M^{(1)-1})$$

We can finally write:

$$\boxed{\langle\Phi_0|\Phi_1\rangle = (-1)^{\frac{n(n+1)}{2}}\langle 0|\Phi_1\rangle\langle\Phi_0|0\rangle \mathrm{pf}(M^{(1)})\mathrm{pf}(-M^{(0)*}+M^{(1)-1})} \tag{5.25}$$

5.1.3 Axial and time-reversal invariance with the same harmonic-oscillator representations

In the special case of axial and time-reversal invariant HFB states, the matrices $\tilde{U}^{(i)}$ and $\tilde{V}^{(i)}$ (with i = 0 or 1) are real and exhibit the following structures:

$$\tilde{U}^{(i)} = \begin{pmatrix} U^{(i)} & 0 \\ 0 & U^{(i)}\end{pmatrix} \qquad \tilde{V}^{(i)} = \begin{pmatrix} 0 & -V^{(i)} \\ V^{(i)} & 0\end{pmatrix} \tag{5.26}$$

Here, the $U^{(i)}$ and $V^{(i)}$ are of dimension $n/2$. Eq.(5.26) implies that the matrices $M^{(i)}$ defined in Eq.(5.11) also have a special structure:

$$M^{(i)} = \begin{pmatrix} 0 & -V^{(i)}U^{(i)-1} \\ V^{(i)}U^{(i)-1} & 0\end{pmatrix} \tag{5.27}$$

It is important to remark that the matrices $M^{(i)}$ are skew-symmetric, while the matrices $V^{(i)}U^{(i)-1}$ are symmetric. Using Pfaffian properties, we write:

$$\mathrm{pf}(M^{(1)}) = (-1)^{\frac{n(\frac{n}{2}-1)}{4}}(-1)^{\frac{n}{2}}\det(V^{(1)}U^{(1)-1}) \tag{5.28}$$

$$\mathrm{pf}(-M^{(0)*}+M^{(1)-1}) = (-1)^{\frac{n(\frac{n}{2}-1)}{4}}\det(V^{(0)}U^{(0)-1}+U^{(1)}V^{(1)-1}) \tag{5.29}$$

With these results we can finally write:

$$\boxed{\langle\Phi_0|\Phi_1\rangle = \langle 0|\Phi_1\rangle\langle\Phi_0|0\rangle\det(I+V^{(0)}U^{(0)-1}V^{(1)}U^{(1)-1})} \tag{5.30}$$

5.1.4 Link with the "Onishi-Yoshida" formula

The "Onishi-Yoshida" formula [68] is often found in the literature. It gives the absolute value of the overlap between two given HFB states and reads as follows:

$$\boxed{|\langle\Phi_0|\Phi_1\rangle| = \sqrt{|\det(U^{(0)+}U^{(1)} + V^{(0)+}V^{(1)})|}} \tag{5.31}$$

In the following, we show the connection between Eq.(5.25) and Eq.(5.31). Starting from Eq.(5.25) and using Pfaffian properties, we write:

$$|\langle\Phi_0|\Phi_1\rangle| = |\langle 0|\Phi_1\rangle\langle\Phi_0|0\rangle|\sqrt{|\det(M^{(1)})\det(-M^{(0)*} + M^{(1)-1})|} \tag{5.32}$$

From Eq.(5.9), it is clear that $|\langle 0|\Phi_i\rangle| = \prod_{k>} u_k^{(i)} = \sqrt{|\det(U^{(i)})|}$. We use this property to transform Eq.(5.32):

$$|\langle\Phi_0|\Phi_1\rangle| = \sqrt{|\det(U^{(1)})\det(U^{(0)+})\det(I - M^{(0)*}M^{(1)})|} \tag{5.33}$$

$$|\langle\Phi_0|\Phi_1\rangle| = \sqrt{|\det(U^{(1)})\det(U^{(0)+})\det(I + (U^{(0)+})^{-1}V^{(0)+}V^{(1)}U^{(1)-1})|} \tag{5.34}$$

Then, we finally recover the "Onishi-Yoshida" formula back:

$$|\langle\Phi_0|\Phi_1\rangle| = \sqrt{|\det(U^{(0)+}U^{(1)} + V^{(0)+}V^{(1)})|} \tag{5.35}$$

5.1.5 Overlap between HFB states built with two different harmonic-oscillator representations

The derivations we present in this section are brand new. They enables us to consider two different harmonic-oscillator representations of different dimensions without completing their rectangular overlap matrix R.

In this case, we consider two HFB states $|\Phi_0\rangle$ and $|\Phi_1\rangle$ associated with the quasiparticle annihilation operators sets $\{\xi_{0,j}\}$ and $\{\xi_{1,j}\}$. The quasiparticle annihilation operators of these two sets are not built on the same harmonic-oscillator representations. More explicitly, they read as follows:

$$\begin{cases} \xi_{0,i} = \sum_l U_{li}^{(0)*} c_{0,l} + V_{li}^{(0)*} c_{0,l}^+ \\ \\ \xi_{1,i} = \sum_l U_{li*}^{(1)} c_{1,l} + V_{li}^{(1)*} c_{1,l}^+ \end{cases} \tag{5.36}$$

We call these two harmonic-oscillator sets $\{0\}$ and $\{1\}$. Both are truncated subsets of the full harmonic-oscillator sets $\{\bar{0}\}$ and $\{\bar{1}\}$. We call $\bar{R}$ the full overlap matrix between them:

$$\begin{cases} c_{0,l} = \sum_k^{+\infty} \bar{R}_{kl}^T c_{1,k} \\ \\ c_{1,l} = \sum_k^{+\infty} \bar{R}_{kl} c_{0,k} \end{cases} \tag{5.37}$$

We start by using the Thouless theorem to transform the overlap $\langle\Phi_0|\Phi_1\rangle$:

$$\langle\Phi_0|\Phi_1\rangle = \langle 0|\Phi_1\rangle\langle\Phi_0|0\rangle\langle 0|e^{\frac{1}{2}\sum_{kk'}(V^{(0)}U^{(0)-1})_{kk'}c_{0,k'}c_{0,k}}e^{\frac{1}{2}\sum_{kk'}(V^{(1)}U^{(1)-1})^*_{kk'}c^+_{1,k}c^+_{1,k'}}|0\rangle \tag{5.38}$$

We use the matrix $\bar{R}$ defined in Eq.(5.37):

$$\langle\Phi_0|\Phi_1\rangle = \langle 0|\Phi_1\rangle\langle\Phi_0|0\rangle\langle 0|e^{\frac{1}{2}\sum_{kk'}(V^{(0)}U^{(0)-1})_{kk'}c_{0,k'}c_{0,k}}e^{\frac{1}{2}\sum_{ll'}^{+\infty}(\bar{R}V^{(1)}U^{(1)-1}\bar{R}^T)^*_{ll'}c^+_{0,l}c^+_{0,l'}}|0\rangle \tag{5.39}$$

The sum is limited to the indices belonging to the truncated harmonic-oscillator representation associated with $\{0\}$, while the sum on the exponential on the right hand side spans the full infinite set $\{\bar{0}\}$. Considering an arbitrary particle operator $c^+_{0,\gamma} \notin \{0\}$, we can write:

$$\begin{aligned} e^{\frac{1}{2}\sum_{ll'}^{+\infty}(\bar{R}V^{(1)}U^{(1)-1}\bar{R}^T)^*_{ll'}c^+_{0,l}c^+_{0,l'}}|0\rangle = (1 + \frac{1}{2}\sum_{l}^{+\infty}(\bar{R}V^{(1)}U^{(1)-1}\bar{R}^T)^*_{l\gamma}c^+_{0,l}c^+_{0,\gamma}) \\ e^{\frac{1}{2}\sum_{ll'(l'\neq\gamma)}^{+\infty}(\bar{R}V^{(1)}U^{(1)-1}\bar{R}^T)^*_{ll'}c^+_{0,l}c^+_{0,l'}}|0\rangle \end{aligned} \tag{5.40}$$

It is clear that the operator $c^+_{0,\gamma}$ commutes with $e^{\frac{1}{2}\sum_{kk'}(V^{(0)}U^{(0)-1})_{kk'}c_{0,k'}c_{0,k}}$. Therefore, we obtain:

$$\langle\Phi_0|\Phi_1\rangle = \langle 0|\Phi_1\rangle\langle\Phi_0|0\rangle\langle 0|e^{\frac{1}{2}\sum_{kk'}(V^{(0)}U^{(0)-1})_{kk'}c_{0,k'}c_{0,k}}e^{\frac{1}{2}\sum_{ll'(l'\neq\gamma)}^{+\infty}(\bar{R}V^{(1)}U^{(1)-1}\bar{R}^T)^*_{ll'}c^+_{0,l}c^+_{0,l'}}|0\rangle \tag{5.41}$$

Repeating this process for all the indices spanning $\{\bar{0}\}/\{0\}$ and for both l and l', we finally find:

$$\langle\Phi_0|\Phi_1\rangle = \langle 0|\Phi_1\rangle\langle\Phi_0|0\rangle\langle 0|e^{\frac{1}{2}\sum_{kk'}(V^{(0)}U^{(0)-1})_{kk'}c_{0,k'}c_{0,k}}e^{\frac{1}{2}\sum_{kk'}(RV^{(1)}U^{(1)-1}R^T)^*_{kk'}c^+_{0,k}c^+_{0,k'}}|0\rangle \tag{5.42}$$

In Eq.(5.42), the matrix R stands for the restriction of $\bar{R}$ to the subsets $\{0\}$ and $\{1\}$. Now, we can define the matrices $M^{(0)}$ and $M^{(1)}_R$ as follows:

$$\begin{cases} M^{(0)} = (V^{(0)}U^{(0)-1})^* \\ M^{(1)}_R = (RV^{(1)}U^{(1)-1}R^T)^* \end{cases} \tag{5.43}$$

Inserting Eq.(5.43) into Eq.(5.42) leads to:

$$\langle\Phi_0|\Phi_1\rangle = \langle 0|\Phi_1\rangle\langle\Phi_0|0\rangle\langle 0|e^{\frac{1}{2}\sum_{kk'}M^{(0)*}_{kk'}c_{0,k'}c_{0,k}}e^{\frac{1}{2}\sum_{kk'}(M^{(1)}_R)_{kk'}c^+_{0,k}c^+_{0,k'}}|0\rangle \tag{5.44}$$

It is clear that both $M^{(0)}$ and $M^{(1)}_R$ are skew-symmetric matrices. Therefore, we directly write the final form of $\langle\Phi_0|\Phi_1\rangle$ by analogy with the derivations done in section 5.1.2:

$$\boxed{\langle\Phi_0|\Phi_1\rangle = (-1)^{\frac{n(n+1)}{2}}\langle 0|\Phi_1\rangle\langle\Phi_0|0\rangle \mathrm{pf}(M^{(1)}_R)\mathrm{pf}(-M^{(0)*} + (M^{(1)}_R)^{-1})} \tag{5.45}$$

5.1.6 Axial and time-reversal invariance with two different harmonic-oscillator representations

Using Eq.(5.45) and by analogy with section 5.1.3, we directly write:

$$\boxed{\langle\Phi_0|\Phi_1\rangle = \langle 0|\Phi_1\rangle\langle\Phi_0|0\rangle \det(I + V^{(0)}U^{(0)-1}RV^{(1)}U^{(1)-1}R^T)} \tag{5.46}$$

This formula is very useful in practice as it does not require to find the inverse matrix of R.

5.1.7 Link with L.M. Robledo formula

We find in [69] the following formula:

$$\boxed{|\langle\Phi_0|\Phi_1\rangle| = \sqrt{|\det(U^{(0)T}(R^T)^{-1}U^{(1)*} + V^{(0)T}RV^{(1)*})\det(R)|}} \tag{5.47}$$

This formula has two major drawbacks. First, it requires to complete R into a square matrix. Then, it does not give the phase of $\langle\Phi_0|\Phi_1\rangle$.

In the following, we show the connection between Eq.(5.47) and Eq.(5.45). Starting from Eq.(5.47), we write:

$$|\langle\Phi_0|\Phi_1\rangle| = \sqrt{|\det(U^{(0)})|}\sqrt{|\det(U^{(1)})|}\sqrt{|\det(I + U^{(0)T-1}V^{(0)T}RV^{(1)*}(U^{(1)-1})^*R^T)|} \tag{5.48}$$

$$|\langle\Phi_0|\Phi_1\rangle| = |\langle 0|\Phi_1\rangle\langle\Phi_0|0\rangle|\sqrt{|\det(I - M^{(0)*}M_R^{(1)})|} \tag{5.49}$$

$$|\langle\Phi_0|\Phi_1\rangle| = |\langle 0|\Phi_1\rangle\langle\Phi_0|0\rangle|\sqrt{|\det(M_R^{(1)})\det(-M^{(0)*} + M_R^{(1)-1})|} \tag{5.50}$$

Then, we finally go back to the Pfaffians:

$$\boxed{|\langle\Phi_0|\Phi_1\rangle| = |\langle 0|\Phi_1\rangle\langle\Phi_0|0\rangle|\mathrm{pf}(M_R^{(1)})\mathrm{pf}(-M^{(0)*} + M_R^{(1)-1})|} \tag{5.51}$$

5.1.8 Link with the "Haider-Gogny" formula

In this section, we link the results obtained previously to the "Haider-Gogny" formula [70]. In the following, we consider two HFB states $|\Phi_0\rangle$ and $|\Phi_1\rangle$ built on the same harmonic-oscillator representations. We start by writing the "canonical transformation" associated with both states:

$$\begin{pmatrix} \eta^{(k)} \\ \bar{\eta}^{(k)} \\ \eta^{(k)+} \\ \bar{\eta}^{(k)+} \end{pmatrix} = \begin{pmatrix} u^{(k)} & 0 & 0 & -v^{(k)} \\ 0 & u^{(k)} & v^{(k)} & 0 \\ 0 & -v^{(k)} & u^{(k)} & 0 \\ v^{(k)} & 0 & 0 & u^{(k)} \end{pmatrix} \begin{pmatrix} a^{(k)} \\ \bar{a}^{(k)} \\ a^{(k)+} \\ \bar{a}^{(k)+} \end{pmatrix} = \begin{pmatrix} \tilde{u}^{(k)} & \tilde{v}^{(k)} \\ \tilde{v}^{(k)} & \tilde{u}^{(k)} \end{pmatrix} \begin{pmatrix} a^{(k)} \\ \bar{a}^{(k)} \\ a^{(k)+} \\ \bar{a}^{(k)+} \end{pmatrix} \tag{5.52}$$

Eq.(5.52) describes a case which is very similar to the one with two different harmonic-oscillator representations. Here, the equivalent of the overlap matrix R is the matrix τ^{01} defined as follows:

$$\boxed{a_{k'}^{(1)+} = \sum_k \tau_{kk'}^{01} a_k^{(0)+}} \tag{5.53}$$

This matrix τ^{01} can be explicitly rewritten using the $D^{(i)}$ Bloch-Messiah matrices associated with both $|\Phi_0\rangle$ and $|\Phi_1\rangle$:

$$a_{k'}^{(1)+} = \sum_l D_{lk'}^{(1)} c_l^+ = \sum_l \sum_k D_{lk'}^{(1)} D_{kl}^{(0)+} a_k^{(0)+} = \sum_k (D^{(0)+} D^{(1)})_{kk'} a_k^{(0)+} \tag{5.54}$$

$$\boxed{\tau_{kk'}^{01} = (D^{(0)+} D^{(1)})_{kk'}} \tag{5.55}$$

Then, we use the analogy with section 5.1.5 to write:

$$\langle \Phi_0 | \Phi_1 \rangle = (-1)^{\frac{n(n+1)}{2}} \langle \Phi_0 | 0 \rangle \langle 0 | \Phi_1 \rangle \mathrm{pf}(M_\tau^{(1)}) \mathrm{pf}(-M^{(0)*} + M_\tau^{(1)-1}) \tag{5.56}$$

We've naturally set:

$$\begin{cases} M^{(0)} = \begin{pmatrix} 0 & -\frac{v^{(0)}}{u^{(0)}} \\ \frac{v^{(0)}}{u^{(0)}} & 0 \end{pmatrix} \\ \\ M_\tau^{(1)} = \begin{pmatrix} 0 & -\tau^{01} \frac{v^{(0)}}{u^{(0)}} \tau^{01T} \\ \tau^{01} \frac{v^{(0)}}{u^{(0)}} \tau^{01T} & 0 \end{pmatrix} \end{cases} \tag{5.57}$$

Because of the special structure of Eq.(5.57), similar to the one of the axial and time-reversal invariant case, we write by analogy with section 5.1.6:

$$\langle \Phi_0 | \Phi_1 \rangle = \langle \Phi_0 | 0 \rangle \langle 0 | \Phi_1 \rangle \det(I + \frac{v^{(0)}}{u^{(0)}} \tau^{(01)} \frac{v^{(1)}}{u^{(1)}} (\tau^{(01)})^T) \tag{5.58}$$

$$\langle \Phi_0 | \Phi_1 \rangle = \prod_{k'} u_{k'}^{(1)} \prod_k u_k^{(0)} \det(I + \frac{v^{(0)}}{u^{(0)}} \tau^{(01)} \frac{v^{(1)}}{u^{(1)}} (\tau^{(01)})^T) \tag{5.59}$$

Finally, we recover the "Haider-Gogny" formula:

$$\boxed{\langle \Phi_0 | \Phi_1 \rangle = \det(\tau^{01}) \det(u^{(1)} (\tau^{(01)})^{-1} u^{(0)} + v^{(1)} (\tau^{(01)})^T v^{(0)})} \tag{5.60}$$

This demonstration shows that the "Haider-Gogny" already considered the phases ambiguity.

5.1.9 The "V phasis"

In our PES calculations using the HFB3+CHICON combo, we've observed strange behaviors of the overlap distance defined in Chapter 2. Indeed, it happened that some neighboring states with almost identical multipole moments presented an important overlap distance (close to one). In addition, these discontinuities detected by the overlap distance were not noticed by the density distance d_ρ defined in Chapter 2.
In panel (a) of Figure (5.1), we've displayed the density distance between each HFB state and its neighbour on the right for the adiabatic set obtained with the $\mathcal{P}_{20}$ procedure in the ^{240}Pu, with respect to the quadrupole deformation. In panel (b), we've represented the overlap distance between each HFB state and its neighbour on the right for the same set, with respect to the quadrupole deformation:

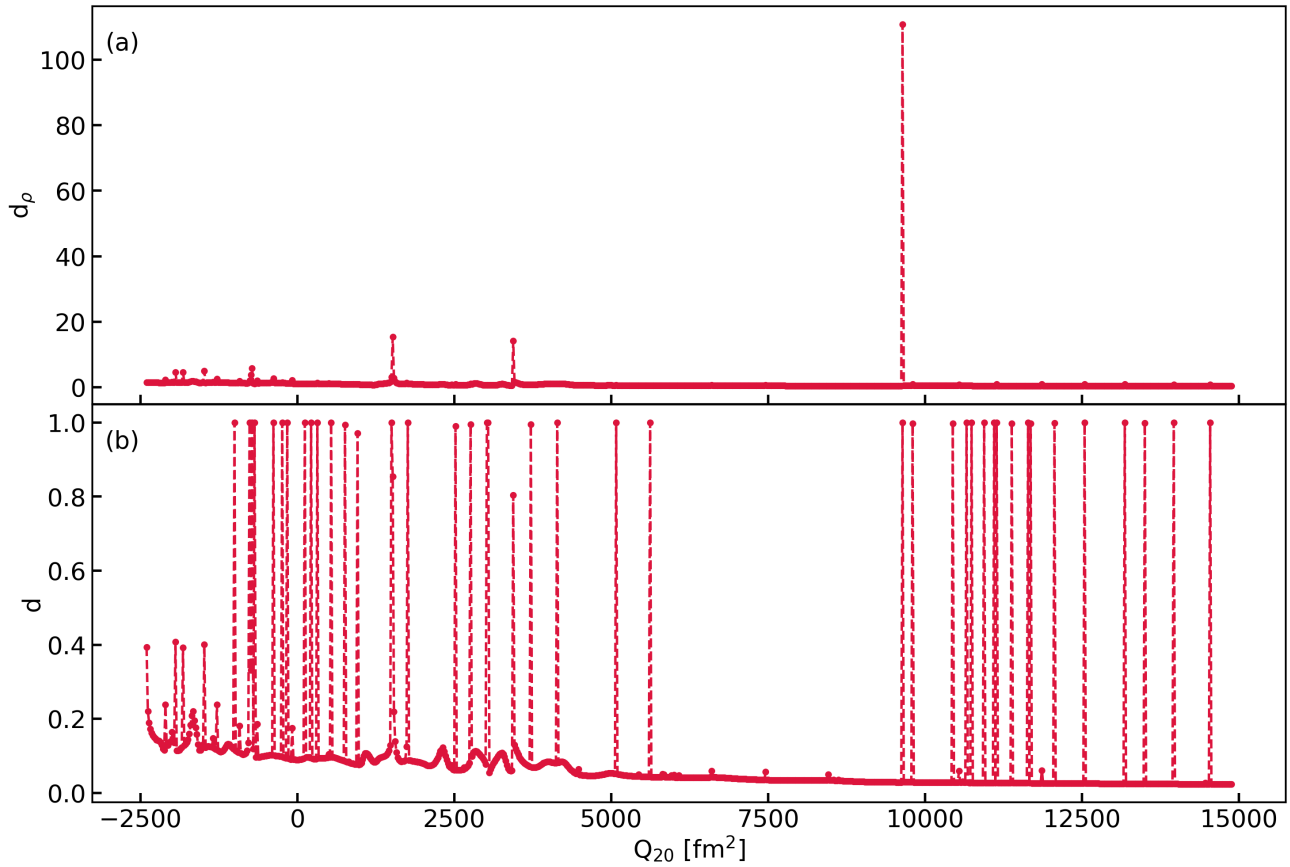

Figure 5.1: Illustration of the unexpected differences between d and d_ρ. Panel (a): the "density distance" d_ρ between each state and its neighbour on the right. Panel (b): the overlap distance d between each state and its neighbour on the right.

We clearly observe in Figure (5.1) that the overlap distance detects much more discontinuities than the density distance does. Insofar as these overlap distance discontinuities seemed to be far too numerous, in addition not being linked to any multipole moment discontinuity, we've assumed that they must be due to phasis issues.
Consequently, we've investigated the U and V Bogoliubov matrices related to the problematic states in detail. We finally found out that the U and V matrices associated with two neighboring states characterized by abnormal overlap distance discontinuities were almost identical, except sign differences in some (Ω,τ) sub-blocks.

Noting $U^{(0)}$, $V^{(0)}$ and $U^{(1)}$, $V^{(1)}$ the Bogoliubov matrices associated with two HFB states $|\Phi_0\rangle$ and $|\Phi_1\rangle$ characterized by an unexpected overlap distance discontinuity, we've evaluated the overlap between $|\Phi_0\rangle$ and $|\Phi_1\rangle$ using the formula given in Eq.(5.30):

$$\langle\Phi_0|\Phi_1\rangle = \langle 0|\Phi_1\rangle\langle\Phi_0|0\rangle \prod_{(\Omega,\tau)} \det(I + V^{(0)\tau\Omega}(U^{(0)\tau\Omega})^{-1}V^{(1)\tau\Omega}(U^{(1)\tau\Omega})^{-1}) \tag{5.61}$$

We've intentionnally developed the (Ω,τ) sub-structure of Eq.(5.61). Clearly, if we change the sign of a $V^{(1)\tau\Omega}$ matrix without changing anything else, the resulting overlap is modified. However, considering only the state $|\Phi_1\rangle$, this sign difference does not imply any change in the one-body observables. This is not a surprise as $\rho = V^{(1)}V^{(1)T}$. When it comes to the total binding energy, the sign difference implies a sign change in the related sub-block of the pairing tensor $\kappa = V^{(1)}U^{(1)T}$. Since the pairing tensor elements are squared in the energy evaluation, this change does not imply any energy variation though.
These observations have led us to replace the overlap formula given in Eq.(5.61) by the following one:

$$\boxed{\langle\Phi_0|\Phi_1\rangle = \langle 0|\Phi_1\rangle\langle\Phi_0|0\rangle \prod_{(\Omega,\tau)} |\max_{\pm}|[\det(I \pm V^{(0)\tau\Omega}(U^{(0)\tau\Omega})^{-1}V^{(1)\tau\Omega}(U^{(1)\tau\Omega})^{-1})]} \tag{5.62}$$

The notation $|\max_{\pm}|$ signifies that we choose the sign $+$ or $-$ in Eq.(5.62) that maximizes the absolute value of the related determinant.
In Figure (5.2), we've represented the differences between the overlap distance evaluation using the customary formula given in Eq.(5.61), already represented in Figure (5.1), and the one using the corrected formula displayed in Eq.(5.62):

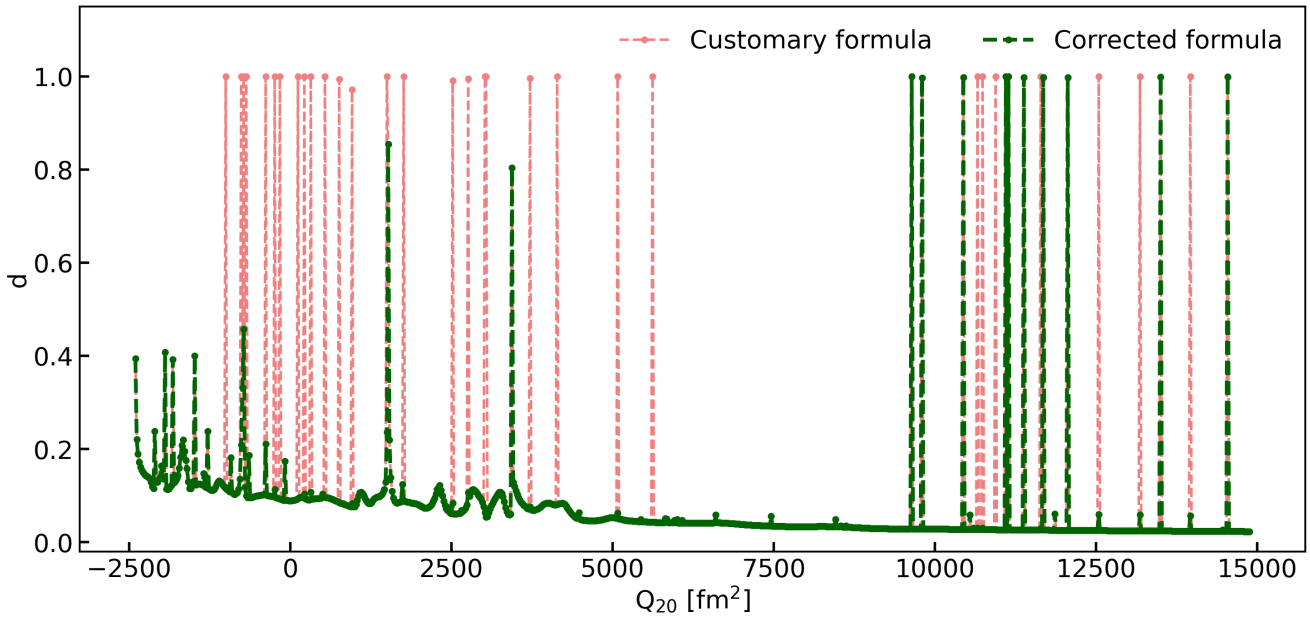

Figure 5.2: Comparison of the overlap distances obtained with the customary overlap formula and with the corrected one, taking explicitly into account the "V phasis", with respect to the quadrupole deformation.

We observe that most of the discontinuities detected using Eq.(5.61) disappear when Eq.(5.62) is used. Besides, the remaining discontinuities on the left hand side of Figure (5.2) correspond to the ones raised by the density distance (see Figure (5.1)). The differences between the corrected overlap distance and the density distance that remain on the right hand side of Figure (5.2) are not related to the "V phasis". As discussed in Chapter 2, they may originate from different causes. We didn't investigated these differences further as we were not interested in the physics of the states belonging to the $\mathcal{P}_{20}$ fusion valley (see Chapter 2). In addition to its evaluation role, Eq.(5.62) can be seen as a prescription to define the "V phasis" of states belonging to the same set. Besides, we are aware that the sign changes observed do change the pairing gaps (they change their signs with respect to the related (Ω, τ) sub-blocks). Even if the pairing gaps are not observables, they could provide us with an interesting prescription to fix the "V phasis" of a given state without considering its neighbors.

We were unable to identify the numerical origin of the sign changes observed. We found that they were most likely to occur when optimizing basis parameters, but we also observed cases of spontaneous changes (starting calculations from an adjacent state without basis parameters optimization).
Nevertheless, we have been able to identify the nature of the "V phasis" phenomenon. It is related to the phases of the different particle number subspaces. Therefore, the "V phasis" accounts for the particle number symmetry breaking. To understand this statement, we can consider a time-even HFB state $|\Phi\rangle$ built with four quasiparticles only:

$$|\Phi\rangle = \mathcal{N}\xi_2\bar{\xi}_2\xi_1\bar{\xi}_1|0\rangle \tag{5.63}$$

We can study the coefficients associated with the different particle states components of $|\Phi\rangle$. We easily figure out that the commutation relations between the particle annihilation and creation operators imply that the coefficient of the state $|0\rangle$ is associated with products of exactly two V elements, while the coefficients of the states $|1\bar{1}\rangle$, $|2\bar{1}\rangle$, $|\bar{2}1\rangle$ and $|2\bar{2}\rangle$ are associated with products of exactly three V elements. Finally, the coefficient of the state $|2\bar{2}1\bar{1}\rangle$ is associated with products of exactly four V elements. These observations signify that changing the sign of V leads to a change in the sign of the coefficients of the states $|1\bar{1}\rangle$, $|2\bar{1}\rangle$, $|\bar{2}1\rangle$ and $|2\bar{2}\rangle$, while the coefficients of the states $|0\rangle$ and $|2\bar{2}1\bar{1}\rangle$ are not impacted.
This example can easily be extended to the general case of an arbitrary time-even HFB state. Noting $2n$ the total number of quasiparticles belonging to the time-even HFB state and p the particle number associated with an arbitrary particle number subspace of the HFB state, changing the sign of the V matrix leads to:

$$\underline{n \text{ even}} \Rightarrow \begin{cases} \text{If } p \equiv 0\ (4),\ \text{the sign of the associated subspace does not change.} \\ \text{If } p \equiv 2\ (4),\ \text{the sign of the associated subspace changes.} \end{cases} \tag{5.64}$$

$$\underline{n \text{ odd}} \Rightarrow \begin{cases} \text{If } p \equiv 0\ (4),\ \text{the sign of the associated subspace changes.} \\ \text{If } p \equiv 2\ (4),\ \text{the sign of the associated subspace does not change.} \end{cases} \tag{5.65}$$

Eq.(5.64) clearly highlights how the nature of the "V phasis" phenomenon is related to the particle number symmetry breaking within the HFB formalism.

We conclude telling a few words about the importance of taking into account the "V phasis"

phenomenon using the overlap constraints methods presented in Chapter 3. Indeed, we have to be sure that the overlaps evaluated reflect a physical distance between the states considered instead of phasis related artifacts. This is especially the case for "Deflation"-based methods, where we need to ensure that orthogonality conditions are not achieved by simple spurious sign changes.

5.2 Projected overlap kernels

In this section, we present and demonstrate the projected overlap formulas used during this PhD thesis work.
Firstly, we explain how to evaluate the projected norm of an HFB state. We've mostly followed [54]. This norm is called "projected diagonal kernel" thereafter. Secondly, we present the new formulas we've developed to evaluate projected overlap kernels between two HFB states built with two different harmonic-oscillator representations. Then, we give the formula related to the most simple case with only one harmonic-oscillator representation. Finally, we display results useful within the POF method (see Chapter 4).

To conclude, we only consider axial and time-reversal HFB states in this section.

5.2.1 Projected HFB states diagonal kernels

In this section, we give the expression of the projected norm defined as follows:

$$\boxed{\langle\Phi|\tilde{\Phi}\rangle = \langle\Phi|\hat{P}^{\tau_n}\hat{P}^{\tau_p}|\Phi\rangle} \tag{5.66}$$

We start by rewriting Eq.(5.66) more explicitly:

$$\boxed{\langle\Phi|\tilde{\Phi}\rangle = \sum_{\varphi_n}\sum_{\varphi_p}\frac{e^{2i\varphi_n\pi N_n}e^{2i\varphi_p\pi N_p}}{n_{\varphi_n}n_{\varphi_p}}\langle\Phi|\Phi(\varphi_n,\varphi_p)\rangle} \tag{5.67}$$

With:

$$|\Phi(\varphi_n,\varphi_p)\rangle = e^{-2i\varphi_p\pi\hat{N}_n}e^{-2i\varphi_p\pi\hat{N}_p}|\Phi\rangle = e^{-2i\varphi_p\pi\hat{N}_n}|\Phi_{\tau_n}\rangle\otimes e^{-2i\varphi_n\pi\hat{N}_p}|\Phi_{\tau_p}\rangle \tag{5.68}$$

To handle Eq.(5.68), we study first how an operator $e^{-2i\varphi_p\pi\hat{N}}$ acts on annihilation and creation particle operators:

$$\begin{cases} e^{-2i\pi\varphi\hat{N}}c_l^+e^{2i\pi\varphi\hat{N}} = c_l^+ - 2i\pi\varphi[\hat{N},c_l^+] + \frac{(2i\pi\varphi)^2}{2}[\hat{N},[\hat{N},c_l^+]] + ... \\ e^{-2i\pi\varphi\hat{N}}c_le^{2i\pi\varphi\hat{N}} = c_l - 2i\pi\varphi[\hat{N},c_l] + \frac{(2i\pi\varphi)^2}{2}[\hat{N},[\hat{N},c_l]] + ... \end{cases} \tag{5.69}$$

Then, we remark the following property:

$$\begin{cases} [\hat{N},c_l^+] = c_l^+ \\ [\hat{N},c_l] = -c_l \end{cases} \tag{5.70}$$

Inserting Eq.(5.70) into Eq.(5.69) leads to:

$$\begin{cases} e^{-2i\pi\varphi\hat{N}} c_l^+ e^{2i\pi\varphi\hat{N}} = c_l^+[1 - 2i\pi\varphi + \frac{(2i\pi\varphi)^2}{2} + ...] = e^{-2i\pi\varphi} c_l^+ \\ e^{-2i\pi\varphi\hat{N}} c_l e^{2i\pi\varphi\hat{N}} = c_l[1 + 2i\pi\varphi + \frac{(2i\pi\varphi)^2}{2} + ...] = e^{2i\pi\varphi} c_l \end{cases} \tag{5.71}$$

In the light of Eq.(5.71), we easily deduce how the operator $e^{-2i\varphi\pi\hat{N}}$ acts on annihilation and creation quasiparticle operators:

$$\begin{cases} e^{-2i\pi\varphi\hat{N}} \xi_j e^{2i\pi\varphi\hat{N}} = \xi_j(\varphi) = \sum_{k>} e^{2i\pi\varphi} U_{kj} c_k + e^{-2i\pi\varphi} V_{kj} \bar{c}_k^+ \\ e^{-2i\pi\varphi\hat{N}} \bar{\xi}_j e^{2i\pi\varphi\hat{N}} = \bar{\xi}_j(\varphi) = \sum_{k>} e^{2i\pi\varphi} U_{kj} \bar{c}_k - e^{-2i\pi\varphi} V_{kj} c_k^+ \end{cases} \tag{5.72}$$

And:

$$\begin{cases} e^{-2i\pi\varphi\hat{N}} \xi_j^+ e^{2i\pi\varphi\hat{N}} = \xi_j^+(\varphi) = \sum_{k>} e^{-2i\pi\varphi} U_{kj} c_k^+ + e^{2i\pi\varphi} V_{kj} \bar{c}_k \\ e^{-2i\pi\varphi\hat{N}} \bar{\xi}_j^+ e^{2i\pi\varphi\hat{N}} = \bar{\xi}_j^+(\varphi) = \sum_{k>} e^{-2i\pi\varphi} U_{kj} \bar{c}_k^+ - e^{2i\pi\varphi} V_{kj} c_k \end{cases} \tag{5.73}$$

These quasiparticle operators verify the following property:

$$\begin{cases} (\xi_j(\varphi))^+ = \xi_j^+(\varphi) \\ (\bar{\xi}_j(\varphi))^+ = \bar{\xi}_j^+(\varphi) \end{cases} \tag{5.74}$$

Besides, the operators $\{\bar{\xi}_j(\varphi)\}$ are no longer the time-reversal counterparts of the operator $\{\xi_j(\varphi)\}$:

$$T^+ \xi_j(\varphi) T = \sum_{k>} e^{-2i\pi\varphi} U_{kj} \bar{c}_k - e^{2i\pi\varphi} V_{kj} c_k^+ = \xi_j(-\varphi) \neq \bar{\xi}_j(\varphi) \tag{5.75}$$

Using Eq.(5.72) and Eq.(5.73), we can write the HFB transformation associated with the quasiparticle annihilation operators $\{\xi_j(\varphi)\}$:

$$\begin{pmatrix} \xi(\varphi) \\ \bar{\xi}(\varphi) \\ \xi^+(\varphi) \\ \bar{\xi}^+(\varphi) \end{pmatrix} = \begin{pmatrix} e^{2i\pi\varphi} U^T & 0 & 0 & e^{-2i\pi\varphi} V^T \\ 0 & e^{2i_p i\varphi} U^T & -e^{-2i\pi\varphi} V^T & 0 \\ 0 & e^{2i\pi\varphi} V^T & e^{-2i\pi\varphi} U^T & 0 \\ -e^{2i\pi\varphi} V^T & 0 & 0 & e^{-2i\pi\varphi} U^T \end{pmatrix} \begin{pmatrix} c \\ \bar{c} \\ c^+ \\ \bar{c}^+ \end{pmatrix} \tag{5.76}$$

Eq.(5.76) can be rewritten in a more compact form:

$$\boxed{\begin{pmatrix} \xi(\varphi) \\ \xi^+(\varphi) \end{pmatrix} = \begin{pmatrix} (U(\varphi))^+ & (V(\varphi))^+ \\ (V(\varphi))^T & (U(\varphi))^T \end{pmatrix} \begin{pmatrix} c \\ c^+ \end{pmatrix}} \tag{5.77}$$

With:

$$\boxed{U(\varphi) = e^{-2i\pi\varphi} \begin{pmatrix} U & 0 \\ 0 & U \end{pmatrix}} \qquad \boxed{V(\varphi) = e^{2i\pi\varphi} \begin{pmatrix} 0 & -V \\ V & 0 \end{pmatrix}} \tag{5.78}$$

Now, we can simply apply the results demonstrated in section 5.1 to the overlap $\langle\Phi|\Phi(\varphi)\rangle$ (we voluntarily neglect the isospin for the sake of simplicity). We find:

$$\boxed{\langle\Phi|\Phi(\varphi)\rangle = \det(U^T U + e^{-4i\pi\varphi} V^T V)} \tag{5.79}$$

With Eq.(5.79), the evaluation of the projected norm $\langle\Phi|\tilde{\Phi}\rangle$ becomes straightforward.

5.2.2 Projected HFB states off-diagonal kernels

This section aims to find the expression of the total off-diagonal projected overlap of two different HFB states $|\Phi_0\rangle$ and $|\Phi_1\rangle$:

$$\boxed{\tilde{\mathcal{O}}^{01}_{00} = \frac{\langle\Phi_0|\hat{P}^{\tau_n}\hat{P}^{\tau_p}|\Phi_1\rangle}{\sqrt{\langle\Phi_0|\tilde{\Phi}_0\rangle\langle\Phi_1|\tilde{\Phi}_1\rangle}}} \tag{5.80}$$

We directly consider the most general case with two different harmonic-oscillator representations $\{0\}$ and $\{1\}$. We start by rewriting Eq.(5.80) more explicitly:

$$\tilde{\mathcal{O}}^{01}_{00} = \frac{1}{\sqrt{\langle\Phi_0|\tilde{\Phi}_0\rangle\langle\Phi_1|\tilde{\Phi}_1\rangle}} \sum_{\varphi_n}\sum_{\varphi_p} \frac{e^{2i\varphi_n\pi N_n} e^{2i\varphi_p\pi N_p}}{n_{\varphi_n} n_{\varphi_p}} \langle\Phi_0|\Phi_1(\varphi_n,\varphi_p)\rangle \tag{5.81}$$

With:

$$|\Phi_1(\varphi_n,\varphi_p)\rangle = e^{-2i\varphi_p\pi\hat{N}_n} e^{-2i\varphi_p\pi\hat{N}_p}|\Phi\rangle = e^{-2i\varphi_p\pi\hat{N}_n}|\Phi_{1_{\tau_n}}\rangle \otimes e^{-2i\varphi_p\pi\hat{N}_p}|\Phi_{1_{\tau_p}}\rangle \tag{5.82}$$

By analogy with the diagonal case, it is clear that the HFB transformation associated with the state $|\Phi_1(\varphi)\rangle$ (we voluntarily neglect the isospin for the sake of simplicity) reads as follows:

$$\boxed{\begin{pmatrix}\xi_1(\varphi)\\ \xi_1^+(\varphi)\end{pmatrix} = \begin{pmatrix}(U^{(1)}(\varphi))^+ & (V^{(1)}(\varphi))^+\\ (V^{(1)}(\varphi))^T & (U^{(1)}(\varphi))^T\end{pmatrix}\begin{pmatrix}c_1\\ c_1^+\end{pmatrix}} \tag{5.83}$$

With:

$$\boxed{U^{(1)}(\varphi) = e^{-2i\pi\varphi}\begin{pmatrix}U^{(1)} & 0\\ 0 & U^{(1)}\end{pmatrix}} \qquad \boxed{V^{(1)}(\varphi) = e^{2i\pi\varphi}\begin{pmatrix}0 & -V^{(1)}\\ V^{(1)} & 0\end{pmatrix}} \tag{5.84}$$

Now, we can simply apply the results demonstrated in section 5.1 to the overlap $\langle\Phi_0|\Phi_1(\varphi)\rangle$. We find:

$$\boxed{\langle\Phi_0|\Phi_1(\varphi)\rangle = \det(U^{(0)T}U^{(1)} + e^{-4i\pi\varphi}V^{(0)T}RV^{(1)}(U^{(1)})^{-1}R^T U^{(1)})} \tag{5.85}$$

With Eq.(5.85), the evaluation of the total projected overlap $\langle\Phi_0|\tilde{\Phi}_1\rangle$ becomes straightforward.

In the most simple case, when only one harmonic-oscillator representation is considered, we directly find:

$$\boxed{\langle\Phi_0|\Phi_1(\varphi)\rangle = \det(U^{(0)T}U^{(1)} + e^{-4i\pi\varphi}V^{(0)T}V^{(1)})} \tag{5.86}$$

5.2.3 POF kernels

In this section, we give the expression of the POF norm defined as follows:

$$\boxed{\langle\Phi|\mathring{\hat{\Phi}}\rangle = \langle\Phi|\hat{P}^{(l)\tau_n}\hat{P}^{(l)\tau_p}\hat{P}^{(r)\tau_n}\hat{P}^{(r)\tau_p}|\Phi\rangle} \tag{5.87}$$

We rewrite Eq.(5.87) more explicitly:

$$\langle\Phi|\mathring{\hat{\Phi}}\rangle = \sum_{\varphi^{(l)}_{\tau_n}}\sum_{\varphi^{(r)}_{\tau_n}} \frac{e^{2i\pi\varphi^{(l)}_{\tau_n}N^{(l)}_{\tau_n}}e^{2i\pi\varphi^{(r)}_{\tau_n}N^{(r)}_{\tau_n}}}{n^{(l)}_{\varphi_{\tau_n}}n^{(r)}_{\varphi_{\tau_n}}} \sum_{\varphi^{(l)}_{\tau_p}}\sum_{\varphi^{(r)}_{\tau_p}} \frac{e^{2i\pi\varphi^{(l)}_{\tau_p}N^{(l)}_{\tau_p}}e^{2i\pi\varphi^{(r)}_{\tau_p}N^{(r)}_{\tau_p}}}{n^{(l)}_{\varphi_{\tau_p}}n^{(r)}_{\varphi_{\tau_p}}} \langle\Phi|\Phi(\varphi^{(l)}_{\tau_n},\varphi^{(r)}_{\tau_n},\varphi^{(l)}_{\tau_p},\varphi^{(r)}_{\tau_p})\rangle \tag{5.88}$$

With:

$$|\Phi(\varphi^{(l)}_{\tau_n},\varphi^{(r)}_{\tau_n},\varphi^{(l)}_{\tau_p},\varphi^{(r)}_{\tau_p})\rangle = e^{2i\pi\varphi^{(l)}_{\tau_n}\hat{N}^{(l)}_{\tau_n}}e^{2i\pi\varphi^{(r)}_{\tau_n}\hat{N}^{(r)}_{\tau_n}}|\Phi_{\tau_n}\rangle \otimes e^{2i\pi\varphi^{(l)}_{\tau_p}N^{(l)}_{\tau_p}}e^{2i\pi\varphi^{(r)}_{\tau_p}N^{(r)}_{\tau_p}}|\Phi_{\tau_p}\rangle \tag{5.89}$$

Noting $\{a^{(l)+}_{k_l}\}$, $\{a^{(l)}_{k_l}\}$ and $\{a^{(r)+}_{k_r}\}$, $\{a^{(r)}_{k_r}\}$ the canonical annihilation and creation particle operators associated with the left and right subspaces of $|\Phi\rangle$ respectively, we can directly write by analogy with section 5.2.1:

$$\begin{cases} e^{-2i\pi\varphi^{(l)}\hat{N}^{(l)}}e^{-2i\pi\varphi^{(r)}\hat{N}^{(r)}}a^{(l)+}_{k_l}e^{2i\pi\varphi^{(r)}\hat{N}^{(r)}}e^{2i\pi\varphi^{(l)}\hat{N}^{(l)}} = e^{-2i\pi\varphi^{(l)}}a^{(l)+}_{k_l} \\ e^{-2i\pi\varphi^{(l)}\hat{N}^{(l)}}e^{-2i\pi\varphi^{(r)}\hat{N}^{(r)}}a^{(l)}_{k_l}e^{2i\pi\varphi^{(r)}\hat{N}^{(r)}}e^{2i\pi\varphi^{(l)}\hat{N}^{(l)}} = e^{2i\pi\varphi^{(l)}}a^{(l)}_{k_l} \\ e^{-2i\pi\varphi^{(l)}\hat{N}^{(l)}}e^{-2i\pi\varphi^{(r)}\hat{N}^{(r)}}a^{(r)+}_{k_l}e^{2i\pi\varphi^{(r)}\hat{N}^{(r)}}e^{2i\pi\varphi^{(l)}\hat{N}^{(l)}} = e^{-2i\pi\varphi^{(r)}}a^{(r)+}_{k_r} \\ e^{-2i\pi\varphi^{(l)}\hat{N}^{(l)}}e^{-2i\pi\varphi^{(r)}\hat{N}^{(r)}}a^{(r)}_{k_r}e^{2i\pi\varphi^{(r)}\hat{N}^{(r)}}e^{2i\pi\varphi^{(l)}\hat{N}^{(l)}} = e^{2i\pi\varphi^{(r)}}a^{(r)}_{k_r} \end{cases} \tag{5.90}$$

Thanks to Eq.(5.90), we can write the HFB transformation associated with the state $|\Phi(\varphi^{(l)},\varphi^{(r)})\rangle$ (we voluntarily neglect the isospin for the sake of simplicity) in the canonical representation:

$$\begin{pmatrix} \eta^{(l)}(\varphi^{(l)}) \\ \eta^{(r)}(\varphi^{(r)}) \\ \bar{\eta}^{(l)}(\varphi^{(l)}) \\ \bar{\eta}^{(r)}(\varphi^{(r)}) \\ \eta^{(l)+}(\varphi^{(l)}) \\ \eta^{(r)+}(\varphi^{(r)}) \\ \bar{\eta}^{(l)+}(\varphi^{(l)}) \\ \bar{\eta}^{(r)+}(\varphi^{(r)}) \end{pmatrix} = \begin{pmatrix} \tilde{u}^{(lr)+}(\varphi^{(l)},\varphi^{(r)}) & \tilde{v}^{(lr)+}(\varphi^{(l)},\varphi^{(r)}) \\ \tilde{v}^{(lr)T}(\varphi^{(l)},\varphi^{(r)}) & \tilde{u}^{(lr)T}(\varphi^{(l)},\varphi^{(r)}) \end{pmatrix} \begin{pmatrix} a^{(l)} \\ a^{(r)} \\ \bar{a}^{(l)} \\ \bar{a}^{(r)} \\ a^{(l)+} \\ a^{(r)+} \\ \bar{a}^{(l)+} \\ \bar{a}^{(r)+} \end{pmatrix} \tag{5.91}$$

With:

$$\boxed{\tilde{u}^{(lr)}(\varphi^{(l)},\varphi^{(r)}) = \begin{pmatrix} e^{-2i\pi\varphi^{(l)}}u^{(l)} & 0 & 0 & 0 \\ 0 & e^{-2i\pi\varphi^{(r)}}u^{(r)} & 0 & 0 \\ 0 & 0 & e^{-2i\pi\varphi^{(l)}}u^{(l)} & 0 \\ 0 & 0 & 0 & e^{-2i\pi\varphi^{(r)}}u^{(r)} \end{pmatrix}} \tag{5.92}$$

And:

$$\boxed{\tilde{v}^{(lr)}(\varphi^{(l)},\varphi^{(r)}) = \begin{pmatrix} 0 & 0 & -e^{2i\pi\varphi^{(l)}}v^{(l)} & 0 \\ 0 & 0 & 0 & -e^{2i\pi\varphi^{(r)}}v^{(r)} \\ e^{2i\pi\varphi^{(l)}}v^{(l)} & 0 & 0 & 0 \\ 0 & e^{2i\pi\varphi^{(r)}}v^{(r)} & 0 & 0 \end{pmatrix}} \tag{5.93}$$

We can rewrite the matrices $\tilde{u}^{(lr)}(\varphi^{(l)},\varphi^{(r)})$ and $\tilde{v}^{(lr)}(\varphi^{(l)},\varphi^{(r)})$:

$$\tilde{u}^{(lr)}(\varphi^{(l)},\varphi^{(r)}) = \begin{pmatrix} u^{(lr)}(\varphi^{(l)},\varphi^{(r)}) & 0 \\ 0 & u^{(lr)}(\varphi^{(l)},\varphi^{(r)}) \end{pmatrix} \tag{5.94}$$

And:

$$\tilde{v}^{(lr)}(\varphi^{(l)},\varphi^{(r)}) = \begin{pmatrix} 0 & -v^{(lr)}(\varphi^{(l)},\varphi^{(r)}) \\ v^{(lr)}(\varphi^{(l)},\varphi^{(r)}) & 0 \end{pmatrix} \tag{5.95}$$

With:

$$u^{(lr)}(\varphi^{(l)},\varphi^{(r)}) = \begin{pmatrix} e^{-2i\pi\varphi^{(l)}}u^{(l)} & 0 \\ 0 & e^{-2i\pi\varphi^{(r)}}u^{(r)} \end{pmatrix} \tag{5.96}$$

And:

$$v^{(lr)}(\varphi^{(l)},\varphi^{(r)}) = \begin{pmatrix} e^{2i\pi\varphi^{(l)}}v^{(l)} & 0 \\ 0 & e^{2i\pi\varphi^{(r)}}v^{(r)} \end{pmatrix} \tag{5.97}$$

Now, we can simply apply the results demonstrated in section 5.1 to the overlap $\langle\Phi|\Phi(\varphi^{(l)},\varphi^{(r)})\rangle$. Firstly, we obtain:

$$\langle\Phi|\Phi(\varphi^{(l)},\varphi^{(r)})\rangle = \det(u^2)\det(I + v^{(lr)*}(\varphi^{(l)},\varphi^{(r)})(u^{(lr)*}(\varphi^{(l)},\varphi^{(r)}))^{-1}vu^{-1}) \tag{5.98}$$

As all the matrices in Eq.(5.98) are diagonal matrices, we can separate the determinant:

$$\boxed{\langle\Phi|\Phi(\varphi^{(l)},\varphi^{(r)})\rangle = \det((u^{(l)})^2 + e^{-4i\pi\varphi^{(l)}}(v^{(l)})^2)\det((u^{(r)})^2 + e^{-4i\pi\varphi^{(r)}}(v^{(r)})^2)} \tag{5.99}$$

We can finally rewrite Eq.(5.99) in a more compact form:

$$\boxed{\langle\Phi|\Phi(\varphi^{(l)},\varphi^{(r)})\rangle = \mathcal{O}^{(l)}(\varphi^{(l)})\mathcal{O}^{(r)}(\varphi^{(r)})} \tag{5.100}$$

With:

$$\boxed{\mathcal{O}^{(l)}(\varphi^{(l)}) = \det((u^{(l)})^2 + e^{-4i\pi\varphi^{(l)}}(v^{(l)})^2)} \tag{5.101}$$

And:

$$\boxed{\mathcal{O}^{(r)}(\varphi^{(r)}) = \det((u^{(r)})^2 + e^{-4i\pi\varphi^{(r)}}(v^{(r)})^2)} \tag{5.102}$$

With these formulas, we can rewrite the POF norm $\langle\Phi|\mathring{\Phi}\rangle$:

$$\langle\Phi_\tau|\mathring{\Phi}_\tau\rangle = \sum_{\varphi_\tau^{(l)}} \frac{e^{2i\pi\varphi_\tau^{(l)}N_\tau^{(l)}}}{n_{\varphi_\tau}^{(l)}}\mathcal{O}^{(l)}(\varphi_\tau^{(l)}) \sum_{\varphi_\tau^{(r)}} \frac{e^{2i\pi\varphi_\tau^{(r)}N_\tau^{(r)}}}{n_{\varphi_\tau}^{(r)}}\mathcal{O}^{(r)}(\varphi_\tau^{(r)}) = \langle\Phi_\tau^{(l)}|\mathring{\Phi}_\tau^{(l)}\rangle\langle\Phi_\tau^{(r)}|\mathring{\Phi}_\tau^{(r)}\rangle \tag{5.103}$$

With:

$$\boxed{\langle\Phi_\tau^{(l)}|\mathring{\Phi}_\tau^{(l)}\rangle = \sum_{\varphi_\tau^{(l)}} \frac{e^{2i\pi\varphi_\tau^{(l)}N_\tau^{(l)}}}{n_{\varphi_\tau}^{(l)}}\mathcal{O}^{(l)}(\varphi_\tau^{(l)})} \qquad \boxed{\langle\Phi_\tau^{(r)}|\mathring{\Phi}_\tau^{(r)}\rangle = \sum_{\varphi_\tau^{(r)}} \frac{e^{2i\pi\varphi_\tau^{(r)}N_\tau^{(r)}}}{n_{\varphi_\tau}^{(r)}}\mathcal{O}^{(r)}(\varphi_\tau^{(r)})} \tag{5.104}$$

5.3 Relevant contractions

In this section, we give the expressions relevant to evaluate the Hamiltonian kernels. We directly consider the general case including two different harmonic-oscillator representations. Indeed, the most simple case with only one harmonic-oscillator representation is trivially obtained from it. In addition, we give the expressions of the 2-quasiparticle excited overlaps as well as the ones of the 2-quasiparticle excited transition densities used in the density-dependent term of the interaction (see Appendix F).
As far as we know, the way we handle the contractions with two different harmonic-oscillator representations is totally new. Our method enables us to consider an arbitrary overlap matrix R between the bases $\{0\}$ and $\{1\}$, while the method presented in [69] requires an invertible overlap matrix. As it is always possible to complete the sets $\{0\}$ and $\{1\}$ to achieve this requirement, our new method does not allow to evaluate quantities that were not accessible before. However, we believe that the new derivations presented in this section are very interesting and our new formulas really convenient.

In the whole section, we've always considered the axial and time-reversal symmetries, except for the derivations of the matrices ρ^{01},κ^{01} and $\bar{\kappa}^{01}$ that we've kept as general as possible. Indeed, these derivations are the heart of our new evaluation method, and we wanted to present it fully.

5.3.1 Expressions of ρ^{01},κ^{01} and $\bar{\kappa}^{01}$

This section aims to give an expression of the following quantities:

$$\boxed{\bar{\kappa}_{\alpha\beta}^{01} = \frac{\langle\Phi_0|c_{0,\alpha}^+c_{0,\beta}^+|\Phi_1\rangle}{\langle\Phi_0|\Phi_1\rangle}} \qquad \boxed{\kappa_{\alpha\beta}^{01} = \frac{\langle\Phi_0|c_{1,\alpha}c_{1,\beta}|\Phi_1\rangle}{\langle\Phi_0|\Phi_1\rangle}} \tag{5.105}$$

And:

$$\boxed{\rho_{\delta\beta}^{01} = \frac{\langle\Phi_0|c_{0,\beta}^+c_{1,\delta}|\Phi_1\rangle}{\langle\Phi_0|\Phi_1\rangle}} \tag{5.106}$$

We start by defining the function $f : \mathbb{R} \to \mathbb{C}$ as follows:

$$f(x) = \langle \Phi_0 | \Phi_1(x) \rangle = \frac{\langle 0 | e^{\frac{1}{2}\sum_{kk'}(V^{(0)}U^{(0)-1})_{kk'}c_{0,k'}c_{0,k}} e^{\frac{1}{2}\sum_{kk'}(RV^{(1)}U^{(1)-1}R^T)^*_{kk'}c^+_{0,k}c^+_{0,k'}x_{kk'}} | 0 \rangle}{\langle 0 | \Phi_1 \rangle \langle \Phi_0 | 0 \rangle} \tag{5.107}$$

Here, R stands for the reduced overlap matrix between the harmonic-oscillator representations $\{0\}$ and $\{1\}$ (see section 5.1). Besides, the notation $x_{kk'}$ is defined as follows:

$$\begin{cases} (k,k') = (\alpha,\beta) \text{ or } (\beta,\alpha) \Rightarrow x_{kk'} = x \\ (k,k') \neq (\alpha,\beta) \text{ or } (\beta,\alpha) \Rightarrow x_{kk'} = 1 \end{cases} \tag{5.108}$$

We can differentiate the function f:

$$f'(x) = (RV^{(1)}U^{(1)-1}R^T)^*_{\alpha\beta} \langle \Phi_0 | c^+_{0,\alpha} c^+_{0,\beta} | \Phi_1(x) \rangle \tag{5.109}$$

Evaluating the function f' at $x = 1$ leads to:

$$\boxed{f'(1) = \langle \Phi_0 | \Phi_1 \rangle (RV^{(1)}U^{(1)-1}R^T)^*_{\alpha\beta} \bar{\kappa}^{01}_{\alpha\beta}} \tag{5.110}$$

Now, we set:

$$(M^{(1)}_R(x))_{kk'} = (RV^{(1)}U^{(1)-1}R^T)^*_{kk'} x_{kk'} \tag{5.111}$$

As $M^{(1)}_R(x)$ is a skew-symmetric matrix for all x, we directly obtain a new expression of f using the results developed in section 5.1:

$$f(x) = (-1)^{\frac{n(n+1)}{2}} \langle 0 | \Phi_1 \rangle \langle \Phi_0 | 0 \rangle \mathrm{pf}(-M^{(0)*}) \mathrm{pf}(M^{(1)}_R(x) - (M^{(0)*})^{-1}) \tag{5.112}$$

We recall the following Pfaffian differentiation formula:

$$\frac{\mathrm{dpf}(A(x))}{\mathrm{d}x} = \frac{\mathrm{pf}(A(x))}{2} \mathrm{tr}[(A(x))^{-1} \frac{\mathrm{d}A(x)}{\mathrm{d}x}] \tag{5.113}$$

Here, we define the function A as follows:

$$A(x) = M^{(1)}_R(x) - (M^{(0)*})^{-1} \tag{5.114}$$

We differentiate the function $A(x)$:

$$(\frac{\mathrm{d}A}{\mathrm{d}x}(x))_{kk'} = [\delta_{((k,k')=(\alpha\beta))} - \delta_{((k,k')=(\beta\alpha))}](RV^{(1)}U^{(1)-1}R^T)^*_{\alpha\beta} \tag{5.115}$$

Then, Eq.(5.115) directly implies:

$$\mathrm{tr}[A(x)^{-1} \frac{\mathrm{d}A}{\mathrm{d}x}(x)] = -2A^{-1}_{\alpha\beta}(x)(RV^{(1)}U^{(1)-1}R^T)^*_{\alpha\beta} \tag{5.116}$$

We use Eq.(5.116) to give an alternative expression of $f'(1)$:

$$f'(1) = \langle\Phi_0|\Phi_1\rangle (RV^{(1)}U^{(1)-1}R^T)^*_{\alpha\beta}[(RV^{(1)}U^{(1)-1}R^T)^* - V^{(0)}U^{(0)-1}]^{-1}_{\alpha\beta} \tag{5.117}$$

We finally find the expression of $\bar{\kappa}^{01}$:

$$\boxed{\bar{\kappa}^{01} = [(RV^{(1)}U^{(1)-1}R^T)^* - (V^{(0)}U^{(0)-1})^{-1}]^{-1}} \tag{5.118}$$

As $\kappa^{01} = -\bar{\kappa}^{10*}$, we directly obtain:

$$\boxed{\kappa^{01} = [-R^T V^{(0)}U^{(0)-1}R + (V^{(1)*}U^{(1)*-1})^{-1}]^{-1}} \tag{5.119}$$

When it comes to the transition density matrix ρ^{01}, we start by writing using the Thouless theorem:

$$\rho^{01}_{\delta\beta} = \frac{\langle\Phi_0|c^+_{0,\beta}c_{1,\delta}|\Phi_1\rangle}{\langle\Phi_0|\Phi_1\rangle} = \frac{\langle 0|\Phi_1\rangle}{\langle\Phi_0|\Phi_1\rangle}\langle\Phi_0|c^+_{0,\beta}c_{1,\delta}e^{\frac{1}{2}\sum_{kk'}(V^{(1)}U^{(1)-1})^*_{kk'}c^+_{1,k}c^+_{1,k'}}|0\rangle \tag{5.120}$$

Then, we remark the following property:

$$e^{-\frac{1}{2}\sum_{kk'}(V^{(1)}U^{(1)-1})^*_{kk'}c^+_{1,k}c^+_{1,k'}}c_{1,\delta}e^{\frac{1}{2}\sum_{kk'}(V^{(1)}U^{(1)-1})^*_{kk'}c^+_{1,k}c^+_{1,k'}} = c_{1,\delta} - \sum_k (V^{(1)}U^{(1)-1})^*_{k\delta}c^+_{1,k} \tag{5.121}$$

Inserting Eq.(5.121) into Eq.(5.120) leads to:

$$\rho^{01}_{\delta\beta} = -\sum_k (V^{(1)}U^{(1)-1})^*_{k\delta}\frac{\langle\Phi_0|c^+_{0,\beta}c^+_{1,k}|\Phi_1\rangle}{\langle\Phi_0|\Phi_1\rangle} \tag{5.122}$$

Now, we use the full transformation matrix $\bar{R}$ between the two harmonic-oscillator representations:

$$\rho^{01}_{\delta\beta} = -\sum_k (V^{(1)}U^{(1)-1})^*_{k\delta}\frac{\langle\Phi_0|c^+_{0,\beta}\sum_l^{+\infty}\bar{R}_{lk}c^+_{0,l}|\Phi_1\rangle}{\langle\Phi_0|\Phi_1\rangle} \tag{5.123}$$

It is clear that all the contributions of the sum labeled by $l \notin \{0\}$ vanish. Therefore, we can write:

$$\rho^{01}_{\delta\beta} = -\sum_l\sum_k R_{lk}(V^{(1)}U^{(1)-1})^*_{k\delta}\frac{\langle\Phi_0|c^+_{0,\beta}c^+_{0,l}|\Phi_1\rangle}{\langle\Phi_0|\Phi_1\rangle} \tag{5.124}$$

We identify the matrix $\bar{\kappa}^{01}$:

$$\rho^{01}_{\delta\beta} = \sum_l\sum_k R_{lk}(V^{(1)}U^{(1)-1})^*_{k\delta}\bar{\kappa}^{01}_{\beta l} \tag{5.125}$$

Thus, the transition matrix ρ^{01} reads:

$$\boxed{\rho^{01} = (V^{(1)}U^{(1)-1})^* R^T \bar{\kappa}^{01}} \tag{5.126}$$

We can rewrite Eq.(5.126) more explicitly:

$$\boxed{\rho^{01} = (V^{(1)}U^{(1)-1})^* R^T [(RV^{(1)}U^{(1)-1}R^T)^* - (V^{(0)}U^{(0)-1})^{-1}]^{-1}} \tag{5.127}$$

Connection with the formulas of L.M. Robledo:

In this part, we show the link between our new formulas and the ones given in [69]. We start with $\bar{\kappa}^{01}$, as it is defined in [69]:

$$\boxed{\bar{\kappa}^{01} = (R^T)^{-1}U^{(1)^*}[V^{(0)T}RV^{(1)*} + U^{(0)T}(R^T)^{-1}U^{(1)*}]^{-1}V^{(0)T}} \tag{5.128}$$

Eq.(5.128) includes the correction to the sign mistake we've found in Eq.(19) of [69]. As R is a square invertible matrix, we can write:

$$\bar{\kappa}^{01} = [RV^{(1)*}(U^{(1)*})^{-1}R^T + (V^{(0)T})^{-1}U^{(0)T}]^{-1} \tag{5.129}$$

Finally, using the skew-symmetry property of the matrix $V^{(0)}U^{(0)-1}$ leads to:

$$\bar{\kappa}^{01} = [RV^{(1)*}(U^{(1)*})^{-1}R^T - (V^{(0)}U^{(0)-1})^{-1}]^{-1} \tag{5.130}$$

Now, we consider the definition of the matrix κ^{01} given in [69]:

$$\boxed{\kappa^{01} = V^{(1)^*}[V^{(0)T}RV^{(1)*} + U^{(0)T}(R^T)^{-1}U^{(1)*}]^{-1}U^{(0)T}(R^T)^{-1}} \tag{5.131}$$

As R is a square invertible matrix, we can write:

$$\kappa^{01} = [R^T(U^{(0)T})^{-1}V^{(0)T}R + U^{(1)*}(V^{(1)*})^{-1}]^{-1} \tag{5.132}$$

Finally, using the skew-symmetry of the matrix $V^{(0)}U^{(0)-1}$ leads to our formula for κ^{01}:

$$\kappa^{01} = [-R^TV^{(0)}U^{(0)-1}R + (V^{(1)*}U^{(1)*-1})^{-1}]^{-1} \tag{5.133}$$

To conclude, we consider the definition of the transition density matrix ρ^{01} given in [69]:

$$\boxed{\rho^{01} = V^{(1)^*}[V^{(0)T}RV^{(1)*} + U^{(0)T}(R^T)^{-1}U^{(1)*}]^{-1}V^{(0)T}} \tag{5.134}$$

Here, the transformation is very straightforward:

$$\rho^{01} = (V^{(1)}U^{(1)-1})^* R^T \bar{\kappa}^{01} \tag{5.135}$$

We've shown that our new formulas are equivalent to the ones given in [69] in the special case of a square invertible overlap matrix R.

Axial and time-reversal case:

In the following, we give the explicit expressions of the matrices ρ^{01}, $\bar{\kappa}^{01}$, and κ^{01} in the axial and time-reversal case. We start by recalling that in this particular case, the Bogoliubov matrices $\tilde{U}^{(0)}$, $\tilde{V}^{(0)}$ and $\tilde{U}^{(1)}$, $\tilde{V}^{(1)}$ associated with the axial and time-reversal HFB states $|\Phi_0\rangle$ and $|\Phi_1\rangle$ have a particular form:

$$\tilde{U}^{(i)} = \begin{pmatrix} U^{(i)} & 0 \\ 0 & U^{(i)} \end{pmatrix} \qquad \text{and} \qquad \tilde{V}^{(i)} = \begin{pmatrix} 0 & -V^{(i)} \\ V^{(i)} & 0 \end{pmatrix} \tag{5.136}$$

Moreover, the overlap matrix R also has a particular form:

$$\tilde{R} = \begin{pmatrix} R & 0 \\ 0 & R \end{pmatrix} \tag{5.137}$$

Thanks to Eq.(5.136), Eq.(5.137) and to the results found for the general case, we directly write:

$$\boxed{\bar{\kappa}^{01} = [-RV^{(1)}U^{(1)-1}R^T - (V^{(0)}U^{(0)-1})^{-1}]^{-1}} \tag{5.138}$$

And:

$$\boxed{\kappa^{01} = [R^TV^{(0)}U^{(0)-1}R + (V^{(1)}U^{(1)-1})^{-1}]^{-1}} \tag{5.139}$$

And, finally:

$$\boxed{\rho^{01} = V^{(1)}U^{(1)-1}R^T\bar{\kappa}^{01}} \tag{5.140}$$

It is important to keep in mind that the matrices $\bar{\kappa}^{01}$ and κ^{01} are the reduced matrices whose elements are the $\bar{\kappa}^{01}_{\alpha\bar{\beta}}$ and $\kappa^{01}_{\alpha\bar{\beta}}$ with $\alpha, \beta > 0$. In addition, the elements of the reduced transition matrix ρ^{01} are the $\rho^{01}_{\alpha\beta}$ with $\alpha, \beta > 0$.

5.3.2 Expressions of W,$\bar{W}$, Z and $\bar{Z}$

In this section, we give the explicit expressions of the following quantities:

$$\boxed{W_{\alpha i} = \frac{\langle\Phi_0|c_{1,\alpha}\xi^+_{1,i}|\Phi_1\rangle}{\langle\Phi_0|\Phi_1\rangle}} \qquad \boxed{\bar{W}_{j\beta} = \frac{\langle\Phi_0|\xi_{0,j}c^+_{0,\beta}|\Phi_1\rangle}{\langle\Phi_0|\Phi_1\rangle}} \tag{5.141}$$

And:

$$\boxed{Z_{\alpha\bar{i}} = \frac{\langle\Phi_0|c^+_{0,\alpha}\bar{\xi}^+_{1,i}|\Phi_1\rangle}{\langle\Phi_0|\Phi_1\rangle}} \qquad \boxed{\bar{Z}_{j\bar{\beta}} = \frac{\langle\Phi_0|\xi_{0,j}\bar{c}_{1,\beta}|\Phi_1\rangle}{\langle\Phi_0|\Phi_1\rangle}} \tag{5.142}$$

All these quantities are easily deduced from the matrices $\bar{\kappa}^{01}$, κ^{01}, and ρ^{01}. Therefore, we only present the derivations concerning W explicitly. Then, we simply give the formulas associated with the other quantities. To evaluate W, we start by writing:

$$W_{\alpha i} = -\sum_l U^{(1)}_{li} \frac{\langle \Phi_0 | c^+_{1,l} c_{1,\alpha} | \Phi_1 \rangle}{\langle \Phi_0 | \Phi_1 \rangle} + [\kappa^{01} V^{(1)}]_{\alpha i} \tag{5.143}$$

Then, we remark that:

$$\frac{\langle \Phi_0 | c^+_{1,l} c_{1,\alpha} | \Phi_1 \rangle}{\langle \Phi_0 | \Phi_1 \rangle} = \sum_m^{+\infty} \bar{R}_{ml} \frac{\langle \Phi_0 | c^+_{0,m} c_{1,\alpha} | \Phi_1 \rangle}{\langle \Phi_0 | \Phi_1 \rangle} = \sum_m R_{ml} \frac{\langle \Phi_0 | c^+_{0,m} c_{1,\alpha} | \Phi_1 \rangle}{\langle \Phi_0 | \Phi_1 \rangle} = [\rho^{01} R]_{\alpha l} \tag{5.144}$$

Inserting Eq.(5.144) into Eq.(5.143) finally leads to:

$$\boxed{W = -\rho^{01} R U^{(1)} + \kappa^{01} V^{(1)}} \tag{5.145}$$

The matrix $\bar{W}$ reads as follows:

$$\boxed{\bar{W} = -U^{(0)T} R \rho^{01} - V^{(0)T} \bar{\kappa}^{01}} \tag{5.146}$$

For the matrix Z, we've found:

$$\boxed{Z = \bar{\kappa}^{01} R U^{(1)} - \rho^{01T} V^{(1)}} \tag{5.147}$$

Finally, the matrix $\bar{Z}$ reads as:

$$\boxed{\bar{Z} = U^{(0)T} R \kappa^{01} + V^{(0)T} \rho^{01T}} \tag{5.148}$$

5.3.3 Expressions of Y,T and S

The goal of this section is to give the expressions of the matrices Y, T, and S defined as follows:

$$\boxed{Y_{j\bar{j}'} = \frac{\langle \Phi_0 | \xi_{0,j} \bar{\xi}_{0,j'} | \Phi_1 \rangle}{\langle \Phi_0 | \Phi_1 \rangle}} \qquad \boxed{T_{i\bar{i}'} = \frac{\langle \Phi_0 | \xi^+_{1,i} \bar{\xi}^+_{1,i'} | \Phi_1 \rangle}{\langle \Phi_0 | \Phi_1 \rangle}} \qquad \boxed{S_{ji} = \frac{\langle \Phi_0 | \xi_{0,j} \xi^+_{1,i} | \Phi_1 \rangle}{\langle \Phi_0 | \Phi_1 \rangle}} \tag{5.149}$$

All these quantities are easily deduced from the W, $\bar{W}$, Z, and $\bar{Z}$ matrices. Concerning Y, we can write:

$$\boxed{Y = \bar{Z} R^T U^{(0)} - \bar{W} V^{(0)}} \tag{5.150}$$

The matrix T reads as:

$$\boxed{T = U^{(1)T} R^T Z + V^{(1)T} W} \tag{5.151}$$

Finally, the matrix S has the following form:

$$\boxed{S = \bar{W} U^{(1)} + \bar{Z} V^{(1)}} \tag{5.152}$$

5.3.4 2-quasiparticle excited state overlaps

This section aims to present all the 2-quasiparticle excited state overlap formulas we've used to peform calculations implying 2-quasiparticle excited states.
The first 2-quasiparticle excited state overlap we consider is $\langle\Phi_0^{(j)}|\Phi_1\rangle$:

$$\boxed{\langle\Phi_0^{(j)}|\Phi_1\rangle = \langle\Phi_0|\bar{\xi}_{0,j}\xi_{0,j}|\Phi_1\rangle = -\langle\Phi_0|\Phi_1\rangle Y_{j\bar{j}}} \tag{5.153}$$

Then, we consider the 2-quasiparticle stateexcited overlap $\langle\Phi_0|\Phi_1^{(i)}\rangle$:

$$\boxed{\langle\Phi_0|\Phi_1^{(i)}\rangle = \langle\Phi_0|\xi_{1,i}^{+}\bar{\xi}_{1,i}^{+}|\Phi_1\rangle = \langle\Phi_0|\Phi_1\rangle T_{i\bar{i}}} \tag{5.154}$$

Finally, we study the more complex 2-quasiparticle excited state overlap $\langle\Phi_0^{(j)}|\Phi_1^{(i)}\rangle$:

$$\boxed{\langle\Phi_0^{(j)}|\Phi_1^{(i)}\rangle = \langle\Phi_0|\bar{\xi}_{0,j}\xi_{0,j}\xi_{1,i}^{+}\bar{\xi}_{1,i}^{+}|\Phi_1\rangle = \langle\Phi_0|\Phi_1\rangle[S_{ji}^2 - Y_{j\bar{j}}T_{i\bar{i}}]} \tag{5.155}$$

5.3.5 Excited transition densities

In this section, we give the expressions of the excited transition densities used in the density-dependent term of the interaction when 2-quasiparticle excited states are considered (see Appendix F). When the states $|\Phi_0^{(j)}\rangle$ and $|\Phi_1\rangle$ are considered, the related excited transition density $\rho^{(j0)}$ reads as follows:

$$\boxed{\rho_{\alpha\beta}^{(j0)} = \frac{\langle\Phi_0^{(j)}|c_{0,\beta}^{+}c_{1,\alpha}|\Phi_1\rangle}{\langle\Phi_0|\Phi_1\rangle} = -Y_{j\bar{j}}\rho_{\alpha\beta}^{01} - \bar{Z}_{j\bar{\alpha}}\bar{W}_{j\beta}} \tag{5.156}$$

Then, if the states $|\Phi_0\rangle$ and $|\Phi_1^{(i)}\rangle$ are considered, the associated excited transition density $\rho^{(0i)}$ has the following expression:

$$\boxed{\rho_{\alpha\beta}^{(0i)} = \frac{\langle\Phi_0|c_{0,\beta}^{+}c_{1,\alpha}|\Phi_1^{(i)}\rangle}{\langle\Phi_0|\Phi_1\rangle} = T_{i\bar{i}}\rho_{\alpha\beta}^{01} + W_{\alpha i}Z_{\beta\bar{i}}} \tag{5.157}$$

Finally, we consider the states $|\Phi_0^{(j)}\rangle$ and $|\Phi_1^{(i)}\rangle$. The excited transition density $\rho^{(ji)}$ reads as:

$$\boxed{\begin{aligned}\rho^{(ji)} = \frac{\langle\Phi_0^{(j)}|c_{0,\beta}^{+}c_{1,\alpha}|\Phi_1^{(i)}\rangle}{\langle\Phi_0|\Phi_1\rangle} = -Y_{j\bar{j}}\rho_{\alpha\beta}^{(0i)} - \bar{Z}_{j\bar{\alpha}}[\bar{W}_{j\beta}T_{i\bar{i}} - S_{ji}Z_{\beta\bar{i}}] \\ +S_{ji}[S_{ji}\rho_{\alpha\beta}^{01} + W_{\alpha i}\bar{W}_{j\beta}]\end{aligned}} \tag{5.158}$$

5.4 Relevant projected contractions

In this section, we present the formulas of all the projected contractions we've used in this PhD thesis work. In the following, we call the quantities that depend on the angle φ the local quantities, while the ones summed over φ are called total.
Firstly, we give the expressions of all the projected quantities associated with ρ^{01},$\bar{\kappa}^{01}$, and κ^{01}. Then, we display the ones related to W,$\bar{W}$, Z and $\bar{Z}$ and the ones associated with Y, T, and S.
Secondly, we present the derivations of the projected 2-quasiparticle excited state overlaps and we give the formulas for the projected excited transition densities used in the density-dependent term of the interaction (see Appendix F).
Finally, we conclude with the contractions related to the POF method developed in this PhD thesis work.

5.4.1 Projected expressions related to ρ^{01},$\bar{\kappa}^{01}$, and κ^{01}

First, we tackle the following local quantities:

$$\boxed{\bar{\kappa}^{01}_{\alpha\bar{\beta}}(\varphi) = \frac{\langle\Phi_0|c^+_{0,\alpha}\bar{c}_{0,\beta}|\Phi_1(\varphi)\rangle}{\langle\Phi_0|\Phi_1(\varphi)\rangle}} \qquad \boxed{\kappa^{01}_{\alpha\bar{\beta}}(\varphi) = \frac{\langle\Phi_0|c_{1,\alpha}\bar{c}_{1,\beta}|\Phi_1(\varphi)\rangle}{\langle\Phi_0|\Phi_1(\varphi)\rangle}} \tag{5.159}$$

And:

$$\boxed{\rho^{01}_{\beta\alpha}(\varphi) = \frac{\langle\Phi_0|c^+_{0,\alpha}c_{1,\beta}|\Phi_1(\varphi)\rangle}{\langle\Phi_0|\Phi_1(\varphi)\rangle}} \tag{5.160}$$

As $|\Phi_1(\varphi)\rangle$ is an HFB state associated with the transformation defined in Eq.(5.76), we can directly write, by analogy with the derivations made in section 5.3.1:

$$\boxed{\bar{\kappa}^{01}(\varphi) = [-e^{-4i\pi\varphi}RV^{(1)}U^{(1)-1}R^T - (V^{(0)}U^{(0)-1})^{-1}]^{-1}} \tag{5.161}$$

And:

$$\boxed{\kappa^{01}(\varphi) = [R^TV^{(0)}U^{(0)-1}R + e^{4i\pi\varphi}(V^{(1)}U^{(1)-1})^{-1}]^{-1}} \tag{5.162}$$

And, finally:

$$\boxed{\rho^{01}(\varphi) = e^{-4i\pi\varphi}V^{(1)}U^{(1)-1}R^T\bar{\kappa}^{01}(\varphi)} \tag{5.163}$$

To conclude, we give the definition of the total projected transition density $\tilde{\rho}^{01}$:

$$\boxed{\tilde{\rho}^{01}_{\alpha\beta} = \frac{\langle\Phi_0|c^+_{0,\beta}c^+_{1,\alpha}|\tilde{\Phi}_1\rangle}{\langle\Phi_0|\tilde{\Phi}_1\rangle}} \tag{5.164}$$

We can rewrite $\tilde{\rho}^{01}$ more explicitly:

$$\boxed{\tilde{\rho}^{01\tau}_{\alpha\beta} = \frac{1}{\tilde{\mathcal{O}}^{01\tau}_{00}\sqrt{\langle\Phi_{0\tau}|\tilde{\Phi}_{0\tau}\rangle\langle\Phi_{1\tau}|\tilde{\Phi}_{1\tau}\rangle}}\sum_{\varphi_\tau}\frac{e^{2i\pi\varphi_\tau N_\tau}}{n_{\varphi_\tau}}\langle\Phi_{0\tau}|\Phi_{1\tau}(\varphi_\tau)\rangle\rho^{01\tau}_{\alpha\beta}(\varphi_\tau)} \tag{5.165}$$

The total projected transition density $\tilde{\rho}^{01}$ is the one we've used in the density-dependent term of the interaction, following the prescription formulated in [54].

5.4.2 Projected expressions related to W,$\bar{W}$, Z and $\bar{Z}$

This part aims to give the expressions of the following local quantities:

$$\boxed{W_{\alpha i}(\varphi) = \frac{\langle\Phi_0|c_{1,\alpha}\xi^+_{1,i}(\varphi)|\Phi_1(\varphi)\rangle}{\langle\Phi_0|\Phi_1(\varphi)\rangle}} \qquad \boxed{\bar{W}_{j\beta}(\varphi) = \frac{\langle\Phi_0|\xi_{0,j}c^+_{0,\beta}|\Phi_1(\varphi)\rangle}{\langle\Phi_0|\Phi_1(\varphi)\rangle}} \tag{5.166}$$

And:

$$\boxed{Z_{\alpha\bar{i}}(\varphi) = \frac{\langle\Phi_0|c^+_{0,\alpha}\bar{\xi}^+_{1,i}(\varphi)|\Phi_1\rangle}{\langle\Phi_0|\Phi_1(\varphi)\rangle}} \qquad \boxed{\bar{Z}_{j\bar{\beta}}(\varphi) = \frac{\langle\Phi_0|\xi_{0,j}\bar{c}_{1,\beta}|\Phi_1(\varphi)\rangle}{\langle\Phi_0|\Phi_1(\varphi)\rangle}} \tag{5.167}$$

These quantities are easily deduced from $\rho^{01}(\varphi)$, $\bar{\kappa}^{01}(\varphi)$, and $\kappa^{01}(\varphi)$. At first, $W(\varphi)$ reads as:

$$\boxed{W(\varphi) = -e^{-2i\pi\varphi}\rho^{01}(\varphi)RU^{(1)} + e^{2i\pi\varphi}\kappa^{01}(\varphi)V^{(1)}} \tag{5.168}$$

Then, $\bar{W}(\varphi)$ has the following expression:

$$\boxed{\bar{W}(\varphi) = -U^{(0)T}R\rho^{01}(\varphi) - V^{(0)T}\bar{\kappa}^{01}(\varphi)} \tag{5.169}$$

Concerning $Z(\varphi)$, we've found:

$$\boxed{Z(\varphi) = e^{-2i\pi\varphi}\bar{\kappa}^{01}(\varphi)RU^{(1)} - e^{2i\pi\varphi}\rho^{01T}(\varphi)V^{(1)}} \tag{5.170}$$

To conclude, $\bar{Z}(\varphi)$ reads as follows:

$$\boxed{\bar{Z}(\varphi) = U^{(0)T}R\kappa^{01}(\varphi) + V^{(0)T}\rho^{01T}(\varphi)} \tag{5.171}$$

5.4.3 Projected expressions related to Y,T and S

Here, we express explicitly the following local quantities:

$$\boxed{Y_{j\bar{j}'}(\varphi) = \frac{\langle\Phi_0|\xi_{0,j}\bar{\xi}_{0,j'}|\Phi_1(\varphi)\rangle}{\langle\Phi_0|\Phi_1(\varphi)\rangle}} \qquad \boxed{T_{i\bar{i}'}(\varphi) = \frac{\langle\Phi_0|\xi^+_{1,i}(\varphi)\bar{\xi}^+_{1,i'}(\varphi)|\Phi_1(\varphi)\rangle}{\langle\Phi_0|\Phi_1(\varphi)\rangle}} \tag{5.172}$$

And:

$$\boxed{S_{ji}(\varphi) = \frac{\langle \Phi_0 | \xi_{0,j} \xi^+_{1,i}(\varphi) | \Phi_1(\varphi) \rangle}{\langle \Phi_0 | \Phi_1(\varphi) \rangle}} \tag{5.173}$$

The latter quantities are easily deduced from the matrices $W(\varphi)$, $\bar{W}(\varphi)$, $Z(\varphi)$ and $\bar{Z}(\varphi)$ derived previously. We find for $Y(\varphi)$:

$$\boxed{Y(\varphi) = \bar{Z}(\varphi) R^T U^{(0)} - \bar{W}(\varphi) V^{(0)}} \tag{5.174}$$

Concerning $T(\varphi)$, we write:

$$\boxed{T(\varphi) = e^{-2i\pi\varphi} U^{(1)T} R^T Z(\varphi) + e^{2i\pi\varphi} V^{(1)T} W(\varphi)} \tag{5.175}$$

Finally, the matrix $S(\varphi)$ reads as follows:

$$\boxed{S(\varphi) = e^{-2i\pi\varphi} \bar{W}(\varphi) U^{(1)} + e^{2i\pi\varphi} \bar{Z}(\varphi) V^{(1)}} \tag{5.176}$$

5.4.4 Projected 2-quasiparticle excited state overlaps

This part is dedicated to the projected 2-quasiparticle state overlaps. We start with the overlap $\tilde{\mathcal{O}}^{01}_{j0}$:

$$\boxed{\tilde{\mathcal{O}}^{01}_{j0} = \frac{\langle \Phi^{(j)}_0 | \tilde{\Phi}_1 \rangle}{\sqrt{\langle \Phi^{(j)}_0 | \tilde{\Phi}^{(j)}_0 \rangle \langle \Phi_1 | \tilde{\Phi}_1 \rangle}}} \tag{5.177}$$

The evaluation of Eq.(5.177) requires the evaluation of the two new quantities $\langle \Phi^{(j)}_{0\tau_j} | \tilde{\Phi}^{(j)}_{0\tau_j} \rangle$, and $\langle \Phi^{(j)}_{0\tau_j} | \tilde{\Phi}_{1\tau_j} \rangle$. We start with the excited norm $\langle \Phi^{(j)}_{0\tau_j} | \tilde{\Phi}^{(j)}_{0\tau_j} \rangle$:

$$\langle \Phi^{(j)}_{0\tau_j} | \tilde{\Phi}^{(j)}_{0\tau_j} \rangle = \frac{1}{n_{\varphi_{\tau_j}}} \sum_{\varphi_j} e^{2i\varphi_{\tau_j}\pi N} \langle \Phi_{0\tau_j} | \bar{\xi}_{0,j} \xi_{0,j} \xi^+_{0,j}(\varphi_{\tau_j}) \bar{\xi}^+_{0,j}(\varphi_{\tau_j}) | \Phi_{0\tau_j}(\varphi_{\tau_j}) \rangle \tag{5.178}$$

Using the Wick theorem in Eq.(5.178) leads to:

$$\boxed{\langle \Phi^{(j)}_{0\tau_j} | \tilde{\Phi}^{(j)}_{0\tau_j} \rangle = \frac{1}{n_{\varphi_{\tau_j}}} \sum_{\varphi_j} e^{2i\varphi_{\tau_j}\pi N} \langle \Phi_{0\tau_j} | \Phi_{\tau_j}(\varphi_{\tau_j}) \rangle [S^2_{jj}(\varphi_{\tau_j}) - Y_{j\bar{j}}(\varphi_{\tau_j}) T_{j\bar{j}}(\varphi_{\tau_j})]} \tag{5.179}$$

Then, we evaluate the overlap $\langle \Phi^{(j)}_{0\tau_j} | \tilde{\Phi}_{1\tau_j} \rangle$:

$$\boxed{\langle \Phi^{(j)}_{0\tau_j} | \tilde{\Phi}_{1\tau_j} \rangle = -\frac{1}{n_{\varphi_{\tau_j}}} \sum_{\varphi_j} e^{2i\varphi_{\tau_j}\pi N} \langle \Phi_{0\tau_j} | \Phi_{\tau_j}(\varphi_{\tau_j}) \rangle Y_{j\bar{j}}(\varphi_{\tau_j})} \tag{5.180}$$

Now, we consider the overlap $\tilde{\mathcal{O}}_{0i}^{01}$:

$$\boxed{\tilde{\mathcal{O}}_{0i}^{01} = \frac{\langle \Phi_0 | \tilde{\Phi}_1^{(i)} \rangle}{\sqrt{\langle \Phi_0 | \tilde{\Phi}_0 \rangle \langle \Phi_1^{(i)} | \tilde{\Phi}_1^{(i)} \rangle}}} \tag{5.181}$$

By analogy with the previous case, we directly give the expression of the excited norm $\langle \Phi_{1\tau_i}^{(i)} | \tilde{\Phi}_{1\tau_i}^{(i)} \rangle$:

$$\boxed{\langle \Phi_{1\tau_i}^{(i)} | \tilde{\Phi}_{1\tau_i}^{(i)} \rangle = \frac{1}{n_{\varphi_{\tau_i}}} \sum_{\varphi_i} e^{2i\varphi_{\tau_i}\pi N} \langle \Phi_{0\tau_i} | \Phi_{0\tau_i}(\varphi_{\tau_i}) \rangle [S_{ii}^2(\varphi_{\tau_i}) - Y_{i\bar{i}}(\varphi_{\tau_i}) T_{i\bar{i}} \varphi_{\tau_i})]} \tag{5.182}$$

Finally, we write the overlap $\langle \Phi_{\tau_i} | \tilde{\Phi}_{1\tau_i}^{(i)} \rangle$:

$$\boxed{\langle \Phi_{0\tau_i} | \tilde{\Phi}_{1\tau_i}^{(i)} \rangle = \frac{1}{n_{\varphi_{\tau_i}}} \sum_{\varphi_i} e^{2i\varphi_{\tau_i}\pi N} \langle \Phi_{0\tau_i} | \Phi_{0\tau_i}(\varphi_{\tau_i}) \rangle T_{i\bar{i}}(\varphi)} \tag{5.183}$$

To conclude, we consider the more complex excited overlap $\tilde{\mathcal{O}}_{ji}^{01}$:

$$\boxed{\tilde{\mathcal{O}}_{ji}^{01} = \frac{\langle \Phi_0^{(j)} | \tilde{\Phi}_1^{(i)} \rangle}{\sqrt{\langle \Phi_0^{(j)} | \tilde{\Phi}_0^{(j)} \rangle \langle \Phi_1^{(i)} | \tilde{\Phi}_1^{(i)} \rangle}}} \tag{5.184}$$

The only new quantity that appears in Eq.(5.184) is the overlap $\langle \Phi_{0\tau_j}^{(j)} | \tilde{\Phi}_{1\tau_i}^{(i)} \rangle$, when $\underline{\tau_j = \tau_i}$. It reads as follows:

$$\boxed{\langle \Phi_{0\tau_i}^{(j)} | \tilde{\Phi}_{1\tau_i}^{(i)} \rangle = \frac{1}{n_{\varphi_{\tau_i}}} \sum_{\varphi_i} e^{2i\varphi_{\tau_i}\pi N} \langle \Phi_{0\tau_i} | \Phi_{0\tau_i}(\varphi_{\tau_i}) \rangle [S_{ji}^2(\varphi_{\tau_i}) - Y_{j\bar{j}}(\varphi_{\tau_i}) T_{i\bar{i}}(\varphi_{\tau_i})]} \tag{5.185}$$

5.4.5 Projected excited transition densities

In this section, we give the expressions of the projected excited transition densities used in the density-dependent term of the interaction when projected 2-quasiparticle excited states are considered. When the states $|\Phi_0^{(j)}\rangle$ and $|\Phi_1\rangle$ are considered, the related projected excited transition density $\tilde{\rho}^{(j0)}$ reads as follows:

$$\boxed{\tilde{\rho}_{\alpha\beta}^{01(j0)} = \sqrt{\frac{\langle \Phi_{0\tau_j} | \tilde{\Phi}_{0\tau_j} \rangle}{\langle \Phi_{0\tau_j}^{(j)} | \tilde{\Phi}_{0\tau_j}^{(j)} \rangle}} \frac{\langle \Phi_0^{(j)} | c_{0,\beta}^+ c_{1,\alpha} | \tilde{\Phi}_1 \rangle}{\langle \Phi_0 | \tilde{\Phi}_1 \rangle}} \tag{5.186}$$

We first assume that $\underline{\tau \neq \tau_j}$, in this case, we find:

$$\boxed{\tilde{\rho}_{\alpha\beta}^{01(j0)\tau} = \frac{\tilde{\mathcal{O}}_{j0}^{01\tau_j}}{\tilde{\mathcal{O}}_{00}^{01\tau_j}} \tilde{\rho}_{\alpha\beta}^{01\tau}} \tag{5.187}$$

Then, we consider that $\underline{\tau = \tau_j}$. In this case, we obtain:

$$\boxed{\tilde{\rho}_{\alpha\beta}^{01(j0)\tau_j} = \frac{1}{\tilde{\mathcal{O}}_{00}^{01\tau_j}\sqrt{\langle\Phi_{1\tau_j}|\tilde{\Phi}_{1\tau_j}\rangle\langle\Phi_{0\tau_j}^{(j)}|\tilde{\Phi}_{0\tau_j}^{(j)}\rangle}}\sum_{\varphi_{\tau_j}}\frac{e^{2i\varphi_{\tau_j}\pi N_{\tau_j}}}{n_{\varphi_{\tau_j}}}\langle\Phi_{0\tau_j}|\Phi_{1\tau_j}(\varphi_{\tau_j})\rangle \\ [-Y_{j\bar{j}}(\varphi_{\tau_j})\rho_{\alpha\beta}^{01}(\varphi_{\tau_j}) - \bar{Z}_{j\bar{\alpha}}(\varphi_{\tau_j})\bar{W}_{j\beta}(\varphi_{\tau_j})]} \tag{5.188}$$

When it comes to the states $|\Phi_0\rangle$ and $|\Phi_1^{(i)}\rangle$, the related projected excited transition density $\tilde{\rho}^{(0i)}$ has the following form:

$$\boxed{\tilde{\rho}_{\alpha\beta}^{01(0i)} = \sqrt{\frac{\langle\Phi_{1\tau_i}|\tilde{\Phi}_{1\tau_i}\rangle}{\langle\Phi_{1\tau_i}^{(i)}|\tilde{\Phi}_{1\tau_i}^{(i)}\rangle}}\frac{\langle\Phi_0|c_{0,\beta}^{+}c_{1,\alpha}|\tilde{\Phi}_1\rangle}{\langle\Phi_0|\tilde{\Phi}_1^{(i)}\rangle}} \tag{5.189}$$

At first, we assume that $\underline{\tau \neq \tau_i}$, in this case, we find:

$$\boxed{\tilde{\rho}_{\alpha\beta}^{01(0i)\tau} = \frac{\tilde{\mathcal{O}}_{0i}^{01\tau_i}}{\tilde{\mathcal{O}}_{00}^{01\tau_i}}\tilde{\rho}_{\alpha\beta}^{01\tau}} \tag{5.190}$$

Then, $\underline{\text{if } \tau = \tau_i}$, we write:

$$\boxed{\tilde{\rho}_{\alpha\beta}^{01(0i)\tau_i} = \frac{1}{\tilde{\mathcal{O}}_{00}^{01\tau_i}\sqrt{\langle\Phi_{0\tau_i}|\tilde{\Phi}_{0\tau_i}\rangle\langle\Phi_{1\tau_i}^{(i)}|\tilde{\Phi}_{1\tau_i}^{(i)}\rangle}}\sum_{\varphi_{\tau_i}}\frac{e^{2i\varphi_{\tau_i}\pi N_{\tau_i}}}{n_{\varphi_{\tau_i}}}\langle\Phi_{0\tau_i}|\Phi_{1\tau_i}(\varphi_{\tau_i})\rangle \\ [\rho_{\alpha\beta}^{01}(\varphi_{\tau_i})T_{i\bar{i}}(\varphi_{\tau_i}) + W_{\alpha i}(\varphi_{\tau_i})Z_{\beta\bar{i}}(\varphi_{\tau_i})]} \tag{5.191}$$

Finally, when it comes to the states $|\Phi_0^{(j)}\rangle$ and $|\Phi_1^{(i)}\rangle$, the related projected excited transition density $\tilde{\rho}^{(ji)}$ reads as:

$$\boxed{\tilde{\rho}_{\alpha\beta}^{01(ji)} = \sqrt{\frac{\langle\Phi_{1\tau_i}|\tilde{\Phi}_{1\tau_i}\rangle\langle\Phi_{0\tau_j}|\tilde{\Phi}_{0\tau_j}\rangle}{\langle\Phi_{1\tau_i}^{(i)}|\tilde{\Phi}_{1\tau_i}^{(i)}\rangle\langle\Phi_{0\tau_j}^{(j)}|\tilde{\Phi}_{0\tau_j}^{(j)}\rangle}}\frac{\langle\Phi_0^{(j)}|c_{0,\alpha}^{+}c_{1,\beta}|\tilde{\Phi}_1^{(i)}\rangle}{\langle\Phi_0|\tilde{\Phi}_1\rangle}} \tag{5.192}$$

First, we assume that $\underline{\tau_i \neq \tau_j \text{ and } \tau = \tau_j}$. In this case, we find:

$$\boxed{\tilde{\rho}_{\alpha\beta}^{01(ji)\tau_j} = \frac{\tilde{\mathcal{O}}_{0i}^{01\tau_i}}{\tilde{\mathcal{O}}_{00}^{01\tau_i}}\tilde{\rho}_{\alpha\beta}^{01(j0)}} \tag{5.193}$$

Then, we suppose that $\underline{\tau_i \neq \tau_j \text{ and } \tau = \tau_i}$. In this case, we obtain:

$$\boxed{\tilde{\rho}_{\alpha\beta}^{01(ji)\tau_i} = \frac{\tilde{\mathcal{O}}_{j0}^{01\tau_j}}{\tilde{\mathcal{O}}_{00}^{01\tau_j}}\tilde{\rho}_{\alpha\beta}^{01(0i)}} \tag{5.194}$$

Now, we consider the case with $\underline{\tau_i = \tau_j \text{ and } \tau \neq \tau_i}$. We find:

$$\boxed{\begin{aligned}\tilde{\rho}^{01(ji)\tau}_{\alpha\beta} = \tilde{\rho}^{01\tau}_{\alpha\beta} \frac{1}{\tilde{\mathcal{O}}^{01\tau_i}_{00} \sqrt{\langle \Phi^{(i)}_{1\tau_i} | \tilde{\Phi}^{(i)}_{1\tau_i} \rangle \langle \Phi^{(j)}_{0\tau_j} | \tilde{\Phi}^{(j)}_{0\tau_j} \rangle}} \sum_{\varphi_{\tau_i}} \frac{e^{2i\varphi_{\tau_i}\pi N_{\tau_i}}}{n_{\varphi_{\tau_i}}} \langle \Phi_{0\tau_i} | \Phi_{1\tau_i}(\varphi_{\tau_i}) \rangle \\ [-Y_{j\bar{j}}(\varphi_{\tau_i}) T_{i\bar{i}}(\varphi_{\tau_i}) + S^2_{ji}(\varphi_{\tau_i})]\end{aligned}} \tag{5.195}$$

Finally, when $\underline{\tau_i = \tau_j \text{ and } \tau = \tau_i}$. We write:

$$\boxed{\begin{aligned}\tilde{\rho}^{01(ji)\tau}_{\alpha\beta} = \frac{1}{\tilde{\mathcal{O}}^{01\tau_i}_{00} \sqrt{\langle \Phi^{(i)}_{1\tau_i} | \tilde{\Phi}^{(i)}_{1\tau_i} \rangle \langle \Phi^{(j)}_{0\tau_j} | \tilde{\Phi}^{(j)}_{0\tau_j} \rangle}} \sum_{\varphi_\tau} \frac{e^{2i\varphi_\tau \pi N_\tau}}{n_{\varphi_\tau}} \langle \Phi_{0\tau} | \Phi_{1\tau}(\varphi_\tau) \rangle \\ [-Y_{j\bar{j}}(\varphi_\tau)[\rho^{01\tau}_{\alpha\beta}(\varphi_\tau) T_{i\bar{i}}(\varphi_\tau) + W_{\alpha i}(\varphi_\tau) Z_{\beta\bar{i}}(\varphi_\tau)] \\ -\bar{Z}_{j\bar{\alpha}}(\varphi_\tau)[\bar{W}_{j\beta}(\varphi_\tau) T_{i\bar{i}}(\varphi_\tau) - S_{ji}(\varphi_\tau) Z_{\beta\bar{i}}(\varphi_\tau)] \\ +S_{ji}(\varphi_\tau)[\bar{W}_{j\beta}(\varphi_\tau) W_{\alpha i}(\varphi_\tau) + S_{ji}(\varphi_\tau) \rho^{01\tau}_{\alpha\beta}(\varphi_\tau)]]\end{aligned}} \tag{5.196}$$

5.4.6 POF contractions

In this section, we present the contractions relevant for the POF method (see Chapter 4). We start with the quantity $\mathring{\rho}(\varphi^{(l)}, \varphi^{(r)})$:

$$\boxed{\mathring{\rho}_{km}(\varphi^{(l)}, \varphi^{(r)}) = \frac{\langle \Phi | a^+_m a_k | \Phi(\varphi^{(l)}, \varphi^{(r)}) \rangle}{\langle \Phi | \Phi(\varphi^{(l)}, \varphi^{(r)}) \rangle}} \tag{5.197}$$

We explicitly write $\langle \Phi | a^+_m a_k | \Phi(\varphi^{(l)}, \varphi^{(r)}) \rangle$:

$$\begin{aligned}\langle \Phi | a^+_m a_k | \Phi(\varphi^{(l)}, \varphi^{(r)}) \rangle = \langle 0 | \prod_{j>0} (u_j + \bar{a}_j a_j) a^+_m a_k \prod_{i_l > 0} (u_{i_l} + v_{i_l} e^{-4i\pi\varphi^{(l)}} a^+_{i_l} \bar{a}^+_{i_l}) \\ \prod_{i_r > 0} (u_{i_r} + v_{i_r} e^{-4i\pi\varphi^{(r)}} a^+_{i_r} \bar{a}^+_{i_r}) | 0 \rangle\end{aligned} \tag{5.198}$$

Looking at Eq.(5.198), it is clear that the following property holds:

$$\langle \Phi | a^+_m a_k | \Phi(\varphi^{(l)}, \varphi^{(r)}) \rangle = \delta_{km} \langle \Phi | \Phi(\varphi^{(l)}, \varphi^{(r)}) \rangle \frac{v^2_k e^{-4i\pi(\delta_{k\in\{l\}}\varphi^{(l)} + \delta_{k\in\{r\}}\varphi^{(r)})}}{u^2_k + v^2_k e^{-4i\pi(\delta_{k\in\{l\}}\varphi^{(l)} + \delta_{k\in\{r\}}\varphi^{(r)})}} \tag{5.199}$$

Therefore, $\mathring{\rho}(\varphi^{(l)}, \varphi^{(r)})$ simply reads as:

$$\boxed{\mathring{\rho}_{km}(\varphi^{(l)}, \varphi^{(r)}) = \delta_{km} \frac{v^2_k e^{-4i\pi(\delta_{k\in\{l\}}\varphi^{(l)} + \delta_{k\in\{r\}}\varphi^{(r)})}}{u^2_k + v^2_k e^{-4i\pi(\delta_{k\in\{l\}}\varphi^{(l)} + \delta_{k\in\{r\}}\varphi^{(r)})}}} \tag{5.200}$$

Now, we consider the quantity $\mathring{\kappa}(\varphi^{(l)}, \varphi^{(r)})$, defined as follows:

$$\boxed{\mathring{\kappa}_{km}(\varphi^{(l)},\varphi^{(r)}) = \frac{\langle\Phi|a_m\bar{a}_k|\Phi(\varphi^{(l)},\varphi^{(r)})\rangle}{\langle\Phi|\Phi(\varphi^{(l)},\varphi^{(r)})\rangle}} \tag{5.201}$$

By analogy, we directly find:

$$\boxed{\mathring{\kappa}_{km}(\varphi^{(l)},\varphi^{(r)}) = \delta_{km}\frac{v_k u_k}{v_k^2 + u_k^2 e^{4i\pi(\delta_{k\in\{l\}}\varphi^{(l)}+\delta_{k\in\{r\}}\varphi^{(r)})}}} \tag{5.202}$$

Then, we search for the quantity $\mathring{\bar{\kappa}}(\varphi^{(l)},\varphi^{(r)})$:

$$\boxed{\mathring{\bar{\kappa}}_{km}(\varphi^{(l)},\varphi^{(r)}) = \frac{\langle\Phi|a_m^+\bar{a}_k^+|\Phi(\varphi^{(l)},\varphi^{(r)})\rangle}{\langle\Phi|\Phi(\varphi^{(l)},\varphi^{(r)})\rangle}} \tag{5.203}$$

By analogy, we easily write:

$$\boxed{\mathring{\bar{\kappa}}_{km}(\varphi^{(l)},\varphi^{(r)}) = -\delta_{km}\frac{v_k u_k}{u_k^2 + v_k^2 e^{-4i\pi(\delta_{k\in\{l\}}\varphi^{(l)}+\delta_{k\in\{r\}}\varphi^{(r)})}}} \tag{5.204}$$

Finally, we study the total POF density matrix $\mathring{\tilde{\rho}}$:

$$\boxed{\mathring{\tilde{\rho}}_{km} = \frac{\langle\Phi|a_m^+ a_k|\mathring{\Phi}\rangle}{\langle\Phi|\mathring{\Phi}\rangle}} \tag{5.205}$$

We rewrite $\mathring{\tilde{\rho}}$ more explicitly:

$$\mathring{\tilde{\rho}}_{km}^{\tau} = \frac{\delta_{km}}{\langle\Phi_\tau|\mathring{\Phi}_\tau\rangle}\sum_{\varphi_\tau^{(l)}}\sum_{\varphi_\tau^{(r)}}\frac{e^{2i\pi\varphi_\tau^{(l)}N_\tau^{(l)}}e^{2i\pi\varphi_\tau^{(r)}N_\tau^{(r)}}}{n_{\varphi_\tau}^{(l)}n_{\varphi_\tau}^{(r)}}\mathcal{O}^{(l)}(\varphi_\tau^{(l)})\mathcal{O}^{(r)}(\varphi_\tau^{(r)})\mathring{\rho}_{kk}^{\tau}(\varphi_\tau^{(l)},\varphi_\tau^{(r)}) \tag{5.206}$$

If we assume that $\underline{k\in\{l\}}$, we obtain:

$$\boxed{\mathring{\tilde{\rho}}_{km}^{(l)\tau} = \frac{\delta_{km}}{\langle\Phi_\tau^{(l)}|\mathring{\Phi}_\tau^{(l)}\rangle}\sum_{\varphi_\tau^{(l)}}\frac{e^{2i\pi\varphi_\tau^{(l)}N_\tau^{(l)}}}{n_{\varphi_\tau}^{(l)}}\mathcal{O}^{(l)}(\varphi_\tau^{(l)})\frac{v_k^2 e^{-4i\pi\varphi^{(l)}}}{u_k^2 + v_k^2 e^{-4i\pi\varphi^{(l)}}}} \tag{5.207}$$

On the other hand, $\underline{\text{if } k\in\{r\}}$, we have:

$$\boxed{\mathring{\tilde{\rho}}_{km}^{(r)\tau} = \frac{\delta_{km}}{\langle\Phi_\tau^{(r)}|\mathring{\Phi}_\tau^{(r)}\rangle}\sum_{\varphi_\tau^{(r)}}\frac{e^{2i\pi\varphi_\tau^{(r)}N_\tau^{(l)}}}{n_{\varphi_\tau}^{(r)}}\mathcal{O}^{(r)}(\varphi_\tau^{(r)})\frac{v_k^2 e^{-4i\pi\varphi^{(r)}}}{u_k^2 + v_k^2 e^{-4i\pi\varphi^{(r)}}}} \tag{5.208}$$

5.5 Hamiltonian kernels

This section is dedicated to the evaluation of Hamiltonian kernels between HFB states and 2-quasiparticle excited states. As they are HFB states, these expressions are also valid for the variational excited states created with the "Continuous Deflation" method introduced in Chapter 3.

5.5.1 HFB states off-diagonal kernels

In this section, we derive the expression of the Hamiltonian kernel between two different HFB states $|\Phi_0\rangle$ and $|\Phi_1\rangle$. We start by defining the Hamiltonian $\hat{H}^{01}$:

$$\boxed{\hat{H}^{01} = \sum_{\alpha\beta} t_{\alpha\beta} c^+_{0,\alpha} c_{1,\beta} + \frac{1}{4} \sum_{\alpha\beta\gamma\delta} v^{(a)}_{\alpha\beta\gamma\delta} c^+_{0,\alpha} c^+_{0,\beta} c_{1,\delta} c_{1,\gamma}} \tag{5.209}$$

In Eq.(5.209), the indices 0 and 1 stand for the two possibly different harmonic-oscillator bases related to the HFB states $|\Phi_0\rangle$ and $|\Phi_1\rangle$. We call E^{01}_{00} the Hamiltonian kernel associated with $\hat{H}^{01}$, $|\Phi_0\rangle$ and $|\Phi_1\rangle$. It reads:

$$E^{01}_{00} = \langle\Phi_0|\hat{H}^{01}|\Phi_1\rangle = \langle\Phi_0| \sum_{\alpha\beta} t_{\alpha\beta} c^+_{0,\alpha} c_{1,\beta} |\Phi_1\rangle + \langle\Phi_0| \frac{1}{4} \sum_{\alpha\beta\gamma\delta} v^{(a)}_{\alpha\beta\gamma\delta} c^+_{0,\alpha} c^+_{0,\beta} c_{1,\delta} c_{1,\gamma} |\Phi_1\rangle \tag{5.210}$$

The kinetic part of the kernel E^{01}_{00} is noted $E^{01}_{00}(t)$ and its two-body part is noted $E^{01}_{00}(v)$. With these notations, Eq.(5.210) reads:

$$\boxed{E^{01}_{00} = E^{01}_{00}(t) + E^{01}_{00}(v)} \tag{5.211}$$

Kinetic part:

The kinetic part of the Hamiltonian kernel is written as:

$$E^{01}_{00}(t) = \sum_{\alpha\beta} t_{\alpha\beta} \langle\Phi_0| c^+_{0,\alpha} c_{1,\beta} |\Phi_1\rangle = \langle\Phi_0|\Phi_1\rangle \sum_{\alpha\beta} t_{\alpha\beta} \rho^{01}_{\beta\alpha} \tag{5.212}$$

We use the time-reversal properties of the transition density matrix $\rho^{01}_{\beta\alpha}$ (see Appendix O) in Eq.(5.212):

$$E^{01}_{00}(t) = 2\langle\Phi_0|\Phi_1\rangle \sum_{\alpha\beta>} t_{\alpha\beta} (-1)^{s_\alpha - s_\beta} \rho^{01}_{\beta\alpha} \tag{5.213}$$

As the $t_{\alpha\beta}$ imposes $s_\alpha = s_\beta$, this part of the Hamiltonian kernel finally reads:

$$\boxed{E^{01}_{00}(t) = 2\langle\Phi_0|\Phi_1\rangle \sum_{\alpha\beta>} t_{\alpha\beta} \rho^{01}_{\beta\alpha}} \tag{5.214}$$

The expression given in Eq.(5.214) stands for the kinetic contribution to the collective mean-field. Its detailed expression is given in Appendix K. To conclude, it is easy to show that the following relation holds:

$$\boxed{E_{00}^{01}(t) = E_{00}^{10}(t)} \tag{5.215}$$

Two-body part:

The two-body part of the Hamiltonian kernel reads as:

$$E_{00}^{01}(v) = \frac{1}{4}\sum_{\alpha\beta\gamma\delta} v_{\alpha\beta\gamma\delta}^{(a)} \langle \Phi_0 | c_{0,\alpha}^{+} c_{0,\beta}^{+} c_{1,\delta} c_{1,\gamma} | \Phi_1 \rangle \tag{5.216}$$

We start by using the generalized Wick theorem:

$$\begin{aligned} E_{00}^{01}(v) = \frac{1}{4}\langle \Phi_0 | \Phi_1 \rangle \sum_{\alpha\beta\gamma\delta} v_{\alpha\beta\gamma\delta}^{(a)} [& \frac{\langle \Phi_0 | c_{0,\alpha}^{+} c_{0,\beta}^{+} | \Phi_1 \rangle}{\langle \Phi_0 | \Phi_1 \rangle} \frac{\langle \Phi_0 | c_{1,\delta} c_{1,\gamma} | \Phi_1 \rangle}{\langle \Phi_0 | \Phi_1 \rangle} \\ + \frac{\langle \Phi_0 | c_{0,\alpha}^{+} c_{1,\gamma} | \Phi_1 \rangle}{\langle \Phi_0 | \Phi_1 \rangle} \frac{\langle \Phi_0 | c_{0,\beta}^{+} c_{1,\delta} | \Phi_1 \rangle}{\langle \Phi_0 | \Phi_1 \rangle} & - \frac{\langle \Phi_0 | c_{0,\alpha}^{+} c_{1,\delta} | \Phi_1 \rangle}{\langle \Phi_0 | \Phi_1 \rangle} \frac{\langle \Phi_0 | c_{0,\beta}^{+} c_{1,\gamma} | \Phi_1 \rangle}{\langle \Phi_0 | \Phi_1 \rangle}] \end{aligned} \tag{5.217}$$

As the interaction matrix elements have been antisymmetrized, the index exchange $\gamma \leftrightarrow \delta$ only changes the sign of the expressions. Using this exchange property in Eq.(5.217) leads to:

$$\begin{aligned} E_{00}^{01}(v) = & \frac{\langle \Phi_0 | \Phi_1 \rangle}{4} \sum_{\alpha\beta\gamma\delta} v_{\alpha\beta\gamma\delta}^{(a)} \frac{\langle \Phi_0 | c_{0,\alpha}^{+} c_{0,\beta}^{+} | \Phi_1 \rangle}{\langle \Phi_0 | \Phi_1 \rangle} \frac{\langle \Phi_0 | c_{1,\delta} c_{1,\gamma} | \Phi_1 \rangle}{\langle \Phi_0 | \Phi_1 \rangle} \\ & + \frac{\langle \Phi_0 | \Phi_1 \rangle}{2} \sum_{\alpha\beta\gamma\delta} v_{\alpha\beta\gamma\delta}^{(a)} \frac{\langle \Phi_0 | c_{0,\alpha}^{+} c_{1,\gamma} | \Phi_1 \rangle}{\langle \Phi_0 | \Phi_1 \rangle} \frac{\langle \Phi_0 | c_{0,\beta}^{+} c_{1,\delta} | \Phi_1 \rangle}{\langle \Phi_0 | \Phi_1 \rangle} \end{aligned} \tag{5.218}$$

Now, we can define the collective fields $\bar{\Gamma}$ and $\bar{\Delta}$:

$$\boxed{\bar{\Gamma}_{\alpha\gamma} = \sum_{\beta\delta} v_{\alpha\beta\gamma\delta}^{(a)} \rho_{\delta\beta}^{01}} \qquad \boxed{\bar{\Delta}_{\alpha\beta} = \frac{1}{2}\sum_{\gamma\delta} (-1)^{s_\beta - s_\delta} v_{\alpha\beta\gamma\delta}^{(a)} \kappa_{\gamma\bar{\delta}}^{01}} \tag{5.219}$$

With the collective fields $\bar{\Gamma}$ and $\bar{\Delta}$, Eq.(5.218) reads:

$$E_{00}^{01}(v) = \frac{\langle \Phi_0 | \Phi_1 \rangle}{2} [\sum_{\alpha\gamma} \bar{\Gamma}_{\alpha\gamma} \rho_{\gamma\alpha}^{01} - \sum_{\alpha\beta} \bar{\Delta}_{\alpha\beta} \bar{\kappa}_{\alpha\bar{\beta}}^{01}] \tag{5.220}$$

Finally, we can use the time-reversal properties of the collective fields along with those of the matrices ρ^{01} and $\bar{\kappa}^{01}$ to write:

$$\boxed{E_{00}^{01}(v) = \langle \Phi_0 | \Phi_1 \rangle [\sum_{\alpha\gamma >} \bar{\Gamma}_{\alpha\gamma} \rho_{\gamma\alpha}^{01} - \sum_{\alpha\beta >} \bar{\Delta}_{\alpha\bar{\beta}} \bar{\kappa}_{\alpha\bar{\beta}}^{01}]} \tag{5.221}$$

The detailed expressions of all the collective mean and pairing fields are given in Appendices E-J. To conclude, it is easy to show that the following relation holds:

$$\boxed{E^{01}_{00}(v) = E^{10}_{00}(v)} \tag{5.222}$$

5.5.2 2-quasiparticle excited state off-diagonal kernels

This section is dedicated to the derivation of the expressions of the Hamiltonian kernels involving 2-quasiparticle excited states. In the following, we derive the expressions of the three different kernels E^{01}_{0i}, E^{01}_{j0} and E^{01}_{ji} defined as follows:

$$\boxed{E^{01}_{0i} = \sum_{\alpha\beta} t_{\alpha\beta} \langle \Phi_0 | c^+_{0,\alpha} c_{1,\beta} \xi^+_{1,i} \bar{\xi}^+_{1,i} | \Phi_1 \rangle + \frac{1}{4} \sum_{\alpha\beta\gamma\delta} v^{(a)}_{\alpha\beta\gamma\delta} \langle \Phi_0 | c^+_{0,\alpha} c^+_{0,\beta} c_{1,\delta} c_{1,\gamma} \xi^+_{1,i} \bar{\xi}^+_{1,i} | \Phi_1 \rangle} \tag{5.223}$$

$$\boxed{E^{01}_{j0} = \sum_{\alpha\beta} t_{\alpha\beta} \langle \Phi_0 | \bar{\xi}_{0,j} \xi_{0,j} c^+_{0,\alpha} c_{1,\beta} | \Phi_1 \rangle + \frac{1}{4} \sum_{\alpha\beta\gamma\delta} v^{(a)}_{\alpha\beta\gamma\delta} \langle \Phi_0 | \bar{\xi}_{0,j} \xi_{0,j} c^+_{0,\alpha} c^+_{0,\beta} c_{1,\delta} c_{1,\gamma} | \Phi_1 \rangle} \tag{5.224}$$

$$\boxed{\begin{aligned} E^{01}_{ji} &= \sum_{\alpha\beta} t_{\alpha\beta} \langle \Phi_0 | \bar{\xi}_{0,j} \xi_{0,j} c^+_{0,\alpha} c_{1,\beta} \xi^+_{1,i} \bar{\xi}^+_{1,i} | \Phi_1 \rangle \\ &+ \frac{1}{4} \sum_{\alpha\beta\gamma\delta} v^{(a)}_{\alpha\beta\gamma\delta} \langle \Phi_0 | \bar{\xi}_{0,j} \xi_{0,j} c^+_{0,\alpha} c^+_{0,\beta} c_{1,\delta} c_{1,\gamma} \xi^+_{1,i} \bar{\xi}^+_{1,i} | \Phi_1 \rangle \end{aligned}} \tag{5.225}$$

All these three kernels can be separated into a kinetic and a two-body parts:

$$\boxed{E^{01}_{0i} = E^{01}_{0i}(t) + E^{01}_{0i}(v)} \tag{5.226}$$

$$\boxed{E^{01}_{j0} = E^{01}_{j0}(t) + E^{01}_{j0}(v)} \tag{5.227}$$

$$\boxed{E^{01}_{ji} = E^{01}_{ji}(t) + E^{01}_{ji}(v)} \tag{5.228}$$

Kinetic part $E^{01}_{0i}(t)$:

We consider here the following kernel:

$$E^{01}_{0i}(t) = \sum_{\alpha\beta} t_{\alpha\beta} \langle \Phi_0 | c^+_{0,\alpha} c_{1,\beta} \xi^+_{1,i} \bar{\xi}^+_{1,i} | \Phi_1 \rangle \tag{5.229}$$

First, we notice the following time-reversal property:

$$\langle \Phi_0 | c^+_{0,\bar{\alpha}} c_{1,\bar{\beta}} \xi^+_{1,i} \bar{\xi}^+_{1,i} | \Phi_1 \rangle = (-1)^{s_\alpha - s_\beta} \langle \Phi_0 | c^+_{0,\alpha} c_{1,\beta} \xi^+_{1,i} \bar{\xi}^+_{1,i} | \Phi_1 \rangle \tag{5.230}$$

Eq.(5.229) is rewritten thanks to this time-reversal property:

$$E_{0i}^{01}(t) = 2\sum_{\alpha\beta>} t_{\alpha\beta}\langle\Phi_0|c_{0,\alpha}^{+}c_{1,\beta}\xi_{1,i}^{+}\bar{\xi}_{1,i}^{+}|\Phi_1\rangle \tag{5.231}$$

We use the generalized Wick theorem in Eq.(5.231):

$$\begin{aligned} E_{0i}^{01}(t) = 2\langle\Phi_0|\Phi_1\rangle\sum_{\alpha\beta>} t_{\alpha\beta}[&\frac{\langle\Phi_0|c_{0,\alpha}^{+}c_{1,\beta}|\Phi_1\rangle}{\langle\Phi_0|\Phi_1\rangle}\frac{\langle\Phi_0|\xi_{1,i}^{+}\bar{\xi}_{1,i}^{+}|\Phi_1\rangle}{\langle\Phi_0|\Phi_1\rangle} \\ &+\frac{\langle\Phi_0|c_{0,\alpha}^{+}\bar{\xi}_{1,i}^{+}|\Phi_1\rangle}{\langle\Phi_0|\Phi_1\rangle}\frac{\langle\Phi_0|c_{1,\beta}\xi_{1,i}^{+}|\Phi_1\rangle}{\langle\Phi_0|\Phi_1\rangle}] \end{aligned} \tag{5.232}$$

Using the matrices T, Z, W and ρ^{01}, the kernel finally reads as:

$$\boxed{E_{0i}^{01}(t) = 2\langle\Phi_0|\Phi_1\rangle[T_{i\bar{i}}\sum_{\alpha\beta>} t_{\alpha\beta}\rho_{\beta\alpha}^{01} + \sum_{\alpha\beta>} t_{\alpha\beta}Z_{\alpha\bar{i}}W_{\beta i}]} \tag{5.233}$$

Kinetic part $E_{j0}^{01}(t)$:

Here, we consider the following kernel:

$$E_{j0}^{01}(t) = \sum_{\alpha\beta} t_{\alpha\beta}\langle\Phi_0|\bar{\xi}_{0,j}\xi_{0,j}c_{0,\alpha}^{+}c_{1,\beta}|\Phi_1\rangle \tag{5.234}$$

We start using the time-reversal properties of the kernel:

$$E_{j0}^{01}(t) = 2\sum_{\alpha\beta>} t_{\alpha\beta}\langle\Phi_0|\bar{\xi}_{0,j}\xi_{0,j}c_{0,\alpha}^{+}c_{1,\beta}|\Phi_1\rangle \tag{5.235}$$

We use the generalized Wick theorem in Eq.(5.235):

$$\begin{aligned} E_{j0}^{01}(t) = 2\langle\Phi_0|\Phi_1\rangle\sum_{\alpha\beta>} t_{\alpha\beta}[&\frac{\langle\Phi_0|\bar{\xi}_{0,j}\xi_{0,j}|\Phi_1\rangle}{\langle\Phi_0|\Phi_1\rangle}\frac{\langle\Phi_0|c_{0,\alpha}^{+}c_{1,\beta}|\Phi_1\rangle}{\langle\Phi_0|\Phi_1\rangle} \\ &+\frac{\langle\Phi_0|\bar{\xi}_{0,j}c_{1,\beta}|\Phi_1\rangle}{\langle\Phi_0|\Phi_1\rangle}\frac{\langle\Phi_0|\xi_{0,j}c_{0,\alpha}^{+}|\Phi_1\rangle}{\langle\Phi_0|\Phi_1\rangle}] \end{aligned} \tag{5.236}$$

Using the matrices Y, $\bar{Z}$, $\bar{W}$ and ρ^{01}, the kernel finally reads as:

$$\boxed{E_{j0}^{01}(t) = -2\langle\Phi_0|\Phi_1\rangle[Y_{j\bar{j}}\sum_{\alpha\beta>} t_{\alpha\beta}\rho_{\beta\alpha}^{01} + \sum_{\alpha\beta>} t_{\alpha\beta}\bar{W}_{j\alpha}\bar{Z}_{j\bar{\beta}}]} \tag{5.237}$$

To conclude, it is clear that the following expression holds:

$$\boxed{E_{0i}^{01}(t) = E_{i0}^{10}(t)} \tag{5.238}$$

Kinetic part $E_{ji}^{01}(t)$:

Here, we consider the following kernel:

$$E_{ji}^{01}(t) = \sum_{\alpha\beta} t_{\alpha\beta} \langle \Phi_0 | \bar{\xi}_{0,j} \xi_{0,j} c_{0,\alpha}^{+} c_{1,\beta} \xi_{1,i}^{+} \bar{\xi}_{1,i}^{+} | \Phi_1 \rangle \tag{5.239}$$

We use the time-reversal properties of Eq.(5.239) to simplify it:

$$E_{ji}^{01}(t) = 2 \sum_{\alpha\beta>} t_{\alpha\beta} \langle \Phi_0 | \xi_{0,\bar{j}} \xi_{0,j} c_{0,\alpha}^{+} c_{1,\beta} \xi_{1,i}^{+} \bar{\xi}_{1,i}^{+} | \Phi_1 \rangle \tag{5.240}$$

Using the generalized Wick theorem in Eq.(5.240) leads to:

$$\begin{aligned} E_{ji}^{01}(t) = 2\langle \Phi_0 | \Phi_1 \rangle \sum_{\alpha\beta>} t_{\alpha\beta} [& \frac{\langle \Phi_0 | \bar{\xi}_{0,j} \xi_{0,j} | \Phi_1 \rangle}{\langle \Phi_0 | \Phi_1 \rangle} \Big(\frac{\langle \Phi_0 | c_{0,\alpha}^{+} c_{1,\beta} | \Phi_1 \rangle}{\langle \Phi_0 | \Phi_1 \rangle} \frac{\langle \Phi_0 | \xi_{1,i}^{+} \bar{\xi}_{1,i}^{+} | \Phi_1 \rangle}{\langle \Phi_0 | \Phi_1 \rangle} \\ & + \frac{\langle \Phi_0 | c_{0,\alpha}^{+} \bar{\xi}_{1,i}^{+} | \Phi_1 \rangle}{\langle \Phi_0 | \Phi_1 \rangle} \frac{\langle \Phi_0 | c_{1,\beta} \xi_{1,i}^{+} | \Phi_1 \rangle}{\langle \Phi_0 | \Phi_1 \rangle} \Big) \\ & + \frac{\langle \Phi_0 | \bar{\xi}_{0,j} c_{1,\beta} | \Phi_1 \rangle}{\langle \Phi_0 | \Phi_1 \rangle} \Big(\frac{\langle \Phi_0 | \xi_{0,j} c_{0,\alpha}^{+} | \Phi_1 \rangle}{\langle \Phi_0 | \Phi_1 \rangle} \frac{\langle \Phi_0 | \xi_{1,i}^{+} \bar{\xi}_{1,i}^{+} | \Phi_1 \rangle}{\langle \Phi_0 | \Phi_1 \rangle} - \frac{\langle \Phi_0 | \xi_{0,j} \xi_{1,i}^{+} | \Phi_1 \rangle}{\langle \Phi_0 | \Phi_1 \rangle} \frac{\langle \Phi_0 | c_{0,\alpha}^{+} \bar{\xi}_{1,i}^{+} | \Phi_1 \rangle}{\langle \Phi_0 | \Phi_1 \rangle} \Big) \\ & + \frac{\langle \Phi_0 | \bar{\xi}_{0,j} \bar{\xi}_{1,i}^{+} | \Phi_1 \rangle}{\langle \Phi_0 | \Phi_1 \rangle} \Big(\frac{\langle \Phi_0 | \xi_{0,j} c_{0,\alpha}^{+} | \Phi_1 \rangle}{\langle \Phi_0 | \Phi_1 \rangle} \frac{\langle \Phi_0 | c_{1,\beta} \xi_{1,i}^{+} | \Phi_1 \rangle}{\langle \Phi_0 | \Phi_1 \rangle} + \frac{\langle \Phi_0 | \xi_{0,j} \xi_{1,i}^{+} | \Phi_1 \rangle}{\langle \Phi_0 | \Phi_1 \rangle} \frac{\langle \Phi_0 | c_{0,\alpha}^{+} c_{1,\beta} | \Phi_1 \rangle}{\langle \Phi_0 | \Phi_1 \rangle} \Big)] \end{aligned} \tag{5.241}$$

Using the matrices T, Y, S, Z, $\bar{Z}$, W, $\bar{W}$ and ρ^{01}, the kernel finally reads as:

$$\boxed{\begin{aligned} E_{ji}^{01}(t) = 2\langle \Phi_0 | \Phi_1 \rangle \sum_{\alpha\beta>} t_{\alpha\beta} [& -(Y_{j\bar{j}} T_{i\bar{i}} \rho_{\beta\alpha}^{01} + Y_{j\bar{j}} Z_{\alpha\bar{i}} W_{\beta i} + T_{i\bar{i}} \bar{W}_{j\alpha} Z_{j\bar{\beta}}) \\ & + S_{ji} (Z_{j\bar{\beta}} Z_{\alpha\bar{i}} + \bar{W}_{j\alpha} W_{\beta i} + S_{ji} \rho_{\beta\alpha}^{01})] \end{aligned}} \tag{5.242}$$

To conclude, the following relation clearly holds:

$$\boxed{E_{ji}^{01}(t) = E_{ij}^{10}(t)} \tag{5.243}$$

Two-body part $E_{0i}^{01}(v)$:

Here, we consider the following kernel:

$$E_{0i}^{01}(v) = \frac{1}{4} \sum_{\alpha\beta\gamma\delta} v_{\alpha\beta\gamma\delta}^{(a)} \langle \Phi_0 | c_{0,\alpha}^{+} c_{0,\beta}^{+} c_{1,\delta} c_{1,\gamma} \xi_{1,i}^{+} \bar{\xi}_{1,i}^{+} | \Phi_1 \rangle \tag{5.244}$$

We start by using the generalized Wick theorem in Eq.(5.244):

$$E_{0i}^{01}(v) = \frac{\langle\Phi_0|\Phi_1\rangle}{4}\sum_{\alpha\beta\gamma\delta} v_{\alpha\beta\gamma\delta}^{(a)}[\frac{\langle\Phi_0|c_{0,\alpha}^{+}c_{0,\beta}^{+}|\Phi_1\rangle}{\langle\Phi_0|\Phi_1\rangle}[\frac{\langle\Phi_0|c_{1,\delta}c_{1,\gamma}|\Phi_1\rangle}{\langle\Phi_0|\Phi_1\rangle}\frac{\langle\Phi_0|\xi_{1,i}^{+}\bar{\xi}_{1,i}^{+}|\Phi_1\rangle}{\langle\Phi_0|\Phi_1\rangle} + 2\frac{\langle\Phi_0|c_{1,\delta}\bar{\xi}_{1,i}^{+}|\Phi_1\rangle}{\langle\Phi_0|\Phi_1\rangle}\frac{\langle\Phi_0|c_{1,\gamma}\xi_{1,i}^{+}|\Phi_1\rangle}{\langle\Phi_0|\Phi_1\rangle}] + 2\frac{\langle\Phi_0|c_{0,\alpha}^{+}c_{1,\gamma}|\Phi_1\rangle}{\langle\Phi_0|\Phi_1\rangle}[\frac{\langle\Phi_0|c_{0,\beta}^{+}c_{1,\delta}|\Phi_1\rangle}{\langle\Phi_0|\Phi_1\rangle}\frac{\langle\Phi_0|\xi_{1,i}^{+}\bar{\xi}_{1,i}^{+}|\Phi_1\rangle}{\langle\Phi_0|\Phi_1\rangle} + 4\frac{\langle\Phi_0|c_{0,\beta}^{+}\bar{\xi}_{1,i}^{+}|\Phi_1\rangle}{\langle\Phi_0|\Phi_1\rangle}\frac{\langle\Phi_0|c_{1,\delta}\xi_{1,i}^{+}|\Phi_1\rangle}{\langle\Phi_0|\Phi_1\rangle}] + 2\frac{\langle\Phi_0|c_{0,\alpha}^{+}\bar{\xi}_{1,i}^{+}|\Phi_1\rangle}{\langle\Phi_0|\Phi_1\rangle}\frac{\langle\Phi_0|c_{0,\beta}^{+}\xi_{1,i}^{+}|\Phi_1\rangle}{\langle\Phi_0|\Phi_1\rangle}\frac{\langle\Phi_0|c_{1,\delta}c_{1,\gamma}|\Phi_1\rangle}{\langle\Phi_0|\Phi_1\rangle}] \tag{5.245}$$

Then, we define the new excited field $\bar{\Delta}^{(i)}(WW)$ as follows:

$$\boxed{\bar{\Delta}_{\alpha\bar{\beta}}^{(i)}(WW) = \sum_{\gamma\delta>}(-1)^{s_\beta - s_\delta} v_{\alpha\bar{\beta}\gamma\bar{\delta}}^{(a)} W_{\gamma i} W_{\delta i}} \tag{5.246}$$

Thanks to this new excited field and using the collective fields $\bar{\Gamma}^{(i)}$ and $\bar{\Delta}$, the kernel finally reads:

$$\boxed{\begin{aligned} E_{0i}^{01}(v) = \langle\Phi_0|\Phi_1\rangle[T_{i\bar{i}}\sum_{\alpha\gamma>}\bar{\Gamma}_{\alpha\gamma}^{(i)}\rho_{\gamma\alpha}^{01} - T_{i\bar{i}}\sum_{\alpha\beta>}\bar{\Delta}_{\alpha\bar{\beta}}\bar{\kappa}_{\alpha\bar{\beta}}^{01} + \sum_{\alpha\beta>}\bar{\Delta}_{\alpha\bar{\beta}}^{(i)}(WW)\bar{\kappa}_{\alpha\bar{\beta}}^{01} \\ +2\sum_{\alpha\gamma>}\bar{\Gamma}_{\alpha\gamma}^{(i)}Z_{\alpha\bar{i}}W_{\gamma i} + \sum_{\alpha\beta>}\bar{\Delta}_{\alpha\bar{\beta}}Z_{\alpha\bar{i}}Z_{\beta\bar{i}}] \end{aligned}} \tag{5.247}$$

In Eq.(5.247), the collective field $\bar{\Gamma}^{(i)}$ depends on the excitation index i through the density-dependent term of the Gogny interaction (see Appendix F). Besides, the derivations associated with the excited field $\bar{\Delta}^{(i)}(WW)$ are given in Appendices E-J.

Two-body part $E_{j0}^{01}(v)$:

We consider the following kernel:

$$E_{j0}^{01}(v) = \frac{1}{4}\sum_{\alpha\beta\gamma\delta} v_{\alpha\beta\gamma\delta}^{(a)}\langle\Phi_0|\bar{\xi}_{0,j}\xi_{0,j}c_{0,\alpha}^{+}c_{0,\beta}^{+}c_{1,\delta}c_{1,\gamma}|\Phi_1\rangle \tag{5.248}$$

Using the generalized Wick theorem in Eq.(5.248) leads to:

$$E_{j0}^{01}(v) = \frac{\langle\Phi_0|\Phi_1\rangle}{4}\sum_{\alpha\beta\gamma\delta} v_{\alpha\beta\gamma\delta}^{(a)}[\frac{\langle\Phi_0|\bar{\xi}_{0,j}\xi_{0,j}|\Phi_1\rangle}{\langle\Phi_0|\Phi_1\rangle}[\frac{\langle\Phi_0|c_{0,\alpha}^{+}c_{0,\beta}^{+}|\Phi_1\rangle}{\langle\Phi_0|\Phi_1\rangle}\frac{\langle\Phi_0|c_{1,\delta}c_{1,\gamma}|\Phi_1\rangle}{\langle\Phi_0|\Phi_1\rangle} + 2\frac{\langle\Phi_0|c_{0,\alpha}^{+}c_{1,\gamma}|\Phi_1\rangle}{\langle\Phi_0|\Phi_1\rangle}\frac{\langle\Phi_0|c_{0,\beta}^{+}c_{1,\delta}|\Phi_1\rangle}{\langle\Phi_0|\Phi_1\rangle}] - 2\frac{\langle\Phi_0|\bar{\xi}_{0,j}c_{0,\alpha}^{+}|\Phi_1\rangle}{\langle\Phi_0|\Phi_1\rangle}[\frac{\langle\Phi_0|\xi_{0,j}c_{0,\beta}^{+}|\Phi_1\rangle}{\langle\Phi_0|\Phi_1\rangle}\frac{\langle\Phi_0|c_{1,\delta}c_{1,\gamma}|\Phi_1\rangle}{\langle\Phi_0|\Phi_1\rangle} + 4\frac{\langle\Phi_0|\xi_{0,j}c_{1,\gamma}|\Phi_1\rangle}{\langle\Phi_0|\Phi_1\rangle}\frac{\langle\Phi_0|c_{0,\beta}^{+}c_{1,\delta}|\Phi_1\rangle}{\langle\Phi_0|\Phi_1\rangle}] - 2\frac{\langle\Phi_0|\bar{\xi}_{0,j}c_{1,\delta}|\Phi_1\rangle}{\langle\Phi_0|\Phi_1\rangle}\frac{\langle\Phi_0|\xi_{0,j}c_{1,\gamma}|\Phi_1\rangle}{\langle\Phi_0|\Phi_1\rangle}\frac{\langle\Phi_0|c_{0,\alpha}^{+}c_{0,\beta}^{+}|\Phi_1\rangle}{\langle\Phi_0|\Phi_1\rangle}] \tag{5.249}$$

We introduce the new excited field $\bar{\Delta}^{(j)}(\bar{Z}\bar{Z})$, which reads as follows:

$$\boxed{\bar{\Delta}^{(j)}_{\alpha\bar{\beta}}(\bar{Z}\bar{Z}) = \sum_{\gamma\delta>}(-1)^{s_\beta - s_\delta} v^{(a)}_{\alpha\bar{\beta}\gamma\bar{\delta}} \bar{Z}_{j\bar{\gamma}} \bar{Z}_{j\bar{\delta}}} \tag{5.250}$$

Thanks to this new field and using the collective fields $\bar{\Gamma}$ and $\bar{\Delta}$, Eq.(5.249) is finally rewritten as:

$$\boxed{\begin{aligned} E^{01}_{j0}(v) = -\langle\Phi_0|\Phi_1\rangle[Y_{j\bar{j}} \sum_{\alpha\gamma>} \bar{\Gamma}^{(j)}_{\alpha\gamma}\rho^{01}_{\gamma\alpha} - Y_{j\bar{j}} \sum_{\alpha\beta>} \bar{\Delta}_{\alpha\bar{\beta}}\bar{\kappa}^{01}_{\alpha\bar{\beta}} + \sum_{\alpha\beta>} \bar{\Delta}^{(j)}_{\alpha\bar{\beta}}(\bar{Z}\bar{Z})\bar{\kappa}^{01}_{\alpha\bar{\beta}} \\ +2\sum_{\alpha\gamma>} \bar{\Gamma}^{(j)}_{\alpha\gamma}\bar{W}_{j\alpha}\bar{Z}_{j\bar{\gamma}} + \sum_{\alpha\beta>} \bar{\Delta}_{\alpha\bar{\beta}}\bar{W}_{j\alpha}\bar{W}_{j\beta}] \end{aligned}} \tag{5.251}$$

Here also, the collective field $\bar{\Gamma}^{(j)}$ depends on the excitation index j through the density-dependent term of the Gogny interaction. Finally, it is obvious that:

$$\boxed{E^{01}_{j0}(v) = E^{10}_{0j}(v)} \tag{5.252}$$

Two-body part $E^{01}_{ji}(v)$:

Here, we consider the following kernel:

$$E^{01}_{ji}(v) = \frac{1}{4}\sum_{\alpha\beta\gamma\delta} v^{(a)}_{\alpha\beta\gamma\delta}\langle\Phi_0|\bar{\xi}_{0,j}\xi_{0,j}c^+_{0,\alpha}c^+_{0,\beta}c_{1,\delta}c_{1,\gamma}\xi^+_{1,i}\bar{\xi}^+_{1,i}|\Phi_1\rangle \tag{5.253}$$

Applying Wick theorem in Eq.(5.253) yields a large number of terms. For this reason, we've separated it into four parts:

$$\boxed{E^{01}_{ji}(v) = E^{01}_{ji}(v,1) + E^{01}_{ji}(v,2) + E^{01}_{ji}(v,3) + E^{01}_{ji}(v,4)} \tag{5.254}$$

With:

$$\begin{cases} E^{01}_{ji}(v,1) = \frac{1}{4}\frac{\langle\Phi_0|\bar{\xi}_{0,j}\xi_{0,j}|\Phi_1\rangle}{\langle\Phi_0|\Phi_1\rangle}\sum_{\alpha\beta\gamma\delta} v^{(a)}_{\alpha\beta\gamma\delta}\langle\Phi_0|c^+_{0,\alpha}c^+_{0,\beta}c_{1,\delta}c_{1,\gamma}\xi^+_{1,i}\bar{\xi}^+_{1,i}|\Phi_1\rangle \\ E^{01}_{ji}(v,2) = -\frac{1}{2}\sum_{\alpha\beta\gamma\delta} v^{(a)}_{\alpha\beta\gamma\delta}\frac{\langle\Phi_0|\bar{\xi}_{0,j}c^+_{0,\alpha}|\Phi_1\rangle}{\langle\Phi_0|\Phi_1\rangle}\langle\Phi_0|\xi_{0,j}c^+_{0,\beta}c_{1,\delta}c_{1,\gamma}\xi^+_{1,i}\bar{\xi}^+_{1,i}|\Phi_1\rangle \\ E^{01}_{ji}(v,3) = \frac{1}{2}\sum_{\alpha\beta\gamma\delta} v^{(a)}_{\alpha\beta\gamma\delta}\frac{\langle\Phi_0|\bar{\xi}_{0,j}c_{1,\gamma}|\Phi_1\rangle}{\langle\Phi_0|\Phi_1\rangle}\langle\Phi_0|\xi_{0,j}c^+_{0,\alpha}c^+_{0,\beta}c_{1,\delta}\xi^+_{1,i}\bar{\xi}^+_{1,i}|\Phi_1\rangle \\ E^{01}_{ji}(v,4) = \frac{1}{4}\frac{\langle\Phi_0|\bar{\xi}_{0,j}\bar{\xi}^+_{1,i}|\Phi_1\rangle}{\langle\Phi_0|\Phi_1\rangle}\sum_{\alpha\beta\gamma\delta} v^{(a)}_{\alpha\beta\gamma\delta}\langle\Phi_0|\xi_{0,j}c^+_{0,\alpha}c^+_{0,\beta}c_{1,\delta}c_{1,\gamma}\xi^+_{1,i}|\Phi_1\rangle \end{cases} \tag{5.255}$$

The first term $E^{01}_{ji}(v,1)$ is very similar to $E^{01}_{0i}(v)$. By analogy, we directly write:

$$\boxed{\begin{aligned} E^{01}_{ji}(v,1) = -\langle\Phi_0|\Phi_1\rangle Y_{j\bar{j}}[T_{i\bar{i}}\sum_{\alpha\gamma>}\bar{\Gamma}^{(ji)}_{\alpha\gamma}\rho^{01}_{\gamma\alpha} - T_{\bar{i}i}\sum_{\alpha\beta>}\bar{\Delta}_{\alpha\bar{\beta}}\bar{\kappa}^{01}_{\alpha\bar{\beta}} \\ +\sum_{\alpha\beta>}\bar{\Delta}^{(i)}_{\alpha\bar{\beta}}(WW)\bar{\kappa}^{01}_{\alpha\bar{\beta}} + 2\sum_{\alpha\gamma>}\bar{\Gamma}^{(ji)}_{\alpha\gamma}Z_{\alpha\bar{i}}W_{\gamma i} + \sum_{\alpha\beta>}\bar{\Delta}_{\alpha\bar{\beta}}Z_{\alpha\bar{i}}Z_{\beta\bar{i}}] \end{aligned}} \tag{5.256}$$

In Eq.(5.256), the collective mean field $\bar{\Gamma}^{(ji)}$ depends on the excitations indices i and j through the density-dependent term of the Gogny interaction.

We fully develop the second term $E^{01}_{ji}(v,2)$ using the generalized Wick theorem:

$$\begin{aligned} E^{01}_{ji}(v,2) = -\frac{1}{2}\langle\Phi_0|\Phi_1\rangle\sum_{\alpha\beta\gamma\delta}v^{(a)}_{\alpha\beta\gamma\delta}\frac{\langle\Phi_0|\bar{\xi}_{0,j}c^+_{0,\alpha}|\Phi_1\rangle}{\langle\Phi_0|\Phi_1\rangle}[\\ \langle\Phi_0|\xi_{0,j}c^+_{0,\beta}|\Phi_1\rangle[\langle\Phi_0|c_{1,\delta}c_{1,\gamma}|\Phi_1\rangle\langle\Phi_0|\xi^+_{1,i}\bar{\xi}^+_{1,i}|\Phi_1\rangle + 2\langle\Phi_0|c_{1,\delta}\bar{\xi}^+_{1,i}|\Phi_1\rangle\langle\Phi_0|c_{1,\gamma}\xi^+_{1,i}|\Phi_1\rangle)] \\ +2\langle\Phi_0|\xi_{0,j}c_{1,\gamma}|\Phi_1\rangle[\langle\Phi_0|c^+_{0,\beta}c_{1,\delta}|\Phi_1\rangle\langle\Phi_0|\xi^+_{1,i}\bar{\xi}^+_{1,\imath}|\Phi_1\rangle - \langle\Phi_0|c^+_{0,\beta}\xi^+_{1,i}|\Phi_1\rangle\langle\Phi_0|c_{1,\delta}\bar{\xi}^+_{1,i}|\Phi_1\rangle \\ +\langle\Phi_0|c^+_{0,\beta}\bar{\xi}^+_{1,i}|\Phi_1\rangle\langle\Phi_0|c_{1,\delta}\xi^+_{1,i}|\Phi_1\rangle] \\ -\langle\Phi_0|\xi_{0,j}\xi^+_{1,i}|\Phi_1\rangle[2\langle\Phi_0|c^+_{0,\beta}c_{1,\delta}|\Phi_1\rangle\langle\Phi_0|c_{1,\gamma}\bar{\xi}^+_{1,i}|\Phi_1\rangle + \langle\Phi_0|c^+_{0,\beta}\bar{\xi}^+_{1,i}|\Phi_1\rangle\langle\Phi_0|c_{1,\delta}c_{1,\gamma}|\Phi_1\rangle]] \end{aligned} \tag{5.257}$$

We introduce the new excited field $\bar{\Gamma}^{(ji)}([W,Z])$:

$$\boxed{\bar{\Gamma}^{(ji)}_{\alpha\gamma}([W,Z]) = \sum_{\beta\delta>}[v^{(a)}_{\alpha\beta\gamma\delta} + (-1)^{s_\beta - s_\delta}v^{(a)}_{\alpha\bar{\beta}\gamma\bar{\delta}}]W_{\delta i}Z_{\beta\bar{i}}} \tag{5.258}$$

Thanks to this new excited field, we can write the final form of $E^{01}_{ji}(v,2)$ as:

$$\boxed{\begin{aligned} E^{01}_{ji}(v,2) = \langle\Phi_0|\Phi_1\rangle[S_{ji}\sum_{\alpha\beta>}\bar{\Delta}_{\alpha\bar{\beta}}\bar{W}_{j\alpha}Z_{\beta\bar{i}} - T_{i\bar{i}}\sum_{\alpha\beta>}\bar{\Delta}_{\alpha\bar{\beta}}\bar{W}_{j\alpha}\bar{W}_{j\beta} \\ +\sum_{\alpha\beta>}\bar{\Delta}^{(i)}_{\alpha\bar{\beta}}(WW)\bar{W}_{j\alpha}\bar{W}_{j\beta} - T_{i\bar{i}}\sum_{\alpha\gamma>}\bar{\Gamma}^{(ji)}_{\alpha\gamma}\bar{W}_{j\alpha}\bar{Z}_{j\bar{\gamma}} - \sum_{\alpha\gamma>}\bar{\Gamma}^{(ji)}_{\alpha\gamma}([W,Z])\bar{W}_{j\alpha}\bar{Z}_{j\bar{\gamma}} \\ +S_{ji}\sum_{\alpha\gamma>}\bar{\Gamma}^{(ji)}_{\alpha\gamma}\bar{W}_{j\alpha}W_{\gamma i}] \end{aligned}} \tag{5.259}$$

Now, we consider the third term $E^{01}_{ji}(v,3)$. This term is developed using the Wick theorem:

$$\begin{aligned} E^{01}_{ji}(v,3) = \frac{1}{2}\langle\Phi_0|\Phi_1\rangle\sum_{\alpha\beta\gamma\delta}v^{(a)}_{\alpha\beta\gamma\delta}\frac{\langle\Phi_0|\bar{\xi}_{0,j}c_{1,\gamma}|\Phi_1\rangle}{\langle\Phi_0|\Phi_1\rangle}[\\ 2\frac{\langle\Phi_0|\xi_{0,j}c^+_{0,\alpha}|\Phi_1\rangle}{\langle\Phi_0|\Phi_1\rangle}[\frac{\langle\Phi_0|c^+_{0,\beta}c_{1,\delta}|\Phi_1\rangle}{\langle\Phi_0|\Phi_1\rangle}\frac{\langle\Phi_0|\xi^+_{1,i}\bar{\xi}^+_{1,i}|\Phi_1\rangle}{\langle\Phi_0|\Phi_1\rangle} \\ -\frac{\langle\Phi_0|c^+_{0,\beta}\xi^+_{1,i}|\Phi_1\rangle}{\langle\Phi_0|\Phi_1\rangle}\frac{\langle\Phi_0|c_{1,\delta}\bar{\xi}^+_{1,i}|\Phi_1\rangle}{\langle\Phi_0|\Phi_1\rangle} + \frac{\langle\Phi_0|c^+_{0,\beta}\bar{\xi}^+_{1,i}|\Phi_1\rangle}{\langle\Phi_0|\Phi_1\rangle}\frac{\langle\Phi_0|c_{1,\delta}\xi^+_{1,i}|\Phi_1\rangle}{\langle\Phi_0|\Phi_1\rangle}] \\ +\frac{\langle\Phi_0|\xi_{0,j}c_{1,\delta}|\Phi_1\rangle}{\langle\Phi_0|\Phi_1\rangle}[\frac{\langle\Phi_0|c^+_{0,\alpha}c^+_{0,\beta}|\Phi_1\rangle}{\langle\Phi_0|\Phi_1\rangle}\frac{\langle\Phi_0|\xi^+_{1,i}\bar{\xi}^+_{1,i}|\Phi_1\rangle}{\langle\Phi_0|\Phi_1\rangle} + 2\frac{\langle\Phi_0|c^+_{0,\alpha}\bar{\xi}^+_{1,i}|\Phi_1\rangle}{\langle\Phi_0|\Phi_1\rangle}\frac{\langle\Phi_0|c^+_{0,\beta}\xi^+_{1,i}|\Phi_1\rangle}{\langle\Phi_0|\Phi_1\rangle}] \\ -\frac{\langle\Phi_0|\xi_{0,j}\xi^+_{1,i}|\Phi_1\rangle}{\langle\Phi_0|\Phi_1\rangle}[\frac{\langle\Phi_0|c^+_{0,\alpha}c^+_{0,\beta}|\Phi_1\rangle}{\langle\Phi_0|\Phi_1\rangle}\frac{\langle\Phi_0|c_{1,\delta}\bar{\xi}^+_{1,i}|\Phi_1\rangle}{\langle\Phi_0|\Phi_1\rangle} + 2\frac{\langle\Phi_0|c^+_{0,\alpha}\bar{\xi}^+_{1,i}|\Phi_1\rangle}{\langle\Phi_0|\Phi_1\rangle}\frac{\langle\Phi_0|c^+_{0,\beta}c_{1,\delta}|\Phi_1\rangle}{\langle\Phi_0|\Phi_1\rangle}]] \end{aligned} \tag{5.260}$$

We make the fields appear in Eq.(5.260):

$$\boxed{\begin{aligned} E^{01}_{ji}(v,3) = \langle\Phi_0|\Phi_1\rangle[S_{ij}\sum_{\alpha\gamma>}\bar{\Gamma}^{(ji)}_{\alpha\gamma}Z_{\alpha\bar{i}}\bar{Z}_{j\bar{\gamma}} - T_{i\bar{i}}\sum_{\alpha\gamma>}\bar{\Gamma}^{(ji)}_{\alpha\gamma}\bar{W}_{j\alpha}\bar{Z}_{j\gamma} \\ -\sum_{\alpha\gamma>}\bar{\Gamma}^{(ji)}_{\alpha\gamma}([W,Z])\bar{W}_{j\alpha}\bar{Z}_{j\gamma} - T_{i\bar{i}}\sum_{\alpha\beta>}\bar{\Delta}^{(j)}_{\alpha\bar{\beta}}(\bar{Z}\bar{Z})\bar{\kappa}^{01}_{\alpha\bar{\beta}} + \sum_{\alpha\beta>}\bar{\Delta}^{(j)}_{\alpha\bar{\beta}}(\bar{Z}\bar{Z})Z_{\alpha\bar{i}}Z_{\beta\bar{i}} \\ -\frac{1}{2}S_{ji}\sum_{\alpha\beta\gamma\delta}v^{(a)}_{\alpha\beta\gamma\delta}\frac{\langle\Phi_0|\bar{\xi}_{0,j}c_{1,\gamma}|\Phi_1\rangle}{\langle\Phi_0|\Phi_1\rangle}\frac{\langle\Phi_0|c^+_{0,\alpha}c^+_{0,\beta}|\Phi_1\rangle}{\langle\Phi_0|\Phi_1\rangle}\frac{\langle\Phi_0|c_{1,\delta}\bar{\xi}^+_{1,i}|\Phi_1\rangle}{\langle\Phi_0|\Phi_1\rangle}]\end{aligned}} \tag{5.261}$$

The last part of $E^{01}_{ji}(v,3)$ has not been developed because it will naturally combine with the term $E^{01}_{ji}(v,4)$.

Now, we treat the fourth and last term $E^{01}_{ji}(v,4)$. We start by using the Wick theorem:

$$\begin{aligned} E^{01}_{ji}(v,4) = \frac{1}{4}\langle\Phi_0|\Phi_1\rangle\frac{\langle\Phi_0|\bar{\xi}_{0,j}\bar{\xi}^+_{1,i}|\Phi_1\rangle}{\langle\Phi_0|\Phi_1\rangle}\sum_{\alpha\beta\gamma\delta}v^{(a)}_{\alpha\beta\gamma\delta}[\\ 2\frac{\langle\Phi_0|\xi_{0,j}c^+_{0,\alpha}|\Phi_1\rangle}{\langle\Phi_0|\Phi_1\rangle}[2\frac{\langle\Phi_0|c^+_{0,\beta}c_{1,\delta}|\Phi_1\rangle}{\langle\Phi_0|\Phi_1\rangle}\frac{\langle\Phi_0|c_{1,\gamma}\xi^+_{1,i}|\Phi_1\rangle}{\langle\Phi_0|\Phi_1\rangle} + \frac{\langle\Phi_0|c^+_{0,\beta}\xi^+_{1,i}|\Phi_1\rangle}{\langle\Phi_0|\Phi_1\rangle}\frac{\langle\Phi_0|c_{1,\delta}c_{1,\gamma}|\Phi_1\rangle}{\langle\Phi_0|\Phi_1\rangle}] \\ +2\frac{\langle\Phi_0|\xi_{0,j}c_{1,\delta}|\Phi_1\rangle}{\langle\Phi_0|\Phi_1\rangle}[\frac{\langle\Phi_0|c^+_{0,\alpha}c^+_{0,\beta}|\Phi_1\rangle}{\langle\Phi_0|\Phi_1\rangle}\frac{\langle\Phi_0|c_{1,\gamma}\xi^+_{1,i}|\Phi_1\rangle}{\langle\Phi_0|\Phi_1\rangle} - 2\frac{\langle\Phi_0|c^+_{0,\alpha}c_{1,\gamma}|\Phi_1\rangle}{\langle\Phi_0|\Phi_1\rangle}\frac{\langle\Phi_0|c^+_{0,\beta}\xi^+_{1,i}|\Phi_1\rangle}{\langle\Phi_0|\Phi_1\rangle}] \\ +\frac{\langle\Phi_0|\xi_{0,j}\xi^+_{1,i}|\Phi_1\rangle}{\langle\Phi_0|\Phi_1\rangle}[\frac{\langle\Phi_0|c^+_{0,\alpha}c^+_{0,\beta}|\Phi_1\rangle}{\langle\Phi_0|\Phi_1\rangle}\frac{\langle\Phi_0|c_{1,\delta}c_{1,\gamma}|\Phi_1\rangle}{\langle\Phi_0|\Phi_1\rangle} + 2\frac{\langle\Phi_0|c^+_{0,\alpha}c_{1,\gamma}|\Phi_1\rangle}{\langle\Phi_0|\Phi_1\rangle}\frac{\langle\Phi_0|c^+_{0,\beta}c_{1,\delta}|\Phi_1\rangle}{\langle\Phi_0|\Phi_1\rangle}]] \end{aligned} \tag{5.262}$$

We make the fields appear in Eq.(5.262):

$$\boxed{\begin{aligned} E^{01}_{ji}(v,4) = S_{ji}\langle\Phi_0|\Phi_1\rangle[\sum_{\alpha\gamma>}\bar{\Gamma}^{(ji)}_{\alpha\gamma}\bar{W}_{j\alpha}W_{\gamma i} + \sum_{\alpha\beta>}\bar{\Delta}_{\alpha\bar{\beta}}\bar{W}_{j\alpha}Z_{\beta\bar{i}} \\ +\sum_{\alpha\gamma>}\bar{\Gamma}^{(ji)}_{\alpha\gamma}Z_{\alpha\bar{i}}\bar{Z}_{j\bar{\gamma}} - S_{ji}\sum_{\alpha\beta>}\bar{\Delta}_{\alpha\bar{\beta}}\bar{\kappa}_{\alpha\bar{\beta}} + S_{ji}\sum_{\alpha\gamma>}\bar{\Gamma}^{(ji)}_{\alpha\gamma}\rho^{01}_{\gamma\alpha} \\ +\frac{1}{2}\sum_{\alpha\beta\gamma\delta}v^{(a)}_{\alpha\beta\gamma\delta}\frac{\langle\Phi_0|\xi_{0,j}c_{1,\delta}|\Phi_1\rangle}{\langle\Phi_0|\Phi_1\rangle}\frac{\langle\Phi_0|c^+_{0,\alpha}c^+_{0,\beta}|\Phi_1\rangle}{\langle\Phi_0|\Phi_1\rangle}\frac{\langle\Phi_0|c_{1,\gamma}\xi^+_{1,i}|\Phi_1\rangle}{\langle\Phi_0|\Phi_1\rangle}]\end{aligned}} \tag{5.263}$$

We now introduce the last new excited field $\bar{\Delta}^{(ji)}_{\alpha\bar{\beta}}([W,\bar{Z}])$:

$$\boxed{\bar{\Delta}^{(ji)}_{\alpha\bar{\beta}}([W,\bar{Z}]) = \sum_{\gamma\delta>}(-1)^{s_\beta - s_\delta}v^{(a)}_{\alpha\bar{\beta}\gamma\bar{\delta}}[W_{\gamma i}\bar{Z}_{j\bar{\delta}} + \bar{Z}_{j\bar{\gamma}}W_{\delta i}]} \tag{5.264}$$

Finally, the whole kernel is expressed as follows:

$$\boxed{\begin{aligned} E^{01}_{ji}(v) = \langle\Phi_0|\Phi_1\rangle[\sum_{\alpha\gamma>}\bar{\Gamma}^{(ji)}_{\alpha\gamma}[-Y_{j\bar{j}}T_{i\bar{i}}\rho^{01}_{\gamma\alpha} - 2Y_{j\bar{j}}Z_{\alpha\bar{i}}W_{\gamma i} - 2T_{i\bar{i}}\bar{W}_{j\alpha}\bar{Z}_{j\bar{\gamma}} \\ +2S_{ji}\bar{W}_{j\alpha}W_{\gamma i} + 2S_{ij}Z_{\alpha\bar{i}}\bar{Z}_{j\bar{\gamma}} + S_{ji}S_{ji}\rho^{01}_{\gamma\alpha}] \\ +\sum_{\alpha\beta>}\bar{\Delta}_{\alpha\bar{\beta}}[Y_{j\bar{j}}T_{i\bar{i}}\bar{\kappa}^{01}_{\alpha\bar{\beta}} - Y_{j\bar{j}}Z_{\alpha\bar{i}}Z_{\beta\bar{i}} + 2S_{ji}\bar{W}_{j\alpha}Z_{\beta\bar{i}} - T_{i\bar{i}}\bar{W}_{j\alpha}\bar{W}_{j\beta} - S_{ji}S_{ji}\bar{\kappa}_{\alpha\bar{\beta}}] \\ +\sum_{\alpha\beta>}\bar{\Delta}^{(i)}_{\alpha\bar{\beta}}(WW)[-Y_{j\bar{j}}\bar{\kappa}^{01}_{\alpha\bar{\beta}} + \bar{W}_{j\alpha}\bar{W}_{j\beta}] + \sum_{\alpha\beta>}\bar{\Delta}^{(j)}_{\alpha\bar{\beta}}(\bar{Z}\bar{Z})[-T_{i\bar{i}}\bar{\kappa}^{01}_{\alpha\bar{\beta}} + Z_{\alpha\bar{i}}Z_{\beta\bar{i}}] \\ +S_{ji}\sum_{\alpha\beta>}\bar{\Delta}^{(ji)}_{\alpha\bar{\beta}}([W,\bar{Z}])\bar{\kappa}^{01}_{\alpha\bar{\beta}} - 2\sum_{\alpha\gamma>}\bar{\Gamma}^{(ji)}_{\alpha\gamma}([W,Z])\bar{W}_{j\alpha}\bar{Z}_{j\bar{\gamma}}] \end{aligned}} \tag{5.265}$$

In addition, we have the following property:

$$\boxed{E^{01}_{ji}(v) = E^{10}_{ij}} \tag{5.266}$$

5.6 Projected Hamiltonian kernels

This section is dedicated to the evaluation of projected Hamiltonian kernels between HFB states and 2-quasiparticle excited states. In addition, we give the derivations for the new POF Hamiltonian kernel developed during this PhD thesis.

5.6.1 Projected HFB states diagonal kernels

The goal of this section is to give an expression of the particle number projected HFB energy $\tilde{E}$, which is defined as follows:

$$\boxed{\tilde{E} = \frac{\langle\Phi|\hat{P}^{\tau_n}\hat{P}^{\tau_p}\hat{H}\hat{P}^{\tau_n}\hat{P}^{\tau_p}|\Phi\rangle}{\langle\Phi|\hat{P}^{\tau_n}\hat{P}^{\tau_p}|\Phi\rangle}} \tag{5.267}$$

As both $\hat{P}^{\tau_n}$ and $\hat{P}^{\tau_p}$ commute with $\hat{H}$, we can write:

$$\tilde{E} = \frac{1}{\langle\Phi|\tilde{\Phi}\rangle}[\langle\Phi|\sum_{\alpha\beta}t_{\alpha\beta}c^+_\alpha c_\beta P^{\tau_n}\hat{P}^{\tau_p}|\Phi\rangle + \langle\Phi|\frac{1}{4}\sum_{\alpha\beta\gamma\delta}v^{(a)}_{\alpha\beta\gamma\delta}c^+_\alpha c^+_\beta c_\delta c_\gamma P^{\tau_n}\hat{P}^{\tau_p}|\Phi\rangle] \tag{5.268}$$

From Eq.(5.268), it is clear that we can separate this kernel into a kinetic and a two-body contributions $\tilde{E}(t)$ and $\tilde{E}(v)$:

$$\boxed{\tilde{E} = \tilde{E}(t) + \tilde{E}(v)} \tag{5.269}$$

Kinetic part:

We start by writing explicitly the discretized particle number projection operators in $\tilde{E}(t)$:

$$\tilde{E}(t) = \frac{1}{\langle\Phi|\tilde{\Phi}\rangle} \sum_{\alpha\beta} t_{\alpha\beta} \sum_{\varphi_n} \sum_{\varphi_p} \frac{e^{2i\varphi_n \pi N_n} e^{2i\varphi_p \pi N_p}}{n_{\varphi_n} n_{\varphi_p}} \langle\Phi|c_\alpha^+ c_\beta|\Phi(\varphi_n,\varphi_p)\rangle \tag{5.270}$$

We introduce the local projected density matrices $\rho^\tau(\varphi_\tau)$ into Eq.(5.270):

$$\tilde{E}(t) = \frac{1}{\langle\Phi|\tilde{\Phi}\rangle} \sum_{\alpha\beta} t_{\alpha\beta} \sum_{\varphi_n} \sum_{\varphi_p} \frac{e^{2i\varphi_n \pi N_n} e^{2i\varphi_p \pi N_p}}{n_{\varphi_n} n_{\varphi_p}} \langle\Phi|\Phi(\varphi_n,\varphi_p)\rangle \rho^\tau_{\beta\alpha}(\varphi_\tau) \tag{5.271}$$

Then, we separate the isospin contributions in Eq.(5.271). The shorthand notation $\bar{\tau}$ refers to the opposite isospin of τ:

$$\tilde{E}(t) = \frac{1}{\langle\Phi|\tilde{\Phi}\rangle} \sum_{\alpha\beta} t_{\alpha\beta} \sum_{\varphi_\tau} \frac{1}{n_{\varphi_\tau}} e^{2i\varphi_\tau \pi N_\tau} \langle\Phi_\tau|\Phi_\tau(\varphi_\tau)\rangle \rho^\tau_{\beta\alpha}(\varphi_\tau) \sum_{\varphi_{\bar{\tau}}} \frac{1}{n_{\varphi_{\bar{\tau}}}} e^{2i\varphi_{\bar{\tau}} \pi N_{\bar{\tau}}} \langle\Phi_{\bar{\tau}}|\Phi_{\bar{\tau}}(\varphi_{\bar{\tau}})\rangle \tag{5.272}$$

We make the total projected density matrices $\tilde{\rho}^\tau$ appear in Eq.(5.272):

$$\tilde{E}(t) = \sum_{\alpha\beta} t_{\alpha\beta} \tilde{\rho}^\tau_{\beta\alpha} \tag{5.273}$$

Finally, we use the time-reversal properties of the matrices $\tilde{\rho}^\tau$ to obtain the final expression of $\tilde{E}(t)$:

$$\boxed{\tilde{E}(t) = 2 \sum_{\alpha\beta>} t_{\alpha\beta} \tilde{\rho}^\tau_{\beta\alpha}} \tag{5.274}$$

Two-body part:

We start by writing explicitly the discretized particle number projection operators in $\tilde{E}(v)$:

$$\tilde{E}(v) = \frac{1}{4\langle\Phi|\tilde{\Phi}\rangle} \sum_{\alpha\beta\gamma\delta} v^{(a)}_{\alpha\beta\gamma\delta} \sum_{\varphi_n} \sum_{\varphi_p} \frac{e^{2i\varphi_n \pi N_n} e^{2i\varphi_p \pi N_p}}{n_{\varphi_n} n_{\varphi_p}} \langle\Phi|c_\alpha^+ c_\beta^+ c_\delta c_\gamma|\Phi(\varphi_n,\varphi_p)\rangle \tag{5.275}$$

We develop Eq.(5.275) using the generalized Wik theorem:

$$\tilde{E}(v) = \frac{1}{4\langle\Phi|\tilde{\Phi}\rangle} \sum_{\alpha\beta\gamma\delta} v^{(a)}_{\alpha\beta\gamma\delta} \sum_{\varphi_n} \sum_{\varphi_p} \frac{e^{2i\varphi_n \pi N_n} e^{2i\varphi_p \pi N_p}}{n_{\varphi_n} n_{\varphi_p} \langle\Phi|\Phi(\varphi_n,\varphi_p)\rangle} \tag{5.276}$$
$$[\langle\Phi|c_\alpha^+ c_\beta^+|\Phi(\varphi_n,\varphi_p)\rangle \langle\Phi|c_\delta c_\gamma|\Phi(\varphi_n,\varphi_p)\rangle + 2\langle\Phi|c_\alpha^+ c_\gamma|\Phi(\varphi_n,\varphi_p)\rangle \langle\Phi|c_\beta^+ c_\delta|\Phi(\varphi_n,\varphi_p)\rangle]$$

In this section, we separate the mean and pairing type contributions to $\tilde{E}(v)$ for pedagogical purposes:

$$\boxed{\tilde{E}_\Delta(v) = \frac{1}{4\langle\Phi|\tilde{\Phi}\rangle} \sum_{\alpha\beta\gamma\delta} v^{(a)}_{\alpha\beta\gamma\delta} \sum_{\varphi_n} \sum_{\varphi_p} \frac{e^{2i\varphi_n \pi N_n} e^{2i\varphi_p \pi N_p}}{n_{\varphi_n} n_{\varphi_p} \langle\Phi|\Phi(\varphi_n,\varphi_p)\rangle} \langle\Phi|c_\alpha^+ c_\beta^+|\Phi(\varphi_n,\varphi_p)\rangle \langle\Phi|c_\delta c_\gamma|\Phi(\varphi_n,\varphi_p)\rangle} \tag{5.277}$$

$$\boxed{\begin{aligned}\tilde{E}_{\Gamma}(v) = \frac{1}{2\langle\Phi|\tilde{\Phi}\rangle}\sum_{\alpha\beta\gamma\delta} v^{(a)}_{\alpha\beta\gamma\delta}\sum_{\varphi_n}\sum_{\varphi_p}\frac{e^{2i\varphi_n\pi N_n}e^{2i\varphi_p\pi N_p}}{n_{\varphi_n}n_{\varphi_p}\langle\Phi|\Phi(\varphi_n,\varphi_p)\rangle} \\ \langle\Phi|c^{+}_{\alpha}c_{\gamma}|\Phi(\varphi_n,\varphi_p)\rangle\langle\Phi|c^{+}_{\beta}c_{\delta}|\Phi(\varphi_n,\varphi_p)\rangle\end{aligned}} \tag{5.278}$$

We start by rewriting $\tilde{E}_{\Delta}(v)$ with explicit isospins:

$$\begin{aligned}\tilde{E}_{\Delta}(v) = \frac{1}{4\langle\Phi|\tilde{\Phi}\rangle}\sum_{\alpha\beta\gamma\delta} v^{(a)}_{\alpha\beta\gamma\delta}\sum_{\varphi_n}\sum_{\varphi_p}\frac{e^{2i\varphi_n\pi N_n}e^{2i\varphi_p\pi N_p}}{n_{\varphi_n}n_{\varphi_p}\langle\Phi|\Phi(\varphi_n,\varphi_p)\rangle} \\ [\langle\Phi|c^{+\tau_n}_{\alpha}c^{+\tau_n}_{\beta}|\Phi(\varphi_n,\varphi_p)\rangle\langle\Phi|c^{\tau_n}_{\delta}c^{\tau_n}_{\gamma}|\Phi(\varphi_n,\varphi_p)\rangle + \langle\Phi|c^{+\tau_n}_{\alpha}c^{+\tau_n}_{\beta}|\Phi(\varphi_n,\varphi_p)\rangle\langle\Phi|c^{\tau_p}_{\delta}c^{\tau_p}_{\gamma}|\Phi(\varphi_n,\varphi_p)\rangle \\ +\langle\Phi|c^{+\tau_p}_{\alpha}c^{+\tau_p}_{\beta}|\Phi(\varphi_n,\varphi_p)\rangle\langle\Phi|c^{\tau_n}_{\delta}c^{\tau_n}_{\gamma}|\Phi(\varphi_n,\varphi_p)\rangle + \langle\Phi|c^{+\tau_p}_{\alpha}c^{+\tau_p}_{\beta}|\Phi(\varphi_n,\varphi_p)\rangle\langle\Phi|c^{\tau_p}_{\delta}c^{\tau_p}_{\gamma}|\Phi(\varphi_n,\varphi_p)\rangle]\end{aligned} \tag{5.279}$$

As the pairing terms of the Gogny interactions we've considered in this PhD thesis do not mix the isospins, we can simplify Eq.(5.279):

$$\begin{aligned}\tilde{E}_{\Delta}(v) = \frac{1}{4\langle\Phi|\tilde{\Phi}\rangle}\sum_{\alpha\beta\gamma\delta} v^{(a)}_{\alpha\beta\gamma\delta}\sum_{\varphi_n}\sum_{\varphi_p}\frac{e^{2i\varphi_n\pi N_n}e^{2i\varphi_p\pi N_p}}{n_{\varphi_n}n_{\varphi_p}\langle\Phi|\Phi(\varphi_n,\varphi_p)\rangle} \\ [\langle\Phi|c^{+\tau_n}_{\alpha}c^{+\tau_n}_{\beta}|\Phi(\varphi_n,\varphi_p)\rangle\langle\Phi|c^{\tau_n}_{\delta}c^{\tau_n}_{\gamma}|\Phi(\varphi_n,\varphi_p)\rangle \\ +\langle\Phi|c^{+\tau_p}_{\alpha}c^{+\tau_p}_{\beta}|\Phi(\varphi_n,\varphi_p)\rangle\langle\Phi|c^{\tau_p}_{\delta}c^{\tau_p}_{\gamma}|\Phi(\varphi_n,\varphi_p)\rangle]\end{aligned} \tag{5.280}$$

We use the time-reversal properties of Eq.(5.280):

$$\begin{aligned}\tilde{E}_{\Delta}(v) = -\frac{1}{\langle\Phi|\tilde{\Phi}\rangle}\sum_{\alpha\beta\gamma\delta>} \sigma_{\beta}\sigma_{\delta}v^{(a)}_{\alpha\bar{\beta}\gamma\bar{\delta}}\sum_{\varphi_n}\sum_{\varphi_p}\frac{e^{2i\varphi_n\pi N_n}e^{2i\varphi_p\pi N_p}}{n_{\varphi_n}n_{\varphi_p}\langle\Phi|\Phi(\varphi_n,\varphi_p)\rangle} \\ [\langle\Phi|c^{+\tau_n}_{\alpha}\bar{c}^{+\tau_n}_{\beta}|\Phi(\varphi_n,\varphi_p)\rangle\langle\Phi|c^{\tau_n}_{\gamma}\bar{c}^{\tau_n}_{\delta}|\Phi(\varphi_n,\varphi_p)\rangle \\ +\langle\Phi|c^{+\tau_p}_{\alpha}\bar{c}^{+\tau_p}_{\beta}|\Phi(\varphi_n,\varphi_p)\rangle\langle\Phi|c^{\tau_p}_{\gamma}\bar{c}^{\tau_p}_{\delta}|\Phi(\varphi_n,\varphi_p)\rangle]\end{aligned} \tag{5.281}$$

Now, we can make the local projected pairing matrices $\kappa(\varphi)$ and $\bar{\kappa}(\varphi)$ appear:

$$\begin{aligned}\tilde{E}_{\Delta}(v) = -\frac{1}{\langle\Phi|\tilde{\Phi}\rangle}\sum_{\alpha\beta\gamma\delta>} \sigma_{\beta}\sigma_{\delta}v^{(a)}_{\alpha\bar{\beta}\gamma\bar{\delta}}\sum_{\varphi_n}\sum_{\varphi_p}\frac{e^{2i\varphi_n\pi N_n}e^{2i\varphi_p\pi N_p}}{n_{\varphi_n}n_{\varphi_p}} \\ \langle\Phi|\Phi(\varphi_n,\varphi_p)\rangle[\kappa^{\tau_n}_{\gamma\bar{\delta}}(\varphi_n)\bar{\kappa}^{\tau_n}_{\alpha\bar{\beta}}(\varphi_n) + \kappa^{\tau_p}_{\gamma\bar{\delta}}(\varphi_p)\bar{\kappa}^{\tau_p}_{\alpha\bar{\beta}}(\varphi_p)]\end{aligned} \tag{5.282}$$

We separate the isospin contributions in Eq.(5.282):

$$\begin{aligned}\tilde{E}_{\Delta}(v) = -\frac{1}{\langle\Phi|\tilde{\Phi}\rangle}\sum_{\alpha\beta>}[\sum_{\varphi_n}\sum_{\gamma\delta>}(-1)^{s_{\beta}-s_{\delta}}v^{(a)}_{\alpha\bar{\beta}\gamma\bar{\delta}}\frac{e^{2i\varphi_n\pi N_n}}{n_{\varphi_n}}\langle\Phi_{\tau_n}|\Phi_{\tau_n}(\varphi_n)\rangle \\ \kappa^{\tau_n}_{\gamma\bar{\delta}}(\varphi_n)\bar{\kappa}^{\tau_n}_{\alpha\bar{\beta}}(\varphi_n)\sum_{\varphi_p}\frac{e^{2i\varphi_p\pi N_p}}{n_{\varphi_p}}\langle\Phi_{\tau_p}|\Phi_{\tau_p}(\varphi_p)\rangle \\ +\sum_{\varphi_p}\sum_{\gamma\delta>}(-1)^{s_{\beta}-s_{\delta}}v^{(a)}_{\alpha\bar{\beta}\gamma\bar{\delta}}\frac{e^{2i\varphi_p\pi N_p}}{n_{\varphi_p}}\langle\Phi_{\tau_p}|\Phi_{\tau_p}(\varphi_p)\rangle \\ \kappa^{\tau_p}_{\gamma\bar{\delta}}(\varphi_p)\bar{\kappa}^{\tau_p}_{\alpha\bar{\beta}}(\varphi_p)\sum_{\varphi_n}\frac{e^{2i\varphi_n\pi N_n}}{n_{\varphi_n}}\langle\Phi_{\tau_n}|\Phi_{\tau_n}(\varphi_n)\rangle]\end{aligned} \tag{5.283}$$

We introduce the local projected pairing fields $\Delta^{(\tau\tau)}(\varphi_\tau)$:

$$\boxed{\Delta^{(\tau\tau)}_{\alpha\bar{\beta}}(\varphi_\tau) = \sum_{\gamma\delta>} (-1)^{s_\beta - s_\delta} v^{(a)}_{\alpha\bar{\beta}\gamma\bar{\delta}} \kappa^{\tau}_{\gamma\bar{\delta}}(\varphi_\tau)} \tag{5.284}$$

Thanks to these projected fields, the quantity $\tilde{E}_\Delta(v)$ finally reads as:

$$\boxed{\tilde{E}_\Delta(v) = -\sum_{\alpha\beta>} \frac{1}{\langle\Phi_\tau|\tilde{\Phi}_\tau\rangle} \sum_{\varphi_\tau} \frac{e^{2i\varphi_\tau \pi N_\tau}}{n_{\varphi_\tau}} \langle\Phi_\tau|\Phi_\tau(\varphi_\tau)\rangle \Delta^{(\tau\tau)}_{\alpha\bar{\beta}}(\varphi_\tau) \bar{\kappa}^{\tau}_{\alpha\bar{\beta}}(\varphi_\tau)} \tag{5.285}$$

Now, we consider the mean field part $\tilde{E}_\Gamma(v)$ of the projected energy:

$$\begin{aligned} \tilde{E}_\Gamma(v) = \frac{1}{2\langle\Phi|\tilde{\Phi}\rangle} \sum_{\alpha\beta\gamma\delta} v^{(a)}_{\alpha\beta\gamma\delta} \sum_{\varphi_n} \sum_{\varphi_p} \frac{e^{2i\varphi_n \pi N_n} e^{2i\varphi_p \pi N_p}}{n_{\varphi_n} n_{\varphi_p} \langle\Phi|\Phi(\varphi_n,\varphi_p)\rangle} \\ \langle\Phi|c^+_\alpha c_\gamma|\Phi(\varphi_n,\varphi_p)\rangle \langle\Phi|c^+_\beta c_\delta|\Phi(\varphi_n,\varphi_p)\rangle \end{aligned} \tag{5.286}$$

We write the isospins explicitly and make the local projected matrices $\rho(\varphi)$ appear in Eq.(5.286):

$$\begin{aligned} \tilde{E}_\Gamma(v) = \frac{1}{2\langle\Phi|\tilde{\Phi}\rangle} \sum_{\alpha\beta\gamma\delta} v^{(a)}_{\alpha\beta\gamma\delta} \sum_{\varphi_n} \sum_{\varphi_p} \frac{e^{2i\varphi_n \pi N_n} e^{2i\varphi_p \pi N_p}}{n_{\varphi_n} n_{\varphi_p}} \langle\Phi|\Phi(\varphi_n,\varphi_p)\rangle \\ [\rho^{\tau_n}_{\gamma\alpha}(\varphi_n)\rho^{\tau_n}_{\delta\beta}(\varphi_n) + \rho^{\tau_p}_{\gamma\alpha}(\varphi_p)\rho^{\tau_p}_{\delta\beta}(\varphi_p) + \rho^{\tau_n}_{\gamma\alpha}(\varphi_n)\rho^{\tau_p}_{\delta\beta}(\varphi_p) + \rho^{\tau_p}_{\gamma\alpha}(\varphi_p)\rho^{\tau_n}_{\delta\beta}(\varphi_n)] \end{aligned} \tag{5.287}$$

The terms that do not mix the isospins are treated differently from the others. For this reason, we isolate them in Eq.(5.287):

$$\begin{aligned} \tilde{E}_\Gamma(v) = \frac{1}{2\langle\Phi|\tilde{\Phi}\rangle} \sum_{\alpha\gamma} [\sum_{\varphi_n} \sum_{\beta\delta} v^{(a)}_{\alpha\beta\gamma\delta} \frac{e^{2i\varphi_n \pi N_n}}{n_{\varphi_n}} \langle\Phi_{\tau_n}|\Phi_{\tau_n}(\varphi_n)\rangle \\ \rho^{\tau_n}_{\gamma\alpha}(\varphi_n)\rho^{\tau_n}_{\delta\beta}(\varphi_n) \sum_{\varphi_p} \frac{e^{2i\varphi_p \pi N_p}}{n_{\varphi_p}} \langle\Phi_{\tau_p}|\Phi_{\tau_p}(\varphi_p)\rangle \\ + \sum_{\varphi_p} \sum_{\beta\delta} v^{(a)}_{\alpha\beta\gamma\delta} \frac{e^{2i\varphi_p \pi N_p}}{n_{\varphi_p}} \langle\Phi_{\tau_p}|\Phi_{\tau_p}(\varphi_p)\rangle \rho^{\tau_p}_{\gamma\alpha}(\varphi_p)\rho^{\tau_p}_{\delta\beta}(\varphi_p) \sum_{\varphi_n} \frac{e^{2i\varphi_n \pi N_n}}{n_{\varphi_n}} \langle\Phi_{\tau_n}|\Phi_{\tau_n}(\varphi_n)\rangle \\ + \sum_{\beta\delta} v^{(a)}_{\alpha\beta\gamma\delta} \sum_{\varphi_p} \frac{e^{2i\varphi_p \pi N_p}}{n_{\varphi_p}} \langle\Phi_{\tau_p}|\Phi_{\tau_p}(\varphi_p)\rangle \rho^{\tau_p}_{\delta\beta}(\varphi_p) \sum_{\varphi_n} \frac{e^{2i\varphi_n \pi N_n}}{n_{\varphi_n}} \langle\Phi_{\tau_n}|\Phi_{\tau_n}(\varphi_n)\rangle \rho^{\tau_n}_{\gamma\alpha}(\varphi_n) \\ + \sum_{\beta\delta} v^{(a)}_{\alpha\beta\gamma\delta} \sum_{\varphi_n} \frac{e^{2i\varphi_n \pi N_n}}{n_{\varphi_n}} \langle\Phi_{\tau_n}|\Phi_{\tau_n}(\varphi_n)\rangle \rho^{\tau_n}_{\delta\beta}(\varphi_n) \sum_{\varphi_p} \frac{e^{2i\varphi_p \pi N_p}}{n_{\varphi_p}} \langle\Phi_{\tau_p}|\Phi_{\tau_p}(\varphi_p)\rangle \rho^{\tau_p}_{\gamma\alpha}(\varphi_p)] \end{aligned} \tag{5.288}$$

In the two last terms of Eq.(5.288) it is possible to directly sum over φ_n and φ_p. These summations make the total projected density matrices $\tilde{\rho}^\tau$ appear:

$$\tilde{E}_\Gamma(v) = \frac{1}{2}\sum_{\alpha\gamma}[\frac{1}{\langle\Phi|\tilde{\Phi}\rangle}\sum_{\varphi_n}\sum_{\beta\delta} v^{(a)}_{\alpha\beta\gamma\delta}\frac{e^{2i\varphi_n\pi N_n}}{n_{\varphi_n}}\langle\Phi_{\tau_n}|\Phi_{\tau_n}(\varphi_n)\rangle \tag{5.289}$$
$$\rho^{\tau_n}_{\gamma\alpha}(\varphi_n)\rho^{\tau_n}_{\delta\beta}(\varphi_n)\sum_{\varphi_p}\frac{e^{2i\varphi_p\pi N_p}}{n_{\varphi_p}}\langle\Phi_{\tau_p}|\Phi_{\tau_p}(\varphi_p)\rangle$$
$$+\frac{1}{\langle\Phi|\tilde{\Phi}\rangle}\sum_{\varphi_p}\sum_{\beta\delta} v^{(a)}_{\alpha\beta\gamma\delta}\frac{e^{2i\varphi_p\pi N_p}}{n_{\varphi_p}}\langle\Phi_{\tau_p}|\Phi_{\tau_p}(\varphi_p)\rangle$$
$$\rho^{\tau_p}_{\gamma\alpha}(\varphi_p)\rho^{\tau_p}_{\delta\beta}(\varphi_p)\sum_{\varphi_n}\frac{e^{2i\varphi_n\pi N_n}}{n_{\varphi_n}}\langle\Phi_{\tau_n}|\Phi_{\tau_n}(\varphi_n)\rangle$$
$$+\sum_{\beta\delta} v^{(a)}_{\alpha\beta\gamma\delta}\tilde{\rho}^{\tau_p}_{\delta\beta}\tilde{\rho}^{\tau_n}_{\gamma\alpha} + \sum_{\beta\delta} v^{(a)}_{\alpha\beta\gamma\delta}\tilde{\rho}^{\tau_n}_{\delta\beta}\tilde{\rho}^{\tau_p}_{\gamma\alpha}]$$

We introduce the local projected mean fields $\Gamma^{(\tau\tau)}(\varphi_\tau)$ and the total projected mean field $\tilde{\Gamma}^{(\bar{\tau}\tau)}$:

$$\boxed{\Gamma^{(\tau\tau)}_{\alpha\gamma}(\varphi_\tau) = \sum_{\beta\delta} v^{(a)}_{\alpha\beta\gamma\delta}\rho^{\tau}_{\delta\beta}(\varphi_\tau)} \tag{5.290}$$

$$\boxed{\tilde{\Gamma}^{(\bar{\tau}\tau)}_{\alpha\gamma} = \sum_{\beta\delta} v^{(a)}_{\alpha\beta\gamma\delta}\tilde{\rho}^{\tau}_{\delta\beta}} \tag{5.291}$$

Thanks to these fields, Eq.(5.289) now reads as:

$$\tilde{E}_\Gamma(v) = \frac{1}{2}\sum_{\alpha\gamma}[\frac{1}{\langle\Phi_\tau|\tilde{\Phi}_\tau\rangle}\sum_{\varphi_\tau}\frac{e^{2i\varphi_\tau\pi N_\tau}}{n_{\varphi_\tau}}\langle\Phi_\tau|\Phi_\tau(\varphi_\tau)\rangle\Gamma^{(\tau\tau)}_{\alpha\gamma}(\varphi_\tau)\rho^{\tau}_{\gamma\alpha}(\varphi_\tau) + \tilde{\Gamma}^{(\bar{\tau}\tau)}_{\alpha\gamma}\tilde{\rho}^{\tau}_{\gamma\alpha}] \tag{5.292}$$

Finally, we use the time-reversal properties Eq.(5.292) to write:

$$\boxed{\tilde{E}_\Gamma(v) = \sum_{\alpha\gamma>}[\frac{1}{\langle\Phi_\tau|\tilde{\Phi}_\tau\rangle}\sum_{\varphi_\tau}\frac{e^{2i\varphi_\tau\pi N_\tau}}{n_{\varphi_\tau}}\langle\Phi_\tau|\Phi_\tau(\varphi_\tau)\rangle\Gamma^{(\tau\tau)}_{\alpha\gamma}(\varphi_\tau)\rho^{\tau}_{\gamma\alpha}(\varphi_\tau) + \tilde{\Gamma}^{(\bar{\tau}\tau)}_{\alpha\gamma}\tilde{\rho}^{\tau}_{\gamma\alpha}]} \tag{5.293}$$

To conclude, the two-body part of the projected Hamiltonian energy reads as follows:

$$\boxed{\begin{aligned}\tilde{E}(v) = &\sum_{\alpha\gamma>}[\frac{1}{\langle\Phi_\tau|\tilde{\Phi}_\tau\rangle}\sum_{\varphi_\tau}\frac{e^{2i\varphi_\tau\pi N_\tau}}{n_{\varphi_\tau}}\langle\Phi_\tau|\Phi_\tau(\varphi_\tau)\rangle\Gamma^{(\tau\tau)}_{\alpha\gamma}(\varphi_\tau)\rho^{\tau}_{\gamma\alpha}(\varphi_\tau) + \tilde{\Gamma}^{(\bar{\tau}\tau)}_{\alpha\gamma}\tilde{\rho}^{\tau}_{\gamma\alpha}] \\ &-\sum_{\alpha\beta>}\frac{1}{\langle\Phi_\tau|\tilde{\Phi}_\tau\rangle}\sum_{\varphi_\tau}\frac{e^{2i\varphi_\tau\pi N_\tau}}{n_{\varphi_\tau}}\langle\Phi_\tau|\Phi_\tau(\varphi_\tau)\rangle\Delta^{(\tau\tau)}_{\alpha\bar{\beta}}(\varphi_\tau)\bar{\kappa}^{\tau}_{\alpha\bar{\beta}}(\varphi_\tau)\end{aligned}} \tag{5.294}$$

5.6.2 Projected HFB states off-diagonal kernels

In this section, we give the expression of the projected Hamiltonian kernel $\tilde{E}^{01}_{00}$ between two different HFB states $|\tilde{\Phi}_0\rangle$ and $|\tilde{\Phi}_1\rangle$. This kernel reads:

$$\boxed{\tilde{E}^{01}_{00} = \frac{\langle\Phi_0|\hat{P}^{\tau_n}\hat{P}^{\tau_p}\hat{H}^{01}\hat{P}^{\tau_n}\hat{P}^{\tau_p}|\Phi_1\rangle}{\sqrt{\langle\Phi_0|\hat{P}^{\tau_n}\hat{P}^{\tau_p}|\Phi_0\rangle\langle\Phi_1|\hat{P}^{\tau_n}\hat{P}^{\tau_p}|\Phi_1\rangle}}} \tag{5.295}$$

As both $\hat{P}^{\tau_n}$ and $\hat{P}^{\tau_p}$ commute with $\hat{H}^{01}$, we write:

$$\begin{aligned}\tilde{E}^{01}_{00} = \frac{1}{\sqrt{\langle\Phi_0|\tilde{\Phi}_0\rangle\langle\Phi_1|\tilde{\Phi}_1\rangle}}[&\langle\Phi_0|\sum_{\alpha\beta} t_{\alpha\beta}c^+_{0,\alpha}c_{1,\beta}\hat{P}^{\tau_n}\hat{P}^{\tau_p}|\Phi\rangle \\ &+\langle\Phi_1|\frac{1}{4}\sum_{\alpha\beta\gamma\delta} v^{(a)}_{\alpha\beta\gamma\delta}c^+_{0,\alpha}c^+_{0,\beta}c_{1,\delta}c_{1,\gamma}\hat{P}^{\tau_n}\hat{P}^{\tau_p}|\Phi_1\rangle]\end{aligned} \tag{5.296}$$

Eq.(5.296) is then separated into a kinetic and a two-body contributions $\tilde{E}^{01}_{00}(t)$ and $\tilde{E}^{01}_{00}(v)$:

$$\boxed{\tilde{E}^{01}_{00} = \tilde{E}^{01}_{00}(t) + \tilde{E}^{01}_{00}(v)} \tag{5.297}$$

Kinetic part:

Writing explicitly the disctretized projection operators, the quantity $\tilde{E}^{01}_{00}(t)$ reads as follows:

$$\boxed{\tilde{E}^{01}_{00}(t) = \frac{1}{\sqrt{\langle\Phi_1|\tilde{\Phi}_1\rangle\langle\Phi_0|\tilde{\Phi}_0\rangle}}\sum_{\alpha\beta} t_{\alpha\beta}\sum_{\varphi_n}\sum_{\varphi_p}\frac{e^{2i\varphi_n\pi N_n}e^{2i\varphi_p\pi N_p}}{n_{\varphi_n}n_{\varphi_p}}\langle\Phi_0|c^+_{0,\alpha}c_{1,\beta}|\Phi_1(\varphi_n,\varphi_p)\rangle} \tag{5.298}$$

We make the local projected matrices $\rho^{01}(\varphi_\tau)$ appear:

$$\tilde{E}^{01}_{00}(t) = \frac{1}{\sqrt{\langle\Phi_1|\tilde{\Phi}_1\rangle\langle\Phi_0|\tilde{\Phi}_0\rangle}}\sum_{\alpha\beta} t_{\alpha\beta}\sum_{\varphi_n}\sum_{\varphi_p}\frac{e^{2i\varphi_n\pi N_n}e^{2i\varphi_p\pi N_p}}{n_{\varphi_n}n_{\varphi_p}}\langle\Phi_{0\bar{\tau}}|\Phi_{1\bar{\tau}}(\varphi_{\bar{\tau}})\rangle\rho^{01\tau}_{\beta\alpha}(\varphi_\tau) \tag{5.299}$$

We separate the sums related to the projections in Eq.(5.299):

$$\begin{aligned}\tilde{E}^{01}_{00}(t) = \frac{1}{\sqrt{\langle\Phi_1|\tilde{\Phi}_1\rangle\langle\Phi_0|\tilde{\Phi}_0\rangle}}\sum_{\alpha\beta} t_{\alpha\beta}\sum_{\varphi_\tau}&\frac{e^{2i\varphi_\tau\pi N_\tau}}{n_{\varphi_\tau}}\langle\Phi_{0\tau}|\Phi_{1\tau}(\varphi_\tau)\rangle\rho^{01\tau}_{\beta\alpha}(\varphi_\tau) \\ &\sum_{\varphi_{\bar{\tau}}}\frac{e^{2i\varphi_{\bar{\tau}}\pi N_{\bar{\tau}}}}{n_{\varphi_{\bar{\tau}}}}\langle\Phi_{0\bar{\tau}}|\Phi_{1\bar{\tau}}(\varphi_{\bar{\tau}})\rangle\end{aligned} \tag{5.300}$$

We identify the total projected overlap and the total projected transition density matrix $\tilde{\rho}^{01}$ in Eq.(5.300):

$$\tilde{E}^{01}_{00}(t) = \tilde{\mathcal{O}}^{01}_{00} \sum_{\alpha\beta} t_{\alpha\beta} \tilde{\rho}^{01\tau}_{\beta\alpha} \tag{5.301}$$

Finally, we use the time-reversal properties of Eq.(5.301) to write:

$$\boxed{\tilde{E}^{01}_{00}(t) = 2\tilde{\mathcal{O}}^{01}_{00} \sum_{\alpha\beta>} t_{\alpha\beta} \tilde{\rho}^{01\tau}_{\beta\alpha}} \tag{5.302}$$

To conclude, the following symmetry clearly holds:

$$\boxed{\tilde{E}^{01}_{00}(t) = \tilde{E}^{10}_{00}(t)} \tag{5.303}$$

Two-body part:

Using the disctretized form of the particle number projection operators, the two-body part $\tilde{E}^{01}_{00}(t)$ is written as:

$$\boxed{\begin{aligned}\tilde{E}^{01}_{00}(v) = & \frac{1}{4\sqrt{\langle\Phi_1|\tilde{\Phi}_1\rangle\langle\Phi_0|\tilde{\Phi}_0\rangle}} \sum_{\alpha\beta\gamma\delta} v^{(a)}_{\alpha\beta\gamma\delta} \sum_{\varphi_n} \sum_{\varphi_p} \\ & \frac{e^{2i\varphi_n\pi N_n} e^{2i\varphi_p\pi N_p}}{n_{\varphi_n} n_{\varphi_p}} \langle\Phi_0|c^+_{0,\alpha} c^+_{0,\beta} c_{1,\delta} c_{1,\gamma}|\Phi_1(\varphi_n,\varphi_p)\rangle\end{aligned}} \tag{5.304}$$

We develop Eq.(5.304) using the generalized Wick theorem:

$$\begin{aligned}\tilde{E}^{01}_{00}(v) = & \frac{1}{4\sqrt{\langle\Phi_1|\tilde{\Phi}_1\rangle\langle\Phi_0|\tilde{\Phi}_0\rangle}} \sum_{\alpha\beta\gamma\delta} v^{(a)}_{\alpha\beta\gamma\delta} \sum_{\varphi_n} \sum_{\varphi_p} \frac{e^{2i\varphi_n\pi N_n} e^{2i\varphi_p\pi N_p}}{n_{\varphi_n} n_{\varphi_p} \langle\Phi_0|\Phi_1(\varphi_n,\varphi_p)\rangle} \\ & [\langle\Phi_0|c^+_{0,\alpha} c^+_{0,\beta}|\Phi_1(\varphi_n,\varphi_p)\rangle\langle\Phi_0|c_{1,\delta} c_{1,\gamma}|\Phi_1(\varphi_n,\varphi_p)\rangle \\ & + 2\langle\Phi_0|c^+_{0,\alpha} c_{0,\gamma}|\Phi_1(\varphi_n,\varphi_p)\rangle\langle\Phi_0|c^+_{0,\beta} c_{1,\delta}|\Phi_1(\varphi_n,\varphi_p)\rangle]\end{aligned} \tag{5.305}$$

We separate Eq.(5.305) into a mean and pairing type contributions:

$$\begin{aligned}\tilde{E}^{01}_{00}(v) = & \frac{1}{4\sqrt{\langle\Phi_1|\tilde{\Phi}_1\rangle\langle\Phi_0|\tilde{\Phi}_0\rangle}} \sum_{\alpha\beta\gamma\delta} v^{(a)}_{\alpha\beta\gamma\delta} \sum_{\varphi_n} \sum_{\varphi_p} \frac{e^{2i\varphi_n\pi N_n} e^{2i\varphi_p\pi N_p}}{n_{\varphi_n} n_{\varphi_p} \langle\Phi_0|\Phi_1(\varphi_n,\varphi_p)\rangle} \\ & \langle\Phi_0|c^+_{0,\alpha} c^+_{0,\beta}|\Phi_1(\varphi_n,\varphi_p)\rangle\langle\Phi_0|c_{1,\delta} c_{1,\gamma}|\Phi_1(\varphi_n,\varphi_p)\rangle \\ & + \frac{1}{2\sqrt{\langle\Phi_1|\tilde{\Phi}_1\rangle\langle\Phi_0|\tilde{\Phi}_0\rangle}} \sum_{\alpha\beta\gamma\delta} v^{(a)}_{\alpha\beta\gamma\delta} \sum_{\varphi_n} \sum_{\varphi_p} \frac{e^{2i\varphi_n\pi N_n} e^{2i\varphi_p\pi N_p}}{n_{\varphi_n} n_{\varphi_p} \langle\Phi_0|\Phi_1(\varphi_n,\varphi_p)\rangle} \\ & \langle\Phi_0|c^+_{0,\alpha} c_{1,\gamma}|\Phi_1(\varphi_n,\varphi_p)\rangle\langle\Phi_0|c^+_{0,\beta} c_{1,\delta}|\Phi_1(\varphi_n,\varphi_p)\rangle\end{aligned} \tag{5.306}$$

We make the projected matrices $\kappa^{01}(\varphi_\tau)$, $\bar{\kappa}^{01}(\varphi_\tau)$, $\rho^{01}(\varphi_\tau)$ and $\tilde{\rho}^{01\tau}$ appear in Eq.(5.306):

$$\begin{aligned}\tilde{E}^{01}_{00}(v) = &-\frac{1}{\sqrt{\langle\Phi_1|\tilde{\Phi}_1\rangle\langle\Phi_0|\tilde{\Phi}_0\rangle}}\sum_{\alpha\beta\gamma\delta>} v^{(a)}_{\alpha\bar{\beta}\gamma\bar{\delta}}(-1)^{s_\beta - s_\delta}\sum_{\varphi_n}\sum_{\varphi_p}\frac{e^{2i\varphi_n\pi N_n}e^{2i\varphi_p\pi N_p}}{n_{\varphi_n}n_{\varphi_p}} \\ &\langle\Phi_0|\Phi_1(\varphi_n,\varphi_p)\rangle[\bar{\kappa}^{01\tau_n}_{\alpha\bar{\beta}}(\varphi_n)\kappa^{01\tau_n}_{\gamma\bar{\delta}}(\varphi_n) + \bar{\kappa}^{01\tau_p}_{\alpha\bar{\beta}}(\varphi_p)\kappa^{01\tau_p}_{\gamma\bar{\delta}}(\varphi_p)] \\ &+\frac{1}{2\sqrt{\langle\Phi_1|\tilde{\Phi}_1\rangle\langle\Phi_0|\tilde{\Phi}_0\rangle}}\sum_{\alpha\beta\gamma\delta} v^{(a)}_{\alpha\beta\gamma\delta}\sum_{\varphi_n}\sum_{\varphi_p}\frac{e^{2i\varphi_n\pi N_n}e^{2i\varphi_p\pi N_p}}{n_{\varphi_n}n_{\varphi_p}}\langle\Phi_0|\Phi_1(\varphi_n,\varphi_p)\rangle \\ &[\rho^{01\tau_n}_{\gamma\alpha}(\varphi_n)\rho^{01\tau_n}_{\delta\beta}(\varphi_n) + \rho^{01\tau_p}_{\gamma\alpha}(\varphi_p)\rho^{01\tau_p}_{\delta\beta}(\varphi_p) + \rho^{01\tau_n}_{\gamma\alpha}(\varphi_n)\rho^{01\tau_p}_{\delta\beta}(\varphi_p) + \rho^{01\tau_p}_{\gamma\alpha}(\varphi_p)\rho^{01\tau_n}_{\delta\beta}(\varphi_n)]\end{aligned} \tag{5.307}$$

We introduce the collective projected local fields $\bar{\Delta}^{(\tau\tau)}(\varphi_\tau)$ and $\bar{\Gamma}^{(\tau\tau)}(\varphi_\tau)$ as well as the projected total field $\tilde{\bar{\Gamma}}^{(\bar{\tau}\tau)}$:

$$\boxed{\bar{\Delta}^{(\tau\tau)}_{\alpha\bar{\beta}}(\varphi_\tau) = \sum_{\gamma\delta>}(-1)^{s_\beta - s_\delta}v^{(a)}_{\alpha\bar{\beta}\gamma\bar{\delta}}\kappa^{01\tau}_{\gamma\bar{\delta}}(\varphi_\tau)} \tag{5.308}$$

$$\boxed{\bar{\Gamma}^{(\tau\tau)}_{\alpha\gamma}(\varphi_\tau) = \sum_{\beta\delta} v^{(a)}_{\alpha\beta\gamma\delta}\rho^{01\tau}_{\delta\beta}(\varphi_\tau)} \tag{5.309}$$

$$\boxed{\tilde{\bar{\Gamma}}^{(\bar{\tau}\tau)}_{\alpha\gamma} = \sum_{\beta\delta} v^{(a)}_{\alpha\beta\gamma\delta}\tilde{\rho}^{01\tau}_{\delta\beta}} \tag{5.310}$$

Thanks to these fields, we finally write:

$$\boxed{\begin{aligned}\tilde{E}^{01}_{00}(v) = &-\sum_{\alpha\beta>}\frac{\tilde{\mathcal{O}}^{01\bar{\tau}}_{00}}{\sqrt{\langle\Phi_{1\tau}|\tilde{\Phi}_{1\tau}\rangle\langle\Phi_{0\tau}|\tilde{\Phi}_{0\tau}\rangle}}\sum_{\varphi_\tau}\frac{e^{2i\varphi_\tau\pi N_\tau}}{n_{\varphi_\tau}}\langle\Phi_{0\tau}|\Phi_{1\tau}(\varphi_\tau)\rangle\bar{\Delta}^{(\tau\tau)}_{\alpha\bar{\beta}}(\varphi_\tau)\bar{\kappa}^{01\tau}_{\alpha\bar{\beta}}(\varphi_\tau) \\ &+\sum_{\alpha\gamma>}\frac{\tilde{\mathcal{O}}^{01\bar{\tau}}_{00}}{\sqrt{\langle\Phi_{1\tau}|\tilde{\Phi}_{1\tau}\rangle\langle\Phi_{0\tau}|\tilde{\Phi}_{0\tau}\rangle}}\sum_{\varphi_\tau}\frac{e^{2i\varphi_\tau\pi N_\tau}}{n_{\varphi_\tau}}\langle\Phi_{0\tau}|\Phi_{1\tau}(\varphi_\tau)\rangle\bar{\Gamma}^{(\tau\tau)}_{\alpha\gamma}(\varphi_\tau)\rho^{01\tau}_{\gamma\alpha}(\varphi_\tau) \\ &+\tilde{\mathcal{O}}^{01}_{00}\sum_{\alpha\gamma>}\tilde{\bar{\Gamma}}^{(\bar{\tau}\tau)}_{\alpha\gamma}\tilde{\rho}^{01\tau}_{\gamma\alpha}\end{aligned}} \tag{5.311}$$

To conclude, we remark the following symmetry:

$$\boxed{\tilde{E}^{01}_{00}(v) = \tilde{E}^{10}_{00}(v)} \tag{5.312}$$

5.6.3 Projected 2-quasiparticle excited state off-diagonal kernels

This section aims to give expressions of the particle number projected Hamiltonian kernels involving 2-quasiparticle excited states. In the following, we derive the expressions of the three different kernels $\tilde{E}^{01}_{0i}$, $\tilde{E}^{01}_{j0}$ and $\tilde{E}^{01}_{ji}$ defined as follows:

$$\boxed{\begin{aligned}\tilde{E}^{01}_{0i} = \frac{1}{\sqrt{\langle\Phi^{(i)}_1|\tilde{\Phi}^{(i)}_1\rangle\langle\Phi_0|\tilde{\Phi}_0\rangle}}[&\sum_{\alpha\beta} t_{\alpha\beta}\langle\Phi_0|c^+_{0,\alpha}c_{1,\beta}\hat{P}^{\tau_n}\hat{P}^{\tau_p}\xi^+_{1,i}\bar{\xi}^+_{1,i}|\Phi_1\rangle \\ &+\frac{1}{4}\sum_{\alpha\beta\gamma\delta} v^{(a)}_{\alpha\beta\gamma\delta}\langle\Phi_0|c^+_{0,\alpha}c^+_{0,\beta}c_{1,\delta}c_{1,\gamma}\hat{P}^{\tau_n}\hat{P}^{\tau_p}\xi^+_{1,i}\bar{\xi}^+_{1,i}|\Phi_1\rangle]\end{aligned}} \tag{5.313}$$

$$\boxed{\begin{aligned}\tilde{E}^{01}_{j0} = \frac{1}{\sqrt{\langle\Phi^{(j)}_0|\tilde{\Phi}^{(j)}_0\rangle\langle\Phi_1|\tilde{\Phi}_1\rangle}}[&\sum_{\alpha\beta} t_{\alpha\beta}\langle\Phi_0|\bar{\xi}_{0,j}\xi_{0,j}c^+_{0,\alpha}c_{1,\beta}\hat{P}^{\tau_n}\hat{P}^{\tau_p}|\Phi_1\rangle \\ &+\frac{1}{4}\sum_{\alpha\beta\gamma\delta} v^{(a)}_{\alpha\beta\gamma\delta}\langle\Phi_0|\bar{\xi}_{0,j}\xi_{0,j}c^+_{0,\alpha}c^+_{0,\beta}c_{1,\delta}c_{1,\gamma}\hat{P}^{\tau_n}\hat{P}^{\tau_p}|\Phi_1\rangle]\end{aligned}} \tag{5.314}$$

$$\boxed{\begin{aligned}\tilde{E}^{01}_{ji} = \frac{1}{\sqrt{\langle\Phi^{(i)}_1|\tilde{\Phi}^{(i)}_1\rangle\langle\Phi^{(j)}_0|\tilde{\Phi}^{(j)}_0\rangle}}&\sum_{\alpha\beta} t_{\alpha\beta}\langle\Phi_0|\bar{\xi}_{0,j}\xi_{0,j}c^+_{0,\alpha}c_{1,\beta}\xi^+_{1,i}\bar{\xi}^+_{1,i}|\Phi_1\rangle \\ &+\frac{1}{4}\sum_{\alpha\beta\gamma\delta} v^{(a)}_{\alpha\beta\gamma\delta}\langle\Phi_0|\bar{\xi}_{0,j}\xi_{0,j}c^+_{0,\alpha}c^+_{0,\beta}c_{1,\delta}c_{1,\gamma}\xi^+_{1,i}\bar{\xi}^+_{1,i}|\Phi_1\rangle\end{aligned}} \tag{5.315}$$

All these three kernels are separated into a kinetic and a two-body parts:

$$\boxed{\tilde{E}^{01}_{0i} = \tilde{E}^{01}_{0i}(t) + \tilde{E}^{01}_{0i}(v)} \tag{5.316}$$

$$\boxed{\tilde{E}^{01}_{j0} = \tilde{E}^{01}_{j0}(t) + \tilde{E}^{01}_{j0}(v)} \tag{5.317}$$

$$\boxed{\tilde{E}^{01}_{ji} = \tilde{E}^{01}_{ji}(t) + \tilde{E}^{01}_{ji}(v)} \tag{5.318}$$

Kinetic part $\tilde{E}^{01}_{0i}(t)$:

We start by writing $\tilde{E}^{01}_{0i}(t)$ explicitly:

$$\boxed{\begin{aligned}\tilde{E}^{01}_{0i}(t) = \frac{1}{\sqrt{\langle\Phi^{(i)}_1|\tilde{\Phi}^{(i)}_1\rangle\langle\Phi_0|\tilde{\Phi}_0\rangle}}&\sum_{\alpha\beta} t_{\alpha\beta}\sum_{\varphi_n}\sum_{\varphi_p}\frac{e^{2i\varphi_n\pi N_n}e^{2i\varphi_p\pi N_p}}{n_{\varphi_n}n_{\varphi_p}} \\ &\langle\Phi_0|c^+_{0,\alpha}c_{1,\beta}\xi^+_{1,i}(\varphi_{\tau_i})\bar{\xi}^+_{1,i}(\varphi_{\tau_i})|\Phi_1(\varphi_n,\varphi_p)\rangle\end{aligned}} \tag{5.319}$$

We directly recognize the excited total projected transition density matrix $\tilde{\rho}^{01(0i)}$:

$$\tilde{E}^{01}_{0i}(t) = \frac{\langle\Phi_0|\tilde{\Phi}_1\rangle}{\sqrt{\langle\Phi_1|\tilde{\Phi}_1\rangle\langle\Phi_0|\tilde{\Phi}_0\rangle}}\sum_{\alpha\beta} t_{\alpha\beta}\tilde{\rho}^{01(0i)\tau}_{\beta\alpha} \tag{5.320}$$

We use the time-reversal properties of Eq.(5.320) to finally write:

$$\boxed{\tilde{E}^{01}_{0i}(t) = 2\tilde{\mathcal{O}}^{01}_{00} \sum_{\alpha\beta>} t_{\alpha\beta} \tilde{\rho}^{01(0i)\tau}_{\beta\alpha}} \tag{5.321}$$

Kinetic part $\tilde{E}^{01}_{j0}(t)$:

We start by writing $\tilde{E}^{01}_{j0}(t)$ explicitly:

$$\boxed{\begin{aligned}\tilde{E}^{01}_{j0}(t) = \frac{1}{\sqrt{\langle\Phi_1|\tilde{\Phi}_1\rangle\langle\Phi_0^{(j)}|\tilde{\Phi}_0^{(j)}\rangle}} \sum_{\alpha\beta} t_{\alpha\beta} \sum_{\varphi_n}\sum_{\varphi_p} \frac{e^{2i\varphi_n\pi N_n} e^{2i\varphi_p\pi N_p}}{n_{\varphi_n} n_{\varphi_p}} \\ \langle\Phi_0|\bar{\xi}_{0,j}\xi_{0,j} c^+_{0,\alpha} c_{1,\beta}|\Phi_1(\varphi_n,\varphi_p)\rangle\end{aligned}} \tag{5.322}$$

We directly recognize the excited total projected transition density matrix $\tilde{\rho}^{01(j0)}$:

$$\tilde{E}^{01}_{j0}(t) = \frac{\langle\Phi_0|\tilde{\Phi}_1\rangle}{\sqrt{\langle\Phi_1|\tilde{\Phi}_1\rangle\langle\Phi_0|\tilde{\Phi}_0\rangle}} \sum_{\alpha\beta} t_{\alpha\beta} \tilde{\rho}^{01(j0)\tau}_{\beta\alpha} \tag{5.323}$$

Using the time-reversal properties of Eq.(5.323) finally leads to:

$$\boxed{\tilde{E}^{01}_{j0}(t) = 2\tilde{\mathcal{O}}^{01}_{00} \sum_{\alpha\beta>} t_{\alpha\beta} \tilde{\rho}^{01(j0)\tau}_{\beta\alpha}} \tag{5.324}$$

To conclude, it is clear that the following symmetry holds:

$$\boxed{\tilde{E}^{01}_{0i}(t) = \tilde{E}^{10}_{i0}(t)} \tag{5.325}$$

Kinetic part $\tilde{E}^{01}_{ji}(t)$:

We start by writing $\tilde{E}^{01}_{ji}(t)$ explicitly:

$$\boxed{\begin{aligned}\tilde{E}^{01}_{ji}(t) = \frac{1}{\sqrt{\langle\Phi_1^{(i)}|\tilde{\Phi}_1^{(i)}\rangle\langle\Phi_0^{(j)}|\tilde{\Phi}_0^{(j)}\rangle}} \sum_{\alpha\beta} t_{\alpha\beta} \sum_{\varphi_n}\sum_{\varphi_p} \frac{e^{2i\varphi_n\pi N_n} e^{2i\varphi_p\pi N_p}}{n_{\varphi_n} n_{\varphi_p}} \\ \langle\Phi_0|\bar{\xi}_{0,j}\xi_{0,j} c^+_{0,\alpha} c_{1,\beta} \xi^+_{1,i}(\varphi_{\tau_i})\bar{\xi}^+_{1,i}(\varphi_{\tau_i})|\Phi_1(\varphi_n,\varphi_p)\rangle\end{aligned}} \tag{5.326}$$

We directly recognize the excited total projected transition density matrix $\tilde{\rho}^{01(ji)}$:

$$\tilde{E}^{01}_{ji}(t) = \frac{\langle\Phi_0|\tilde{\Phi}_1\rangle}{\sqrt{\langle\Phi_1|\tilde{\Phi}_1\rangle\langle\Phi_0|\tilde{\Phi}_0\rangle}} \sum_{\alpha\beta} t_{\alpha\beta} \tilde{\rho}^{01(ji)\tau}_{\beta\alpha} \tag{5.327}$$

We finally use the time-reversal properties of Eq.(5.327) to give the final expression of $\tilde{E}^{01}_{ji}(t)$:

$$\boxed{\tilde{E}^{01}_{ji}(t) = 2\tilde{\mathcal{O}}^{01}_{00}\sum_{\alpha\beta>} t_{\alpha\beta}\tilde{\rho}^{01(ji)\tau}_{\beta\alpha}} \tag{5.328}$$

To conclude, the following symmetry clearly holds:

$$\boxed{\tilde{E}^{01}_{ji}(t) = \tilde{E}^{10}_{ij}(t)} \tag{5.329}$$

Two-body part $\tilde{E}^{01}_{0i}(v)$:

We start by writing $\tilde{E}^{01}_{0i}(v)$ explicitly:

$$\boxed{\begin{aligned}\tilde{E}^{01}_{0i}(v) = \frac{1}{4\sqrt{\langle\Phi^{(i)}_1|\tilde{\Phi}^{(i)}_1\rangle\langle\Phi_0|\tilde{\Phi}_0\rangle}}\sum_{\alpha\beta\gamma\delta} v^{(a)}_{\alpha\beta\gamma\delta}\sum_{\varphi_n}\sum_{\varphi_p}\frac{e^{2i\varphi_n\pi N_n}e^{2i\varphi_p\pi N_p}}{n_{\varphi_n}n_{\varphi_p}} \\ \langle\Phi_0|c^+_{0,\alpha}c^+_{0,\beta}c_{1,\delta}c_{1,\gamma}\xi^+_{1,i}(\varphi_{\tau_i})\bar{\xi}^+_{1,i}(\varphi_{\tau_i})|\Phi_1(\varphi_n,\varphi_p)\rangle\end{aligned}} \tag{5.330}$$

We develop Eq.(5.330) using the Wick theorem and we make the projected matrices $T(\varphi_\tau)$, $Z(\varphi_\tau)$, $W(\varphi_\tau)$, $\kappa^{01}(\varphi_\tau)$, $\bar{\kappa}^{01}(\varphi_\tau)$ and $\rho^{01}(\varphi_\tau)$ appear:

$$\begin{aligned}\tilde{E}^{01}_{0i}(v) = \frac{1}{4\sqrt{\langle\Phi^{(i)}_1|\tilde{\Phi}^{(i)}_1\rangle\langle\Phi_0|\tilde{\Phi}_0\rangle}}\sum_{\alpha\beta\gamma\delta} v^{(a)}_{\alpha\beta\gamma\delta}\sum_{\varphi_n}\sum_{\varphi_p}\frac{e^{2i\varphi_n\pi N_n}e^{2i\varphi_p\pi N_p}}{n_{\varphi_n}n_{\varphi_p}}\langle\Phi_0|\Phi_1(\varphi_n,\varphi_p)\rangle \\ [2\rho^{01}_{\gamma\alpha}(\varphi_{\tau_{\gamma\alpha}})\rho^{01}_{\delta\beta}(\varphi_{\tau_{\delta\beta}})T_{i\bar{i}}(\varphi_{\tau_i}) + 8\rho^{01}_{\delta\beta}(\varphi_{\tau_{\delta\beta}})Z_{\alpha\bar{i}}(\varphi_{\tau_i})W_{\gamma i}(\varphi_{\tau_i}) \\ -(-1)^{s_\beta-s_\delta}\bar{\kappa}^{01}_{\alpha\bar{\beta}}(\varphi_{\tau_{\alpha\beta}})\kappa^{01}_{\gamma\bar{\delta}}(\varphi_{\tau_{\gamma\delta}})T_{i\bar{i}}(\varphi_{\tau_i}) + 2(-1)^{s_\beta-s_\delta}\kappa^{01}_{\gamma\bar{\delta}}(\varphi_{\tau_{\gamma\delta}})Z_{\alpha\bar{i}}(\varphi_{\tau_i})Z_{\beta\bar{i}}(\varphi_{\tau_i}) \\ +2(-1)^{s_\beta-s_\delta}\bar{\kappa}^{01}_{\alpha\bar{\beta}}(\varphi_{\tau_{\alpha\beta}})W_{\gamma i}(\varphi_{\tau_i})W_{\delta i}(\varphi_{\tau_i})]\end{aligned} \tag{5.331}$$

Now, we introduce the excited local projected field $\bar{\Delta}^{(i)}(WW)(\varphi_{\tau_i})$:

$$\boxed{\bar{\Delta}^{(i)}_{\alpha\bar{\beta}}(WW)(\varphi_{\tau_i}) = \sum_{\gamma\delta>}(-1)^{s_\beta-s_\delta}v^{(a)}_{\alpha\bar{\beta}\gamma\bar{\delta}}W_{\gamma i}(\varphi_{\tau_i})W_{\delta i}(\varphi_{\tau_i})} \tag{5.332}$$

We can finally write the two-body kernel part $\tilde{E}^{01}_{0i}(v)$ in its final form:

$$
\begin{aligned}
\tilde{E}^{01}_{0i}(v) = &\frac{2\tilde{\mathcal{O}}^{01\bar{\tau}_i}_{00}}{\sqrt{\langle\Phi^{(i)}_{1\tau_i}|\tilde{\Phi}^{(i)}_{1\tau_i}\rangle\langle\Phi_{0\tau_i}|\tilde{\Phi}_{0\tau_i}\rangle}}\sum_{\varphi_{\tau_i}}\frac{e^{2i\varphi_{\tau_i}\pi N_{\tau_i}}}{n_{\varphi_{\tau_i}}}\langle\Phi_{0\tau_i}|\Phi_{1\tau_i}(\varphi_{\tau_i})\rangle \\
&\sum_{\alpha\gamma>}\bar{\Gamma}^{(i)(\tau_i\tau_i)}_{\alpha\gamma}(\varphi_{\tau_i})Z_{\alpha\bar{i}}(\varphi_{\tau_i})W_{\gamma i}(\varphi_{\tau_i}) \\
+&\frac{2\tilde{\mathcal{O}}^{01\bar{\tau}_i}_{00}}{\sqrt{\langle\Phi^{(i)}_{1\tau_i}|\tilde{\Phi}^{(i)}_{1\tau_i}\rangle\langle\Phi_{0\tau_i}|\tilde{\Phi}_{0\tau_i}\rangle}}\sum_{\alpha\gamma>}\tilde{\bar{\Gamma}}^{(i)(\bar{\tau}_i\tau_i)}_{\alpha\gamma}\sum_{\varphi_{\tau_i}}\frac{e^{2i\varphi_{\tau_i}\pi N_{\tau_i}}}{n_{\varphi_{\tau_i}}}\langle\Phi_{0\tau_i}|\Phi_{1\tau_i}(\varphi_{\tau_i})\rangle Z_{\alpha\bar{i}}(\varphi_{\tau_i})W_{\gamma i}(\varphi_{\tau_i}) \\
+&\frac{\tilde{\mathcal{O}}^{01\bar{\tau}_i}_{00}}{\sqrt{\langle\Phi^{(i)}_{1\tau_i}|\tilde{\Phi}^{(i)}_{1\tau_i}\rangle\langle\Phi_{0\tau_i}|\tilde{\Phi}_{0\tau_i}\rangle}}\sum_{\varphi_{\tau_i}}\frac{e^{2i\varphi_{\tau_i}\pi N_{\tau_i}}}{n_{\varphi_{\tau_i}}}\langle\Phi_{0\tau_i}|\Phi_{1\tau_i}(\varphi_{\tau_i})\rangle T_{i\bar{i}}(\varphi_{\tau_i})\sum_{\alpha\gamma>}\bar{\Gamma}^{(i)(\tau_i\tau_i)}_{\alpha\gamma}(\varphi_{\tau_i})\rho^{01\tau_i}_{\gamma\alpha}(\varphi_{\tau_i}) \\
+&\frac{\tilde{\mathcal{O}}^{01\tau_i}_{0i}}{\sqrt{\langle\Phi_{1\bar{\tau}_i}|\tilde{\Phi}_{1\bar{\tau}_i}\rangle\langle\Phi_{0\bar{\tau}_i}|\tilde{\Phi}_{0\bar{\tau}_i}\rangle}}\sum_{\varphi_{\bar{\tau}_i}}\frac{e^{2i\varphi_{\bar{\tau}_i}\pi N_{\bar{\tau}_i}}}{n_{\varphi_{\bar{\tau}_i}}}\langle\Phi_{0\bar{\tau}_i}|\Phi_{1\bar{\tau}_i}(\varphi_{\bar{\tau}_i})\rangle\sum_{\alpha\gamma>}\bar{\Gamma}^{(i)(\bar{\tau}_i\bar{\tau}_i)}_{\alpha\gamma}(\varphi_{\bar{\tau}_i})\rho^{01\bar{\tau}_i}_{\gamma\alpha}(\varphi_{\bar{\tau}_i}) \\
+&\frac{2\tilde{\mathcal{O}}^{01\bar{\tau}_i}_{00}}{\sqrt{\langle\Phi^{(i)}_{1\tau_i}|\tilde{\Phi}^{(i)}_{1\tau_i}\rangle\langle\Phi_{0\tau_i}|\tilde{\Phi}_{0\tau_i}\rangle}}\sum_{\varphi_{\tau_i}}\frac{e^{2i\varphi_{\tau_i}\pi N_{\tau_i}}}{n_{\varphi_{\tau_i}}}\langle\Phi_{0\tau_i}|\Phi_{1\tau_i}(\varphi_{\tau_i})\rangle T_{i\bar{i}}(\varphi_{\tau_i})\sum_{\alpha\gamma>}\tilde{\bar{\Gamma}}^{(i)(\bar{\tau}_i\tau_i)}_{\alpha\gamma}\rho^{01\tau_i}_{\gamma\alpha}(\varphi_{\tau_i}) \\
+&\frac{\tilde{\mathcal{O}}^{01\bar{\tau}_i}_{00}}{\sqrt{\langle\Phi^{(i)}_{1\tau_i}|\tilde{\Phi}^{(i)}_{1\tau_i}\rangle\langle\Phi_{0\tau_i}|\tilde{\Phi}_{0\tau_i}\rangle}}\sum_{\varphi_{\tau_i}}\frac{e^{2i\varphi_{\tau_i}\pi N_{\tau_i}}}{n_{\varphi_{\tau_i}}}\langle\Phi_{0\tau_i}|\Phi_{1\tau_i}(\varphi_{\tau_i})\rangle\sum_{\alpha\beta>}\bar{\Delta}^{(i)}_{\alpha\bar{\beta}}(WW)(\varphi_{\tau_i})\bar{\kappa}^{01\tau_i}_{\alpha\bar{\beta}}(\varphi_{\tau_i}) \\
-&\frac{\tilde{\mathcal{O}}^{01\bar{\tau}_i}_{00}}{\sqrt{\langle\Phi^{(i)}_{1\tau_i}|\tilde{\Phi}^{(i)}_{1\tau_i}\rangle\langle\Phi_{0\tau_i}|\tilde{\Phi}_{0\tau_i}\rangle}}\sum_{\varphi_{\tau_i}}\frac{e^{2i\varphi_{\tau_i}\pi N_{\tau_i}}}{n_{\varphi_{\tau_i}}}\langle\Phi_{0\tau_i}|\Phi_{1\tau_i}(\varphi_{\tau_i})\rangle T_{i\bar{i}}(\varphi_{\tau_i})\sum_{\alpha\beta>}\bar{\Delta}^{(\tau_i\tau_i)}_{\alpha\bar{\beta}}(\varphi_{\tau_i})\bar{\kappa}^{01\tau_i}_{\alpha\bar{\beta}}(\varphi_{\tau_i}) \\
-&\frac{\tilde{\mathcal{O}}^{01\tau_i}_{0i}}{\sqrt{\langle\Phi_{1\bar{\tau}_i}|\tilde{\Phi}_{1\bar{\tau}_i}\rangle\langle\Phi_{0\bar{\tau}_i}|\tilde{\Phi}_{0\bar{\tau}_i}\rangle}}\sum_{\varphi_{\bar{\tau}_i}}\frac{e^{2i\varphi_{\bar{\tau}_i}\pi N_{\bar{\tau}_i}}}{n_{\varphi_{\bar{\tau}_i}}}\langle\Phi_{0\bar{\tau}_i}|\Phi_{1\bar{\tau}_i}(\varphi_{\bar{\tau}_i})\rangle\sum_{\alpha\beta>}\bar{\Delta}^{(\bar{\tau}_i\bar{\tau}_i)}_{\alpha\bar{\beta}}(\varphi_{\bar{\tau}_i})\bar{\kappa}^{01\bar{\tau}_i}_{\alpha\bar{\beta}}(\varphi_{\bar{\tau}_i}) \\
+&\frac{\tilde{\mathcal{O}}^{01\bar{\tau}_i}_{00}}{\sqrt{\langle\Phi^{(i)}_{1\tau_i}|\tilde{\Phi}^{(i)}_{1\tau_i}\rangle\langle\Phi_{0\tau_i}|\tilde{\Phi}_{0\tau_i}\rangle}}\sum_{\varphi_{\tau_i}}\frac{e^{2i\varphi_{\tau_i}\pi N_{\tau_i}}}{n_{\varphi_{\tau_i}}}\langle\Phi_{0\tau_i}|\Phi_{1\tau_i}(\varphi_{\tau_i})\rangle\sum_{\alpha\beta>}\bar{\Delta}^{(\tau_i\tau_i)}_{\alpha\bar{\beta}}(\varphi_{\tau_i})Z_{\alpha\bar{i}}(\varphi_{\tau_i})Z_{\beta\bar{i}}(\varphi_{\tau_i})
\end{aligned}
\tag{5.333}
$$

Two-body part $\tilde{E}^{01}_{j0}(v)$:

We start by writing $\tilde{E}^{01}_{j0}(v)$ explicitly:

$$
\begin{aligned}
\tilde{E}^{01}_{j0}(v) = &\frac{1}{4\sqrt{\langle\Phi^{(j)}_0|\tilde{\Phi}^{(j)}_0\rangle\langle\Phi_1|\tilde{\Phi}_1\rangle}}\sum_{\alpha\beta\gamma\delta}v^{(a)}_{\alpha\beta\gamma\delta}\sum_{\varphi_n}\sum_{\varphi_p}\frac{e^{2i\varphi_n\pi N_n}e^{2i\varphi_p\pi N_p}}{n_{\varphi_n}n_{\varphi_p}} \\
&\langle\Phi_0|\bar{\xi}_{0,j}\xi_{0,j}c^+_{0,\alpha}c^+_{0,\beta}c_{1,\delta}c_{1,\gamma}|\Phi_1(\varphi_n,\varphi_p)\rangle
\end{aligned}
\tag{5.334}
$$

We develop Eq.(5.334) using the Wick theorem and we make the projected matrices $Y(\varphi_\tau)$, $\bar{Z}(\varphi_\tau)$, $\bar{W}(\varphi_\tau)$, $\kappa^{01}(\varphi_\tau)$, $\bar{\kappa}^{01}(\varphi_\tau)$ and $\rho^{01}(\varphi_\tau)$ appear:

$$
\begin{aligned}
\tilde{E}^{01}_{j0}(v) = &\frac{1}{4\sqrt{\langle\Phi^{(j)}_0|\tilde{\Phi}^{(j)}_0\rangle\langle\Phi_1|\tilde{\Phi}_1\rangle}}\sum_{\alpha\beta\gamma\delta}v^{(a)}_{\alpha\beta\gamma\delta}\sum_{\varphi_n}\sum_{\varphi_p}\frac{e^{2i\varphi_n\pi N_n}e^{2i\varphi_p\pi N_p}}{n_{\varphi_n}n_{\varphi_p}}\langle\Phi_0|\Phi_1(\varphi_n,\varphi_p)\rangle[\\
&-2\rho^{01}_{\delta\beta}(\varphi_{\tau_{\delta\beta}})\rho^{01}_{\gamma\alpha}(\varphi_{\tau_{\gamma\alpha}})Y_{j\bar{j}}(\varphi_{\tau_j}) - 8\rho^{01}_{\delta\beta}(\varphi_{\tau_{\delta\beta}})\bar{W}_{j\alpha}(\varphi_{\tau_j})\bar{Z}_{j\bar{\gamma}}(\varphi_{\tau_j}) \\
&+(-1)^{s_\beta-s_\delta}\bar{\kappa}^{01}_{\alpha\bar{\beta}}(\varphi_{\tau_{\alpha\beta}})\kappa^{01}_{\gamma\bar{\delta}}(\varphi_{\tau_{\gamma\delta}})Y_{j\bar{j}}(\varphi_{\tau_j}) - 2(-1)^{s_\beta-s_\delta}\kappa^{01}_{\gamma\bar{\delta}}(\varphi_{\tau_{\gamma\delta}})\bar{W}_{j\alpha}(\varphi_{\tau_j})\bar{W}_{j\beta}(\varphi_{\tau_j}) \\
&-2\bar{\kappa}^{01}_{\alpha\bar{\beta}}(\varphi_{\tau_{\alpha\beta}})\bar{Z}_{j\bar{\gamma}}(\varphi_{\tau_j})\bar{Z}_{j\bar{\delta}}(\varphi_{\tau_j})]
\end{aligned}
\tag{5.335}
$$

We introduce the excited local projected field $\bar{\Delta}^{(j)}(\bar{Z}\bar{Z})(\varphi_{\tau_j})$:

$$\boxed{\bar{\Delta}^{(j)}_{\alpha\bar{\beta}}(\bar{Z}\bar{Z})(\varphi_{\tau_j}) = \sum_{\gamma\delta>}(-1)^{s_\beta - s_\delta} v^{(a)}_{\alpha\bar{\beta}\gamma\bar{\delta}} \bar{Z}_{j\bar{\gamma}}(\varphi_{\tau_j})\bar{Z}_{j\bar{\delta}}(\varphi_{\tau_j})} \tag{5.336}$$

Now, we can write the final expression of $\tilde{E}^{01}_{j0}(v)$:

$$\begin{aligned}
\tilde{E}^{01}_{j0}(v) = &-\frac{2\tilde{\mathcal{O}}^{01\bar{\tau}_j}_{00}}{\sqrt{\langle\Phi^{(j)}_{0\tau_j}|\tilde{\Phi}^{(j)}_{0\tau_j}\rangle\langle\Phi_{1\tau_j}|\tilde{\Phi}_{1\tau_j}\rangle}}\sum_{\varphi_{\tau_j}}\frac{e^{2i\varphi_{\tau_j}\pi N_{\tau_j}}}{n_{\varphi_{\tau_j}}}\langle\Phi_{0\tau_j}|\Phi_{1\tau_j}(\varphi_{\tau_j})\rangle \\
&\sum_{\alpha\gamma>}\bar{\Gamma}^{(j)(\tau_j\tau_j)}_{\alpha\gamma}(\varphi_{\tau_j})\bar{W}_{j\alpha}(\varphi_{\tau_j})\bar{Z}_{j\bar{\gamma}}(\varphi_{\tau_j}) \\
&-\frac{2\tilde{\mathcal{O}}^{01\bar{\tau}_j}_{00}}{\sqrt{\langle\Phi^{(j)}_{0\tau_j}|\tilde{\Phi}^{(j)}_{0\tau_j}\rangle\langle\Phi_{1\tau_j}|\tilde{\Phi}_{1\tau_j}\rangle}}\sum_{\alpha\gamma>}\tilde{\bar{\Gamma}}^{(j)(\bar{\tau}_j\tau_j)}_{\alpha\gamma}\sum_{\varphi_{\tau_j}}\frac{e^{2i\varphi_{\tau_j}\pi N_{\tau_j}}}{n_{\varphi_{\tau_j}}}\langle\Phi_{0\tau_j}|\Phi_{1\tau_j}(\varphi_{\tau_j})\rangle\bar{W}_{j\alpha}(\varphi_{\tau_j})\bar{Z}_{j\bar{\gamma}}(\varphi_{\tau_j}) \\
&-\frac{\tilde{\mathcal{O}}^{01\bar{\tau}_j}_{00}}{\sqrt{\langle\Phi^{(j)}_{0\tau_j}|\tilde{\Phi}^{(j)}_{0\tau_j}\rangle\langle\Phi_{1\tau_j}|\tilde{\Phi}_{1\tau_j}\rangle}}\sum_{\varphi_{\tau_j}}\frac{e^{2i\varphi_{\tau_j}\pi N_{\tau_j}}}{n_{\varphi_{\tau_j}}}\langle\Phi_{0\tau_j}|\Phi_{1\tau_j}(\varphi_{\tau_j})\rangle Y_{j\bar{j}}(\varphi_{\tau_j})\sum_{\alpha\gamma>}\bar{\Gamma}^{(j)(\tau_j\tau_j)}_{\alpha\gamma}(\varphi_{\tau_j})\rho^{01\tau_j}_{\gamma\alpha}(\varphi_{\tau_j}) \\
&-\frac{\tilde{\mathcal{O}}^{01\tau_j}_{j0}}{\sqrt{\langle\Phi_{1\bar{\tau}_j}|\tilde{\Phi}_{1\bar{\tau}_j}\rangle\langle\Phi_{0\bar{\tau}_j}|\tilde{\Phi}_{0\bar{\tau}_j}\rangle}}\sum_{\varphi_{\bar{\tau}_j}}\frac{e^{2i\varphi_{\bar{\tau}_j}\pi N_{\bar{\tau}_j}}}{n_{\varphi_{\bar{\tau}_j}}}\langle\Phi_{0\bar{\tau}_j}|\Phi_{1\bar{\tau}_j}(\varphi_{\bar{\tau}_j})\rangle\sum_{\alpha\gamma>}\bar{\Gamma}^{(j)(\bar{\tau}_j\tau_j)}_{\alpha\gamma}(\varphi_{\bar{\tau}_j})\rho^{01\bar{\tau}_j}_{\gamma\alpha}(\varphi_{\bar{\tau}_j}) \\
&-\frac{2\tilde{\mathcal{O}}^{01\bar{\tau}_j}_{00}}{\sqrt{\langle\Phi^{(j)}_{0\tau_j}|\tilde{\Phi}^{(j)}_{0\tau_j}\rangle\langle\Phi_{1\tau_j}|\tilde{\Phi}_{1\tau_j}\rangle}}\sum_{\varphi_{\tau_j}}\frac{e^{2i\varphi_{\tau_j}\pi N_{\tau_j}}}{n_{\varphi_{\tau_j}}}\langle\Phi_{0\tau_j}|\Phi_{1\tau_j}(\varphi_{\tau_j})\rangle Y_{j\bar{j}}(\varphi_{\tau_j})\sum_{\alpha\gamma>}\tilde{\bar{\Gamma}}^{(j)(\bar{\tau}_j\tau_j)}_{\alpha\gamma}\rho^{01\tau_j}_{\gamma\alpha}(\varphi_{\tau_j}) \\
&-\frac{\tilde{\mathcal{O}}^{01\bar{\tau}_j}_{00}}{\sqrt{\langle\Phi^{(j)}_{0\tau_j}|\tilde{\Phi}^{(j)}_{0\tau_j}\rangle\langle\Phi_{1\tau_j}|\tilde{\Phi}_{1\tau_j}\rangle}}\sum_{\varphi_{\tau_j}}\frac{e^{2i\varphi_{\tau_j}\pi N_{\tau_j}}}{n_{\varphi_{\tau_j}}}\langle\Phi_{0\tau_j}|\Phi_{1\tau_j}(\varphi_{\tau_j})\rangle\sum_{\alpha\beta>}\bar{\Delta}^{(j)}_{\alpha\bar{\beta}}(\bar{Z}\bar{Z})(\varphi_{\tau_j})\bar{\kappa}^{01\tau_j}_{\alpha\bar{\beta}}(\varphi_{\tau_j}) \\
&+\frac{\tilde{\mathcal{O}}^{01\bar{\tau}_j}_{00}}{\sqrt{\langle\Phi^{(j)}_{0\tau_j}|\tilde{\Phi}^{(j)}_{0\tau_j}\rangle\langle\Phi_{1\tau_j}|\tilde{\Phi}_{1\tau_j}\rangle}}\sum_{\varphi_{\tau_j}}\frac{e^{2i\varphi_{\tau_j}\pi N_{\tau_j}}}{n_{\varphi_{\tau_j}}}\langle\Phi_{0\tau_j}|\Phi_{1\tau_j}(\varphi_{\tau_j})\rangle Y_{j\bar{j}}(\varphi_{\tau_j})\sum_{\alpha\beta>}\bar{\Delta}^{(\tau_j\tau_j)}_{\alpha\bar{\beta}}(\varphi_{\tau_j})\bar{\kappa}^{01\tau_j}_{\alpha\bar{\beta}}(\varphi_{\tau_j}) \\
&+\frac{\tilde{\mathcal{O}}^{01\tau_j}_{j0}}{\sqrt{\langle\Phi_{1\bar{\tau}_j}|\tilde{\Phi}_{1\bar{\tau}_j}\rangle\langle\Phi_{0\bar{\tau}_j}|\tilde{\Phi}_{0\bar{\tau}_j}\rangle}}\sum_{\varphi_{\bar{\tau}_j}}\frac{e^{2i\varphi_{\bar{\tau}_j}\pi N_{\bar{\tau}_j}}}{n_{\varphi_{\bar{\tau}_j}}}\langle\Phi_{0\bar{\tau}_j}|\Phi_{1\bar{\tau}_j}(\varphi_{\bar{\tau}_j})\rangle\sum_{\alpha\beta>}\bar{\Delta}^{(\bar{\tau}_j\bar{\tau}_j)}_{\alpha\bar{\beta}}(\varphi_{\bar{\tau}_j})\bar{\kappa}^{01\bar{\tau}_j}_{\alpha\bar{\beta}}(\varphi_{\bar{\tau}_j}) \\
&-\frac{\tilde{\mathcal{O}}^{01\bar{\tau}_j}_{00}}{\sqrt{\langle\Phi^{(j)}_{0\tau_j}|\tilde{\Phi}^{(j)}_{0\tau_j}\rangle\langle\Phi_{1\tau_j}|\tilde{\Phi}_{1\tau_j}\rangle}}\sum_{\varphi_{\tau_j}}\frac{e^{2i\varphi_{\tau_j}\pi N_{\tau_i}}}{n_{\varphi_{\tau_j}}}\langle\Phi_{0\tau_j}|\Phi_{1\tau_j}(\varphi_{\tau_j})\rangle\sum_{\alpha\beta>}\bar{\Delta}^{(\tau_j\tau_j)}_{\alpha\bar{\beta}}(\varphi_{\tau_j})\bar{W}_{j\alpha}(\varphi_{\tau_j})\bar{W}_{j\gamma}(\varphi_{\tau_j})
\end{aligned} \tag{5.337}$$

To conclude, it's clear that the following symmetry holds:

$$\boxed{\tilde{E}^{01}_{j0}(v) = \tilde{E}^{10}_{0j}(v)} \tag{5.338}$$

Two-body part $\tilde{E}^{01}_{ji}(v)$:

We start by writing $\tilde{E}^{01}_{j0}(v)$ explicitly:

$$\begin{aligned}
\boxed{\tilde{E}^{01}_{ji}(v) = &\frac{1}{4\sqrt{\langle\Phi^{(j)}_0|\tilde{\Phi}^{(j)}_0\rangle\langle\Phi^{(i)}_1|\tilde{\Phi}^{(i)}_1\rangle}}\sum_{\alpha\beta\gamma\delta}v^{(a)}_{\alpha\beta\gamma\delta}\sum_{\varphi_n}\sum_{\varphi_p}\frac{e^{2i\varphi_n\pi N_n}e^{2i\varphi_p\pi N_p}}{n_{\varphi_n}n_{\varphi_p}} \\
&\langle\Phi_0|\bar{\xi}_{0,j}\xi_{0,j}c^+_{0,\alpha}c^+_{0,\beta}c_{1,\delta}c_{1,\gamma}\xi^+_{1,i}(\varphi_{\tau_i})\bar{\xi}^+_{1,i}(\varphi_{\tau_i})|\Phi_1(\varphi_n,\varphi_p)\rangle}
\end{aligned} \tag{5.339}$$

The development of Eq.(5.339) gives rise to a monstruous number of terms. To simplify the expressions as much as possible, we consider separately different cases with respect to τ_i, τ_j, Ω_i, and Ω_j. We first tackle the case $\underline{\tau_i = \tau_j \text{ and } \Omega_i = \Omega_j}$:

$$
\begin{aligned}
\tilde{E}^{01}_{ji}(v) = \frac{\tilde{\mathcal{O}}^{01\tau_i}_{ji}}{\sqrt{\langle\Phi^{(j)}_{0\bar{\tau}_i}|\tilde{\Phi}^{(j)}_{0\bar{\tau}_i}\rangle\langle\Phi^{(i)}_{1\bar{\tau}_i}|\tilde{\Phi}^{(i)}_{1\bar{\tau}_i}\rangle}}[&\sum_{\varphi_{\bar{\tau}_i}}\frac{e^{2i\varphi_{\bar{\tau}_i}\pi N_{\bar{\tau}_i}}}{n_{\varphi_{\bar{\tau}_i}}}\langle\Phi_{0\bar{\tau}_i}|\Phi_{1\bar{\tau}_i}(\varphi_{\bar{\tau}_i})\rangle\sum_{\alpha\beta>}\bar{\Gamma}^{(ji)(\bar{\tau}_i\bar{\tau}_i)}_{\alpha\gamma}(\varphi_{\bar{\tau}_i})\rho^{01\bar{\tau}_i}_{\gamma\alpha}(\varphi_{\bar{\tau}_i})\\
&-\sum_{\varphi_{\bar{\tau}_i}}\frac{e^{2i\varphi_{\bar{\tau}_i}\pi N_{\bar{\tau}_i}}}{n_{\varphi_{\bar{\tau}_i}}}\langle\Phi_{0\bar{\tau}_i}|\Phi_{1\bar{\tau}_i}(\varphi_{\bar{\tau}_i})\rangle\sum_{\alpha\beta>}\bar{\Delta}^{(\bar{\tau}_i\bar{\tau}_i)}_{\alpha\bar{\beta}}(\varphi_{\bar{\tau}_i})\bar{\kappa}^{01\bar{\tau}_i}_{\alpha\bar{\beta}}(\varphi_{\bar{\tau}_i})]\\
+\frac{\tilde{\mathcal{O}}^{01\bar{\tau}_i}_{00}}{\sqrt{\langle\Phi^{(j)}_{0\tau_i}|\tilde{\Phi}^{(j)}_{0\tau i}\rangle\langle\Phi^{(i)}_{1\tau_i}|\tilde{\Phi}^{(i)}_{1\tau_i}\rangle}}[&\sum_{\alpha\gamma>}\tilde{\bar{\Gamma}}^{(ji)(\bar{\tau}_i\tau_i)}_{\alpha\gamma}\sum_{\varphi_{\tau_i}}\frac{e^{2i\varphi_{\tau_i}\pi N_{\tau_i}}}{n_{\varphi_{\tau_i}}}\langle\Phi_{0\tau_i}|\Phi_{1\tau_i}(\varphi_{\tau_i})\rangle\\
[2S_{ji}(\varphi_{\tau_i})[\bar{W}_{j\alpha}(\varphi_{\tau_i})W_{\gamma i}(\varphi_{\tau_i})+Z_{\alpha\bar{i}}(\varphi_{\tau_i})\bar{Z}_{j\bar{\gamma}}(\varphi_{\tau_i})]-2Y_{j\bar{j}}(\varphi_{\tau_i})Z_{\alpha\bar{i}}(\varphi_{\tau_i})W_{\gamma i}(\varphi_{\tau_i})\\
-2T_{i\bar{i}}(\varphi_{\tau_i})\bar{W}_{j\alpha}(\varphi_{\tau_i})\bar{Z}_{j\bar{\gamma}}(\varphi_{\tau_i})+2[S_{ji}(\varphi_{\tau_i})S_{ji}(\varphi_{\tau_i})-T_{i\bar{i}}(\varphi_{\tau_i})Y_{j\bar{j}}(\varphi_{\tau_i})]\rho^{01\tau_i}_{\gamma\alpha}(\varphi_{\tau_i})]\\
&+\sum_{\varphi_{\tau_i}}\frac{e^{2i\varphi_{\tau_i}\pi N_{\tau_i}}}{n_{\varphi_{\tau_i}}}\langle\Phi_{0\tau_i}|\Phi_{1\tau_i}(\varphi_{\tau_i})\rangle[[S_{ji}(\varphi_{\tau_i})S_{ji}(\varphi_{\tau_i})\\
&-T_{i\bar{i}}(\varphi_{\tau_i})Y_{j\bar{j}}(\varphi_{\tau_i})]\sum_{\alpha\gamma>}\bar{\Gamma}^{(ji)(\tau_i\tau_i)}_{\alpha\gamma}(\varphi_{\tau_i})\rho^{01\tau_i}_{\gamma\alpha}(\varphi_{\tau_i})\\
&-2T_{i\bar{i}}(\varphi_{\tau_i})\sum_{\alpha\gamma>}\bar{\Gamma}^{(ji)(\tau_i\tau_i)}_{\alpha\gamma}(\varphi_{\tau_i})\bar{W}_{j\alpha}(\varphi_{\tau_i})\bar{Z}_{j\bar{\gamma}}(\varphi_{\tau_i})\\
&-2Y_{j\bar{j}}(\varphi_{\tau_i})\sum_{\alpha\gamma>}\bar{\Gamma}^{(ji)(\tau_i\tau_i)}_{\alpha\gamma}(\varphi_{\tau_i})Z_{\alpha\bar{i}}(\varphi_{\tau_i})W_{\gamma i}(\varphi_{\tau_i})\\
&+2S_{ji}(\varphi_{\tau_i})\sum_{\alpha\gamma>}\bar{\Gamma}^{(ji)(\tau_i\tau_i)}_{\alpha\gamma}(\varphi_{\tau_i})[\bar{W}_{j\alpha}(\varphi_{\tau_i})W_{\gamma i}(\varphi_{\tau_i})+Z_{\alpha\bar{i}}(\varphi_{\tau_i})\bar{Z}_{j\bar{\gamma}}(\varphi_{\tau_i})]]\\
&+\sum_{\varphi_{\tau_i}}\frac{e^{2i\varphi_{\tau_i}\pi N_{\tau_i}}}{n_{\varphi_{\tau_i}}}\langle\Phi_{0\tau_i}|\Phi_{1\tau_i}(\varphi_{\tau_i})\rangle[[T_{i\bar{i}}(\varphi_{\tau_i})Y_{j\bar{j}}(\varphi_{\tau_i})\\
&-S_{ji}(\varphi_{\tau_i})S_{ji}(\varphi_{\tau_i})]\sum_{\alpha\beta>}\bar{\Delta}^{(\tau_i\tau_i)}_{\alpha\bar{\beta}}(\varphi_{\tau_i})\bar{\kappa}^{01\tau_i}_{\alpha\bar{\beta}}(\varphi_{\tau_i})\\
&-T_{i\bar{i}}(\varphi_{\tau_i})\sum_{\alpha\beta>}\bar{\Delta}^{(\tau_i\tau_i)}_{\alpha\bar{\beta}}(\varphi_{\tau_i})\bar{W}_{j\alpha}(\varphi_{\tau_i})\bar{W}_{j\beta}(\varphi_{\tau_i})\\
&-Y_{j\bar{j}}(\varphi_{\tau_i})\sum_{\alpha\beta>}\bar{\Delta}^{(\tau_i\tau_i)}_{\alpha\bar{\beta}}(\varphi_{\tau_i})Z_{\alpha\bar{i}}(\varphi_{\tau_i})Z_{\beta\bar{i}}(\varphi_{\tau_i})\\
&+2S_{ji}(\varphi_{\tau_i})\sum_{\alpha\beta>}\bar{\Delta}^{(\tau_i\tau_i)}_{\alpha\bar{\beta}}(\varphi_{\tau_i})\bar{W}_{j\alpha}(\varphi_{\tau_i})Z_{\beta\bar{i}}(\varphi_{\tau_i})]\\
&+\sum_{\varphi_{\tau_i}}\frac{e^{2i\varphi_{\tau_i}\pi N_{\tau_i}}}{n_{\varphi_{\tau_i}}}\langle\Phi_{0\tau_i}|\Phi_{1\tau_i}(\varphi_{\tau_i})\rangle[\sum_{\alpha\beta>}\bar{\Delta}^{(j)}_{\alpha\bar{\beta}}(\bar{Z}\bar{Z})(\varphi_{\tau_i})Z_{\alpha\bar{i}}(\varphi_{\tau_i})Z_{\beta\bar{i}}(\varphi_{\tau_i})\\
&-T_{i\bar{i}}(\varphi_{\tau_i})\sum_{\alpha\beta>}\bar{\Delta}^{(j)}_{\alpha\bar{\beta}}(\bar{Z}\bar{Z})(\varphi_{\tau_i})\bar{\kappa}^{01\tau_i}_{\alpha\bar{\beta}}(\varphi_{\tau_i})]\\
&+\sum_{\varphi_{\tau_i}}\frac{e^{2i\varphi_{\tau_i}\pi N_{\tau_i}}}{n_{\varphi_{\tau_i}}}\langle\Phi_{0\tau_i}|\Phi_{1\tau_i}(\varphi_{\tau_i})\rangle[\sum_{\alpha\beta>}\bar{\Delta}^{(i)}_{\alpha\bar{\beta}}(WW)(\varphi_{\tau_i})\bar{W}_{j\alpha}(\varphi_{\tau_i})\bar{W}_{j\beta}(\varphi_{\tau_i})\\
&-Y_{j\bar{j}}(\varphi_{\tau_i})\sum_{\alpha\beta>}\bar{\Delta}^{(i)}_{\alpha\bar{\beta}}(WW)(\varphi_{\tau_i})\bar{\kappa}^{01\tau_i}_{\alpha\bar{\beta}}(\varphi_{\tau_i})]\\
&+\sum_{\varphi_{\tau_i}}\frac{e^{2i\varphi_{\tau_i}\pi N_{\tau_i}}}{n_{\varphi_{\tau_i}}}\langle\Phi_{0\tau_i}|\Phi_{1\tau_i}(\varphi_{\tau_i})\rangle S_{ji}(\varphi_{\tau_i})\sum_{\alpha\beta>}\bar{\Delta}^{(ji)}_{\alpha\bar{\beta}}([W,\bar{Z}])(\varphi_{\tau_i})\bar{\kappa}^{01\tau_i}_{\alpha\bar{\beta}}(\varphi_{\tau_i})\\
&-2\sum_{\varphi_{\tau_i}}\frac{e^{2i\varphi_{\tau_i}\pi N_{\tau_i}}}{n_{\varphi_{\tau_i}}}\langle\Phi_{0\tau_i}|\Phi_{1\tau_i}(\varphi_{\tau_i})\rangle\sum_{\alpha\gamma>}\bar{\Gamma}^{(ji)}_{\alpha\gamma}([W,Z])(\varphi_{\tau_i})\bar{W}_{j\alpha}(\varphi_{\tau_i})\bar{Z}_{j\bar{\gamma}}(\varphi_{\tau_i})]
\end{aligned}
\tag{5.340}
$$

In Eq.(5.340), we've introduced the two projected excited fields and, defined as follows:

$$\boxed{\bar{\Delta}^{(ji)}_{\alpha\bar{\beta}}([W,\bar{Z}])(\varphi_{\tau_i}) = \sum_{\gamma\delta>}(-1)^{s_\beta - s_\delta} v^{(a)}_{\alpha\bar{\beta}\gamma\bar{\delta}}[W_{\gamma i}(\varphi_{\tau_i})\bar{Z}_{j\bar{\delta}}(\varphi_{\tau_i}) + \bar{Z}_{j\bar{\gamma}}(\varphi_{\tau_i})W_{\delta i}(\varphi_{\tau_i})]} \tag{5.341}$$

$$\boxed{\bar{\Gamma}^{(ji)}_{\alpha\gamma}([W,Z])(\varphi_{\tau_i}) = \sum_{\beta\delta>}[v^{(a)}_{\alpha\beta\gamma\delta} + (-1)^{s_\beta - s_\delta} v^{(a)}_{\alpha\bar{\beta}\gamma\bar{\delta}}]W_{\delta i}(\varphi_{\tau_i})Z_{\beta\bar{i}}(\varphi_{\tau_i})} \tag{5.342}$$

Now, we consider the case $\underline{\tau_i = \tau_j \text{ and } \Omega_i \neq \Omega_j}$:

$$\begin{aligned}
\tilde{E}^{01}_{ji}(v) = \frac{\tilde{\mathcal{O}}^{01\tau_i}_{ji}}{\sqrt{\langle\Phi^{(j)}_{0\bar{\tau}_i}|\tilde{\Phi}^{(j)}_{0\bar{\tau}_i}\rangle\langle\Phi^{(i)}_{1\bar{\tau}_i}|\tilde{\Phi}^{(i)}_{1\bar{\tau}_i}\rangle}}&[\sum_{\varphi_{\bar{\tau}_i}}\frac{e^{2i\varphi_{\bar{\tau}_i}\pi N_{\bar{\tau}_i}}}{n_{\varphi_{\bar{\tau}_i}}}\langle\Phi_{0\bar{\tau}_i}|\Phi_{1\bar{\tau}_i}(\varphi_{\bar{\tau}_i})\rangle\sum_{\alpha\beta>}\bar{\Gamma}^{(ji)(\bar{\tau}_i\bar{\tau}_i)}_{\alpha\gamma}(\varphi_{\bar{\tau}_i})\rho^{01\bar{\tau}_i}_{\gamma\alpha}(\varphi_{\bar{\tau}_i})\\
&-\sum_{\varphi_{\bar{\tau}_i}}\frac{e^{2i\varphi_{\bar{\tau}_i}\pi N_{\bar{\tau}_i}}}{n_{\varphi_{\bar{\tau}_i}}}\langle\Phi_{0\bar{\tau}_i}|\Phi_{1\bar{\tau}_i}(\varphi_{\bar{\tau}_i})\rangle\sum_{\alpha\beta>}\bar{\Delta}^{(\bar{\tau}_i\bar{\tau}_i)}_{\alpha\bar{\beta}}(\varphi_{\bar{\tau}_i})\bar{\kappa}^{01\bar{\tau}_i}_{\alpha\bar{\beta}}(\varphi_{\bar{\tau}_i})]\\
&+\frac{\tilde{\mathcal{O}}^{01\bar{\tau}_i}_{00}}{\sqrt{\langle\Phi^{(j)}_{0\tau_i}|\tilde{\Phi}^{(j)}_{0\tau i}\rangle\langle\Phi^{(i)}_{1\tau_i}|\tilde{\Phi}^{(i)}_{1\tau_i}\rangle}}[\sum_{\alpha\gamma>}\tilde{\bar{\Gamma}}^{(ji)(\bar{\tau}_i\tau_i)}_{\alpha\gamma}\sum_{\varphi_{\tau_i}}\frac{e^{2i\varphi_{\tau_i}\pi N_{\tau_i}}}{n_{\varphi_{\tau_i}}}\langle\Phi_{0\tau_i}|\Phi_{1\tau_i}(\varphi_{\tau_i})\rangle\\
&[-2Y_{j\bar{j}}(\varphi_{\tau_i})Z_{\alpha\bar{i}}(\varphi_{\tau_i})W_{\gamma i}(\varphi_{\tau_i}) - 2T_{i\bar{i}}(\varphi_{\tau_i})\bar{W}_{j\alpha}(\varphi_{\tau_i})\bar{Z}_{j\bar{\gamma}}(\varphi_{\tau_i}) - 2T_{i\bar{i}}(\varphi_{\tau_i})Y_{j\bar{j}}(\varphi_{\tau_i})]\rho^{01\tau_i}_{\gamma\alpha}(\varphi_{\tau_i})]\\
&+\sum_{\varphi_{\tau_i}}\frac{e^{2i\varphi_{\tau_i}\pi N_{\tau_i}}}{n_{\varphi_{\tau_i}}}\langle\Phi_{0\tau_i}|\Phi_{1\tau_i}(\varphi_{\tau_i})\rangle[-T_{i\bar{i}}(\varphi_{\tau_i})Y_{j\bar{j}}(\varphi_{\tau_i})\sum_{\alpha\gamma>}\bar{\Gamma}^{(ji)(\tau_i\tau_i)}_{\alpha\gamma}(\varphi_{\tau_i})\rho^{01\tau_i}_{\gamma\alpha}(\varphi_{\tau_i})\\
&-2T_{i\bar{i}}(\varphi_{\tau_i})\sum_{\alpha\gamma>}\bar{\Gamma}^{(ji)(\tau_i\tau_i)}_{\alpha\gamma}(\varphi_{\tau_i})\bar{W}_{j\alpha}(\varphi_{\tau_i})\bar{Z}_{j\bar{\gamma}}(\varphi_{\tau_i})\\
&-2Y_{j\bar{j}}(\varphi_{\tau_i})\sum_{\alpha\gamma>}\bar{\Gamma}^{(ji)(\tau_i\tau_i)}_{\alpha\gamma}(\varphi_{\tau_i})Z_{\alpha\bar{i}}(\varphi_{\tau_i})W_{\gamma i}(\varphi_{\tau_i})]\\
&+\sum_{\varphi_{\tau_i}}\frac{e^{2i\varphi_{\tau_i}\pi N_{\tau_i}}}{n_{\varphi_{\tau_i}}}\langle\Phi_{0\tau_i}|\Phi_{1\tau_i}(\varphi_{\tau_i})\rangle[T_{i\bar{i}}(\varphi_{\tau_i})Y_{j\bar{j}}(\varphi_{\tau_i})\sum_{\alpha\beta>}\bar{\Delta}^{(\tau_i\tau_i)}_{\alpha\bar{\beta}}(\varphi_{\tau_i})\bar{\kappa}^{01\tau_i}_{\alpha\bar{\beta}}(\varphi_{\tau_i})\\
&-T_{i\bar{i}}(\varphi_{\tau_i})\sum_{\alpha\beta>}\bar{\Delta}^{(\tau_i\tau_i)}_{\alpha\bar{\beta}}(\varphi_{\tau_i})\bar{W}_{j\alpha}(\varphi_{\tau_i})\bar{W}_{j\beta}(\varphi_{\tau_i}) - Y_{j\bar{j}}(\varphi_{\tau_i})\sum_{\alpha\beta>}\bar{\Delta}^{(\tau_i\tau_i)}_{\alpha\bar{\beta}}(\varphi_{\tau_i})Z_{\alpha\bar{i}}(\varphi_{\tau_i})Z_{\beta\bar{i}}(\varphi_{\tau_i})]\\
&+\sum_{\varphi_{\tau_i}}\frac{e^{2i\varphi_{\tau_i}\pi N_{\tau_i}}}{n_{\varphi_{\tau_i}}}\langle\Phi_{0\tau_i}|\Phi_{1\tau_i}(\varphi_{\tau_i})\rangle[\sum_{\alpha\beta>}\bar{\Delta}^{(j)}_{\alpha\bar{\beta}}(\bar{Z}\bar{Z})(\varphi_{\tau_i})Z_{\alpha\bar{i}}(\varphi_{\tau_i})Z_{\beta\bar{i}}(\varphi_{\tau_i})\\
&-T_{i\bar{i}}(\varphi_{\tau_i})\sum_{\alpha\beta>}\bar{\Delta}^{(j)}_{\alpha\bar{\beta}}(\bar{Z}\bar{Z})(\varphi_{\tau_i})\bar{\kappa}^{01\tau_i}_{\alpha\bar{\beta}}(\varphi_{\tau_i})]\\
&+\sum_{\varphi_{\tau_i}}\frac{e^{2i\varphi_{\tau_i}\pi N_{\tau_i}}}{n_{\varphi_{\tau_i}}}\langle\Phi_{0\tau_i}|\Phi_{1\tau_i}(\varphi_{\tau_i})\rangle[\sum_{\alpha\beta>}\bar{\Delta}^{(i)}_{\alpha\bar{\beta}}(WW)(\varphi_{\tau_i})\bar{W}_{j\alpha}(\varphi_{\tau_i})\bar{W}_{j\beta}(\varphi_{\tau_i})\\
&-Y_{j\bar{j}}(\varphi_{\tau_i})\sum_{\alpha\beta>}\bar{\Delta}^{(i)}_{\alpha\bar{\beta}}(WW)(\varphi_{\tau_i})\bar{\kappa}^{01\tau_i}_{\alpha\bar{\beta}}(\varphi_{\tau_i})]\\
&-2\sum_{\varphi_{\tau_i}}\frac{e^{2i\varphi_{\tau_i}\pi N_{\tau_i}}}{n_{\varphi_{\tau_i}}}\langle\Phi_{0\tau_i}|\Phi_{1\tau_i}(\varphi_{\tau_i})\rangle\sum_{\alpha\gamma>}\bar{\Gamma}^{(ji)}_{\alpha\gamma}([W,Z])(\varphi_{\tau_i})\bar{W}_{j\alpha}(\varphi_{\tau_i})\bar{Z}_{j\bar{\gamma}}(\varphi_{\tau_i})]
\end{aligned} \tag{5.343}$$

Finally, we treat the case $\underline{\tau_i \neq \tau_j}$:

$$
\begin{aligned}
\tilde{E}^{01}_{ji}(v) = -2\frac{1}{\sqrt{\langle\Phi^{(j)}_0|\tilde{\Phi}^{(j)}_0\rangle\langle\Phi^{(i)}_1|\tilde{\Phi}^{(i)}_1\rangle}}\sum_{\alpha\gamma>}\sum_{\varphi_{\tau_j}}\frac{e^{2i\varphi_{\tau_j}\pi N_{\tau_j}}}{n_{\varphi_{\tau_j}}}\langle\Phi_{0\tau_j}|\Phi_{1\tau_j}(\varphi_{\tau_j})\rangle Y_{j\bar{j}}(\varphi_{\tau_j})\rho^{01\tau_j}_{\gamma\alpha}(\varphi_{\tau_j}) \\
\sum_{\varphi_{\tau_i}}\frac{e^{2i\varphi_{\tau_i}\pi N_{\tau_i}}}{n_{\varphi_{\tau_i}}}\langle\Phi_{0\tau_i}|\Phi_{1\tau_i}(\varphi_{\tau_i})\rangle\bar{\Gamma}^{(ji)(\tau_i\tau_i)}_{\alpha\gamma}(\varphi_{\tau_i})T_{i\bar{i}}(\varphi_{\tau_i}) \\
-\frac{\tilde{\mathcal{O}}^{01\tau_i}_{0i}}{\sqrt{\langle\Phi^{(j)}_{0\tau_j}|\tilde{\Phi}^{(j)}_{0\tau_j}\rangle\langle\Phi^{(i)}_{1\tau_j}|\tilde{\Phi}^{(i)}_{1\tau_j}\rangle}}\sum_{\varphi_{\tau_j}}\frac{e^{2i\varphi_{\tau_j}\pi N_{\tau_j}}}{n_{\varphi_{\tau_j}}}\langle\Phi_{0\tau_j}|\Phi_{1\tau_j}(\varphi_{\tau_j})\rangle Y_{j\bar{j}}(\varphi_{\tau_j})\sum_{\alpha\gamma>}\bar{\Gamma}^{(ji)(\tau_j\tau_j)}_{\alpha\gamma}(\varphi_{\tau_j})\rho^{01\tau_j}_{\gamma\alpha}(\varphi_{\tau_j}) \\
-\frac{\tilde{\mathcal{O}}^{01\tau_j}_{j0}}{\sqrt{\langle\Phi^{(j)}_{0\tau_i}|\tilde{\Phi}^{(j)}_{0\tau_i}\rangle\langle\Phi^{(i)}_{1\tau_i}|\tilde{\Phi}^{(i)}_{1\tau_i}\rangle}}\sum_{\varphi_{\tau_i}}\frac{e^{2i\varphi_{\tau_i}\pi N_{\tau_i}}}{n_{\varphi_{\tau_i}}}\langle\Phi_{0\tau_i}|\Phi_{1\tau_i}(\varphi_{\tau_i})\rangle T_{i\bar{i}}(\varphi_{\tau_i})\sum_{\alpha\gamma>}\bar{\Gamma}^{(ji)(\tau_i\tau_i)}_{\alpha\gamma}(\varphi_{\tau_i})\rho^{01\tau_i}_{\gamma\alpha}(\varphi_{\tau_i}) \\
-2\frac{1}{\sqrt{\langle\Phi^{(j)}_0|\tilde{\Phi}^{(j)}_0\rangle\langle 0\Phi^{(i)}_1|\tilde{\Phi}^{(i)}_1\rangle}}\sum_{\varphi_{\tau_j}}\frac{e^{2i\varphi_{\tau_j}\pi N_{\tau_j}}}{n_{\varphi_{\tau_j}}}\langle\Phi_{0\tau_j}|\Phi_{1\tau_j}(\varphi_{\tau_j})\rangle\bar{W}_{j\alpha}(\varphi_{\tau_j})\bar{Z}_{j\bar{\gamma}}(\varphi_{\tau_j}) \\
\sum_{\varphi_{\tau_i}}\frac{e^{2i\varphi_{\tau_i}\pi N_{\tau_i}}}{n_{\varphi_{\tau_i}}}\langle\Phi_{0\tau_i}|\Phi_{1\tau_i}(\varphi_{\tau_i})\rangle\sum_{\alpha\gamma>}\bar{\Gamma}^{(ji)(\tau_i\tau_i)}_{\alpha\gamma}(\varphi_{\tau_i})T_{i\bar{i}}(\varphi_{\tau_i}) \\
-2\frac{1}{\sqrt{\langle\Phi^{(j)}_0|\tilde{\Phi}^{(j)}_0\rangle\langle\Phi^{(i)}_1|\tilde{\Phi}^{(i)}_1\rangle}}\sum_{\varphi_{\tau_i}}\frac{e^{2i\varphi_{\tau_i}\pi N_{\tau_i}}}{n_{\varphi_{\tau_i}}}\langle\Phi_{0\tau_i}|\Phi_{1\tau_i}(\varphi_{\tau_i})\rangle Z_{\alpha\bar{i}}(\varphi_{\tau_i})W_{\gamma i}(\varphi_{\tau_i}) \\
\sum_{\varphi_{\tau_j}}\frac{e^{2i\varphi_{\tau_j}\pi N_{\tau_j}}}{n_{\varphi_{\tau_j}}}\langle\Phi_{0\tau_j}|\Phi_{1\tau_j}(\varphi_{\tau_j})\rangle\sum_{\alpha\gamma>}\bar{\Gamma}^{(ji)(\tau_j\tau_j)}_{\alpha\gamma}(\varphi_{\tau_j})Y_{j\bar{j}}(\varphi_{\tau_j}) \\
-2\frac{\tilde{\mathcal{O}}^{01\tau_j}_{j0}}{\sqrt{\langle\Phi^{(j)}_{0\tau_i}|\tilde{\Phi}^{(j)}_{0\tau_i}\rangle\langle\Phi^{(i)}_{1\tau_i}|\tilde{\Phi}^{(i)}_{1\tau_i}\rangle}}\sum_{\varphi_{\tau_i}}\frac{e^{2i\varphi_{\tau_i}\pi N_{\tau_i}}}{n_{\varphi_{\tau_i}}}\langle\Phi_{0\tau_i}|\Phi_{1\tau_i}(\varphi_{\tau_i})\rangle\sum_{\alpha\gamma>}\bar{\Gamma}^{(ji)(\tau_i\tau_i)}_{\alpha\gamma}(\varphi_{\tau_i})Z_{\alpha\bar{i}}(\varphi_{\tau_i})W_{\gamma i}(\varphi_{\tau_i}) \\
-2\frac{\tilde{\mathcal{O}}^{01\tau_i}_{0i}}{\sqrt{\langle\Phi^{(j)}_{0\tau_j}|\tilde{\Phi}^{(j)}_{0\tau_j}\rangle\langle\Phi^{(i)}_{1\tau_j}|\tilde{\Phi}^{(i)}_{1\tau_j}\rangle}}\sum_{\varphi_{\tau_j}}\frac{e^{2i\varphi_{\tau_j}\pi N_{\tau_j}}}{n_{\varphi_{\tau_j}}}\langle\Phi_{0\tau_j}|\Phi_{1\tau_j}(\varphi_{\tau_j})\rangle\sum_{\alpha\gamma>}\bar{\Gamma}^{(ji)(\tau_j\tau_j)}_{\alpha\gamma}(\varphi_{\tau_j})\bar{W}_{j\alpha}(\varphi_{\tau_j})\bar{Z}_{j\bar{\gamma}}(\varphi_{\tau_j}) \\
+\frac{\tilde{\mathcal{O}}^{01\tau_j}_{j0}}{\sqrt{\langle\Phi^{(j)}_{0\tau_i}|\tilde{\Phi}^{(j)}_{0\tau_i}\rangle\langle\Phi^{(i)}_{1\tau_i}|\tilde{\Phi}^{(i)}_{1\tau_i}\rangle}}\sum_{\varphi_{\tau_i}}\frac{e^{2i\varphi_{\tau_i}\pi N_{\tau_i}}}{n_{\varphi_{\tau_i}}}\langle\Phi_{0\tau_i}|\Phi_{1\tau_i}(\varphi_{\tau_i})\rangle T_{i\bar{i}}(\varphi_{\tau_i})\sum_{\alpha\beta>}\bar{\Delta}^{(\tau_i\tau_i)}_{\alpha\bar{\beta}}(\varphi_{\tau_i})\bar{\kappa}^{01\tau_i}_{\alpha\bar{\beta}}(\varphi_{\tau_i}) \\
+\frac{\tilde{\mathcal{O}}^{01\tau_i}_{0i}}{\sqrt{\langle\Phi^{(j)}_{0\tau_j}|\tilde{\Phi}^{(j)}_{0\tau_j}\rangle\langle\Phi^{(i)}_{1\tau_j}|\tilde{\Phi}^{(i)}_{1\tau_j}\rangle}}\sum_{\varphi_{\tau_j}}\frac{e^{2i\varphi_{\tau_j}\pi N_{\tau_j}}}{n_{\varphi_{\tau_j}}}\langle\Phi_{0\tau_j}|\Phi_{1\tau_j}(\varphi_{\tau_j})\rangle Y_{j\bar{j}}(\varphi_{\tau_j})\sum_{\alpha\beta>}\bar{\Delta}^{(\tau_j\tau_j)}_{\alpha\bar{\beta}}(\varphi_{\tau_j})\bar{\kappa}^{01\tau_j}_{\alpha\bar{\beta}}(\varphi_{\tau_j}) \\
-\frac{\tilde{\mathcal{O}}^{01\tau_i}_{0i}}{\sqrt{\langle\Phi^{(j)}_{0\tau_j}|\tilde{\Phi}^{(j)}_{0\tau_j}\rangle\langle\Phi^{(i)}_{1\tau_j}|\tilde{\Phi}^{(i)}_{1\tau_j}\rangle}}\sum_{\varphi_{\tau_j}}\frac{e^{2i\varphi_{\tau_j}\pi N_{\tau_j}}}{n_{\varphi_{\tau_j}}}\langle\Phi_{0\tau_j}|\Phi_{1\tau_j}(\varphi_{\tau_j})\rangle\sum_{\alpha\beta>}\bar{\Delta}^{(\tau_j\tau_j)}_{\alpha\bar{\beta}}(\varphi_{\tau_j})\bar{W}_{j\alpha}(\varphi_{\tau_j})\bar{W}_{j\beta}(\varphi_{\tau_j}) \\
-\frac{\tilde{\mathcal{O}}^{01\tau_j}_{j0}}{\sqrt{\langle\Phi^{(j)}_{0\tau_i}|\tilde{\Phi}^{(j)}_{0\tau_i}\rangle\langle\Phi^{(i)}_{1\tau_i}|\tilde{\Phi}^{(i)}_{1\tau_i}\rangle}}\sum_{\varphi_{\tau_i}}\frac{e^{2i\varphi_{\tau_i}\pi N_{\tau_i}}}{n_{\varphi_{\tau_i}}}\langle\Phi_{0\tau_i}|\Phi_{1\tau_i}(\varphi_{\tau_i})\rangle\sum_{\alpha\beta>}\bar{\Delta}^{(\tau_i\tau_i)}_{\alpha\bar{\beta}}(\varphi_{\tau_i})Z_{\alpha\bar{i}}(\varphi_{\tau_i})Z_{\beta\bar{i}}(\varphi_{\tau_i}) \\
-\frac{\tilde{\mathcal{O}}^{01\tau_i}_{0i}}{\sqrt{\langle\Phi^{(j)}_{0\tau_j}|\tilde{\Phi}^{(j)}_{0\tau_j}\rangle\langle\Phi^{(i)}_{1\tau_j}|\tilde{\Phi}^{(i)}_{1\tau_j}\rangle}}\sum_{\varphi_{\tau_j}}\frac{e^{2i\varphi_{\tau_j}\pi N_{\tau_j}}}{n_{\varphi_{\tau_j}}}\langle\Phi_{0\tau_j}|\Phi_{1\tau_j}(\varphi_{\tau_j})\rangle\sum_{\alpha\beta>}\bar{\Delta}^{(j)}_{\alpha\bar{\beta}}(\bar{Z}\bar{Z})(\varphi_{\tau_j})\bar{\kappa}^{01\tau_j}_{\alpha\bar{\beta}}(\varphi_{\tau_j}) \\
-\frac{\tilde{\mathcal{O}}^{01\tau_j}_{j0}}{\sqrt{\langle\Phi^{(j)}_{0\tau_i}|\tilde{\Phi}^{(j)}_{0\tau_i}\rangle\langle\Phi^{(i)}_{1\tau_i}|\tilde{\Phi}^{(i)}_{1\tau_i}\rangle}}\sum_{\varphi_{\tau_i}}\frac{e^{2i\varphi_{\tau_i}\pi N_{\tau_i}}}{n_{\varphi_{\tau_i}}}\langle\Phi_{0\tau_i}|\Phi_{1\tau_i}(\varphi_{\tau_i})\rangle\sum_{\alpha\beta>}\bar{\Delta}^{(i)}_{\alpha\bar{\beta}}(WW)(\varphi_{\tau_i})\bar{\kappa}^{01\tau_i}_{\alpha\bar{\beta}}(\varphi_{\tau_i}) \\
-\frac{2}{\sqrt{\langle\Phi^{(j)}_0|\tilde{\Phi}^{(j)}_0\rangle\langle\Phi^{(i)}_1|\tilde{\Phi}^{(i)}_1\rangle}}\sum_{\alpha\gamma>}\tilde{\bar{\Gamma}}^{(ji)}_{\alpha\gamma}([W,Z])\sum_{\varphi_{\tau_j}}\frac{e^{2i\varphi_{\tau_j}\pi N_{\tau_j}}}{n_{\varphi_{\tau_j}}}\langle\Phi_{0\tau_j}|\Phi_{1\tau_j}(\varphi_{\tau_j})\rangle\bar{W}_{j\alpha}(\varphi_{\tau_j})\bar{Z}_{j\bar{\gamma}}(\varphi_{\tau_j})
\end{aligned}
\tag{5.344}
$$

We've introduced the excited total projected field $\tilde{\bar{\Gamma}}^{(ji)}([W,Z])$, defined as follows:

$$\boxed{\begin{aligned}\tilde{\tilde{\Gamma}}^{(ji)}_{\alpha\gamma}([W,Z]) &= \sum_{\beta\delta>}[v^{(a)}_{\alpha\beta\gamma\delta} + (-1)^{s_\beta - s_\delta} v^{(a)}_{\alpha\bar{\beta}\gamma\bar{\delta}}] \\ \sum_{\varphi_{\tau_i}} &\frac{e^{2i\varphi_{\tau_i}\pi N_{\tau_i}}}{n_{\varphi_{\tau_i}}} \langle \Phi_{0\tau_i} | \Phi_{1\tau_i}(\varphi_{\tau_i}) \rangle W_{\delta i}(\varphi_{\tau_i}) Z_{\beta\bar{i}}(\varphi_{\tau_i})\end{aligned}} \tag{5.345}$$

To conclude this section, it is clear that the following symmetry holds:

$$\boxed{\tilde{E}^{01}_{ji}(v) = \tilde{E}^{10}_{ij}} \tag{5.346}$$

5.6.4 POF kernels:

In this section an expression of the POF HFB energy $\mathring{E}$ is derived. This quantity is defined as follows:

$$\boxed{\mathring{E} = \frac{\langle \Phi | \hat{P}^{(l)\tau_n} \hat{P}^{(l)\tau_p} \hat{P}^{(r)\tau_n} \hat{P}^{(r)\tau_p} \hat{H} | \mathring{\Phi} \rangle}{\langle \Phi | \mathring{\Phi} \rangle}} \tag{5.347}$$

We can separate $\mathring{E}$ into a kinetic and a two-body contribution $\mathring{E}(t)$ and $\mathring{E}(v)$:

$$\boxed{\mathring{E}(t) = \frac{1}{\langle \Phi | \mathring{\Phi} \rangle} \sum_{ij} \mathring{t}_{ij} \langle \Phi | \hat{P}^{(l)\tau_n} \hat{P}^{(l)\tau_p} \hat{P}^{(r)\tau_n} \hat{P}^{(r)\tau_p} a_i^+ a_j | \mathring{\Phi} \rangle} \tag{5.348}$$

$$\boxed{\mathring{E}(v) = \frac{1}{4\langle \Phi | \mathring{\Phi} \rangle} \sum_{abcd} \mathring{v}^{(a)}_{abcd} \langle \Phi | \hat{P}^{(l)\tau_n} \hat{P}^{(l)\tau_p} \hat{P}^{(r)\tau_n} \hat{P}^{(r)\tau_p} a_a^+ a_b^+ a_d a_c | \mathring{\Phi} \rangle} \tag{5.349}$$

As the POF projection operators are built with the canonical basis particle operators, the Hamiltonian has been written with respect to it. Therefore $\mathring{t}$ and $\mathring{v}^{(a)}$ are the counterparts of t and $v^{(a)}$ in the canonical basis. Besides, in Eq.(5.348) and Eq.(5.349) we didn't commute the POF projection operators and the Hamiltonian. Indeed, their commutation relations are not trivial. We will start by studying them.

One-body commutation relation:

$$\mathring{A}_{ij} = \langle \mathring{\Phi} | a_i^{+\tau_i} a_j^{\tau_j} | \mathring{\Phi} \rangle \tag{5.350}$$

$$A_{ij} = \langle \Phi | a_i^{+\tau_i} a_j^{\tau_j} | \mathring{\Phi} \rangle \tag{5.351}$$

If $\tau_i \neq \tau_j$, then it is clear that $A_{ij} = 0$ and $\mathring{A}_{ij} = 0$. Thus, $A_{ij} = \mathring{A}_{ij}$ in this case.

If $\tau_i = \tau_j$ and $i \neq j$, then $A_{ij} = 0$ and $\mathring{A}_{ij} = 0$. Thus, $A_{ij} = \mathring{A}_{ij}$ in this case also.

If $\tau_i = \tau_j$ and $i \neq j$, then the operator $a_i^{+\tau_i} a_i^{\tau_i}$ does not modify the particle numbers associated with the left and right subspaces of $|\mathring{\Phi}\rangle$. Therefore, we can write:

$$A_{ij} = \langle \Phi | a_i^{+\tau_i} a_i^{\tau_i} | \mathring{\Phi} \rangle = \langle \Phi | \hat{P}^{(l)\tau_n} \hat{P}^{(r)\tau_n} \hat{P}^{(l)\tau_p} \hat{P}^{(r)\tau_p} a_i^{+\tau_i} a_j^{\tau_j} | \mathring{\Phi} \rangle = \mathring{A}_{ij} \tag{5.352}$$

We've demonstrated the following commutation relation:

$$\boxed{\langle \Phi | \hat{P}^{(l)\tau_n} \hat{P}^{(r)\tau_n} \hat{P}^{(l)\tau_p} \hat{P}^{(r)\tau_p} a_i^{+\tau_i} a_i^{\tau_j} | \mathring{\Phi} \rangle = \langle \Phi | a_i^{+\tau_i} a_i^{\tau_j} | \mathring{\Phi} \rangle} \tag{5.353}$$

Two-body commutation relation:

$$\mathring{B}_{ab}^{cd} = \langle \mathring{\Phi} | a_a^{+\tau_a} a_b^{+\tau_b} a_d^{\tau_d} a_c^{\tau_c} | \mathring{\Phi} \rangle \tag{5.354}$$

$$B_{ab}^{cd} = \langle \Phi | a_a^{+\tau_a} a_b^{+\tau_b} a_d^{\tau_d} a_c^{\tau_c} | \mathring{\Phi} \rangle \tag{5.355}$$

If $\tau_a = \tau_b = \tau_c \neq \tau_d$, then $\mathring{B}_{ab}^{cd} = B_{ab}^{cd} = 0$.

If $\tau_a = \tau_b = \tau_d \neq \tau_c$, then $\mathring{B}_{ab}^{cd} = B_{ab}^{cd} = 0$.

If $\tau_a = \tau_c = \tau_d \neq \tau_b$, then $\mathring{B}_{ab}^{cd} = B_{ab}^{cd} = 0$.

If $\tau_b = \tau_c = \tau_d \neq \tau_a$, then $\mathring{B}_{ab}^{cd} = B_{ab}^{cd} = 0$.

If $\tau_a = \tau_c \neq \tau_b = \tau_d$, it is easy to observe using the one-body commutation relation that $\mathring{B}_{ab}^{cd} = B_{ab}^{cd}$.

If $\tau_a = \tau_d \neq \tau_b = \tau_c$, it is easy to observe using the one-body commutation relation that $\mathring{B}_{ab}^{cd} = B_{ab}^{cd}$.

If $\tau_a = \tau_b \neq \tau_c = \tau_d$, then $\mathring{B}_{ab}^{cd} = 0$, but B_{ab}^{cd} does not necessarily equal 0. We call this special case (k_τ).

If $\tau_a = \tau_b = \tau_c = \tau_d$ and $c = d$, then $\mathring{B}_{ab}^{cd} = B_{ab}^{cd} = 0$.

If $\tau_a = \tau_b = \tau_c = \tau_d$ and $c \neq \bar{d}$ and $c \neq d$:

- If $a \neq c$ and $a \neq d$ or $b \neq c$ and $b \neq d$, then $\mathring{B}_{ab}^{cd} = B_{ab}^{cd} = 0$.
- If $a = c$ and $b = c$ or $a = d$ and $b = d$, then $\mathring{B}_{ab}^{cd} = B_{ab}^{cd} = 0$.
- If $a = c$ and $b = d$ or $a = d$ and $a = c$, then the particle numbers related to the different subspaces of $|\mathring{\Phi}\rangle$ are not changed and $\mathring{B}_{ab}^{cd} = B_{ab}^{cd}$.

If $\tau_a = \tau_b = \tau_c = \tau_d$ and $c = \bar{d}$:

- If $a \neq \bar{b}$, then $\mathring{B}_{ab}^{cd} = B_{ab}^{cd} = 0$.

- If $a = \bar{b}$ and a and c belongs to the same subsapce of $|\mathring{\Phi}\rangle$, then the particle numbers related to the different subspaces of $|\mathring{\Phi}\rangle$ are not changed and $\mathring{B}^{cd}_{ab} = B^{cd}_{ab}$.
- If $a = \bar{b}$ and a and c does not belong to the same subsapce of $|\mathring{\Phi}\rangle$, $\mathring{B}^{cd}_{ab} = 0$, but B^{cd}_{ab} does not necessarily equal 0. We call this special case (k_{lr}).

We've spotted two problematic cases (k_τ) and (k_{lr}), because of them $\mathring{B}^{cd}_{ab}$ does not equal B^{cd}_{ab} in general. However, setting $\delta_{(\bar{k}_\tau)} = (1 - \delta_{(k_\tau)})$ and $\delta_{(\bar{k}_{lr})} = (1 - \delta_{(k_{lr})})$, the following relation holds:

$$\mathring{B}^{cd}_{ab} = \delta_{(\bar{k}_\tau)}\delta_{(\bar{k}_{lr})}B^{cd}_{ab} \tag{5.356}$$

We can rewrite Eq.(5.356) more explicitly to end up with the desired commutation relation:

$$\boxed{\langle\Phi|\hat{P}^{(l)\tau_n}\hat{P}^{(r)\tau_n}\hat{P}^{(l)\tau_p}\hat{P}^{(r)\tau_p}a_a^{+\tau_a}a_b^{+\tau_b}a_d^{\tau_d}a_c^{\tau_c}|\mathring{\Phi}\rangle = \delta_{(\bar{k}_\tau)}\delta_{(\bar{k}_{lr})}\langle\Phi|a_a^{+\tau_a}a_b^{+\tau_b}a_d^{\tau_d}a_c^{\tau_c}|\mathring{\Phi}\rangle} \tag{5.357}$$

Kinetic part:

As demonstrated, we can commute the POF projection operators and the particle operators in the expression of $\mathring{E}(t)$:

$$\mathring{E}(t) = \frac{1}{\langle\Phi|\mathring{\Phi}\rangle}\sum_{ij}\mathring{t}_{ij}\langle\Phi|a_i^+a_j|\mathring{\Phi}\rangle \tag{5.358}$$

We rewrite Eq.(5.358) more explicitly:

$$\mathring{E}(t) = \frac{1}{\langle\Phi|\mathring{\Phi}\rangle}\sum_{ij}\mathring{t}_{ij}\sum_{\varphi_\tau^{(l)}}\sum_{\varphi_\tau^{(r)}}\frac{e^{2i\pi\varphi_\tau^{(l)}N_\tau^{(l)}}e^{2i\pi\varphi_\tau^{(r)}N_\tau^{(r)}}}{n^{(l)}_{\varphi_\tau}n^{(r)}_{\varphi_\tau}}\langle\Phi_\tau|a_i^{+\tau}a_j^\tau|\Phi_\tau(\varphi_\tau^{(l)},\varphi_\tau^{(r)})\rangle \tag{5.359}$$
$$\sum_{\varphi_{\bar{\tau}}^{(l)}}\sum_{\varphi_{\bar{\tau}}^{(r)}}\frac{e^{2i\pi\varphi_{\bar{\tau}}^{(l)}N_{\bar{\tau}}^{(l)}}e^{2i\pi\varphi_{\bar{\tau}}^{(r)}N_{\bar{\tau}}^{(r)}}}{n^{(l)}_{\varphi_{\bar{\tau}}}n^{(r)}_{\varphi_{\bar{\tau}}}}\langle\Phi_{\bar{\tau}}|\Phi_{\bar{\tau}}(\varphi_{\bar{\tau}}^{(l)},\varphi_{\bar{\tau}}^{(r)})\rangle$$

As shown in section 5.4, the matrices $\mathring{\rho}^\tau(\varphi_\tau^{(l)},\varphi_\tau^{(r)})$ are diagonal. We use this property to simplify Eq.(5.359):

$$\mathring{E}(t) = \frac{1}{\langle\Phi|\mathring{\Phi}\rangle}\sum_i\mathring{t}_{ii}\langle\Phi_{\bar{\tau}}|\mathring{\Phi}_{\bar{\tau}}\rangle\sum_{\varphi_\tau^{(l)}}\sum_{\varphi_\tau^{(r)}}\frac{e^{2i\pi\varphi_\tau^{(l)}N_\tau^{(l)}}e^{2i\pi\varphi_\tau^{(r)}N_\tau^{(r)}}}{n^{(l)}_{\varphi_\tau}n^{(r)}_{\varphi_\tau}}\langle\Phi_\tau|\Phi_\tau(\varphi_{\bar{\tau}}^{(l)},\varphi_{\bar{\tau}}^{(r)})\rangle\mathring{\rho}^\tau_{ii}(\varphi_\tau^{(l)},\varphi_\tau^{(r)}) \tag{5.360}$$

We make the matrices $\mathring{\tilde{\rho}}$ appear in Eq.(5.360):

$$\mathring{E}(t) = \sum_i\mathring{t}_{ii}\mathring{\tilde{\rho}}_{ii} \tag{5.361}$$

We now separate the matrices $\mathring{\tilde{\rho}}$ with respect to the left and right subspaces of $|\Phi\rangle$, which are noted $\{l\}$ and $\{r\}$:

$$\mathring{E}(t) = \sum_i \mathring{t}_{ii}(\mathring{\tilde{\rho}}_{ii}\delta_{i\in\{l\}} + \mathring{\tilde{\rho}}_{ii}\delta_{i\in\{r\}}) \tag{5.362}$$

We bring Eq.(5.362) back to the harmonic-oscillator representation:

$$\mathring{E}(t) = \sum_{\alpha\beta} t_{\alpha\beta}\tilde{\rho}^{(l)}_{\alpha\beta} + \sum_{\alpha\beta} t_{\alpha\beta}\tilde{\rho}^{(r)}_{\alpha\beta} \tag{5.363}$$

Using the time-reversal properties of Eq.(5.363) finally leads to:

$$\boxed{\mathring{E}(t) = 2(\sum_{\alpha\beta} t_{\alpha\beta}\tilde{\rho}^{(l)}_{\alpha\beta} + \sum_{\alpha\beta} t_{\alpha\beta}\tilde{\rho}^{(r)}_{\alpha\beta}) = \mathring{E}^{(l)}(t) + \mathring{E}^{(r)}(t)} \tag{5.364}$$

Eq.(5.364) clearly highlights that the POF HFB energy is separated into a left and right contributions.

Two-body part:

We start by using the commutation relation given in Eq.(5.357) to rewrite $\mathring{E}(v)$:

$$\mathring{E}(v) = \frac{1}{4\langle\Phi|\mathring{\Phi}\rangle}\sum_{abcd}\delta_{(\bar{k}_\tau)}\delta_{(\bar{k}_{lr})}\mathring{v}^{(a)}_{abcd}\langle\Phi|a^+_a a^+_b a_d a_c|\mathring{\Phi}\rangle \tag{5.365}$$

We transform the sum to take into account explicitly the commutation relation:

$$\begin{aligned}\mathring{E}(v) = \frac{1}{4\langle\Phi|\mathring{\Phi}\rangle}[&2\sum_{ab}\mathring{v}^{(a)}_{abba}\langle\Phi|a^{+\tau}_a a^{+\bar{\tau}}_b a^\tau_a a^{\bar{\tau}}_b|\mathring{\Phi}\rangle + 2\sum_{ab,\ a\neq\bar{b}}\mathring{v}^{(a)}_{abba}\langle\Phi|a^{+\tau}_a a^{+\tau}_b a^\tau_a a^\tau_b|\mathring{\Phi}\rangle \\ &+ \sum_{ac\in\{l\}}\mathring{v}^{(a)}_{a\bar{a}\bar{c}c}\langle\Phi|a^{+\tau}_a a^{+\tau}_{\bar{a}} a^\tau_c a^\tau_{\bar{c}}|\mathring{\Phi}\rangle + \sum_{ac\in\{r\}}\mathring{v}^{(a)}_{a\bar{a}\bar{c}c}\langle\Phi|a^{+\tau}_a a^{+\tau}_{\bar{a}} a^\tau_c a^\tau_{\bar{c}}|\mathring{\Phi}\rangle]\end{aligned} \tag{5.366}$$

Now, we can write Eq.(5.366) explicitly:

$$\begin{aligned}\mathring{E}(v) = \frac{1}{4\langle\Phi|\mathring{\Phi}\rangle}[&2\sum_{ab}\mathring{v}^{(a)}_{abba}\sum_{\varphi^{(l)}_\tau}\sum_{\varphi^{(r)}_\tau}\frac{e^{2i\pi\varphi^{(l)}_\tau N^{(l)}_\tau}e^{2i\pi\varphi^{(r)}_\tau N^{(r)}_\tau}}{n^{(l)}_{\varphi_\tau}n^{(r)}_{\varphi_\tau}} \\ &\sum_{\varphi^{(l)}_{\bar{\tau}}}\sum_{\varphi^{(r)}_{\bar{\tau}}}\frac{e^{2i\pi\varphi^{(l)}_{\bar{\tau}} N^{(l)}_{\bar{\tau}}}e^{2i\pi\varphi^{(r)}_{\bar{\tau}} N^{(r)}_{\bar{\tau}}}}{n^{(l)}_{\varphi_{\bar{\tau}}}n^{(r)}_{\varphi_{\bar{\tau}}}}\langle\Phi|a^{+\tau}_a a^{+\bar{\tau}}_b a^\tau_a a^{\bar{\tau}}_b|\Phi(\varphi^{(l)}_\tau,\varphi^{(r)}_\tau,\varphi^{(l)}_{\bar{\tau}},\varphi^{(r)}_{\bar{\tau}})\rangle \\ +2\sum_{ab}\mathring{v}^{(a)}_{abba}&\langle\Phi_{\bar{\tau}}|\mathring{\Phi}_{\bar{\tau}}\rangle\sum_{\varphi^{(l)}_\tau}\sum_{\varphi^{(r)}_\tau}\frac{e^{2i\pi\varphi^{(l)}_\tau N^{(l)}_\tau}e^{2i\pi\varphi^{(r)}_\tau N^{(r)}_\tau}}{n^{(l)}_{\varphi_\tau}n^{(r)}_{\varphi_\tau}}\langle\Phi_\tau|a^{+\tau}_a a^{+\tau}_b a^\tau_a a^\tau_b|\Phi_\tau(\varphi^{(l)}_\tau,\varphi^{(r)}_\tau)\rangle \\ +\sum_{ac\in\{l\}}\mathring{v}^{(a)}_{a\bar{a}\bar{c}c}&\langle\Phi_{\bar{\tau}}|\mathring{\Phi}_{\bar{\tau}}\rangle\sum_{\varphi^{(l)}_\tau}\sum_{\varphi^{(r)}_\tau}\frac{e^{2i\pi\varphi^{(l)}_\tau N^{(l)}_\tau}e^{2i\pi\varphi^{(r)}_\tau N^{(r)}_\tau}}{n^{(l)}_{\varphi_\tau}n^{(r)}_{\varphi_\tau}}\langle\Phi_\tau|a^{+\tau}_a a^{+\tau}_{\bar{a}} a^\tau_c a^\tau_{\bar{c}}|\Phi_\tau(\varphi^{(l)}_\tau,\varphi^{(r)}_\tau)\rangle \\ +\sum_{ac\in\{r\}}\mathring{v}^{(a)}_{a\bar{a}\bar{c}c}&\langle\Phi_{\bar{\tau}}|\mathring{\Phi}_{\bar{\tau}}\rangle\sum_{\varphi^{(l)}_\tau}\sum_{\varphi^{(r)}_\tau}\frac{e^{2i\pi\varphi^{(l)}_\tau N^{(l)}_\tau}e^{2i\pi\varphi^{(r)}_\tau N^{(r)}_\tau}}{n^{(l)}_{\varphi_\tau}n^{(r)}_{\varphi_\tau}}\langle\Phi_\tau|a^{+\tau}_a a^{+\tau}_{\bar{a}} a^\tau_c a^\tau_{\bar{c}}|\Phi_\tau(\varphi^{(l)}_\tau,\varphi^{(r)}_\tau)\rangle]\end{aligned} \tag{5.367}$$

We make the matrices $\mathring{\rho}(\varphi_\tau^{(l)},\varphi_\tau^{(r)})$, $\mathring{\kappa}(\varphi_\tau^{(l)},\varphi_\tau^{(r)})$ and $\mathring{\bar{\kappa}}(\varphi_\tau^{(l)},\varphi_\tau^{(r)})$ appear using the Wick theorem in Eq.(5.366):

$$\begin{aligned}
\mathring{E}(v) = \frac{1}{4\langle\Phi|\mathring{\Phi}\rangle}[2\sum_{ab}\mathring{v}^{(a)}_{abba}\sum_{\varphi_\tau^{(l)}}\sum_{\varphi_\tau^{(r)}}\frac{e^{2i\pi\varphi_\tau^{(l)}N_\tau^{(l)}}e^{2i\pi\varphi_\tau^{(r)}N_\tau^{(r)}}}{n^{(l)}_{\varphi_\tau}n^{(r)}_{\varphi_\tau}}\mathring{\rho}^{\tau}_{aa}(\varphi_\tau^{(l)},\varphi_\tau^{(r)})\langle\Phi_\tau|\Phi_\tau(\varphi_\tau^{(l)},\varphi_\tau^{(r)})\rangle \\
\sum_{\varphi_{\bar\tau}^{(l)}}\sum_{\varphi_{\bar\tau}^{(r)}}\frac{e^{2i\pi\varphi_{\bar\tau}^{(l)}N_{\bar\tau}^{(l)}}e^{2i\pi\varphi_{\bar\tau}^{(r)}N_{\bar\tau}^{(r)}}}{n^{(l)}_{\varphi_{\bar\tau}}n^{(r)}_{\varphi_{\bar\tau}}}\mathring{\rho}^{\bar\tau}_{bb}(\varphi_{\bar\tau}^{(l)},\varphi_{\bar\tau}^{(r)})\langle\Phi_{\bar\tau}|\Phi_{\bar\tau}(\varphi_{\bar\tau}^{(l)},\varphi_{\bar\tau}^{(r)})\rangle \\
+2\sum_{ab}\mathring{v}^{(a)}_{abba}\langle\Phi_{\bar\tau}|\mathring{\Phi}_{\bar\tau}\rangle\sum_{\varphi_\tau^{(l)}}\sum_{\varphi_\tau^{(r)}}\frac{e^{2i\pi\varphi_\tau^{(l)}N_\tau^{(l)}}e^{2i\pi\varphi_\tau^{(r)}N_\tau^{(r)}}}{n^{(l)}_{\varphi_\tau}n^{(r)}_{\varphi_\tau}}\langle\Phi_\tau|\Phi_\tau(\varphi_\tau^{(l)},\varphi_\tau^{(r)})\rangle \\
\mathring{\rho}^{\tau}_{aa}(\varphi_\tau^{(l)},\varphi_\tau^{(r)})\mathring{\rho}^{\tau}_{bb}(\varphi_\tau^{(l)},\varphi_\tau^{(r)}) \\
-\sum_{ac\in\{l\}}\mathring{v}^{(a)}_{a\bar a c\bar c}\langle\Phi_{\bar\tau}|\mathring{\Phi}_{\bar\tau}\rangle(-1)^{s_a-s_c}\sum_{\varphi_\tau^{(l)}}\sum_{\varphi_\tau^{(r)}}\frac{e^{2i\pi\varphi_\tau^{(l)}N_\tau^{(l)}}e^{2i\pi\varphi_\tau^{(r)}N_\tau^{(r)}}}{n^{(l)}_{\varphi_\tau}n^{(r)}_{\varphi_\tau}}\langle\Phi_\tau|\Phi_\tau(\varphi_\tau^{(l)},\varphi_\tau^{(r)})\rangle \\
\mathring{\bar\kappa}^{\tau}_{a\bar a}(\varphi_\tau^{(l)},\varphi_\tau^{(r)})\mathring{\kappa}^{\tau}_{c\bar c}(\varphi_\tau^{(l)},\varphi_\tau^{(r)}) \\
-\sum_{ac\in\{r\}}\mathring{v}^{(a)}_{a\bar a c\bar c}\langle\Phi_{\bar\tau}|\mathring{\Phi}_{\bar\tau}\rangle(-1)^{s_a-s_c}\sum_{\varphi_\tau^{(l)}}\sum_{\varphi_\tau^{(r)}}\frac{e^{2i\pi\varphi_\tau^{(l)}N_\tau^{(l)}}e^{2i\pi\varphi_\tau^{(r)}N_\tau^{(r)}}}{n^{(l)}_{\varphi_\tau}n^{(r)}_{\varphi_\tau}}\langle\Phi_\tau|\Phi_\tau(\varphi_\tau^{(l)},\varphi_\tau^{(r)})\rangle \\
\mathring{\bar\kappa}^{\tau}_{a\bar a}(\varphi_\tau^{(l)},\varphi_\tau^{(r)})\mathring{\kappa}^{\tau}_{c\bar c}(\varphi_\tau^{(l)},\varphi_\tau^{(r)})]
\end{aligned} \tag{5.368}$$

Thanks to the properties demonstrated in section 5.4.6, we can separate $\mathring{E}(v)$:

$$\boxed{\mathring{E}(v) = \mathring{E}^{(l)}(v) + \mathring{E}^{(r)}(v) + \mathring{E}_{int}(v)} \tag{5.369}$$

With:

$$\begin{aligned}
\mathring{E}^{(l)}(v) = &+\sum_{ab\in\{l\}}\frac{1}{2\langle\Phi_\tau^{(l)}|\mathring{\Phi}_\tau^{(l)}\rangle}\mathring{v}^{(a)}_{abba}\sum_{\varphi_\tau^{(l)}}\frac{e^{2i\pi\varphi_\tau^{(l)}N_\tau^{(l)}}}{n^{(l)}_{\varphi_\tau}}\mathcal{O}^{(l)}(\varphi_l)\mathring{\rho}^{(l)\tau}_{aa}(\varphi_\tau^{(l)})\mathring{\rho}^{(l)\tau}_{bb}(\varphi_\tau^{(l)}) \\
&-\sum_{ac\in\{l\}}\frac{1}{4\langle\Phi_\tau^{(l)}|\mathring{\Phi}_\tau^{(l)}\rangle}\mathring{v}^{(a)}_{a\bar a c\bar c}(-1)^{s_a-s_c}\sum_{\varphi_\tau^{(l)}}\frac{e^{2i\pi\varphi_\tau^{(l)}N_\tau^{(l)}}}{n^{(l)}_{\varphi_\tau}}\mathcal{O}^{(l)}(\varphi_l)\mathring{\bar\kappa}^{(l)\tau}_{a\bar a}(\varphi_\tau^{(l)})\mathring{\kappa}^{(l)\tau}_{c\bar c}(\varphi_\tau^{(l)}) \\
&+\frac{1}{2}\sum_{a\in\{l\}}\sum_{b\in\{l\}}\mathring{v}^{(a)}_{abba}\mathring{\tilde\rho}^{(l)\tau}_{aa}\mathring{\tilde\rho}^{(l)\bar\tau}_{bb}
\end{aligned} \tag{5.370}$$

And:

$$\begin{aligned}
\mathring{E}^{(r)}(v) = &+\sum_{ab,\ a\neq\bar b,\ ab\in\{r\}}\frac{1}{2\langle\Phi_\tau^{(r)}|\mathring{\Phi}_\tau^{(r)}\rangle}\mathring{v}^{(a)}_{abba}\sum_{\varphi_\tau^{(r)}}\frac{e^{2i\pi\varphi_\tau^{(r)}N_\tau^{(r)}}}{n^{(r)}_{\varphi_\tau}}\mathcal{O}^{(r)}(\varphi_r)\mathring{\rho}^{(r)\tau}_{aa}(\varphi_\tau^{(r)})\mathring{\rho}^{(r)\tau}_{bb}(\varphi_\tau^{(r)}) \\
&-\sum_{ac\in\{r\}}\frac{1}{4\langle\Phi_\tau^{(r)}|\mathring{\Phi}_\tau^{(r)}\rangle}\mathring{v}^{(a)}_{a\bar a c\bar c}(-1)^{s_a-s_c}\sum_{\varphi_\tau^{(r)}}\frac{e^{2i\pi\varphi_\tau^{(r)}N_\tau^{(r)}}}{n^{(r)}_{\varphi_\tau}}\mathcal{O}^{(r)}(\varphi_r)\mathring{\bar\kappa}^{(r)\tau}_{a\bar a}(\varphi_\tau^{(r)})\mathring{\kappa}^{(r)\tau}_{c\bar c}(\varphi_\tau^{(r)}) \\
&+\frac{1}{2}\sum_{a\in\{r\}}\sum_{b\in\{r\}}\mathring{v}^{(a)}_{abba}\mathring{\tilde\rho}^{(r)\tau}_{aa}\mathring{\tilde\rho}^{(r)\bar\tau}_{bb}
\end{aligned} \tag{5.371}$$

And, finally:

$$\mathring{E}_{int}(v) = \sum_{a\in\{l\}}\sum_{b\in\{r\}} \mathring{v}^{(a)}_{abba}\mathring{\tilde{\rho}}^{(l)\tau}_{aa}\mathring{\tilde{\rho}}^{(r)\bar{\tau}}_{bb} + \sum_{a\in\{l\}}\sum_{b\in\{r\}} \mathring{v}^{(a)}_{abba}\mathring{\tilde{\rho}}^{(l)\tau}_{aa}\mathring{\tilde{\rho}}^{(r)\tau}_{bb} \tag{5.372}$$

We transform these three expressions into the harmonic-oscillator representation:

$$\begin{aligned}\mathring{E}^{(l)}(v) = &+\sum_{\varphi^{(l)}_\tau}\frac{1}{2\langle\Phi^{(l)}_\tau|\mathring{\Phi}^{(l)}_\tau\rangle}\sum_{\alpha\beta\gamma\delta} v^{(a)}_{\alpha\beta\gamma\delta}\frac{e^{2i\pi\varphi^{(l)}_\tau N^{(l)}_\tau}}{n^{(l)}_{\varphi_\tau}}\mathcal{O}^{(l)}(\varphi_l)\rho^{(l)\tau}_{\delta\beta}(\varphi^{(l)}_\tau)\rho^{(l)\tau}_{\gamma\alpha}(\varphi^{(l)}_\tau) \\ &-\sum_{\alpha\beta\gamma\delta}\frac{1}{4\langle\Phi^{(l)}_\tau|\mathring{\Phi}^{(l)}_\tau\rangle}v^{(a)}_{\alpha\bar{\beta}\gamma\bar{\delta}}(-1)^{s_\delta-s_\beta}\sum_{\varphi^{(l)}_\tau}\frac{e^{2i\pi\varphi^{(l)}_\tau N^{(l)}_\tau}}{n^{(l)}_{\varphi_\tau}}\mathcal{O}^{(l)}(\varphi_l)\bar{\kappa}^{(l)\tau}_{\alpha\bar{\beta}}(\varphi^{(l)}_\tau)\kappa^{(l)\tau}_{\gamma\bar{\delta}}(\varphi^{(l)}_\tau) \\ &+\frac{1}{2}\sum_{\alpha\beta\gamma\delta} v^{(a)}_{\alpha\beta\gamma\delta}\tilde{\rho}^{(l)\tau}_{\delta\beta}\tilde{\rho}^{(l)\bar{\tau}}_{\gamma\delta}\end{aligned} \tag{5.373}$$

And:

$$\begin{aligned}\mathring{E}^{(r)}(v) = &+\sum_{\alpha\beta\gamma\delta}\frac{1}{2\langle\Phi^{(r)}_\tau|\mathring{\Phi}^{(r)}_\tau\rangle}v^{(a)}_{\alpha\beta\gamma\delta}\sum_{\varphi^{(r)}_\tau}\frac{e^{2i\pi\varphi^{(r)}_\tau N^{(r)}_\tau}}{n^{(r)}_{\varphi_\tau}}\mathcal{O}^{(r)}(\varphi_r)\rho^{(r)\tau}_{\delta\beta}(\varphi^{(r)}_\tau)\rho^{(r)\tau}_{\gamma\alpha}(\varphi^{(r)}_\tau) \\ &-\sum_{\alpha\beta\gamma\delta}\frac{1}{4\langle\Phi^{(r)}_\tau|\mathring{\Phi}^{(r)}_\tau\rangle}v^{(a)}_{\alpha\bar{\beta}\gamma\bar{\delta}}(-1)^{s_\delta-s_\beta}\sum_{\varphi^{(r)}_\tau}\frac{e^{2i\pi\varphi^{(r)}_\tau N^{(r)}_\tau}}{n^{(r)}_{\varphi_\tau}}\mathcal{O}^{(r)}(\varphi_r)\bar{\kappa}^{(r)\tau}_{\alpha\bar{\beta}}(\varphi^{(r)}_\tau)\kappa^{(r)\tau}_{\gamma\bar{\delta}}(\varphi^{(r)}_\tau) \\ &+\frac{1}{2}\sum_{\alpha\beta\gamma\delta} v^{(a)}_{\alpha\beta\gamma\delta}\tilde{\rho}^{(r)\tau}_{\delta\beta}\tilde{\rho}^{(r)\bar{\tau}}_{\gamma\delta}\end{aligned} \tag{5.374}$$

And finally,

$$\mathring{E}_{int}(v) = \sum_{\alpha\beta\gamma\delta} v^{(a)}_{\alpha\beta\gamma\delta}\tilde{\rho}^{(l)\tau}_{\delta\beta}\tilde{\rho}^{(r)\bar{\tau}}_{\gamma\delta} + \sum_{\alpha\beta\gamma\delta} v^{(a)}_{\alpha\beta\gamma\delta}\tilde{\rho}^{(l)\tau}_{\delta\beta}\tilde{\rho}^{(r)\tau}_{\gamma\delta} \tag{5.375}$$

Now, we introduce the related left and right POF fields. We start with the local POF fields:

$$\boxed{\Gamma^{(l)\tau\tau}_{\alpha\gamma}(\varphi^{(l)}_\tau) = \sum_{\delta\beta} v^{(a)}_{\alpha\beta\gamma\delta}\rho^{(l)\tau}_{\delta\beta}(\varphi^{(l)}_\tau)} \qquad \boxed{\Gamma^{(r)\tau\tau}_{\alpha\gamma}(\varphi^{(r)}_\tau) = \sum_{\delta\beta} v^{(a)}_{\alpha\beta\gamma\delta}\rho^{(r)\tau}_{\delta\beta}(\varphi^{(r)}_\tau)} \tag{5.376}$$

And:

$$\boxed{\Delta^{(l)\tau\tau}_{\alpha\bar{\beta}}(\varphi^{(l)}_\tau) = \frac{1}{2}\sum_{\alpha\beta} v^{(a)}_{\alpha\bar{\beta}\gamma\bar{\delta}}(-1)^{s_\delta-s_\beta}\kappa^{(l)\tau}_{\gamma\bar{\delta}}(\varphi^{(l)}_\tau)} \tag{5.377}$$

$$\boxed{\Delta^{(r)\tau\tau}_{\alpha\bar{\beta}}(\varphi^{(r)}_\tau) = \frac{1}{2}\sum_{\alpha\beta} v^{(a)}_{\alpha\bar{\beta}\gamma\bar{\delta}}(-1)^{s_\delta-s_\beta}\kappa^{(r)\tau}_{\gamma\bar{\delta}}(\varphi^{(r)}_\tau)} \tag{5.378}$$

Finally, we display the expression of the total POF fields:

$$\boxed{\tilde{\Gamma}^{(l)\tau\bar{\tau}}_{\alpha\gamma} = \sum_{\delta\beta} v^{(a)}_{\alpha\beta\gamma\delta}\tilde{\rho}^{(l)\tau}_{\delta\beta}} \qquad \boxed{\tilde{\Gamma}^{(r)\tau\bar{\tau}}_{\alpha\gamma} = \sum_{\delta\beta} v^{(a)}_{\alpha\beta\gamma\delta}\tilde{\rho}^{(r)\tau}_{\delta\beta}} \tag{5.379}$$

Thanks to these new fields, we can finally write:

$$\begin{aligned}\boxed{\begin{aligned}\mathring{E}^{(l)}(v) = &+\sum_{\varphi^{(l)}_\tau} \frac{e^{2i\pi\varphi^{(l)}_\tau N^{(l)}_\tau}}{n^{(l)}_{\varphi_\tau}} \mathcal{O}^{(l)}(\varphi_l) \sum_{\alpha\gamma>} \frac{1}{\langle \Phi^{(l)}_\tau | \mathring{\Phi}^{(l)}_\tau \rangle} \Gamma^{(l)\tau\tau}_{\alpha\gamma}(\varphi^{(l)}_\tau)\rho^{(l)\tau}_{\gamma\alpha}(\varphi^{(l)}_\tau) \\ &-\sum_{\varphi^{(l)}_\tau} \frac{e^{2i\pi\varphi^{(l)}_\tau N^{(l)}_\tau}}{n^{(l)}_{\varphi_\tau}} \mathcal{O}^{(l)}(\varphi_l) \sum_{\alpha\beta>} \frac{1}{\langle \Phi^{(l)}_\tau | \mathring{\Phi}^{(l)}_\tau \rangle} \Delta^{(l)\tau\tau}_{\alpha\beta}(\varphi^{(l)}_\tau)\bar{\kappa}^{(l)\tau}_{\alpha\bar{\beta}}(\varphi^{(l)}_\tau) \\ &+\sum_{\alpha\gamma>} \tilde{\Gamma}^{(l)\tau\bar{\tau}}_{\alpha\gamma}\tilde{\rho}^{(l)\bar{\tau}}_{\gamma\delta}\end{aligned}}\end{aligned} \tag{5.380}$$

And:

$$\begin{aligned}\boxed{\begin{aligned}\mathring{E}^{(r)}(v) = &+\sum_{\varphi^{(r)}_\tau} \frac{e^{2i\pi\varphi^{(r)}_\tau N^{(r)}_\tau}}{n^{(r)}_{\varphi_\tau}} \mathcal{O}^{(r)}(\varphi_r) \sum_{\alpha\gamma>} \frac{1}{\langle \Phi^{(r)}_\tau | \mathring{\Phi}^{(r)}_\tau \rangle} \Gamma^{(r)\tau\tau}_{\alpha\gamma}(\varphi^{(r)}_\tau)\rho^{(r)\tau}_{\gamma\alpha}(\varphi^{(r)}_\tau) \\ &-\sum_{\varphi^{(r)}_\tau} \frac{e^{2i\pi\varphi^{(r)}_\tau N^{(r)}_\tau}}{n^{(r)}_{\varphi_\tau}} \mathcal{O}^{(r)}(\varphi_l) \sum_{\alpha\beta>} \frac{1}{\langle \Phi^{(r)}_\tau | \mathring{\Phi}^{(r)}_\tau \rangle} \Delta^{(r)\tau\tau}_{\alpha\beta}(\varphi^{(r)}_\tau)\bar{\kappa}^{(r)\tau}_{\alpha\bar{\beta}}(\varphi^{(r)}_\tau) \\ &+\sum_{\alpha\gamma} \tilde{\Gamma}^{(r)\tau\bar{\tau}}_{\alpha\gamma>}\tilde{\rho}^{(r)\bar{\tau}}_{\gamma\delta}\end{aligned}}\end{aligned} \tag{5.381}$$

And finally,

$$\boxed{\mathring{E}_{int}(v) = 2\sum_{\alpha\gamma>} \tilde{\Gamma}^{(l)\tau\bar{\tau}}_{\alpha\gamma}\tilde{\rho}^{(r)\bar{\tau}}_{\gamma\delta} + 2\sum_{\alpha\gamma} \tilde{\Gamma}^{(l)\tau\bar{\tau}}_{\alpha\gamma>}\tilde{\rho}^{(r)\tau}_{\gamma\delta}} \tag{5.382}$$

5.7 Divergences

In practice, we didn't face any particular difficulty calculating the overlap and Hamiltonian kernels, except in the cases of Hamiltonian kernels between adiabatic states and variational excited states and between two different variational excited states (each belonging to a different excited set). Indeed, in these cases, we try to evaluate fractions whose numerator and denominator tend towards zero. In addition, the denominator tends towards zero faster than the numerator does (a quadratic difference [71]).
Initially, we thought that the numerical precision of the orthogonality obtained with the overlap constraints (see Chapter 3) would enable us to avoid the issue. However, the problem has always arisen, albeit with varying degrees of severity. In panel (a) of Figure (5.3), we've represented the Hamiltonian kernel $\langle \Phi^{(i)}(220-s)|\hat{H}|\Phi(220+s)\rangle$, the superscript (i) standing for the neutron $\Omega = 1/2$ variational excitation, with respect to s. In panel (b), we've represented the overlap kernel $\langle \Phi^{(i)}(220-s)|\Phi(220+s)\rangle$, with respect to s:

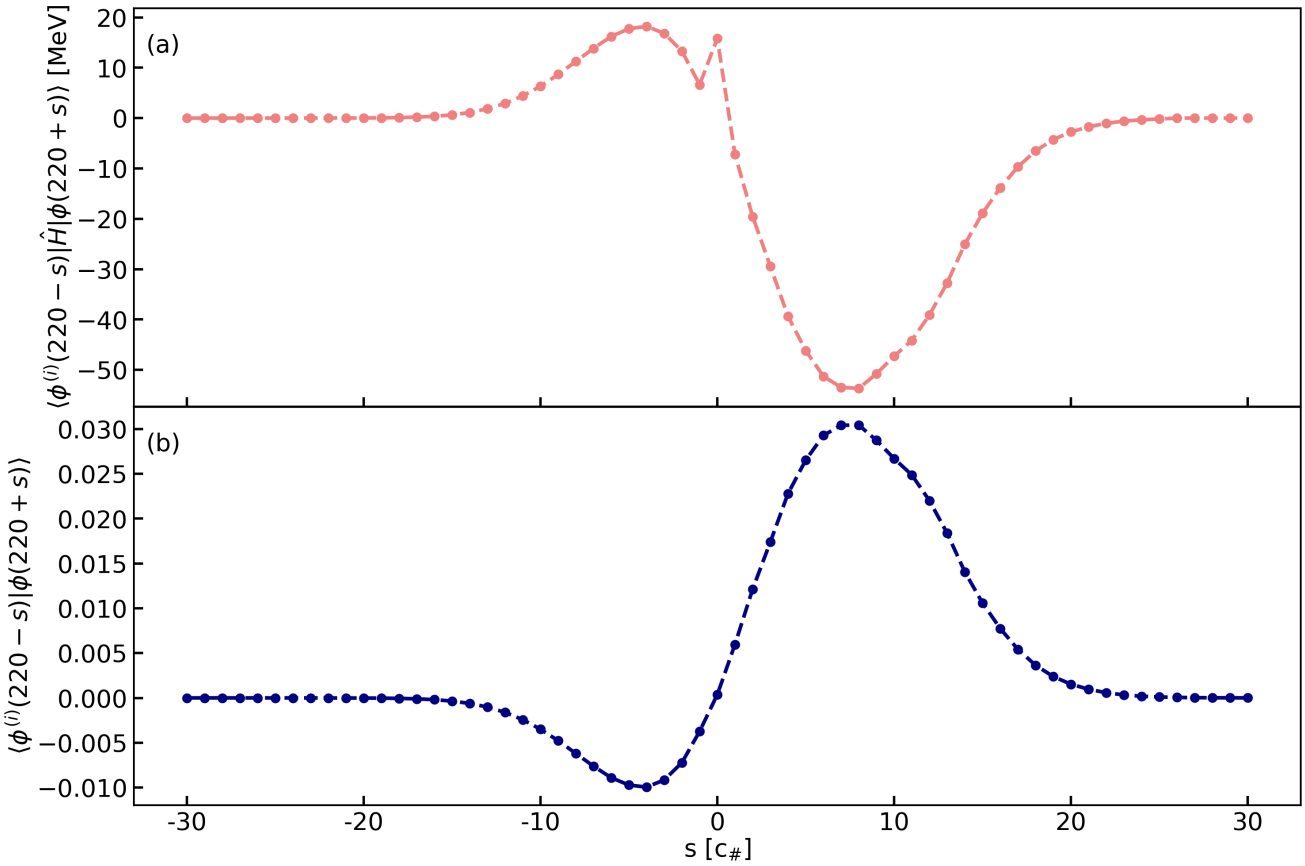

Figure 5.3: Illustration of small Hamiltonian kernel divergences. Panel (a): representation of the Hamiltonian kernel $\langle\Phi^{(i)}(220-s)|\hat{H}|\Phi(220+s)\rangle$, the superscript (i) standing for the neutron $\Omega = 1/2$ variational excitation, with respect to s [c$_\#$]. Panel (b): representation of the overlap kernel $\langle\Phi^{(i)}(220-s)|\Phi(220+s)\rangle$, with respect to s [c$_\#$].

In panel (a), we clearly observe the divergence problem at $s = 0$. However, it is both well-localized and very reasonable compared to the overall amplitude of the curve. Besides, we see that both the Hamiltonian kernels and the overlap ones vary accordingly.
On the contrary, in Figure (5.4), we've represented much more severe divergences. In panel (a), we've plotted the Hamiltonian kernel $\langle\Phi^{(i)}(320-s)|\hat{H}|\Phi(320+s)\rangle$, with respect to s. In panel (b), we've displayed the overlap kernel $\langle\Phi^{(i)}(320-s)|\Phi(320+s)\rangle$, with respect to s. In this case, we see that the amplitude of the anomalies are very problematic. Moreover, the anomalies are spread and not only localized at $s = 0$, as observed in Figure (5.3). We attribute this feature to the fact that the associated overlap kernel values are very small in the range $s \in [-1, 10]$. Finally, we remark, here also, that the Hamiltonian and overlap kernels tend to vary accordingly (if we don't focus on the divergent part):

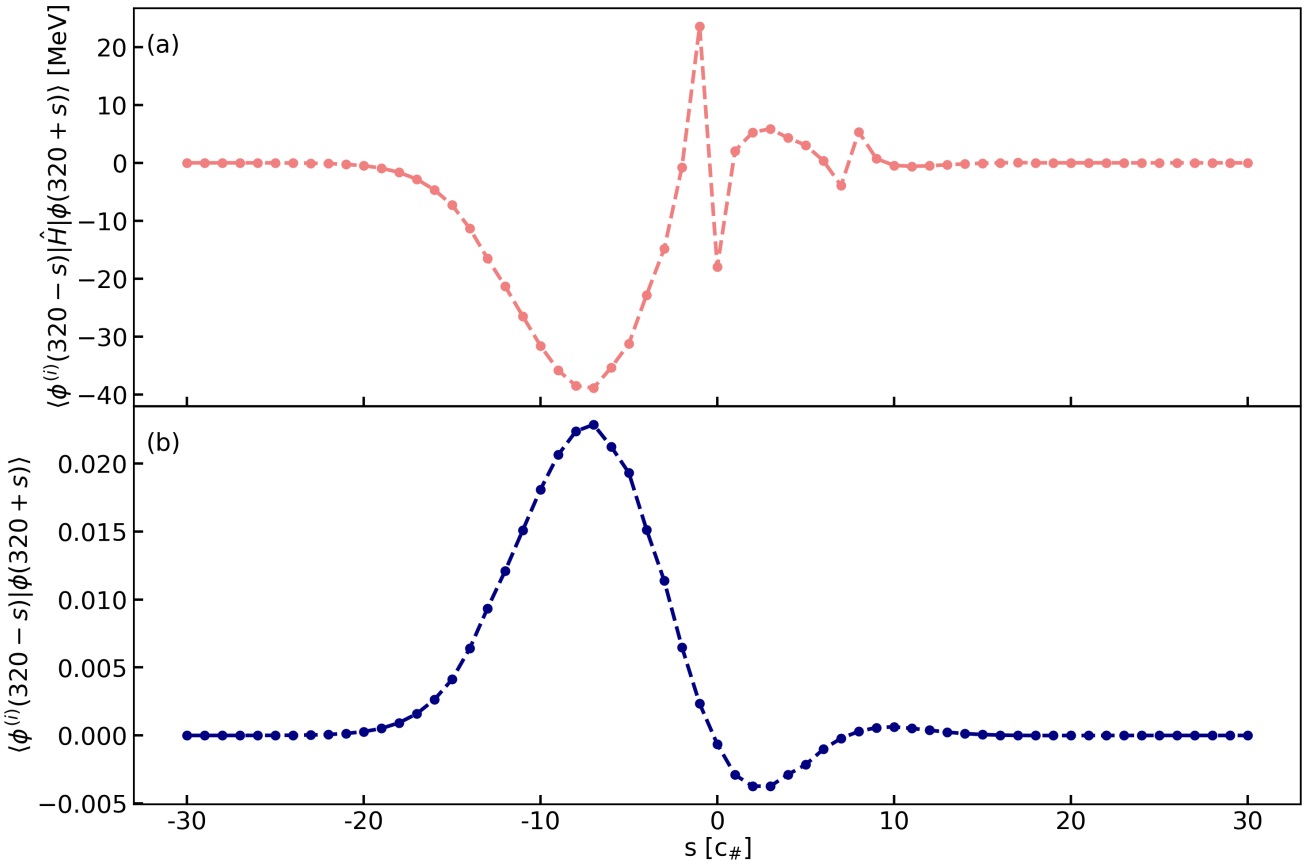

Figure 5.4: Illustration of severe Hamiltonian kernel divergences. Panel (a): representation of the Hamiltonian kernel $\langle\Phi^{(i)}(320-s)|\hat{H}|\Phi(320+s)\rangle$, with the superscript (i) standing for the neutron $\Omega = 1/2$ variational excitation, with respect to s [c$_\#$]. Panel (b): representation of the overlap kernel $\langle\Phi^{(i)}(320-s)|\Phi(320+s)\rangle$, with respect to s [c$_\#$].

To tackle these issues, we've tested three different prescriptions. The first one comes from the similarity between the Hamiltonian and overlap kernel behaviors. It is a straightforward extension of the local approximation, and we refer to it the overlap prescription. It reads as follows:

$$\boxed{\langle\Phi^{(i)}(\bar{q}-s)|\hat{H}|\Phi(\bar{q}+s)\rangle_{cor} = \frac{E^{(i)}(\bar{q})+E(\bar{q})}{2}\langle\Phi^{(i)}(\bar{q}-s)|\Phi(\bar{q}+s)\rangle} \tag{5.383}$$

The two other prescriptions have been inspired by [71]. The idea is to multiply the divergent quantities by their associated overlap kernel in order to compensate for the quadratic speed of the divergent denominator. We've tried two different ways to apply this idea in practice. The first prescription is to correct only the term associated with $s = 0$. Therefore, we call this prescription the zero prescription. It reads explicitly as:

$$\boxed{\langle\Phi^{(i)}(\bar{q}-s)|\hat{H}|\Phi(\bar{q}+s)\rangle_{cor} = \langle\Phi^{(i)}(\bar{q}-s)|\hat{H}|\Phi(\bar{q}+s)\rangle[\delta_{s\neq 0}+\delta_{s=0}\langle\Phi^{(i)}(\bar{q}-s)|\Phi(\bar{q}+s)\rangle]} \tag{5.384}$$

In addition, because of the very spread anomalies displayed in Figure (5.4), we've thought that correcting at $s = 0$ only would surely not be sufficient. Thus, we've defined the threshold prescription:

$$\boxed{\langle\Phi^{(i)}(\bar{q}-s)|\hat{H}|\Phi(\bar{q}+s)\rangle_{cor} = \langle\Phi^{(i)}(\bar{q}-s)|\hat{H}|\Phi(\bar{q}+s)\rangle[\delta_{s>\epsilon} + \delta_{s\leq\epsilon}\langle\Phi^{(i)}(\bar{q}-s)|\Phi(\bar{q}+s)\rangle]} \quad (5.385)$$

In panels (a-c) of Figure (5.5), we've displayed the results of the three mentioned prescriptions in the Hamiltonian kernels related to the small divergences observed in Figure (5.3). Concerning the threshold prescription, we've chosen $\epsilon = 5 \times 10^{-3}$:

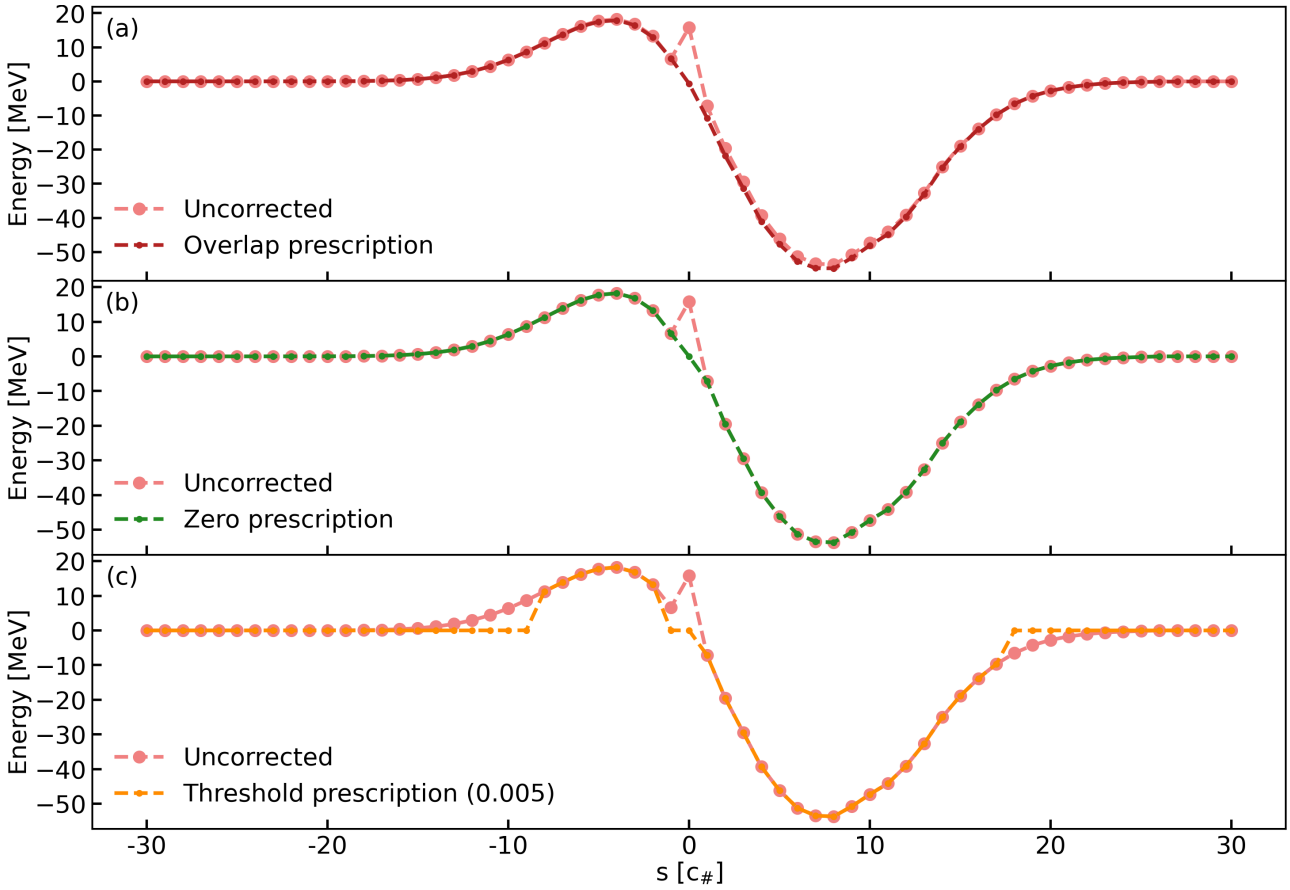

Figure 5.5: Illustration of the Hamiltonian kernel prescriptions at $\bar{q} = 220$ [$c_{\#}$]. Panel (a): the overlap prescription. Panel (b): the zero prescription. Panel (c): the threshold prescription.

We clearly observe in panels (a-b) that both the overlap and the zero prescriptions work very well to smooth the divergence out. On the other hand, the threshold prescription exhibits threshold discontinuities.
In panels (a-c) of Figure (5.6), we've plotted the results of the three prescriptions in the Hamiltonian kernels related to the severe divergences observed in Figure (5.4). We've kept $\epsilon = 5 \times 10^{-3}$ in the threshold prescription:

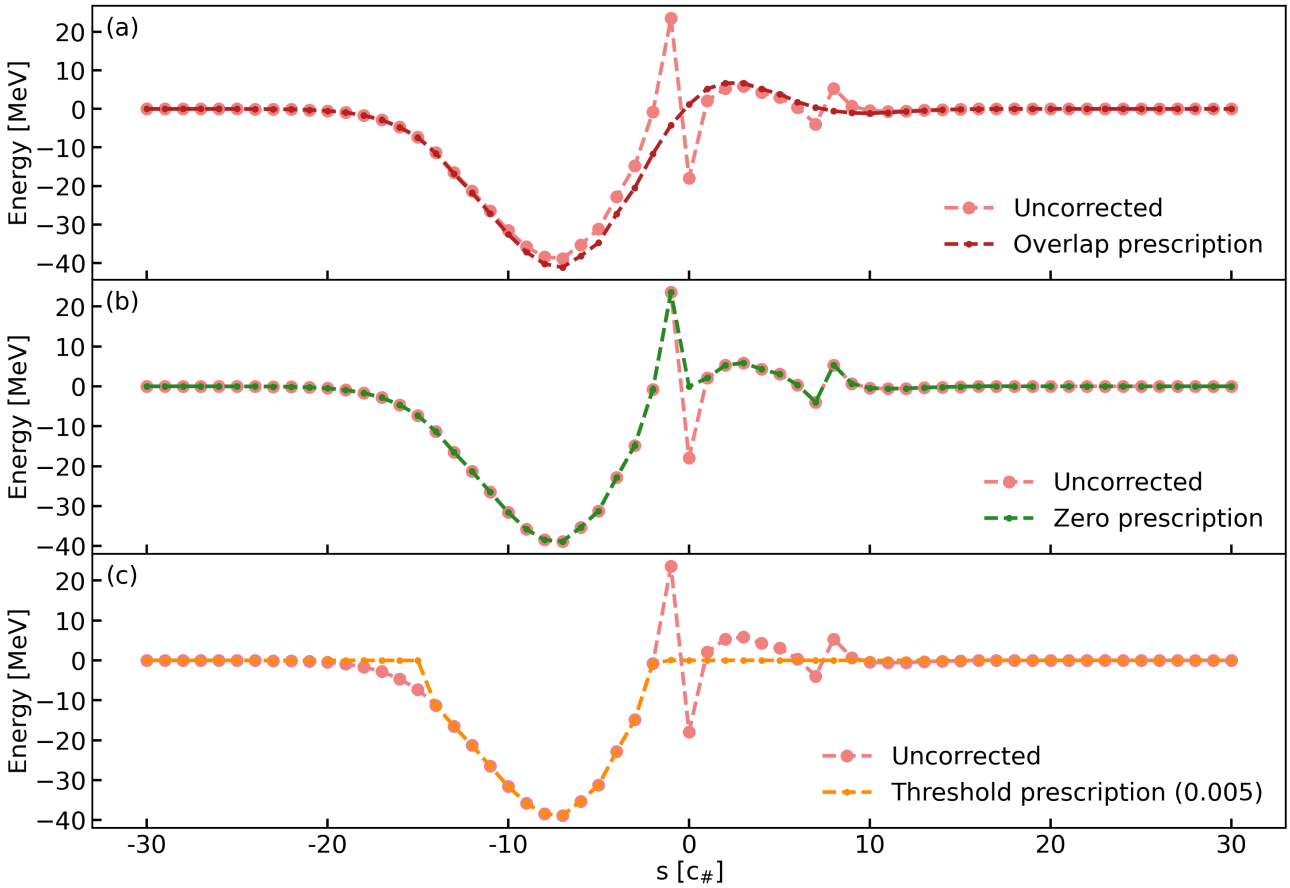

Figure 5.6: Illustration of the Hamiltonian kernel prescriptions at $\bar{q} = 320$ [$c_{\#}$]. Panel (a): the overlap prescription. Panel (b): the zero prescription. Panel (c): the threshold prescription.

This time, it seems that the overlap prescription displayed in panel (a) has the smoothest and most natural behaviour. In panel (b), we see as expected that the zero prescription is not sufficient to treat spread divergences. Finally, in panel (c), we observe that the threshold prescription behaves in a more regular way than the zero one. However, it is also clear that it neglects a part of the Hamiltonian kernel behaviour, due to threshold effects.

In the light of these observations, we've naturally chosen the overlap prescription to evaluate the problematic Hamiltonian kernels. A very interesting and convenient feature of this prescription lies in the fact that only the numerical evaluations of the diagonal Hamiltonian kernels (in terms of excitations) are then required within the SCIM formalism. It is a real advantage when numerous variational excitations are considered.
A more in depth study would be required to characterize thoroughly the quality of the overlap prescription. However, we do believe that it is a good starting point for the first applications of the SCIM approach.

Chapter 6

Dynamical description of ^{240}Pu fission along an asymmetric path

This Chapter aims to discuss the SCIM "dynamics". Firstly, we explain how the SCIM potential, dissipation tensor, and inertia tensor are evaluated in practice. Then, we analyze these three dynamical ingredients. In particular, we compare the SCIM potential and the SCIM inertia tensor at the adiabatic limit (without considering any excitation), to the ones obtained within the GOA formalism, with and without approximations.
Besides, the SCIM inertia tensor analysis reveals that some excitations are well suited for the "dynamics" while other are not. This observation leads to define the scenario (*), which corresponds to the inclusion of six different excitations in the "dynamics" in addition to the adiabatic states.
Secondly, we focus on the collective-intrinsic Schrödinger equation associated with the SCIM Hamiltonian $\mathcal{H}_{SCIM}$. We first detail the numerical solution of the collective-intrinsic Schrödinger equation. Then, we present the formalism developed in this PhD thesis to extract the different adiabatic and excited probability fluxes.
Finally, we analyze the "dynamics" results associated with the scenario (*). We start by analyzing the probability fluxes and the associated excited yields. Then, we study the excitation impact on the fragments particle number distributions at scission. At last, the energy balance at scission is discussed.

6.1 Dynamical ingredients

This section is dedicated to the SCIM Hamtilonian ingredients. Namely, we study the potential V, the dissipation tensor D, and the inertia tensor B. The formalism leading to these three different quantities is detailed in Chapter 1, and their explicit formulas are presented in Appendix M.

In practice, we've found out that even with an appropriate collective coordinate as $c_{\#}$ (see Chapter 2 and Chapter 3), the regularity of the kernel moments was not good enough to obtain the dynamical ingredients V, D and B with the method presented in Chapter 1. To tackle this issue, we've implemented the Savitzky-Golay filter [72], called SG-differentiation in the following. The SG-differentiation is a well-known tool in numerical analysis and is commonly used to smooth-out high frequency fluctuations in order to focus on longer trends. In the first part of this section, we therefore precisely discuss why we had to use the SG-differentiation and how we've used it.

Then, we analyze the dynamical quantities obtained. Our studies of the SCIM potential V and the SCIM inertia tensor B share the same structures. Firstly, we compare their adiabatic limit to the ZPE and inertial masses obtained with the GOA (without approximation), GOA+Cranking, and GOA+ATDHFB. As far as we know, it is the first time that relevant GOA ZPE and GOA inertial mass are calculated without approximations in the fission context.
Following this analysis, we propose a complete study of the different quantities V and B associated with each variational excitation in the limit case where each of them is treated alone. We call this case the "adiabatic-excited" limit, as we treat the different excited sets as if they were the adiabatic one. Then, we study how the adiabatic quantities are renormalized by the addition of the variational excitations within the scenario $(*)$. Finally, we discuss the order of magnitude of the new off-diagonal parts of V and B in the scenario $(*)$.
To conclude, when it comes to the dissipation tensor D, we simply discuss the order of magnitude of its different components in the scenario $(*)$.

6.1.1 The SG-differentiation

As stated in introduction, the Savitzky-Golay filter or SG-differentiation is a powerful tool to treat the unwanted fluctuations of a given function when differentiating it. In the literature, this method is often used to get rid of noise issues associated with experimental data sets. In practice, the application of the method to the differentiation of a finite set representing the values of a function f reads as follows:

- At each point c, we consider the set of points $\{x_c\}$ in the range $[c - \frac{(r-1)}{2}, c + \frac{(r-1)}{2}]$. The importance of the parameter r is discussed in the following.
- Then, we build the polynomial P_c of order n, which minimizes the linear least squares error with respect to the set $\{x_c\}$. We've chosen $n = 3$ in this PhD thesis work.
- Finally, we set $f'(c) = P'_c(c)$, $f''(c) = P''_c(c)$, and $f'''(c) = P'''_c(c)$.

In our case, we've desired to separate the physics contained in the kernel moments into two parts. The first part is the one associated with the physical phenomena of medium and low frequency. These phenomena correspond to the physics the SCIM approach has been designed to treat. Therefore, this part is the one we want to keep.
On the other hand, the higher-frequency phenomena cannot be studied using the SCIM method. This limitation is related to the order 2 trunctation used for the SOPO (see Chapter 1). Thus, this part is the one we want to filter.
Finally, we highlight that the SG-differentiation only applies to differentiation. It means that the non-derivated quantities are kept as they are. In practice, it is not a problem as the higher frequency components naturally vanish in the ratios between Hamiltonian kernel moments and overlap ones (see Chapter 2 as well as the introduction of Chapter 3).

To better understand why the SG-differentiation method is necessary, we can observe the diagonal adiabatic zero-order moment of the overlap kernel $\mathcal{N}_{00}^{(0)}$. In Figure (6.1), we've displayed $\mathcal{N}_{00}^{(0)}(c_\#)$, with respect to the collective coordinate $c_\#$:

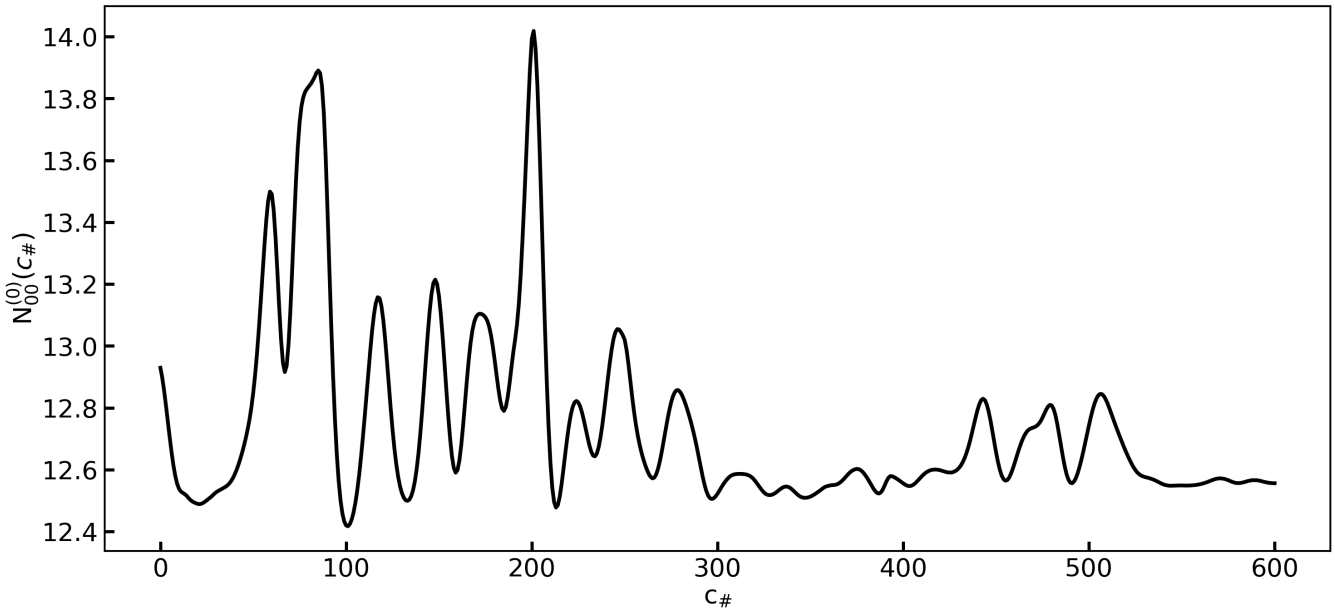

Figure 6.1: Adiabatic zero-order moment of the overlap kernel $\mathcal{N}_{00}^{(0)}(c_\#)$, with respect to the collective coordinate $c_\#$.

Looking at Figure (6.1), we clearly see the presence of high frequency components in the overlap moment $\mathcal{N}_{00}^{(0)}$. In practice, using the customary finite difference method, it was not even possible to achieve the iterative factorization process required to obtain the inverse square root of the operator $\bar{\mathcal{N}}$ described in Chapter 1.
In Figure (6.2), we've compared the first derivative of $\mathcal{N}_{00}^{(0)}$ obtained with the finite difference method and three different filtered versions of $\mathcal{N}_{00}^{(0)}$ evaluated using the SG-differentiation method with different r parameters:

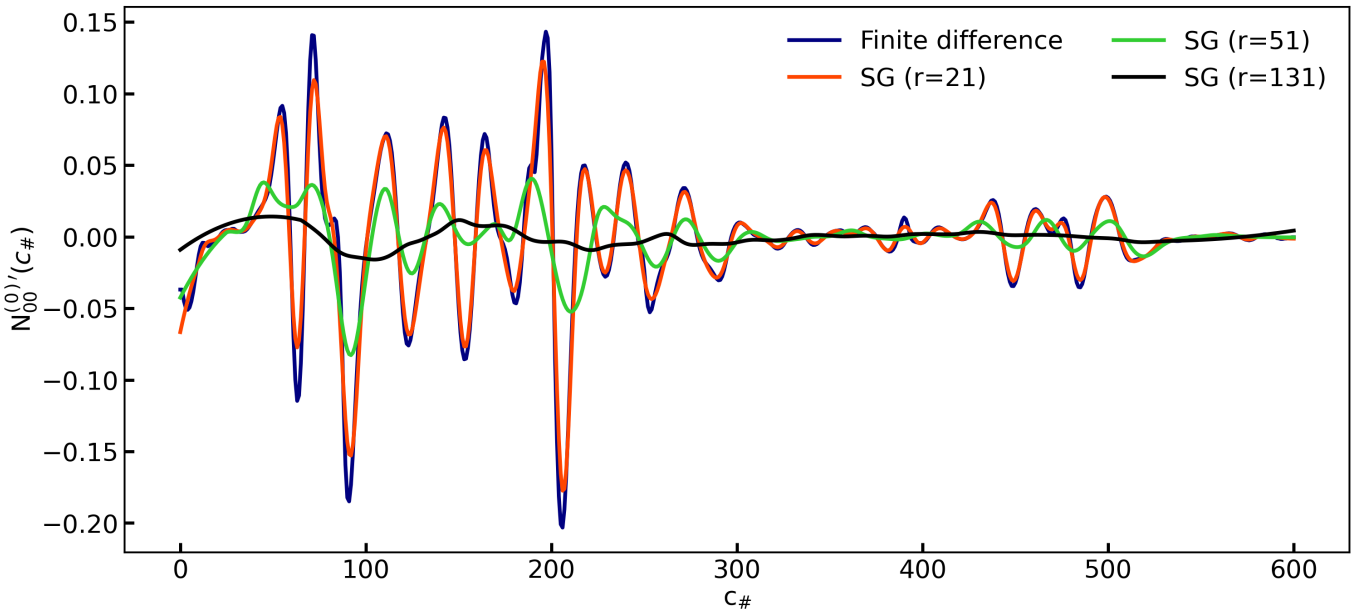

Figure 6.2: Comparison between the finite difference method and the SG-differentiation method, with different r parameters, in the calculation of $N_{00}^{(0)\prime}$.

In Figure (6.2), we directly observe how the SG-differentiation method attenuates the fluctuations of the derivative $\mathcal{N}_{00}^{'(0)}$. The greater the r parameter, the smaller the fluctuations. For r values greater than 25, it was possible to get the inverse square root of $\bar{\mathcal{N}}$.
With this inverse square root $\bar{\mathcal{N}}^{-1/2}$, it is then easy to evaluate the dynamical quantities V and B. We naturally sought to address the impact of the choice of the parameter r on these latter quantities. In panel (a) of Figure (6.3), we've plotted the values $B(c_{\#})$ obtained with different r parameters with respect to $c_{\#}$. In panel (b), we've represented the values $V(c_{\#})$ obtained with different r parameters with respect to $c_{\#}$:

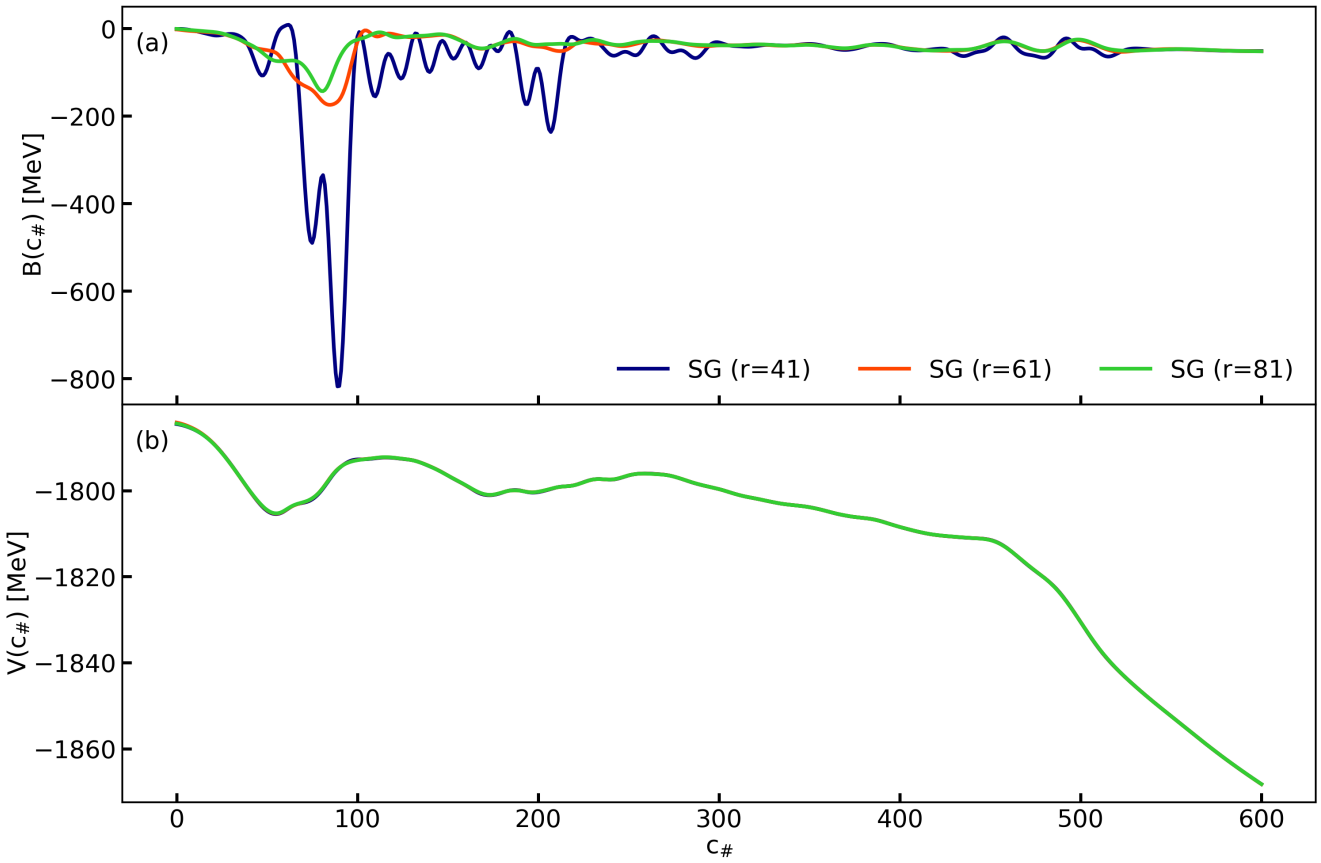

Figure 6.3: Illustration of the impact of the r parameter of the SG-differentiation on both the potential V and the inertia tensor B. Panel (a): values of the inertia tensor B, with respect to $c_{\#}$ and for different r parameters. Panel (b): values of the potential V, with respect to $c_{\#}$ and for different r parameters.

First of all, it is striking to observe in panel (b) that the values of the potential V do not seem to depend on the choice of the parameter r. This behaviour was expected. Indeed, as already stated in the introduction of Chapter 3, the leading term of the potential V approximately equals the quantity $\mathcal{N}^{(0)-1/2}\mathcal{H}^{(0)}\mathcal{N}^{(0)-1/2}$, which does not depend on derivatives.
On the contrary, we see in panel (a) that the values of the inertia tensor B do vary a lot with respect to the choice of the parameter r. This feature was also expected. We remarked in the introduction of Chapter 3 that the inertia tensor values mostly depend on the derivatives, as its different non-derivatives components tend to cancel out.
Given the large variations in the values of the inertia tensor B displayed in panel (a), it is *a priori* difficult to determine a relevant value for the parameter r. However, looking at the

orange and green curves standing respectively for $r = 61$ and $r = 81$, we can guess that the values of B may converge, increasing the parameter r.
In Figure (6.4), we've displayed the test of this convergence assumption. In panel (a), we've represented the values $B(c_\#)$ obtained with different higher values of the r parameter with respect to $c_\#$. In panel (b), we've represented the corresponding values $V(c_\#)$, with respect to $c_\#$:

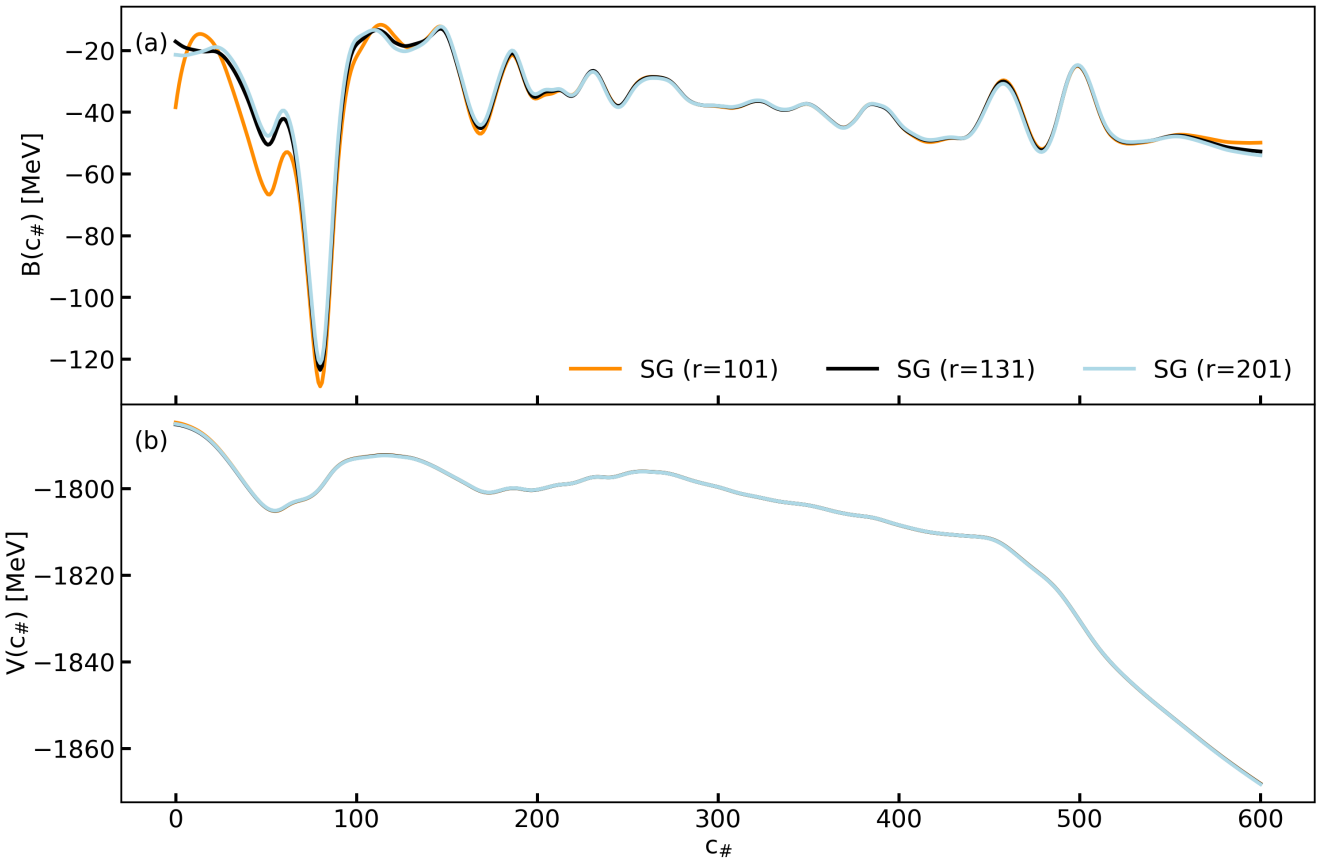

Figure 6.4: Test of the convergence assumption with regard to the inertia tensor B. Panel (a): values of the inertia tensor B, with respect to $c_\#$ and for different r parameters. Panel (b): values of the potential V, with respect to $c_\#$ and for different r parameters.

The results displayed in panel (b) confirm that the potential V is still not impacted by the choice of the parameter r. Besides, we observe in panel (a) the convergence of the $B(c_\#)$ values we've supposed earlier.
In the light of these results, we've chosen the parameter value $r = 131$ for the applications presented in this PhD thesis. Indeed, this value ensures a good convergence of the inertia tensor B. Besides, as we will see in the following sections, the good agreement between the ZPE and the inertial mass obtained with the SCIM method using this parameter value and the ones coming from the GOA (and its associated approximations), clearly highlights the relevance of this choice.

6.1.2 Potential

This section is dedicated to the study of the SCIM potential V.

Comparison with the GOA:

Firstly, we want to compare it at the adiabatic limit (considering no excitation) with the GOA potential, obtained with and without approximation. To do so, we have to express the SCIM Hamiltonian $\mathcal{H}_{SCIM}$ at the adiabatic limit and the GOA Hamiltonian $\mathcal{H}_{GOA}$ in the form. We start recalling their expressions:

$$\boxed{\mathcal{H}_{SCIM}(c_\#) = V_{SCIM}(c_\#) + [B_{SCIM}(c_\#)\frac{\partial}{\partial c_\#}]^{(2)}} \tag{6.1}$$

And:

$$\boxed{\mathcal{H}_{GOA}(c_\#) = V_{GOA}(c_\#) + \frac{\partial}{\partial c_\#}B_{GOA}(c_\#)\frac{\partial}{\partial c_\#}} \tag{6.2}$$

There is no dissipation tensor D in Eq.(6.1) because it vanishes at the adiabatic limit. Moreover, it is necessary to develop the SOPO in this same equation in order to find a form similar to Eq.(6.2):

$$\boxed{\mathcal{H}_{scim}(c_\#) = \big(V_{SCIM}(c_\#) + B''_{SCIM}(c_\#)\big) + 4\frac{\partial}{\partial c_\#}B_{SCIM}(c_\#)\frac{\partial}{\partial c_\#}} \tag{6.3}$$

From Eq.(6.3), it is clear that the quantities to compare are $V_{SCIM} + B''_{SCIM}$ and V_{GOA}. To evaluate B''_{SCIM}, we use the finite difference method and not the SG-differentiation one. It is important to keep in mind that the SG-differentiation method is only used within the SCIM formalism to obtain the expression of the quantities V, D and B. Once the latter are determined, we go back to using the customary differentiation.
Now, we focus on V_{GOA}. In Chapter 1, we've demonstrated that it can be expressed as follows:

$$\boxed{V_{GOA}(c_\#) = E_{HFB}(c_\#) + \frac{1}{2\gamma_0}h^{(2,0)}(c_\#, c_\#) + \frac{1}{8\gamma_0^2}\frac{\partial^2}{\partial c_\#^2}[h^{(2,0)}(c_\#, c_\#)]} \tag{6.4}$$

With:

$$h(c_\#, c'_\#) = \frac{\langle\Phi(c_\#)|\hat{H}|\Phi_(c'_\#)\rangle}{\langle\Phi(c_\#)|\Phi_(c'_\#)\rangle} \qquad \text{and} \qquad h^{(2,0)}(c_\#, c'_\#) = \frac{\partial^2}{\partial c_\#^2}h(c_\#, c'_\#) \tag{6.5}$$

The different derivatives appearing in Eq.(6.4) are evaluated using the finite difference method. Besides, the constant γ_0 is defined as follows within the GOA formalism:

$$\langle\Phi(c_\#)|\Phi(c'_\#)\rangle = e^{-\frac{1}{2}\gamma_0(c_\# - c'_\#)^2} \tag{6.6}$$

Eq.(6.6) does not hold exactly, since the overlap kernels related to our adiabatic set do not perfectly follow the GOA (see Chapter 2). However, as the overlap between two adjacent

states is always 0.995 in the adiabatic set obtained with the $\tilde{\mathcal{P}}_{20}$ procedure, it is reasonable to determine γ_0 through the following equation:

$$\boxed{\langle \Phi(c_\#) | \Phi(c_\# + 1) \rangle = e^{-\frac{1}{2}\gamma_0} \qquad \Rightarrow \qquad \gamma_0 = -2\ln(0.995)} \tag{6.7}$$

In addition to the exact GOA potential V_{GOA} presented above. We've evaluated both the potentials associated with the GOA+Cranking approximation and with the GOA+ATDHFB approximation. The related formulas are given in Chapter 1.
In the following, we've decided to compare the ZPE and not directly the potentials. Indeed, the differences between the quantities are much clearer considering the ZPE. The ZPE associated with a potential V simply reads as follows:

$$\boxed{\mathrm{ZPE}(c_\#) = V(c_\#) - E_{HFB}(c_\#)} \tag{6.8}$$

In Figure (6.5), we've represented the ZPE associated with the SCIM formalism, the ZPE associated with the GOA formalism without approximation (noted exact GOA), and both the ZPE associated with the GOA+Cranking and GOA+ATDHFB approximations:

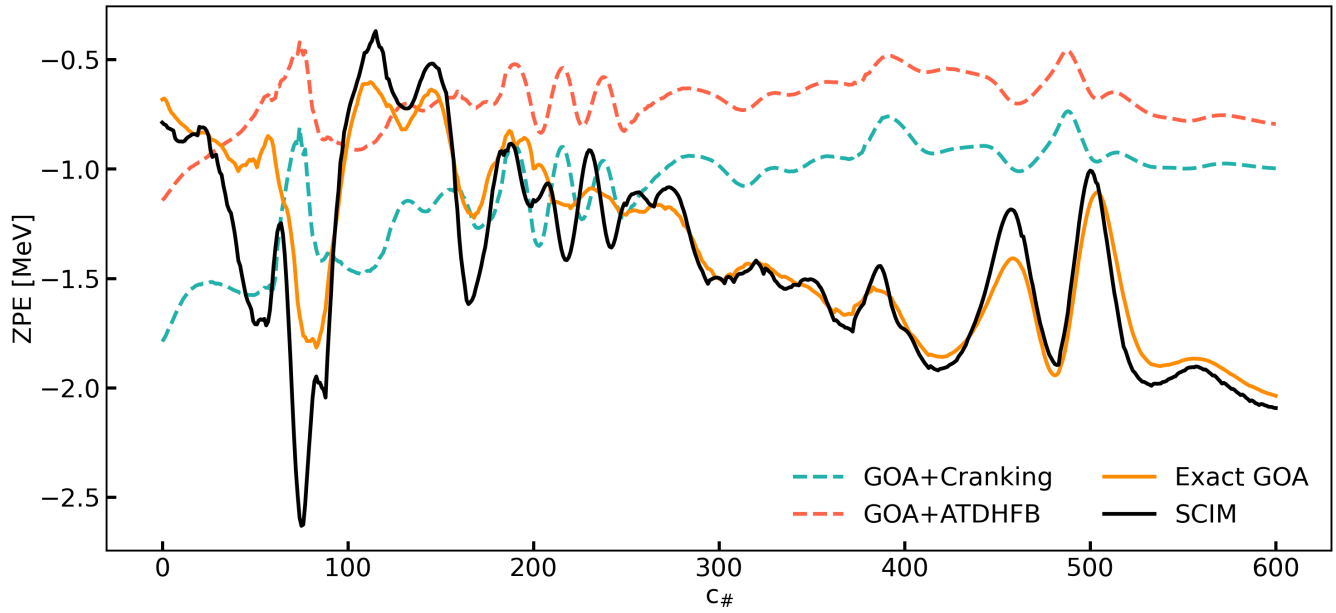

Figure 6.5: Comparison between the ZPE obtained with the SCIM formalism, the ZPE obtained with the GOA formalism without approximation, and both the ZPE associated with the GOA+Cranking and GOA+ATDHFB approximations.

The most striking phenomenon observed in Figure (6.5) is the very good overall agreement between the SCIM ZPE and the GOA ZPE evaluated without approximation. This agreement clearly underlines the revelance of the SCIM formalism. That said, we observe significant differences at the level of the ground state well ($c_\# \approx 80$) and at the first barrier ($c_\# \approx 120$). These differences lead to a "collective" first barrier 1 MeV higher in the case of the SCIM potential.
When it comes to the ZPE related to the GOA+Cranking and GOA+ATDHFB approximations, it is first important to remark that they only imply a shift in the scission descent

(comparing the HFB energy with the resulting collective potential), while the other ZPE correspond to a steeper scission descent. This feature may lead to different dynamical properties. Then, we observe something like a slight horizontal shift in the patterns of both the approximated ZPE compared to the patterns of the SCIM and exact GOA ones. We attribute this shift to the fact that the approximated ZPE are local quantities (with respect to $c_{\#}$), while the others take into account non-local effects.

Study of the adiabatic-excited limit:

We've compared the SCIM potential at the "adiabatic limit" with the different SCIM potentials associated with the variational excitations at the "adiabatic-excited" limit. We recall that, in the "adiabatic-excited" limit, we consider a variational excited set alone, as if it were the adiabatic one.
This study is designed as a first check of the variational excitations dynamical properties. Its goal is to perform an early detection of possible pathologies. In panel (a) of Figure (6.6), we've displayed the SCIM potential at the adiabatic limit and the SCIM potentials at the "adiabatic-excited" limit associated with the neutron variational excitations, with respect to $c_{\#}$. In panel (b), we've represented the same for proton variational excitations:

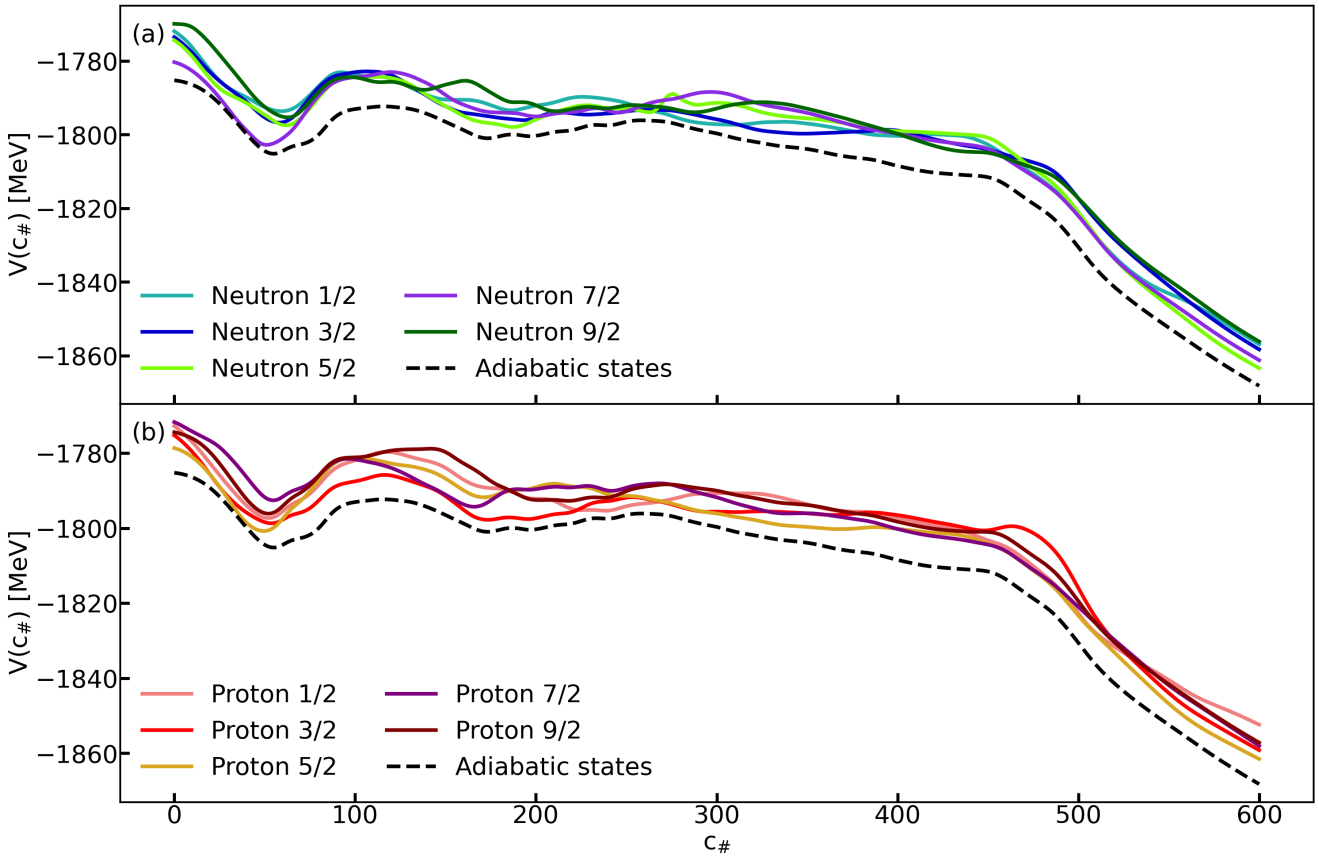

Figure 6.6: Comparison between the SCIM potential at the adiabatic limit and the SCIM potentials associated with the variational excitations at the "adiabatic-excited" limit. Panel (a): the SCIM potential at the adiabatic limit with SCIM potentials at the "adiabatic-excited" limit associated with the neutron variational excitations. Panel (b): same as panel (a), but for proton variational excitations.

Neither panel (a) nor panel (b) shows any particular pathologies. The differences between the potentials are overall comparable to the ones between their related HFB energies (see Chapter 3).

Study of the adiabatic renormalization in the scenario (*):

We've studied how the SCIM potential at the adiabatic limit is renormalized when excitations are considered. More explicitly, in Figure (6.7), we've compared the SCIM potential V at the adiabatic limit with the V_{00} component of the SCIM potential V in the scenario (*).

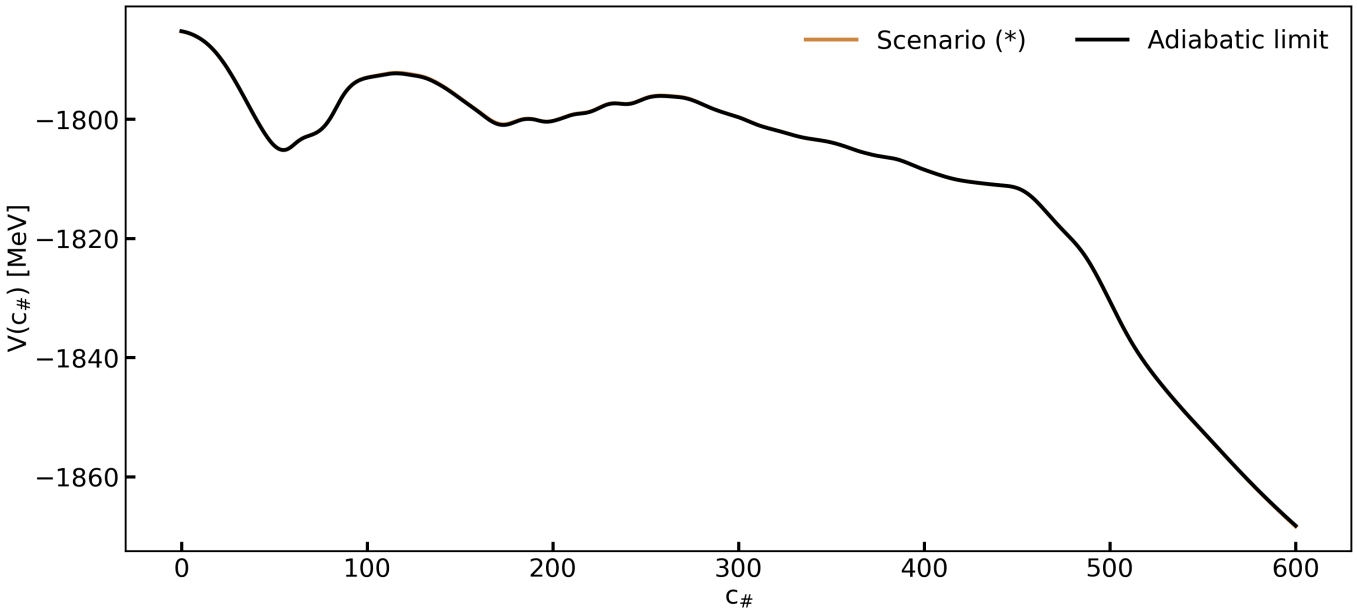

Figure 6.7: Study of the renormalization of the diagonal adiabatic potential induced by the variational excitations in the scenario (*).

We observe that the SCIM potential V is almost not renormalized at all by the variational excitations. This feature originate from the non-differentiated nature of the SCIM potential leading term. Indeed, the order of magnitude of the diagonal components of both the Hamiltonian kernel moment $\mathcal{H}^{(0)}$ and the overlap kernel moment $\mathcal{N}^{(0)}$ is much greater than the off-diagonal ones.

Study of the off-diagonal SCIM potential components in the scenario (*):

Finally, in Table (6.1), we've displayed the maximum absolute values of the different components of the SCIM potential V in the scenario (*):

	a	$n_{1/2}$	$n_{3/2}$	$n_{7/2}$	$p_{1/2}$	$p_{5/2}$	$p_{7/2}$
a	1868.34	0.57	0.83	0.02	0.17	0.28	1.85
$n_{1/2}$	-	1856.93	0.20	0.02	0.03	0.07	0.09
$n_{3/2}$	-	-	1858.34	0.04	0.00	0.03	0.3
$n_{7/2}$	-	-	-	1861.25	0.00	0.00	0.00
$p_{1/2}$	-	-	-	-	1852.38	0.26	0.04
$p_{5/2}$	-	-	-	-	-	1861.55	0.21
$p_{7/2}$	-	-	-	-	-	-	1858.07

Table 6.1: Maximum absolute values of the different components of the SCIM potential V in the scenario (*).

Here, the shorthand notation a stands for the adiabatic level. It is clear that the off-diagonal components are much smaller than the diagonal ones. In addition, the off-diagonal adiabatic-excited components are overall greater than the off-diagonal excited-excited ones. This feature signifies that the static couplings between the adiabatic states and the excitations are stronger than the static couplings between two different excitations. Besides, we observe that the neutron $\Omega = 7/2$ variational excitation does not exhibit any relevant static coupling (the associated values are smaller than 10^{-2}).
Finally, we've represented in Figure (6.8) the adiabatic-excited off-diagonal potential component $V_{(a,n_{1/2})}$ and the excited-excited off-diagonal potential component $V_{(n_{1/2},n_{3/2})}$, with respect to $c_{\#}$:

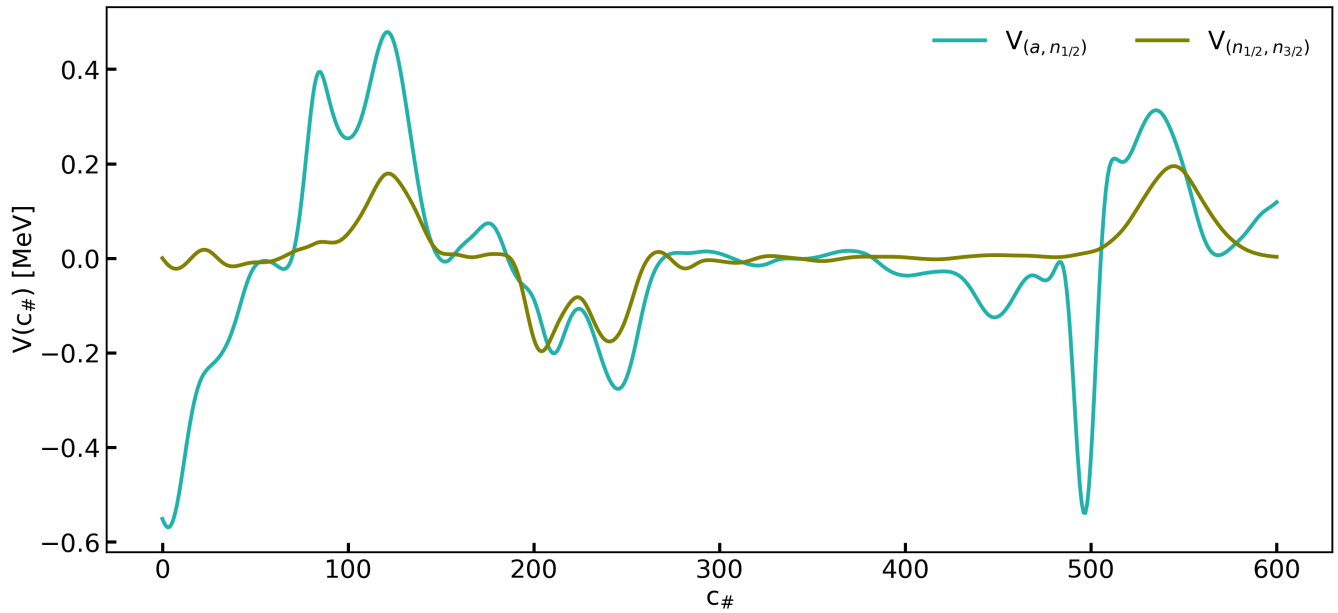

Figure 6.8: Comparison between the off-diagonal potential component $V_{(a,n_{1/2})}$ and the off-diagonal potential component $V_{(n_{1/2},n_{3/2})}$, with respect to $c_{\#}$.

Figure (6.8) confirms the observations made in Table(6.1). Indeed, we observe a greater amplitude in the case of the adiabatic-excited potential. Besides, we notice ineresting patterns around the first barrier ($c_{\#} \approx 120$), near the saddle point ($c_{\#} \approx 267$), and near scission ($c_{\#} \approx 495$). These patterns signify that the static couplings are relatively stronger in these areas.

6.1.3 Inertia tensor

In this section, we study the SCIM inertia tensor B.

Comparison with the GOA:

We start by comparing B_{SCIM} with the GOA inertia tensor B_{GOA} obtained without approximation and with the GOA inertia tensors obtained with the GOA+Cranking and GOA+ATDHFB approximations.
In the light of Eq.(6.2) and Eq.(6.3) of the previous section, it is clear that the quantities relevant to compare are $4B_{SCIM}$ and B_{GOA}. In Chapter 1, we've shown that the quantity B_{GOA} reads as:

$$\boxed{B_{GOA}(c_\#) = \frac{1}{4\gamma_0^2}(h^{(2,0)}(c_\#, c_\#) - h^{(1,1)}(c_\#, c_\#))} \tag{6.9}$$

The quantities γ_0 and $h^{(2,0)}$ have been defined in the previous section and $h^{(1,1)}$ corresponds to:

$$h^{(1,1)}(c_\#, c'_\#) = \frac{\partial}{\partial c_\#}\frac{\partial}{\partial c'_\#}h(c_\#, c'_\#) \tag{6.10}$$

We've evaluated the inertia tensor B_{GOA}, as defined in Eq.(6.9), simply using the finite difference method.
The inertia tensors $B_{Cranking}$ and B_{ATDHFB} related to the GOA+Cranking and the GOA+ATDHFB approximations are more complex to compare with the quantity $4B_{SCIM}$. Indeed, both the GOA+Cranking and the GOA+ATDHFB approximations rely on the multipole moments. Therefore, the inertia tensors $B_{Cranking}$ and B_{ATDHFB} obtained with the formulas provided in Chapter 1 are expressed with respect to multipole moments related collective coordinates. As the collective coordinate $c_\#$ spans a one-dimensional path, we've decided to consider only the part of the inertia tensors $B_{Cranking}$ and B_{ATDHFB} related to the quadrupole moment Q_{20} (in practice we've tested to include Q_{30} also, and it didn't change the results in a significant way).
Noting q_{20} the collective coordinate associated with the quadrupole moment Q_{20} and $\tilde{B}_{Cranking}$ and $\tilde{B}_{ATDHFB}$ the GOA+Cranking and GOA+ATDHFB inertia tensors in the $c_\#$ representation, we can write at first order:

$$\begin{cases} \tilde{B}_{Cranking}(c_\#) = (\frac{\partial c_\#}{\partial q_{20}})^2 B_{Cranking}(c_\#) \\ \\ \tilde{B}_{ATDHFB}(c_\#) = (\frac{\partial c_\#}{\partial q_{20}})^2 B_{ATDHFB}(c_\#) \end{cases} \tag{6.11}$$

In addition, we've chosen to present the results of the comparison in terms of inertial masses and not in terms of inertia tensors. Indeed, it appeared that inertial masses are more common in the literature. We recall the general expression linking an inertia tensor B to its related inertial mass M:

$$\boxed{M(c_\#) = -\frac{1}{2B(c_\#)}} \tag{6.12}$$

In Figure (6.9), we've represented the inertial mass obtained with the SCIM method, the inertial mass associated with the GOA formalism without approximation (called exact GOA), and the GOA+Cranking and GOA+ATDHFB inertial masses, with respect to $c_{\#}$:

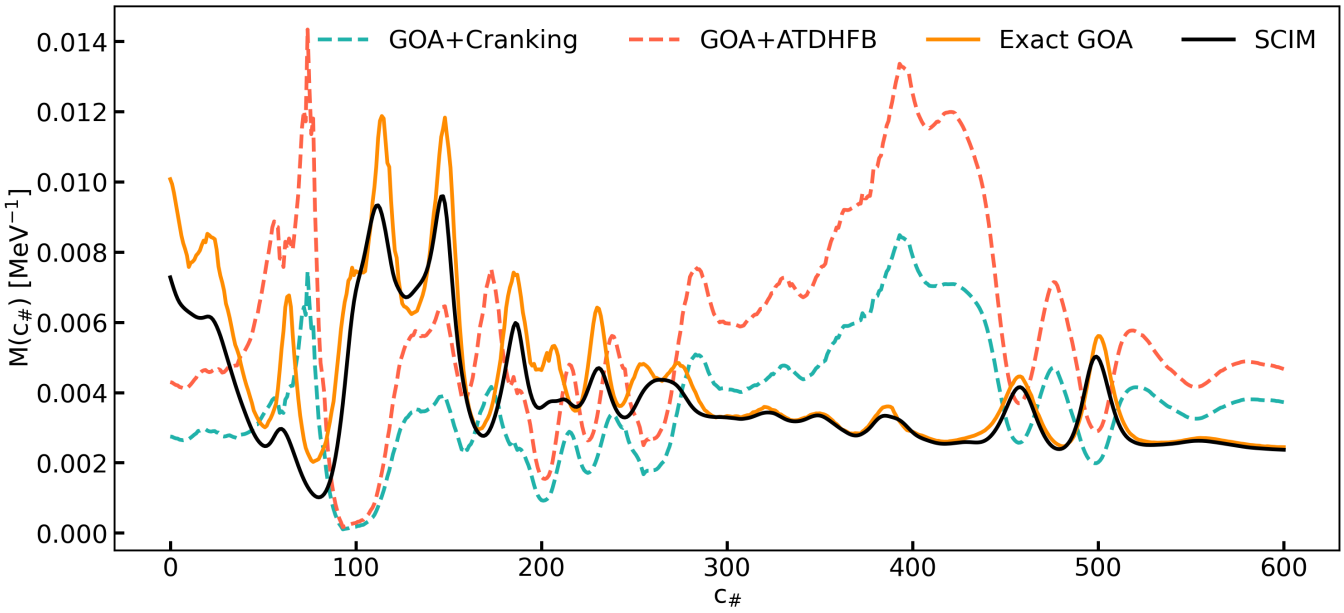

Figure 6.9: Comparison between the inertial mass obtained with the SCIM method, the inertial mass associated with the GOA formalism without approximation, and the GOA+Cranking and GOA+ATDHFB inertial masses, with respect to $c_{\#}$.

It is first striking to observe that the exact GOA inertial mass and the SCIM inertial mass are very similar, as already noticed in the case of the ZPE (see Figure (6.5)). This phenomenon confirms both the overall relevance of the SCIM approach and the particular choice we've done concerning the r parameter of the SG-differentiation. In fact, we think that choosing a large r parameter for the SG-differentiation method is comparable to the Taylor series expansion of h truncated at order 2 achieved in the GOA formalism (see Chapter 1). Indeed, both methods boil down to filtering high-frequency components.
Besides, the comparison between the SCIM and the exact GOA inertial masses on the one hand, and the GOA+Cranking and GOA+ATDHFB ones on the other hand, is very instructive. First of all, we observe that the SCIM and the exact GOA inertial masses are much greater than the approximated ones close to the first barrier ($c_{\#} \approx 120$). This property is very important, as the GOA+Cranking inertial mass is often criticized for being too small to describe spontaneous fission lifetimes accurately. It is the reason why the GOA+ATDHFB inertial mass are often preferred. The results displayed in Figure (6.9) suggest that the exact GOA masses would be even more appropriate for spontaneous fission lifetime evaluation purposes. It signifies that the physics corresponding to the exact treatment of the non-locality, which is included in the SCIM and the exact GOA inertial masses, is probably more important than the time-odd physics added thanks to the ATDHFB approximation.
Then, we still notice an horizontal shift in the approximated inertial masses patterns compared to the other ones. This observation is in line with the one made in the case of the ZPE (see Figure (6.5)). Once again, we attribute this feature to non-local phenomena (with respect to $c_{\#}$), which are taken into account by both the SCIM and the exact GOA inertial masses, but neglected in the case of both the GOA+Cranking and GOA+ATDHFB approximations.

Finally, the reader may be surprised by the huge bumps appearing in both approximated inertial masses around $c_{\#} \approx 400$. These two bumps directly come from the quantity $(\frac{\partial c_{\#}}{\partial q_{20}})^2$ in Eq.(6.11). Indeed, we've displayed in Figure (6.10) the GOA+Cranking and the GOA+ATDHFB inertial masses in the representation associated with the quadrupole moment Q_{20}. In this representation, there is no sign of the bumps observed in Figure (6.9):

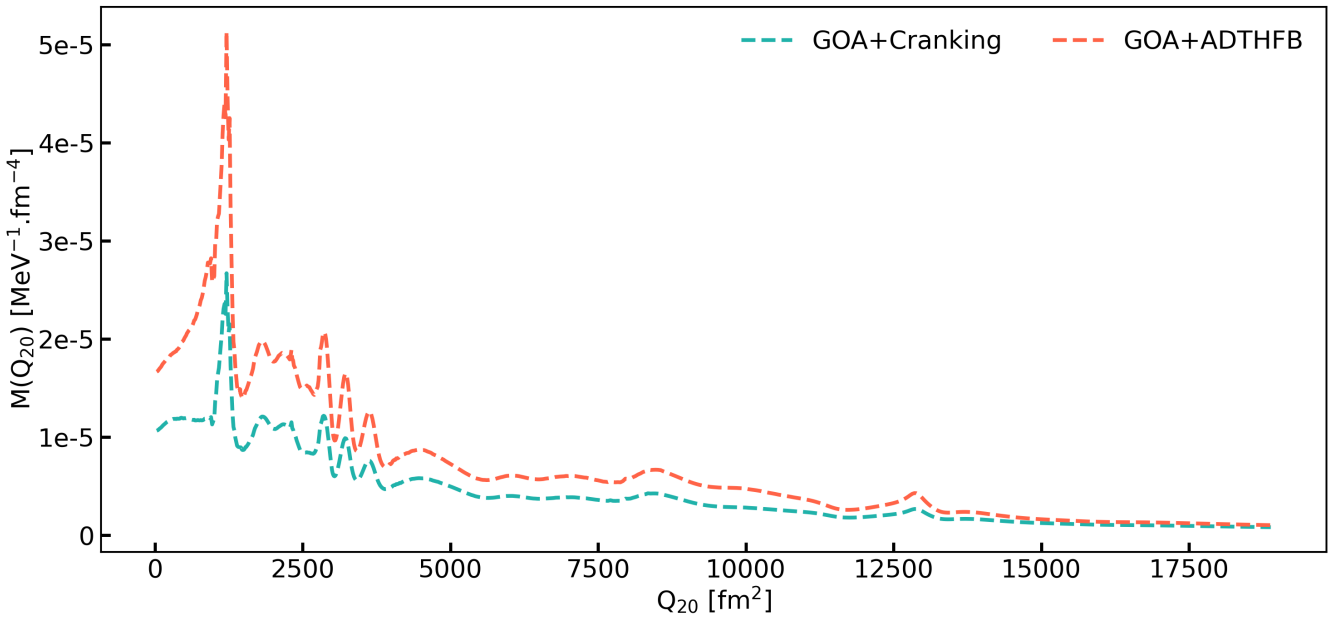

Figure 6.10: GOA+Cranking and GOA+ATDHFB inertial masses in the Q_{20} representation, with respect to Q_{20}.

The quantity $(\frac{\partial c_{\#}}{\partial q_{20}})^2$ describes how the quadrupole moment varies locally with respect to an overlap variation in the direction defined by the adiabatic path obtained with the $\tilde{\mathcal{P}}_{20}$ procedure. Therefore, it contains non-local informations missed by both the GOA+Cranking and the GOA+ATDHFB approximations. As this missing information leads to huge consequences in terms of inertial mass, we do think that taking into account the exact inertial mass in the GOA would lead to important improvements in the results provided by the method.

Study of the adiabatic-excited limit:

Then, we've studied the different SCIM inertia tensors associated with the variational excitations at the "adiabatic-excited" limit. In panel (a) of Figure (6.11), we've plotted the SCIM inertia tensor at the adiabatic limit and the SCIM inertia tensors associated with the "adiabatic-excited" limit of the neutron variational excitations. In panel (b), we've represented the same thing for the proton variational excitations:

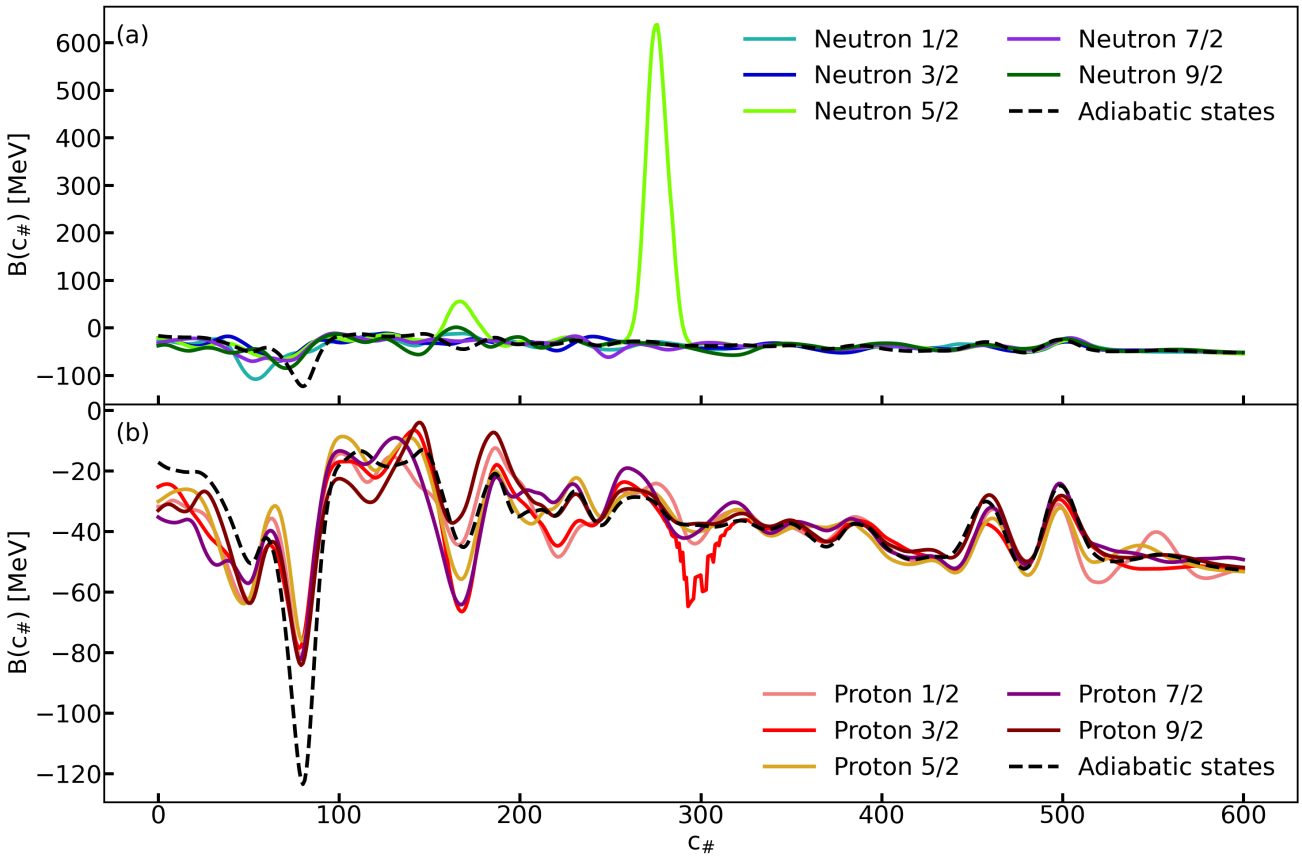

Figure 6.11: Comparison between the SCIM inertia tensor at the adiabatic limit and the SCIM inertia tensors associated with the variational excitations at the "adiabatic-excited" limit. Panel (a): the SCIM inertia tensor at the adiabatic limit with SCIM inertia tensors at the "adiabatic-excited" limit associated with the neutron variational excitations. Panel (b): the SCIM inertia tensor at the adiabatic limit with the SCIM inertia tensors at the "adiabatic-excited" limit associated with the proton variational excitations.

In panel (a), we observe that most of the inertia tensors related to the neutron variational excitations are comparable to the adiabatic one, but we can't miss the prominent light green peak associated with the neutron $\Omega = 5/2$ variational excitation. This peak remains the same when the parameter r of the SG-differentiation increases. In addition, it is clearly related to the local-approximation anomaly observed in Chapter 3. Therefore, we assume that the neutron $\Omega = 5/2$ variational excitation locally includes a peculiar physics that cannot be described accurately by the SCIM approach. Further investigations will have to be carried out in the future.
Of course, the positive values of the inertia tensors are not relevant as they lead to negative inertial mass values (and to divergences when the sign changes). Consequently, we didn't keep this excitation for the scenario (*).
In addition, some positive values are also found for the inertia tensor associated with the neutron $\Omega = 9/2$ variational excitation. Even if this peak is much smaller than the light green one, the neutron $\Omega = 9/2$ variational excitation is not suitable for dynamical pruposes. Thus, it is not included in the scenario (*).
In panel (b), the inertia tensors related to the proton variational excitations are comparable to the adiabatic one, and we don't observe pathologies similar to the ones noticed in panel (a). However, the inertia tensor associated with the proton $\Omega = 3/2$ variational excitation presents some surprising discontinuities. We were not able to clearly identify their origin,

which has probably a numerical nature. Therefore, we didn't keep this variational excitation in the scenario (*).
To conclude on the scenario (*), we wanted to use the same number of neutron and proton variational excitations within the "dynamics". For this reason, we didn't keep the proton $\Omega = 9/2$ variational excitation in the scenario (*). This choice has been motivated by the fact that this variational excitation has the highest excitation energy in average.
Finally, in order to analyze the neutron variational excitation inertia tensors kept in the scenario (*) in a clearer manner, we've represented them in Figure (6.12) without the other ones:

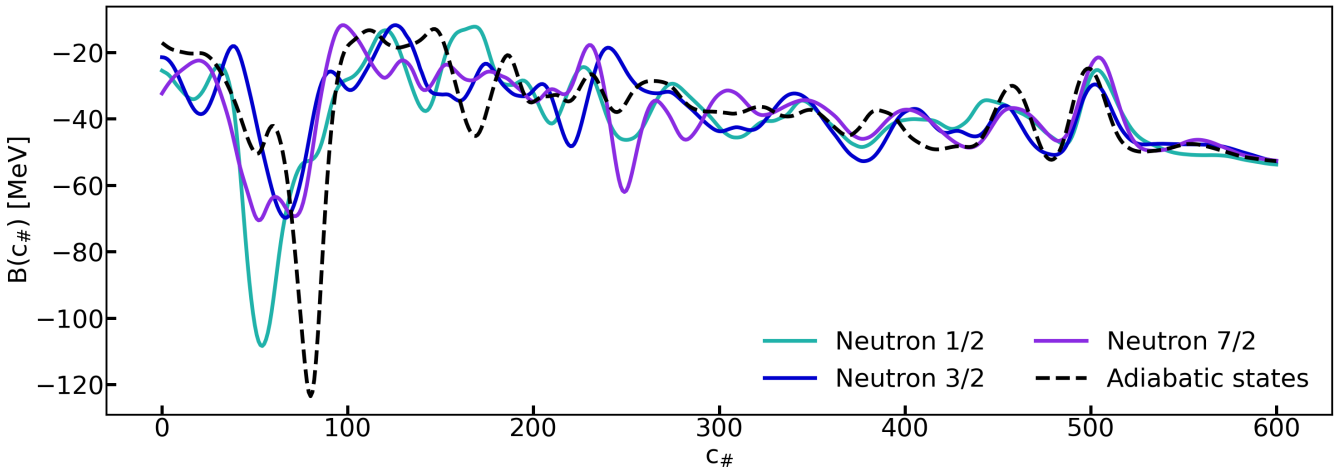

Figure 6.12: Comparison between the inertia tensor at the adiabatic limit and the adiabatic-excited inertia tensors related to the neutron variational excitations included in the scenario (*).

We clearly observe that the inertia tensors associated with the remaining neutron variational excitations behave in a way comparable to that of the inertia tensor at the adiabatic limit.

Study of the adiabatic renormalization in the scenario (*):

We've studied the renormalization of the diagonal adiabatic part of the SCIM inertia tensor B induced by the variational excitations in the case of the scenario (*). In Figure (6.13), we've displayed both the SCIM inertia tensor B at the adiabatic limit and the diagonal adiabatic component B_{00} of the SCIM inertia tensor in the scenario (*):

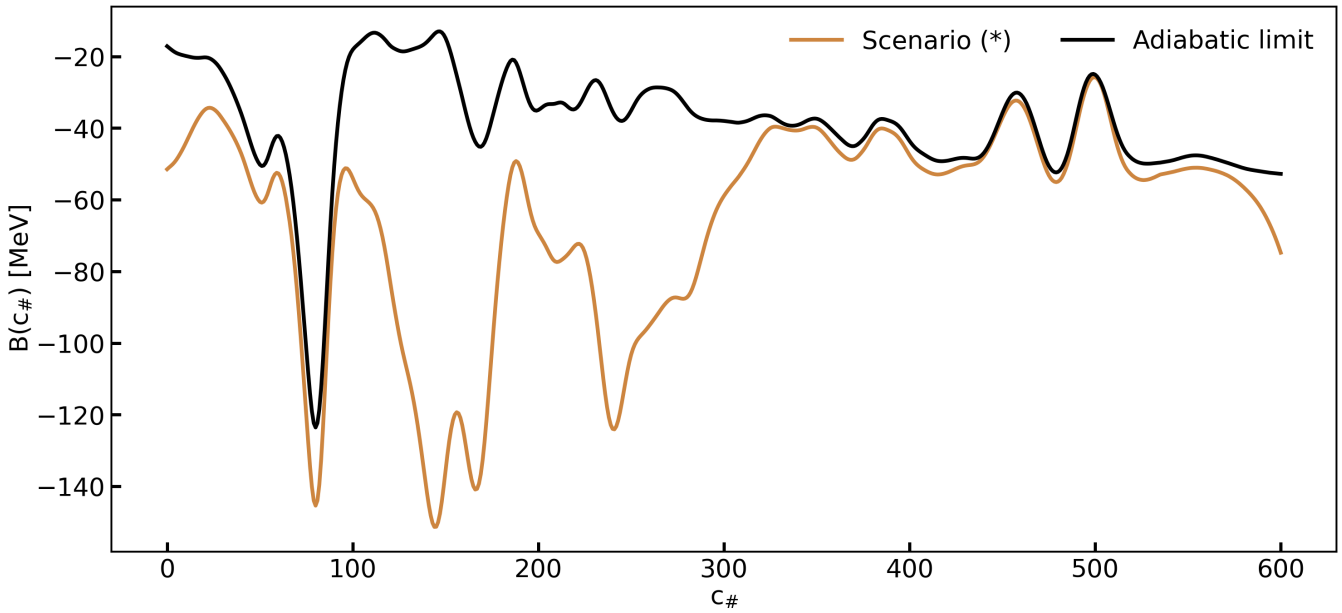

Figure 6.13: Comparison between the SCIM inertia tensor at the adiabatic limit and the diagonal adiabatic part of the SCIM inertia tensor in the scenario (*).

In contrast with the observations concerning the renormalization of the SCIM potential, the inclusion of the variational excitations has a huge impact on the diagonal adiabatic part B_{00} of the SCIM inertia tensor in the scenario (*). We've noticed two interesting properties of the renormalization effect. Firstly, there is a global increase in the inertia tensor values (in absolute). Secondly, the effect is mostly localized between $c_\# = 100$ and $c_\# = 350$ approximately.
To help a clearer physical interpretation of these two properties, we've represented in Figure (6.14) the mass associated with the inertia tensor displayed in Figure (6.13):

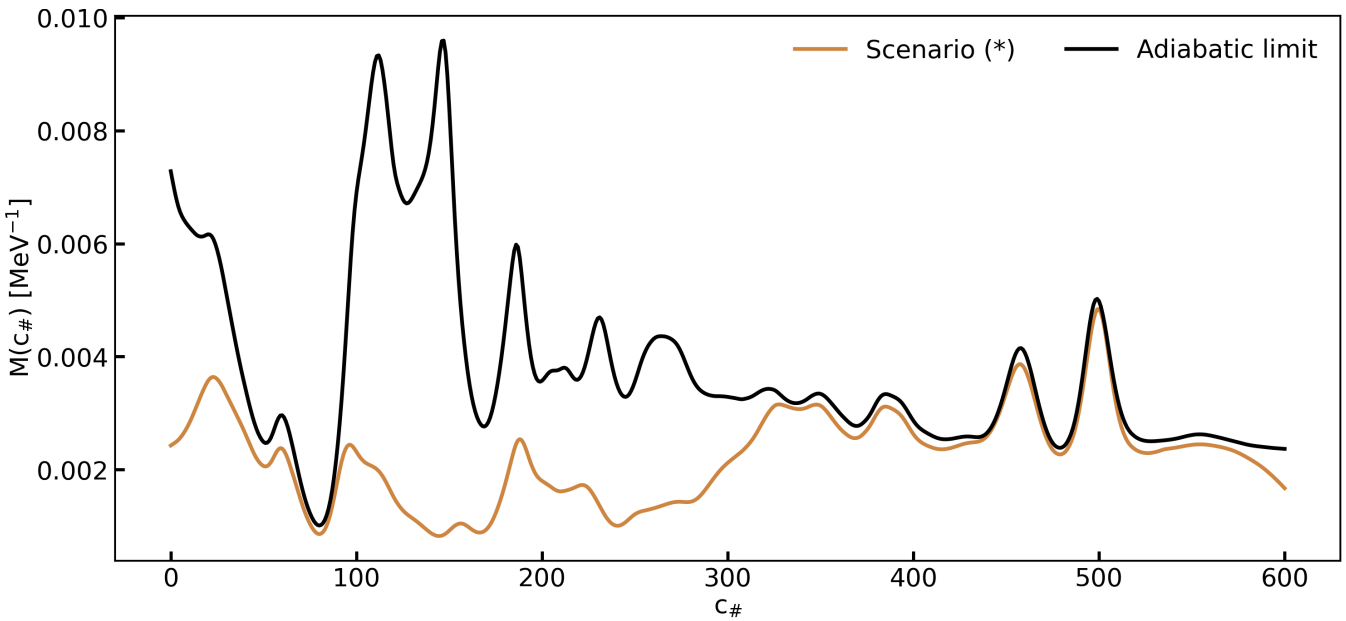

Figure 6.14: Comparison between the SCIM inertial mass at the adiabatic limit and the diagonal adiabatic part of the SCIM inertial mass in the scenario (*).

We clearly observe that the SCIM adiabatic inertial mass is locally much smaller after renormalization. This feature reflects the fact that the variational excitation presence makes it comparatively easier for a wave packet to propagate on the adiabatic potential energy surface, *ceteris paribus*. Indeed, when excitations are included in the "dynamics", the diagonal adiabatic inertial mass is no longer the only relevant quantity to figure out how well and how fast a wave packet will propagate on the adiabatic potential energy surface. Indeed, all the components of the potential, inertial mass and dissipation tensor play a role in the propagation. Therefore, a much complete investigation of the SCIM wave packet propagation is required to go further. We didn't have the time to realize this study during this PhD thesis, but it would be a very interesting topic to treat.

Study of the off-diagonal SCIM inertia tensor components in the scenario (*):

In Table (6.2), we've displayed the maximum absolute values of the different components of the SCIM inertia tensor B in the scenario (*):

	a	$n_{1/2}$	$n_{3/2}$	$n_{7/2}$	$p_{1/2}$	$p_{5/2}$	$p_{7/2}$
a	151.31	27.72	45.53	1.16	4.51	22.28	49.15
$n_{1/2}$	-	112.51	21.81	0.49	1.80	13.59	11.02
$n_{3/2}$	-	-	81.23	0.82	0.89	14.23	59.02
$n_{7/2}$	-	-	-	70.65	0.02	0.25	0.37
$p_{1/2}$	-	-	-	-	81.16	3.50	1.69
$p_{5/2}$	-	-	-	-	-	90.50	9.98
$p_{7/2}$	-	-	-	-	-	-	103.84

Table 6.2: Maximum absolute values of the different components of the SCIM inertia tensor B in the scenario (*).

We observe in Table (6.2) that the diagonal components of the inertia tensor B are greater than the off-diagonal ones. However, they are in general 5 to 50 times greater, which is a smaller difference than in the case of the SCIM potential (see Table (6.1)). In addition, the adiabatic-excited off-diagonal components are in general greater than the excited-excited off-diagonal ones, as already observed for the SCIM potential.
To conclude, we've plotted in Figure (6.15) the adiabatic-excited off-diagonal inertia tensor component $B_{(a,n_{1/2})}$ and the excited-excited off-diagonal inertia tensor component $B_{(n_{1/2},n_{3/2})}$, with respect to $c_{\#}$:

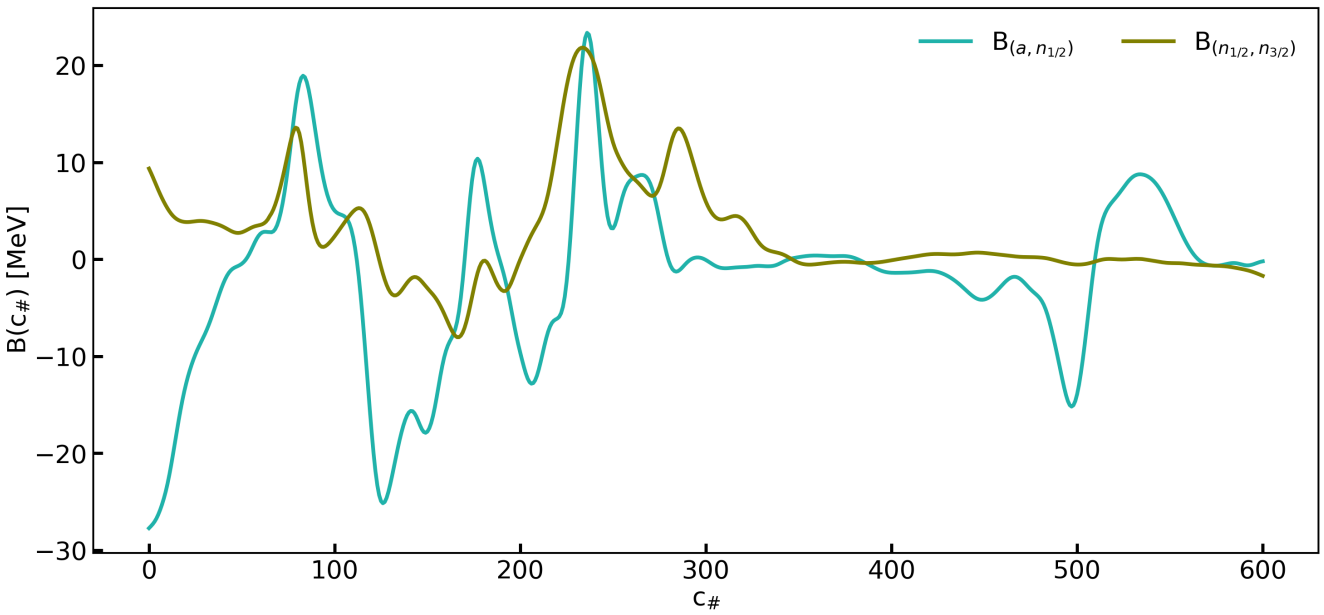

Figure 6.15: Comparison between the off-diagonal inertia tensor component $B_{(a,n_{1/2})}$ and the off-diagonal inertia tensor component $B_{(n_{1/2},n_{3/2})}$, with respect to $c_{\#}$.

As in the case of the potential components observed in Figure (6.8), we observe a greater amplitude in the case of the adiabatic-excited inertia tensor. In addition, relevant fluctuations are mostly observed around the first barrier ($c_{\#} \approx 120$), near the saddle point ($c_{\#} \approx 267$), and near scission ($c_{\#} \approx 495$). It means that the dynamical couplings are relatively stronger in these areas.

6.1.4 Dissipation tensor

This section is dedicated to the study of the SCIM dissipation tensor D. In Table (6.3), we've displayed the maximum absolute values of the different components of the SCIM dissipation tensor D in the scenario (*):

	a	$n_{1/2}$	$n_{3/2}$	$n_{7/2}$	$p_{1/2}$	$p_{5/2}$	$p_{7/2}$
a	0	7.78	11.70	0.12	3.68	9.04	12.59
$n_{1/2}$	-	0	2.00	0.10	0.03	0.24	0.66
$n_{3/2}$	-	-	0	0.06	0.02	0.63	1.02
$n_{7/2}$	-	-	-	0	0.00	0.01	0.02
$p_{1/2}$	-	-	-	-	0	0.33	0.07
$p_{5/2}$	-	-	-	-	-	0	0.54
$p_{7/2}$	-	-	-	-	-	-	0

Table 6.3: Maximum absolute values of the different components of the SCIM dissipation tensor D in the scenario (*).

Once again, the off-diagonal adiabatic-excited components are greater than the excited-excited ones. In addition, the order of magnitude of the values displayed is smaller than the one of the off-diagonal components of the inertia tensor B.
Finally, we've represented in Figure (6.15) the adiabatic-excited off-diagonal dissipation tensor component $B_{(a,n_{1/2})}$ and the excited-excited off-diagonal inertia tensor component $B_{(n_{1/2},n_{3/2})}$, with respect to $c_{\#}$:

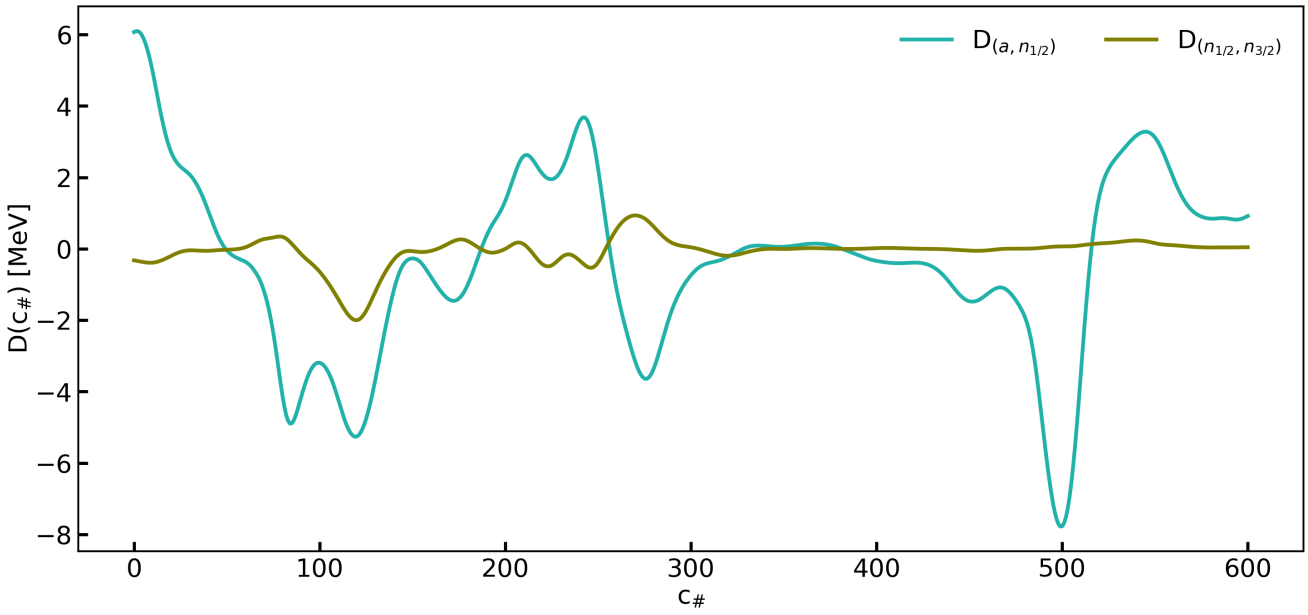

Figure 6.16: Comparison between the off-diagonal inertia tensor component $D_{(a,n_{1/2})}$ and the off-diagonal inertia tensor component $D_{(n_{1/2},n_{3/2})}$, with respect to $c_\#$.

The adiabatic-excited off-diagonal component of the dissipation tensor D represented in Figure (6.16) clearly exhibit variations of a greater magnitude than the ones of the excited-excited off-diagonal component. One more time, the fluctuations are mostly localized around the first barrier ($c_\# \approx 120$), near the saddle point ($c_\# \approx 267$), and near scission ($c_\# \approx 495$). It would be interesting to study the extent to which static and dynamical couplings are correlated in general, as in the case of the examples presented in this section.

6.2 The collective-intrinsic Schrödinger equation

Once the SCIM Hamiltonian is obtained, the "dynamics" consists in using the Schrödinger equation to make a well-chosen initial wave function g evolve over time (see Chapter 1). We call "collective-intrinsic" Schrödinger equation the Schrödinger equation associated with the SCIM Hamiltonian $\mathcal{H}_{SCIM}$. It reads as:

$$\boxed{\mathcal{H}_{SCIM}g(t) = i\hbar\frac{\partial}{\partial t}g(t)} \tag{6.13}$$

Of course, when excitations are included in the "dynamics", Eq.(6.13) has a more complex explicit structure:

$$\boxed{\begin{pmatrix} (\mathcal{H}_{SCIM})_{00} & \dots & (\mathcal{H}_{SCIM})_{0n} \\ \vdots & \ddots & \vdots \\ (\mathcal{H}_{SCIM})_{n0} & \dots & (\mathcal{H}_{SCIM})_{nn} \end{pmatrix} \begin{pmatrix} g_0(t) \\ \vdots \\ g_n(t) \end{pmatrix} = i\hbar\frac{\partial}{\partial t}g(t) \begin{pmatrix} g_0(t) \\ \vdots \\ g_n(t) \end{pmatrix}} \tag{6.14}$$

In the following, we detail how Eq.(6.14) is treated numerically. We start by explaining how the initial wave function $g(t = 0)$ is built. Then, we discuss how the collective-intrinsic

Shrödinger equation is solved using the Crank-Nicolson method [27, 73, 74]. Finally, we explain how the boundary conditions are defined.
To conclude, we present the derivations leading to the different probability fluxes. These quantities are very important as they enable us to evaluate the excited yields at scission. As far as we know, these derivations are totally new.

6.2.1 Numerical solution of the collective-intrinsic Schrödinger equation

This section is dedicated to the numerical solution of the collective-intrinsic Schrödinger equation. First of all, we explain how the initial wave function $g(t = 0)$ is built.

Construction of the initial wave function:

In the literature, we generally find two ways of constructing the initial state $g(t = 0)$. The first is basically to create a wave packet in the extrapolated ground state potential well (see for instance [27]). The second method is based on the first one, but an additional "boost" is given to the initial wave packet in the fission direction (this topic is discussed in [28]).
Considering the inherent complexity of the SCIM approach, we've decided to keep the "dynamics" as simple as possible. Therefore, we've only tested the first method described above. In addition, we've decided to create only fully adiabatic initial wave functions.

The creation of the initial wave function starts with the definition of the Hamiltonian corresponding to the extrapolated ground state well. We note this Hamiltonian $\mathcal{H}_{ext}$. It reads as follows:

$$\boxed{\mathcal{H}_{ext}(c_{\#}) = V_{ext}(c_{\#}) + [B_{00}(c_{\#})\frac{\partial}{\partial c_{\#}}]^{(2)}} \tag{6.15}$$

As already stated, $\mathcal{H}_{ext}$ only operates at the adiabatic level. It is the reason why there is no dissipation tensor in Eq.(6.15). The extrapolated potential V_{ext} is defined as a simple parabola. In practice, we build this parabola using the point corresponding to the ground state well minimum and two other different arbitrary points belonging to the well. Moreover, the inertia tensor that appears in Eq.(6.15) is nothing but the diagonal adiabatic component of the SCIM inertia tensor B.

Once $\mathcal{H}_{ext}$ is defined, we can diagonalize it and find both its eigenvectors v and its eigenvalues E_v. The eigenvectors of $\mathcal{H}_{ext}$ are the static wave functions of the extrapolated ground state well and the eigenvalues are their related energies.
Now, the goal is to build a gaussian wave packet v_G, with the average energy $\bar{E}_G$ and an approximated energy standard deviation σ_G, using the static wave functions v. It is important to keep in mind that the average energy desired is the energy corresponding to the SCIM Hamiltonian $\mathcal{H}_{SCIM}$ and not the one related to the extrapolated Hamiltonian $\mathcal{H}_{ext}$. Therefore, the eigenvalues E_v are useless, and we have to evaluate the energies $\tilde{E}_v$ associated with the SCIM Hamiltonian $\mathcal{H}_{SCIM}$ instead:

$$\boxed{\tilde{E}_v = \sum_{c_{\#}} v(c_{\#})\mathcal{H}_{SCIM}(c_{\#})v(c_{\#})} \tag{6.16}$$

Then, we consider the Gaussian wave packet $v(E)$ defined as follows:

$$\boxed{v(E) = \sum_i v_i e^{-\frac{(\bar{E}_v - E)^2}{2\sigma_G^2}}} \tag{6.17}$$

We use a dichotomy approach to find the energy E_d such that the average energy of the Gaussian wave packet $v(E_d)$ equals the desired average energy $\bar{E}_G$. Moreover, the way $v(E_d)$ is built ensure that its energy standard deviation is close to σ_G. Therefore, we have $v_G = v(E_d)$.

In this PhD thesis study, we've chosen to build a Gaussian wave packet with an average energy equal to the potential energy at the top of the first barrier ($\bar{E}_G = -1792.21$ MeV). In addition, we've imposed an energy standard deviation $\sigma_G = 0.5$ MeV. These choices have been made in coherence with the low-energy fission phenomena the SCIM aims to describe. Finally, we can express the SCIM initial wave function used in practice as follows:

$$\boxed{g(t=0) = v_G(\bar{E}_G = -1792.21, \sigma_G = 0.5)} \tag{6.18}$$

Numerical propagation of the wave function:

The Crank-Nicolson method applied to the collective-intrinsic Schrödinger equation leads to the following expression:

$$\boxed{\frac{g(c_\#, t+\Delta t) - g(c_\#, t)}{\Delta t} = -\frac{i\mathcal{H}_{SCIM}(c_\#)}{2\hbar}[g(c_\#, t+\Delta t) + g(c_\#, t)]} \tag{6.19}$$

Eq.(6.19) is then easily transformed into the following linear system:

$$\boxed{(1 + i\frac{\mathcal{H}_{SCIM}(c_\#)\Delta t}{2\hbar})g(c_\#, t+\Delta t) = (1 - i\frac{\mathcal{H}_{SCIM}(c_\#)\Delta t}{2\hbar})g(c_\#, t)} \tag{6.20}$$

This system is solved iteratively using the method proposed in [27]. Noting $(g^{(i)}(t+\Delta t))_i$ the corresponding sequence and setting $g^{(0)} = g(c_\#, t)$, we define $(g^{(i+1)}(t+\Delta t))_i$ as follows:

$$\boxed{g^{(i+1)}(c_\#, t+\Delta t) = (1 - i\frac{\mathcal{H}_{SCIM}(c_\#)\Delta t}{2\hbar})g(c_\#, t) - i\frac{\mathcal{H}_{SCIM}(c_\#)\Delta t}{2\hbar}g^{(i)}(c_\#, t+\Delta t)} \tag{6.21}$$

In practice, the iterative process described in Eq.(6.21) stops when the following condition is fulfilled:

$$\boxed{||g^{(i+1)}(t+\Delta t) - g^{(i)}(t+\Delta t)||^2 < 10^{-16}} \tag{6.22}$$

In practice, we've chosen the time step $\Delta t = 6\hbar \times 10^{-4}$, which was in practice numerically relevant.

Boundary conditions:

The numerical method presented above applied to finite sets (in terms of $c_\#$) leads to unphysical reflections of the wave functions at the edges of these sets ($c_\# = 0$ and $c_\# = 600$). To avoid this problem, we complete the SCIM Hamiltonian $\mathcal{H}_{SCIM}$ with a new part $\mathcal{H}_{abs}$ including a complex potential. This additional part of the SCIM Hamiltonian corresponds to indices $c_\# = 601$ to $c_\# = 800$ and allows the wave function to be progressively absorbed in this area.

In practice, we've chosen to set all the off-diagonal components of V_{abs}, D_{abs}, and B_{abs} to zero. It avoids irrelevant excitation phenomena in the absorption zone. Concerning the diagonal components of B_{abs}, we simply set:

$$\boxed{(B_{abs})_{ii}(c_\#) = (B_{SCIM})_{ii}(600)} \tag{6.23}$$

Finally, when it comes to the diagonal components of the potential V_{abs}, their real part is defined as the natural linear extrapolation of V_{SCIM}. Their complex part is a second order polynomial whose coefficients are chosen to ensure a smooth absorption. These coefficients have been found in practice as the result of a trial and error process. Eventually, the diagonal components of the potential V_{abs} explicitly read as:

$$\boxed{\begin{aligned}(V_{abs})_{ii}(c_\#) = c_\#[(V_{SCIM})_{ii}(600) - (V_{SCIM})_{ii}(599)] + (V_{SCIM})_{ii}(600) \\ -600[(V_{SCIM})_{ii}(600) - (V_{SCIM})_{ii}(599)] \\ -i[-5 \times 10^{-6} c_\#^2 + 0.1 c_\# - 62]\end{aligned}} \tag{6.24}$$

6.2.2 Probability flux evaluation

We call probability flux evaluated at (c_s, t_f) the quantity defined as follows:

$$\boxed{\phi(c_s, t_f) = \int_0^{t_f} \mathrm{d}t \frac{\mathrm{dP}(c_\# > c_s)}{\mathrm{d}t}(t)} \tag{6.25}$$

With:

$$\mathrm{P}(c_\# > c_s)(t) = \int_{c_s}^{800} \mathrm{d}c_\# \sum_i |g_i(c_\#, t)|^2 \tag{6.26}$$

The physical interpretation of the probability flux $\phi(c_s, t_f)$ is rather straightforward. It represents the total amount of probability (counted with a sign) that has passed through the point c_s during the time t_f.
Of course, the integral associated with $\phi(c_s, t_f)$ does not converge with respect to t_f for any c_s. However, as we've included absorption to the SCIM Hamiltonian, and given the SCIM potential topology, it is clear that if a component of the wave function goes through the first potential barrier, it will eventually be absorbed. Therefore, the total probability flux $\phi_{tot}(c_s)$ is well defined for large enough c_s values. It reads as:

$$\boxed{\phi_{tot}(c_s) = \int_0^{+\infty} \mathrm{d}t \frac{\mathrm{dP}(c_\# > c_s)}{\mathrm{d}t}(t)} \tag{6.27}$$

This section aims first to express the total probability flux $\phi_{tot}(c_s)$ explicitly. Then, we demonstrate that $\phi_{tot}(c_s)$ can be divided into different adiabatic and excited components as follows:

$$\boxed{\phi_{tot}(c_s) = \sum_{i=0} \phi_i(c_s)} \tag{6.28}$$

Eq.(6.28) is very precious as it directly gives access to the different adiabatic and excited yields evaluated at c_s, $\mathrm{Y}_i(c_s)$. Indeed, the latter are defined as:

$$\boxed{\mathrm{Y}_i(c_s) = \frac{\phi_i(c_s)}{\phi_{tot}(c_s)}} \tag{6.29}$$

Continuity equation:

To express the quantity $\phi_{tot}(c_s)$, we start by developing the integrand $\mathrm{d}t\frac{\mathrm{dP}(c_\# > c_s)}{\mathrm{d}t}(t)$:

$$\frac{\mathrm{dP}(c_\# > c_s)}{\mathrm{d}t}(t) = \int_{c_s}^{800} \mathrm{d}c_\# \ \sum_i (g_i(c_\#, t)\frac{\partial}{\partial t}g_i^*(c_\#, t) + g_i^*(c_\#, t)\frac{\partial}{\partial t}g_i(c_\#, t)) \tag{6.30}$$

To get rid of the integral in Eq.(6.30), we want to write the integrand in the following form:

$$\boxed{\sum_i (g_i(c_\#, t)\frac{\partial}{\partial t}g_i^*(c_\#, t) + g_i^*(c_\#, t)\frac{\partial}{\partial t}g_i(c_\#, t) = -\frac{\partial}{\partial c_\#}J(c_\#, t)} \tag{6.31}$$

Eq.(6.31) is called the continuity equation and J is called the probability current. To perform this transformation, we start by rephrasing the derivatives in Eq.(6.30) thanks to the collective-intrinsic Schrödinger equation. We find:

$$\frac{\partial}{\partial t}g_i(c_\#, t) = -\frac{i}{\hbar}\sum_j (\mathcal{H}_{SCIM})_{ij}(c_\#)g_j(c_\#, t) \tag{6.32}$$

And:

$$\frac{\partial}{\partial t}g_i^*(c_\#, t) = \frac{i}{\hbar}\sum_j (\mathcal{H}_{SCIM})_{ij}(c_\#)g_j^*(c_\#, t) \tag{6.33}$$

Inserting Eq.(6.32) and Eq.(6.33) into Eq.(6.31) leads to:

$$\begin{aligned} -\frac{\partial}{\partial c_\#}J(c_\#, t) = \frac{i}{\hbar}\sum_{ij}[&g_i(c_\#, t)(V_{ij}(c_\#) + [D_{ij}(c_\#)\frac{\partial}{\partial c_\#}]^{(1)} + [B_{ij}(c_\#)\frac{\partial}{\partial c_\#}]^{(2)})g_j^*(c_\#, t) \\ &- g_i^*(c_\#, t)(V_{ij}(c_\#) + [D_{ij}(c_\#)\frac{\partial}{\partial c_\#}]^{(1)} + [B_{ij}(c_\#)\frac{\partial}{\partial c_\#}]^{(2)})g_j(c_\#, t)] \end{aligned} \tag{6.34}$$

Then, we separate Eq.(6.34) into three parts:

$$\boxed{-\frac{\partial}{\partial c_\#}J(c_\#,t) = -\frac{\partial}{\partial c_\#}J_V(c_\#,t) - \frac{\partial}{\partial c_\#}J_D(c_\#,t) - \frac{\partial}{\partial c_\#}J_B(c_\#,t)} \tag{6.35}$$

With:

$$\boxed{-\frac{\partial}{\partial c_\#}J_V(c_\#,t) = \frac{i}{\hbar}\sum_{ij}[g_i(c_\#,t)V_{ij}(c_\#)g_j^*(c_\#,t) - g_i^*(c_\#,t)V_{ij}(c_\#)g_j(c_\#,t)]} \tag{6.36}$$

And:

$$\boxed{\begin{aligned}-\frac{\partial}{\partial c_\#}J_D(c_\#,t) = \frac{i}{\hbar}\sum_{ij}[&g_i(c_\#,t)[D_{ij}(c_\#)\frac{\partial}{\partial c_\#}]^{(1)}g_j^*(c_\#,t)\\ &-g_i^*(c_\#,t)[D_{ij}(c_\#)\frac{\partial}{\partial c_\#}]^{(1)}(c_\#)g_j(c_\#,t)]\end{aligned}} \tag{6.37}$$

And, finally:

$$\boxed{\begin{aligned}-\frac{\partial}{\partial c_\#}J_B(c_\#,t) = \frac{i}{\hbar}\sum_{ij}[&g_i(c_\#,t)[B_{ij}(c_\#)\frac{\partial}{\partial c_\#}]^{(2)}g_j^*(c_\#,t)\\ &-g_i^*(c_\#,t)[B_{ij}(c_\#)\frac{\partial}{\partial c_\#}]^{(2)}(c_\#)g_j(c_\#,t)]\end{aligned}}$$

Calculation of J_V:

The symmetry of the SCIM potential V directly leads to:

$$\boxed{J_V(c_\#,t) = 0} \tag{6.38}$$

We've chosen zero in Eq.(6.38) as the constant part of $J_V(c_\#,t)$ is irrelevant in the following.

Calculation of J_D:

The quantity $-\frac{\partial}{\partial c_\#}J_D(c_\#,t)$ explicitly reads as follows:

$$\begin{aligned}-\frac{\partial}{\partial c_\#}J_D(c_\#,t) = \frac{i}{\hbar}\sum_i[&g_i(c_\#,t)\sum_j(\frac{\partial}{\partial c_\#}D_{ij}(c_\#) + D_{ij}(c_\#)\frac{\partial}{\partial c_\#})g_j^*(c_\#,t)\\ &-g_i^*(c_\#,t)\sum_j(\frac{\partial}{\partial c_\#}D_{ij}(c_\#) + D_{ij}(c_\#)\frac{\partial}{\partial c_\#})g_j(c_\#,t)]\end{aligned} \tag{6.39}$$

We remark that:

$$\sum_{ij} g_i(c_\#,t)\frac{\partial}{\partial c_\#}(D_{ij}(c_\#)g_j^*(c_\#,t)) = \frac{\partial}{\partial c_\#}(\sum_{ij} g_i(c_\#,t)D_{ij}(c_\#)g_j^*(c_\#,t)) - \sum_{ij}\frac{\partial}{\partial c_\#}(g_i(c_\#,t))D_{ij}(c_\#)g_j^*(c_\#,t) \tag{6.40}$$

And, similarly:

$$-\sum_{ij} g_i^*(c_\#,t)\frac{\partial}{\partial c_\#}(D_{ij}(c_\#)g_j(c_\#,t)) = -\frac{\partial}{\partial c_\#}(\sum_{ij} g_i^*(c_\#,t)D_{ij}(c_\#)g_j(c_\#,t)) + \sum_{ij}\frac{\partial}{\partial c_\#}(g_i^*(c_\#,t))D_{ij}(c_\#)g_j(c_\#,t) \tag{6.41}$$

Inserting Eq.(6.40) and Eq.(6.41) into Eq.(6.39) and using the skew-symmetry of the dissipation tensor D leads to:

$$-\frac{\partial}{\partial c_\#}J_D(c_\#,t) = \frac{i}{\hbar}\frac{\partial}{\partial c_\#}(\sum_{ij} g_i(c_\#,t)D_{ij}(c_\#)g_j^*(c_\#,t) - g_i^*(c_\#,t)D_{ij}(c_\#)g_j(c_\#,t)) \tag{6.42}$$

Consequently, $J_D(c_\#,t)$ reads as follows:

$$\boxed{J_D(c_\#,t) = -\frac{2i}{\hbar}\Im[\sum_{ij} g_i(c_\#,t)D_{ij}(c_\#)g_j^*(c_\#,t)]} \tag{6.43}$$

Calculation of J_B:

The quantity $-\frac{\partial}{\partial c_\#}J_B(c_\#,t)$ can be expressed as:

$$\begin{aligned}-\frac{\partial}{\partial c_\#}J_B(c_\#,t) = \frac{i}{\hbar}\sum_i [g_i(c_\#,t)\sum_j (\frac{\partial^2}{\partial c_\#^2}B_{ij}(c_\#) + 2\frac{\partial}{\partial c_\#}B_{ij}(c_\#)\frac{\partial}{\partial c_\#} + B_{ij}(c_\#)\frac{\partial^2}{\partial c_\#^2})g_j^*(c_\#,t) \\ -g_i^*(c_\#,t)\sum_j (\frac{\partial^2}{\partial c_\#^2}B_{ij}(c_\#) + 2\frac{\partial}{\partial c_\#}B_{ij}(c_\#)\frac{\partial}{\partial c_\#} + B_{ij}(c_\#)\frac{\partial^2}{\partial c_\#^2})g_j(c_\#,t)]\end{aligned} \tag{6.44}$$

We remark that:

$$\sum_{ij} g_i(c_\#,t)\frac{\partial^2}{\partial c_\#^2}B_{ij}(c_\#)g_j^*(c_\#,t) = \frac{\partial^2}{\partial c_\#^2}(\sum_{ij} g_i(c_\#,t)B_{ij}(c_\#)g_j^*(c_\#,t)) \tag{6.45}$$
$$+\sum_{ij}\frac{\partial^2}{\partial c_\#^2}(g_i(c_\#,t))B_{ij}(c_\#)g_j^*(c_\#,t) - 2\frac{\partial}{\partial c_\#}(\sum_{ij}\frac{\partial}{\partial c_\#}(g_i(c_\#,t))B_{ij}(c_\#)g_j^*(c_\#,t))$$

And, similarly:

$$-\sum_{ij} g_i^*(c_\#,t)\frac{\partial^2}{\partial c_\#^2}B_{ij}(c_\#)g_j(c_\#,t) = -\frac{\partial^2}{\partial c_\#^2}(\sum_{ij} g_i^*(c_\#,t)B_{ij}(c_\#)g_j(c_\#,t)) \quad (6.46)$$
$$-\sum_{ij}\frac{\partial^2}{\partial c_\#^2}(g_i^*(c_\#,t))B_{ij}(c_\#)g_j(c_\#,t) + 2\frac{\partial}{\partial c_\#}(\sum_{ij}\frac{\partial}{\partial c_\#}(g_i^*(c_\#,t))B_{ij}(c_\#)g_j(c_\#,t))$$

In addition, the following property holds:

$$2\sum_{ij} g_i(c_\#,t)\frac{\partial}{\partial c_\#}(B_{ij}(c_\#)\frac{\partial}{\partial c_\#}g_j^*(c_\#,t)) = 2\frac{\partial}{\partial c_\#}(\sum_{ij} g_i(c_\#,t)B_{ij}(c_\#)\frac{\partial}{\partial c_\#}g_j^*(c_\#,t)) \quad (6.47)$$
$$-2\sum_{ij}\frac{\partial}{\partial c_\#}(g_i(c_\#,t))B_{ij}(c_\#)\frac{\partial}{\partial c_\#}g_j^*(c_\#,t)$$

And, similarly:

$$-2\sum_{ij} g_i^*(c_\#,t)\frac{\partial}{\partial c_\#}(B_{ij}(c_\#)\frac{\partial}{\partial c_\#}g_j^*(c_\#,t)) = -2\frac{\partial}{\partial c_\#}(\sum_{ij} g_i^*(c_\#,t)B_{ij}(c_\#)\frac{\partial}{\partial c_\#}g_j(c_\#,t)) \quad (6.48)$$
$$+2\sum_{ij}\frac{\partial}{\partial c_\#}(g_i^*(c_\#,t))B_{ij}(c_\#)\frac{\partial}{\partial c_\#}g_j(c_\#,t)$$

Using Eq.(6.45 - 6.48) along with the symmetry of the inertia tensor B leads to:

$$-\frac{\partial}{\partial c_\#}J_B(c_\#,t) = \frac{4i}{\hbar}\frac{\partial}{\partial c_\#}(\sum_{ij} g_i(c_\#,t)B_{ij}(c_\#)\frac{\partial}{\partial c_\#}g_j^* - g_i^*(c_\#,t)B_{ij}(c_\#)\frac{\partial}{\partial c_\#}g_j(c_\#,t)) \quad (6.49)$$

By identification, $J_B(c_\#,t)$ eventually reads as:

$$\boxed{J_B(c_\#,t) = -\frac{8i}{\hbar}\Im[\sum_{ij} g_i(c_\#,t)B_{ij}(c_\#)\frac{\partial}{\partial c_\#}g_j^*(c_\#,t)]} \quad (6.50)$$

Expression of the total probability flux:

Now, it is clear that the probability current J reads as:

$$\boxed{\begin{aligned}J(c_\#,t) = &-\frac{2i}{\hbar}\Im[\sum_{ij} g_i(c_\#,t)D_{ij}(c_\#)g_j^*(c_\#,t)]\\ &-\frac{8i}{\hbar}\Im[\sum_{ij} g_i(c_\#,t)B_{ij}(c_\#)\frac{\partial}{\partial c_\#}g_j^*(c_\#,t)]\end{aligned}} \quad (6.51)$$

Inserting this result into Eq.(6.30) leads to:

$$\frac{\mathrm{dP}(c_\# > c_s)}{\mathrm{d}t}(t) = -J(800,t) + J(c_s,t) \quad (6.52)$$

Because of the absorption, $J(800,t)=0,\ \forall t$. Thus:

$$\frac{\mathrm{dP}(c_{\#}>c_s)}{\mathrm{d}t}(t) = -\frac{2i}{\hbar}\Im[\sum_{ij} g_i(c_s,t)D_{ij}(c_s)g_j^*(c_s,t)] \\ -\frac{8i}{\hbar}\Im[\sum_{ij} g_i(c_s,t)B_{ij}(c_{\#})\frac{\partial}{\partial c_s}g_j^*(c_s,t)] \tag{6.53}$$

Using Eq.(6.53), the total probability flux $\phi_{tot}(c_s)$ is now easy to express:

$$\boxed{\phi_{tot}(c_s) = \int_0^{+\infty}\mathrm{d}t[-\frac{2i}{\hbar}\Im[\sum_{ij} g_i(c_s,t)D_{ij}(c_s)g_j^*(c_s,t)] \\ -\frac{8i}{\hbar}\Im[\sum_{ij} g_i(c_s,t)B_{ij}(c_{\#})\frac{\partial}{\partial c_s}g_j^*(c_s,t)]]} \tag{6.54}$$

In addition, it is clear that the total probability flux components noted $\phi_i(c_s)$ and defined in Eq.(6.28) can be expressed as:

$$\boxed{\phi_i(c_s) = \int_0^{+\infty}\mathrm{d}t[-\frac{2i}{\hbar}\Im[g_i(c_s,t)\sum_{j} D_{ij}(c_s)g_j^*(c_s,t)] \\ -\frac{8i}{\hbar}\Im[g_i(c_s,t)\sum_{j} B_{ij}(c_{\#})\frac{\partial}{\partial c_s}g_j^*(c_s,t)]]} \tag{6.55}$$

6.3 "Dynamics" results associated with the scenario (*)

In this final section, we discuss the results obtained performing the "dynamics" associated with the scenario (*). We recall that the scenario (*) includes six variational excitations in addition to the adiabatic states. More precisely, we've considered the neutron $\Omega=1/2$, $\Omega=3/2$, and $\Omega=7/2$ variational excitations and the proton $\Omega=1/2$, $\Omega=5/2$, and $\Omega=7/2$ variational excitations.

In Figure (6.17), we've represented the local squared norm of the different wave function components g_i at different times, with respect to $c_{\#}$. The plots end at $c_{\#}=600$ as the greater values of $c_{\#}$ are physically irrelevant (it is the absorption area). The first five plots from top to bottom are evenly spaced in time. They are intended to give an idea of how the wave function propagates. The last plot corresponds to the last iteration of the "dynamics". It aims to describe the remaining part of the wave function after propagation. Finally, in Figure (6.18), we've zoomed in on the plots displayed in Figure (6.17) to provide the reader with clearer details:

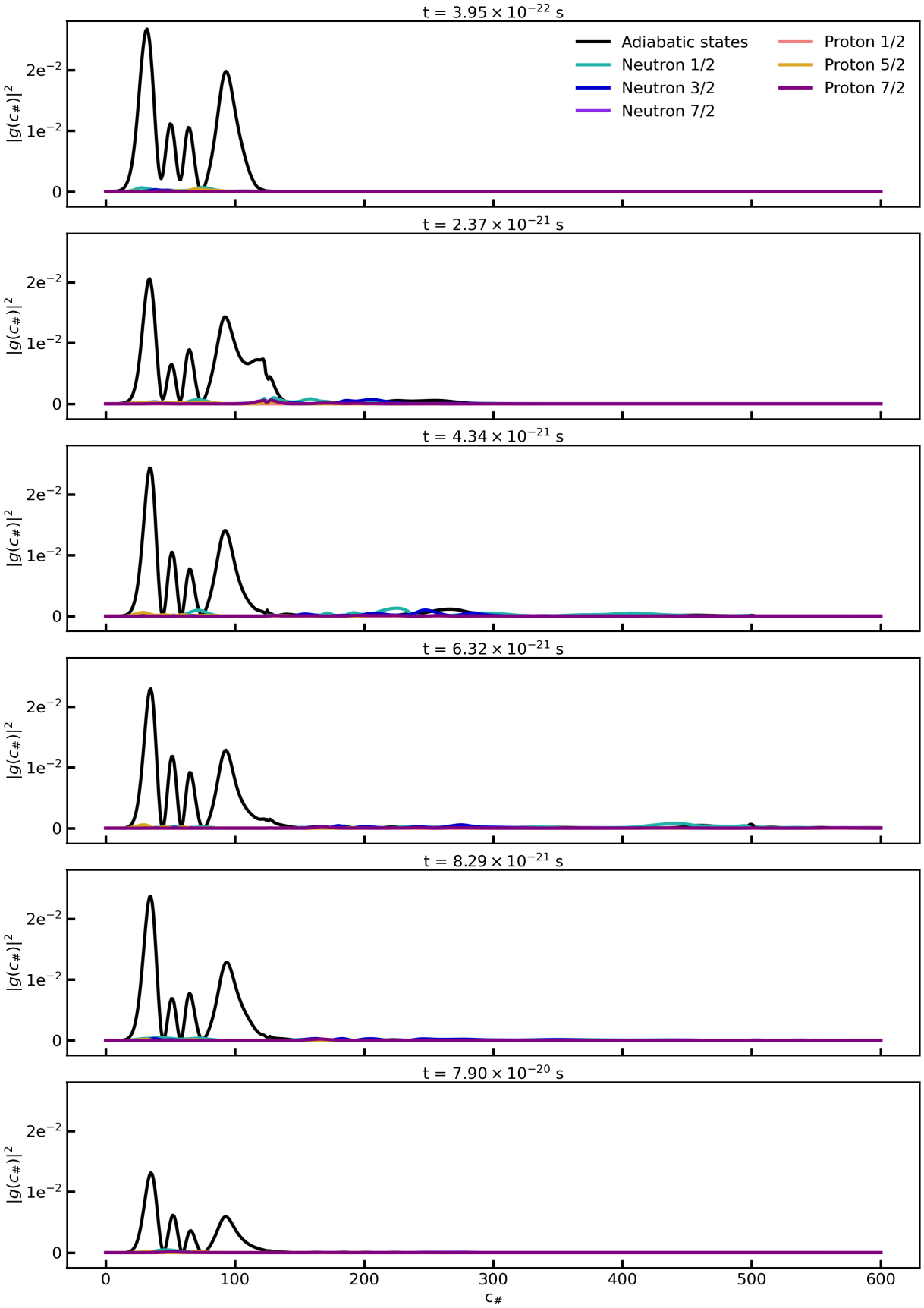

Figure 6.17: Illustration of the "dynamics" associated with the scenario (*). The different local squared norms of the wave function components g_i are represented with respect to $c_\#$ at different times.

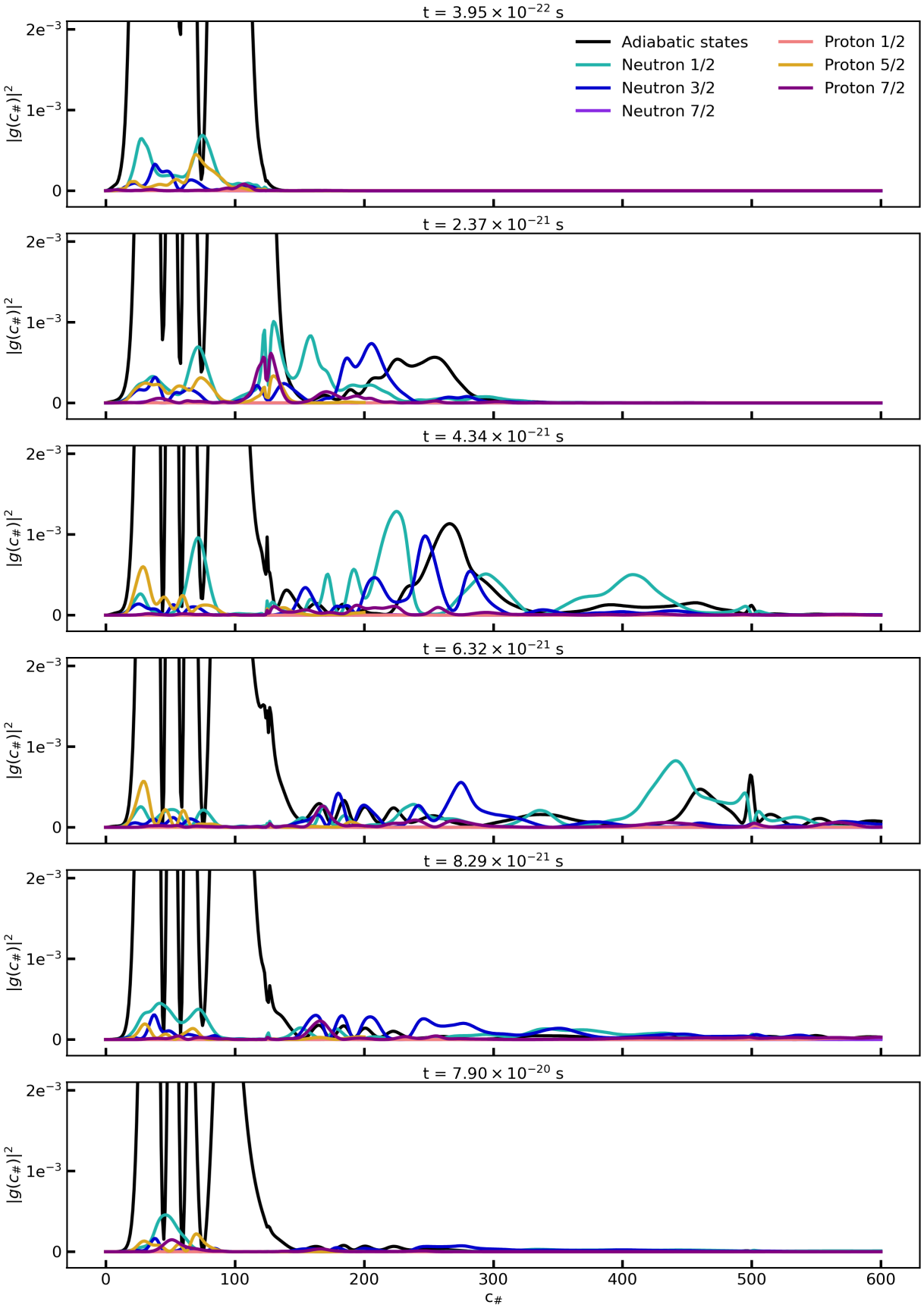

Figure 6.18: Illustration of the "dynamics" associated with the scenario (*) with a relevant zoom. The different local squared norms of the wave function components g_i are represented with respect to $c_\#$ at different times.

First of all, in Figure (6.17), we mostly observe that a non negligible part of the initial wave function has been absorbed at the end of the propagation. More precisely, the total squared norm of the remaining part of the wave function accounts for only 39.4 % of the initial one. The order of magnitude of this result was expected. Indeed, the initial wave function had an average energy equal to the SCIM potential energy at the top of the first barrier.
Then, looking at Figure (6.18), it is possible to figure out how the different adiabatic and excited components of the wave function evolve over time. We namely observe two interesting phenomena. Firstly, we see on the right hand side of the plots how the different contributions of the wave functions behave towards scission. It is striking to remark that the adiabatic component of the wave function is no longer the most important one after the saddle point ($c_{\#} = 267$). When it comes to scission, the neutron $\Omega = 1/2$ variational excitation seems to be the leading component of the wave function.
Secondly, on the left hand side of the plots, we observe how the different adiabatic and excited wave function components oscillate in the ground state well. It is also interesting to observe in the last plot that the remaining part of the wave function is still slowly leaking out of the ground state well, through the first barrier. We attribute this phenomenon of minor amplitude to the tunneling effect.

6.3.1 Excited yields

In this section, we first discuss the different probability fluxes extracted from the "dynamics" using the method presented earlier. Then, we use these probability fluxes to deduce the excited yields, i.e. the probability of obtaining a given excitation at scission.

In Figure (6.19), we've displayed the total probability flux, the adiabatic probability flux and the excited probability flux (the sum of all the ϕ_i) after $t = 7.90 \times 10^{-20}$s, and evaluated at different $c_{\#}$ values:

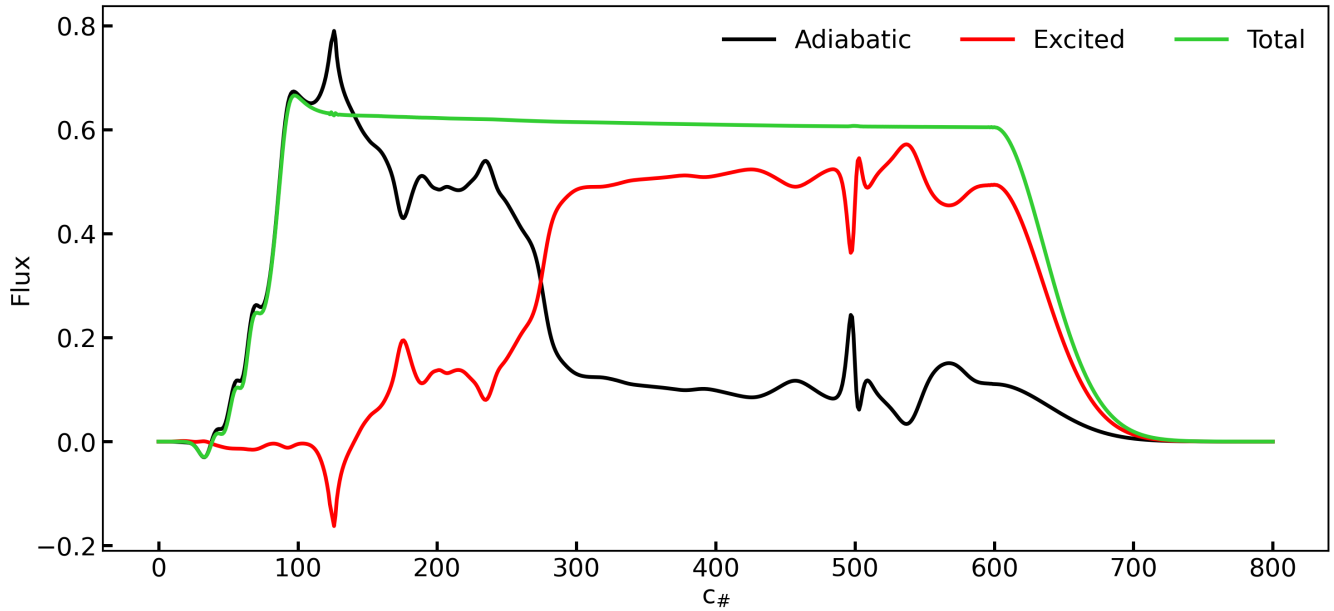

Figure 6.19: Total probability flux, adiabatic probability flux and the excited probability flux after $t = 7.90 \times 10^{-20}$s, and evaluated at different $c_{\#}$ values.

First of all, the rader may be surprised to see a negative excited flux near $c_{\#} = 120$. In fact this phenomenon is easy to understand. It's due to some adiabatic components rising towards

the first barrier (counted with a plus sign), which then transform into excited components and finally fall back down towards the ground state well (counted with a minus sign).
Then, it is striking to observe that the excited flux increases rapidly, approximatively from the saddle point ($c_\# = 267$). It exceeds the adiabatic flux at $c_\# = 280$. After this initial rapid increase, the excited flux continues to rise slowly, until it reaches the scission area (around $c_\# = 495$). Near scission, both the adiabatic and the excited fluxes are disrupted. We attribute this feature to the violent phenomena occuring in this area.
Besides, it is interesting to look at the total flux represented by the green curve. Indeed, the plateau that begins after the first barrier ($c_\# = 120$) directly reflects that almost all the wave function components that have passed through the first barrier have been absorbed. Moreover, at $c_\# = 600$, we find a total flux value of 0.606. It means that, at the end of the propagation, 60.6 % of the initial wave function has been absorbed. This result is the counterpart of the 39.4 % found for the total squared norm of the remaining wave function. Finally, we clearly see the effect of the absorption after $c_\# = 600$.

In Figure (6.20), we've represented the different adiabatic and excited probability fluxes after $t = 7.90 \times 10^{-20}$s, and evaluated at different $c_\#$ values:

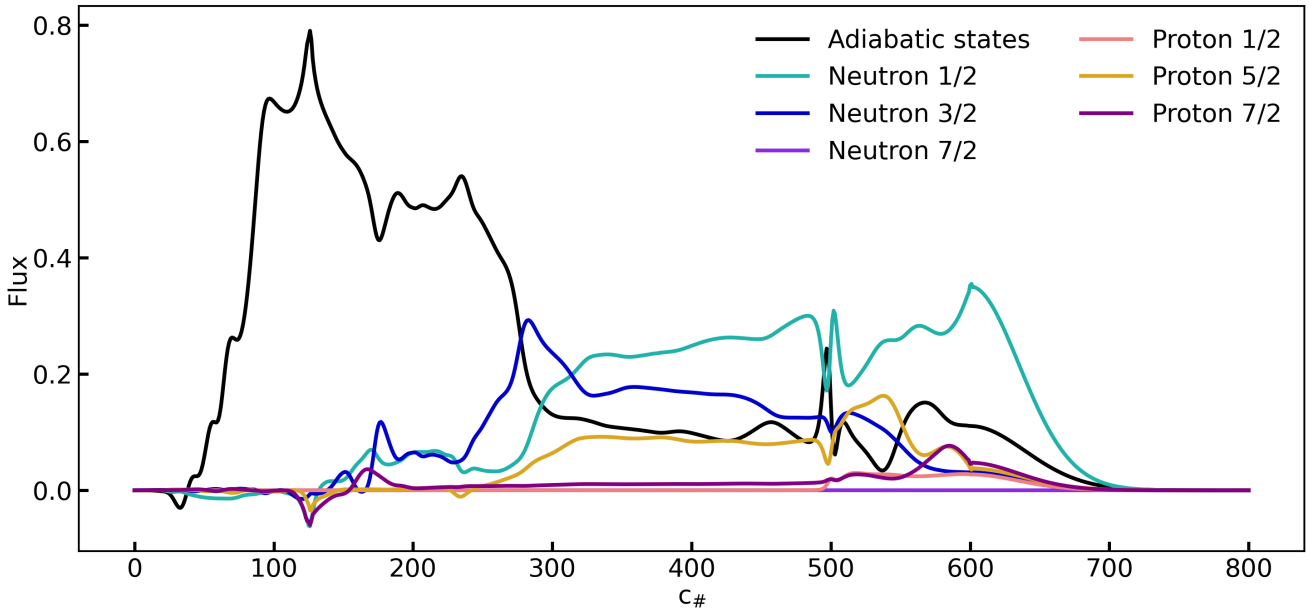

Figure 6.20: Adiabatic and excited probability fluxes after $t = 7.90 \times 10^{-20}$s, and evaluated at different $c_\#$ values.

With this plot, we can analyze how the different excitations contribute to the total excited flux. Without surprise, the contribution of the neutron $\Omega = 1/2$ excitation, already identified in the previous section, is the most important after $c_\# = 315$. We also observe that the contributions associated with the neutron $\Omega = 3/2$ and proton $\Omega = 5/2$ excitations are also relevant overall. Besides, the contributions of the proton $\Omega = 1/2$ and proton $\Omega = 7/2$ excitations are much smaller than the others but are not negligible near scission. Finally, we cannot distinguish in Figure (6.20) any flux associated with the neutron $\Omega = 7/2$ excitation. For this reason, we've plotted the probability flux related to this excitation alone in Figure (6.21):

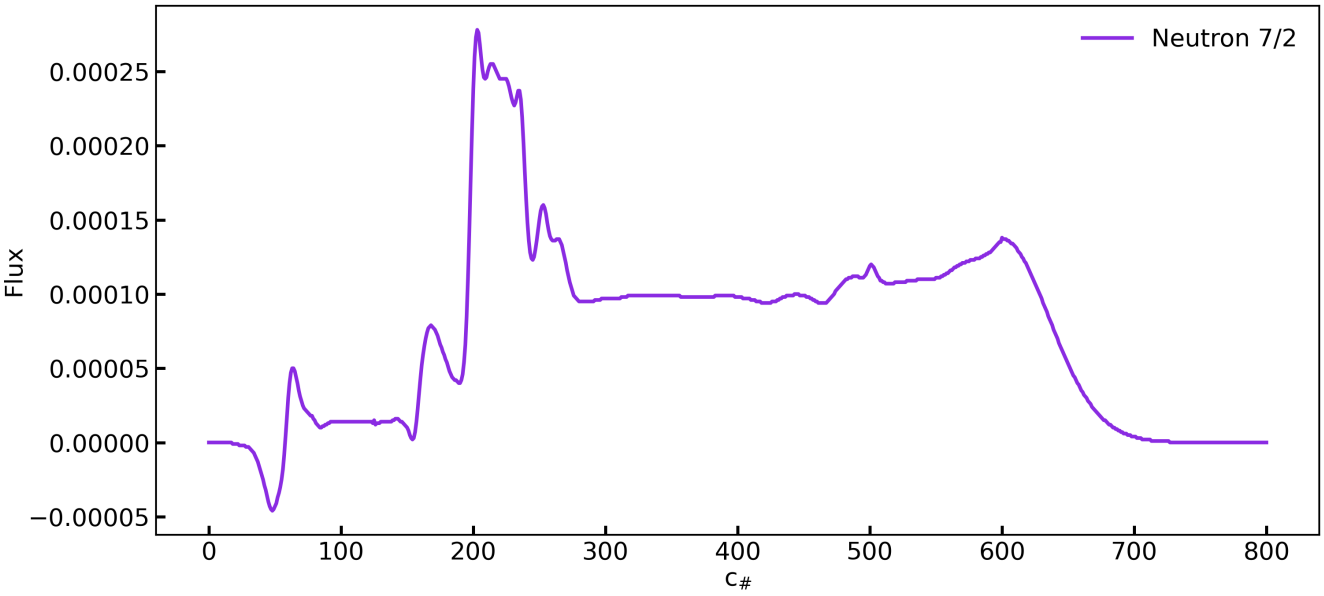

Figure 6.21: Probability flux associated with the neutron $\Omega = 7/2$ excitation after $t = 7.90 \times 10^{-20}$s, and evaluated at different $c_{\#}$ values.

We observe that the probability flux associated with the neutron $\Omega = 7/2$ excitation is very small. More precisely, it is approximately three orders of magnitude smaller than the others. This result was expected. Indeed, considering the data displayed in Tables (6.1 - 6.3), it was already clear that the couplings related to the neutron $\Omega = 7/2$ excitation were much smaller than the others overall.

In Figure (6.20), we've also remarked that the neutron excitations contribute more than the proton ones to the total excited flux. In order to illustrate more clearly the latter statement, we've represented in Figure (6.22) the total excited probability fluxes associated with both isospins:

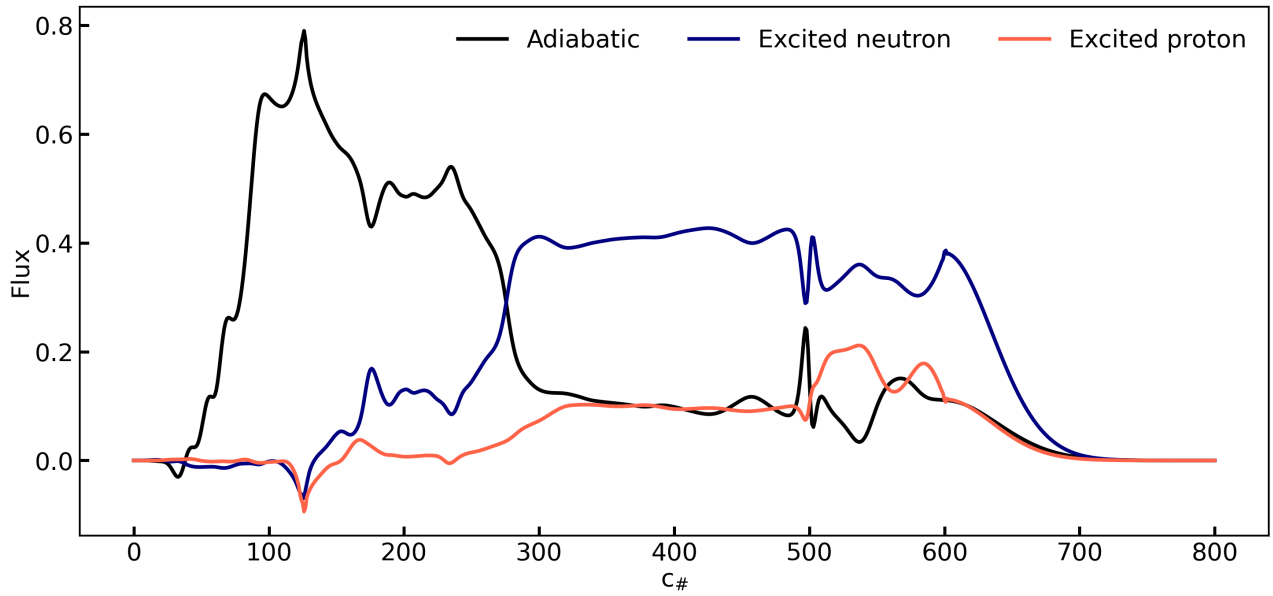

Figure 6.22: Adiabatic and excited probability fluxes associated with both isospins, after $t = 7.90 \times 10^{-20}$s, and evaluated at different $c_{\#}$ values.

It is difficult to tell whether the marked difference in favor of the neutron excitations that appears in Figure (6.22) indicates a real physical phenomenon, or whether it is simply related to a bias in the excitation choice.
An argument pleading for a physical cause may be found in the proton odd-even staggering observed at scission (around $c_{\#} = 495$). Indeed, this feature implies that proton pairs are comparatively harder to break than neutron ones. As we've observed that the low-energy variational excitations created generally include pair-breaking phenomena, we do believe that the results displayed in Figure (6.22) may not be the result of chance. A more in-depth study on this topic would be of great interest.

To conclude, we've evaluated the excited yields associated with the different probability fluxes. Because of the flux pertubations near scission, we've decided to consider the average flux values in the range $[c_{\#} - 50, c_{\#} + 50]$. In Figure (6.23), we've represented the different excited yields obtained:

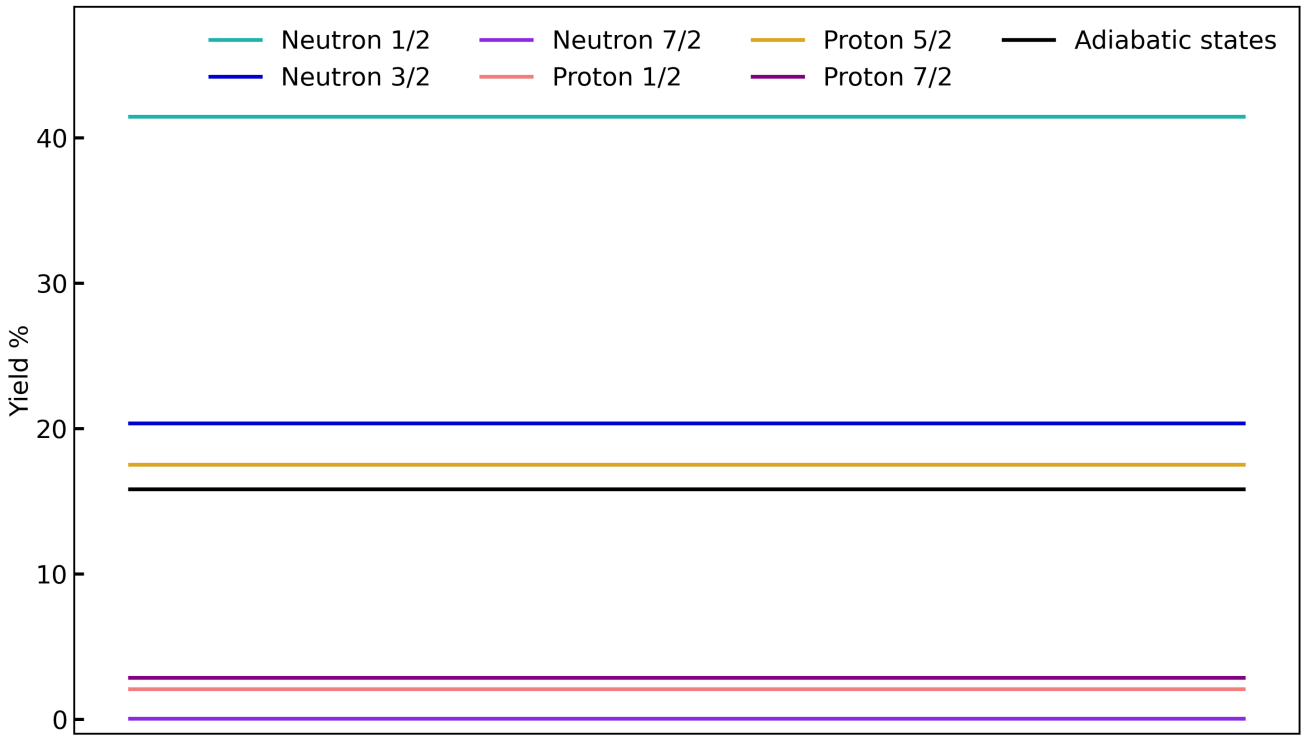

Figure 6.23: Excited yields associated with the scenario (*).

More precisely, we've found 15.8 % for the adiabatic states, 41.5 % for the neutron $\Omega = 1/2$ excitation, 20.3 % for the neutron $\Omega = 3/2$ excitation, 0.0 % for the neutron $\Omega = 7/2$ excitation, 2.1 % for the proton $\Omega = 1/2$ excitation, 17.5 % for the proton $\Omega = 5/2$ excitation, and 2.8 % for the proton $\Omega = 7/2$ excitation.
The different excitations represent 84.2 % of the total yield. This fact unequivocally highlights how important it is to include intrinsic excitations within the description of the fission process.

6.3.2 Particle number and proton and neutron yields

In this section, we compare the light fragment neutron and proton yields associated with the adiabatic states to the ones associated with the SCIM states. In addition, we provide

both the experimental light fragment neutron and proton yields related to the ^{239}Pu(n_{th},f) reaction [61].
The light fragment neutron and proton yields associated with the SCIM states are simply deduced from the excited yields given in Figure (6.23) using the following formulas:

$$\boxed{\mathrm{Y}_{SCIM}(N_l) = \sum_{i=0}^{6} \mathrm{Y}_i c_i^2(N_l)} \qquad \boxed{\mathrm{Y}_{SCIM}(Z_l) = \sum_{i=0}^{6} \mathrm{Y}_i c_i^2(Z_l)} \tag{6.56}$$

In Eq.(6.56), the notation Y_i stands for the excited yield associated with the i-th excitation (i=0 corresponds to the adiabatic states). The coefficients $c_i^2(N_l)$ and $c_i^2(Z_l)$ are the probability amplitudes of the i-th excitation associated with the light fragments characterized by the neutron number N_l and the proton number Z_l, respectively (see Chapter 3).

In Figure (6.24), we've displayed the adiabatic and the SCIM light fragment neutron yields (evaluated at $c_{\#} = 495$), in addition to the experimental one [61]:

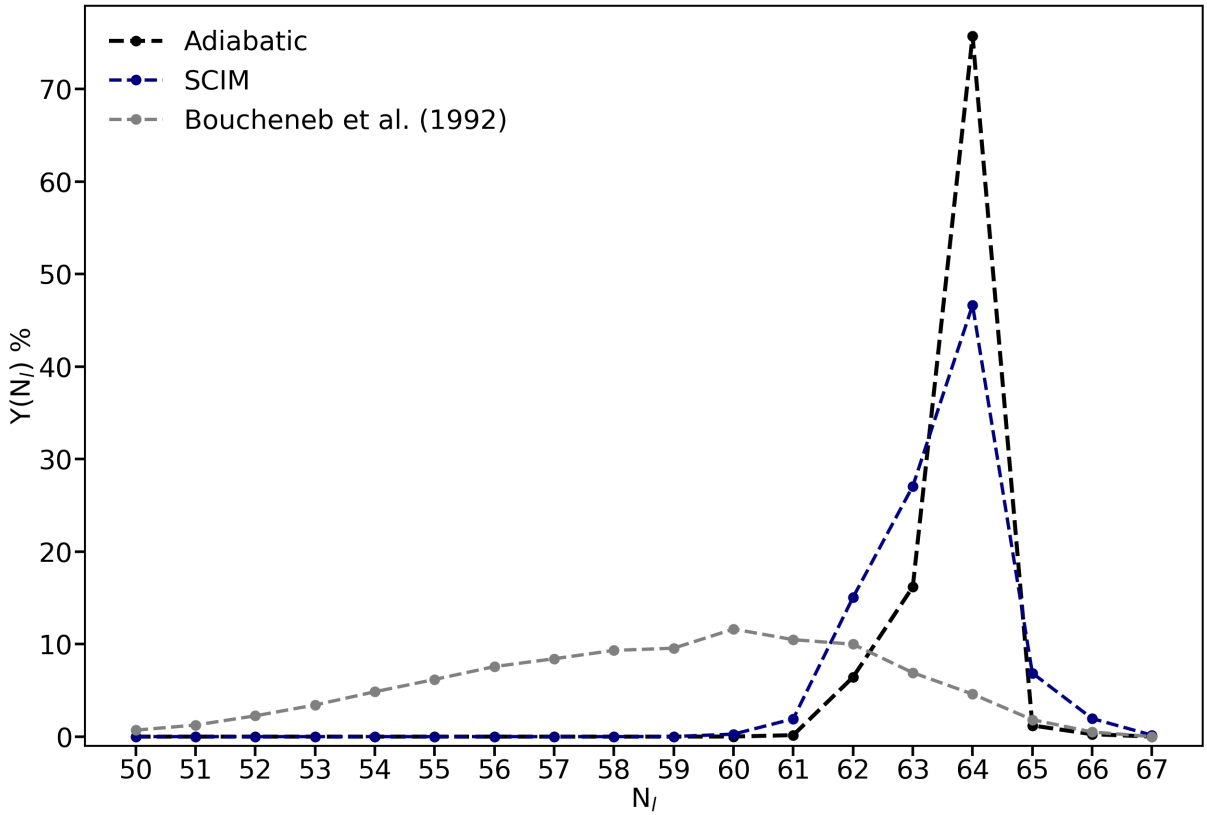

Figure 6.24: Comparison between the adiabatic, the SCIM, and the experimental neutron yields.

We clearly observe that including intrinsic excitations within the fission description tends to broaden the neutron yields. This result is very promising, as the adiabatic TDGCM yields are often criticized for being too narrow compared to the experimental ones. Moreover, the odd components of the neutron yields are increased in a significant way, taking into account the excitations. We attribute this feature to the fact that the variational excitations created include pair breaking phenomena.

However, both the adiabatic and the SCIM neutron yields are still far from the experimental ones. This is not a surprise, as our description misses another collective degree of freedom.

In Figure (6.25), we've represented the adiabatic and the SCIM light fragment proton yields (evaluated at $c_{\#} = 495$), in addition to the experimental one [61]:

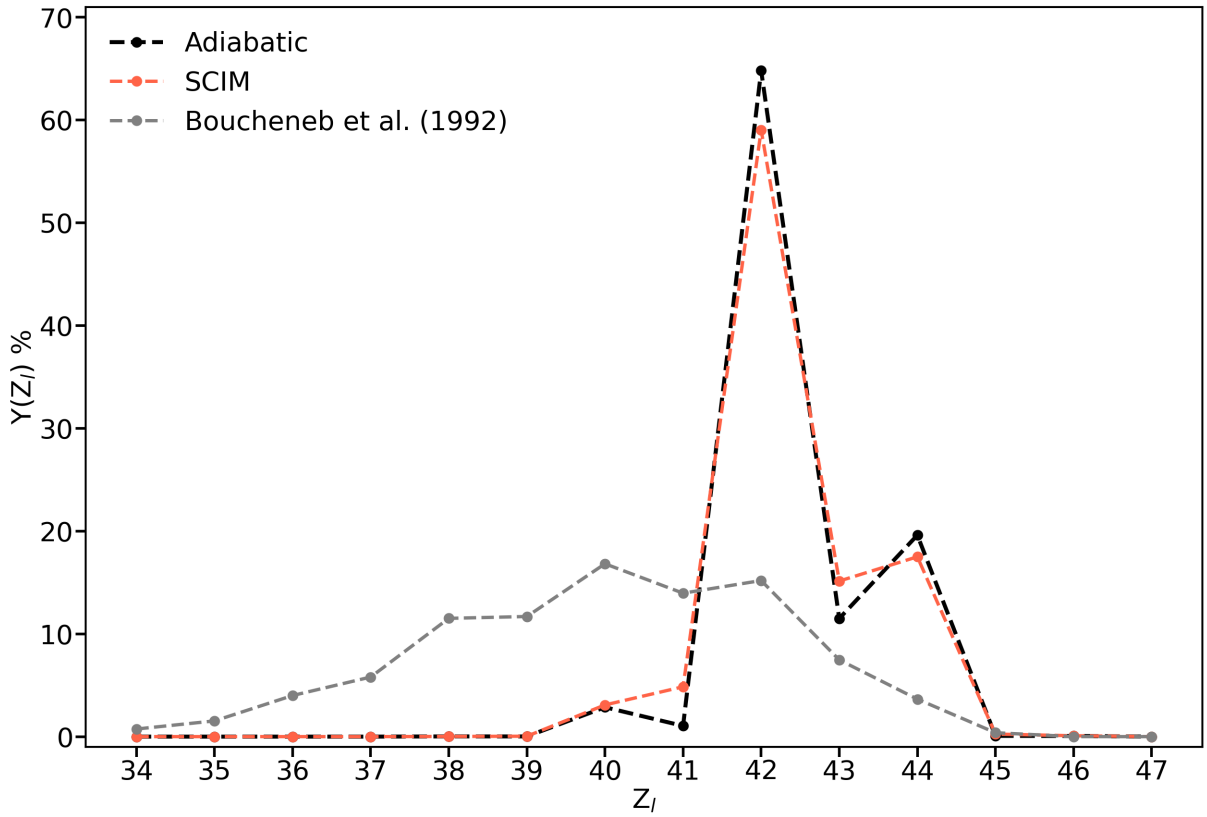

Figure 6.25: Comparison between the adiabatic, the SCIM, and the experimental proton yields.

As in the case of neutrons, the light fragment proton yields is broaden by the excitations, and proton pairs are clearly broken. These effects are of a much smaller magnitude than in the neutron case, though. This feature is trivially related to the smaller total proton excited yield extracted from the "dynamics". As stated previously, further studies would be required to determine precisely whether this phenomenon has any physical significance, or if it is just an artifact related to the scenario (*).
Here also, both the adiabatic and the SCIM proton yields are compatible with the experiments but are not able to recover fully experimental results. Therefore, it will be of paramount importance to include a second collective coordinate in the future SCIM applications.

6.3.3 Energy balance

Finally, we study the energy balance at scission in the light of the "dynamics" results. First of all, we analyze the total excitation energy associated with the variational excitations included in the scenario (*).
In order to have access to local informations about the total intrinsic excitation energy, we've chosen to define the local total intrinsic excitation energy $E^*(c_{\#})$ as follows:

$$\boxed{E^*(c_\#) = \sum_{i=1}^{6} \frac{\phi_i(c_\#)}{\phi_{tot}(c_\#)} (E^{(i)}_{HFB}(c_\#) - E_{HFB}(c_\#))} \tag{6.57}$$

In Eq.(6.57), the quantity $E^{(i)}_{HFB}(c_\#)$ simply stands for the total binding energy related to the i-th excitation and evaluated at $c_\#$. Regarding the relevant intrinsic excitation energy to use within the energy balance at scission, we've chosen to consider the average of $E^*(c_\#)$ in the range $[c_\# - 50, c_\# + 50]$. This choice allows to avoid issues related to flux pertubations near scission and is made in coherence with the method used to extract the excited yields.
In Figure (6.26), we've represented the local intrinsic excitation energy $E^*(c_\#)$, with respect to $c_\#$. In addition, we've plotted the intrinsic excitation energy at scission E^*_s, which has been defined just above:

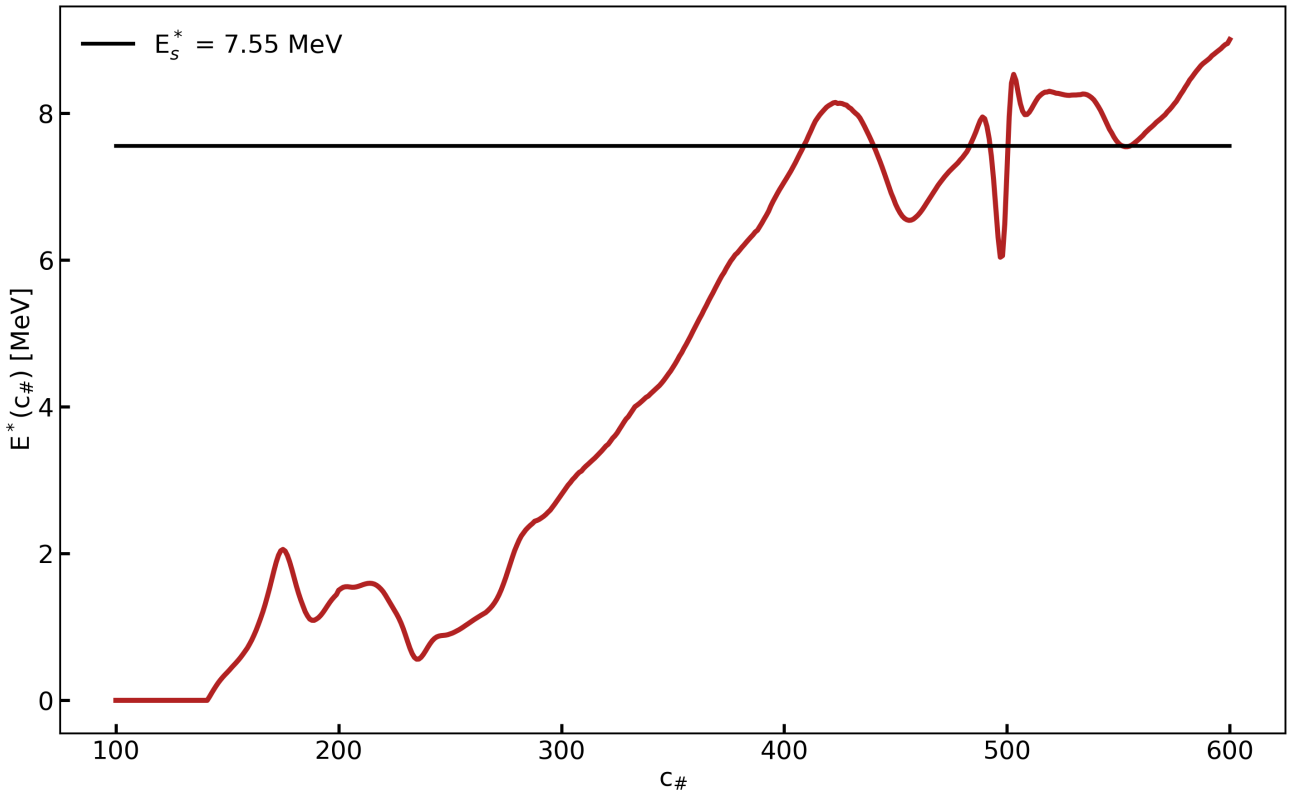

Figure 6.26: Evolution of the local intrinsic excitation energy $E^*(c_\#)$, with respect to $c_\#$.

First of all, Figure (6.26) definitely confirms the fact that the excitation process really starts from the saddle point ($c_\# = 267$). Moreover, the red curve reveals a very important new piece of information. Indeed, it is clear that the excitation energy increases almost linearly from the saddle point to the scission area. When we studied the total excited probability flux, we saw a rapid increase after the saddle point, followed by a much slower increase. Figure (6.26) highlights that these speed differences in the scission descent are mostly related to the fact that the local excitation energy differences $\Delta E^*_i(c_\#) = E^{(i)}_{HFB}(c_\#) - E_{HFB}(c_\#)$ tend to increase overall after the saddle point.
In addition, the regular behaviour of the local intrinsic excitation energy in the scission descent naturally leads to the definition of the dissipation coefficient $\gamma^*_{c_\#}$:

$$\boxed{\gamma^*_{c_\#} = \frac{E^*(420) - E^*(267)}{420 - 267} = 4.50 \times 10^{-2} \text{ MeV}} \tag{6.58}$$

It is clear that the coefficient $\gamma^*_{c_\#}$ characterizes the amount of collective energy which is transformed into intrinsic energy with respect to an overlap variation of 0.995 in the scission direction (after the saddle point). Obviously, the same quantity can be expressed in terms of the quadrupole moment Q_{20}:

$$\boxed{\gamma^*_{Q_{20}} = \frac{E^*(420) - E^*(267)}{Q_{20}(420) - Q_{20}(267)} = \gamma^*_{Q_{20}} = 1.22 \times 10^{-3} \text{ MeV.fm}^{-2}} \tag{6.59}$$

We are aware that further studies are needed to confirm the physical relevance of this kind of coefficients. In particular, they may strongly vary depending on the nucleus and on the initial conditions of the "dynamics" (especially the initial wave function average energy). Besides, it is possible that the linear behaviour observed only originates from the choice of the scenario (*). That said, in the case of a given nucleus and with given initial conditions, we assume that this kind of coefficients could provide interesting qualitative estimations of the intrinsic excitation energies related to different fission paths (obviously not too far from the adiabatic one).
Finally, the intrinsic excitation energy E^*_s, which will be considered within the energy balance equals 7.55 MeV. This amount of energy is relatively important as it represents approximatively the emission of one neutron after scission.

Now, we have everything needed to formulate the energy balance at scission. We start by recalling the informations obtained in Chapter 3:

- The excitation energy coming from the deformation of the fragments E_D has been estimated at 26.85 MeV (at $c_\# = 495$).
- The Coulomb interaction energy between the fragments E_C has been estimated at 178.743 MeV (at $c_\# = 495$).
- The total interaction energy between the fragments E_{int} has been estimated at 152.50 MeV (at $c_\# = 495$).
- The energy difference ΔE_{1s} between the top of the first barrier and the scission point ($c_\# = 495$) is 33.31 MeV.

First of all, we evaluate the Total Excitation Energy (TXE) related to the scenario (*):

$$\boxed{\text{TXE} = E_D + E^*_s = 34.40 \text{ MeV}} \tag{6.60}$$

This TXE is slightly overvalued. Indeed, the experimental data related to the ^{239}Pu(n_{th},f) reaction indicate a neutron multiplicity $\bar{\nu} \approx 3$ plus a few gamma emissions leading to a TXE of approximately 30 MeV [75]. This over-estimation may originate from the deformation energy E_D, which appears to be a very sensitive quantity as stated in Chapter 4.

Then, we've calculated the pre-scission kinetic energy E_{PS}:

$$\boxed{E_{PS} = \Delta E_{1s} - E_s^* = 25.76 \text{ MeV}} \tag{6.61}$$

Thanks to E_{PS}, we can evaluate the Total Kinetic Energy (TKE) associated with the two different hypotheses made in Chapter 3. In the first case, which is the customary assumption, we only adds the Coulomb interaction energy to the pre-scission kinetic energy. The related TKE is noted TKE_C and reads as:

$$\boxed{\text{TKE}_C = E_{PS} + E_C = 204.50 \text{ MeV}} \tag{6.62}$$

In the second case, we add the whole interaction energy E_{int} to the pre-scission kinetic energy E_{PS}. The related TKE is noted TKE_{int}:

$$\boxed{\text{TKE}_{int} = E_{PS} + E_{int} = 178.26 \text{ MeV}} \tag{6.63}$$

To compare these two different TKE with the experimental data, we've reproduced in Figure (6.27) the results found in [76]. The average TKE associated with the ^{239}Pu(n_{th},f) reaction are displayed with respect to the light fragment proton number Z_l. In addition, we've added a black line standing for the "goal TKE", which is the TKE we should find according to the light fragment proton particle number distribution of the SCIM wave function at scission ($c_\# = 495$):

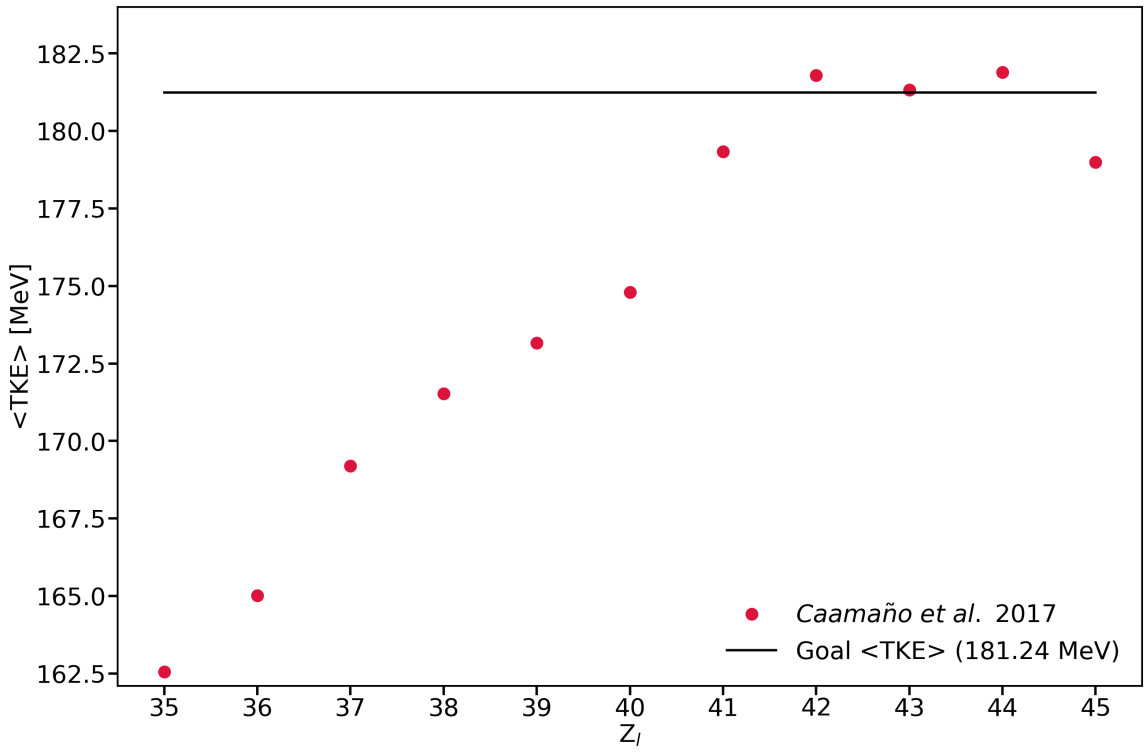

Figure 6.27: Average TKE associated with the ^{239}Pu(n_{th},f) reaction, displayed with respect to the light fragment proton number Z_l.

The TKE evaluated with the whole interaction energy is much closer to the "goal TKE" than the one evaluated using the Coulomb interaction energy only. This result suggests that

the nuclear interaction energy should not be neglected when evaluating the energy balance at scission.
To conclude, the pre-scission kinetic energy found accounts for 14.4 % of TKE_{int}. This order of magnitude is in line with the results obtained in the recent work of Y. Tanimura and D. Lacroix [77, 78], using an original stochastic mean-field approach to explore the nucleus phase-space.

Conclusion

The path that scientific research follows day after day is not known for being straightforward and easy. And that's a good thing. It's what makes the job of a researcher so exciting, and the history of science is full of twists and turns eventually as fruitful as they were unexpected. The PhD thesis that these present lines conclude is no exception to the rule.

The journey of this PhD thesis began with the study of R. Bernard et al. [33, 34], which led to the formulation of the Schrödinger Collective-Intrinsic Model (SCIM) in 2011. The aim of the first Chapter was to recall these earlier theoretical developments, while situating them in relation with the Time-Dependent Generator Coordinate Model (TDGCM), from which they originate.

Our first attempts to implement the SCIM formalism ended in failure. In Chapter 2, we told the story of these difficulties and the lessons we learned from them.
At first, we thought that the main problem with the original formulation of the SCIM was that the 2-quasiparticle excitations broke the average particle number, leading to unrealistic Hamiltonian kernel values. For this reason, we implemented the Projection on particle number After Variation (PAV) method in the SCIM formalism. Using this tool, we were able to successfully correct the problems observed in Hamiltonian kernels previously mentioned. Unfortunately, these improvements were still not enough to use the SCIM in practice. At this point, we realized that, due to level repulsions, the 2-quasiparticle excitations were by nature not regular enough to match the SCIM assumptions. Besides, we discovered that this regularity issue also occured at the adiabatic level, albeit to a lesser extent. These observations finally led us to the formulation of the concepts of intrinsic and extrinsic regularities, which enabled us to better define the problems to be solved.

In this manuscript, Chapter 2 and Chapter 3 follow on from each other, but they were, in fact, separated by many long months. The central idea for solving SCIM problems - adding new constraints on overlaps to the constrained Hartree Fock Bogoliubov (HFB) theory - was initially a matter of chance.
Although we've thought about constraining overlaps in the past, it was during a discussion with D. Lacroix at a workshop in late november 2023 that we first heard about the concrete possibility of doing so. Indeed, Y. Beaujeault-Taudière and D. Lacroix had just completed a quantum computing study [58] in which they used a method called "Deflation", originating in quantum chemistry [59], to create variational excited states, by imposing orthogonality constraints on overlaps. We then integrated this new idea into the HFB theory, and we extended its scope by making it possible to constrain not only the orthogonality but the precise value of the overlaps. From there, we created the three new methods - the "Link", the "Drop" and the "Continuous Deflation" methods [60] - that finally made the SCIM possible in practice.

As we showed in Chapter 3, the "Link" method efficiently connects two non-orthogonal HFB states. Indeed, we demonstrated in the case of ^{240}Pu that this method is particularly well suited for correcting the discontinuities usually found in PES. The "Drop" method, on the other hand, provides a continuous and easy description of phenomena characterized by a descending energy gradient. In particular, it enabled us to continuously describe the entire scission process in the case of the ^{240}Pu nucleus, which was totally new in TDGCM-type approaches. The combination of these two approaches allowed to create an adiabatic and asymmetric fission path associated with the ^{240}Pu nucleus, which was both continuous and as regular as possible (it included a fixed overlap between two adjacent states). This path being characterized by the new collective coordinate $c_{\#}$, naturally deduced from the regular sequence of states. In addition, thanks to the "Continuous Deflation" method, we successfully built ten continuous and regular variational excitations on top of the previously mentioned adiabatic path. Finally, we extensively studied the physical content of these variational excitations and showed that they were mostly made up of 2- and 4-quasiparticle excitations.

In Chapter 4, we presented the new results on the physics of scission area that obtained from the states created using the "Link", the "Drop", and the "Continuous Deflation" methods in the ^{240}Pu nucleus. Firstly, we studied the chemical potentials near scission and noticed very clear peaks at the adiabatic level, for both neutrons and protons. We interpreted these peaks as a signature of the scission phenomenon, linked to the comparatively lower binding energy of particles in the neck between the two pre-fragments.
Secondly, we showed a remarkable neutron/proton asymmetry in the neck between the pre-fragments at the adiabatic level. This phenomenon proved even more important for neutron variational excitations, where we found a maximum ratio of approximately forty to one. We believe that these observations represent a step forward in our understanding of neutron emission at scission. Besides, we observed a greater nucleon density in the neck for most of the variational excited states compared with their associated adiabatic states. These results suggest that intrinsic excitations might play a role in the binding of the compound nucleus in the utlimate moments before scission.
Thirdly, we focused on fragment particle number distributions around scission. At the adiabatic level, we observed a very interesting proton odd-even staggering, in line with the experimental data [61]. Regarding variational excited states, we found that they generally broaden the fragment particle number distributions. Additionally, the significant number of odd components that appear in most of the particle number distributions associated with variational excitations indicate that they include pair-breaking phenomena, which are expected for low-energy intrinsic excitations [29, 30].
Finally, we conducted a static energy balance at scission using a new method called "RC-separation", which we developed inspired by the work of W. Younes and D. Gogny [35]. This method allowed for the extraction of the deformation energies of the fragments at scission, as well as the evaluation of their reciprocal interaction energy. We realized that the residual nuclear interaction energy between the fragments at scission was far from being negligible compared to the Coulomb interaction energy (around 20 %). This latter observation led us to hypothesize the necessity of explicitly considering the total interaction energy in the energy balance at scission in order to describe the post-scission kinetic energy more accurately.

To obtain the results presented throughout this PhD thesis, meticulous theoretical and numerical works on the calculation of both Hamiltonian and overlap kernels was carried out. In Chapter 5, we detailed the approaches used and gave the explicit formulas for these calculations. Notably, we presented new theoretical results that allow for easier evaluation of

kernels when two different 1- or 2-center harmonic-oscillator bases are considered.
Moreover, we specifically investigated two numerical problems encountered in practice. The first concerns a phasis, which we have called "V-phasis", related to the particle number breaking in HFB theory. This phasis can lead to the evaluation of nearly zero overlaps between states that are otherwise very similar. We proposed a prescription, in the form of a new overlap formula, which allowed us to fully correct the problem in practice.
The second issue we faced involved the divergence of Hamiltonian kernels between two orthogonal states. We also proposed a prescription, which we called "overlap prescription", directly derived from the "local approximation", that enabled us to circumvent this difficulty.

In our final Chapter, we presented the first dynamical application of the SCIM formalism in the realistic case of an asymmetric fission path of the ^{240}Pu nucleus. Firstly, we described the Savitzky-Golay filter [72] that allowed us to obtain the quantities needed for constructing the SCIM Hamiltonian, namely the SCIM potential, the SCIM dissipation tensor, and the SCIM inertia tensor. Then, we studied these quantities in details. We started by comparing them with their counterparts in the Gaussian Overlap Approximation (GOA) formalism. We presented this comparison for the exact GOA inertial mass and the exact GOA zero point energy (ZPE), which is a first in the context of fission, as well as for the inertial masses and ZPE related to the customary approximations knwon as GOA+Cranking and GOA+ATDHFB. The results clearly demonstrated the agreement between the SCIM adiabatic limit and the exact GOA, highlighting the relevance of the SCIM formalism. Regarding the ZPE and inertial masses related to the GOA+Cranking and GOA+ATDHFB approximations, the significant differences between them and the ones associated with the SCIM and the exact GOA underline the need to account for non-local collective effects in the evaluation of these quantities.
Finally, the study of the SCIM inertia tensors related to the variational excitations at the "adiabatic-excited" limit revealed that only certain excitations were suitable for the dynamics. This led us to formulate a scenario, called scenario (*), including six different variational excitations in addition to the adiabatic states.
Secondly, we detailed the numerical solution of the collective-intrinsic Schrödinger equation of the SCIM formalism, using the Crank-Nicolson method [27, 73, 74]. We also derived new formulas for evaluating probability fluxes associated with the excitations considered in the dynamics.
Finally, we analyzed the results obtained by performing the SCIM dynamics in the case of the scenario (*). This involved considering an adiabatic asymmetric fission path of the ^{240}Pu nucleus as well as six associated variational excitations. The probability fluxes obtained allowed us to make several observations. Indeed, we observed that from the saddle point onwards, the propagation of the SCIM wave function was highly diabatic, with the probability flux associated with the adiabatic states generally representing less than 20 % of the total probability flux near scission. Then, we noticed a significantly higher excited probability flux for neutrons than for protons around scission. We hypothesized that this difference correlates with the greater binding of proton pairs at the adiabatic level, as evidenced by the proton odd-even staggering phenomenon observed. In addition, the probability fluxes enabled us to deduce excited yields, *i.e.* the probability of obtaining a given excited or adiabatic state at scission during a fission event. Using these excited yields, we were able to study the impact of taking intrinsic excitations into account on fragment particle number distributions at scission. In particular, we showed that mass yields could be significantly broaden by intrinsic excitations, which calls for future SCIM dynamics studies including two collective degrees of freedom.
Chapter 6 concludes with the dynamical energy balance at scission. First of all, during this

first SCIM dynamics, we were able to dissipate 7.55 MeV as intrinsic excitation energy. This represents a significant amount of energy, roughly equivalent to the emission of a neutron by the scission fragments. Then, we found a slightly overvalued TXE of 34.40 MeV and a slightly undervalued TKE of 178.26 MeV. To give an idea, the experimental results indicate approximatively 30 MeV in the first case [75] and 181 MeV in the second [76]. Besides, we were eventually able to demonstrate the crucial need to include the nuclear interaction energy between the fragments in addition to the Coulomb one within the energy balance at scission, in order to obtain reliable predictions regarding the TKE of the fragments.

Regarding the perspectives opened by this work, avenues for future studies have been already proposed throughout the Chapters. We will now focus on highlighting and elaborating on those we believe to be the most relevant and necessary.

With regard to the new methods based on the overlap constraints, we believe that the most beneficial study for a better understanding of the "Link" method would be to provide an interpretation in terms of action. Indeed, we are convinced that this study would aid all subsequent numerical developments aimed at improving the performances of the method.
Concerning the "Drop" method, we believe it would be both easy and extremely instructive to use the "Guided Drop" method with a fixed octupole moment Q_{30} to conduct a two-dimensional topological study of a relevant actinide PES around scission.
Next, it would be of great interest to further analyze the composition of the variational excited states created with the "Deflation"-type methods. In particular, a description in terms of 2n-quasiparticle excited states with n>2 could be provided, and a more detailed study of the quasiparticle states included in each component would be very enlightening too.
Finally, it is clear that developing a new overlap constraint method for constructing two-dimensional continuous and regular PES (in terms of collective coordinates) is of utmost importance. In this regard, we would like to share with the reader several ideas that form the basis of a new method we have called Nuclear Paving (NP method). Indeed, we believe that implementing a new collective coordinate, which we will denote as $c_\flat$ in the following, could be achieved based on a few very simple ideas. First, a notion of a direction "orthogonal" to another could be obtained using the GOA predictions. In Figure (6.28), we have provided a schematic view of what we have in mind. We consider three states, A, B and C, described by the collective coordinate $c_\#$ (thus characterized by a fixed overlap x_0 between them). The method would consist in searching for a state D, which would have an overlap of x_0 with the state B and such that its overlap with the state A would be equal to its overlap with the state C. The overlap value between the states D and A, and the states D and C, that satisfies these conditions, while being consistent with the GOA, equals x_0^2 (see chapter 2):

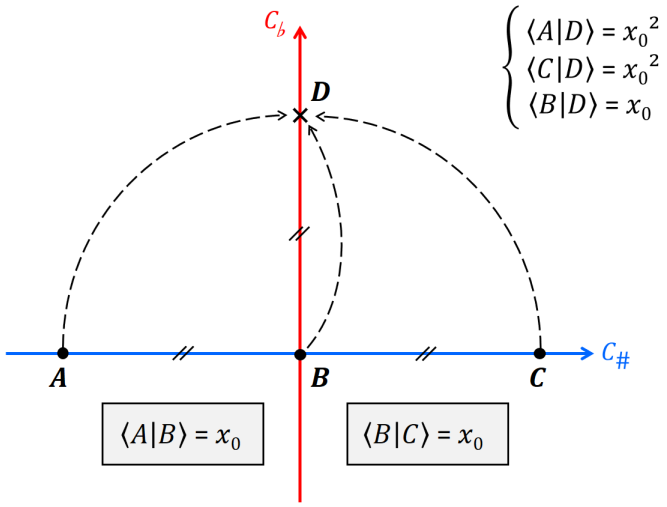

Figure 6.28: Schematic view of the definition of a direction "orthogonal" to another.

Consequently, imposing simultaneously the three constraints $\langle A|D\rangle = x_0^2$, $\langle C|D\rangle = x_0^2$, and $\langle B|D\rangle = x_0$ could define a state D that would be adjacent to the state B, but with respect to the direction associated with $c_\flat$ geometrically orthognal to the one related to $c_\#$.
Once such an orthogonal direction is defined, one can easily imagine creating a two-dimensional grid, still using the GOA predictions. In Figure (6.29), we have illustrated this idea by showing how a state E could be defined from three different states D, B, and C, forming an isosceles triangle in the $c_\flat - c_\#$ plane:

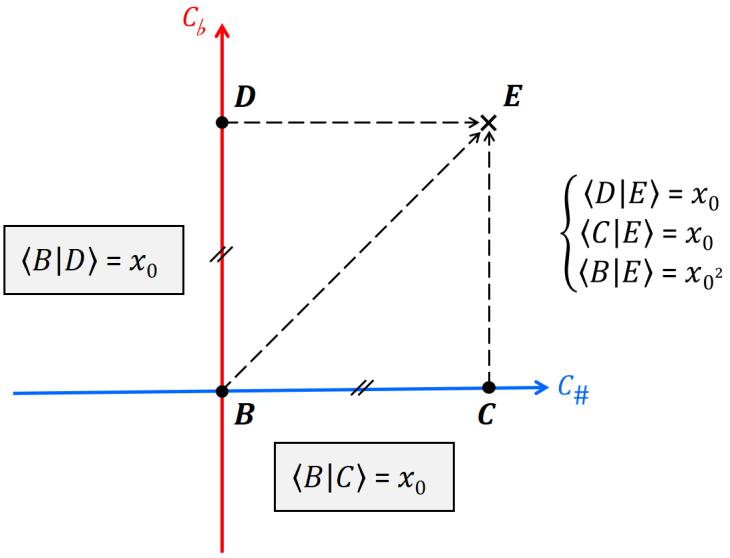

Figure 6.29: Schematic view of a $c_\flat - c_\#$ grid construction using overlap constraints in combo with the GOA predictions.

In this case also, three different overlap constraints would be imposed at a same time, namely $\langle D|E\rangle = x_0$, $\langle C|E\rangle = x_0$, and $\langle B|E\rangle = x_0^2$.

Finally, it would be possible to jump from a $c_\flat$ level to another using GOA predictions once again. In Figure (6.30), we have represented this latter idea showing how a state E ($c_\#$,$c_\flat$) could be defined from two other states D ($c_\#$,$c_\flat - 1$) and B ($c_\#$,$c_\flat - 2$):

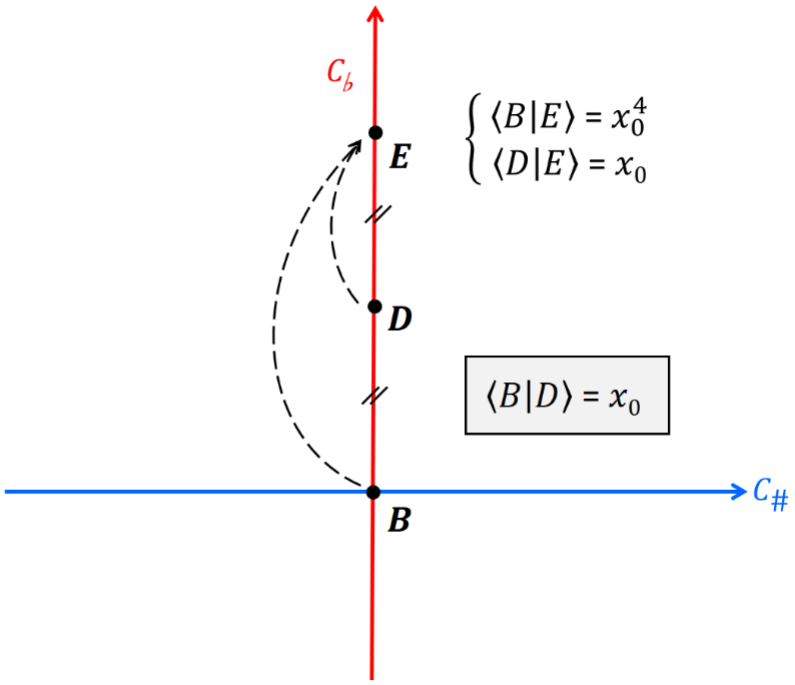

Figure 6.30: Schematic view of $c_\flat$ climbing using the GOA predictions.

We have tested these ideas locally around the scission point ($c_\# = 495$). In Figure (6.31) and Figure (6.32), we have displayed a 5×5 grid created with the NP method with respect to $c_\#$ and $c_\flat$ and $c_\#$ and $|Q_{30}|$ respectively:

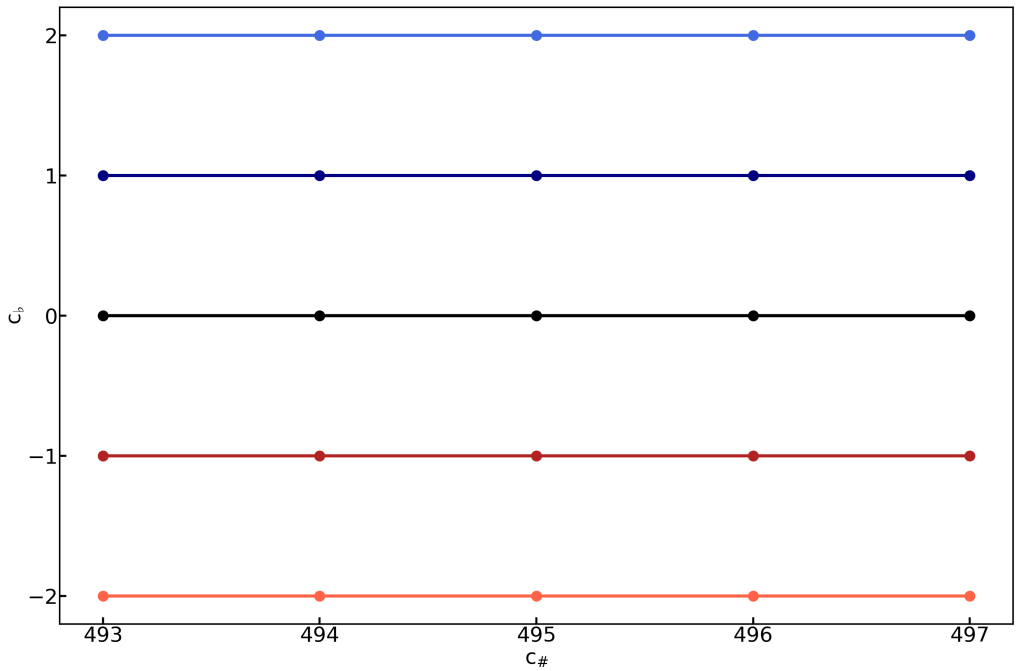

Figure 6.31: 5×5 grid made using the NP method and displayed with respect to $c_\#$ and $c_\flat$.

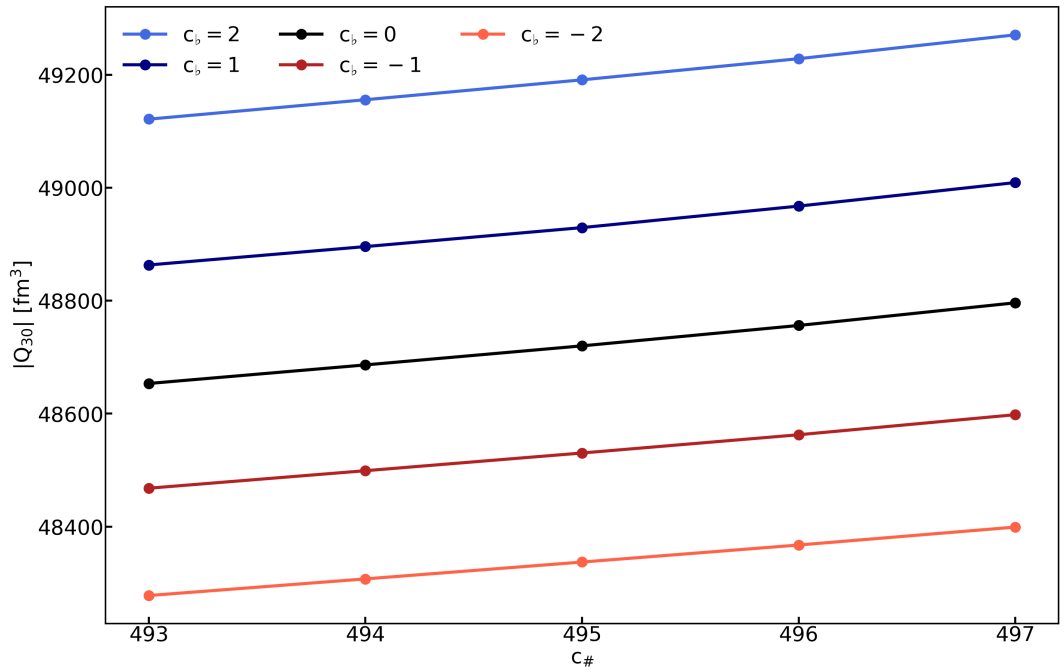

Figure 6.32: 5×5 grid made using the NP method and displayed with respect to $c_\#$ and $|Q_{30}|$.

We clearly observe in Figure (6.32) that the new collective coordinate $c_\flat$ generated by the NP method accounts for an asymmetry gradient.
In Figure (6.33), we have represented the energy of all the states belonging to the 5×5 grid. The study is still too local to obtain any relevant physical information, but we note that the states labeled by $c_\flat = 0$, generated by the "Drop" method, are associated with the strongest energy gradient (in parentheses), which was expected:

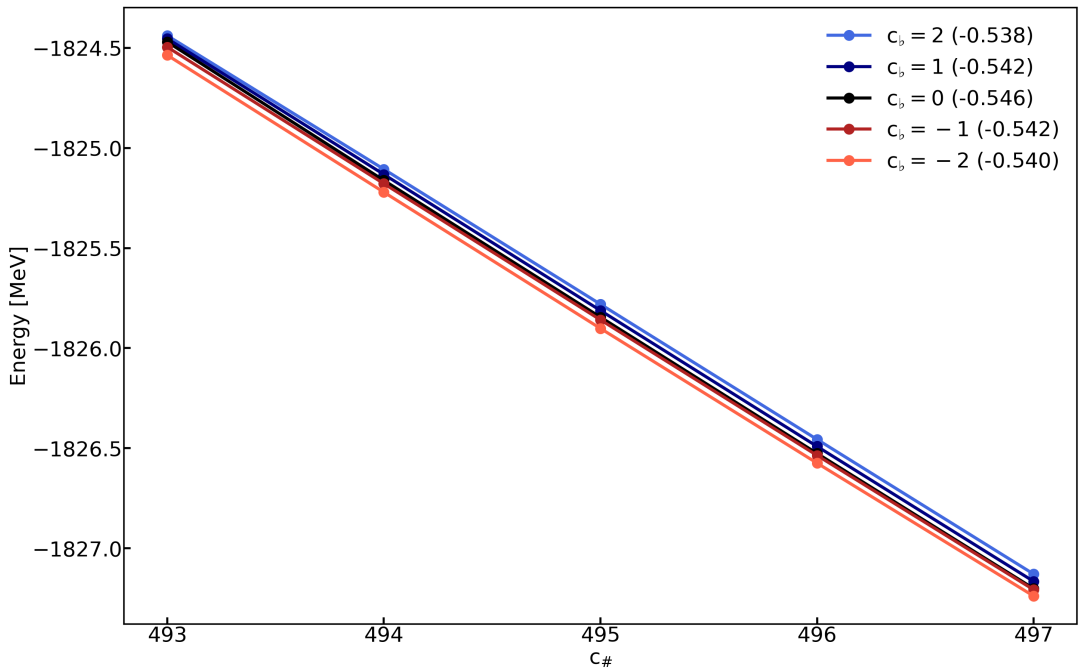

Figure 6.33: Energy of the states belonging to the 5×5 grid made using the NP method.

The NP method will likely need to be refined and adapted for practical applications. In particular, topological problems could arise when moving from local to global. Nevertheless,

it will probably be possible to circumvent these topological issues by weakening certain constraints with wisdom.
We are convinced that the ideas presented above are a viable avenue for extending the methods based on the overlap constraints to the creation of two-dimensional PES.

With regard to the themes developed in Chapter 4, we believe that the most important challenge would be to find a method to obtain the deformation energies of the fragments and the interaction energy between the fragments associated with the variational excitations. Indeed, since the variational excitations account for more than 80 % of the SCIM wave function at scission, a better evaluation of these quantities could have a significant impact on the energy balance at scission.

Finally, it is clear that the last Chapter calls for the most new studies and developments. First, it would be interesting to evaluate the impact of considering the exact GOA inertial mass and ZPE in the case of lifetime calculations, as well as for two-dimensional adiabatic dynamics using the TDGCM+GOA formalism.
Furthermore, as we address the topic of lifetimes, it would be interesting to study the impact of the intrinsic excitations on them. To do this, we could diagonalize the SCIM Hamiltonian and analyze the complex parts of the eigenvalues obtained. More generally, in the case of induced fission (considering an initial state with an energy close to the first barrier), it would be of great interest to quantify the velocity of the SCIM wave function components with respect to the intrinsic excitations included. This could be done by studying the probability flux evolution over time.
Then, as with any numerical model, it would be important to evaluate the sensitivity to initial conditions. In particular, at the adiabatic level, the impact of both the average energy and the energy standard deviation of the initial wave packet should be studied. When it comes to variational excitations, it would be necessary to compare the results obtained across a large number of scenarios to determine, for example, whether saturation of the dissipation appears. This phenomenon would help to define both the nature and the number of the excitations to consider for accurately describing the dissipation physics in low-energy fission. Besides, it would be interesting to investigate whether the observed asymmetry between the probability fluxes associated with the neutron excitations and the ones associated with the proton excitations really reflects a physical phenomenon, rather than simply being a consequence of the choice of the scenario (*).

To conclude, it is clear that the most crucial development suggested by the SCIM dynamics results is the application of the SCIM formalism in the case of two collective degrees of freedom. This extension would lead to mass and charge yields directly comparable to the experimental data, while providing a consistent and fully microscopic evaluation of the energy balance at scission.

Appendix A

The SOPO

The SOPO or Symmetric Ordered Product of Operators is a way to write product of operators in a compact form. It is defined as follows:

$$\boxed{[AB]^{(n)} = \sum_{k=0}^{n} \binom{n}{k} B^k A B^{n-k} \qquad \forall n \in \mathbb{N}} \tag{A.1}$$

It is clear that a SOPO is $\mathbb{C}$-linear on the left:

$$[\lambda(A+C)B]^{(n)} = \lambda([AB]^{(n)} + [CB]^{(n)}) \qquad \forall \lambda \in \mathbb{C},\ \forall n \in \mathbb{N} \tag{A.2}$$

In this PhD thesis, the SOPOs are always used with a derivative operator on the right:

$$[A(q)\frac{\partial}{\partial q}]^{(n)} = \sum_{k=0}^{n} \binom{n}{k} \frac{\partial^k}{\partial q^k} A(q) \frac{\partial^{n-k}}{\partial q^{n-k}} \tag{A.3}$$

Note that the derivative operator $\frac{\partial}{\partial q}$ in Eq.(A.3) does not only act on A but on anything on its right.

A.1 Product of SOPO

Products of SOPOs frequently appear in the SCIM [33,34], it is thus useful to derive a closed formula to handle them. It explicitly reads:

$$[A(q)\frac{\partial}{\partial q}]^{(n)}[B(q)\frac{\partial}{\partial q}]^{(p)} = \sum_{k=0}^{n}\sum_{l=0}^{p} \binom{n}{k}\binom{p}{l} \frac{\partial^k}{\partial q^k} A(q) \frac{\partial^{n-k}}{\partial q^{n-k}} \frac{\partial^l}{\partial q^l} B(q) \frac{\partial^{p-l}}{\partial q^{p-l}} \tag{A.4}$$

Commuting the derivatives in the middle of Eq.(A.4) leads to:

$$\begin{aligned}[A(q)\frac{\partial}{\partial q}]^{(n)}[B(q)\frac{\partial}{\partial q}]^{(p)} = \sum_{k=0}^{n}\sum_{l=0}^{p}\sum_{\alpha=0}^{l}\sum_{s=0}^{n-k} \binom{n}{k}\binom{p}{l}\binom{l}{\alpha}\binom{n-k}{s} \\ \frac{\partial^{(k+l)-\alpha}}{\partial q^{(k+l)-\alpha}}(-1)^\alpha A^{(\alpha)}(q) B^{(s)}(q) \frac{\partial^{(p+n)-(k+l)-s}}{\partial q^{(p+n)-(k+l)-s}}\end{aligned} \tag{A.5}$$

We change the order of the sums:

$$[A(q)\frac{\partial}{\partial q}]^{(n)}[B(q)\frac{\partial}{\partial q}]^{(p)} = \sum_{s=0}^{n}\sum_{\alpha=0}^{p}\sum_{l=\alpha}^{p}\sum_{k=0}^{n-s}\binom{n}{k}\binom{p}{l}\binom{l}{\alpha}\binom{n-k}{s} \frac{\partial^{(k+l)-\alpha}}{\partial q^{(k+l)-\alpha}}(-1)^{\alpha}A^{(\alpha)}(q)B^{(s)}(q)\frac{\partial^{(p+n)-(k+l)-s}}{\partial q^{(p+n)-(k+l)-s}} \tag{A.6}$$

We set $l' = l - \alpha$:

$$[A(q)\frac{\partial}{\partial q}]^{(n)}[B(q)\frac{\partial}{\partial q}]^{(p)} = \sum_{s=0}^{n}\sum_{\alpha=0}^{p}\sum_{l=0}^{p-\alpha}\sum_{k=0}^{n-s}\binom{n}{k}\binom{p}{l+\alpha}\binom{l+\alpha}{\alpha}\binom{n-k}{s} \frac{\partial^{(k+l)}}{\partial q^{(k+l)}}(-1)^{\alpha}A^{(\alpha)}(q)B^{(s)}(q)\frac{\partial^{(p+n)-(k+l)-(s+\alpha)}}{\partial q^{(p+n)-(k+l)-(s+\alpha)}} \tag{A.7}$$

We set $z = k + l$:

$$[A(q)\frac{\partial}{\partial q}]^{(n)}[B(q)\frac{\partial}{\partial q}]^{(p)} = \sum_{s=0}^{n}\sum_{\alpha=0}^{p}\sum_{z=0}^{p+n-(s+\alpha)}\frac{\partial^{z}}{\partial q^{z}}(-1)^{\alpha}A^{(\alpha)}(q)B^{(s)}(q)\frac{\partial^{(p+n)-(s+\alpha)-z}}{\partial q^{(p+n)-(s+\alpha)-z}} \sum_{k=\max(0,z-(p-\alpha))}^{\min(z,n-s)}\binom{n}{k}\binom{p}{z-k+\alpha}\binom{z-k+\alpha}{\alpha}\binom{n-k}{s} \tag{A.8}$$

The binomial coefficients are then reorganized:

$$[A(q)\frac{\partial}{\partial q}]^{(n)}[B(q)\frac{\partial}{\partial q}]^{(p)} = \sum_{s=0}^{n}\sum_{\alpha=0}^{p}\sum_{z=0}^{p+n-(s+\alpha)}\frac{\partial^{z}}{\partial q^{z}}(-1)^{\alpha}A^{(\alpha)}(q)B^{(s)}(q)\frac{\partial^{(p+n)-(s+\alpha)-z}}{\partial q^{(p+n)-(s+\alpha)-z}} \binom{n}{s}\binom{p}{\alpha}\sum_{k=\max(0,z-(p-\alpha))}^{\min(z,n-s)}\binom{n-s}{k}\binom{p-\alpha}{z-k} \tag{A.9}$$

Remarking that:

$$\sum_{k=\max(0,z-(p-\alpha))}^{\min(z,n-s)}\binom{n-s}{k}\binom{p-\alpha}{z-k} = \binom{n+p-(s+\alpha)}{k} \tag{A.10}$$

And inserting Eq.(A.10) in Eq.(A.9), we get:

$$[A(q)\frac{\partial}{\partial q}]^{(n)}[B(q)\frac{\partial}{\partial q}]^{(p)} = \sum_{s=0}^{n}\sum_{\alpha=0}^{p}\binom{n}{s}\binom{p}{\alpha}\sum_{z=0}^{p+n-(s+\alpha)}\binom{n+p-(s+\alpha)}{k} \frac{\partial^{z}}{\partial q^{z}}(-1)^{\alpha}A^{(\alpha)}(q)B^{(s)}(q)\frac{\partial^{(p+n)-(s+\alpha)-z}}{\partial q^{(p+n)-(s+\alpha)-z}} \tag{A.11}$$

We clearly identify the expression of a SOPO on the right hand side of Eq.(A.11):

$$[A(q)\frac{\partial}{\partial q}]^{(n)}[B(q)\frac{\partial}{\partial q}]^{(p)} = \sum_{s=0}^{n}\sum_{\alpha=0}^{p}\binom{n}{s}\binom{p}{\alpha}(-1)^{\alpha}[A^{(\alpha)}(q)B^{(s)}(q)\frac{\partial}{\partial q}]^{(n+p-(s+\alpha))} \quad \text{(A.12)}$$

Setting $i = \alpha + s$, we finally have:

$$\boxed{[A(q)\frac{\partial}{\partial q}]^{(n)}[B(q)\frac{\partial}{\partial q}]^{(p)} = \sum_{i=0}^{n+p}\sum_{s=\max(0,i-p)}^{\min(i,n)}\binom{n}{s}\binom{p}{i-s}(-1)^{i-s}[A^{(i-s)}(q)B^{(s)}(q)\frac{\partial}{\partial q}]^{(n+p-i)}} \quad \text{(A.13)}$$

To conclude, Eq.(A.13) can be generalized to handle the product of 3 SOPOs:

$$\boxed{\begin{aligned}[A(q)\frac{\partial}{\partial q}]^{(n)}[B(q)\frac{\partial}{\partial q}]^{(p)}[C(q)\frac{\partial}{\partial q}]^{(r)} = \sum_{i=0}^{n+p}\sum_{s=\max(0,i-p)}^{\min(i,n)}\binom{n}{s}\binom{p}{i-s}(-1)^{i-s}\sum_{j=0}^{n+p+r-i}\\ \sum_{z=\max(0,j-r)}^{\min(j,n+p-i)}\binom{n+p-i}{z}\binom{r}{j-z}(-1)^{j-z}[(A^{(i-s)}(q)B^{(s)}(q))^{(j-z)}C^{(z)}(q)\frac{\partial}{\partial q}]^{(n+p+r-i-j)}\end{aligned}} \quad \text{(A.14)}$$

Appendix B

Thouless theorem

This appendix aims to present different forms of the famous Thouless theorem [79] used all along this PhD thesis for HFB states. The first form uses the particle vacuum $|0\rangle$:

$$\boxed{|\Phi\rangle = \langle 0|\Phi\rangle e^{\frac{1}{2}\sum_{kk'}(VU^{-1})^*_{kk'}c^+_k c^+_{k'}}|0\rangle} \tag{B.1}$$

The second one links two non-orthogonal HFB states $|\Phi_0\rangle$ and $|\Phi_1\rangle$:

$$\boxed{|\Phi_1\rangle = \langle \Phi_0|\Phi_1\rangle e^{\frac{1}{2}\sum_{kk'} Z_{kk'}\xi^+_{0,k}\xi^+_{0,k'}}|\Phi_0\rangle} \tag{B.2}$$

Both demonstrations work the same way. We first show that the states defined on the right hand side of Eq.(B.1) and Eq.(B.2) are vacua for the quasiparticles annihilation operators of the states on the left hand side of Eq.(B.1) and Eq.(B.2) respectively. It guarantees that both states are equal up to a non-zero constant when they share the same dimension. We finally show that this constant equals 1.
In the following, we assume that the HFB matrices U of the states considered are always invertible. If it is not the case the theorems still hold but the derivations become denser (see [45]).

B.1 Thouless theorem using the particle vacuum

In this part, we present a demonstration of the Thouless theorem using the particle vacuum $|0\rangle$. We then give a closed formula for the overlap $\langle 0|\Phi\rangle$.

B.1.1 Demonstration of the theorem

We first perform a transformation of the quasiparticles $\{\xi^+_i\}$ of $|\Phi\rangle$:

$$\tilde{\xi}^+_j = \sum_i U^{-1}_{ij}\xi^+_i = \sum_i U^{-1}_{ij}(\sum_l U_{li}c^+_l + V_{li}c_l) = c^+_j + \sum_l (VU^{-1})_{lj}c_l \tag{B.3}$$

Since this transformation is linear and invertible, it is clear that a vacuum of the $\{\xi_i\}$ is also a vacuum of the $\{\tilde{\xi}_j\}$. We now demonstrate that the right hand side of Eq.(B.1) is also a vacuum of the $\{\tilde{\xi}_j\}$:

$$\tilde{\xi}_j e^{\frac{1}{2}\sum_{kk'}(VU^{-1})^*_{kk'}c^+_k c^+_{k'}}|0\rangle = (c_j + \sum_l (VU^{-1})^*_{lj} c^+_l) e^{\frac{1}{2}\sum_{kk'}(VU^{-1})^*_{kk'}c^+_k c^+_{k'}}|0\rangle \qquad \forall j \tag{B.4}$$

As $\forall i,j\ [c^+_i, c^+_j]_+ = 0$, the right hand side of Eq.(B.4) can be written as follows:

$$[c_j e^{\frac{1}{2}\sum_{kk'}(VU^{-1})^*_{kk'}c^+_k c^+_{k'}} + e^{\frac{1}{2}\sum_{kk'}(VU^{-1})^*_{kk'}c^+_k c^+_{k'}} \sum_l (VU^{-1})^*_{lj} c^+_l]|0\rangle \tag{B.5}$$

We factorize by the exponential term:

$$e^{\frac{1}{2}\sum_{kk'}(VU^{-1})^*_{kk'}c^+_k c^+_{k'}}[e^{-\frac{1}{2}\sum_{kk'}(VU^{-1})^*_{kk'}c^+_k c^+_{k'}} c_j e^{\frac{1}{2}\sum_{kk'}(VU^{-1})^*_{kk'}c^+_k c^+_{k'}} + \sum_l (VU^{-1})^*_{lj} c^+_l]|0\rangle \tag{B.6}$$

We then remark that:

$$e^{-\frac{1}{2}\sum_{kk'}(VU^{-1})^*_{kk'}c^+_k c^+_{k'}} c_j e^{\frac{1}{2}\sum_{kk'}(VU^{-1})^*_{kk'}c^+_k c^+_{k'}} = c_j - \frac{1}{2}\sum_k (VU^{-1})^*_{kj} c^+_k + \frac{1}{2}\sum_k (VU^{-1})^*_{jk'} c^+_{k'} \tag{B.7}$$

Using the following property of the U and V matrices:

$$U^+V^* + V^+U^* = 0 \tag{B.8}$$

And including Eq.(B.8) in Eq.(B.7) we find:

$$e^{-\frac{1}{2}\sum_{kk'}(VU^{-1})^*_{kk'}c^+_k c^+_{k'}} c_j e^{\frac{1}{2}\sum_{kk'}(VU^{-1})^*_{kk'}c^+_k c^+_{k'}} = c_j - \sum_k (VU^{-1})^*_{kj} c^+_k \tag{B.9}$$

Injecting Eq.(B.9) in Eq.(B.6), we get:

$$\tilde{\xi}_j e^{\frac{1}{2}\sum_{kk'}(VU^{-1})^*_{kk'}c^+_k c^+_{k'}}|0\rangle = e^{\frac{1}{2}\sum_{kk'}(VU^{-1})^*_{kk'}c^+_k c^+_{k'}}[c_j - \sum_k (VU^{-1})^*_{kj} c^+_k + \sum_l (VU^{-1})^*_{lj} c^+_l]|0\rangle \tag{B.10}$$

Thus:

$$\boxed{\tilde{\xi}_j e^{\frac{1}{2}\sum_{kk'}(VU^{-1})^*_{kk'}c^+_k c^+_{k'}}|0\rangle = 0 \qquad \forall j} \tag{B.11}$$

We can therefore write:

$$\exists \lambda \neq 0 \in \mathbb{C} \qquad ; \qquad |\Phi\rangle = \lambda \langle 0|\Phi\rangle e^{\frac{1}{2}\sum_{kk'}(VU^{-1})^*_{kk'}c^+_k c^+_{k'}}|0\rangle \tag{B.12}$$

Moreover:

$$\langle 0|\Phi\rangle = \lambda \langle 0|\Phi\rangle \langle 0|e^{\frac{1}{2}\sum_{kk'}(VU^{-1})^*_{kk'}c^+_k c^+_{k'}}|0\rangle = \lambda \langle 0|\Phi\rangle \tag{B.13}$$

It shows that $\lambda = 1$. We finally found back the Thouless theorem with the particle vacuum:

$$\boxed{|\Phi\rangle = \langle 0|\Phi\rangle e^{\frac{1}{2}\sum_{kk'}(VU^{-1})^*_{kk'}c^+_k c^+_{k'}}|0\rangle} \tag{B.14}$$

B.1.2 Evaluation of $\langle 0|\Phi\rangle$

The reader may now be curious about the expression of the quantity $\langle 0|\Phi\rangle$. This derivation uses the well-known Bloch-Messiah theorem (Appendix C) which states that the matrices U and V can be separated into three matrices:

$$U = DuC \qquad V = D^* vC \tag{B.15}$$

The matrices D et C are unitary and the matrices u and v have the special form :

$$u = \begin{pmatrix} u_1 & 0 & & & \\ 0 & u_1 & & & \\ & & \ddots & & \\ & & & u_n & 0 \\ & & & 0 & u_n \end{pmatrix} \qquad v = \begin{pmatrix} 0 & v_1 & & & \\ -v_1 & 0 & & & \\ & & \ddots & & \\ & & & 0 & v_n \\ & & & -v_n & 0 \end{pmatrix} \tag{B.16}$$

We can then write the creation and annihilation operators in the canonical basis:

$$\begin{cases} \xi_i = \sum_k C^*_{ki} \eta_k \\ \eta_k = u_k a_k + v_k \bar{a}^+_k \\ a^+_k = \sum_l D_{lk} c^+_l \end{cases} \tag{B.17}$$

With the definitions of Eq.(B.17), the state $|\Phi\rangle$ reads:

$$|\Phi\rangle = \frac{\det(C)}{\prod_{k=1}^n v_k} (\prod_{i=1}^n \xi_i)|0\rangle = \frac{\det(C)}{\prod_{k=1}^n v_k} (\prod_{i=1}^n \sum_k C^*_{ki} \eta_k)|\Phi\rangle = \frac{1}{\prod_{k=1}^n v_k} (\prod_{i=1}^n \eta_k)|0\rangle \tag{B.18}$$

$$|\Phi\rangle = (\prod_{k=1}^n u_k + v_k a^+_k \bar{a}^+_k)|0\rangle \tag{B.19}$$

In that form, we directly have access to the desired quantity:

$$\boxed{\langle 0|\Phi\rangle = \prod_{k=1}^n u_k = (det(U))^{1/2}} \tag{B.20}$$

B.2 Thouless theorem for two HFB states

In this part we present a demonstration of the Thouless theorem using two non-orthogonal HFB states. To do so, we follow [45]. We also present the converse of this theorem which is useful in HFB derivations.

B.2.1 Demonstration of the theorem

Two non-orthogonal HFB states $|\Phi_1\rangle$ and $|\Phi_0\rangle$ being given, we can write the related HFB transformations for their quasiparticles:

$$\begin{cases} \begin{pmatrix} \xi_0 \\ \xi_0^+ \end{pmatrix} = \begin{pmatrix} U^{(0)+} & V^{(0)+} \\ V^{(0)T} & U^{(0)T} \end{pmatrix} \begin{pmatrix} c \\ c^+ \end{pmatrix} = B_0 \begin{pmatrix} c \\ c^+ \end{pmatrix} \\ \begin{pmatrix} \xi_1 \\ \xi_1^+ \end{pmatrix} = \begin{pmatrix} U^{(1)+} & V^{(1)+} \\ V^{(1)T} & U^{(1)T} \end{pmatrix} \begin{pmatrix} c \\ c^+ \end{pmatrix} = B_1 \begin{pmatrix} c \\ c^+ \end{pmatrix} \end{cases} \tag{B.21}$$

Mixing both transformations of Eq.(B.21) we can write the $\{\xi_1^+\}$ and the $\{\xi_1\}$ operators with respect to the $\{\xi_0^+\}$ and $\{\xi_0\}$ ones:

$$\begin{pmatrix} \xi_1 \\ \xi_1^+ \end{pmatrix} = \begin{pmatrix} U^{(1)+}U^{(0)} + V^{(1)+}V^{(0)} & U^{(1)+}V^{(0)*} + V^{(1)+}U^{(0)*} \\ V^{(1)T}U^{(0)} + U^{(1)T}V^{(0)} & U^{(1)T}U^{(0)*} + V^{(1)T}V^{(0)*} \end{pmatrix} \begin{pmatrix} \xi_0 \\ \xi_0^+ \end{pmatrix} = B_1 B_0^+ \begin{pmatrix} \xi_0 \\ \xi_0^+ \end{pmatrix} \tag{B.22}$$

Note that since $B_1 B_0^+ (B_1 B_0^+)^+ = I$, the transformation of Eq.(B.22) is unitary. We then set:

$$\begin{cases} \tilde{U} = U^{(0)+}U^{(1)} + V^{(0)+}V^{(1)} \\ \tilde{V} = V^{(0)T}U^{(1)} + U^{(0)T}V^{(1)} \end{cases} \tag{B.23}$$

We therefore have:

$$\xi_{1,i}^+ = \sum_k \tilde{U}_{ki}\xi_{0,k}^+ + \tilde{V}_{ki}\xi_{0,k} \qquad \forall i \tag{B.24}$$

We transform the operators $\{\xi_1^+\}$ and $\{\xi_1\}$ and in the same way as in Eq.(B.3) :

$$\tilde{\xi}_{1,j}^+ = \sum_i \tilde{U}_{ij}^{-1}\xi_{1,i}^+ = \xi_{0,j}^+ + \sum_k Z_{kj}^*\xi_{0,k} \qquad \forall j \tag{B.25}$$

The transformation of Eq.(B.25) is linear and invertible. Thus, a vacuum of the $\{\xi_1\}$ is also a vacuum of the $\{\tilde{\xi}_1\}$. We can now excplicitly give the Z matrix evoked in Eq.(B.2):

$$Z = (\tilde{V}\tilde{U}^{-1})^* \tag{B.26}$$

As the transformation $B_1 B_0^+$ is unitary, $\tilde{U}$ and $\tilde{V}$ verify the so called Bogoliubov equations (see Chapter 1). In particular, we can write:

$$\tilde{U}^+\tilde{V}^* + \tilde{V}^+\tilde{U}^* = 0 \qquad \Rightarrow \qquad Z^T = -Z \tag{B.27}$$

Then, we want to evaluate to following quantity:

$$\tilde{\xi}_{1,j} e^{\frac{1}{2}\sum_{kk'} Z_{kk'}\xi_{0,k}^+\xi_{0,k'}^+}|\Phi_0\rangle = (\xi_{0,j} + \sum_k Z_{kj}\xi_{0,k}^+) e^{\frac{1}{2}\sum_{kk'} Z_{kk'}\xi_{0,k}^+\xi_{0,k'}^+}|\Phi_0\rangle \tag{B.28}$$

As ξ_0^+ commutes with the exponential, we focus on $\xi_{0,j}$ and write:

$$\xi_{0,j} e^{\frac{1}{2}\sum_{kk'} Z_{kk'}\xi^+_{0,k}\xi^+_{0,k'}}|\Phi_0\rangle = e^{\frac{1}{2}\sum_{kk'} Z_{kk'}\xi^+_{0,k}\xi^+_{0,k'}} e^{-\frac{1}{2}\sum_{kk'} Z_{kk'}\xi^+_{0,k}\xi^+_{0,k'}} \xi_{0,j} e^{\frac{1}{2}\sum_{kk'} Z_{kk'}\xi^+_{0,k}\xi^+_{0,k'}}|\Phi_0\rangle \quad \text{(B.29)}$$

It is then easy to show that:

$$e^{-\frac{1}{2}\sum_{kk'} Z_{kk'}\xi^+_{0,k}\xi^+_{0,k'}} \xi_{0,j} e^{\frac{1}{2}\sum_{kk'} Z_{kk'}\xi^+_{0,k}\xi^+_{0,k'}} = \xi_{0,j} - \sum_k Z_{kj}\xi^+_{0,k} \quad \text{(B.30)}$$

Injecting Eq.(B.30) in Eq.(B.29), we find:

$$\xi_{0,j} e^{\frac{1}{2}\sum_{kk'} Z_{kk'}\xi^+_{0,k}\xi^+_{0,k'}}|\Phi_0\rangle = -e^{\frac{1}{2}\sum_{kk'} Z_{kk'}\xi^+_{0,k}\xi^+_{0,k'}} \sum_k Z_{kj}\xi^+_{0,k}|\Phi_0\rangle \quad \text{(B.31)}$$

Using Eq(B.31) in Eq.(B.28), we finally find:

$$\boxed{\tilde{\xi}_{1,j} e^{\frac{1}{2}\sum_{kk'} Z_{kk'}\xi^+_{0,k}\xi^+_{0,k'}}|\Phi_0\rangle = 0 \qquad \forall j} \quad \text{(B.32)}$$

We can therefore write:

$$\exists \lambda \neq 0 \in \mathbb{C}\ ; \qquad |\Phi_1\rangle = \lambda \langle\Phi_0|\Phi_1\rangle e^{\frac{1}{2}\sum_{kk'} Z_{kk'}\xi^+_{0,k}\xi^+_{0,k'}}|\Phi_0\rangle \quad \text{(B.33)}$$

We then remark that:

$$\langle\Phi_0| e^{\frac{1}{2}\sum_{kk'} Z_{kk'}\xi^+_{0,k}\xi^+_{0,k'}}|\Phi_0\rangle = \langle\Phi_0|\Phi_0\rangle = 1 \qquad \Rightarrow \qquad \lambda = 1 \quad \text{(B.34)}$$

We found back the expression announced in Eq.(B.2):

$$\boxed{|\Phi_1\rangle = \langle\Phi_0|\Phi_1\rangle e^{\frac{1}{2}\sum_{kk'} Z_{kk'}\xi^+_{0,k}\xi^+_{0,k'}}|\Phi_0\rangle} \quad \text{(B.35)}$$

B.2.2 Converse of the theorem

The converse of the theorem Eq.(B.2) is very important as it plays a role in the HFB derivations (see chapter 2). What we call the converse is the statement that given a Z skew-symmetric matrix and a HFB state $|\Phi_0\rangle$, the state $|\Phi_1\rangle$ defined as follows is a HFB vacuum :

$$|\Phi_1\rangle = \langle\Phi_0|\Phi(Z)\rangle e^{\frac{1}{2}\sum_{kk'} Z_{kk'}\xi^+_{0,k}\xi^+_{0,k'}}|\Phi_0\rangle \quad \text{(B.36)}$$

We would like to find $U^{(1)}$ and $V^{(1)}$ matrices that verify the Bogoliubov equations and such that the related matrices $\tilde{U}$ and $\tilde{V}$ defined from Eq.(B.23) are related to Z, as in Eq.(B.26). We will show that it is verified, setting:

$$\boxed{\begin{cases} U^{(1)} = (U^{(0)} + V^{(0)*}Z^*)(I - ZZ^*)^{-1/2} \\ V^{(1)} = (V^{(0)} + U^{(0)*}Z^*)(I - ZZ^*)^{-1/2} \end{cases}} \quad \text{(B.37)}$$

These $U^{(1)}$ and $V^{(1)}$ matrices can be written in a more compact form:

$$B_1^+ = B_0^+ \begin{pmatrix} I & Z \\ Z^* & I \end{pmatrix} \begin{pmatrix} (I - ZZ^*)^{-1/2} & 0 \\ 0 & (I - Z^*Z)^{-1/2} \end{pmatrix} \tag{B.38}$$

Therefore, we just have to show that B_1 is unitary to prove that the Bogoliubov equations hold:

$$B_1 B_1^+ = \begin{pmatrix} (I - ZZ^*)^{-1/2} & 0 \\ 0 & (I - Z^*Z)^{-1/2} \end{pmatrix} \begin{pmatrix} I & -Z \\ -Z^* & I \end{pmatrix} \begin{pmatrix} I & Z \\ Z^* & I \end{pmatrix} \begin{pmatrix} (I - ZZ^*)^{-1/2} & 0 \\ 0 & (I - Z^*Z)^{-1/2} \end{pmatrix}$$

$$B_1 B_1^+ = \begin{pmatrix} (I - ZZ^*)^{-1/2} & 0 \\ 0 & (I - Z^*Z)^{-1/2} \end{pmatrix} \begin{pmatrix} I - ZZ^* & 0 \\ 0 & I - Z^*Z \end{pmatrix} \begin{pmatrix} (I - ZZ^*)^{-1/2} & 0 \\ 0 & (I - Z^*Z)^{-1/2} \end{pmatrix}$$

$$\boxed{B_1 B_1^+ = I} \tag{B.39}$$

We now have to check that $Z = (\tilde{V}\tilde{U}^{-1})^*$. Using Eq.($B$.38), we first remark that:

$$\begin{pmatrix} \tilde{U} & \tilde{V}^* \\ \tilde{V} & \tilde{U}^* \end{pmatrix} = \begin{pmatrix} I & Z \\ Z^* & I \end{pmatrix} \begin{pmatrix} (I - ZZ^*)^{-1/2} & 0 \\ 0 & (I - Z^*Z)^{-1/2} \end{pmatrix} \tag{B.40}$$

Eq.(B.40) leads to:

$$\boxed{\begin{cases} \tilde{U} = (I - ZZ^*)^{-1/2} \\ \tilde{V} = Z^*(I - ZZ^*)^{-1/2} \end{cases} \quad \Rightarrow \quad (\tilde{V}\tilde{U}^{-1})^* = Z} \tag{B.41}$$

Thus, $|\Phi_1\rangle$ is a HFB state.

Appendix C

Bloch-Messiah theorem

The objective of this appendix is to give a clear and complete demonstration of the Bloch-Messiah theorem [80], both in the general case and in the special case of time-reversal invariance. The Bloch-Messiah theorem is a central pillar of many developments made on top of the HFB theory. Indeed, it enables to connect the HFB quasiparticle representation to an equivalent canonical quasiparticle representation of BCS type. This BCS interpretation of the HFB theory often simplifies both theoretical developments and numerical calculations. In the general case, the Bloch-Messiah theorem states that there exists two unitary matrices D and C such that the matrices of the HFB transformation U and V read:

$$\boxed{U = DuC} \qquad \boxed{V = D^{*}vC} \tag{C.1}$$

Here, the matrices u and v have the following form:

$$u = \begin{pmatrix} 0 & \cdots & \cdots & \cdots & \cdots & \cdots & \cdots & \cdots & \cdots & \cdots & 0 \\ \vdots & \ddots & & & & & & & & & \vdots \\ \vdots & & 0 & & & & & 0 & & & \vdots \\ \vdots & & & u_1 & & & & & & & \vdots \\ \vdots & & & & u_1 & & & & & & \vdots \\ \vdots & & & & & \ddots & & & & & \vdots \\ \vdots & & & & & & u_t & & & & \vdots \\ \vdots & & & & & & & u_t & & & \vdots \\ \vdots & & & 0 & & & & & 1 & & \vdots \\ \vdots & & & & & & & & & \ddots & \vdots \\ 0 & \cdots & \cdots & \cdots & \cdots & \cdots & \cdots & \cdots & \cdots & \cdots & 1 \end{pmatrix} \quad \text{with } 1 > u_i > 0 \tag{C.2}$$

$$
v = \begin{pmatrix}
1 & 0 & \dots & \dots & \dots & \dots & \dots & \dots & \dots & \dots & 0 \\
0 & \ddots & & & & & & & & & \vdots \\
\vdots & & 1 & & & & & 0 & & & \vdots \\
\vdots & & & 0 & v_1 & & & & & & \vdots \\
\vdots & & & -v_1 & 0 & & & & & & \vdots \\
\vdots & & & & & \ddots & & & & & \vdots \\
\vdots & & & & & & 0 & v_t & & & \vdots \\
\vdots & & & & & & -v_t & 0 & & & \vdots \\
\vdots & & & 0 & & & & & 0 & & \vdots \\
\vdots & & & & & & & & & \ddots & \vdots \\
0 & \dots & \dots & \dots & \dots & \dots & \dots & \dots & \dots & \dots & 0
\end{pmatrix} \quad \text{with } 1 > v_i > 0 \tag{C.3}
$$

With Eq.(C.1), the full HFB transformation (see Chapter 2) reads:

$$
\boxed{\begin{pmatrix} \xi \\ \xi^+ \end{pmatrix} = \begin{pmatrix} C^+ & 0 \\ 0 & C^T \end{pmatrix} \begin{pmatrix} u & v^T \\ v^T & u \end{pmatrix} \begin{pmatrix} D^+ & 0 \\ 0 & D^T \end{pmatrix} \begin{pmatrix} c \\ c^+ \end{pmatrix}} \tag{C.4}
$$

The unitary transformation C defines a rotation among the HFB quastiparticles and the transformation D rotates the operators of the orthonormal particle basis. We call the rotated quasiparticle operators "η" and the rotated particle operators "a":

$$
\boxed{\begin{pmatrix} \eta \\ \eta^+ \end{pmatrix} = \begin{pmatrix} C & 0 \\ 0 & C* \end{pmatrix} \begin{pmatrix} \xi \\ \xi^+ \end{pmatrix}} \qquad \boxed{\begin{pmatrix} a \\ a^+ \end{pmatrix} = \begin{pmatrix} D^+ & 0 \\ 0 & D^T \end{pmatrix} \begin{pmatrix} c \\ c^+ \end{pmatrix}} \tag{C.5}
$$

With Eq.(C.5), the HFB transformation can be written in a more compact form:

$$
\boxed{\begin{pmatrix} \eta \\ \eta^+ \end{pmatrix} = \begin{pmatrix} u & v^T \\ v^T & u \end{pmatrix} \begin{pmatrix} a \\ a^+ \end{pmatrix}} \tag{C.6}
$$

This final representation is called "canonical" as it defines a BCS transformation.

In the case of time-reversal invariance and axial symmetry, the matrices U and V are real and reduced to the subspace corresponding to $\Omega > 0$. In this subspace, the density matrix ρ and the pairing tensor κ are both real and symmetric matrices and the Bloch-Messiah theorem reads as follows:

$$
\boxed{U = \bar{D}\bar{u}\bar{C}} \qquad \boxed{V = \bar{D}\bar{v}\bar{C}} \tag{C.7}
$$

Here, $\bar{D}$ and $\bar{C}$ are orthogonal matrices and $\bar{u}$ and $\bar{v}$ read as follows:

$$\boxed{\bar{u} = \begin{pmatrix} u_1 & 0 & \dots & 0 \\ 0 & \ddots & 0 & \vdots \\ \vdots & 0 & \ddots & 0 \\ 0 & \dots & 0 & u_n \end{pmatrix} \qquad \text{with } 1 \geq u_i \geq 0} \tag{C.8}$$

$$\boxed{\bar{v} = \begin{pmatrix} v_1 & 0 & \dots & 0 \\ 0 & \ddots & 0 & \vdots \\ \vdots & 0 & \ddots & 0 \\ 0 & \dots & 0 & v_n \end{pmatrix} \qquad \text{with } 1 \geq v_i \geq -1} \tag{C.9}$$

Both $\bar{u}$ and $\bar{v}$ are diagonal. However, the elements of $\bar{v}$ are not necessarily positive. In the associated "canonical" representation, the full HFB transformation reads as follows:

$$\boxed{\begin{pmatrix} \eta \\ \bar{\eta} \\ \eta^+ \\ \bar{\eta}^+ \end{pmatrix} = \begin{pmatrix} \bar{u} & 0 & 0 & \bar{v} \\ 0 & \bar{u} & -\bar{v} & 0 \\ 0 & \bar{v} & \bar{u} & 0 \\ -\bar{v} & 0 & 0 & \bar{u} \end{pmatrix} \begin{pmatrix} a \\ \bar{a} \\ a^+ \\ \bar{a}^+ \end{pmatrix}} \tag{C.10}$$

In Eq.(C.10), we clearly see that the particle operators paired by the "canonical" BCS transformation are also the particle operators paired by the time-reversal transformation:

$$\boxed{\begin{cases} \eta_i = u_i a_i + v_i \bar{a}_i^+ \\ \bar{\eta}_i = u_i \bar{a}_i - v_i a_i^+ \end{cases}} \tag{C.11}$$

In the following, we prove first the linear algebra results required to show the Bloch-Messiah theorem. Then, we demonstrate it in both the general and the axial symmetric time-reversal invariant case.

C.1 Diagonalization of a Hermitian matrix

The objective of this part is to show the following property:

$$\boxed{\forall X \in \mathcal{M}_n(\mathbb{C}),\ X^+ = X \qquad \Rightarrow \qquad \exists Q \in U(n),\ \exists D = \mathrm{diag}(\lambda_1, ..., \lambda_n),\ X = QDQ^+} \tag{C.12}$$

With $\lambda_i \in \mathbb{R}$, $\forall i$. To do so, we first present the Schur decomposition of a matrix and then use it in the case of normal matrices.

C.1.1 Schur decomposition

We want to demonstrate the proposition below which is called the Schur decomposition of a matrix:

$$\boxed{\forall X \in \mathcal{M}_n(\mathbb{C}),\ \exists Q \in U(n),\ \exists T \in \mathcal{M}_n(\mathbb{C}) \text{ upper triangular };\ X = QTQ^+} \tag{C.13}$$

We first rephrase this proposition in terms of linear applications:

" *$\mathcal{P}_n$: Let E be a $\mathbb{C}$ vector space ($dim(E) = n$), with a Hermitian dot product. Let ψ be an endomorphism of E, $\exists$ $(f_1, ..., f_n)$ an orthonormal family of E such that $\forall i$, $\psi(f_i) = \sum_{k=i}^{n} t_{ik} f_k$ with $\forall i, \forall k$, $t_{ik} \in \mathbb{C}$.*"

We show the proposition $\mathcal{P}$ using complete induction for $n \geq 1$:

Initial case:

Let E_1 a $\mathbb{C}$ vector space of dimension 1 with an Hermitian dot product and ψ_1 an endomorphism of E_1. We choose the vector f_1 such that $||f_1|| = 1$. Doing so, (f_1) forms an orthonormal family of E_1. Moreover, $\psi_1(f_1) = kf_1$ with $k \in \mathbb{C}$. It concludes the initial case.

Induction step:

We assume that $\mathcal{P}_n$ holds up to n, we show that it implies that $\mathcal{P}_{n+1}$ also holds. Let E_{n+1} be a $\mathbb{C}$ vector space of dimension $n+1$ with an Hermitian dot product and ψ_{n+1} an endomorphism of E_{n+1}. If $\psi_{n+1} = 0$, the property directly holds. We assume therefore that $\psi_{n+1} \neq 0$ in the following.
As $\psi_{n+1} \neq 0$, $\exists f_{n+1} \in E_{n+1}$ such that $\psi_{n+1}(f_{n+1}) \neq 0$ and $||f_{n+1}|| = 1$. Let $F = \text{Vect}(f_{n+1})^\perp$ the orthogonal complement of $\text{Vect}(f_{n+1})$, we define the following endomorphism:

$$\psi_F = \pi_F \circ \psi_{n+1}|_F \tag{C.14}$$

As ψ_F is an endomorphism of F whose dimension is n, $\mathcal{P}_n$ applies. We therefore have access to an orthonormal family $(f_1, ..., f_n)$ such that $\psi_F(f_i) = \sum_{k=i}^{n} t_{ik} f_k$ with $t_{ik} \in \mathbb{C}$. If we complete this family with f_{n+1}, it remains orthonormal since f_{n+1} is normalized and orthogonal to all the vectors of F by definition. The following result is now completely straightforward:

$$\boxed{\forall i\ ;\ n+1 \geq i \geq 0, \qquad \psi_{n+1}(f_i) = \sum_{k=i}^{n+1} t_{ik} f_k \qquad \text{with} \qquad t_{ik} \in \mathbb{C}} \tag{C.15}$$

This result concludes the induction as well as the demonstration of the Schur decomposition.

C.1.2 Normal matrix

A normal matrix is a matrix that verifies the well-known property:

$$\boxed{X \in \mathcal{M}_n(\mathbb{C})\ ;\ X^+X = XX^+} \tag{C.16}$$

We want to demonstrate here the following result:

$$\boxed{\forall X \in \mathcal{M}_n(\mathbb{C}),\ X \text{ normal} \quad \Rightarrow \quad \exists Q \in U(n),\ \exists D = \text{diag}(\lambda_1, ..., \lambda_n)\ ;\ X = QDQ^+} \tag{C.17}$$

Let $M \in \mathcal{M}_n(\mathbb{C})$ be a normal matrix. We write its Schur decomposition:

$$M = QTQ^+ \tag{C.18}$$

The following equivalence clearly holds:

$$MM^+ = M^+M \leftrightarrow TT^+ = T^+T \tag{C.19}$$

In other words, a matrix is normal if and only if the upper triangular matrix of its Schur decomposition is normal. Moreover, considering the diagonal coefficients of T^+T and TT^+ and using Eq.(C.19), we find the following equation:

$$\sum_{k=i}^{n} |t_{ik}|^2 = \sum_{k=1}^{i} |t_{ki}|^2 \tag{C.20}$$

We now show using a complete induction on i that Eq.(C.20) implies that the off-diagonal coefficients of the matrix T are all equal to zero.

Initial case:

For $i = 1$, we have:

$$\sum_{k=1}^{n} |t_{1k}|^2 = |t_{11}|^2 \quad \Rightarrow \quad \forall k > 1,\ t_{1k} = 0 \tag{C.21}$$

Induction step:

For an i such that $1 < i - 1 < n$, the induction hypotheses holds up to $i - 1$ and gives:

$$\sum_{k=i}^{n} |t_{ik}|^2 = \sum_{k=1}^{i} |t_{ki}|^2 = |t_{ii}|^2 \quad \Rightarrow \quad \forall k > i,\ t_{ki} = 0 \tag{C.22}$$

It concludes the complete induction. We showed that the upper triangular matrix in the Schur decomposition of a normal matrix is always diagonal. Note that the converse is straightforward.

C.1.3 Conclusion

Let M be a Hermitian matrix, it is clear that M is also a normal matrix. Using the previously demonstrated results, we can write:

$$\boxed{\exists Q \in U(n), \exists D = \text{diag}(\lambda_1, ..., \lambda_n)\ ;\ M = QDQ^+} \tag{C.23}$$

Moreover, if we call X an eigenvector of M associated with the eigenvalue λ, we can write:

$$\boxed{(X, MX) = (MX, X) \qquad \Rightarrow \qquad \lambda^* = \lambda} \tag{C.24}$$

We proved that a Hermitian matrix can be diagonalized by a unitary matrix and has only real eigenvalues as announced in Eq.(C.12).

C.2 Diagonalization of a unitary matrix

Let W be a unitary matrix, then W is also a normal matrix:

$$\boxed{W^+W = WW^+ = I} \tag{C.25}$$

Using the results demonstrated for the normal matrices, the following property directly holds:

$$\boxed{\exists Q \in U(n), \exists D = \text{diag}(\lambda_1, ..., \lambda_n) \ ; \ W = QDQ^+} \tag{C.26}$$

Moreover, we can give a characterization of the eingenvalues of W. Indeed, if we call X an eigenvector of W associated with the eigenvalue λ, we have:

$$\boxed{X^+W^+WX = |\lambda|^2 = 1 \qquad \Rightarrow \qquad |\lambda| = 1} \tag{C.27}$$

We showed that the modulus of all the eigenvalues of a unitary matrix is 1.

C.3 Diagonalization of a real symmetric matrix

In the case of real symmetric matrices, the Schur decomposition reads as follows:

$$\boxed{\forall X \in \mathcal{M}_n(\mathbb{R}), \ \exists Q \in O(n), \ \exists T \in \mathcal{M}_n(\mathbb{R}) \text{ upper triangular } ; \ X = QTQ^T} \tag{C.28}$$

The demonstration directly follows the one of the Hermitian case, the only difference being that we consider a real dot product and a real vector space. As the real symmetric matrices are also normal matrices, the following property holds:

$$\boxed{\forall X \in \mathcal{M}_n(\mathbb{R}), \ X^T = X \qquad \Rightarrow \qquad \exists Q \in O(n), \ \exists D = \text{diag}(\lambda_1, ..., \lambda_n), \ X = QDQ^T} \tag{C.29}$$

As they are also Hermitian, all the eigenvalues of the real symmetric matrices are real numbers as proved in Eq.(C.27).

C.4 Diagonalization of an orthogonal matrix

Let O be an orthogonal matrix, then O is also a normal matrix:

$$\boxed{O^T O = O O^T = I} \tag{C.30}$$

Using the results demonstrated for the normal matrices, the following property directly holds:

$$\boxed{\exists Q \in O(n), \exists D = \text{diag}(\lambda_1, ..., \lambda_n) \ ; \ O = QDQ^+} \tag{C.31}$$

Moreover, we can give a characterization of the eingenvalues of O. Indeed, if we call X an eigenvector of O associated with the real eigenvalue λ, we have:

$$\boxed{X^T O^T O X = \lambda^2 = 1 \qquad \Rightarrow \qquad \lambda = \pm 1} \tag{C.32}$$

C.5 Square root of a positive semi-definite Hermitian matrix

Let $M \in \mathcal{M}_n(\mathbb{C})$ be a positive semi-definite Hermitian matrix. As demonstrated in Eq.(C.23), we can find a unitary matrix Q such that:

$$M = Q\text{diag}(m)Q^+ \tag{C.33}$$

As M is a positive semi-definite Hermitian matrix, all its eigenvalues m_i are positive. We use this property to define $M^{1/2}$ as follows:

$$\begin{cases} M^{1/2} = Q\text{diag}(\sqrt{m})Q^+ \\ M = M^{1/2}M^{1/2} \end{cases} \tag{C.34}$$

$M^{1/2}$ is called the semi-definite Hermitian square root of M. We show that $M^{1/2}$ is unique. We assume that $N^{1/2}$ is another semi-definite positive Hermitian square root of M. As $N^{1/2}$ is hermitian, there exists a unitary matrix P such that:

$$N^{1/2} = P\text{diag}(n)P^+ \tag{C.35}$$

The following equation gives the expression of diag(n):

$$N^{1/2}N^{1/2} = M \qquad \Rightarrow \qquad \text{diag}(n^2) = \text{diag}(m) \qquad \Rightarrow \qquad \text{diag}(n) = \text{diag}(\sqrt{m}) \tag{C.36}$$

Note that the last implication holds because $N^{1/2}$ is semi-definite positive. Moreover, as $N^{1/2}$ and $M^{1/2}$ are both square roots of M, we have:

$$N^{1/2}N^{1/2} = M^{1/2}M^{1/2} \qquad \Rightarrow \qquad P^+Q\text{diag}(\sqrt{m})Q^+P = \text{diag}(\sqrt{m}) \tag{C.37}$$

Inserting Eq.(C.37) into Eq.(C.35), we finally write:

$$\boxed{N^{1/2} = P\text{diag}(n)P^+ = PP^+Q\text{diag}(\sqrt{m})Q^+PP^+ = M^{1/2}} \tag{C.38}$$

C.6 Singular value decomposition of a complex square matrix

The following property is called the singular value decomposition of a complex square matrix:

$$\boxed{\forall M \in \mathcal{M}_n(\mathbb{C}),\ \ \exists B, A \in U(n)\ \ ;\ \ M = B\mathrm{diag}(s)A^+} \tag{C.39}$$

The s_i are the singular value of M. They are the square roots of the positive eigenvalues of the positive semi-definite Hermitian matrix MM^+. To show this result, we start diagonalizing MM^+ with a unitary matrix B:

$$B^+MM^+B = \begin{pmatrix} D & 0 \\ 0 & 0 \end{pmatrix} \tag{C.40}$$

Here $D \in GL_r(\mathbb{C})$ with $r = \mathrm{rank}(MM^+)$. We separate the matrix B in two parts, B_1 cointaining the first r columns of B and B_2 containing the other ones:

$$B = \begin{pmatrix} B_1 & | & B_2 \end{pmatrix} \tag{C.41}$$

Then, Eq.(C.40) reads:

$$\begin{pmatrix} B_1^+MM^+B_1 & B_1^+MM^+B_2 \\ B_1^+MM^+B_2 & B_2^+MM^+B_2 \end{pmatrix} = \begin{pmatrix} D & 0 \\ 0 & 0 \end{pmatrix} \tag{C.42}$$

From Eq.(C.42) we exctract:

$$B_1^+MM^+B_1 = D \tag{C.43}$$

$$B_2^+MM^+B_2 = (M^+B_2)^+(M^+B_2) = 0 \qquad \Rightarrow \qquad M^+B_2 = 0 \tag{C.44}$$

Moreover, from the unitarity of B, we get for B_1 and B_2:

$$\begin{cases} B_1^+B_1 = I_r \\ B_2^+B_2 = I_{n-r} \end{cases} \tag{C.45}$$

We now define the matrix A_1:

$$A_1 = M^+B_1D^{-1/2} \tag{C.46}$$

Using Eq.(C.43), we directly have:

$$A_1^+A_1 = I_r \tag{C.47}$$

A_1 is not a unitary matrix in general since it is a rectangular $n \times r$ matrix. However, We can always complete it with another $n \times (n-r)$ matrix A_2 such that:

$$\begin{cases} AA^+ = I \\ A = \begin{pmatrix} A_1 & | & A_2 \end{pmatrix} \end{cases} \tag{C.48}$$

Using Eq.(C.48) and Eq.(C.44), we finally write:

$$B^+MA = \begin{pmatrix} B_1^+MA_1 & B_1^+MA_2 \\ B_2^+MA_1 & B_2^+MA_2 \end{pmatrix} = \begin{pmatrix} B_1^+MA_1 & D^{1/2}A_1^+A_2 \\ (M^+B_2)^+A_2 & (B_2M^+)A_2 \end{pmatrix} = \begin{pmatrix} D^{1/2} & 0 \\ 0 & 0 \end{pmatrix} \tag{C.49}$$

Eq.(C.49) is easily transformed into:

$$\boxed{M = B\text{diag}(s)A^+ \qquad \text{with} \qquad \text{diag}(s) = \begin{pmatrix} D^{1/2} & 0 \\ 0 & 0 \end{pmatrix}} \tag{C.50}$$

C.7 Singular value decomposition of a real square matrix

The following property is called the singular value decomposition of a real square matrix:

$$\boxed{\forall M \in \mathcal{M}_n(\mathbb{R}),\ \ \exists B, A \in O(n)\ \ ;\ \ M = B\text{diag}(s)A^T} \tag{C.51}$$

Here the s_i are the singular value of M. They are the square roots of the positive eigenvalues of the positive semi-definite symmetric matrix MM^T. To prove Eq.(C.51), we first diagonalize MM^T with an orthogonal matrix B:

$$B^TMM^TB = \begin{pmatrix} D & 0 \\ 0 & 0 \end{pmatrix} \tag{C.52}$$

Here, $D \in GL_r(\mathbb{R})$ with $r = \text{rank}(MM^T)$. We separate the matrix B in two parts, B_1 cointaining the first r columns of B and B_2 containing the other ones:

$$B = \begin{pmatrix} B_1 & | & B_2 \end{pmatrix} \tag{C.53}$$

Then, Eq.(C.52) reads:

$$\begin{pmatrix} B_1^TMM^TB_1 & B_1^TMM^TB_2 \\ B_1^TMM^TB_2 & B_2^TMM^TB_2 \end{pmatrix} = \begin{pmatrix} D & 0 \\ 0 & 0 \end{pmatrix} \tag{C.54}$$

From Eq.(C.54), we exctract:

$$B_1^TMM^TB_1 = D \tag{C.55}$$

$$B_2^TMM^TB_2 = (M^TB_2)^T(M^TB_2) = 0 \qquad \Rightarrow \qquad M^TB_2 = 0 \tag{C.56}$$

Moreover, from the orthogonality of B, we get for B_1 and B_2:

$$\begin{cases} B_1^T B_1 = I_r \\ B_2^T B_2 = I_{n-r} \end{cases} \tag{C.57}$$

We now define the matrix A_1:

$$A_1 = M^T B_1 D^{-1/2} \tag{C.58}$$

Using Eq.(C.55), we directly have:

$$A_1^T A_1 = I_r \tag{C.59}$$

A_1 is not an orthogonal matrix in general since it is a rectangular $n \times r$ matrix. However, can always complete it with a $n \times (n-r)$ matrix A_2 such that:

$$\begin{cases} AA^T = I \\ A = \begin{pmatrix} A_1 & | & A_2 \end{pmatrix} \end{cases} \tag{C.60}$$

Using Eq.(C.60) and Eq.(C.56), we finally write:

$$B^T M A = \begin{pmatrix} B_1^T M A_1 & B_1^T M A_2 \\ B_2^T M A_1 & B_2^T M A_2 \end{pmatrix} = \begin{pmatrix} B_1^T M A_1 & D^{1/2} A_1^T A_2 \\ (M^T B_2)^T A_2 & (B_2 M^T) A_2 \end{pmatrix} = \begin{pmatrix} D^{1/2} & 0 \\ 0 & 0 \end{pmatrix} \tag{C.61}$$

Then, Eq.(C.61) is easily transformed into:

$$\boxed{M = B \mathrm{diag}(s) A^T \qquad \text{with} \qquad \mathrm{diag}(s) = \begin{pmatrix} D^{1/2} & 0 \\ 0 & 0 \end{pmatrix}} \tag{C.62}$$

C.8 Canonical form of a skew-symmetric matrix

The objective of this part is to show the following property:

$$\boxed{\forall M \in \mathcal{M}_n(\mathbb{C}),\ M^T = -M \qquad \Rightarrow \qquad \exists Q \in U(n),\ \exists \Sigma,\ Q^T M Q = \Sigma} \tag{C.63}$$

Here, the matrix Σ takes the special form:

$$\boxed{\Sigma = \begin{pmatrix} \Lambda_1 & 0 & \dots & \dots & \dots & 0 \\ 0 & \ddots & & & & \vdots \\ \vdots & & \Lambda_p & & & \vdots \\ \vdots & & & 0 & & \vdots \\ \vdots & & & & \ddots & \vdots \\ 0 & \dots & \dots & \dots & \dots & 0 \end{pmatrix} \qquad \text{with} \qquad \Lambda_i = \begin{pmatrix} 0 & \lambda_i \\ -\lambda_i & 0 \end{pmatrix},\ \forall i \in [\![1, r]\!]} \tag{C.64}$$

Note that each $\lambda_i \in \mathbb{R}$ and $\lambda_i > 0$. Moreover, these λs are the positive square roots of the non-zero eigenvalues of the matrix M^+M. It is a well-known linear algebra theorem. We follow thereafter the proof of [81] as it is both short and elegant.

Let $M \in \mathcal{M}_n(\mathcal{C})$ be a skew-symmetric matrix. The matrix M^+M is Hermitian with only real positive eigenvalues. Indeed, with the natural Hermitian dot product of $\mathcal{M}_{n,1}(\mathbb{C})$:

$$(V, W) = \sum_{i=1}^{n} V_i^* W_i \tag{C.65}$$

Considering X_i an eigenvector of M^+M associated with the non-zero eigenvalue λ_i, we find:

$$(X_i, M^+MX_i) = ||MX_i|| = \lambda ||X_i|| \qquad \Rightarrow \qquad \lambda_i \geq 0 \tag{C.66}$$

Moreover, if we set:

$$X_i' = \frac{1}{\sqrt{\lambda_i}} M^+ X_i^* \tag{C.67}$$

We observe that X_i' is also an eigenvector of M associated with the eigenvalue λ_i:

$$M^+MX_i' = \frac{1}{\sqrt{\lambda_i}} M^+MM^+X_i^* = \lambda_i \frac{1}{\sqrt{\lambda_i}} M^+X_i^* = \lambda_i X_i' \tag{C.68}$$

As each eigenvector X_i associated with a non-zero eigenvalue is paired with another eigenvector X_i', the matrix M^+M has an even rank $r = 2p$. Now, we focus on the action of M on each X_i and X_i':

$$\boxed{\begin{cases} MX_i = -(M^+X_i^*)^* = -\sqrt{\lambda_i} X_i'^* \\ MX_i' = \frac{1}{\sqrt{\lambda_i}} MM^+X_i^* = \sqrt{\lambda_i} X_i^* \end{cases}} \tag{C.69}$$

Moreover, it is easy to see that the eigenvectors Y_i of M^+M associated with a zero eigenvalue are also eigenvectors of M associated with a zero eigenvalue:

$$\boxed{(Y_i, M^+MY_i) = ||MY_i|| = 0 \qquad \Rightarrow \qquad MY_i = 0} \tag{C.70}$$

We can now consider the following matrix Q:

$$Q = \left(X_1 \;\middle|\; X_1' \;\middle|\; \dots \;\middle|\; X_p \;\middle|\; X_p' \;\middle|\; Y_1 \;\middle|\; \dots \;\middle|\; Y_{n-2p}\right) \tag{C.71}$$

The product Q^TMQ reads:

$$\begin{pmatrix} X_1^TMX_1 & X_1^TMX_1' & \dots & X_1^TMX_p & X_1^TMX_p' & X_1^TMY_1 & \dots & X_1^TMY_{n-2p} \\ X_1'^TMX_1 & X_1'^TMX_1' & \dots & X_1'^TMX_p & X_1'^TMX_p' & X_1'^TMY_1 & \dots & X_1'^TMY_{n-2p} \\ \vdots & \vdots & \ddots & \vdots & \vdots & \vdots & & \vdots \\ X_p^TMX_1 & X_p^TMX_1' & \dots & X_p^TMX_p & X_p^TMX_p' & X_p^TMY_1 & \dots & X_p^TMY_{n-2p} \\ X_p'^TMX_1 & X_p'^TMX_1' & \dots & X_p'^TMX_p & X_p'^TMX_p' & X_p'^TMY_1 & \dots & X_p'^TMY_{n-2p} \\ Y_1^TMX_1 & Y_1^TMX_1' & \dots & Y_1^TMX_p & Y_1^TMX_p' & Y_1^TMY_1^+ & \dots & Y_1^TMY_{n-2p} \\ \vdots & \vdots & & \vdots & \vdots & \vdots & \ddots & \vdots \\ Y_{n-2p}^TMX_1 & Y_{n-2p}^TMX_1' & \dots & Y_{n-2p}^TMX_p & Y_{n-2p}^TMX_p' & Y_{n-2p}^TMY_1 & \dots & Y_{n-2p}^TMY_{n-2p} \end{pmatrix} \tag{C.72}$$

Using Eq.($C.69$), Eq.($C.70$) and the orthogonality of the eigenvectors of M^+M, we finally find:

$$\boxed{Q^T M Q = \begin{pmatrix} \Lambda_1 & 0 & \dots & \dots & \dots & 0 \\ 0 & \ddots & & & & \vdots \\ \vdots & & \Lambda_p & & & \vdots \\ \vdots & & & 0 & & \vdots \\ \vdots & & & & \ddots & \vdots \\ 0 & \dots & \dots & \dots & \dots & 0 \end{pmatrix} \quad \text{with} \quad \Lambda_i = \begin{pmatrix} 0 & \lambda_i \\ -\lambda_i & 0 \end{pmatrix} \ , \ \forall i \in [\![1, r]\!]} \tag{C.73}$$

C.9 Demonstration of the Bloch-Messiah theorem

C.9.1 General case

This part aims to demonstrate the Bloch-Messiah theorem in the general case of Eq.($C.1$). We first recall some useful results from the HFB theory developed in Chapter 2. The unitary Bogoliubov transformation reads as follows:

$$B = \begin{pmatrix} U^+ & V^+ \\ V^T & U^T \end{pmatrix} \tag{C.74}$$

The unitarity of B implies the following conditions:

$$\begin{cases} U^+U + V^+V = I \\ UU^+ + V^*V^T = I \end{cases} \qquad \begin{cases} V^TU + U^TV = 0 \\ UV^+ + V^*U^T = 0 \end{cases} \tag{C.75}$$

We define the matrices ρ and κ as follows:

$$\begin{cases} \rho = V^*V^T = I - UU^+ \\ \kappa = V^*U^T = -\kappa^T \end{cases} \tag{C.76}$$

Using Eq.($C.75$) in Eq.($C.76$), we find:

$$\begin{cases} \rho = I - UU^+ \\ \kappa = -\kappa^T \end{cases} \tag{C.77}$$

Moreover, the property $R^2 = R$ of the generalized density matrix defined in the HFB theory gives two important equations connecting ρ and κ:

$$\rho\kappa = \kappa\rho^* \tag{C.78}$$

$$\rho^2 - \rho = \kappa\kappa^* \tag{C.79}$$

The three equations Eq.($C.77$), Eq.($C.78$) and Eq.($C.79$) are required to demonstrate the Bloch-Messiah theorem. We start by considering Eq.($C.77$).

Consequences of Eq.($C.77$):

We first observe from Eq.($C.77$) that ρ is a positive semi-definite Hermitian matrix. Indeed, if X is an eigenvector of ρ associated with the eigenvalue λ, we have:

$$X^+V^*V^TX = \lambda = ||V^TX|| \geq 0 \tag{C.80}$$

Because of that, we call v_i^2 the eigenvalues of ρ thereafter. We diagonalize ρ with the unitary matrix Q in Eq.($C.77$):

$$Q^+\rho Q = Q^+V^*V^TQ = I - QUU^+Q = \text{diag}(v^2) \tag{C.81}$$

It is clear from Eq.($C.81$) that the matrix Q also diagonalizes the positive semi-definite Hermitian matrix UU^+. Denoting u_i^2 the eigenvalues of UU^+ we find:

$$\boxed{\forall i, \qquad u_i^2 + v_i^2 = 1} \tag{C.82}$$

Consequences of Eq.($C.78$):

We now diagonalize ρ in Eq.($C.78$):

$$\text{diag}(v^2)Q^+\kappa Q^* = Q^+\kappa Q^*\text{diag}(v^2) \tag{C.83}$$

Here, $\text{diag}(v^2)$ is the diagonal matrix whose elements are the v_i^2. We set:

$$\tilde{\kappa} = Q^+\kappa Q^* \tag{C.84}$$

Using Eq.($C.83$), we deduce conditions constraining the elements of $\tilde{\kappa}$:

$$\forall i,j, \qquad (v_i^2 - v_j^2)\tilde{\kappa}_{ij} = 0 \tag{C.85}$$

Therefore, the following property holds:

$$\boxed{\forall i,j, \qquad v_i^2 \neq v_j^2 \qquad \Rightarrow \qquad \tilde{\kappa}_{ij} = 0} \tag{C.86}$$

We consider the index $1 \leq k \leq p$ that spans the different eigenvalues v_k^2 with multiplicity α_k. With these notations, $\text{diag}(v^2)$ and $\tilde{\kappa}$ read (up to a permutation we implicitly include in Q):

$$\text{diag}(v^2) = \begin{pmatrix} v_1^2 I_{\alpha_1} & 0 & \dots & \dots & 0 \\ 0 & \ddots & & & \vdots \\ \vdots & & v_k^2 I_{\alpha_k} & & \vdots \\ \vdots & & & \ddots & 0 \\ 0 & \dots & \dots & 0 & v_p^2 I_{\alpha_p} \end{pmatrix} \quad \text{and} \quad \tilde{\kappa} = \begin{pmatrix} \tilde{\kappa}_1 & 0 & \dots & \dots & 0 \\ 0 & \ddots & & & \vdots \\ \vdots & & \tilde{\kappa}_k & & \vdots \\ \vdots & & & \ddots & 0 \\ 0 & \dots & \dots & 0 & \tilde{\kappa}_p \end{pmatrix} \tag{C.87}$$

As the matrices $\tilde{\kappa}_k$ are all skew-symmetric, we transform them into their canonical forms K_k thanks to the unitary matrices S_k. The total matrix made with the K_k is called K. The unitaty matrix whose blocks are the S_k is called S:

$$K = S^{+}\tilde{\kappa}S^{*} = \begin{pmatrix} K_1 & 0 & \dots & \dots & 0 \\ 0 & \ddots & & & \vdots \\ \vdots & & K_k & & \vdots \\ \vdots & & & \ddots & 0 \\ 0 & \dots & \dots & 0 & K_p \end{pmatrix} \tag{C.88}$$

Here, each matrix K_k has the canonical form defined in Eq.(C.64):

$$\boxed{K_k = \begin{pmatrix} \Lambda_1^{(k)} & 0 & \dots & \dots & \dots & 0 \\ 0 & \ddots & & & & \vdots \\ \vdots & & \Lambda_{z(k)}^{(k)} & & & \vdots \\ \vdots & & & 0 & & \vdots \\ \vdots & & & & \ddots & \vdots \\ 0 & \dots & \dots & \dots & \dots & 0 \end{pmatrix} \quad \text{with} \quad \Lambda_i^{(k)} = \begin{pmatrix} 0 & \lambda_i^{(k)} \\ -\lambda_i^{(k)} & 0 \end{pmatrix}} \tag{C.89}$$

Besides, as the S_k are all unitary matrices and operate only on the degenerate subspaces of $\mathrm{diag}(v^2)$, $\mathrm{diag}(v^2)$ is thus invariant under the following transformations:

$$\boxed{S^{+}\mathrm{diag}(v^2)S = S^{T}\mathrm{diag}(v^2)S^{*} = \mathrm{diag}(v^2)} \tag{C.90}$$

Therefore, we find a representation in which both ρ and κ are in their canonical forms (to a permutation). We associate this representation with the unitary matrix $D = QS$.

Consequences of Eq.(C.79):

We now consider Eq.(C.79) in the D representation newly defined:

$$\mathrm{diag}(v^4) - \mathrm{diag}(v^2) = KK \tag{C.91}$$

In an arbitrary degenerate subspace k of $\mathrm{diag}(v^2)$ of multiplicity α_k, Eq.(C.91) reads:

$$(v_k^4 - v_k^2)I_{\alpha_k} = \begin{pmatrix} \Lambda_1^{(k)2} & 0 & \dots & \dots & \dots & 0 \\ 0 & \ddots & & & & \vdots \\ \vdots & & \Lambda_{z(k)}^{(k)2} & & & \vdots \\ \vdots & & & 0 & & \vdots \\ \vdots & & & & \ddots & \vdots \\ 0 & \dots & \dots & \dots & \dots & 0 \end{pmatrix} \quad \text{with} \quad \Lambda_i^{(k)2} = -\lambda_i^{(k)2} I_2 \tag{C.92}$$

There exist two possibilites:

- If $v_k^2 = 0$ or $v_k^2 = 1$, it is clear that $K_k = 0$.

- If $v_k^2 \neq 0$ and $v_k^2 \neq 1$, using Eq.(C.92) and Eq.(C.82), K_k reads:

$$K_k = \begin{pmatrix} \Lambda^{(k)} & 0 & \dots & \dots & 0 \\ 0 & \ddots & & & \vdots \\ \vdots & & \Lambda^{(k)} & & \vdots \\ \vdots & & & \ddots & 0 \\ 0 & \dots & \dots & 0 & \Lambda^{(k)} \end{pmatrix} \qquad \text{with} \qquad \Lambda^{(k)} = \begin{pmatrix} 0 & |v_k u_k| \\ -|v_k u_k| & 0 \end{pmatrix} \tag{C.93}$$

In particular, Eq.(C.93) implies that all the eigenvalues v_k^2 such that $v_k^2 \neq 0$ and $v_k^2 \neq 1$ have an even multiplicity α_k. We can now write explicitly the form of ρ and κ in the representation defined by D (up to a permutation we implicitly include in D):

$$D^+ \rho D = \begin{pmatrix} 1 & 0 & \dots & \dots & \dots & \dots & \dots & \dots & \dots & \dots & 0 \\ 0 & \ddots & & & & & & & & & \vdots \\ \vdots & & 1 & & & & & 0 & & & \vdots \\ \vdots & & & v_1^2 & & & & & & & \vdots \\ \vdots & & & & v_1^2 & & & & & & \vdots \\ \vdots & & & & & \ddots & & & & & \vdots \\ \vdots & & & & & & v_t^2 & & & & \vdots \\ \vdots & & & & & & & v_t^2 & & & \vdots \\ \vdots & & & 0 & & & & & 0 & & \vdots \\ \vdots & & & & & & & & & \ddots & \vdots \\ 0 & \dots & \dots & \dots & \dots & \dots & \dots & \dots & \dots & \dots & 0 \end{pmatrix} \tag{C.94}$$

$$D^+ \kappa D^* = \begin{pmatrix} 0 & \dots & \dots & \dots & \dots & \dots & \dots & \dots & \dots & \dots & 0 \\ \vdots & \ddots & & & & & & & & & \vdots \\ \vdots & & 0 & & & & & 0 & & & \vdots \\ \vdots & & & 0 & |v_1 u_1| & & & & & & \vdots \\ \vdots & & & -|v_1 u_1| & 0 & & & & & & \vdots \\ \vdots & & & & & \ddots & & & & & \vdots \\ \vdots & & & & & & 0 & |v_t u_t| & & & \vdots \\ \vdots & & & & & & -|v_t u_t| & 0 & & & \vdots \\ \vdots & & & 0 & & & & & 0 & & \vdots \\ \vdots & & & & & & & & & \ddots & \vdots \\ 0 & \dots & \dots & \dots & \dots & \dots & \dots & \dots & \dots & \dots & 0 \end{pmatrix} \tag{C.95}$$

Here, $v_i^2 \neq 0$ and $v_i^2 \neq 1$, $\forall i \in [\![1, t]\!]$. We have everything in hands to transform U and V into their special form given by the Bloch-Messiah theorem.

Special form of U:

As seen in Eq.(C.81), the transformation that diagonalizes ρ diagonalizes also UU^+:

$$D^+UU^+D = \text{diag}(u^2) \tag{C.96}$$

As $(UU^+)^{1/2}$ is a positive semi-definite Hermitian matrix, its positive semi-definite Hermitian square root is unique:

$$\boxed{(UU^+)^{1/2} = D\text{diag}(u)D^+ \qquad \text{with} \qquad u_i \geq 0 \ \ \forall i} \tag{C.97}$$

The singular value decomposition of U reads:

$$U = B\text{diag}(u)A^+ \tag{C.98}$$

Here B and A are unitary matrices. Using Eq.(C.98), we write:

$$UU^+ = B\text{diag}(u)A^+A\text{diag}(u)B^+ = (B\text{diag}(u)B^+)(B\text{diag}(u)B^+) \tag{C.99}$$

Eq.(C.99) shows that $B\text{diag}(u)B^+$ is also the positive semi-definite square root of UU^+. Using Eq.(C.97) and the uniqueness of the positive semi-definite Hermitian square root, we have:

$$\boxed{B\text{diag}(u)B^+ = D\text{diag}(u)D^+} \tag{C.100}$$

At this stage, it could be tempting to state that $B = D$, but it is not necessarily the case. Instead, we write from Eq.(C.98):

$$U = B\text{diag}(u)A^+ = B\text{diag}(u)B^+BA^+ = D\text{diag}(u)D^+BA^+ \tag{C.101}$$

Using the notation $\text{diag}(u) = u$, we finally write U in its special form:

$$\boxed{\begin{cases} U = DuC \\ C = D^+BA^+ \end{cases}} \tag{C.102}$$

Here, C is obviously a unitary matrix. Thanks to Eq.(C.82) and Eq.(C.94), u explicitly reads:

$$u = \begin{pmatrix} 0 & \dots & \dots & \dots & \dots & \dots & \dots & \dots & \dots & \dots & 0 \\ \vdots & \ddots & & & & & & & & & \vdots \\ \vdots & & 0 & & & & & 0 & & & \vdots \\ \vdots & & & u_1 & & & & & & & \vdots \\ \vdots & & & & u_1 & & & & & & \vdots \\ \vdots & & & & & \ddots & & & & & \vdots \\ \vdots & & & & & & u_t & & & & \vdots \\ \vdots & & & & & & & u_t & & & \vdots \\ \vdots & & & 0 & & & & & 1 & & \vdots \\ \vdots & & & & & & & & & \ddots & \vdots \\ 0 & \dots & \dots & \dots & \dots & \dots & \dots & \dots & \dots & \dots & 1 \end{pmatrix} \tag{C.103}$$

Here, $1 > u_i > 0,\ \forall i \in [\![1, t]\!]$. We can now focus on the special form of V.

Special form of V:

In the representation that sets κ in its canonical form, we write thanks to Eq.(C.76):

$$K = D^{+}V^{*}U^{T}D^{*} = D^{+}V^{*}C^{T}u \tag{C.104}$$

We take the complex conjugate of Eq.(C.104), and define the matrix $\tilde{v} = D^{T}VC^{+}$:

$$K = \tilde{v}u \tag{C.105}$$

As u is not invertible in general, the equation Eq.(C.105) only describes the subspace where $u_i > 0$. We note u_{22} the matrix corresponding to this subspace and separate the matrices v and K in blocks accordingly:

$$\begin{pmatrix} 0 & 0 \\ 0 & K_{22} \end{pmatrix} = \begin{pmatrix} \tilde{v}_{11} & \tilde{v}_{12} \\ \tilde{v}_{21} & \tilde{v}_{22} \end{pmatrix} \begin{pmatrix} 0 & 0 \\ 0 & u_{22} \end{pmatrix} \tag{C.106}$$

Here the form of K is due to Eq.(C.95) implying that $K_{ij} = 0$ in the subspaces where $u_i = 0$. Using the inverse matrix of u_{22}, Eq.(C.106) leads to:

$$\boxed{\begin{cases} \tilde{v}_{22} = K_{22}u_{22}^{-1} \\ \tilde{v}_{12} = 0 \end{cases}} \tag{C.107}$$

To determine the other blocks of $\tilde{v}$, we use Eq.(C.76):

$$D^{+}\rho D = D^{+}V^{*}V^{T}D = D^{+}V^{*}C^{T}C^{*}V^{T}D = u^{*}u^{T} = uu^{+} \tag{C.108}$$

Then, the blocks structure of Eq.(C.108) reads:

$$\begin{pmatrix} I_{11} & 0 \\ 0 & \mathrm{diag}(v^2)_{22} \end{pmatrix} = \begin{pmatrix} \tilde{v}_{11} & 0 \\ \tilde{v}_{21} & K_{22}u_{22}^{-1} \end{pmatrix} \begin{pmatrix} \tilde{v}_{11}^{+} & \tilde{v}_{21}^{+} \\ 0 & (K_{22}u_{22}^{-1})^{+} \end{pmatrix} \tag{C.109}$$

It implies:

$$\begin{cases} \tilde{v}_{11}\tilde{v}_{11}^{+} = I_{11} \\ \tilde{v}_{21}\tilde{v}_{11}^{+} = 0 \end{cases} \qquad \Rightarrow \qquad \tilde{v}_{21} = 0 \tag{C.110}$$

The matrix $\tilde{v}$ has therefore the following form:

$$\tilde{v} = \begin{pmatrix} \tilde{v}_{11} & 0 \\ 0 & K_{22}u_{22}^{-1} \end{pmatrix} \tag{C.111}$$

Using the result in Eq.(C.26), $\tilde{v}_{11}$ can be diagonalized by a untiary matrix F_{11}. Moreover, the eigenvalues of $\tilde{v}_{11}$ all have a modulus equal to 1 as seen in Eq.(C.27). Thus:

$$F_{11}\tilde{v}_{11}F_{11}^{+} = \mathrm{diag}(e^{i\varphi}) \tag{C.112}$$

We can include the phases matrix $\mathrm{diag}(e^{i\varphi})$ in the matrix F_{11}:

$$\boxed{\begin{cases} F_{11}\tilde{v}_{11}\tilde{F}_{11}^{+} = I_{11} \\ \tilde{F}_{11} = e^{i\varphi}F_{11} \end{cases}} \tag{C.113}$$

The resulting matrix $\tilde{F}_{11}$ is clearly still unitary. Then, we complete F_{11} and $\tilde{F}_{11}$ to build the full matrices F and $\tilde{F}$:

$$\boxed{\begin{cases} F = \begin{pmatrix} F_{11} & 0 \\ 0 & I_{22} \end{pmatrix} \\ \tilde{F} = \begin{pmatrix} \tilde{F}_{11} & 0 \\ 0 & I_{22} \end{pmatrix} \end{cases}} \tag{C.114}$$

Using Eq.(C.114) in Eq.(C.111) enables to define the final matrix v:

$$\boxed{v = F\tilde{v}\tilde{F}^{+} = \begin{pmatrix} I_{11} & 0 \\ 0 & K_{22}u_{22}^{-1} \end{pmatrix}} \tag{C.115}$$

This matrix v explicitly reads:

$$
\boxed{
v = \begin{pmatrix}
1 & 0 & \dots & \dots & \dots & \dots & \dots & \dots & \dots & \dots & 0 \\
0 & \ddots & & & & & & & & & \vdots \\
\vdots & & 1 & & & & & 0 & & & \vdots \\
\vdots & & & 0 & v_1 & & & & & & \vdots \\
\vdots & & & -v_1 & 0 & & & & & & \vdots \\
\vdots & & & & & \ddots & & & & & \vdots \\
\vdots & & & & & & 0 & v_t & & & \vdots \\
\vdots & & & & & & -v_t & 0 & & & \vdots \\
\vdots & & & 0 & & & & & 0 & & \vdots \\
\vdots & & & & & & & & & \ddots & \vdots \\
0 & \dots & \dots & \dots & \dots & \dots & \dots & \dots & \dots & \dots & 0
\end{pmatrix}
}
\tag{C.116}
$$

Here, $1 > v_i > 0$, $\forall i \in [\![1, t]\!]$. There is one thing left to be done. We have to verify that the new unitary transformations defined by $D' = DF^*$ and $C' = \tilde{F}C$ don't change the special forms of ρ, κ and U. It is in fact very easy to check. We start by considering Eq.(C.94):

$$
\boxed{
D'^{+}\rho D' = \begin{pmatrix} F_{11}^T & 0 \\ 0 & I \end{pmatrix} \begin{pmatrix} I_{11} & 0 \\ 0 & \mathrm{diag}(v^2)_{22} \end{pmatrix} \begin{pmatrix} F_{11}^* & 0 \\ 0 & I \end{pmatrix} = \begin{pmatrix} I_{11} & 0 \\ 0 & \mathrm{diag}(v^2)_{22} \end{pmatrix}
}
\tag{C.117}
$$

From Eq.(C.95), we then have:

$$
\boxed{
D'^{+}\kappa D'^{*} = \begin{pmatrix} F_{11}^T & 0 \\ 0 & I \end{pmatrix} \begin{pmatrix} 0 & 0 \\ 0 & K_{22} \end{pmatrix} \begin{pmatrix} F_{11} & 0 \\ 0 & I \end{pmatrix} = \begin{pmatrix} 0 & 0 \\ 0 & K_{22} \end{pmatrix}
}
\tag{C.118}
$$

Finally, we use Eq.(C.103) to show that the special form of U doesn't change:

$$
\boxed{
D'^{+}UC'^{+} = \begin{pmatrix} F_{11}^T & 0 \\ 0 & I \end{pmatrix} \begin{pmatrix} 0 & 0 \\ 0 & u_{22} \end{pmatrix} \begin{pmatrix} \tilde{F}_{11}^{+} & 0 \\ 0 & I \end{pmatrix} = \begin{pmatrix} 0 & 0 \\ 0 & u_{22} \end{pmatrix}
}
\tag{C.119}
$$

Conclusion:

We demonstrated the Bloch-Messiah theorem in the general case. We built two unitary matrices D' and C' such that the matrices U anv V write:

$$
\boxed{U = D'uC'} \qquad \boxed{V = D'^{*}vC'}
\tag{C.120}
$$

Moreover, the matrices u and v have the special forms explicitly described in Eq.(C.103) and Eq.(C.116).

C.9.2 Time-reversal invariance and axial symmetry

The goal of this part is to demonstrate the Bloch-Messiah theorem in the special case of time-reversal invariance and axial symmetry Eq.(C.7). As for the general case, we will first recall some results from the time-reversal invariant HFB theory. The following relations between U and V hold:

$$\begin{cases} U^TU + V^TV = I \\ UU^T + VV^T = I \end{cases} \qquad \begin{cases} V^TU - U^TV = 0 \\ UV^T - VU^T = 0 \end{cases} \tag{C.121}$$

The $\Omega > 0$ part of the density and the pairing tensor are defined as follows:

$$\begin{cases} \rho = VV^T = I - UU^T \\ \kappa = VU^T = \kappa^T \end{cases} \tag{C.122}$$

The matrices ρ and κ are connected by two equations similar to Eq.(C.78) and Eq.(C.79):

$$\rho\kappa = \kappa\rho \tag{C.123}$$

$$\rho^2 - \rho = -\kappa^2 \tag{C.124}$$

The three equations Eq.(C.122), Eq.(C.123) and Eq.(C.124) are required to demonstrate the Bloch-Messiah theorem in the case of axial symmetry and time reversal-invariance. We start with Eq.(C.122).

Consequences of Eq.(C.122):

It is clear that the matrix ρ is a positive semi-definite matrix. Indeed if we consider X an eigenvector of ρ associated with the eigenvalue λ we have:

$$X^T\rho X = \lambda = ||V^TX|| \qquad \Rightarrow \qquad \lambda \geq 0 \tag{C.125}$$

Moreover, as ρ is real and symmetric, it can be diagonalized by an orthogonal matrix Q:

$$Q^T\rho Q = Q^TVV^TQ = I - Q^TUU^TQ = \mathrm{diag}(v^2) \tag{C.126}$$

From Eq.(C.126), it is clear that the matrix Q also diagonalizes the positive semi-definite matrix UU^T. Denoting u_i^2 the eigenvalues of UU^T, we have:

$$\boxed{\forall i, \qquad u_i^2 + v_i^2 = 1} \tag{C.127}$$

Consequences of Eq.(C.123):

We diagonalize ρ in Eq.(C.123):

$$\begin{cases} \text{diag}(v^2)\tilde{\kappa} = \tilde{\kappa}\text{diag}(v^2) \\ \tilde{\kappa} = Q^T \kappa Q \end{cases} \tag{C.128}$$

This relation directly implies constraints on the elements of $\tilde{\kappa}$:

$$\boxed{(v_i^2 - v_j^2)\tilde{\kappa}_{ij} = 0} \tag{C.129}$$

It implies that $\tilde{\kappa}$ is diagonal in all the non-degenerate subspaces of $\text{diag}(v^2)$:

$$\boxed{\forall i, j, \qquad v_i^2 \neq v_j^2 \qquad \Rightarrow \qquad \tilde{\kappa}_{ij} = 0} \tag{C.130}$$

We consider the index $1 \leq k \leq p$ that spans the different eigenvalues v_k^2 with multiplicity α_k. With these notations $\text{diag}(v^2)$ and $\tilde{\kappa}$ read (up to a permutation we implicitly include in Q):

$$\text{diag}(v^2) = \begin{pmatrix} v_1^2 I_{\alpha_1} & 0 & \dots & 0 \\ 0 & \ddots & 0 & \vdots \\ \vdots & 0 & \ddots & 0 \\ 0 & \dots & 0 & v_p^2 I_{\alpha_p} \end{pmatrix} \qquad \text{and} \qquad \tilde{\kappa} = \begin{pmatrix} \tilde{\kappa}_1 & 0 & \dots & 0 \\ 0 & \ddots & 0 & \vdots \\ \vdots & 0 & \ddots & 0 \\ 0 & \dots & 0 & \tilde{\kappa}_p \end{pmatrix} \tag{C.131}$$

Since the matrices $\tilde{\kappa}_k$ are real and symmetric, we can diagonalize them thanks to the orthogonal matrices S_k into the matrices $\text{diag}(K_k)$. The total matrix made with the $\text{diag}(K_k)$ is called $\text{diag}(K)$. The orthogonal matrix whose blocks are the S_k is called S:

$$\boxed{\text{diag}(K) = S^T \tilde{\kappa} S = \begin{pmatrix} \text{diag}(K_1) & 0 & \dots & 0 \\ 0 & \ddots & 0 & \vdots \\ \vdots & 0 & \ddots & 0 \\ 0 & \dots & 0 & \text{diag}(K_p) \end{pmatrix}} \tag{C.132}$$

Moreover, as the S_k are all orthogonal matrices and operate only on the degenerate subspaces of $\text{diag}(v^2)$, $\text{diag}(v^2)$ is invariant under the following transformations:

$$\boxed{S^T \text{diag}(v^2) S = \text{diag}(v^2)} \tag{C.133}$$

In the representation defined by the matrix $\bar{D} = QS$, the matrices ρ and κ are both diagonal.

Consequences of Eq.(C.124):

We transform Eq.(C.123) thanks to the matrix $\bar{D}$:

$$\text{diag}(v^4) - \text{diag}(v^2) = -\text{diag}(K^2) \tag{C.134}$$

This equation explicitly gives the form of the elements of $\text{diag}(K^2)$:

$$\mathrm{diag}(K^2) = \begin{pmatrix} v_1^2 u_1^2 & 0 & \dots & 0 \\ 0 & \ddots & 0 & \vdots \\ \vdots & 0 & \ddots & 0 \\ 0 & \dots & 0 & v_n^2 u_n^2 \end{pmatrix} \tag{C.135}$$

The matrix κ is not in general positive semi-definite. Therefore, the elements of $\mathrm{diag}(K)$ can be negative. If we integrate this sign in the elements v_i and set $u_i \geq 0$, we have:

$$\boxed{\mathrm{diag}(K) = \mathrm{diag}(vu) = \begin{pmatrix} v_1 u_1 & 0 & \dots & 0 \\ 0 & \ddots & 0 & \vdots \\ \vdots & 0 & \ddots & 0 \\ 0 & \dots & 0 & v_n u_n \end{pmatrix}} \tag{C.136}$$

We have now developed everything to describe the special forms of the matrices U and V.

Special form of U:

From Eq.(C.126), we know that the matrix $\bar{D}$ diagonalizes UU^T:

$$\bar{D}^T U U^T \bar{D} = \mathrm{diag}(u^2) \tag{C.137}$$

Therefore, the matrix $\bar{D}^T \mathrm{diag}(u) D$ is a positive semi-definite Hermitian square root of UU^T. Moreover, using the real singular value decomposition of the matrix U, we can find orthogonal matrices A and B such that:

$$U = B \mathrm{diag}(u) A^T \tag{C.138}$$

Using Eq.(C.138), we find:

$$UU^T = B \mathrm{diag}(u^2) B^T = B \mathrm{diag}(u) A^T A \mathrm{diag}(u) B^T = B \mathrm{diag}(u^2) B^T \tag{C.139}$$

Eq.(C.139) proves that $B^T \mathrm{diag}(u) B$ is also a positive semi-definite Hermitian square root of UU^T. Because of the uniqueness of this square root, we have:

$$\bar{D} \mathrm{diag}(u) \bar{D}^T = B \mathrm{diag}(u) B^T \tag{C.140}$$

Inserting Eq.(C.140) in Eq.(C.138), we get:

$$U = B \mathrm{diag}(u) A^T = B \mathrm{diag}(u) B^T B A^T = \bar{D} \mathrm{diag}(u) \bar{D}^T B A^T \tag{C.141}$$

If we define the matric $\bar{C} = \bar{D}^T B A^T$ and $\bar{u} = \mathrm{diag}(u)$, we can finally write:

$$\boxed{U = \bar{D}\bar{u}\bar{C}} \qquad \text{with} \qquad \boxed{\bar{u} = \begin{pmatrix} u_1 & 0 & \dots & 0 \\ 0 & \ddots & 0 & \vdots \\ \vdots & 0 & \ddots & 0 \\ 0 & \dots & 0 & u_n \end{pmatrix} \qquad \forall i,\ 1 \geq u_i \geq 0} \tag{C.142}$$

Special form of V:

To determine the special form of V, we inject the definition of U in the expression of κ Eq.(C.122):

$$\kappa = VU^T = V\bar{C}^T\bar{u}\bar{D}^T \tag{C.143}$$

We diagonlize κ using the matrix $\bar{D}$:

$$\begin{cases} \text{diag}(vu) = \tilde{v}\bar{u} \\ \tilde{v} = \bar{D}^T V \bar{C}^T \end{cases} \tag{C.144}$$

Unfortunately, $\bar{u}$ is not invertible in general. We use permutations that we implicitly integrate in $\bar{D}$ and $\bar{C}$ to explicitly write the invertible part of $\bar{u}$ as follows:

$$\bar{u} = \begin{pmatrix} 0 & 0 \\ 0 & \bar{u}_{22} \end{pmatrix} \tag{C.145}$$

Now, Eq.(C.144) reads:

$$\begin{pmatrix} 0 & 0 \\ 0 & \text{diag}(vu)_{22} \end{pmatrix} = \begin{pmatrix} 0 & \tilde{v}_{12}\bar{u}_{22} \\ 0 & \tilde{v}_{22}\bar{u}_{22} \end{pmatrix} \tag{C.146}$$

We deduce:

$$\begin{cases} \tilde{v}_{22} = \text{diag}(v)_{22} \\ \tilde{v}_{12} = 0 \end{cases} \tag{C.147}$$

In order to have access to the other elements of V, we use the definition of ρ Eq.(C.122) and the matrices $\bar{D}$ and $\bar{C}$:

$$\text{diag}(v^2) = \bar{D}^T V \bar{C}^T C V^T \bar{D} = \tilde{v}\tilde{v}^T \tag{C.148}$$

We obtain for the elements of $\tilde{v}$:

$$\begin{cases} \tilde{v}_{11}\tilde{v}_{11}^T = I_{11} \\ \tilde{v}_{21}\tilde{v}_{11}^T = 0 \end{cases} \qquad \Rightarrow \qquad \tilde{v}_{21} = 0 \tag{C.149}$$

The matrix $\tilde{v}$ therefore reads:

$$\tilde{v} = \begin{pmatrix} \tilde{v}_{11} & 0 \\ 0 & \mathrm{diag}(v)_{22} \end{pmatrix} \tag{C.150}$$

From Eq.(C.149), we know that $\tilde{v}_{11}$ is orthogonal. We can diagonalize it with an orthogonal matrix F_{11} as stated in Eq.(C.31):

$$F_{11}^T \tilde{v}_{11} F_{11} = \begin{pmatrix} \pm 1 & 0 & \dots & 0 \\ 0 & \ddots & 0 & \vdots \\ \vdots & 0 & \ddots & 0 \\ 0 & \dots & 0 & \pm 1 \end{pmatrix} \tag{C.151}$$

Now, we complete the matrix F_{11} :

$$F = \begin{pmatrix} F_{11} & 0 \\ 0 & I_{22} \end{pmatrix} \tag{C.152}$$

With these additional transformations, the matrix $\tilde{v}$ is fully diagonal. We call this diagonal matrix $\bar{v}$ and define the matrices $\bar{D}' = \bar{D}F$ and $\bar{C}' = F\bar{C}$. With these notations we have:

$$\boxed{V = \bar{D}'\bar{v}\bar{C}'} \qquad \text{with} \qquad \boxed{\bar{v} = \begin{pmatrix} v_1 & 0 & \dots & 0 \\ 0 & \ddots & 0 & \vdots \\ \vdots & 0 & \ddots & 0 \\ 0 & \dots & 0 & v_n \end{pmatrix} \qquad \forall i,\ 1 \geq v_i \geq -1} \tag{C.153}$$

Finally, we have to verify that the orthogonal transformations defined by $\bar{D}' = \bar{D}F$ and $\bar{C}' = F\bar{C}$ don't change the special forms of ρ, κ and U. It is in fact very easy to see that it is the case. We start with Eq.(C.94):

$$\boxed{\bar{D}'^T \rho \bar{D} = \begin{pmatrix} F_{11}^T & 0 \\ 0 & I \end{pmatrix} \begin{pmatrix} I_{11} & 0 \\ 0 & \mathrm{diag}(v^2)_{22} \end{pmatrix} \begin{pmatrix} F_{11} & 0 \\ 0 & I \end{pmatrix} = \begin{pmatrix} I_{11} & 0 \\ 0 & \mathrm{diag}(v^2)_{22} \end{pmatrix}} \tag{C.154}$$

From Eq.(C.95), we then have:

$$\boxed{\bar{D}'^T \kappa \bar{D}' = \begin{pmatrix} F_{11}^T & 0 \\ 0 & I \end{pmatrix} \begin{pmatrix} 0 & 0 \\ 0 & \mathrm{diag}(vu)_{22} \end{pmatrix} \begin{pmatrix} F_{11} & 0 \\ 0 & I \end{pmatrix} = \begin{pmatrix} 0 & 0 \\ 0 & \mathrm{diag}(vu)_{22} \end{pmatrix}} \tag{C.155}$$

Finally, we use Eq.(C.103) to show that the special form of U doesn't change:

$$\boxed{\bar{D}'^T U \bar{C}'^T = \begin{pmatrix} F_{11}^T & 0 \\ 0 & I \end{pmatrix} \begin{pmatrix} 0 & 0 \\ 0 & \bar{u}_{22} \end{pmatrix} \begin{pmatrix} F_{11}^T & 0 \\ 0 & I \end{pmatrix} = \begin{pmatrix} 0 & 0 \\ 0 & \bar{u}_{22} \end{pmatrix}} \tag{C.156}$$

Conclusion:

We demonstrated the Bloch-Messiah theorem in the axial symmetric time-reversal invariant case. We built two orthogonal matrices $\bar{D}'$ and $\bar{C}'$ such that the matrices U anv V write:

$$\boxed{U = D'\bar{u}C'} \qquad \boxed{V = D'\bar{v}C'} \tag{C.157}$$

Moreover, the matrices $\bar{u}$ and $\bar{v}$ have the special forms explicitly described in Eq.(C.142) and Eq.(C.153).

Appendix D

Harmonic-oscillator wave function properties

In this appendix are gathered the important formulas related to the harmonic oscillator wave functions used all along this PhD thesis work. Here, we consider two different types of harmonic oscillator wave functions. The first one is the one-dimensional harmonic oscillator wave function, called z-harmonic oscillator wave function in the following:

$$\boxed{\varphi_{n_z}(z+d,b_z) = \frac{1}{\sqrt{2^{n_z} b_z n_z! \sqrt{\pi}}} e^{-\frac{1}{2}(\frac{z}{b_z})^2} H_{n_z}(\frac{z+d}{b_z})} \tag{D.1}$$

Here, n_z is the quantum number related to the number of energy quanta of the wave function in the z direction and b_z is the oscillator length that characterizes the spreading of the wave function. The H_{n_z} are the well-known Hermite polynomials:

$$H_{n_z}(\frac{z+d}{b_z}) = (-1)^{n_z} e^{(\frac{z+d}{b_z})^2} \frac{d^{n_z}}{dz^{n_z}} e^{-(\frac{z+d}{b_z})^2} \tag{D.2}$$

We also use the cylindrical harmonic oscillator wave functions named thereafter the $r_\perp$-harmonic oscillator wave functions. They read as follows:

$$\boxed{\phi_{(m,n_\perp)}(\vec{r}_\perp, b_r) = \frac{1}{b_r\sqrt{\pi}} \sqrt{\frac{n_\perp!}{(n_\perp+|m|)!}} e^{im\phi} (\frac{r_\perp}{b_r})^{|m|} L_{n_\perp}^{|m|}[(\frac{r_\perp}{b_r})^2] e^{-\frac{1}{2}(\frac{r_\perp}{b_r})^2}} \tag{D.3}$$

Here, m is the projection of the angular momentum of the wave function, $n_\perp$ defines its energy quantua in the $r_\perp$ direction and the oscillator length b_r defines its spreading. The $L_{n_\perp}^{|m|}$ are the generalized Laguerre polynomials:

$$L_{n_\perp}^{|m|}[(\frac{r_\perp}{b_r})^2] = \frac{(\frac{r_\perp}{b_r})^{-2|m|} e^{(\frac{r_\perp}{b_r})^2}}{n_\perp!} \frac{d^{n_\perp}}{dr_\perp^{n_\perp}} (e^{-(\frac{r_\perp}{b_r})^2} (\frac{r_\perp}{b_r})^{2(n_\perp+|m|)}) \tag{D.4}$$

Some of the formulas related to the behaviour of these wave functions are already well documented in the literature. In this case, we just provide the reader with the references of these formulas. The new contributions of this PhD thesis work concern the behaviour of the wave functions with different oscillator lengths in the 2-center case. These derivations have been inspired by the work of L. Robledo [69] who treated the 1-center case.

D.1 Rescaling

The aim of this part is to rescale the harmonic oscillator wave functions. In the case of z-harmonic oscillator wave functions with $d \neq 0$, this rescaling also includes translations which don't imply further difficulties.

D.1.1 z-harmonic oscillator wave functions

The most important result to know concerning the Hermite polnyomials in order to rescale the z-harmonic oscillator wave functions is their generating-functions property:

$$\boxed{\sum_{n_z=0}^{+\infty} \frac{t^{n_z}}{n_z!} H_{n_z}(z) = e^{-t^2+2tz}} \tag{D.5}$$

In the following, we use the Eq.(D.5) to transform a Hermite polynomial associated with the quantum number n_z and evaluated at $\frac{z}{b_z}$ into a sum of Hermite polynomials associated with other quantum numbers n'_z and evaluated at $\frac{z}{b'_z}$. We start by writting:

$$\sum_{n_z=0}^{+\infty} \frac{t^{n_z}}{n_z!} H_{n_z}(\frac{z}{b_z}) = e^{-t^2+2t\frac{z}{b_z}} \tag{D.6}$$

We factorize the exponential in the right hand side of Eq.(D.6):

$$e^{-t^2+2t\frac{z}{b_z}} = e^{-(\frac{b'_z t}{b_z})^2+2\frac{b'_z t}{b_z}\frac{z}{b'_z}} e^{-t^2(1-(\frac{b'_z}{b_z})^2} \tag{D.7}$$

We recognize the right hand side of Eq.(D.6) in the first term of Eq.(D.7). We expand the other term in series:

$$\sum_{n_z=0}^{+\infty} \frac{t^{n_z}}{n_z!} H_{n_z}(\frac{z}{b_z}) = \sum_{n'_z}^{+\infty} \frac{(\frac{b'_z t}{b_z})^{n'_z}}{n'_z!} H_{n'_z}(\frac{z}{b'_z}) \sum_{k}^{+\infty} \frac{1}{k!}((\frac{b'_z}{b_z})^2 - 1)^k t^{2k} \tag{D.8}$$

We can now find the expression of $H_{n_z}(\frac{z}{b_z})$ by identifying the different powers of t in Eq.(D.8):

$$\boxed{H_{n_z}(\frac{z}{b_z}) = \sum_{n'_z=0}^{n_z} \Delta_{(n_z,n'_z)} \frac{n_z!}{n'_z!(\frac{n_z-n'_z}{2})!} (\frac{b'_z}{b_z})^{n'_z} ((\frac{b'_z}{b_z})^2 - 1)^{\frac{n_z-n'_z}{2}} H_{n'_z}(\frac{z}{b'_z})} \tag{D.9}$$

$$\Delta_{(n_z,n_{z_0})} = \frac{1}{2}[1 + (-1)^{n_z+n_{z_0}}] \tag{D.10}$$

From Eq.(D.9), we deduce the expression of the L transition matrix:

$$\boxed{L_{(n_z,n\prime_z)}(b_z, b'_z) = \Delta_{(n_z,n'_z)} \sqrt{\frac{n_z!}{n'_z! 2^{n_z-n'_z}}} \frac{1}{(\frac{n_z-n'_z}{2})!} (\frac{b'_z}{b_z})^{n'_z+1/2} ((\frac{b'_z}{b_z})^2 - 1)^{\frac{n_z-n'_z}{2}}} \tag{D.11}$$

Thanks to this L matrix, we can finally rescale a z-harmonic oscillator wave function in the case $d = 0$:

$$\boxed{\varphi_{n_z}(z, b_z) = e^{-\frac{1}{2}(\frac{z}{b_z})^2} e^{\frac{1}{2}(\frac{z}{b'_z})^2} \sum_{n'_z=0}^{n_z} L_{(n_z n'_z)}(b_z, b'_z)\varphi_{n'_z}(z, b'_z)} \tag{D.12}$$

To treat the case $d \neq 0$, we have to study the translations of a Hermite polynomial. Using Eq.(D.5), we write:

$$\sum_{n_z=0}^{+\infty} \frac{t^{n_z}}{n_z!} H_{n_z}(\frac{z+d}{b_z}) = e^{-t^2+2t\frac{z+d}{b_z}} \tag{D.13}$$

Again, we factorize the exponential in Eq.(D.13):

$$e^{-t^2+2t\frac{z+d}{b_z}} = e^{-t^2+2t\frac{z+d'}{b_z}} e^{2t\frac{d-d'}{b_z}} \tag{D.14}$$

We recognize the right hand side of Eq.(D.6) in the first term of Eq.(D.14). We expand the other term in series:

$$\sum_{n_z=0}^{+\infty} \frac{t^{n_z}}{n_z!} H_{n_z}(\frac{z+d}{b_z}) = \sum_{n'_z}^{+\infty} \frac{t^{n'_z}}{n'_z!} H_{n'_z}(\frac{z+d'}{b_z}) \sum_{k}^{+\infty} \frac{(2\frac{d-d'}{b_z})^k}{k!} t^k \tag{D.15}$$

We now identify the different powers of t in Eq.(D.15):

$$\boxed{H_{n_z}(\frac{z+d}{b_z}) = \sum_{n'_z=0}^{n_z} \binom{n_z}{n'_z} (2\frac{d-d'}{b_z})^{n_z-n'_z} H_{n'_z}(\frac{z+d'}{b_z})} \tag{D.16}$$

We mix this translation result with the L matrix defined in Eq.(D.11) to obtain the more general $\bar{L}$ transition matrix:

$$\boxed{\bar{L}_{(n_z,n'_z)}(b_z, b'_z, d, d') = \sum_{n''_z=n'_z}^{n_z} \binom{n_z}{n''_z} \sqrt{\frac{n''_z! 2^{n_z-n''_z}}{n_z!}} (\frac{d-d'}{b_z})^{n_z-n''_z} L_{n_{zp} n'_z}(b'_z, b_z)} \tag{D.17}$$

Thanks to Eq.(D.17), we can finally rescale and translate the z-harmonic oscillator wave functions:

$$\boxed{\varphi_{n_z}(z+d, b_z) = e^{-\frac{1}{2}(\frac{z+d}{b_z})^2} e^{\frac{1}{2}(\frac{z+d'}{b'_z})^2} \sum_{n_{z'}=0}^{n_z} \bar{L}_{(n_z n'_z)}(b_z, b'_z, d, d')\varphi_{n'_z}(z+d', b'_z)} \tag{D.18}$$

As far as we know, the result displayed in Eq.(D.18) is totally new and very useful in our work.

D.1.2 $r_\perp$-harmonic oscillator wave functions

The $r_\perp$-harmonic oscillator wave functions also have their generating-functions property:

$$\boxed{\sum_{n_\perp}\sum_{m}\chi^{(2)*}_{(m,n_\perp)}(\vec{t})\phi_{(m,n_\perp)}(\vec{r}_\perp,b_r)=\frac{1}{b_r\sqrt{\pi}}e^{-\frac{1}{2}(\frac{r}{b_r})^2+2\frac{\vec{r}_\perp}{b_r}.\vec{t}-t^2}} \tag{D.19}$$

$$\chi^{(2)}_{(m,n_\perp)}(\vec{t})=\frac{(-1)^{n_\perp}}{\sqrt{n_\perp!(n_\perp+|m|)!}}e^{im\theta}t^{2n_\perp+|m|} \tag{D.20}$$

We factorize in the exponential of Eq.(D.19):

$$\frac{1}{b_r\sqrt{\pi}}e^{-\frac{1}{2}(\frac{r}{b_r})^2+2\frac{\vec{r}_\perp}{b_r}.\vec{t}-t^2}=e^{-\frac{1}{2}(\frac{r}{b_r})^2+\frac{1}{2}(\frac{r}{b'_r})^2}\frac{1}{b_r\sqrt{\pi}}e^{-\frac{1}{2}(\frac{r}{b'_r})^2+2\frac{\vec{r}_\perp}{b'_r}.\frac{b'_r\vec{t}}{b_r}-(\frac{b'_rt}{b_r})^2}e^{-t^2(1-(\frac{b'_r}{b_r})^2)} \tag{D.21}$$

We recognize the Eq.(D.19) in the exponential on the middle of Eq.(D.21). In addition, we expand the last term in series:

$$\begin{aligned}\sum_{n_\perp}\sum_{m}\chi^{(2)*}_{(m,n_\perp)}(\vec{t})\phi_{(m,n_\perp)}(\vec{r}_\perp,b_r)=e^{-\frac{1}{2}(\frac{r}{b_r})^2+\frac{1}{2}(\frac{r}{b'_r})^2}\frac{b'_r}{b_r}\sum_{n'_\perp}\sum_{m'}\frac{(-1)^{n'_\perp}}{\sqrt{n'_\perp!(n'_\perp+|m'|)!}}\\ e^{-im'\theta}(\frac{b'_rt}{b_r})^{2n'_\perp+|m'|}\phi_{(m',n'_\perp)}(\vec{r}_\perp,b'_r)\sum_k\frac{((\frac{b'_r}{b_r})^2-1)^kt^{2k}}{k!}\end{aligned} \tag{D.22}$$

Then, we identify with respect to t and θ:

$$\boxed{\begin{aligned}\phi_{(m,n_\perp)}(\vec{r}_\perp,b_r)=e^{-\frac{1}{2}(\frac{r}{b_r})^2+\frac{1}{2}(\frac{r}{b'_r})^2}\sum_{n'_\perp=0}^{n_\perp}\frac{\sqrt{n_\perp!(n_\perp+|m|)!}}{(n_\perp-n'_\perp)!\sqrt{n'_\perp!(n'_\perp+|m|)!}}\\ (\frac{b'_r}{b_r})^{2n'_\perp+|m|+1}(1-(\frac{b'_r}{b_r})^2)^{n_\perp-n'_\perp}\phi_{(m,n'_\perp)}(\vec{r}_\perp,b'_r)\end{aligned}} \tag{D.23}$$

From Eq.(D.23), we deduce the following $\mathring{L}$ transition matrix:

$$\boxed{\mathring{L}^{|m|}_{(n_\perp,n'_\perp)}(b_r,b'_r)=\frac{\sqrt{n_\perp!(n_\perp+|m|)!}}{(n_\perp-n'_\perp)!\sqrt{n'_\perp!(n'_\perp+|m|)!}}(\frac{b'_r}{b_r})^{2n'_\perp+|m|+1}(1-(\frac{b'_r}{b_r})^2)^{n_\perp-n'_\perp}} \tag{D.24}$$

Thanks to the $\mathring{L}$ matrix, it is easy to rescale the $r_\perp$-harmonic oscillator wave functions:

$$\boxed{\phi_{(m,n_\perp)}(\vec{r}_\perp,b_r)=e^{-\frac{1}{2}(\frac{r}{b_r})^2+\frac{1}{2}(\frac{r}{b'_r})^2}\sum_{n'_\perp=0}^{n_\perp}\mathring{L}^{|m|}_{(n_\perp,n'_\perp)}(b_r,b'_r)\phi_{(m,n'_\perp)}(\vec{r}_\perp,b'_r)} \tag{D.25}$$

D.2 Derivatives

The behaviours of the harmonic oscillator wave-functions with respect to differentiation is directly deduced from the properties of the Hermite and generalized Laguerre polynomials [48].

z-harmonic oscillator wave function:

In the case of the z-harmonic oscillator wave function, the following property holds:

$$\boxed{\nabla_z \varphi_{(n_z)}(z+d,b_z) = \frac{1}{b_z\sqrt{2}}(\delta_{(n_z>0)}\sqrt{n_z}\varphi_{(n_z-1)}(z+d,b_z) - \sqrt{n_z+1}\varphi_{(n_z+1)}(z+d,b_z))} \quad \text{(D.26)}$$

Moreover, applying the derivative operator two times leads to:

$$\boxed{\begin{aligned}\nabla_z^2\varphi_{n_z}(z,b_z) = \frac{1}{2b_z^2}[&\sqrt{n_z(n_z-1)}\varphi_{n_z-2}(z,b_z) \\ -(2n_z+1)\varphi_{n_z}(z,b_z) + &\sqrt{(n_z+1)(n_z+2)}\varphi_{n_z+2}(z,b_z)]\end{aligned}} \quad \text{(D.27)}$$

$r_\perp$-harmonic oscillator wave function:

In the case of the $r_\perp$-harmonic oscillator wave function, the following properties hold:

$$\boxed{\begin{aligned}\nabla_-\phi_{(m,n_\perp)}(\vec{r}_\perp,b_r) = \frac{1}{b_r\sqrt{2}}[&\delta_{(m\geq 1)}(\sqrt{m+n_\perp}\phi_{(m-1,n_\perp)}(\vec{r}_\perp,b_r) \\ &+\sqrt{n_\perp+1}\phi_{(m-1,n_\perp+1)}(\vec{r}_\perp,b_r)) \\ &-\delta_{(m<1)}(\sqrt{|m|+n_\perp+1}\phi_{(m-1,n_\perp)}(\vec{r}_\perp,b_r) \\ &+\delta_{(n_\perp>0)}\sqrt{n_\perp}\phi_{(m-1,n_\perp-1)}(\vec{r}_\perp,b_r))]\end{aligned}} \quad \text{(D.28)}$$

And:

$$\boxed{\begin{aligned}\nabla_+\phi_{(m,n_\perp)}(\vec{r}_\perp,b_r) = \frac{1}{b_r\sqrt{2}}[&\delta_{(m\geq 0)}(\sqrt{m+n_\perp+1}\phi_{(m+1,n_\perp)}(\vec{r}_\perp,b_r) \\ &+\delta_{(n_\perp>0)}\sqrt{n_\perp}\phi_{(m+1,n_\perp-1)}(\vec{r}_\perp,b_r)) \\ &-\delta_{(m<0)}(\sqrt{|m|+n_\perp}\phi_{(m+1,n_\perp)}(\vec{r}_\perp,b_r) \\ &+\sqrt{n_\perp+1}\phi_{(m+1,n_\perp+1)}(\vec{r}_\perp,b_r))]\end{aligned}} \quad \text{(D.29)}$$

Here, the operators ∇_- and ∇_+ are the spherical derivative operators whose expressions in cylindrical coordinates are:

$$\begin{cases}\nabla_- = \frac{e^{-i\varphi}}{\sqrt{2}}(\frac{\partial}{\partial r} - \frac{i}{r}\frac{\partial}{\partial\varphi}) \\ \nabla_+ = -\frac{e^{i\varphi}}{\sqrt{2}}(\frac{\partial}{\partial r} + \frac{i}{r}\frac{\partial}{\partial\varphi})\end{cases} \quad \text{(D.30)}$$

From Eq.(D.29), it is clear that:

$$\boxed{\nabla_-\phi_{(m,n_\perp)} = -(\nabla_+\phi_{(-m,n_\perp)})^*} \quad \text{(D.31)}$$

To conclude, we give the following final property:

$$\boxed{\begin{aligned}\nabla_\perp^2\phi_{(m,n)}(\vec{r}_\perp,b_r) = -\frac{1}{b_r^2}[&\sqrt{n(n+|m|)}\phi_{(m,n-1)}(\vec{r}_\perp,b_r) + (2n+|m|+1)\phi_{(m,n)}(\vec{r}_\perp,b_r)\\ &+\sqrt{(n+1)(n+|m|+1)}\phi_{(m,n+1)}(\vec{r}_\perp,b_r)]\end{aligned}} \tag{D.32}$$

Here, the operator $\nabla_\perp^2$ stands for the $r_\perp$ part of the scalar product $\vec{\nabla}^2$ which explicitly reads:

$$\nabla_\perp^2 = -2\nabla_-\nabla_+ \tag{D.33}$$

D.3 Generating-function formalism

We have presented a part of the generating-function formalism in the section D.1 of this appendix where we used it to rescale the harmonic oscillator wave functions. This formalism is always used with the same philosophy. The target wave functions are transformed into exponentials through the generating-functions formalism. Factorizations are operated in the exponentials. Then, the generating-functions formalism is used to come back to a summation where the target wave functions are finally identified with their new desired form.
In addition to the main properties of the generating-functions already displayed in Eq.(D.5) and Eq.(D.19), it is important to know their scaling properties:

$$\boxed{\chi_{n_z}^{(1)}(\gamma t) = \sqrt{\frac{2^{n_z}}{n_z!}}(\gamma t)^{n_z} = \gamma^{n_z}\chi_{n_z}^{(1)}(t)} \tag{D.34}$$

$$\boxed{\chi_{(m,n_\perp)}^{(2)}(\gamma\vec{t}) = \frac{(-1)^{n_\perp}}{\sqrt{n_\perp!(n_\perp+|m|)!}}e^{im\theta}(\gamma t)^{2n_\perp+|m|} = \gamma^{2n_\perp+|m|}\chi_{(m,n_\perp)}^{(2)}(\vec{t})} \tag{D.35}$$

Note that the generating-functions associated with the z-harmonic oscillator wave functions Eq.(D.34) are not exactly the same as the generating-functions of the Hermite polynomials Eq.(D.5). This feature is due to the normalization coefficients added in the z-harmonic oscillator wave functions.

D.4 Talman coefficients

The Talman coefficients enable us to transform the product of two harmonic oscillator wave functions into a sum of harmonic oscillator wave functions. It's a precious help in the derivations of the fields. In this section, we present first the Talman coefficients that transform the product of two wave functions with the same oscillator length into a sum. Then we discuss the generalization in the case of different oscillator lengths.

D.4.1 Talman coefficients

The Talman coefficients are obtained using the generating-function formalism. We only present here the way they operate on harmonic oscillator wave functions, as it is our main

concern (for further informations, see [47] and [48]).

Talman-z coefficients:

The Talman-z coefficients are defined by the following expression:

$$\boxed{\varphi_{n_{z_\alpha}}(z+d_\alpha,b_z)\varphi_{n_{z_\beta}}(z+d_\beta,b_z)=\frac{1}{\sqrt{b_z\sqrt{\pi}}}e^{-\frac{1}{2}(\frac{z+k_{\alpha\beta}}{b_z})^2}\sum_{n_{z_a}}T^{n_{z_a}}_{(n_{z\alpha},d_\alpha)(n_{z_\beta},d_\beta)}\varphi_{n_{z_a}}(z+k_{\alpha\beta})} \quad \text{(D.36)}$$

$$k_{\alpha\beta}=\frac{d_\alpha+d_\beta}{2} \quad \text{(D.37)}$$

Talman-r coefficients:

The Talman-r coefficients operate on the $r_\perp$-harmonic oscillator wave functions as follows:

$$\boxed{\phi^*_{(m_\alpha,n_{\perp\alpha})}(\vec{r}_\perp,b_r)\phi_{(m_\beta,n_{\perp\beta})}(\vec{r}_\perp,b_r)=\frac{1}{b_r\sqrt{\pi}}e^{-\frac{1}{2}(\frac{r_\perp}{b_r})^2}\sum_{n_{\perp a}}T^{n_{\perp a}}_{(m_\alpha,n_{\perp\alpha})(m_\beta,n_{\perp\beta})}\phi_{(m_a,n_{\perp a})}(\vec{r}_\perp,b_r)} \quad \text{(D.38)}$$

Here, $m_a=m_\beta-m_\alpha$.

D.4.2 Generalized Talman coefficients

In this PhD thesis work, we have generalized the Talman coefficients to the product of two wave functions with different oscillator lengths.

Generalized Talman-z coefficients:

We start by transforming the product of two z-harmonic oscillator wave functions with different oscillator lengths thanks to the $\bar{L}$ matrix defined in Eq.(D.17):

$$\varphi_{n_{z\alpha}}(z+d_\alpha,b_{z_0})\varphi_{n_{z_\beta}}(z+d_\beta,b_{z_1})=e^{-\frac{1}{2}(\frac{z+d_\alpha}{b_{z_0}})^2}e^{\frac{1}{2}(\frac{z+d'_\alpha}{B_z})^2}e^{-\frac{1}{2}(\frac{z+d_\beta}{b_{z_1}})^2}e^{\frac{1}{2}(\frac{z+d'_\beta}{B_z})^2}\sum_{n_{z_0}=0}^{n_{z_\alpha}}\sum_{n_{z_1}=0}^{n_{z_\beta}} \quad \text{(D.39)}$$
$$\bar{L}_{(n_{z\alpha},n_{z_0})}(b_{z_0},B_z,d_\alpha,d'_\alpha)\bar{L}_{(n_{z_\beta},n_{z_1})}(b_{z_1},B_z,d_\beta,d'_\beta)\varphi_{n_{z_0}}(z+d'_\alpha,B_z)\varphi_{n_{z_1}}(z+d'_\beta,B_z)$$

We can choose any value B_z, d'_α and d'_β. We therefore search for special values that simplify Eq.(D.39):

$$\boxed{B_z=\frac{b_{z_0}b_{z_1}\sqrt{2}}{\sqrt{b^2_{z_0}+b^2_{z_1}}}} \qquad \boxed{d'_\alpha=d'_\beta=d'=\frac{b^2_{z_1}d_\alpha+b^2_{z_0}d_\beta}{b^2_{z_0}+b^2_{z_1}}} \quad \text{(D.40)}$$

These special values allow us to cancel the z dependency of the exponentials in Eq.(D.39):

$$\varphi_{n_{z\alpha}}(z+d_\alpha,b_{z_0})\varphi_{n_{z_\beta}}(z+d_\beta,b_{z_1})=e^{-\frac{1}{2}\frac{(d_\alpha-d_\beta)^2}{b^2_{z_0}+b^2_{z_1}}}\sum_{n_{z_0}}\sum_{n_{z_1}}\bar{L}_{(n_{z\alpha},n_{z_0})}(b_{z_0},B_z,d_\alpha,d') \quad \text{(D.41)}$$
$$\bar{L}_{(n_{z_\beta},n_{z_1})}(b_{z_1},B_z,d_\beta,d')\varphi_{n_{z_0}}(z+d',B_z)\varphi_{n_{z_1}}(z+d',B_z)$$

Using the customary Talman-z coefficient in Eq.(D.41), we get:

$$\varphi_{n_{z_\alpha}}(z+d_\alpha,b_{z_0})\varphi_{n_{z_\beta}}(z+d_\beta,b_{z_1}) = \frac{1}{\sqrt{B_z\sqrt{\pi}}} e^{-\frac{1}{2}\frac{(d_\alpha-d_\beta)^2}{b_{z_0}^2+b_{z_1}^2}} e^{-\frac{1}{2}(\frac{z+d'}{B_z})^2} \sum_{n_{z_0}}\sum_{n_{z_1}} \tag{D.42}$$
$$\bar{L}_{(n_{z_\alpha},n_{z_0})}(b_{z_0},B_z,d_\alpha,d')\bar{L}_{(n_{z_\beta},n_{z_1})}(b_{z_1},B_z,d_\beta,d')\sum_{n_{z_a}} T^{n_{z_a}}_{(n_{z_0},d')(n_{z_1},d')}\varphi_{n_{z_a}}(z+d',B_z)$$

Eq.(D.42) naturally leads to define the generalized Talman-z coefficients as follows:

$$\boxed{\begin{aligned}\bar{T}^{n_{z_a}}_{(n_{z_\alpha},d_\alpha)(n_{z_\beta},d_\beta)} = e^{-\frac{1}{2}\frac{(d_\alpha-d_\beta)^2}{b_{z_0}^2+b_{z_1}^2}} \sum_{n_{z_0}=0}^{n_{z_\alpha}}\sum_{n_{z_1}=0}^{n_{z_\beta}} \bar{L}_{(n_{z_\alpha},n_{z_0})}(b_{z_0},B_z,d_\alpha,d') \\ \bar{L}_{(n_{z_\beta},n_{z_1})}(b_{z_1},B_z,d_\beta,d')T^{n_{z_a}}_{(n_{z_0},d')(n_{z_1},d')}\end{aligned}} \tag{D.43}$$

Thanks to Eq.(D.43), the product of the wave functions in Eq.(D.39) finally reduces to:

$$\boxed{\begin{aligned}\varphi_{n_{z_\alpha}}(z+d_\alpha,b_{z_0})\varphi_{n_{z_\beta}}(z+d_\beta,b_{z_1}) = \frac{1}{\sqrt{B_z\sqrt{\pi}}} e^{-\frac{1}{2}(\frac{z+d'}{B_z})^2} \\ \sum_{n_{z_a}} \bar{T}^{n_{z_a}}_{(n_{z_\alpha},d_\alpha)(n_{z_\beta},d_\beta)}\varphi_{n_{z_a}}(z+d',B_z)\end{aligned}} \tag{D.44}$$

As far as we know, these generalized Talman-z coefficients are expressed for the first time.

Generalized Talman-r coefficients:

We start by transforming the product of two $r_\perp$-harmonic oscillator wave functions with different oscillator lengths thanks to the $\mathring{L}$ matrix defined in Eq.(D.24):

$$\phi^*_{(m_\alpha,n_{\perp_\alpha})}(\vec{r}_\perp,b_{r_0})\phi_{(m_\beta,n_{\perp_\beta})}(\vec{r}_\perp,b_{r_1}) = e^{-\frac{1}{2}(\frac{r}{b_{r_0}})^2+\frac{1}{2}(\frac{r}{B_r})^2} e^{-\frac{1}{2}(\frac{r}{b_{r_1}})^2+\frac{1}{2}(\frac{r}{B_r})^2} \tag{D.45}$$
$$\sum_{n_{\perp_0}}\sum_{n_{\perp_1}} \mathring{L}^{|m_\alpha|}_{(n_{\perp_\alpha},n_{\perp_0})}(b_{r_0},B_r)\mathring{L}^{|m_\beta|}_{(n_{\perp_\beta},n_{\perp_1})}(b_{r_1},B_r)\phi^*_{(m_\alpha,n_{\perp_0})}(\vec{r}_\perp,B_r)\phi_{(m_\beta,n_{\perp_1})}(\vec{r}_\perp,B_r)$$

The quantity B_r is chosen to cancel the exponentials of Eq.(D.45):

$$\boxed{B_r = \frac{b_{r_0}b_{r_1}\sqrt{2}}{\sqrt{b_{r_0}^2+b_{r_1}^2}}} \tag{D.46}$$

Using Eq.(D.46) in Eq.(D.45), we get:

$$\phi^*_{(m_\alpha,n_{\perp_\alpha})}(\vec{r}_\perp,b_{r_0})\phi_{(m_\beta,n_{\perp_\beta})}(\vec{r}_\perp,b_{r_1}) = \sum_{n_{\perp_0}}\sum_{n_{\perp_1}} \mathring{L}^{|m_\alpha|}_{(n_{\perp_\alpha},n_{\perp_0})}(b_{r_0},B_r)\mathring{L}^{|m_\beta|}_{(n_{\perp_\beta},n_{\perp_1})}(b_{r_1},B_r) \tag{D.47}$$
$$\phi^*_{(m_\alpha,n_{\perp_0})}(\vec{r}_\perp,B_r)\phi_{(m_\beta,n_{\perp_1})}(\vec{r}_\perp,B_r)$$

Inserting the customary Talman-r coefficients in Eq.(D.47), we find:

$$\phi^*_{(m_\alpha,n_{\perp_\alpha})}(\vec{r}_\perp,b_{r_0})\phi_{(m_\beta,n_{\perp_\beta})}(\vec{r}_\perp,b_{r_1}) = \frac{1}{B_r\sqrt{\pi}}e^{-\frac{1}{2}(\frac{r}{B_r})^2}\sum_{n_{\perp_0}}\sum_{n_{\perp_1}}\mathring{L}^{|m_\alpha|}_{(n_{\perp_\alpha},n_{\perp_0})}(b_{r_0},B_r) \tag{D.48}$$
$$\mathring{L}^{|m_\beta|}_{(n_{\perp_\beta},n_{\perp_1})}(b_{r_1},B_r)\sum_{n_{\perp_a}}T^{n_{\perp_a}}_{(m_\alpha,n_{\perp_0})(m_\beta,n_{\perp_1})}\phi_{(m_\beta-m_\alpha,n_{\perp_a})}(\vec{r}_\perp,B_r)$$

Eq.(D.48) leads to a natural definition of the generalized Talman-r coefficients:

$$\boxed{\bar{T}^{n_{\perp_a}}_{(m_\alpha,n_{\perp_\alpha})(m_\beta,n_{\perp_\beta})} = \sum_{n_{\perp_0}=0}^{n_{\perp_\alpha}}\sum_{n_{\perp_1}=0}^{n_{\perp_\beta}}\mathring{L}^{|m_\alpha|}_{(n_{\perp_\alpha},n_{\perp_0})}(b_{r_0},B_r)\mathring{L}^{|m_\beta|}_{(n_{\perp_\beta},n_{\perp_1})}(b_{r_1},B_r)T^{n_{\perp_a}}_{(m_\alpha,n_{\perp_0})(m_\beta,n_{\perp_1})}} \tag{D.49}$$

Thanks to Eq.(D.49), the product of harmonic oscillator wave functions in Eq.(D.45) eventually reads:

$$\boxed{\begin{aligned}\phi^*_{(m_\alpha,n_{\perp_\alpha})}(\vec{r}_\perp,b_{r_0})\phi_{(m_\beta,n_{\perp_\beta})}(\vec{r}_\perp,b_{r_1}) &= \frac{1}{B_r\sqrt{\pi}}e^{-\frac{1}{2}(\frac{r}{B_r})^2}\\ &\sum_{n_{\perp_a}}\bar{T}^{n_{\perp_a}}_{(m_\alpha,n_{\perp_\alpha})(m_\beta,n_{\perp_\beta})}\phi_{(m_\beta-m_\alpha,n_{\perp_a})}(\vec{r}_\perp,B_r)\end{aligned}} \tag{D.50}$$

As far as we know, these generalized Talman-r coefficients are also totally new.

D.5 Moshinsky coefficients

The Moshinsky coeffcients are used to transform a product of two harmonic oscillator wave functions depending on two coordinates $\vec{r}_0$ and $\vec{r}_1$ into a sum of products of two harmonic oscillator wave functions in the associated center of mass and relative representation. The Moshinsky coefficients are also obtained using the generating-function formalism. As for the customary Talman coefficients, we only describe how the Moshinsky coefficients operate on the harmonic oscillator wave functions (see [47] and [48] for more details).

Moshinsky-z coefficients:

The Moshinsky-z coefficients operate on the z-harmonic oscillator wave functions in the following way:

$$\boxed{\varphi_{n_{z_\alpha}}(z_0+d_\alpha,b_z)\varphi_{n_{z_\beta}}(z_1+d_\beta,b_z) = \sum_{n_{z_a}}\sum_{n_{z_b}}M^{n_{z_a}n_{z_b}}_{n_{z_\alpha}n_{z_\beta}}\varphi_{n_{z_a}}(Z+D_{\alpha\beta})\varphi_{n_{z_b}}(z+d_{\alpha\beta},b_z)} \tag{D.51}$$

$$\begin{cases}Z = \frac{z_0+z_1}{\sqrt{2}}\\ z = \frac{z_0-z_1}{\sqrt{2}}\end{cases}\qquad\qquad\begin{cases}D_{\alpha\beta} = \frac{d_\alpha+d_\beta}{\sqrt{2}}\\ d_{\alpha\beta} = \frac{d_\alpha-d_\beta}{\sqrt{2}}\end{cases} \tag{D.52}$$

Moshinsky-r coefficients:

In this PhD thesis work, the Moshinsky-r coefficients operate only on wave functions depending on the same coordinate $\vec{r}_\perp$. In this case, the center of mass and relative representation is very convenient:

$$\boxed{\begin{aligned}&\phi^*_{(m_\alpha,n_{\perp_\alpha})}(\vec{r}_\perp,b_r)\phi_{(m_\beta,n_{\perp_\beta})}(\vec{r}_\perp,b_r)=\sum_{(m_a,n_{\perp_a})}\sum_{(m_b,n_{\perp_b})}\\&M^{(m_c,n_{\perp_c})(m_d,n_{\perp_d})}_{(m_\alpha,n_{\perp_\alpha})(m_\beta,n_{\perp_\beta})}\phi^*_{(m_c,n_{\perp_c})}(\sqrt{2}\vec{r}_\perp,b_r)\phi_{(m_d,n_{\perp_d})}(0,b_r)\end{aligned}} \tag{D.53}$$

Note that a special case is found in the spatial part of the Central term where the wave functions have two different oscillator lengths (see Appendix E). The related formulas are then specified.

D.6 Overlap of two harmonic oscillator wave functions

The analytic expressions of the overlaps between two harmonic oscillator wave functions are very useful. They are required to orthonormalize the 2-center representation and to give a closed formula for the kinetic and the two-body center of mass correction fields.

D.6.1 z-harmonic oscillator wave functions

Same b_z:

In the case of two z-harmonic oscillator wave functions sharing the same b_z, the overlap matrix is called S and defined by:

$$S_{(n_{z_\alpha},d_\alpha)(n_{z_\beta},d_\beta)}=\int dz\varphi_{n_{z_\alpha}}(z+d_\alpha,b_z)\varphi_{n_{z_\beta}}(z+d_\beta,b_z) \tag{D.54}$$

We use the $\bar{L}$ matrix defined in Eq.(D.17):

$$\begin{aligned}S_{(n_{z_\alpha},d_\alpha)(n_{z_\beta},d_\beta)}=e^{-\frac{1}{2}\frac{(d_\alpha-d_\beta)^2}{2b_z^2}}\sum_{n_{z_a}=0}^{n_{z_\alpha}}\sum_{n_{z_b}=0}^{n_{z_\beta}}\bar{L}_{(n_{z_\alpha},n_{z_a})}(b_z,b_z,d_\alpha,d')\\\bar{L}_{(n_{z_\beta},n_{z_b})}(b_z,b_z,d_\beta,d')\int dz\varphi_{n_{z_a}}(z+d')\varphi_{n_{z_b}}(z+d')\end{aligned} \tag{D.55}$$

The value of d' is deduced from Eq.(D.40):

$$d'=\frac{d_\alpha+d_\beta}{2} \tag{D.56}$$

Inserting the orthonormality relations of the z-harmonic oscillator wave functions in Eq.(D.55), we finally find:

$$\boxed{S_{(n_{z_\alpha},d_\alpha)(n_{z_\beta},d_\beta)}=e^{-\frac{1}{2}\frac{(d_\alpha-d_\beta)^2}{2b_z^2}}\sum_{n_z=0}^{\min(n_{z_\alpha},n_{z_\beta})}\bar{L}_{(n_{z_\alpha},n_z)}(b_z,b_z,d_\alpha,d')\bar{L}_{(n_{z_\beta},n_z)}(b_z,b_z,d_\beta,d')} \tag{D.57}$$

Different b_z:

In the case of two different oscillator lengths, the overlap matrix is called $\bar{S}_z$:

$$\bar{S}_{z_{(n_{z_\alpha},d_\alpha)(n_{z_\beta},d_\beta)}}(b_{z_0},b_{z_1}) = \int dz \varphi_{n_{z_\alpha}}(z+d_\alpha,b_{z_0})\varphi_{n_{z_\beta}}(z+d_\beta,b_{z_1}) \tag{D.58}$$

We transform Eq.(D.58) thanks to the $\bar{L}$ matrix defined in Eq.(D.17):

$$\begin{aligned}\bar{S}_{z_{(n_{z_\alpha},d_\alpha)(n_{z_\beta},d_\beta)}}(b_{z_0},b_{z_1}) = e^{-\frac{1}{2}\frac{(d_\alpha-d_\beta)^2}{b_{z_0}^2+b_{z_1}^2}} \sum_{n_{z_0}=0}^{n_{z_\alpha}} \sum_{n_{z_1}=0}^{n_{z_\beta}} \bar{L}_{(n_{z_\alpha},n_{z_0})}(b_{z_0},B_z,d_\alpha,d') \\ \bar{L}_{(n_{z_\beta},n_{z_1})}(b_{z_1},B_z,d_\beta,d') \int dz \varphi_{n_{z_0}}(z+d',B_z)\varphi_{n_{z_1}}(z+d',B_z)\end{aligned} \tag{D.59}$$

The expression of B_z and d' are given in Eq.(D.40). We use the orthonormality relations of the z-harmonic oscillator wave functions to finally write:

$$\boxed{\begin{aligned}\bar{S}_{z_{(n_{z_\alpha},d_\alpha)(n_{z_\beta},d_\beta)}}(b_{z_0},b_{z_1}) = e^{-\frac{1}{2}\frac{(d_\alpha-d_\beta)^2}{b_{z_0}^2+b_{z_1}^2}} \sum_{n_z=0}^{\min(n_{z_\alpha},n_{z_\beta})} \bar{L}_{(n_{z_\alpha},n_z)}(b_{z_0},B_z,d_\alpha,d') \\ \bar{L}_{(n_{z_\beta},n_z)}(b_{z_1},B_z,d_\beta,d')\end{aligned}} \tag{D.60}$$

D.6.2 $r_\perp$-harmonic oscillator wave functions

Same b_r:

The overlap between two $r_\perp$-harmonic oscillator wave functions with the same oscillator lengths is trivial due to the orthonormality relations of these functions:

$$\boxed{\int d\vec{r}_\perp \phi^*_{(m_\alpha,n_{\perp_\alpha})}(\vec{r}_\perp,b_r)\phi_{(m_\beta,n_{\perp_\beta})}(\vec{r}_\perp,b_r) = \delta_{(m_\alpha,m_\beta)}\delta_{(n_{\perp_\alpha},n_{\perp_\beta})}} \tag{D.61}$$

Different b_r:

In the case of two different oscillator lengths, the overlap matrix is called $\bar{S}_r$ and reads as follows:

$$\bar{S}_{r_{(m_\alpha,n_{\perp_\alpha})(m_\beta,n_{\perp_\beta})}}(b_{r_0},b_{r_1}) = \int d\vec{r}_\perp \phi^*_{(m_\alpha,n_{\perp_\alpha})}(\vec{r}_\perp,b_{r_0})\phi_{(m_\beta,n_{\perp_\beta})}(\vec{r}_\perp,b_{r_1}) \tag{D.62}$$

We transform Eq.(D.62) thanks to the $\mathring{L}$ matrix defined in Eq.(D.24):

$$\begin{aligned}\bar{S}_{r_{(m_\alpha,n_{\perp_\alpha})(m_\beta,n_{\perp_\beta})}}(b_{r_0},b_{r_1}) = \sum_{n_{\perp_0}=0}^{n_{\perp_\alpha}} \sum_{n_{\perp_1}=0}^{n_{\perp_\beta}} \mathring{L}^{|m_\alpha|}_{(n_{\perp_\alpha},n_{\perp_0})}(b_{r_0},B_r)\mathring{L}^{|m_\beta|}_{(n_{\perp_\beta},n_{\perp_1})}(b_{r_1},B_r) \\ \int d\vec{r}_\perp \phi^*_{(m_\alpha,n_{\perp_0})}(\vec{r}_\perp,B_r)\phi_{(m_\beta,n_{\perp_1})}(\vec{r}_\perp,B_r)\end{aligned} \tag{D.63}$$

The expression of B_r is given in Eq.(D.46). We use the orthonormality relations of the $r_\perp$-harmonic oscillator wave functions to finally write:

$$\boxed{\bar{S}_{r_{(m_\alpha,n_{\perp_\alpha})(m_\beta,n_{\perp_\beta})}}(b_{r_0},b_{r_1}) = \delta_{(m_\alpha,m_\beta)} \sum_{n_\perp=0}^{\min(n_{\perp_\alpha},n_{\perp_\beta})} \mathring{L}^{|m_\alpha|}_{(n_{\perp_\alpha},n_\perp)}(b_{r_0},B_r)\mathring{L}^{|m_\beta|}_{(n_{\perp_\beta},n_\perp)}(b_{r_1},B_r)} \quad \text{(D.64)}$$

D.6.3 Full harmonic oscillator wave functions

Same oscillator lengths:

The full overlap between two harmonic oscillator wave functions with the same oscillator lengths is called $\mathcal{O}$. This matrix is easily deduced from the result of Eq.(D.57) and Eq.(D.61):

$$\boxed{\mathcal{O}_{\alpha\beta} = \delta_{(m_\alpha,m_\beta)}\delta_{(n_{perp_\alpha},n_{\perp_\beta})}S_{(n_{z_\alpha},d_\alpha)(n_{z_\beta},d_\beta)}} \quad \text{(D.65)}$$

Different oscillator lengths:

In the case of different oscillator lengths, the overlap matrix $\bar{\mathcal{O}}$ is determined using Eq.(D.60) and Eq.(D.64):

$$\boxed{\bar{\mathcal{O}}_{\alpha\beta}(b_0,b_1) = \bar{S}_{r_{(m_\alpha,n_{\perp_\alpha})(m_\beta,n_{\perp_\beta})}}(b_{r_0},b_{r_1})\bar{S}_{z_{(nz_\alpha,d_\alpha)(nz_\beta,d_\beta)}}(b_{z_0},b_{z_1})} \quad \text{(D.66)}$$

Appendix E

Central fields

The central part of the antisymmetrized Gogny interaction reads as follows:

$$\boxed{V^{(Ctrl)}(1-P_rP_\sigma P_\tau)=\sum_{i=1}^{2}e^{-(|\vec{r}_1-\vec{r}_2|)^2/\mu_i^2}(W_i+B_iP_\sigma-H_iP_\tau-M_iP_\sigma P_\tau)(1-P_rP_\sigma P_\tau)} \quad \text{(E.1)}$$

The operators P_r, P_σ and P_τ represent the exchange of the spatial, spin and isospin part, respectively. The matrix elements of the central part of the interaction can be separated into a spatial part and a spin-isospin one:

$$\boxed{{}_0\langle\alpha\beta|V^{(Ctrl)}(1-P_rP_\sigma P_\tau)|\gamma\delta\rangle_1=\sum_{i=1}^{2}\bar{E}^{(i)\gamma\delta}_{\alpha\beta}S^{(i)\gamma\delta}_{\alpha\beta}-\bar{E}^{(i)\delta\gamma}_{\alpha\beta}S^{(i)\delta\gamma}_{\alpha\beta}} \quad \text{(E.2)}$$

$$\begin{cases}\bar{E}^{(i)\gamma\delta}_{\alpha\beta}={}_0\langle\alpha\beta|e^{-(|\vec{r}_1-\vec{r}_2|)^2/\mu_i^2}|\gamma\delta\rangle_1\\ S^{(i)\gamma\delta}_{\alpha\beta}={}_0\langle(s_\alpha,\tau_\alpha)(s_\beta,\tau_\beta)|(W_i+B_iP_\sigma-H_iP_\tau-M_iP_\sigma P_\tau)|(s_\gamma,\tau_\gamma)(s_\delta,\tau_\delta)\rangle_1\end{cases} \quad \text{(E.3)}$$

The indices 0 and 1 stand for the fact that the particle bases on the right and on the left can be different. When they are the same, the expression reduces to the more common one :

$$\boxed{\langle\alpha\beta|V^{(Ctrl)}(1-P_rP_\sigma P_\tau)|\gamma\delta\rangle=\sum_{i=1}^{2}E^{(i)\gamma\delta}_{\alpha\beta}S^{(i)\gamma\delta}_{\alpha\beta}-E^{(i)\delta\gamma}_{\alpha\beta}S^{(i)\delta\gamma}_{\alpha\beta}} \quad \text{(E.4)}$$

$$E^{(i)\gamma\delta}_{\alpha\beta}=\langle\alpha\beta|e^{-(|\vec{r}_1-\vec{r}_2|)^2/\mu_i^2}|\gamma\delta\rangle \quad \text{(E.5)}$$

This appendix aims to give an analytic expression of all the Central fields involved in this PhD thesis.

E.1 Spatial part

We give an analytic expression of the spatial part of the central matrix element. The case with the same bases on the left hand side and on the right hand side is treated first.Then derivations are given for the general case.

E.1.1 Same bases

This part aims to give an explicit expression of the following quantity:

$$E_{\alpha\beta}^{(i)\gamma\delta} = \langle \alpha\beta | e^{-(|\vec{r}_1 - \vec{r}_2|)^2/\mu_i^2} | \gamma\delta \rangle \tag{E.6}$$

It could be rewritten:

$$E_{\alpha\beta}^{(i)\gamma\delta} = \int\int d\vec{r}_1 d\vec{r}_2 e^{-(|\vec{r}_1 - \vec{r}_2|)^2/\mu_i^2} \psi_\alpha^*(\vec{r}_1)\psi_\beta^*(\vec{r}_2)\psi_\gamma(\vec{r}_1)\psi_\delta(\vec{r}_2) \tag{E.7}$$

We can then separate with respect to $\vec{r}_\perp$ and z:

$$\boxed{\begin{aligned} E_{\alpha\beta}^{(i)\gamma\delta} = \int\int d\vec{r}_{\perp_1} d\vec{r}_{\perp_2} e^{-(r_{\perp_1} - r_{\perp_2})^2/\mu_i^2} \phi_\alpha^*(\vec{r}_{\perp_1})\phi_\beta^*(\vec{r}_{\perp_2})\phi_\gamma(\vec{r}_{\perp_1})\phi_\delta(\vec{r}_{\perp_2}) \\ \int\int dz_1 dz_2 e^{-(\vec{z}_1 - \vec{z}_2)^2/\mu_i^2} \varphi_{n_{z_\alpha}}(z + d_\alpha)\varphi_{n_{z_\beta}}(z + d_\beta)\varphi_{n_{z_\gamma}}(z + d_\gamma)\varphi_{n_{z_\delta}}(z + d_\delta) \end{aligned}} \tag{E.8}$$

Both integrals are treated separately thereafter.

Calculation of the z-integral:

We'd like to evaluate the following integral:

$$I_z = \int\int dz_1 dz_2 e^{-(\vec{z}_1 - \vec{z}_2)^2/\mu_i^2} \varphi_{n_{z_\alpha}}(z + d_\alpha)\varphi_{n_{z_\beta}}(z + d_\beta)\varphi_{n_{z_\gamma}}(z + d_\gamma)\varphi_{n_{z_\delta}}(z + d_\delta) \tag{E.9}$$

We start using the Talman-z coefficients (see Appendix D):

$$I_z = \frac{1}{b_z\sqrt{\pi}} \sum_{n_{z_a}} \sum_{n_{z_b}} T^{n_{z_a}}_{(n_{z_\alpha}, d_\alpha)(n_{z_\gamma}, d_\gamma)} T^{n_{z_b}}_{(n_{z_\beta}, d_\beta)(n_{z_\delta}, d_\delta)} \tag{E.10}$$
$$\int\int dz_1 dz_2 e^{-(\vec{z}_1 - \vec{z}_2)^2/\mu_i^2} e^{-\frac{1}{2}(\frac{z_1 + k_{\alpha\gamma}}{b_z})^2} e^{-\frac{1}{2}(\frac{z_2 + k_{\beta\delta}}{b_z})^2} \varphi_{n_{z_a}}(z_1 + k_{\alpha\gamma})\varphi_{n_{z_b}}(z_2 + k_{\beta\delta})$$

$$\begin{cases} k_{\alpha\gamma} = \frac{d_\alpha + d_\gamma}{2} \\ k_{\beta\delta} = \frac{d_\beta + d_\delta}{2} \end{cases} \tag{E.11}$$

We then use the Moshinsky-z coefficients (see Appendix D):

$$I_z = \frac{1}{b_z\sqrt{\pi}} \sum_{n_z a} \sum_{n_z b} T^{n_{z_a}}_{(n_{z_\alpha}, d_\alpha)(n_{z_\gamma}, d_\gamma)} T^{n_{z_b}}_{(n_{z_\beta}, d_\beta)(n_{z_\delta}, d_\delta)} \sum_{n_{z_c}} \sum_{n_z d} M^{n_{z_c} n_{z_d}}_{n_{z_a}, n_{z_b}} \tag{E.12}$$
$$\int\int dz_1 dz_2 e^{-(\vec{z}_1 - \vec{z}_2)^2/\mu_i^2} e^{-\frac{1}{2}(\frac{z_1 + k_{\alpha\gamma}}{b_z})^2} e^{-\frac{1}{2}(\frac{z_2 + k_{\beta\delta}}{b_z})^2} \varphi_{n_{z_c}}(Z + D^{\gamma\delta}_{\alpha\beta})\varphi_{n_{z_d}}(z + d^{\gamma\delta}_{\alpha\beta})$$

$$\begin{cases} Z = \frac{z_0 + z_1}{\sqrt{2}} \\ z = \frac{z_0 - z_1}{\sqrt{2}} \end{cases} \qquad \begin{cases} D^{\gamma\delta}_{\alpha\beta} = \frac{k_{\alpha\gamma} + k_{\beta\delta}}{\sqrt{2}} \\ d^{\gamma\delta}_{\alpha\beta} = \frac{k_{\alpha\gamma} - k_{\beta\delta}}{\sqrt{2}} \end{cases} \tag{E.13}$$

We perform the following change of variable $(z_0, z_1) \longrightarrow (Z, z)$:

$$I_z = \frac{1}{b_z\sqrt{\pi}} \sum_{n_z a} \sum_{n_z b} T^{n_{z_a}}_{(n_{z_\alpha}, d_\alpha)(n_{z_\gamma}, d_\gamma)} T^{n_{z_b}}_{(n_{z_\beta}, d_\beta)(n_{z_\delta}, d_\delta)} \sum_{n_{z_c}} \sum_{n_z d} M^{n_{z_c} n_{z_d}}_{n_{z_a}, n_{z_b}} \tag{E.14}$$
$$\int dZ e^{-\frac{1}{2}(\frac{Z + D^{\gamma\delta}_{\alpha\beta}}{b_z})^2} \varphi_{n_{z_c}}(Z + D^{\gamma\delta}_{\alpha\beta}) \int dz e^{-(\sqrt{2}z)^2/\mu_i^2} e^{-\frac{1}{2}(\frac{z_2 + k_{\beta\delta}}{b_z})^2} \varphi_{n_{z_d}}(z + d^{\gamma\delta}_{\alpha\beta})$$

Due to the orthonormality of the harmonic oscillator wave functions, the Z-integral take a very simple form:

$$\int dZ e^{-\frac{1}{2}(\frac{Z + D^{\gamma\delta}_{\alpha\beta}}{b_z})^2} \varphi_{n_{z_c}}(Z + D^{\gamma\delta}_{\alpha\beta}) = \delta_{0 n_{z_c}} \sqrt{b_z\sqrt{\pi}} \tag{E.15}$$

Inserting Eq.(E.14) in Eq.(E.15) we find:

$$\boxed{\begin{aligned} I_z = \frac{1}{\sqrt{b_z\sqrt{\pi}}} \sum_{n_z a} \sum_{n_z b} T^{n_{z_a}}_{(n_{z_\alpha}, d_\alpha)(n_{z_\gamma}, d_\gamma)} T^{n_{z_b}}_{(n_{z_\beta}, d_\beta)(n_{z_\delta}, d_\delta)} M^{0 n_{z_d}}_{n_{z_a}, n_{z_b}} \\ \int dz e^{-(\sqrt{2}z)^2/\mu_i^2} e^{-\frac{1}{2}(\frac{z_2 + k_{\beta\delta}}{b_z})^2} \varphi_{n_{z_d}}(z + d^{\gamma\delta}_{\alpha\beta}) \end{aligned}} \tag{E.16}$$

The remaining integral requires to use generating functions (see Appendix D). We set:

$$I_{gz} = \int dz e^{-(\sqrt{2}z)^2/\mu_i^2} e^{-\frac{1}{2}(\frac{z_2 + k_{\beta\delta}}{b_z})^2} \varphi_{n_{z_d}}(z + d^{\gamma\delta}_{\alpha\beta}) \tag{E.17}$$

We perform the change of variable $(z) \to (z + d^{\gamma\delta}_{\alpha\beta})$:

$$I_{gz} = \int dz e^{-2(z - d^{\gamma\delta}_{\alpha\beta})^2/\mu_i^2} e^{-\frac{1}{2}(\frac{z}{b_z})^2} \varphi_{n_{z_d}}(z) \tag{E.18}$$

We add the generating functions:

$$\sum_{n_z} \chi_{n_z}(t) I_{gz} = \frac{1}{\sqrt{b_z\sqrt{\pi}}} \int dz e^{-2(z - d^{\gamma\delta}_{\alpha\beta})^2/\mu_i^2} e^{-(\frac{z}{b_z})^2 + 2z\frac{t}{b_z} - t^2} \tag{E.19}$$

We factorize in the exponential:

$$\sum_{n_z} \chi_{n_z}(t) I_{gz} = \frac{1}{\sqrt{b_z\sqrt{\pi}}} e^{-2(d^{\gamma\delta}_{\alpha\beta})^2/\mu_i^2} e^{\frac{(\frac{t}{b_z} + \frac{2d^{\gamma\delta}_{\alpha\beta}}{\mu_i^2})^2}{\frac{2}{\mu_i^2} + \frac{1}{b_z^2}} - t^2} \int dz e^{-(z\sqrt{\frac{2}{\mu_i^2} + \frac{1}{b_z^2}} - \frac{\frac{t}{b_z} + \frac{2d^{\gamma\delta}_{\alpha\beta}}{\mu_i^2}}{\sqrt{\frac{2}{\mu_i^2} + \frac{1}{b_z^2}}})^2} \tag{E.20}$$

Now, we use the change of variable $(z) \longrightarrow (z\sqrt{\frac{2}{\mu_i^2} + \frac{1}{b_z^2}} - \frac{\frac{t}{b_z} + \frac{2d^{\gamma\delta}_{\alpha\beta}}{\mu_i^2}}{\sqrt{\frac{2}{\mu_i^2} + \frac{1}{b_z^2}}})$:

$$\sum_{n_z}\chi_{n_z}(t)I_{gz}=\frac{1}{\sqrt{b_z\sqrt{\pi}}}\frac{1}{\sqrt{\frac{2}{\mu_i^2}+\frac{1}{b_z^2}}}e^{-2(d_{\alpha\beta}^{\gamma\delta})^2/\mu_i^2}e^{\frac{(\frac{t}{b_z}+\frac{2d_{\alpha\beta}^{\gamma\delta}}{\mu_i^2})^2}{\frac{2}{\mu_i^2}+\frac{1}{b_z^2}}-t^2}\int dze^{-z^2} \tag{E.21}$$

We recall the well-known result:

$$\int dze^{-z^2}=\sqrt{\pi} \tag{E.22}$$

Introducing Eq.(E.22) into Eq.(E.21), we obtain:

$$\sum_{n_z}\chi_{n_z}(t)I_{gz}=\sqrt{\frac{\sqrt{\pi}}{b_z}}\frac{1}{\sqrt{\frac{2}{\mu_i^2}+\frac{1}{b_z^2}}}e^{-2(d_{\alpha\beta}^{\gamma\delta})^2/\mu_i^2}e^{\frac{(\frac{t}{b_z}+\frac{2d_{\alpha\beta}^{\gamma\delta}}{\mu_i^2})^2}{\frac{2}{\mu_i^2}+\frac{1}{b_z^2}}-t^2} \tag{E.23}$$

We factorize again in the exponential:

$$\sum_{n_z}\chi_{n_z}(t)I_{gz}=\sqrt{\frac{\sqrt{\pi}}{b_z}}\frac{\mu_i}{\sqrt{2K_z}}e^{-2(d_{\alpha\beta}^{\gamma\delta})^2/\mu_i^2}e^{\frac{2(d_{\alpha\beta}^{\gamma\delta})^2}{\mu_i^2K_z}+\frac{1}{2}\frac{(d_{\alpha\beta}^{\gamma\delta})^2}{b_z^2K_z}}e^{-(\frac{t}{\sqrt{K_z}})^2+2(\frac{t}{\sqrt{K_z}})(\frac{d_{\alpha\beta}^{\gamma\delta}}{b_z\sqrt{K_z}})-\frac{1}{2}\frac{(d_{\alpha\beta}^{\gamma\delta})^2}{b_z^2K_z}} \tag{E.24}$$

With:

$$K_z=\frac{2b_z^2+\mu_i^2}{2b_z^2} \tag{E.25}$$

Now, we can go back to the generating functions:

$$\sum_{n_z}\chi_{n_z}(t)I_{gz}=\frac{\sqrt{\pi}\mu_i}{\sqrt{2K_z}}e^{-2(d_{\alpha\beta}^{\gamma\delta})^2/\mu_i^2}e^{\frac{2(d_{\alpha\beta}^{\gamma\delta})^2}{\mu_i^2K_z}+\frac{1}{2}\frac{(d_{\alpha\beta}^{\gamma\delta})^2}{b_z^2K_z}}\sum_{n_z}\chi_{n_z}(\frac{t}{\sqrt{K_z}})\varphi_{n_z}(\frac{d_{\alpha\beta}^{\gamma\delta}}{\sqrt{K_z}},b_z) \tag{E.26}$$

Then, we rescale the generating functions:

$$\sum_{n_z}\chi_{n_z}(t)I_{gz}=\frac{\sqrt{\pi}\mu_i}{\sqrt{2K_z}}e^{-2(d_{\alpha\beta}^{\gamma\delta})^2/\mu_i^2}e^{\frac{2(d_{\alpha\beta}^{\gamma\delta})^2}{\mu_i^2K_z}+\frac{1}{2}\frac{(d_{\alpha\beta}^{\gamma\delta})^2}{b_z^2K_z}}\sum_{n_z}\frac{1}{\sqrt{K_z}^{n_z}}\chi_{n_z}(t)\varphi_{n_z}(\frac{d_{\alpha\beta}^{\gamma\delta}}{\sqrt{K_z}},b_z) \tag{E.27}$$

It becomes possible to identify I_{gz}:

$$\boxed{I_{gz}=\mu_i\sqrt{\frac{\pi}{2}}\frac{e^{-\frac{(d_{\alpha\beta}^{\gamma\delta})^2}{2b_z^2K_z}}}{\sqrt{K_z}^{n_{z_d}+1}}\varphi_{n_{z_d}}(\frac{d_{\alpha\beta}^{\gamma\delta}}{\sqrt{K_z}},b_z)} \tag{E.28}$$

We can finally write:

$$\boxed{I_z = \frac{\mu_i \pi^{1/4}}{\sqrt{2b_z}} e^{-\frac{(d^{\gamma\delta}_{\alpha\beta})^2}{2b_z^2 K_z}} \sum_{n_z a} \sum_{n_z b} T^{n_{z_a}}_{(n_{z_\alpha},d_\alpha)(n_{z_\gamma},d_\gamma)} T^{n_{z_b}}_{(n_{z_\beta},d_\beta)(n_{z_\delta},d_\delta)} M^{0n_{z_d}}_{n_{z_a},n_{z_b}} \frac{1}{\sqrt{K_z}^{n_{z_d}+1}} \varphi_{n_{z_d}}(\frac{d^{\gamma\delta}_{\alpha\beta}}{\sqrt{K_z}}, b_z)} \quad \text{(E.29)}$$

This expression is factorized one more time using the J coefficients to give the expression used in the HFB3 code:

$$\boxed{I_z = \sum_{n_z a} T^{n_{z_a}}_{(n_{z_\alpha},d_\alpha)(n_{z_\gamma},d_\gamma)} J^{n_{z_a}}_{(n_{z_\beta},d_\beta)(n_{z_\delta},d_\delta)(d_\alpha,d_\gamma)}} \quad \text{(E.30)}$$

With:

$$J^{n_{z_a}}_{(n_{z_\beta},d_\beta)(n_{z_\delta},d_\delta)(d_\alpha,d_\gamma)} = \frac{\mu_i \pi^{1/4}}{\sqrt{2b_z}} e^{-\frac{(d^{\gamma\delta}_{\alpha\beta})^2}{2b_z^2 K_z}} \sum_{n_z b} T^{n_{z_b}}_{(n_{z_\beta},d_\beta)(n_{z_\delta},d_\delta)} M^{0n_{z_d}}_{n_{z_a},n_{z_b}} \frac{1}{\sqrt{K_z}^{n_{z_d}+1}} \varphi_{n_{z_d}}(\frac{d^{\gamma\delta}_{\alpha\beta}}{\sqrt{K_z}}, b_z) \quad \text{(E.31)}$$

Calculation of the $\vec{r}_\perp$-integral:

The goal here is to evaluate the following quantity:

$$I_r = \int\int d\vec{r}_{\perp_1} d\vec{r}_{\perp_2} e^{-(r_{\perp_1}-r_{\perp_2})^2/\mu_i^2} \phi^*_\alpha(\vec{r}_{\perp_1}) \phi^*_\beta(\vec{r}_{\perp_2}) \phi_\gamma(\vec{r}_{\perp_1}) \phi_\delta(\vec{r}_{\perp_2}) \quad \text{(E.32)}$$

We start using the Talman-r coefficients (see Appendix D):

$$I_r = \frac{1}{b_r^2 \pi} \sum_{n_{\perp a}} \sum_{n_{\perp b}} T^{n_{\perp_a}}_{(m_\alpha,n_{\perp\alpha})(m_\gamma,n_{\perp\gamma})} T^{n_{\perp_b}}_{(m_\beta,n_{\perp\beta})(m_\delta,n_{\perp\delta})} \int d\vec{r}_{\perp_2} e^{-\frac{1}{2}(\frac{r_{\perp_2}}{b_r})^2} \phi_{(m_b,n_{\perp_b})}(\vec{r}_{\perp_2}) \quad \text{(E.33)}$$
$$\int d\vec{r}_{\perp_1} e^{-(\vec{r}_{\perp_1}-\vec{r}_{\perp_2})^2/\mu_i^2} e^{-\frac{1}{2}(\frac{r_{\perp_1}}{b_r})^2} \phi_{(m_a,n_{\perp_a})}(\vec{r}_{\perp_1})$$

We will have to use the generating functions to tackle the last integral. We set:

$$I_{gr} = \int d\vec{r}_{\perp_1} e^{-(\vec{r}_{\perp_1}-\vec{r}_{\perp_2})^2/\mu_i^2} e^{-\frac{1}{2}(\frac{r_{\perp_1}}{b_r})^2} \phi_{(m_a,n_{\perp_a})}(\vec{r}_{\perp_1}) \quad \text{(E.34)}$$

We add the generating functions:

$$\sum_{(m,n_\perp)} \chi^*_{(m,n_\perp)}(\vec{t}) I_{gr} = \frac{1}{b_r\sqrt{\pi}} \int d\vec{r}_{\perp_1} e^{-(\vec{r}_{\perp_1}-\vec{r}_{\perp_2})^2/\mu_i^2} e^{-(\frac{\vec{r}_{\perp_1}}{b_r})^2 + 2\frac{\vec{r}_{\perp_1}}{b_r}.\vec{t} - \vec{t}^2} \quad \text{(E.35)}$$

We factorize in the exponential:

$$\sum_{(m,n_\perp)} \chi^*_{(m,n_\perp)}(\vec{t}) I_{gr} = \frac{1}{b_r\sqrt{\pi}} e^{-\frac{\vec{r}_{\perp_2}^2}{\mu_i^2}} e^{\frac{(\frac{\vec{t}}{b_r}+\frac{\vec{r}_{\perp_2}}{\mu_i^2})^2}{\frac{1}{\mu_i^2}+\frac{1}{b_r^2}} - \vec{t}^2} \int d\vec{r}_{\perp_1} e^{-(\vec{r}_{\perp_1}\sqrt{\frac{1}{\mu_i^2}+\frac{1}{b_r^2}} - \frac{\frac{\vec{t}}{b_r}+\frac{\vec{r}_{\perp_2}}{\mu_i^2}}{\sqrt{\frac{1}{\mu_i^2}+\frac{1}{b_r^2}}})^2} \quad \text{(E.36)}$$

We perform the change of variable $(\vec{r}_{\perp_1}) \longrightarrow (\vec{r}_{\perp_1}\sqrt{\frac{1}{\mu_i^2}+\frac{1}{b_r^2}} - \frac{\frac{\vec{t}}{b_r}+\frac{\vec{r}_{\perp_2}}{\mu_i^2}}{\sqrt{\frac{1}{\mu_i^2}+\frac{1}{b_r^2}}})$:

$$\sum_{(m,n_\perp)} \chi^*_{(m,n_\perp)}(\vec{t}) I_{gr} = \frac{1}{b_r\sqrt{\pi}} \frac{1}{\frac{1}{\mu_i^2}+\frac{1}{b_r^2}} e^{-\frac{\vec{r}_{\perp_2}^2}{\mu_i^2}} e^{\frac{(\frac{\vec{t}}{b_r}+\frac{\vec{r}_{\perp_2}}{\mu_i^2})^2}{\frac{1}{\mu_i^2}+\frac{1}{b_r^2}} - \vec{t}^2} \int d\vec{r}_{\perp_1} e^{-\vec{r}_{\perp_1}^2} \tag{E.37}$$

We recall the well-known result:

$$\int d\vec{r}_{\perp_1} e^{-\vec{r}_{\perp_1}^2} = \int_0^{+\infty} r dr e^{-r^2} \int_0^{2\pi} d\theta = \pi \tag{E.38}$$

Then, inserting Eq.$(E.38)$ into Eq.$(E.37)$ leads to:

$$\sum_{(m,n_\perp)} \chi^*_{(m,n_\perp)}(\vec{t}) I_{gr} = \frac{\sqrt{\pi}}{b_r} \frac{1}{\frac{1}{\mu_i^2}+\frac{1}{b_r^2}} e^{-\frac{\vec{r}_{\perp_2}^2}{\mu_i^2}} e^{\frac{(\frac{\vec{t}}{b_r}+\frac{\vec{r}_{\perp_2}}{\mu_i^2})^2}{\frac{1}{\mu_i^2}+\frac{1}{b_r^2}} - \vec{t}^2} \tag{E.39}$$

We factorize in the exponential again:

$$\sum_{(m,n_\perp)} \chi^*_{(m,n_\perp)}(\vec{t}) I_{gr} = \frac{\sqrt{\pi}}{b_r} \frac{\mu_i^2}{K_r} e^{-(\frac{\vec{t}}{\sqrt{K_r}})^2 + 2\frac{\vec{t}}{\sqrt{K_r}} \frac{\vec{r}_{\perp_2}}{b_r\sqrt{K_r}} - \frac{1}{2}\frac{\vec{r}_{\perp_2}^2}{b_r^2 K_r}} e^{-\frac{1}{2}\frac{\vec{r}_{\perp_2}^2}{b_r^2 K_r}} \tag{E.40}$$

$$K_r = \frac{b_r^2+\mu_i^2}{b_r^2} \tag{E.41}$$

We can go back to the generating functions:

$$\sum_{(m,n_\perp)} \chi^*_{(m,n_\perp)}(\vec{t}) I_{gr} = \frac{\pi\mu_i^2}{\sqrt{K_r}} e^{-\frac{1}{2}\frac{\vec{r}_{\perp_2}^2}{b_r^2 K_r}} \sum_{(m,n_\perp)} \chi^*_{(m,n_\perp)}(\frac{\vec{t}}{\sqrt{K_r}}) \phi_{(m,n_\perp)}(\vec{r}_{\perp_2}, b_r\sqrt{K_r}) \tag{E.42}$$

Then, we rescale the generating functions:

$$\sum_{(m,n_\perp)} \chi^*_{(m,n_\perp)}(\vec{t}) I_{gr} = \frac{\pi\mu_i^2}{\sqrt{K_r}} e^{-\frac{1}{2}\frac{\vec{r}_{\perp_2}^2}{b_r^2 K_r}} \sum_{(m,n_\perp)} \frac{1}{\sqrt{K_r}^{2n_\perp+|m|}} \chi^*_{(m,n_\perp)}(\vec{t}) \phi_{(m,n_\perp)}(\vec{r}_{\perp_2}, b_r\sqrt{K_r}) \tag{E.43}$$

We can now identify I_{gr}:

$$\boxed{I_{gr} = \frac{\pi\mu_i^2}{\sqrt{K_r}^{2n_{\perp_a}+|m_a|+1}} e^{-\frac{1}{2}\frac{\vec{r}_{\perp_2}^2}{b_r^2 K_r}} \phi_{(m_a,n_{\perp_a})}(\vec{r}_{\perp_2}, b_r\sqrt{K_r})} \tag{E.44}$$

We inject Eq.$(E.44)$ into Eq.$(E.32)$:

$$I_r = \frac{\mu_i^2}{b_r^2} \sum_{n_{\perp_a}} \sum_{n_{\perp_b}} T^{n_{\perp_a}}_{(m_\alpha, n_{\perp_\alpha})(m_\gamma, n_{\perp_\gamma})} T^{n_{\perp_b}}_{(m_\beta, n_{\perp_\beta})(m_\delta, n_{\perp_\delta})} \frac{1}{\sqrt{K_r}^{2n_{\perp_a}+|m_a|+1}} \tag{E.45}$$
$$\int d\vec{r}_{\perp_2} e^{-\frac{1}{2}\vec{r}^2_{\perp_2}(\frac{1}{b_r^2}+\frac{1}{b_r^2 K_r})} \phi_{(m_b, n_{\perp_b})}(\vec{r}_{\perp_2}, b_r) \phi_{(m_a, n_{\perp_a})}(\vec{r}_{\perp_2}, b_r\sqrt{K_r})$$

We now use the Moschinsky-r coefficients (see Appendix D):

$$I_r = \frac{\mu_i^2}{b_r^2} \sum_{n_{\perp_a}} \sum_{n_{\perp_b}} T^{n_{\perp_a}}_{(m_\alpha, n_{\perp_\alpha})(m_\gamma, n_{\perp_\gamma})} T^{n_{\perp_b}}_{(m_\beta, n_{\perp_\beta})(m_\delta, n_{\perp_\delta})} \frac{1}{\sqrt{K_r}^{2n_{\perp_a}+|m_a|+1}} \tag{E.46}$$
$$\sum_{(m_c, n_{\perp_c})} \sum_{(m_d, n_{\perp_d})} M^{(m_c, n_{\perp_c})(m_d, n_{\perp_d})}_{(m_a, n_{\perp_a})(m_b, n_{\perp_b})}(b_r\sqrt{K_r}, b_r) \phi_{(m_d, n_{\perp_d})}(0, b_r\sqrt{\frac{1+K_r}{2}})$$
$$\int d\vec{r}_{\perp_2} e^{-\frac{1}{2}(\sqrt{2}\vec{r}_{\perp_2})^2(\frac{\sqrt{1+K_r}}{b_r\sqrt{2K_r}})^2} \phi_{(m_c, n_{\perp_c})}(\sqrt{2}\vec{r}_{\perp_2}, b_r\frac{\sqrt{2K_r}}{\sqrt{1+K_r}})$$

We know from the harmonic oscillator wave functions properties that:

$$\phi_{(m_d, n_{\perp_d})}(0, b_r\sqrt{\frac{1+K_r}{2}}) = \frac{\sqrt{2}}{b_r\sqrt{\pi(1+K_r)}} \tag{E.47}$$

$$\int d\vec{r}_{\perp_2} e^{-\frac{1}{2}(\sqrt{2}\vec{r}_{\perp_2})^2(\frac{\sqrt{1+K_r}}{b_r\sqrt{2K_r}})^2} \phi_{(m_c, n_{\perp_c})}(\sqrt{2}\vec{r}_{\perp_2}, b_r\frac{\sqrt{2K_r}}{\sqrt{1+K_r}}) = \delta_{0,n_{\perp_c}}\delta_{0,m_c}\frac{b_r\sqrt{\pi}}{2}\frac{\sqrt{2K_r}}{\sqrt{1+K_r}} \tag{E.48}$$

Both Eq.(E.47) and Eq.(E.48) are used in Eq.(E.46):

$$I_r = \frac{\mu_i^2}{b_r^2(1+K_r)} \sum_{n_{\perp_a}} \sum_{n_{\perp_b}} T^{n_{\perp_a}}_{(m_\alpha, n_{\perp_\alpha})(m_\gamma, n_{\perp_\gamma})} T^{n_{\perp_b}}_{(m_\beta, n_{\perp_\beta})(m_\delta, n_{\perp_\delta})} \tag{E.49}$$
$$\frac{1}{\sqrt{K_r}^{2n_{\perp_a}+|m_a|}} M^{(0,0)(0,n_{\perp_d})}_{(m_a, n_{\perp_a})(m_b, n_{\perp_b})}(b_r\sqrt{K_r}, b_r)$$

We recall the following property of the Moshinsky-r coefficients:

$$\frac{1}{\sqrt{K_r}^{2n_{\perp_a}+|m_a|}} M^{(0,0)(0,n_{\perp_d})}_{(m_a, n_{\perp_a})(m_b, n_{\perp_b})}(b_r\sqrt{K_r}, b_r) = \delta_{(m_a, -m_b)}(\frac{2}{2+\frac{\mu_i^2}{b_r^2}})^{n_{\perp_a}+n_{\perp_b}+|m_a|} M^{(0,0)(0,n_{\perp_d})}_{(m_a, n_{\perp_a})(m_b, n_{\perp_b})} \tag{E.50}$$

Using Eq.(E.50) we finally write:

$$\boxed{I_r = \delta_{(m_\alpha+m_\beta, m_\gamma+m_\delta)} \frac{\mu_i^2}{b_r^2(1+K_r)} \sum_{n_{\perp_a}} \sum_{n_{\perp_b}} T^{n_{\perp_a}}_{(m_\alpha, n_{\perp_\alpha})(m_\gamma, n_{\perp_\gamma})} T^{n_{\perp_b}}_{(m_\beta, n_{\perp_\beta})(m_\delta, n_{\perp_\delta})} (\frac{2}{2+\frac{\mu_i^2}{b_r^2}})^{n_{\perp_a}+n_{\perp_b}+|m_a|} M^{(0,0)(0,n_{\perp_d})}_{(m_a, n_{\perp_a})(m_b, n_{\perp_b})}} \tag{E.51}$$

As for the z-integral, we set J coefficients to end up with the formula used in the HFB3 solver:

$$\boxed{I_r = \delta_{(m_\alpha+m_\beta,m_\gamma+m_\delta)} \sum_{n_{\perp a}} \sum_{n_{\perp b}} T^{n_{\perp a}}_{(m_\alpha,n_{\perp\alpha})(m_\gamma,n_{\perp\gamma})} J^{n_{\perp a}}_{(m_\beta,n_{\perp\beta})(m_\delta,n_{\perp\delta})}} \tag{E.52}$$

With:

$$J^{n_{\perp a}}_{(m_\beta,n_{\perp\beta})(m_\delta,n_{\perp\delta})} = \frac{\mu_i^2}{b_r^2(1+K_r)} \sum_{n_{\perp b}} T^{n_{\perp b}}_{(m_\beta,n_{\perp\beta})(m_\delta,n_{\perp\delta})} \left(\frac{2}{2+\frac{\mu_i^2}{b_r^2}}\right)^{n_{\perp a}+n_{\perp b}+|m_a|} M^{(0,0)(0,n_{\perp d})}_{(m_a,n_{\perp a})(m_b,n_{\perp b})} \tag{E.53}$$

E.1.2 Different bases

Here, we want to find an analytic expression for the following term:

$$\bar{E}^{(i)\gamma\delta}_{\alpha\beta} = {}_0\langle\alpha\beta|e^{-(|\vec{r}_1-\vec{r}_2|)^2/\mu_i^2}|\gamma\delta\rangle_1 \tag{E.54}$$

We rewrite it as an integral:

$$\bar{E}^{(i)\gamma\delta}_{\alpha\beta} = \int\int d\vec{r}_1 d\vec{r}_2 e^{-(|\vec{r}_1-\vec{r}_2|)^2/\mu_i^2} \psi^*_\alpha(\vec{r}_1,b_0)\psi^*_\beta(\vec{r}_2,b_0)\psi_\gamma(\vec{r}_1,b_1)\psi_\delta(\vec{r}_2,b_1) \tag{E.55}$$

As for Eq.(E.8) this integral is separated with respect to $\vec{r}_\perp$ and z:

$$\boxed{\begin{aligned}\bar{E}^{(i)\gamma\delta}_{\alpha\beta} = \int\int d\vec{r}_{\perp_1} d\vec{r}_{\perp_2} e^{-(r_{\perp_1}-r_{\perp_2})^2/\mu_i^2} \phi^*_\alpha(\vec{r}_{\perp_1},b_{r_0})\phi^*_\beta(\vec{r}_{\perp_2},b_{r_0})\phi_\gamma(\vec{r}_{\perp_1},b_{r_1})\phi_\delta(\vec{r}_{\perp_2},b_{r_1}) \\ \int\int dz_1 dz_2 e^{-(\vec{z}_1-\vec{z}_2)^2/\mu_i^2} \varphi_{n_{z_\alpha}}(z+d_\alpha,b_{z_0})\varphi_{n_{z_\beta}}(z+d_\beta,b_{z_0})\varphi_{n_{z_\gamma}}(z+d_\gamma,b_{z_1})\varphi_{n_{z_\delta}}(z+d_\delta,b_{z_1})\end{aligned}} \tag{E.56}$$

Calculation of the z-integral:

The goals is to evaluate the integral:

$$\begin{aligned}\bar{I}_z = \int\int dz_1 dz_2 e^{-(z_1-z_2)^2/\mu_i^2} \varphi_{n_{z_\alpha}}(z_1+d_\alpha,b_{z_0})\varphi_{n_{z_\beta}}(z_2+d_\beta,b_{z_0}) \\ \varphi_{n_{z_\gamma}}(z_1+d_\gamma,b_{z_1})\varphi_{n_{z_\delta}}(z_2+d_\delta,b_{z_1})\end{aligned} \tag{E.57}$$

We start by using the generalyzed Talman-z coefficients (see Appendix D):

$$\begin{aligned}\bar{I}_z = \frac{1}{B_z\sqrt{\pi}} \sum_{n_{za}} \sum_{n_{z_b}} \bar{T}^{n_{za}}_{(n_{z_\alpha},d_\alpha)(n_{z_\gamma},d_\gamma)} \bar{T}^{n_{z_b}}_{(n_{z_\beta},d_\beta)(n_{z_\delta},d_\delta)} \int\int dz_1 dz_2 e^{-(\vec{z}_1-\vec{z}_2)^2/\mu_i^2} \\ e^{-\frac{1}{2}(\frac{z_1+d_{\alpha\gamma}}{B_z})^2} e^{-\frac{1}{2}(\frac{z_2+d_{\beta\delta}}{B_z})^2} \varphi_{n_{z_a}}(z_1+d_{\alpha\gamma},B_z)\varphi_{n_{z_b}}(z_2+d_{\beta\delta},B_z)\end{aligned} \tag{E.58}$$

With:

$$\begin{cases} B_z = \sqrt{\frac{2b_{z_0}^2 b_{z_1}^2}{b_{z_0}^2+b_{z_1}^2}} \\ d_{\alpha\gamma} = \frac{b_{z_1}^2 d_\alpha + b_{z_0}^2 d_\gamma}{b_{z_1}^2+b_{z_0}^2} \end{cases} \tag{E.59}$$

We observe that this expression is formally equivalent to the one of Eq.(E.10). We therefore directly write:

$$\boxed{\begin{aligned} \bar{I}_z = \frac{\mu_i \pi^{1/4}}{\sqrt{2B_z}} e^{-\frac{(\bar{d}_{\alpha\beta}^{\gamma\delta})^2}{2B_z^2 K_z}} \sum_{n_{z_a}} \sum_{n_{z_b}} \bar{T}^{n_{z_a}}_{(n_{z_\alpha},d_\alpha)(n_{z_\gamma},d_\gamma)} \bar{T}^{n_{z_b}}_{(n_{z_\beta},d_\beta)(n_{z_\delta},d_\delta)} \\ M^{0 n_{z_d}}_{n_{z_a},n_{z_b}} \frac{1}{\sqrt{K_z}^{n_{z_d}+1}} \varphi_{n_{z_d}}(\frac{\bar{d}_{\alpha\beta}^{\gamma\delta}}{\sqrt{K_z}}, B_z) \end{aligned}} \tag{E.60}$$

With:

$$\bar{d}_{\alpha\beta}^{\gamma\delta} = \frac{d_{\alpha\gamma} - d_{\beta\delta}}{\sqrt{2}} \tag{E.61}$$

Factorizing with the $\bar{J}$ coefficients we find the expression used in practice in the SCIM:

$$\boxed{\bar{I}_z = \sum_{n_{z_a}} \bar{T}^{n_{z_a}}_{(n_{z_\alpha},d_\alpha)(n_{z_\gamma},d_\gamma)} \bar{J}^{n_{z_a}}_{(n_{z_\beta},d_\beta)(n_{z_\delta},d_\delta)(d_\alpha,d_\gamma)}} \tag{E.62}$$

With:

$$\bar{J}^{n_{z_a}}_{(n_{z_\beta},d_\beta)(n_{z_\delta},d_\delta)(d_\alpha,d_\gamma)} = \frac{\mu_i \pi^{1/4}}{\sqrt{2B_z}} e^{-\frac{(\bar{d}_{\alpha\beta}^{\gamma\delta})^2}{2B_z^2 K_z}} \sum_{n_{z_b}} \bar{T}^{n_{z_b}}_{(n_{z_\beta},d_\beta)(n_{z_\delta},d_\delta)} M^{0 n_{z_d}}_{n_{z_a},n_{z_b}} \frac{1}{\sqrt{K_z}^{n_{z_d}+1}} \varphi_{n_{z_d}}(\frac{\bar{d}_{\alpha\beta}^{\gamma\delta}}{\sqrt{K_z}}, B_z) \tag{E.63}$$

Calculation of the $\vec{r}_\perp$-integral:

We want to find a formula for the following expression :

$$\bar{I}_r = \int\int d\vec{r}_{\perp_1} d\vec{r}_{\perp_2} e^{-(r_{\perp_1}-r_{\perp_2})^2/\mu_i^2} \phi_\alpha^*(\vec{r}_{\perp_1}, b_{r_0}) \phi_\beta^*(\vec{r}_{\perp_2}, b_{r_0}) \phi_\gamma(\vec{r}_{\perp_1}, b_{r_1}) \phi_\delta(\vec{r}_{\perp_2}, b_{r_1}) \tag{E.64}$$

We start using the generalyzed Talman-r coefficients:

$$\begin{aligned} \bar{I}_r = \frac{1}{B_r^2 \pi} \sum_{n_{\perp_a}} \sum_{n_{\perp_b}} \bar{T}^{n_{\perp_a}}_{(m_\alpha,n_{\perp_\alpha})(m_\gamma,n_{\perp_\gamma})} \bar{T}^{n_{\perp_b}}_{(m_\beta,n_{\perp_\beta})(m_\delta,n_{\perp_\delta})} \int d\vec{r}_{\perp_2} e^{-\frac{1}{2}(\frac{r_{\perp_2}}{B_r})^2} \phi_{(m_b,n_{\perp_b})}(\vec{r}_{\perp_2}, B_r) \\ \int d\vec{r}_{\perp_1} e^{-(\vec{r}_{\perp_1}-\vec{r}_{\perp_2})^2/\mu_i^2} e^{-\frac{1}{2}(\frac{r_{\perp_1}}{B_r})^2} \phi_{(m_a,n_{\perp_a})}(\vec{r}_{\perp_1}, B_r) \end{aligned} \tag{E.65}$$

With:

$$B_r = \sqrt{\frac{2b_{r_0}^2 b_{r_1}^2}{b_{r_0}^2 + b_{r_1}^2}} \tag{E.66}$$

As for the z-integral case, this formulation is now equivalent to the one of Eq.($E.33$). We can therefore directly write:

$$\boxed{\bar{I}_r = \delta_{(m_\alpha+m_\beta,m_\gamma+m_\delta)} \frac{\mu_i^2}{B_r^2(1+K_r)} \sum_{n_{\perp_a}} \sum_{n_{\perp_b}} \bar{T}^{n_{\perp_a}}_{(m_\alpha,n_{\perp_\alpha})(m_\gamma,n_{\perp_\gamma})} \bar{T}^{n_{\perp_b}}_{(m_\beta,n_{\perp_\beta})(m_\delta,n_{\perp_\delta})} \left(\frac{2}{2+\frac{\mu_i^2}{B_r^2}}\right)^{n_{\perp_a}+n_{\perp_b}+|m_a|} M^{(0,0)(0,n_{\perp_d})}_{(m_a,n_{\perp_a})(m_b,n_{\perp_b})}} \tag{E.67}$$

Introducing the $\bar{J}$ coefficients, we finally find the expression used in the SCIM code:

$$\boxed{\bar{I}_r = \delta_{(m_\alpha+m_\beta,m_\gamma+m_\delta)} \sum_{n_{\perp_a}} \sum_{n_{\perp_b}} \bar{T}^{n_{\perp_a}}_{(m_\alpha,n_{\perp_\alpha})(m_\gamma,n_{\perp_\gamma})} \bar{J}^{n_{\perp_a}}_{(m_\beta,n_{\perp_\beta})(m_\delta,n_{\perp_\delta})}} \tag{E.68}$$

With:

$$\bar{J}^{n_{\perp_a}}_{(m_\beta,n_{\perp_\beta})(m_\delta,n_{\perp_\delta})} = \frac{\mu_i^2}{B_r^2(1+K_r)} \sum_{n_{\perp_b}} \bar{T}^{n_{\perp_b}}_{(m_\beta,n_{\perp_\beta})(m_\delta,n_{\perp_\delta})} \left(\frac{2}{2+\frac{\mu_i^2}{B_r^2}}\right)^{n_{\perp_a}+n_{\perp_b}+|m_a|} M^{(0,0)(0,n_{\perp_d})}_{(m_a,n_{\perp_a})(m_b,n_{\perp_b})} \tag{E.69}$$

E.2 HFB fields

In this part, the direct mean field, exchange mean field and pairing field are derived in great details. Thoses derivations are the one used in the HFB3 code.

E.2.1 Direct mean field

The central part of the direct mean field reads:

$$\Gamma_{\alpha\gamma}(D) = \sum_{\beta\delta} \langle\alpha\beta|V^{(Ctrl)}|\gamma\delta\rangle \rho_{\delta\beta} \tag{E.70}$$

We use the time-reversal properties of ρ:

$$\Gamma_{\alpha\gamma}(D) = \sum_{\beta\delta>} [\langle\alpha\beta|V^{(Ctrl)}|\gamma\delta\rangle + (-1)^{s_\delta - s_\beta} \langle\alpha\bar{\beta}|V^{(Ctrl)}|\gamma\bar{\delta}\rangle] \rho_{\delta\beta} \tag{E.71}$$

We separate the spatial part and the spin-isospin one:

$$\Gamma_{\alpha\gamma}(D) = \sum_{\beta\delta>} \sum_{i=1}^{2} [E^{(i)\gamma\delta}_{\alpha\beta} . S^{(i)\gamma\delta}_{\alpha\beta} + (-1)^{s_\delta - s_\beta} E^{(i)\gamma\bar{\delta}}_{\alpha\bar{\beta}} . S^{(i)\gamma\bar{\delta}}_{\alpha\bar{\beta}}] \rho_{\delta\beta} \tag{E.72}$$

It is then easy to see that:

$$E^{(i)\gamma\bar{\delta}}_{\alpha\bar{\beta}} = E^{(i)\gamma\beta}_{\alpha\delta} \tag{E.73}$$

Using Eq.($E.73$), we use the symmetry of the density matrix to write:

$$\boxed{\Gamma_{\alpha\gamma}(D) = \sum_{\beta\delta>}\sum_{i=1}^{2} E^{(i)\gamma\delta}_{\alpha\beta}.[S^{(i)\gamma\delta}_{\alpha\beta} + (-1)^{s_\delta - s_\beta} S^{(i)\gamma\bar{\beta}}_{\alpha\bar{\delta}}]\rho_{\delta\beta}} \tag{E.74}$$

In the following, we will explicitly consider the spins of α and γ.

Block ++:

In this part, we consider $(\alpha\uparrow, \gamma\uparrow)$. We start by investigating the spin-isospin part:

$$\begin{cases} (S^{(i)\gamma\delta}_{\alpha\beta})^{++} = \delta_{s_\beta s_\delta}[W_i - \delta_{\tau\tau'}H_i] + \delta_{s_{\beta+}s_{\delta+}}[B_i - \delta_{\tau\tau'}M_i] \\ (S^{(i)\gamma\bar{\beta}}_{\alpha\bar{\delta}})^{++} = \delta_{s_\beta s_\delta}[W_i - \delta_{\tau\tau'}H_i] + \delta_{s_{\beta-}s_{\delta-}}[B_i - \delta_{\tau\tau'}M_i] \end{cases} \tag{E.75}$$

Here $\delta_{\tau\tau'}$ means that the density matrix has to have the same isospin as the direct mean field matrix. Then, we can write with Eq.($E.75$):

$$\begin{aligned} \Gamma^{\tau++}_{\alpha\gamma}(D) = \sum_{\beta\delta>}\sum_{i=1}^{2} E^{(i)\gamma\delta}_{\alpha\beta}[[2(W_i - H_i) + B_i - M_i](\rho^{\tau++}_{\delta\beta} + \rho^{\tau--}_{\delta\beta}) \\ +[2W_i + B_i](\rho^{\bar{\tau}++}_{\delta\beta} + \rho^{\bar{\tau}--}_{\delta\bar{\beta}})] \end{aligned} \tag{E.76}$$

It can be transformed into a more compact form:

$$\Gamma^{\tau++}_{\alpha\gamma}(D) = \sum_{\beta\delta>}\sum_{i=1}^{2} E^{(i)\gamma\delta}_{\alpha\beta} R^{(i)\tau++}_{\delta\beta}(D) \tag{E.77}$$

$$R^{(i)\tau++}_{\delta\beta}(D) = [2(W_i - H_i) + B_i - M_i](\rho^{\tau++}_{\delta\beta} + \rho^{\tau--}_{\delta\beta}) + [2W_i + B_i](\rho^{\bar{\tau}++}_{\delta\beta} + \rho^{\bar{\tau}--}_{\delta\bar{\beta}}) \tag{E.78}$$

To conclude, we explicitly write the spatial part:

$$\boxed{\Gamma^{\tau++}_{\alpha\gamma}(D) = \sum_{\beta\delta>}\sum_{i=1}^{2} (I^{(i)}_r)^{\gamma\delta}_{\alpha\beta}(I^{(i)}_z)^{\gamma\delta}_{\alpha\beta} R^{(i)\tau++}_{\delta\beta}(D)} \tag{E.79}$$

Block −−:

Here we consider the spins $(\alpha\downarrow, \gamma\downarrow)$. We observe that the central part of the direct mean field is invariant under the spin change $(\uparrow,\uparrow) \to (\downarrow,\downarrow)$. This property is straightforward looking at the R matrix defined in Eq.($E.78$). We thus have:

$$\boxed{\Gamma^{\tau--}_{\alpha\gamma}(D) = \Gamma^{\tau++}_{\alpha\gamma}(D)}$$

Block $-+$:

Here we consider the spins $(\alpha\downarrow, \gamma\uparrow)$. We start with the spin-isospin part:

$$\begin{cases} (S^{(i)\gamma\delta}_{\alpha\beta})^{-+} = \delta_{s_{\beta^+}s_{\delta^-}}[B_i - \delta_{\tau\tau'}M_i] \\ (-1)^{s_\delta - s_\beta}(S^{(i)\delta\bar{\beta}}_{\alpha\bar{\delta}})^{-+} = -\delta_{s_{\beta^+}s_{\delta^-}}[B_i - \delta_{\tau\tau'}M_i] \end{cases} \tag{E.80}$$

Injected in Eq.$(E.74)$, it directly implies that :

$$\boxed{\Gamma^{\tau-+}_{\alpha\gamma}(D) = 0} \tag{E.81}$$

Block $+-$:

Here we consider the spins $(\alpha\uparrow, \gamma\downarrow)$. Symmetry arguments directly give:

$$\boxed{\Gamma^{+-}_{\alpha\gamma}(D) = 0} \tag{E.82}$$

E.2.2 Exchange mean field

The central part of the exchange mean field take the following form:

$$\Gamma_{\alpha\gamma}(E) = -\sum_{\beta\delta}\langle\alpha\beta|V^{(Ctrl)}|\delta\gamma\rangle\rho_{\delta\beta} \tag{E.83}$$

We first use the time-reversal properties of ρ:

$$\Gamma_{\alpha\gamma}(E) = -\sum_{\beta\delta>}[\langle\alpha\beta|V^{(Ctrl)}|\delta\gamma\rangle + (-1)^{s_\delta - s_\beta}\langle\alpha\bar{\beta}|V^{(ctrl)}|\bar{\delta}\gamma\rangle]\rho_{\delta\beta} \tag{E.84}$$

We then separate the spatial part and the spin-isospin one:

$$\boxed{\Gamma_{\alpha\gamma}(E) = -\sum_{\beta\delta>}\sum_{i=1}^{2}[E^{(i)\delta\gamma}_{\alpha\beta}.S^{(i)\delta\gamma}_{\alpha\beta} + (-1)^{s_\delta - s_\beta}E^{(i)\bar{\delta}\gamma}_{\alpha\bar{\beta}}.S^{(i)\bar{\delta}\gamma}_{\alpha\bar{\beta}}]\rho_{\delta\beta}} \tag{E.85}$$

We now consider explicitly the spins of α and γ.

Block $++$:

Here we consider the spins $(\alpha\uparrow, \gamma\uparrow)$. We start witht the spin-isospin part:

$$\begin{cases} (S^{(i)\delta\gamma}_{\alpha\beta})^{++} = \delta_{s_{\beta^+}s_{\delta^+}}[\delta_{\tau\tau'}W_i - H_i] + \delta_{s_\beta s_\delta}[\delta_{\tau\tau'}B_i - M_i] \\ (S^{(i)\bar{\delta}\gamma}_{\alpha\bar{\beta}})^{++} = \delta_{s_{\beta^-}s_{\delta^-}}[\delta_{\tau\tau'}W_i - H_i] + \delta_{s_\beta s_\delta}[\delta_{\tau\tau'}B_i - M_i] \end{cases} \tag{E.86}$$

The exchange mean field then reads:

$$\Gamma^{\tau++}_{\alpha\gamma}(E) = \sum_{\beta\delta>}\sum_{i=1}^{2} E^{(i)\delta\gamma}_{\alpha\beta}([H_i + M_i - W_i - B_i]\rho^{\tau++}_{\delta\beta} + [H_i + M_i]\rho^{\bar{\tau}++}_{\delta\beta} \\ +[M_i - B_i]\rho^{\tau--}_{\delta\beta} + M_i\rho^{\bar{\tau}--}_{\delta\beta}) \\ +E^{(i)\bar{\delta}\gamma}_{\alpha\bar{\beta}}([H_i + M_i - W_i - B_i]\rho^{\tau--}_{\delta\bar{\beta}} + [H_i + M_i]\rho^{\bar{\tau}--}_{\delta\bar{\beta}} \\ +[M_i - B_i]\rho^{\tau++}_{\delta\bar{\beta}} + M_i\rho^{\bar{\tau}++}_{\delta\bar{\beta}}) \tag{E.87}$$

It takes a more compact form:

$$\Gamma^{\tau++}_{\alpha\gamma}(E) = \sum_{\beta\delta>}\sum_{i=1}^{2} E^{(i)\delta\gamma}_{\alpha\beta}\tilde{R}^{(i)\tau++}_{\delta\beta}(E) + E^{(i)\bar{\delta}\gamma}_{\alpha\bar{\beta}}\bar{R}^{(i)\tau++}_{\delta\beta}(E) \tag{E.88}$$

$$\begin{cases} \tilde{R}^{(i)\tau++}_{\delta\beta}(E) = [H_i + M_i - W_i - B_i]\rho^{\tau++}_{\delta\beta} + [H_i + M_i]\rho^{\bar{\tau}++}_{\delta\beta} + [M_i - B_i]\rho^{\tau--}_{\delta\beta} + M_i\rho^{\bar{\tau}--}_{\delta\beta} \\ \bar{R}^{(i)\tau++}_{\delta\beta}(E) = [H_i + M_i - W_i - B_i]\rho^{\tau--}_{\delta\beta} + [H_i + M_i]\rho^{\bar{\tau}--}_{\delta\beta} + [M_i - B_i]\rho^{\tau++}_{\delta\beta} + M_i\rho^{\bar{\tau}++}_{\delta\beta} \end{cases} \tag{E.89}$$

We now perform the summation not only on the positive m_β and m_δ but on all the possible values. It enables us to gather the different part of Eq.(E.88):

$$\Gamma^{\tau++}_{\alpha\gamma}(E) = \sum_{\beta\delta>}\sum_{m'}\sum_{i=1}^{2} E^{(i)\delta\gamma}_{\alpha\beta}R^{(i)\tau++}_{\delta\beta}(E) \tag{E.90}$$

$$\begin{cases} (m' > 0) \rightarrow R^{(i)\tau++}_{\delta\beta}(E) = \tilde{R}^{(i)\tau++}_{\delta\beta}(E) \\ (m' = 0) \rightarrow R^{(i)\tau++}_{\delta\beta}(E) = \bar{R}^{(i)\tau++}_{\delta\beta}(E) + \tilde{R}^{(i)\tau++}_{\delta\beta}(E) \\ (m' < 0) \rightarrow R^{(i)\tau++}_{\delta\beta}(E) = \bar{R}^{(i)\tau++}_{\delta\beta}(E) \end{cases} \tag{E.91}$$

At least, the result concerning the spatial part are integrated:

$$\boxed{\Gamma^{\tau++}_{\alpha\gamma}(E) = \sum_{\beta\delta>}\sum_{m'}\sum_{i=1}^{2}(I^{(i)}_r)^{\delta\gamma}_{\alpha\beta}(I^{(i)}_z)^{\delta\gamma}_{\alpha\beta}R^{(i)\tau++}_{\delta\beta}(E)} \tag{E.92}$$

Block $--$:

Here we consider the spins $(\alpha\uparrow, \gamma\uparrow)$. The only difference with the $++$ case is the following exchange $\tilde{R} \leftrightarrow \bar{R}$. This block of the central exchange mean field then reads:

$$\boxed{\Gamma^{\tau--}_{\alpha\gamma}(E) = \sum_{\beta\delta>}\sum_{m'}\sum_{i=1}^{2}(I^{(i)}_r)^{\bar{\delta}\gamma}_{\alpha\bar{\beta}}(I^{(i)}_z)^{\delta\gamma}_{\alpha\beta}R^{(i)\tau++}_{\delta\beta}(E)} \tag{E.93}$$

Block $-+$:

Here we consider the spins $(\alpha\downarrow, \gamma\uparrow)$. We start witht the spin-isospin part:

$$\begin{cases}(S^{(i)\delta\gamma}_{\alpha\beta})^{-+} = \delta_{s_{\beta^+}s_{\delta^-}}[\delta_{\tau\tau'}W_i - H_i] \\ (S^{(i)\bar{\delta}\gamma}_{\alpha\bar{\beta}})^{-+} = \delta_{s_{\beta^-}s_{\delta^+}}[\delta_{\tau\tau'}W_i - H_i]\end{cases} \tag{E.94}$$

The field then reads:

$$\Gamma^{-+}_{\alpha\gamma}(E) = \sum_{\beta\delta>}\sum_{i=1}^{2} E^{(i)\delta\gamma}_{\alpha\beta}([-W_i + H_i]\rho^{\tau-+}_{\delta\beta} + H_i\rho^{\bar{\tau}-+}_{\delta\beta}) + E^{(i)\bar{\delta}\gamma}_{\alpha\bar{\beta}}([W_i - H_i]\rho^{\tau+-}_{\delta\beta} - H_i\rho^{\bar{\tau}+-}_{\delta\beta}) \tag{E.95}$$

We set:

$$\begin{cases}\tilde{R}^{(i)\tau-+}_{\delta\beta}(E) = [-W_i + H_i]\rho^{\tau-+}_{\delta\beta} + H_i\rho^{\bar{\tau}-+}_{\delta\beta} \\ \bar{R}^{(i)\tau-+}_{\delta\beta}(E) = [W_i - H_i]\rho^{\tau+-}_{\delta\beta} - H_i\rho^{\bar{\tau}+-}_{\delta\beta}\end{cases} \tag{E.96}$$

$\tilde{R}$ and $\bar{R}$ of Eq.(E.96) naturally combine:

$$\begin{cases}(m' > 0) \rightarrow R^{(i)\tau-+}_{\delta\beta}(E) = \tilde{R}^{(i)\tau-+}_{\delta\beta}(E) \\ (m' \leq 0) \rightarrow R^{(i)\tau-+}_{\delta\beta}(E) = \bar{R}^{(i)\tau-+}_{\delta\beta}(E)\end{cases} \tag{E.97}$$

We finally find:

$$\boxed{\Gamma^{\tau-+}_{\alpha\gamma}(E) = \sum_{\beta\delta>}\sum_{m'}\sum_{i=1}^{2}(I^{(i)}_r)^{\delta\gamma}_{\alpha\beta}(I^{(i)}_z)^{\delta\gamma}_{\alpha\beta}R^{(i)\tau-+}_{\delta\beta}(E)} \tag{E.98}$$

Block $+-$:

Here we consider the spins $(\alpha\uparrow, \gamma\downarrow)$. Symmetry arguments directly give:

$$\boxed{\Gamma^{\tau+-}_{\alpha\gamma}(E) = \Gamma^{\tau-+}_{\gamma\alpha}(E)} \tag{E.99}$$

E.2.3 Pairing field

The strategy of the pairing field derivations is very simple. We want to put it in a form equivalent to the central exchange field in order to evaluate them numerically in parallel. With he conventions of the HFB3 code, the central pairing field take the following form:

$$\Delta_{\alpha\bar{\beta}} = \sum_{\gamma\delta}(-1)^{s_\beta - s_\delta}\langle\alpha\bar{\beta}|V^{(Ctrl)}|\gamma\bar{\delta}\rangle\kappa_{\gamma\bar{\delta}} \tag{E.100}$$

We use the time-reversal properties of κ:

$$\boxed{\Delta_{\alpha\bar{\beta}} = \sum_{\gamma\delta>}[(-1)^{s_\beta - s_\delta}E^{(i)\gamma\bar{\delta}}_{\alpha\bar{\beta}}.S^{(i)\gamma\bar{\delta}}_{\alpha\bar{\beta}} + (-1)^{s_\beta + s_\gamma}E^{(i)\bar{\gamma}\delta}_{\alpha\bar{\beta}}.S^{(i)\bar{\gamma}\delta}_{\alpha\bar{\beta}}]\kappa_{\gamma\bar{\delta}}} \tag{E.101}$$

To go further we will explicitly consider the spins of α and $\bar{\beta}$.

Block ++:

Here we consider the spins $(\alpha\uparrow, \bar{\beta}\uparrow)$. We first develop the spin-isospin part:

$$\begin{cases} (-1)^{s_\beta - s_\delta}(S^{\gamma\bar{\delta}}_{\alpha\bar{\beta}})^{++} = \delta_{\tau\tau'}(\delta_{s_{\gamma^+}s_{\delta^+}}[W_i - H_i] + \delta_{s_{\gamma^-}s_{\delta^-}}[M_i - B_i]) \\ (-1)^{s_\beta + s_\gamma}(S^{\bar{\gamma}\delta}_{\alpha\bar{\beta}})^{++} = \delta_{\tau\tau'}(\delta_{s_{\gamma^-}s_{\delta^-}}[W_i - H_i] + \delta_{s_{\gamma^+}s_{\delta^+}}[M_i - B_i]) \end{cases} \tag{E.102}$$

We then write the field:

$$\begin{aligned} \Delta^{\tau++}_{\alpha\bar{\beta}} = \sum_{\gamma\delta>} & E^{\gamma\bar{\delta}}_{\alpha\bar{\beta}}(\kappa^{\tau++}_{\gamma\bar{\delta}}[W_i - H_i] + \kappa^{\tau--}_{\gamma\bar{\delta}}[M_i - B_i]) \\ & + E^{\bar{\gamma}\delta}_{\alpha\bar{\beta}}(\kappa^{\tau--}_{\gamma\bar{\delta}}[W_i - H_i] + \kappa^{\tau++}_{\gamma\bar{\delta}}[M_i - B_i]) \end{aligned} \tag{E.103}$$

We use the symmetries of E and κ to put the field in a form similar to the one of the exchange mean field:

$$\begin{aligned} \Delta^{\tau++}_{\alpha\bar{\beta}} = \sum_{\gamma\delta>} & E^{\gamma\beta}_{\alpha\delta}(\kappa^{\tau++}_{\gamma\bar{\delta}}[W_i - H_i] + \kappa^{\tau--}_{\gamma\bar{\delta}}[M_i - B_i]) \\ & + E^{\bar{\gamma}\beta}_{\alpha\bar{\delta}}(\kappa^{\tau--}_{\gamma\bar{\delta}}[W_i - H_i] + \kappa^{\tau++}_{\gamma\bar{\delta}}[M_i - B_i]) \end{aligned} \tag{E.104}$$

We then set:

$$\begin{aligned} \tilde{K}^{(i)\tau++}_{\gamma\bar{\delta}} &= \kappa^{\tau++}_{\gamma\bar{\delta}}[W_i - H_i] + \kappa^{\tau--}_{\gamma\bar{\delta}}[M_i - B_i] \\ \bar{K}^{(i)\tau++}_{\gamma\bar{\delta}} &= \kappa^{\tau--}_{\gamma\bar{\delta}}[W_i - H_i] + \kappa^{\tau++}_{\gamma\bar{\delta}}[M_i - B_i] \end{aligned} \tag{E.105}$$

$\tilde{K}$ and $\bar{K}$ naturally combine:

$$\begin{cases} (m' > 0) \to K^{(i)\tau++}_{\gamma\bar{\delta}} = \tilde{K}^{(i)\tau++}_{\gamma\bar{\delta}} \\ (m' = 0) \to K^{(i)\tau++}_{\gamma\bar{\delta}} = \bar{K}^{(i)\tau++}_{\gamma\bar{\delta}} + \tilde{K}^{(i)\tau++}_{\gamma\bar{\delta}} \\ (m' < 0) \to K^{(i)\tau++}_{\gamma\bar{\delta}} = \bar{K}^{(i)\tau++}_{\gamma\bar{\delta}} \end{cases} \tag{E.106}$$

We finally get:

$$\boxed{\Delta^{\tau++}_{\alpha\bar{\beta}} = \sum_{\gamma\delta>}\sum_{m'}\sum_{i=1}^{2}(I^{(i)}_r)^{\gamma\beta}_{\alpha\delta}(I^{(i)}_z)^{\gamma\beta}_{\alpha\delta}K^{(i)\tau++}_{\gamma\bar{\delta}}} \tag{E.107}$$

Block −−:

Here we consider the spins $(\alpha\downarrow, \bar{\beta}\downarrow)$. As the pairing field and the exchange mean field behave the same, we directly have:

$$\boxed{\Delta^{\tau--}_{\alpha\bar{\beta}} = \sum_{\gamma\delta>}\sum_{m'}\sum_{i=1}^{2}(I_r^{(i)})^{\bar{\gamma}\beta}_{\alpha\bar{\delta}}(I_z^{(i)})^{\gamma\beta}_{\alpha\delta}K^{(i)\tau++}_{\gamma\bar{\delta}}} \tag{E.108}$$

Block $-+$:

Here we consider the spins $(\alpha\downarrow, \bar{\beta}\uparrow)$. We start with the spin-isospin part:

$$\begin{cases}(-1)^{s_\beta - s_\delta}(S^{\gamma\bar{\delta}}_{\alpha\bar{\beta}})^{-+} = \delta_{\tau\tau'}(\delta_{s_{\gamma^-}s_{\delta^+}}[W_i - H_i] + \delta_{s_{\gamma^-}s_{\delta^+}}[B_i - M_i]) \\ (-1)^{s_\beta + s_\gamma}(S^{\bar{\gamma}\delta}_{\alpha\bar{\beta}})^{-+} = -\delta_{\tau\tau'}(-\delta_{s_{\gamma^+}s_{\delta^-}}[W_i - H_i] + \delta_{s_{\gamma^+}s_{\delta^-}}[B_i - M_i])\end{cases} \tag{E.109}$$

The field write:

$$\Delta^{\tau-+}_{\alpha\bar{\beta}} = \sum_{\gamma\delta>} E^{\gamma\bar{\delta}}_{\alpha\bar{\beta}}(W_i - H_i + B_i - M_i)\kappa^{\tau-+}_{\gamma\bar{\delta}} + E^{\bar{\gamma}\delta}_{\alpha\bar{\beta}}(-W_i + H_i - B_i + M_i)\kappa^{\tau+-}_{\gamma\bar{\delta}} \tag{E.110}$$

We set:

$$\begin{cases}\tilde{K}^{(i)\tau-+}_{\gamma\bar{\delta}} = (W_i - H_i + B_i - M_i)\kappa^{\tau-+}_{\gamma\bar{\delta}} \\ \bar{K}^{(i)\tau-+}_{\gamma\bar{\delta}} = (-W_i + H_i - B_i + M_i)\kappa^{\tau+-}_{\gamma\bar{\delta}}\end{cases} \tag{E.111}$$

The latter naturally combine:

$$\begin{cases}(m' > 0)K^{(i)\tau-+}_{\gamma\bar{\delta}} = \tilde{K}^{(i)\tau-+}_{\gamma\bar{\delta}} \\ (m' \leq 0)K^{(i)\tau-+}_{\gamma\bar{\delta}} = \bar{K}^{(i)\tau-+}_{\gamma\bar{\delta}}\end{cases} \tag{E.112}$$

We end up with the field:

$$\boxed{\Delta^{\tau-+}_{\alpha\bar{\beta}} = \sum_{\gamma\delta>}\sum_{m'}\sum_{i=1}^{2}(I_r^{(i)})^{\gamma\beta}_{\alpha\delta}(I_z^{(i)})^{\gamma\beta}_{\alpha\delta}K^{(i)\tau-+}_{\gamma\bar{\delta}}} \tag{E.113}$$

Block $+-$:

Here we consider the spins $(\alpha\uparrow, \bar{\beta}\downarrow)$. Symmetry arguments directly give:

$$\boxed{\Delta^{\tau+-}_{\alpha\bar{\beta}} = \Delta^{\tau-+}_{\beta\bar{\alpha}}} \tag{E.114}$$

E.3 Collective fields

This part aims to give an expression of the direct mean field, exchange mean field and pairing field in the more complex case when ρ^{01} is not symmetric anymore and the two harmonic oscillator bases $\{0\}$ and $\{1\}$ are different. This derivations are useful to evaluate quantities of the following type :

$$\langle\Phi_0|\hat{H}|\Phi_1\rangle \tag{E.115}$$

Those quantities are not only useful in the SCIM approach but appear in many situations as for instance in the expression of the true TDGCM mass and collective potential.

E.3.1 Collective direct mean field

The collective central direct mean field reads as follows:

$$\bar{\Gamma}_{\alpha\gamma}(D) = \sum_{\beta\delta} {}_0\langle\alpha\beta|V^{(Ctrl)}|\gamma\delta\rangle_1 \rho^{01}_{\delta\beta} \tag{E.116}$$

First, we use the time-reversal properties of ρ^{01}:

$$\bar{\Gamma}_{\alpha\gamma}(D) = \sum_{\beta\delta>} [{}_0\langle\alpha\beta|V^{(Ctrl)}|\gamma\delta\rangle_1 + (-1)^{s_\delta - s_\beta} {}_0\langle\alpha\bar{\beta}|V^{(Ctrl)}|\gamma\bar{\delta}\rangle_1] \rho^{01}_{\delta\beta} \tag{E.117}$$

We then separate the spatial part and the spin-isospin one:

$$\boxed{\bar{\Gamma}_{\alpha\gamma}(D) = \sum_{\beta\delta>} \sum_{i=1}^{2} [\bar{E}^{(i)\gamma\delta}_{\alpha\beta} . S^{(i)\gamma\delta}_{\alpha\beta} + (-1)^{s_\delta - s_\beta} \bar{E}^{(i)\gamma\bar{\delta}}_{\alpha\bar{\beta}} . S^{(i)\gamma\bar{\delta}}_{\alpha\bar{\beta}}] \rho^{01}_{\delta\beta}} \tag{E.118}$$

We explicitly consider the spins of α and γ.

Block ++:

Here we consider the spins $(\alpha\uparrow, \gamma\uparrow)$. The ++ spin-isopsin part of the collective exchange mean field is the same as the non-collective one:

$$\begin{cases} (S^{(i)\gamma\delta}_{\alpha\beta})^{++} = \delta_{s_\beta s_\delta}[W_i - \delta_{\tau\tau'} H_i] + \delta_{s_{\beta^+} s_{\delta^+}}[B_i - \delta_{\tau\tau'} M_i] \\ (S^{(i)\gamma\bar{\delta}}_{\alpha\bar{\beta}})^{++} = \delta_{s_\beta s_\delta}[W_i - \delta_{\tau\tau'} H_i] + \delta_{s_{\beta^-} s_{\delta^-}}[B_i - \delta_{\tau\tau'} M_i] \end{cases} \tag{E.119}$$

As we always have $(m_\beta = m_\delta)$, we get the following result:

$$\bar{E}^{(i)\gamma\bar{\delta}}_{\alpha\bar{\beta}} = \bar{E}^{(i)\gamma\delta}_{\alpha\beta} \tag{E.120}$$

The field thus reads:

$$\begin{aligned} \bar{\Gamma}^{\tau++}_{\alpha\gamma}(D) = \sum_{\beta\delta>} \sum_{i=1}^{2} \bar{E}^{(i)\gamma\delta}_{\alpha\beta} [[2(W_i - H_i) + B_i - M_i](\rho^{01\tau++}_{\delta\beta} + \rho^{01\tau--}_{\delta\beta}) \\ + [2W_i + B_i](\rho^{01\bar{\tau}++}_{\delta\beta} + \rho^{01\bar{\tau}--}_{\delta\beta})] \end{aligned} \tag{E.121}$$

We put it in the more compact form:

$$\bar{\Gamma}^{\tau++}_{\alpha\gamma}(D) = \sum_{\beta\delta>} \sum_{i=1}^{2} \bar{E}^{(i)\gamma\delta}_{\alpha\beta} R^{01(i)\tau++}_{\delta\beta}(D) \tag{E.122}$$

$$\begin{aligned} R^{01(i)\tau++}_{\delta\beta}(D) = [2(W_i - H_i) + B_i - M_i](\rho^{01\tau++}_{\delta\beta} + \rho^{01\tau--}_{\delta\beta}) \\ + [2W_i + B_i](\rho^{01\bar{\tau}++}_{\delta\beta} + \rho^{01\bar{\tau}--}_{\delta\beta}) \end{aligned} \tag{E.123}$$

Including the results of the spatial part we finally get:

$$\boxed{\bar{\Gamma}^{\tau++}_{\alpha\gamma}(D) = \sum_{\beta\delta>}\sum_{i=1}^{2}(\bar{I}_r^{(i)})^{\gamma\delta}_{\alpha\beta}(\bar{I}_z^{(i)})^{\gamma\delta}_{\alpha\beta}R^{01(i)\tau++}_{\delta\beta}(D)} \tag{E.124}$$

Block $--$:

Here we consider the spins $(\alpha\downarrow, \gamma\downarrow)$. As for the non-collective case, we directly find for this part of the field:

$$\boxed{\bar{\Gamma}^{\tau--}_{\alpha\gamma}(D) = \bar{\Gamma}^{\tau++}_{\alpha\gamma}(D)} \tag{E.125}$$

Block $-+$:

Here we consider the spins $(\alpha\downarrow, \gamma\uparrow)$. We start looking at the spin-isospin part of the field:

$$\begin{cases}(S^{(i)\gamma\delta}_{\alpha\beta})^{-+} = \delta_{s_{\beta^+}s_{\delta^-}}[B_i - \delta_{\tau\tau'}M_i] \\ (-1)^{s_\delta - s_\beta}(S^{(i)\gamma\bar{\delta}}_{\alpha\bar{\beta}})^{-+} = -\delta_{s_{\beta^-}s_{\delta^+}}[B_i - \delta_{\tau\tau'}M_i]\end{cases} \tag{E.126}$$

Even if this spin-isospin part is the same as the non-collective one Eq.$(E.80)$, since ρ^{01} is not symmetric it is not possible to simplify anymore. We end up with:

$$\begin{aligned}\bar{\Gamma}^{\tau-+}_{\alpha\gamma}(D) = \sum_{\beta\delta>}\sum_{i=1}^{2}&\bar{E}^{(i)\gamma\delta}_{\alpha\beta}[(B_i - M_i)\rho^{01\tau-+}_{\delta\beta} + B_i\rho^{01\bar{\tau}-+}_{\delta\beta}] \\ &-\bar{E}^{(i)\gamma\bar{\delta}}_{\alpha\bar{\beta}}[(B_i - M_i)\rho^{01\tau+-}_{\delta\beta} + B_i\rho^{01\bar{\tau}+-}_{\delta\beta}]\end{aligned} \tag{E.127}$$

We set:

$$\begin{cases}\tilde{R}^{01(i)\tau-+}_{\delta\beta}(D) = [(B_i - M_i)\rho^{01\tau-+}_{\delta\beta} + B_i\rho^{01\bar{\tau}-+}_{\delta\beta}] \\ \bar{R}^{01(i)\tau-+}_{\delta\beta}(D) = -[(B_i - M_i)\rho^{01\tau+-}_{\delta\beta} + B_i\rho^{01\bar{\tau}+-}_{\delta\beta}]\end{cases} \tag{E.128}$$

$\tilde{R}$ and $\bar{R}$ are combined:

$$\begin{cases}(m' > 0) \to R^{01(i)\tau-+}_{\delta\beta}(D) = \tilde{R}^{01(i)\tau-+}_{\delta\beta}(D) \\ (m' \leq 0) \to R^{01(i)\tau-+}_{\delta\beta}(D) = \bar{R}^{01(i)\tau-+}_{\delta\beta}(D)\end{cases} \tag{E.129}$$

We finally write:

$$\boxed{\bar{\Gamma}^{\tau-+}_{\alpha\gamma}(D) = \sum_{\beta\delta>}\sum_{m'}\sum_{i=1}^{2}(\bar{I}_r^{(i)})^{\gamma\delta}_{\alpha\beta}(\bar{I}_z^{(i)})^{\gamma\delta}_{\alpha\beta}R^{01(i)\tau-+}_{\delta\beta}(D)} \tag{E.130}$$

Block $+-$:

Here we consider the spins $(\alpha\uparrow, \gamma\downarrow)$. As the direct mean field is not symmetric anymore, we have to treat explicitly this spin block. We start looking at the spin-isospin part of the field:

$$\begin{cases} (S_{\alpha\beta}^{(i)\delta\gamma})^{+-} = \delta_{s_{\beta^-}s_{\delta^+}}[B_i - \delta_{\tau\tau'}M_i] \\ (-1)^{s_\delta - s_\beta}(S_{\alpha\bar{\beta}}^{(i)\gamma\bar{\delta}})^{+-} = -\delta_{s_{\beta^+}s_{\delta^-}}[B_i - \delta_{\tau\tau'}M_i] \end{cases} \tag{E.131}$$

By analogy with Eq.(E.127) we directly know that the field take the following form:

$$\boxed{\bar{\Gamma}_{\alpha\gamma}^{\tau+-}(D) = -\sum_{\beta\delta>}\sum_{m'}\sum_{i=1}^{2}(\bar{I}_r^{(i)})_{\alpha\bar{\beta}}^{\gamma\bar{\delta}}(\bar{I}_z^{(i)})_{\alpha\beta}^{\gamma\delta}R_{\delta\beta}^{01(i)\tau-+}(D)} \tag{E.132}$$

E.3.2 Collective exchange mean field

The exchange part of the collective central mean field reads as follows:

$$\bar{\Gamma}_{\alpha\gamma}(E) = -\sum_{\beta\delta}{}_0\langle\alpha\beta|V^{(Ctrl)}|\delta\gamma\rangle_1\rho_{\delta\beta}^{01} \tag{E.133}$$

We use the time-reversal properties of ρ^{01}:

$$\bar{\Gamma}_{\alpha\gamma}(E) = -\sum_{\beta\delta>}[{}_0\langle\alpha\beta|V^{(Ctrl)}|\delta\gamma\rangle_1 + (-1)^{s_\delta - s_\beta}{}_0\langle\alpha\bar{\beta}|V^{(Ctrl)}|\bar{\delta}\gamma\rangle_1]\rho_{\delta\beta}^{01} \tag{E.134}$$

We separate into a spatial and a spin-isospin part:

$$\boxed{\bar{\Gamma}_{\alpha\gamma}(E) = -\sum_{\beta\delta>}\sum_{i=1}^{2}[\bar{E}_{\alpha\beta}^{(i)\delta\gamma}.S_{\alpha\beta}^{(i)\delta\gamma} + (-1)^{s_\delta - s_\beta}\bar{E}_{\alpha\bar{\beta}}^{(i)\bar{\delta}\gamma}.S_{\alpha\bar{\beta}}^{(i)\bar{\delta}\gamma}]\rho_{\delta\beta}^{01}} \tag{E.135}$$

We now consider the spins explicitly.

Block $++$:

Here, we consider the spins $(\alpha\uparrow, \gamma\uparrow)$. We first look at the spin-isospin part:

$$\begin{cases} (S_{\alpha\beta}^{(i)\delta\gamma})^{++} = \delta_{s_{\beta^+}s_{\delta^+}}[\delta_{\tau\tau'}W_i - H_i] + \delta_{s_\beta s_\delta}[\delta_{\tau\tau'}B_i - M_i] \\ (S_{\alpha\bar{\beta}}^{(i)\bar{\delta}\gamma})^{++} = \delta_{s_{\beta^-}s_{\delta^-}}[\delta_{\tau\tau'}W_i - H_i] + \delta_{s_\beta s_\delta}[\delta_{\tau\tau'}B_i - M_i] \end{cases} \tag{E.136}$$

The field then reads:

$$\begin{aligned} \bar{\Gamma}_{\alpha\gamma}^{\tau++}(E) = \sum_{\beta\delta>}\sum_{i=1}^{2}\bar{E}_{\alpha\beta}^{(i)\delta\gamma}([H_i + M_i - W_i - B_i]\rho_{\delta\beta}^{01\tau++} + [H_i + M_i]\rho_{\delta\beta}^{01\bar{\tau}++} \\ +[M_i - B_i]\rho_{\delta\beta}^{01\tau--} + M_i\rho_{\delta\beta}^{01\bar{\tau}--}) \\ +\bar{E}_{\alpha\bar{\beta}}^{(i)\bar{\delta}\gamma}([H_i + M_i - W_i - B_i]\rho_{\delta\beta}^{01\tau--} + [H_i + M_i]\rho_{\delta\beta}^{01\bar{\tau}--} \\ +[M_i - B_i]\rho_{\delta\beta}^{01\tau++} + M_i\rho_{\delta\beta}^{01\bar{\tau}++}) \end{aligned} \tag{E.137}$$

We set:

$$\tilde{R}^{01(i)\tau++}_{\delta\beta}(E) = [H_i + M_i - W_i - B_i]\rho^{01\tau++}_{\delta\beta} + [H_i + M_i]\rho^{01\bar{\tau}++}_{\delta\beta} + [M_i - B_i]\rho^{01\tau--}_{\delta\beta} + M_i\rho^{01\bar{\tau}--}_{\delta\beta} \tag{E.138}$$

$$\bar{R}^{01(i)\tau++}_{\delta\beta}(E) = [H_i + M_i - W_i - B_i]\rho^{01\tau--}_{\delta\beta} + [H_i + M_i]\rho^{01\bar{\tau}--}_{\delta\beta} + [M_i - B_i]\rho^{01\tau++}_{\delta\beta} + M_i\rho^{01\bar{\tau}++}_{\delta\beta} \tag{E.139}$$

Those quantities are combined:

$$\begin{cases} (m' > 0) \rightarrow R^{01(i)\tau++}_{\delta\beta}(E) = \tilde{R}^{01(i)\tau++}_{\delta\beta}(E) \\ (m' = 0) \rightarrow R^{01(i)\tau++}_{\delta\beta}(E) = \bar{R}^{01(i)\tau++}_{\delta\beta}(E) + \tilde{R}^{01(i)\tau++}_{\delta\beta}(E) \\ (m' < 0) \rightarrow R^{01(i)\tau++}_{\delta\beta}(E) = \bar{R}^{01(i)\tau++}_{\delta\beta}(E) \end{cases} \tag{E.140}$$

We finally write:

$$\boxed{\bar{\Gamma}^{\tau++}_{\alpha\gamma}(E) = \sum_{\beta\delta>}\sum_{m'}\sum_{i=1}^{2}(\bar{I}^{(i)}_{r})^{\delta\gamma}_{\alpha\beta}(\bar{I}^{(i)}_{z})^{\delta\gamma}_{\alpha\beta}R^{01(i)\tau++}_{\delta\beta}(E)} \tag{E.141}$$

Block $--$:

Here, we consider the spins $(\alpha\downarrow, \gamma\downarrow)$. By analogy with the non-collective case we directly write:

$$\boxed{\bar{\Gamma}^{\tau--}_{\alpha\gamma}(E) = \sum_{\beta\delta>}\sum_{m'}\sum_{i=1}^{2}(\bar{I}^{(i)}_{r})^{\bar{\delta}\gamma}_{\alpha\bar{\beta}}(\bar{I}^{(i)}_{z})^{\delta\gamma}_{\alpha\beta}R^{01(i)\tau++}_{\delta\beta}(E)} \tag{E.142}$$

Block $-+$:

Here, we consider the spins $(\alpha\downarrow, \gamma\uparrow)$. We write for the spin-isospin part:

$$\begin{cases} (S^{(i)\delta\gamma}_{\alpha\beta})^{-+} = \delta_{s_{\beta^+}s_{\delta^-}}[\delta_{\tau\tau'}W_i - H_i] \\ (-1)^{s_\delta - s_\beta}(S^{(i)\bar{\delta}\gamma}_{\alpha\bar{\beta}})^{-+} = -\delta_{s_{\beta^-}s_{\delta^+}}[\delta_{\tau\tau'}W_i - H_i] \end{cases} \tag{E.143}$$

The field then reads:

$$\bar{\Gamma}^{-+}_{\alpha\gamma}(E) = \sum_{\beta\delta>}\sum_{i=1}^{2}\bar{E}^{(i)\delta\gamma}_{\alpha\beta}([-W_i + H_i]\rho^{01\tau-+}_{\delta\beta} + H_i\rho^{01\bar{\tau}-+}_{\delta\beta}) + \bar{E}^{(i)\bar{\delta}\gamma}_{\alpha\bar{\beta}}([W_i - H_i]\rho^{01\tau+-}_{\delta\beta} - H_i\rho^{01\bar{\tau}+-}_{\delta\beta}) \tag{E.144}$$

We set:

$$\begin{cases} \tilde{R}^{01(i)\tau-+}_{\delta\beta}(E) = [-W_i + H_i]\rho^{01\tau-+}_{\delta\beta} + H_i\rho^{01\bar{\tau}-+}_{\delta\beta} \\ \bar{R}^{01(i)\tau-+}_{\delta\beta}(E) = [W_i - H_i]\rho^{01\tau+-}_{\delta\beta} - H_i\rho^{01\bar{\tau}+-}_{\delta\beta} \end{cases} \tag{E.145}$$

Both terms are combined:

$$\begin{cases} (m' > 0) \rightarrow R^{01(i)\tau-+}_{\delta\beta}(E) = \tilde{R}^{01(i)\tau-+}_{\delta\beta}(E) \\ (m' \leq 0) \rightarrow R^{01(i)\tau-+}_{\delta\beta}(E) = \bar{R}^{01(i)\tau-+}_{\delta\beta}(E) \end{cases} \tag{E.146}$$

We finally write:

$$\boxed{\bar{\Gamma}^{\tau-+}_{\alpha\gamma}(E) = \sum_{\beta\delta>}\sum_{m'}\sum_{i=1}^{2}(\bar{I}^{(i)}_{r})^{\delta\gamma}_{\alpha\beta}(\bar{I}^{(i)}_{z})^{\delta\gamma}_{\alpha\beta}R^{01(i)\tau-+}_{\delta\beta}(E)} \tag{E.147}$$

Block $+-$:

Here, we consider the spins ($\alpha\uparrow, \gamma\downarrow$). Unfortunately, this spin block has to be considered explicitly as for the collective mean direct field. We first consider the spin-isospin part:

$$\begin{cases} (S^{(i)\delta\gamma}_{\alpha\beta})^{+-} = \delta_{s_{\beta^-}s_{\delta^+}}[\delta_{\tau\tau'}W_i - H_i] \\ (-1)^{s_\delta - s_\beta}(S^{(i)\bar{\delta}\gamma}_{\alpha\bar{\beta}})^{-+} = -\delta_{s_{\beta^+}s_{\delta^-}}[\delta_{\tau\tau'}W_i - H_i] \end{cases} \tag{E.148}$$

By analogy with the $-+$ part we directly write:

$$\boxed{\bar{\Gamma}^{\tau+-}_{\alpha\gamma}(E) = -\sum_{\beta\delta>}\sum_{m'}\sum_{i=1}^{2}(\bar{I}^{(i)}_{r})^{\bar{\delta}\gamma}_{\alpha\bar{\beta}}(\bar{I}^{(i)}_{z})^{\delta\gamma}_{\alpha\beta}R^{01(i)\tau-+}_{\delta\beta}(E)} \tag{E.149}$$

E.3.3 Collective pairing field

The collective central pairing field reads as follows:

$$\bar{\Delta}_{\alpha\bar{\beta}} = \sum_{\gamma\delta}(-1)^{s_\beta - s_\delta}\langle\alpha\bar{\beta}|V^{(Ctrl)}|\gamma\bar{\delta}\rangle\kappa^{01}_{\gamma\bar{\delta}} \tag{E.150}$$

We use the time-reversal properties of κ^{01} to write:

$$\boxed{\bar{\Delta}_{\alpha\bar{\beta}} = \sum_{\gamma\delta>}[(-1)^{s_\beta - s_\delta}\bar{E}^{(i)\gamma\bar{\delta}}_{\alpha\bar{\beta}}.S^{(i)\gamma\bar{\delta}}_{\alpha\bar{\beta}} + (-1)^{s_\beta + s_\gamma}\bar{E}^{(i)\bar{\gamma}\delta}_{\alpha\bar{\beta}}.S^{(i)\bar{\gamma}\delta}_{\alpha\bar{\beta}}]\kappa^{01}_{\gamma\bar{\delta}}} \tag{E.151}$$

We then consider explicitly the spin blocks.

Block $++$:

Here, we consider the spins $(\alpha\uparrow, \bar{\beta}\uparrow)$. We first look at the spin-isospin part:

$$\begin{cases} (-1)^{s_\beta - s_\delta}(S^{\gamma\bar{\delta}}_{\alpha\bar{\beta}})^{++} = \delta_{\tau\tau'}(\delta_{s_{\gamma^+}s_{\delta^+}}[W_i - H_i] + \delta_{s_{\gamma^-}s_{\delta^-}}[M_i - B_i]) \\ (-1)^{s_\beta + s_\gamma}(S^{\bar{\gamma}\delta}_{\alpha\bar{\beta}})^{++} = \delta_{\tau\tau'}(\delta_{s_{\gamma^-}s_{\delta^-}}[W_i - H_i] + \delta_{s_{\gamma^+}s_{\delta^+}}[M_i - B_i]) \end{cases} \tag{E.152}$$

The field then reads:

$$\begin{aligned} \bar{\Delta}^{\tau++}_{\alpha\bar{\beta}} = \sum_{\gamma\delta>} & \bar{E}^{\gamma\bar{\delta}}_{\alpha\bar{\beta}}(\kappa^{01\tau++}_{\gamma\bar{\delta}}[W_i - H_i] + \kappa^{01\tau--}_{\gamma\bar{\delta}}[M_i - B_i]) \\ & + \bar{E}^{\bar{\gamma}\delta}_{\alpha\bar{\beta}}(\kappa^{01\tau--}_{\gamma\bar{\delta}}[W_i - H_i] + \kappa^{01\tau++}_{\gamma\bar{\delta}}[M_i - B_i]) \end{aligned} \tag{E.153}$$

We set:

$$\begin{cases} \tilde{K}^{01(i)\tau++}_{\gamma\bar{\delta}} = \kappa^{01\tau++}_{\gamma\bar{\delta}}[W_i - H_i] + \kappa^{01\tau--}_{\gamma\bar{\delta}}[M_i - B_i] \\ \bar{K}^{01(i)\tau++}_{\gamma\bar{\delta}} = \kappa^{01\tau--}_{\gamma\bar{\delta}}[W_i - H_i] + \kappa^{01\tau++}_{\gamma\bar{\delta}}[M_i - B_i] \end{cases} \tag{E.154}$$

These quantities are combined:

$$\begin{cases} (m' > 0) \to K^{01(i)\tau++}_{\gamma\bar{\delta}} = \tilde{K}^{01(i)\tau++}_{\gamma\bar{\delta}} \\ (m' = 0) \to K^{01(i)\tau++}_{\gamma\bar{\delta}} = \bar{K}^{01(i)\tau++}_{\gamma\bar{\delta}} + \tilde{K}^{01(i)\tau++}_{\gamma\bar{\delta}} \\ (m' < 0) \to K^{01(i)\tau++}_{\gamma\bar{\delta}} = \bar{K}^{01(i)\tau++}_{\gamma\bar{\delta}} \end{cases} \tag{E.155}$$

We finally get:

$$\boxed{\bar{\Delta}^{\tau++}_{\alpha\bar{\beta}} = \sum_{\gamma\delta>}\sum_{m'}\sum_{i=1}^{2}(\bar{I}^{(i)}_r)^{\gamma\bar{\delta}}_{\alpha\bar{\beta}}(\bar{I}^{(i)}_z)^{\gamma\delta}_{\alpha\beta}K^{01(i)\tau++}_{\gamma\bar{\delta}}} \tag{E.156}$$

Block $--$:

Here, we consider the spins $(\alpha\downarrow, \bar{\beta}\downarrow)$. By analogy with the non-collective case we directly find:

$$\boxed{\bar{\Delta}^{\tau--}_{\alpha\bar{\beta}} = \sum_{\gamma\delta>}\sum_{m'}\sum_{i=1}^{2}(\bar{I}^{(i)}_r)^{\bar{\gamma}\delta}_{\alpha\bar{\beta}}(\bar{I}^{(i)}_z)^{\gamma\delta}_{\alpha\beta}K^{01(i)\tau++}_{\gamma\bar{\delta}}} \tag{E.157}$$

Block $-+$:

Here, we consider the spins $(\alpha\downarrow, \bar{\beta}\uparrow)$. We start wtih the spin-isospin part:

$$\begin{cases} (-1)^{s_\beta - s_\delta}(S^{\gamma\bar{\delta}}_{\alpha\bar{\beta}})^{-+} = \delta_{\tau\tau'}(\delta_{s_{\gamma^-}s_{\delta^+}}[W_i - H_i] + \delta_{s_{\gamma^-}s_{\delta^+}}[B_i - M_i]) \\ (-1)^{s_\beta + s_\gamma}(S^{\bar{\gamma}\delta}_{\alpha\bar{\beta}})^{-+} = -\delta_{\tau\tau'}(-\delta_{s_{\gamma^+}s_{\delta^-}}[W_i - H_i] + \delta_{s_{\gamma^+}s_{\delta^-}}[B_i - M_i]) \end{cases} \tag{E.158}$$

The field then reads:

$$\bar{\Delta}^{\tau-+}_{\alpha\bar{\beta}} = \sum_{\gamma\delta>} \bar{E}^{\gamma\bar{\delta}}_{\alpha\bar{\beta}}(W_i - H_i + B_i - M_i)\kappa^{01\tau-+}_{\gamma\bar{\delta}} + \bar{E}^{\bar{\gamma}\delta}_{\alpha\bar{\beta}}(-W_i + H_i - B_i + M_i)\kappa^{01\tau+-}_{\gamma\bar{\delta}} \quad \text{(E.159)}$$

We set:

$$\begin{cases} \tilde{K}^{01(i)\tau-+}_{\gamma\bar{\delta}} = (W_i - H_i + B_i - M_i)\kappa^{01\tau-+}_{\gamma\bar{\delta}} \\ \bar{K}^{01(i)\tau-+}_{\gamma\bar{\delta}} = (-W_i + H_i - B_i + M_i)\kappa^{01\tau+-}_{\gamma\bar{\delta}} \end{cases} \quad \text{(E.160)}$$

We then combine those latter quantities:

$$\begin{cases} (m' > 0)K^{01(i)\tau-+}_{\gamma\bar{\delta}} = \tilde{K}^{01(i)\tau-+}_{\gamma\bar{\delta}} \\ (m' \leq 0)K^{01(i)\tau-+}_{\gamma\bar{\delta}} = \bar{K}^{01(i)\tau-+}_{\gamma\bar{\delta}} \end{cases} \quad \text{(E.161)}$$

We finally find:

$$\boxed{\bar{\Delta}^{\tau-+}_{\alpha\bar{\beta}} = \sum_{\gamma\delta>}\sum_{m'}\sum_{i=1}^{2}(\bar{I}^{(i)}_r)^{\gamma\bar{\delta}}_{\alpha\bar{\beta}}(\bar{I}^{(i)}_z)^{\gamma\delta}_{\alpha\beta}K^{01(i)\tau-+}_{\gamma\bar{\delta}}} \quad \text{(E.162)}$$

Block $+-$:

Here, we consider the spins ($\alpha\uparrow, \bar{\beta}\downarrow$). Even if $\bar{\Gamma}$ is not symmetric anymore, $\bar{\Delta}$ is still symmetric, we thus have:

$$\boxed{\bar{\Delta}^{\tau+-}_{\alpha\bar{\beta}} = \bar{\Delta}^{\tau-+}_{\beta\bar{\alpha}}} \quad \text{(E.163)}$$

E.4 Excited collective fields

The goal of this part is to give an expression of the new central fields that appear when intrinsic excitations are added. They are useful to evaluate quantities of the following type :

$$\langle\Phi_0|\bar{\xi}_j\xi_j\hat{H}\xi^+_i\bar{\xi}^+_i|\Phi_1\rangle \quad \text{(E.164)}$$

E.4.1 Excited collective field $\bar{\Gamma}^{(i)}([W,Z])$

This central excited field reads as follows:

$$\boxed{\begin{aligned}&\bar{\Gamma}^{(i)}_{\alpha\gamma}([W,Z]) = \sum_{\beta\delta>}[{}_0\langle\alpha\beta|V^{(Ctrl)}(1 - P_rP_\sigma P_\tau)|\gamma\delta\rangle_1 \\ &+(-1)^{s_\beta - s_\delta}{}_0\langle\alpha\bar{\beta}|V^{(Ctrl)}(1 - P_rP_\sigma P_\tau)|\gamma\bar{\delta}\rangle_1]W_{\delta i}Z_{\beta\bar{i}}\end{aligned}} \quad \text{(E.165)}$$

The choice of an excitation fixes a specific Ω and a specific isospin. We therefore have $(\tau_\beta = \tau_\delta = \tau_i)$ and $(\Omega_\beta = \Omega_\delta = \Omega_i \geq 0)$. We can separate the spatial part and the spin-isospin part:

$$\begin{aligned}\bar{\Gamma}^{(i)}_{\alpha\gamma}([W,Z]) = \sum_{\delta\beta\in(\Omega_i,\tau_i)}\sum_{\mu=1}^{2}[\bar{E}^{(\mu)\gamma\delta}_{\alpha\beta}.S^{(\mu)\gamma\delta}_{\alpha\beta} - \bar{E}^{(\mu)\delta\gamma}_{\alpha\beta}.S^{(\mu)\delta\gamma}_{\alpha\beta} \\ +(-1)^{s_\beta - s_\delta}(\bar{E}^{(\mu)\gamma\bar{\delta}}_{\alpha\bar{\beta}}.S^{(\mu)\gamma\bar{\delta}}_{\alpha\bar{\beta}} - \bar{E}^{(\mu)\bar{\delta}\gamma}_{\alpha\bar{\beta}}.S^{(\mu)\bar{\delta}\gamma}_{\alpha\bar{\beta}})]W_{\delta i}Z_{\beta\bar{i}}\end{aligned} \tag{E.166}$$

We now consider the spins explicitly.

Block ++:

Here, we consider the spins $(\alpha\uparrow, \gamma\uparrow)$. The associated spin-isospin part reads:

$$\begin{cases}(S^{(\mu)\gamma\delta}_{\alpha\beta})^{++} = \delta_{s_\beta s_\delta}[W_\mu - \delta_{\tau\tau_i}H_i] + \delta_{s_{\beta^+}s_{\delta^+}}[B_\mu - \delta_{\tau\tau_i}M_\mu] \\ (S^{(\mu)\gamma\bar{\delta}}_{\alpha\bar{\beta}})^{++} = \delta_{s_\beta s_\delta}[W_\mu - \delta_{\tau\tau_i}H_\mu] + \delta_{s_{\beta^-}s_{\delta^-}}[B_\mu - \delta_{\tau\tau_i}M_\mu] \\ (S^{(\mu)\delta\gamma}_{\alpha\beta})^{++} = \delta_{s_{\beta^+}s_{\delta^+}}[\delta_{\tau\tau_i}W_\mu - H_\mu] + \delta_{s_\beta s_\delta}[\delta_{\tau\tau_i}B_\mu - M_\mu] \\ (S^{(\mu)\bar{\delta}\gamma}_{\alpha\bar{\beta}})^{++} = \delta_{s_{\beta^-}s_{\delta^-}}[\delta_{\tau\tau_i}W_\mu - H_\mu] + \delta_{s_\beta s_\delta}[\delta_{\tau\tau_i}B_\mu - M_\mu]\end{cases} \tag{E.167}$$

As $(m_\beta = m_\delta)$ always holds, we have in addition:

$$\bar{E}^{(\mu)\gamma\bar{\delta}}_{\alpha\bar{\beta}} = \bar{E}^{(\mu)\gamma\delta}_{\alpha\beta} \tag{E.168}$$

Due to the result of Eq.$(E.168)$, the field takes the following form:

$$\begin{aligned}\bar{\Gamma}^{(i)++\tau}_{\alpha\gamma}([W,Z]) = \sum_{\delta\beta\in(\Omega_i,\tau_i)}\sum_{\mu=1}^{2}\bar{E}^{(\mu)\gamma\delta}_{\alpha\beta}[2W_\mu + B_\mu - \delta_{\tau\tau_i}(2H_\mu + M_\mu)][W^+_{\delta i}Z^+_{\beta\bar{i}} + W^-_{\delta i}Z^-_{\beta\bar{i}}] \\ +\bar{E}^{(\mu)\delta\gamma}_{\alpha\beta}([H_\mu + M_\mu - \delta_{\tau\tau_i}(W_\mu + B_\mu)][W^+_{\delta i}Z^+_{\beta\bar{i}}] + [M_\mu - \delta_{\tau\tau_i}B_\mu][W^-_{\delta i}Z^-_{\beta\bar{i}}]) \\ +\bar{E}^{(\mu)\bar{\delta}\gamma}_{\alpha\bar{\beta}}([H_\mu + M_\mu - \delta_{\tau\tau_i}(W_\mu + B_\mu)][W^-_{\delta i}Z^-_{\beta\bar{i}}] + [M_\mu - \delta_{\tau\tau_i}B_\mu][W^+_{\delta i}Z^+_{\beta\bar{i}}])\end{aligned} \tag{E.169}$$

We set:

$$[W,Z]^{(\mu)\tau++}_{\delta\beta}(D) = (2H_\mu + M_\mu)][W^+_{\delta i}Z^+_{\beta\bar{i}} + W^-_{\delta i}Z^-_{\beta\bar{i}}] \tag{E.170}$$

$$\begin{aligned}(\Omega_i > 0) \to [W,Z]^{(\mu)\tau++}_{\delta\beta}(E) = [H_\mu + M_\mu - \delta_{\tau\tau_i}(W_\mu + B_\mu)][W^+_{\delta i}Z^+_{\beta\bar{i}}] \\ +[M_\mu - \delta_{\tau\tau_i}B_\mu][W^-_{\delta i}Z^-_{\beta\bar{i}}]\end{aligned} \tag{E.171}$$

$$\begin{aligned}(\Omega_i < 0) \to [W,Z]^{(\mu)\tau++}_{\delta\beta}(E) = [H_\mu + M_\mu - \delta_{\tau\tau_i}(W_\mu + B_\mu)][W^-_{\delta i}Z^-_{\beta\bar{i}}] \\ +[M_\mu - \delta_{\tau\tau_i}B_\mu][W^+_{\delta i}Z^+_{\beta\bar{i}}]\end{aligned} \tag{E.172}$$

We finally end up with the expression:

$$\boxed{\begin{aligned}\bar{\Gamma}^{(i)++\tau}_{\alpha\gamma}([W,Z]) = \sum_{\mu=1}^{2}[&\sum_{\delta\beta\in(\Omega_i,\tau_i)} (\bar{I}_r^{(\mu)})^{\gamma\delta}_{\alpha\beta}(\bar{I}_z^{(\mu)})^{\gamma\delta}_{\alpha\beta}[W,Z]^{(\mu)\tau++}_{\delta\beta}(D) \\ &+ \sum_{\delta\beta\in(\pm\Omega_i,\tau_i)} (\bar{I}_r^{(\mu)})^{\delta\gamma}_{\alpha\beta}(\bar{I}_z^{(\mu)})^{\delta\gamma}_{\alpha\beta}[W,Z]^{(\mu)\tau++}_{\delta\beta}(E)]\end{aligned}} \tag{E.173}$$

Block $--$:

Here, we consider the spins $(\alpha\downarrow,\gamma\downarrow)$. We directly have:

$$\begin{aligned}\bar{\Gamma}^{(i)--\tau}_{\alpha\gamma}([W,Z]) = &\sum_{\delta\beta\in(\Omega_i,\tau_i)}\sum_{\mu=1}^{2}\bar{E}^{(\mu)\gamma\delta}_{\alpha\beta}[2W_\mu + B_\mu - \delta_{\tau\tau_i}(2H_\mu + M_\mu)][W^+_{\delta\bar{i}}Z^+_{\beta\bar{i}} + W^-_{\delta i}Z^-_{\beta\bar{i}}] \\ &+\bar{E}^{(\mu)\delta\gamma}_{\alpha\beta}([H_\mu + M_\mu - \delta_{\tau\tau_i}(W_\mu + B_\mu)][W^-_{\delta i}Z^-_{\beta\bar{i}}] + [M_\mu - \delta_{\tau\tau_i}B_\mu][W^+_{\delta\bar{i}}Z^+_{\beta\bar{i}}]) \\ &+\bar{E}^{(\mu)\delta\bar{\gamma}}_{\alpha\bar{\beta}}([H_\mu + M_\mu - \delta_{\tau\tau_i}(W_\mu + B_\mu)][W^+_{\delta\bar{i}}Z^+_{\beta\bar{i}}] + [M_\mu - \delta_{\tau\tau_i}B_\mu][W^-_{\delta i}Z^-_{\beta\bar{i}}])\end{aligned} \tag{E.174}$$

The first part of the sum is the same as for the $++$ block. It finally reads:

$$\boxed{\begin{aligned}\bar{\Gamma}^{(i)--\tau}_{\alpha\gamma}([W,Z]) = \sum_{\mu=1}^{2}[&\sum_{\delta\beta\in(\Omega_i,\tau_i)} (\bar{I}_r^{(\mu)})^{\gamma\delta}_{\alpha\beta}(\bar{I}_z^{(\mu)})^{\gamma\delta}_{\alpha\beta}[W,Z]^{(\mu)\tau++}_{\delta\beta}(D) \\ &+ \sum_{\delta\beta\in(\pm\Omega_i,\tau_i)} (\bar{I}_r^{(\mu)})^{\bar{\delta}\gamma}_{\alpha\bar{\beta}}(\bar{I}_z^{(\mu)})^{\delta\gamma}_{\alpha\beta}[W,Z]^{(\mu)\tau++}_{\delta\beta}(E)]\end{aligned}} \tag{E.175}$$

Block $-+$:

Here, we consider the spins $(\alpha\downarrow,\gamma\uparrow)$. The spin-isospin part reads:

$$\begin{cases}(S^{(\mu)\gamma\delta}_{\alpha\beta})^{-+} = \delta_{s_{\beta^+}s_{\delta^-}}[B_\mu - \delta_{\tau\tau_i}M_\mu] \\ (-1)^{s_\delta - s_\beta}(S^{(\mu)\gamma\bar{\delta}}_{\alpha\bar{\beta}})^{-+} = -\delta_{s_{\beta^-}s_{\delta^+}}[B_\mu - \delta_{\tau\tau_i}M_\mu] \\ (S^{(\mu)\delta\gamma}_{\alpha\beta})^{-+} = \delta_{s_{\beta^+}s_{\delta^-}}[\delta_{\tau\tau_i}W_\mu - H_\mu] \\ (-1)^{s_\delta - s_\beta}(S^{(\mu)\bar{\delta}\gamma}_{\alpha\bar{\beta}})^{-+} = -\delta_{s_{\beta^-}s_{\delta^+}}[\delta_{\tau\tau_i}W_\mu - H_\mu]\end{cases} \tag{E.176}$$

We then write:

$$\begin{aligned}\bar{\Gamma}^{(i)-+\tau}_{\alpha\gamma}([W,Z]) = &\sum_{\delta\beta\in(\Omega_i,\tau_i)}\sum_{\mu=1}^{2}\bar{E}^{(\mu)\gamma\delta}_{\alpha\beta}[B_\mu - \delta_{\tau\tau_i}M_\mu][W^-_{\delta i}Z^+_{\beta\bar{i}}] \\ -\bar{E}^{(\mu)\gamma\bar{\delta}}_{\alpha\bar{\beta}}[B_\mu - \delta_{\tau\tau_i}M_\mu][W^+_{\delta\bar{i}}Z^-_{\beta\bar{i}}] &+ \bar{E}^{(\mu)\delta\gamma}_{\alpha\beta}[H_\mu - \delta_{\tau\tau_i}W_\mu][W^-_{\delta i}Z^+_{\beta\bar{i}}] \\ &-\bar{E}^{(\mu)\bar{\delta}\gamma}_{\alpha\bar{\beta}}[H_\mu - \delta_{\tau\tau_i}W_\mu][W^+_{\delta\bar{i}}Z^-_{\beta\bar{i}}]\end{aligned} \tag{E.177}$$

We set:

$$\begin{cases} (\Omega_i > 0) \rightarrow [W,Z]^{(\mu)\tau -+}_{\delta\beta}(D) = [B_\mu - \delta_{\tau\tau_i} M_\mu][W^-_{\delta i} Z^+_{\beta\bar{i}}] \\ (\Omega_i < 0) \rightarrow [W,Z]^{(\mu)\tau -+}_{\delta\beta}(D) = -[B_\mu - \delta_{\tau\tau_i} M_\mu][W^+_{\delta i} Z^-_{\beta\bar{i}}] \end{cases} \tag{E.178}$$

$$\begin{cases} (\Omega_i > 0) \rightarrow [W,Z]^{(\mu)\tau -+}_{\delta\beta}(E) = [H_\mu - \delta_{\tau\tau_i} W_\mu][W^-_{\delta i} Z^+_{\beta\bar{i}}] \\ (\Omega_i < 0) \rightarrow [W,Z]^{(\mu)\tau -+}_{\delta\beta}(E) = -[H_\mu - \delta_{\tau\tau_i} W_\mu][W^+_{\delta i} Z^-_{\beta\bar{i}}] \end{cases} \tag{E.179}$$

We finally write the field:

$$\boxed{\begin{aligned} \bar{\Gamma}^{(i)-+\tau}_{\alpha\gamma}([W,Z]) = \sum_{\mu=1}^{2} \sum_{\delta\beta\in(\pm\Omega_i,\tau_i)} & (\bar{I}^{(\mu)}_r)^{\gamma\delta}_{\alpha\beta} (\bar{I}^{(\mu)}_z)^{\gamma\delta}_{\alpha\beta} [W,Z]^{(\mu)\tau -+}_{\delta\beta}(D) \\ & + (\bar{I}^{(\mu)}_r)^{\delta\gamma}_{\alpha\beta} (\bar{I}^{(\mu)}_z)^{\delta\gamma}_{\alpha\beta} [W,Z]^{(\mu)\tau -+}_{\delta\beta}(E) \end{aligned}} \tag{E.180}$$

Block $+-$:

Here, we consider the spins ($\alpha\uparrow, \gamma\downarrow$). By analogy with the $-+$ part, we can directly write:

$$\boxed{\begin{aligned} \bar{\Gamma}^{(i)+-\tau}_{\alpha\gamma}([W,Z]) = -\sum_{\mu=1}^{2} \sum_{\delta\beta\in(\pm\Omega_i,\tau_i)} & (\bar{I}^{(\mu)}_r)^{\gamma\bar{\delta}}_{\alpha\bar{\beta}} (\bar{I}^{(\mu)}_z)^{\gamma\delta}_{\alpha\beta} [W,Z]^{(\mu)\tau -+}_{\delta\beta}(D) \\ & + (\bar{I}^{(\mu)}_r)^{\bar{\delta}\gamma}_{\alpha\bar{\beta}} (\bar{I}^{(\mu)}_z)^{\delta\gamma}_{\alpha\beta} [W,Z]^{(\mu)\tau -+}_{\delta\beta}(E) \end{aligned}} \tag{E.181}$$

E.4.2 Excited collective field $\bar{\Delta}^{(i)}(WW)$

This field is defined as the following contraction:

$$\boxed{\bar{\Delta}^{(i)}_{\alpha\bar{\beta}}(WW) = \sum_{\gamma\delta>} (-1)^{s_\beta - s_\delta}{}_0\langle \alpha\bar{\beta}|V^{(Ctrl)}(1 - P_r P_\sigma P_\tau)|\gamma\bar{\delta}\rangle_1 W_{\gamma i} W_{\delta i}} \tag{E.182}$$

Using the symmetries of the interaction we find:

$$\bar{\Delta}^{(i)}_{\alpha\bar{\beta}}(WW) = \sum_{\gamma\delta>} [(-1)^{s_\beta - s_\delta}{}_0\langle \alpha\bar{\beta}|V^{(Ctrl)}|\gamma\bar{\delta}\rangle_1 - (-1)^{s_\beta - s_\gamma}{}_0\langle \alpha\bar{\beta}|V^{(Ctrl)}|\bar{\gamma}\delta\rangle_1] W_{\gamma i} W_{\delta i} \tag{E.183}$$

We separate the spatial and the spin-isospin part:

$$\boxed{\bar{\Delta}^{(i)}_{\alpha\bar{\beta}}(WW) = \sum_{\gamma\delta\in(\Omega_i,\tau_i)} \sum_{\mu=1}^{2} [(-1)^{s_\beta - s_\delta} \bar{E}^{(\mu)\gamma\bar{\delta}}_{\alpha\bar{\beta}} . S^{(\mu)\gamma\bar{\delta}}_{\alpha\bar{\beta}} + (-1)^{s_\beta + s_\gamma} \bar{E}^{(\mu)\bar{\gamma}\delta}_{\alpha\bar{\beta}} . S^{(\mu)\bar{\gamma}\delta}_{\alpha\bar{\beta}}] W_{\gamma i} W_{\delta i}} \tag{E.184}$$

We then consider explicitly the spins.

Block ++:

Here, we consider the spins $(\alpha\uparrow,\bar{\beta}\uparrow)$. The spin-isospin reads:

$$\begin{cases}(-1)^{s_\beta-s_\delta}(S^{(\mu)\gamma\bar{\delta}}_{\alpha\bar{\beta}})^{++}=\delta_{\tau\tau_i}(\delta_{s_{\gamma^+}s_{\delta^+}}[W_\mu-H_\mu]+\delta_{s_{\gamma^-}s_{\delta^-}}[M_\mu-B_\mu])\\(-1)^{s_\beta+s_\gamma}(S^{(\mu)\bar{\gamma}\delta}_{\alpha\bar{\beta}})^{++}=\delta_{\tau\tau_i}(\delta_{s_{\gamma^-}s_{\delta^-}}[W_\mu-H_\mu]+\delta_{s_{\gamma^+}s_{\delta^+}}[M_\mu-B_\mu])\end{cases}\tag{E.185}$$

We then write the field:

$$\begin{aligned}\bar{\Delta}^{(i)++\tau}_{\alpha\bar{\beta}}(WW)=\delta_{\tau\tau_i}\sum_{\gamma\delta\in(\Omega_i,\tau_i)}\sum_{\mu=1}^{2}&\bar{E}^{(\mu)\gamma\bar{\delta}}_{\alpha\bar{\beta}}[(W_\mu-H_\mu)W^+_{\gamma i}W^+_{\delta i}+(M_\mu-B_\mu)W^-_{\gamma i}W^-_{\delta i}]\\&+\bar{E}^{(\mu)\bar{\gamma}\delta}_{\alpha\bar{\beta}}[(W_\mu-H_\mu)W^-_{\gamma i}W^-_{\delta i}+(M_\mu-B_\mu)W^+_{\gamma i}W^+_{\delta i}]\end{aligned}\tag{E.186}$$

We set:

$$\begin{cases}(\Omega_i>0)\rightarrow WW^{(\mu)\tau++}_{\gamma\bar{\delta}}=(W_\mu-H_\mu)W^+_{\gamma i}W^+_{\delta i}+(M_\mu-B_\mu)W^-_{\gamma i}W^-_{\delta i}\\(\Omega_i<0)\rightarrow WW^{(\mu)\tau++}_{\gamma\bar{\delta}}=(W_\mu-H_\mu)W^-_{\gamma i}W^-_{\delta i}+(M_\mu-B_\mu)W^+_{\gamma i}W^+_{\delta i}\end{cases}\tag{E.187}$$

We finally have:

$$\boxed{\bar{\Delta}^{(i)++\tau}_{\alpha\bar{\beta}}(WW)=\delta_{\tau\tau_i}\sum_{\gamma\delta\in(\pm\Omega_i,\tau_i)}\sum_{\mu=1}^{2}(\bar{I}^{(\mu)}_r)^{\gamma\bar{\delta}}_{\alpha\bar{\beta}}(\bar{I}^{(\mu)}_z)^{\gamma\delta}_{\alpha\beta}WW^{(\mu)\tau++}_{\gamma\bar{\delta}}}\tag{E.188}$$

Block −−:

Here, we consider the spins $(\alpha\downarrow,\bar{\beta}\downarrow)$.By analogy with the ++ part we directly write:

$$\boxed{\bar{\Delta}^{(i)--\tau}_{\alpha\bar{\beta}}(WW)=\delta_{\tau\tau_i}\sum_{\gamma\delta\in(\pm\Omega_i,\tau_i)}\sum_{\mu=1}^{2}(\bar{I}^{(\mu)}_r)^{\bar{\gamma}\delta}_{\alpha\bar{\beta}}(\bar{I}^{(\mu)}_z)^{\gamma\delta}_{\alpha\beta}WW^{(\mu)\tau++}_{\gamma\bar{\delta}}}\tag{E.189}$$

Block −+:

Here, we consider the spins $(\alpha\downarrow,\bar{\beta}\uparrow)$. We first write the spin-isospin part:

$$\begin{cases}(-1)^{s_\beta-s_\delta}(S^{(\mu)\gamma\bar{\delta}}_{\alpha\bar{\beta}})^{-+}=\delta_{\tau\tau_i}(\delta_{s_{\gamma^-}s_{\delta^+}}[W_\mu-H_\mu]+\delta_{s_{\gamma^-}s_{\delta^+}}[B_\mu-M_\mu])\\(-1)^{s_\beta+s_\gamma}(S^{(\mu)\bar{\gamma}\delta}_{\alpha\bar{\beta}})^{-+}=-\delta_{\tau\tau_i}(\delta_{s_{\gamma^+}s_{\delta^-}}[W_\mu-H_\mu]+\delta_{s_{\gamma^+}s_{\delta^-}}[B_\mu-M_\mu])\end{cases}\tag{E.190}$$

The field then reads:

$$\begin{aligned}\bar{\Delta}^{(i)-+\tau}_{\alpha\bar{\beta}}(WW)=\delta_{\tau\tau_i}\sum_{\gamma\delta\in(\Omega_i,\tau_i)}\sum_{\mu=1}^{2}&\bar{E}^{(\mu)\gamma\bar{\delta}}_{\alpha\bar{\beta}}[W_\mu-H_\mu+B_\mu-M_\mu]W^-_{\gamma i}W^+_{\delta i}\\&+\bar{E}^{(\mu)\bar{\gamma}\delta}_{\alpha\bar{\beta}}[-W_\mu+H_\mu-B_\mu+M_\mu]W^+_{\gamma i}W^-_{\delta i}\end{aligned}\tag{E.191}$$

We set:

$$\begin{cases} (\Omega_i > 0) \to WW_{\gamma\bar{\delta}}^{(\mu)\tau-+} = [W_\mu - H_\mu + B_\mu - M_\mu] W_{\gamma i}^- W_{\delta i}^+ \\ (\Omega_i < 0) \to WW_{\gamma\bar{\delta}}^{(\mu)\tau-+} = -[W_\mu - H_\mu + B_\mu - M_\mu] W_{\gamma i}^+ W_{\delta i}^- \end{cases} \tag{E.192}$$

We finally write:

$$\boxed{\bar{\Delta}_{\alpha\bar{\beta}}^{(i)-+\tau}(WW) = \delta_{\tau\tau_i} \sum_{\gamma\delta\in(\pm\Omega_i,\tau_i)} \sum_{\mu=1}^{2} (\bar{I}_r^{(\mu)})_{\alpha\bar{\beta}}^{\gamma\bar{\delta}} (\bar{I}_z^{(\mu)})_{\alpha\beta}^{\gamma\delta} WW_{\gamma\bar{\delta}}^{(\mu)\tau-+}} \tag{E.193}$$

Block $+-$:

Here, we consider the spins $(\alpha\uparrow, \bar{\beta}\downarrow)$. Symmetry arguments directly leads to:

$$\boxed{\bar{\Delta}_{\alpha\bar{\beta}}^{(i)+-\tau}(WW) = \bar{\Delta}_{\beta\bar{\alpha}}^{(i)-+\tau}(WW)} \tag{E.194}$$

E.4.3 Excited collective field $\bar{\Delta}^{(j)}(\bar{Z}\bar{Z})$

This excited field is defined as follows:

$$\boxed{\bar{\Delta}_{\alpha\bar{\beta}}^{(j)}(\bar{Z}\bar{Z}) = \sum_{\gamma\delta>} (-1)^{s_\beta - s_\delta} {}_0\langle \alpha\bar{\beta}|V^{(Ctrl)}(1 - P_r P_\sigma P_\tau)|\gamma\bar{\delta}\rangle_1 \bar{Z}_{j\bar{\gamma}} \bar{Z}_{j\bar{\delta}}} \tag{E.195}$$

By analogy with $\bar{\Delta}^{(i)}(WW)$, we directly get the results for each spin block.

Block $++$:

Here, we consider the spins $(\alpha\uparrow, \bar{\beta}\uparrow)$. The field reads:

$$\boxed{\bar{\Delta}_{\alpha\bar{\beta}}^{(j)++\tau}(\bar{Z}\bar{Z}) = \delta_{\tau\tau_j} \sum_{\gamma\delta\in(\pm\Omega_j,\tau_j)} \sum_{\mu=1}^{2} (\bar{I}_r^{(\mu)})_{\alpha\bar{\beta}}^{\gamma\bar{\delta}} (\bar{I}_z^{(\mu)})_{\alpha\beta}^{\gamma\delta} \bar{Z}\bar{Z}_{\gamma\bar{\delta}}^{(\mu)\tau++}} \tag{E.196}$$

With:

$$\begin{cases} (\Omega_j > 0) \to \bar{Z}\bar{Z}_{\gamma\bar{\delta}}^{(\mu)\tau++} = (W_\mu - H_\mu)\bar{Z}_{j\bar{\gamma}}^+ \bar{Z}_{j\bar{\delta}}^+ + (M_\mu - B_\mu)\bar{Z}_{j\bar{\gamma}}^- \bar{Z}_{j\bar{\delta}}^- \\ (\Omega_j < 0) \to \bar{Z}\bar{Z}_{\gamma\bar{\delta}}^{(\mu)\tau++} = (W_\mu - H_\mu)\bar{Z}_{j\bar{\gamma}}^- \bar{Z}_{j\bar{\delta}}^- + (M_\mu - B_\mu)\bar{Z}_{j\bar{\gamma}}^+ \bar{Z}_{j\bar{\delta}}^+ \end{cases} \tag{E.197}$$

Block $--$:

Here, we consider the spins $(\alpha\downarrow, \bar{\beta}\downarrow)$. The field reads:

$$\boxed{\bar{\Delta}_{\alpha\bar{\beta}}^{(j)++\tau}(\bar{Z}\bar{Z}) = \delta_{\tau\tau_j} \sum_{\gamma\delta\in(\pm\Omega_j,\tau_j)} \sum_{\mu=1}^{2} (\bar{I}_r^{(\mu)})_{\alpha\bar{\beta}}^{\bar{\gamma}\delta} (\bar{I}_z^{(\mu)})_{\alpha\beta}^{\gamma\delta} \bar{Z}\bar{Z}_{\gamma\bar{\delta}}^{(\mu)\tau++}} \tag{E.198}$$

Block $-+$:

Here, we consider the spins $(\alpha\downarrow, \bar{\beta}\uparrow)$. The field reads:

$$\boxed{\bar{\Delta}^{(j)-+\tau}_{\alpha\bar{\beta}}(\bar{Z}\bar{Z}) = \delta_{\tau\tau_j} \sum_{\gamma\delta\in(\pm\Omega_j,\tau_j)} \sum_{\mu=1}^{2} (\bar{I}_r^{(\mu)})^{\bar{\gamma}\delta}_{\alpha\bar{\beta}} (\bar{I}_z^{(\mu)})^{\gamma\delta}_{\alpha\beta} \bar{Z}\bar{Z}^{(\mu)\tau-+}_{\gamma\bar{\delta}}} \tag{E.199}$$

With:

$$\begin{cases} (\Omega_j > 0) \to \bar{Z}\bar{Z}^{(\mu)\tau-+}_{\gamma\bar{\delta}} = [W_\mu - H_\mu + B_\mu - M_\mu]\bar{Z}^{-}_{j\bar{\gamma}}\bar{Z}^{+}_{j\bar{\delta}} \\ (\Omega_j < 0) \to \bar{Z}\bar{Z}^{(\mu)\tau-+}_{\gamma\bar{\delta}} = -[W_\mu - H_\mu + B_\mu - M_\mu]\bar{Z}^{+}_{j\bar{\gamma}}\bar{Z}^{-}_{j\bar{\delta}} \end{cases} \tag{E.200}$$

Block $+-$:

Here, we consider the spins $(\alpha\uparrow, \bar{\beta}\downarrow)$. We use a symmetry argument to write:

$$\boxed{\bar{\Delta}^{(j)+-\tau}_{\alpha\bar{\beta}}(\bar{Z}\bar{Z}) = \bar{\Delta}^{(j)-+\tau}_{\beta\bar{\alpha}}(\bar{Z}\bar{Z})} \tag{E.201}$$

E.4.4 Excited collective field $\bar{\Delta}^{(ji)}([W, \bar{Z}])$

This excited field is defined as follows:

$$\boxed{\bar{\Delta}^{(ji)}_{\alpha\bar{\beta}}([W,\bar{Z}]) = \sum_{\gamma\delta>} (-1)^{s_\beta - s_\delta} {}_0\langle\alpha\bar{\beta}|V^{(Ctrl)}(1 - P_r P_\sigma P_\tau)|\gamma\bar{\delta}\rangle_1 [W_{\gamma i}\bar{Z}_{j\bar{\delta}} + \bar{Z}_{j\bar{\gamma}}W_{\delta i}]} \tag{E.202}$$

This field comes with the special conditions $(\tau_i = \tau_j = \tau_{ji})$ and $(\Omega_i = \Omega_j = \Omega_{ji})$.For the rest, we can use an analogy with the previous excited fields.

Block $++$:

Here, we consider the spins $(\alpha\uparrow, \bar{\beta}\uparrow)$.This part of the field reads:

$$\boxed{\bar{\Delta}^{(ji)++\tau}_{\alpha\bar{\beta}}([W,\bar{Z}]) = \delta_{\tau\tau_{ji}} \sum_{\gamma\delta\in(\pm\Omega_{ji},\tau_{ji})} \sum_{\mu=1}^{2} (\bar{I}_r^{(\mu)})^{\gamma\bar{\delta}}_{\alpha\bar{\beta}} (\bar{I}_z^{(\mu)})^{\gamma\delta}_{\alpha\beta} [W,\bar{Z}]^{(\mu)\tau++}_{\gamma\bar{\delta}}} \tag{E.203}$$

With:

$$\begin{aligned} (\Omega_{ji} > 0) \to [W,\bar{Z}]^{(\mu)\tau++}_{\gamma\bar{\delta}} &= (W_\mu - H_\mu)[W^{+}_{\gamma i}\bar{Z}^{+}_{j\bar{\delta}} + \bar{Z}^{+}_{j\bar{\gamma}}W^{+}_{\delta i}] \\ &+(M_\mu - B_\mu)[W^{-}_{\gamma i}\bar{Z}^{-}_{j\bar{\delta}} + \bar{Z}^{-}_{j\bar{\gamma}}W^{-}_{\delta i}] \end{aligned} \tag{E.204}$$

$$\begin{aligned} (\Omega_{ji} < 0) \to [W,\bar{Z}]^{(\mu)\tau++}_{\gamma\bar{\delta}} &= (W_\mu - H_\mu)[W^{-}_{\gamma i}\bar{Z}^{-}_{j\bar{\delta}} + \bar{Z}^{-}_{j\bar{\gamma}}W^{-}_{\delta i}] \\ &+(M_\mu - B_\mu)[W^{+}_{\gamma i}\bar{Z}^{+}_{j\bar{\delta}} + \bar{Z}^{+}_{j\bar{\gamma}}W^{+}_{\delta i}] \end{aligned} \tag{E.205}$$

Block $--$:

Here, we consider the spins $(\alpha\downarrow, \bar{\beta}\downarrow)$.This part of the field reads:

$$\boxed{\bar{\Delta}^{(ji)--\tau}_{\alpha\bar{\beta}}([W,\bar{Z}]) = \delta_{\tau\tau_{ji}} \sum_{\gamma\delta\in(\pm\Omega_{ji},\tau_{ji})} \sum_{\mu=1}^{2} (\bar{I}_r^{(\mu)})^{\bar{\gamma}\delta}_{\alpha\bar{\beta}} (\bar{I}_z^{(\mu)})^{\gamma\delta}_{\alpha\beta} [W,\bar{Z}]^{(\mu)\tau++}_{\gamma\bar{\delta}}} \tag{E.206}$$

Block $-+$:

Here, we consider the spins $(\alpha\downarrow, \bar{\beta}\uparrow)$.This part of the field reads:

$$\boxed{\bar{\Delta}^{(ji)-+\tau}_{\alpha\bar{\beta}}([W,\bar{Z}]) = \delta_{\tau\tau_{ji}} \sum_{\gamma\delta\in(\pm\Omega_{ji},\tau_{ji})} \sum_{\mu=1}^{2} (\bar{I}_r^{(\mu)})^{\gamma\bar{\delta}}_{\alpha\bar{\beta}} (\bar{I}_z^{(\mu)})^{\gamma\delta}_{\alpha\beta} [W,\bar{Z}]^{(\mu)\tau-+}_{\gamma\bar{\delta}}} \tag{E.207}$$

With:

$$\begin{cases} (\Omega_{ji} > 0) \to [W,\bar{Z}]^{(\mu)\tau-+}_{\gamma\bar{\delta}} = [W_\mu - H_\mu + B_\mu - M_\mu][W^-_{\gamma i}\bar{Z}^+_{j\bar{\delta}} + \bar{Z}^-_{j\bar{\gamma}} W^+_{\delta i}] \\ (\Omega_{ji} < 0) \to [W,\bar{Z}]^{(\mu)\tau-+}_{\gamma\bar{\delta}} = -[W_\mu - H_\mu + B_\mu - M_\mu][W^+_{\gamma i}\bar{Z}^-_{j\bar{\delta}} + \bar{Z}^+_{j\bar{\gamma}} W^-_{\delta i}] \end{cases} \tag{E.208}$$

Block $+-$:

Here, we consider the spins $(\alpha\uparrow, \bar{\beta}\downarrow)$. Symmetry arguments give for this field:

$$\boxed{\bar{\Delta}^{(ji)+-\tau}_{\alpha\bar{\beta}}([W,\bar{Z}]) = \bar{\Delta}^{(ji)-+\tau}_{\beta\bar{\alpha}}([W,\bar{Z}])} \tag{E.209}$$

Appendix F

Contact density-dependent fields

The contact density-dependent part of the antisymmetrized interaction reads as follows:

$$\boxed{V^{(D)}(1-P_rP_\sigma P_\tau) = t_3(1+x_0P_\sigma)\delta(\vec{r}_1-\vec{r}_2)[\rho(\frac{\vec{r}_1+\vec{r}_2}{2})]^\alpha(1-P_rP_\sigma P_\tau)} \tag{F.1}$$

The operators P_r, P_σ and P_τ represent the exchange of the spatial, spin and isospin part, respectively. As this part of the interaction depends on the state considered through its one-body density, it is a pseudo-operator. In the general case, when the the Hamiltonian is evaluated between two different states, the density-dependent matrix elements take the folowing form:

$$\boxed{\begin{aligned}{}_0\langle\alpha\beta|V^{(D)}(1-P_rP_\sigma P_\tau)|\gamma\delta\rangle_1 = {}_0\langle\alpha\beta|t_3(1+x_0P_\sigma)\delta(\vec{r}_1-\vec{r}_2)\\ [\rho^{01}(\frac{\vec{r}_1+\vec{r}_2}{2})]^\alpha(1-P_rP_\sigma P_\tau)|\gamma\delta\rangle_1\end{aligned}} \tag{F.2}$$

Using the local transition density matrix in the density-dependent term as done in Eq.(F.2) is a standard prescription in the literature [82]. This appendix aims to give the expression of all the contact density-dependent fields involved in this PhD thesis.

F.1 HFB fields

In this part, the HFB density-dependent mean field is explicitly derived. As the local density at the power $\alpha = 1/3$ is involved, there is no analytic expression for this part of the mean field. Therefore, we start giving a reduced expression of the field. Then, we explain how it is evaluated numerically.

F.1.1 Mean field reduced expression

First, we give the expression of the local density in the interaction:

$$\boxed{\rho(\vec{r}) = \sum_{\sigma\tau}\rho(\vec{r},\sigma,\tau) = \sum_{\sigma\tau}\langle\Phi|\Psi^+(\vec{r},\sigma,\tau)\Psi(\vec{r},\sigma,\tau)|\Phi\rangle} \tag{F.3}$$

Here Ψ^+ and Ψ are the field creation and annihilation operators [83] and can be written in the harmonic oscillator basis:

$$\begin{cases} \Psi^+(\vec{r},\sigma,\tau) = \sum_\alpha \delta_{\tau_\alpha\tau}\delta_{\sigma_\alpha\sigma}\psi^*_\alpha(\vec{r})c^+_\alpha \\ \Psi(\vec{r},\sigma,\tau) = \sum_\beta \delta_{\tau_\beta\tau}\delta_{\sigma_\beta\sigma}\psi_\beta(\vec{r})c_\beta \end{cases} \tag{F.4}$$

Injecting Eq.(F.4) in Eq.(F.3), we find:

$$\boxed{\rho(\vec{r}) = \sum_{\alpha\beta} \delta_{\sigma_\beta\sigma_\alpha}\delta_{\tau_\beta\tau_\alpha}\psi^*_\alpha(\vec{r})\psi_\beta(\vec{r})\rho_{\beta\alpha}} \tag{F.5}$$

The contact density-dependent part of the mean field reads as follows:

$$\boxed{\Gamma_{\alpha\gamma} = \sum_{\delta\beta} \langle\alpha\beta|V^{(D)}(1 - P_r P_\sigma P_\tau)|\gamma\delta\rangle\rho_{\delta\beta}} \tag{F.6}$$

The tradition [47] is to evaluate the direct part and the part of the mean field all together as they combine to give a simpler expression. Applying explicitly the operators P_σ and P_τ we find:

$$\Gamma^\tau_{\alpha\gamma} = t_3\langle\alpha|[\rho(\vec{r})]^\alpha \sum_{\delta\beta} \psi^*_\beta(\vec{r})\psi_\delta(\vec{r})[(1 - x_0\delta_{\tau\tau'})\delta_{s_\alpha s_\gamma}\delta_{s_\beta s_\delta} + (x_0 - \delta_{\tau\tau'})\delta_{s_\alpha s_\delta}\delta_{s_\beta s_\gamma}]\rho^{\tau'}_{\delta\beta}|\gamma\rangle \tag{F.7}$$

We now introduce S_L and S_R standing respectively for the first and the second contributions of Eq.(F.7). We start evaluating S_L :

$$S^\tau_L = \delta_{s_\alpha s_\gamma} \sum_{\delta\beta} \psi^*_\beta(\vec{r})\psi_\delta(\vec{r})(1 - x_0\delta_{\tau\tau'})\delta_{s_\beta s_\delta}\rho^{\tau'}_{\delta\beta} \tag{F.8}$$

We easily find back the local density:

$$\boxed{S^\tau_L = \delta_{s_\alpha s_\gamma}(\rho(\vec{r}) - x_0\rho^\tau(\vec{r}))} \tag{F.9}$$

We now focus on S_R:

$$S^\tau_R = \sum_{\delta\beta} \psi^*_\beta(\vec{r})\psi_\delta(\vec{r})(x_0 - \delta_{\tau\tau'})\delta_{s_\alpha s_\delta}\delta_{s_\beta s_\gamma}\rho_{\delta\beta} \tag{F.10}$$

We use the time-reversal property of the matrix ρ:

$$\begin{aligned} S^\tau_R = \sum_{\delta\beta>} [&\psi^*_\beta(\vec{r})\psi_\delta(\vec{r})(x_0 - \delta_{\tau\tau'})\delta_{s_\alpha s_\delta}\delta_{s_\beta s_\gamma} \\ &+(-1)^{s_\beta - s_\delta}\psi_\beta(\vec{r})\psi^*_\delta(\vec{r})(x_0 - \delta_{\tau\tau'})\delta_{s_\alpha \bar{s_\delta}}\delta_{\bar{s_\beta} s_\gamma}]\rho_{\delta\beta} \end{aligned} \tag{F.11}$$

We then use the symmetry of ρ to exchange δ and β in the last term of the sum. The conditions on the spins then give:

$$S_R^\tau = \delta_{s_\alpha s_\gamma} \sum_{\delta\beta>} \delta_{s_\beta s_\delta} \psi_\beta^*(\vec{r})\psi_\delta(\vec{r})(x_0 - \delta_{\tau\tau'})\rho_{\delta\beta} \tag{F.12}$$

We separate the sum in Eq.(F.12) in two parts in order to span the full space:

$$S_R^\tau = \delta_{s_\alpha s_\gamma} \frac{1}{2}(\sum_{\delta\beta>} \delta_{s_\beta s_\delta} \psi_\beta^*(\vec{r})\psi_\delta(\vec{r})(x_0 - \delta_{\tau\tau'})\rho_{\delta\beta} + \sum_{\delta\beta<} \delta_{s_{\bar{\beta}} s_{\bar{\delta}}} \psi_\beta(\vec{r})\psi_\delta^*(\vec{r})(x_0 - \delta_{\tau\tau'})\rho_{\bar{\delta}\bar{\beta}}) \tag{F.13}$$

We then find using the time-reversal properties of the density:

$$S_R^\tau = \delta_{s_\alpha s_\gamma} \frac{1}{2} \sum_{\delta\beta} \delta_{s_\beta s_\delta} \psi_\beta^*(\vec{r})\psi_\delta(\vec{r})(x_0 - \delta_{\tau\tau'})\rho_{\delta\beta} \tag{F.14}$$

Here also, we find back the local density:

$$\boxed{S_R^\tau = \delta_{s_\alpha s_\gamma} \frac{1}{2}(x_0\rho(\vec{r}) - \rho^\tau(\vec{r}))} \tag{F.15}$$

The field finally reads:

$$\boxed{\Gamma_{\alpha\gamma}^\tau = t_3 \delta_{s_\alpha s_\gamma} \langle\alpha|(1 + \frac{x_0}{2})[\rho(\vec{r})]^{\alpha+1} - (\frac{1}{2} + x_0)\rho^\tau(\vec{r})[\rho(\vec{r})]^\alpha|\gamma\rangle} \tag{F.16}$$

We can now explicitly consider the spins.

Block ++:

Here, we consider ($\alpha\uparrow$,$\gamma\uparrow$). Looking at Eq.(F.16), the expression we search for is straightforward:

$$\boxed{\Gamma_{\alpha\gamma}^{\tau++} = t_3 \langle\alpha|(1 + \frac{x_0}{2})[\rho(\vec{r})]^{\alpha+1} - (\frac{1}{2} + x_0)\rho^\tau(\vec{r})[\rho(\vec{r})]^\alpha|\gamma\rangle} \tag{F.17}$$

Block −−:

Here, we consider ($\alpha\downarrow$,$\gamma\downarrow$). It is clear that this spin block is the same as the ++ one:

$$\boxed{\Gamma_{\alpha\gamma}^{\tau--} = \Gamma_{\alpha\gamma}^{\tau++}} \tag{F.18}$$

Block −+:

Here, we consider ($\alpha\downarrow$,$\gamma\uparrow$). The $\delta_{s_\alpha s_\gamma}$ in Eq.(F.16) directly implies:

$$\boxed{\Gamma_{\alpha\gamma}^{\tau-+} = 0} \tag{F.19}$$

Block +−:

Here, we consider ($\alpha\uparrow$,$\gamma\downarrow$). The $\delta_{s_\alpha s_\gamma}$ in Eq.($F.16$) directly implies:

$$\boxed{\Gamma^{\tau+-}_{\alpha\gamma} = 0} \tag{F.20}$$

Remark on the isospin symmetry:

It is interesting to observe that the HFB energy coming from the density-dependent term won't depend on the isospin. Indeed, the energy reads:

$$\begin{aligned} E^\tau = \sum_{\alpha\gamma} \Gamma^\tau_{\alpha\gamma}\rho^\tau_{\alpha\gamma} = \sum_{\alpha\gamma}\int d\vec{r} t_3[(1+\frac{x_0}{2})[\rho(\vec{r})]^{\alpha+1} \\ -(\frac{1}{2}+x_0)\rho^\tau(\vec{r})[\rho(\vec{r})]^\alpha]\psi^*_\alpha(\vec{r})\psi_\gamma(\vec{r})\rho^\tau_{\alpha\gamma}\delta_{s_\alpha s_\gamma} \end{aligned} \tag{F.21}$$

We exchange the sum and the integral and we find back the local density:

$$E^\tau = \int d\vec{r} t_3[(1+\frac{x_0}{2})[\rho(\vec{r})]^{\alpha+1} - (\frac{1}{2}+x_0)\rho^\tau(\vec{r})[\rho(\vec{r})]^\alpha]\rho^\tau(\vec{r}) \tag{F.22}$$

We can rewrite:

$$E^\tau = \int d\vec{r} t_3[\rho(\vec{r})]^\alpha[(1+\frac{x_0}{2})[(\rho(\vec{r})^\tau)^2 + \rho(\vec{r})^{\bar{\tau}}\rho(\vec{r})^\tau] - (\frac{1}{2}+x_0)(\rho^\tau(\vec{r}))^2] \tag{F.23}$$

We finally find:

$$\boxed{E^\tau = \int d\vec{r} t_3[\rho(\vec{r})]^\alpha(1+\frac{x_0}{2})\rho(\vec{r})^{\bar{\tau}}\rho(\vec{r})^\tau} \tag{F.24}$$

It is clear that this expression does not depend on the isospin.

F.1.2 Mean field numerical evaluation

Now, we focus on the numerical evaluation of the contact density-dependent mean field. This evaluation is done using the quadratures methods (see Appendix N). The integral we have to evaluate reads as follows:

$$\boxed{I = t_3\int d\vec{r}\psi^*_\alpha(\vec{r})\psi_\gamma(\vec{r})((1+\frac{x_0}{2})[\rho(\vec{r})]^{\alpha+1} - (\frac{1}{2}+x_0)\rho^\tau(\vec{r})[\rho(\vec{r})]^\alpha)} \tag{F.25}$$

We set:

$$R^\tau(\vec{r}) = t_3(1+\frac{x_0}{2})[\rho(\vec{r})]^{\alpha+1} - t_3(\frac{1}{2}+x_0)\rho^\tau(\vec{r})[\rho(\vec{r})]^\alpha \tag{F.26}$$

The integral then reduces:

$$I = \int d\vec{r}\psi^*_\alpha(\vec{r})\psi_\gamma(\vec{r})R^\tau(\vec{r}) \tag{F.27}$$

It is clear that R has the axial symmetry just as ρ. Moreover, as we always have ($m_\alpha = m_\gamma$), we can write:

$$\psi^*_\alpha(\vec{r})\psi_\gamma(\vec{r}) = Re[\psi_\alpha(\vec{r})\psi_\gamma(\vec{r})] \tag{F.28}$$

Using Eq.(F.28), the integral can be expressed as follows:

$$I = \int_{-\infty}^{+\infty} dz\varphi_\alpha(z+d_\alpha)\varphi_\gamma(z+d_\gamma)\int_0^{+\infty} r_\perp dr_\perp Re[\phi_\alpha(r_\perp)\phi_\gamma(r_\perp)]R^\tau(r_\perp,z)\int_0^{2\pi} d\theta \tag{F.29}$$

The last integral with respect to θ is straightforward:

$$I = 2\pi\int_{-\infty}^{+\infty} dz\varphi_\alpha(z+d_\alpha)\varphi_\gamma(z+d_\gamma)\int_0^{+\infty} r_\perp dr_\perp Re[\phi_\alpha(r_\perp)\phi_\gamma(r_\perp)]R^\tau(r_\perp,z) \tag{F.30}$$

We can separate the expression into a $r_\perp$ part and a z part:

$$I = 2\pi e^{-\frac{1}{2b_z^2}(\frac{d_\alpha-d_\gamma}{\sqrt{2}})^2}\int_{-\infty}^{+\infty} dz e^{-\frac{1}{2b_z^2}(\sqrt{2}z+\frac{d_\alpha+d_\gamma}{\sqrt{2}})^2}\bar{\varphi}_\alpha(z+d_\alpha)\bar{\varphi}_\gamma(z+d_\gamma) \tag{F.31}$$
$$\int_0^{+\infty} r_\perp dr_\perp \bar{\phi}_\alpha(r_\perp)\bar{\phi}_\gamma(r_\perp)R^\tau(r_\perp,z)$$

The bars above the harmonic oscillator wave functions stand for the fact we consider only their real part without their exponential factor. It is natural to apply a Gauss-Hermite quadrature on the z-integral and a Gauss-Laguerre quadrature on the $r_\perp$-integral.
When it comes to the z-integral with the 2-center representation, two possibilities do exist. We can either explicitly use the exponential of the wave functions in the quadrature or we can just perform the quadrature "brute force". The first method seems to be more elegant but requires to perform a tedious change of variables. The "brute force" method is way simpler but has a bad reputation since it is claimed that the change of variable in the wave functions is not only elegant but also makes the quadrature more efficient. We tried both methods and found indeed better performances using the change of variable in the case of highly deformed nuclei. It means that less points were required in the quadrature to reach the same precision. However this advantage was in fact small compared to its non negligible additional complexity. For this reason, the "brute force" method has been preferred wherever we were dealing with new quantities, which are more complex to calculate. For the rest, we showed respect for the tradition.

We therefore set the following change of variable:

$$\begin{cases} (\frac{r_\perp}{b_r})^2 \to r_\perp \\ \frac{z+\frac{d_\alpha+d_\gamma}{2}}{b_z} \to z \end{cases} \tag{F.32}$$

It brings:

$$I = \pi b_z b_r^2 c_{\alpha\gamma} e^{-\frac{1}{2b_z^2}(\frac{d_\alpha - d_\gamma}{\sqrt{2}})^2} \int_{-\infty}^{+\infty} dz e^{-z^2} H_{n_{z_\alpha}}(z + \frac{d_\alpha - d_\gamma}{2b_z}) H_{n_{z_\gamma}}(z + \frac{-d_\alpha + d_\gamma}{2b_z}) \quad \text{(F.33)}$$
$$\int_0^{+\infty} dr_\perp e^{-r_\perp} r_\perp^m L_{n_{\perp_\alpha}}^m[r_\perp] L_{n_{\perp_\gamma}}^m[r_\perp] R^\tau(b_r\sqrt{r_\perp}, z b_z - \frac{d_\alpha + d_\gamma}{2})$$

With:

$$c_{\alpha\gamma} = \frac{1}{b_r^2 \pi} \sqrt{\frac{n_{\perp_\alpha}!}{(n_{\perp_\alpha} + |m_\alpha|)!}} \sqrt{\frac{n_{\perp_\gamma}!}{(n_{\perp_\gamma} + |m_\gamma|)!}} \frac{1}{b_z \sqrt{\pi} \sqrt{2^{n_{z_\alpha}} n_{z_\alpha}! 2^{n_{z_\gamma}} n_{z_\gamma}!}} \quad \text{(F.34)}$$

We then finally apply the quadratures:

$$\boxed{\begin{aligned} I \approx \pi b_z b_r^2 c_{\alpha\gamma} e^{-\frac{1}{2b_z^2}(\frac{d_\alpha - d_\gamma}{\sqrt{2}})^2} \sum_{j=1}^{n_{GLA}} w_{GLA_j} r_j^m L_{n_{\perp_\alpha}}^m[r_j] L_{n_{\perp_\gamma}}^m[r_j] \\ \sum_{i=1}^{n_{GHE}} w_{GHE_i} H_{n_{z_\alpha}}(z_i + \frac{d_\alpha - d_\gamma}{2b_z}) H_{n_{z_\gamma}}(z_i + \frac{-d_\alpha + d_\gamma}{2b_z}) R^\tau(b_r\sqrt{r_j}, z_i b_z - \frac{d_\alpha + d_\gamma}{2}) \end{aligned}} \quad \text{(F.35)}$$

For the sake of numerical performances, it is important to do the calculations in the order given in Eq.(F.35). Here n_{GLA} and n_{GHE} represent the number of points chosen for the Gauss-Laguerre and Gauss-Hermite quadratures respectively. The definition of z_i, r_j, w_{GHE_i}, w_{GLA_j} are given in the dedicated Appendix N.

F.1.3 Pairing field

The contact density-dependent part of the pairing field reads as follows:

$$\boxed{\Delta_{\alpha\bar{\beta}} = \sum_{\gamma\delta} (-1)^{s_\beta - s_\delta} \langle \alpha\bar{\beta} | V^{(D)} (1 - P_r P_\sigma P_\tau) | \gamma\bar{\delta} \rangle \kappa_{\gamma\bar{\delta}}} \quad \text{(F.36)}$$

We write this expression more explicitly applying P_σ and P_τ:

$$\Delta_{\alpha\bar{\beta}} = t_3 \sum_{\gamma\delta} (-1)^{s_\beta - s_\delta} \langle (s_\alpha, \tau_\beta)(\bar{s_\beta}, \tau_\beta) | (1 - x_0) \quad \text{(F.37)}$$
$$+ (x_0 - 1) P_\sigma | (s_\gamma, \tau_\gamma)(\bar{s_\delta}, \tau_\delta) \rangle \langle \alpha\bar{\beta} | [\rho(\vec{r})]^\alpha | \gamma\bar{\delta} \rangle \kappa_{\gamma\bar{\delta}}$$

In the D1-type Gogny interactions, $x_0 = 1$. Because of that, it is straightforward to see from Eq.(F.37) that the pairing field is always equals to zero:

$$\boxed{\Delta_{\alpha\bar{\beta}} = 0} \quad \text{(F.38)}$$

Note that the parameter x_0 has been specially chosen to give this result, as firstly pairing correlations are very little renormalized by medium effect (bare interaction) and secondly in order to avoid the ultraviolet divergences we may encounter evaluating pairing energies coming from contact forces.

F.1.4 Rearrangement field reduced expression

Rearrangement field is defined as follows:

$$\boxed{\partial\Gamma^{\tau}_{\alpha\beta} = \sum_{\gamma\delta}\sum_{\eta\mu}\langle\gamma\eta|\frac{\partial V^{(D)}}{\partial\rho^{\tau}_{\alpha\beta}}(1-P_rP_\sigma P_\tau)|\delta\mu\rangle\rho_{\gamma\delta}\rho_{\eta\mu}} \tag{F.39}$$

We first want to give an expression of the derivative of the local density with respect to the $\rho_{\alpha\beta}$. Using Eq.(F.5), we find:

$$\boxed{\frac{\partial\rho(\vec{r})}{\partial\rho_{\alpha\beta}} = \delta_{\sigma_\beta\sigma_\alpha}\delta_{\tau_\beta\tau_\alpha}\psi^*_\alpha(\vec{r})\psi_\beta(\vec{r})} \tag{F.40}$$

Note that we can already observe that the rearrangement field won't depend on the isospin. We can now rewrite the field:

$$\begin{aligned}\partial\Gamma_{\alpha\beta} = \delta_{\sigma_\beta\sigma_\alpha}\sum_{\gamma\delta}\sum_{\eta\mu}\langle\gamma\eta|t_3\alpha[\rho(\vec{r}_1)]^{\alpha-1}\delta_{\vec{r}_1-\vec{r}_2}\psi^*_\alpha(\vec{r}_1)\psi_\beta(\vec{r}_1)[(1-x_0\delta_{\tau\tau'})\delta_{s_\gamma s_\delta}\delta_{s_\mu s_\eta} \\ +(x_0-\delta_{\tau\tau'})\delta_{s_\gamma s_\mu}\delta_{s_\delta s_\eta}]|\delta\mu\rangle\rho^{\tau}_{\gamma\delta}\rho^{\tau'}_{\eta\mu}\end{aligned} \tag{F.41}$$

We rephrase:

$$\begin{aligned}\partial\Gamma_{\alpha\beta} = \delta_{\sigma_\beta\sigma_\alpha}t_3\alpha\langle\alpha|[\rho(\vec{r}_1)]^{\alpha-1}\sum_{\gamma\delta}\sum_{\eta\mu}\psi^*_\gamma(\vec{r})\psi_\delta(\vec{r})\psi^*_\eta(\vec{r})\psi_\mu(\vec{r})\rho^{\tau}_{\gamma\delta}\rho^{\tau'}_{\eta\mu}[(1-x_0\delta_{\tau\tau'})\delta_{s_\gamma s_\delta}\delta_{s_\mu s_\eta} \\ +(x_0-\delta_{\tau\tau'})\delta_{s_\gamma s_\mu}\delta_{s_\delta s_\eta}]|\beta\rangle\end{aligned} \tag{F.42}$$

We separate the first and last parts of Eq.(F.42). We start with the first one:

$$S_L = \sum_{\gamma\delta}\sum_{\eta\mu}\psi^*_\gamma(\vec{r})\psi_\delta(\vec{r})\psi^*_\eta(\vec{r})\psi_\mu(\vec{r})\rho^{\tau}_{\gamma\delta}\rho^{\tau'}_{\eta\mu}(1-x_0\delta_{\tau\tau'})\delta_{s_\gamma s_\delta}\delta_{s_\mu s_\eta} \tag{F.43}$$

We find back the local density:

$$S_L = \sum_{\tau}\sum_{\tau'}(1-x_0\delta_{\tau\tau'})\rho^{\tau}(\vec{r})\rho^{\tau'}(\vec{r}) \tag{F.44}$$

It eventually reads:

$$\boxed{S_L = [\rho(\vec{r})]^2 - x_0([\rho^{\tau}(\vec{r})]^2 + [\rho^{\bar{\tau}}(\vec{r})]^2)} \tag{F.45}$$

Concerning the right part, we write:

$$S_R = \sum_{\gamma\delta}\psi^*_\gamma(\vec{r})\psi_\delta(\vec{r})\rho^{\tau}_{\gamma\delta}\sum_{\eta\mu}\psi^*_\eta(\vec{r})\psi_\mu(\vec{r})\rho^{\tau'}_{\eta\mu}(x_0-\delta_{\tau\tau'})\delta_{s_\gamma s_\mu}\delta_{s_\delta s_\eta} \tag{F.46}$$

We use the time-reversal properties of ρ:

$$S_R = \sum_{\gamma\delta} \psi^*_\gamma(\vec{r})\psi_\delta(\vec{r})\rho^\tau_{\gamma\delta} \sum_{\eta\mu>} (x_0 - \delta_{\tau\tau'})\psi^*_\eta(\vec{r})\psi_\mu(\vec{r})[\delta_{s_\gamma s_\mu}\delta_{s_\delta s_\eta} + (-1)^{s_\eta - s_\mu}\delta_{s_\gamma \bar{s_\eta}}\delta_{s_\delta \bar{s_\mu}}]\rho^{\tau'}_{\eta\mu} \quad \text{(F.47)}$$

The conditions on the spins then directly give:

$$S_R = \sum_{\gamma\delta} \psi^*_\gamma(\vec{r})\psi_\delta(\vec{r})\rho^\tau_{\gamma\delta}\delta_{s_\gamma s_\delta} \sum_{\eta\mu>} (x_0 - \delta_{\tau\tau'})\psi^*_\eta(\vec{r})\psi_\mu(\vec{r})\rho^{\tau'}_{\eta\mu}\delta_{s_\eta s_\mu} \quad \text{(F.48)}$$

We find back the local density:

$$S_R = \frac{1}{2}\sum_\tau \sum_{\tau'} \rho^\tau(\vec{r})\rho^{\tau'}(\vec{r})(x_0 - \delta_{\tau\tau'}) \quad \text{(F.49)}$$

We finally end up with:

$$\boxed{S_R = \frac{x_0}{2}[\rho(\vec{r})]^2 - \frac{1}{2}([\rho^\tau(\vec{r})]^2 + [\rho^{\bar{\tau}}(\vec{r})]^2)} \quad \text{(F.50)}$$

Integrating Eq.(F.50) and Eq.(F.45) in the expression of the field Eq.(F.42), we can find its reduced form:

$$\boxed{\partial\Gamma_{\alpha\beta} = \delta_{\sigma_\beta\sigma_\alpha} t_3\alpha\langle\alpha|[\rho(\vec{r}_1)]^{\alpha-1}[[\rho(\vec{r})]^2(1+\frac{x_0}{2}) - ([\rho^\tau(\vec{r})]^2 + [\rho^{\bar{\tau}}(\vec{r})]^2)(\frac{1}{2}+x_0)]|\beta\rangle} \quad \text{(F.51)}$$

This expression is then treated using quadratures.

F.1.5 Rearrangement field numerical evaluation

This part aims to explain the numerical evaluation of the following quantity accounting for the contact density-dependent rearrangement fied:

$$\boxed{I = \int d\vec{r}\psi^*_\alpha(\vec{r})\psi_\beta(\vec{r})\alpha t_3[\rho(\vec{r}_1)]^{\alpha-1}[[\rho(\vec{r})]^2(1+\frac{x_0}{2}) - ([\rho^\tau(\vec{r})]^2 + [\rho^{\bar{\tau}}(\vec{r})]^2)(\frac{1}{2}+x_0)]} \quad \text{(F.52)}$$

We set:

$$R(\vec{r}) = t_3\alpha[\rho(\vec{r}_1)]^{\alpha-1}[[\rho(\vec{r})]^2(1+\frac{x_0}{2}) - ([\rho^\tau(\vec{r})]^2 + [\rho^{\bar{\tau}}(\vec{r})]^2)(\frac{1}{2}+x_0)] \quad \text{(F.53)}$$

With Eq.(F.53), Eq.(F.52) reduces to:

$$I = \int d\vec{r}\psi^*_\alpha(\vec{r})\psi_\beta(\vec{r})R(\vec{r}) \quad \text{(F.54)}$$

As $(m_\alpha = m_\gamma)$ always holds, we get:

$$\psi^*_\alpha(\vec{r})\psi_\gamma(\vec{r}) = Re[\psi_\alpha(\vec{r})\psi_\gamma(\vec{r})] \tag{F.55}$$

The inegral therefore reads:

$$I = 2\pi \int_{-\infty}^{+\infty} dz \varphi_\alpha(z+d_\alpha)\varphi_\beta(z+d_\beta) \int_0^{+\infty} r_\perp dr_\perp \phi_\alpha(r_\perp)\phi_\beta(r_\perp) R(r_\perp, z) \tag{F.56}$$

We'd like to perform a Gauss-Hermite quadrature on the z-integral and a Gauss-Laguerre in the $r_\perp$-integral. Before that, we set the following change of variable:

$$\begin{cases} (\frac{r_\perp}{b_r})^2 \to r_\perp \\ \frac{z}{b_z} \to z \end{cases} \tag{F.57}$$

We rewrite the integral using Eq.(F.57) :

$$\begin{aligned} I = \pi b_z b_r^2 c_{\alpha\beta} \int_{-\infty}^{+\infty} dz e^{-z^2} e^{z^2} \varphi_\alpha(zb_z + d_\alpha)\varphi_\beta(zb_z + d_\beta) \\ \int_0^{+\infty} dr_\perp e^{-r_\perp} r_\perp^m L^m_{n_{\perp_\alpha}}[r_\perp] L^m_{n_{\perp_\beta}}[r_\perp] R^\tau(b_r\sqrt{r_\perp}, zb_z) \end{aligned} \tag{F.58}$$

With:

$$c_{\alpha\beta} = \frac{1}{b_r^2\pi} \sqrt{\frac{n_{\perp_\alpha}!}{(n_{\perp_\alpha} + |m_\alpha|)!}} \sqrt{\frac{n_{\perp_\beta}!}{(n_{\perp_\beta} + |m_\beta|)!}} \tag{F.59}$$

We finally apply the quadratures:

$$\boxed{\begin{aligned} I \approx \pi b_z b_r^2 c_{\alpha\beta} \sum_{j=1}^{n_{GLA}} w_{GLA_j} r_j^m L^m_{n_{\perp_\alpha}}[r_j] L^m_{n_{\perp_\gamma}}[r_j] \\ \sum_{i=1}^{n_{GHE}} w_{GHE_i} e^{z_i^2} \varphi_\alpha(z_i b_z + d_\alpha)\varphi_\beta(z_i b_z + d_\beta) R^\tau(b_r\sqrt{r_j}, z_i b_z) \end{aligned}} \tag{F.60}$$

For the sake of numerical performances, it is important to do the calculations in the order given in Eq.(F.35). Here n_{GLA} and n_{GHE} represent the number of points chosen for the Gauss-Laguerre and Gauss-Hermite quadratures respectively. The definition of z_i, r_j, w_{GHE_i}, w_{GLA_j} are given in the dedicated Appendix N.

F.2 Collective fields

This part aims to give an expression of the collective fields in the more complex case when ρ^{01} is not symmetric anymore and the two harmonic oscillator bases $\{0\}$ and $\{1\}$ are different. This derivations are useful to evaluate quantities of the following type :

$$\langle \Phi_0 | \hat{H} | \Phi_1 \rangle \tag{F.61}$$

Those quantities are not only useful in the SCIM approach but appear in many situations as for instance in the expression of the true TDGCM mass and collective potential.

F.2.1 Collective mean field reduced expression

There is now straightforward way to choose which local density should be put in the density-dependent term when the states on the left and on the right are different. The only certainty we have is that the $\{0\} \to \{1\}$ limit has to give back the traditional local density associated with the state $\{1\}$. With this condition, we could for example set:

$$\rho^{01}(\vec{r}) := \frac{\rho^{00}(\vec{r}) + \rho^{11}(\vec{r})}{2} \tag{F.62}$$

However, this local density doesn't work properly in practice. This is the reason why we've choosen in this PhD thesis the following definition of the transition local density [82]:

$$\rho^{01}(\vec{r}) = \sum_{\sigma\tau} \rho^{01}(\vec{r},\sigma,\tau) := \sum_{\sigma\tau} \frac{\langle \Phi_0 | \Psi_0^+(\vec{r},\sigma,\tau)\Psi_1(\vec{r},\sigma,\tau)|\Phi_1\rangle}{\langle \Phi_0|\Phi_1\rangle} \tag{F.63}$$

Here Ψ_0^+ and Ψ_1 are the field operators associated with the bases $\{0\}$ and $\{1\}$ respectively. They read as follows:

$$\begin{cases} \Psi_0^+(\vec{r},\sigma,\tau) = \sum_\alpha \delta_{\tau_\alpha\tau}\delta_{\sigma_\alpha\sigma}\psi_\alpha^*(\vec{r},b_0)c_{0,\alpha}^+ \\ \Psi_1(\vec{r},\sigma,\tau) = \sum_\beta \delta_{\tau_\beta\tau}\delta_{\sigma_\beta\sigma}\psi_\beta(\vec{r},b_1)c_{1,\beta} \end{cases} \tag{F.64}$$

Using this result in Eq.(F.63), we find:

$$\rho^{01}(\vec{r}) = \sum_{\alpha\beta} \delta_{\sigma_\beta\sigma_\alpha}\delta_{\tau_\beta\tau_\alpha}\psi_\alpha^*(\vec{r},b_0)\psi_\beta(\vec{r},b_1)\frac{\langle \Phi_0|c_{0,\alpha}^+ c_{1,\beta}|\Phi_1\rangle}{\langle \Phi_0|\Phi_1\rangle} \tag{F.65}$$

Then:

$$\boxed{\rho^{01}(\vec{r}) = \sum_{\alpha\beta} \delta_{\sigma_\beta\sigma_\alpha}\psi_\alpha^*(\vec{r},b_0)\psi_\beta(\vec{r},b_1)\rho_{\beta\alpha}^{01}} \tag{F.66}$$

Note that with this definition some negative values at the power $\alpha = 1/3$ may appear. In that case, we naturally chose to set:

$$(\rho^{01}(\vec{r}))^\alpha := (\frac{\rho^{01}(\vec{r})}{|\rho^{01}(\vec{r})|})^{1/\alpha}(|\rho^{01}(\vec{r})|)^\alpha \tag{F.67}$$

We now have everything in hands to consider the collective field in itself. The latter reads:

$$\boxed{\bar{\Gamma}_{\alpha\gamma} = \sum_{\delta\beta} {}_0\langle \alpha\beta|V^{(D)}(1 - P_r P_\sigma P_\tau)|\gamma\delta\rangle_1 \rho_{\delta\beta}^{01}} \tag{F.68}$$

We apply the operators P_σ and P_τ :

$$\bar{\Gamma}^{\tau}_{\alpha\gamma} = t_{30}\langle\alpha|[\rho^{01}(\vec{r})]^{\alpha}\sum_{\delta\beta}\psi^{*}_{\beta}(\vec{r},b_0)\psi_{\delta}(\vec{r},b_1)[(1-x_0\delta_{\tau\tau'})\delta_{s_\alpha s_\gamma}\delta_{s_\beta s_\delta} + (x_0-\delta_{\tau\tau'})\delta_{s_\alpha s_\delta}\delta_{s_\beta s_\gamma}]\rho^{01\tau'}_{\delta\beta}|\gamma\rangle_1 \tag{F.69}$$

We separate Eq.(*F*.69) into a left $\bar{S}_L$ and a right $\bar{S}_R$. We start with $\bar{S}_L$:

$$\bar{S}^{\tau}_{L} = \delta_{s_\alpha s_\gamma}\sum_{\delta\beta}\psi^{*}_{\beta}(\vec{r},b_0)\psi_{\delta}(\vec{r},b_1)(1-x_0\delta_{\tau\tau'})\delta_{s_\beta s_\delta}\rho^{01\tau'}_{\delta\beta} \tag{F.70}$$

We find back the transition local density:

$$\boxed{\bar{S}^{\tau}_{L} = \delta_{s_\alpha s_\gamma}(\rho^{01}(\vec{r}) - x_0\rho^{01\tau}(\vec{r}))} \tag{F.71}$$

We now focus on $\bar{S}_R$:

$$\bar{S}^{\tau}_{R} = \sum_{\delta\beta}\psi^{*}_{\beta}(\vec{r},b_0)\psi_{\delta}(\vec{r},b_1)(x_0-\delta_{\tau\tau'})\delta_{s_\alpha s_\delta}\delta_{s_\beta s_\gamma}\rho^{01\tau'}_{\delta\beta} \tag{F.72}$$

We use the time-reversal properties of ρ^{01}:

$$\boxed{\begin{aligned}\bar{S}^{\tau}_{R} = \sum_{\delta\beta>}&[\psi^{*}_{\beta}(\vec{r},b_0)\psi_{\delta}(\vec{r},b_1)(x_0-\delta_{\tau\tau'})\delta_{s_\alpha s_\delta}\delta_{s_\beta s_\gamma} \\ &+(-1)^{s_\beta - s_\delta}\psi_{\beta}(\vec{r},b_0)\psi^{*}_{\delta}(\vec{r},b_1)(x_0-\delta_{\tau\tau'})\delta_{s_\alpha \bar{s_\delta}}\delta_{\bar{s_\beta} s_\gamma}]\rho^{01\tau'}_{\delta\beta}\end{aligned}} \tag{F.73}$$

As the transition density matrix is no more symmetric, we can not exchange δ and β as done in Eq.(*F*.14). Because of that, the spin blocks $-+$ and $+-$ won't be zero as in the case of the non-collective mean field. We now explicitly consider the spins.

Block ++:

Here, we consider ($\alpha\uparrow$,$\gamma\uparrow$). We first want to reduce $\bar{S}_R$:

$$\bar{S}^{\tau++}_{R} = \sum_{\delta\beta>}[\psi^{*}_{\beta}(\vec{r},b_0)\psi_{\delta}(\vec{r},b_1)(x_0-\delta_{\tau\tau'})\delta_{s^{+}_{\beta}s^{+}_{\delta}} + \psi_{\beta}(\vec{r},b_0)\psi^{*}_{\delta}(\vec{r},b_1)(x_0-\delta_{\tau\tau'})\delta_{s^{-}_{\beta}s^{-}_{\delta}}]\rho^{01\tau'}_{\delta\beta} \tag{F.74}$$

Because of the axial symmetry, we always have $(s_\beta = s_\delta) \Rightarrow (m_\beta = m_\delta)$. This implies:

$$\psi_{\beta}(\vec{r},b_0)\psi^{*}_{\delta}(\vec{r},b_1) = \psi^{*}_{\beta}(\vec{r},b_0)\psi_{\delta}(\vec{r},b_1) \tag{F.75}$$

We can therefore write:

$$\bar{S}^{\tau++}_{R} = \sum_{\delta\beta>}\psi^{*}_{\beta}(\vec{r},b_0)\psi_{\delta}(\vec{r},b_1)(x_0-\delta_{\tau\tau'})\delta_{s_\beta s_\delta}\rho^{01\tau'}_{\delta\beta} \tag{F.76}$$

Now, we can perform the same process as in Eq.($F.14$):

$$\bar{S}_R^{\tau++} = \frac{1}{2}(\sum_{\delta\beta>} \psi_\beta^*(\vec{r},b_0)\psi_\delta(\vec{r},b_1)(x_0-\delta_{\tau\tau'})\delta_{s_\beta s_\delta}\rho_{\delta\beta}^{01\tau'} + \sum_{\delta\beta<} \psi_\beta(\vec{r},b_0)\psi_\delta^*(\vec{r},b_1)(x_0-\delta_{\tau\tau'})\delta_{s_\beta s_\delta}\rho_{\delta\beta}^{01\tau'}) \tag{F.77}$$

Then:

$$\bar{S}_R^{\tau++} = \frac{1}{2}\sum_{\delta\beta} \psi_\beta^*(\vec{r},b_0)\psi_\delta(\vec{r},b_1)(x_0-\delta_{\tau\tau'})\delta_{s_\beta s_\delta}\rho_{\delta\beta}^{01\tau'} \tag{F.78}$$

We find back the transition local density:

$$\boxed{\bar{S}_R^{\tau++} = \frac{1}{2}(x_0\rho^{01}(\vec{r}) - \rho^{01\tau}(\vec{r}))} \tag{F.79}$$

It is now straightforward to write the field:

$$\boxed{\bar{\Gamma}_{\alpha\gamma}^{\tau++} = t_{30}\langle\alpha|(1+\frac{x_0}{2})[\rho^{01}(\vec{r})]^{\alpha+1} - (\frac{1}{2}+x_0)\rho^{01\tau}(\vec{r})[\rho^{01}(\vec{r})]^{\alpha}|\gamma\rangle_1} \tag{F.80}$$

Block $--$:

Here, we consider ($\alpha\downarrow$,$\gamma\downarrow$). It is clear that:

$$\boxed{\bar{\Gamma}_{\alpha\gamma}^{\tau--} = \bar{\Gamma}_{\alpha\gamma}^{\tau++}} \tag{F.81}$$

Block $-+$:

Here, we consider ($\alpha\downarrow$,$\gamma\uparrow$). In contrast with the non-collective case, this part of the field is not equal to zero. We start by writing $\bar{S}_R$:

$$\bar{S}_R^{\tau-+} = \sum_{\delta\beta>}(x_0-\delta_{\tau\tau'})[\psi_\beta^*(\vec{r},b_0)\psi_\delta(\vec{r},b_1)\rho_{\delta\beta}^{01-+\tau'}\delta_{s_\delta^- s_\beta^+} - \psi_\beta(\vec{r},b_0)\psi_\delta^*(\vec{r},b_1)\rho_{\delta\beta}^{01+-\tau'}\delta_{s_\delta^+ s_\beta^-}] \tag{F.82}$$

Then, we define a new spin off-diagonal local transition density:

$$\boxed{\tilde{\rho}^{01\tau}(\vec{r}) = \sum_{\delta\beta>}[\psi_\beta^*(\vec{r},b_0)\psi_\delta(\vec{r},b_1)\rho_{\delta\beta}^{01-+\tau}\delta_{s_\delta^- s_\beta^+} - \psi_\beta(\vec{r},b_0)\psi_\delta^*(\vec{r},b_1)\rho_{\delta\beta}^{01+-\tau}\delta_{s_\delta^+ s_\beta^-}]} \tag{F.83}$$

We observe that this new quantity explicitly reads:

$$\tilde{\rho}^{01\tau}(\vec{r}) = e^{i\varphi_r}Re[\sum_{\delta\beta>}[\psi_\beta^*(\vec{r},b_0)\psi_\delta(\vec{r},b_1)\rho_{\delta\beta}^{01-+\tau}\delta_{s_\delta^- s_\beta^+} - \psi_\beta(\vec{r},b_0)\psi_\delta^*(\vec{r},b_1)\rho_{\delta\beta}^{01+-\tau}\delta_{s_\delta^+ s_\beta^-}]] \tag{F.84}$$

However, in the field, the complex exponential cancels with the ones of the remaining wave functions:

$$\psi^*_\alpha(\vec{r},b_0)\psi_\gamma(\vec{r},b_1)\tilde{\rho}^{01\tau}(\vec{r}) = Re[\psi^*_\alpha(\vec{r},b_0)\psi_\gamma(\vec{r},b_1)\sum_{\delta\beta>}[\psi^*_\beta(\vec{r},b_0)\psi_\delta(\vec{r},b_1)\rho^{01-+\tau}_{\delta\beta}\delta_{s^-_\delta s^+_\beta} - \psi_\beta(\vec{r},b_0)\psi^*_\delta(\vec{r},b_1)\rho^{01+-\tau}_{\delta\beta}\delta_{s^+_\delta s^-_\beta}]] \quad \text{(F.85)}$$

This is the reason why we keep considering inly the real part of $\tilde{\rho}(\vec{r})$. We have fo $\bar{S}_R$:

$$\boxed{\bar{S}^{\tau-+}_R = x_0\tilde{\rho}^{01}(\vec{r}) - \tilde{\rho}^{01\tau}(\vec{r})} \quad \text{(F.86)}$$

The field finally reduces to:

$$\boxed{\bar{\Gamma}^{\tau-+}_{\alpha\gamma} = t_{30}\langle\alpha|(x_0\tilde{\rho}^{01}(\vec{r}) - \tilde{\rho}^{01\tau}(\vec{r}))[\rho^{01}(\vec{r})]^\alpha|\gamma\rangle_1} \quad \text{(F.87)}$$

Block $+-$:

Here, we consider ($\alpha\uparrow$,$\gamma\downarrow$). By analogy with the previous $-+$ block, we directly find:

$$\boxed{\bar{\Gamma}^{\tau+-}_{\alpha\gamma} = -t_{30}\langle\alpha|(x_0\tilde{\rho}^{01}(\vec{r}) - \tilde{\rho}^{01\tau}(\vec{r}))[\rho^{01}(\vec{r})]^\alpha|\gamma\rangle_1} \quad \text{(F.88)}$$

Remark on the $-+$ and $+-$ blocks:

Because of the differences in the bases, the $+-$ part is not simply the opposite of the $-+$ part. However in practice, considering similar $\{0\}$ and $\{1\}$ bases, the sum of the energy coming from the $-+$ and $+-$ part of the field tends to be close to zero.

F.2.2 Collective mean field numerical evaluation

This part aims to explain how the collective mean field is evaluated numerically with the quadrature method (see Appendix N). We give the derivations for each spin block.

Block $++$:

Here, we consider ($\alpha\uparrow$,$\gamma\uparrow$). We search to evaluate the following quantity:

$$\bar{I}^{++} = t_{30}\langle\alpha|(1+\frac{x_0}{2})[\rho^{01}(\vec{r})]^{\alpha+1} - (\frac{1}{2}+x_0)\rho^{01\tau}(\vec{r})[\rho^{01}(\vec{r})]^\alpha|\gamma\rangle_1 \quad \text{(F.89)}$$

We set:

$$\bar{R}^{\tau++}(\vec{r}) = t_3(1+\frac{x_0}{2})[\rho^{01}(\vec{r})]^{\alpha+1} - t_3(\frac{1}{2}+x_0)\rho^{01\tau}(\vec{r})[\rho^{01}(\vec{r})]^\alpha \quad \text{(F.90)}$$

Doing so, Eq.(F.89) reads:

$$\bar{I}^{++} = \int d\vec{r}\psi^*_\alpha(\vec{r}, b_0)\psi_\gamma(\vec{r}, b_1)\bar{R}^{\tau++}(\vec{r}) \tag{F.91}$$

As $(m_\alpha = m_\gamma)$, we obtain:

$$\psi^*_\alpha(\vec{r}, b_0)\psi_\gamma(\vec{r}, b_1) = Re[\psi_\alpha(\vec{r}, b_0)\psi_\gamma(\vec{r}, b_1)] \tag{F.92}$$

We then rewrite the integral Eq.$(F.91)$:

$$\bar{I}^{++} = 2\pi \int_{-\infty}^{+\infty} dz\varphi_\alpha(z + d_\alpha, b_{z_0})\varphi_\gamma(z + d_\gamma, b_{z_1}) \tag{F.93}$$
$$\int_0^{+\infty} r_\perp dr_\perp Re[\phi_\alpha(r_\perp, b_{r_0})\phi_\gamma(r_\perp, b_{r_1})]\bar{R}^{\tau++}(r_\perp, z)$$

We simply set the following change of variable:

$$r^2_\perp \to r_\perp \tag{F.94}$$

We then write:

$$\bar{I}^{++} = \pi \frac{c_{\alpha\gamma}}{(b_{r_0} b_{r_1})^{2m}} \int_{-\infty}^{+\infty} dz\varphi_\alpha(z + d_\alpha, b_{z_0})\varphi_\gamma(z + d_\gamma, b_{z_1}) \tag{F.95}$$
$$\int_0^{+\infty} dr_\perp e^{-r_\perp(\frac{1}{2b^2_{r_0}} + \frac{1}{2b^2_{r_1}})} r^m_\perp L^m_{n_{\perp_\alpha}}[\frac{r_\perp}{b^2_{r_0}}] L^m_{n_{\perp_\gamma}}[\frac{r_\perp}{b^2_{r_1}}]\bar{R}^{\tau++}(\sqrt{r_\perp}, z)$$

With:

$$c_{\alpha\gamma} = \frac{1}{b_{r_0} b_{r_1}\pi} \sqrt{\frac{n_{\perp_\alpha}!}{(n_{\perp_\alpha} + |m_\alpha|)!}} \sqrt{\frac{n_{\perp_\gamma}!}{(n_{\perp_\gamma} + |m_\gamma|)!}} \tag{F.96}$$

We rescale the $r_\perp$ part:

$$\bar{I}^{++} = \pi \frac{c_{\alpha\gamma} B^{2+2m}_r}{(b_{r_0} b_{r_1})^{2m}} \int_{-\infty}^{+\infty} dz\varphi_\alpha(z + d_\alpha, b_{z_0})\varphi_\gamma(z + d_\gamma, b_{z_1}) \tag{F.97}$$
$$\int_0^{+\infty} dr_\perp e^{-r_\perp} r^m_\perp L^m_{n_{\perp_\alpha}}[\frac{r_\perp B^2_r}{b^2_{r_0}}] L^m_{n_{\perp_\gamma}}[\frac{r_\perp B^2_r}{b^2_{r_1}}]\bar{R}^{\tau++}(B_r\sqrt{r_\perp}, z)$$

With:

$$B_r = \frac{\sqrt{2} b_{r_0} b_{r_1}}{\sqrt{b^2_{r_0} + b^2_{r_1}}} \tag{F.98}$$

We finally apply the quadratures:

$$\boxed{\begin{aligned}\bar{I}^{++} \approx \pi \frac{c_{\alpha\gamma} B_r^{2+2m}}{(b_{r_0} b_{r_1})^{2m}} \sum_{j=1}^{n_{GLA}} w_{GLA_j} r_j^m L_{n_{\perp\alpha}}^m [\frac{r_j B_r^2}{b_{r_0}^2}] L_{n_{\perp\gamma}}^m [\frac{r_j B_r^2}{b_{r_1}^2}] \\ \sum_{i=1}^{n_{GHE}} w_{GHE_i} e^{z_i^2} \varphi_\alpha(z_i + d_\alpha, b_{z_0}) \varphi_\gamma(z_i + d_\gamma, b_{z_1}) \bar{R}^{\tau++}(B_r \sqrt{r_j}, z_i)\end{aligned}} \tag{F.99}$$

Block $--$:

Here, we consider ($\alpha\downarrow$,$\gamma\downarrow$). We directly have:

$$\boxed{\bar{I}^{--} = \bar{I}^{++}} \tag{F.100}$$

Block $-+$:

Here, we consider ($\alpha\downarrow$,$\gamma\uparrow$). We want to evaluate the following quantity:

$$\bar{I}^{-+} = t_{30} \langle \alpha | (x_0 \tilde{\rho}^{01}(\vec{r}) - \tilde{\rho}^{01\tau}(\vec{r}))[\rho^{01}(\vec{r})]^\alpha | \gamma \rangle_1 \tag{F.101}$$

We set:

$$\bar{R}^{\tau-+}(\vec{r}) = t_3 (x_0 \tilde{\rho}^{01}(\vec{r}) - \tilde{\rho}^{01\tau}(\vec{r}))[\rho^{01}(\vec{r})]^\alpha \tag{F.102}$$

Then, the integral of Eq.(F.101) reads:

$$\bar{I}^{-+} = \int d\vec{r} \psi_\alpha^*(\vec{r}, b_0) \psi_\gamma(\vec{r}, b_1) \bar{R}^{\tau-+}(\vec{r}) \tag{F.103}$$

As the complex part of Eq.(F.101) vanishes, we end up with:

$$\begin{aligned}\bar{I}^{-+} = 2\pi \int_{-\infty}^{+\infty} dz \varphi_\alpha(z + d_\alpha, b_{z_0}) \varphi_\gamma(z + d_\gamma, b_{z_1}) \\ \int_0^{+\infty} r_\perp dr_\perp Re[\phi_\alpha(r_\perp, b_{r_0}) \phi_\gamma(r_\perp, b_{r_1})] \bar{R}^{\tau-+}(r_\perp, z)\end{aligned} \tag{F.104}$$

We set the change of variable:

$$r_\perp^2 \to r_\perp \tag{F.105}$$

The integral then reads:

$$\begin{aligned}\bar{I}^{-+} = \pi \frac{c_{\alpha\gamma}}{b_{r_0}^{2m_\alpha} b_{r_1}^{2m_\gamma}} \int_{-\infty}^{+\infty} dz \varphi_\alpha(z + d_\alpha, b_{z_0}) \varphi_\gamma(z + d_\gamma, b_{z_1}) \\ \int_0^{+\infty} dr_\perp e^{-r_\perp (\frac{1}{2b_{r_0}^2} + \frac{1}{2b_{r_1}^2})} r_\perp^{\frac{m_\alpha + m_\gamma}{2}} L_{n_{\perp\alpha}}^{m_\alpha} [\frac{r_\perp}{b_{r_0}^2}] L_{n_{\perp\gamma}}^{m_\gamma} [\frac{r_\perp}{b_{r_1}^2}] \bar{R}^{\tau-+}(\sqrt{r_\perp}, z)\end{aligned} \tag{F.106}$$

With:

$$c_{\alpha\gamma} = \frac{1}{b_{r_0} b_{r_1} \pi} \sqrt{\frac{n_{\perp_\alpha}!}{(n_{\perp_\alpha} + |m_\alpha|)!}} \sqrt{\frac{n_{\perp_\gamma}!}{(n_{\perp_\gamma} + |m_\gamma|)!}} \tag{F.107}$$

We rescale the $r_\perp$ part:

$$\bar{I}^{-+} = \pi \frac{c_{\alpha\gamma} B_r^{2+m_\alpha+m_\gamma}}{b_{r_0}^{2m_\alpha} b_{r_1}^{2m_\gamma}} \int_{-\infty}^{+\infty} dz \varphi_\alpha(z + d_\alpha, b_{z_0}) \varphi_\gamma(z + d_\gamma, b_{z_1}) \tag{F.108}$$
$$\int_0^{+\infty} dr_\perp e^{-r_\perp} r_\perp^{\frac{m_\alpha+m_\gamma}{2}} L_{n_{\perp_\alpha}}^{m_\alpha}[\frac{r_\perp B_r^2}{b_{r_0}^2}] L_{n_{\perp_\gamma}}^{m_\gamma}[\frac{r_\perp B_r^2}{b_{r_1}^2}] \bar{R}^{\tau-+}(B_r\sqrt{r_\perp}, z)$$

With:

$$B_r = \frac{\sqrt{2} b_{r_0} b_{r_1}}{\sqrt{b_{r_0}^2 + b_{r_1}^2}} \tag{F.109}$$

We finally use the quadratures:

$$\boxed{\begin{aligned}\bar{I}^{-+} \approx \pi \frac{c_{\alpha\gamma} B_r^{2+m_\alpha+m_\gamma}}{b_{r_0}^{2m_\alpha} b_{r_1}^{2m_\gamma}} \sum_{j=1}^{n_{GLA}} w_{GLA_j} r_j^{\frac{m_\alpha+m_\gamma}{2}} L_{n_{\perp_\alpha}}^{m_\alpha}[\frac{r_j B_r^2}{b_{r_0}^2}] L_{n_{\perp_\gamma}}^{m_\gamma}[\frac{r_j B_r^2}{b_{r_1}^2}] \\ \sum_{i=1}^{n_{GHE}} w_{GHE_i} e^{z_i^2} \varphi_\alpha(z_i + d_\alpha, b_{z_0}) \varphi_\gamma(z_i + d_\gamma, b_{z_1}) \bar{R}^{\tau-+}(B_r\sqrt{r_j}, z_i)\end{aligned}} \tag{F.110}$$

Block $+-$:

Here, we consider ($\alpha\uparrow$,$\gamma\downarrow$). By analogy with the $-+$ part, we directly have:

$$\boxed{\begin{aligned}\bar{I}^{+-} \approx -\pi \frac{c_{\alpha\gamma} B_r^{2+m_\alpha+m_\gamma}}{b_{r_0}^{2m_\alpha} b_{r_1}^{2m_\gamma}} \sum_{j=1}^{n_{GLA}} w_{GLA_j} r_j^{\frac{m_\alpha+m_\gamma}{2}} L_{n_{\perp_\alpha}}^{m_\alpha}[\frac{r_j B_r^2}{b_{r_0}^2}] L_{n_{\perp_\gamma}}^{m_\gamma}[\frac{r_j B_r^2}{b_{r_1}^2}] \\ \sum_{i=1}^{n_{GHE}} w_{GHE_i} e^{z_i^2} \varphi_\alpha(z_i + d_\alpha, b_{z_0}) \varphi_\gamma(z_i + d_\gamma, b_{z_1}) \bar{R}^{\tau-+}(B_r\sqrt{r_j}, z_i)\end{aligned}} \tag{F.111}$$

F.2.3 Collective pairing field

The collective contact density-dependent pairing field reads as follows:

$$\boxed{\bar{\Delta}_{\alpha\bar{\beta}} = \sum_{\gamma\delta} (-1)^{s_\beta - s_\delta} {}_0\langle \alpha\bar{\beta}|V^{(D)}(1 - P_r P_\sigma P_\tau)|\gamma\bar{\delta}\rangle_1 \kappa_{\gamma\bar{\delta}}^{01}} \tag{F.112}$$

By analogy with the non-collective case, we write:

$$\bar{\Delta}_{\alpha\bar{\beta}} = t_3 \sum_{\gamma\delta} (-1)^{s_\beta - s_\delta} \langle (s_\alpha, \tau_\beta)(\bar{s_\beta}, \tau_\beta)| (1 - x_0) \tag{F.113}$$
$$+ (x_0 - 1) P_\sigma |(s_\gamma, \tau_\gamma)(\bar{s_\delta}, \tau_\delta)\rangle_0 \langle \alpha\bar{\beta}|[\rho(\vec{r})]^\alpha |\gamma\bar{\delta}\rangle_1 \kappa^{01}_{\gamma\bar{\delta}}$$

Since in the D1-type Gogny interactions $x_0 = 1$, we have:

$$\boxed{\bar{\Delta}_{\alpha\bar{\beta}} = 0} \tag{F.114}$$

F.3 Excited collective fields

The goal of this part is to give an expression of the new contact density-dependent fields that appear when intrinsic excitations are added. They are useful to evaluate quantities of the following type:

$$\langle \Phi_0 | \bar{\xi}_j \xi_j \hat{H} \xi_i^+ \bar{\xi}_i^+ | \Phi_1 \rangle \tag{F.115}$$

Note that these excited fields are peculiar compared with the others since the local excited density is involved. It could be tempting to define this excited local density as follows:

$$\rho^{01(ji)}(\vec{r}) := \sum_{\sigma\tau} \frac{\langle \Phi_0 | \bar{\xi}_{0,j} \xi_{0,j} \Psi_0^+(\vec{r}, \sigma, \tau) \Psi_1(\vec{r}, \sigma, \tau) \xi_{1,i}^+ \bar{\xi}_{1,i}^+ | \Phi_1 \rangle}{\langle \Phi_0 | \bar{\xi}_{0,j} \xi_{0,j} \xi_{1,i}^+ \bar{\xi}_{1,i}^+ | \Phi_1 \rangle} \tag{F.116}$$

However, this quantity diverges when $\{0\} \to \{1\}$. For this reason, we've chosen the following definition, which is a new prescription:

$$\boxed{\rho^{01(ji)}(\vec{r}) := \sum_{\sigma\tau} \frac{\langle \Phi_0 | \bar{\xi}_{0,j} \xi_{0,j} \Psi_0^+(\vec{r}, \sigma, \tau) \Psi_1(\vec{r}, \sigma, \tau) \xi_{1,i}^+ \bar{\xi}_{1,i}^+ | \Phi_1 \rangle}{\langle \Phi_0 | \Phi_1 \rangle}} \tag{F.117}$$

We treat the negative values as presented in Eq.(F.67). This definition is straightforward to extend to the case where only one excitation is considered. Performing Hamiltonian kernel calculations we never faced any problems coming from these density definitions. We can rewrite Eq.(F.117):

$$\rho^{01(ji)}(\vec{r}) = \sum_{\alpha\beta} \delta_{\sigma_\alpha\sigma_\beta} \delta_{\tau_\alpha\tau_\beta} \psi_\alpha^*(\vec{r}, b_0) \psi_\beta(\vec{r}, b_1) \frac{\langle \Phi_0 | \bar{\xi}_{0,j} \xi_{0,j} c_{0,\alpha}^+ c_{1,\beta} \xi_{1,i}^+ \bar{\xi}_{1,i}^+ | \Phi_1 \rangle}{\langle \Phi_0 | \Phi_1 \rangle} \tag{F.118}$$

Using the Y,T,S, Z and W matrices defined in Chapter 5, we can explicitly write:

$$\boxed{\begin{aligned} \frac{\langle \Phi_0 | \bar{\xi}_{0,j} \xi_{0,j} c_{0,\alpha}^+ c_{1,\beta} \xi_{1,i}^+ \bar{\xi}_{1,i}^+ | \Phi_1 \rangle}{\langle \Phi_0 | \Phi_1 \rangle} &= -Y_{j\bar{j}} [\rho^{01\tau}_{\beta\alpha} T_{i\bar{i}} + W_{\beta i} Z_{\alpha\bar{i}} \delta_{\tau\tau_i}] - \delta_{\tau\tau_j} \bar{Z}_{j\bar{\beta}} [\bar{W}_{j\alpha} T_{i\bar{i}} - S_{ji} Z_{\alpha\bar{i}}] \\ &\quad + S_{ji} [\bar{W}_{j\alpha} W_{\beta i} + S_{ji} \rho^{01\tau}_{\beta\alpha}] \end{aligned}} \tag{F.119}$$

In the case where only one excitation is considered, we write:

$$\rho^{01(i)}(\vec{r}) = \sum_{\alpha\beta} \delta_{\sigma_\alpha\sigma_\beta}\delta_{\tau_\alpha\tau_\beta}\psi^*_\alpha(\vec{r},b_0)\psi_\beta(\vec{r},b_1)\frac{\langle\Phi_0|c^+_{0,\alpha}c_{1,\beta}\xi^+_{1,i}\bar{\xi}^+_{1,i}|\Phi_1\rangle}{\langle\Phi_0|\Phi_1\rangle} \tag{F.120}$$

Then, the last part of this equation reads:

$$\boxed{\frac{\langle\Phi_0|c^+_{0,\alpha}c_{1,\beta}\xi^+_{1,i}\bar{\xi}^+_{1,i}|\Phi_1\rangle}{\langle\Phi_0|\Phi_1\rangle} = \rho^{01\tau}_{\beta\alpha}T_{i\bar{i}} + W_{\beta i}Z_{\alpha\bar{i}}\delta_{\tau\tau_i}} \tag{F.121}$$

Finally, as for the non-collective and collective case, there is no excited contact density-dependent pairing field.

F.3.1 Excited collective field $\bar{\Gamma}^{(ji)}$ reduced expression

This excited field is quasi equivalent to the collective one Eq.(F.68). The only difference is in the local density that is used in the interaction. We write:

$$\boxed{\bar{\Gamma}^{(ji)}_{\alpha\gamma} = \sum_{\delta\beta} {}_0\langle\alpha\beta|V^{(D)(ji)}(1-P_rP_\sigma P_\tau)|\gamma\delta\rangle_1\rho^{01}_{\delta\beta}} \tag{F.122}$$

We then consider the spins. Each result is directly obtain by analogy with the collective case.

Block ++:

Here, we consider ($\alpha\uparrow$,$\gamma\uparrow$). This part reads:

$$\boxed{\bar{\Gamma}^{(ji)\tau++}_{\alpha\gamma} = t_{30}\langle\alpha|[\rho^{01(ji)}(\vec{r})]^\alpha[(1+\frac{x_0}{2})\rho^{01}(\vec{r}) - (\frac{1}{2}+x_0)\rho^{01\tau}(\vec{r})]|\gamma\rangle_1} \tag{F.123}$$

Block −−:

Here, we consider ($\alpha\downarrow$,$\gamma\downarrow$). We directly have:

$$\boxed{\bar{\Gamma}^{(ji)\tau--}_{\alpha\gamma} = \bar{\Gamma}^{(ji)\tau++}_{\alpha\gamma}} \tag{F.124}$$

Block −+:

Here, we consider ($\alpha\downarrow$,$\gamma\uparrow$). We find:

$$\boxed{\bar{\Gamma}^{(ji)\tau-+}_{\alpha\gamma} = t_{30}\langle\alpha|[\rho^{01(ji)}(\vec{r})]^\alpha[x_0\tilde{\rho}^{01}(\vec{r}) - \tilde{\rho}^{01\tau}(\vec{r})]|\gamma\rangle_1} \tag{F.125}$$

Block +−:

Here, we consider ($\alpha\uparrow$,$\gamma\downarrow$). We get:

$$\boxed{\bar{\Gamma}^{(ji)\tau+-}_{\alpha\gamma} = -t_{30}\langle\alpha|[\rho^{01(ji)}(\vec{r})]^\alpha[x_0\tilde{\rho}^{01}(\vec{r}) - \tilde{\rho}^{01\tau}(\vec{r})]|\gamma\rangle_1} \tag{F.126}$$

F.3.2 Excited collective field $\bar{\Gamma}^{(ji)}$ numerical evaluation

In this part also, we directly use the analogy with the collective part to find the expression of the quadratures.

Block ++:

Here, we consider ($\alpha\uparrow$,$\gamma\uparrow$). We search for the following quantity:

$$\bar{I}^{(ji)++} = t_{30}\langle\alpha|[\rho^{01(ji)}(\vec{r})]^{\alpha}[(1+\frac{x_0}{2})\rho^{01}(\vec{r}) - (\frac{1}{2}+x_0)\rho^{01\tau}(\vec{r})]|\gamma\rangle_1 \tag{F.127}$$

We set:

$$\bar{R}^{(ji)\tau++}(\vec{r}) = t_3[\rho^{01(ji)}(\vec{r})]^{\alpha}[(1+\frac{x_0}{2})\rho^{01}(\vec{r}) - (\frac{1}{2}+x_0)\rho^{01\tau}(\vec{r})] \tag{F.128}$$

Eq.(F.127) eventually reads:

$$\boxed{\begin{aligned}\bar{I}^{(ji)++} \approx \pi\frac{c_{\alpha\gamma}B_r^{2+2m}}{(b_{r_0}b_{r_1})^{2m}}\sum_{j=1}^{n_{GLA}} w_{GLA_j} r_j^m L^m_{n_{\perp_\alpha}}[\frac{r_jB_r^2}{b_{r_0}^2}]L^m_{n_{\perp_\gamma}}[\frac{r_jB_r^2}{b_{r_1}^2}] \\ \sum_{i=1}^{n_{GHE}} w_{GHE_i}e^{z_i^2}\varphi_\alpha(z_i+d_\alpha,b_{z_0})\varphi_\gamma(z_i+d_\gamma,b_{z_1})\bar{R}^{(ji)\tau++}(B_r\sqrt{r_j},z_i)\end{aligned}} \tag{F.129}$$

Block −−:

Here, we consider ($\alpha\downarrow$,$\gamma\downarrow$). We directly have:

$$\boxed{\bar{I}^{(ji)--} = \bar{I}^{(ji)++}} \tag{F.130}$$

Block −+:

Here, we consider ($\alpha\downarrow$,$\gamma\uparrow$). We want to evaluate the following quantity:

$$\bar{I}^{(ji)-+} = t_{30}\langle\alpha|[\rho^{01(ji)}(\vec{r})]^{\alpha}[x_0\tilde{\rho}^{01}(\vec{r}) - \tilde{\rho}^{01\tau}(\vec{r})]|\gamma\rangle_1 \tag{F.131}$$

We set:

$$\bar{R}^{(ji)\tau-+}(\vec{r}) = t_3[\rho^{01(ji)}(\vec{r})]^{\alpha}[x_0\tilde{\rho}^{01}(\vec{r}) - \tilde{\rho}^{01\tau}(\vec{r})] \tag{F.132}$$

We finally write:

$$\boxed{\begin{aligned}\bar{I}^{(ji)-+} \approx \pi\frac{c_{\alpha\gamma}B_r^{2+m_\alpha+m_\gamma}}{b_{r_0}^{2m_\alpha}b_{r_1}^{2m_\gamma}}\sum_{j=1}^{n_{GLA}} w_{GLA_j} r_j^{\frac{m_\alpha+m_\gamma}{2}} L^{m_\alpha}_{n_{\perp_\alpha}}[\frac{r_jB_r^2}{b_{r_0}^2}]L^{m_\gamma}_{n_{\perp_\gamma}}[\frac{r_jB_r^2}{b_{r_1}^2}] \\ \sum_{i=1}^{n_{GHE}} w_{GHE_i}e^{z_i^2}\varphi_\alpha(z_i+d_\alpha,b_{z_0})\varphi_\gamma(z_i+d_\gamma,b_{z_1})\bar{R}^{(ji)\tau-+}(B_r\sqrt{r_j},z_i)\end{aligned}} \tag{F.133}$$

Block +−:

Here, we consider ($\alpha\uparrow$,$\gamma\downarrow$). We directly have:

$$\boxed{\begin{aligned}\bar{I}^{(ji)+-} \approx -\pi\frac{c_{\alpha\gamma}B_r^{2+m_\alpha+m_\gamma}}{b_{r_0}^{2m_\alpha}b_{r_1}^{2m_\gamma}}\sum_{j=1}^{n_{GLA}} w_{GLA_j} r_j^{\frac{m_\alpha+m_\gamma}{2}} L_{n_{\perp_\alpha}}^{m_\alpha}[\frac{r_jB_r^2}{b_{r_0}^2}]L_{n_{\perp_\gamma}}^{m_\gamma}[\frac{r_jB_r^2}{b_{r_1}^2}] \\ \sum_{i=1}^{n_{GHE}} w_{GHE_i}e^{z_i^2}\varphi_\alpha(z_i+d_\alpha,b_{z_0})\varphi_\gamma(z_i+d_\gamma,b_{z_1})\bar{R}^{(ji)\tau-+}(B_r\sqrt{r_j},z_i)\end{aligned}} \tag{F.134}$$

F.3.3 Excited collective field $\bar{\Gamma}^{(ji)}([W,Z])$ reduced expression

This excited field is defined as follows:

$$\boxed{\begin{aligned}\bar{\Gamma}_{\alpha\gamma}^{(ji)}([W,Z]) = \sum_{\delta\beta}[{}_1\langle\alpha\beta|V^{((ji)D)}(1-P_rP_\sigma P_\tau)|\gamma\delta\rangle_0 \\ +(-1)^{s_\beta-s_\delta}{}_1\langle\alpha\bar{\beta}|V^{((ji)D)}(1-P_rP_\sigma P_\tau)|\gamma\bar{\delta}\rangle_0]W_{\delta i}Z_{\beta\bar{i}}\end{aligned}} \tag{F.135}$$

The excitation fixes the isospin and the Ω block considered. Indeed, we have ($\tau_\beta=\tau_\delta=\tau_i$) and ($\Omega_\beta=\Omega_\delta=\Omega_i\geq 0$). We used the analogy with the previously derived fields to consider directly the spin blocks.

Block ++:

Here, we consider ($\alpha\uparrow$,$\gamma\uparrow$). We first set:

$$WZ(\vec{r}) = \sum_{\delta\beta\in(\Omega_i,\tau_i)}\delta_{\sigma_\beta\sigma_\delta}\psi_\beta^*(\vec{r},b_0)\psi_\delta(\vec{r},b_1)W_{\delta i}Z_{\beta\bar{i}} \tag{F.136}$$

The field then reads:

$$\boxed{\bar{\Gamma}_{\alpha\gamma}^{(ji)\tau++}([W,Z]) = \delta_{\tau\neq\tau_i}\frac{3t_3}{2}{}_0\langle\alpha|[\rho^{01(ji)}(\vec{r})]^\alpha WZ(\vec{r})|\gamma\rangle_1} \tag{F.137}$$

Block −−:

Here, we consider ($\alpha\downarrow$,$\gamma\downarrow$). We directly have:

$$\boxed{\bar{\Gamma}_{\alpha\gamma}^{(ji)\tau--}([W,Z]) = \bar{\Gamma}_{\alpha\gamma}^{(ji)\tau++}([W,Z])} \tag{F.138}$$

Block −+:

Here, we consider ($\alpha\downarrow$,$\gamma\uparrow$). We set:

$$\tilde{WZ}(\vec{r}) = \sum_{\delta\beta\in(\Omega_i,\tau_i)}[\psi_\beta^*(\vec{r},b_0)\psi_\delta(\vec{r},b_1)\delta_{s_\delta^-s_\beta^+}W_{\delta i}^-Z_{\beta\bar{i}}^+ - \psi_\beta(\vec{r},b_0)\psi_\delta^*(\vec{r},b_1)\delta_{s_\delta^+s_\beta^-}W_{\delta i}^+Z_{\beta\bar{i}}^-] \tag{F.139}$$

Then, the field reads:

$$\boxed{\bar{\Gamma}^{(ji)\tau-+}_{\alpha\gamma}([W,Z]) = \delta_{\tau\neq\tau_i} t_{30} \langle\alpha|[\rho^{01(ji)}(\vec{r})]^{\alpha} \tilde{WZ}(\vec{r})|\gamma\rangle_1} \tag{F.140}$$

Block $+-$:

Here, we consider ($\alpha\uparrow$,$\gamma\downarrow$). We directly write:

$$\boxed{\bar{\Gamma}^{(ji)\tau+-}_{\alpha\gamma}([W,Z]) = -\delta_{\tau\neq\tau_i} t_{30} \langle\alpha|[\rho^{01(ji)}(\vec{r})]^{\alpha} \tilde{WZ}(\vec{r})|\gamma\rangle_1} \tag{F.141}$$

F.3.4 Excited collective field $\bar{\Gamma}^{(ji)}([W,Z])$ numerical evaluation

We use the analogy with the results of the previously derived fields to directly consider the spin blocks.

Block $++$:

Here, we consider ($\alpha\uparrow$,$\gamma\uparrow$). We search for the following quantity:

$$\bar{I}^{(ji)++}([W,Z]) = \delta_{\tau\neq\tau_i} \frac{3t_3}{2} {}_0\langle\alpha|[\rho^{01(ji)}(\vec{r})]^{\alpha} WZ(\vec{r})|\gamma\rangle_1 \tag{F.142}$$

We set:

$$WZ^{(ji)++}(\vec{r}) = \frac{3t_3}{2} [\rho^{01(ji)}(\vec{r})]^{\alpha} WZ(\vec{r}) \tag{F.143}$$

We apply the quadratures:

$$\boxed{\begin{aligned}\bar{I}^{(ji)++}([W,Z]) \approx \delta_{\tau\neq\tau_i} \pi \frac{c_{\alpha\gamma} B_r^{2+2m}}{(b_{r_0} b_{r_1})^{2m}} \sum_{j=1}^{n_{GLA}} w_{GLA_j} r_j^m L^m_{n_{\perp_\alpha}}[\frac{r_j B_r^2}{b_{r_0}^2}] L^m_{n_{\perp_\gamma}}[\frac{r_j B_r^2}{b_{r_1}^2}] \\ \sum_{i=1}^{n_{GHE}} w_{GHE_i} e^{z_i^2} \varphi_\alpha(z_i + d_\alpha, b_{z_0}) \varphi_\gamma(z_i + d_\gamma, b_{z_1}) WZ^{(ji)++}(B_r\sqrt{r_j}, z_i)\end{aligned}} \tag{F.144}$$

Block $--$:

Here, we consider ($\alpha\downarrow$,$\gamma\downarrow$). This part directly reads:

$$\boxed{\bar{I}^{(ji)--}([W,Z]) = \bar{I}^{(ji)++}([W,Z])} \tag{F.145}$$

Block $-+$:

Here, we consider ($\alpha\downarrow$,$\gamma\uparrow$). We want to evaluate:

$$\bar{I}^{(ji)-+}([W,Z]) = \delta_{\tau\neq\tau_i} t_{30} \langle\alpha|[\rho^{01(ji)}(\vec{r})]^{\alpha} \tilde{WZ}(\vec{r})|\gamma\rangle_1 \tag{F.146}$$

We set:

$$WZ^{(ji)-+}(\vec{r}) = t_3[\rho^{01(ji)}(\vec{r})]^{\alpha}\tilde{WZ}(\vec{r}) \tag{F.147}$$

Using the quadratures we find:

$$\begin{aligned}\bar{I}^{(ji)-+}([W,Z]) \approx \delta_{\tau\neq\tau_i}\pi\frac{c_{\alpha\gamma}B_r^{2+m_\alpha+m_\gamma}}{b_{r_0}^{2m_\alpha}b_{r_1}^{2m_\gamma}}\sum_{j=1}^{n_{GLA}} w_{GLA_j} r_j^{\frac{m_\alpha+m_\gamma}{2}} L_{n_{\perp_\alpha}}^{m_\alpha}[\frac{r_jB_r^2}{b_{r_0}^2}]L_{n_{\perp_\gamma}}^{m_\gamma}[\frac{r_jB_r^2}{b_{r_1}^2}] \\ \sum_{i=1}^{n_{GHE}} w_{GHE_i}e^{z_i^2}\varphi_\alpha(z_i+d_\alpha,b_{z_0})\varphi_\gamma(z_i+d_\gamma,b_{z_1})WZ^{(ji)-+}(B_r\sqrt{r_j},z_i)\end{aligned} \tag{F.148}$$

Block $+-$:

Here, we consider $(\alpha\uparrow,\gamma\downarrow)$. We directly have:

$$\begin{aligned}\bar{I}^{(ji)+-}([W,Z]) \approx -\delta_{\tau\neq\tau_i}\pi\frac{c_{\alpha\gamma}B_r^{2+m_\alpha+m_\gamma}}{b_{r_0}^{2m_\alpha}b_{r_1}^{2m_\gamma}}\sum_{j=1}^{nGLA} w_{GLA_j} r_j^{\frac{m_\alpha+m_\gamma}{2}} L_{n_{\perp_\alpha}}^{m_\alpha}[\frac{r_jB_r^2}{b_{r_0}^2}]L_{n_{\perp_\gamma}}^{m_\gamma}[\frac{r_jB_r^2}{b_{r_1}^2}] \\ \sum_{i=1}^{nGHE} w_{GHE_i}e^{z_i^2}\varphi_\alpha(z_i+d_\alpha,b_{z_0})\varphi_\gamma(z_i+d_\gamma,b_{z_1})WZ^{(ji)-+}(B_r\sqrt{r_j},z_i)\end{aligned} \tag{F.149}$$

Appendix G

Finite-range density fields

In the case of the D2 Gogny interaction, the finite-range density part of the antisymmetrized interaction reads as follows:

$$\boxed{\begin{aligned} V^{(D2)}(1-P_rP_\sigma P_\tau) = \frac{1}{2(\mu_3\sqrt{\pi})^3}(W_3 + B_3P_\sigma - H_3P_\tau - M_3P_\sigma P_\tau) \\ e^{-\frac{(\vec{r}_1-\vec{r}_2)^2}{\mu_3^2}}([\rho(\vec{r}_1)]^\alpha + [\rho(\vec{r}_2)]^\alpha)(1-P_rP_\sigma P_\tau) \end{aligned}} \tag{G.1}$$

The matrix elements of the finite-range density part of the interaction can be separated into a spatial part and a spin-isospin part:

$$\boxed{\langle\alpha\beta|V^{(D2)}(1-P_rP_\sigma P_\tau)|\gamma\delta\rangle = E^{\gamma\delta}_{\alpha\beta}S^{\gamma\delta}_{\alpha\beta} - E^{\delta\gamma}_{\alpha\beta}S^{\delta\gamma}_{\alpha\beta}} \tag{G.2}$$

With:

$$\begin{cases} E^{\gamma\delta}_{\alpha\beta} = \frac{1}{2(\mu_3\sqrt{\pi})^3}\langle\alpha\beta|e^{-\frac{(\vec{r}_1-\vec{r}_2)^2}{\mu_3^2}}([\rho(\vec{r}_1)]^\alpha + [\rho(\vec{r}_2)]^\alpha)|\gamma\delta\rangle \\ \\ S^{\gamma\delta}_{\alpha\beta} = \langle\alpha\beta|W_3 + B_3P_\sigma - H_3P_\tau - M_3P_\sigma P_\tau|\gamma\delta\rangle \end{cases} \tag{G.3}$$

The local density which appears in Eq.(G.3) reads as follows (see Appendix F):

$$\boxed{\rho(\vec{r}) = \sum_{\alpha\beta}\delta_{\sigma_\beta\sigma_\alpha}\delta_{\tau_\beta\tau_\alpha}\psi^*_\alpha(\vec{r})\psi_\beta(\vec{r})\rho_{\beta\alpha}} \tag{G.4}$$

Besides, when the interaction matrix elements are differentiated with respect to the elements of the density matrix ρ, we find:

$$\boxed{\langle\gamma\eta|\frac{\partial V^{(D2)}}{\partial\rho_{\alpha\beta}}(1-P_rP_\sigma P_\tau)|\delta\mu\rangle = E^{(\gamma\delta)(\eta\mu)}_{\alpha\beta}S^{\delta\mu}_{\gamma\eta} - E^{(\gamma\mu)(\eta\delta)}_{\alpha\beta}S^{\mu\delta}_{\gamma\eta}} \tag{G.5}$$

With:

$$E^{(\gamma\delta)(\eta\mu)}_{\alpha\beta} = \frac{\alpha\delta_{s_\alpha s_\beta}\delta_{\tau_\alpha\tau_\beta}}{2(\mu_3\sqrt{\pi})^3}\langle\gamma\eta|e^{-\frac{(\vec{r}_1-\vec{r}_2)^2}{\mu_3^2}}([\rho(\vec{r}_1)]^{\alpha-1}\psi^*_\alpha(\vec{r}_1)\psi^*_\beta(\vec{r}_1) + [\rho(\vec{r}_2)]^{\alpha-1}\psi^*_\alpha(\vec{r}_2)\psi^*_\beta(\vec{r}_2))|\delta\mu\rangle \tag{G.6}$$

G.1 Spatial parts

In this section, we study the two spatial parts defined in Eq.(G.3) and Eq.(G.6). We first develop the expression of the first one, which then naturally gives the expression of the second one:

$$E^{\gamma\delta}_{\alpha\beta} = \frac{1}{2(\mu_3\sqrt{\pi})^3}\langle\alpha\beta|e^{-\frac{(\vec{r}_1-\vec{r}_2)^2}{\mu_3^2}}([\rho(\vec{r}_1)]^\alpha + [\rho(\vec{r}_2)]^\alpha)|\gamma\delta\rangle \tag{G.7}$$

We rewrite Eq.(G.7) more explicitly:

$$\begin{aligned} E^{\gamma\delta}_{\alpha\beta} = \frac{1}{2(\mu_3\sqrt{\pi})^3}&\int d\vec{r}_1[\rho(\vec{r}_1)]^\alpha\psi^*_\alpha(\vec{r}_1)\psi_\gamma(\vec{r}_1)\int d\vec{r}_2 e^{-\frac{(\vec{r}_1-\vec{r}_2)^2}{\mu_3^2}}\psi^*_\beta(\vec{r}_2)\psi_\delta(\vec{r}_2) \\ &+\int d\vec{r}_2[\rho(\vec{r}_2)]^\alpha\psi^*_\beta(\vec{r}_2)\psi_\delta(\vec{r}_2)\int d\vec{r}_1 e^{-\frac{(\vec{r}_1-\vec{r}_2)^2}{\mu_3^2}}\psi^*_\alpha(\vec{r}_1)\psi_\gamma(\vec{r}_1) \end{aligned} \tag{G.8}$$

We focus on the two integrals of Eq.(G.8) that do not depend on the local density. They both share the same structure, which we call I:

$$I_{\alpha\gamma} = \int d\vec{r}_1 e^{-\frac{(\vec{r}_1-\vec{r}_2)^2}{\mu_3^2}}\psi^*_\alpha(\vec{r}_1)\psi_\gamma(\vec{r}_1) \tag{G.9}$$

We separate I into a z and a $\vec{r}_\perp$ part:

$$\boxed{I_{\alpha\gamma} = \int d\vec{r}_{\perp_1} e^{-(r_{\perp_1}-r_{\perp_2})^2/\mu_i^2}\phi^*_\alpha(\vec{r}_{\perp_1})\phi_\gamma(\vec{r}_{\perp_1})\int dz_1 e^{-(\vec{z}_1-\vec{z}_2)^2/\mu_i^2}\varphi_{n_{z_\alpha}}(z_2+d_\alpha)\varphi_{n_{z_\gamma}}(z_2+d_\gamma)} \tag{G.10}$$

Calculation of the z-integral:

The goal is to evaluate I_z, the z part of I:

$$(I_z)_{(n_{z_\alpha},d_\alpha)(n_{z_\gamma},d_\gamma)}(z_2) = \int dz_1 e^{-(\vec{z}_1-\vec{z}_2)^2/\mu_i^2}\varphi_{n_{z_\alpha}}(z_2+d_\alpha)\varphi_{n_{z_\gamma}}(z_2+d_\gamma) \tag{G.11}$$

The analytic expression of Eq.(G.11) is found using the same techniques as for the spatial part of the central term of the interaction (see Appendix E). We find:

$$\boxed{(I_z)_{(n_{z_\alpha},d_\alpha)(n_{z_\gamma},d_\gamma)}(z_2) = \frac{\mu_3\sqrt{\pi}}{\sqrt{b_z\sqrt{\pi}}}e^{-\frac{1}{2}(\frac{z_2+k_{\alpha\gamma}}{b_z\sqrt{K_z}})^2}\sum_{n_{z_a}} T^{n_{z_a}}_{(n_{z_\alpha},d_\alpha)(n_{z_\gamma},d_\gamma)}\frac{1}{\sqrt{K_z}^{n_{z_a}+1}}\varphi_{n_{z_a}}(\frac{z_2+k_{\alpha\gamma}}{\sqrt{K_z}})} \tag{G.12}$$

With:

$$K_z = \frac{\mu_3^2+b_z^2}{b_z^2} \tag{G.13}$$

Calculation of the $\vec{r}_\perp$-integral:

The goal is to evaluate I_r, the $\vec{r}_\perp$ part of I defined as:

$$(I_r)_{(m_\alpha,n_{\perp\alpha})(m_\gamma,n_{\perp\gamma})}(\vec{r}_{\perp 2}) = \int d\vec{r}_{\perp 1} e^{-\frac{(\vec{r}_{\perp 1}-\vec{r}_{\perp 2})^2}{\mu_3^2}} \phi^*_{(m_\alpha,n_{\perp\alpha})}(\vec{r}_{\perp 1})\phi_{(m_\gamma,n_{\perp\gamma})}(\vec{r}_{\perp 1}) \tag{G.14}$$

The analytic expression of Eq.(G.14) is found using the same techniques as for the spatial part of the central term of the interaction (see Appendix E). We find:

$$\boxed{\begin{aligned}(I_r)_{(m_\alpha,n_{\perp\alpha})(m_\gamma,n_{\perp\gamma})}(\vec{r}_{\perp 2}) = \frac{\mu_3^2\sqrt{\pi}}{b_r} e^{-\frac{1}{2}(\frac{\vec{r}_{\perp 2}}{b_r\sqrt{K_r}})^2} \sum_{n_{\perp a}} T^{n_{\perp a}}_{(m_\alpha,n_{\perp\alpha})(m_\gamma,n_{\perp\gamma})} \\ \frac{1}{\sqrt{K_r}^{2n_{\perp a}+|m_a|+2}} \phi_{(m_a,n_{\perp a})}(\frac{\vec{r}_{\perp 2}}{\sqrt{K_r}})\end{aligned}} \tag{G.15}$$

With:

$$K_r = \frac{\mu_3^2 + b_r^2}{b_r^2} \tag{G.16}$$

Final expression of the first spatial part:

Eventually, the spatial part of the finite-range density dependent term of the interaction reads as follows:

$$\boxed{\begin{aligned}E^{\gamma\delta}_{\alpha\beta} = \frac{1}{2(\mu_3\sqrt{\pi})^3} \int d\vec{r}[\rho(\vec{r})]^\alpha \psi^*_\alpha(\vec{r})\psi_\gamma(\vec{r})(I_r)_{(m_\beta,n_{\perp\beta})(m_\delta,n_{\perp\delta})}(\vec{r}_\perp)(I_z)_{(n_{z\beta},d_\beta)(n_{z\delta},d_\delta)}(z) \\ + \int d\vec{r}[\rho(\vec{r})]^\alpha \psi^*_\beta(\vec{r})\psi_\delta(\vec{r})(I_r)_{(m_\alpha,n_{\perp\alpha})(m_\gamma,n_{\perp\gamma})}(\vec{r}_\perp)(I_z)_{(n_{z\alpha},d_\alpha)(n_{z\gamma},d_\gamma)}(z)\end{aligned}} \tag{G.17}$$

Final expression of the second spatial part:

By analogy, it is easy to write:

$$\boxed{E^{(\gamma\delta)(\eta\mu)}_{\alpha\beta} = \frac{\delta_{s_\alpha s_\beta}\delta_{\tau_\alpha\tau_\beta}}{2(\mu_3\sqrt{\pi})^3} \int d\vec{r}\alpha[\rho(\vec{r})]^{\alpha-1}\psi^*_\alpha(\vec{r})\psi_\beta(\vec{r})[\psi^*_\gamma(\vec{r})\psi_\delta(\vec{r})I_{\eta\mu}(\vec{r}) + \psi^*_\eta(\vec{r})\psi_\mu(\vec{r})I_{\gamma\delta}(\vec{r})]} \tag{G.18}$$

G.2 HFB fields

In this part, the finite-range density dependent mean field, exchange field and pairing field are explicitly derived. As the local density at the power $\alpha = 1/3$ is involved, there is no analytic expressions for these different fields. In this section, we give the reduced expressions of the fields, which are then numerically evaluated using the quadrature techniques presented in Appendix F.

G.2.1 Direct mean field

The direct mean field reads as follows:

$$\boxed{\Gamma_{\alpha\gamma}(D) = \sum_{\delta\beta} \langle \alpha\beta | V^{(D2)} | \gamma\delta \rangle \rho_{\delta\beta}} \tag{G.19}$$

We separate the spatial and spin-isospin parts of Eq.(G.19) and we use its time-reversal properties:

$$\Gamma_{\alpha\gamma}(D) = \sum_{\delta\beta>} [E^{\gamma\delta}_{\alpha\beta}.S^{\gamma\delta}_{\alpha\beta} + (-1)^{s_\beta - s_\delta} E^{\gamma\bar{\delta}}_{\alpha\bar{\beta}}.S^{\gamma\bar{\delta}}_{\alpha\bar{\beta}}]\rho_{\delta\beta} \tag{G.20}$$

We remark that:

$$E^{\gamma\delta}_{\alpha\beta} = E^{\gamma\bar{\beta}}_{\alpha\bar{\delta}} \tag{G.21}$$

Using Eq.(G.21) into Eq.(G.20) finally leads to:

$$\boxed{\Gamma_{\alpha\gamma}(D) = \sum_{\delta\beta>} E^{\gamma\delta}_{\alpha\beta}[S^{\gamma\delta}_{\alpha\beta} + (-1)^{s_\beta - s_\delta} S^{\gamma\bar{\beta}}_{\alpha\bar{\delta}}]\rho_{\delta\beta}} \tag{G.22}$$

We can now explicitly consider the spins.

Block ++:

Here, we consider ($\alpha\uparrow$,$\gamma\uparrow$). We first evaluate the associated spin-isospin part:

$$(S^{\gamma\delta}_{\alpha\beta})^{\tau++} = [W_3 - H_3\delta_{\tau\tau'}]\delta_{s_\beta s_\delta} + [B_3 - M_3\delta_{\tau\tau'}]\delta_{s^+_\delta s^+_\beta} \tag{G.23}$$

$$(-1)^{s_\beta - s_\delta}(S^{\gamma\bar{\beta}}_{\alpha\bar{\delta}})^{\tau++} = [W_3 - H_3\delta_{\tau\tau'}]\delta_{s_\beta s_\delta} + [B_3 - M_3\delta_{\tau\tau'}]\delta_{s^-_\delta s^-_\beta} \tag{G.24}$$

Therefore, the related part of the direct mean field reads:

$$\begin{aligned}\Gamma^{\tau++}_{\alpha\gamma}(D) = \sum_{\delta\beta>} E^{\gamma\delta}_{\alpha\beta}[(2W_3 + B_3)(\rho^{\tau++}_{\delta\beta} + \rho^{\tau--}_{\delta\beta} + \rho^{\bar{\tau}++}_{\delta\beta} + \rho^{\bar{\tau}--}_{\delta\beta}) \\ -(2H_3 + M_3)(\rho^{\tau++}_{\delta\beta} + \rho^{\tau--}_{\delta\beta})]\end{aligned} \tag{G.25}$$

We set the following quantity:

$$R^{\tau++}_{\delta\beta}(D) = (2W_3 + B_3)(\rho^{\tau++}_{\delta\beta} + \rho^{\tau--}_{\delta\beta} + \rho^{\bar{\tau}++}_{\delta\beta} + \rho^{\bar{\tau}--}_{\delta\beta}) - (2H_3 + M_3)(\rho^{\tau++}_{\delta\beta} + \rho^{\tau--}_{\delta\beta}) \tag{G.26}$$

Using this quantity in Eq.(G.25) leads to:

$$\Gamma^{\tau++}_{\alpha\gamma}(D) = \sum_{\delta\beta>} E^{\gamma\delta}_{\alpha\beta} R^{\tau++}_{\delta\beta}(D) \tag{G.27}$$

We can rewrite Eq.(G.27) more explicitly:

$$\boxed{\begin{aligned}\Gamma^{\tau++}_{\alpha\gamma}(D) = \int d\vec{r}[\rho(\vec{r})]^{\alpha}(I_r)_{(m_\alpha,n_{\perp_\alpha})(m_\gamma,n_{\perp_\gamma})}(\vec{r}_\perp)(I_z)_{(n_{z_\alpha},d_\alpha)(n_{z_\gamma},d_\gamma)}(z)R^{\tau++}(D,\vec{r}) \\ + \int d\vec{r}[\rho(\vec{r})]^{\alpha}\psi^*_\alpha(\vec{r})\psi_\gamma(\vec{r})\mathcal{R}^{\tau++}(D,\vec{r})\end{aligned}} \tag{G.28}$$

With:

$$\begin{cases} R^{\tau++}(D,\vec{r}) = \frac{1}{2(\mu_3\sqrt{\pi})^3}\sum_{\delta\beta>}\psi^*_\beta(\vec{r})\psi_\delta(\vec{r})R^{\tau++}_{\delta\beta}(D) \\ \\ \mathcal{R}^{\tau++}(D,\vec{r}) = \frac{1}{2(\mu_3\sqrt{\pi})^3}\sum_{\delta\beta>}(I_r)_{(m_\beta,n_{\perp_\beta})(m_\delta,n_{\perp_\delta})}(\vec{r}_\perp)(I_z)_{(n_{z_\beta},d_\beta)(n_{z_\delta},d_\delta)}(z)R^{\tau++}_{\delta\beta}(D) \end{cases} \tag{G.29}$$

Block $--$:

Here, we consider ($\alpha\downarrow$,$\gamma\downarrow$). This block is clearly the same as the $++$ one:

$$\boxed{\Gamma^{\tau++}_{\alpha\gamma}(D) = \Gamma^{\tau--}_{\alpha\gamma}(D)} \tag{G.30}$$

Block $-+$:

Here, we consider ($\alpha\downarrow$,$\gamma\uparrow$). We first evaluate the associated spin-isospin part:

$$(S^{\gamma\delta}_{\alpha\beta})^{\tau-+} = [B_3 - M_3\delta_{\tau\tau'}]\delta_{s^-_\delta s^+_\beta} \tag{G.31}$$

$$(-1)^{s_\beta - s_\delta}(S^{\gamma\bar{\beta}}_{\alpha\bar{\delta}})^{\tau-+} = -[B_3 - M_3\delta_{\tau\tau'}]\delta_{s^-_\delta s^+_\beta} \tag{G.32}$$

As the two terms cancel each other out, we finally find:

$$\boxed{\Gamma^{\tau-+}_{\alpha\gamma}(D) = 0} \tag{G.33}$$

Block $+-$:

Here, we consider ($\alpha\uparrow$,$\gamma\downarrow$). For symmetry purposes, we directly have:

$$\boxed{\Gamma^{\tau+-}_{\alpha\gamma}(D) = 0} \tag{G.34}$$

G.2.2 Exchange mean field

The exchange mean field reads as follows:

$$\boxed{\Gamma_{\alpha\gamma}(E) = -\sum_{\delta\beta} \langle \alpha\beta | V^{(D2)} | \delta\gamma \rangle \rho_{\delta\beta}} \tag{G.35}$$

We separate the spatial and spin-isospin parts of Eq.(G.35) and we use its time-reversal properties:

$$\boxed{\Gamma_{\alpha\gamma}(E) = \sum_{\delta\beta>} [E^{\delta\gamma}_{\alpha\beta}.S^{\delta\gamma}_{\alpha\beta} + (-1)^{s_\beta - s_\delta} E^{\bar{\delta}\gamma}_{\alpha\bar{\beta}}.S^{\bar{\delta}\gamma}_{\alpha\bar{\beta}}]\rho_{\delta\beta}} \tag{G.36}$$

We now consider the spin blocks.

Block ++:

Here, we consider ($\alpha\uparrow$,$\gamma\uparrow$). We first evaluate the associated spin-isospin part:

$$(S^{\delta\gamma}_{\alpha\beta})^{\tau++} = [W_3\delta_{\tau\tau'} - H_3]\delta_{s^+_\beta s^+_\delta} + [B_3\delta_{\tau\tau'} - M_3]\delta_{s_\delta s_\beta} \tag{G.37}$$

$$(-1)^{s_\beta - s_\delta}(S^{\bar{\delta}\gamma}_{\alpha\bar{\beta}})^{\tau++} = [W_3\delta_{\tau\tau'} - H_3]\delta_{s^-_\beta s^-_\delta} + [B_3\delta_{\tau\tau'} - M_3]\delta_{s_\delta s_\beta} \tag{G.38}$$

Thanks to Eq.(G.37) and Eq.(G.38), the related part of the exchange mean field reads:

$$\begin{aligned}\Gamma^{\tau++}_{\alpha\gamma}(E) = &\sum_{\delta\beta>} E^{\delta\gamma}_{\alpha\beta}([W_3\delta_{\tau\tau'} - H_3]\delta_{s^+_\beta s^+_\delta} + [B_3\delta_{\tau\tau'} - M_3]\delta_{s_\delta s_\beta})\rho_{\delta\beta} \\ &+ \sum_{\delta\beta>} E^{\bar{\delta}\gamma}_{\alpha\bar{\beta}}([W_3\delta_{\tau\tau'} - H_3]\delta_{s^-_\beta s^-_\delta} + [B_3\delta_{\tau\tau'} - M_3]\delta_{s_\delta s_\beta})\rho_{\delta\beta}\end{aligned} \tag{G.39}$$

We naturally set:

$$\begin{cases} \tilde{R}^{++}_{\delta\beta}(E) = ([W_3\delta_{\tau\tau'} - H_3]\delta_{s^+_\beta s^+_\delta} + [B_3\delta_{\tau\tau'} - M_3]\delta_{s_\delta s_\beta})\rho_{\delta\beta} \\ \\ \bar{R}^{++}_{\delta\beta}(E) = ([W_3\delta_{\tau\tau'} - H_3]\delta_{s^-_\beta s^-_\delta} + [B_3\delta_{\tau\tau'} - M_3]\delta_{s_\delta s_\beta})\rho_{\delta\beta} \end{cases} \tag{G.40}$$

Thanks to these quantity, the field now reads:

$$\Gamma^{\tau++}_{\alpha\gamma}(E) = \sum_{\delta\beta>} E^{\delta\gamma}_{\alpha\beta}\tilde{R}^{++}_{\delta\beta}(E) + E^{\bar{\delta}\gamma}_{\alpha\bar{\beta}}\bar{R}^{++}_{\delta\beta}(E) \tag{G.41}$$

We then combine the quantities $\tilde{R}$ and $\bar{R}$ together:

$$\begin{cases} (m'>0) \rightarrow R^{++}_{\delta\beta}(E) = \tilde{R}^{++}_{\delta\beta}(E) \\ (m'=0) \rightarrow R^{++}_{\delta\beta}(E) = \tilde{R}^{++}_{\delta\beta}(E) + \bar{R}^{++}_{\delta\beta}(E) \\ (m'<0) \rightarrow R^{++}_{\delta\beta}(E) = \bar{R}^{++}_{\delta\beta}(E) \end{cases} \tag{G.42}$$

Using these notations, we write:

$$\Gamma^{\tau++}_{\alpha\gamma}(E) = \sum_{\delta\beta>} \sum_{m'} E^{\delta\gamma}_{\alpha\beta} R^{++}_{\delta\beta}(E) \tag{G.43}$$

We finally write the spatial part of Eq.(G.43) more explicitly:

$$\boxed{\Gamma^{\tau++}_{\alpha\gamma}(E) = \int d\vec{r}[\rho(\vec{r})]^{\alpha} \psi^{*}_{\alpha}(\vec{r}) R^{++}_{\gamma}(E,\vec{r}) + \int d\vec{r}[\rho(\vec{r})]^{\alpha} \psi_{\gamma}(\vec{r}) R^{++}_{\alpha}(E,\vec{r})} \tag{G.44}$$

We've set:

$$\begin{cases} R^{++}_{\gamma}(E,\vec{r}) = \frac{1}{2(\mu_3\sqrt{\pi})^3} \sum_{\delta\beta>} \sum_{m'} \psi_{\delta}(\vec{r}) (I_r)_{(m_\beta, n_{\perp_\beta})(m_\gamma, n_{\perp_\gamma})}(\vec{r}_\perp) (I_z)_{(n_{z_\beta}, d_\beta)(n_{z_\gamma}, d_\gamma)}(z) R^{++}_{\delta\beta}(E) \\ \\ R^{++}_{\alpha}(E,\vec{r}) = \frac{1}{2(\mu_3\sqrt{\pi})^3} \sum_{\delta\beta>} \sum_{m'} \psi^{*}_{\beta}(\vec{r}) (I_r)_{(m_\alpha, n_{\perp_\alpha})(m_\delta, n_{\perp_\delta})}(\vec{r}_\perp) (I_z)_{(n_{z_\alpha}, d_\alpha)(n_{z_\delta}, d_\delta)}(z) R^{++}_{\delta\beta}(E) \end{cases} \tag{G.45}$$

Block $--$:

Here, we consider ($\alpha\downarrow$,$\gamma\downarrow$). We first evaluate the associated spin-isospin part:

$$(S^{\delta\gamma}_{\alpha\beta})^{\tau--} = [W_3\delta_{\tau\tau'} - H_3]\delta_{s^-_\beta s^-_\delta} + [B_3\delta_{\tau\tau'} - M_3]\delta_{s_\delta s_\beta} \tag{G.46}$$

$$(-1)^{s_\beta - s_\delta}(S^{\bar{\delta}\gamma}_{\alpha\bar{\beta}})^{\tau--} = [W_3\delta_{\tau\tau'} - H_3]\delta_{s^+_\beta s^+_\delta} + [B_3\delta_{\tau\tau'} - M_3]\delta_{s_\delta s_\beta} \tag{G.47}$$

Then, we set:

$$\begin{cases} \tilde{R}^{--}_{\delta\beta}(E) = ([W_3\delta_{\tau\tau'} - H_3]\delta_{s^-_\beta s^-_\delta} + [B_3\delta_{\tau\tau'} - M_3]\delta_{s_\delta s_\beta})\rho_{\delta\beta} \\ \\ \bar{R}^{--}_{\delta\beta}(E) = ([W_3\delta_{\tau\tau'} - H_3]\delta_{s^+_\beta s^+_\delta} + [B_3\delta_{\tau\tau'} - M_3]\delta_{s_\delta s_\beta})\rho_{\delta\beta} \end{cases} \tag{G.48}$$

We combine the quantities defined in Eq.(G.48)

$$\begin{cases} (m'>0) \rightarrow R^{--}_{\delta\beta}(E) = \tilde{R}^{--}_{\delta\beta}(E) \\ (m'=0) \rightarrow R^{--}_{\delta\beta}(E) = \tilde{R}^{--}_{\delta\beta}(E) + \bar{R}^{--}_{\delta\beta}(E) \\ (m'<0) \rightarrow R^{--}_{\delta\beta}(E) = \bar{R}^{--}_{\delta\beta}(E) \end{cases} \tag{G.49}$$

Using these notations, we write:

$$\Gamma^{\tau--}_{\alpha\gamma}(E) = \sum_{\delta\beta>}\sum_{m'} E^{\delta\gamma}_{\alpha\beta} R^{--}_{\delta\beta}(E) \tag{G.50}$$

We develop the spatial part of Eq.(G.50):

$$\boxed{\Gamma^{\tau--}_{\alpha\gamma}(E) = \int d\vec{r}[\rho(\vec{r})]^{\alpha}\psi^{*}_{\alpha}(\vec{r})R^{--}_{\gamma}(E,\vec{r}) + \int d\vec{r}[\rho(\vec{r})]^{\alpha}\psi_{\gamma}(\vec{r})R^{--}_{\alpha}(E,\vec{r})} \tag{G.51}$$

With:

$$\begin{cases} R^{--}_{\gamma}(E,\vec{r}) = \frac{1}{2(\mu_3\sqrt{\pi})^3}\sum_{\delta\beta>}\sum_{m'}\psi_{\delta}(\vec{r})(I_r)_{(m_\beta,n_{\perp_\beta})(m_\gamma,n_{\perp_\gamma})}(\vec{r}_{\perp})(I_z)_{(n_{z_\beta},d_\beta)(n_{z_\gamma},d_\gamma)}(z)R^{--}_{\delta\beta}(E) \\ R^{--}_{\alpha}(E,\vec{r}) = \frac{1}{2(\mu_3\sqrt{\pi})^3}\sum_{\delta\beta>}\sum_{m'}\psi^{*}_{\beta}(\vec{r})(I_r)_{(m_\alpha,n_{\perp_\alpha})(m_\delta,n_{\perp_\delta})}(\vec{r}_{\perp})(I_z)_{(n_{z_\alpha},d_\alpha)(n_{z_\delta},d_\delta)}(z)R^{--}_{\delta\beta}(E) \end{cases} \tag{G.52}$$

Block $-+$:

Here, we consider $(\alpha\downarrow,\gamma\uparrow)$. We first evaluate the associated spin-isospin part:

$$(S^{\delta\gamma}_{\alpha\beta})^{\tau-+} = [W_3\delta_{\tau\tau'} - H_3]\delta_{s^{+}_{\beta}s^{-}_{\delta}} \tag{G.53}$$

$$(-1)^{s_\beta - s_\delta}(S^{\bar{\delta}\gamma}_{\alpha\bar{\beta}})^{\tau-+} = -[W_3\delta_{\tau\tau'} - H_3]\delta_{s^{-}_{\beta}s^{+}_{\delta}} \tag{G.54}$$

Using Eq.(G.53) and Eq.(G.54), the related part of the exchange mean field reads:

$$\Gamma^{\tau-+}_{\alpha\gamma}(E) = \sum_{\delta\beta>} E^{\delta\gamma}_{\alpha\beta}[W_3\delta_{\tau\tau'} - H_3]\rho^{-+}_{\delta\beta} - \sum_{\delta\beta>} E^{\bar{\delta}\gamma}_{\alpha\bar{\beta}}[W_3\delta_{\tau\tau'} - H_3]\rho^{+-}_{\delta\beta} \tag{G.55}$$

Then we set:

$$\begin{cases} \tilde{R}^{-+}_{\delta\beta}(E) = ([W_3\delta_{\tau\tau'} - H_3]\rho^{-+}_{\delta\beta} \\ \bar{R}^{-+}_{\delta\beta}(E) = -[W_3\delta_{\tau\tau'} - H_3]\rho^{+-}_{\delta\beta} \end{cases} \tag{G.56}$$

The quantities defined in Eq.(G.56) are then combined:

$$\begin{cases} (m' > 0) \rightarrow R^{-+}_{\delta\beta}(E) = \tilde{R}^{-+}_{\delta\beta}(E) \\ (m' \leq 0) \rightarrow R^{-+}_{\delta\beta}(E) = \bar{R}^{-+}_{\delta\beta}(E) \end{cases} \tag{G.57}$$

Thanks to these notations, we write:

$$\Gamma^{\tau-+}_{\alpha\gamma}(E) = \sum_{\delta\beta>}\sum_{m'} E^{\delta\gamma}_{\alpha\beta} R^{-+}_{\delta\beta}(E) \tag{G.58}$$

Finally, we develop the spatial part of Eq.(G.58):

$$\boxed{\Gamma^{\tau -+}_{\alpha\gamma}(E) = \int d\vec{r}[\rho(\vec{r})]^{\alpha}\psi^{*}_{\alpha}(\vec{r})R^{-+}_{\gamma}(E,\vec{r}) + \int d\vec{r}[\rho(\vec{r})]^{\alpha}\psi_{\gamma}(\vec{r})R^{-+}_{\alpha}(E,\vec{r})} \tag{G.59}$$

With:

$$\begin{cases} R^{-+}_{\gamma}(E,\vec{r}) = \frac{1}{2(\mu_3\sqrt{\pi})^3}\sum_{\delta\beta>}\sum_{m'}\psi_{\delta}(\vec{r})(I_r)_{(m_\beta,n_{\perp_\beta})(m_\gamma,n_{\perp_\gamma})}(\vec{r}_{\perp})(I_z)_{(n_{z_\beta},d_\beta)(n_{z_\gamma},d_\gamma)}(z)R^{-+}_{\delta\beta}(E) \\ R^{-+}_{\alpha}(E,\vec{r}) = \frac{1}{2(\mu_3\sqrt{\pi})^3}\sum_{\delta\beta>}\sum_{m'}\psi^{*}_{\beta}(\vec{r})(I_r)_{(m_\alpha,n_{\perp_\alpha})(m_\delta,n_{\perp_\delta})}(\vec{r}_{\perp})(I_z)_{(n_{z_\alpha},d_\alpha)(n_{z_\delta},d_\delta)}(z)R^{-+}_{\delta\beta}(E) \end{cases} \tag{G.60}$$

Block +−:

Here, we consider ($\alpha\uparrow$,$\gamma\downarrow$). For symmetry purposes, we directly have:

$$\boxed{\Gamma^{\tau +-}_{\alpha\gamma}(E) = \Gamma^{\tau -+}_{\gamma\alpha}(E)} \tag{G.61}$$

G.2.3 Pairing field

The pairing field reads as follows:

$$\boxed{\Delta_{\alpha\bar{\beta}} = \sum_{\gamma\delta}(-1)^{s_\beta - s_\delta}\langle\alpha\bar{\beta}|V^{(D2)}|\gamma\bar{\delta}\rangle\kappa_{\gamma\bar{\delta}}} \tag{G.62}$$

We separate the spin and isospin parts of Eq.(G.62) and we use its time-reversal properties:

$$\boxed{\Delta_{\alpha\bar{\beta}} = \sum_{\gamma\delta>}[(-1)^{s_\beta - s_\delta}E^{\gamma\bar{\delta}}_{\alpha\bar{\beta}}.S^{\gamma\bar{\delta}}_{\alpha\bar{\beta}} + (-1)^{s_\beta + s_\gamma}E^{\bar{\gamma}\delta}_{\alpha\bar{\beta}}.S^{\bar{\gamma}\delta}_{\alpha\bar{\beta}}]\kappa_{\gamma\bar{\delta}}} \tag{G.63}$$

Now, we consider the spins.

Block ++:

Here, we consider ($\alpha\uparrow$,$\bar{\beta}\uparrow$). We first evaluate the associated spin-isospin part:

$$(-1)^{s_\beta - s_\delta}(S^{\gamma\bar{\delta}}_{\alpha\bar{\beta}})^{\tau ++} = \delta_{\tau\tau'}([W_3 - H_3]\delta_{s^+_\gamma s^+_\delta} - [B_3\ - M_3]\delta_{s^-_\gamma s^-_\delta}) \tag{G.64}$$

$$(-1)^{s_\beta + s_\gamma}(S^{\bar{\gamma}\delta}_{\alpha\bar{\beta}})^{\tau ++} = \delta_{\tau\tau'}([W_3 - H_3]\delta_{s^-_\gamma s^-_\delta} - [B_3\ - M_3]\delta_{s^+_\gamma s^+_\delta}) \tag{G.65}$$

Thanks to Eq.(G.64) and Eq.(G.65), the related part of the pairing field reads:

$$\begin{aligned}\Delta^{\tau ++}_{\alpha\bar{\beta}} = &\sum_{\gamma\delta>}E^{\gamma\bar{\delta}}_{\alpha\bar{\beta}}([W_3 - H_3]\delta_{s^+_\gamma s^+_\delta} - [B_3\ - M_3]\delta_{s^-_\gamma s^-_\delta})\kappa^{\tau}_{\gamma\bar{\delta}} \\ &+\sum_{\gamma\delta>}E^{\bar{\gamma}\delta}_{\alpha\bar{\beta}}([W_3 - H_3]\delta_{s^-_\gamma s^-_\delta} - [B_3\ - M_3]\delta_{s^+_\gamma s^+_\delta})\kappa^{\tau}_{\bar{\gamma}\delta}\end{aligned} \tag{G.66}$$

We note:

$$\begin{cases} \tilde{K}^{++}_{\gamma\bar{\delta}} = ([W_3 - H_3]\delta_{s^+_\gamma s^+_\delta} - [B_3 \ - M_3]\delta_{s^-_\gamma s^-_\delta})\kappa^\tau_{\gamma\bar{\delta}} \\ \\ \bar{K}^{++}_{\gamma\bar{\delta}} = ([W_3 - H_3]\delta_{s^-_\gamma s^-_\delta} - [B_3 \ - M_3]\delta_{s^+_\gamma s^+_\delta})\kappa^\tau_{\gamma\bar{\delta}} \end{cases} \tag{G.67}$$

The quantities defined in Eq.(G.67) are then combined:

$$\begin{cases} (m' > 0) \rightarrow K^{++}_{\gamma\bar{\delta}} = \tilde{K}^{++}_{\gamma\bar{\delta}} \\ (m' = 0) \rightarrow K^{++}_{\gamma\bar{\delta}} = \tilde{K}^{++}_{\gamma\bar{\delta}} + \bar{K}^{++}_{\gamma\bar{\delta}} \\ (m' < 0) \rightarrow K^{++}_{\gamma\bar{\delta}} = \bar{K}^{++}_{\gamma\bar{\delta}} \end{cases} \tag{G.68}$$

Using Eq.(G.68) in the field leads to:

$$\Delta^{\tau++}_{\alpha\bar{\beta}} = \sum_{\gamma\delta>} \sum_{m'} E^{\gamma\bar{\delta}}_{\alpha\bar{\beta}} K^{++}_{\gamma\bar{\delta}} \tag{G.69}$$

Finally, we develop the spatial part of Eq.(G.69):

$$\boxed{\Delta^{\tau++}_{\alpha\bar{\beta}} = \int d\vec{r}[\rho(\vec{r})]^\alpha \psi^*_\alpha(\vec{r}) K^{++}_\beta(\vec{r}) + \int d\vec{r}[\rho(\vec{r})]^\alpha \psi^*_\beta(\vec{r}) K^{++}_\alpha(\vec{r})} \tag{G.70}$$

With:

$$\begin{cases} K^{++}_\beta(\vec{r}) = \frac{1}{2(\mu_3\sqrt{\pi})^3} \sum_{\gamma\delta>} \sum_{m'} \psi_\gamma(\vec{r}) (I_r)_{(m_\beta, n_{\perp_\beta})(m_\delta, n_{\perp_\delta})}(\vec{r}_\perp) (I_z)_{(n_{z_\beta}, d_\beta)(n_{z_\delta}, d_\delta)}(z) K^{++}_{\gamma\bar{\delta}} \\ \\ K^{++}_\alpha(\vec{r}) = \frac{1}{2(\mu_3\sqrt{\pi})^3} \sum_{\gamma\delta>} \sum_{m'} \psi_\delta(\vec{r}) (I_r)_{(m_\alpha, n_{\perp_\alpha})(m_\gamma, n_{\perp_\gamma})}(\vec{r}_\perp) (I_z)_{(n_{z_\alpha}, d_\alpha)(n_{z_\gamma}, d_\gamma)}(z) K^{++}_{\gamma\bar{\delta}} \end{cases} \tag{G.71}$$

Block $--$:

Here, we consider $(\alpha\downarrow, \bar{\beta}\downarrow)$. We first evaluate the associated spin-isospin part:

$$(-1)^{s_\beta - s_\delta} (S^{\gamma\bar{\delta}}_{\alpha\bar{\beta}})^{\tau--} = \delta_{\tau\tau'}([W_3 - H_3]\delta_{s^-_\gamma s^-_\delta} - [B_3 \ - M_3]\delta_{s^+_\gamma s^+_\delta}) \tag{G.72}$$

$$(-1)^{s_\beta + s_\gamma} (S^{\bar{\gamma}\delta}_{\alpha\bar{\beta}})^{\tau--} = \delta_{\tau\tau'}([W_3 - H_3]\delta_{s^+_\gamma s^+_\delta} - [B_3 \ - M_3]\delta_{s^-_\gamma s^-_\delta}) \tag{G.73}$$

Using Eq.(G.72) and Eq.(G.73), the related part of the pairing field reads:

$$\begin{aligned} \Delta^{\tau--}_{\alpha\bar{\beta}} = &\sum_{\gamma\delta>} E^{\gamma\bar{\delta}}_{\alpha\bar{\beta}} ([W_3 - H_3]\delta_{s^-_\gamma s^-_\delta} - [B_3 \ - M_3]\delta_{s^+_\gamma s^+_\delta})\kappa^\tau_{\gamma\bar{\delta}} \\ &+ \sum_{\gamma\delta>} E^{\bar{\gamma}\delta}_{\alpha\bar{\beta}} ([W_3 - H_3]\delta_{s^+_\gamma s^+_\delta} - [B_3 \ - M_3]\delta_{s^-_\gamma s^-_\delta})\kappa^\tau_{\gamma\bar{\delta}} \end{aligned} \tag{G.74}$$

We set:

$$\begin{cases} \tilde{K}^{--}_{\gamma\bar{\delta}} = ([W_3 - H_3]\delta_{s^-_\gamma s^-_\delta} - [B_3 \ - M_3]\delta_{s^+_\gamma s^+_\delta})\kappa^\tau_{\gamma\bar{\delta}} \\ \\ \bar{K}^{--}_{\gamma\bar{\delta}} = ([W_3 - H_3]\delta_{s^+_\gamma s^+_\delta} - [B_3 \ - M_3]\delta_{s^-_\gamma s^-_\delta})\kappa^\tau_{\gamma\bar{\delta}} \end{cases} \tag{G.75}$$

The quantities defined in Eq.(G.75) are combined:

$$\begin{cases} (m' > 0) \rightarrow K^{--}_{\gamma\bar{\delta}} = \tilde{K}^{--}_{\gamma\bar{\delta}} \\ (m' = 0) \rightarrow K^{--}_{\gamma\bar{\delta}} = \tilde{K}^{++}_{\gamma\bar{\delta}} + \bar{K}^{--}_{\gamma\bar{\delta}} \\ (m' < 0) \rightarrow K^{--}_{\gamma\bar{\delta}} = \bar{K}^{--}_{\gamma\bar{\delta}} \end{cases} \tag{G.76}$$

Thanks to Eq.(G.76), the field reads:

$$\Delta^{\tau--}_{\alpha\bar{\beta}} = \sum_{\gamma\delta>} \sum_{m'} E^{\gamma\bar{\delta}}_{\alpha\bar{\beta}} K^{--}_{\gamma\bar{\delta}} \tag{G.77}$$

Finally, we develop the spatial part of Eq.(G.77):

$$\boxed{\Delta^{\tau--}_{\alpha\bar{\beta}} = \int d\vec{r}[\rho(\vec{r})]^\alpha \psi^*_\alpha(\vec{r}) K^{--}_\beta(\vec{r}) + \int d\vec{r}[\rho(\vec{r})]^\alpha \psi^*_\beta(\vec{r}) K^{--}_\alpha(\vec{r})} \tag{G.78}$$

With:

$$\begin{cases} K^{--}_\beta(\vec{r}) = \frac{1}{2(\mu_3\sqrt{\pi})^3} \sum_{\gamma\delta>} \sum_{m'} \psi_\gamma(\vec{r}) (I_r)_{(m_\beta, n_{\perp_\beta})(m_\delta, n_{\perp_\delta})}(\vec{r}_\perp)(I_z)_{(n_{z_\beta}, d_\beta)(n_{z_\delta}, d_\delta)}(z) K^{--}_{\gamma\bar{\delta}} \\ \\ K^{--}_\alpha(\vec{r}) = \frac{1}{2(\mu_3\sqrt{\pi})^3} \sum_{\gamma\delta>} \sum_{m'} \psi_\delta(\vec{r}) (I_r)_{(m_\alpha, n_{\perp_\alpha})(m_\gamma, n_{\perp_\gamma})}(\vec{r}_\perp)(I_z)_{(n_{z_\alpha}, d_\alpha)(n_{z_\gamma}, d_\gamma)}(z) K^{--}_{\gamma\bar{\delta}} \end{cases} \tag{G.79}$$

Block $-+$:

Here, we consider $(\alpha\downarrow, \bar{\beta}\uparrow)$. We first evaluate the associated spin-isospin part:

$$(-1)^{s_\beta - s_\delta}(S^{\gamma\bar{\delta}}_{\alpha\bar{\beta}})^{\tau-+} = \delta_{\tau\tau'}[W_3 - H_3 + B_3 - M_3]\delta_{s^-_\gamma s^+_\delta} \tag{G.80}$$

$$(-1)^{s_\beta + s_\gamma}(S^{\bar{\gamma}\delta}_{\alpha\bar{\beta}})^{\tau-+} = -\delta_{\tau\tau'}[W_3 - H_3 + B_3 - M_3]\delta_{s^+_\gamma s^-_\delta} \tag{G.81}$$

Using Eq.(G.80) and Eq.(G.81), the related part of the pairing field reads:

$$\begin{aligned} \Delta^{\tau-+}_{\alpha\bar{\beta}} = &\sum_{\gamma\delta>} E^{\gamma\bar{\delta}}_{\alpha\bar{\beta}}[W_3 - H_3 + B_3 - M_3]\delta_{s^-_\gamma s^+_\delta}\kappa^\tau_{\gamma\bar{\delta}} \\ &- \sum_{\gamma\delta>} E^{\bar{\gamma}\delta}_{\alpha\bar{\beta}}[W_3 - H_3 + B_3 - M_3]\delta_{s^+_\gamma s^-_\delta}\kappa^\tau_{\gamma\bar{\delta}} \end{aligned} \tag{G.82}$$

We then set:

$$\begin{cases} \tilde{K}^{-+}_{\gamma\bar{\delta}} = [W_3 - H_3 + B_3 - M_3]\delta_{s^-_\gamma s^+_\delta}\kappa^\tau_{\gamma\bar{\delta}} \\ \\ \bar{K}^{-+}_{\gamma\bar{\delta}} = -[W_3 - H_3 + B_3 - M_3]\delta_{s^+_\gamma s^-_\delta}\kappa^\tau_{\gamma\bar{\delta}} \end{cases} \tag{G.83}$$

The quantities defined in Eq.(G.83) are combined:

$$\begin{cases} (m' > 0) \rightarrow K^{-+}_{\gamma\bar{\delta}} = \tilde{K}^{-+}_{\gamma\bar{\delta}} \\ (m' \leq 0) \rightarrow K^{-+}_{\gamma\bar{\delta}} = \bar{K}^{-+}_{\gamma\bar{\delta}} \end{cases} \tag{G.84}$$

Thanks to Eq.(G.84), we rewrite the field:

$$\Delta^{\tau-+}_{\alpha\bar{\beta}} = \sum_{\gamma\delta>}\sum_{m'} E^{\gamma\bar{\delta}}_{\alpha\bar{\beta}} K^{-+}_{\gamma\bar{\delta}} \tag{G.85}$$

We finally develop the spatial part of Eq.(G.85)

$$\boxed{\Delta^{\tau-+}_{\alpha\bar{\beta}} = \int d\vec{r}[\rho(\vec{r})]^\alpha \psi^*_\alpha(\vec{r}) K^{-+}_\beta(\vec{r}) + \int d\vec{r}[\rho(\vec{r})]^\alpha \psi^*_\beta(\vec{r}) K^{-+}_\alpha(\vec{r})} \tag{G.86}$$

With:

$$\begin{cases} K^{-+}_\beta(\vec{r}) = \frac{1}{2(\mu_3\sqrt{\pi})^3}\sum_{\gamma\delta>}\sum_{m'}\psi_\gamma(\vec{r})(I_r)_{(m_\beta,n_{\perp_\beta})(m_\delta,n_{\perp_\delta})}(\vec{r}_\perp)(I_z)_{(n_{z_\beta},d_\beta)(n_{z_\delta},d_\delta)}(z)K^{-+}_{\gamma\bar{\delta}} \\ \\ K^{-+}_\alpha(\vec{r}) = \frac{1}{2(\mu_3\sqrt{\pi})^3}\sum_{\gamma\delta>}\sum_{m'}\psi_\delta(\vec{r})(I_r)_{(m_\alpha,n_{\perp_\alpha})(m_\gamma,n_{\perp_\gamma})}(\vec{r}_\perp)(I_z)_{(n_{z_\alpha},d_\alpha)(n_{z_\gamma},d_\gamma)}(z)K^{-+}_{\gamma\bar{\delta}} \end{cases} \tag{G.87}$$

Block $+-$:

Here, we consider ($\alpha\uparrow$,$\bar{\beta}\downarrow$). For symmetry purposes, we directly have:

$$\boxed{\Delta^{\tau+-}_{\alpha\bar{\beta}} = \Delta^{\tau-+}_{\beta\bar{\alpha}}} \tag{G.88}$$

G.2.4 Direct rearrangement field

The direct rearrangement field reads as follows:

$$\boxed{\partial\Gamma_{\alpha\beta}(D) = \sum_{\gamma\delta}\sum_{\eta\mu}\langle\gamma\eta|\frac{\partial V^{(D2)}}{\partial\rho_{\alpha\beta}}|\delta\mu\rangle\rho_{\gamma\delta}\rho_{\eta\mu}} \tag{G.89}$$

We can separate the spatial and the spin-isospin part of Eq.(G.89):

$$\partial\Gamma_{\alpha\beta}(D) = \sum_{\gamma\delta}\sum_{\eta\mu} E^{(\gamma\delta)(\eta\mu)}_{\alpha\beta} S^{\delta\mu}_{\gamma\eta}\rho_{\gamma\delta}\rho_{\eta\mu} \tag{G.90}$$

Using the time-reversal properties of Eq.(G.90) associated with the indices η and μ leads to:

$$\partial\Gamma_{\alpha\beta}(D) = \sum_{\gamma\delta}\sum_{\eta\mu>}[E_{\alpha\beta}^{(\gamma\delta)(\eta\mu)}S_{\gamma\eta}^{\delta\mu} + (-1)^{s_\eta - s_\mu}E_{\alpha\beta}^{(\gamma\delta)(\bar{\eta}\bar{\mu})}S_{\gamma\bar{\eta}}^{\delta\bar{\mu}}]\rho_{\gamma\delta}\rho_{\eta\mu} \tag{G.91}$$

We then remark the following property:

$$E_{\alpha\beta}^{(\gamma\delta)(\bar{\eta}\bar{\mu})} = E_{\alpha\beta}^{(\gamma\delta)(\mu\eta)} \tag{G.92}$$

Inserting this property into Eq.(G.91), we get:

$$\partial\Gamma_{\alpha\beta}(D) = \sum_{\gamma\delta}\sum_{\eta\mu>}E_{\alpha\beta}^{(\gamma\delta)(\eta\mu)}[S_{\gamma\eta}^{\delta\mu} + (-1)^{s_\eta - s_\mu}S_{\gamma\bar{\mu}}^{\delta\bar{\eta}}]\rho_{\gamma\delta}\rho_{\eta\mu} \tag{G.93}$$

Then, we use the time-reversal properties of Eq.(G.93) associated with the indices γ and δ:

$$\begin{aligned}\partial\Gamma_{\alpha\beta}(D) = \sum_{\gamma\delta>}\sum_{\eta\mu>}E_{\alpha\beta}^{(\gamma\delta)(\eta\mu)}([S_{\gamma\eta}^{\delta\mu} + (-1)^{s_\eta - s_\mu}S_{\gamma\bar{\mu}}^{\delta\bar{\eta}}] \\ +(-1)^{s_\delta - s_\gamma}[S_{\bar{\delta}\eta}^{\bar{\gamma}\mu} + (-1)^{s_\eta - s_\mu}S_{\bar{\delta}\bar{\mu}}^{\bar{\gamma}\bar{\eta}}])\rho_{\gamma\delta}\rho_{\eta\mu}\end{aligned} \tag{G.94}$$

Besides, we remark the following property concerning the spin-isospin part of $\partial\Gamma(D)$:

$$(-1)^{s_\delta - s_\gamma}(-1)^{s_\eta - s_\mu}S_{\bar{\delta}\bar{\mu}}^{\bar{\gamma}\bar{\eta}} = (W_3 - H_3\delta_{\tau_\gamma\tau_\mu})\delta_{s_\gamma s_\delta}\delta_{s_\eta s_\mu} + (B_3 - M_3\delta_{\tau_\gamma\tau_\mu})\delta_{s_\gamma s_\mu}\delta_{s_\eta s_\delta} = S_{\gamma\eta}^{\delta\mu} \tag{G.95}$$

Thanks to the property displayed in Eq.(G.95), we write:

$$\partial\Gamma_{\alpha\beta}(D) = \sum_{\gamma\delta>}\sum_{\eta\mu>}E_{\alpha\beta}^{(\gamma\delta)(\eta\mu)}(2S_{\gamma\eta}^{\delta\mu} + (-1)^{s_\eta - s_\mu}S_{\gamma\bar{\mu}}^{\delta\bar{\eta}} + (-1)^{s_\delta - s_\gamma}S_{\bar{\delta}\eta}^{\bar{\gamma}\mu})\rho_{\gamma\delta}\rho_{\eta\mu} \tag{G.96}$$

Performing the indice exchange $\gamma\delta \leftrightarrow \eta\mu$ on the term in the middle of Eq.(G.96), we obtain:

$$\partial\Gamma_{\alpha\beta}(D) = 2\sum_{\gamma\delta>}\sum_{\eta\mu>}E_{\alpha\beta}^{(\gamma\delta)(\eta\mu)}(S_{\gamma\eta}^{\delta\mu} + (-1)^{s_\eta - s_\mu}S_{\gamma\bar{\mu}}^{\delta\bar{\eta}})\rho_{\gamma\delta}\rho_{\eta\mu} \tag{G.97}$$

Unlike the other fields discussed previously, the summation applies to all the indices of the spin-isospin part. Therefore it does not depend on the field anymore. In addition, we remark for this spin-isospin part:

$$\begin{cases} S_{\gamma\eta}^{\delta\mu} = (W_3 - H_3\delta_{\tau_\gamma\tau_\mu})\delta_{s_\gamma s_\delta}\delta_{s_\eta s_\mu} + (B_3 - M_3\delta_{\tau_\gamma\tau_\mu})\delta_{s_\gamma s_\mu}\delta_{s_\eta s_\delta} \\ \\ (-1)^{s_\eta - s_\mu}S_{\gamma\bar{\mu}}^{\delta\bar{\eta}} = (W_3 - H_3\delta_{\tau_\gamma\tau_\mu})\delta_{s_\gamma s_\delta}\delta_{s_\eta s_\mu} + (-1)^{s_\eta - s_\mu}(B_3 - M_3\delta_{\tau_\gamma\tau_\mu})\delta_{s_\gamma\bar{s}_\eta}\delta_{\bar{s}_\mu s_\delta} \end{cases} \tag{G.98}$$

Thanks to Eq.(G.98), the field now reads:

$$\partial\Gamma_{\alpha\beta}(D) = 2\sum_{\gamma\delta>}\sum_{\eta\mu>} E_{\alpha\beta}^{(\gamma\delta)(\eta\mu)}[2(W_3 - H_3\delta_{\tau_\gamma\tau_\mu}) \\ +(B_3 - M_3\delta_{\tau_\gamma\tau_\mu})](\rho_{\mu\eta}^{++} + \rho_{\mu\eta}^{--})(\rho_{\delta\gamma}^{++} + \rho_{\delta\gamma}^{--}) \tag{G.99}$$

We can explicitly develop the isospin conditions:

$$\partial\Gamma_{\alpha\beta}(D) = 2\sum_{\gamma\delta>}\sum_{\eta\mu>} E_{\alpha\beta}^{(\gamma\delta)(\eta\mu)}([2W_3 + B_3](\rho_{\mu\eta}^{++\tau} + \rho_{\mu\eta}^{++\bar{\tau}} + \rho_{\mu\eta}^{--\tau} + \rho_{\mu\eta}^{--\bar{\tau}}) \\ (\rho_{\delta\gamma}^{++\tau} + \rho_{\delta\gamma}^{++\bar{\tau}} + \rho_{\delta\gamma}^{--\tau} + \rho_{\delta\gamma}^{--\bar{\tau}}) \\ -[2H_3 + M_3][(\rho_{\mu\eta}^{++\tau} + \rho_{\mu\eta}^{--\tau})(\rho_{\delta\gamma}^{++\tau} + \rho_{\delta\gamma}^{--\tau}) + (\rho_{\mu\eta}^{++\bar{\tau}} + \rho_{\mu\eta}^{--\bar{\tau}})(\rho_{\delta\gamma}^{++\bar{\tau}} + \rho_{\delta\gamma}^{--\bar{\tau}})]) \tag{G.100}$$

Then, we set:

$$\begin{cases} \partial R_{\mu\eta}^{tot}(D) = \rho_{\mu\eta}^{++\tau} + \rho_{\mu\eta}^{++\bar{\tau}} + \rho_{\mu\eta}^{--\tau} + \rho_{\mu\eta}^{--\bar{\tau}} \\ \\ \partial R_{\mu\eta}^{\tau}(D) = \rho_{\mu\eta}^{++\tau} + \rho_{\mu\eta}^{--\tau} \end{cases} \tag{G.101}$$

Inserting Eq.(G.101) into the rearrangement field leads to:

$$\partial\Gamma_{\alpha\beta}(D) = 2\sum_{\gamma\delta>}\sum_{\eta\mu>} E_{\alpha\beta}^{(\gamma\delta)(\eta\mu)}([2W_3 + B_3]\partial R_{\mu\eta}^{tot}(D)\partial R_{\delta\gamma}^{tot}(D) \\ -[2H_3 + M_3]\partial R_{\mu\eta}^{\tau}(D)\partial R_{\delta\gamma}^{\tau}(D) - [2H_3 + M_3]\partial R_{\mu\eta}^{\bar{\tau}}(D)\partial R_{\delta\gamma}^{\bar{\tau}}(D)) \tag{G.102}$$

We develop the spatial part of Eq.(G.102):

$$\partial\Gamma_{\alpha\beta}(D) = \frac{2\delta_{s_\alpha s_\beta}}{2(\mu_3\sqrt{\pi})^3}\int d\vec{r}\alpha[\rho(\vec{r})]^{\alpha-1}\psi_\alpha^*(\vec{r})\psi_\beta(\vec{r})\sum_{\gamma\delta>}\sum_{\eta\mu>}[\psi_\gamma^*(\vec{r})\psi_\delta(\vec{r})I_{\eta\mu}(\vec{r}) + \psi_\eta^*(\vec{r})\psi_\mu(\vec{r})I_{\gamma\delta}(\vec{r})] \\ ([2W_3 + B_3]\partial R_{\mu\eta}^{tot}(D)\partial R_{\delta\gamma}^{tot}(D) - [2H_3 + M_3]\partial R_{\mu\eta}^{\tau}(D)\partial R_{\delta\gamma}^{\tau}(D) \\ -[2H_3 + M_3]\partial R_{\mu\eta}^{\bar{\tau}}(D)\partial R_{\delta\gamma}^{\bar{\tau}}(D)) \tag{G.103}$$

We use the change of indices $\gamma\delta \leftrightarrow \eta\mu$ to simplify Eq.(G.103):

$$\partial\Gamma_{\alpha\beta}(D) = \frac{4\delta_{s_\alpha s_\beta}}{2(\mu_3\sqrt{\pi})^3}\int d\vec{r}\alpha[\rho(\vec{r})]^{\alpha-1}\psi_\alpha^*(\vec{r})\psi_\beta(\vec{r})\sum_{\gamma\delta>}\sum_{\eta\mu>}\psi_\gamma^*(\vec{r})\psi_\delta(\vec{r})I_{\eta\mu}(\vec{r}) \\ ([2W_3 + B_3]\partial R_{\mu\eta}^{tot}(D)\partial R_{\delta\gamma}^{tot}(D) - [2H_3 + M_3]\partial R_{\mu\eta}^{\tau}(D)\partial R_{\delta\gamma}^{\tau}(D) \\ -[2H_3 + M_3]\partial R_{\mu\eta}^{\bar{\tau}}(D)\partial R_{\delta\gamma}^{\bar{\tau}}(D)) \tag{G.104}$$

We then naturally set:

$$\partial R(D,\vec{r}) = \frac{1}{2(\mu_3\sqrt{\pi})^3}[[2W_3 + B_3]\sum_{\gamma\delta>}\psi_\gamma^*(\vec{r})\psi_\delta(\vec{r})\partial R_{\delta\gamma}^{tot}(D)\sum_{\eta\mu>}I_{\eta\mu}(\vec{r})\partial R_{\mu\eta}^{tot}(D) \\ -[2H_3 + M_3]\sum_{\gamma\delta>}\psi_\gamma^*(\vec{r})\psi_\delta(\vec{r})\partial R_{\delta\gamma}^{\tau}(D)\sum_{\eta\mu>}I_{\eta\mu}(\vec{r})\partial R_{\mu\eta}^{\tau}(D) \\ -[2H_3 + M_3]\sum_{\gamma\delta>}\psi_\gamma^*(\vec{r})\psi_\delta(\vec{r})\partial R_{\delta\gamma}^{\bar{\tau}}(D)\sum_{\eta\mu>}I_{\eta\mu}(\vec{r})\partial R_{\mu\eta}^{\bar{\tau}}(D)] \tag{G.105}$$

Using Eq.(G.105), we can give the final reduced expression of the direct rearrangement field (it does not depend on the isospins):

$$\boxed{\partial\Gamma_{\alpha\beta}(D) = 4\delta_{s_\alpha s_\beta}\int d\vec{r}\alpha[\rho(\vec{r})]^{\alpha-1}\psi^*_\alpha(\vec{r})\psi_\beta(\vec{r})\partial R(D,\vec{r})} \tag{G.106}$$

This expression is the one evaluated numerically in the HFB3 code.

G.2.5 Exchange rearrangement field

The exchange rearrangement field reads as follows:

$$\boxed{\partial\Gamma_{\alpha\beta}(E) = -\sum_{\gamma\delta}\sum_{\eta\mu}\langle\gamma\eta|\frac{\partial V^{(D2)}}{\partial\rho_{\alpha\beta}}|\mu\delta\rangle\rho_{\delta\gamma}\rho_{\mu\eta}} \tag{G.107}$$

We start by separating the spatial and spin-isospin part of Eq.(G.107):

$$\partial\Gamma_{\alpha\beta}(E) = -\sum_{\gamma\delta}\sum_{\eta\mu}E^{(\gamma\mu)(\eta\delta)}_{\alpha\beta}S^{\mu\delta}_{\gamma\eta}\rho_{\delta\gamma}\rho_{\mu\eta} \tag{G.108}$$

We first use the time-reversal properties of Eq.(G.108) associated with the indices η and μ:

$$\partial\Gamma_{\alpha\beta}(E) = -\sum_{\gamma\delta}\sum_{\eta\mu>}[E^{(\gamma\mu)(\eta\delta)}_{\alpha\beta}S^{\mu\delta}_{\gamma\eta} + (-1)^{s_\eta - s_\mu}E^{(\gamma\bar{\mu})(\bar{\eta}\delta)}_{\alpha\beta}S^{\bar{\mu}\delta}_{\gamma\bar{\eta}}]\rho_{\delta\gamma}\rho_{\mu\eta} \tag{G.109}$$

Then, we use the time-reversal properties associated with the indices γ and δ:

$$\begin{aligned}\partial\Gamma_{\alpha\beta}(E) = -\sum_{\gamma\delta>}\sum_{\eta\mu>}([E^{(\gamma\mu)(\eta\delta)}_{\alpha\beta}S^{\mu\delta}_{\gamma\eta} + (-1)^{s_\eta - s_\mu}E^{(\gamma\bar{\mu})(\bar{\eta}\delta)}_{\alpha\beta}S^{\bar{\mu}\delta}_{\gamma\bar{\eta}}] \\ +(-1)^{s_\delta - s_\gamma}[E^{(\bar{\gamma}\mu)(\eta\bar{\delta})}_{\alpha\beta}S^{\mu\bar{\delta}}_{\bar{\gamma}\eta} + (-1)^{s_\eta - s_\mu}E^{(\bar{\gamma}\bar{\mu})(\bar{\eta}\bar{\delta})}_{\alpha\beta}S^{\bar{\mu}\bar{\delta}}_{\bar{\gamma}\bar{\eta}}])\rho_{\delta\gamma}\rho_{\mu\eta}\end{aligned} \tag{G.110}$$

We remark the following properties:

$$\begin{cases}E^{(\bar{\gamma}\bar{\mu})(\bar{\eta}\bar{\delta})}_{\alpha\beta} = E^{(\gamma\mu)(\eta\delta)}_{\alpha\beta} \\ E^{(\bar{\gamma}\mu)(\eta\bar{\delta})}_{\alpha\beta} = E^{(\gamma\bar{\mu})(\bar{\eta}\delta)}_{\alpha\beta}\end{cases} \qquad \begin{cases}(-1)^{s_\delta - s_\gamma + s_\eta - s_\mu}S^{\bar{\mu}\bar{\delta}}_{\bar{\gamma}\bar{\eta}} = S^{\mu\delta}_{\gamma\eta} \\ (-1)^{s_\gamma - s_\delta}S^{\mu\bar{\delta}}_{\bar{\gamma}\eta} = (-1)^{s_\eta - s_\mu}S^{\bar{\mu}\delta}_{\gamma\bar{\eta}}\end{cases} \tag{G.111}$$

Thanks to these properties, $\partial\Gamma(E)$ reads:

$$\partial\Gamma_{\alpha\beta}(E) = -2\sum_{\gamma\delta>}\sum_{\eta\mu>}[E^{(\gamma\mu)(\eta\delta)}_{\alpha\beta}S^{\mu\delta}_{\gamma\eta} + (-1)^{s_\eta - s_\mu}E^{(\gamma\bar{\mu})(\bar{\eta}\delta)}_{\alpha\beta}S^{\bar{\mu}\delta}_{\gamma\bar{\eta}}]\rho_{\delta\gamma}\rho_{\mu\eta} \tag{G.112}$$

We develop the spatial part of Eq.(G.112):

$$\partial\Gamma_{\alpha\beta}(E) = \frac{-2\delta_{s_\alpha s_\beta}\delta_{\tau_\alpha\tau_\beta}}{2(\mu_3\sqrt{\pi})^3}\int d\vec{r}\alpha[\rho(\vec{r})]^{\alpha-1}\psi^*_\alpha(\vec{r})\psi_\beta(\vec{r}) \tag{G.113}$$
$$[\sum_{\gamma\delta>}\sum_{\eta\mu>}[\psi^*_\gamma(\vec{r})\psi_\mu(\vec{r})I_{\eta\delta}(\vec{r}) + \psi^*_\eta(\vec{r})\psi_\delta(\vec{r})I_{\gamma\mu}(\vec{r})]S^{\mu\delta}_{\gamma\eta}\rho_{\delta\gamma}\rho_{\mu\eta}$$
$$+\sum_{\gamma\delta>}\sum_{\eta\mu>}(-1)^{s_\eta - s_\mu}[\psi^*_\gamma(\vec{r})\psi^*_\mu(\vec{r})I_{\bar{\eta}\delta}(\vec{r}) + \psi_\eta(\vec{r})\psi_\delta(\vec{r})I_{\gamma\bar{\mu}}(\vec{r})]S^{\bar{\mu}\delta}_{\gamma\bar{\eta}}\rho_{\delta\gamma}\rho_{\mu\eta}]$$

Thanks to the indice exchange $\gamma\delta \leftrightarrow \eta\mu$, we obtain:

$$\partial\Gamma_{\alpha\beta}(E) = \frac{-2\delta_{s_\alpha s_\beta}\delta_{\tau_\alpha\tau_\beta}}{2(\mu_3\sqrt{\pi})^3}\int d\vec{r}\alpha[\rho(\vec{r})]^{\alpha-1}\psi^*_\alpha(\vec{r})\psi_\beta(\vec{r}) \tag{G.114}$$
$$[\sum_{\gamma\delta>}\sum_{\eta\mu>}\psi^*_\eta(\vec{r})\psi_\delta(\vec{r})I_{\gamma\mu}(\vec{r})[S^{\mu\delta}_{\gamma\eta} + S^{\delta\mu}_{\eta\gamma}]\rho_{\delta\gamma}\rho_{\mu\eta}$$
$$+\sum_{\gamma\delta>}\sum_{\eta\mu>}\psi_\eta(\vec{r})\psi_\delta(\vec{r})I_{\gamma\bar{\mu}}(\vec{r})[(-1)^{s_\eta - s_\mu}S^{\bar{\mu}\delta}_{\gamma\bar{\eta}} + (-1)^{s_\gamma - s_\delta}S^{\bar{\delta}\mu}_{\eta\bar{\gamma}}]\rho_{\delta\gamma}\rho_{\mu\eta}]$$

Then, we find for the spin-isospin part:

$$S^{\mu\delta}_{\gamma\eta} = (W_3\delta_{\tau_\gamma\tau_\mu} - H_3)\delta_{s_\gamma s_\mu}\delta_{s_\eta s_\delta} + (B_3\delta_{\tau_\gamma\tau_\mu} - M_3)\delta_{s_\gamma s_\delta}\delta_{s_\eta s_\mu} = S^{\delta\mu}_{\eta\gamma} \tag{G.115}$$

And:

$$(-1)^{s_\eta - s_\mu}S^{\bar{\mu}\delta}_{\gamma\bar{\eta}} == (-1)^{s_\gamma - s_\delta}S^{\bar{\delta}\mu}_{\eta\bar{\gamma}} \tag{G.116}$$

Thanks to these results, Eq.(G.114) finally reads:

$$\boxed{\begin{aligned}\partial\Gamma_{\alpha\beta}(E) = \frac{-4\delta_{s_\alpha s_\beta}\delta_{\tau_\alpha\tau_\beta}}{2(\mu_3\sqrt{\pi})^3}\int d\vec{r}\alpha[\rho(\vec{r})]^{\alpha-1}\psi^*_\alpha(\vec{r})\psi_\beta(\vec{r})[\sum_{\gamma\delta>}\sum_{\eta\mu>}\psi^*_\eta(\vec{r})\psi_\delta(\vec{r})I_{\gamma\mu}(\vec{r})S^{\mu\delta}_{\gamma\eta}\rho_{\delta\gamma}\rho_{\mu\eta}\\ +\sum_{\gamma\delta>}\sum_{\eta\mu>}(-1)^{s_\eta - s_\mu}\psi_\eta(\vec{r})\psi_\delta(\vec{r})I_{\gamma\bar{\mu}}(\vec{r})(\vec{r})S^{\bar{\mu}\delta}_{\gamma\bar{\eta}}\rho_{\delta\gamma}\rho_{\mu\eta}]\end{aligned}} \tag{G.117}$$

It is numerically relevant to separate the different contributions of the sum with respect to the spins associated with γ and δ:

$$\partial\Gamma_{\alpha\beta}(E) = \partial\Gamma^{++}_{\alpha\beta}(E) + \partial\Gamma^{--}_{\alpha\beta}(E) + \partial\Gamma^{-+}_{\alpha\beta}(E) + \partial\Gamma^{-+}_{\alpha\beta}(E) \tag{G.118}$$

This spin separation does not account for the different spin blocks of the exchange rearrangement field, as for the direct mean, exchange mean, and pairing fields.

Block ++:

Here, we consider ($\gamma\uparrow$,$\delta\uparrow$). The related part of the exchange rearrangement field reads:

$$\boxed{\begin{aligned}\partial\Gamma^{++}_{\alpha\beta}(E) = \frac{-4\delta_{s_\alpha s_\beta}\delta_{\tau_\alpha\tau_\beta}}{2(\mu_3\sqrt{\pi})^3}\int d\vec{r}\alpha[\rho(\vec{r})]^{\alpha-1}\psi^*_\alpha(\vec{r})\psi_\beta(\vec{r})\sum_{\gamma\delta>}\psi_\delta(\vec{r})\rho^{++\tau}_{\delta\gamma}\\ [\sum_{\eta\mu>}\psi^*_\eta(\vec{r})I_{\gamma\mu}(\vec{r})[(W_3\delta_{\tau\tau'}-H_3)\delta_{s^+_\eta s^+_\mu}+(B_3\delta_{\tau\tau'}-M_3)\delta_{s_\eta s_\mu}]\rho_{\mu\eta}\\ +\sum_{\eta\mu>}\psi_\eta(\vec{r})I_{\gamma\bar{\mu}}(\vec{r})[(W_3\delta_{\tau\tau'}-H_3)\delta_{s^-_\eta s^-_\mu}+(B_3\delta_{\tau\tau'}-M_3)\delta_{s_\eta s_\mu}]\rho_{\mu\eta}]\end{aligned}} \quad (G.119)$$

Block $--$:

Here, we consider ($\gamma\downarrow$,$\delta\downarrow$). The related part of the exchange rearrangement field reads:

$$\boxed{\begin{aligned}\partial\Gamma^{--}_{\alpha\beta}(E) = \frac{-4\delta_{s_\alpha s_\beta}\delta_{\tau_\alpha\tau_\beta}}{2(\mu_3\sqrt{\pi})^3}\int d\vec{r}\alpha[\rho(\vec{r})]^{\alpha-1}\psi^*_\alpha(\vec{r})\psi_\beta(\vec{r})\sum_{\gamma\delta>}\psi_\delta(\vec{r})\rho^{--\tau}_{\delta\gamma}\\ [\sum_{\eta\mu>}\psi^*_\eta(\vec{r})I_{\gamma\mu}(\vec{r})[(W_3\delta_{\tau\tau'}-H_3)\delta_{s^-_\eta s^-_\mu}+(B_3\delta_{\tau\tau'}-M_3)\delta_{s_\eta s_\mu}]\rho_{\mu\eta}\\ +\sum_{\eta\mu>}\psi_\eta(\vec{r})I_{\gamma\bar{\mu}}(\vec{r})[(W_3\delta_{\tau\tau'}-H_3)\delta_{s^+_\eta s^+_\mu}+(B_3\delta_{\tau\tau'}-M_3)\delta_{s_\eta s_\mu}]\rho_{\mu\eta}]\end{aligned}} \quad (G.120)$$

Block $-+$:

Here, we consider ($\gamma\downarrow$,$\delta\uparrow$). The related part of the exchange rearrangement field reads:

$$\boxed{\begin{aligned}\partial\Gamma^{-+}_{\alpha\beta}(E) = \frac{-4\delta_{s_\alpha s_\beta}\delta_{\tau_\alpha\tau_\beta}}{2(\mu_3\sqrt{\pi})^3}\int d\vec{r}\alpha[\rho(\vec{r})]^{\alpha-1}\psi^*_\alpha(\vec{r})\psi_\beta(\vec{r})\sum_{\gamma\delta>}\psi_\delta(\vec{r})\rho^{+-\tau}_{\delta\gamma}\\ [\sum_{\eta\mu>}\psi^*_\eta(\vec{r})I_{\gamma\mu}(\vec{r})(W_3\delta_{\tau\tau'}-H_3)\rho^{-+}_{\mu\eta}-\sum_{\eta\mu>}\psi_\eta(\vec{r})I_{\gamma\bar{\mu}}(\vec{r})(W_3\delta_{\tau\tau'}-H_3)\rho^{+-}_{\mu\eta}]\end{aligned}} \quad (G.121)$$

Block $+-$:

Here, we consider ($\gamma\uparrow$,$\delta\downarrow$). For symmetry purposes, we directly have:

$$\boxed{\partial\Gamma^{+-}_{\alpha\beta}(E) = \partial\Gamma^{-+}_{\alpha\beta}(E)} \quad (G.122)$$

G.2.6 Pairing rearrangement field

The pairing rearrangement field reads as follows:

$$\boxed{\partial\Delta_{\alpha\beta} = \sum_{\gamma\eta}\sum_{\delta\mu}(-1)^{s_\mu-s_\eta}\langle\gamma\bar{\eta}|\frac{\partial V^{(D2)}}{\partial\rho_{\alpha\beta}}|\delta\bar{\mu}\rangle\kappa_{\delta\bar{\mu}}\kappa_{\gamma\bar{\eta}}} \quad (G.123)$$

This term is called "pairing rearrangement field" because it includes the pairing tensor κ. However, it is not really a pairing field as it comes from $\frac{\partial\mathcal{E}}{\partial\rho}$. Note that the "pairing

rearrangement field" is included in h and not in Δ within the HFB theory. This field can be written using the following expression:

$$\partial\Delta_{\alpha\beta} = \sum_{\gamma\eta}\sum_{\delta\mu}(-1)^{s_\mu - s_\eta} E^{(\gamma\delta)(\bar{\eta}\bar{\mu})}_{\alpha\beta} S^{\delta\bar{\mu}}_{\gamma\bar{\eta}} \kappa_{\delta\bar{\mu}}\kappa_{\gamma\bar{\eta}} \tag{G.124}$$

We first use the time-reversal properties of Eq.(G.124) associated with the indices δ and μ:

$$\partial\Delta_{\alpha\beta} = \sum_{\gamma\eta}\sum_{\delta\mu>}[(-1)^{s_\mu - s_\eta} E^{(\gamma\delta)(\bar{\eta}\bar{\mu})}_{\alpha\beta} S^{\delta\bar{\mu}}_{\gamma\bar{\eta}} + (-1)^{s_\delta - s_\eta} E^{(\gamma\bar{\delta})(\bar{\eta}\mu)}_{\alpha\beta} S^{\bar{\delta}\mu}_{\gamma\bar{\eta}}]\kappa_{\delta\bar{\mu}}\kappa_{\gamma\bar{\eta}} \tag{G.125}$$

Then, we use the time-reversal properties associated with the indices γ and η:

$$\begin{aligned}\partial\Delta_{\alpha\beta} = \sum_{\gamma\eta>}\sum_{\delta\mu>}([(-1)^{s_\mu - s_\eta} E^{(\gamma\delta)(\bar{\eta}\bar{\mu})}_{\alpha\beta} S^{\delta\bar{\mu}}_{\gamma\bar{\eta}} + (-1)^{s_\delta + s_\eta} E^{(\gamma\bar{\delta})(\bar{\eta}\mu)}_{\alpha\beta} S^{\bar{\delta}\mu}_{\gamma\bar{\eta}}] \\ +(-1)^{s_\gamma - s_\eta}[(-1)^{s_\mu + s_\eta} E^{(\bar{\gamma}\delta)(\eta\bar{\mu})}_{\alpha\beta} S^{\delta\bar{\mu}}_{\bar{\gamma}\eta} + (-1)^{s_\delta - s_\eta} E^{(\bar{\gamma}\bar{\delta})(\eta\mu)}_{\alpha\beta} S^{\bar{\delta}\mu}_{\bar{\gamma}\eta}])\kappa_{\delta\bar{\mu}}\kappa_{\gamma\bar{\eta}}\end{aligned} \tag{G.126}$$

We remark the following properties:

$$\begin{cases} E^{(\bar{\gamma}\bar{\delta})(\eta\mu)}_{\alpha\beta} = E^{(\gamma\delta)(\bar{\eta}\bar{\mu})}_{\alpha\beta} \\ \\ E^{(\bar{\gamma}\delta)(\eta\bar{\mu})}_{\alpha\beta} = E^{(\gamma\bar{\delta})(\bar{\eta}\mu)}_{\alpha\beta} \end{cases} \qquad \begin{cases} (-1)^{s_\delta - s_\gamma} S^{\bar{\delta}\mu}_{\bar{\gamma}\eta} = (-1)^{s_\mu - s_\eta} S^{\delta\bar{\mu}}_{\gamma\bar{\eta}} \\ \\ (-1)^{s_\gamma - s_\eta} S^{\delta\bar{\mu}}_{\bar{\gamma}\eta} = (-1)^{s_\eta - s_\delta} S^{\bar{\delta}\mu}_{\gamma\bar{\eta}} \end{cases} \tag{G.127}$$

Thanks to these properties, $\partial\Delta$ reads:

$$\partial\Delta_{\alpha\beta} = 2\sum_{\gamma\eta>}\sum_{\delta\mu>}[(-1)^{s_\mu - s_\eta} E^{(\gamma\delta)(\bar{\eta}\bar{\mu})}_{\alpha\beta} S^{\delta\bar{\mu}}_{\gamma\bar{\eta}} + (-1)^{s_\delta + s_\eta} E^{(\gamma\bar{\delta})(\bar{\eta}\mu)}_{\alpha\beta} S^{\bar{\delta}\mu}_{\gamma\bar{\eta}}]\kappa_{\delta\bar{\mu}}\kappa_{\gamma\bar{\eta}} \tag{G.128}$$

We transform Eq.(G.128) into a form similar to the one of the exchange rearrangement term:

$$\partial\Delta_{\alpha\beta} = 2\sum_{\gamma\delta>}\sum_{\eta\mu>}[(-1)^{s_\eta - s_\delta} E^{(\gamma\mu)(\eta\delta)}_{\alpha\beta} S^{\mu\bar{\eta}}_{\gamma\bar{\delta}} + (-1)^{s_\delta + s_\mu} E^{(\gamma\bar{\mu})(\bar{\eta}\delta)}_{\alpha\beta} S^{\bar{\mu}\eta}_{\gamma\bar{\delta}}]\kappa_{\mu\bar{\eta}}\kappa_{\gamma\bar{\delta}} \tag{G.129}$$

We develop the spatial part of Eq.(G.129):

$$\begin{aligned}\partial\Delta_{\alpha\beta} = \frac{2\delta_{s_\alpha s_\beta}\delta_{\tau_\alpha\tau_\beta}}{2(\mu_3\sqrt{\pi})^3}\int d\vec{r}\alpha[\rho(\vec{r})]^{\alpha-1}\psi^*_\alpha(\vec{r})\psi_\beta(\vec{r}) \\ [\sum_{\gamma\delta>}\sum_{\eta\mu>}[\psi^*_\gamma(\vec{r})\psi_\mu(\vec{r})I_{\eta\delta}(\vec{r}) + \psi^*_\eta(\vec{r})\psi_\delta(\vec{r})I_{\gamma\mu}(\vec{r})](-1)^{s_\eta - s_\delta} S^{\mu\bar{\eta}}_{\gamma\bar{\delta}}\kappa_{\mu\bar{\eta}}\kappa_{\gamma\bar{\delta}} \\ +\sum_{\gamma\delta>}\sum_{\eta\mu>}[\psi^*_\gamma(\vec{r})\psi^*_\mu(\vec{r})I_{\bar{\eta}\delta}(\vec{r}) + \psi_\eta(\vec{r})\psi_\delta(\vec{r})I_{\gamma\bar{\mu}}(\vec{r})](-1)^{s_\delta + s_\mu} S^{\bar{\mu}\eta}_{\gamma\bar{\delta}}\kappa_{\mu\bar{\eta}}\kappa_{\gamma\bar{\delta}}]\end{aligned} \tag{G.130}$$

Thanks to the indice exchange $\gamma\delta \leftrightarrow \eta\mu$, we obtain:

$$\partial\Delta_{\alpha\beta} = \frac{2\delta_{s_\alpha s_\beta}\delta_{\tau_\alpha\tau_\beta}}{2(\mu_3\sqrt{\pi})^3}\int d\vec{r}\alpha[\rho(\vec{r})]^{\alpha-1}\psi^*_\alpha(\vec{r})\psi_\beta(\vec{r}) \tag{G.131}$$
$$[\sum_{\gamma\delta>}\sum_{\eta\mu>}\psi^*_\eta(\vec{r})\psi_\delta(\vec{r})I_{\gamma\mu}(\vec{r})[(-1)^{s_\gamma-s_\mu}S^{\delta\bar{\gamma}}_{\eta\bar{\mu}}+(-1)^{s_\eta-s_\delta}S^{\mu\bar{\eta}}_{\gamma\bar{\delta}}]\kappa_{\mu\bar{\eta}}\kappa_{\delta\bar{\gamma}}$$
$$+\sum_{\gamma\delta>}\sum_{\eta\mu>}\psi_\eta(\vec{r})\psi_\delta(\vec{r})I_{\gamma\bar{\mu}}(\vec{r})[(-1)^{s_\delta+s_\mu}S^{\bar{\delta}\gamma}_{\eta\bar{\mu}}+(-1)^{s_\delta+s_\mu}S^{\bar{\mu}\eta}_{\gamma\bar{\delta}}]\kappa_{\mu\bar{\eta}}\kappa_{\delta\bar{\gamma}}]$$

Then, we find for the spin-isospin part:

$$(-1)^{s_\gamma-s_\mu}S^{\delta\bar{\gamma}}_{\eta\bar{\mu}} = (-1)^{s_\eta-s_\delta}S^{\mu\bar{\eta}}_{\gamma\bar{\delta}} \tag{G.132}$$

$$(-1)^{s_\delta+s_\mu}S^{\bar{\delta}\gamma}_{\eta\bar{\mu}} = (-1)^{s_\delta+s_\mu}S^{\bar{\mu}\eta}_{\gamma\bar{\delta}} \tag{G.133}$$

Thanks to these results, Eq.(G.131) finally reads:

$$\boxed{\begin{aligned}\partial\Delta_{\alpha\beta} &= \frac{4\delta_{s_\alpha s_\beta}\delta_{\tau_\alpha\tau_\beta}}{2(\mu_3\sqrt{\pi})^3}\int d\vec{r}\alpha[\rho(\vec{r})]^{\alpha-1}\psi^*_\alpha(\vec{r})\psi_\beta(\vec{r})\\ &[\sum_{\gamma\delta>}\sum_{\eta\mu>}\psi^*_\eta(\vec{r})\psi_\delta(\vec{r})I_{\gamma\mu}(\vec{r})(-1)^{s_\eta-s_\delta}S^{\mu\bar{\eta}}_{\gamma\bar{\delta}}\kappa_{\mu\bar{\eta}}\kappa_{\delta\bar{\gamma}}\\ &+\sum_{\gamma\delta>}\sum_{\eta\mu>}\psi_\eta(\vec{r})\psi_\delta(\vec{r})I_{\gamma\bar{\mu}}(\vec{r})(-1)^{s_\delta+s_\mu}S^{\bar{\mu}\eta}_{\gamma\bar{\delta}}\kappa_{\mu\bar{\eta}}\kappa_{\delta\bar{\gamma}}]\end{aligned}} \tag{G.134}$$

It is numerically relevant to separate the different contributions of the sum with respect to the spins of γ and δ:

$$\partial\Delta_{\alpha\beta} = \partial\Delta^{++}_{\alpha\beta} + \partial\Delta^{--}_{\alpha\beta} + \partial\Delta^{-+}_{\alpha\beta} + \partial\Delta^{--}_{\alpha\beta} \tag{G.135}$$

Once again, this spin separation does not account for the different spin blocks of the pairing rearrangement field.

Block ++:

Here, we consider ($\gamma\uparrow$,$\delta\uparrow$). The related part of the exchange rearrangement field reads:

$$\boxed{\begin{aligned}\partial\Delta^{++}_{\alpha\beta} &= \frac{4\delta_{s_\alpha s_\beta}\delta_{\tau_\alpha\tau_\beta}}{2(\mu_3\sqrt{\pi})^3}\int d\vec{r}\alpha[\rho(\vec{r})]^{\alpha-1}\psi^*_\alpha(\vec{r})\psi_\beta(\vec{r})\sum_{\gamma\delta>}\psi_\delta(\vec{r})\kappa^{++\tau}_{\delta\bar{\gamma}}\\ &[\sum_{\eta\mu>}\psi^*_\eta(\vec{r})I_{\gamma\mu}(\vec{r})[(W_3-H_3)\delta_{s^+_\eta s^+_\mu}-(B_3-M_3)\delta_{s^-_\eta s^-_\mu}]\kappa^\tau_{\mu\bar{\eta}}\\ &+\sum_{\eta\mu>}\psi_\eta(\vec{r})I_{\gamma\bar{\mu}}(\vec{r})[(W_3-H_3)\delta_{s^-_\eta s^-_\mu}-(B_3-M_3)\delta_{s^+_\eta s^+_\mu}]\kappa^\tau_{\mu\bar{\eta}}]\end{aligned}} \tag{G.136}$$

Block −−:

Here, we consider ($\gamma\downarrow$,$\delta\downarrow$). The related part of the exchange rearrangement field reads:

$$\boxed{\begin{aligned}\partial\Delta^{--}_{\alpha\beta} = \frac{4\delta_{s_\alpha s_\beta}\delta_{\tau_\alpha\tau_\beta}}{2(\mu_3\sqrt{\pi})^3}\int d\vec{r}\alpha[\rho(\vec{r})]^{\alpha-1}\psi^*_\alpha(\vec{r})\psi_\beta(\vec{r})\sum_{\gamma\delta>}\psi_\delta(\vec{r})\kappa^{--\tau}_{\delta\bar{\gamma}} \\ [\sum_{\eta\mu>}\psi^*_\eta(\vec{r})I_{\gamma\mu}(\vec{r})[(W_3-H_3)\delta_{s^-_\eta s^-_\mu}-(B_3-M_3)\delta_{s^+_\eta s^+_\mu}]\kappa^\tau_{\mu\bar{\eta}} \\ +\sum_{\eta\mu>}\psi_\eta(\vec{r})I_{\gamma\bar{\mu}}(\vec{r})[(W_3-H_3)\delta_{s^+_\eta s^+_\mu}-(B_3-M_3)\delta_{s^-_\eta s^-_\mu}]\kappa^\tau_{\mu\bar{\eta}}]\end{aligned}} \tag{G.137}$$

Block $-+$:

Here, we consider ($\gamma\downarrow$,$\delta\uparrow$). The related part of the exchange rearrangement field reads:

$$\boxed{\begin{aligned}\partial\Delta^{-+}_{\alpha\beta} = \frac{4\delta_{s_\alpha s_\beta}\delta_{\tau_\alpha\tau_\beta}}{2(\mu_3\sqrt{\pi})^3}\int d\vec{r}\alpha[\rho(\vec{r})]^{\alpha-1}\psi^*_\alpha(\vec{r})\psi_\beta(\vec{r})\sum_{\gamma\delta>}\psi_\delta(\vec{r})\kappa^{+-\tau}_{\delta\gamma} \\ [\sum_{\eta\mu>}\psi^*_\eta(\vec{r})I_{\gamma\mu}(\vec{r})(W_3-H_3+B_3-M_3)\kappa^{-+}_{\mu\eta} \\ -\sum_{\eta\mu>}\psi_\eta(\vec{r})I_{\gamma\bar{\mu}}(\vec{r})(W_3-H_3+B_3-M_3)\kappa^{+-}_{\mu\eta}]\end{aligned}} \tag{G.138}$$

Block $+-$:

Here, we consider ($\gamma\uparrow$,$\delta\downarrow$). By analogy with the exchange rearrangement term, we directly write:

$$\boxed{\partial\Delta^{+-}_{\alpha\beta} = \partial\Delta^{-+}_{\alpha\beta}} \tag{G.139}$$

Appendix H

Spin-orbit fields

The contact spin-isospin part of the antisymmetrized interaction reads as follows:

$$\boxed{V^{(SO)}(1-P_rP_\sigma P_\tau) = iW_{LS}\overleftarrow{\nabla}_{12}\delta(\vec{r}_1-\vec{r}_2)\wedge\overrightarrow{\nabla}_{12}.(\vec{\sigma}_1+\vec{\sigma}_2)(1-P_rP_\sigma P_\tau)} \tag{H.1}$$

The operators P_r , P_σ et P_τ represent the exchange of the spatial, spin and isospin part respectively and the operators $\overrightarrow{\nabla}_{12}$ and $\overleftarrow{\nabla}_{12}$ have the following definition:

$$\overrightarrow{\nabla}_{12} = \frac{\overrightarrow{\nabla}_1 - \overrightarrow{\nabla}_2}{2} \qquad \overleftarrow{\nabla}_{12} = \frac{\overleftarrow{\nabla}_1 - \overleftarrow{\nabla}_2}{2} \tag{H.2}$$

The operator $\overleftarrow{\nabla}$ operates on the left hand side and $\overrightarrow{\nabla}$ operates on the right hand side. In the general case of two different harmonic oscillator bases, the matrix elements of the contact spin-orbit term of the interaction read as follows:

$$\boxed{\begin{aligned}{}_0\langle\alpha\beta|V^{(SO)}(1-P_rP_\sigma P_\tau)|\gamma\delta\rangle_1 = {}_0\langle\alpha\beta|iW_{LS}\overleftarrow{\nabla}_{12}\delta(\vec{r}_1-\vec{r}_2)\\ \wedge\overrightarrow{\nabla}_{12}.(\vec{\sigma}_1+\vec{\sigma}_2)(1-P_rP_\sigma P_\tau)|\gamma\delta\rangle_1\end{aligned}} \tag{H.3}$$

Here 0 and 1 stand for the two different harmonic oscillator bases $\{0\}$ and $\{1\}$ respectively. We separate the spatial, the spin and the isospin part of Eq.(H.3):

$$\begin{aligned}{}_0\langle\alpha\beta|V^{(SO)}(1-P_rP_\sigma P_\tau)|\gamma\delta\rangle_1 = {}&{}_0\langle\vec{r}_\alpha\vec{r}_\beta|iW_{LS}\overleftarrow{\nabla}_{12}\delta(\vec{r}_1-\vec{r}_2)\wedge\overrightarrow{\nabla}_{12}|\vec{r}_\gamma\vec{r}_\delta\rangle_1\\ &.\langle s_\alpha s_\beta|(\vec{\sigma}_1+\vec{\sigma}_2)|s_\gamma s_\delta\rangle\delta_{\tau_\alpha\tau_\gamma}\delta_{\tau_\beta\tau_\delta}\\ &-{}_0\langle\vec{r}_\alpha\vec{r}_\beta|iW_{LS}\overleftarrow{\nabla}_{12}\delta(\vec{r}_1-\vec{r}_2)\wedge\overrightarrow{\nabla}_{12}|\vec{r}_\delta\vec{r}_\gamma\rangle_1\\ &.\langle s_\alpha s_\beta|(\vec{\sigma}_1+\vec{\sigma}_2)|s_\delta s_\gamma\rangle\delta_{\tau_\alpha\tau_\delta}\delta_{\tau_\beta\tau_\gamma}\end{aligned} \tag{H.4}$$

Note that only the spatial part of Eq.(H.4) is impacted by the difference between the bases. We set for the spatial and spin part:

$$\begin{cases}\bar{E}^{\gamma\delta}_{\alpha\beta} = {}_0\langle\vec{r}_\alpha\vec{r}_\beta|iW_{LS}\overleftarrow{\nabla}_{12}\delta(\vec{r}_1-\vec{r}_2)\wedge\overrightarrow{\nabla}_{12}|\vec{r}_\gamma\vec{r}_\delta\rangle_1\\ S^{\gamma\delta}_{\alpha\beta} = \langle s_\alpha s_\beta|(\vec{\sigma}_1+\vec{\sigma}_2)|s_\gamma s_\delta\rangle\end{cases} \tag{H.5}$$

$\bar{E}$ and S verify the following properties:

$$\begin{cases} \bar{E}^{\gamma\delta}_{\alpha\beta} = -\bar{E}^{\delta\gamma}_{\alpha\beta} \\ S^{\gamma\delta}_{\alpha\beta} = S^{\delta\gamma}_{\alpha\beta} \end{cases} \tag{H.6}$$

These properties are demonstrated in section H.1.2 and section H.2, respectively. Using them, we can rewrite Eq.(H.4):

$$\boxed{{}_0\langle\alpha\beta|V^{(SO)}(1-P_rP_\sigma P_\tau)|\gamma\delta\rangle_1 = \bar{E}^{\gamma\delta}_{\alpha\beta}.S^{\gamma\delta}_{\alpha\beta}[\delta_{\tau_\alpha\tau_\gamma}\delta_{\tau_\beta\tau_\delta}+\delta_{\tau_\alpha\tau_\delta}\delta_{\tau_\beta\tau_\gamma}]} \tag{H.7}$$

When only one harmonic oscillator basis is involved, the matrix elements of the contact spin-orbit part of the interaction reads:

$$\boxed{\langle\alpha\beta|V^{(SO)}(1-P_rP_\sigma P_\tau)|\gamma\delta\rangle = \langle\alpha\beta|iW_{LS}\overleftarrow{\nabla}_{12}\delta(\vec{r}_1-\vec{r}_2)\wedge\overrightarrow{\nabla}_{12}.(\vec{\sigma}_1+\vec{\sigma}_2)(1-P_rP_\sigma P_\tau)|\gamma\delta\rangle} \tag{H.8}$$

We set:

$$E^{\gamma\delta}_{\alpha\beta} = \langle\vec{r}_\alpha\vec{r}_\beta|iW_{LS}\overleftarrow{\nabla}_{12}\delta(\vec{r}_1-\vec{r}_2)\wedge\overrightarrow{\nabla}_{12}|\vec{r}_\gamma\vec{r}_\delta\rangle \tag{H.9}$$

Then, by analogy with the general case, we directly find:

$$\boxed{\langle\alpha\beta|V^{(SO)}(1-P_rP_\sigma P_\tau)|\gamma\delta\rangle = E^{\gamma\delta}_{\alpha\beta}.S^{\gamma\delta}_{\alpha\beta}[\delta_{\tau_\alpha\tau_\gamma}\delta_{\tau_\beta\tau_\delta}+\delta_{\tau_\alpha\tau_\delta}\delta_{\tau_\beta\tau_\gamma}]} \tag{H.10}$$

This Appendix aims to give an analytic expression of all the contact spin-orbit fields involved in this PhD thesis.

H.1 Spatial part

We give in this section an analytic expression of the spatial part of the contact spin-orbit matrix elements. The case with only one basis is treated first, then derivations are given for the general case.

H.1.1 Same bases

We want to give an explicit expression of the following quantity:

$$\boxed{E^{\gamma\delta}_{\alpha\beta} = i\frac{W_{LS}}{4}\langle\vec{r}_\alpha\vec{r}_\beta|(\overleftarrow{\nabla}_1-\overleftarrow{\nabla}_2)\delta(\vec{r}_1-\vec{r}_2)(\overrightarrow{\nabla}_1-\overrightarrow{\nabla}_2)\wedge|\vec{r}_\gamma\vec{r}_\delta\rangle} \tag{H.11}$$

We rewrite Eq.(H.11):

$$\begin{aligned} E^{\gamma\delta}_{\alpha\beta} = i\frac{W_{LS}}{4}\int d\vec{r}(&\vec{\nabla}(\psi^*_\alpha(\vec{r}))\psi^*_\beta(\vec{r})-\vec{\nabla}(\psi^*_\beta(\vec{r}))\psi^*_\alpha(\vec{r})) \\ &\wedge(\vec{\nabla}(\psi_\gamma(\vec{r}))\psi_\delta(\vec{r})-\vec{\nabla}(\psi_\delta(\vec{r}))\psi_\gamma(\vec{r})) \end{aligned} \tag{H.12}$$

From Eq.(H.11), it is clear that the property $E^{\gamma\delta}_{\alpha\beta} = -E^{\delta\gamma}_{\alpha\beta}$ holds. To go further, we have to use the Stokes theorem. Before applying it, we tranform Eq.(H.11) in the following:

$$E^{\gamma\delta}_{\alpha\beta} = i\frac{W_{LS}}{4}\int d\vec{r}\psi^*_\beta(\vec{r})\psi_\delta(\vec{r})(\overrightarrow{\nabla}\psi^*_\alpha(\vec{r})\wedge\overrightarrow{\nabla}\psi_\gamma(\vec{r})) - \psi^*_\beta(\vec{r})\psi_\gamma(\vec{r})(\overrightarrow{\nabla}\psi^*_\alpha(\vec{r})\wedge\overrightarrow{\nabla}\psi_\delta(\vec{r})) \quad \text{(H.13)}$$
$$-\psi^*_\alpha(\vec{r})\psi_\delta(\vec{r})(\overrightarrow{\nabla}\psi^*_\beta(\vec{r})\wedge\overrightarrow{\nabla}\psi_\gamma(\vec{r})) + \psi^*_\alpha(\vec{r})\psi_\gamma(\vec{r})(\overrightarrow{\nabla}\psi^*_\beta(\vec{r})\wedge\overrightarrow{\nabla}\psi_\delta(\vec{r}))$$

We recall a fundamental formula of vector calculus:

$$\overrightarrow{\nabla}\wedge f(\overrightarrow{\nabla}g) = (\overrightarrow{\nabla}f)\wedge(\overrightarrow{\nabla}g) \quad \text{(H.14)}$$

Using Eq.(H.14) as well as the usual commutation relations of derivative operators we get:

$$-\psi^*_\beta(\vec{r})\psi_\gamma(\vec{r})(\overrightarrow{\nabla}\psi^*_\alpha(\vec{r})\wedge\overrightarrow{\nabla}\psi_\delta(\vec{r})) = -\overrightarrow{\nabla}\wedge\psi^*_\alpha(\vec{r})\psi^*_\beta(\vec{r})\psi_\gamma(\vec{r})\overrightarrow{\nabla}(\psi_\delta(\vec{r})) \quad \text{(H.15)}$$
$$+\psi^*_\alpha(\vec{r})\psi^*_\beta(\vec{r})(\overrightarrow{\nabla}\psi_\gamma(\vec{r}))\wedge\overrightarrow{\nabla}\psi_\delta(\vec{r})) + \psi^*_\alpha(\vec{r})\psi_\gamma(\vec{r})(\overrightarrow{\nabla}\psi^*_\beta(\vec{r}))\wedge\overrightarrow{\nabla}\psi_\delta(\vec{r}))$$

And:

$$-\psi^*_\alpha(\vec{r})\psi_\delta(\vec{r})(\overrightarrow{\nabla}\psi^*_\beta(\vec{r})\wedge\overrightarrow{\nabla}\psi_\gamma(\vec{r})) = -\overrightarrow{\nabla}\wedge\psi^*_\beta(\vec{r})\psi^*_\alpha(\vec{r})\psi_\delta(\vec{r})\overrightarrow{\nabla}(\psi_\gamma(\vec{r})) \quad \text{(H.16)}$$
$$+\psi^*_\beta(\vec{r})\psi^*_\alpha(\vec{r})(\overrightarrow{\nabla}\psi_\delta(\vec{r}))\wedge\overrightarrow{\nabla}\psi_\gamma(\vec{r})) + \psi^*_\beta(\vec{r})\psi_\delta(\vec{r})(\overrightarrow{\nabla}\psi^*_\alpha(\vec{r}))\wedge\overrightarrow{\nabla}\psi_\gamma(\vec{r}))$$

Thanks to Eq.(H.15) and Eq.(H.16), the Eq.(H.13) is rewritten as follows:

$$E^{\gamma\delta}_{\alpha\beta} = i\frac{W_{LS}}{4}\int d\vec{r}\,2[\psi^*_\beta(\vec{r})\psi_\delta(\vec{r})(\overrightarrow{\nabla}\psi^*_\alpha(\vec{r})\wedge\overrightarrow{\nabla}\psi_\gamma(\vec{r})) \quad \text{(H.17)}$$
$$+\psi^*_\alpha(\vec{r})\psi_\gamma(\vec{r})(\overrightarrow{\nabla}\psi^*_\beta(\vec{r})\wedge\overrightarrow{\nabla}\psi_\delta(\vec{r}))]$$
$$-\overrightarrow{\nabla}\wedge\psi^*_\beta(\vec{r})\psi^*_\alpha(\vec{r})\overrightarrow{\nabla}(\psi_\delta(\vec{r})\psi_\gamma(\vec{r}))$$

It is now possible to use the Stokes theorem on the last part of Eq.(H.17):

$$\int_V d\vec{r}\,\overrightarrow{\nabla}\wedge\psi^*_\beta(\vec{r})\psi^*_\alpha(\vec{r})\overrightarrow{\nabla}(\psi_\delta(\vec{r})\psi_\gamma(\vec{r})) = \int_{\partial V}\psi^*_\beta(\vec{r})\psi^*_\alpha(\vec{r})\overrightarrow{\nabla}(\psi_\delta(\vec{r})\psi_\gamma(\vec{r})).d\vec{S} \quad \text{(H.18)}$$

As the oscillator harmonic wave functions are bounded functions, all the quantities in the second part of Eq.(H.18) are equal to zero when they are evaluated in ∂V:

$$\int_{\partial V}\psi^*_\beta(\vec{r})\psi^*_\alpha(\vec{r})\overrightarrow{\nabla}(\psi_\delta(\vec{r})\psi_\gamma(\vec{r})).d\vec{S} = 0 \quad \text{(H.19)}$$

With this result, we can write Eq.(H.18) in a more compact form:

$$\boxed{E^{\gamma\delta}_{\alpha\beta} = i\frac{W_{LS}}{2}\int d\vec{r}\psi^*_\beta(\vec{r})\psi_\delta(\vec{r})(\overrightarrow{\nabla}\psi^*_\alpha(\vec{r})\wedge\overrightarrow{\nabla}\psi_\gamma(\vec{r})) + \psi^*_\alpha(\vec{r})\psi_\gamma(\vec{r})(\overrightarrow{\nabla}\psi^*_\beta(\vec{r})\wedge\overrightarrow{\nabla}\psi_\delta(\vec{r}))} \quad \text{(H.20)}$$

Now, we want to write explicitly the gradient operators in order to apply the wedge products.

Gradient operators expression:

We give an expression of the gradient in the $(z,+,-)$ coordinate system. We choose this system as it allows us to use powerful formulas (see Appendix D) to express harmonic oscillator wave functions derivatives. We set the following change of variables:

$$\begin{cases} z_- = \frac{1}{\sqrt{2}}(x - iy) \\ z_+ = -\frac{1}{\sqrt{2}}(x + iy) \end{cases} \tag{H.21}$$

As this change of variables is linear, we easily find:

$$\begin{pmatrix} \nabla_- \\ \nabla_+ \end{pmatrix} = \frac{1}{\sqrt{2}} \begin{pmatrix} 1 & -i \\ -1 & -i \end{pmatrix} \begin{pmatrix} \frac{\partial}{\partial_x} \\ \frac{\partial}{\partial_y} \end{pmatrix} \qquad \Rightarrow \qquad \begin{pmatrix} \frac{\partial}{\partial_x} \\ \frac{\partial}{\partial_y} \end{pmatrix} = \frac{1}{\sqrt{2}} \begin{pmatrix} 1 & -1 \\ i & i \end{pmatrix} \begin{pmatrix} \nabla_- \\ \nabla_+ \end{pmatrix} \tag{H.22}$$

Thanks to Eq.(H.22), the wedge products in Eq.(H.20) now reads:

$$\overrightarrow{\nabla}\psi^*_\alpha(\vec{r}) \wedge \overrightarrow{\nabla}\psi_\gamma(\vec{r}) = \begin{pmatrix} \frac{1}{\sqrt{2}}(\nabla_- - \nabla_+)\psi^*_\alpha(\vec{r}) \\ \frac{i}{\sqrt{2}}(\nabla_- + \nabla_+)\psi^*_\alpha(\vec{r}) \\ \nabla_0\psi^*_\alpha(\vec{r}) \end{pmatrix} \wedge \begin{pmatrix} \frac{1}{\sqrt{2}}(\nabla_- - \nabla_+)\psi_\gamma(\vec{r}) \\ \frac{i}{\sqrt{2}}(\nabla_- + \nabla_+)\psi_\gamma(\vec{r}) \\ \nabla_0\psi_\gamma(\vec{r}) \end{pmatrix} \tag{H.23}$$

We finally find:

$$\boxed{\overrightarrow{\nabla}\psi^*_\alpha(\vec{r}) \wedge \overrightarrow{\nabla}\psi_\gamma(\vec{r}) = \begin{pmatrix} \frac{i}{\sqrt{2}}[(\nabla_- + \nabla_+)\psi^*_\alpha(\vec{r})\nabla_0\psi_\gamma(\vec{r}) - \nabla_0\psi^*_\alpha(\vec{r})(\nabla_- + \nabla_+)\psi_\gamma(\vec{r})] \\ \frac{1}{\sqrt{2}}[\nabla_0\psi^*_\alpha(\vec{r})(\nabla_- - \nabla_+)\psi_\gamma(\vec{r}) - (\nabla_- - \nabla_+)\psi^*_\alpha(\vec{r})\nabla_0\psi_\gamma(\vec{r})] \\ i[\nabla_-\psi^*_\alpha(\vec{r})\nabla_+\psi_\gamma(\vec{r}) - \nabla_+\psi^*_\alpha(\vec{r})\nabla_-\psi_\gamma(\vec{r})] \end{pmatrix}} \tag{H.24}$$

H.1.2 Different bases

In this part, we search for a reduced expression of the following quantity:

$$\boxed{\bar{E}^{\gamma\delta}_{\alpha\beta} = i\frac{W_{LS}}{4}{}_0\langle \vec{r}_\alpha \vec{r}_\beta | (\overleftarrow{\nabla}_1 - \overleftarrow{\nabla}_2)\delta(\vec{r}_1 - \vec{r}_2)(\overrightarrow{\nabla}_1 - \overrightarrow{\nabla}_2) \wedge |\vec{r}_\gamma \vec{r}_\delta\rangle_1} \tag{H.25}$$

Eq.(H.25) is rewritten:

$$\begin{aligned} \bar{E}^{\gamma\delta}_{\alpha\beta} = i\frac{W_{LS}}{4} \int d\vec{r} (\vec{\nabla}(\psi^*_\alpha(\vec{r}, b_0))\psi^*_\beta(\vec{r}, b_0) - \vec{\nabla}(\psi^*_\beta(\vec{r}, b_0))\psi^*_\alpha(\vec{r}, b_0)) \\ \wedge (\vec{\nabla}(\psi_\gamma(\vec{r}, b_1))\psi_\delta(\vec{r}, b_1) - \vec{\nabla}(\psi_\delta(\vec{r}, b_1))\psi_\gamma(\vec{r}, b_1)) \end{aligned} \tag{H.26}$$

From Eq.(H.26), it is clear that the property $\bar{E}^{\gamma\delta}_{\alpha\beta} = -\bar{E}^{\delta\gamma}_{\alpha\beta}$ stated in Eq.(H.6) holds. It is then easy to verify that the whole process involving the Stokes theorem from Eq.(H.13) to Eq.(H.20) is still fully applicable in the case of two different bases. We end up with the following equation:

$$\boxed{\begin{aligned}\bar{E}^{\gamma\delta}_{\alpha\beta} = i\frac{W_{LS}}{2}\int d\vec{r}\psi^*_\beta(\vec{r},b_0)\psi_\delta(\vec{r},b_1)(\overrightarrow{\nabla}\psi^*_\alpha(\vec{r},b_0)\wedge\overrightarrow{\nabla}\psi_\gamma(\vec{r},b_1)) \\ +\psi^*_\alpha(\vec{r},b_0)\psi_\gamma(\vec{r},b_1)(\overrightarrow{\nabla}\psi^*_\beta(\vec{r},b_0)\wedge\overrightarrow{\nabla}\psi_\delta(\vec{r},b_1))\end{aligned}} \tag{H.27}$$

Finally, we give an explicit expression of the gradient operators and wedge products implied in Eq.(H.27) thanks to the results developed from Eq.(H.21) to Eq.(H.24):

$$\boxed{\begin{aligned}\overrightarrow{\nabla}\psi^*_\alpha(\vec{r},b_0)\wedge\overrightarrow{\nabla}\psi_\gamma(\vec{r},b_1) &= \begin{pmatrix}\frac{1}{\sqrt{2}}(\nabla_- - \nabla_+)\psi^*_\alpha(\vec{r},b_0)\\ \frac{i}{\sqrt{2}}(\nabla_- + \nabla_+)\psi^*_\alpha(\vec{r},b_0)\\ \nabla_0\psi^*_\alpha(\vec{r},b_0)\end{pmatrix}\wedge\begin{pmatrix}\frac{1}{\sqrt{2}}(\nabla_- - \nabla_+)\psi_\gamma(\vec{r},b_1)\\ \frac{i}{\sqrt{2}}(\nabla_- + \nabla_+)\psi_\gamma(\vec{r},b_1)\\ \nabla_0\psi_\gamma(\vec{r},b_1)\end{pmatrix} \\ &= \begin{pmatrix}\frac{i}{\sqrt{2}}[(\nabla_- + \nabla_+)\psi^*_\alpha(\vec{r},b_0)\nabla_0\psi_\gamma(\vec{r},b_1) - \nabla_0\psi^*_\alpha(\vec{r},b_0)(\nabla_- + \nabla_+)\psi_\gamma(\vec{r},b_1)]\\ \frac{1}{\sqrt{2}}[\nabla_0\psi^*_\alpha(\vec{r},b_0)(\nabla_- - \nabla_+)\psi_\gamma(\vec{r},b_1) - (\nabla_- - \nabla_+)\psi^*_\alpha(\vec{r},b_0)\nabla_0\psi_\gamma(\vec{r},b_1)]\\ i[\nabla_-\psi^*_\alpha(\vec{r},b_0)\nabla_+\psi_\gamma(\vec{r},b_1) - \nabla_+\psi^*_\alpha(\vec{r},b,0)\nabla_-\psi_\gamma(\vec{r},b_1)]\end{pmatrix}\end{aligned}} \tag{H.28}$$

H.2 Spin part

This section is dedicated to the spin part of the contact spin-orbit term. We want to rewrite the following quantity:

$$S^{\gamma\delta}_{\alpha\beta} = \langle s_\alpha s_\beta|(\vec{\sigma}_1 + \vec{\sigma}_2)|s_\gamma s_\delta\rangle \tag{H.29}$$

Eq.(H.29) is easily separated in two parts:

$$\boxed{S^{\gamma\delta}_{\alpha\beta} = \langle s_\alpha|\vec{\sigma}|s_\gamma\rangle\delta_{s_\beta s_\delta} + \langle s_\beta|\vec{\sigma}|s_\delta\rangle\delta_{s_\alpha s_\gamma}} \tag{H.30}$$

Now, we express the operator $\vec{\sigma}$ in coordinates:

$$\vec{\sigma} = \begin{pmatrix}\sigma_x\\ \sigma_y\\ \sigma_z\end{pmatrix} \tag{H.31}$$

The elements of $\vec{\sigma}$ are the well-known Pauli matrices:

$$\sigma_x = \begin{pmatrix}0 & 1\\ 1 & 0\end{pmatrix}; \qquad \sigma_y = \begin{pmatrix}0 & -i\\ i & 0\end{pmatrix}; \qquad \sigma_z = \begin{pmatrix}1 & 0\\ 0 & -1\end{pmatrix} \tag{H.32}$$

From Eq.(H.32), we know that these matrices operate on spin states as follows:

$$\begin{cases}\sigma_x|+\rangle = |-\rangle\\ \sigma_x|-\rangle = |+\rangle\end{cases}; \qquad \begin{cases}\sigma_y|+\rangle = i|-\rangle\\ \sigma_y|-\rangle = -i|+\rangle\end{cases}; \qquad \begin{cases}\sigma_z|+\rangle = |+\rangle\\ \sigma_z|-\rangle = -|-\rangle\end{cases} \tag{H.33}$$

It is easy to give an expression of the quantities of the type $\langle s_\alpha|\vec{\sigma}|s_\gamma\rangle$:

$$\langle s_\alpha|\vec{\sigma}|s_\gamma\rangle = \begin{pmatrix} \delta_{s_{\alpha_+}s_{\gamma_-}} + \delta_{s_{\alpha_-}s_{\gamma_+}} \\ -i(\delta_{s_{\alpha_+}s_{\gamma_-}} - \delta_{s_{\alpha_-}s_{\gamma_+}}) \\ \delta_{s_{\alpha_+}s_{\gamma_+}} - \delta_{s_{\alpha_-}s_{\gamma_-}} \end{pmatrix} \tag{H.34}$$

Thanks to Eq.(H.34), we find for $S^{\gamma\delta}_{\alpha\beta}$:

$$\boxed{S^{\gamma\delta}_{\alpha\beta} = \begin{pmatrix} \delta_{s_{\alpha_+}s_{\gamma_-}} + \delta_{s_{\alpha_-}s_{\gamma_+}} \\ -i(\delta_{s_{\alpha_+}s_{\gamma_-}} - \delta_{s_{\alpha_-}s_{\gamma_+}}) \\ \delta_{s_{\alpha_+}s_{\gamma_+}} - \delta_{s_{\alpha_-}s_{\gamma_-}} \end{pmatrix} \delta_{s_\beta s_\delta} + \begin{pmatrix} \delta_{s_{\beta_+}s_{\delta_-}} + \delta_{s_{\beta_-}s_{\delta_+}} \\ -i(\delta_{s_{\beta_+}s_{\delta_-}} - \delta_{s_{\beta_-}s_{\delta_+}}) \\ \delta_{s_{\beta_+}s_{\delta_+}} - \delta_{s_{\beta_-}s_{\delta_-}} \end{pmatrix} \delta_{s_\alpha s_\gamma}} \tag{H.35}$$

Now, we have everything to demonstrate the property $S^{\gamma\delta}_{\alpha\beta} = S^{\delta\gamma}_{\alpha\beta}$ stated in Eq.(H.6). To do so, we fully develop the expressions of $S^{\gamma\delta}_{\alpha\beta}$ and $S^{\delta\gamma}_{\alpha\beta}$. We start with $S^{\gamma\delta}_{\alpha\beta}$:

$$\begin{aligned} S^{\gamma\delta}_{\alpha\beta} = &\begin{pmatrix} [\delta_{s_{\alpha_+}s_{\gamma_-}} + \delta_{s_{\alpha_-}s_{\gamma_+}}][\delta_{s_{\beta_+}s_{\delta_+}} + \delta_{s_{\beta_-}s_{\delta_-}}] \\ -i[\delta_{s_{\alpha_+}s_{\gamma_-}} - \delta_{s_{\alpha_-}s_{\gamma_+}}][\delta_{s_{\beta_+}s_{\delta_+}} + \delta_{s_{\beta_-}s_{\delta_-}}] \\ [\delta_{s_{\alpha_+}s_{\gamma_+}} - \delta_{s_{\alpha_-}s_{\gamma_-}}][\delta_{s_{\beta_+}s_{\delta_+}} + \delta_{s_{\beta_-}s_{\delta_-}}] \end{pmatrix} \\ &+ \begin{pmatrix} [\delta_{s_{\beta_+}s_{\delta_-}} + \delta_{s_{\beta_-}s_{\delta_+}}][\delta_{s_{\alpha_+}s_{\gamma_+}} + \delta_{s_{\alpha_-}s_{\gamma_-}}] \\ -i[\delta_{s_{\beta_+}s_{\delta_-}} - \delta_{s_{\beta_-}s_{\delta_+}}][\delta_{s_{\alpha_+}s_{\gamma_+}} + \delta_{s_{\alpha_-}s_{\gamma_-}}] \\ [\delta_{s_{\beta_+}s_{\delta_+}} - \delta_{s_{\beta_-}s_{\delta_-}}][\delta_{s_{\alpha_+}s_{\gamma_+}} + \delta_{s_{\alpha_-}s_{\gamma_-}}] \end{pmatrix} \end{aligned} \tag{H.36}$$

Thus, the different elements of $S^{\gamma\delta}_{\alpha\beta}$ read:

$$\begin{aligned} (S^{\gamma\delta}_{\alpha\beta})_x = &\delta_{s_{\alpha_+}s_{\gamma_+}s_{\beta_+}s_{\delta_-}} + \delta_{s_{\alpha_+}s_{\gamma_+}s_{\beta_-}s_{\delta_+}} + \delta_{s_{\alpha_-}s_{\gamma_-}s_{\beta_+}s_{\delta_-}} + \delta_{s_{\alpha_-}s_{\gamma_-}s_{\beta_-}s_{\delta_+}} \\ &\delta_{s_{\alpha_+}s_{\gamma_-}s_{\beta_+}s_{\delta_+}} + \delta_{s_{\alpha_-}s_{\gamma_+}s_{\beta_+}s_{\delta_+}} + \delta_{s_{\alpha_+}s_{\gamma_-}s_{\beta_-}s_{\delta_-}} + \delta_{s_{\alpha_-}s_{\gamma_+}s_{\beta_-}s_{\delta_-}} \end{aligned} \tag{H.37}$$

$$\begin{aligned} (S^{\gamma\delta}_{\alpha\beta})_y = -i(&\delta_{s_{\alpha_+}s_{\gamma_+}s_{\beta_+}s_{\delta_-}} - \delta_{s_{\alpha_+}s_{\gamma_+}s_{\beta_-}s_{\delta_+}} + \delta_{s_{\alpha_-}s_{\gamma_-}s_{\beta_+}s_{\delta_-}} - \delta_{s_{\alpha_-}s_{\gamma_-}s_{\beta_-}s_{\delta_+}} \\ &\delta_{s_{\alpha_+}s_{\gamma_-}s_{\beta_+}s_{\delta_+}} - \delta_{s_{\alpha_-}s_{\gamma_+}s_{\beta_+}s_{\delta_+}} + \delta_{s_{\alpha_+}s_{\gamma_-}s_{\beta_-}s_{\delta_-}} - \delta_{s_{\alpha_-}s_{\gamma_+}s_{\beta_-}s_{\delta_-}}) \end{aligned} \tag{H.38}$$

$$(S^{\gamma\delta}_{\alpha\beta})_z = 2(\delta_{s_{\alpha_+}s_{\gamma_+}s_{\beta_+}s_{\delta_+}} - \delta_{s_{\alpha_-}s_{\gamma_-}s_{\beta_-}s_{\delta_-}}) \tag{H.39}$$

We develop $S^{\delta\gamma}_{\alpha\beta}$:

$$\begin{aligned} S^{\delta\gamma}_{\alpha\beta} = &\begin{pmatrix} [\delta_{s_{\alpha_+}s_{\delta_-}} + \delta_{s_{\alpha_-}s_{\delta_+}}][\delta_{s_{\beta_+}s_{\gamma_+}} + \delta_{s_{\beta_-}s_{\gamma_-}}] \\ -i[\delta_{s_{\alpha_+}s_{\delta_-}} - \delta_{s_{\alpha_-}s_{\delta_+}}][\delta_{s_{\beta_+}s_{\gamma_+}} + \delta_{s_{\beta_-}s_{\gamma_-}}] \\ [\delta_{s_{\alpha_+}s_{\delta_+}} - \delta_{s_{\alpha_-}s_{\delta_-}}][\delta_{s_{\beta_+}s_{\gamma_+}} + \delta_{s_{\beta_-}s_{\gamma_-}}] \end{pmatrix} \\ &+ \begin{pmatrix} [\delta_{s_{\beta_+}s_{\gamma_-}} + \delta_{s_{\beta_-}s_{\gamma_+}}][\delta_{s_{\alpha_+}s_{\delta_+}} + \delta_{s_{\alpha_-}s_{\delta_-}}] \\ -i[\delta_{s_{\beta_+}s_{\gamma_-}} - \delta_{s_{\beta_-}s_{\gamma_+}}][\delta_{s_{\alpha_+}s_{\delta_+}} + \delta_{s_{\alpha_-}s_{\delta_-}}] \\ [\delta_{s_{\beta_+}s_{\gamma_+}} - \delta_{s_{\beta_-}s_{\gamma_-}}][\delta_{s_{\alpha_+}s_{\delta_+}} + \delta_{s_{\alpha_-}s_{\delta_-}}] \end{pmatrix} \end{aligned} \tag{H.40}$$

Isolating the elements of $S^{\delta\gamma}_{\alpha\beta}$, we finally get:

$$\begin{aligned}(S^{\delta\gamma}_{\alpha\beta})_x = \delta_{s_{\alpha_+}s_{\gamma_+}s_{\beta_+}s_{\delta_-}} + \delta_{s_{\alpha_+}s_{\gamma_+}s_{\beta_-}s_{\delta_+}} + \delta_{s_{\alpha_-}s_{\gamma_-}s_{\beta_+}s_{\delta_-}} + \delta_{s_{\alpha_-}s_{\gamma_-}s_{\beta_-}s_{\delta_+}} \\ \delta_{s_{\alpha_+}s_{\gamma_-}s_{\beta_+}s_{\delta_+}} + \delta_{s_{\alpha_-}s_{\gamma_+}s_{\beta_+}s_{\delta_+}} + \delta_{s_{\alpha_+}s_{\gamma_-}s_{\beta_-}s_{\delta_-}} + \delta_{s_{\alpha_-}s_{\gamma_+}s_{\beta_-}s_{\delta_-}}\end{aligned} \tag{H.41}$$

$$\begin{aligned}(S^{\delta\gamma}_{\alpha\beta})_y = -i(\delta_{s_{\alpha_+}s_{\gamma_+}s_{\beta_+}s_{\delta_-}} - \delta_{s_{\alpha_+}s_{\gamma_+}s_{\beta_-}s_{\delta_+}} + \delta_{s_{\alpha_-}s_{\gamma_-}s_{\beta_+}s_{\delta_-}} - \delta_{s_{\alpha_-}s_{\gamma_-}s_{\beta_-}s_{\delta_+}} \\ \delta_{s_{\alpha_+}s_{\gamma_-}s_{\beta_+}s_{\delta_+}} - \delta_{s_{\alpha_-}s_{\gamma_+}s_{\beta_+}s_{\delta_+}} + \delta_{s_{\alpha_+}s_{\gamma_-}s_{\beta_-}s_{\delta_-}} - \delta_{s_{\alpha_-}s_{\gamma_+}s_{\beta_-}s_{\delta_-}})\end{aligned} \tag{H.42}$$

$$(S^{\delta\gamma}_{\alpha\beta})_z = 2(\delta_{s_{\alpha_+}s_{\gamma_+}s_{\beta_+}s_{\delta_+}} - \delta_{s_{\alpha_-}s_{\gamma_-}s_{\beta_-}s_{\delta_-}}) \tag{H.43}$$

It is now really easy to observe that $S^{\gamma\delta}_{\alpha\beta} = S^{\delta\gamma}_{\alpha\beta}$.

H.3 HFB fields

In this part, only the expression of the mean field is derived in great details. The pairing field is not included in the calculations because of the zero-range nature of the spin-orbit term in D1-type Gogny interactions. Indeed, we want to avoid ultraviolet divergences that may occur evaluating pairing energies coming from contact forces. The derivations thereafter are the ones used in the HFB3 code.

H.3.1 Mean field

The contact spin-isospin part of the mean field reads:

$$\Gamma_{\alpha\gamma} = \sum_{\beta\delta} E^{\gamma\delta}_{\alpha\beta}.S^{\gamma\delta}_{\alpha\beta}[\delta_{\tau_\alpha\tau_\gamma}\delta_{\tau_\beta\tau_\delta} + \delta_{\tau_\alpha\tau_\delta}\delta_{\tau_\beta\tau_\gamma}]\rho_{\delta\beta} \tag{H.44}$$

The isospin part of Eq.(H.44) is easily handled:

$$\Gamma^{\tau}_{\alpha\gamma} = \sum_{\beta\delta} E^{\gamma\delta}_{\alpha\beta}.S^{\gamma\delta}_{\alpha\beta}[1 + \delta_{\tau\tau'}]\rho^{\tau'}_{\delta\beta} \tag{H.45}$$

Then, we decompose the spatial part E:

$$\begin{cases} E^{\gamma\delta}_{\alpha\beta} = A^{\gamma\delta}_{\alpha\beta} + A^{\delta\gamma}_{\beta\alpha} \\ A^{\gamma\delta}_{\alpha\beta} = i\frac{W_{LS}}{2}\int d\vec{r}\psi^*_\alpha(\vec{r})\psi_\gamma(\vec{r})(\overrightarrow{\nabla}\psi^*_\beta(\vec{r}) \wedge \overrightarrow{\nabla}\psi_\delta(\vec{r})) \end{cases} \tag{H.46}$$

We give the full expression of A:

$$A^{\gamma\delta}_{\alpha\beta} = i\frac{W_{LS}}{2}\int d\vec{r}\psi^*_\alpha(\vec{r})\psi_\gamma(\vec{r}) \begin{pmatrix} \frac{i}{\sqrt{2}}[(\nabla_- + \nabla_+)\psi^*_\beta(\vec{r})\nabla_0\psi_\delta(\vec{r}) - \nabla_0\psi^*_\beta(\vec{r})(\nabla_- + \nabla_+)\psi_\delta(\vec{r})] \\ \frac{1}{\sqrt{2}}[\nabla_0\psi^*_\beta(\vec{r})(\nabla_- - \nabla_+)\psi_\delta(\vec{r}) - (\nabla_- - \nabla_+)\psi^*_\beta(\vec{r})\nabla_0\psi_\delta(\vec{r})] \\ i[\nabla_-\psi^*_\beta(\vec{r})\nabla_+\psi_\delta(\vec{r}) - \nabla_+\psi^*_\beta(\vec{r})\nabla_-\psi_\delta(\vec{r})] \end{pmatrix} \tag{H.47}$$

Thanks to Eq.(H.46), the field reads:

$$\Gamma^{\tau}_{\alpha\gamma} = \sum_{\beta\delta} [A^{\gamma\delta}_{\alpha\beta} + A^{\delta\gamma}_{\beta\alpha}].S^{\gamma\delta}_{\alpha\beta}[1+\delta_{\tau\tau'}]\rho^{\tau'}_{\delta\beta} \tag{H.48}$$

Using the the time-reversal properties of the density, we find:

$$\Gamma^{\tau}_{\alpha\gamma} = \sum_{\beta\delta>} [(A^{\gamma\delta}_{\alpha\beta} + A^{\delta\gamma}_{\beta\alpha}).S^{\gamma\delta}_{\alpha\beta} + (-1)^{s_\delta - s_\beta}(A^{\gamma\bar{\delta}}_{\alpha\bar{\beta}} + A^{\bar{\delta}\gamma}_{\bar{\beta}\alpha}).S^{\gamma\bar{\delta}}_{\alpha\bar{\beta}}][1+\delta_{\tau\tau'}]\rho^{\tau'}_{\delta\beta} \tag{H.49}$$

From Eq.(H.46) we extract the following properties:

$$\begin{cases} A^{\gamma\delta}_{\alpha\beta} = -A^{\gamma\bar{\beta}}_{\alpha\bar{\delta}} \\ A^{\delta\gamma}_{\beta\alpha} = A^{\bar{\beta}\gamma}_{\bar{\delta}\alpha} \end{cases} \tag{H.50}$$

Combining Eq.(H.50) with the symmetry of ρ, we simplify Eq.(H.49):

$$\boxed{\Gamma^{\tau}_{\alpha\gamma} = \sum_{\beta\delta>} [(A^{\gamma\delta}_{\alpha\beta}.(S^{\gamma\delta}_{\alpha\beta} - S^{\gamma\bar{\beta}}_{\alpha\bar{\delta}}(-1)^{s_\delta - s_\beta}) + A^{\delta\gamma}_{\beta\alpha}.(S^{\gamma\delta}_{\alpha\beta} + S^{\gamma\bar{\beta}}_{\alpha\bar{\delta}}(-1)^{s_\delta - s_\beta})][1+\delta_{\tau\tau'}]\rho^{\tau'}_{\delta\beta}} \tag{H.51}$$

In the following, we will explicitly consider the spins of α and γ.

Block ++:

Here, we consider the spins $(\alpha\uparrow, \gamma\uparrow)$. We start looking at the spin part of the ++ mean field:

$$\begin{cases} (S^{\gamma\delta}_{\alpha\beta})^{++} = \begin{pmatrix} \delta_{s_{\beta_+} s_{\delta_-}} + \delta_{s_{\beta_-} s_{\delta_+}} \\ -i(\delta_{s_{\beta_+} s_{\delta_-}} - \delta_{s_{\beta_-} s_{\delta_+}}) \\ 2\delta_{s_{\beta_+} s_{\delta_+}} \end{pmatrix} \\ (-1)^{s_\delta - s_\beta}(S^{\gamma\bar{\beta}}_{\alpha\bar{\delta}})^{++} = \begin{pmatrix} -\delta_{s_{\beta_+} s_{\delta_-}} - \delta_{s_{\beta_-} s_{\delta_+}} \\ i(\delta_{s_{\beta_+} s_{\delta_-}} - \delta_{s_{\beta_-} s_{\delta_+}}) \\ 2\delta_{s_{\beta_-} s_{\delta_-}} \end{pmatrix} \end{cases} \tag{H.52}$$

Eq.(H.52) directly implies:

$$\begin{cases} (S^{\gamma\delta}_{\alpha\beta})^{++} - (S^{\gamma\bar{\beta}}_{\alpha\bar{\delta}})^{++}(-1)^{s_\delta - s_\beta} = 2\begin{pmatrix} \delta_{s_{\beta_+} s_{\delta_-}} + \delta_{s_{\beta_-} s_{\delta_+}} \\ -i(\delta_{s_{\beta_+} s_{\delta_-}} - \delta_{s_{\beta_-} s_{\delta_+}}) \\ \delta_{s_{\beta_+} s_{\delta_+}} - \delta_{s_{\beta_-} s_{\delta_-}} \end{pmatrix} \\ (S^{\gamma\delta}_{\alpha\beta})^{++} + (S^{\gamma\bar{\beta}}_{\alpha\bar{\delta}})^{++}(-1)^{s_\delta - s_\beta} = 2\begin{pmatrix} 0 \\ 0 \\ \delta_{s_{\beta_+} s_{\delta_+}} + \delta_{s_{\beta_-} s_{\delta_-}} \end{pmatrix} \end{cases} \tag{H.53}$$

It is now possible to develop the dot products bewteen the spatial part and the spin part of the field:

$$A^{\delta\gamma}_{\beta\alpha}.((S^{\gamma\delta}_{\alpha\beta})^{++}+(S^{\gamma\bar{\beta}}_{\alpha\bar{\delta}})^{++}(-1)^{s_\delta-s_\beta}) = W_{LS}\int d\vec{r}\psi^*_\beta(\vec{r})\psi_\delta(\vec{r})[\nabla_+\psi^*_\alpha(\vec{r})\nabla_-\psi_\gamma(\vec{r}) - \nabla_-\psi^*_\alpha(\vec{r})\nabla_+\psi_\gamma(\vec{r})](\delta_{s_{\beta_+}s_{\delta_+}}+\delta_{s_{\beta_-}s_{\delta_-}}) \tag{H.54}$$

$$\begin{aligned}A^{\gamma\delta}_{\alpha\beta}.((S^{\gamma\delta}_{\alpha\beta})^{++}-(S^{\gamma\bar{\beta}}_{\alpha\bar{\delta}})^{++}(-1)^{s_\delta-s_\beta}) = W_{LS}\int d\vec{r}\psi^*_\alpha(\vec{r})\psi_\gamma(\vec{r})(\sqrt{2}[\nabla_0\psi^*_\beta(\vec{r})\nabla_+\psi_\delta(\vec{r}) \\ -\nabla_+\psi^*_\beta(\vec{r})\nabla_0\psi_\delta(\vec{r})]\delta_{s_{\beta_-}s_{\delta_+}} \\ +\sqrt{2}[\nabla_0\psi^*_\beta(\vec{r})\nabla_-\psi_\delta(\vec{r})-\nabla_-\psi^*_\beta(\vec{r})\nabla_0\psi_\delta(\vec{r})]\delta_{s_{\beta_+}s_{\delta_-}} \\ +[\nabla_+\psi^*_\beta(\vec{r})\nabla_-\psi_\delta(\vec{r})-\nabla_-\psi^*_\beta(\vec{r})\nabla_+\psi_\delta(\vec{r})](\delta_{s_{\beta_+}s_{\delta_+}}-\delta_{s_{\beta_-}s_{\delta_-}}))\end{aligned} \tag{H.55}$$

Because $s_\alpha = s_\gamma \Rightarrow m_\alpha = m_\gamma$, we can write:

$$e^{i(m_\gamma-m_\alpha)\phi}=1 \qquad \Rightarrow \qquad \psi^*_\alpha(\vec{r})\psi_\gamma(\vec{r}) = \psi_\alpha(\vec{r})\psi^*_\gamma(\vec{r}) \tag{H.56}$$

Moreover, the following property holds for the derivative operators:

$$-\nabla_0\psi_\delta(\vec{r})\nabla_-\psi^*_\beta(\vec{r}) = \nabla_0\psi^*_\delta(\vec{r})(\nabla_+\psi_\beta(\vec{r}))^* \tag{H.57}$$

Using Eq.(H.56) and Eq.(H.57) along with the symmetry of ρ we find:

$$\begin{aligned}&\sum_{\beta\delta>}\int d\vec{r}\psi^*_\alpha(\vec{r})\psi_\gamma(\vec{r})[\nabla_0\psi^*_\beta(\vec{r})\nabla_-\psi_\delta(\vec{r})-\nabla_-\psi^*_\beta(\vec{r})\nabla_0\psi_\delta(\vec{r})]\rho^{-+}_{\delta\beta} \\ =&\sum_{\beta\delta>}\int d\vec{r}\psi^*_\alpha(\vec{r})\psi_\gamma(\vec{r})[\nabla_0\psi^*_\beta(\vec{r})\nabla_+\psi_\delta(\vec{r})-\nabla_+\psi^*_\beta(\vec{r})\nabla_0\psi_\delta(\vec{r})]\rho^{+-}_{\delta\beta}\end{aligned} \tag{H.58}$$

Inserting Eq.(H.58) in the expression of the field, we get:

$$\boxed{\begin{aligned}\Gamma^{\tau++}_{\alpha\gamma} = W_{LS}\sum_{\beta\delta>}[2\sqrt{2}\int d\vec{r}\psi^*_\alpha(\vec{r})\psi_\gamma(\vec{r})[\nabla_0\psi^*_\beta(\vec{r})\nabla_+\psi_\delta(\vec{r})-\nabla_+\psi^*_\beta(\vec{r})\nabla_0\psi_\delta(\vec{r})][\rho^{\bar{\tau}+-}_{\delta\beta}+2\rho^{\tau+-}_{\delta\beta}] \\ +\int d\vec{r}\psi^*_\alpha(\vec{r})\psi_\gamma(\vec{r})[\nabla_+\psi^*_\beta(\vec{r})\nabla_-\psi_\delta(\vec{r})-\nabla_-\psi^*_\beta(\vec{r})\nabla_+\psi_\delta(\vec{r})][\rho^{\bar{\tau}++}_{\delta\beta}-\rho^{\bar{\tau}--}_{\delta\beta}+2(\rho^{\tau++}_{\delta\beta}-\rho^{\tau--}_{\delta\beta})] \\ +\int d\vec{r}\psi^*_\beta(\vec{r})\psi_\delta(\vec{r})[\nabla_+\psi^*_\alpha(\vec{r})\nabla_-\psi_\gamma(\vec{r})-\nabla_-\psi^*_\alpha(\vec{r})\nabla_+\psi_\gamma(\vec{r})][\rho^{\bar{\tau}++}_{\delta\beta}+\rho^{\bar{\tau}--}_{\delta\beta}+2(\rho^{\tau++}_{\delta\beta}+\rho^{\tau--}_{\delta\beta})]]\end{aligned}} \tag{H.59}$$

Eq.(H.59) is then decomposed using the X and Y matrices defined in section H.6.1. The formula below is the final formula which is implemented in the HFB3 code. Note that this decomposition is essential for the sake of numerical performances:

$$\boxed{\begin{aligned}\Gamma^{\tau++}_{\alpha\gamma} = W_{LS}\sum_{\beta\delta>}2\sqrt{2}Y^{(0)}_{z_{\alpha\gamma}}Y^{(0)}_{r_{\alpha\gamma}}[X^{(0)}_{r_{\delta\beta}}X^{(0)}_{z_{\delta\beta}}-X^{(1)}_{r_{\delta\beta}}X^{(1)}_{z_{\delta\beta}}]R^{(0)}_{\delta\beta} \\ +Y^{(0)}_{z_{\alpha\gamma}}Y^{(0)}_{r_{\alpha\gamma}}X^{(2)}_{r_{\delta\beta}}X^{(2)}_{z_{\delta\beta}}R^{(1)}_{\delta\beta}+Y^{(0)}_{z_{\alpha\gamma}}Y^{(1)}_{r_{\alpha\gamma}}X^{(3)}_{r_{\delta\beta}}X^{(2)}_{z_{\delta\beta}}R^{(2)}_{\delta\beta}\end{aligned}} \tag{H.60}$$

In addition to the X and Y matrices, we used the following quantities in Eq.(H.60):

$$\begin{cases} R^{(0)}_{\delta\beta} = \rho^{\bar{\tau}+-}_{\delta\beta} + 2\rho^{\tau+-}_{\delta\beta} \\ R^{(1)}_{\delta\beta} = \rho^{\bar{\tau}++}_{\delta\beta} - \rho^{\bar{\tau}--}_{\delta\beta} - 2(\rho^{\tau++}_{\delta\beta} + \rho^{\tau--}_{\delta\beta}) \\ R^{(2)}_{\delta\beta} = \rho^{\bar{\tau}++}_{\delta\beta} + \rho^{\bar{\tau}--}_{\delta\beta} + 2(\rho^{\tau++}_{\delta\beta} + \rho^{\tau--}_{\delta\beta}) \end{cases} \tag{H.61}$$

Block $--$:

Here, we consider the spins $(\alpha\downarrow, \gamma\downarrow)$. We start looking at the spin part of the $--$ mean field:

$$\begin{cases} (S^{\gamma\delta}_{\alpha\beta})^{--} = \begin{pmatrix} \delta_{s_{\beta_+}s_{\delta_-}} + \delta_{s_{\beta_-}s_{\delta_+}} \\ -i(\delta_{s_{\beta_+}s_{\delta_-}} - \delta_{s_{\beta_-}s_{\delta_+}}) \\ -2\delta_{s_{\beta_-}s_{\delta_-}} \end{pmatrix} \\ (-1)^{s_\delta - s_\beta}(S^{\gamma\bar{\beta}}_{\alpha\bar{\delta}})^{--} = \begin{pmatrix} -\delta_{s_{\beta_+}s_{\delta_-}} - \delta_{s_{\beta_-}s_{\delta_+}} \\ i(\delta_{s_{\beta_+}s_{\delta_-}} - \delta_{s_{\beta_-}s_{\delta_+}}) \\ -2\delta_{s_{\beta_+}s_{\delta_+}} \end{pmatrix} \end{cases} \tag{H.62}$$

Eq.(H.62) directly implies:

$$\begin{cases} ((S^{\gamma\delta}_{\alpha\beta})^{--} - (S^{\gamma\bar{\beta}}_{\alpha\bar{\delta}})^{--}(-1)^{s_\delta - s_\beta}) = 2\begin{pmatrix} \delta_{s_{\beta_+}s_{\delta_-}} + \delta_{s_{\beta_-}s_{\delta_+}} \\ -i(\delta_{s_{\beta_+}s_{\delta_-}} - \delta_{s_{\beta_-}s_{\delta_+}}) \\ \delta_{s_{\beta_+}s_{\delta_+}} - \delta_{s_{\beta_-}s_{\delta_-}} \end{pmatrix} \\ ((S^{\gamma\delta}_{\alpha\beta})^{--} + (S^{\gamma\bar{\beta}}_{\alpha\bar{\delta}})^{--}(-1)^{s_\delta - s_\beta}) = -2\begin{pmatrix} 0 \\ 0 \\ \delta_{s_{\beta_+}s_{\delta_+}} + \delta_{s_{\beta_-}s_{\delta_-}} \end{pmatrix} \end{cases} \tag{H.63}$$

Then, we develop the dot products between the sparial and the spin parts:

$$\begin{aligned} A^{\delta\gamma}_{\beta\alpha}.((S^{\gamma\delta}_{\alpha\beta})^{--} + (S^{\gamma\bar{\beta}}_{\alpha\bar{\delta}})^{--}(-1)^{s_\delta - s_\beta}) = -W_{LS}\int d\vec{r}\psi^*_\beta(\vec{r})\psi_\delta(\vec{r})[\nabla_+\psi^*_\alpha(\vec{r})\nabla_-\psi_\gamma(\vec{r}) \\ -\nabla_-\psi^*_\alpha(\vec{r})\nabla_+\psi_\gamma(\vec{r})](\delta_{s_{\beta_+}s_{\delta_+}} + \delta_{s_{\beta_-}s_{\delta_-}}) \end{aligned} \tag{H.64}$$

$$\begin{aligned} A^{\gamma\delta}_{\alpha\beta}.((S^{\gamma\delta}_{\alpha\beta})^{--} - (S^{\gamma\bar{\beta}}_{\alpha\bar{\delta}})^{--}(-1)^{s_\delta - s_\beta}) = W_{LS}\int d\vec{r}\psi^*_\alpha(\vec{r})\psi_\gamma(\vec{r})(\sqrt{2}[\nabla_0\psi^*_\beta(\vec{r})\nabla_+\psi_\delta(\vec{r}) \\ -\nabla_+\psi^*_\beta(\vec{r})\nabla_0\psi_\delta(\vec{r})]\delta_{s_{\beta_-}s_{\delta_+}} \\ +\sqrt{2}[\nabla_0\psi^*_\beta(\vec{r})\nabla_-\psi_\delta(\vec{r}) - \nabla_-\psi^*_\beta(\vec{r})\nabla_0\psi_\delta(\vec{r})]\delta_{s_{\beta_+}s_{\delta_-}} \\ +[\nabla_+\psi^*_\beta(\vec{r})\nabla_-\psi_\delta(\vec{r}) - \nabla_-\psi^*_\beta(\vec{r})\nabla_+\psi_\delta(\vec{r})](\delta_{s_{\beta_+}s_{\delta_+}} - \delta_{s_{\beta_-}s_{\delta_-}})) \end{aligned} \tag{H.65}$$

By analogy with the $++$ part, we write the field as follows:

$$\boxed{\begin{aligned} \Gamma^{\tau--}_{\alpha\gamma} = W_{LS}\sum_{\beta\delta>}[2\sqrt{2}\int d\vec{r}\psi^*_\alpha(\vec{r})\psi_\gamma(\vec{r})[\nabla_0\psi^*_\beta(\vec{r})\nabla_+\psi_\delta(\vec{r}) - \nabla_+\psi^*_\beta(\vec{r})\nabla_0\psi_\delta(\vec{r})][\rho^{\bar{\tau}+-}_{\delta\beta} + 2\rho^{\tau+-}_{\delta\beta}] \\ + \int d\vec{r}\psi^*_\alpha(\vec{r})\psi_\gamma(\vec{r})[\nabla_+\psi^*_\beta(\vec{r})\nabla_-\psi_\delta(\vec{r}) - \nabla_-\psi^*_\beta(\vec{r})\nabla_+\psi_\delta(\vec{r})][\rho^{\bar{\tau}++}_{\delta\beta} - \rho^{\bar{\tau}--}_{\delta\beta} + 2(\rho^{\tau++}_{\delta\beta} - \rho^{\tau--}_{\delta\beta})] \\ - \int d\vec{r}\psi^*_\beta(\vec{r})\psi_\delta(\vec{r})[\nabla_+\psi^*_\alpha(\vec{r})\nabla_-\psi_\gamma(\vec{r}) - \nabla_-\psi^*_\alpha(\vec{r})\nabla_+\psi_\gamma(\vec{r})][\rho^{\bar{\tau}++}_{\delta\beta} + \rho^{\bar{\tau}--}_{\delta\beta} + 2(\rho^{\tau++}_{\delta\beta} + \rho^{\tau--}_{\delta\beta})]] \end{aligned}} \tag{H.66}$$

We observe that the components of the $--$ block are similar to the ones of the $++$ block with the exception of the last term, which comes with a minus sign. It is important to keep it in mind when programming the fields. We decompose Eq.(H.66) thanks to the X and Y matrices defined in section H.6.1. We end up with the final expression implemented in the HFB3 code:

$$\boxed{\begin{aligned}\Gamma^{\tau--}_{\alpha\gamma} = W_{LS}\sum_{\beta\delta>} 2\sqrt{2}Y^{(0)}_{z_{\alpha\gamma}}Y^{(0)}_{r_{\alpha\gamma}}[X^{(0)}_{r_{\delta\beta}}X^{(0)}_{z_{\delta\beta}} - X^{(1)}_{r_{\delta\beta}}X^{(1)}_{z_{\delta\beta}}]R^{(0)}_{\delta\beta} \\ +Y^{(0)}_{z_{\alpha\gamma}}Y^{(0)}_{r_{\alpha\gamma}}X^{(2)}_{r_{\delta\beta}}X^{(2)}_{z_{\delta\beta}}R^{(1)}_{\delta\beta} - Y^{(0)}_{z_{\alpha\gamma}}Y^{(1)}_{r_{\alpha\gamma}}X^{(3)}_{r_{\delta\beta}}X^{(2)}_{z_{\delta\beta}}R^{(2)}_{\delta\beta}\end{aligned}} \tag{H.67}$$

Block $-+$:

Here, we consider the spins $(\alpha\downarrow, \gamma\uparrow)$. We start looking at the spin part of the $-+$ mean field:

$$\begin{cases}(S^{\gamma\delta}_{\alpha\beta})^{-+} = \begin{pmatrix}\delta_{s_{\beta_+}s_{\delta_+}} + \delta_{s_{\beta_-}s_{\delta_-}} \\ i(\delta_{s_{\beta_+}s_{\delta_+}} + \delta_{s_{\beta_-}s_{\delta_-}}) \\ 0\end{pmatrix} \\ (-1)^{s_\delta - s_\beta}(S^{\gamma\bar{\beta}}_{\alpha\bar{\delta}})^{-+} = \begin{pmatrix}\delta_{s_{\beta_+}s_{\delta_+}} + \delta_{s_{\beta_-}s_{\delta_-}} \\ i(\delta_{s_{\beta_+}s_{\delta_+}} + \delta_{s_{\beta_-}s_{\delta_-}}) \\ 0\end{pmatrix}\end{cases} \tag{H.68}$$

Eq.(H.68) implies:

$$\begin{cases}((S^{\gamma\delta}_{\alpha\beta})^{-+} - (S^{\gamma\bar{\beta}}_{\alpha\bar{\delta}})^{-+}(-1)^{s_\delta - s_\beta}) = 0 \\ ((S^{\gamma\delta}_{\alpha\beta})^{-+} + (S^{\gamma\bar{\beta}}_{\alpha\bar{\delta}})^{-+}(-1)^{s_\delta - s_\beta}) = 2\begin{pmatrix}\delta_{s_{\beta_+}s_{\delta_+}} + \delta_{s_{\beta_-}s_{\delta_-}} \\ i(\delta_{s_{\beta_+}s_{\delta_+}} + \delta_{s_{\beta_-}s_{\delta_-}}) \\ 0\end{pmatrix}\end{cases} \tag{H.69}$$

Now, we develop the dot products between the spatial and spin parts:

$$\begin{aligned}A^{\delta\gamma}_{\beta\alpha}.((S^{\gamma\delta}_{\alpha\beta})^{-+} + (S^{\gamma\bar{\beta}}_{\alpha\bar{\delta}})^{-+}(-1)^{s_\delta - s_\beta}) = W_{LS}\sqrt{2}\int d\vec{r}\psi^*_\beta(\vec{r})\psi_\delta(\vec{r})[\nabla_0\psi^*_\alpha(\vec{r})\nabla_+\psi_\gamma(\vec{r}) \\ -\nabla_+\psi^*_\alpha(\vec{r})\nabla_0\psi_\gamma(\vec{r})](\delta_{s_{\beta_+}s_{\delta_+}} + \delta_{s_{\beta_-}s_{\delta_-}})\end{aligned} \tag{H.70}$$

$$A^{\gamma\delta}_{\alpha\beta}.((S^{\gamma\delta}_{\alpha\beta})^{-+} - (S^{\gamma\bar{\beta}}_{\alpha\bar{\delta}})^{-+}(-1)^{s_\delta - s_\beta}) = 0 \tag{H.71}$$

Then, the field reads:

$$\boxed{\begin{aligned}\Gamma^{\tau-+}_{\alpha\gamma} = W_{LS}\sqrt{2}\sum_{\beta\delta>}\int d\vec{r}\psi^*_\beta(\vec{r})\psi_\delta(\vec{r})[\nabla_0\psi^*_\alpha(\vec{r})\nabla_+\psi_\gamma(\vec{r}) \\ -\nabla_+\psi^*_\alpha(\vec{r})\nabla_0\psi_\gamma(\vec{r})][\rho^{\bar{\tau}++}_{\delta\beta} + \rho^{\bar{\tau}--}_{\delta\beta} + 2(\rho^{\tau++}_{\delta\beta} + \rho^{\tau--}_{\delta\beta})]\end{aligned}} \tag{H.72}$$

We decompose Eq.(H.72) with the X and Y matrices defined in section H.6.1 and eventually find the formula used in the HFB3 code:

$$\boxed{\Gamma^{\tau-+}_{\alpha\gamma} = W_{LS} \sum_{\beta\delta>} \sqrt{2}[Y^{(1)}_{z_{\alpha\gamma}} Y^{(2)}_{r_{\alpha\gamma}} - Y^{(2)}_{z_{\alpha\gamma}} Y^{(3)}_{r_{\alpha\gamma}}] X^{(3)}_{r_{\delta\beta}} X^{(2)}_{z_{\delta\beta}} R^{(2)}_{\delta\beta}}$$

Block $+-$:

Here, we consider the spins ($\alpha \uparrow, \gamma \downarrow$). Thanks to the symmetry of the mean field, we directly have:

$$\boxed{\Gamma^{\tau+-}_{\alpha\gamma} = \Gamma^{\tau-+}_{\gamma\alpha}} \tag{H.73}$$

H.4 Collective fields

This part aims to give an expression of the collective contact spin-orbit mean field in the more complex case when ρ^{01} is no longer symmetric and the two harmonic oscillator bases $\{0\}$ and $\{1\}$ are different. These derivations are useful to evaluate quantities of the following type :

$$\langle \Phi_0 | \hat{H} | \Phi_1 \rangle \tag{H.74}$$

These quantities are not only useful in the SCIM approach but appear in many situations as for instance in the expression of the true TDGCM mass and collective potential.

H.4.1 Collective mean field

The collective contact spin-orbit mean field reads as follows:

$$\bar{\Gamma}_{\alpha\gamma} = \sum_{\beta\delta} \bar{E}^{\gamma\delta}_{\alpha\beta} . S^{\gamma\delta}_{\alpha\beta} [\delta_{\tau_\alpha\tau_\gamma}\delta_{\tau_\beta\tau_\delta} + \delta_{\tau_\alpha\tau_\delta}\delta_{\tau_\beta\tau_\gamma}] \rho^{01}_{\delta\beta} \tag{H.75}$$

The isospin is handled easily:

$$\bar{\Gamma}^{\tau}_{\alpha\gamma} = \sum_{\beta\delta} \bar{E}^{\gamma\delta}_{\alpha\beta} . S^{\gamma\delta}_{\alpha\beta} [1 + \delta_{\tau\tau'}] \rho^{01\tau'}_{\delta\beta} \tag{H.76}$$

By analogy with Eq.(H.46), we decompose the spatial part $\bar{E}$:

$$\begin{cases} \bar{E}^{\gamma\delta}_{\alpha\beta} = \bar{A}^{\gamma\delta}_{\alpha\beta} + \bar{A}^{\delta\gamma}_{\beta\alpha} \\ \bar{A}^{\gamma\delta}_{\alpha\beta} = i\frac{W_{LS}}{2} \int d\vec{r} \psi^*_\alpha(\vec{r}, b_0) \psi_\gamma(\vec{r}, b_1) (\overrightarrow{\nabla} \psi^*_\beta(\vec{r}, b_0) \wedge \overrightarrow{\nabla} \psi_\delta(\vec{r}, b_1)) \end{cases} \tag{H.77}$$

The full expression of the wedge product $\overrightarrow{\nabla} \psi^*_\beta(\vec{r}, b_0) \wedge \overrightarrow{\nabla} \psi_\delta(\vec{r}, b_1)$ will be useful in the following:

$$\begin{pmatrix} \frac{i}{\sqrt{2}}[(\nabla_- + \nabla_+)\psi^*_\beta(\vec{r},b_0)\nabla_0\psi_\delta(\vec{r},b_1) - \nabla_0\psi^*_\beta(\vec{r},b_0)(\nabla_- + \nabla_+)\psi_\delta(\vec{r},b_1)] \\ \frac{1}{\sqrt{2}}[\nabla_0\psi^*_\beta(\vec{r},b_0)(\nabla_- - \nabla_+)\psi_\delta(\vec{r},b_1) - (\nabla_- - \nabla_+)\psi^*_\beta(\vec{r},b_0)\nabla_0\psi_\delta(\vec{r},b_1)] \\ i[\nabla_-\psi^*_\beta(\vec{r},b_0)\nabla_+\psi_\delta(\vec{r},b_1) - \nabla_+\psi^*_\beta(\vec{r},b_0)\nabla_-\psi_\delta(\vec{r},b_1)] \end{pmatrix} \tag{H.78}$$

Thanks to Eq.(H.77), the field reads:

$$\bar{\Gamma}^\tau_{\alpha\gamma} = \sum_{\beta\delta}[\bar{A}^{\gamma\delta}_{\alpha\beta} + \bar{A}^{\delta\gamma}_{\beta\alpha}].S^{\gamma\delta}_{\alpha\beta}[1+\delta_{\tau\tau'}]\rho^{01\tau'}_{\delta\beta} \tag{H.79}$$

Then, we use the time-reversal properties of the matrix ρ^{01}:

$$\boxed{\bar{\Gamma}^\tau_{\alpha\gamma} = \sum_{\beta\delta>}[(\bar{A}^{\gamma\delta}_{\alpha\beta} + \bar{A}^{\delta\gamma}_{\beta\alpha}).S^{\gamma\delta}_{\alpha\beta} + (-1)^{s_\delta - s_\beta}(\bar{A}^{\gamma\bar{\delta}}_{\alpha\bar{\beta}} + \bar{A}^{\bar{\delta}\gamma}_{\bar{\beta}\alpha}).S^{\gamma\bar{\delta}}_{\alpha\bar{\beta}}][1+\delta_{\tau\tau'}]\rho^{01\tau'}_{\delta\beta}} \tag{H.80}$$

As ρ^{01} is not symmetric anymore, it is not possible to obtain a more reduced expression. In the following, we explicitly consider the spin blocks.

Block ++:

Here, we consider the spins $(\alpha\uparrow, \gamma\uparrow)$. We start looking at the spin part of the ++ collective mean field:

$$\begin{cases} (S^{\gamma\delta}_{\alpha\beta})^{++} = \begin{pmatrix} \delta_{s_{\beta_+}s_{\delta_-}} + \delta_{s_{\beta_-}s_{\delta_+}} \\ -i(\delta_{s_{\beta_+}s_{\delta_-}} - \delta_{s_{\beta_-}s_{\delta_+}}) \\ 2\delta_{s_{\beta_+}s_{\delta_+}} \end{pmatrix} \\ (-1)^{s_\delta - s_\beta}(S^{\gamma\bar{\delta}}_{\alpha\bar{\beta}})^{++} = \begin{pmatrix} -\delta_{s_{\beta_+}s_{\delta_-}} - \delta_{s_{\beta_-}s_{\delta_+}} \\ i(\delta_{s_{\beta_-}s_{\delta_+}} - \delta_{s_{\beta_+}s_{\delta_-}}) \\ 2\delta_{s_{\beta_-}s_{\delta_-}} \end{pmatrix} \end{cases} \tag{H.81}$$

Then, we develop the dot products between the spatial and spin parts:

$$\begin{aligned} \bar{A}^{\gamma\delta}_{\alpha\beta}.(S^{\gamma\delta}_{\alpha\beta})^{++} = \frac{W_{LS}}{2}\int d\vec{r}\psi^*_\alpha(\vec{r},b_0)\psi_\gamma(\vec{r},b_1)[\sqrt{2}(\nabla_0\psi^*_\beta(\vec{r},b_0)\nabla_-\psi_\delta(\vec{r},b_1) \\ -\nabla_-\psi^*_\beta(\vec{r},b_0)\nabla_0\psi_\delta(\vec{r},b_1))\delta_{s^-_\delta s^+_\beta} \\ +\sqrt{2}(\nabla_0\psi^*_\beta(\vec{r},b_0)\nabla_+\psi_\delta(\vec{r},b_1) - \nabla_+\psi^*_\beta(\vec{r},b_0)\nabla_0\psi_\delta(\vec{r},b_1))\delta_{s^+_\delta s^-_\beta} \\ -2(\nabla_-\psi^*_\beta(\vec{r},b_0)\nabla_+\psi_\delta(\vec{r},b_1) - \nabla_+\psi^*_\beta(\vec{r},b_0)\nabla_-\psi_\delta(\vec{r},b_1))\delta_{s^+_\delta s^+_\beta}] \end{aligned} \tag{H.82}$$

$$\begin{aligned} (-1)^{s_\delta - s_\beta}\bar{A}^{\gamma\bar{\delta}}_{\alpha\bar{\beta}}.(S^{\gamma\bar{\delta}}_{\alpha\bar{\beta}})^{++} = \frac{W_{LS}}{2}\int d\vec{r}\psi^*_\alpha(\vec{r},b_0)\psi_\gamma(\vec{r},b_1)[\sqrt{2}(\nabla_-\psi_\beta(\vec{r},b_0)\nabla_0\psi^*_\delta(\vec{r},b_1) \\ -\nabla_0\psi_\beta(\vec{r},b_0)\nabla_-\psi^*_\delta(\vec{r},b_1))\delta_{s^+_\delta s^-_\beta} \\ +\sqrt{2}(\nabla_+\psi_\beta(\vec{r},b_0)\nabla_0\psi^*_\delta(\vec{r},b_1) - \nabla_0\psi_\beta(\vec{r},b_0)\nabla_+\psi^*_\delta(\vec{r},b_1))\delta_{s^-_\delta s^+_\beta} \\ -2(\nabla_-\psi_\beta(\vec{r},b_0)\nabla_+\psi^*_\delta(\vec{r},b_1) - \nabla_+\psi_\beta(\vec{r},b_0)\nabla_-\psi^*_\delta(\vec{r},b_1))\delta_{s^-_\delta s^-_\beta}] \end{aligned} \tag{H.83}$$

$$\bar{A}^{\delta\gamma}_{\beta\alpha}.(S^{\gamma\delta}_{\alpha\beta})^{++} = \frac{W_{LS}}{2}\int d\vec{r}\psi^*_\beta(\vec{r},b_0)\psi_\delta(\vec{r},b_1)[\sqrt{2}(\nabla_0\psi^*_\alpha(\vec{r},b_0)\nabla_-\psi_\gamma(\vec{r},b_1) \tag{H.84}$$
$$-\nabla_-\psi^*_\alpha(\vec{r},b_0)\nabla_0\psi_\gamma(\vec{r},b_1))\delta_{s^-_\delta s^+_\beta}$$
$$+\sqrt{2}(\nabla_0\psi^*_\alpha(\vec{r},b_0)\nabla_+\psi_\gamma(\vec{r},b_1) - \nabla_+\psi^*_\alpha(\vec{r},b_0)\nabla_0\psi_\gamma(\vec{r},b_1))\delta_{s^+_\delta s^-_\beta}$$
$$-2(\nabla_-\psi^*_\alpha(\vec{r},b_0)\nabla_+\psi_\gamma(\vec{r},b_1) - \nabla_+\psi^*_\alpha(\vec{r},b_0)\nabla_-\psi_\gamma(\vec{r},b_1))\delta_{s^+_\delta s^+_\beta}]$$

$$(-1)^{s_\delta - s_\beta}\bar{A}^{\bar{\delta}\gamma}_{\bar{\beta}\alpha}.(S^{\gamma\bar{\delta}}_{\alpha\bar{\beta}})^{++} = \frac{W_{LS}}{2}\int d\vec{r}\psi_\beta(\vec{r},b_0)\psi^*_\delta(\vec{r},b_1)[-\sqrt{2}(\nabla_0\psi^*_\alpha(\vec{r},b_0)\nabla_-\psi_\gamma(\vec{r},b_1) \tag{H.85}$$
$$-\nabla_-\psi^*_\alpha(\vec{r},b_0)\nabla_0\psi_\gamma(\vec{r},b_1))\delta_{s^+_\delta s^-_\beta}$$
$$-\sqrt{2}(\nabla_0\psi^*_\alpha(\vec{r},b_0)\nabla_+\psi_\gamma(\vec{r},b_1) - \nabla_+\psi^*_\alpha(\vec{r},b_0)\nabla_0\psi_\gamma(\vec{r},b_1))\delta_{s^-_\delta s^+_\beta}$$
$$-2(\nabla_-\psi^*_\alpha(\vec{r},b_0)\nabla_+\psi_\gamma(\vec{r},b_1) - \nabla_+\psi^*_\alpha(\vec{r},b_0)\nabla_-\psi_\gamma(\vec{r},b_1))\delta_{s^-_\delta s^-_\beta}]$$

We gather the equations from Eq.(H.82) to Eq.(H.85) in order to rewrite the collective field:

$$\begin{aligned}
\bar{\Gamma}^{++\tau}_{\alpha\gamma} = W_{LS}\sum_{\delta\beta>}\sqrt{2}\int d\vec{r}\psi^*_\alpha(\vec{r},b_0)\psi_\gamma(\vec{r},b_1)(\nabla_0\psi^*_\beta(\vec{r},b_0)\nabla_-\psi_\delta(\vec{r},b_1)\\
-\nabla_-\psi^*_\beta(\vec{r},b_0)\nabla_0\psi_\delta(\vec{r},b_1))(\rho^{01\bar{\tau}-+}_{\delta\beta} + 2\rho^{01\tau-+}_{\delta\beta})\\
+\sqrt{2}\int d\vec{r}\psi^*_\alpha(\vec{r},b_0)\psi_\gamma(\vec{r},b_1)(\nabla_0\psi^*_\beta(\vec{r},b_0)\nabla_+\psi_\delta(\vec{r},b_1)\\
-\nabla_+\psi^*_\beta(\vec{r},b_0)\nabla_0\psi_\delta(\vec{r},b_1))(\rho^{01\bar{\tau}+-}_{\delta\beta} + 2\rho^{01\tau+-}_{\delta\beta})\\
+\int d\vec{r}\psi^*_\alpha(\vec{r},b_0)\psi_\gamma(\vec{r},b_1)(\nabla_+\psi^*_\beta(\vec{r},b_0)\nabla_-\psi_\delta(\vec{r},b_1)\\
-\nabla_-\psi^*_\beta(\vec{r},b_0)\nabla_+\psi_\delta(\vec{r},b_1))(\rho^{01\bar{\tau}++}_{\delta\beta} - \rho^{01\bar{\tau}--}_{\delta\beta} + 2(\rho^{01\tau++}_{\delta\beta} - \rho^{01\tau--}_{\delta\beta}))\\
+\int d\vec{r}\psi^*_\beta(\vec{r},b_0)\psi_\delta(\vec{r},b_1)(\nabla_+\psi^*_\alpha(\vec{r},b_0)\nabla_-\psi_\gamma(\vec{r},b_1)\\
-\nabla_-\psi^*_\alpha(\vec{r},b_0)\nabla_+\psi_\gamma(\vec{r},b_1))(\rho^{01\bar{\tau}++}_{\delta\beta} + \rho^{01\bar{\tau}--}_{\delta\beta} + 2(\rho^{01\tau++}_{\delta\beta} + \rho^{01\tau--}_{\delta\beta}))\\
+\frac{\sqrt{2}}{2}\int d\vec{r}\psi^*_\beta(\vec{r},b_0)\psi_\delta(\vec{r},b_1)(\nabla_0\psi^*_\alpha(\vec{r},b_0)\nabla_-\psi_\gamma(\vec{r},b_1)\\
-\nabla_-\psi^*_\alpha(\vec{r},b_0)\nabla_0\psi_\gamma(\vec{r},b_1))(\rho^{01\bar{\tau}-+}_{\delta\beta} + 2\rho^{01\tau-+}_{\delta\beta})\\
+\frac{\sqrt{2}}{2}\int d\vec{r}\psi^*_\beta(\vec{r},b_0)\psi_\delta(\vec{r},b_1)(\nabla_0\psi^*_\alpha(\vec{r},b_0)\nabla_+\psi_\gamma(\vec{r},b_1)\\
-\nabla_+\psi^*_\alpha(\vec{r},b_0)\nabla_0\psi_\gamma(\vec{r},b_1))(\rho^{01\bar{\tau}+-}_{\delta\beta} + 2\rho^{01\tau+-}_{\delta\beta})\\
+\frac{\sqrt{2}}{2}\int d\vec{r}\psi^*_\beta(\vec{r},b_0)\psi_\delta(\vec{r},b_1)(\nabla_0\psi_\alpha(\vec{r},b_0)\nabla_-\psi^*_\gamma(\vec{r},b_1)\\
-\nabla_-\psi_\alpha(\vec{r},b_0)\nabla_0\psi^*_\gamma(\vec{r},b_1))(\rho^{01\bar{\tau}-+}_{\delta\beta} + 2\rho^{01\tau-+}_{\delta\beta})\\
+\frac{\sqrt{2}}{2}\int d\vec{r}\psi^*_\beta(\vec{r},b_0)\psi_\delta(\vec{r},b_1)(\nabla_0\psi_\alpha(\vec{r},b_0)\nabla_+\psi^*_\gamma(\vec{r},b_1)\\
-\nabla_+\psi_\alpha(\vec{r},b_0)\nabla_0\psi^*_\gamma(\vec{r},b_1))(\rho^{01\bar{\tau}+-}_{\delta\beta} + 2\rho^{01\tau+-}_{\delta\beta})
\end{aligned} \tag{H.86}$$

The two first integrals in Eq.(H.86) are separated, whereas there are not in the non-collective fields. Moreover, the four last integrals vanish in the non-collective case. We decompose the collective mean field using the matrices $\bar{X}$ and $\bar{Y}$ defined in section H.6.2. The resulting formula is the one implemented in the SCIM code:

$$\begin{aligned}\boxed{\bar{\Gamma}^{++\tau}_{\alpha\gamma} = W_{LS}\sum_{\delta\beta>} \bar{Y}^{(0)}_{z_{\alpha\gamma}}\bar{Y}^{(0)}_{r_{\alpha\gamma}}[\bar{X}^{(4)}_{r_{\delta\beta}}\bar{X}^{(0)}_{z_{\delta\beta}} - \bar{X}^{(5)}_{r_{\delta\beta}}\bar{X}^{(1)}_{z_{\delta\beta}}]\bar{R}^{\tau(3)}_{\delta\beta} + \bar{Y}^{(0)}_{z_{\alpha\gamma}}\bar{Y}^{(1)}_{r_{\alpha\gamma}}\bar{X}^{(3)}_{r_{\delta\beta}}\bar{X}^{(2)}_{z_{\delta\beta}}\bar{R}^{\tau(2)}_{\delta\beta}} \\ +\bar{Y}^{(0)}_{z_{\alpha\gamma}}\bar{Y}^{(0)}_{r_{\alpha\gamma}}[\bar{X}^{(0)}_{r_{\delta\beta}}\bar{X}^{(0)}_{z_{\delta\beta}} - \bar{X}^{(1)}_{r_{\delta\beta}}\bar{X}^{(1)}_{z_{\delta\beta}}]\bar{R}^{\tau(0)}_{\delta\beta} + \bar{Y}^{(0)}_{z_{\alpha\gamma}}\bar{Y}^{(0)}_{r_{\alpha\gamma}}\bar{X}^{(2)}_{r_{\delta\beta}}\bar{X}^{(2)}_{z_{\delta\beta}}\bar{R}^{\tau(1)}_{\delta\beta} \\ +\frac{1}{2}\bar{Y}^{(1)}_{z_{\alpha\gamma}}[\bar{Y}^{(4)}_{r_{\alpha\gamma}} + \bar{Y}^{(6)}_{r_{\alpha\gamma}}][\bar{X}^{(6)}_{r_{\delta\beta}}\bar{X}^{(2)}_{z_{\delta\beta}}\bar{R}^{\tau(0)}_{\delta\beta} - \bar{X}^{(7)}_{r_{\delta\beta}}\bar{X}^{(2)}_{z_{\delta\beta}}\bar{R}^{\tau(3)}_{\delta\beta}] \\ -\frac{1}{2}\bar{Y}^{(2)}_{z_{\alpha\gamma}}[\bar{Y}^{(7)}_{r_{\alpha\gamma}} + \bar{Y}^{(5)}_{r_{\alpha\gamma}}][\bar{X}^{(6)}_{r_{\delta\beta}}\bar{X}^{(2)}_{z_{\delta\beta}}\bar{R}^{\tau(0)}_{\delta\beta} - \bar{X}^{(7)}_{r_{\delta\beta}}\bar{X}^{(2)}_{z_{\delta\beta}}\bar{R}^{\tau(3)}_{\delta\beta}]\end{aligned} \tag{H.87}$$

In addition to the $\bar{X}$ and $\bar{Y}$ we used the following quantities:

$$\begin{cases}\bar{R}^{\tau(0)}_{\delta\beta} = \sqrt{2}(\rho^{01\bar{\tau}+-}_{\delta\beta} + 2\rho^{01\tau+-}_{\delta\beta}) \\ \bar{R}^{\tau(1)}_{\delta\beta} = \rho^{01\bar{\tau}++}_{\delta\beta} - \rho^{01\bar{\tau}--}_{\delta\beta} + 2(\rho^{01\tau++}_{\delta\beta} - \rho^{01\tau--}_{\delta\beta}) \\ \bar{R}^{\tau(2)}_{\delta\beta} = \rho^{01\bar{\tau}++}_{\delta\beta} + \rho^{01\bar{\tau}--}_{\delta\beta} + 2(\rho^{01\tau++}_{\delta\beta} + \rho^{01\tau--}_{\delta\beta}) \\ \bar{R}^{\tau(3)}_{\delta\beta} = \sqrt{2}(\rho^{01\bar{\tau}-+}_{\delta\beta} + 2\rho^{01\tau-+}_{\delta\beta})\end{cases} \tag{H.88}$$

Block $--$:

Here, we consider the spins $(\alpha\downarrow, \gamma\downarrow)$. We start looking at the spin part of the $--$ collective contact spin-orbit mean field:

$$\begin{cases}(S^{\gamma\delta}_{\alpha\beta})^{--} = \begin{pmatrix}\delta_{s_{\beta_+}s_{\delta_-}} + \delta_{s_{\beta_-}s_{\delta_+}} \\ -i(\delta_{s_{\beta_+}s_{\delta_-}} - \delta_{s_{\beta_-}s_{\delta_+}}) \\ -2\delta_{s_{\beta_-}s_{\delta_-}}\end{pmatrix} \\ (-1)^{s_\delta - s_\beta}(S^{\gamma\bar{\delta}}_{\alpha\bar{\beta}})^{--} = \begin{pmatrix}-\delta_{s_{\beta_-}s_{\delta_+}} - \delta_{s_{\beta_+}s_{\delta_-}} \\ i(\delta_{s_{\beta_-}s_{\delta_+}} - \delta_{s_{\beta_+}s_{\delta_-}}) \\ -2\delta_{s_{\beta_+}s_{\delta_+}}\end{pmatrix}\end{cases} \tag{H.89}$$

We then develop the dot products between the spatial and spin parts:

$$\begin{aligned}\bar{A}^{\gamma\delta}_{\alpha\beta}.(S^{\gamma\delta}_{\alpha\beta})^{--} = \frac{W_{LS}}{2}\int d\vec{r}\psi^*_\alpha(\vec{r},b_0)\psi_\gamma(\vec{r},b_1)[\sqrt{2}(\nabla_0\psi^*_\beta(\vec{r},b_0)\nabla_-\psi_\delta(\vec{r},b_1) \\ -\nabla_-\psi^*_\beta(\vec{r},b_0)\nabla_0\psi_\delta(\vec{r},b_1))\delta_{s_\delta^- s_\beta^+} \\ +\sqrt{2}(\nabla_0\psi^*_\beta(\vec{r},b_0)\nabla_+\psi_\delta(\vec{r},b_1) - \nabla_+\psi^*_\beta(\vec{r},b_0)\nabla_0\psi_\delta(\vec{r},b_1))\delta_{s_\delta^+ s_\beta^-} \\ +2(\nabla_-\psi^*_\beta(\vec{r},b_0)\nabla_+\psi_\delta(\vec{r},b_1) - \nabla_+\psi^*_\beta(\vec{r},b_0)\nabla_-\psi_\delta(\vec{r},b_1))\delta_{s_\delta^- s_\beta^-}]\end{aligned} \tag{H.90}$$

$$\begin{aligned}(-1)^{s_\delta - s_\beta}\bar{A}^{\gamma\bar{\delta}}_{\alpha\bar{\beta}}.(S^{\gamma\bar{\delta}}_{\alpha\bar{\beta}})^{--} = \frac{W_{LS}}{2}\int d\vec{r}\psi^*_\alpha(\vec{r},b_0)\psi_\gamma(\vec{r},b_1)[\sqrt{2}(\nabla_-\psi_\beta(\vec{r},b_0)\nabla_0\psi^*_\delta(\vec{r},b_1) \\ -\nabla_0\psi_\beta(\vec{r},b_0)\nabla_-\psi^*_\delta(\vec{r},b_1))\delta_{s_\delta^+ s_\beta^-} \\ +\sqrt{2}(\nabla_+\psi_\beta(\vec{r},b_0)\nabla_0\psi^*_\delta(\vec{r},b_1) - \nabla_0\psi_\beta(\vec{r},b_0)\nabla_+\psi^*_\delta(\vec{r},b_1))\delta_{s_\delta^- s_\beta^+} \\ +2(\nabla_-\psi_\beta(\vec{r},b_0)\nabla_+\psi^*_\delta(\vec{r},b_1) - \nabla_+\psi_\beta(\vec{r},b_0)\nabla_-\psi^*_\delta(\vec{r},b_1))\delta_{s_\delta^+ s_\beta^+}]\end{aligned} \tag{H.91}$$

$$\bar{A}^{\delta\gamma}_{\beta\alpha}.(S^{\gamma\delta}_{\alpha\beta})^{--} = \frac{W_{LS}}{2}\int d\vec{r}\psi^*_\beta(\vec{r},b_0)\psi_\delta(\vec{r},b_1)[\sqrt{2}(\nabla_0\psi^*_\alpha(\vec{r},b_0)\nabla_-\psi_\gamma(\vec{r},b_1) \tag{H.92}$$
$$-\nabla_-\psi^*_\alpha(\vec{r},b_0)\nabla_0\psi_\gamma(\vec{r},b_1))\delta_{s^-_\delta s^+_\beta}$$
$$+\sqrt{2}(\nabla_0\psi^*_\alpha(\vec{r},b_0)\nabla_+\psi_\gamma(\vec{r},b_1) - \nabla_+\psi^*_\alpha(\vec{r},b_0)\nabla_0\psi_\gamma(\vec{r},b_1))\delta_{s^+_\delta s^-_\beta}$$
$$+2(\nabla_-\psi^*_\alpha(\vec{r},b_0)\nabla_+\psi_\gamma(\vec{r},b_1) - \nabla_+\psi^*_\alpha(\vec{r},b_0)\nabla_-\psi_\gamma(\vec{r},b_1))\delta_{s^-_\delta s^-_\beta}]$$

$$(-1)^{s_\delta - s_\beta}\bar{A}^{\bar{\delta}\gamma}_{\bar{\beta}\alpha}.(S^{\gamma\bar{\delta}}_{\alpha\bar{\beta}})^{--} = \frac{W_{LS}}{2}\int d\vec{r}\psi_\beta(\vec{r},b_0)\psi^*_\delta(\vec{r},b_1)[-\sqrt{2}(\nabla_0\psi^*_\alpha(\vec{r},b_0)\nabla_-\psi_\gamma(\vec{r},b_1) \tag{H.93}$$
$$-\nabla_-\psi^*_\alpha(\vec{r},b_0)\nabla_0\psi_\gamma(\vec{r},b_1))\delta_{s^+_\delta s^-_\beta}$$
$$-\sqrt{2}(\nabla_0\psi^*_\alpha(\vec{r},b_0)\nabla_+\psi_\gamma(\vec{r},b_1) - \nabla_+\psi^*_\alpha(\vec{r},b_0)\nabla_0\psi_\gamma(\vec{r},b_1))\delta_{s^-_\delta s^+_\beta}$$
$$+2(\nabla_-\psi^*_\alpha(\vec{r},b_0)\nabla_+\psi_\gamma(\vec{r},b_1) - \nabla_+\psi^*_\alpha(\vec{r},b_0)\nabla_-\psi_\gamma(\vec{r},b_1))\delta_{s^+_\delta s^+_\beta}]$$

We gather the equations from Eq.(H.90) to Eq.(H.93) and write the collective field:

$$\begin{aligned}
\bar{\Gamma}^{--\tau}_{\alpha\gamma} = W_{LS}\sum_{\delta\beta>}\sqrt{2}\int d\vec{r}\psi^*_\alpha(\vec{r},b_0)\psi_\gamma(\vec{r},b_1)(\nabla_0\psi^*_\beta(\vec{r},b_0)\nabla_-\psi_\delta(\vec{r},b_1)\\
-\nabla_-\psi^*_\beta(\vec{r},b_0)\nabla_0\psi_\delta(\vec{r},b_1))(\rho^{01\bar{\tau}-+}_{\delta\beta} + 2\rho^{01\tau-+}_{\delta\beta})\\
+\sqrt{2}\int d\vec{r}\psi^*_\alpha(\vec{r},b_0)\psi_\gamma(\vec{r},b_1)(\nabla_0\psi^*_\beta(\vec{r},b_0)\nabla_+\psi_\delta(\vec{r},b_1)\\
-\nabla_+\psi^*_\beta(\vec{r},b_0)\nabla_0\psi_\delta(\vec{r},b_1))(\rho^{01\bar{\tau}+-}_{\delta\beta} + 2\rho^{01\tau+-}_{\delta\beta})\\
+\int d\vec{r}\psi^*_\alpha(\vec{r},b_0)\psi_\gamma(\vec{r},b_1)(\nabla_+\psi^*_\beta(\vec{r},b_0)\nabla_-\psi_\delta(\vec{r},b_1)\\
-\nabla_-\psi^*_\beta(\vec{r},b_0)\nabla_+\psi_\delta(\vec{r},b_1))(\rho^{01\bar{\tau}++}_{\delta\beta} - \rho^{01\bar{\tau}--}_{\delta\beta} + 2(\rho^{01\tau++}_{\delta\beta} - \rho^{01\tau--}_{\delta\beta}))\\
-\int d\vec{r}\psi^*_\beta(\vec{r},b_0)\psi_\delta(\vec{r},b_1)(\nabla_+\psi^*_\alpha(\vec{r},b_0)\nabla_-\psi_\gamma(\vec{r},b_1)\\
-\nabla_-\psi^*_\alpha(\vec{r},b_0)\nabla_+\psi_\gamma(\vec{r},b_1))(\rho^{01\bar{\tau}++}_{\delta\beta} + \rho^{01\bar{\tau}--}_{\delta\beta} + 2(\rho^{01\tau++}_{\delta\beta} + \rho^{01\tau--}_{\delta\beta}))\\
+\frac{\sqrt{2}}{2}\int d\vec{r}\psi^*_\beta(\vec{r},b_0)\psi_\delta(\vec{r},b_1)(\nabla_0\psi^*_\alpha(\vec{r},b_0)\nabla_-\psi_\gamma(\vec{r},b_1)\\
-\nabla_-\psi^*_\alpha(\vec{r},b_0)\nabla_0\psi_\gamma(\vec{r},b_1))(\rho^{01\bar{\tau}-+}_{\delta\beta} + 2\rho^{01\tau-+}_{\delta\beta})\\
+\frac{\sqrt{2}}{2}\int d\vec{r}\psi^*_\beta(\vec{r},b_0)\psi_\delta(\vec{r},b_1)(\nabla_0\psi^*_\alpha(\vec{r},b_0)\nabla_+\psi_\gamma(\vec{r},b_1)\\
-\nabla_+\psi^*_\alpha(\vec{r},b_0)\nabla_0\psi_\gamma(\vec{r},b_1))(\rho^{01\bar{\tau}+-}_{\delta\beta} + 2\rho^{01\tau+-}_{\delta\beta})\\
+\frac{\sqrt{2}}{2}\int d\vec{r}\psi^*_\beta(\vec{r},b_0)\psi_\delta(\vec{r},b_1)(\nabla_0\psi_\alpha(\vec{r},b_0)\nabla_-\psi^*_\gamma(\vec{r},b_1)\\
-\nabla_-\psi_\alpha(\vec{r},b_0)\nabla_0\psi^*_\gamma(\vec{r},b_1))(\rho^{01\bar{\tau}-+}_{\delta\beta} + 2\rho^{01\tau-+}_{\delta\beta})\\
+\frac{\sqrt{2}}{2}\int d\vec{r}\psi^*_\beta(\vec{r},b_0)\psi_\delta(\vec{r},b_1)(\nabla_0\psi_\alpha(\vec{r},b_0)\nabla_+\psi^*_\gamma(\vec{r},b_1)\\
-\nabla_+\psi_\alpha(\vec{r},b_0)\nabla_0\psi^*_\gamma(\vec{r},b_1))(\rho^{01\bar{\tau}+-}_{\delta\beta} + 2\rho^{01\tau+-}_{\delta\beta})
\end{aligned} \tag{H.94}$$

The only difference with the block ++ is the minus sign in the fourth integral. Using the $\bar{X}$ and $\bar{Y}$ matrices defined in section H.6.2, we can finally write the formula implemented in the SCIM code:

$$\begin{aligned}\bar{\Gamma}^{--\tau}_{\alpha\gamma} = W_{LS}\sum_{\delta\beta>} &\bar{Y}^{(0)}_{z_{\alpha\gamma}}\bar{Y}^{(0)}_{r_{\alpha\gamma}}[\bar{X}^{(4)}_{r_{\delta\beta}}\bar{X}^{(0)}_{z_{\delta\beta}} - \bar{X}^{(5)}_{r_{\delta\beta}}\bar{X}^{(1)}_{z_{\delta\beta}}]\bar{R}^{\tau(3)}_{\delta\beta} - \bar{Y}^{(0)}_{z_{\alpha\gamma}}\bar{Y}^{(1)}_{r_{\alpha\gamma}}\bar{X}^{(3)}_{r_{\delta\beta}}\bar{X}^{(2)}_{z_{\delta\beta}}\bar{R}^{\tau(2)}_{\delta\beta} \\ &+\bar{Y}^{(0)}_{z_{\alpha\gamma}}\bar{Y}^{(0)}_{r_{\alpha\gamma}}[\bar{X}^{(0)}_{r_{\delta\beta}}\bar{X}^{(0)}_{z_{\delta\beta}} - \bar{X}^{(1)}_{r_{\delta\beta}}\bar{X}^{(1)}_{z_{\delta\beta}}]\bar{R}^{\tau(0)}_{\delta\beta} + \bar{Y}^{(0)}_{z_{\alpha\gamma}}\bar{Y}^{(0)}_{r_{\alpha\gamma}}\bar{X}^{(2)}_{r_{\delta\beta}}\bar{X}^{(2)}_{z_{\delta\beta}}\bar{R}^{\tau(1)}_{\delta\beta} \\ &+\frac{1}{2}\bar{Y}^{(1)}_{z_{\alpha\gamma}}[\bar{Y}^{(4)}_{r_{\alpha\gamma}} + \bar{Y}^{(6)}_{r_{\alpha\gamma}}][\bar{X}^{(6)}_{r_{\delta\beta}}\bar{X}^{(2)}_{z_{\delta\beta}}\bar{R}^{\tau(0)}_{\delta\beta} - \bar{X}^{(7)}_{r_{\delta\beta}}\bar{X}^{(2)}_{z_{\delta\beta}}\bar{R}^{\tau(3)}_{\delta\beta}] \\ &-\frac{1}{2}\bar{Y}^{(2)}_{z_{\alpha\gamma}}[\bar{Y}^{(7)}_{r_{\alpha\gamma}} + \bar{Y}^{(5)}_{r_{\alpha\gamma}}][\bar{X}^{(6)}_{r_{\delta\beta}}\bar{X}^{(2)}_{z_{\delta\beta}}\bar{R}^{\tau(0)}_{\delta\beta} - \bar{X}^{(7)}_{r_{\delta\beta}}\bar{X}^{(2)}_{z_{\delta\beta}}\bar{R}^{\tau(3)}_{\delta\beta}]\end{aligned} \tag{H.95}$$

Block −+:

Here, we consider the spins ($\alpha\downarrow, \gamma\uparrow$). We start looking at the spin part of the −+ collective mean field:

$$\begin{cases}(S^{\gamma\delta}_{\alpha\beta})^{-+} = \begin{pmatrix}\delta_{s_{\beta_+}s_{\delta_+}} + \delta_{s_{\beta_-}s_{\delta_-}} \\ i(\delta_{s_{\beta_+}s_{\delta_+}} + \delta_{s_{\beta_-}s_{\delta_-}}) \\ 0\end{pmatrix} \\ (-1)^{s_\delta - s_\beta}(S^{\gamma\bar{\delta}}_{\alpha\bar{\beta}})^{-+} = \begin{pmatrix}\delta_{s_{\beta_+}s_{\delta_+}} + \delta_{s_{\beta_-}s_{\delta_-}} \\ i(\delta_{s_{\beta_+}s_{\delta_+}} + \delta_{s_{\beta_-}s_{\delta_-}}) \\ 0\end{pmatrix}\end{cases} \tag{H.96}$$

We develop the dot products between the spatial and spin parts:

$$\begin{aligned}\bar{A}^{\gamma\delta}_{\alpha\beta}.(S^{\gamma\delta}_{\alpha\beta})^{-+} = \frac{W_{LS}}{\sqrt{2}}\int d\vec{r}\psi^*_\alpha(\vec{r},b_0)\psi_\gamma(\vec{r},b_1)(\nabla_0\psi^*_\beta(\vec{r},b_0)\nabla_+\psi_\delta(\vec{r},b_1) \\ -\nabla_+\psi^*_\beta(\vec{r},b_0)\nabla_0\psi_\delta(\vec{r},b_1))\delta_{s_\delta s_\beta}\end{aligned} \tag{H.97}$$

$$\begin{aligned}(-1)^{s_\delta - s_\beta}\bar{A}^{\gamma\bar{\delta}}_{\alpha\bar{\beta}}.(S^{\gamma\bar{\delta}}_{\alpha\bar{\beta}})^{-+} = \frac{W_{LS}}{\sqrt{2}}\int d\vec{r}\psi^*_\alpha(\vec{r},b_0)\psi_\gamma(\vec{r},b_1)(\nabla_0\psi_\beta(\vec{r},b_0)\nabla_+\psi^*_\delta(\vec{r},b_1) \\ -\nabla_+\psi_\beta(\vec{r},b_0)\nabla_0\psi^*_\delta(\vec{r},b_1))\delta_{s_\delta s_\beta}\end{aligned} \tag{H.98}$$

$$\begin{aligned}\bar{A}^{\delta\gamma}_{\beta\alpha}.(S^{\gamma\delta}_{\alpha\beta})^{-+} = \frac{W_{LS}}{\sqrt{2}}\int d\vec{r}\psi^*_\beta(\vec{r},b_0)\psi_\delta(\vec{r},b_1)(\nabla_0\psi^*_\alpha(\vec{r},b_0)\nabla_+\psi_\gamma(\vec{r},b_1) \\ -\nabla_+\psi^*_\alpha(\vec{r},b_0)\nabla_0\psi_\gamma(\vec{r},b_1))\delta_{s_\delta s_\beta}\end{aligned} \tag{H.99}$$

$$\begin{aligned}(-1)^{s_\delta - s_\beta}\bar{A}^{\bar{\delta}\gamma}_{\bar{\beta}\alpha}.(S^{\gamma\bar{\delta}}_{\alpha\bar{\beta}})^{-+} = \frac{W_{LS}}{\sqrt{2}}\int d\vec{r}\psi_\beta(\vec{r},b_0)\psi^*_\delta(\vec{r},b_1)(\nabla_0\psi^*_\alpha(\vec{r},b_0)\nabla_+\psi_\gamma(\vec{r},b_1) \\ -\nabla_+\psi^*_\alpha(\vec{r},b_0)\nabla_0\psi_\gamma(\vec{r},b_1))\delta_{s_\delta s_\beta}\end{aligned} \tag{H.100}$$

We gather the equations from Eq.(H.97) to Eq.(H.100) to rewrite the collective field:

$$\begin{aligned}\bar{\Gamma}^{-+\tau}_{\alpha\gamma} = W_{LS}\sum_{\delta\beta>}\frac{1}{\sqrt{2}}\int d\vec{r}\psi^*_\alpha(\vec{r},b_0)\psi_\gamma(\vec{r},b_1)[\nabla_0\psi^*_\beta(\vec{r},b_0)\nabla_+\psi_\delta(\vec{r},b_1)\\ -\nabla_+\psi^*_\beta(\vec{r},b_0)\nabla_0\psi_\delta(\vec{r},b_1)+\nabla_0\psi_\beta(\vec{r},b_0)\nabla_+\psi^*_\delta(\vec{r},b_1)\\ -\nabla_+\psi_\beta(\vec{r},b_0)\nabla_0\psi^*_\delta(\vec{r},b_1)](\rho^{01\bar{\tau}++}_{\delta\beta}+\rho^{01\bar{\tau}--}_{\delta\beta}+2(\rho^{01\tau++}_{\delta\beta}+\rho^{01\tau--}_{\delta\beta}))\\ +\sqrt{2}\int d\vec{r}\psi^*_\beta(\vec{r},b_0)\psi_\delta(\vec{r},b_1)(\nabla_0\psi^*_\alpha(\vec{r},b_0)\nabla_+\psi_\gamma(\vec{r},b_1)\\ -\nabla_+\psi^*_\alpha(\vec{r},b_0)\nabla_0\psi_\gamma(\vec{r},b_1))(\rho^{01\bar{\tau}++}_{\delta\beta}+\rho^{01\bar{\tau}--}_{\delta\beta}+2(\rho^{01\tau++}_{\delta\beta}+\rho^{01\tau--}_{\delta\beta}))\end{aligned} \tag{H.101}$$

With the $\bar{X}$ and $\bar{Y}$ matrices defined in section H.6.2 we eventually find the expression used in the SCIM code:

$$\begin{aligned}\bar{\Gamma}^{-+\tau}_{\alpha\gamma} = W_{LS}\sum_{\delta\beta>}\sqrt{2}[\bar{Y}^{(1)}_{z_{\alpha\gamma}}\bar{Y}^{(2)}_{r_{\alpha\gamma}}-\bar{Y}^{(2)}_{z_{\alpha\gamma}}\bar{Y}^{(3)}_{z_{\alpha\gamma}}]\bar{X}^{(3)}_{r_{\delta\beta}}\bar{X}^{(2)}_{z_{\delta\beta}}\bar{R}^{\tau(2)}_{\delta\beta}\\ +\frac{1}{\sqrt{2}}\bar{Y}^{(0)}_{z_{\alpha\gamma}}\bar{Y}^{(10)}_{r_{\alpha\gamma}}[\bar{X}^{(8)}_{r_{\delta\beta}}\bar{X}^{(0)}_{z_{\delta\beta}}-\bar{X}^{(9)}_{r_{\delta\beta}}\bar{X}^{(1)}_{z_{\delta\beta}}+\bar{X}^{(10)}_{r_{\delta\beta}}\bar{X}^{(0)}_{z_{\delta\beta}}-\bar{X}^{(11)}_{r_{\delta\beta}}\bar{X}^{(1)}_{z_{\delta\beta}}]\bar{R}^{\tau(2)}_{\delta\beta}\end{aligned} \tag{H.102}$$

Block $+-$:

Here, we consider the spins ($\alpha\uparrow,\gamma\downarrow$). We start looking at the spin part of the $+-$ collective mean field:

$$\begin{cases}(S^{\gamma\delta}_{\alpha\beta})^{+-} = \begin{pmatrix}\delta_{s_{\beta_+}s_{\delta_+}}+\delta_{s_{\beta_-}s_{\delta_-}}\\ -i(\delta_{s_{\beta_+}s_{\delta_+}}+\delta_{s_{\beta_-}s_{\delta_-}})\\ 0\end{pmatrix}\\ (-1)^{s_\delta-s_\beta}(S^{\gamma\bar{\delta}}_{\alpha\bar{\beta}})^{+-} = \begin{pmatrix}\delta_{s_{\beta_+}s_{\delta_+}}+\delta_{s_{\beta_-}s_{\delta_-}}\\ -i(\delta_{s_{\beta_+}s_{\delta_+}}+\delta_{s_{\beta_-}s_{\delta_-}})\\ 0\end{pmatrix}\end{cases} \tag{H.103}$$

By analogy with the $+-$ part, we directly write the collective field:

$$\begin{aligned}\bar{\Gamma}^{+-\tau}_{\alpha\gamma} = W_{LS}\sum_{\delta\beta>}\frac{1}{\sqrt{2}}\int d\vec{r}\psi^*_\alpha(\vec{r},b_0)\psi_\gamma(\vec{r},b_1)[\nabla_0\psi^*_\beta(\vec{r},b_0)\nabla_-\psi_\delta(\vec{r},b_1)\\ -\nabla_-\psi^*_\beta(\vec{r},b_0)\nabla_0\psi_\delta(\vec{r},b_1)+\nabla_0\psi_\beta(\vec{r},b_0)\nabla_-\psi^*_\delta(\vec{r},b_1)\\ -\nabla_-\psi_\beta(\vec{r},b_0)\nabla_0\psi^*_\delta(\vec{r},b_1)](\rho^{01\bar{\tau}++}_{\delta\beta}+\rho^{01\bar{\tau}--}_{\delta\beta}+2(\rho^{01\tau++}_{\delta\beta}+\rho^{01\tau--}_{\delta\beta}))\\ +\sqrt{2}\int d\vec{r}\psi^*_\beta(\vec{r},b_0)\psi_\delta(\vec{r},b_1)(\nabla_0\psi^*_\alpha(\vec{r},b_0)\nabla_-\psi_\gamma(\vec{r},b_1)\\ -\nabla_-\psi^*_\alpha(\vec{r},b_0)\nabla_0\psi_\gamma(\vec{r},b_1))(\rho^{01\bar{\tau}++}_{\delta\beta}+\rho^{01\bar{\tau}--}_{\delta\beta}+2(\rho^{01\tau++}_{\delta\beta}+\rho^{01\tau--}_{\delta\beta}))\end{aligned} \tag{H.104}$$

With the $\bar{X}$ and $\bar{Y}$ matrices defined in section H.6.2 we eventually find the expression used in the SCIM code:

$$\boxed{\begin{aligned}\bar{\Gamma}^{+-\tau}_{\alpha\gamma} = W_{LS}\sum_{\delta\beta>}\sqrt{2}[\bar{Y}^{(1)}_{z_{\alpha\gamma}}\bar{Y}^{(8)}_{r_{\alpha\gamma}} - \bar{Y}^{(2)}_{z_{\alpha\gamma}}\bar{Y}^{(9)}_{z_{\alpha\gamma}}]\bar{X}^{(3)}_{r_{\delta\beta}}\bar{X}^{(2)}_{z_{\delta\beta}}\bar{R}^{\tau(2)}_{\delta\beta}\\ -\frac{1}{\sqrt{2}}\bar{Y}^{(0)}_{z_{\alpha\gamma}}\bar{Y}^{(11)}_{r_{\alpha\gamma}}[\bar{X}^{(8)}_{r_{\delta\beta}}\bar{X}^{(0)}_{z_{\delta\beta}} - \bar{X}^{(9)}_{r_{\delta\beta}}\bar{X}^{(1)}_{z_{\delta\beta}} + \bar{X}^{(10)}_{r_{\delta\beta}}\bar{X}^{(0)}_{z_{\delta\beta}} - \bar{X}^{(11)}_{r_{\delta\beta}}\bar{X}^{(1)}_{z_{\delta\beta}}]\bar{R}^{\tau(2)}_{\delta\beta}\end{aligned}} \tag{H.105}$$

H.5 Excited collective fields

The goal of this part is to give an expression of the new contact spin-orbit fields that appear when intrinsic excitations are added. They are useful to evaluate quantities of the following type :

$$\langle\Phi_0|\bar{\xi}_j\xi_j\hat{H}\xi^+_i\bar{\xi}^+_i|\Phi_1\rangle \tag{H.106}$$

In coherence with the adiabatic fields, the excited pairing fields are intentionally omitted.

H.5.1 Excited collective field $\bar{\Gamma}^{(i)}([W,Z])$

The $\bar{\Gamma}^{(i)}([W,Z])$ contact spin-orbit excited field is defined as follows:

$$\boxed{\begin{aligned}\bar{\Gamma}^{(i)}_{\alpha\gamma}([W,Z]) = \sum_{\beta\delta>}[{}_0\langle\alpha\beta|V^{(SO)}(1-P_rP_\sigma P_\tau)|\gamma\delta\rangle_1\\ +(-1)^{s_\beta-s_\delta}{}_0\langle\alpha\bar{\beta}|V^{(SO)}(1-P_rP_\sigma P_\tau)|\gamma\bar{\delta}\rangle_1]W_{\delta i}Z_{\beta\bar{i}}\end{aligned}} \tag{H.107}$$

Choosing an excitation, we set a specific Ω_i and τ_i. We have therefore $\tau_\beta = \tau_\delta = \tau_i$ and $\Omega_\beta = \Omega_\delta = \Omega_i \geq 0$. Using the quantities $\bar{A}$ defined in Eq.(H.77) and S defined Eq.(H.36), we can separate the spatial and spin parts of the excited field:

$$\boxed{\begin{aligned}\bar{\Gamma}^{(i)\tau}_{\alpha\gamma}([W,Z]) = \sum_{\delta\beta\in(\Omega_i,\tau_i)}[(\bar{A}^{\gamma\delta}_{\alpha\beta} + \bar{A}^{\delta\gamma}_{\beta\alpha}).S^{\gamma\delta}_{\alpha\beta}\\ +(-1)^{s_\delta-s_\beta}(\bar{A}^{\gamma\bar{\delta}}_{\alpha\bar{\beta}} + \bar{A}^{\bar{\delta}\gamma}_{\bar{\beta}\alpha}).S^{\gamma\bar{\delta}}_{\alpha\bar{\beta}}][1+\delta_{\tau\tau_i}]W_{\delta i}Z_{\beta\bar{i}}\end{aligned}} \tag{H.108}$$

We now consider the different spin blocks.

Block ++:

Here, we consider the spins $(\alpha\uparrow, \gamma\uparrow)$. By analogy with the collective mean field, we directly write:

$$
\begin{aligned}
\bar{\Gamma}^{(i)++\tau}_{\alpha\gamma}([W,Z]) = \sum_{\delta\beta\in(\Omega_i,\tau_i)} [\sqrt{2}\int d\vec{r}\psi^*_\alpha(\vec{r},b_0)\psi_\gamma(\vec{r},b_1)(\nabla_0\psi^*_\beta(\vec{r},b_0)\nabla_-\psi_\delta(\vec{r},b_1) \\
-\nabla_-\psi^*_\beta(\vec{r},b_0)\nabla_0\psi_\delta(\vec{r},b_1))W^-_{\delta i}Z^+_{\beta\bar{i}} \\
+\sqrt{2}\int d\vec{r}\psi^*_\alpha(\vec{r},b_0)\psi_\gamma(\vec{r},b_1)(\nabla_0\psi^*_\beta(\vec{r},b_0)\nabla_+\psi_\delta(\vec{r},b_1) \\
-\nabla_+\psi^*_\beta(\vec{r},b_0)\nabla_0\psi_\delta(\vec{r},b_1))W^+_{\delta i}Z^-_{\beta\bar{i}} \\
+\int d\vec{r}\psi^*_\alpha(\vec{r},b_0)\psi_\gamma(\vec{r},b_1)(\nabla_+\psi^*_\beta(\vec{r},b_0)\nabla_-\psi_\delta(\vec{r},b_1) \\
-\nabla_-\psi^*_\beta(\vec{r},b_0)\nabla_+\psi_\delta(\vec{r},b_1))(W^+_{\delta i}Z^+_{\beta\bar{i}} - W^-_{\delta i}Z^-_{\beta\bar{i}}) \\
+\int d\vec{r}\psi^*_\beta(\vec{r},b_0)\psi_\delta(\vec{r},b_1)(\nabla_+\psi^*_\alpha(\vec{r},b_0)\nabla_-\psi_\gamma(\vec{r},b_1) \\
-\nabla_-\psi^*_\alpha(\vec{r},b_0)\nabla_+\psi_\gamma(\vec{r},b_1))(W^+_{\delta i}Z^+_{\beta\bar{i}} + W^-_{\delta i}Z^-_{\beta\bar{i}}) \\
+\frac{\sqrt{2}}{2}\int d\vec{r}\psi^*_\beta(\vec{r},b_0)\psi_\delta(\vec{r},b_1)(\nabla_0\psi^*_\alpha(\vec{r},b_0)\nabla_-\psi_\gamma(\vec{r},b_1) \\
-\nabla_-\psi^*_\alpha(\vec{r},b_0)\nabla_0\psi_\gamma(\vec{r},b_1))W^-_{\delta i}Z^+_{\beta\bar{i}} \\
+\frac{\sqrt{2}}{2}\int d\vec{r}\psi^*_\beta(\vec{r},b_0)\psi_\delta(\vec{r},b_1)(\nabla_0\psi^*_\alpha(\vec{r},b_0)\nabla_+\psi_\gamma(\vec{r},b_1) \\
-\nabla_+\psi^*_\alpha(\vec{r},b_0)\nabla_0\psi_\gamma(\vec{r},b_1))W^+_{\delta i}Z^-_{\beta\bar{i}} \\
+\frac{\sqrt{2}}{2}\int d\vec{r}\psi^*_\beta(\vec{r},b_0)\psi_\delta(\vec{r},b_1)(\nabla_0\psi_\alpha(\vec{r},b_0)\nabla_-\psi^*_\gamma(\vec{r},b_1) \\
-\nabla_-\psi_\alpha(\vec{r},b_0)\nabla_0\psi^*_\gamma(\vec{r},b_1))W^-_{\delta i}Z^+_{\beta\bar{i}} \\
+\frac{\sqrt{2}}{2}\int d\vec{r}\psi^*_\beta(\vec{r},b_0)\psi_\delta(\vec{r},b_1)(\nabla_0\psi_\alpha(\vec{r},b_0)\nabla_+\psi^*_\gamma(\vec{r},b_1) \\
-\nabla_+\psi_\alpha(\vec{r},b_0)\nabla_0\psi^*_\gamma(\vec{r},b_1))W^+_{\delta i}Z^-_{\beta\bar{i}}]W_{LS}[1+\delta_{\tau\tau_i}]
\end{aligned}
\tag{H.109}
$$

With the $\bar{X}$ and $\bar{Y}$ matrices defined in section H.6.2, we eventually find the expression used in the SCIM code:

$$
\begin{aligned}
\bar{\Gamma}^{(i)++\tau}_{\alpha\gamma}([W,Z]) = W_{LS}[1+\delta_{\tau\tau_i}] \sum_{\delta\beta\in(\Omega_i,\tau_i)} \bar{Y}^{(0)}_{z_{\alpha\gamma}}\bar{Y}^{(0)}_{r_{\alpha\gamma}}[\bar{X}^{(4)}_{r_{\delta\beta}}\bar{X}^{(0)}_{z_{\delta\beta}} - \bar{X}^{(5)}_{r_{\delta\beta}}\bar{X}^{(1)}_{z_{\delta\beta}}]WZ^{(3)}_{\delta\beta} \\
+\bar{Y}^{(0)}_{z_{\alpha\gamma}}\bar{Y}^{(0)}_{r_{\alpha\gamma}}[\bar{X}^{(0)}_{r_{\delta\beta}}\bar{X}^{(0)}_{z_{\delta\beta}} - \bar{X}^{(1)}_{r_{\delta\beta}}\bar{X}^{(1)}_{z_{\delta\beta}}]WZ^{(0)}_{\delta\beta} \\
+\bar{Y}^{(0)}_{z_{\alpha\gamma}}\bar{Y}^{(0)}_{r_{\alpha\gamma}}\bar{X}^{(2)}_{r_{\delta\beta}}\bar{X}^{(2)}_{z_{\delta\beta}}WZ^{(1)}_{\delta\beta} + \bar{Y}^{(0)}_{z_{\alpha\gamma}}\bar{Y}^{(1)}_{r_{\alpha\gamma}}\bar{X}^{(3)}_{r_{\delta\beta}}\bar{X}^{(2)}_{z_{\delta\beta}}WZ^{(2)}_{\delta\beta} \\
+\frac{1}{2}\bar{Y}^{(1)}_{z_{\alpha\gamma}}[\bar{Y}^{(4)}_{r_{\alpha\gamma}} + \bar{Y}^{(6)}_{r_{\alpha\gamma}}][\bar{X}^{(6)}_{r_{\delta\beta}}\bar{X}^{(2)}_{z_{\delta\beta}}WZ^{(0)}_{\delta\beta} - \bar{X}^{(7)}_{r_{\delta\beta}}\bar{X}^{(2)}_{z_{\delta\beta}}WZ^{(3)}_{\delta\beta}] \\
-\frac{1}{2}\bar{Y}^{(2)}_{z_{\alpha\gamma}}[\bar{Y}^{(7)}_{r_{\alpha\gamma}} + \bar{Y}^{(5)}_{r_{\alpha\gamma}}][\bar{X}^{(6)}_{r_{\delta\beta}}\bar{X}^{(2)}_{z_{\delta\beta}}WZ^{(0)}_{\delta\beta} - \bar{X}^{(7)}_{r_{\delta\beta}}\bar{X}^{(2)}_{z_{\delta\beta}}WZ^{(3)}_{\delta\beta}]
\end{aligned}
\tag{H.110}
$$

In addition to the $\bar{X}$ and $\bar{Y}$ matrices, we used the following quantities in Eq.(H.110):

$$\begin{cases} WZ^{(0)}_{\delta\beta} = \sqrt{2} W^{+}_{\delta i} Z^{-}_{\beta\bar{i}} \\ WZ^{(1)}_{\delta\beta} = W^{+}_{\delta i} Z^{+}_{\beta\bar{i}} - W^{-}_{\delta i} Z^{-}_{\beta\bar{i}} \\ WZ^{(2)}_{\delta\beta} = W^{+}_{\delta i} Z^{+}_{\beta\bar{i}} + W^{-}_{\delta i} Z^{-}_{\beta\bar{i}} \\ WZ^{(3)}_{\delta\beta} = \sqrt{2} W^{-}_{\delta i} Z^{+}_{\beta\bar{i}} \end{cases} \tag{H.111}$$

Block $--$:

Here, we consider the spins $(\alpha\downarrow, \gamma\downarrow)$. By analogy with the collective mean field, we directly write:

$$\begin{aligned} \bar{\Gamma}^{(i)--\tau}_{\alpha\gamma}([W,Z]) = \sum_{\delta\beta\in(\Omega_i,\tau_i)} [\sqrt{2} \int d\vec{r} \psi^*_\alpha(\vec{r},b_0)\psi_\gamma(\vec{r},b_1)(\nabla_0\psi^*_\beta(\vec{r},b_0)\nabla_-\psi_\delta(\vec{r},b_1) \\ -\nabla_-\psi^*_\beta(\vec{r},b_0)\nabla_0\psi_\delta(\vec{r},b_1))W^-_{\delta i}Z^+_{\beta\bar{i}} \\ +\sqrt{2}\int d\vec{r}\psi^*_\alpha(\vec{r},b_0)\psi_\gamma(\vec{r},b_1)(\nabla_0\psi^*_\beta(\vec{r},b_0)\nabla_+\psi_\delta(\vec{r},b_1) \\ -\nabla_+\psi^*_\beta(\vec{r},b_0)\nabla_0\psi_\delta(\vec{r},b_1))W^+_{\delta i}Z^-_{\beta\bar{i}} \\ +\int d\vec{r}\psi^*_\alpha(\vec{r},b_0)\psi_\gamma(\vec{r},b_1)(\nabla_+\psi^*_\beta(\vec{r},b_0)\nabla_-\psi_\delta(\vec{r},b_1) \\ -\nabla_-\psi^*_\beta(\vec{r},b_0)\nabla_+\psi_\delta(\vec{r},b_1))(W^+_{\delta i}Z^+_{\beta\bar{i}} - W^-_{\delta i}Z^-_{\beta\bar{i}}) \\ -\int d\vec{r}\psi^*_\beta(\vec{r},b_0)\psi_\delta(\vec{r},b_1)(\nabla_+\psi^*_\alpha(\vec{r},b_0)\nabla_-\psi_\gamma(\vec{r},b_1) \\ -\nabla_-\psi^*_\alpha(\vec{r},b_0)\nabla_+\psi_\gamma(\vec{r},b_1))(W^+_{\delta i}Z^+_{\beta\bar{i}} + W^-_{\delta i}Z^-_{\beta\bar{i}}) \\ +\frac{\sqrt{2}}{2}\int d\vec{r}\psi^*_\beta(\vec{r},b_0)\psi_\delta(\vec{r},b_1)(\nabla_0\psi^*_\alpha(\vec{r},b_0)\nabla_-\psi_\gamma(\vec{r},b_1) \\ -\nabla_-\psi^*_\alpha(\vec{r},b_0)\nabla_0\psi_\gamma(\vec{r},b_1))W^-_{\delta i}Z^+_{\beta\bar{i}} \\ +\frac{\sqrt{2}}{2}\int d\vec{r}\psi^*_\beta(\vec{r},b_0)\psi_\delta(\vec{r},b_1)(\nabla_0\psi^*_\alpha(\vec{r},b_0)\nabla_+\psi_\gamma(\vec{r},b_1) \\ -\nabla_+\psi^*_\alpha(\vec{r},b_0)\nabla_0\psi_\gamma(\vec{r},b_1))W^+_{\delta i}Z^-_{\beta\bar{i}} \\ +\frac{\sqrt{2}}{2}\int d\vec{r}\psi^*_\beta(\vec{r},b_0)\psi_\delta(\vec{r},b_1)(\nabla_0\psi_\alpha(\vec{r},b_0)\nabla_-\psi^*_\gamma(\vec{r},b_1) \\ -\nabla_-\psi_\alpha(\vec{r},b_0)\nabla_0\psi^*_\gamma(\vec{r},b_1))W^-_{\delta i}Z^+_{\beta\bar{i}} \\ +\frac{\sqrt{2}}{2}\int d\vec{r}\psi^*_\beta(\vec{r},b_0)\psi_\delta(\vec{r},b_1)(\nabla_0\psi_\alpha(\vec{r},b_0)\nabla_+\psi^*_\gamma(\vec{r},b_1) \\ -\nabla_+\psi_\alpha(\vec{r},b_0)\nabla_0\psi^*_\gamma(\vec{r},b_1))W^+_{\delta i}Z^-_{\beta\bar{i}}]W_{LS}[1+\delta_{\tau\tau_i}] \end{aligned} \tag{H.112}$$

With the $\bar{X}$ and $\bar{Y}$ matrices defined in section H.6.2 we eventually find the expression used in the SCIM code:

$$\begin{aligned}\bar{\Gamma}^{(i)--\tau}_{\alpha\gamma}([W,Z]) = W_{LS}[1+\delta_{\tau\tau_i}] \sum_{\delta\beta\in(\Omega_i,\tau_i)} & \bar{Y}^{(0)}_{z_{\alpha\gamma}}\bar{Y}^{(0)}_{r_{\alpha\gamma}}[\bar{X}^{(4)}_{r_{\delta\beta}}\bar{X}^{(0)}_{z_{\delta\beta}} - \bar{X}^{(5)}_{r_{\delta\beta}}\bar{X}^{(1)}_{z_{\delta\beta}}]WZ^{(3)}_{\delta\beta} \\ & + \bar{Y}^{(0)}_{z_{\alpha\gamma}}\bar{Y}^{(0)}_{r_{\alpha\gamma}}[\bar{X}^{(0)}_{r_{\delta\beta}}\bar{X}^{(0)}_{z_{\delta\beta}} - \bar{X}^{(1)}_{r_{\delta\beta}}\bar{X}^{(1)}_{z_{\delta\beta}}]WZ^{(0)}_{\delta\beta} \\ & + \bar{Y}^{(0)}_{z_{\alpha\gamma}}\bar{Y}^{(0)}_{r_{\alpha\gamma}}\bar{X}^{(2)}_{r_{\delta\beta}}\bar{X}^{(2)}_{z_{\delta\beta}}WZ^{(1)}_{\delta\beta} - \bar{Y}^{(0)}_{z_{\alpha\gamma}}\bar{Y}^{(1)}_{r_{\alpha\gamma}}\bar{X}^{(3)}_{r_{\delta\beta}}\bar{X}^{(2)}_{z_{\delta\beta}}WZ^{(2)}_{\delta\beta} \\ & + \frac{1}{2}\bar{Y}^{(1)}_{z_{\alpha\gamma}}[\bar{Y}^{(4)}_{r_{\alpha\gamma}} + \bar{Y}^{(6)}_{r_{\alpha\gamma}}][\bar{X}^{(6)}_{r_{\delta\beta}}\bar{X}^{(2)}_{z_{\delta\beta}}WZ^{(0)}_{\delta\beta} - \bar{X}^{(7)}_{r_{\delta\beta}}\bar{X}^{(2)}_{z_{\delta\beta}}WZ^{(3)}_{\delta\beta}] \\ & - \frac{1}{2}\bar{Y}^{(2)}_{z_{\alpha\gamma}}[\bar{Y}^{(7)}_{r_{\alpha\gamma}} + \bar{Y}^{(5)}_{r_{\alpha\gamma}}][\bar{X}^{(6)}_{r_{\delta\beta}}\bar{X}^{(2)}_{z_{\delta\beta}}WZ^{(0)}_{\delta\beta} - \bar{X}^{(7)}_{r_{\delta\beta}}\bar{X}^{(2)}_{z_{\delta\beta}}WZ^{(3)}_{\delta\beta}]\end{aligned} \tag{H.113}$$

Block $-+$:

Here, we consider the spins $(\alpha\downarrow, \gamma\uparrow)$. By analogy with the collective mean field, we directly write:

$$\begin{aligned}\bar{\Gamma}^{(i)-+\tau}_{\alpha\gamma}([W,Z]) = \sum_{\delta\beta\in(\Omega_i,\tau_i)} & [\frac{1}{\sqrt{2}}\int d\vec{r}\psi^*_\alpha(\vec{r},b_0)\psi_\gamma(\vec{r},b_1)[\nabla_0\psi^*_\beta(\vec{r},b_0)\nabla_+\psi_\delta(\vec{r},b_1) \\ & - \nabla_+\psi^*_\beta(\vec{r},b_0)\nabla_0\psi_\delta(\vec{r},b_1) + \nabla_0\psi_\beta(\vec{r},b_0)\nabla_+\psi^*_\delta(\vec{r},b_1) \\ & - \nabla_+\psi_\beta(\vec{r},b_0)\nabla_0\psi^*_\delta(\vec{r},b_1)](W^+_{\delta i}Z^+_{\beta\bar{i}} + W^-_{\delta i}Z^-_{\beta\bar{i}}) \\ & + \sqrt{2}\int d\vec{r}\psi^*_\beta(\vec{r},b_0)\psi_\delta(\vec{r},b_1)(\nabla_0\psi^*_\alpha(\vec{r},b_0)\nabla_+\psi_\gamma(\vec{r},b_1) \\ & - \nabla_+\psi^*_\alpha(\vec{r},b_0)\nabla_0\psi_\gamma(\vec{r},b_1))(W^+_{\delta i}Z^+_{\beta\bar{i}} + W^-_{\delta i}Z^-_{\beta\bar{i}})]W_{LS}[1+\delta_{\tau\tau_i}]\end{aligned} \tag{H.114}$$

With the $\bar{X}$ and $\bar{Y}$ matrices defined in section H.6.2 we eventually find the expression used in the SCIM code:

$$\begin{aligned}\bar{\Gamma}^{(i)-+\tau}_{\alpha\gamma}([W,Z]) = W_{LS}[1+\delta_{\tau\tau_i}] \sum_{\delta\beta\in(\Omega_i,\tau_i)} & \sqrt{2}[\bar{Y}^{(1)}_{z_{\alpha\gamma}}\bar{Y}^{(2)}_{r_{\alpha\gamma}} - \bar{Y}^{(2)}_{z_{\alpha\gamma}}\bar{Y}^{(3)}_{z_{\alpha\gamma}}]\bar{X}^{(3)}_{r_{\delta\beta}}\bar{X}^{(2)}_{z_{\delta\beta}}WZ^{(2)}_{\delta\beta} \\ & + \frac{1}{\sqrt{2}}\bar{Y}^{(0)}_{z_{\alpha\gamma}}\bar{Y}^{(10)}_{r_{\alpha\gamma}}[\bar{X}^{(8)}_{r_{\delta\beta}}\bar{X}^{(0)}_{z_{\delta\beta}} - \bar{X}^{(9)}_{r_{\delta\beta}}\bar{X}^{(1)}_{z_{\delta\beta}} + \bar{X}^{(10)}_{r_{\delta\beta}}\bar{X}^{(0)}_{z_{\delta\beta}} - \bar{X}^{(11)}_{r_{\delta\beta}}\bar{X}^{(1)}_{z_{\delta\beta}}]WZ^{(2)}_{\delta\beta}\end{aligned} \tag{H.115}$$

Block $+-$:

Here, we consider the spins $(\alpha\uparrow, \gamma\downarrow)$. By analogy with the collective mean field, we directly write:

$$\begin{aligned}\bar{\Gamma}^{(i)+-\tau}_{\alpha\gamma}([W,Z]) = \sum_{\delta\beta\in(\Omega_i,\tau_i)} & [\frac{1}{\sqrt{2}}\int d\vec{r}\psi^*_\alpha(\vec{r},b_0)\psi_\gamma(\vec{r},b_1)[\nabla_0\psi^*_\beta(\vec{r},b_0)\nabla_-\psi_\delta(\vec{r},b_1) \\ & - \nabla_-\psi^*_\beta(\vec{r},b_0)\nabla_0\psi_\delta(\vec{r},b_1) + \nabla_0\psi_\beta(\vec{r},b_0)\nabla_-\psi^*_\delta(\vec{r},b_1) \\ & - \nabla_-\psi_\beta(\vec{r},b_0)\nabla_0\psi^*_\delta(\vec{r},b_1)](W^+_{\delta i}Z^+_{\beta\bar{i}} + W^-_{\delta i}Z^-_{\beta\bar{i}}) \\ & + \sqrt{2}\int d\vec{r}\psi^*_\beta(\vec{r},b_0)\psi_\delta(\vec{r},b_1)(\nabla_0\psi^*_\alpha(\vec{r},b_0)\nabla_-\psi_\gamma(\vec{r},b_1) \\ & - \nabla_-\psi^*_\alpha(\vec{r},b_0)\nabla_0\psi_\gamma(\vec{r},b_1))(W^+_{\delta i}Z^+_{\beta\bar{i}} + W^-_{\delta i}Z^-_{\beta\bar{i}})]W_{LS}[1+\delta_{\tau\tau_i}]\end{aligned} \tag{H.116}$$

With the $\bar{X}$ and $\bar{Y}$ matrices defined in section H.6.2 we eventually find the expression used in the SCIM code:

$$\begin{aligned}\bar{\Gamma}^{(i)+-\tau}_{\alpha\gamma}([W,Z]) = W_{LS}[1+\delta_{\tau\tau_i}] \sum_{\delta\beta\in(\Omega_i,\tau_i)} \sqrt{2}[\bar{Y}^{(1)}_{z_{\alpha\gamma}}\bar{Y}^{(8)}_{r_{\alpha\gamma}} - \bar{Y}^{(2)}_{z_{\alpha\gamma}}\bar{Y}^{(9)}_{z_{\alpha\gamma}}]\bar{X}^{(3)}_{r_{\delta\beta}}\bar{X}^{(2)}_{z_{\delta\beta}}WZ^{(2)}_{\delta\beta} \\ -\frac{1}{\sqrt{2}}\bar{Y}^{(0)}_{z_{\alpha\gamma}}\bar{Y}^{(11)}_{r_{\alpha\gamma}}[\bar{X}^{(8)}_{r_{\delta\beta}}\bar{X}^{(0)}_{z_{\delta\beta}} - \bar{X}^{(9)}_{r_{\delta\beta}}\bar{X}^{(1)}_{z_{\delta\beta}} + \bar{X}^{(10)}_{r_{\delta\beta}}\bar{X}^{(0)}_{z_{\delta\beta}} - \bar{X}^{(11)}_{r_{\delta\beta}}\bar{X}^{(1)}_{z_{\delta\beta}}]WZ^{(2)}_{\delta\beta}\end{aligned} \tag{H.117}$$

H.6 Integral calculations

All the formulas of the integrals used in the derivations of the contact spin-orbit fields are given here. This section is divided into two parts: the first one is dedicated to the non-collective case, the second one tackles the collective one.

H.6.1 Same bases

In this part, four different integrals have to be evaluated. Each one of these integrals is divided into different X_z, X_r, Y_z and Y_r matrices. This separation is essential to guarantee the numerical performances of the field calculations. We recall thereafter the four integrals we want to evaluate along with their specific m conditions:

Case $(m_\alpha = m_\gamma)$ **and** $(m_\delta = m_\beta - 1)$**:**

$$\begin{aligned}\int d\vec{r}\psi^*_\alpha(\vec{r})\psi_\gamma(\vec{r})[\nabla_0\psi^*_\beta(\vec{r})\nabla_+\psi_\delta(\vec{r}) - \nabla_+\psi^*_\beta(\vec{r})\nabla_0\psi_\delta(\vec{r})] \\ = Y^{(0)}_z Y^{(0)}_r [X^{(0)}_r X^{(0)}_z - X^{(1)}_r X^{(1)}_z]\end{aligned} \tag{H.118}$$

Case $(m_\alpha = m_\gamma)$ **and** $(m_\delta = m_\beta)$**:**

$$\int d\vec{r}\psi^*_\alpha(\vec{r})\psi_\gamma(\vec{r})[\nabla_+\psi^*_\beta(\vec{r})\nabla_-\psi_\delta(\vec{r}) - \nabla_-\psi^*_\beta(\vec{r})\nabla_+\psi_\delta(\vec{r})] = Y^{(0)}_z Y^{(0)}_r X^{(2)}_r X^{(2)}_z \tag{H.119}$$

$$\int d\vec{r}\psi^*_\beta(\vec{r})\psi_\delta(\vec{r})[\nabla_+\psi^*_\alpha(\vec{r})\nabla_-\psi_\gamma(\vec{r}) - \nabla_-\psi^*_\alpha(\vec{r})\nabla_+\psi_\gamma(\vec{r})] = Y^{(0)}_z Y^{(1)}_r X^{(3)}_r X^{(2)}_z \tag{H.120}$$

Case $(m_\alpha = m_\gamma + 1)$ **and** $(m_\delta = m_\beta)$**:**

$$\begin{aligned}\int d\vec{r}\psi^*_\beta(\vec{r})\psi_\delta(\vec{r})[\nabla_0\psi^*_\alpha(\vec{r})\nabla_+\psi_\gamma(\vec{r}) - \nabla_+\psi^*_\alpha(\vec{r})\nabla_0\psi_\gamma(\vec{r})] \\ = [Y^{(1)}_z Y^{(2)}_r - Y^{(2)}_z Y^{(3)}_r]X^{(3)}_r X^{(2)}_z\end{aligned} \tag{H.121}$$

For the sake of compacity, we only present the derivations of the z-integrals and the $r_\perp$-integrals in the most general case, without considering the peculiarities brought by the derivative operators. Once these general formulas are obtained, it is really easy to find the expressions of the X and Y matrices applying the derivative formulas given in Appendix D.

Calculation of the z-integral:

The general model to evaluate all the z-integrals involved in this section reads as follows:

$$\boxed{I_z = \int dz \varphi_{n_{z_\alpha}}(z+d_\alpha)\varphi_{n_{z_\gamma}}(z+d_\gamma)\varphi_{n_{z_\delta}}(z+d_\delta)\varphi_{n_{z_\beta}}(z+d_\beta)} \tag{H.122}$$

We start reducing Eq.(H.122) with the Talman-z coefficients (see Appendix D):

$$I_z = \frac{1}{b_z\sqrt{\pi}} \sum_{n_{z_a}} T^{n_{z_a}}_{(n_{z_\alpha},d_\alpha)(n_{z_\gamma},d_\gamma)} \sum_{n_{z_b}} T^{n_{z_b}}_{(n_{z_\delta},d_\delta)(n_{z_\beta},d_\beta)} \tag{H.123}$$
$$\int dz e^{-\frac{1}{2}(\frac{z+k_{\alpha\gamma}}{b_z})^2} e^{-\frac{1}{2}(\frac{z+k_{\beta\delta}}{b_z})^2} \varphi_{n_{z_a}}(z+k_{\alpha\gamma})\varphi_{n_{z_b}}(z+k_{\beta\delta})$$

With:

$$\begin{cases} k_{\alpha\gamma} = \frac{d_\alpha + d_\gamma}{2} \\ k_{\beta\delta} = \frac{d_\beta + d_\delta}{2} \end{cases} \tag{H.124}$$

Introducing the Moshinsky-z coefficients (see Appendix D) in Eq.(H.123), we get:

$$I_z = \frac{1}{b_z\sqrt{\pi}} \sum_{n_{z_a}} T^{n_{z_a}}_{(n_{z_\alpha},d_\alpha)(n_{z_\gamma},d_\gamma)} \sum_{n_{z_b}} T^{n_{z_b}}_{(n_{z_\delta},d_\delta)(n_{z_\beta},d_\beta)} \sum_{n_{z_c}} \sum_{n_{z_d}} M^{n_{z_c}n_{z_d}}_{n_{z_a}n_{z_b}} \varphi_{n_{z_d}}(d^{\beta\delta}_{\alpha\gamma}) e^{-\frac{1}{2}(\frac{d^{\beta\delta}_{\alpha\gamma}}{b_z})^2} \tag{H.125}$$
$$\int dz e^{-\frac{1}{2}(\frac{\sqrt{2}z+D^{\beta\delta}_{\alpha\gamma}}{b_z})^2} \varphi_{n_{z_c}}(\sqrt{2}z + D^{\beta\delta}_{\alpha\gamma})$$

With:

$$\begin{cases} D^{\beta\delta}_{\alpha\gamma} = \frac{k_{\alpha\gamma}+k_{\beta\delta}}{\sqrt{2}} \\ d^{\beta\delta}_{\alpha\gamma} = \frac{k_{\alpha\gamma}-k_{\beta\delta}}{\sqrt{2}} \end{cases} \tag{H.126}$$

We now set the change of variables ($\sqrt{2}z + D^{\beta\delta}_{\alpha\gamma} \longrightarrow z$) and use the orthonormality of the harmonic oscillator wave functions:

$$I_z = \frac{1}{\sqrt{2b_z\sqrt{\pi}}} \sum_{n_{z_a}} T^{n_{z_a}}_{(n_{z_\alpha},d_\alpha)(n_{z_\gamma},d_\gamma)} \sum_{n_{z_b}} T^{n_{z_b}}_{(n_{z_\delta},d_\delta)(n_{z_\beta},d_\beta)} \sum_{n_{z_d}} M^{0n_{z_d}}_{n_{z_a}n_{z_b}} e^{-\frac{1}{2}(\frac{d^{\beta\delta}_{\alpha\gamma}}{b_z})^2} \varphi_{n_{z_d}}(d^{\beta\delta}_{\alpha\gamma}) \tag{H.127}$$

In Eq.(H.127), n_{z_d} is fully defined by n_{z_a} and n_{z_b}. Indeed, the following relation holds $n_{z_d} = n_{z_a} + n_{z_b}$. Thus, we finally write:

$$\boxed{I_z = \frac{1}{\sqrt{2b_z\sqrt{\pi}}} \sum_{n_{z_a}} T^{n_{z_a}}_{(n_{z_\alpha},d_\alpha)(n_{z_\gamma},d_\gamma)} \sum_{n_{z_b}} T^{n_{z_b}}_{(n_{z_\delta},d_\delta)(n_{z_\beta},d_\beta)} M^{0n_{z_d}}_{n_{z_a}n_{z_b}} e^{-\frac{1}{2}(\frac{d^{\beta\delta}_{\alpha\gamma}}{b_z})^2} \varphi_{n_{z_d}}(d^{\beta\delta}_{\alpha\gamma})} \tag{H.128}$$

Calculation of the $r_\perp$-integral:

The general model to evaluate all the $r_\perp$-integrals involved in this section reads as follows:

$$\boxed{I_r = \int d\vec{r}_\perp \phi^*_{(m_\alpha,n_{\perp_\alpha})}(\vec{r}_\perp)\phi^*_{(m_\beta,n_{\perp_\beta})}(\vec{r}_\perp)\phi_{(m_\delta,n_{\perp_\delta})}(\vec{r}_\perp)\phi_{(m_\gamma,n_{\perp_\gamma})}(\vec{r}_\perp)} \tag{H.129}$$

We start using the Talman-r coefficients (see Appendix D):

$$I_r = \frac{1}{b_r^2\pi}\sum_{n_{\perp_a}} T^{(m_\gamma-m_\alpha,n_{\perp_a})}_{(m_\alpha,n_{\perp_\alpha})(m_\gamma,n_{\perp_\gamma})}\sum_{n_{\perp_b}} T^{(m_\delta-m_\beta,n_{\perp_b})}_{(m_\beta,n_{\perp_\beta})(m_\delta,n_{\perp_\delta})} \tag{H.130}$$
$$\int d\vec{r}_\perp e^{-\frac{1}{2}(\frac{\sqrt{2}r}{b_r})^2}\phi_{(m_\gamma-m_\alpha,n_{\perp_a})}(\vec{r}_\perp)\phi_{(m_\delta-m_\beta,n_{\perp_b})}(\vec{r}_\perp)$$

Introducing the Moshinsky-r coefficients (see Appendix D) in Eq.(H.130), we find:

$$I_r = \frac{1}{b_r^2\pi}\sum_{n_{\perp_a}} T^{(m_\gamma-m_\alpha,n_{\perp_a})}_{(m_\alpha,n_{\perp_\alpha})(m_\gamma,n_{\perp_\gamma})}\sum_{n_{\perp_b}} T^{(m_\delta-m_\beta,n_{\perp_b})}_{(m_\beta,n_{\perp_\beta})(m_\delta,n_{\perp_\delta})}\sum_{m_c}\sum_{m_d}\sum_{n_{\perp_c}}\sum_{n_{\perp_d}} \tag{H.131}$$
$$M^{(m_c,n_{\perp_c})(m_d,n_{\perp_d})}_{(m_\gamma-m_\alpha,n_{\perp_a})(m_\delta-m_\beta,n_{\perp_b})}\phi_{(m_d,n_{\perp_d})}(0)\int d\vec{r}_\perp e^{-\frac{1}{2}(\frac{\sqrt{2}r}{b_r})^2}\phi_{(m_c,n_{\perp_c})}(\sqrt{2}\vec{r}_\perp)$$

We recall the following result:

$$\phi_{(m_d,n_{\perp_d})}(0) = \frac{\delta_{m_d0}}{b_r\sqrt{\pi}} \tag{H.132}$$

Using Eq.(H.132) in combination with the orthonormality of the harmonic oscillator wave functions and a straightforward rescaling, we get:

$$I_r = \frac{\delta_{(m_\alpha+m_\beta=m_\gamma+m_\delta)}}{2b_r^2\pi}\sum_{n_{\perp_a}} T^{(m_\gamma-m_\alpha,n_{\perp_a})}_{(m_\alpha,n_{\perp_\alpha})(m_\gamma,n_{\perp_\gamma})} \tag{H.133}$$
$$\sum_{n_{\perp_b}} T^{(m_\delta-m_\beta,n_{\perp_b})}_{(m_\beta,n_{\perp_\beta})(m_\delta,n_{\perp_\delta})}\sum_{n_{\perp_d}} M^{(0,0)(0,n_{\perp_d})}_{(m_\gamma-m_\alpha,n_{\perp_a})(m_\delta-m_\beta,n_{\perp_b})} \tag{H.134}$$

In Eq.(H.133), the summation over $n_{\perp_d}$ vanishes as it is fully determined by $n_{\perp_a}$ and $n_{\perp_b}$:

$$n_{\perp_d} = n_{\perp_a} + n_{\perp_b} \tag{H.135}$$

We eventually write for the $r_\perp$-integral:

$$\boxed{\begin{aligned} I_r = \frac{\delta_{(m_\alpha+m_\beta=m_\gamma+m_\delta)}}{2b_r^2\pi}\sum_{n_{\perp_a}} T^{(m_\gamma-m_\alpha,n_{\perp_a})}_{(m_\alpha,n_{\perp_\alpha})(m_\gamma,n_{\perp_\gamma})} \\ \sum_{n_{\perp_b}} T^{(m_\delta-m_\beta,n_{\perp_b})}_{(m_\beta,n_{\perp_\beta})(m_\delta,n_{\perp_\delta})} M^{(0,0)(0,n_{\perp_d})}_{(m_\gamma-m_\alpha,n_{\perp_a})(m_\delta-m_\beta,n_{\perp_b})} \end{aligned}} \tag{H.136}$$

We now have everything in hands to give the explicit formulas of the X and Y matrices.

Expression of the X_z quantities:

The expression of the different X_z are given thereafter:

$$\boxed{\begin{aligned} X_z^{(0)} = \frac{1}{2b_z^{3/2}\pi^{1/4}}[\delta_{(n_{z_\beta}>0)}\sqrt{n_{z_\beta}}\sum_{n_{z_b}} T^{n_{z_b}}_{(n_{z_\beta-1},d_\beta)(n_{z_\delta},d_\delta)} \\ -\sqrt{n_{z_\beta}+1}\sum_{n_{z_b}} T^{n_{z_b}}_{(n_{z_\beta+1},d_\beta)(n_{z_\delta},d_\delta)}]M^{0n_{z_d}}_{n_{z_a}n_{z_b}}e^{-\frac{1}{2}(\frac{d^{\beta\delta}_{\alpha\gamma}}{b_z})^2}\varphi_{n_{z_d}}(d^{\beta\delta}_{\alpha\gamma})] \end{aligned}} \tag{H.137}$$

$$\boxed{\begin{aligned} X_z^{(1)} = \frac{1}{2b_z^{3/2}\pi^{1/4}}[\delta_{(n_{z_\delta}>0)}\sqrt{n_{z_\delta}}\sum_{n_{z_b}} T^{n_{z_b}}_{(n_{z_\delta-1},d_\delta)(n_{z_\beta},d_\beta)} \\ -\sqrt{n_{z_\delta}+1}\sum_{n_{z_b}} T^{n_{z_b}}_{(n_{z_\delta+1},d_\delta)(n_{z_\beta},d_\beta)}]M^{0n_{z_d}}_{n_{z_a}n_{z_b}}e^{-\frac{1}{2}(\frac{d^{\beta\delta}_{\alpha\gamma}}{b_z})^2}\varphi_{n_{z_d}}(d^{\beta\delta}_{\alpha\gamma})] \end{aligned}} \tag{H.138}$$

$$\boxed{X_z^{(2)} = \frac{1}{\sqrt{2b_z\sqrt{\pi}}}\sum_{n_{z_b}} T^{n_{z_b}}_{(n_{z_\beta},d_\beta)(n_{z_\delta},d_\delta)}M^{0n_{z_d}}_{n_{z_a}n_{z_b}}e^{-\frac{1}{2}(\frac{d^{\beta\delta}_{\alpha\gamma}}{b_z})^2}\varphi_{n_{z_d}}(d^{\beta\delta}_{\alpha\gamma})} \tag{H.139}$$

Expression of the Y_z quantities:

The expression of the different Y_z are given thereafter:

$$\boxed{Y_z^{(0)} = T^{n_{z_a}}_{(n_{z_\alpha},d_\alpha)(n_{z_\gamma},d_\gamma)}} \tag{H.140}$$

$$\boxed{Y_z^{(1)} = \frac{1}{b_z\sqrt{2}}(\delta_{(n_{z_\alpha}>0)}\sqrt{n_{z_\alpha}}\sum_{n_{z_b}} T^{n_{z_b}}_{(n_{z_\alpha-1},d_\alpha)(n_{z_\gamma},d_\gamma)} - \sqrt{n_{z_\alpha}+1}\sum_{n_{z_b}} T^{n_{z_b}}_{(n_{z_\alpha+1},d_\alpha)(n_{z_\gamma},d_\gamma)})} \tag{H.141}$$

$$\boxed{Y_z^{(2)} = \frac{1}{b_z\sqrt{2}}(\delta_{(n_{z_\gamma}>0)}\sqrt{n_{z_\gamma}}\sum_{n_{z_b}} T^{n_{z_b}}_{(n_{z_\gamma-1},d_\gamma)(n_{z_\alpha},d_\alpha)} - \sqrt{n_{z_\gamma}+1}\sum_{n_{z_b}} T^{n_{z_b}}_{(n_{z_\gamma+1},d_\gamma)(n_{z_\alpha},d_\alpha)})} \tag{H.142}$$

Expression of the X_r quantities:

The expression of the different X_r are given thereafter:

$$\boxed{\begin{aligned} X_r^{(0)} = \frac{1}{b_r^3\pi 2^{3/2}}[\sqrt{m'+n_{\perp_\delta}+1}\sum_{n_{\perp_b}} T^{n_{\perp_b}}_{(m'+1,n_{\perp_\beta})(m'+1,n_{\perp_\delta})} \\ +\delta_{(n_{\perp_\delta}>0)}\sqrt{n_{\perp_\delta}}\sum_{n_{\perp_b}} T^{n_{\perp_b}}_{(m'+1,n_{\perp_\beta})(m'+1,n_{\perp_\delta}-1)}]M^{(0,0)(0,n_{\perp_d})}_{(0,n_{\perp_a})(0,n_{\perp_b})} \end{aligned}} \tag{H.143}$$

$$\boxed{\begin{aligned} X_r^{(1)} = -\frac{1}{b_r^3 \pi 2^{3/2}} [& \sqrt{m' + n_{\perp_\beta} + 1} \sum_{n_{\perp_b}} T^{n_{\perp_b}}_{(m', n_{\perp_\beta})(m', n_{\perp_\delta})} \\ & + \sqrt{n_{\perp_\beta} + 1} \sum_{n_{\perp_b}} T^{n_{\perp_b}}_{(m', n_{\perp_\beta}+1)(m', n_{\perp_\delta})}] M^{(0,0)(0,n_{\perp_d})}_{(0,n_{\perp_a})(0,n_{\perp_b})} \end{aligned}} \tag{H.144}$$

$$\boxed{\begin{aligned} X_r^{(2)} = \frac{\delta_{(m'>0)}}{4 b_r^4 \pi} \sum_{n_{\perp_b}} [& - \sqrt{(m' + n_{\perp_\beta})(m' + n_{\perp_\delta})} T^{n_{\perp_b}}_{(m'-1, n_{\perp_\beta})(m'-1, n_{\perp_\delta})} \\ & - \sqrt{(m' + n_{\perp_\beta})(n_{\perp_\delta} + 1)} T^{n_{\perp_b}}_{(m'-1, n_{\perp_\beta})(m'-1, n_{\perp_\delta}+1)} \\ & - \sqrt{(n_{\perp_\beta} + 1)(m' + n_{\perp_\delta})} T^{n_{\perp_b}}_{(m'-1, n_{\perp_\beta}+1)(m'-1, n_{\perp_\delta})} \\ & - \sqrt{(n_{\perp_\beta} + 1)(n_{\perp_\delta} + 1)} T^{n_{\perp_b}}_{(m'-1, n_{\perp_\beta}+1)(m'-1, n_{\perp_\delta}+1)} \\ & + \sqrt{(m' + n_{\perp_\beta} + 1)(m' + n_{\perp_\delta} + 1)} T^{n_{\perp_b}}_{(m'+1, n_{\perp_\beta})(m'+1, n_{\perp_\delta})} \\ & + \delta_{(n_{\perp_\delta}>0)} \sqrt{(m' + n_{\perp_\beta} + 1) n_{\perp_\delta}} T^{n_{\perp_b}}_{(m'+1, n_{\perp_\beta})(m'+1, n_{\perp_\delta}-1)} \\ & + \delta_{(n_{\perp_\beta}>0)} \sqrt{n_{\perp_\beta} (m' + n_{\perp_\delta} + 1)} T^{n_{\perp_b}}_{(m'+1, n_{\perp_\beta}-1)(m'+1, n_{\perp_\delta})} \\ & + \delta_{(n_{\perp_\delta}>0)} \delta_{(n_{\perp_\beta}>0)} \sqrt{n_{\perp_\beta} n_{\perp_\delta}} T^{n_{\perp_b}}_{(m'+1, n_{\perp_\beta}-1)(m'+1, n_{\perp_\delta}-1)}] M^{(0,0)(0,n_{\perp_d})}_{(0,n_{\perp_a})(0,n_{\perp_b})} \end{aligned}} \tag{H.145}$$

$$\boxed{X_r^{(3)} = T^{n_{\perp_b}}_{(m', n_{\perp_\beta})(m', n_{\perp_\delta})}} \tag{H.146}$$

Expression of the Y_r quantities:

The expression of the different Y_r are given thereafter:

$$\boxed{Y_r^{(0)} = T^{n_{\perp_b}}_{(m, n_{\perp_\alpha})(m, n_{\perp_\gamma})}} \tag{H.147}$$

$$\boxed{\begin{aligned} Y_r^{(1)} = \frac{\delta_{(m>0)}}{4 b_r^4 \pi} \sum_{n_{\perp_b}} [& - \sqrt{(m + n_{\perp_\alpha})(m + n_{\perp_\gamma})} T^{n_{\perp_b}}_{(m-1, n_{\perp_\alpha})(m-1, n_{\perp_\gamma})} \\ & - \sqrt{(m + n_{\perp_\alpha})(n_{\perp_\gamma} + 1)} T^{n_{\perp_b}}_{(m-1, n_{\perp_\alpha})(m-1, n_{\perp_\gamma}+1)} \\ & - \sqrt{(n_{\perp_\alpha} + 1)(m + n_{\perp_\gamma})} T^{n_{\perp_b}}_{(m-1, n_{\perp_\alpha}+1)(m-1, n_{\perp_\gamma})} \\ & - \sqrt{(n_{\perp_\alpha} + 1)(n_{\perp_\gamma} + 1)} T^{n_{\perp_b}}_{(m-1, n_{\perp_\alpha}+1)(m-1, n_{\perp_\gamma}+1)} \\ & + \sqrt{(m + n_{\perp_\alpha} + 1)(m + n_{\perp_\gamma} + 1)} T^{n_{\perp_b}}_{(m+1, n_{\perp_\alpha})(m+1, n_{\perp_\gamma})} \\ & + \delta_{(n_{\perp_\gamma}>0)} \sqrt{(m + n_{\perp_\alpha} + 1) n_{\perp_\gamma}} T^{n_{\perp_b}}_{(m+1, n_{\perp_\alpha})(m+1, n_{\perp_\gamma}-1)} \\ & + \delta_{(n_{\perp_\alpha}>0)} \sqrt{n_{\perp_\alpha} (m' + n_{\perp_\gamma} + 1)} T^{n_{\perp_b}}_{(m+1, n_{\perp_\alpha}-1)(m+1, n_{\perp_\gamma})} \\ & + \delta_{(n_{\perp_\gamma}>0)} \delta_{(n_{\perp_\alpha}>0)} \sqrt{n_{\perp_\alpha} n_{\perp_\gamma}} T^{n_{\perp_b}}_{(m+1, n_{\perp_\alpha}-1)(m+1, n_{\perp_\gamma}-1)}] M^{(0,0)(0,n_{\perp_d})}_{(0,n_{\perp_a})(0,n_{\perp_b})} \end{aligned}} \tag{H.148}$$

$$\boxed{\begin{aligned} Y_r^{(2)} &= \frac{1}{b_r^3\pi 2^{3/2}}[\sqrt{m+n_{\perp_\gamma}}\sum_{n_{\perp_b}} T^{n_{\perp_b}}_{(m,n_{\perp_\alpha})(m,n_{\perp_\gamma})} \\ &+\delta_{(n_{\perp_\gamma}>0)}\sqrt{n_{\perp_\gamma}}\sum_{n_{\perp_b}} T^{n_{\perp_b}}_{(m,n_{\perp_\alpha})(m,n_{\perp_\gamma}-1)}]M^{(0,0)(0,n_{\perp_d})}_{(0,n_{\perp_a})(0,n_{\perp_b})} \end{aligned}} \tag{H.149}$$

$$\boxed{\begin{aligned} Y_r^{(3)} &= -\frac{1}{b_r^3\pi 2^{3/2}}[\sqrt{m+n_{\perp_\alpha}}\sum_{n_{\perp_b}} T^{n_{\perp_b}}_{(m-1,n_{\perp_\alpha})(m-1,n_{\perp_\gamma})} \\ &+\sqrt{n_{\perp_\alpha}+1}\sum_{n_{\perp_b}} T^{n_{\perp_b}}_{(m-1,n_{\perp_\alpha}+1)(m-1,n_{\perp_\gamma})}]M^{(0,0)(0,n_{\perp_d})}_{(0,n_{\perp_a})(0,n_{\perp_b})} \end{aligned}} \tag{H.150}$$

H.6.2 Different bases

In this part, twelve different integrals have to be evaluated. Each one of these integrals is divided into different $\bar{X}_z$, $\bar{X}_r$, $\bar{Y}_z$ and $\bar{Y}_r$ matrices. This separation is essential to guarantee the numerical performances of the field calculations. We recall thereafter the twelve integrals we want to evaluate along with their specific m conditions:

Case $(m_\alpha = m_\gamma)$ **and** $(m_\delta = m_\beta - 1)$**:**

$$\begin{aligned} \int d\vec{r}\psi^*_\alpha(\vec{r},b_0)\psi_\gamma(\vec{r},b_1)(\nabla_0\psi^*_\beta(\vec{r},b_0)\nabla_+\psi_\delta(\vec{r},b_1) - \nabla_+\psi^*_\beta(\vec{r},b_0)\nabla_0\psi_\delta(\vec{r},b_1)) \\ = \bar{Y}_z^{(0)}\bar{Y}_r^{(0)}[\bar{X}_r^{(0)}\bar{X}_z^{(0)} - \bar{X}_r^{(1)}\bar{X}_z^{(1)}] \end{aligned} \tag{H.151}$$

$$\begin{aligned} \int d\vec{r}\psi^*_\beta(\vec{r},b_0)\psi_\delta(\vec{r},b_1)(\nabla_0\psi_\alpha(\vec{r},b_0)\nabla_+\psi^*_\gamma(\vec{r},b_1) - \nabla_+\psi_\alpha(\vec{r},b_0)\nabla_0\psi^*_\gamma(\vec{r},b_1)) \\ = [\bar{Y}_z^{(1)}\bar{Y}_r^{(4)} - \bar{Y}_z^{(2)}\bar{Y}_r^{(5)}]\bar{X}_r^{(6)}\bar{X}_z^{(2)} \end{aligned} \tag{H.152}$$

$$\begin{aligned} \int d\vec{r}\psi^*_\beta(\vec{r},b_0)\psi_\delta(\vec{r},b_1)(\nabla_0\psi^*_\alpha(\vec{r},b_0)\nabla_+\psi_\gamma(\vec{r},b_1) - \nabla_+\psi^*_\alpha(\vec{r},b_0)\nabla_0\psi_\gamma(\vec{r},b_1)) \\ = [\bar{Y}_z^{(1)}\bar{Y}_r^{(6)} - \bar{Y}_z^{(2)}\bar{Y}_r^{(7)}]\bar{X}_r^{(6)}\bar{X}_z^{(2)} \end{aligned} \tag{H.153}$$

Case $(m_\alpha = m_\gamma)$ **and** $(m_\delta = m_\beta + 1)$**:**

$$\begin{aligned} \int d\vec{r}\psi^*_\alpha(\vec{r},b_0)\psi_\gamma(\vec{r},b_1)(\nabla_0\psi^*_\beta(\vec{r},b_0)\nabla_-\psi_\delta(\vec{r},b_1) - \nabla_-\psi^*_\beta(\vec{r},b_0)\nabla_0\psi_\delta(\vec{r},b_1)) \\ = \bar{Y}_z^{(0)}\bar{Y}_r^{(0)}[\bar{X}_r^{(4)}\bar{X}_z^{(0)} - \bar{X}_r^{(5)}\bar{X}_z^{(1)}] \end{aligned} \tag{H.154}$$

$$\begin{aligned} \int d\vec{r}\psi^*_\beta(\vec{r},b_0)\psi_\delta(\vec{r},b_1)(\nabla_0\psi_\alpha(\vec{r},b_0)\nabla_-\psi^*_\gamma(\vec{r},b_1) - \nabla_-\psi_\alpha(\vec{r},b_0)\nabla_0\psi^*_\gamma(\vec{r},b_1)) \\ = -[\bar{Y}_z^{(1)}\bar{Y}_r^{(6)} - \bar{Y}_z^{(2)}\bar{Y}_r^{(7)}]\bar{X}_r^{(7)}\bar{X}_z^{(2)} \end{aligned} \tag{H.155}$$

$$\begin{aligned} \int d\vec{r}\psi^*_\beta(\vec{r},b_0)\psi_\delta(\vec{r},b_1)(\nabla_0\psi^*_\alpha(\vec{r},b_0)\nabla_-\psi_\gamma(\vec{r},b_1) - \nabla_-\psi^*_\alpha(\vec{r},b_0)\nabla_0\psi_\gamma(\vec{r},b_1)) \\ = -[\bar{Y}_z^{(1)}\bar{Y}_r^{(4)} - \bar{Y}_z^{(2)}\bar{Y}_r^{(5)}]\bar{X}_r^{(7)}\bar{X}_z^{(2)} \end{aligned} \tag{H.156}$$

Case $(m_\alpha = m_\gamma)$ and $(m_\delta = m_\beta)$:

$$\int d\vec{r}\psi^*_\alpha(\vec{r},b_0)\psi_\gamma(\vec{r},b_1)(\nabla_+\psi^*_\beta(\vec{r},b_0)\nabla_-\psi_\delta(\vec{r},b_1) - \nabla_-\psi^*_\beta(\vec{r},b_0)\nabla_+\psi_\delta(\vec{r},b_1)) \quad \text{(H.157)}$$
$$= \bar{Y}^{(0)}_z\bar{Y}^{(0)}_r\bar{X}^{(2)}_r\bar{X}^{(2)}_z$$

$$\int d\vec{r}\psi^*_\beta(\vec{r},b_0)\psi_\delta(\vec{r},b_1)(\nabla_+\psi^*_\alpha(\vec{r},b_0)\nabla_-\psi_\gamma(\vec{r},b_1) - \nabla_-\psi^*_\alpha(\vec{r},b_0)\nabla_+\psi_\gamma(\vec{r},b_1)) \quad \text{(H.158)}$$
$$= \bar{Y}^{(0)}_z\bar{Y}^{(1)}_r\bar{X}^{(3)}_r\bar{X}^{(2)}_z$$

Case $(m_\alpha = m_\gamma + 1)$ and $(m_\delta = m_\beta)$:

$$\int d\vec{r}\psi^*_\beta(\vec{r},b_0)\psi_\delta(\vec{r},b_1)(\nabla_0\psi^*_\alpha(\vec{r},b_0)\nabla_+\psi_\gamma(\vec{r},b_1) - \nabla_+\psi^*_\alpha(\vec{r},b_0)\nabla_0\psi_\gamma(\vec{r},b_1)) \quad \text{(H.159)}$$
$$= [\bar{Y}^{(1)}_z\bar{Y}^{(2)}_r - \bar{Y}^{(2)}_z\bar{Y}^{(3)}_r]\bar{X}^{(3)}_r\bar{X}^{(2)}_z$$

$$\int d\vec{r}\psi^*_\alpha(\vec{r},b_0)\psi_\gamma(\vec{r},b_1)[\nabla_0\psi^*_\beta(\vec{r},b_0)\nabla_+\psi_\delta(\vec{r},b_1) - \nabla_+\psi^*_\beta(\vec{r},b_0)\nabla_0\psi_\delta(\vec{r},b_1) \quad \text{(H.160)}$$
$$+\nabla_0\psi_\beta(\vec{r},b_0)\nabla_+\psi^*_\delta(\vec{r},b_1) - \nabla_+\psi_\beta(\vec{r},b_0)\nabla_0\psi^*_\delta(\vec{r},b_1)]$$
$$= \bar{Y}^{(0)}_z\bar{Y}^{(10)}_r[\bar{X}^{(8)}_r\bar{X}^{(0)}_z - \bar{X}^{(9)}_r\bar{X}^{(1)}_z + \bar{X}^{(10)}_r\bar{X}^{(0)}_z - \bar{X}^{(11)}_r\bar{X}^{(1)}_z]$$

Case $(m_\alpha = m_\gamma - 1)$ and $(m_\delta = m_\beta)$:

$$\int d\vec{r}\psi^*_\beta(\vec{r},b_0)\psi_\delta(\vec{r},b_1)(\nabla_0\psi^*_\alpha(\vec{r},b_0)\nabla_-\psi_\gamma(\vec{r},b_1) - \nabla_-\psi^*_\alpha(\vec{r},b_0)\nabla_0\psi_\gamma(\vec{r},b_1)) \quad \text{(H.161)}$$
$$= [\bar{Y}^{(1)}_z\bar{Y}^{(8)}_r - \bar{Y}^{(2)}_z\bar{Y}^{(9)}_r]\bar{X}^{(3)}_r\bar{X}^{(2)}_z$$

$$\int d\vec{r}\psi^*_\alpha(\vec{r},b_0)\psi_\gamma(\vec{r},b_1)[\nabla_0\psi^*_\beta(\vec{r},b_0)\nabla_-\psi_\delta(\vec{r},b_1) - \nabla_-\psi^*_\beta(\vec{r},b_0)\nabla_0\psi_\delta(\vec{r},b_1) \quad \text{(H.162)}$$
$$+\nabla_0\psi_\beta(\vec{r},b_0)\nabla_-\psi^*_\delta(\vec{r},b_1) - \nabla_-\psi_\beta(\vec{r},b_0)\nabla_0\psi^*_\delta(\vec{r},b_1)]$$
$$= -\bar{Y}^{(0)}_z\bar{Y}^{(11)}_r[\bar{X}^{(8)}_r\bar{X}^{(0)}_z - \bar{X}^{(9)}_r\bar{X}^{(1)}_z + \bar{X}^{(10)}_r\bar{X}^{(0)}_z - \bar{X}^{(11)}_r\bar{X}^{(1)}_z]$$

As for the non-collective case, we present models for the z-integrals and the $r_\perp$-integrals that enables to evaluate the $\bar{X}$ and $\bar{Y}$ matrices easily.

Calculation of the z-integral:

The general model to evaluate all the z-integrals involved in this section reads as follows:

$$\boxed{\bar{I}_z = \int dz\varphi_{n_{z_\alpha}}(z+d_\alpha,b_{z_0})\varphi_{n_{z_\gamma}}(z+d_\gamma,b_{z_1})\varphi_{n_{z_\delta}}(z+d_\delta,b_{z_1})\varphi_{n_{z_\beta}}(z+d_\beta,b_{z_0})} \quad \text{(H.163)}$$

We start using the generalized Talman-z coefficients (see Appendix D) to reduce Eq.(H.163):

$$\bar{I}_z = \frac{1}{B_z\sqrt{\pi}} \sum_{n_{z_a}} \bar{T}^{n_{z_a}}_{(n_{z_\alpha},d_\alpha)(n_{z_\gamma},d_\gamma)} \sum_{n_{z_b}} \bar{T}^{n_{z_b}}_{(n_{z_\delta},d_\delta)(n_{z_\beta},d_\beta)} \tag{H.164}$$
$$\int dz e^{-\frac{1}{2}(\frac{z+d_{\alpha\gamma}}{B_z})^2} e^{-\frac{1}{2}(\frac{z+d_{\beta\delta}}{B_z})^2} \varphi_{n_{z_a}}(z+d_{\alpha\gamma},B_z)\varphi_{n_{z_b}}(z+d_{\beta\delta},B_z)$$

With:

$$\begin{cases} B_z = \frac{b_{z_0} b_{z_1}\sqrt{2}}{\sqrt{b_{z_0}^2+b_{z_1}^2}} \\ d_{\beta\delta} = \frac{b_{z_1}^2 d_\beta + b_{z_0}^2 d_\delta}{b_{z_1}^2+b_{z_0}^2} \end{cases} \tag{H.165}$$

Using the Moshinsky-z coefficients in Eq.(H.164), we get:

$$\bar{I}_z = \frac{1}{B_z\sqrt{\pi}} \sum_{n_{z_a}} \bar{T}^{n_{z_a}}_{(n_{z_\alpha},d_\alpha)(n_{z_\gamma},d_\gamma)} \sum_{n_{z_b}} \bar{T}^{n_{z_b}}_{(n_{z_\delta},d_\delta)(n_{z_\beta},d_\beta)} \sum_{n_{z_c}} \sum_{n_{z_d}} \tag{H.166}$$
$$M^{n_{z_c}n_{z_d}}_{n_{z_a}n_{z_b}} \varphi_{n_{z_d}}(\bar{d}^{\beta\delta}_{\alpha\gamma},B_z) e^{-\frac{1}{2}(\frac{\bar{d}^{\beta\delta}_{\alpha\gamma}}{b_z})^2} \int dz e^{-\frac{1}{2}(\frac{\sqrt{2}z+\bar{D}^{\beta\delta}_{\alpha\gamma}}{B_z})^2} \varphi_{n_{z_c}}(\sqrt{2}z+\bar{D}^{\beta\delta}_{\alpha\gamma})$$

With:

$$\begin{cases} \bar{D}^{\beta\delta}_{\alpha\gamma} = \frac{d_{\alpha\gamma}+d_{\beta\delta}}{\sqrt{2}} \\ \bar{d}^{\beta\delta}_{\alpha\gamma} = \frac{d_{\alpha\gamma}-d_{\beta\delta}}{\sqrt{2}} \end{cases} \tag{H.167}$$

As Eq.(H.166) is now similar to the Eq.(H.125) derived previously, we deduce by analogy:

$$\boxed{\bar{I}_z = \frac{1}{\sqrt{2B_z\sqrt{\pi}}} \sum_{n_{z_a}} \bar{T}^{n_{z_a}}_{(n_{z_\alpha},d_\alpha)(n_{z_\gamma},d_\gamma)} \sum_{n_{z_b}} \bar{T}^{n_{z_b}}_{(n_{z_\delta},d_\delta)(n_{z_\beta},d_\beta)} M^{0n_{z_d}}_{n_{z_a}n_{z_b}} e^{-\frac{1}{2}(\frac{\bar{d}^{\beta\delta}_{\alpha\gamma}}{B_z})^2} \varphi_{n_{z_d}}(\bar{d}^{\beta\delta}_{\alpha\gamma},B_z)} \tag{H.168}$$

Calculation of the $r_\perp$-integral:

The general model to evaluate all the $r_\perp$-integrals involved in this section reads as follows:

$$\boxed{\bar{I}_r = \int d\vec{r}_\perp \phi^*_{(m_\alpha,n_{\perp_\alpha})}(\vec{r}_\perp,b_{r_0})\phi^*_{(m_\beta,n_{\perp_\beta})}(\vec{r}_\perp,b_{r_0})\phi_{(m_\delta,n_{\perp_\delta})}(\vec{r}_\perp,b_{r_1})\phi_{(m_\gamma,n_{\perp_\gamma})}(\vec{r}_\perp,b_{r_1})} \tag{H.169}$$

First, we use the generalized Talman-r coefficients (see Appendix D):

$$\bar{I}_r = \frac{1}{B_r^2\pi} \sum_{n_{\perp_a}} \bar{T}^{(m_\gamma-m_\alpha,n_{\perp_a})}_{(m_\alpha,n_{\perp_\alpha})(m_\gamma,n_{\perp_\gamma})} \sum_{n_{\perp_b}} \bar{T}^{(m_\delta-m_\beta,n_{\perp_b})}_{(m_\beta,n_{\perp_\beta})(m_\delta,n_{\perp_\delta})} \tag{H.170}$$
$$\int d\vec{r}_\perp e^{-\frac{1}{2}(\frac{\sqrt{2}r}{B_r})^2} \phi_{(m_\gamma-m_\alpha,n_{\perp_a})}(\vec{r}_\perp,B_r)\phi_{(m_\delta-m_\beta,n_{\perp_b})}(\vec{r}_\perp,B_r)$$

As Eq.(H.170) is similar to the Eq.(H.130) previously treated, we find by analogy:

$$\boxed{\begin{array}{l}\bar{I}_r = \dfrac{\delta_{(m_\alpha+m_\beta=m_\gamma+m_\delta)}}{2B_r^2\pi}\displaystyle\sum_{n_{\perp_a}} \bar{T}^{(m_\gamma-m_\alpha,n_{\perp_a})}_{(m_\alpha,n_{\perp_\alpha})(m_\gamma,n_{\perp_\gamma})} \\ \displaystyle\sum_{n_{\perp_b}} \bar{T}^{(m_\delta-m_\beta,n_{\perp_b})}_{(m_\beta,n_{\perp_\beta})(m_\delta,n_{\perp_\delta})} M^{(0,0)(0,n_{\perp_d})}_{(m_\gamma-m_\alpha,n_{\perp_a})(m_\delta-m_\beta,n_{\perp_b})}\end{array}} \tag{H.171}$$

It is now possible to give formulas for both the $\bar{X}$ and the $\bar{Y}$ matrices.

Expression of the $\bar{X}_z$ quantities:

The expression of the different $\bar{X}_z$ are given thereafter:

$$\boxed{\begin{array}{r}\bar{X}_z^{(0)} = \dfrac{1}{2b_{z_0}\sqrt{B_z\sqrt{\pi}}}[\delta_{(n_{z_\beta}>0)}\sqrt{n_{z_\beta}}\displaystyle\sum_{n_{z_b}} \bar{T}^{n_{z_b}}_{(n_{z_\beta-1},d_\beta)(n_{z_\delta},d_\delta)} \\ -\sqrt{n_{z_\beta}+1}\displaystyle\sum_{n_{z_b}} \bar{T}^{n_{z_b}}_{(n_{z_\beta+1},d_\beta)(n_{z_\delta},d_\delta)}]M^{0n_{z_d}}_{n_{z_a}n_{z_b}} e^{-\frac{1}{2}(\frac{\bar{d}^{\beta\delta}_{\alpha\gamma}}{B_z})^2}\varphi_{n_{z_d}}(\bar{d}^{\beta\delta}_{\alpha\gamma}, B_z)]\end{array}} \tag{H.172}$$

$$\boxed{\begin{array}{r}\bar{X}_z^{(1)} = \dfrac{1}{2b_{z_1}\sqrt{B_z\sqrt{\pi}}}[\delta_{(n_{z_\delta}>0)}\sqrt{n_{z_\delta}}\displaystyle\sum_{n_{z_b}} \bar{T}^{n_{z_b}}_{(n_{z_\delta-1},d_\delta)(n_{z_\beta},d_\beta)} \\ -\sqrt{n_{z_\delta}+1}\displaystyle\sum_{n_{z_b}} \bar{T}^{n_{z_b}}_{(n_{z_\delta+1},d_\delta)(n_{z_\beta},d_\beta)}]M^{0n_{z_d}}_{n_{z_a}n_{z_b}} e^{-\frac{1}{2}(\frac{\bar{d}^{\beta\delta}_{\alpha\gamma}}{B_z})^2}\varphi_{n_{z_d}}(\bar{d}^{\beta\delta}_{\alpha\gamma}, B_z)]\end{array}} \tag{H.173}$$

$$\boxed{\bar{X}_z^{(2)} = \frac{1}{\sqrt{2B_z\sqrt{\pi}}}\sum_{n_{z_b}} \bar{T}^{n_{z_b}}_{(n_{z_\beta},d_\beta)(n_{z_\delta},d_\delta)} M^{0n_{z_d}}_{n_{z_a}n_{z_b}} e^{-\frac{1}{2}(\frac{d^{\beta\delta}_{\alpha\gamma}}{b_z})^2}\varphi_{n_{z_d}}(\bar{d}^{\beta\delta}_{\alpha\gamma}, B_z)} \tag{H.174}$$

Expression of the $\bar{Y}_z$ quantities:

The expression of the different $\bar{Y}_z$ are given thereafter:

$$\boxed{\bar{Y}_z^{(0)} = \bar{T}^{n_{z_a}}_{(n_{z_\alpha},d_\alpha)(n_{z_\gamma},d_\gamma)}} \tag{H.175}$$

$$\boxed{\bar{Y}_z^{(1)} = \frac{1}{b_{z_0}\sqrt{2}}(\delta_{(n_{z_\alpha}>0)}\sqrt{n_{z_\alpha}}\sum_{n_{z_b}} \bar{T}^{n_{z_b}}_{(n_{z_\alpha-1},d_\alpha)(n_{z_\gamma},d_\gamma)} - \sqrt{n_{z_\alpha}+1}\sum_{n_{z_b}} \bar{T}^{n_{z_b}}_{(n_{z_\alpha+1},d_\alpha)(n_{z_\gamma},d_\gamma)})} \tag{H.176}$$

$$\boxed{\bar{Y}_z^{(2)} = \frac{1}{b_{z_1}\sqrt{2}}(\delta_{(n_{z_\gamma}>0)}\sqrt{n_{z_\gamma}}\sum_{n_{z_b}} \bar{T}^{n_{z_b}}_{(n_{z_\gamma-1},d_\gamma)(n_{z_\alpha},d_\alpha)} - \sqrt{n_{z_\gamma}+1}\sum_{n_{z_b}} \bar{T}^{n_{z_b}}_{(n_{z_\gamma+1},d_\gamma)(n_{z_\alpha},d_\alpha)})} \tag{H.177}$$

Expression of the $\bar{X}_r$ quantities:

The expression of the different $\bar{X}_r$ are given thereafter:

$$\boxed{\begin{aligned}\bar{X}_r^{(0)} = \frac{1}{b_{r_1} B_r^2 \pi 2^{3/2}} [& \sqrt{m' + n_{\perp_\delta} + 1} \sum_{n_{\perp_b}} \bar{T}^{n_{\perp_b}}_{(m'+1, n_{\perp_\beta})(m'+1, n_{\perp_\delta})} \\ & + \delta_{(n_{\perp_\delta} > 0)} \sqrt{n_{\perp_\delta}} \sum_{n_{\perp_b}} \bar{T}^{n_{\perp_b}}_{(m'+1, n_{\perp_\beta})(m'+1, n_{\perp_\delta}-1)}] M^{(0,0)(0,n_{\perp_d})}_{(0,n_{\perp_a})(0,n_{\perp_b})}\end{aligned}} \tag{H.178}$$

$$\boxed{\begin{aligned}\bar{X}_r^{(1)} = -\frac{1}{b_{r_0} B_r^2 \pi 2^{3/2}} [& \sqrt{m' + n_{\perp_\beta} + 1} \sum_{n_{\perp_b}} \bar{T}^{n_{\perp_b}}_{(m', n_{\perp_\beta})(m', n_{\perp_\delta})} \\ & + \sqrt{n_{\perp_\beta} + 1} \sum_{n_{\perp_b}} \bar{T}^{n_{\perp_b}}_{(m', n_{\perp_\beta}+1)(m', n_{\perp_\delta})}] M^{(0,0)(0,n_{\perp_d})}_{(0,n_{\perp_a})(0,n_{\perp_b})}\end{aligned}} \tag{H.179}$$

$$\begin{aligned}\bar{X}_r^{(2)} = \frac{\delta_{(m'>0)}}{b_{r_2} b_{r_1} B_r^2 4\pi} \sum_{n_{\perp_b}} [& - \sqrt{(m' + n_{\perp_\beta})(m' + n_{\perp_\delta})} \bar{T}^{n_{\perp_b}}_{(m'-1, n_{\perp_\beta})(m'-1, n_{\perp_\delta})} \\ & - \sqrt{(m' + n_{\perp_\beta})(n_{\perp_\delta} + 1)} \bar{T}^{n_{\perp_b}}_{(m'-1, n_{\perp_\beta})(m'-1, n_{\perp_\delta}+1)} \\ & - \sqrt{(n_{\perp_\beta} + 1)(m' + n_{\perp_\delta})} \bar{T}^{n_{\perp_b}}_{(m'-1, n_{\perp_\beta}+1)(m'-1, n_{\perp_\delta})} \\ & - \sqrt{(n_{\perp_\beta} + 1)(n_{\perp_\delta} + 1)} \bar{T}^{n_{\perp_b}}_{(m'-1, n_{\perp_\beta}+1)(m'-1, n_{\perp_\delta}+1)} \\ & + \sqrt{(m' + n_{\perp_\beta} + 1)(m' + n_{\perp_\delta} + 1)} \bar{T}^{n_{\perp_b}}_{(m'+1, n_{\perp_\beta})(m'+1, n_{\perp_\delta})} \\ & + \delta_{(n_{\perp_\delta} > 0)} \sqrt{(m' + n_{\perp_\beta} + 1) n_{\perp_\delta}} \bar{T}^{n_{\perp_b}}_{(m'+1, n_{\perp_\beta})(m'+1, n_{\perp_\delta}-1)} \\ & + \delta_{(n_{\perp_\beta} > 0)} \sqrt{n_{\perp_\beta} (m' + n_{\perp_\delta} + 1)} \bar{T}^{n_{\perp_b}}_{(m'+1, n_{\perp_\beta}-1)(m'+1, n_{\perp_\delta})} \\ & + \delta_{(n_{\perp_\delta} > 0)} \delta_{(n_{\perp_\beta} > 0)} \sqrt{n_{\perp_\beta} n_{\perp_\delta}} \bar{T}^{n_{\perp_b}}_{(m'+1, n_{\perp_\beta}-1)(m'+1, n_{\perp_\delta}-1)}] M^{(0,0)(0,n_{\perp_d})}_{(0,n_{\perp_a})(0,n_{\perp_b})}\end{aligned} \tag{H.180}$$

$$\boxed{\bar{X}_r^{(3)} = \bar{T}^{n_{\perp_b}}_{(m', n_{\perp_\beta})(m', n_{\perp_\delta})}} \tag{H.181}$$

$$\boxed{\begin{aligned}\bar{X}_r^{(4)} = \frac{1}{b_{r_1} B_r^2 \pi 2^{3/2}} [& \sqrt{m' + n_{\perp_\delta}} \sum_{n_{\perp_b}} \bar{T}^{n_{\perp_b}}_{(m'-1, n_{\perp_\beta})(m'-1, n_{\perp_\delta})} \\ & + \sqrt{n_{\perp_\delta} + 1} \sum_{n_{\perp_b}} \bar{T}^{n_{\perp_b}}_{(m'-1, n_{\perp_\beta})(m'-1, n_{\perp_\delta}+1)}] M^{(0,0)(0,n_{\perp_d})}_{(0,n_{\perp_a})(0,n_{\perp_b})}\end{aligned}} \tag{H.182}$$

$$\boxed{\begin{aligned}\bar{X}_r^{(5)} = -\frac{1}{b_{r_0} B_r^2 \pi 2^{3/2}} [& \sqrt{m' + n_{\perp_\beta}} \sum_{n_{\perp_b}} \bar{T}^{n_{\perp_b}}_{(m', n_{\perp_\beta})(m', n_{\perp_\delta})} \\ & + \sqrt{n_{\perp_\beta}} \sum_{n_{\perp_b}} \bar{T}^{n_{\perp_b}}_{(m', n_{\perp_\beta}-1)(m', n_{\perp_\delta})}] M^{(0,0)(0,n_{\perp_d})}_{(0,n_{\perp_a})(0,n_{\perp_b})}\end{aligned}} \tag{H.183}$$

$$\boxed{\bar{X}_r^{(6)} = \bar{T}^{n_{\perp_b}}_{(m'+1,n_{\perp_\beta})(m',n_{\perp_\delta})}} \tag{H.184}$$

$$\boxed{\bar{X}_r^{(7)} = \bar{T}^{n_{\perp_b}}_{(m'-1,n_{\perp_\beta})(m',n_{\perp_\delta})}} \tag{H.185}$$

$$\begin{aligned}\boxed{\bar{X}_r^{(8)} = \frac{1}{b_{r_1} B_r^2 \pi 2^{3/2}} [\sqrt{m' + n_{\perp_\delta} + 1} \sum_{n_{\perp_b}} \bar{T}^{n_{\perp_b}}_{(m',n_{\perp_\beta})(m'+1,n_{\perp_\delta})} \\ + \delta_{(n_{\perp_\delta}>0)} \sqrt{n_{\perp_\delta}} \sum_{n_{\perp_b}} \bar{T}^{n_{\perp_b}}_{(m',n_{\perp_\beta})(m'+1,n_{\perp_\delta}-1)}] M^{(0,0)(0,n_{\perp_d})}_{(0,n_{\perp_a})(0,n_{\perp_b})}}\end{aligned} \tag{H.186}$$

$$\begin{aligned}\boxed{\begin{aligned}\bar{X}_r^{(9)} = \frac{1}{b_{r_0} B_r^2 \pi 2^{3/2}} [\delta_{m_\delta=0} [\sqrt{n_{\perp_\beta} + 1} \sum_{n_{\perp_b}} \bar{T}^{n_{\perp_b}}_{(1,n_{\perp_\beta})(0,n_{\perp_\delta})} \\ + \delta_{(n_{\perp_\beta}>0)} \sqrt{n_{\perp_\beta}} \sum_{n_{\perp_b}} \bar{T}^{n_{\perp_b}}_{(1,n_{\perp_\beta}-1)(0,n_{\perp_\delta})}] \\ - \delta_{m_\delta>0} [\sqrt{m' + n_{\perp_\beta}} \sum_{n_{\perp_b}} \bar{T}^{n_{\perp_b}}_{(m'-1,n_{\perp_\beta})(m',n_{\perp_\delta})} \\ + \sqrt{n_{\perp_\beta} + 1} \sum_{n_{\perp_b}} \bar{T}^{n_{\perp_b}}_{(m'-1,n_{\perp_\beta}+1)(m',n_{\perp_\delta})}]] M^{(0,0)(0,n_{\perp_d})}_{(0,n_{\perp_a})(0,n_{\perp_b})}\end{aligned}}\end{aligned} \tag{H.187}$$

$$\begin{aligned}\boxed{\begin{aligned}\bar{X}_r^{(10)} = \frac{1}{b_{r_1} B_r^2 \pi 2^{3/2}} [\delta_{m_\delta=0} [\sqrt{n_{\perp_\delta} + 1} \sum_{n_{\perp_b}} \bar{T}^{n_{\perp_b}}_{(0,n_{\perp_\beta})(1,n_{\perp_\delta})} \\ + \delta_{(n_{\perp_\delta}>0)} \sqrt{n_{\perp_\delta}} \sum_{n_{\perp_b}} \bar{T}^{n_{\perp_b}}_{(0,n_{\perp_\beta})(1,n_{\perp_\delta}-1)}] \\ - \delta_{m_\delta>0} [\sqrt{m' + n_{\perp_\delta}} \sum_{n_{\perp_b}} \bar{T}^{n_{\perp_b}}_{(m',n_{\perp_\beta})(m'-1,n_{\perp_\delta})} \\ + \sqrt{n_{\perp_\delta} + 1} \sum_{n_{\perp_b}} \bar{T}^{n_{\perp_b}}_{(m',n_{\perp_\beta})(m'-1,n_{\perp_\delta}+1)}]] M^{(0,0)(0,n_{\perp_d})}_{(0,n_{\perp_a})(0,n_{\perp_b})}\end{aligned}}\end{aligned} \tag{H.188}$$

$$\begin{aligned}\boxed{\bar{X}_r^{(11)} = \frac{1}{b_{r_0} B_r^2 \pi 2^{3/2}} [\sqrt{m' + n_{\perp_\beta} + 1} \sum_{n_{\perp_b}} \bar{T}^{n_{\perp_b}}_{(m'+1,n_{\perp_\beta})(m',n_{\perp_\delta})} \\ + \delta_{(n_{\perp_\beta}>0)} \sqrt{n_{\perp_\beta}} \sum_{n_{\perp_b}} \bar{T}^{n_{\perp_b}}_{(m'+1,n_{\perp_\beta}-1)(m',n_{\perp_\delta})}] M^{(0,0)(0,n_{\perp_d})}_{(0,n_{\perp_a})(0,n_{\perp_b})}}\end{aligned} \tag{H.189}$$

Expression of the $\bar{Y}_r$ quantities:

The expression of the different $\bar{Y}_r$ are given thereafter:

$$\boxed{\bar{Y}_r^{(0)} = \bar{T}^{n_{\perp_b}}_{(m,n_{\perp_\alpha})(m,n_{\perp_\gamma})}} \tag{H.190}$$

$$\bar{Y}_r^{(1)} = \frac{\delta_{(m>0)}}{b_{r_1} b_{r_0} B_r^2 4\pi} \sum_{n_{\perp_b}} [-\sqrt{(m+n_{\perp_\alpha})(m+n_{\perp_\gamma})}\bar{T}^{n_{\perp_b}}_{(m-1,n_{\perp_\alpha})(m-1,n_{\perp_\gamma})}$$
$$-\sqrt{(m+n_{\perp_\alpha})(n_{\perp_\gamma}+1)}\bar{T}^{n_{\perp_b}}_{(m-1,n_{\perp_\alpha})(m-1,n_{\perp_\gamma}+1)}$$
$$-\sqrt{(n_{\perp_\alpha}+1)(m+n_{\perp_\gamma})}\bar{T}^{n_{\perp_b}}_{(m-1,n_{\perp_\alpha}+1)(m-1,n_{\perp_\gamma})}$$
$$-\sqrt{(n_{\perp_\alpha}+1)(n_{\perp_\gamma}+1)}\bar{T}^{n_{\perp_b}}_{(m-1,n_{\perp_\alpha}+1)(m-1,n_{\perp_\gamma}+1)}$$
$$+\sqrt{(m+n_{\perp_\alpha}+1)(m+n_{\perp_\gamma}+1)}\bar{T}^{n_{\perp_b}}_{(m+1,n_{\perp_\alpha})(m+1,n_{\perp_\gamma})}$$
$$+\delta_{(n_{\perp_\gamma}>0)}\sqrt{(m+n_{\perp_\alpha}+1)n_{\perp_\gamma}}\bar{T}^{n_{\perp_b}}_{(m+1,n_{\perp_\alpha})(m+1,n_{\perp_\gamma}-1)}$$
$$+\delta_{(n_{\perp_\alpha}>0)}\sqrt{n_{\perp_\alpha}(m'+n_{\perp_\gamma}+1)}\bar{T}^{n_{\perp_b}}_{(m+1,n_{\perp_\alpha}-1)(m+1,n_{\perp_\gamma})}$$
$$+\delta_{(n_{\perp_\gamma}>0)}\delta_{(n_{\perp_\alpha}>0)}\sqrt{n_{\perp_\alpha}n_{\perp_\gamma}}\bar{T}^{n_{\perp_b}}_{(m+1,n_{\perp_\alpha}-1)(m+1,n_{\perp_\gamma}-1)}]M^{(0,0)(0,n_{\perp_d})}_{(0,n_{\perp_a})(0,n_{\perp_b})} \tag{H.191}$$

$$\bar{Y}_r^{(2)} = \frac{1}{b_{r_1} B_r^2 \pi 2^{3/2}} [\sqrt{m+n_{\perp_\gamma}} \sum_{n_{\perp_b}} \bar{T}^{n_{\perp_b}}_{(m,n_{\perp_\alpha})(m,n_{\perp_\gamma})}$$
$$+\delta_{(n_{\perp_\gamma}>0)}\sqrt{n_{\perp_\gamma}} \sum_{n_{\perp_b}} \bar{T}^{n_{\perp_b}}_{(m,n_{\perp_\alpha})(m,n_{\perp_\gamma}-1)}]M^{(0,0)(0,n_{\perp_d})}_{(0,n_{\perp_a})(0,n_{\perp_b})} \tag{H.192}$$

$$\bar{Y}_r^{(3)} = -\frac{1}{b_{r_0} B_r^2 \pi 2^{3/2}} [\sqrt{m+n_{\perp_\alpha}} \sum_{n_{\perp_b}} \bar{T}^{n_{\perp_b}}_{(m-1,n_{\perp_\alpha})(m-1,n_{\perp_\gamma})}$$
$$+\sqrt{n_{\perp_\alpha}+1} \sum_{n_{\perp_b}} \bar{T}^{n_{\perp_b}}_{(m-1,n_{\perp_\alpha}+1)(m-1,n_{\perp_\gamma})}]M^{(0,0)(0,n_{\perp_d})}_{(0,n_{\perp_a})(0,n_{\perp_b})} \tag{H.193}$$

$$\bar{Y}_r^{(4)} = \frac{1}{b_{r_1} B_r^2 \pi 2^{3/2}} [\delta_{m_\alpha=0}[\sqrt{n_{\perp_\gamma}+1} \sum_{n_{\perp_b}} \bar{T}^{n_{\perp_b}}_{(0,n_{\perp_\alpha})(1,n_{\perp_\gamma})}$$
$$+\delta_{(n_{\perp_\gamma}>0)}\sqrt{n_{\perp_\gamma}} \sum_{n_{\perp_b}} \bar{T}^{n_{\perp_b}}_{(0,n_{\perp_\alpha})(1,n_{\perp_\gamma}-1)}]$$
$$-\delta_{m_\alpha>0}[\sqrt{m+n_{\perp_\gamma}} \sum_{n_{\perp_b}} \bar{T}^{n_{\perp_b}}_{(m,n_{\perp_\alpha})(m-1,n_{\perp_\gamma})}$$
$$+\sqrt{n_{\perp_\gamma}+1} \sum_{n_{\perp_b}} \bar{T}^{n_{\perp_b}}_{(m,n_{\perp_\alpha})(m-1,n_{\perp_\gamma}+1)}]]M^{(0,0)(0,n_{\perp_d})}_{(0,n_{\perp_a})(0,n_{\perp_b})} \tag{H.194}$$

$$\bar{Y}_r^{(5)} = \frac{1}{b_{r_0} B_r^2 \pi 2^{3/2}} [\sqrt{m+n_{\perp_\alpha}+1} \sum_{n_{\perp_b}} \bar{T}^{n_{\perp_b}}_{(m+1,n_{\perp_\alpha})(m,n_{\perp_\gamma})}$$
$$+\delta_{n_\alpha>0}\sqrt{n_{\perp_\alpha}} \sum_{n_{\perp_b}} \bar{T}^{n_{\perp_b}}_{(m+1,n_{\perp_\alpha}-1)(m,n_{\perp_\gamma})}]M^{(0,0)(0,n_{\perp_d})}_{(0,n_{\perp_a})(0,n_{\perp_b})} \tag{H.195}$$

$$\boxed{\begin{aligned}\bar{Y}_r^{(6)} = \frac{1}{b_{r_1} B_r^2 \pi 2^{3/2}} [& \sqrt{m + n_{\perp_\gamma} + 1} \sum_{n_{\perp_b}} \bar{T}^{n_{\perp_b}}_{(m,n_{\perp_\alpha})(m+1,n_{\perp_\gamma})} \\ & + \delta_{n_\gamma > 0} \sqrt{n_{\perp_\gamma}} \sum_{n_{\perp_b}} \bar{T}^{n_{\perp_b}}_{(m,n_{\perp_\alpha})(m+1,n_{\perp_\gamma}-1)}] M^{(0,0)(0,n_{\perp_d})}_{(0,n_{\perp_a})(0,n_{\perp_b})}\end{aligned}} \tag{H.196}$$

$$\boxed{\begin{aligned}\bar{Y}_r^{(7)} = \frac{1}{b_{r_0} B_r^2 \pi 2^{3/2}} [& \delta_{m_\alpha = 0} [\sqrt{n_{\perp_\alpha} + 1} \sum_{n_{\perp_b}} \bar{T}^{n_{\perp_b}}_{(1,n_{\perp_\alpha})(0,n_{\perp_\gamma})} \\ & + \delta_{(n_{\perp_\alpha} > 0)} \sqrt{n_{\perp_\alpha}} \sum_{n_{\perp_b}} \bar{T}^{n_{\perp_b}}_{(1,n_{\perp_\alpha}-1)(0,n_{\perp_\gamma})}] \\ & - \delta_{m_\alpha > 0} [\sqrt{m + n_{\perp_\alpha}} \sum_{n_{\perp_b}} \bar{T}^{n_{\perp_b}}_{(m-1,n_{\perp_\alpha})(m,n_{\perp_\gamma})} \\ & + \sqrt{n_{\perp_\alpha} + 1} \sum_{n_{\perp_b}} \bar{T}^{n_{\perp_b}}_{(m-1,n_{\perp_\alpha}+1)(m,n_{\perp_\gamma})}]] M^{(0,0)(0,n_{\perp_d})}_{(0,n_{\perp_a})(0,n_{\perp_b})}\end{aligned}} \tag{H.197}$$

$$\boxed{\begin{aligned}\bar{Y}_r^{(8)} = \frac{1}{b_{r_1} B_r^2 \pi 2^{3/2}} [& \sqrt{m + n_{\perp_\gamma} + 1} \sum_{n_{\perp_b}} \bar{T}^{n_{\perp_b}}_{(m,n_{\perp_\alpha})(m,n_{\perp_\gamma})} \\ & + \sqrt{n_{\perp_\gamma} + 1} \sum_{n_{\perp_b}} \bar{T}^{n_{\perp_b}}_{(m,n_{\perp_\alpha})(m,n_{\perp_\gamma}+1)}] M^{(0,0)(0,n_{\perp_d})}_{(0,n_{\perp_a})(0,n_{\perp_b})}\end{aligned}} \tag{H.198}$$

$$\boxed{\begin{aligned}\bar{Y}_r^{(9)} = -\frac{1}{b_{r_0} B_r^2 \pi 2^{3/2}} [& \sqrt{m + n_{\perp_\alpha} + 1} \sum_{n_{\perp_b}} \bar{T}^{n_{\perp_b}}_{(m+1,n_{\perp_\alpha})(m+1,n_{\perp_\gamma})} \\ & + \delta_{n_\alpha > 0} \sqrt{n_{\perp_\alpha}} \sum_{n_{\perp_b}} \bar{T}^{n_{\perp_b}}_{(m+1,n_{\perp_\alpha}-1)(m+1,n_{\perp_\gamma})}] M^{(0,0)(0,n_{\perp_d})}_{(0,n_{\perp_a})(0,n_{\perp_b})}\end{aligned}} \tag{H.199}$$

$$\boxed{\bar{Y}_r^{(10)} = \bar{T}^{n_{\perp_b}}_{(m,n_{\perp_\alpha})(m-1,n_{\perp_\gamma})}} \tag{H.200}$$

$$\boxed{\bar{Y}_r^{(11)} = \bar{T}^{n_{\perp_b}}_{(m,n_{\perp_\alpha})(m+1,n_{\perp_\gamma})}} \tag{H.201}$$

Appendix I

Coulomb fields

The antisymmetrized Coulomb interaction reads as follows:

$$\boxed{V^{(Clmb)}(1 - P_r P_\sigma P_\tau) = e^2 \frac{\delta_{\tau_p \tau'_p}}{|\vec{r}_1 - \vec{r}_2|}(1 - P_r P_\sigma P_\tau)} \tag{I.1}$$

The operators P_r, P_σ and P_τ represent the exchange of the spatial, spin and isospin part, respectively. The operator $\delta_{\tau_p \tau'_p}$ implies that the Coulomb interaction only operates in the proton-proton channel. The quantity e is the electrostatic constant. The matrix elements of the Coulomb interaction can be separated into a spatial part and a spin-isospin one:

$$\boxed{{}_0\langle \alpha\beta | V^{(Clmb)}(1 - P_r P_\sigma P_\tau) | \gamma\delta \rangle_1 = (\bar{E}^{\gamma\delta}_{\alpha\beta} - \bar{E}^{\delta\gamma}_{\alpha\beta}) e^2 \delta_{\tau_p \tau'_p}} \tag{I.2}$$

$$\bar{E}^{\gamma\delta}_{\alpha\beta} = {}_0\langle \alpha\beta | \frac{1}{|\vec{r}_1 - \vec{r}_2|} | \gamma\delta \rangle_1 \tag{I.3}$$

The indices 0 and 1 stand for the fact that the particle bases $\{0\}$ and $\{1\}$ on the right and on the left side can be different. When they are the same, the expression reduces to the more common one:

$$\boxed{\langle \alpha\beta | V^{(Clmb)}(1 - P_r P_\sigma P_\tau) | \gamma\delta \rangle = (E^{\gamma\delta}_{\alpha\beta} - E^{\delta\gamma}_{\alpha\beta}) e^2 \delta_{\tau_p \tau'_p}} \tag{I.4}$$

$$E^{\gamma\delta}_{\alpha\beta} = \langle \alpha\beta | \frac{1}{|\vec{r}_1 - \vec{r}_2|} | \gamma\delta \rangle \tag{I.5}$$

This appendix aims to give an analytic expression of all the Coulomb fields involved in this PhD thesis. It is important to know that, in practice, the Coulomb exchange contribution to the energy is often evaluated with the Slater approximation [49] and the Coulomb pairing contribution is neglected. This approximation is therefore discussed in section I.3 and extended to the collective case in section I.5.

I.1 Spatial part

We give a reduced expression of the spatial part of the Coulomb interaction matrix elements. The case with only one basis is treated first, then derivations are given for the general case.

I.1.1 Same bases

This part aims to give a reduced expression of the following quantity:

$$E_{\alpha\beta}^{\gamma\delta} = \langle\alpha\beta|\frac{1}{|\vec{r}_1 - \vec{r}_2|}|\gamma\delta\rangle \tag{I.6}$$

We develop Eq.(I.6):

$$\begin{aligned} E_{\alpha\beta}^{\gamma\delta} = \int\int dz_0 dz_1 \varphi_{n_{z\alpha}}(z_0 + d_\alpha)\varphi_{n_{z\beta}}(z_1 + d_\beta) \\ \varphi_{n_{z\gamma}}(z_0 + d_\gamma)\varphi_{n_{z\delta}}(z_1 + d_\delta) \\ \int\int d\vec{r}_{\perp_0} d\vec{r}_{\perp_1} \phi^*_{n_{\perp\alpha},m_\alpha}(\vec{r}_{\perp_0})\phi^*_{n_{\perp\beta},m_\beta}(\vec{r}_{\perp_1}) \\ \phi_{n_{\perp\gamma},m_\gamma}(\vec{r}_{\perp_0})\phi_{n_{\perp\delta},m_\delta}(\vec{r}_{\perp_1})\frac{1}{|\vec{r}_{\perp_0} - \vec{r}_{\perp_1} + (z_0 - z_1)\vec{u}_z|} \end{aligned} \tag{I.7}$$

We then introduce the Talman-z and Talman-r (see Appendix D) coefficients in Eq.(I.7):

$$\begin{aligned} E_{\alpha\beta}^{\gamma\delta} = \frac{1}{b_z b_r^2 \pi^{3/2}} \sum_{n_{z_a}} T^{n_{z_a}}_{(n_{z\alpha},d_\alpha)(n_{z\gamma},d_\gamma)} \sum_{n_{z_b}} T^{n_{z_b}}_{(n_{z\delta},d_\delta)(n_{z\beta},d_\beta)} \\ \int\int dz_0 dz_1 e^{-\frac{1}{2}(\frac{z_0 + k_{\alpha\gamma}}{b_z})^2} e^{-\frac{1}{2}(\frac{z_1 + k_{\beta\delta}}{b_z})^2} \varphi_{n_{z_a}}(z_0 + k_{\alpha\gamma})\varphi_{n_{z_b}}(z_1 + k_{\beta\delta}) \\ \sum_{n_{\perp_a}} T^{(m_\gamma - m_\alpha, n_{\perp_a})}_{(m_\alpha,n_{\perp\alpha})(m_\gamma,n_{\perp\gamma})} \sum_{n_{\perp_b}} T^{(m_\delta - m_\beta, n_{\perp_b})}_{(m_\beta,n_{\perp\beta})(m_\delta,n_{\perp\delta})} \\ \int\int d\vec{r}_{\perp_0} d\vec{r}_{\perp_1} e^{-\frac{1}{2}(\frac{\vec{r}_{\perp_1}}{b_r})^2} e^{-\frac{1}{2}(\frac{\vec{r}_{\perp_0}}{b_r})^2} \frac{\phi_{n_{\perp_a},m_a}(\vec{r}_{\perp_0})\phi_{n_{\perp_b},m_b}(\vec{r}_{\perp_1})}{|\vec{r}_{\perp_0} - \vec{r}_{\perp_1} + (z_0 - z_1)\vec{u}_z|} \end{aligned} \tag{I.8}$$

The Moshinsky-z and Moshinsky-r (see Appendix D) are used to rewrite Eq.(I.8):

$$\begin{aligned} E_{\alpha\beta}^{\gamma\delta} = \frac{1}{b_z b_r^2 \pi^{3/2}} \sum_{n_{z_a}} T^{n_{z_a}}_{(n_{z\alpha},d_\alpha)(n_{z\gamma},d_\gamma)} \sum_{n_{z_b}} T^{n_{z_b}}_{(n_{z\delta},d_\delta)(n_{z\beta},d_\beta)} \sum_{n_{z_c}} \sum_{n_{z_d}} M^{n_{z_c} n_{z_d}}_{n_{z_a} n_{z_b}} \\ \int\int dz_0 dz_1 e^{-\frac{1}{2}(\frac{z_0 + k_{\alpha\gamma}}{b_z})^2} e^{-\frac{1}{2}(\frac{z_1 + k_{\beta\delta}}{b_z})^2} \varphi_{n_{z_c}}(Z + D^{\beta\delta}_{\alpha\gamma})\varphi_{n_{z_d}}(z + d^{\beta\delta}_{\alpha\gamma}) \\ \sum_{n_{\perp_a}} T^{(m_\gamma - m_\alpha, n_{\perp_a})}_{(m_\alpha,n_{\perp\alpha})(m_\gamma,n_{\perp\gamma})} \sum_{n_{\perp_b}} T^{(m_\delta - m_\beta, n_{\perp_b})}_{(m_\beta,n_{\perp\beta})(m_\delta,n_{\perp\delta})} \sum_{m_c} \sum_{m_d} \sum_{n_{\perp_c}} \sum_{n_{\perp_d}} M^{(m_c,n_{\perp_c})(m_d,n_{\perp_d})}_{(m_a,n_{\perp_a})(m_b,n_{\perp_b})} \\ \int\int d\vec{r}_{\perp_0} d\vec{r}_{\perp_1} e^{-\frac{1}{2}(\frac{\vec{r}_{\perp_1}}{b_r})^2} e^{-\frac{1}{2}(\frac{\vec{r}_{\perp_0}}{b_r})^2} \frac{\phi_{n_{\perp_c},m_c}(\vec{R}_\perp)\phi_{n_{\perp_d},m_d}(\vec{r}_\perp)}{|\vec{r}_{\perp_0} - \vec{r}_{\perp_1} + (z_0 - z_1)\vec{u}_z|} \end{aligned} \tag{I.9}$$

With:

$$\begin{cases} \vec{R}_\perp = \frac{\vec{r}_{\perp_0} + \vec{r}_{\perp_1}}{\sqrt{2}} \\ \vec{r}_\perp = \frac{\vec{r}_{\perp_0} - \vec{r}_{\perp_1}}{\sqrt{2}} \end{cases} \quad ; \quad \begin{cases} Z = \frac{z_0 + z_1}{\sqrt{2}} \\ z = \frac{z_0 - z_1}{\sqrt{2}} \end{cases} \quad ; \quad \begin{cases} D^{\beta\delta}_{\alpha\gamma} = \frac{k_{\alpha\gamma} + k_{\beta\delta}}{\sqrt{2}} \\ d^{\beta\delta}_{\alpha\gamma} = \frac{k_{\alpha\gamma} - k_{\beta\delta}}{\sqrt{2}} \end{cases} \tag{I.10}$$

We then operate two changes of variables $(z_0, z_1) \longrightarrow (Z, z)$ and $(\vec{r}_{\perp_0}, \vec{r}_{\perp_1}) \longrightarrow (\vec{R}_\perp, \vec{r}_\perp)$:

$$E_{\alpha\beta}^{\gamma\delta} = \frac{1}{b_z b_r^2 \pi^{3/2}} \sum_{n_{z_a}} T^{n_{z_a}}_{(n_{z_\alpha},d_\alpha)(n_{z_\gamma},d_\gamma)} \sum_{n_{z_b}} T^{n_{z_b}}_{(n_{z_\delta},d_\delta)(n_{z_\beta},d_\beta)} \sum_{n_{z_c}} \sum_{n_{z_d}} M^{n_{z_c} n_{z_d}}_{n_{z_a} n_{z_b}} \tag{I.11}$$
$$\int dZ e^{-\frac{1}{2}(\frac{Z+D_{\alpha\gamma}^{\beta\delta}}{b_z})^2} \varphi_{n_{z_c}}(Z + D_{\alpha\gamma}^{\beta\delta}) \int dz e^{-\frac{1}{2}(\frac{z+d_{\alpha\gamma}^{\beta\delta}}{b_z})^2} \varphi_{n_{z_d}}(z + d_{\alpha\gamma}^{\beta\delta})$$
$$\sum_{n_{\perp_a}} T^{(m_\gamma - m_\alpha, n_{\perp_a})}_{(m_\alpha,n_{\perp_\alpha})(m_\gamma,n_{\perp_\gamma})} \sum_{n_{\perp_b}} T^{(m_\delta - m_\beta, n_{\perp_b})}_{(m_\beta,n_{\perp_\beta})(m_\delta,n_{\perp_\delta})} \sum_{m_c} \sum_{m_d} \sum_{n_{\perp_c}} \sum_{n_{\perp_d}} M^{(m_c,n_{\perp_c})(m_d,n_{\perp_d})}_{(m_a,n_{\perp_a})(m_b,n_{\perp_b})}$$
$$\int d\vec{r}_\perp e^{-\frac{1}{2}(\frac{\vec{r}_\perp}{b_r})^2} \frac{\phi_{n_{\perp_d},m_d}(\vec{r}_\perp)}{\sqrt{2}|\vec{r}_\perp + z\vec{u}_z|} \int d\vec{R}_\perp e^{-\frac{1}{2}(\frac{\vec{R}_\perp}{b_r})^2} \phi_{n_{\perp_c},m_c}(\vec{R}_\perp)$$

We recall the following properties coming from the orthonormality of the harmonic oscillator wave functions:

$$\begin{cases} \int dZ e^{-\frac{1}{2}(\frac{Z+D_{\alpha\gamma}^{\beta\delta}}{b_z})^2} \varphi_{n_{z_c}}(Z + D_{\alpha\gamma}^{\beta\delta}) = \sqrt{b_z\sqrt{\pi}} \delta_{n_{z_c}0} \\ \int d\vec{R}_\perp e^{-\frac{1}{2}(\frac{\vec{R}_\perp}{b_r})^2} \phi_{n_{\perp_c},m_c}(\vec{R}_\perp) = b_r\sqrt{\pi} \delta_{n_{\perp_c}0} \delta_{m_c 0} \end{cases} \tag{I.12}$$

Using Eq.(I.12) in Eq.(I.11), we obtain:

$$E_{\alpha\beta}^{\gamma\delta} = \frac{1}{b_r\sqrt{2b_z}\pi^{3/4}} \sum_{n_{za}} T^{n_{z_a}}_{(n_{z_\alpha},d_\alpha)(n_{z_\gamma},d_\gamma)} \sum_{n_{z_b}} T^{n_{z_b}}_{(n_{z_\delta},d_\delta)(n_{z_\beta},d_\beta)} \tag{I.13}$$
$$M^{n_{z_d}}_{n_{z_a} n_{z_b}} \int dz e^{-\frac{1}{2}(\frac{z+d_{\alpha\gamma}^{\beta\delta}}{b_z})^2} \varphi_{n_{z_d}}(z + d_{\alpha\gamma}^{\beta\delta})$$
$$\sum_{n_{\perp_a}} T^{(m_\gamma - m_\alpha, n_{\perp_a})}_{(m_\alpha,n_{\perp_\alpha})(m_\gamma,n_{\perp_\gamma})} \sum_{n_{\perp_b}} T^{(m_\delta - m_\beta, n_{\perp_b})}_{(m_\beta,n_{\perp_\beta})(m_\delta,n_{\perp_\delta})}$$
$$M^{(m_d,n_{\perp_d})}_{(m_a,n_{\perp_a})(m_b,n_{\perp_b})} \int d\vec{r}_\perp e^{-\frac{1}{2}(\frac{\vec{r}_\perp}{b_r})^2} \frac{\phi_{n_{\perp_d},m_d}(\vec{r}_\perp)}{|\vec{r}_\perp + z\vec{u}_z|}$$

Moreover, the following relations hold and define n_{z_d}, m_d and $n_{\perp_d}$:

$$\begin{cases} n_{z_d} = n_{z_a} + n_{z_b} \\ m_d = m_a + m_b \\ n_{\perp_d} = n_{\perp_a} + n_{\perp_b} + \frac{|m_a|+|m_b|-|m_a+m_b|}{2} \end{cases} \tag{I.14}$$

We consider now the denominator in the last part of Eq.(I.13). We use the following property:

$$\boxed{\frac{1}{|\vec{r}_\perp + z\vec{u}_z|} = \frac{1}{\sqrt{r_\perp^2 + z^2}} = \frac{2}{\sqrt{\pi}} \int_0^\infty dx e^{-(r_\perp^2 + z^2)x^2}} \tag{I.15}$$

Thanks to Eq.(I.15), Eq.(I.13) now reads:

$$
\begin{aligned}
E_{\alpha\beta}^{\gamma\delta} = \frac{\sqrt{2}}{b_r\sqrt{b_z}\pi^{5/4}} \sum_{n_{z_a}} T^{n_{z_a}}_{(n_{z_\alpha},d_\alpha)(n_{z_\gamma},d_\gamma)} \sum_{n_{z_b}} T^{n_{z_b}}_{(n_{z_\delta},d_\delta)(n_{z_\beta},d_\beta)} \\
M^{n_{z_d}}_{n_{z_a}n_{z_b}} \int_0^\infty dx \int dz e^{-\frac{1}{2}(\frac{z+d^{\beta\delta}_{\alpha\gamma}}{b_z})^2} e^{-z^2x^2} \varphi_{n_{z_d}}(z+d^{\beta\delta}_{\alpha\gamma}) \\
\sum_{n_{\perp_a}} T^{(m_\gamma-m_\alpha,n_{\perp_a})}_{(m_\alpha,n_{\perp_\alpha})(m_\gamma,n_{\perp_\gamma})} \sum_{n_{\perp_b}} T^{(m_\delta-m_\beta,n_{\perp_b})}_{(m_\beta,n_{\perp_\beta})(m_\delta,n_{\perp_\delta})} \\
M^{(m_d,n_{\perp_d})}_{(m_a,n_{\perp_a})(m_b,n_{\perp_b})} \int d\vec{r}_\perp e^{-\frac{1}{2}(\frac{\vec{r}_\perp}{b_r})^2} e^{-r_\perp^2x^2} \phi_{n_{\perp_d},m_d}(\vec{r}_\perp)
\end{aligned}
\tag{I.16}
$$

In the following, we treat separately the z-integral and the $r_\perp$-integral.

Calculation of the z-integral:

We want to evaluate the following integral:

$$
I_z = \int dz e^{-\frac{1}{2}(\frac{z+d^{\beta\delta}_{\alpha\gamma}}{b_z})^2} e^{-z^2x^2} \varphi_{n_{z_d}}(z+d^{\beta\delta}_{\alpha\gamma}) \tag{I.17}
$$

We start rescaling the integral in Eq.(I.17):

$$
I_z = \int dz e^{-\frac{1}{2}(\frac{z}{b_z})^2} e^{-(z-d^{\beta\delta}_{\alpha\gamma})^2x^2} \varphi_{n_{z_d}}(z) \tag{I.18}
$$

We now use the generating-function formalism:

$$
\sum_{n_{z_\mu}} \chi^{(1)}_\mu(t_1) I_z = \frac{1}{\sqrt{b_z\sqrt{\pi}}} \int dz e^{-z^2(\frac{1}{b_z^2}+x^2)+2z(\frac{t_1}{b_z}+d^{\beta\delta}_{\alpha\gamma}x^2)-t_1^2-(d^{\beta\delta}_{\alpha\gamma}x)^2} \tag{I.19}
$$

We factorize the exponential in Eq.(I.19):

$$
\sum_{n_{z_\mu}} \chi^{(1)}_\mu(t_1) I_z = \frac{1}{\sqrt{b_z\sqrt{\pi}}} e^{\frac{(t_1+b_zd^{\beta\delta}_{\alpha\gamma}x^2)^2}{1+b_z^2x^2}-t_1^2-(d^{\beta\delta}_{\alpha\gamma}x)^2} \int dz e^{-(z\sqrt{\frac{1}{b_z^2}+x^2}-\frac{(\frac{t_1}{b_z}+d^{\beta\delta}_{\alpha\gamma}x^2)}{\sqrt{\frac{1}{b_z^2}+x^2}})^2} \tag{I.20}
$$

We perform the following change of variables $z \longrightarrow (z\sqrt{\frac{1}{b_z^2}+x^2} - \frac{(\frac{t_1}{b_z}+d^{\beta\delta}_{\alpha\gamma}x^2)}{\sqrt{\frac{1}{b_z^2}+x^2}})$:

$$
\sum_{n_{z_\mu}} \chi^{(1)}_\mu(t_1) I_z = \frac{\sqrt{b_z}}{\pi^{1/4}\sqrt{1+b_z^2x^2}} e^{\frac{(t_1+b_zd^{\beta\delta}_{\alpha\gamma}x^2)^2}{1+b_z^2x^2}-t_1^2-(d^{\beta\delta}_{\alpha\gamma}x)^2} \int dz e^{-z^2} \tag{I.21}
$$

The last integral in Eq.(I.21) is trivial:

$$
\sum_{n_{z_\mu}} \chi^{(1)}_\mu(t_1) I_z = \frac{\sqrt{b_z}\pi^{1/4}}{\sqrt{1+b_z^2x^2}} e^{\frac{(t_1+b_zd^{\beta\delta}_{\alpha\gamma}x^2)^2}{1+b_z^2x^2}-t_1^2-(d^{\beta\delta}_{\alpha\gamma}x)^2} \tag{I.22}
$$

We factorize in the exponential of Eq.(I.22):

$$\sum_{n_{z_\mu}} \chi_\mu^{(1)}(t_1) I_z = \frac{\sqrt{b_z}\pi^{1/4}}{\sqrt{1+b_z^2x^2}} e^{-t_1^2(\frac{b_z^2x^2}{1+b_z^2x^2})+2(\frac{t_1 b_z x}{\sqrt{1+b_z^2x^2}})\frac{d_{\alpha\gamma}^{\beta\delta}x}{\sqrt{1+b_z^2x^2}}-\frac{(d_{\alpha\gamma}^{\beta\delta}x)^2}{1+b_z^2x^2}} \tag{I.23}$$

We rewrite the second part of Eq.(I.23) using the generating-functions:

$$\sum_{n_{z_\mu}} \chi_\mu^{(1)}(t_1) I_z = e^{-\frac{1}{2}\frac{(d_{\alpha\gamma}^{\beta\delta}x)^2}{1+b_z^2x^2}} \frac{\sqrt{b_z\pi}}{\sqrt{1+b_z^2x^2}} \sum_{n_{z_\mu}} \chi_\mu^{(1)}(\frac{t_1 b_z x}{\sqrt{1+b_z^2x^2}})\varphi_{n_{z_\mu}}(\frac{d_{\alpha\gamma}^{\beta\delta}x}{\sqrt{1+b_z^2x^2}},1) \tag{I.24}$$

We rescale the generating-functions in the right part of Eq.(I.24):

$$\sum_{n_{z_\mu}} \chi_\mu^{(1)}(t_1) I_z = e^{-\frac{1}{2}\frac{(d_{\alpha\gamma}^{\beta\delta}x)^2}{1+b_z^2x^2}} \frac{\sqrt{b_z\pi}}{\sqrt{1+b_z^2x^2}} \sum_{n_{z_\mu}} \chi_\mu^{(1)}(t_1)(\frac{b_z x}{\sqrt{1+b_z^2x^2}})^{n_{z_\mu}}\varphi_{n_{z_\mu}}(\frac{d_{\alpha\gamma}^{\beta\delta}x}{\sqrt{1+b_z^2x^2}},1) \tag{I.25}$$

It's finally possible to identify:

$$\boxed{I_z = e^{-\frac{1}{2}\frac{(d_{\alpha\gamma}^{\beta\delta}x)^2}{1+b_z^2x^2}} \frac{\sqrt{b_z\pi}}{\sqrt{1+b_z^2x^2}}(\frac{b_z x}{\sqrt{1+b_z^2x^2}})^{n_{z_d}}\varphi_{n_{z_d}}(\frac{d_{\alpha\gamma}^{\beta\delta}x}{\sqrt{1+b_z^2x^2}},1)} \tag{I.26}$$

Calculation of the $r_\perp$-integral:

We want to evaluate the following integral:

$$I_r = \int d\vec{r}_\perp e^{-\vec{r}_\perp^2(\frac{1}{2b_r}+x^2)}\phi_{n_{\perp_d},m_d}(\vec{r}_\perp) \tag{I.27}$$

We start using the generating-functions formalism:

$$\sum_{n_{\perp_\mu}}\sum_{m_\mu} \chi_\mu^{(2)*}(\vec{t_1}) I_r = \frac{1}{b_r\sqrt{\pi}} \int d\vec{r}_\perp e^{-\vec{r}_\perp^2(\frac{1}{2b_r^2}+x^2)} e^{-\frac{1}{2}(\frac{\vec{r}_\perp}{b_r})^2+2\frac{\vec{r}_\perp}{b_r}.\vec{t_1}-t_1^2} \tag{I.28}$$

We factorize in the exponential of Eq.(I.28):

$$\sum_{n_{\perp_\mu}}\sum_{m_\mu} \chi_\mu^{(2)*}(\vec{t_1}) I_r = \frac{1}{b_r\sqrt{\pi}} e^{-t_1^2(\frac{b_r^2x^2}{1+b_r^2x^2})} \int d\vec{r}_\perp e^{-(\vec{r}_\perp\sqrt{\frac{1}{b_r^2}+x^2}-\frac{\vec{t}_1}{b_r\sqrt{\frac{1}{b_r^2}+x^2}})^2} \tag{I.29}$$

We operate the following change of variables $(\vec{r}_\perp) \longrightarrow (\vec{r}_\perp\sqrt{\frac{1}{b_r^2}+x^2} - \frac{\vec{t}_1}{b_r\sqrt{\frac{1}{b_r^2}+x^2}})$:

$$\sum_{n_{\perp_\mu}}\sum_{m_\mu} \chi_\mu^{(2)*}(\vec{t_1}) I_r = \frac{1}{b_r\sqrt{\pi}} e^{-t_1^2(\frac{b_r^2x^2}{1+b_r^2x^2})} \frac{b_r^2}{1+x^2b_r^2} \int d\vec{r}_\perp e^{-\vec{r}_\perp^2} \tag{I.30}$$

The last integral in Eq.(I.30) is trivial:

$$\sum_{n_{\perp_\mu}}\sum_{m_\mu}\chi_\mu^{(2)*}(\vec{t}_1)I_r=\frac{b_r\sqrt{\pi}}{1+x^2b_r^2}e^{-t_1^2(\frac{b_r^2x^2}{1+b_r^2x^2})} \tag{I.31}$$

We now rewrite the right part of Eq.(I.31) using the generating-functions:

$$\sum_{n_{\perp_\mu}}\sum_{m_\mu}\chi_\mu^{(2)*}(\vec{t}_1)I_r=\sum_{n_{\perp_\mu}}\sum_{m_\mu}\chi_\mu^{(2)*}(\vec{t}_1\frac{b_rx}{\sqrt{1+b_r^2x^2}})\frac{\pi b_r}{1+x^2b_r^2}\phi_{n_{\perp_\mu},m_\mu}(0,1) \tag{I.32}$$

We rescale the generating-functions on the right part of Eq.(I.32):

$$\sum_{n_{\perp_\mu}}\sum_{m_\mu}\chi_\mu^{(2)*}(\vec{t}_1)I_r=\sum_{n_{\perp_\mu}}\sum_{m_\mu}\chi_\mu^{(2)*}(\vec{t}_1)(\frac{b_rx}{\sqrt{1+b_r^2x^2}})^{2n_{\perp_mu}+|m_\mu|}\frac{\pi b_r}{1+x^2b_r^2}\phi_{n_{\perp_\mu},m_\mu}(0,1) \tag{I.33}$$

By identification, we obtain:

$$I_r=(\frac{b_rx}{\sqrt{1+b_r^2x^2}})^{2n_{\perp_d}+|m_d|}\frac{\pi b_r}{1+x^2b_r^2}\phi_{n_{\perp_d},m_d}(0,1) \tag{I.34}$$

Moreover, the following property holds:

$$\phi_{n_{\perp_d},m_d}(0,1)=\frac{1}{\sqrt{\pi}}\delta_{m_d0} \tag{I.35}$$

Using Eq.(I.35) in Eq.(I.34), we eventually find:

$$\boxed{I_r=\delta_{m_d0}(\frac{b_rx}{\sqrt{1+b_r^2x^2}})^{2n_{\perp_d}}\frac{\sqrt{\pi}b_r}{1+x^2b_r^2}} \tag{I.36}$$

Evaluation of the Coulomb integral:

Gathering the results obtained in Eq.(I.26) and Eq.(I.36), we can rewrite:

$$\begin{aligned}E_{\alpha\beta}^{\gamma\delta}=\frac{\sqrt{2}\delta_{m_am_b}}{\pi^{1/4}}\sum_{n_{z_a}}T_{(n_{z_\alpha},d_\alpha)(n_{z_\gamma},d_\gamma)}^{n_{z_a}}\sum_{n_{z_b}}T_{(n_{z_\delta},d_\delta)(n_{z_\beta},d_\beta)}^{n_{z_b}} \\ M_{n_{z_a}n_{z_b}}^{n_{z_d}}\sum_{n_{\perp_a}}T_{(m_\alpha,n_{\perp_\alpha})(m_\gamma,n_{\perp_\gamma})}^{(m_\gamma-m_\alpha,n_{\perp_a})}\sum_{n_{\perp_b}}T_{(m_\beta,n_{\perp_\beta})(m_\delta,n_{\perp_\delta})}^{(m_\delta-m_\beta,n_{\perp_b})}M_{(m_a,n_{\perp_a})(m_b,n_{\perp_b})}^{(0,n_{\perp_d})} \\ \int_0^\infty dxe^{-\frac{1}{2}\frac{(d_{\alpha\gamma}^{\beta\delta}x)^2}{1+b_z^2x^2}}\frac{(b_rx)^{2n_{\perp_d}}}{(1+b_r^2x^2)^{n_{\perp_d}+1}}\frac{(b_zx)^{n_{z_d}}}{(1+b_z^2x^2)^{\frac{n_{z_d}+1}{2}}}\varphi_{n_{z_d}}(\frac{d_{\alpha\gamma}^{\beta\delta}x}{\sqrt{1+b_z^2x^2}},1)\end{aligned} \tag{I.37}$$

The integral in Eq.(I.37) is called the Coulomb integral, noted I_c:

$$\boxed{I_c = \int_0^\infty dx e^{-\frac{1}{2}\frac{(d_{\alpha\gamma}^{\beta\delta}x)^2}{1+b_z^2x^2}} \frac{(b_r x)^{2n_{\perp_d}}}{(1+b_r^2x^2)^{n_{\perp_d}+1}} \frac{(b_z x)^{n_{z_d}}}{(1+b_z^2x^2)^{\frac{n_{z_d}+1}{2}}} \varphi_{n_{z_d}}(\frac{d_{\alpha\gamma}^{\beta\delta}x}{\sqrt{1+b_z^2x^2}}, 1)} \tag{I.38}$$

There is no analytic expression of the Coulomb integral. Thus, we perform a quadrature on it. However, the integration domain is not optimal. For this reason, we rescale the integral with the change of variables $(x) \rightarrow (\frac{xb_z}{\sqrt{1+b_z^2x^2}})$:

$$I_c = \frac{1}{b_z}(\frac{b_r}{b_z})^{2n_{\perp_d}} \int_0^1 dx e^{-\frac{1}{2}\frac{(d_{\alpha\gamma}^{\beta\delta}x)^2}{b_z^2}} \frac{x^{2n_{\perp_d}+n_{z_d}}}{(1+x^2[(\frac{b_r}{b_z})^2-1])^{n_{\perp_d}+1}} \varphi_{n_{z_d}}(\frac{d_{\alpha\gamma}^{\beta\delta}x}{b_z}, 1) \tag{I.39}$$

With:

$$\begin{cases} x' = \frac{xb_z}{\sqrt{1+b_z^2x^2}} \iff x = \frac{1}{b_z}\frac{x'}{\sqrt{1-x'^2}} \\ dx = \frac{dx'}{b_z(1-x'^2)^{3/2}} \end{cases} \tag{I.40}$$

Moreover, we set:

$$\gamma = (\frac{b_r}{b_z})^2 - 1 \tag{I.41}$$

We observe that the integrand in Eq.(I.39) is an even function. Thanks to that, the integration domain of the integral in Eq.(I.39) is tranformed to fit the Gauss-Legendre quadrature method:

$$\boxed{I_c = \frac{1}{2b_z}(\frac{b_r}{b_z})^{2n_{\perp_d}} \int_{-1}^1 dx e^{-\frac{1}{2}\frac{(d_{\alpha\gamma}^{\beta\delta}x)^2}{b_z^2}} \frac{x^{2n_{\perp_d}+n_{z_d}}}{(1+\gamma x^2)^{n_{\perp_d}+1}} \varphi_{n_{z_d}}(\frac{d_{\alpha\gamma}^{\beta\delta}x}{b_z}, 1)} \tag{I.42}$$

Applying explicitly the Gauss-Legendre quadrature in Eq.(I.42), we eventually find:

$$\boxed{I_c \approx \frac{1}{2b_z}(\frac{b_r}{b_z})^{2n_{\perp_d}} \sum_{i=1}^{n_{GLE}} w_i e^{-\frac{1}{2}\frac{(d_{\alpha\gamma}^{\beta\delta}x_i)^2}{b_z^2}} \frac{x_i^{2n_{\perp_d}+n_{z_d}}}{(1+\gamma x_i^2)^{n_{\perp_d}+1}} \varphi_{n_{z_d}}(\frac{d_{\alpha\gamma}^{\beta\delta}x_i}{b_z}, 1)} \tag{I.43}$$

Here, n_{GLE} is the number of points in the quadrature. The w_i and x_i are defined in the Appendix N.

Factorization of the spatial part for the direct mean field:

For the direct mean field, we choose to evaluate the Coulomb integral first and to contract it with the Talman and Moshinsky coefficients:

$$\boxed{J_{\delta\beta}^{n_{z_a}n_{\perp_a}} = \sum_{n_{z_b}} T_{(n_{z_\delta},d_\delta)(n_{z_\beta},d_\beta)}^{n_{z_b}} M_{n_{z_a}n_{z_b}}^{n_{z_d}} \sum_{n_{\perp_b}} T_{(m_\beta,n_{\perp_\beta})(m_\delta,n_{\perp_\delta})}^{(m_\delta-m_\beta,n_{\perp_b})} M_{(m_a,n_{\perp_a})(m_b,n_{\perp_b})}^{(0,n_{\perp_d})} I_c^{n_{z_d}n_{\perp_d}}} \tag{I.44}$$

The numerical evaluation of Eq.(I.44) may require some time, but it is only performed once in a HFB convergence process as it only depends on the harmonic oscillator basis we chose. In this case, the spatial part eventually reads:

$$\boxed{E^{\gamma\delta}_{\alpha\beta} = \delta_{(m_\alpha+m_\gamma)(m_\delta+m_\beta)} \frac{\sqrt{2}}{\pi^{1/4}} \sum_{n_{za}} T^{n_{za}}_{(n_{z\alpha},d_\alpha)(n_{z\gamma},d_\gamma)} \sum_{n_{\perp a}} T^{(m_\gamma - m_\alpha, n_{\perp a})}_{(m_\alpha,n_{\perp\alpha})(m_\gamma,n_{\perp\gamma})} J^{n_{za}n_{\perp a}}_{\delta\beta}} \tag{I.45}$$

Factorization of the spatial part for the exchange mean and pairing fields:

In the case of the exchange mean and pairing fields, it's not possible anymore to contract the Coulomb integral with the Talman and Moshinsky coefficients and to store the result once and for all. Indeed, in that case, the Coulomb integral no longer depend solely on the basis, but also on the density matrix (or pairing tensor in the case of the pairing field). Because of that peculiarity and for the sake of numerical performances, the factorization of the spatial part is done in a totally different way for the exchange and pairing fields.
The objective is to transform the spatial part of the Coulomb term into a form similar to the spatial part of the central term. We start writting the spatial part:

$$E^{\gamma\delta}_{\alpha\beta} = \int d\vec{r} \psi^*_\alpha(\vec{r}) \psi^*_\beta(\vec{r}) \frac{1}{|\vec{r}_1 - \vec{r}_2|} \psi_\gamma(\vec{r}) \psi_\delta(\vec{r}) \tag{I.46}$$

We directly transform the fraction in Eq.(I.46) into the integral of an exponential term:

$$\frac{1}{|\vec{r}_1 - \vec{r}_2|} = \frac{2}{\sqrt{\pi}} \int_0^\infty dx e^{-(\vec{r}_1 - \vec{r}_2)^2 x^2} \tag{I.47}$$

Inserting Eq.(I.47) in Eq.(I.46), we get:

$$E^{\gamma\delta}_{\alpha\beta} = \frac{2}{\sqrt{\pi}} \int_0^\infty dx \int d\vec{r} e^{-(\vec{r}_1 - \vec{r}_2)^2 x^2} \psi^*_\alpha(\vec{r}) \psi^*_\beta(\vec{r}) \psi_\gamma(\vec{r}) \psi_\delta(\vec{r}) \tag{I.48}$$

The last integral of Eq.(I.48) is precisely the spatial part of a central term whose parameter is $\mu(x) = \frac{1}{x}$. The key point to achieve good numerical performances is to rescale the integral from $[0, \infty]$ to $[-1, 1]$. To do so, we set the change of variables $(x) \to (\frac{1-x}{1+x})$:

$$E^{\gamma\delta}_{\alpha\beta} = \frac{4}{\sqrt{\pi}} \int_{-1}^1 dx \frac{1}{(1+x)^2} \int d\vec{r} e^{-(\frac{\vec{r}_1 - \vec{r}_2}{\mu(x)})^2} \psi^*_\alpha(\vec{r}) \psi^*_\beta(\vec{r}) \psi_\gamma(\vec{r}) \psi_\delta(\vec{r}) \tag{I.49}$$

$$\mu(x) = \frac{1+x}{1-x} \tag{I.50}$$

Using the derivations of the spatial part of the central term in Appendix E, we write:

$$\boxed{E^{\gamma\delta}_{\alpha\beta} = \frac{4}{\sqrt{\pi}} \int_{-1}^1 dx \frac{1}{(1+x)^2} (I_{rx})^{\gamma\delta}_{\alpha\beta} (I_{zx})^{\gamma\delta}_{\alpha\beta}} \tag{I.51}$$

Here, I_{rx} and I_{zx} are nothing but spatial central terms depending on the parameter $\mu(x)$. Using a Gauss-Legendre quadrature in Eq.(I.51), we finally write:

$$\boxed{E^{\gamma\delta}_{\alpha\beta} \approx \frac{4}{\sqrt{\pi}} \sum_{i=0}^{n_{GLE}} \frac{w_i}{(1+x_i)^2} (I_{rx_i})^{\gamma\delta}_{\alpha\beta} (I_{zx_i})^{\gamma\delta}_{\alpha\beta}} \tag{I.52}$$

Note that in Eq.(I.52), the z part and the r part are separated when they are mixed in the evaluation of the Coulomb integral. It's an important property that explains the performances of this factorization method. In practice, a good numerical accuracy can be achieved with around twelve points.

We'd like to thank L. Robledo here for his excellent comments that inspired these derivations.

I.1.2 Different bases

In the collective case, we choose to factorize all the terms as for the non-collective exchange and pairing terms. By analogy with the non-collective case, we directly write:

$$\boxed{\bar{E}^{\gamma\delta}_{\alpha\beta} = \frac{4}{\sqrt{\pi}} \int_{-1}^{1} dx \frac{1}{(1+x)^2} (\bar{I}_{rx})^{\gamma\delta}_{\alpha\beta} (\bar{I}_{zx})^{\gamma\delta}_{\alpha\beta}} \tag{I.53}$$

The $\bar{I}$ quantities correspond to the collective spatial part of central terms depending on the parameter $\mu(x)$. We finally rewrite Eq.(I.53) using a Gauss-Legendre quadrature:

$$\boxed{\bar{E}^{\gamma\delta}_{\alpha\beta} \approx \frac{4}{\sqrt{\pi}} \sum_{i=0}^{n_{GLE}} \frac{w_i}{(1+x_i)^2} (\bar{I}_{rx_i})^{\gamma\delta}_{\alpha\beta} (\bar{I}_{zx_i})^{\gamma\delta}_{\alpha\beta}} \tag{I.54}$$

I.2 HFB fields

In this part, the direct mean field, exchange mean field and pairing field are derived in great details. These derivations are the one used in the HFB3 code.

I.2.1 Direct mean field

The Coulomb contribution to the direct mean field reads as follows:

$$\Gamma^{\tau_p}_{\alpha\gamma}(D) = e^2 \sum_{\delta\beta} \langle \alpha\beta | \frac{1}{|\vec{r}_1 - \vec{r}_2|} | \gamma\delta \rangle \rho^{\tau_p}_{\delta\beta} \tag{I.55}$$

We rewrite Eq.(I.55) developing the spin and isospin conditions:

$$\Gamma^{\tau_p}_{\alpha\gamma}(D) = e^2 \delta_{s_\alpha s_\gamma} \sum_{\delta\beta} \langle \alpha\beta | \frac{1}{|\vec{r}_1 - \vec{r}_2|} | \gamma\delta \rangle [\rho^{\tau_p --}_{\delta\beta} + \rho^{\tau_p ++}_{\delta\beta}] \tag{I.56}$$

We then use the time-reversal properties of the density:

$$\boxed{\Gamma^{\tau_p}_{\alpha\gamma}(D) = 2e^2\delta_{s_\alpha s_\gamma}\sum_{\delta\beta>}\langle\alpha\beta|\frac{1}{|\vec{r}_1-\vec{r}_2|}|\gamma\delta\rangle[\rho^{\tau_p--}_{\delta\beta}+\rho^{\tau_p++}_{\delta\beta}]} \tag{I.57}$$

In the following, we explicitly consider the spins of α and γ.

Block ++:

Here, we consider the spins ($\alpha\uparrow$,$\gamma\uparrow$). In this case, the direct mean field reads:

$$\Gamma^{\tau_p++}_{\alpha\gamma}(D) = 2e^2\sum_{\delta\beta>}\langle\alpha\beta|\frac{1}{|\vec{r}_1-\vec{r}_2|}|\gamma\delta\rangle[\rho^{\tau_p--}_{\delta\beta}+\rho^{\tau_p++}_{\delta\beta}] \tag{I.58}$$

We set:

$$R_{\delta\beta}(D) = [\rho^{\tau_p--}_{\delta\beta}+\rho^{\tau_p++}_{\delta\beta}] \tag{I.59}$$

Developing the spatial part of Eq.(I.58), we finally find the expression of the Coulomb direct mean field used in the HFB3 code:

$$\boxed{\Gamma^{\tau_p++}_{\alpha\gamma}(D) = 2e^2\sum_{n_{za}}T^{n_{za}}_{(d_\alpha,n_{z_\alpha})(d_\gamma,n_{z_\gamma})}\sum_{n_a}T^{(0,n_a)}_{(m,n_\alpha)(m,n_\gamma)}\sum_{\delta\beta>}J^{n_a n_{za}}_{(d_\alpha,d_\gamma)\delta\beta}R_{\delta\beta}(D)} \tag{I.60}$$

Block −−:

Here, we consider the spins ($\alpha\downarrow$,$\gamma\downarrow$). Lookin at Eq.(I.57), it is clear that we have:

$$\boxed{\Gamma^{\tau_p--}_{\alpha\gamma}(D) = \Gamma^{\tau_p++}_{\alpha\gamma}(D)} \tag{I.61}$$

Block −+:

Here, we consider the spins ($\alpha\downarrow$,$\gamma\uparrow$). From Eq.(I.57), it is clear that we have:

$$\boxed{\Gamma^{\tau_p-+}_{\alpha\gamma}(D) = 0} \tag{I.62}$$

Block +−:

Here, we consider the spins ($\alpha\uparrow$,$\gamma\downarrow$). From Eq.(I.57), it is clear that we have:

$$\boxed{\Gamma^{\tau_p+-}_{\alpha\gamma}(D) = 0} \tag{I.63}$$

I.2.2 Exchange mean field

The Coulomb contribution to the exchange mean field reads as follows:

$$\Gamma^{\tau_p}_{\alpha\gamma}(E) = -e^2 \sum_{\delta\beta} \langle\alpha\beta| \frac{1}{|\vec{r}_1 - \vec{r}_2|} |\delta\gamma\rangle \rho^{\tau_p}_{\delta\beta} \tag{I.64}$$

We start writting explicitly the spin conditions:

$$\Gamma^{\tau_p}_{\alpha\gamma}(E) = -e^2 \sum_{\delta\beta} \langle\alpha\beta| \frac{1}{|\vec{r}_1 - \vec{r}_2|} |\delta\gamma\rangle \delta_{s_\alpha s_\delta} \delta_{s_\beta s_\gamma} \rho^{\tau_p}_{\delta\beta} \tag{I.65}$$

We then use the time-reversal properties of the density:

$$\boxed{\begin{aligned}\Gamma^{\tau_p}_{\alpha\gamma}(E) = -e^2 \sum_{\delta\beta>} [&\langle\alpha\beta| \frac{1}{|\vec{r}_1 - \vec{r}_2|} |\delta\gamma\rangle \delta_{s_\alpha s_\delta} \delta_{s_\beta s_\gamma} \\ &+ (-1)^{s_\delta - s_\beta} \langle\alpha\bar{\beta}| \frac{1}{|\vec{r}_1 - \vec{r}_2|} |\bar{\delta}\gamma\rangle \delta_{s_\alpha \bar{s_\delta}} \delta_{\bar{s_\beta} s_\gamma}] \rho^{\tau_p}_{\delta\beta}\end{aligned}} \tag{I.66}$$

In the following, we explicitly consider the spins of α and γ.

Block ++:

Here, we consider the spins (α $\uparrow$,γ $\uparrow$). In this case, the Coulomb exchange mean field reads:

$$\Gamma^{\tau_p ++}_{\alpha\gamma}(E) = -e^2 \sum_{\delta\beta>} [\langle\alpha\beta| \frac{1}{|\vec{r}_1 - \vec{r}_2|} |\delta\gamma\rangle \delta_{s^+_\delta s^+_\beta} + \langle\alpha\bar{\beta}| \frac{1}{|\vec{r}_1 - \vec{r}_2|} |\bar{\delta}\gamma\rangle \delta_{s^-_{\bar{\delta}} s^-_{\bar{\beta}}}] \rho^{\tau_p}_{\delta\beta} \tag{I.67}$$

We set:

$$R^{++}_{\delta\beta}(E) = \begin{cases} \rho^{\tau_p ++}_{\delta\beta} & m' \geq 0 \\ \rho^{\tau_p --}_{\delta\beta} & m' < 0 \end{cases} \tag{I.68}$$

Thanks to Eq.(I.68), we write:

$$\Gamma^{\tau_p ++}_{\alpha\gamma}(E) = -e^2 \sum_{\delta\beta>} \sum_{m'} \langle\alpha\beta| \frac{1}{|\vec{r}_1 - \vec{r}_2|} |\delta\gamma\rangle R^{++}_{\delta\beta}(E) \tag{I.69}$$

As explained in section I.1.1, we tranform the spatial part of Eq.(I.69) into an integral of Central terms, then we perform a quadrature:

$$\boxed{\Gamma^{\tau_p ++}_{\alpha\gamma}(E) \approx -\frac{4e^2}{\sqrt{\pi}} \sum_{i=0}^{n_{GLE}} \frac{w_i}{(1+x_i)^2} \sum_{n_\delta n_\beta} \sum_{m'} (I_{r x_i})^{\delta\gamma}_{\alpha\beta} \sum_{d_\delta d_\beta} \sum_{n_{z_\delta} n_{z_\beta}} (I_{z x_i})^{\delta\gamma}_{\alpha\beta} R^{++}_{\delta\beta}(E)} \tag{I.70}$$

Block $--$:

Here, we consider the spins ($\alpha\ \downarrow$,$\gamma\ \downarrow$). In this case, the Coulomb exchange mean field reads:

$$\Gamma^{\tau_p --}_{\alpha\gamma}(E) = -e^2 \sum_{\delta\beta>} [\langle\alpha\beta| \frac{1}{|\vec{r}_1 - \vec{r}_2|} |\delta\gamma\rangle \delta_{s_\delta^- s_\beta^-} + \langle\alpha\bar{\beta}| \frac{1}{|\vec{r}_1 - \vec{r}_2|} |\bar{\delta}\gamma\rangle \delta_{s_\delta^+ s_\beta^+}] \rho^{\tau_p}_{\delta\beta} \tag{I.71}$$

It is easy to deduce the expression of the $--$ exchange mean field from the one of the $++$ exchange mean field. Indeed, we just have to inverse the $m' < 0$ and $m' \geq 0$ contributions:

$$\boxed{\Gamma^{\tau_p --}_{\alpha\gamma}(E) \approx -\frac{4e^2}{\sqrt{\pi}} \sum_{i=0}^{n_{GLE}} \frac{w_i}{(1+x_i)^2} \sum_{n_\delta n_\beta} \sum_{m'} (I_{rx_i})^{\bar{\delta}\gamma}_{\alpha\bar{\beta}} \sum_{d_\delta d_\beta} \sum_{n_{z_\delta} n_{z_\beta}} (I_{zx_i})^{\delta\gamma}_{\alpha\beta} R^{++}_{\delta\beta}(E)} \tag{I.72}$$

We remark that the contraction of I_{zx} and R is the same as in the $++$ case. Thus, this contraction is calculated only one time in the HFB3 code.

Block $-+$:

Here, we consider the spins ($\alpha\ \downarrow$,$\gamma\ \uparrow$). In this case, the Coulomb exchange mean field reads:

$$\Gamma^{\tau_p -+}_{\alpha\gamma}(E) = -e^2 \sum_{\delta\beta>} [\langle\alpha\beta| \frac{1}{|\vec{r}_1 - \vec{r}_2|} |\delta\gamma\rangle \delta_{s_\delta^- s_\beta^+} - \langle\alpha\bar{\beta}| \frac{1}{|\vec{r}_1 - \vec{r}_2|} |\bar{\delta}\gamma\rangle \delta_{s_\delta^+ s_\beta^-}] \rho^{\tau_p}_{\delta\beta} \tag{I.73}$$

We set:

$$R^{-+}_{\delta\beta}(E) = \begin{cases} \rho^{\tau_p -+}_{\delta\beta} & m' > 0 \\ -\rho^{\tau_p +-}_{\delta\beta} & m' \leq 0 \end{cases} \tag{I.74}$$

Using Eq.(I.74), we write for this part of the exchange mean field:

$$\boxed{\Gamma^{\tau_p -+}_{\alpha\gamma}(E) \approx -\frac{4e^2}{\sqrt{\pi}} \sum_{i=0}^{n_{GLE}} \frac{w_i}{(1+x_i)^2} \sum_{n_\delta n_\beta} \sum_{m'} (I_{rx_i})^{\delta\gamma}_{\alpha\beta} \sum_{d_\delta d_\beta} \sum_{n_{z_\delta} n_{z_\beta}} (I_{zx_i})^{\delta\gamma}_{\alpha\beta} R^{-+}_{\delta\beta}(E)} \tag{I.75}$$

Block $+-$:

Here, we consider the spins ($\alpha\ \uparrow$,$\gamma\ \downarrow$). Thanks to the symmetry of the exchange mean field, we directly have:

$$\boxed{\Gamma^{\tau_p +-}_{\alpha\gamma}(E) = \Gamma^{\tau_p -+}_{\gamma\alpha}(E)} \tag{I.76}$$

I.2.3 Pairing field

The Coulomb contribution to the pairing field reads as follows:

$$\Delta^{\tau_p}_{\alpha\bar{\beta}} = e^2 \sum_{\delta\gamma} (-1)^{s_\beta - s_\delta} \langle \alpha\bar{\beta}| \frac{1}{|\vec{r}_1 - \vec{r}_2|} |\gamma\bar{\delta}\rangle \kappa^{\tau_p}_{\gamma\bar{\delta}} \tag{I.77}$$

We start developing the spin conditions:

$$\Delta^{\tau_p}_{\alpha\bar{\beta}} = e^2 \sum_{\delta\gamma} (-1)^{s_\beta - s_\delta} \langle \alpha\bar{\beta}| \frac{1}{|\vec{r}_1 - \vec{r}_2|} |\gamma\bar{\delta}\rangle \delta_{s_\alpha s_\gamma} \delta_{s_\beta s_\delta} \kappa^{\tau_p}_{\gamma\bar{\delta}} \tag{I.78}$$

We use the time-reversal properties of the pairing tensor:

$$\boxed{\begin{aligned}\Delta^{\tau_p}_{\alpha\bar{\beta}} = e^2 \sum_{\delta\gamma>} [&(-1)^{s_\beta - s_\delta} \langle \alpha\bar{\beta}| \frac{1}{|\vec{r}_1 - \vec{r}_2|} |\gamma\bar{\delta}\rangle \delta_{s_\alpha s_\gamma} \delta_{s_\beta s_\delta} \\ &+ (-1)^{s_\beta + s_\gamma} \langle \alpha\bar{\beta}| \frac{1}{|\vec{r}_1 - \vec{r}_2|} |\bar{\gamma}\delta\rangle \delta_{s_\alpha \bar{s_\gamma}} \delta_{s_\beta \bar{s_\delta}}] \kappa^{\tau_p}_{\gamma\bar{\delta}}\end{aligned}} \tag{I.79}$$

In the following, we explicitly consider the spins of α and $\bar{\beta}$.

Block ++:

Here, we consider the spins ($\alpha\uparrow$,$\bar{\beta}\uparrow$). In this case, the pairing field reads:

$$\Delta^{\tau_p ++}_{\alpha\bar{\beta}} = e^2 \sum_{\delta\gamma>} [\langle \alpha\bar{\beta}| \frac{1}{|\vec{r}_1 - \vec{r}_2|} |\gamma\bar{\delta}\rangle \delta_{s^+_\gamma s^+_\delta} + \langle \alpha\bar{\beta}| \frac{1}{|\vec{r}_1 - \vec{r}_2|} |\bar{\gamma}\delta\rangle \delta_{s^-_\gamma s^-_\delta}] \kappa^{\tau_p}_{\gamma\bar{\delta}} \tag{I.80}$$

We set:

$$K^{++}_{\gamma\bar{\delta}} = \begin{cases} \kappa^{\tau_p ++}_{\gamma\bar{\delta}} & m' \geq 0 \\ \kappa^{\tau_p --}_{\gamma\bar{\delta}} & m' < 0 \end{cases} \tag{I.81}$$

Thanks to Eq.(I.81) and developing the spatial part of the pairing field, we get:

$$\boxed{\Delta^{\tau_p ++}_{\alpha\bar{\beta}} \approx \frac{4e^2}{\sqrt{\pi}} \sum_{i=0}^{n_{GLE}} \frac{w_i}{(1+x_i)^2} \sum_{n_\gamma n_\delta} \sum_{m'} (I_{rx_i})^{\gamma\bar{\delta}}_{\alpha\bar{\beta}} \sum_{d_\gamma d_\delta} \sum_{n_{z_\gamma} n_{z_\delta}} (I_{zx_i})^{\gamma\delta}_{\alpha\beta} K^{++}_{\gamma\bar{\delta}}} \tag{I.82}$$

Block −−:

Here, we consider the spins ($\alpha\downarrow$,$\bar{\beta}\downarrow$). In this case, the pairing field reads:

$$\Delta^{\tau_p --}_{\alpha\bar{\beta}} = e^2 \sum_{\delta\gamma>} [\langle \alpha\bar{\beta}| \frac{1}{|\vec{r}_1 - \vec{r}_2|} |\gamma\bar{\delta}\rangle \delta_{s^-_\gamma s^-_\delta} + \langle \alpha\bar{\beta}| \frac{1}{|\vec{r}_1 - \vec{r}_2|} |\bar{\gamma}\delta\rangle \delta_{s^+_\gamma s^+_\delta}] \kappa^{\tau_p}_{\gamma\bar{\delta}} \tag{I.83}$$

As for the exchange mean field, it is enough to inverse the $m' < 0$ and $m' \geq 0$ contributions:

$$\boxed{\Delta^{\tau_p --}_{\alpha\bar{\beta}} \approx \frac{4e^2}{\sqrt{\pi}} \sum_{i=0}^{n_{GLE}} \frac{w_i}{(1+x_i)^2} \sum_{n_\gamma n_\delta} \sum_{m'} (I_{rx_i})^{\bar{\gamma}\delta}_{\alpha\bar{\beta}} \sum_{d_\gamma d_\delta} \sum_{n_{z_\gamma} n_{z_\delta}} (I_{zx_i})^{\gamma\delta}_{\alpha\beta} K^{++}_{\gamma\bar{\delta}}} \tag{I.84}$$

Block $-+$:

Here, we consider the spins ($\alpha\downarrow$,$\bar{\beta}\uparrow$). In this case, the pairing field reads:

$$\Delta^{\tau_p -+}_{\alpha\bar{\beta}} = e^2 \sum_{\delta\gamma>} [\langle\alpha\bar{\beta}| \frac{1}{|\vec{r}_1 - \vec{r}_2|} |\gamma\bar{\delta}\rangle \delta_{s^-_\gamma s^+_\delta} - \langle\alpha\bar{\beta}| \frac{1}{|\vec{r}_1 - \vec{r}_2|} |\bar{\gamma}\delta\rangle \delta_{s^+_\gamma s^-_\delta}] \kappa^{\tau_p}_{\gamma\bar{\delta}} \tag{I.85}$$

We set:

$$K^{-+}_{\gamma\bar{\delta}} = \begin{cases} \kappa^{\tau_p -+}_{\gamma\delta} & m' > 0 \\ -\kappa^{\tau_p +-}_{\gamma\delta} & m' \leq 0 \end{cases} \tag{I.86}$$

The pairing field then reads:

$$\boxed{\Delta^{\tau_p -+}_{\alpha\bar{\beta}} \approx \frac{4e^2}{\sqrt{\pi}} \sum_{i=0}^{n_{GLE}} \frac{w_i}{(1+x_i)^2} \sum_{n_\gamma n_\delta} \sum_{m'} (I_{rx_i})^{\gamma\bar{\delta}}_{\alpha\bar{\beta}} \sum_{d_\gamma d_\delta} \sum_{n_{z_\gamma} n_{z_\delta}} (I_{zx_i})^{\gamma\delta}_{\alpha\beta} K^{-+}_{\gamma\bar{\delta}}} \tag{I.87}$$

Block $+-$:

Here, we consider the spins ($\alpha\uparrow$,$\bar{\beta}\downarrow$). Thanks to the symmetry of the pairing field, we directly find:

$$\boxed{\Delta^{\tau_p +-}_{\alpha\bar{\beta}} = \Delta^{\tau_p -+}_{\beta\bar{\alpha}}} \tag{I.88}$$

I.3 The Slater approximation

The Slater approximation [49] gives a simple and convenient expression of the Coulomb exchange contribution to the energy:

$$\boxed{E_S = -\frac{3}{4} e^2 (\frac{3}{\pi})^{1/3} \int d^3\vec{r} (\rho(\vec{r})^{\tau_p})^{4/3}} \tag{I.89}$$

As Eq.(I.89) depends on the density, it is possible to build an associated rearrangement field as done in [46]. We tried this method but didn't observe significant changes in the HFB calculations. For this reason, we decided not to keep this associated rearrangement field. In Figure (I.1), we displayed an evaluation of the Slater approximation's accuracy in an adiabatic ^{240}Pu set obtained with the $\tilde{\mathcal{P}}_{20}$ procedure. In panel (a), the black curve represents the Slater energy whereas the blue and purple dashed curves account respectively for the

Coulomb exchange and Coulomb pairing+exchange contributions to the energy. In panel (b), we've isolated the Coulomb pairing contribution to the energy. For this evaluation, we considered HFB states built with the slater approximation and then evaluated the Coulomb energy with the exact treatment of all the Coulomb fields, without redoing any convergence. This way to evaluate the Slater approximation may seem a bit naive, as it is not self-consistent (the differences when considering self-consistency are studied in Chapter 4). However, here we wanted to focus on the simple energy difference we may find evaluating the same state with the two different methods:

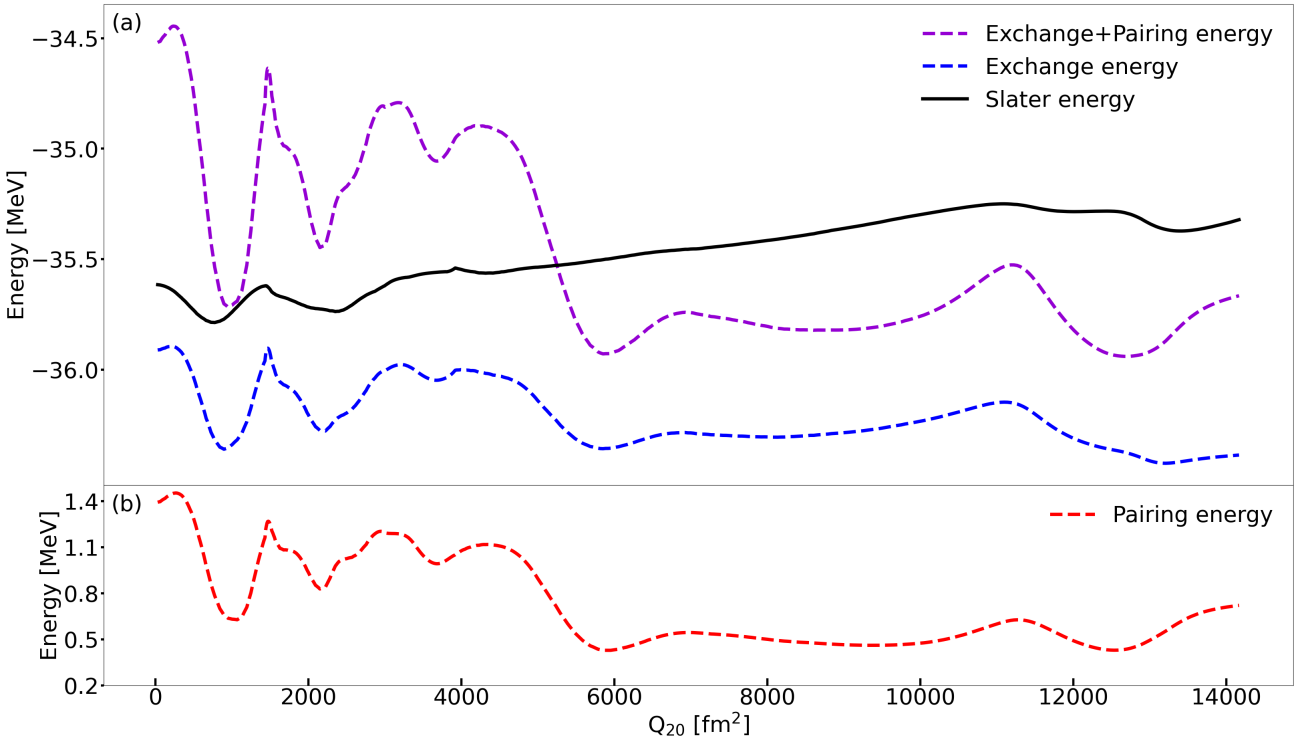

Figure I.1: Evaluation of the Slater approximation in the ^{240}Pu adiabatic set obtained with the procedure $\tilde{\mathcal{P}}_{20}$ and displayed with respect to the quadrupole deformation. Panel (a): the Slater energy compared to the exchange and exchange+pairing contributions to the energy. Panel (b): the Coulomb contribution th the pairing energy.

The differences between the black and the purple curves are rather small, especially when we compare them with the total binding energy of the ^{240}Pu. The curves accounting for the exact treatment of the Coulomb interaction display variations that are not in line with what is usually found for the energy coming from a field. It suggests that the nucleus has locally behaved in a way which wouldn't have been favored with an exact treatment of the Coulomb interaction.

I.4 Collective fields

This part aims to give an expression of the Coulomb contribution to the direct mean field, exchange mean field and pairing field in the more complex case when ρ^{01} is not symmetric anymore and the two harmonic oscillator bases $\{0\}$ and $\{1\}$ are different. These derivations allows us to evaluate quantities of the following type :

$$\langle\Phi_0|\hat{H}|\Phi_1\rangle \tag{I.90}$$

These quantities are not only useful in the SCIM approach but appear in many situations as for instance in the expression of the true TDGCM mass and collective potential.

I.4.1 Collective direct mean field

The Coulomb contribution to the collective direct mean field reads as follows:

$$\bar{\Gamma}^{\tau_p}_{\alpha\gamma}(D) = e^2 \sum_{\delta\beta} {}_0\langle\alpha\beta|\frac{1}{|\vec{r}_1-\vec{r}_2|}|\gamma\delta\rangle_1 \rho^{01\tau_p}_{\delta\beta} \tag{I.91}$$

We first develop the spin conditions:

$$\bar{\Gamma}^{\tau_p}_{\alpha\gamma}(D) = e^2\delta_{s_\alpha s_\gamma} \sum_{\delta\beta} {}_0\langle\alpha\beta|\frac{1}{|\vec{r}_1-\vec{r}_2|}|\gamma\delta\rangle_1 [\rho^{01\tau_p --}_{\delta\beta} + \rho^{01\tau_p ++}_{\delta\beta}] \tag{I.92}$$

We then use the time-reversal properties of the matrix ρ^{01}:

$$\boxed{\bar{\Gamma}^{\tau_p}_{\alpha\gamma}(D) = 2e^2\delta_{s_\alpha s_\gamma} \sum_{\delta\beta>} {}_0\langle\alpha\beta|\frac{1}{|\vec{r}_1-\vec{r}_2|}|\gamma\delta\rangle_1 [\rho^{01\tau_p --}_{\delta\beta} + \rho^{01\tau_p ++}_{\delta\beta}]} \tag{I.93}$$

Here, we used the fact that $m_\beta = m_\delta$ in order to write ${}_0\langle\alpha\beta|\frac{1}{|\vec{r}_1-\vec{r}_2|}|\gamma\delta\rangle_1 = {}_0\langle\alpha\bar{\beta}|\frac{1}{|\vec{r}_1-\vec{r}_2|}|\gamma\bar{\delta}\rangle_1$. In the following, we explicitly consider the spins of α and γ.

Block ++:

Here, we consider the spins ($\alpha\uparrow$,$\gamma\uparrow$). In this case, the collective direct mean field reads:

$$\bar{\Gamma}^{\tau_p ++}_{\alpha\gamma}(D) = 2e^2 \sum_{\delta\beta>} {}_0\langle\alpha\beta|\frac{1}{|\vec{r}_1-\vec{r}_2|}|\gamma\delta\rangle_1 [\rho^{01\tau_p --}_{\delta\beta} + \rho^{01\tau_p ++}_{\delta\beta}] \tag{I.94}$$

We set:

$$R^{01}_{\delta\beta}(D) = [\rho^{01\tau_p --}_{\delta\beta} + \rho^{01\tau_p ++}_{\delta\beta}] \tag{I.95}$$

Thanks to Eq.(I.95) and developing the spatial part of the collective field, we find:

$$\boxed{\bar{\Gamma}^{\tau_p ++}_{\alpha\gamma}(D) \approx \frac{8e^2}{\sqrt{\pi}} \sum_{i=0}^{n_{GLE}} \frac{w_i}{(1+x_i)^2} \sum_{n_\delta n_\beta} \sum_{m'>} (\bar{I}_{rx_i})^{\gamma\delta}_{\alpha\beta} \sum_{d_\delta d_\beta} \sum_{n_{z_\delta} n_{z_\beta}} (I_{zx_i})^{\gamma\delta}_{\alpha\beta} R^{01}_{\delta\beta}(D)} \tag{I.96}$$

Block −−:

Here, we consider the spins ($\alpha\downarrow$,$\gamma\downarrow$). As for the non-collective case, we directly find:

$$\boxed{\bar{\Gamma}^{\tau_p --}_{\alpha\gamma}(D) = \bar{\Gamma}^{\tau_p ++}_{\alpha\gamma}(D)} \tag{I.97}$$

Block $-+$:

Here, we consider the spins ($\alpha\downarrow$,$\gamma\uparrow$). As for the non-collective case, we directly find:

$$\boxed{\bar{\Gamma}^{\tau_p -+}_{\alpha\gamma}(D) = 0} \tag{I.98}$$

Block $+-$:

Here, we consider the spins ($\alpha\uparrow$,$\gamma\downarrow$). As for the non-collective case, we directly find:

$$\boxed{\bar{\Gamma}^{\tau_p +-}_{\alpha\gamma}(D) = 0} \tag{I.99}$$

I.4.2 Collective exchange mean field

The Coulomb contribution to the collective exchange mean field reads as follows:

$$\bar{\Gamma}^{\tau_p}_{\alpha\gamma}(E) = -e^2 \sum_{\delta\beta} {}_0\langle\alpha\beta| \frac{1}{|\vec{r}_1 - \vec{r}_2|} |\delta\gamma\rangle_1 \rho^{01\tau_p}_{\delta\beta} \tag{I.100}$$

We start developing the spin conditions:

$$\bar{\Gamma}^{\tau_p}_{\alpha\gamma}(E) = -e^2 \sum_{\delta\beta} {}_0\langle\alpha\beta| \frac{1}{|\vec{r}_1 - \vec{r}_2|} |\delta\gamma\rangle_1 \delta_{s_\alpha s_\delta} \delta_{s_\beta s_\gamma} \rho^{01\tau_p}_{\delta\beta} \tag{I.101}$$

We then use the time-reversal properties of ρ^{01}:

$$\boxed{\begin{aligned} \bar{\Gamma}^{\tau_p}_{\alpha\gamma}(E) = -e^2 \sum_{\delta\beta>} [& {}_0\langle\alpha\beta| \frac{1}{|\vec{r}_1 - \vec{r}_2|} |\delta\gamma\rangle_1 \delta_{s_\alpha s_\delta} \delta_{s_\beta s_\gamma} \\ & + (-1)^{s_\delta - s_\beta} {}_0\langle\alpha\bar{\beta}| \frac{1}{|\vec{r}_1 - \vec{r}_2|} |\bar{\delta}\gamma\rangle_1 \delta_{s_\alpha \bar{s_\delta}} \delta_{\bar{s_\beta} s_\gamma}] \rho^{01\tau_p}_{\delta\beta} \end{aligned}} \tag{I.102}$$

In the following, we explicitly consider the spins of α and γ.

Block $++$:

Here, we consider the spins ($\alpha\uparrow$,$\gamma\uparrow$). In this case, the collective exchange mean field reads:

$$\bar{\Gamma}^{\tau_p ++}_{\alpha\gamma}(E) = -e^2 \sum_{\delta\beta>} [{}_0\langle\alpha\beta| \frac{1}{|\vec{r}_1 - \vec{r}_2|} |\delta\gamma\rangle_1 \delta_{s^+_\delta s^+_\beta} + {}_0\langle\alpha\bar{\beta}| \frac{1}{|\vec{r}_1 - \vec{r}_2|} |\bar{\delta}\gamma\rangle_1 \delta_{s^-_\delta s^-_\beta}] \rho^{01\tau_p}_{\delta\beta} \tag{I.103}$$

We set:

$$R_{\delta\beta}^{01++}(E) = \begin{cases} \rho_{\delta\beta}^{01\tau_p++} & m' \geq 0 \\ \rho_{\delta\beta}^{01\tau_p--} & m' < 0 \end{cases} \tag{I.104}$$

Thanks to Eq.(I.104), we write:

$$\bar{\Gamma}_{\alpha\gamma}^{\tau_p++}(E) = -e^2 \sum_{\delta\beta>} \sum_{m'} {}_0\langle\alpha\beta| \frac{1}{|\vec{r}_1 - \vec{r}_2|} |\delta\gamma\rangle_1 R_{\delta\beta}^{01++}(E) \tag{I.105}$$

Developing the spatial part of Eq.(I.105), we eventually find:

$$\boxed{\bar{\Gamma}_{\alpha\gamma}^{\tau_p++}(E) \approx -\frac{4e^2}{\sqrt{\pi}} \sum_{i=0}^{n_{GLE}} \frac{w_i}{(1+x_i)^2} \sum_{n_\delta n_\beta} \sum_{m'} (\bar{I}_{rx_i})_{\alpha\beta}^{\delta\gamma} \sum_{d_\delta d_\beta} \sum_{n_{z_\delta} n_{z_\beta}} (\bar{I}_{zx_i})_{\alpha\beta}^{\delta\gamma} R_{\delta\beta}^{01++}(E)} \tag{I.106}$$

Block $--$:

Here, we consider the spins ($\alpha\downarrow$,$\gamma\downarrow$). By analogy with the non-collective case we directly write:

$$\boxed{\bar{\Gamma}_{\alpha\gamma}^{\tau_p--}(E) \approx -\frac{4e^2}{\sqrt{\pi}} \sum_{i=0}^{n_{GLE}} \frac{w_i}{(1+x_i)^2} \sum_{n_\delta n_\beta} \sum_{m'} (\bar{I}_{rx_i})_{\alpha\bar{\beta}}^{\bar{\delta}\gamma} \sum_{d_\delta d_\beta} \sum_{n_{z_\delta} n_{z_\beta}} (\bar{I}_{zx_i})_{\alpha\beta}^{\delta\gamma} R_{\delta\beta}^{01++}(E)} \tag{I.107}$$

Block $-+$:

Here, we consider the spins ($\alpha\downarrow$,$\gamma\uparrow$). In this case, the collective exchange mean field reads:

$$\bar{\Gamma}_{\alpha\gamma}^{\tau_p-+}(E) = -e^2 \sum_{\delta\beta>} [{}_0\langle\alpha\beta| \frac{1}{|\vec{r}_1 - \vec{r}_2|} |\delta\gamma\rangle_1 \delta_{s_\delta^- s_\beta^+} - {}_0\langle\alpha\bar{\beta}| \frac{1}{|\vec{r}_1 - \vec{r}_2|} |\bar{\delta}\gamma\rangle_1 \delta_{s_\delta^+ s_\beta^-}] \rho_{\delta\beta}^{01\tau_p} \tag{I.108}$$

We set:

$$R_{\delta\beta}^{01-+}(E) = \begin{cases} \rho_{\delta\beta}^{01\tau_p-+} & m' > 0 \\ -\rho_{\delta\beta}^{01\tau_p+-} & m' \leq 0 \end{cases} \tag{I.109}$$

Developing the spatial part of Eq.(I.108) and using Eq.(I.109), we eventually find:

$$\boxed{\bar{\Gamma}_{\alpha\gamma}^{\tau_p-+}(E) \approx -\frac{4e^2}{\sqrt{\pi}} \sum_{i=0}^{n_{GLE}} \frac{w_i}{(1+x_i)^2} \sum_{n_\delta n_\beta} \sum_{m'} (\bar{I}_{rx_i})_{\alpha\beta}^{\delta\gamma} \sum_{d_\delta d_\beta} \sum_{n_{z_\delta} n_{z_\beta}} (\bar{I}_{zx_i})_{\alpha\beta}^{\delta\gamma} R_{\delta\beta}^{01-+}(E)} \tag{I.110}$$

Block $+-$:

Here, we consider the spins ($\alpha\uparrow$,$\gamma\downarrow$). As the matrix ρ^{01} is no more symmetric in general, we have to consider explicitly this case. However, by analogy with the $-+$ part, we easily find:

$$\boxed{\bar{\Gamma}^{\tau_p+-}_{\alpha\gamma}(E) \approx \frac{4e^2}{\sqrt{\pi}} \sum_{i=0}^{n_{GLE}} \frac{w_i}{(1+x_i)^2} \sum_{n_\delta n_\beta} \sum_{m'} (\bar{I}_{rx_i})^{\bar{\delta}\gamma}_{\alpha\bar{\beta}} \sum_{d_\delta d_\beta} \sum_{n_{z_\delta} n_{z_\beta}} (\bar{I}_{zx_i})^{\delta\gamma}_{\alpha\beta} R^{01-+}_{\delta\beta}(E)} \tag{I.111}$$

I.4.3 Collective pairing field

The Coulomb contribution to the collective pairing field reads as follows:

$$\bar{\Delta}^{\tau_p}_{\alpha\bar{\beta}} = e^2 \sum_{\delta\gamma} (-1)^{s_\beta - s_\delta} {}_0\langle\alpha\bar{\beta}| \frac{1}{|\vec{r}_1 - \vec{r}_2|} |\gamma\bar{\delta}\rangle_1 \kappa^{01\tau_p}_{\gamma\bar{\delta}} \tag{I.112}$$

We start developing the spin conditions:

$$\bar{\Delta}^{\tau_p}_{\alpha\bar{\beta}} = e^2 \sum_{\delta\gamma} (-1)^{s_\beta - s_\delta} {}_0\langle\alpha\bar{\beta}| \frac{1}{|\vec{r}_1 - \vec{r}_2|} |\gamma\bar{\delta}\rangle_1 \delta_{s_\alpha s_\gamma} \delta_{s_\beta s_\delta} \kappa^{01\tau_p}_{\gamma\bar{\delta}} \tag{I.113}$$

We then use the time-reversal properties of the matrix κ^{01}:

$$\boxed{\begin{aligned}\bar{\Delta}^{\tau_p}_{\alpha\bar{\beta}} = e^2 \sum_{\delta\gamma>} [&(-1)^{s_\beta - s_\delta} {}_0\langle\alpha\bar{\beta}| \frac{1}{|\vec{r}_1 - \vec{r}_2|} |\gamma\bar{\delta}\rangle_1 \delta_{s_\alpha s_\gamma} \delta_{s_\beta s_\delta} \\ &+ (-1)^{s_\beta + s_\gamma} {}_0\langle\alpha\bar{\beta}| \frac{1}{|\vec{r}_1 - \vec{r}_2|} |\bar{\gamma}\delta\rangle_1 \delta_{s_\alpha \bar{s_\gamma}} \delta_{s_\beta \bar{s_\delta}}] \kappa^{01\tau_p}_{\gamma\bar{\delta}}\end{aligned}} \tag{I.114}$$

In the following, we explicitly consider the spins of α and $\bar{\beta}$.

Block ++:

Here, we consider the spins ($\alpha\uparrow$,$\bar{\beta}\uparrow$). In this case, the collective pairing field reads:

$$\bar{\Delta}^{\tau_p++}_{\alpha\bar{\beta}} = e^2 \sum_{\delta\gamma>} [{}_0\langle\alpha\bar{\beta}| \frac{1}{|\vec{r}_1 - \vec{r}_2|} |\gamma\bar{\delta}\rangle_1 \delta_{s^+_\gamma s^+_\delta} + {}_0\langle\alpha\bar{\beta}| \frac{1}{|\vec{r}_1 - \vec{r}_2|} |\bar{\gamma}\delta\rangle_1 \delta_{s^-_\gamma s^-_\delta}] \kappa^{01\tau_p}_{\gamma\bar{\delta}} \tag{I.115}$$

We set:

$$K^{01++}_{\gamma\bar{\delta}} = \begin{cases} \kappa^{01\tau_p++}_{\gamma\bar{\delta}} & m' \geq 0 \\ \kappa^{01\tau_p--}_{\gamma\bar{\delta}} & m' < 0 \end{cases} \tag{I.116}$$

Using Eq.(I.116) and developing the spatial part of Eq.(I.115), we write:

$$\boxed{\bar{\Delta}^{\tau_p++}_{\alpha\bar{\beta}} \approx \frac{4e^2}{\sqrt{\pi}} \sum_{i=0}^{n_{GLE}} \frac{w_i}{(1+x_i)^2} \sum_{n_\gamma n_\delta} \sum_{m'} (\bar{I}_{rx_i})^{\gamma\bar{\delta}}_{\alpha\bar{\beta}} \sum_{d_\gamma d_\delta} \sum_{n_{z_\gamma} n_{z_\delta}} (\bar{I}_{zx_i})^{\gamma\delta}_{\alpha\beta} K^{01++}_{\gamma\bar{\delta}}} \tag{I.117}$$

Block $--$:

Here, we consider the spins ($\alpha\downarrow$,$\bar{\beta}\downarrow$). By analogy with the non-collective case, we directly have:

$$\boxed{\bar{\Delta}^{\tau_p--}_{\alpha\bar{\beta}} \approx \frac{4e^2}{\sqrt{\pi}} \sum_{i=0}^{n_{GLE}} \frac{w_i}{(1+x_i)^2} \sum_{n_\gamma n_\delta} \sum_{m'} (\bar{I}_{rx_i})^{\bar{\gamma}\delta}_{\alpha\bar{\beta}} \sum_{d_\gamma d_\delta} \sum_{n_{z_\gamma} n_{z_\delta}} (\bar{I}_{zx_i})^{\gamma\delta}_{\alpha\beta} K^{01++}_{\gamma\bar{\delta}}} \tag{I.118}$$

Block $-+$:

Here, we consider the spins ($\alpha\downarrow$,$\bar{\beta}\uparrow$). In this case, the collective pairing field reads:

$$\bar{\Delta}^{\tau_p-+}_{\alpha\bar{\beta}} = e^2 \sum_{\delta\gamma>} [{}_0\langle\alpha\bar{\beta}|\frac{1}{|\vec{r}_1-\vec{r}_2|}|\gamma\bar{\delta}\rangle_1 \delta_{s^-_\gamma s^+_\delta} - {}_0\langle\alpha\bar{\beta}|\frac{1}{|\vec{r}_1-\vec{r}_2|}|\bar{\gamma}\delta\rangle_1 \delta_{s^+_\gamma s^-_\delta}] \kappa^{01\tau_p}_{\gamma\bar{\delta}} \tag{I.119}$$

We set:

$$K^{01-+}_{\gamma\bar{\delta}} = \begin{cases} \kappa^{01\tau_p-+}_{\gamma\delta} & m' > 0 \\ -\kappa^{01\tau_p+-}_{\gamma\delta} & m' \leq 0 \end{cases} \tag{I.120}$$

Thanks to Eq.(I.120) and developing the spatial part of Eq.(I.119), we finally get:

$$\boxed{\bar{\Delta}^{\tau_p-+}_{\alpha\bar{\beta}} \approx \frac{4e^2}{\sqrt{\pi}} \sum_{i=0}^{n_{GLE}} \frac{w_i}{(1+x_i)^2} \sum_{n_\gamma n_\delta} \sum_{m'} (\bar{I}_{rx_i})^{\gamma\bar{\delta}}_{\alpha\bar{\beta}} \sum_{d_\gamma d_\delta} \sum_{n_{z_\gamma} n_{z_\delta}} (\bar{I}_{zx_i})^{\gamma\delta}_{\alpha\beta} K^{01-+}_{\gamma\bar{\delta}}} \tag{I.121}$$

Block $+-$:

Here, we consider the spins ($\alpha\uparrow$,$\bar{\beta}\downarrow$). Using the symmetry of the collective pairing field, we directly have:

$$\boxed{\bar{\Delta}^{\tau_p+-}_{\alpha\bar{\beta}} = \bar{\Delta}^{\tau_p-+}_{\beta\bar{\alpha}}} \tag{I.122}$$

I.5 The collective Slater approximation

In this PhD thesis work, we wanted to give an extension to the Slater approximation in the collective case. It has been done to allow a full consistency beyond the mean field level using the D1S interaction. This collective approximation is more an ansatz than a physically guided approximation as in the non-collective case. The expression of the collective approximation is trivial as the transition density is simply considered instead of the usual density:

$$\boxed{\bar{E}_S = -\frac{3}{4}e^2(\frac{3}{\pi})^{1/3} \int d^3\vec{r} (\rho(\vec{r})^{01\tau_p})^{4/3}} \tag{I.123}$$

In Figure (I.2), we proposed an evaluation of the collective Slater approximation for the ^{240}Pu adiabatic set obtained with the procedure $\tilde{\mathcal{P}}_{20}$ and with respect to the quadrupole deformation. In panel (a), we've displayed the collective Slater contribution to the Hamiltonian kernel along with the collective Coulomb exchange and Coulomb exchange+pairing contributions to the Hamiltonian kernel. In panel (b), we've represented the collective Coulomb pairing contribution the the Hamiltonian kernel. Note that the calculations have been made for the following terms $\langle\Phi(7583)|V^{Coul}|\Phi(Q_{20})\rangle$, the value $Q_{20} = 7583$ fm^2 being randomly chosen:

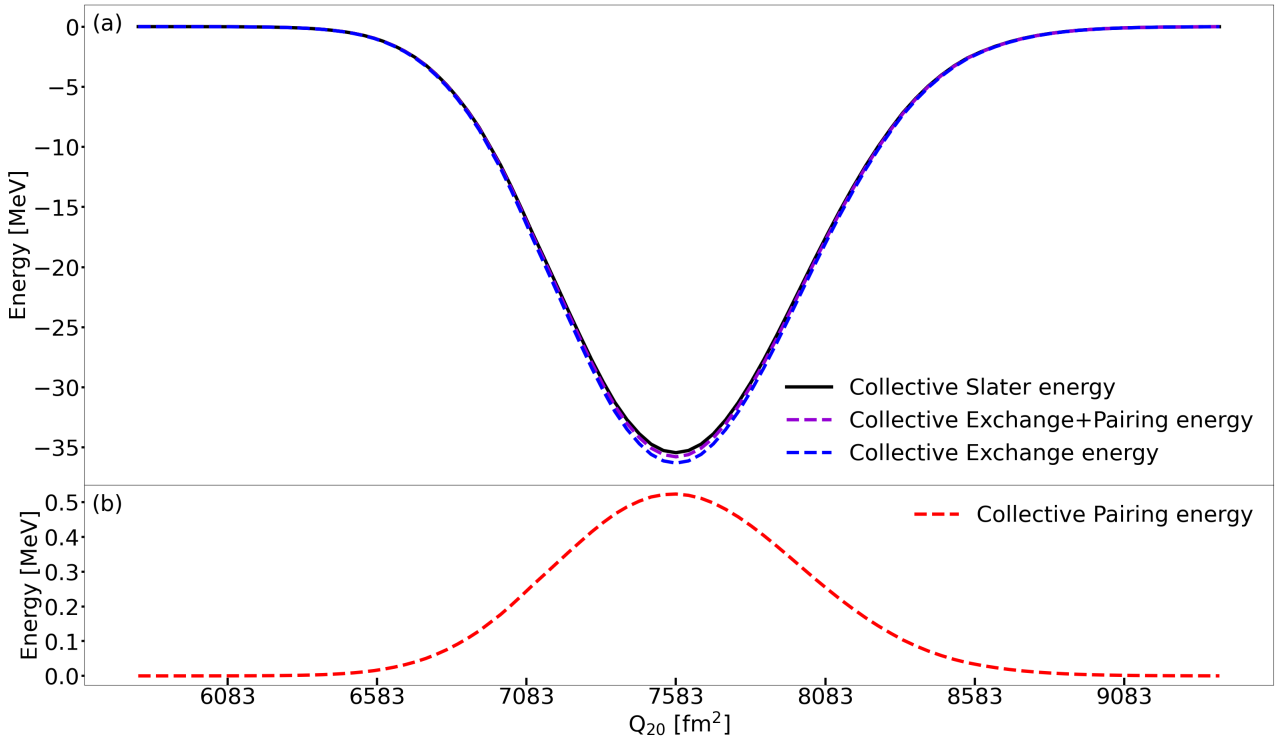

Figure I.2: Evaluation of the collective Slater approximation in the kernels $\langle\Phi(7583)|V^{Coul}|\Phi(Q_{20})\rangle$ with respect to quadrupole deformation in the ^{240}Pu. Panel (a): collective Slater, collective Coulomb exchange and collective Coulomb exchange+pairing contributions to the kernels. Panel (b): collective Coulomb pairing contribution to the kernels.

We observe that the collective Slater approximation seems to be a rather accurate approximation.

I.6 Excited collective fields

The goal of this part is to give an expression of the new central fields that appear when intrinsic excitations are added. They are useful to evaluate quantities of the following type:

$$\langle\Phi_0|\bar{\xi}_j\xi_j\hat{H}\xi_i^+\bar{\xi}_i^+|\Phi_1\rangle \tag{I.124}$$

Note that all the Coulomb excited fields vanishe when a neutron intrinsic excitation is considered.

I.6.1 Excited collective field $\Gamma^{(i)}([W,Z])$

This Coulomb excited field is defined as follows:

$$\boxed{\begin{aligned}\bar{\Gamma}^{(i)\tau_p}_{\alpha\gamma}([W,Z]) = \sum_{\beta\delta>}[{}_0\langle\alpha\beta|V^{(Clmb)}(1-P_rP_\sigma P_\tau)|\gamma\delta\rangle_1 \\ +(-1)^{s_\beta - s_\delta}{}_0\langle\alpha\bar{\beta}|V^{(Clmb)}(1-P_rP_\sigma P_\tau)|\gamma\bar{\delta}\rangle_1]W_{\delta i}Z_{\beta\bar{i}}\end{aligned}} \tag{I.125}$$

The choice of an excitation fixes a specific Ω and a specific isospin. We therefore have $(\tau_\beta = \tau_\delta = \tau_i = \tau_p)$ and $(\Omega_\beta = \Omega_\delta = \Omega_i \geq 0)$. We can separate the spatial part and the spin-isospin part:

$$\begin{aligned}\bar{\Gamma}^{(i)\tau_p}_{\alpha\gamma}([W,Z]) = \delta_{\tau_i\tau_p}\sum_{\delta\beta\in(\Omega_i,\tau_i)}[\bar{E}^{\gamma\delta}_{\alpha\beta}\delta_{s_\alpha s_\gamma}\delta_{s_\beta s_\delta} - \bar{E}^{\delta\gamma}_{\alpha\beta}\delta_{s_\alpha s_\delta}\delta_{s_\beta s_\gamma} \\ +(-1)^{s_\beta - s_\delta}(\bar{E}^{\gamma\bar{\delta}}_{\alpha\bar{\beta}}\delta_{s_\alpha s_\gamma}\delta_{s_\beta s_\delta} - \bar{E}^{\bar{\delta}\gamma}_{\alpha\bar{\beta}}\delta_{s_\alpha\bar{s}_\delta}\delta_{\bar{s}_\beta s_\gamma})]W_{\delta i}Z_{\beta\bar{i}}\end{aligned} \tag{I.126}$$

We now consider the spins explicitly.

Block ++:

Here, we consider the spins ($\alpha\uparrow$,$\gamma\uparrow$). In this case, the excited field reads:

$$\bar{\Gamma}^{(i)\tau_p++}_{\alpha\gamma}([W,Z]) = \delta_{\tau_i\tau_p}\sum_{\delta\beta\in(\Omega_i,\tau_i)}[(\bar{E}^{\gamma\delta}_{\alpha\beta}+\bar{E}^{\gamma\bar{\delta}}_{\alpha\bar{\beta}})\delta_{s_\beta s_\delta} - \bar{E}^{\delta\gamma}_{\alpha\beta}\delta_{s^+_\beta s^+_\delta} - \bar{E}^{\bar{\delta}\gamma}_{\alpha\bar{\beta}}\delta_{s^-_{\bar{\beta}}s^-_{\bar{\delta}}}]W_{\delta i}Z_{\beta\bar{i}} \tag{I.127}$$

As $(m_\beta = m_\delta)$, we have in addition:

$$\bar{E}^{\gamma\bar{\delta}}_{\alpha\bar{\beta}} = \bar{E}^{\gamma\delta}_{\alpha\beta} \tag{I.128}$$

Using Eq.(I.128) in Eq.(I.127), we write:

$$\bar{\Gamma}^{(i)\tau_p++}_{\alpha\gamma}([W,Z]) = \delta_{\tau_i\tau_p}\sum_{\delta\beta\in(\Omega_i,\tau_i)}2\bar{E}^{\gamma\delta}_{\alpha\beta}[W^+_{\delta i}Z^+_{\beta\bar{i}} + W^-_{\delta i}Z^-_{\beta\bar{i}}] - \bar{E}^{\delta\gamma}_{\alpha\beta}W^+_{\delta i}Z^+_{\beta\bar{i}} - \bar{E}^{\bar{\delta}\gamma}_{\alpha\bar{\beta}}W^-_{\delta i}Z^-_{\beta\bar{i}} \tag{I.129}$$

We set:

$$[W,Z]^{++}_{\delta\beta}(D) = W^+_{\delta i}Z^+_{\beta\bar{i}} + W^-_{\delta i}Z^-_{\beta\bar{i}} \tag{I.130}$$

And:

$$\begin{cases}(\Omega_i > 0) \to [W,Z]^{++}_{\delta\beta}(E) = [W^+_{\delta i}Z^+_{\beta\bar{i}}] \\ (\Omega_i < 0) \to [W,Z]^{++}_{\delta\beta}(E) = [W^-_{\delta i}Z^-_{\beta\bar{i}}]\end{cases} \tag{I.131}$$

Eq.(I.130) and Eq.(I.131) lead to the final form of the field:

$$\boxed{\bar{\Gamma}^{(i)\tau_p++}_{\alpha\gamma}([W,Z]) \approx \delta_{\tau_i\tau_p}\frac{4e^2}{\sqrt{\pi}}\sum_{\mu=0}^{n_{GLE}}\frac{w_\mu}{(1+x_\mu)^2}[2\sum_{\delta\beta\in(\Omega_i,\tau_i)}(\bar{I}_{rx_\mu})^{\gamma\delta}_{\alpha\beta}(\bar{I}_{zx_\mu})^{\gamma\delta}_{\alpha\beta}[W,Z]^{++}_{\delta\beta}(D) - \sum_{\delta\beta\in(\pm\Omega_i,\tau_i)}(\bar{I}_{rx_\mu})^{\delta\gamma}_{\alpha\beta}(\bar{I}_{zx_\mu})^{\delta\gamma}_{\alpha\beta}[W,Z]^{++}_{\delta\beta}(E)]} \quad \text{(I.132)}$$

Block $--$:

Here, we consider the spins ($\alpha\downarrow$,$\gamma\downarrow$). By analogy with the $++$ spin block, we directly write:

$$\boxed{\bar{\Gamma}^{(i)\tau_p--}_{\alpha\gamma}([W,Z]) \approx \delta_{\tau_i\tau_p}\frac{4e^2}{\sqrt{\pi}}\sum_{\mu=0}^{n_{GLE}}\frac{w_\mu}{(1+x_\mu)^2}[2\sum_{\delta\beta\in(\Omega_i,\tau_i)}(\bar{I}_{rx_\mu})^{\gamma\delta}_{\alpha\beta}(\bar{I}_{zx_\mu})^{\gamma\delta}_{\alpha\beta}[W,Z]^{++}_{\delta\beta}(D) - \sum_{\delta\beta\in(\pm\Omega_i,\tau_i)}(\bar{I}_{rx_\mu})^{\bar{\delta}\gamma}_{\alpha\bar{\beta}}(\bar{I}_{zx_\mu})^{\delta\gamma}_{\alpha\beta}[W,Z]^{++}_{\delta\beta}(E)]} \quad \text{(I.133)}$$

Block $-+$:

Here, we consider the spins ($\alpha\downarrow$,$\gamma\uparrow$). In this case, the excited field reads:

$$\bar{\Gamma}^{(i)\tau_p-+}_{\alpha\gamma}([W,Z]) = -\delta_{\tau_i\tau_p}\sum_{\delta\beta\in(\Omega_i,\tau_i)}[\bar{E}^{\delta\gamma}_{\alpha\beta}\delta_{s^+_\beta s^-_\delta} - \bar{E}^{\bar{\delta}\gamma}_{\alpha\bar{\beta}}\delta_{s^-_{\bar{\beta}} s^+_\delta}]W_{\delta i}Z_{\beta\bar{i}} \quad \text{(I.134)}$$

We apply the spin conditions in Eq.(I.134):

$$\bar{\Gamma}^{(i)\tau_p-+}_{\alpha\gamma}([W,Z]) = -\delta_{\tau_i\tau_p}\sum_{\delta\beta\in(\Omega_i,\tau_i)}\bar{E}^{\delta\gamma}_{\alpha\beta}W^-_{\delta i}Z^+_{\beta\bar{i}} - \bar{E}^{\bar{\delta}\gamma}_{\alpha\bar{\beta}}W^+_{\delta i}Z^-_{\beta\bar{i}} \quad \text{(I.135)}$$

We set:

$$\begin{cases}(\Omega_i>0)\rightarrow[W,Z]^{-+}_{\delta\beta}(E) = W^-_{\delta i}Z^+_{\beta\bar{i}}\\(\Omega_i<0)\rightarrow[W,Z]^{-+}_{\delta\beta}(E) = -W^+_{\delta i}Z^-_{\beta\bar{i}}\end{cases} \quad \text{(I.136)}$$

Thanks to Eq.(I.136), we finally write:

$$\boxed{\bar{\Gamma}^{(i)\tau_p-+}_{\alpha\gamma}([W,Z]) \approx -\delta_{\tau_i\tau_p}\frac{4e^2}{\sqrt{\pi}}\sum_{\mu=0}^{n_{GLE}}\frac{w_\mu}{(1+x_\mu)^2}\sum_{\delta\beta\in(\pm\Omega_i,\tau_i)}(\bar{I}_{rx_\mu})^{\delta\gamma}_{\alpha\beta}(\bar{I}_{zx_\mu})^{\delta\gamma}_{\alpha\beta}[W,Z]^{-+}_{\delta\beta}(E)]} \quad \text{(I.137)}$$

Block $+-$:

Here, we consider the spins ($\alpha\uparrow$,$\gamma\downarrow$). By analogy with the $-+$ spin block, we directly write:

$$\boxed{\bar{\Gamma}^{(i)\tau_p+-}_{\alpha\gamma}([W,Z]) \approx \delta_{\tau_i\tau_p}\frac{4e^2}{\sqrt{\pi}}\sum_{\mu=0}^{n_{GLE}}\frac{w_\mu}{(1+x_\mu)^2}\sum_{\delta\beta\in(\pm\Omega_i,\tau_i)}(\bar{I}_{rx_\mu})^{\bar{\delta}\gamma}_{\alpha\bar{\beta}}(\bar{I}_{zx_\mu})^{\delta\gamma}_{\alpha\beta}[W,Z]^{-+}_{\delta\beta}(E)]} \quad \text{(I.138)}$$

I.6.2 Excited collective field $\bar{\Delta}^{(i)}(WW)$

This Coulomb excited field reads as follows:

$$\boxed{\bar{\Delta}^{(i)\tau_p}_{\alpha\bar{\beta}}(WW) = \sum_{\gamma\delta>}(-1)^{s_\beta - s_\delta}{}_0\langle\alpha\bar{\beta}|V^{(Clmb)}(1 - P_r P_\sigma P_\tau)|\gamma\bar{\delta}\rangle_1 W_{\gamma i}W_{\delta i}} \tag{I.139}$$

Thanks to the symmetries of Eq.(I.139), we write:

$$\bar{\Delta}^{(i)\tau_p}_{\alpha\bar{\beta}}(WW) = \sum_{\gamma\delta>}[(-1)^{s_\beta - s_\delta}{}_0\langle\alpha\bar{\beta}|V^{(Clmb)}|\gamma\bar{\delta}\rangle_1 - (-1)^{s_\beta - s_\gamma}{}_0\langle\alpha\bar{\beta}|V^{(Clmb)}|\bar{\gamma}\delta\rangle_1]W_{\gamma i}W_{\delta i} \tag{I.140}$$

$$\bar{\Delta}^{(i)\tau_p}_{\alpha\bar{\beta}}(WW) = \delta_{\tau_i\tau_p}\sum_{\gamma\delta\in(\Omega_i,\tau_i)}[\bar{E}^{\gamma\bar{\delta}}_{\alpha\bar{\beta}}\delta_{s_\alpha s_\gamma}\delta_{s_\beta s_\delta} + (-1)^{s_\beta + s_\gamma}\bar{E}^{(\mu)\bar{\gamma}\delta}_{\alpha\bar{\beta}}\delta_{s_\alpha\bar{s}_\gamma}\delta_{s_\beta\bar{s}_\delta}]W_{\gamma i}W_{\delta i} \tag{I.141}$$

We now consider the spins explicitly.

Block ++:

Here, we consider the spins ($\alpha\uparrow$,$\bar{\beta}\uparrow$). In this case, the excited field reads:

$$\bar{\Delta}^{(i)\tau_p ++}_{\alpha\bar{\beta}}(WW) = \delta_{\tau_i\tau_p}\sum_{\gamma\delta\in(\Omega_i,\tau_i)}[\bar{E}^{\gamma\bar{\delta}}_{\alpha\bar{\beta}}\delta_{s^+_\delta s^+_\gamma} + \bar{E}^{\bar{\gamma}\delta}_{\alpha\bar{\beta}}\delta_{s^-_\delta s^-_\gamma}]W_{\gamma i}W_{\delta i} \tag{I.142}$$

We apply the spin conditions in Eq.(I.142):

$$\bar{\Delta}^{(i)\tau_p ++}_{\alpha\bar{\beta}}(WW) = \delta_{\tau_i\tau_p}\sum_{\gamma\delta\in(\Omega_i,\tau_i)}\bar{E}^{\gamma\bar{\delta}}_{\alpha\bar{\beta}}W^+_{\gamma i}W^+_{\delta i} + \bar{E}^{\bar{\gamma}\delta}_{\alpha\bar{\beta}}W^-_{\gamma i}W^-_{\delta i} \tag{I.143}$$

We set:

$$\begin{cases}(\Omega_i > 0) \rightarrow WW^{++}_{\gamma\bar{\delta}} = W^+_{\gamma i}W^+_{\delta i}\\ (\Omega_i < 0) \rightarrow WW^{++}_{\gamma\bar{\delta}} = W^-_{\gamma i}W^-_{\delta i}\end{cases} \tag{I.144}$$

Thanks to Eq.(I.144), we finally write:

$$\boxed{\bar{\Delta}^{(i)\tau_p ++}_{\alpha\bar{\beta}}(WW) \approx \delta_{\tau_i\tau_p}\frac{4e^2}{\sqrt{\pi}}\sum_{\mu=0}^{n_{GLE}}\frac{w_\mu}{(1+x_\mu)^2}\sum_{\gamma\delta\in(\pm\Omega_i,\tau_i)}(\bar{I}_{rx_\mu})^{\gamma\bar{\delta}}_{\alpha\bar{\beta}}(\bar{I}_{zx_\mu})^{\gamma\delta}_{\alpha\beta}WW^{++}_{\gamma\bar{\delta}}} \tag{I.145}$$

Block −−:

Here, we consider the spins ($\alpha\downarrow$,$\bar{\beta}\downarrow$). By analogy with the ++ spin block, we directly find:

$$\boxed{\bar{\Delta}^{(i)\tau_p--}_{\alpha\bar{\beta}}(WW) \approx \delta_{\tau_i\tau_p}\frac{4e^2}{\sqrt{\pi}}\sum_{\mu=0}^{n_{GLE}}\frac{w_\mu}{(1+x_\mu)^2}\sum_{\gamma\delta\in(\pm\Omega_i,\tau_i)}(\bar{I}_{rx_\mu})^{\bar{\gamma}\delta}_{\alpha\bar{\beta}}(\bar{I}_{zx_\mu})^{\gamma\delta}_{\alpha\beta}WW^{++}_{\gamma\bar{\delta}}} \tag{I.146}$$

Block $-+$:

Here, we consider the spins ($\alpha\downarrow$,$\bar{\beta}\uparrow$). In this case, the excited field reads:

$$\bar{\Delta}^{(i)\tau_p-+}_{\alpha\bar{\beta}}(WW) = \delta_{\tau_i\tau_p}\sum_{\gamma\delta\in(\Omega_i,\tau_i)}[\bar{E}^{\gamma\bar{\delta}}_{\alpha\bar{\beta}}\delta_{s^+_\delta s^-_\gamma} - \bar{E}^{\bar{\gamma}\delta}_{\alpha\bar{\beta}}\delta_{s^-_\delta s^+_\gamma}]W_{\gamma i}W_{\delta i} \tag{I.147}$$

We apply the spin conditions in Eq.(I.147):

$$\bar{\Delta}^{(i)\tau_p-+}_{\alpha\bar{\beta}}(WW) = \delta_{\tau_i\tau_p}\sum_{\gamma\delta\in(\Omega_i,\tau_i)}\bar{E}^{\gamma\bar{\delta}}_{\alpha\bar{\beta}}W^-_{\gamma i}W^+_{\delta i} - \bar{E}^{\bar{\gamma}\delta}_{\alpha\bar{\beta}}W^+_{\gamma i}W^-_{\delta i} \tag{I.148}$$

We set:

$$\begin{cases}(\Omega_i > 0) \rightarrow WW^{-+}_{\gamma\bar{\delta}} = W^-_{\gamma i}W^+_{\delta i}\\ (\Omega_i < 0) \rightarrow WW^{-+}_{\gamma\bar{\delta}} = -W^+_{\gamma i}W^-_{\delta i}\end{cases} \tag{I.149}$$

Thanks to Eq.(I.149), the field eventually reads:

$$\boxed{\bar{\Delta}^{(i)\tau_p-+}_{\alpha\bar{\beta}}(WW) \approx \delta_{\tau_i\tau_p}\frac{4e^2}{\sqrt{\pi}}\sum_{\mu=0}^{n_{GLE}}\frac{w_\mu}{(1+x_\mu)^2}\sum_{\gamma\delta\in(\pm\Omega_i,\tau_i)}(\bar{I}_{rx_\mu})^{\gamma\bar{\delta}}_{\alpha\bar{\beta}}(\bar{I}_{zx_\mu})^{\gamma\delta}_{\alpha\beta}WW^{-+}_{\gamma\bar{\delta}}} \tag{I.150}$$

Block $+-$:

Here, we consider the spins ($\alpha\uparrow$,$\bar{\beta}\downarrow$). Because of the symmetry of the field, we directly write:

$$\boxed{\bar{\Delta}^{(i)\tau_p+-}_{\alpha\bar{\beta}}(WW) = \bar{\Delta}^{(i)\tau_p-+}_{\beta\bar{\alpha}}(WW)} \tag{I.151}$$

I.6.3 Excited collective field $\bar{\Delta}^{(j)}(\bar{Z}\bar{Z})$

This Coulomb excited field reads as follows:

$$\boxed{\bar{\Delta}^{(j)}_{\alpha\bar{\beta}}(\bar{Z}\bar{Z}) = \sum_{\gamma\delta>}(-1)^{s_\beta - s_\delta}{}_0\langle\alpha\bar{\beta}|V^{(Clmb)}(1-P_rP_\sigma P_\tau)|\gamma\bar{\delta}\rangle_1\bar{Z}_{j\bar{\gamma}}\bar{Z}_{j\bar{\delta}}} \tag{I.152}$$

By analogy with the $\bar{\Delta}^{(i)}(WW)$ excited field, we can directly consider the spin blocks.

Block $++$:

Here, we consider the spins ($\alpha\uparrow$,$\bar{\beta}\uparrow$). In this case, we directly set:

$$\begin{cases} (\Omega_j > 0) \rightarrow \bar{Z}\bar{Z}^{++}_{\gamma\bar{\delta}} = \bar{Z}^{+}_{j\bar{\gamma}}\bar{Z}^{+}_{j\bar{\delta}} \\ (\Omega_j < 0) \rightarrow \bar{Z}\bar{Z}^{++}_{\gamma\bar{\delta}} = \bar{Z}^{-}_{j\bar{\gamma}}\bar{Z}^{-}_{j\bar{\delta}} \end{cases} \tag{I.153}$$

Thanks to Eq.(I.153), the excited field reads:

$$\boxed{\bar{\Delta}^{(j)\tau_p++}_{\alpha\bar{\beta}}(\bar{Z}\bar{Z}) \approx \delta_{\tau_j\tau_p}\frac{4e^2}{\sqrt{\pi}}\sum_{\mu=0}^{n_{GLE}}\frac{w_\mu}{(1+x_\mu)^2}\sum_{\gamma\delta\in(\pm\Omega_j,\tau_j)}(\bar{I}_{rx_\mu})^{\gamma\bar{\delta}}_{\alpha\bar{\beta}}(\bar{I}_{zx_\mu})^{\gamma\delta}_{\alpha\beta}\bar{Z}\bar{Z}^{++}_{\gamma\bar{\delta}}} \tag{I.154}$$

Block $--$:

Here, we consider the spins ($\alpha\downarrow$,$\bar{\beta}\downarrow$). By analogy with the $++$ spin block, we directly write:

$$\boxed{\bar{\Delta}^{(j)\tau_p--}_{\alpha\bar{\beta}}(\bar{Z}\bar{Z}) \approx \delta_{\tau_j\tau_p}\frac{4e^2}{\sqrt{\pi}}\sum_{\mu=0}^{n_{GLE}}\frac{w_\mu}{(1+x_\mu)^2}\sum_{\gamma\delta\in(\pm\Omega_j,\tau_j)}(\bar{I}_{rx_\mu})^{\bar{\gamma}\delta}_{\alpha\bar{\beta}}(\bar{I}_{zx_\mu})^{\gamma\delta}_{\alpha\beta}\bar{Z}\bar{Z}^{++}_{\gamma\bar{\delta}}} \tag{I.155}$$

Block $-+$:

Here, we consider the spins ($\alpha\downarrow$,$\bar{\beta}\uparrow$). In this case, we directly set:

$$\begin{cases} (\Omega_j > 0) \rightarrow \bar{Z}\bar{Z}^{-+}_{\gamma\bar{\delta}} = \bar{Z}^{-}_{j\bar{\gamma}}\bar{Z}^{+}_{j\bar{\delta}} \\ (\Omega_j < 0) \rightarrow \bar{Z}\bar{Z}^{-+}_{\gamma\bar{\delta}} = -\bar{Z}^{+}_{j\bar{\gamma}}\bar{Z}^{-}_{j\bar{\delta}} \end{cases} \tag{I.156}$$

Using equation Eq.(I.156), the field eventually reads:

$$\boxed{\bar{\Delta}^{(j)\tau_p-+}_{\alpha\bar{\beta}}(\bar{Z}\bar{Z}) \approx \delta_{\tau_j\tau_p}\frac{4e^2}{\sqrt{\pi}}\sum_{\mu=0}^{n_{GLE}}\frac{w_\mu}{(1+x_\mu)^2}\sum_{\gamma\delta\in(\pm\Omega_j,\tau_j)}(\bar{I}_{rx_\mu})^{\gamma\bar{\delta}}_{\alpha\bar{\beta}}(\bar{I}_{zx_\mu})^{\gamma\delta}_{\alpha\beta}\bar{Z}\bar{Z}^{-+}_{\gamma\bar{\delta}}} \tag{I.157}$$

Block $+-$:

Here, we consider the spins ($\alpha\uparrow$,$\bar{\beta}\downarrow$). Because of the symmetry of the field, we directly write:

$$\boxed{\bar{\Delta}^{(j)\tau_p+-}_{\alpha\bar{\beta}}(\bar{Z}\bar{Z}) = \bar{\Delta}^{(j)\tau_p-+}_{\beta\bar{\alpha}}(\bar{Z}\bar{Z})} \tag{I.158}$$

I.6.4 Excited collective field $\bar{\Delta}^{(ji)}([W,\bar{Z}])$

This Coulomb excited field reads as follows:

$$\boxed{\bar{\Delta}^{(ji)}_{\alpha\bar{\beta}}([W,\bar{Z}]) = \sum_{\gamma\delta>}(-1)^{s_\beta - s_\delta}{}_0\langle\alpha\bar{\beta}|V^{(Clmb)}(1-P_rP_\sigma P_\tau)|\gamma\bar{\delta}\rangle_1[W_{\gamma i}\bar{Z}_{j\bar{\delta}} + \bar{Z}_{j\bar{\gamma}}W_{\delta i}]} \quad \text{(I.159)}$$

In this field, special conditions on the isospin and on Ω hold. Indeed, we have $\tau_i = \tau_j = \tau_{ji} = \tau_p$ and $\Omega_i = \Omega_j = \Omega_{ji}$. That said, we can consider the spin blocks by analogy with the previously derived excited fields.

Block ++:

Here, we consider the spins ($\alpha\uparrow$,$\bar{\beta}\uparrow$). In this case, we directly set:

$$\begin{cases}(\Omega_{ji} > 0) \rightarrow [W,\bar{Z}]^{++}_{\gamma\bar{\delta}} = W^+_{\gamma i}\bar{Z}^+_{j\bar{\delta}} + \bar{Z}^+_{j\bar{\gamma}}W^+_{\delta i}\\ (\Omega_{ji} < 0) \rightarrow [W,\bar{Z}]^{++}_{\gamma\bar{\delta}} = W^-_{\gamma i}\bar{Z}^-_{j\bar{\delta}} + \bar{Z}^-_{j\bar{\gamma}}W^-_{\delta i}\end{cases} \quad \text{(I.160)}$$

Thanks to Eq.(I.160), the field reads:

$$\boxed{\bar{\Delta}^{(ji)\tau_p++}_{\alpha\bar{\beta}}([W,\bar{Z}]) = \delta_{\tau_{ji}\tau_p}\frac{4e^2}{\sqrt{\pi}}\sum_{\mu=0}^{n_{GLE}}\frac{w_\mu}{(1+x_\mu)^2}\sum_{\gamma\delta\in(\pm\Omega_{ji},\tau_{ji})}(\bar{I}_{rx_\mu})^{\gamma\bar{\delta}}_{\alpha\bar{\beta}}(\bar{I}_{zx_\mu})^{\gamma\delta}_{\alpha\beta}[W,\bar{Z}]^{++}_{\gamma\bar{\delta}}} \quad \text{(I.161)}$$

Block −−:

Here, we consider the spins ($\alpha\downarrow$,$\bar{\beta}\downarrow$). By analogy with the ++ spin block, we directly write:

$$\boxed{\bar{\Delta}^{(ji)\tau_p--}_{\alpha\bar{\beta}}([W,\bar{Z}]) = \delta_{\tau_{ji}\tau_p}\frac{4e^2}{\sqrt{\pi}}\sum_{\mu=0}^{n_{GLE}}\frac{w_\mu}{(1+x_\mu)^2}\sum_{\gamma\delta\in(\pm\Omega_{ji},\tau_{ji})}(\bar{I}_{rx_\mu})^{\bar{\gamma}\delta}_{\alpha\bar{\beta}}(\bar{I}_{zx_\mu})^{\gamma\delta}_{\alpha\beta}[W,\bar{Z}]^{++}_{\gamma\bar{\delta}}} \quad \text{(I.162)}$$

Block −+:

Here, we consider the spins ($\alpha\downarrow$,$\bar{\beta}\uparrow$). In this case, we directly set:

$$\begin{cases}(\Omega_{ji} > 0) \rightarrow [W,\bar{Z}]^{-+}_{\gamma\bar{\delta}} = W^-_{\gamma i}\bar{Z}^+_{j\bar{\delta}} + \bar{Z}^-_{j\bar{\gamma}}W^+_{\delta i}\\ (\Omega_{ji} < 0) \rightarrow [W,\bar{Z}]^{-+}_{\gamma\bar{\delta}} = -(W^+_{\gamma i}\bar{Z}^-_{j\bar{\delta}} + \bar{Z}^+_{j\bar{\gamma}}W^-_{\delta i})\end{cases} \quad \text{(I.163)}$$

Using Eq.(I.163), the field eventually reads:

$$\boxed{\bar{\Delta}^{(ji)\tau_p-+}_{\alpha\bar{\beta}}([W,\bar{Z}]) = \delta_{\tau_{ji}\tau_p}\frac{4e^2}{\sqrt{\pi}}\sum_{\mu=0}^{n_{GLE}}\frac{w_\mu}{(1+x_\mu)^2}\sum_{\gamma\delta\in(\pm\Omega_{ji},\tau_{ji})}(\bar{I}_{rx_\mu})^{\gamma\bar{\delta}}_{\alpha\bar{\beta}}(\bar{I}_{zx_\mu})^{\gamma\delta}_{\alpha\beta}[W,\bar{Z}]^{-+}_{\gamma\bar{\delta}}} \quad \text{(I.164)}$$

Block +−:

Here, we consider the spins ($\alpha\uparrow$,$\bar{\beta}\downarrow$). Because of the symmetry of the field, we directly write:

$$\boxed{\bar{\Delta}^{(ji)\tau_p+-}_{\alpha\bar{\beta}}([W,\bar{Z}]) = \bar{\Delta}^{(ji)\tau_p-+}_{\beta\bar{\alpha}}([W,\bar{Z}])} \quad \text{(I.165)}$$

Appendix J

Two-body center of mass correction fields

We want to correct the spurious energy contributions coming from the motion of the center of mass of the nuclei. To do so, we introduce the following operator:

$$\boxed{V^{(Cdm)} = -\frac{1}{2MA}\vec{P}^2} \tag{J.1}$$

A stands for the number of nucleons and M for the mass of these nucleons. We develop the operator $\vec{P}^2$:

$$V^{(Cdm)} = -\frac{1}{2MA}(\sum_{i=1}^{A}\vec{P}_i^2 + \sum_{i\neq j=1}^{A}\vec{P}_i.\vec{P}_j) \tag{J.2}$$

It is easy to rewrite Eq.(J.2) in second quantization:

$$V^{(Cdm)} = -\frac{1}{2MA}(\sum_{\alpha\beta}{}_0\langle\alpha|\vec{P}^2|\beta\rangle_1 c^+_{0,\alpha}c_{1,\beta} + \sum_{\alpha\beta\gamma\delta}{}_0\langle\alpha\beta|\vec{P}_1.\vec{P}_2|\gamma\delta\rangle_1 c^+_{0,\alpha}c^+_{0,\beta}c_{1,\delta}c_{1,\gamma}) \tag{J.3}$$

We wrote Eq.(J.3) with respect to two different harmonic oscillator bases on the left and on the right side. On the left of Eq.(J.3), we recognize the one-body kinetic operator (see Appendix K):

$$-\frac{1}{2MA}\sum_{\alpha\beta}{}_0\langle\alpha|\vec{P}^2|\beta\rangle_1 c^+_{0,\alpha}c_{1,\beta} = -\frac{1}{A}\sum_{\alpha\beta}t_{\alpha\beta}c^+_{0,\alpha}c_{1,\beta} \tag{J.4}$$

The term on the right side of Eq.(J.3), is antisymmetryzed:

$$\sum_{\alpha\beta\gamma\delta}{}_0\langle\alpha\beta|\vec{P}_1.\vec{P}_2|\gamma\delta\rangle_1 c^+_{0,\alpha}c^+_{0,\beta}c_{1,\delta}c_{1,\gamma} = \frac{1}{2}\sum_{\alpha\beta\gamma\delta}{}_0\langle\alpha\beta|\vec{P}_1.\vec{P}_2(1-P_rP_\sigma P_\tau)|\gamma\delta\rangle_1 c^+_{0,\alpha}c^+_{0,\beta}c_{1,\delta}c_{1,\gamma} \tag{J.5}$$

Thanks to Eq.(J.4) and Eq.(J.5), the full Hamiltonian of the system can be rewritten as:

$$\boxed{\hat{H} = (1 - \frac{1}{A}) \sum_{\alpha\beta} t_{\alpha\beta} c^+_{0,\alpha} c_{1,\beta} + \frac{1}{4} \sum_{\alpha\beta\gamma\delta} (v^{(a)}_{\alpha\beta\gamma\delta} + v^{(Cdm)}_{\alpha\beta\gamma\delta}) c^+_{0,\alpha} c^+_{0,\beta} c_{1,\delta} c_{1,\gamma}} \tag{J.6}$$

In Eq.(J.6), the quantities $v^{(Cdm)}_{\alpha\beta\gamma\delta}$ stand for the matrix elements of the two-body antisymmetrized center of mass correction operator and reads as follows:

$$\boxed{v^{(Cdm)}_{\alpha\beta\gamma\delta} = -\frac{1}{MA} {}_0\langle \alpha\beta | \vec{P}_1 . \vec{P}_2 (1 - P_r P_\sigma P_\tau) | \gamma\delta \rangle_1} \tag{J.7}$$

In practice, most of the time in the derivations, the notation $v^{(a)}$ already stands for the sum $v^{(a)} + v^{(Cdm)}$. This Appendix is dedicated to the research of an analytic expression for $v^{(Cdm)}$. Besides, the one-body component of the center of mass correction is proportional to the customary kinetic operator, both are therefore calculated together (see Appendix K).
The two-body center of mass matrix elements can be separated into a spatial and a spin-isospin part. In the general case of two different harmonic oscillator bases, it reads:

$$\boxed{v^{(Cdm)}_{\alpha\beta\gamma\delta} = -\frac{1}{MA} [\bar{E}^{\gamma\delta}_{\alpha\beta} S^{\gamma\delta}_{\alpha\beta} - \bar{E}^{\delta\gamma}_{\alpha\beta} S^{\delta\gamma}_{\alpha\beta}]} \tag{J.8}$$

Where the spatial part $\bar{E}$ and the spin-isospin part S are defined as follows:

$$\begin{cases} \bar{E}^{\gamma\delta}_{\alpha\beta} = {}_0\langle \alpha | \vec{P} | \gamma \rangle_1 . {}_0\langle \beta | \vec{P} | \delta \rangle_1 \\ S^{\gamma\delta}_{\alpha\beta} = \delta_{s_\alpha s_\gamma} \delta_{\tau_\alpha \tau_\gamma} \delta_{s_\beta s_\delta} \delta_{\tau_\beta \tau_\delta} \end{cases} \tag{J.9}$$

In the customary non-collective case, Eq.(J.8) is simply transformed into:

$$\boxed{v^{(Cdm)}_{\alpha\beta\gamma\delta} = -\frac{1}{MA} [E^{\gamma\delta}_{\alpha\beta} S^{\gamma\delta}_{\alpha\beta} - E^{\delta\gamma}_{\alpha\beta} S^{\delta\gamma}_{\alpha\beta}]} \tag{J.10}$$

With the non-collective spatial part E:

$$E^{\gamma\delta}_{\alpha\beta} = \langle \alpha | \vec{P} | \gamma \rangle . \langle \beta | \vec{P} | \delta \rangle \tag{J.11}$$

J.1 Spatial part

This part aims to give an analytic expression of the spatial part of the two-body center of mass correction matrix elements. First of all, we recall some properties of the gradient operators.

Gradient operators properties:

In Cartesian coordinates, the dot product of two gradient operators reads:

$$\overrightarrow{\nabla}_1.\overrightarrow{\nabla}_2 = \begin{pmatrix} \frac{\partial}{\partial_{x_1}} \\ \frac{\partial}{\partial_{y_1}} \\ \frac{\partial}{\partial_{z_1}} \end{pmatrix} . \begin{pmatrix} \frac{\partial}{\partial_{x_2}} \\ \frac{\partial}{\partial_{y_2}} \\ \frac{\partial}{\partial_{z_2}} \end{pmatrix} = \frac{\partial}{\partial_{x_1}}\frac{\partial}{\partial_{x_2}} + \frac{\partial}{\partial_{y_1}}\frac{\partial}{\partial_{y_2}} + \frac{\partial}{\partial_{z_1}}\frac{\partial}{\partial_{z_2}} \tag{J.12}$$

We want to rewrite Eq.(J.12) in the spherical coordinate system $(z, -, +)$, in which we have access to powerful formulas to treat the derivatives of the harmonic oscillator wave functions (see Appendix D). To do so, we set the following change of variables:

$$\begin{cases} z_- = \frac{1}{\sqrt{2}}(x - iy) \\ z_+ = -\frac{1}{\sqrt{2}}(x + iy) \end{cases} \tag{J.13}$$

It is now easy to tranform the Cartesian derivative operators $\frac{\partial}{\partial_x}$ and $\frac{\partial}{\partial_y}$ into ∇_+ and ∇_-:

$$\begin{pmatrix} \nabla_- \\ \nabla_+ \end{pmatrix} = \frac{1}{\sqrt{2}} \begin{pmatrix} 1 & -i \\ -1 & -i \end{pmatrix} \begin{pmatrix} \frac{\partial}{\partial_x} \\ \frac{\partial}{\partial_y} \end{pmatrix} \qquad \Rightarrow \qquad \begin{pmatrix} \frac{\partial}{\partial_x} \\ \frac{\partial}{\partial_y} \end{pmatrix} = \frac{1}{\sqrt{2}} \begin{pmatrix} 1 & -1 \\ i & i \end{pmatrix} \begin{pmatrix} \nabla_- \\ \nabla_+ \end{pmatrix} \tag{J.14}$$

Inserting Eq.(J.14) in Eq.(J.12) and writting $\frac{\partial}{\partial_z} = \nabla_z$, we finally get:

$$\overrightarrow{\nabla}_1.\overrightarrow{\nabla}_2 = \nabla_{z_1}\nabla_{z_2} + \frac{1}{2}(\nabla_{-_1} - \nabla_{+_1})(\nabla_{-_2} - \nabla_{+_2}) - \frac{1}{2}(\nabla_{-_1} + \nabla_{+_1})(\nabla_{-_2} + \nabla_{+_2}) \tag{J.15}$$

$$\boxed{\overrightarrow{\nabla}_1.\overrightarrow{\nabla}_2 = \nabla_{z_1}\nabla_{z_2} - \nabla_{-_1}\nabla_{+_2} - \nabla_{-_2}\nabla_{+_1}} \tag{J.16}$$

Polar point of view:

We show the link between the complex change of variables Eq.(J.13) and the customary real polar change of variables:

$$\begin{cases} x = rcos(\varphi) \\ y = rsin(\varphi) \end{cases} \qquad \Rightarrow \qquad \begin{cases} \frac{\partial}{\partial_r} = \frac{\partial x}{\partial_r}\frac{\partial}{\partial_x} + \frac{\partial y}{\partial_r}\frac{\partial}{\partial_y} \\ \frac{\partial}{\partial_\varphi} = \frac{\partial x}{\partial_\varphi}\frac{\partial}{\partial_x} + \frac{\partial y}{\partial_\varphi}\frac{\partial}{\partial_y} \end{cases} \tag{J.17}$$

Eq.(J.17) leads to:

$$\begin{pmatrix} \frac{\partial}{\partial_r} \\ \frac{\partial}{\partial_\varphi} \end{pmatrix} = \begin{pmatrix} cos(\varphi) & sin(\varphi) \\ -rsin(\varphi) & rcos(\varphi) \end{pmatrix} \begin{pmatrix} \frac{\partial}{\partial_x} \\ \frac{\partial}{\partial_y} \end{pmatrix} \qquad \Rightarrow \qquad \begin{pmatrix} \frac{\partial}{\partial_x} \\ \frac{\partial}{\partial_y} \end{pmatrix} = \begin{pmatrix} cos(\varphi) & -\frac{sin(\varphi)}{r} \\ sin(\varphi) & \frac{cos(\varphi)}{r} \end{pmatrix} \begin{pmatrix} \frac{\partial}{\partial_r} \\ \frac{\partial}{\partial_\varphi} \end{pmatrix} \tag{J.18}$$

Combining Eq.(J.14) and Eq.(J.18), we find:

$$\begin{pmatrix} \nabla_- \\ \nabla_+ \end{pmatrix} = \frac{1}{\sqrt{2}} \begin{pmatrix} 1 & -i \\ -1 & -i \end{pmatrix} \begin{pmatrix} cos(\varphi) & -\frac{sin(\varphi)}{r} \\ sin(\varphi) & \frac{cos(\varphi)}{r} \end{pmatrix} \begin{pmatrix} \frac{\partial}{\partial_r} \\ \frac{\partial}{\partial_\varphi} \end{pmatrix} \tag{J.19}$$

$$\begin{pmatrix} \nabla_- \\ \nabla_+ \end{pmatrix} = \frac{1}{\sqrt{2}} \begin{pmatrix} e^{-i\varphi} & -\frac{i}{r}e^{-i\varphi} \\ -e^{i\varphi} & -\frac{i}{r}e^{i\varphi} \end{pmatrix} \begin{pmatrix} \frac{\partial}{\partial_r} \\ \frac{\partial}{\partial_\varphi} \end{pmatrix} \tag{J.20}$$

From Eq.(J.20), we finally extract:

$$\boxed{\begin{cases}\nabla_- = \frac{e^{-i\varphi}}{\sqrt{2}}(\frac{\partial}{\partial r} - \frac{i}{r}\frac{\partial}{\partial \varphi}) \\ \nabla_+ = -\frac{e^{i\varphi}}{\sqrt{2}}(\frac{\partial}{\partial r} + \frac{i}{r}\frac{\partial}{\partial \varphi})\end{cases}} \tag{J.21}$$

Eq.(J.21) is a useful link between the polar and the spherical representations.

J.1.1 Same bases

Developing the dot product, the spatial part E defined in Eq.(J.21) reads:

$$\boxed{E_{\alpha\beta}^{\gamma\delta} = \hbar^2[-\langle\alpha|\nabla_z|\gamma\rangle\langle\beta|\nabla_z|\delta\rangle + \langle\alpha|\nabla_-|\gamma\rangle\langle\beta|\nabla_+|\delta\rangle + \langle\alpha|\nabla_+|\gamma\rangle\langle\beta|\nabla_-|\delta\rangle]} \tag{J.22}$$

In the following, we derive an analytic expression for all the terms appearing in Eq.(J.22).

Calculation of $\langle\alpha|\nabla_z|\beta\rangle$:

We start developing $\langle\alpha|\nabla_z|\beta\rangle$:

$$\langle\alpha|\nabla_z|\beta\rangle = \int d\vec{r}_\perp \phi^*_{(n_{\perp_\alpha}, m_\alpha)}(\vec{r}_\perp)\phi_{(n_{\perp_\beta}, m_\beta)}(\vec{r}_\perp) \int dz \varphi_{n_{z_\alpha}}(z + d_\alpha)\nabla_z \varphi_{n_{z_\beta}}(z + d_\beta) \tag{J.23}$$

Thanks to the orthonormality relations of the $r_\perp$-harmonic oscillator wave functions, Eq.(J.23) is simplified:

$$\langle\alpha|\nabla_z|\beta\rangle = \delta_{m_\alpha m_\beta}\delta_{n_{\perp_\alpha} n_{\perp_\beta}} \int dz \varphi_{n_{z_\alpha}}(z + d_\alpha)\nabla_z \varphi_{n_{z_\beta}}(z + d_\beta) \tag{J.24}$$

To tackle the z part, we first apply ∇_z:

$$\begin{aligned}\langle\alpha|\nabla_z|\beta\rangle = \delta_{m_\alpha m_\beta}\delta_{n_{\perp_\alpha} n_{\perp_\beta}} \frac{1}{b_z\sqrt{2}} \int dz \varphi_{n_{z_\alpha}}(z + d_\alpha)[\delta_{(n_{z_\beta}>0)}\sqrt{n_{z_\beta}}\varphi_{(n_{z_\beta}-1)}(z + d_\beta) \\ -\sqrt{n_{z_\beta}+1}\varphi_{(n_{z_\beta}+1)}(z + d_\beta)]\end{aligned} \tag{J.25}$$

We then insert the S matrix standing for the overlap between two z-harmonic oscillator wave functions (see Appendix D) in Eq.(J.25). We finally find:

$$\boxed{\begin{aligned}\langle\alpha|\nabla_z|\beta\rangle = \delta_{m_\alpha m_\beta}\delta_{n_{\perp_\alpha} n_{\perp_\beta}} \frac{1}{b_z\sqrt{2}}[\delta_{(n_{z_\beta}>0)}\sqrt{n_{z_\beta}}S_{(n_{z_\alpha}, d_\alpha)(n_{z_\beta}-1, d_\beta)} \\ -\sqrt{n_{z_\beta}+1}S_{(n_{z_\alpha}, d_\alpha)(n_{z_\beta}+1, d_\beta)}]\end{aligned}} \tag{J.26}$$

Calculation of $\langle\alpha|\nabla_+|\beta\rangle$:

We start developing $\langle\alpha|\nabla_+|\beta\rangle$:

$$\langle\alpha|\nabla_+|\beta\rangle = \int d\vec{r}_\perp \phi^*_{(n_{\perp_\alpha},m_\alpha)}(\vec{r}_\perp)\nabla_+\phi_{(n_{\perp_\beta},m_\beta)}(\vec{r}_\perp)\int dz\varphi_{n_{z_\alpha}}(z+d_\alpha)\varphi_{n_{z_\beta}}(z+d_\beta) \quad \text{(J.27)}$$

The z-part is easily handled using the S matrix defined previously:

$$\langle\alpha|\nabla_+|\beta\rangle = S_{(n_{z_\alpha},d_\alpha)(n_{z_\beta},d_\beta)}\int d\vec{r}_\perp \phi^*_{(n_{\perp_\alpha},m_\alpha)}(\vec{r}_\perp)\nabla_+\phi_{(n_{\perp_\beta},m_\beta)}(\vec{r}_\perp) \quad \text{(J.28)}$$

Applying the gradient ∇_+ and using the orthonormality relations of the $r_\perp$-harmonic oscillator wave functions, we eventually find:

$$\boxed{\begin{aligned}\langle\alpha|\nabla_+|\beta\rangle = S_{(n_{z_\alpha},d_\alpha)(n_{z_\beta},d_\beta)}\frac{1}{b_r\sqrt{2}}\delta_{(m_\alpha,m_\beta+1)}\\ [\delta_{(m_\beta\geq 0)}(\delta_{(n_{\perp_\beta},n_{\perp_\alpha})}\sqrt{m_\beta+n_{\perp_\beta}+1}+\delta_{(n_{\perp_\beta}>0)}\delta_{(n_{\perp_\beta}-1,n_{\perp_\alpha})}\sqrt{n_{\perp_\beta}})\\ -\delta_{(m_\beta<0)}(\delta_{(n_{\perp_\beta},n_{\perp_\alpha})}\sqrt{|m_\beta|+n_{\perp_\beta}}+\delta_{(n_{\perp_\beta}+1,n_{\perp_\alpha})}\sqrt{n_{\perp_\beta}+1})]\end{aligned}} \quad \text{(J.29)}$$

Calculation of $\langle\alpha|\nabla_-|\beta\rangle$:

We start developing $\langle\alpha|\nabla_-|\beta\rangle$:

$$\langle\alpha|\nabla_-|\beta\rangle = \int d\vec{r}_\perp \phi^*_{(n_{\perp_\alpha},m_\alpha)}(\vec{r}_\perp)\nabla_-\phi_{(n_{\perp_\beta},m_\beta)}(\vec{r}_\perp)\int dz\varphi_{n_{z_\alpha}}(z+d_\alpha)\varphi_{n_{z_\beta}}(z+d_\beta) \quad \text{(J.30)}$$

The z-part is easily handled using the S matrix previously defined:

$$\langle\alpha|\nabla_-|\beta\rangle = S_{(n_{z_\alpha},d_\alpha)(n_{z_\beta},d_\beta)}\int d\vec{r}_\perp \phi^*_{(n_{\perp_\alpha},m_\alpha)}(\vec{r}_\perp)\nabla_-\phi_{(n_{\perp_\beta},m_\beta)}(\vec{r}_\perp) \quad \text{(J.31)}$$

Applying the gradient ∇_- and using the orthonormality relations of the $r_\perp$-harmonic oscillator wave functions, we eventually find:

$$\boxed{\begin{aligned}\langle\alpha|\nabla_-|\beta\rangle = S_{(n_{z_\alpha},d_\alpha)(n_{z_\beta},d_\beta)}\frac{1}{b_r\sqrt{2}}\delta_{(m_\alpha,m_\beta-1)}\\ [\delta_{(m_\beta\geq 1)}(\delta_{(n_{\perp_\beta},n_{\perp_\alpha})}\sqrt{m_\beta+n_{\perp_\beta}}+\delta_{(n_{\perp_\beta}+1,n_{\perp_\alpha})}\sqrt{n_{\perp_\beta}+1})\\ -\delta_{(m_\beta<1)}(\delta_{(n_{\perp_\beta},n_{\perp_\alpha})}\sqrt{|m_\beta|+n_{\perp_\beta}+1}+\delta_{(n_{\perp_\beta}>0)}\delta_{(n_{\perp_\beta}-1,n_{\perp_\alpha})}\sqrt{n_{\perp_\beta}})]\end{aligned}} \quad \text{(J.32)}$$

To conclude, we observe the following property which is useful in practice:

$$\boxed{\langle\alpha|\nabla_+|\beta\rangle = \langle\beta|\nabla_-|\alpha\rangle} \quad \text{(J.33)}$$

J.1.2 Different bases

Developing the dot product in the collective spatial part $\bar{E}$ defined in Eq.(J.11), we find:

$$\boxed{\bar{E}^{\gamma\delta}_{\alpha\beta} = \hbar^2[-{}_0\langle\alpha|\nabla_z|\gamma\rangle_{10}\langle\beta|\nabla_z|\delta\rangle_1 + {}_0\langle\alpha|\nabla_-|\gamma\rangle_{10}\langle\beta|\nabla_+|\delta\rangle_1 + {}_0\langle\alpha|\nabla_+|\gamma\rangle_{10}\langle\beta|\nabla_-|\delta\rangle_1]} \quad \text{(J.34)}$$

Calculation of ${}_0\langle\alpha|\nabla_z|\beta\rangle_1$:

We start developing ${}_0\langle\alpha|\nabla_z|\beta\rangle_1$:

$$\begin{aligned} {}_0\langle\alpha|\nabla_z|\beta\rangle_1 = &\int d\vec{r}_\perp \phi^*_{(n_{\perp_\alpha},m_\alpha)}(\vec{r}_\perp, b_{r_0})\phi_{(n_{\perp_\beta},m_\beta)}(\vec{r}_\perp, b_{r_1}) \\ &\int dz \varphi_{n_{z_\alpha}}(z + d_\alpha, b_{z_0})\nabla_z \varphi_{n_{z_\beta}}(z + d_\beta, b_{z_1}) \end{aligned} \quad \text{(J.35)}$$

The $r_\perp$-part is handled using the $\bar{S}_r$ matrix that stands for the overlap between two $r_\perp$-harmonic oscillator wave functions with two different oscillator lengths (see Appendix D):

$${}_0\langle\alpha|\nabla_z|\beta\rangle_1 = \bar{S}_{r_{(m_\alpha,n_{\perp_\alpha})(m_\beta,n_{\perp_\beta})}}(b_{r_0}, b_{r_1}) \int dz \varphi_{n_{z_\alpha}}(z + d_\alpha, b_{z_0})\nabla_z \varphi_{n_{z_\beta}}(z + d_\beta, b_{z_1}) \quad \text{(J.36)}$$

For the z-part, we first apply ∇_z and then use the matrix $\bar{S}_z$ standing for the overlap between two z-harmonic oscillator wave functions with different oscillator lengths (see Appendix D). We eventually find:

$$\boxed{\begin{aligned} {}_0\langle\alpha|\nabla_z|\beta\rangle_1 = \frac{1}{b_{z_1}\sqrt{2}}\bar{S}_{r_{(m_\alpha,n_{\perp_\alpha})(m_\beta,n_{\perp_\beta})}}(b_{r_0}, b_{r_1})[&\delta_{(n_{z_\beta}>0)}\sqrt{n_{z_\beta}}\bar{S}_{z_{(n_{z_\alpha},d_\alpha)(n_{z_\beta}-1,d_\beta)}}(b_{z_0}, b_{z_1}) \\ &-\sqrt{n_{z_\beta}+1}\bar{S}_{z_{(n_{z_\alpha},d_\alpha)(n_{z_\beta}+1,d_\beta)}}(b_{z_0}, b_{z_1})] \end{aligned}} \quad \text{(J.37)}$$

Calculation of ${}_0\langle\alpha|\nabla_+|\beta\rangle_1$:

We start developing ${}_0\langle\alpha|\nabla_+|\beta\rangle_1$:

$$\begin{aligned} {}_0\langle\alpha|\nabla_+|\beta\rangle_1 = &\int d\vec{r}_\perp \phi^*_{(n_{\perp_\alpha},m_\alpha)}(\vec{r}_\perp, b_{r_0})\nabla_+\phi_{(n_{\perp_\beta},m_\beta)}(\vec{r}_\perp, b_{r_1}) \\ &\int dz \varphi_{n_{z_\alpha}}(z + d_\alpha, b_{z_0})\varphi_{n_{z_\beta}}(z + d_\beta, b_{z_1}) \end{aligned} \quad \text{(J.38)}$$

The z-part is easily handled using the $\bar{S}_z$ matrix defined previously:

$${}_0\langle\alpha|\nabla_+|\beta\rangle_1 = \bar{S}_{z_{(n_{z_\alpha},d_\alpha)(n_{z_\beta},d_\beta)}}(b_{z_0}, b_{z_1}) \int d\vec{r}_\perp \phi^*_{(n_{\perp_\alpha},m_\alpha)}(\vec{r}_\perp, b_{r_0})\nabla_+\phi_{(n_{\perp_\beta},m_\beta)}(\vec{r}_\perp, b_{r_1}) \quad \text{(J.39)}$$

Applying the gradient ∇_+ and using the matrix $\bar{S}_r$, we eventually find:

$$
\boxed{
\begin{aligned}
{}_0\langle\alpha|\nabla_+|\beta\rangle_1 = \delta_{(m_\alpha,m_\beta+1)}\frac{1}{b_{r_1}\sqrt{2}}\bar{S}_{z_{(n_{z_\alpha},d_\alpha)(n_{z_\beta},d_\beta)}}(b_{z_0},b_{z_1})[\\
\delta_{(m_\beta\geq 0)}[\sqrt{m_\beta+n_{\perp_\beta}+1}\bar{S}_{r_{(m_\alpha,n_{\perp_\alpha})(m_\beta+1,n_{\perp_\beta})}}(b_{r_0},b_{r_1})\\
+\delta_{(n_{\perp_\beta}>0)}\sqrt{n_{\perp_\beta}}\bar{S}_{r_{(m_\alpha,n_{\perp_\alpha})(m_\beta+1,n_{\perp_\beta}-1)}}(b_{r_0},b_{r_1})]\\
-\delta_{(m_\beta<0)}[\sqrt{|m_\beta|+n_{\perp_\beta}}\bar{S}_{r_{(m_\alpha,n_{\perp_\alpha})(m_\beta+1,n_{\perp_\beta})}}(b_{r_0},b_{r_1})\\
+\sqrt{n_{\perp_\beta}+1}\bar{S}_{r_{(m_\alpha,n_{\perp_\alpha})(m_\beta+1,n_{\perp_\beta}+1)}}(b_{r_0},b_{r_1})]]
\end{aligned}
} \tag{J.40}
$$

Calculation of ${}_0\langle\alpha|\nabla_-|\beta\rangle_1$:

We start developing ${}_0\langle\alpha|\nabla_-|\beta\rangle_1$:

$$
\begin{aligned}
{}_0\langle\alpha|\nabla_-|\beta\rangle_1 = \int d\vec{r}_\perp \phi^*_{(n_{\perp_\alpha},m_\alpha)}(\vec{r}_\perp,b_{r_0})\nabla_-\phi_{(n_{\perp_\beta},m_\beta)}(\vec{r}_\perp,b_{r_1})\\
\int dz\varphi_{n_{z_\alpha}}(z+d_\alpha,b_{z_0})\varphi_{n_{z_\beta}}(z+d_\beta,b_{z_1})
\end{aligned} \tag{J.41}
$$

The z-part is treated thanks to the $\bar{S}_z$ matrix:

$$
{}_0\langle\alpha|\nabla_-|\beta\rangle_1 = \bar{S}_{z_{(n_{z_\alpha},d_\alpha)(n_{z_\beta},d_\beta)}}(b_{z_0},b_{z_1})\int d\vec{r}_\perp\phi^*_{(n_{\perp_\alpha},m_\alpha)}(\vec{r}_\perp,b_{r_0})\nabla_-\phi_{(n_{\perp_\beta},m_\beta)}(\vec{r}_\perp,b_{r_1}) \tag{J.42}
$$

Applying ∇_+ and introducing the matrix $\bar{S}_r$, Eq.(J.42) eventually reads:

$$
\boxed{
\begin{aligned}
{}_0\langle\alpha|\nabla_-|\beta\rangle_1 = \delta_{(m_\alpha,m_\beta-1)}\frac{1}{b_{r_1}\sqrt{2}}\bar{S}_{z_{(n_{z_\alpha},d_\alpha)(n_{z_\beta},d_\beta)}}(b_{z_0},b_{z_1})[\\
\delta_{(m_\beta\geq 1)}[\sqrt{m_\beta+n_{\perp_\beta}}\bar{S}_{r_{(m_\alpha,n_{\perp_\alpha})(m_\beta-1,n_{\perp_\beta})}}(b_{r_0},b_{r_1})\\
+\sqrt{n_{\perp_\beta}+1}\bar{S}_{r_{(m_\alpha,n_{\perp_\alpha})(m_\beta-1,n_{\perp_\beta}+1)}}(b_{r_0},b_{r_1})]\\
-\delta_{(m_\beta<1)}[\sqrt{|m_\beta|+n_{\perp_\beta}+1}\bar{S}_{r_{(m_\alpha,n_{\perp_\alpha})(m_\beta-1,n_{\perp_\beta})}}(b_{r_0},b_{r_1})\\
+\delta_{(n_{\perp_\beta}>0)}\sqrt{n_{\perp_\beta}}\bar{S}_{r_{(m_\alpha,n_{\perp_\alpha})(m_\beta-1,n_{\perp_\beta}-1)}}(b_{r_0},b_{r_1})]]
\end{aligned}
} \tag{J.43}
$$

J.2 HFB fields

In this part, the direct mean field, exchange mean field and pairing field are derived in great details. Thoses derivations are the one used in the HFB3 code.

J.2.1 Direct mean field

The direct mean field reads:

$$
\Gamma_{\alpha\gamma}(D) = -\frac{1}{AM}\langle\alpha|\vec{P}|\gamma\rangle.\sum_{\delta\beta}\langle\beta|\vec{P}|\delta\rangle\rho_{\delta\beta} \tag{J.44}
$$

We first use the time-reversal properties of the density matrix:

$$\Gamma_{\alpha\gamma}(D) = -\frac{1}{AM}\langle\alpha|\vec{P}|\gamma\rangle.\sum_{\delta\beta>}[\langle\beta|\vec{P}|\delta\rangle + (-1)^{s_\delta - s_\beta}\langle\bar{\beta}|\vec{P}|\bar{\delta}\rangle]\rho_{\delta\beta} \tag{J.45}$$

In Eq.(J.45), the spin condition $\delta_{s_\delta s_\beta}$ implies that $(-1)^{s_\delta - s_\beta} = 1$. Moreover, as the operator $\vec{P}$ is time-odd, we write:

$$\langle\bar{\beta}|\vec{P}|\bar{\delta}\rangle = (\langle\beta|T^+)\vec{P}T|\delta\rangle = (\langle\beta|T^+\vec{P}T|\delta\rangle)^* = -(\langle\beta|\vec{P}|\delta\rangle)^* = -\langle\delta|\vec{P}|\beta\rangle \tag{J.46}$$

Eq.(J.46) naturally leads to:

$$\Gamma_{\alpha\gamma}(D) = -\frac{1}{AM}\sum_{\delta\beta>}\langle\alpha|\vec{P}|\gamma\rangle.\langle\beta|\vec{P}|\delta\rangle\rho_{\delta\beta} - -\frac{1}{AM}\sum_{\delta\beta>}\langle\alpha|\vec{P}|\gamma\rangle\langle\delta|\vec{P}|\beta\rangle\rho_{\delta\beta} \tag{J.47}$$

As ρ is symmetric, the following property is now straightforward:

$$\boxed{\Gamma_{\alpha\gamma}(D) = 0} \tag{J.48}$$

J.2.2 Exchange mean field

The exchange mean fields reads as follows:

$$\Gamma_{\alpha\gamma}(E) = \frac{1}{AM}\sum_{\delta\beta}\langle\alpha|\vec{P}|\delta\rangle.\langle\beta|\vec{P}|\gamma\rangle\rho_{\delta\beta} \tag{J.49}$$

We start using the time-reversal property of ρ:

$$\Gamma_{\alpha\gamma}(E) = \frac{1}{AM}\sum_{\delta\beta>}[\langle\alpha|\vec{P}|\delta\rangle.\langle\beta|\vec{P}|\gamma\rangle + (-1)^{s_\delta - s_\beta}\langle\alpha|\vec{P}|\bar{\delta}\rangle.\langle\bar{\beta}|\vec{P}|\gamma\rangle]\rho_{\delta\beta} \tag{J.50}$$

Then, we develop the operator $\vec{P}$ and implicitly consider the spin-isospin part:

$$\begin{aligned}\Gamma_{\alpha\gamma}(E) = \frac{\hbar^2}{AM}\sum_{\delta\beta>}[&(-\langle\alpha|\nabla_z|\delta\rangle.\langle\beta|\nabla_z|\gamma\rangle + \langle\alpha|\nabla_+|\delta\rangle.\langle\beta|\nabla_-|\gamma\rangle + \langle\alpha|\nabla_-|\delta\rangle.\langle\beta|\nabla_+|\gamma\rangle) \\ &+(-1)^{s_\delta - s_\beta}(-\langle\alpha|\nabla_z|\bar{\delta}\rangle.\langle\bar{\beta}|\nabla_z|\gamma\rangle + \langle\alpha|\nabla_+|\bar{\delta}\rangle.\langle\bar{\beta}|\nabla_-|\gamma\rangle + \langle\alpha|\nabla_-|\bar{\delta}\rangle.\langle\bar{\beta}|\nabla_+|\gamma\rangle)]\rho_{\delta\beta}\end{aligned} \tag{J.51}$$

We have to perform a meticulous analysis of the conditions implied by both the derivative operators and the spin parts. First, $\langle\alpha|\nabla_z|\bar{\delta}\rangle \Rightarrow (m_\alpha = -m_\delta) \Rightarrow (m_\alpha = m_\delta = 0)$ and $(s_\alpha = -s_\delta)$. Similarly, $\langle\bar{\beta}|\nabla_z|\gamma\rangle \Rightarrow (-m_\beta = m_\gamma) \Rightarrow (m_\beta = m_\gamma = 0)$ and $(s_\beta = -s_\gamma)$. As we only consider $\Omega \geq 0$, $(m_\alpha = m_\gamma = 0) \Rightarrow (s_\alpha = s_\gamma = +) \Rightarrow (s_\beta = s_\delta = -)$ while $(m_\delta = m_\beta = 0) \Rightarrow (s_\beta = s_\delta = +)$. It is clear that both conditions cannot hold at the same time. Then the term equals zero. Besides, $\langle\alpha|\nabla_-|\bar{\delta}\rangle \Rightarrow (m_\alpha = -m_\delta - 1)$, which is not

possible as ($m_\alpha \geq 0$) and ($m_\delta \geq 0$). Therefore, the related term also equals zero. Finally, we observe that the isospin condition always imposes a global $\delta_{\tau\tau'}$. Eq.(J.51) eventually reads:

$$\boxed{\begin{aligned}\Gamma^\tau_{\alpha\gamma}(E) = \frac{\hbar^2}{AM}\sum_{\delta\beta>}[&-\langle\alpha|\nabla_z|\delta\rangle.\langle\beta|\nabla_z|\gamma\rangle + \langle\alpha|\nabla_+|\delta\rangle.\langle\beta|\nabla_-|\gamma\rangle \\ &+\langle\alpha|\nabla_-|\delta\rangle.\langle\beta|\nabla_+|\gamma\rangle + (-1)^{s_\delta - s_\beta}\langle\alpha|\nabla_+|\bar{\delta}\rangle.\langle\bar{\beta}|\nabla_-|\gamma\rangle]\rho^\tau_{\delta\beta}\end{aligned}} \tag{J.52}$$

To conclude this part, we explicitly consider the spins of the last term including time-reversed components. The latter is called $\tilde{\Gamma}$:

$$\tilde{\Gamma}^\tau_{\alpha\gamma} = \sum_{\delta\beta>}(-1)^{s_\delta - s_\beta}\langle\alpha|\nabla_+|\bar{\delta}\rangle.\langle\bar{\beta}|\nabla_-|\gamma\rangle\rho^\tau_{\delta\beta} \tag{J.53}$$

Case $(m_\alpha = m_\gamma = 0) \Rightarrow (s_\alpha = s_\gamma = +)$:

It directly implies $(m_\delta = m_\beta = 1) \Rightarrow (s_\delta = s_\beta = -)$. Therefore, introducing obvious notations:

$$\tilde{\Gamma}^{\tau++}_{(0,0)} = \sum_{\delta\beta>}\langle 0_\alpha|\nabla_+|\bar{1_\delta}\rangle.\langle\bar{1_\beta}|\nabla_-|0_\gamma\rangle\rho^{\tau--}_{\delta\beta} \tag{J.54}$$

Case $(m_\alpha = m_\gamma = 1)$:

It directly implies $(m_\delta = m_\beta = 0) \Rightarrow (s_\delta = s_\beta = +) \Rightarrow (s_\alpha = s_\gamma = -)$. Then:

$$\tilde{\Gamma}^{\tau--}_{(1,1)} = \sum_{\delta\beta>}\langle 1_\alpha|\nabla_+|\bar{0_\delta}\rangle.\langle\bar{0_\beta}|\nabla_-|1_\gamma\rangle\rho^{\tau++}_{\delta\beta} \tag{J.55}$$

Case $(m_\alpha = 1, m_\gamma = 0) \Rightarrow (s_\alpha = -, s_\gamma = +)$:

It directly implies $(m_\delta = 0, m_\beta = 1) \Rightarrow (s_\delta = +, s_\beta = -)$. Then:

$$\tilde{\Gamma}^{\tau-+}_{(1,0)} = -\sum_{\delta\beta>}\langle 1_\alpha|\nabla_+|\bar{0_\delta}\rangle.\langle\bar{1_\beta}|\nabla_-|0_\gamma\rangle\rho^{\tau+-}_{\delta\beta} \tag{J.56}$$

Case $(m_\alpha = 0, m_\gamma = 1) \Rightarrow (s_\alpha = +, s_\gamma = -)$:

It directly implies $(m_\delta = 1, m_\beta = 0) \Rightarrow (s_\delta = -, s_\beta = +)$, such that:

$$\tilde{\Gamma}^{\tau+-}_{(0,1)} = -\sum_{\delta\beta>}\langle 0_\alpha|\nabla_+|\bar{1_\delta}\rangle.\langle\bar{0_\beta}|\nabla_-|1_\gamma\rangle\rho^{\tau-+}_{\delta\beta} \tag{J.57}$$

The only existing Ω block ($\Omega = 0$) then reads:

$$\tilde{\Gamma}^{\tau(\Omega=0)} = \begin{pmatrix} 0 & \langle 0|\nabla_+|\bar{1}\rangle \\ -\langle 1|\nabla_+|0\rangle & 0 \end{pmatrix}\begin{pmatrix} \rho^{\tau++}_{00} & \rho^{\tau+-}_{01} \\ \rho^{\tau-+}_{01} & \rho^{\tau--}_{00} \end{pmatrix}\begin{pmatrix} 0 & -\langle 0|\nabla_-|1\rangle \\ \langle\bar{1}|\nabla_-|0\rangle & 0 \end{pmatrix} \tag{J.58}$$

We use the following relations:

$$\langle\alpha|\nabla_+|\beta\rangle = \langle\beta|\nabla_-|\alpha\rangle \qquad \langle\alpha|\nabla_+|\beta\rangle = -\langle\bar{\beta}|\nabla_+|\bar{\alpha}\rangle \tag{J.59}$$

Thanks to Eq.(J.59), $\tilde{\Gamma}$ eventually reads:

$$\boxed{\tilde{\Gamma}^{\tau(\Omega=0)} = \begin{pmatrix} 0 & \langle 1|\nabla_+|0\rangle \\ \langle 1|\nabla_+|0\rangle & 0 \end{pmatrix} \begin{pmatrix} \rho_{00}^{\tau++} & \rho_{01}^{\tau+-} \\ \rho_{01}^{\tau-+} & \rho_{00}^{\tau--} \end{pmatrix} \begin{pmatrix} 0 & \langle 1|\nabla_+|0\rangle \\ \langle 1|\nabla_+|0\rangle & 0 \end{pmatrix} = p\rho^{\tau(\Omega=0)}p} \tag{J.60}$$

Where the matrix p is defined as follows:

$$p = \begin{pmatrix} 0 & \langle 1|\nabla_+|0\rangle \\ \langle 1|\nabla_+|0\rangle & 0 \end{pmatrix} \tag{J.61}$$

Using Eq.(J.60), the exchange mean field is eventually written in its final form:

$$\boxed{\begin{aligned}\Gamma^{\tau}_{\alpha\gamma}(E) = \frac{\hbar^2}{AM}\sum_{\delta\beta>} &-(P_0)_{\alpha\delta}\rho^{\tau}_{\delta\beta}(P_0)_{\beta\gamma} + (P_+)_{\alpha\delta}\rho^{\tau}_{\delta\beta}(P_-)_{\beta\gamma} \\ &+(P_-)_{\alpha\delta}\rho^{\tau}_{\delta\beta}(P_+)_{\beta\gamma} + p_{\alpha\delta}\rho^{\tau}_{\delta\beta}p_{\beta\gamma}\end{aligned}} \tag{J.62}$$

In Eq.(J.62), we have introduced the following notations:

$$\begin{cases} (P_0)_{\alpha\gamma} = \langle\alpha|\nabla_z|\gamma\rangle \\ (P_+)_{\alpha\gamma} = \langle\alpha|\nabla_+|\gamma\rangle \\ (P_-)_{\alpha\gamma} = \langle\alpha|\nabla_-|\gamma\rangle \end{cases} \tag{J.63}$$

J.2.3 Pairing field

The pairing field reads as follows:

$$\Delta_{\alpha\bar{\beta}} = \frac{1}{AM}\sum_{\gamma\delta}(-1)^{s_\beta+s_\delta}\langle\alpha|\vec{P}|\gamma\rangle.\langle\bar{\beta}|\vec{P}|\bar{\delta}\rangle\kappa_{\gamma\bar{\delta}} \tag{J.64}$$

We use the time-reversal property of the pairing tensor:

$$\Delta_{\alpha\bar{\beta}} = \frac{1}{AM}\sum_{\gamma\delta>}[(-1)^{s_\beta+s_\delta}\langle\alpha|\vec{P}|\gamma\rangle.\langle\bar{\beta}|\vec{P}|\bar{\delta}\rangle + (-1)^{s_\beta-s_\gamma}\langle\alpha|\vec{P}|\bar{\gamma}\rangle.\langle\bar{\beta}|\vec{P}|\delta\rangle]\kappa_{\gamma\bar{\delta}} \tag{J.65}$$

It is clear that $\delta_{s_\beta s_\delta}$ implies $(-1)^{s_\beta+s_\delta} = -1$. We then use the time-reversal relations $\langle\bar{\beta}|\vec{P}|\bar{\delta}\rangle = -\langle\delta|\vec{P}|\beta\rangle$ and $\langle\bar{\beta}|\vec{P}|\delta\rangle = -\langle\bar{\delta}|\vec{P}|\beta\rangle$, such that Eq.(J.65) reads:

$$\Delta_{\alpha\bar{\beta}} = \frac{1}{AM}\sum_{\gamma\delta>}[\langle\alpha|\vec{P}|\gamma\rangle.\langle\delta|\vec{P}|\beta\rangle + (-1)^{s_\beta+s_\gamma}\langle\alpha|\vec{P}|\bar{\gamma}\rangle.\langle\bar{\delta}|\vec{P}|\beta\rangle]\kappa_{\gamma\bar{\delta}} \tag{J.66}$$

Now, we transform Eq.(J.66) into a form very similar to the one of the exchange mean field in Eq.(J.51) :

$$\Delta_{\alpha\bar{\beta}} = \frac{\hbar^2}{AM}\sum_{\gamma\delta>}[-\langle\alpha|\nabla_z|\gamma\rangle.\langle\delta|\nabla_z|\beta\rangle + \langle\alpha|\nabla_+|\gamma\rangle.\langle\delta|\nabla_-|\beta\rangle + \langle\alpha|\nabla_-|\gamma\rangle.\langle\delta|\nabla_+|\beta\rangle \quad \text{(J.67)}$$
$$+(-1)^{s_\beta+s_\gamma}(-\langle\alpha|\nabla_z|\bar{\gamma}\rangle.\langle\bar{\delta}|\nabla_z|\beta\rangle + \langle\alpha|\nabla_+|\bar{\gamma}\rangle.\langle\bar{\delta}|\nabla_-|\beta\rangle + \langle\alpha|\nabla_-|\bar{\gamma}\rangle.\langle\bar{\delta}|\nabla_+|\beta\rangle)]\kappa_{\gamma\bar{\delta}}$$

By analogy with the exchange mean field, we eventually write for the pairing field:

$$\boxed{\begin{aligned}\Delta^\tau_{\alpha\bar{\beta}} = \frac{\hbar^2}{AM}\sum_{\gamma\delta>}[&-\langle\alpha|\nabla_z|\gamma\rangle.\langle\delta|\nabla_z|\beta\rangle + \langle\alpha|\nabla_+|\gamma\rangle.\langle\delta|\nabla_-|\beta\rangle + \langle\alpha|\nabla_-|\gamma\rangle.\langle\delta|\nabla_+|\beta\rangle \\ &+(-1)^{s_\beta+s_\gamma}\langle\alpha|\nabla_+|\bar{\gamma}\rangle.\langle\bar{\delta}|\nabla_-|\beta\rangle]\kappa^\tau_{\gamma\bar{\delta}}\end{aligned}} \quad \text{(J.68)}$$

In the following, we explicitly consider the spins of the last term including time-reversed components. The latter is called $\tilde{\Delta}$:

$$\tilde{\Delta}^\tau_{\alpha\bar{\beta}} = \sum_{\gamma\delta>}(-1)^{s_\beta+s_\gamma}\langle\alpha|\nabla_+|\bar{\gamma}\rangle.\langle\bar{\delta}|\nabla_-|\beta\rangle]\kappa^\tau_{\gamma\bar{\delta}} \quad \text{(J.69)}$$

Case $(m_\alpha = m_\beta = 0) \Rightarrow (s_\alpha = s_\beta = +)$:

It directly implies $(m_\delta = m_\gamma = 1) \Rightarrow (s_\delta = s_\gamma = -)$. Then:

$$\tilde{\Delta}^{\tau++}_{(0,0)} = \sum_{\delta\gamma>}\langle 0_\alpha|\nabla_+|\bar{1_\gamma}\rangle.\langle\bar{1_\delta}|\nabla_-|0_\beta\rangle\kappa^{\tau--}_{\gamma\bar{\delta}} \quad \text{(J.70)}$$

Case $(m_\alpha = m_\beta = 1)$:

It directly implies $(m_\delta = m_\gamma = 0) \Rightarrow (s_\delta = s_\gamma = +) \Rightarrow (s_\alpha = s_\beta = -)$. Therefore:

$$\tilde{\Delta}^{\tau--}_{(1,\bar{1})} = \sum_{\delta\gamma>}\langle 1_\alpha|\nabla_+|\bar{0_\gamma}\rangle.\langle\bar{0_\delta}|\nabla_-|1_\beta\rangle\kappa^{\tau++}_{\gamma\bar{\delta}} \quad \text{(J.71)}$$

Case $(m_\alpha = 1, m_\beta = 0) \Rightarrow (s_\alpha = -, s_\beta = +)$:

It directly implies $(m_\delta = 1, m_\gamma = 0) \Rightarrow (s_\delta = -, s_\gamma = +)$. So:

$$\tilde{\Delta}^{\tau-+}_{(1,0)} = -\sum_{\delta\gamma>}\langle 1_\alpha|\nabla_+|\bar{0_\gamma}\rangle.\langle\bar{1_\delta}|\nabla_-|0_\beta\rangle\kappa^{\tau+-}_{\gamma\bar{\delta}} \quad \text{(J.72)}$$

Case $(m_\alpha = 0, m_\beta = 1) \Rightarrow (s_\alpha = +, s_\beta = -)$:

It directly implies $(m_\delta = 0, m_\gamma = 1) \rightarrow (s_\delta = +, s_\gamma = -)$, such that:

$$\tilde{\Delta}^{\tau+-}_{(0,\bar{1})} = -\sum_{\delta\gamma>}\langle 0_\alpha|\nabla_+|\bar{1_\gamma}\rangle.\langle\bar{0_\delta}|\nabla_-|1_\beta\rangle\kappa^{\tau-+}_{\gamma\bar{\delta}} \quad \text{(J.73)}$$

With these results, the only existing Ω block ($\Omega = 0$) reads:

$$\tilde{\Delta}^{\tau(\Omega=0)} = \begin{pmatrix} 0 & \langle 0|\nabla_+|\bar{1}\rangle \\ -\langle 1|\nabla_+|0\rangle & 0 \end{pmatrix} \begin{pmatrix} \kappa_{00}^{\tau++} & \kappa_{01}^{\tau+-} \\ \kappa_{01}^{\tau-+} & \kappa_{00}^{\tau--} \end{pmatrix} \begin{pmatrix} 0 & -\langle 0|\nabla_-|1\rangle \\ \langle \bar{1}|\nabla_-|0\rangle & 0 \end{pmatrix} \tag{J.74}$$

Then, we use the relations:

$$\langle \alpha|\nabla_+|\beta\rangle = \langle \beta|\nabla_-|\alpha\rangle \qquad \langle \alpha|\nabla_+|\beta\rangle = -\langle \bar{\beta}|\nabla_+|\bar{\alpha}\rangle \tag{J.75}$$

Using Eq.(J.75), we eventually find:

$$\boxed{\tilde{\Delta}^{\tau(\Omega=0)} = \begin{pmatrix} 0 & \langle 1|\nabla_+|0\rangle \\ \langle 1|\nabla_+|0\rangle & 0 \end{pmatrix} \begin{pmatrix} \kappa_{00}^{\tau++} & \kappa_{01}^{\tau+-} \\ \kappa_{01}^{\tau-+} & \kappa_{00}^{\tau--} \end{pmatrix} \begin{pmatrix} 0 & \langle 1|\nabla_+|0\rangle \\ \langle 1|\nabla_+|0\rangle & 0 \end{pmatrix} = p\kappa^{\tau(\Omega=0)}p} \tag{J.76}$$

With the matrices P_0, P_+ and P_- defined in Eq.(J.63), the pairing field take the following form:

$$\boxed{\Delta_{\alpha\bar{\beta}}^{\tau} = \frac{\hbar^2}{AM} \sum_{\delta\gamma>} -(P_0)_{\alpha\gamma}\kappa_{\gamma\delta}^{\tau}(P_0)_{\delta\beta} + (P_+)_{\alpha\gamma}\kappa_{\gamma\delta}^{\tau}(P_-)_{\delta\beta} + (P_-)_{\alpha\gamma}\kappa_{\gamma\delta}^{\tau}(P_+)_{\delta\beta} + p_{\alpha\gamma}\kappa_{\gamma\delta}^{\tau}p_{\delta\beta}} \tag{J.77}$$

J.2.4 Programming of the fields

The goal of this section is to explain the special way the fields are evaluated in the HFB3 code. We want to find a convenient block structure to express the equations Eq.(J.62) and Eq.(J.77). We start writting Eq.(J.62) in matrix form:

$$\Gamma^{\tau}(E) = \frac{\hbar^2}{AM}(-P_0\rho P_0 + P_+\rho P_+^T + P_+^T\rho P_+ + p\rho p) \tag{J.78}$$

In Eq.(J.78), P_0 et p clearly have an Ω block structure. In order to understand how to characterize the substructure of P_+, we write schematically $P_+\rho P_+^T$ ordering the columns with respect to m and s:

$$\begin{pmatrix} 0 & 0 & 0 & 0 & 0 \\ 0 & 0 & 0 & 0 & 0 \\ 0 & 0 & \langle 1|\nabla_+|0\rangle\rho_{00}^{++}\langle 0|\nabla_-|1\rangle & \langle 1|\nabla_+|0\rangle\rho_{01}^{+-}\langle 1|\nabla_-|2\rangle & 0 \\ 0 & 0 & \langle 2|\nabla_+|1\rangle\rho_{10}^{-+}\langle 0|\nabla_-|1\rangle & \langle 2|\nabla_+|1\rangle\rho_{11}^{--}\langle 1|\nabla_-|2\rangle & 0 \\ 0 & 0 & 0 & 0 & \langle 2|\nabla_+|1\rangle\rho_{11}^{++}\langle 1|\nabla_-|2\rangle \end{pmatrix} \tag{J.79}$$

Then, we do the same for $P_+^T\rho P_+$:

$$\begin{pmatrix} \langle 0|\nabla_-|1\rangle\rho_{11}^{++}\langle 1|\nabla_+|0\rangle & \langle 0|\nabla_-|1\rangle\rho_{12}^{+-}\langle 2|\nabla_+|1\rangle & 0 & 0 & 0 \\ \langle 1|\nabla_-|2\rangle\rho_{21}^{-+}\langle 1|\nabla_+|0\rangle & \langle 1|\nabla_-|2\rangle\rho_{22}^{--}\langle 2|\nabla_+|1\rangle & 0 & 0 & 0 \\ 0 & 0 & \langle 1|\nabla_-|2\rangle\rho_{22}^{++}\langle 2|\nabla_+|1\rangle & 0 & 0 \\ 0 & 0 & 0 & 0 & 0 \\ 0 & 0 & 0 & 0 & 0 \end{pmatrix} \tag{J.80}$$

Even if P_+ alone does not have an Ω block structure, the full products do have this structure. More precisely, if we label a block of $\Gamma(E)$ with the indices $(m_\alpha, m_\gamma, s_\alpha, s_\gamma)$, the contribution $\Gamma^{s_\alpha s_\beta}_{m_\alpha m_\beta}$ of the term $(P_+\rho P_+^T + P_+^T\rho P_+)$ to $\Gamma(E)$ reads:

$$\boxed{\begin{aligned}\Gamma^{s_\alpha s_\beta}_{m_\alpha m_\beta} = &\langle m_\alpha|\nabla_+|m_\alpha - 1\rangle\rho^{s_\alpha,s_\beta}_{(m_\alpha-1)(m_\beta-1)}\langle m_\beta - 1|\nabla_-|m_\beta\rangle \\ &+\langle m_\alpha|\nabla_-|m_\alpha + 1\rangle\rho^{s_\alpha,s_\beta}_{(m_\alpha+1)(m_\beta+1)}\langle m_\beta + 1|\nabla_+|m_\beta\rangle\end{aligned}} \tag{J.81}$$

Eq.(J.81) defines the way the special block structures of all the two-body center of mass correction fields are handled in HFB3.

J.3 Collective fields

This part aims to give an expression of the direct mean field, exchange mean field and pairing field in the more complex case when ρ^{01} is not symmetric anymore and the two harmonic oscillator bases $\{0\}$ and $\{1\}$ are different. This derivations are useful to evaluate quantities of the following type:

$$\langle\Phi_0|\hat{H}|\Phi_1\rangle \tag{J.82}$$

Those quantities are not only useful in the SCIM approach but appear in many situations as for instance in the expression of the true TDGCM mass and collective potential.

J.3.1 Collective direct mean field

The collective direct mean field reads:

$$\bar{\Gamma}_{\alpha\gamma}(D) = -\frac{1}{AM}{}_0\langle\alpha|\vec{P}|\gamma\rangle_1.\sum_{\delta\beta}{}_0\langle\beta|\vec{P}|\delta\rangle_1\rho^{01}_{\delta\beta} \tag{J.83}$$

We use the time-reversal property of the matrix ρ^{01}:

$$\bar{\Gamma}_{\alpha\gamma}(D) = -\frac{1}{AM}{}_0\langle\alpha|\vec{P}|\gamma\rangle_1.\sum_{\delta\beta>}[{}_0\langle\beta|\vec{P}|\delta\rangle_1 + (-1)^{s_\delta - s_\beta}{}_0\langle\bar{\beta}|\vec{P}|\bar{\delta}\rangle_1]\rho^{01}_{\delta\beta} \tag{J.84}$$

In Eq.(J.84), it is clear that $\delta_{s_\delta s_\beta} \Rightarrow ((-1)^{s_\delta - s_\beta} = 1)$. Besides, as the operator $\vec{P}$ is time-odd, we eventually write:

$$\bar{\Gamma}_{\alpha\gamma}(D) = -\frac{1}{AM}{}_0\langle\alpha|\vec{P}|\gamma\rangle_1.\sum_{\delta\beta>}[{}_0\langle\beta|\vec{P}|\delta\rangle_1 - {}_1\langle\delta|\vec{P}|\beta\rangle_0]\rho^{01}_{\delta\beta} \tag{J.85}$$

As ρ^{01} is not symmetric in general, it is not possible to reduce the expression to zero anymore. Instead, we develop the operator $\vec{P}$:

$$\bar{\Gamma}_{\alpha\gamma}(D) = \frac{\hbar^2}{AM}\sum_{\delta\beta>}[{}_0\langle\alpha|\nabla_z|\gamma\rangle_{10}\langle\beta|\nabla_z|\delta\rangle_1 - {}_0\langle\alpha|\nabla_+|\gamma\rangle_{10}\langle\beta|\nabla_-|\delta\rangle_1 \tag{J.86}$$
$$-{}_0\langle\alpha|\nabla_-|\gamma\rangle_{10}\langle\beta|\nabla_+|\delta\rangle_1 - {}_0\langle\alpha|\nabla_z|\gamma\rangle_{11}\langle\delta|\nabla_z|\beta\rangle_0 + {}_0\langle\alpha|\nabla_+|\gamma\rangle_{11}\langle\delta|\nabla_-|\beta\rangle_0$$
$$+{}_0\langle\alpha|\nabla_-|\gamma\rangle_{11}\langle\delta|\nabla_+|\beta\rangle_0]\rho^{01}_{\delta\beta}$$

We observe that $(s_\beta = s_\delta) \Rightarrow (m_\beta = m_\delta)$. Therefore, all the term of the type $({}_0\langle\beta|\nabla_+|\delta\rangle_1,{}_0\langle\beta|\nabla_-|\delta\rangle_1)$ equal zero. In addition, using the relation ${}_1\langle\delta|\nabla_z|\beta\rangle_0 = -{}_0\langle\beta|\nabla_z|\delta\rangle_1$, Eq.(J.86) is simplified:

$$\bar{\Gamma}_{\alpha\gamma}(D) = 2\frac{\hbar^2}{AM}{}_0\langle\alpha|\nabla_z|\gamma\rangle_1\sum_{\delta\beta>}{}_0\langle\beta|\nabla_z|\delta\rangle_1[\rho^{01\tau}_{\delta\beta} + \rho^{01\bar{\tau}}_{\delta\beta}] \tag{J.87}$$

Now, we set:

$$(P^{01}_0)_{\alpha\gamma} = {}_0\langle\alpha|\nabla_z|\gamma\rangle_1 \tag{J.88}$$

We eventually write the field:

$$\boxed{\bar{\Gamma}_{\alpha\gamma}(D) = 2\frac{\hbar^2}{AM}Tr(P^{01}_0[\rho^{01\tau} + \rho^{01\bar{\tau}}])(P^{01}_0)_{\alpha\gamma}} \tag{J.89}$$

We observe that the field is the same for both isospins.

J.3.2 Collective exchange mean field

The collective exchange mean field reads as follows:

$$\bar{\Gamma}_{\alpha\gamma}(E) = \frac{1}{AM}\sum_{\delta\beta}{}_0\langle\alpha|\vec{P}|\delta\rangle_1\cdot{}_0\langle\beta|\vec{P}|\gamma\rangle_1\rho^{01}_{\delta\beta} \tag{J.90}$$

We use the time-reversal property of ρ^{01}:

$$\bar{\Gamma}_{\alpha\gamma}(E) = \frac{1}{AM}\sum_{\delta\beta>}[{}_0\langle\alpha|\vec{P}|\delta\rangle_1\cdot{}_0\langle\beta|\vec{P}|\gamma\rangle_1 + (-1)^{s_\delta - s_\beta}{}_0\langle\alpha|\vec{P}|\bar{\delta}\rangle_1\cdot{}_0\langle\bar{\beta}|\vec{P}|\gamma\rangle_1]\rho^{01}_{\delta\beta} \tag{J.91}$$

Then, we develop the operator $\vec{P}$:

$$\bar{\Gamma}_{\alpha\gamma}(E) = \frac{\hbar^2}{AM}\sum_{\delta\beta>}[-{}_0\langle\alpha|\nabla_z|\delta\rangle_{10}\langle\beta|\nabla_z|\gamma\rangle_1 + {}_0\langle\alpha|\nabla_+|\delta\rangle_{10}\langle\beta|\nabla_-|\gamma\rangle_1 \tag{J.92}$$
$$+{}_0\langle\alpha|\nabla_-|\delta\rangle_{10}\langle\beta|\nabla_+|\gamma\rangle_1 + (-1)^{s_\delta - s_\beta}(-{}_0\langle\alpha|\nabla_z|\bar{\delta}\rangle_{10}\langle\bar{\beta}|\nabla_z|\gamma\rangle_1$$
$$+{}_0\langle\alpha|\nabla_+|\bar{\delta}\rangle_{10}\langle\bar{\beta}|\nabla_-|\gamma\rangle_1 + {}_0\langle\alpha|\nabla_-|\bar{\delta}\rangle_{10}\langle\bar{\beta}|\nabla_+|\gamma\rangle_1)]\rho^{01}_{\delta\beta}$$

As done for the non-collective case, we perform an analysis of the conditions implied by both the derivative operators and the spin parts.

First, ${}_0\langle\alpha|\nabla_z|\bar{\delta}\rangle_1 \Rightarrow (m_\alpha = -m_\delta) \Rightarrow (m_\alpha = m_\delta = 0)$ and $(s_\alpha = -s_\delta)$. Then, ${}_0\langle\bar{\beta}|\nabla_z|\gamma\rangle_1 \Rightarrow (-m_\beta = -m_\gamma) \Rightarrow (m_\beta = m_\gamma = 0)$ and $(s_\beta = -s_\gamma)$. Furthermore, as $\Omega \geq 0$,
$(m_\alpha = m_\gamma = 0) \Rightarrow (s_\alpha = s_\gamma = +) \Rightarrow (s_\beta = s_\delta = -)$. This last condition combines with the condition $(m_\beta = m_\delta = 0)$, such that the term finally equals zero. Besides, the condition ${}_0\langle\alpha|\nabla_-|\bar{\delta}\rangle_1 \Rightarrow (m_\alpha = -m_\delta - 1)$ cannot hold since $(m_\alpha \geq 0)$ and $(m_\delta \geq 0)$. Therefore this part also equals zero. Finally, a global $\delta_{\tau\tau'}$ holds:

$$\boxed{\begin{aligned}\bar{\Gamma}^{\tau}_{\alpha\gamma}(E) = \frac{\hbar^2}{AM}\sum_{\delta\beta>}[&-{}_0\langle\alpha|\nabla_z|\delta\rangle_1 {}_0\langle\beta|\nabla_z|\gamma\rangle_1 + {}_0\langle\alpha|\nabla_+|\delta\rangle_1 {}_0\langle\beta|\nabla_-|\gamma\rangle_1 \\ &+{}_0\langle\alpha|\nabla_-|\delta\rangle_1 {}_0\langle\beta|\nabla_+|\gamma\rangle_1 + (-1)^{s_\delta - s_\beta}{}_0\langle\alpha|\nabla_+|\bar{\delta}\rangle_1 {}_0\langle\bar{\beta}|\nabla_-|\gamma\rangle_1]\rho^{01\tau}_{\delta\beta}\end{aligned}} \tag{J.93}$$

In the following, we explicitly consider the spins of the last term including time-reversed components. The latter is called $\tilde{\bar{\Gamma}}$.

Case $(m_\alpha = m_\gamma = 0) \Rightarrow (s_\alpha = s_\gamma = +)$:

It directly implies $(m_\delta = m_\beta = 1) \Rightarrow (s_\delta = s_\beta = -)$. Then:

$$\tilde{\bar{\Gamma}}^{\tau++}_{(0,0)} = \sum_{\delta\beta>} {}_0\langle 0_\alpha|\nabla_+|\bar{1_\delta}\rangle_1 {}_0\langle\bar{1_\beta}|\nabla_-|0_\gamma\rangle_1 \rho^{01\tau--}_{\delta\beta} \tag{J.94}$$

Case $(m_\alpha = m_\gamma = 1)$:

It directly implies $(m_\delta = m_\beta = 0) \Rightarrow (s_\delta = s_\beta = +) \Rightarrow (s_\alpha = s_\gamma = -)$. Therefore:

$$\tilde{\bar{\Gamma}}^{\tau--}_{(1,1)} = \sum_{\delta\beta>} {}_0\langle 1_\alpha|\nabla_+|\bar{0_\delta}\rangle_1 {}_0\langle\bar{0_\beta}|\nabla_-|1_\gamma\rangle_1 \rho^{01\tau++}_{\delta\beta} \tag{J.95}$$

Case $(m_\alpha = 1, m_\gamma = 0) \Rightarrow (s_\alpha = -, s_\gamma = +)$:

It directly implies $(m_\delta = 0, m_\beta = 1) \Rightarrow (s_\delta = +, s_\beta = -)$. Then:

$$\tilde{\bar{\Gamma}}^{\tau-+}_{(0,1)} = -\sum_{\delta\beta>} {}_0\langle 1_\alpha|\nabla_+|\bar{0_\delta}\rangle_1 {}_0\langle\bar{1_\beta}|\nabla_-|0_\gamma\rangle_1 \rho^{01\tau+-}_{\delta\beta} \tag{J.96}$$

Case $(m_\alpha = 0, m_\gamma = 1) \Rightarrow (s_\alpha = +, s_\gamma = -)$:

It directly implies $(m_\delta = 1, m_\beta = 0) \Rightarrow (s_\delta = -, s_\beta = +)$, such that:

$$\tilde{\bar{\Gamma}}^{\tau+-}_{(1,0)} = -\sum_{\delta\beta>} {}_0\langle 0_\alpha|\nabla_+|\bar{1_\delta}\rangle_1 {}_0\langle\bar{0_\beta}|\nabla_-|1_\gamma\rangle_1 \rho^{01\tau-+}_{\delta\beta} \tag{J.97}$$

The only existing Ω block $(\Omega = 0)$ then reads:

$$\tilde{\bar{\Gamma}}^{\tau(\Omega=0)} = \begin{pmatrix} 0 & {}_0\langle 0|\nabla_+|\bar{1}\rangle_1 \\ -{}_0\langle 1|\nabla_+|0\rangle_1 & 0 \end{pmatrix} \begin{pmatrix} \rho^{01\tau++}_{00} & \rho^{01\tau+-}_{01} \\ \rho^{01\tau-+}_{01} & \rho^{01\tau--}_{00} \end{pmatrix} \begin{pmatrix} 0 & -{}_0\langle 0|\nabla_-|1\rangle_1 \\ {}_0\langle\bar{1}|\nabla_-|0\rangle_1 & 0 \end{pmatrix} \tag{J.98}$$

We transform Eq.(J.98) thanks to the gradients properties:

$$\tilde{\bar{\Gamma}}^{\tau(\Omega=0)} = \begin{pmatrix} 0 & {}_0\langle 0|\nabla_-|1\rangle_1 \\ {}_0\langle 1|\nabla_+|0\rangle_1 & 0 \end{pmatrix} \begin{pmatrix} \rho_{00}^{01\tau++} & \rho_{01}^{01\tau+-} \\ \rho_{01}^{01\tau-+} & \rho_{00}^{01\tau--} \end{pmatrix} \begin{pmatrix} 0 & {}_0\langle 0|\nabla_-|1\rangle_1 \\ {}_0\langle 1|\nabla_+|0\rangle_1 & 0 \end{pmatrix} \quad \text{(J.99)}$$

We eventually find:

$$\boxed{\tilde{\bar{\Gamma}}^{\tau(\Omega=0)} = \bar{p}\rho^{01\tau(\Omega=0)}\bar{p}} \quad \text{(J.100)}$$

Where we have set:

$$\bar{p} = \begin{pmatrix} 0 & {}_0\langle 0|\nabla_-|1\rangle_1 \\ {}_0\langle 1|\nabla_+|0\rangle_1 & 0 \end{pmatrix} \quad \text{(J.101)}$$

With these results, the full collective exchange mean field eventually reads:

$$\boxed{\begin{aligned} \bar{\Gamma}^{\tau}_{\alpha\gamma}(E) = \frac{\hbar^2}{AM} \sum_{\delta\beta>} & -(P_0^{01})_{\alpha\delta}\rho^{01\tau}_{\delta\beta}(P_0^{01})_{\beta\gamma} + (P_+^{01})_{\alpha\delta}\rho^{01\tau}_{\delta\beta}(P_-^{01})_{\beta\gamma} \\ & +(P_-^{01})_{\alpha\delta}\rho^{01\tau}_{\delta\beta}(P_+^{01})_{\beta\gamma} + \bar{p}_{\alpha\delta}\rho^{01\tau}_{\delta\beta}\bar{p}_{\beta\gamma} \end{aligned}} \quad \text{(J.102)}$$

With the following notations:

$$(P_+^{01})_{\alpha\gamma} = {}_0\langle\alpha|\nabla_+|\gamma\rangle_1 \qquad (P_-^{01})_{\alpha\gamma} = {}_0\langle\alpha|\nabla_-|\gamma\rangle_1 \quad \text{(J.103)}$$

J.3.3 Collective pairing field

The collective pairing field reads as follows:

$$\bar{\Delta}_{\alpha\bar{\beta}} = \frac{1}{AM} \sum_{\gamma\delta} (-1)^{s_\beta+s_\delta} {}_0\langle\alpha|\vec{P}|\gamma\rangle_1 \cdot {}_0\langle\bar{\beta}|\vec{P}|\bar{\delta}\rangle_1 \kappa^{01}_{\gamma\bar{\delta}} \quad \text{(J.104)}$$

We use the time-reversal properties of κ^{01}:

$$\bar{\Delta}_{\alpha\bar{\beta}} = \frac{1}{AM} \sum_{\gamma\delta>} [(-1)^{s_\beta+s_\delta} {}_0\langle\alpha|\vec{P}|\gamma\rangle_1 \cdot {}_0\langle\bar{\beta}|\vec{P}|\bar{\delta}\rangle_1 + (-1)^{s_\beta-s_\gamma} {}_0\langle\alpha|\vec{P}|\bar{\gamma}\rangle_1 \cdot {}_0\langle\bar{\beta}|\vec{P}|\delta\rangle_1] \kappa^{01}_{\gamma\bar{\delta}} \quad \text{(J.105)}$$

In Eq.(J.105), it is clear that $(-1)^{s_\beta+s_\delta} = -1$. We then develop the operator $\vec{P}$:

$$\begin{aligned} \bar{\Delta}_{\alpha\bar{\beta}} = \frac{\hbar^2}{AM} \sum_{\gamma\delta>} & [{}_0\langle\alpha|\nabla_z|\gamma\rangle_1 \cdot {}_0\langle\bar{\beta}|\nabla_z|\bar{\delta}\rangle_1 - {}_0\langle\alpha|\nabla_+|\gamma\rangle_1 {}_0\langle\bar{\beta}|\nabla_-|\bar{\delta}\rangle_1 \nabla_-|\gamma\rangle_1 {}_0\langle\bar{\beta}|\nabla_+|\bar{\delta}\rangle_1 \\ & -{}_0\langle\alpha| + (-1)^{s_\beta+s_\gamma} ({}_0\langle\alpha|\nabla_z|\bar{\gamma}\rangle_1 {}_0\langle\bar{\beta}|\nabla_z|\delta\rangle_1 \nabla_-|\gamma\rangle_1 {}_0\langle\bar{\beta}|\nabla_+|\bar{\delta}\rangle_1 \\ & -{}_0\langle\alpha|\nabla_+|\bar{\gamma}\rangle_1 {}_0\langle\bar{\beta}|\nabla_-|\delta\rangle_1 - {}_0\langle\alpha|\nabla_-|\bar{\gamma}\rangle_1 {}_0\langle\bar{\beta}|\nabla_+|\delta\rangle_1)] \kappa^{01}_{\gamma\bar{\delta}} \end{aligned} \quad \text{(J.106)}$$

By analogy with the collective exchange term, we write:

$$\boxed{\begin{array}{l}\bar{\Delta}_{\alpha\bar{\beta}} = \dfrac{\hbar^2}{AM}\displaystyle\sum_{\gamma\delta>}[{}_0\langle\alpha|\nabla_z|\gamma\rangle_1 {}_0\langle\bar{\beta}|\nabla_z|\bar{\delta}\rangle_1 - {}_0\langle\alpha|\nabla_+|\gamma\rangle_1 {}_0\langle\bar{\beta}|\nabla_-|\bar{\delta}\rangle_1 \\ -{}_0\langle\alpha|\nabla_-|\gamma\rangle_1 {}_0\langle\bar{\beta}|\nabla_+|\bar{\delta}\rangle_1 - (-1)^{s_\beta+s_\gamma}{}_0\langle\alpha|\nabla_+|\bar{\gamma}\rangle_1 {}_0\langle\bar{\beta}|\nabla_-|\delta\rangle_1]\kappa^{01}_{\gamma\bar{\delta}}\end{array}} \tag{J.107}$$

In the following, we explicitly consider the spins of the last term including time-reversal components. The latter is called $\tilde{\bar{\Delta}}$.

Case $(m_\alpha = m_\beta = 0) \Rightarrow (s_\alpha = s_\beta = +)$:

It directly implies $(m_\delta = m_\gamma = 1) \Rightarrow (s_\delta = s_\gamma = -)$. Thus:

$$\tilde{\bar{\Delta}}^{\tau++}_{(0,0)} = \sum_{\delta\gamma>} {}_0\langle 0_\alpha|\nabla_+|\bar{1_\gamma}\rangle_1 {}_0\langle\bar{0_\beta}|\nabla_-|1_\delta\rangle_1 \kappa^{01\tau--}_{\gamma\bar{\delta}} \tag{J.108}$$

Case $(m_\alpha = m_\beta = 1)$:

It directly implies $(m_\delta = m_\gamma = 0) \Rightarrow (s_\delta = s_\gamma = +) \Rightarrow (s_\alpha = s_\beta = -)$. Therefore:

$$\tilde{\bar{\Delta}}^{\tau--}_{(1,\bar{1})} = \sum_{\delta\gamma>} {}_0\langle 1_\alpha|\nabla_+|\bar{0_\gamma}\rangle_1 {}_0\langle\bar{1_\beta}|\nabla_-|0_\delta\rangle_1 \kappa^{01\tau++}_{\gamma\bar{\delta}} \tag{J.109}$$

Case $(m_\alpha = 1, m_\beta = 0) \Rightarrow (s_\alpha = -, s_\beta = +)$:

It directly implies $(m_\delta = 1, m_\gamma = 0) \Rightarrow (s_\delta = -, s_\gamma = +)$. Then:

$$\tilde{\bar{\Delta}}^{\tau-+}_{(1,0)} = -\sum_{\delta\gamma>} {}_0\langle 1_\alpha|\nabla_+|\bar{0_\gamma}\rangle_1 {}_0\langle\bar{0_\beta}|\nabla_-|1_\delta\rangle_1 \kappa^{01\tau+-}_{\gamma\bar{\delta}} \tag{J.110}$$

Case $(m_\alpha = 0, m_\beta = 1) \Rightarrow (s_\alpha = +, s_\beta = -)$:

It directly implies $(m_\delta = 0, m_\gamma = 1) \Rightarrow (s_\delta = +, s_\gamma = -)$, such that:

$$\tilde{\bar{\Delta}}^{\tau+-}_{(0,\bar{1})} = -\sum_{\delta\gamma>} {}_0\langle 0_\alpha|\nabla_+|\bar{1_\gamma}\rangle_1 {}_0\langle\bar{1_\beta}|\nabla_-|0_\delta\rangle_1 \kappa^{01\tau-+}_{\gamma\bar{\delta}} \tag{J.111}$$

The only existing Ω block ($\Omega = 0$) then reads:

$$\tilde{\bar{\Delta}}^{\tau(\Omega=0)} = \begin{pmatrix} 0 & {}_0\langle 0|\nabla_+|\bar{1}\rangle_1 \\ -{}_0\langle 1|\nabla_+|0\rangle_1 & 0 \end{pmatrix} \begin{pmatrix} \kappa^{01\tau++}_{00} & \kappa^{01\tau+-}_{01} \\ \kappa^{01\tau-+}_{01} & \kappa^{01\tau--}_{00} \end{pmatrix} \begin{pmatrix} 0 & -[{}_0\langle\bar{1}|\nabla_-|0\rangle_1]^T \\ [{}_0\langle 0|\nabla_-|1\rangle_1]^T & 0 \end{pmatrix} \tag{J.112}$$

We tranform Eq.(J.112) using the gradients properties:

$$\tilde{\bar{\Delta}}^{\tau(\Omega=0)} = -\begin{pmatrix} 0 & {}_0\langle 0|\nabla_-|1\rangle_1 \\ {}_0\langle 1|\nabla_+|0\rangle_1 & 0 \end{pmatrix} \begin{pmatrix} \kappa^{01\tau++}_{00} & \kappa^{01\tau+-}_{01} \\ \kappa^{01\tau-+}_{01} & \kappa^{01\tau--}_{00} \end{pmatrix} \begin{pmatrix} 0 & [{}_0\langle 1|\nabla_+|0\rangle_1]^T \\ [{}_0\langle 0|\nabla_-|1\rangle_1]^T & 0 \end{pmatrix} \tag{J.113}$$

Using the matrix $\bar{p}$ defined in Eq.(J.101), we finally write:

$$\boxed{\tilde{\bar{\Delta}}^{(\Omega=0)} = -\bar{p}\kappa^{01\tau(\Omega=0)}\bar{p}^T} \tag{J.114}$$

With these results, the collective pairing field eventually reads:

$$\boxed{\begin{aligned}\bar{\Delta}^{\tau}_{\alpha\bar{\beta}} = \frac{\hbar^2}{AM}\sum_{\gamma\delta>}(P_0^{01})_{\alpha\gamma}\kappa^{01\tau}_{\gamma\delta}(P_0^{01T})_{\delta\beta} + (P_+^{01})_{\alpha\gamma}\kappa^{01\tau}_{\gamma\delta}(P_+^{01T})_{\delta\beta} \\ +(P_-^{01})_{\alpha\gamma}\kappa^{01\tau}_{\gamma\delta}(P_-^{01T})_{\delta\beta} + \bar{p}_{\alpha\gamma}\kappa^{01\tau}_{\gamma\delta}\bar{p}^T_{\delta\beta}\end{aligned}} \tag{J.115}$$

J.4 Excited collective fields

The goal of this part is to give an expression of the new two-body center of mass correction fields that appear when intrinsic excitations are added. They are useful to evaluate quantities of the following type :

$$\langle\Phi_0|\bar{\xi}_j\xi_j\hat{H}\xi_i^+\bar{\xi}_i^+|\Phi_1\rangle \tag{J.116}$$

J.4.1 Excited collective field $\bar{\Gamma}^{(i)}([W,Z])$

This field is defined as follows:

$$\boxed{\begin{aligned}\bar{\Gamma}^{(i)}_{\alpha\gamma}([W,Z]) = \frac{1}{AM}\sum_{\delta\beta\in(\Omega_i,\tau_i)}[-{}_0\langle\alpha|\vec{P}|\gamma\rangle_1.({}_0\langle\beta|\vec{P}|\delta\rangle_1 + (-1)^{s_\beta-s_\delta}{}_0\langle\bar{\beta}|\vec{P}|\bar{\delta}\rangle_1) \\ +{}_0\langle\alpha|\vec{P}|\delta\rangle_1.{}_0\langle\beta|\vec{P}|\gamma\rangle_1 + (-1)^{s_\beta-s_\delta}{}_0\langle\alpha|\vec{P}|\bar{\delta}\rangle_1.{}_0\langle\bar{\beta}|\vec{P}|\gamma\rangle_1]W_{\delta i}Z_{\beta\bar{i}}\end{aligned}} \tag{J.117}$$

By analogy with the fields previously derived, we directly write:

$$\boxed{\begin{aligned}\bar{\Gamma}^{(i)\tau}_{\alpha\gamma}([W,Z]) = \frac{\hbar^2}{AM}[2Tr(Z^TP_0^{01}W)(P_0^{01})_{\alpha\gamma} + \delta_{\tau\tau_i}\sum_{\delta\beta\in(\Omega_i,\tau_i)}[-(P_0^{01})_{\alpha\delta}WZ_{\delta\beta}(P_0^{01})_{\beta\gamma} \\ +(P_+^{01})_{\alpha\delta}WZ_{\delta\beta}(P_-^{01})_{\beta\gamma} + (P_-^{01})_{\alpha\delta}WZ_{\delta\beta}(P_+^{01})_{\beta\gamma} + \bar{p}_{\alpha\delta}WZ_{\delta\beta}\bar{p}_{\beta\gamma}]]\end{aligned}} \tag{J.118}$$

Here, we have set:

$$WZ_{\delta\beta} = W_{\delta i}Z_{\beta\bar{i}} \tag{J.119}$$

J.4.2 Excited collective field $\bar{\Delta}^{(i)}(WW)$

This field is defined as follows:

$$\boxed{\begin{aligned}\bar{\Delta}^{(i)}_{\alpha\bar{\beta}}(WW) = \frac{1}{AM}\sum_{\gamma\delta\in(\Omega_i,\tau_i)}[(-1)^{s_\beta+s_\delta}{}_0\langle\alpha|\vec{P}|\gamma\rangle_1.{}_0\langle\bar{\beta}|\vec{P}|\bar{\delta}\rangle_1 \\ +(-1)^{s_\beta-s_\gamma}{}_0\langle\alpha|\vec{P}|\bar{\gamma}\rangle_1.{}_0\langle\bar{\beta}|\vec{P}|\delta\rangle_1]W_{\gamma i}W_{\delta i}\end{aligned}} \tag{J.120}$$

By analogy with the fields previously derived, we directly write:

$$\boxed{\begin{aligned}\bar{\Delta}^{(i)\tau}_{\alpha\bar{\beta}}(WW) = \delta_{\tau\tau_i}\frac{\hbar^2}{AM}\sum_{\gamma\delta\in(\Omega_i,\tau_i)}&(P_0^{01})_{\alpha\gamma}WW_{\gamma\delta}(P_0^{01T})_{\delta\beta} + (P_+^{01})_{\alpha\gamma}WW_{\gamma\delta}(P_+^{01T})_{\delta\beta}\\ &+(P_-^{01})_{\alpha\gamma}WW_{\gamma\delta}(P_-^{01T})_{\delta\beta} + \bar{p}_{\alpha\gamma}WW_{\gamma\delta}\bar{p}^T_{\delta\beta}\end{aligned}} \tag{J.121}$$

Here, we have set:

$$WW_{\gamma\delta} = W_{\gamma i}W_{\delta i} \tag{J.122}$$

J.4.3 Excited collective field $\bar{\Delta}^{(j)}(\bar{Z}\bar{Z})$

This field is defined as follows:

$$\boxed{\begin{aligned}\bar{\Delta}^{(j)}_{\alpha\bar{\beta}}(\bar{Z}\bar{Z}) = \frac{1}{AM}\sum_{\gamma\delta\in(\Omega_j,\tau_j)}&[(-1)^{s_\beta+s_\delta}{}_0\langle\alpha|\vec{P}|\gamma\rangle_1{}_{\cdot 0}\langle\bar{\beta}|\vec{P}|\bar{\delta}\rangle_1\\ &+(-1)^{s_\beta-s_\gamma}{}_0\langle\alpha|\vec{P}|\bar{\gamma}\rangle_1{}_{\cdot 0}\langle\bar{\beta}|\vec{P}|\delta\rangle_1]\bar{Z}_{j\bar{\gamma}}\bar{Z}_{j\bar{\delta}}\end{aligned}} \tag{J.123}$$

By analogy with the fields previously derived, we directly write:

$$\boxed{\begin{aligned}\bar{\Delta}^{(j)\tau}_{\alpha\bar{\beta}}(\bar{Z}\bar{Z}) = \delta_{\tau\tau_j}\frac{\hbar^2}{AM}\sum_{\gamma\delta\in(\Omega_j,\tau_j)}&(P_0^{01})_{\alpha\gamma}\bar{Z}\bar{Z}_{\gamma\delta}(P_0^{01T})_{\delta\beta} + (P_+^{01})_{\alpha\gamma}\bar{Z}\bar{Z}_{\gamma\delta}(P_+^{01T})_{\delta\beta}\\ &+(P_-^{01})_{\alpha\gamma}\bar{Z}\bar{Z}_{\gamma\delta}(P_-^{01T})_{\delta\beta} + \bar{p}_{\alpha\gamma}\bar{Z}\bar{Z}_{\gamma\delta}\bar{p}^T_{\delta\beta}\end{aligned}} \tag{J.124}$$

Here, we have set:

$$\bar{Z}\bar{Z}_{\gamma\delta} = \bar{Z}_{j\bar{\gamma}}\bar{Z}_{j\bar{\delta}} \tag{J.125}$$

J.4.4 Excited collective field $\bar{\Delta}^{(ji)}([W,\bar{Z}])$

This excited field reads as follows:

$$\boxed{\begin{aligned}\bar{\Delta}^{(ji)}_{\alpha\bar{\beta}}([W,\bar{Z}]) = \frac{1}{AM}\sum_{\gamma\delta\in(\Omega_{ji},\tau_{ji})}&[(-1)^{s_\beta+s_\delta}{}_0\langle\alpha|\vec{P}|\gamma\rangle_1{}_{\cdot 0}\langle\bar{\beta}|\vec{P}|\bar{\delta}\rangle_1\\ &+(-1)^{s_\beta-s_\gamma}{}_0\langle\alpha|\vec{P}|\bar{\gamma}\rangle_1{}_{\cdot 0}\langle\bar{\beta}|\vec{P}|\delta\rangle_1][W_{\gamma i}\bar{Z}_{j\bar{\delta}} + \bar{Z}_{j\bar{\gamma}}W_{\delta i}]\end{aligned}} \tag{J.126}$$

By analogy with the fields previously derived, we directly write:

$$\boxed{\begin{aligned}\bar{\Delta}^{(ji)\tau}_{\alpha\bar{\beta}}([W,\bar{Z}]) = \delta_{\tau\tau_{ji}}\frac{\hbar^2}{AM}\sum_{\gamma\delta\in(\Omega_{ji},\tau_{ji})}&(P_0^{01})_{\alpha\gamma}[W,\bar{Z}]_{\gamma\delta}(P_0^{01T})_{\delta\beta}\\ +(P_+^{01})_{\alpha\gamma}[W,\bar{Z}]_{\gamma\delta}(P_+^{01T})_{\delta\beta} &+ (P_-^{01})_{\alpha\gamma}[W,\bar{Z}]_{\gamma\delta}(P_-^{01T})_{\delta\beta} + \bar{p}_{\alpha\gamma}[W,\bar{Z}]_{\gamma\delta}\bar{p}^T_{\delta\beta}\end{aligned}} \tag{J.127}$$

Here, we have set:

$$[W, \bar{Z}]_{\gamma\delta} = W_{\gamma i}\bar{Z}_{j\bar{\delta}} + \bar{Z}_{j\bar{\gamma}}W_{\delta i} \tag{J.128}$$

Appendix K

Kinetic fields

The kinetic fields are the easiest to treat. Indeed, as the kinetic operator is a one-body operator, the fields only depend on the harmonic oscillator bases considered. In addition to the customary kinetic operator, we include the one-body center of mass correction (see Appendix J) in the derivations thereafter, such that the final corrected kinetic operator reads:

$$\boxed{T = \frac{1}{2M}(1 - \frac{1}{A})P^2} \tag{K.1}$$

Here, M stands for the mass of the nucleons and A for the number of nulceons.

K.1 HFB field

As the kinetic operator is a one-body operator, its matrix elements directly stand for its mean field contribution:

$$\boxed{\Gamma_{\alpha\beta} = \langle\alpha|T|\beta\rangle = -\frac{\hbar^2}{2M}(1 - \frac{1}{A})\delta_{\tau_\alpha,\tau_\beta}\delta_{s_\alpha,s_\beta}\int d\vec{r}\psi^*_\alpha(\vec{r})(\vec{\nabla}^2_\perp + \nabla^2_z)\psi_\beta(\vec{r})} \tag{K.2}$$

The evaluation of Eq.(K.2) requires to calculate two different integrals:

$$\begin{cases} I_z = \int d\vec{r}\psi^*_\alpha(\vec{r})\nabla^2_z\psi_\beta(\vec{r}) \\ I_r = \int d\vec{r}\psi^*_\alpha(\vec{r})\vec{\nabla}^2_\perp\psi_\beta(\vec{r}) \end{cases} \tag{K.3}$$

The definitions in Eq.(K.3) lead to:

$$\boxed{\Gamma_{\alpha\beta} = -\frac{\hbar^2}{2M}(1 - \frac{1}{A})\delta_{\tau_\alpha,\tau_\beta}\delta_{s_\alpha,s_\beta}(I_r + I_z)} \tag{K.4}$$

Calculation of the z-integral:

We want to find an analytic expression for the following quantity:

$$I_z = \int d\vec{r}\psi^*_\alpha(\vec{r})\nabla^2_z\psi_\beta(\vec{r}) \tag{K.5}$$

We separate Eq.(K.5) into a z part and a $r_\perp$ one:

$$I_z = \int d\vec{r}_\perp \phi^*_\alpha(\vec{r}_\perp)\phi_\beta(\vec{r}_\perp) \int dz \varphi_{n_{z_\alpha}}(z+d_\alpha)\nabla^2_z \varphi_{n_{z_\beta}}(z+d_\beta) \tag{K.6}$$

The left part of Eq.(K.6) is easily handled thanks to the orthonormality relations of the $r_\perp$-harmonic oscillator wave functions:

$$I_z = \delta_{m_\alpha m_\beta}\delta_{n_\alpha n_\beta} \int dz \varphi_{n_{z_\alpha}}(z+d_\alpha)\nabla^2_z \varphi_{n_{z_\beta}}(z+d_\beta) \tag{K.7}$$

We recall the formula on the squared derivative operator ∇^2_z given in Appendix D:

$$\begin{aligned}\nabla^2_z \varphi_{n_z}(z,b_z) = \frac{1}{2b_z^2}[&\sqrt{n_z(n_z-1)}\varphi_{n_z-2}(z,b_z) - (2n_z+1)\varphi_{n_z}(z,b_z) \\ &+\sqrt{(n_z+1)(n_z+2)}\varphi_{n_z+2}(z,b_z)]\end{aligned} \tag{K.8}$$

Using Eq.(K.8) and introducing the S matrix standing for the overlap between z-harmonic oscillator wave functions (see Appendix D), we finally get:

$$\boxed{\begin{aligned}I_z = \delta_{m_\alpha m_\beta}\delta_{n_\alpha n_\beta}\frac{1}{2b_z^2}[&\sqrt{n_{z_\beta}(n_{z_\beta}-1)}S_{(n_{z_\alpha},d_\alpha)(n_{z_\beta}-2,d_\beta)} - (2n_{z_\beta}+1)S_{(n_{z_\alpha},d_\alpha)(n_{z_\beta},d_\beta)} \\ &+\sqrt{(n_{z_\beta}+1)(n_{z_\beta}+2)}S_{(n_{z_\alpha},d_\alpha)(n_{z_\beta}+2,d_\beta)}]\end{aligned}} \tag{K.9}$$

Calculation of the $r_\perp$-integral:

We want to find an analytic expression for the following quantity:

$$I_r = \int d\vec{r}\psi^*_\alpha(\vec{r})\vec{\nabla}^2_\perp \psi_\beta(\vec{r}) \tag{K.10}$$

We separate the Eq.(K.10) into a z part and a $r_\perp$ one:

$$I_r = \int d\vec{r}_\perp \phi^*_\alpha(\vec{r}_\perp)\vec{\nabla}^2_\perp \phi_\beta(\vec{r}_\perp) \int dz \varphi_{n_{z_\alpha}}(z+d_\alpha)\varphi_{n_{z_\beta}}(z+d_\beta) \tag{K.11}$$

The right integral in Eq.(K.11) is directly handled with the S matrix:

$$I_r = S_{(n_{z_\alpha},d_\alpha)(n_{z_\beta},d_\beta)} \int d\vec{r}_\perp \phi^*_\alpha(\vec{r}_\perp)\vec{\nabla}^2_\perp \phi_\beta(\vec{r}_\perp) \tag{K.12}$$

We recall the formula on the squared derivative operator $\nabla^2_\perp$ given in Appendix D:

$$\begin{aligned}\nabla^2_\perp \phi_{m,n}(\vec{r}_\perp,b_r) = -\frac{1}{b_r^2}[&\sqrt{n(n+|m|)}\phi_{m,n-1}(\vec{r}_\perp,b_r) + (2n+|m|+1)\phi_{m,n}(\vec{r}_\perp,b_r) \\ &+\sqrt{(n+1)(n+|m|+1)}\phi_{m,n+1}(\vec{r}_\perp,b_r)]\end{aligned} \tag{K.13}$$

Using Eq.(K.13) along with the orthonormality relations of the $r_\perp$-harmonic oscillator wave functions, we finally find:

$$\boxed{\begin{aligned} I_r = -S_{(n_{z_\alpha},d_\alpha)(n_{z_\beta},d_\beta)}\delta_{m_\alpha m_\beta}\frac{1}{b_r^2}[\sqrt{n_\beta(n_\beta+|m_\beta|)}]\delta_{n_\alpha n_\beta-1} + (2n_\beta+|m_\beta|+1)\delta_{n_\alpha n_\beta} \\ +\sqrt{(n_\beta+1)(n_\beta+|m_\beta|+1)}\delta_{n_\alpha n_\beta+1}] \end{aligned}} \tag{K.14}$$

K.2 Collective fields

As for the non-collective case, the matrix elements of the kinetic operator considered in the case of two different harmonic oscillator bases $\{0\}$ and $\{1\}$ directly stand for its collective mean field contribution:

$$\boxed{\bar{\Gamma}_{\alpha\beta} = {}_0\langle\alpha|T|\beta\rangle_1 = -\frac{\hbar^2}{2M}(1-\frac{1}{A})\delta_{\tau_\alpha,\tau_\beta}\delta_{s_\alpha,s_\beta}\int d\vec{r}\psi^*_\alpha(\vec{r},b_0)(\vec{\nabla}^2_\perp+\nabla^2_z)\psi_\beta(\vec{r},b_1)} \tag{K.15}$$

We start dividing Eq.(K.15) into two integrals:

$$\begin{cases} \bar{I}_z = \int d\vec{r}\psi^*_\alpha(\vec{r},b_0)\nabla^2_z\psi_\beta(\vec{r},b_1) \\ \bar{I}_r = \int d\vec{r}\psi^*_\alpha(\vec{r},b_0)\vec{\nabla}^2_\perp\psi_\beta(\vec{r},b_1) \end{cases} \tag{K.16}$$

Eq.(K.16) leads to rewrite the field:

$$\boxed{\bar{\Gamma}_{\alpha\beta} = -\frac{\hbar^2}{2M}(1-\frac{1}{A})\delta_{\tau_\alpha,\tau_\beta}\delta_{s_\alpha,s_\beta}(\bar{I}_r+\bar{I}_z)} \tag{K.17}$$

Calculation of the z-integral:

We want to find an analytic expression for the following quantity:

$$\bar{I}_z = \int d\vec{r}\psi^*_\alpha(\vec{r},b_0)\nabla^2_z\psi_\beta(\vec{r},b_1) \tag{K.18}$$

We start separating Eq.(K.18) into a z and a $r_\perp$ part:

$$\bar{I}_z = \int d\vec{r}_\perp\phi^*_\alpha(\vec{r}_\perp,b_{r_0})\phi_\beta(\vec{r}_\perp,b_{r_1})\int dz\varphi_{n_{z_\alpha}}(z+d_\alpha,b_{z_0})\nabla^2_z\varphi_{n_{z_\beta}}(z+d_\beta,b_{z_1}) \tag{K.19}$$

The left part of the Eq.(K.19) is easily handled using the $\bar{S}_r$ matrix defined in Appendix D, and standing for the overlap of two $r_\perp$-harmonic oscillator wave functions in the case of two different b_r:

$$\bar{I}_z = \bar{S}_{r_{(m_\alpha,n_{\perp_\alpha})(m_\beta,n_{\perp_\beta})}}(b_{r_0},b_{r_1})\int dz\varphi_{n_{z_\alpha}}(z+d_\alpha,b_{z_0})\nabla^2_z\varphi_{n_{z_\beta}}(z+d_\beta,b_{z_1}) \tag{K.20}$$

We now apply the formula on the squared derivative operator ∇_z^2 given in Eq.(K.8):

$$\begin{aligned}\bar{I}_z = \bar{S}_{r_{(m_\alpha,n_{\perp_\alpha})(m_\beta,n_{\perp_\beta})}}(b_{r_0},b_{r_1})\frac{1}{2b_{z_1}^2}[&\sqrt{n_{z_\beta}(n_{z_\beta}-1)}\int dz\varphi_{n_{z_\alpha}}(z+d_\alpha,b_{z_0})\varphi_{n_{z_\beta}-2}(z+d_\beta,b_{z_1})\\ &-(2n_{z_\beta}+1)\int dz\varphi_{n_{z_\alpha}}(z+d_\alpha,b_{z_0})\varphi_{n_{z_\beta}}(z+d_\beta,b_{z_1})\\ &+\sqrt{(n_{z_\beta}+1)(n_{z_\beta}+2)}\int dz\varphi_{n_{z_\alpha}}(z+d_\alpha,b_{z_0})\varphi_{n_{z_\beta}+2}(z+d_\beta,b_{z_1})]\end{aligned} \tag{K.21}$$

We finally use the $\bar{S}_z$ matrices defined in Appendix D, standing for the overlap of z-harmonic oscillator wave functions in the case of different b_z:

$$\boxed{\begin{aligned}\bar{I}_z = \bar{S}_{r_{(m_\alpha,n_{\perp_\alpha})(m_\beta,n_{\perp_\beta})}}(b_{r_0},b_{r_1})\frac{1}{2b_{z_1}^2}[&\sqrt{n_{z_\beta}(n_{z_\beta}-1)}\bar{S}_{z_{(n_{z_\alpha},d_\alpha)(n_{z_\beta}-2,d_\beta)}}(b_{z_0},b_{z_1})\\ &-(2n_{z_\beta}+1)\bar{S}_{z_{(n_{z_\alpha},d_\alpha)(n_{z_\beta},d_\beta)}}(b_{z_0},b_{z_1})\\ &+\sqrt{(n_{z_\beta}+1)(n_{z_\beta}+2)}\bar{S}_{z_{(n_{z_\alpha},d_\alpha)(n_{z_\beta}+2,d_\beta)}}(b_{z_0},b_{z_1})]\end{aligned}} \tag{K.22}$$

Calculation of the $r_\perp$-integral:

We want to find an analytic expression for the following quantity:

$$\bar{I}_r = \int d\vec{r}\psi_\alpha^*(\vec{r},b_0)\vec{\nabla}_\perp^2\psi_\beta(\vec{r},b_1) \tag{K.23}$$

We start separating Eq.(K.23) into a z and a $r_\perp$ part:

$$\bar{I}_r = \int d\vec{r}_\perp\phi_\alpha^*(\vec{r}_\perp,b_{r_0})\vec{\nabla}_\perp^2\phi_\beta(\vec{r}_\perp,b_{r_1})\int dz\varphi_{n_{z_\alpha}}(z+d_\alpha,b_{z_0})\varphi_{n_{z_\beta}}(z+d_\beta,b_{z_1}) \tag{K.24}$$

The right hand side of Eq.(K.24) is directly handled using the $\bar{S}_z$ matrix:

$$\bar{I}_r = \int d\vec{r}_\perp\phi_\alpha^*(\vec{r}_\perp,b_{r_0})\vec{\nabla}_\perp^2\phi_\beta(\vec{r}_\perp,b_{r_1})\bar{S}_{z_{(n_{z_\alpha},d_\alpha)(n_{z_\beta},d_\beta)}}(b_{z_0},b_{z_1}) \tag{K.25}$$

We now use the formula on the squared derivative operator $\nabla_\perp^2$ given in Eq.(K.13):

$$\begin{aligned}\bar{I}_r = -\bar{S}_{z_{(n_{z_\alpha},d_\alpha)(n_{z_\beta},d_\beta)}}(b_{z_0},b_{z_1})\frac{1}{b_{r_1}^2}[&\sqrt{n_\beta(n_\beta+|m_\beta|)}\int d\vec{r}_\perp\phi_{(m_\alpha,n_\alpha)}^*(\vec{r}_\perp,b_{r_0})\phi_{(m_\beta,n_\beta-1)}(\vec{r}_\perp,b_{r_1})\\ &+(2n_\beta+|m_\beta|+1)\int d\vec{r}_\perp\phi_{(m_\alpha,n_\alpha)}^*(\vec{r}_\perp,b_{r_0})\phi_{(m_\beta,n_\beta)}(\vec{r}_\perp,b_{r_1})\\ &+\sqrt{(n_\beta+1)(n_\beta+|m_\beta|+1)}\int d\vec{r}_\perp\phi_{(m_\alpha,n_\alpha)}^*(\vec{r}_\perp,b_{r_0})\phi_{(m_\beta,n_\beta+1)}(\vec{r}_\perp,b_{r_1})]\end{aligned} \tag{K.26}$$

We finally use the $\bar{S}_r$ matrix to rewrite Eq.(K.26):

$$\boxed{\begin{aligned}\bar{I}_r = -\bar{S}_{z_{(n_{z_\alpha},d_\alpha)(n_{z_\beta},d_\beta)}}(b_{z_0},b_{z_1})\frac{1}{b_{r_1}^2}[&\sqrt{n_\beta(n_\beta+|m_\beta|)}\bar{S}_{r_{(m_\alpha,n_{\perp_\alpha})(m_\beta,n_{\perp_\beta}-1)}}(b_{r_0},b_{r_1})\\ &+(2n_\beta+|m_\beta|+1)\bar{S}_{r_{(m_\alpha,n_{\perp_\alpha})(m_\beta,n_{\perp_\beta})}}(b_{r_0},b_{r_1})\\ &+\sqrt{(n_\beta+1)(n_\beta+|m_\beta|+1)}\bar{S}_{r_{(m_\alpha,n_{\perp_\alpha})(m_\beta,n_{\perp_\beta}+1)}}(b_{r_0},b_{r_1})]\end{aligned}} \tag{K.27}$$

Appendix L

Grassmann algebra

This Appendix aims to present Grassmann algebra and some results on the associated Berezin integration theory. These results are used in this PhD thesis work to evaluate overlap kernels. The development presented in the following has been mostly inspired by [84].

L.1 Grassmann algebra definition

In this section, we construct Grassmann algebras from finite-dimensional vector spaces. Then, we show some elementary properties of these algebras.

L.1.1 Intuitive definition

Let E be a $\mathbb{C}$ vector space of dimension n generated by the $\{\theta_i\}$. We build ΛE, the Grassmann algebra on E, as the $\mathbb{C}$ unital associative algebra generated by the $\{\theta_i\}$ and such that the following relation holds:

$$\forall(i,j) \qquad \theta_i\theta_j = -\theta_j\theta_i \tag{L.1}$$

L.1.2 Definition using the associated tensor algebra

The intuitive definition presented above can be reformulated more rigorously using tensor algebra. We call $T(E)$ the tensor algebra on the vector space E. $T(E)$ is the set of all the words that can be built with the elements of E. Therefore, the product associated with this algebra is nothing but the juxtaposition of the elements of $T(E)$.

For instance, an arbitrary element of the tensor algebra $t \in T(E)$ reads:

$$t = \theta_1\theta_5\theta_2\theta_3 \tag{L.2}$$

To define the Grassmann algebra ΛE, we have to consider the quotient of $T(E)$ by the two-sided ideal $I \subset T(E)$, which is generated by the pairs of the type $\theta\theta$ (with $\theta \in T(E)$). This quotient reproduces the condition given in Eq.(L.1). We give an example below:

$$(\theta_i+\theta_j)(\theta_i+\theta_j) = 0 \qquad \rightarrow \qquad \theta_i\theta_i + \theta_j\theta_j + \theta_i\theta_j + \theta_j\theta_i = 0 \qquad \rightarrow \qquad \theta_i\theta_j = -\theta_j\theta_i \tag{L.3}$$

We can finally write ΛE:

$$\boxed{\Lambda E = T(E)/I} \tag{L.4}$$

L.1.3 Dimension of a Grassmann algebra

Because of the way the product is defined on the Grassmann algebra, we understand that the elements of ΛE are generated by the k-tuples built with k different elements belonging to the vector space E of dimension n. For a given k, there exist $\binom{n}{k}$ different k-tuples. With this remark, it is easy to find the dimension of ΛE:

$$\boxed{|\Lambda E| = \sum_{k=0}^{n} \binom{n}{k} = 2^n} \tag{L.5}$$

L.1.4 Decomposition of an element in a Grassmann algebra

An element belonging to a Grassmann algebra ΛE can be decomposed thanks to the algebra generators. To make this decomposition unique, it is sufficient to impose an order among the elements of the basis of the vector space E. The shorthand notation θ^ϵ refers to a given generator of ΛE, and $|\epsilon|$ corresponds to the number k of elements composing the k-tuple θ^ϵ. With these notations, the decomposition of a given element $\gamma \in \Lambda E$ reads as follows:

$$\boxed{\gamma \in \Lambda E \qquad \rightarrow \qquad \exists!\ (c_\epsilon(\gamma))_\epsilon \in \mathbb{K}^{2^n}\ ,\ \gamma = \sum_\epsilon c_\epsilon(\gamma)\theta^\epsilon} \tag{L.6}$$

L.1.5 An exemple

We can build a Grassmann algebra on the following $\mathbb{C}$ vector space E:

$$E = \mathrm{Vect}(\theta_1, \theta_2, \theta_3) \tag{L.7}$$

In this case, the dimension of the Grassmann algebra is $2^3 = 8$. In addition, we can write ΛE as follows:

$$\Lambda E = \mathrm{Vect}(1, \theta_1, \theta_2, \theta_3, \theta_1\theta_2, \theta_1\theta_3, \theta_2\theta_3, \theta_1\theta_2\theta_3) \tag{L.8}$$

An arbitrary element $\gamma \in \Lambda E$ has a unique decomposition considering the natural ordering of the integers. For instance, we can write:

$$\gamma = 5 + 3\theta_1 + i\theta_1\theta_2 \tag{L.9}$$

In this case, the different $|\epsilon|$ read:

$$|\epsilon|_1 = 0 \qquad |\epsilon|_{\theta_1} = 1 \qquad |\epsilon|_{\theta_1\theta_2} = 2 \tag{L.10}$$

L.2 Differentiation on a Grassmann algebra

It is possible to define a differentiation operation on a Grassmann algebra. We start by noticing that for a given $\theta_i \in E$, each element $\gamma \in \Lambda E$ can be written as:

$$\gamma = \gamma_i + \theta_i \gamma_i' \qquad (\gamma_i, \gamma_i') \in \Lambda(E - \{\theta_i\})^2 \tag{L.11}$$

The notation $\Lambda(E - \{\theta_i\})$ simply stands for the Grassmann algebra built on the vector space E/θ_i. It means that θ_i does not appear in γ_i nor in γ_i'. Now, we can define the differentiation with respect to θ_i:

$$\forall i, \quad \frac{\partial}{\partial \theta_i} : \begin{cases} \Lambda E \to \Lambda E \\ \gamma \to \gamma_i' \end{cases} \tag{L.12}$$

It is clear that this differentiation is a linear application. Unfortunately, it does not respect the Leibniz rule. However, we can show that a very similar property holds. The latter requires to introduce the parity operator.

L.2.1 Parity operator

Each element $\gamma \in \Lambda E$ can be decomposed on the generators of ΛE:

$$\gamma = \sum_{\epsilon} c_\epsilon(\gamma) \theta^\epsilon \tag{L.13}$$

We can separate the sum in Eq.(L.13) in two parts. The first one contains the generators such that $|\epsilon| \equiv 0\ (2)$, the second one contains the others:

$$\gamma = \sum_{|\epsilon| \equiv 0(2)} c_\epsilon(\gamma) \theta^\epsilon + \sum_{|\epsilon| \equiv 1(2)} c_\epsilon(\gamma) \theta^\epsilon = \gamma^+ + \gamma^- \tag{L.14}$$

In the light of Eq.(L.14), it is natural to define the following parity operator $\hat{P}$:

$$\boxed{\hat{P} : \begin{cases} \Lambda E \to \Lambda E \\ \gamma \to \gamma^+ - \gamma^- \end{cases}} \tag{L.15}$$

L.2.2 The Leibniz-like rule for the Grassmann algebra differentiation

The Leibniz-like rule for the Grassmann algebra differentiation reads as follows:

$$\boxed{\forall (\gamma, g) \in \Lambda E^2, \qquad \frac{\partial}{\partial \theta_i}(\gamma g) = \hat{P}(\gamma) \frac{\partial}{\partial \theta_i} g + \frac{\partial}{\partial \theta_i}(\gamma) g} \tag{L.16}$$

We demonstrate this relation in the following. We start by making θ_i appear in the product γg:

$$\gamma g = (\gamma_i + \theta_i \gamma_i')(g_i + \theta_i g_i') = \gamma_i g_i + \theta_i \gamma_i' g_i + \gamma_i \theta_i g_i' \tag{L.17}$$

We remark the following property:

$$\gamma_i \theta_i = (\gamma_i^+ + \gamma_i^-)\theta_i = \theta_i(\gamma_i^+ - \gamma_i^-) = \theta_i \hat{P}(\gamma) \tag{L.18}$$

This property directly leads to:

$$\boxed{\gamma g = \gamma_i g_i + \theta_i(\hat{P}(\gamma_i) g_i' + \gamma_i' g_i) \qquad \Rightarrow \qquad \frac{\partial}{\partial \theta_i}(\gamma g) = \hat{P}(\gamma_i) g_i' + \gamma_i' g_i} \tag{L.19}$$

Now, we develop the right hand side of Eq.(L.16):

$$\hat{P}(\gamma)\frac{\partial}{\partial \theta_i} g + \frac{\partial}{\partial \theta_i}(\gamma) g = [\hat{P}(\gamma_i) - \theta_i \hat{P}(\gamma_i')] g_i' + \gamma_i'(g_i + \theta_i g_i) \tag{L.20}$$

$$\hat{P}(\gamma)\frac{\partial}{\partial \theta_i} g + \frac{\partial}{\partial \theta_i}(\gamma) g = \hat{P}(\gamma_i) g_i' + \gamma_i' g_i - \theta_i \hat{P}(\gamma_i') g_i' + \gamma_i' \theta_i g_i \tag{L.21}$$

Commuting θ_i towards the left hand side in the last term of Eq.(L.21), we obtain:

$$\boxed{\hat{P}(\gamma)\frac{\partial}{\partial \theta_i} g + \frac{\partial}{\partial \theta_i}(\gamma) g = \hat{P}(\gamma_i) g_i' + \gamma_i' g_i - \theta_i \hat{P}(\gamma_i') g_i' + \theta_i \hat{P}(\gamma_i') g_i = \frac{\partial}{\partial \theta_i}(\gamma g)} \tag{L.22}$$

L.2.3 Schwartz theorem within a Grassmann algebra

In the case of the Grassmann algebra differentiation, two different differentiation operators $\frac{\partial}{\theta_j}$ and $\frac{\partial}{\theta_i}$ commute just as their related elements θ_j and θ_i. Indeed, if we consider an arbitrary element $\gamma \in \Lambda E$, we can write:

$$\boxed{\begin{cases} \frac{\partial}{\partial \theta_j}\frac{\partial}{\partial \theta_i}\gamma = \frac{\partial}{\partial \theta_j}\frac{\partial}{\partial \theta_i}(\gamma_{ij} + \theta_i\theta_j\gamma_{ij}') = \gamma_{ij}' \\ \frac{\partial}{\partial \theta_i}\frac{\partial}{\partial \theta_j}\gamma = \frac{\partial}{\partial \theta_j}\frac{\partial}{\partial \theta_i}(\gamma_{ij} - \theta_j\theta_i\gamma_{ij}') = -\gamma_{ij}' \end{cases} \qquad \Rightarrow \qquad \frac{\partial}{\partial \theta_j}\frac{\partial}{\partial \theta_i}\gamma = -\frac{\partial}{\partial \theta_i}\frac{\partial}{\partial \theta_j}\gamma} \tag{L.23}$$

L.2.4 Multiplication on the left operator

We call $\hat{\theta}_i$ the operator standing for the multiplication on the left by θ_i:

$$\boxed{\hat{\theta}_i : \begin{cases} \Lambda E \to \Lambda E \\ \gamma \to \theta_i \gamma \end{cases}} \tag{L.24}$$

We remark the following property:

$$\forall \gamma \in \Lambda E,\ \frac{\partial}{\partial \theta_i}\hat{\theta}_j\gamma = \frac{\partial}{\partial \theta_i}\theta_j\gamma = -\theta_j\frac{\partial}{\partial \theta_i}\gamma + \delta_{ij}\gamma = [-\hat{\theta}_j\frac{\partial}{\partial \theta_i} + \delta_{ij}]\gamma \tag{L.25}$$

In other words:

$$\boxed{[\frac{\partial}{\partial \theta_i}, \hat{\theta}_j]_+ = \delta_{ij}} \tag{L.26}$$

It is clear that the commutation relations displayed in Eq.(L.26) are the ones characterizing the fermionic operators.

L.3 Integration on a Grassmann algebra (Berezin integration)

Surprisingly, integration on a Grassmann algebra is the same thing as differentiation. For instance:

$$\int \gamma d\theta_3 d\theta_2 d\theta_1 = \frac{\partial}{\partial \theta_3}\frac{\partial}{\partial \theta_2}\frac{\partial}{\partial \theta_1}\gamma \tag{L.27}$$

In the light of Eq.(L.27), we understand that the order of the volume elements has an impact on the result. Their commutation is handled with the Schwartz theorem demonstrated previously.

As they are equivalent, the choice between integration and differentiation symbols depends on the situation. For instance, it is more natural to write the Leibniz-like rule we've demonstrated using differentiation symbol, while dot products are more naturally written with the integration one.

Most of the time, we use the integration symbol when all the $\{\theta_i\}$ are considered at the same time. We call this operation the "total integration".

L.3.1 Total integration

The total integration refers to a situation where all the volume elements possible are used. For instance, for an arbitrary $\gamma \in \Lambda E$, the total integration operation reads as follows:

$$I(\gamma) = \int \gamma d\theta_n ... d\theta_1 = \int \gamma d\theta \tag{L.28}$$

We can develop Eq.(L.28):

$$I(\gamma) = \sum_\epsilon c_\epsilon(\gamma) \int \theta^\epsilon d\theta \tag{L.29}$$

It is clear that $I(\gamma) \neq 0$ only when the coefficient associated with the unique n-tuple θ^{ϵ_n} (n being the dimension of E) in the decomposition of γ does not equal 0. Indeed, the following relation holds:

$$\boxed{I(\gamma) = c_{\epsilon_n}(\gamma)} \tag{L.30}$$

L.3.2 Exponential application on a Grassmann algebra

We naturally define the exponential application using the Taylor series:

$$\exp : \begin{cases} \Lambda E \to \Lambda E \\ \gamma \to \sum_{k=0}^{n} \frac{\gamma^k}{k!} \end{cases} \tag{L.31}$$

The sum stops at n, which is the dimension of E. Indeed, $\forall k > n, \;\; \gamma^k = 0$.

L.3.3 Gaussian integral of a skew-symmetric matrix

Let E be a vector space of dimension $2n$ and M be a $2n \times 2n$ skew-symmetric matrix. We call Gaussian integral of M the following quantity:

$$I(M) = \int e^{\frac{1}{2}\sum_{ij=0}^{2n} \theta_i M_{ij} \theta_j} d\theta = \int e^{\frac{1}{2}\theta^T M \theta} d\theta \tag{L.32}$$

As the integration displayed in Eq.(L.32) is total, the only non-zero term in the series decomposition associated with the exponential is the one at the power n. Thus, we write:

$$I(M) = \frac{1}{2^n n!} \int (\sum_{ij=0}^{n} \theta_i M_{ij} \theta_j)^n d\theta = \frac{1}{2^n n!} \sum_{\sigma \in S_{2n}} \text{sgn}(\sigma) \prod_{i=1}^{n} M_{\sigma(2i-1)\sigma(2i)} = \text{pf}(M) \tag{L.33}$$

In L.33, pf(M) stands for the Pfaffian of the matrix M. We've therefore demonstrated the following essential result:

$$\boxed{\int e^{\frac{1}{2}\sum_{ij=0}^{2n} \theta_i M_{ij} \theta_j} d\theta = \text{pf}(M)} \tag{L.34}$$

L.4 Super Hilbert space $\mathcal{H}^{(n)}$:

We want to define a super Hilbert space $\mathcal{H}^{(n)}$ being isomorphic to the Fock space $\mathcal{F}^{(n)}$. We consider a Grassmann algebra ΛE built on a $\mathbb{C}$ vector space E. In the following, we start by defining a complex structure on the Grassmann algebra ΛE in order to build an Hermitian dot product on it.

L.4.1 Complex structure on a Grassmann algebra

The goal of this section is to define a complex structure on a given Grassmann algebra ΛE associated with a $\mathbb{C}$ vector space E of dimension n. The vector space E reads as follows:

$$E = \text{Vect}(\theta_1, ..., \theta_n) \tag{L.35}$$

We can build another vector space $E^c = E + E$:

$$E^c = \text{Vect}(\theta_1, ..., \theta_n, \theta_1^*, ..., \theta_n^*) \tag{L.36}$$

We voluntarily paired the generators of the vector space E^c. It defines a complex involution $(*)$ on E^c:

$$(*) : \begin{cases} E^c \to E^c \\ \lambda\theta_i \to \lambda^*\theta_i^* \\ \lambda\theta_i^* \to \lambda^*\theta_i \end{cases} \tag{L.37}$$

In Eq.(L.37), λ is an arbitrary complex number and λ^* is simply its conjugate complex number. To extend this involution on ΛE^c, it is sufficient to define how it operates on an arbitrary pair of two elements of ΛE^c:

$$\forall(\gamma, g) \in (\Lambda E^c)^2,\ (\gamma g)^* = g^*\gamma^* \tag{L.38}$$

We call ΛE^c with the involution $(*)$ the complex structure on the Grassmann algebra ΛE.

L.4.2 Definition of a dot product

We define a dot product on $\mathcal{H}^{(n)}$ as follows:

$$\boxed{\forall(\gamma, g) \in \Lambda E^2, \qquad \langle\gamma|g\rangle := \int \gamma^* g e^{\theta^*.\theta} \prod_{k=1}^{n} (d\theta_k d\theta_k^*)} \tag{L.39}$$

Eq.(L.39) clearly highlights that the super Hilbert space $\mathcal{H}^{(n)}$ is nothing but the Grassmann algebra ΛE with its complex structure and the dot product defined in Eq.(L.39). Besides, it is clear that this dot product is 1-Hermitian with respect to $(*)$.
Now, we show that the generators of ΛE are an orthonormal family with respect to the dot product defined in Eq.(L.39). We consider the following general expression with two arbitrary generators θ^ϵ and $\theta^{\epsilon'}$:

$$\langle\theta^\epsilon|\theta^{\epsilon'}\rangle = \int (\theta^\epsilon)^* \theta^{\epsilon'} e^{\theta^*.\theta} \prod_{k=1}^{n} (d\theta_k d\theta_k^*) \tag{L.40}$$

We can rewrite Eq.(L.43) more explicitly:

$$\langle\theta^\epsilon|\theta^{\epsilon'}\rangle = \int (\theta^\epsilon)^*\theta^{\epsilon'} \sum_p \frac{(\sum_{i=1}^n \theta_i^*\theta_i)^p}{p!} \prod_{k=1}^n (d\theta_k d\theta_k^*) \tag{L.41}$$

As the integration is total, the terms of Eq.(L.41) are non-zero only when the generators coming from the exponential combine simultaneously with θ^ϵ and $(\theta^\epsilon)^*$ to give θ^{ϵ_n} and $(\theta^{\epsilon_n})^*$. We observe that it is only possible when $\epsilon = \epsilon'$. Therefore:

$$\langle\theta^\epsilon|\theta^{\epsilon'}\rangle = \delta_{\epsilon\epsilon'} \int (\theta^\epsilon)^*\theta^{\epsilon'} \sum_p \frac{(\sum_{i=1}^n \theta_i^*\theta_i)^p}{p!} \prod_{k=1}^n (d\theta_k d\theta_k^*) \tag{L.42}$$

We introduce $\theta^{\bar{\epsilon}}$, the complementary generator of θ^ϵ defined as follows:

$$\theta^\epsilon\theta^{\bar{\epsilon}} = (-1)^{\varphi(\epsilon)}\theta_1...\theta_n \tag{L.43}$$

Using this definition, Eq.(L.42) reads:

$$\langle\theta^\epsilon|\theta^{\epsilon'}\rangle = \delta_{\epsilon\epsilon'} \int (\theta^\epsilon)^*\theta^{\epsilon} \frac{(\sum_{i=1}^n \theta_i^*\theta_i)^{|\bar{\epsilon}|}}{|\bar{\epsilon}|!} \prod_{k=1}^n (d\theta_k d\theta_k^*) \tag{L.44}$$

As the pairs $\theta_i^*\theta_i$ commute between each other, there are $|\bar{\epsilon}|!$ ways to build the complementary operators of $(\theta^\epsilon)^*$ and θ^ϵ. In addition, we can write $(\theta^\epsilon)^*\theta^\epsilon$ as a product of pairs:

$$(\theta^\epsilon)^*\theta^\epsilon = \theta^*_{\epsilon_{|\epsilon|}}...\theta^*_{\epsilon_1}\theta_{\epsilon_1}...\theta_{\epsilon_{|\epsilon|}} = (-1)^{\frac{|\epsilon|(|\epsilon|-1)}{2}}\theta^*_{\epsilon_1}...\theta^*_{\epsilon_{|\epsilon|}}\theta_{\epsilon_1}...\theta_{\epsilon_{|\epsilon|}} \tag{L.45}$$

$$(\theta^\epsilon)^*\theta^\epsilon = (-1)^{\frac{|\epsilon|(|\epsilon|-1)}{2}}(-1)^{\frac{|\epsilon|(|\epsilon|-1)}{2}}\theta^*_{\epsilon_1}\theta_{\epsilon_1}...\theta^*_{\epsilon_{|\epsilon|}}\theta_{\epsilon_{|\epsilon|}} \tag{L.46}$$

$$(\theta^\epsilon)^*\theta^\epsilon = \theta^*_{\epsilon_1}\theta_{\epsilon_1}...\theta^*_{\epsilon_{|\epsilon|}}\theta_{\epsilon_{|\epsilon|}} \tag{L.47}$$

Thanks to these results, we finally find:

$$\boxed{\langle\theta^\epsilon|\theta^{\epsilon'}\rangle = \delta_{\epsilon\epsilon'} \int \theta_1^*\theta_1...\theta_n^*\theta_n \prod_{k=1}^n (d\theta_k d\theta_k^*) = \delta_{\epsilon\epsilon'}} \tag{L.48}$$

L.4.3 Conjugation of the differentiation operators and of the mutliplication on the left operators

We show that the differentiation operators and the multiplication on the left operators are conjugated with respect to the dot product defined above. More explicitly, we demonstrate the following property:

$$\forall i,\ \forall(\gamma, g) \in \Lambda E^2, \qquad \langle\gamma|\frac{\partial}{\partial\theta_i}g\rangle = \langle\hat{\theta}_i\gamma|g\rangle \tag{L.49}$$

We develop the left and the right hand side of Eq.(L.49):

$$\langle\gamma|\frac{\partial}{\partial\theta_i}g\rangle = (\langle\gamma_i| + \langle\theta_i\gamma_i'|)|\frac{\partial}{\partial\theta_i}g\rangle = \langle\gamma_i|g_i'\rangle = \sum_\epsilon c_\epsilon^*(\gamma_i)c_\epsilon(g_i') \tag{L.50}$$

$$\langle\hat{\theta}_i\gamma|g\rangle = \langle\theta_i(\gamma_i+\theta_i\gamma_i')|g_i+\theta_i g_i'\rangle = \langle\theta_i\gamma_i|\theta_i g_i'\rangle = \sum_\epsilon c_\epsilon^*(\theta_i\gamma_i)c_\epsilon(\theta_i g_i') = \sum_\epsilon c_\epsilon^*(\gamma_i)c_\epsilon(g_i') \tag{L.51}$$

L.4.4 Isomorphism between $\mathcal{H}^{(n)}$ and $\mathcal{F}^{(n)}$

In this section, we build an isomorphism ϕ between $\mathcal{H}^{(n)}$ and $\mathcal{F}^{(n)}$:

$$\boxed{\phi : \begin{cases}\mathcal{H}^{(n)} \to \mathcal{F}^{(n)} \\ \lambda\theta^\epsilon \to \lambda(a^+)^\epsilon|0\rangle\end{cases}} \tag{L.52}$$

Here, $\lambda \in \mathbb{C}$. Besides, the shorthand notation $(a^+)^\epsilon$ is defined as follows:

$$(a^+)^\epsilon|0\rangle = a^+_{\epsilon_1}...a^+_{\epsilon_{|\epsilon|}}|0\rangle \tag{L.53}$$

We remark that the identity element of ΛE is transformed into the particle vacuum:

$$\phi(1) = |0\rangle \tag{L.54}$$

Moreover, we can associate the creation and annihilation operators with the multiplication on the left and the differentiation operator respectively:

$$\boxed{\gamma \in \mathcal{H}^{(n)},\ |\psi\rangle \in \mathcal{F}^{(n)}, \qquad \begin{cases}a_i^+|\psi\rangle = \phi(\hat{\theta}_i\phi^{-1}(|\psi\rangle)) \\ a_i|\psi\rangle = \phi(\frac{\partial}{\partial\theta_i}\phi^{-1}(|\psi\rangle))\end{cases}} \tag{L.55}$$

To conclude, we observe that the customary bra-ket is nothing but the dot product we've defined on $\mathcal{H}^{(n)}$.

L.5 Fermionic coherent states

The fermionic coherent states are by definition the eigenstates of the annihilation operators:

$$\boxed{a|z\rangle = z|z\rangle \qquad \langle z|a^+ = \langle z|z^*} \tag{L.56}$$

Without specifying further for the moment, the construction of these coherent states will require a richer structure than that of $\mathcal{H}^{(n)}$, which is simply isomorphic to $\mathcal{F}^{(n)}$. This new structure is called $\tilde{\mathcal{H}}^{(n)}$.

L.5.1 Super Hilbert space $\tilde{\mathcal{H}}^{(n)}$

For the moment, we've only considered Grassmann algebras built on top of a $\mathbb{C}$ vector space. However, it is possible to consider other structures to define the Grassmann algebra coefficients. In the present work, we choose to consider coefficients coming from another Grassmann algebra:

$$\tilde{\mathcal{H}}^{(n)} = \Lambda E^c \times \Lambda E \tag{L.57}$$

In the light of Eq.(L.57), we can interpret $\tilde{\mathcal{H}}^{(n)}$ as a ΛE^c module on the left built on ΛE. The relation between the elements of ΛE^c and those of ΛE is simply defined as follows:

$$\forall z \in \Lambda E^c,\ \forall \gamma \in \Lambda E, \qquad z\gamma = -\gamma z \tag{L.58}$$

Consequently, we can also consider $\tilde{\mathcal{H}}^{(n)}$ as the Grassmann algebra built on the vector space $\tilde{h}^{(n)}$ (plus the involution among the sets $\{z_i\}$ and $\{z_i^*\}$), which is defined thereafter:

$$\tilde{h}^{(n)} = \text{Vect}(z_1, ...z_n, z_1^*, ..., z_n^*, \theta_1, ..., \theta_n) \tag{L.59}$$

In the light of Eq.(L.59), we understand that it is possible to decompose an arbitrary element $s \in \tilde{\mathcal{H}}^{(n)}$:

$$\boxed{\exists!\ (c_\epsilon(s))_\epsilon \in (\Lambda E^c)^{2^n}\ ,\ \ s = \sum_\epsilon c_\epsilon(s)\theta^\epsilon} \tag{L.60}$$

The involution $(*)$ of $\mathcal{H}^{(n)}$ is trivially extended to $\tilde{\mathcal{H}}^{(n)}$, as well as the dot product:

$$\boxed{\forall (s,r) \in \tilde{\mathcal{H}}^{(n)}, \qquad \langle s|r\rangle := \int s^* r e^{\theta^*.\theta} \prod_{k=1}^{n} (d\theta_k d\theta_k^*)} \tag{L.61}$$

A dot product always gives elements belonging to the coefficients space:

$$\forall (s,r) \in \tilde{\mathcal{H}}^{(n)}, \qquad \langle s|r\rangle \in \Lambda E^c \tag{L.62}$$

We observe that the dot product is still 1-Hermitian with respect to the involution $(*)$ of $\tilde{\mathcal{H}}^{(n)}$. More precisely, it means:

$$\forall (s,r,v) \in (\tilde{\mathcal{H}}^{(n)})^3,\ \forall x \in \Lambda E^c, \qquad \begin{cases} \langle s|r+v\rangle = \langle s|r\rangle + \langle s|v\rangle \\ \langle s+v|r\rangle = \langle s|r\rangle + \langle v|r\rangle \\ \langle sx|r\rangle = x^*\langle s|r\rangle \\ \langle s|rx\rangle = \langle s|r\rangle x \\ \langle s|r\rangle = (\langle r|s\rangle)^* \end{cases} \tag{L.63}$$

L.5.2 Translation operator on $\tilde{\mathcal{H}}^{(n)}$

We define the translation operator $\hat{T}(z)$ on $\tilde{\mathcal{H}}^{(n)}$ as follows :

$$\boxed{\hat{T}(z) = e^{\hat{\theta}.z - z^*.\frac{\partial}{\partial\theta}}} \tag{L.64}$$

The following relation originate naturally from the Taylor series definition of the exponential application:

$$e^{\hat{A}}e^{\hat{B}}e^{-\frac{1}{2}[\hat{A},\hat{B}]} = e^{\hat{A}+\hat{B}} \tag{L.65}$$

Thanks to Eq.(L.65), we easily write:

$$(\hat{T}(z))^*\hat{T}(z) = e^{-\hat{\theta}.z+z^*.\frac{\partial}{\partial\theta}}e^{\hat{\theta}.z-z^*.\frac{\partial}{\partial\theta}} = id \tag{L.66}$$

The two most important properties of the translation operator are given below:

$$\boxed{\begin{cases} (\hat{T}(z))^*\frac{\partial}{\partial\theta_i}\hat{T}(z) = \frac{\partial}{\partial\theta_i} + z_i \\ \\ (\hat{T}(z))^*\hat{\theta}_i\hat{T}(z) = \hat{\theta}_i + z_i^* \end{cases}} \tag{L.67}$$

In the following, we only demonstrate the first property in Eq.(L.67). Indeed, the second one is then easily deduced by conjugation. We write:

$$(\hat{T}(z))^*\frac{\partial}{\partial\theta_i}\hat{T}(z) = \frac{\partial}{\partial\theta_i} - [\hat{\theta}.z - z^*.\frac{\partial}{\partial\theta_i}, \frac{\partial}{\partial\theta_i}] \tag{L.68}$$

$$(\hat{T}(z))^*\frac{\partial}{\partial\theta_i}\hat{T}(z) = \frac{\partial}{\partial\theta_i} - (\hat{\theta}.z - z^*.\frac{\partial}{\partial\theta_i})\frac{\partial}{\partial\theta_i} + \frac{\partial}{\partial\theta_i}(\hat{\theta}.z - z^*.\frac{\partial}{\partial\theta_i}) \tag{L.69}$$

$$(\hat{T}(z))^*\frac{\partial}{\partial\theta_i}\hat{T}(z) = \frac{\partial}{\partial\theta_i} - \hat{\theta}.z\frac{\partial}{\partial\theta_i} + \frac{\partial}{\partial\theta}\hat{\theta}.z = \frac{\partial}{\partial\theta_i} - \hat{\theta}.z\frac{\partial}{\partial\theta_i} + P(\hat{\theta}.z)\frac{\partial}{\partial\theta_i} + \frac{\partial}{\partial\theta_i}(\hat{\theta}.z) \tag{L.70}$$

$$(\hat{T}(z))^*\frac{\partial}{\partial\theta_i}\hat{T}(z) = \frac{\partial}{\partial\theta_i} + z_i \tag{L.71}$$

Finally, we show that $T(z)$ is ΛE^c linear:

$$s \in \Lambda E^c, \qquad \hat{T}(z)s = e^{\hat{\theta}.z-z^*.\frac{\partial}{\partial\theta}}s = \sum_p \frac{(\sum_k \hat{\theta}_k.z_k - z_k^*.\frac{\partial}{\partial\theta_k})^p}{p!}s \tag{L.72}$$

As $s \in \Lambda E^c$, we get:

$$\forall k, \qquad \frac{\partial}{\partial\theta_k}s = -s\frac{\partial}{\partial\theta_k} \tag{L.73}$$

Finally, we obtain:

$$\boxed{s \in \Lambda E^c, \qquad \hat{T}(z)s = s\hat{T}(z)} \tag{L.74}$$

L.5.3 Construction of the fermionic coherent states

The fermionic coherent state ψ_z is defined as the element of $\tilde{\mathcal{H}}^{(n)}$ resulting from the application of $\hat{T}(z)$ onto the identity element of $\tilde{\mathcal{H}}^{(n)}$:

$$\psi_z = \hat{T}(z)(1) \tag{L.75}$$

The following property is then really clear:

$$\frac{\partial}{\partial\theta_k}\psi_z = \hat{T}(z)(\hat{T}(z))^* \frac{\partial}{\partial\theta_k}\hat{T}(z)(1) = \hat{T}(z)(\frac{\partial}{\partial\theta_k}(1) + (z_k.1)) = \hat{T}(z)(z_k.1) = z_k\psi_z \tag{L.76}$$

Now, we consider the super Fock space $\tilde{\mathcal{F}}^{(n)}$ which is isomorphic to $\tilde{\mathcal{H}}^{(n)}$. This space is nothing but the customary Fock space, but with elements of ΛE^c as coefficients. We set:

$$\tilde{\mathcal{F}}^{(n)} = \Lambda E^c \times \mathcal{F}^{(n)} \tag{L.77}$$

It is clear that $\tilde{\mathcal{F}}^{(n)}$ and $\tilde{\mathcal{H}}^{(n)}$ are isomorphic. We call the extended isomorphism $\tilde{\phi}$. We can write:

$$\boxed{\tilde{\phi}(\psi_z) = |z\rangle \qquad a_k|z\rangle = z_k|z\rangle \qquad \langle z|a_k^+ = \langle z|z_k^*} \tag{L.78}$$

In Eq.(L.78), the last relation is found using conjugation.

L.5.4 Reformulation of the coherent fermionic states

We can rewrite the fermionic coherent states in a more convenient way:

$$\boxed{\psi_z = e^{(\theta - z^*/2).z}} \tag{L.79}$$

To demonstrate Eq.(L.79), we perform an induction on the n of $\tilde{\mathcal{H}}^{(n)}$, whose related hypothesis is the following:

$$P^{(n)} \ : \ \{\ \psi_z^{(n)} \in \tilde{\mathcal{H}}^{(n)}, \qquad \psi_z^{(n)} = e^{(\theta - z^*/2).z}\ \} \tag{L.80}$$

Initial case:

For $(n = 1)$, we find:

$$\psi_z^{(1)} = e^{\hat{\theta}_1 z_1 - z_1^* \frac{\partial}{\partial\theta_1}}(1) = [1 + \hat{\theta}_1 z_1 - z_1^*\frac{\partial}{\partial\theta_1} + \frac{1}{2}(\hat{\theta}_1 z_1 - z_1^*\frac{\partial}{\partial\theta_1})(\hat{\theta}_1 z_1 - z_1^*\frac{\partial}{\partial\theta_1})](1) \tag{L.81}$$

$$\psi_z^{(1)} = [1 + \hat{\theta}_1 z_1 + -\frac{1}{2}z_1^*\frac{\partial}{\partial\theta_1}\hat{\theta}_1 z_1](1) \tag{L.82}$$

Using the Leibniz-like rule into Eq.(L.82) leads to:

$$\boxed{\psi_z^{(1)} = 1 + \theta_1 z_1 + -\frac{1}{2} z_1^* z_1 = e^{(\theta_1 - z_1^*/2) z_1}} \tag{L.83}$$

Induction step:

We assume that $P^{(n)}$ is true and we show that it implies that $P^{(n+1)}$ is also true. We start by writing:

$$\psi_z^{(n+1)} = e^{\sum_{k=1}^{n+1} \hat{\theta}_k z_k - z_k^* \frac{\partial}{\partial \theta_k}}(1) = e^{\hat{\theta}_{n+1} z_{n+1} - z_{n+1}^* \frac{\partial}{\partial \theta_{n+1}} + \sum_{k=1}^{n} \hat{\theta}_k z_k - z_k^* \frac{\partial}{\partial \theta_k}}(1) \tag{L.84}$$

It is clear that the operators outside of the sum do commute with those inside of it. Therefore, we can separate the exponential in two parts:

$$\psi_z^{(n+1)} = e^{\hat{\theta}_{n+1} z_{n+1} - z_{n+1}^* \frac{\partial}{\partial \theta_{n+1}}} e^{\sum_{k=1}^{n} \hat{\theta}_k z_k - z_k^* \frac{\partial}{\partial \theta_k}}(1) \tag{L.85}$$

We identify $\psi_z^{(n)}$ on the right hand side of Eq.(L.85):

$$\psi_z^{(n+1)} = e^{\hat{\theta}_{n+1} z_{n+1} - z_{n+1}^* \frac{\partial}{\partial \theta_{n+1}}}(\psi_z^{(n)}) \tag{L.86}$$

Then, we develop the exponential:

$$\psi_z^{(n+1)} = [1 + \hat{\theta}_{n+1} z_{n+1} - z_{n+1}^* \frac{\partial}{\partial \theta_{n+1}} + \frac{1}{2}(\hat{\theta}_{n+1} z_{n+1} - z_{n+1}^* \frac{\partial}{\partial \theta_{n+1}})(\hat{\theta}_{n+1} z_{n+1} - z_{n+1}^* \frac{\partial}{\partial \theta_{n+1}})](\psi_z^{(n)}) \tag{L.87}$$

As $\psi_z^{(n)}$ does not contain θ_{n+1}, we can write:

$$\psi_z^{(n+1)} = [1 + \hat{\theta}_{n+1} z_{n+1} - \frac{1}{2} z_{n+1}^* \frac{\partial}{\partial \theta_{n+1}} \hat{\theta}_{n+1} z_{n+1}](\psi_z^{(n)}) \tag{L.88}$$

We use the Leibniz-like rule into Eq.(L.88):

$$\psi_z^{(n+1)} = (1 + \theta_{n+1} z_{n+1} - \frac{1}{2} z_{n+1}^* z_{n+1}) \psi_z^{(n)} = e^{(\theta_{n+1} - z_{n+1}^*/2) z_{n+1}} \psi_z^{(n)} \tag{L.89}$$

Inserting the induction hypothesis on Eq.(L.89) leads to:

$$\psi_z^{(n+1)} = e^{(\theta_{n+1} - z_{n+1}^*/2) z_{n+1}} e^{\sum_{k=1}^{n} (\theta_k - z_k^*/2).z_k} \tag{L.90}$$

It is straightforward that we can combine both exponentials:

$$\boxed{\psi_z^{(n+1)} = e^{\sum_{k=1}^{n+1} (\theta_k - z_k^*/2).z_k}} \tag{L.91}$$

L.5.5 Dot product of the coherent fermionic states

In this section, we consider the dot product of the coherent states ψ_z with an arbitrary element of $\tilde{\mathcal{H}}^{(n)}$. It is clear that it is sufficient to determine the dot product of ψ_z with all the generators θ^ϵ. We start by separating ψ_z into two exponentials:

$$\psi_z = e^{(\theta - z^*/2).z} = e^{-z^*.z/2} e^{\theta.z} \tag{L.92}$$

We develop the last exponential on the right hand side of Eq.(L.92):

$$\psi_z = e^{(\theta - z^*/2).z} = e^{-z^*.z/2} \sum_{k=0}^{n} \frac{(\sum_{i=1}^{n} \theta_i z_i)^k}{k!} \tag{L.93}$$

It is clear that the sum in Eq.(L.93) generates all the θ^ϵ. Moreover, as the expression is symmetric with respect to θ and z, each θ^ϵ comes with its related z^ϵ plus a commutation phase. This phase is rather straightforward to determine from the commutation relations. We find $(-1)^{\frac{|\epsilon|(|\epsilon|-1)}{2}}$. Thus:

$$\psi_z = e^{(\theta - z^*/2).z} = \sum_{\epsilon} (-1)^{\frac{|\epsilon|(|\epsilon|-1)}{2}} \theta^\epsilon z^\epsilon e^{-z^*.z/2} \tag{L.94}$$

Now, the dot product of ψ_z with an arbitrary generator θ^ϵ is easily handled:

$$\langle \theta^\epsilon | \psi_z \rangle = \sum_{\epsilon'} (-1)^{\frac{|\epsilon'|(|\epsilon'|-1)}{2}} \langle \theta^\epsilon | \theta^{\epsilon'} z^{\epsilon'} e^{-z^*.z/2} \rangle = \sum_{\epsilon'} (-1)^{\frac{|\epsilon'|(|\epsilon'|-1)}{2}} \langle \theta^\epsilon | \theta^{\epsilon'} \rangle z^{\epsilon'} e^{-z^*.z/2} \tag{L.95}$$

$$\boxed{\langle \theta^\epsilon | \psi_z \rangle = e^{-z^*.z/2} (-1)^{\frac{|\epsilon|(|\epsilon|-1)}{2}} z^\epsilon} \tag{L.96}$$

Therefore, the dot product of ψ_z with an arbitrary $s \in \tilde{\mathcal{H}}^{(n)}$ reads as:

$$\boxed{\langle s | \psi_z \rangle = e^{-z^*.z/2} \sum_{\epsilon} (-1)^{\frac{|\epsilon|(|\epsilon|-1)}{2}} c_\epsilon(s)^* z^\epsilon} \tag{L.97}$$

In particular, we find for the identity element:

$$\langle 1 | \psi_z \rangle = e^{-z^*.z/2} \tag{L.98}$$

The result displayed in Eq.(L.98) is very important and its equivalent in $\tilde{\mathcal{F}}^{(n)}$ reads as:

$$\boxed{\langle 0 | z \rangle = e^{-z^*.z/2}} \tag{L.99}$$

L.5.6 Completness of the fermionic coherent states

To conclude, it is remarkable that the coherent states verify the following completness property:

$$\boxed{\forall s \in \tilde{\mathcal{H}}^{(n)}, \qquad s = \int \langle \psi_z | s \rangle \psi_z \prod_{k=1}^{n} (dz_k^* dz_k)} \tag{L.100}$$

As the dot product is 1-Hermitian, it is sufficient to show Eq.(L.100) for an arbitrary generator θ^ϵ. We start by writing:

$$\int \langle \psi_z | \theta^\epsilon \rangle \psi_z \prod_{k=1}^{n} (dz_k dz_k^*) = (-1)^{\frac{|\epsilon|(|\epsilon|-1)}{2}} \int (z^\epsilon)^* e^{-z^*.z/2} e^{(\theta - z^*/2).z} \prod_{k=1}^{n} (dz_k^* dz_k) \tag{L.101}$$

We gather the exponentials in Eq.(L.101):

$$\int \langle \psi_z | \theta^\epsilon \rangle \psi_z \prod_{k=1}^{n} (dz_k dz_k^*) = (-1)^{\frac{|\epsilon|(|\epsilon|-1)}{2}} \int (z^\epsilon)^* e^{\theta.z + z.z^*} \prod_{k=1}^{n} (dz_k^* dz_k) \tag{L.102}$$

Now, we have to complete $(z^\epsilon)^*$. It requires $|\bar{\epsilon}|$ times the pair $z.z^*$, then $|\epsilon|$ times the pair $\theta.z$. Therefore, n is the only power remaining in the Taylor series decomposition of the exponential in the right hand side of Eq.(L.102):

$$\int \langle \psi_z | \theta^\epsilon \rangle \psi_z \prod_{k=1}^{n} (dz_k dz_k^*) = (-1)^{\frac{|\epsilon|(|\epsilon|-1)}{2}} \int (z^\epsilon)^* \frac{(\theta.z + z.z^*)^n}{n!} \prod_{k=1}^{n} (dz_k^* dz_k) \tag{L.103}$$

There are $n!$ ways to build the complementary of $(z^\epsilon)^*$. Moreover, as the pairs commute between each other, we can get θ^ϵ out of the integral adding the phase $(-1)^{|\epsilon|}$. Then, we build pairs from $(z^\epsilon)^*$ and z^ϵ. This process brings the phase $(-1)^{\frac{|\epsilon|(|\epsilon+1|}{2})}$. Finally, we can write:

$$\int \langle \psi_z | \theta^\epsilon \rangle \psi_z \prod_{k=1}^{n} (dz_k dz_k^*) = (-1)^{\frac{|\epsilon|(|\epsilon|-1)}{2}} (-1)^{|\epsilon|} (-1)^{\frac{|\epsilon|(|\epsilon+1|}{2})} \theta^\epsilon \int \prod_{k=1}^{n} (z_k z_k^*) \prod_{k=1}^{n} (dz_k^* dz_k) \tag{L.104}$$

Then:

$$\boxed{\int \langle \psi_z | \theta^\epsilon \rangle \psi_z \prod_{k=1}^{n} (dz_k dz_k^*) = \theta^\epsilon} \tag{L.105}$$

Appendix M

Expression of the dynamical ingredients

This appendix aims to give the explicit formulas of the SCIM potential V, dissipation tensor D, and inertia tensor B that appear in the SCIM Hamiltonian $\mathcal{H}_{SCIM}$:

$$\boxed{\mathcal{H}_{SCIM}(\bar{q}) = V(\bar{q}) + [D(\bar{q})\frac{\partial}{\partial q}]^{(1)} + [B(\bar{q})\frac{\partial}{\partial q}]^{(2)}} \tag{M.1}$$

In Chapter 1, we've defined the SCIM Hamiltonian as the result of the following product:

$$\mathcal{H}_{SCIM}(\bar{q}) = \bar{\mathcal{N}}^{-1/2}(\bar{q})\bar{\mathcal{H}}(\bar{q})\bar{\mathcal{N}}^{-1/2T}(\bar{q}) \tag{M.2}$$

In Eq.(M.2), the operator $\bar{\mathcal{N}}^{-1/2}$ appears as the product of two different terms:

$$\mathcal{N}^{-1/2}(\bar{q}) = \mathcal{J}^{-1/2}(\bar{q})\mathcal{F}^{-1}(\bar{q}) \tag{M.3}$$

The quantities $\mathcal{F}(\bar{q})$ are simple matrices (they do not contain any differentiation operator). They are easily obtained through an iterative factorization process described in Chapter 1. On the other hand, the operator $\mathcal{J}^{-1/2}$ is more complex to evaluate. It is defined as the inverse square root of the operator $\mathcal{J}$, which reads as follows:

$$\mathcal{J}(\bar{q}) = I + [\mathcal{N}_R^{(1)}(\bar{q})\frac{\partial}{\partial q}]^{(1)} + [\mathcal{N}_R^{(2)}(\bar{q})\frac{\partial}{\partial q}]^{(2)} = I + \mathcal{U}(\bar{q}) \tag{M.4}$$

In Eq.(M.4), the quantities $\mathcal{N}_R^{(1)}$ and $\mathcal{N}_R^{(2)}$ come directly from the factorization process described in Chapter 1.

In the following, we start by presenting the derivations leading to the explicit formula of $\mathcal{J}^{-1/2}$. Then, we use this result to express the potential V, the dissipation tensor D, and the intertia tensor B.

M.1 Expression of $\mathcal{J}^{-1/2}$

In this section, we give the explicit expression of the operator $\mathcal{J}^{-1/2}$, which reads as follows:

$$\boxed{\mathcal{J}^{-1/2}(\bar{q}) = j_0(\bar{q}) + [j_1(\bar{q})\frac{\partial}{\partial q}]^{(1)} + [j_2(\bar{q})\frac{\partial}{\partial q}]^{(2)}} \tag{M.5}$$

From Eq.(M.4), we calculate the inverse square root of the operator $\mathcal{J}$, thanks to a Taylor series expansion truncated at the second order:

$$\mathcal{J}^{-1/2}(\bar{q}) = I - \frac{1}{2}\mathcal{U}(\bar{q}) + \frac{3}{8}\mathcal{U}^2(\bar{q}) \tag{M.6}$$

For the sake of clarity, we omit the $\bar{q}$ dependency of the operators, and we write for $\mathcal{U}$:

$$\mathcal{U} = [\mathcal{N}_R^{(1)}\frac{\partial}{\partial q}]^{(1)} + [\mathcal{N}_R^{(2)}\frac{\partial}{\partial q}]^{(2)} = [u_1\frac{\partial}{\partial q}]^{(1)} + [u_2\frac{\partial}{\partial q}]^{(2)} \tag{M.7}$$

In addition, the shorthand notation superscript (p) stands for the derivative of order p of a given quantity in the following. We start by giving the expression of j_0:

$$\boxed{j_0 = I - \frac{3}{8}u_1^{(1)}u_1^{(1)} + \frac{3}{8}(u_1^{(2)}u_2^{(1)} - u_2^{(1)}u_1^{(2)}) + \frac{3}{8}u_2^{(2)}u_2^{(2)}} \tag{M.8}$$

Then, we give the quantity j_1:

$$\boxed{j_1 = \frac{3}{8}[u_1u_1^{(1)} - u_1^{(1)}u_1 + u_1^{(2)}u_2 + u_2u_1^{(2)} - 2(u_1^{(1)}u_2^{(1)} + u_2^{(1)}u_1^{(1)}) + 2(u_2^{(2)}u_2^{(1)} - u_2^{(1)}u_2^{(2)})]} \tag{M.9}$$

Finally, we express the quantity j_2:

$$\boxed{j_2 = \frac{3}{8}[u_1u_1 + u_1u_2^{(1)} - u_2^{(1)}u_1 - 2(u_1^{(1)}u_2 - u_2u_1^{(1)}) + u_2^{(2)}u_2 + u_2u_2^{(2)} - 4(u_2^{(1)}u_2^{(1)}]} \tag{M.10}$$

Of course, in the previous expression, we've truncated the expression of $\mathcal{J}^{-1/2}$ at the second order in SOPO, in coherence with the SCIM formalism.

M.2 Expression of $\mathcal{H}_{SCIM}$

This section aims to give the explicit formula of the SCIM Hamiltonian $\mathcal{H}_{SCIM}$:

$$\boxed{\mathcal{H}_{SCIM}(\bar{q}) = V(\bar{q}) + [D(\bar{q})\frac{\partial}{\partial q}]^{(1)} + [B(\bar{q})\frac{\partial}{\partial q}]^{(2)}} \tag{M.11}$$

We start by rewriting the expression of $\mathcal{H}_{SCIM}$ in terms of the quantities $\mathcal{F}$ and $\mathcal{J}^{-1/2}$:

$$\mathcal{H}_{SCIM}(\bar{q}) = \mathcal{J}^{-1/2}(\bar{q})\mathcal{F}^{-1}(\bar{q})\bar{\mathcal{H}}(\bar{q})\mathcal{F}^{-1T}(\bar{q})\mathcal{J}^{-1/2}(\bar{q}) \tag{M.12}$$

The quantity $\bar{\mathcal{H}}$ is defined as follows:

$$\boxed{\bar{\mathcal{H}}(\bar{q}) = \mathcal{H}^{(0)}(\bar{q}) + [\mathcal{H}^{(1)}(\bar{q})\frac{\partial}{\partial q}]^{(1)} + \frac{1}{2}[\mathcal{H}^{(2)}(\bar{q})\frac{\partial}{\partial q}]^{(2)}} \tag{M.13}$$

Now, we define the operator h:

$$\boxed{h(\bar{q}) = h_0(\bar{q}) + [h_1(\bar{q})\frac{\partial}{\partial q}]^{(1)} + [h_2(\bar{q})\frac{\partial}{\partial q}]^{(2)}} \tag{M.14}$$

With:

$$h(\bar{q}) = \mathcal{F}^{-1}(\bar{q})[\mathcal{H}^{(0)}(\bar{q}) + [\mathcal{H}^{(1)}(\bar{q})\frac{\partial}{\partial q}]^{(1)} + \frac{1}{2}[\mathcal{H}^{(2)}(\bar{q})\frac{\partial}{\partial q}]^{(2)}]\mathcal{F}^{-1T}(\bar{q}) \tag{M.15}$$

In the following, we omit the $\bar{q}$ dependency of the operators for simplification purposes. The quantity h_0 reads as:

$$\boxed{\begin{aligned} h_0 = \mathcal{F}^{-1}\mathcal{H}^{(0)}\mathcal{F}^{-1T} + \mathcal{F}^{-1}\mathcal{H}^{(1)}(\mathcal{F}^{-1T})^{(1)} - (\mathcal{F}^{-1})^{(1)}\mathcal{H}^{(1)}\mathcal{F}^{-1T} \\ +\mathcal{F}^{-1}\mathcal{H}^{(2)}(\mathcal{F}^{-1T})^{(2)} + (\mathcal{F}^{-1})^{(2)}\mathcal{H}^{(2)}\mathcal{F}^{-1T} \\ -2(\mathcal{F}^{-1})^{(1)}\mathcal{H}^{(2)}(\mathcal{F}^{-1T})^{(1)} \end{aligned}} \tag{M.16}$$

Then, we express h_1:

$$\boxed{h_1 = \mathcal{F}^{-1}\mathcal{H}^{(1)}\mathcal{F}^{-1T} + 2[\mathcal{F}^{-1}\mathcal{H}^{(2)}(\mathcal{F}^{-1T})^{(1)} - (\mathcal{F}^{-1})^{(1)}\mathcal{H}^{(2)}\mathcal{F}^{-1T}]} \tag{M.17}$$

Finally, we write h_2:

$$\boxed{h_2 = \mathcal{F}^{-1}\mathcal{H}^{(2)}\mathcal{F}^{-1T}} \tag{M.18}$$

The definition of h in Eq.(M.14) leads to the following equation:

$$\mathcal{H}_{SCIM} = (j_0 + [j_1\frac{\partial}{\partial q}]^{(1)} + [j_2\frac{\partial}{\partial q}]^{(2)})(h_0 + [h_1\frac{\partial}{\partial q}]^{(1)} + [h_2\frac{\partial}{\partial q}]^{(2)})(j_0 + [j_1\frac{\partial}{\partial q}]^{(1)} + [j_2\frac{\partial}{\partial q}]^{(2)}) \tag{M.19}$$

We start by writing explicitly the potential V, whose expression is very complex:

$$
\begin{aligned}
V = {} & j_0 h_0 j_0 + j_0 h_1 j_0^{(1)} - j_0^{(1)} h_1 j_0 - j_0 h_0^{(1)} j_1 + j_1 h_0^{(1)} j_0 - j_0^{(1)} h_0 j_1 + j_1 h_0 j_0^{(1)} \\
& + j_0 h_2 j_0^{(2)} + j_0^{(2)} h_2 j_0 - 2 j_0^{(1)} h_2 j_0^{(1)} \\
& + j_0^{(2)} h_0 j_2 + j_2 h_0 j_0^{(2)} + j_0 h_0^{(2)} j_2 + j_2 h_0^{(2)} j_0 + 2(j_0^{(1)} h_0^{(1)} j_2 + j_2 h_0^{(1)} j_0^{(1)}) \\
& - j_1 h_0^{(1)} j_1^{(1)} - j_1^{(1)} h_0^{(1)} j_1 - j_1^{(1)} h_0 j_1^{(1)} - j_1 h_0^{(2)} j_1 \\
& - j_0^{(1)} h_1 j_1^{(1)} - j_1^{(1)} h_1 j_0^{(1)} + j_0^{(2)} h_1 j_1 + j_1 h_1 j_0^{(2)} - j_0 h_1^{(1)} j_1^{(1)} - j_1^{(1)} h_1^{(1)} j_0 \\
& + j_0^{(1)} h_1^{(1)} j_1 + j_1 h_1^{(1)} j_0^{(1)} - j_2^{(1)} h_0 j_1^{(2)} + j_1^{(2)} h_0 j_2^{(1)} + 2(- j_2^{(1)} h_0^{(1)} j_1^{(1)} + j_1^{(1)} h_0^{(1)} j_2^{(1)}) \\
& - j_2 h_0^{(1)} j_1^{(2)} + j_1^{(2)} h_0^{(1)} j_2 + 2(- j_2 h_0^{(2)} j_1^{(1)} + j_1^{(1)} h_0^{(2)} j_2) \\
& - j_2^{(1)} h_0^{(2)} j_1 + j_1 h_0^{(2)} j_2^{(1)} - j_2 h_0^{(3)} j_1 + j_1 h_0^{(3)} j_2 \\
& + j_0^{(2)} h_1 j_2^{(1)} - j_2^{(1)} h_1 j_0^{(2)} - j_0^{(3)} h_1 j_2 + j_2 h_1 j_0^{(3)} + 2(j_0^{(1)} h_1^{(1)} j_2^{(1)} - j_2^{(1)} h_1^{(1)} j_0^{(1)}) \\
& + 2(- j_0^{(2)} h_1^{(1)} j_2 + j_2 h_1^{(1)} j_0^{(2)}) + j_0 h_1^{(2)} j_2^{(1)} - j_2^{(1)} h_1^{(2)} j_0 - j_0^{(1)} h_1^{(2)} j_2 + j_2 h_1^{(2)} j_0^{(1)} \\
& - j_0^{(1)} h_2 j_1^{(2)} + j_1^{(2)} h_2 j_0^{(1)} + 2(j_0^{(2)} h_2 j_1^{(1)} - j_1^{(1)} h_2 j_0^{(2)}) - j_0^{(3)} h_2 j_1 + j_1 h_2 j_0^{(3)} \\
& + 2(j_0^{(1)} h_2^{(1)} j_1^{(1)} - j_1^{(1)} h_2^{(1)} j_0^{(1)}) - j_0 h_2^{(1)} j_1^{(2)} + j_1^{(2)} h_2^{(1)} j_0 - j_0^{(2)} h_2^{(1)} j_1 + j_1 h_2^{(1)} j_0^{(2)} \\
& + 2(j_2^{(1)} h_0^{(1)} j_2^{(2)} + j_2^{(2)} h_0^{(1)} j_2^{(1)}) + j_2 h_0^{(2)} j_2^{(2)} + j_2^{(2)} h_0^{(2)} j_2 + 2(j_2 h_2^{(3)} j_2^{(1)} + j_2^{(1)} h_2^{(3)} j_2) \\
& + j_2^{(2)} h_2 j_2^{(2)} + 4 j_2^{(1)} h_2^{(2)} j_2^{(1)} + j_2 h_2^{(4)} j_2 \\
& + j_0^{(2)} h_2 j_2^{(2)} + j_2^{(2)} h_2 j_0^{(2)} + 2(- j_0^{(3)} h_2 j_2^{(1)} - j_2^{(1)} h_2 j_0^{(3)}) + j_0^{(4)} h_2 j_2 + j_2 h_2 j_0^{(4)} \\
& + 2(j_0^{(1)} h_2^{(1)} j_2^{(2)} + j_2^{(2)} h_2^{(1)} j_0^{(1)}) + 4(- j_0^{(2)} h_2^{(1)} j_2^{(1)} - j_2^{(1)} h_2^{(1)} j_0^{(2)}) + 2(j_0^{(3)} h_2^{(1)} j_2 + j_2 h_2^{(1)} j_0^{(3)}) \\
& + j_0 h_2^{(2)} j_2^{(2)} + j_2^{(2)} h_2^{(2)} j_0 + 2(- j_0^{(1)} h_2^{(2)} j_2^{(1)} - j_2^{(1)} h_2^{(2)} j_0^{(1)}) + j_0^{(2)} h_2^{(2)} j_2 + j_2 h_2^{(2)} j_0^{(2)} \\
& - j_1^{(1)} h_1 j_1^{(2)} + j_1^{(2)} h_1 j_1^{(1)} - j_1 h_1^{(1)} j_1^{(2)} + j_1^{(2)} h_1^{(1)} j_1 - j_1 h_1^{(2)} j_1^{(1)} + j_1^{(1)} h_1^{(2)} j_1 \\
& - j_1^{(1)} h_2 j_1^{(3)} - j_1^{(3)} h_2 j_1^{(1)} + 2 j_1^{(2)} h_2 j_1^{(2)} - j_1 h_1^{(1)} j_1^{(3)} - j_1^{(3)} h_1^{(1)} j_1 \\
& + j_1^{(1)} h_2^{(1)} j_1^{(2)} + j_1^{(2)} h_2^{(1)} j_1^{(1)} - j_1 h_2^{(2)} j_1^{(2)} - j_1^{(2)} h_2^{(2)} j_1 + 2 j_1^{(1)} h_2^{(2)} j_1^{(1)} \\
& - j_2 h_1^{(1)} j_1^{(3)} - j_1^{(3)} h_1^{(1)} j_2 + 2(- j_2 h_1^{(2)} j_1^{(2)} - j_1^{(2)} h_1^{(2)} j_2) - j_2 h_1^{(3)} j_1^{(1)} - j_1^{(1)} h_1^{(3)} j_2 \\
& - j_2^{(1)} h_1 j_1^{(3)} - j_1^{(3)} h_1 j_2^{(1)} + j_2^{(2)} h_1^{(2)} j_1 + j_1 h_1^{(2)} j_2^{(2)} + j_2^{(1)} h_1^{(3)} j_1 + j_1 h_1^{(3)} j_2^{(1)} \\
& - j_2^{(1)} h_1^{(1)} j_1^{(2)} - j_1^{(2)} h_1^{(1)} j_2^{(1)} + j_2^{(2)} h_1 j_1^{(2)} + j_1^{(2)} h_1 j_2^{(2)} + j_2^{(1)} h_1^{(2)} j_1^{(1)} + j_1^{(1)} h_1^{(2)} j_2^{(1)} \\
& + 2(j_2^{(2)} h_1^{(1)} j_1^{(1)} + j_1^{(1)} h_1^{(1)} j_2^{(2)}) + j_2^{(2)} h_2 j_2^{(4)} + j_2^{(4)} h_2 j_2^{(2)} + 2(- j_2^{(2)} h_2^{(1)} j_2^{(3)} - j_2^{(3)} h_2^{(1)} j_2^{(2)}) \\
& + 2(j_2 h_2^{(3)} j_2^{(3)} + j_2^{(3)} h_2^{(3)} j_2) + 2(j_2^{(1)} h_2^{(1)} j_2^{(4)} + j_2^{(4)} h_2^{(1)} j_2^{(1)}) + j_2 h_2^{(2)} j_2^{(4)} + j_2^{(4)} h_2^{(2)} j_2 \\
& + 2(- j_2^{(1)} h_2^{(3)} j_2^{(2)} - j_2^{(2)} h_2^{(3)} j_2^{(1)}) + j_2 h_2^{(4)} j_2^{(2)} + j_2^{(2)} h_2^{(4)} j_2 + 2(j_2^{(1)} h_2^{(2)} j_2^{(3)} + j_2^{(3)} h_2^{(2)} j_2^{(1)}) \\
& + 2(- j_2^{(1)} h_2^{(4)} j_2^{(1)} - j_2^{(3)} h_2 j_2^{(3)}) - 6 j_2^{(2)} h_2^{(2)} j_2^{(2)} \\
& + j_2^{(2)} h_1 j_2^{(3)} - j_2^{(3)} h_1 j_2^{(2)} + 2(j_2^{(1)} h_1^{(1)} j_2^{(3)} - j_2^{(3)} h_1^{(1)} j_2^{(1)}) + 3(j_2^{(1)} h_1^{(2)} j_2^{(2)} - j_2^{(2)} h_1^{(2)} j_2^{(1)}) \\
& + j_2 h_1^{(2)} j_2^{(3)} - j_2^{(3)} h_1^{(2)} j_2 + 2(j_2 h_1^{(3)} j_2^{(2)} - j_2^{(2)} h_1^{(3)} j_2) + j_2 h_1^{(4)} j_2^{(1)} - j_2^{(1)} h_1^{(4)} j_2 \\
& - j_2^{(1)} h_2 j_1^{(4)} + j_1^{(4)} h_2 j_2^{(1)} + 2(j_2^{(2)} h_2 j_1^{(3)} - j_1^{(3)} h_2 j_2^{(2)}) - j_2^{(3)} h_2 j_1^{(2)} + j_1^{(2)} h_2 j_2^{(3)} \\
& - j_2 h_2^{(1)} j_2^{(4)} + j_2^{(4)} h_2^{(1)} j_2 + 3(j_2^{(2)} h_2^{(1)} j_1^{(2)} - j_1^{(2)} h_2^{(1)} j_2^{(2)}) + 2(- j_2^{(3)} h_2^{(1)} j_1^{(1)} + j_1^{(1)} h_2^{(1)} j_2^{(3)}) \\
& + 2(- j_2 h_2^{(2)} j_1^{(3)} + j_1^{(3)} h_2^{(2)} j_2) - j_2^{(3)} h_2^{(2)} j_1 + j_1 h_2^{(2)} j_2^{(3)} + 3(j_2^{(1)} h_2^{(2)} j_1^{(2)} - j_1^{(2)} h_2^{(2)} j_2^{(1)}) \\
& + 2(j_2^{(1)} h_2^{(3)} j_1^{(1)} - j_1^{(1)} h_2^{(3)} j_2^{(1)}) - j_2 h_2^{(3)} j_1^{(2)} + j_1^{(2)} h_2^{(3)} j_2 - j_2^{(2)} h_2^{(3)} j_1 + j_1 h_2^{(3)} j_2^{(2)}
\end{aligned}
\tag{M.20}
$$

Then, we give the expression of the dissipation tensor D:

$$
\begin{aligned}
D = {} & j_0h_1j_0 + j_0h_0j_1 + j_1h_0j_0 + 2(j_0h_2j_0^{(1)} - j_0^{(1)}h_2j_0) + 2(-j_0h_0^{(1)}j_2 - j_2h_0^{(1)}j_0) \\
& +2(-j_0^{(1)}h_0j_2 - j_2h_0j_0^{(1)}) + j_1h_0j_1^{(1)} - j_1^{(1)}h_0j_1 \\
& -j_0h_1^{(1)}j_1 + j_1h_1^{(1)}j_0 + 2(-j_0^{(1)}h_1j_1 + j_1h_1j_0^{(1)}) + j_0h_1j_1^{(1)} - j_1^{(1)}h_1j_0 \\
& +2(-j_2^{(1)}h_0j_1^{(1)} - j_1^{(1)}h_0j_2^{(1)}) + j_2h_0j_1^{(2)} + j_1^{(2)}h_0j_2 \\
& +2(-j_2^{(1)}h_0^{(1)}j_1 - j_1h_0^{(1)}j_2^{(1)}) - j_2h_0^{(2)}j_1 - j_1h_0^{(2)}j_2 \\
& +3(j_0^{(2)}h_1j_2 + j_2h_1j_0^{(2)}) + 2(-j_0^{(1)}h_1j_2^{(1)} - j_2^{(1)}h_1j_0^{(1)}) + 4(j_0^{(1)}h_1^{(1)}j_2 + j_2h_1^{(1)}j_0^{(1)}) \\
& +2(-j_0h_1^{(1)}j_2^{(1)} - j_2^{(1)}h_1^{(1)}j_0) + j_0h_1^{(2)}j_2 + j_2h_1^{(2)}j_0 \\
& +4(-j_0^{(1)}h_2j_1^{(1)} - j_1^{(1)}h_2j_0^{(1)}) + j_0h_2j_1^{(2)} + j_1^{(2)}h_2j_0 + 3(j_0^{(2)}h_2j_1 + j_1h_2j_0^{(2)}) \\
& +2(-j_0h_2^{(1)}j_1^{(1)} - j_1^{(1)}h_2^{(1)}j_0) + 2(j_0^{(1)}h_2^{(1)}j_1 + j_1h_2^{(1)}j_0^{(1)}) \\
& +2(j_2^{(2)}h_0j_2^{(1)} - j_2^{(1)}h_0j_2^{(2)}) + 2(-j_2h_0^{(1)}j_2^{(2)} + j_2^{(2)}h_0^{(1)}j_2) + 2(-j_2h_0^{(2)}j_2^{(1)} + j_2^{(1)}h_0^{(2)}j_2) \\
& +2(-j_0^{(1)}h_2j_2^{(2)} + j_2^{(2)}h_2j_0^{(1)}) + 4(-j_0^{(3)}h_2j_2 + j_2h_2j_0^{(3)}) + 6(j_0^{(2)}h_2j_2^{(1)} - j_2^{(1)}h_2j_0^{(2)}) \\
& +2(-j_0h_2^{(1)}j_2^{(2)} + j_2^{(2)}h_2^{(1)}j_0) + 8(j_0^{(1)}h_2^{(1)}j_2^{(1)} - j_2^{(1)}h_2^{(1)}j_0^{(1)}) + 6(-j_0^{(2)}h_2^{(1)}j_2 + j_2h_2^{(1)}j_0^{(2)}) \\
& +2(j_0h_2^{(2)}j_2^{(1)} - j_2^{(1)}h_2^{(2)}j_0) + 2(-j_0^{(1)}h_2^{(2)}j_2 + j_2h_2^{(2)}j_0^{(1)}) \\
& +j_1h_1j_1^{(2)} + j_1^{(2)}h_1j_1 - j_1h_1^{(1)}j_1^{(1)} - j_1^{(1)}h_1^{(1)}j_1 - j_1h_1^{(2)}j_1 - 3j_1^{(1)}h_1j_1^{(1)} \\
& +5(-j_1^{(1)}h_2j_1^{(2)} + j_1^{(2)}h_2j_1^{(1)}) + 2(-j_1h_2^{(1)}j_1^{(2)} + j_1^{(2)}h_2^{(1)}j_1) \\
& +2(-j_1h_2^{(2)}j_1^{(1)} + j_1^{(1)}h_2^{(2)}j_1) + j_1h_2j_1^{(3)} - j_1^{(3)}h_2j_1 \\
& -j_2h_1^{(1)}j_1^{(2)} + j_1^{(2)}h_1^{(1)}j_2 + 4(-j_2^{(1)}h_1j_1^{(2)} + j_1^{(2)}h_1j_2^{(1)}) + j_2h_1j_1^{(3)} - j_1^{(3)}h_1j_2 \\
& +2(j_2^{(2)}h_1j_1^{(1)} - j_1^{(1)}h_1j_2^{(2)}) - j_2h_1^{(3)}j_1 + j_1h_1^{(3)}j_2 + 4(-j_2^{(1)}h_1^{(1)}j_1^{(1)} + j_1^{(1)}h_1^{(1)}j_2^{(1)}) \\
& +3(-j_2h_1^{(2)}j_1^{(1)} + j_1^{(1)}h_1^{(2)}j_2) + 2(j_2^{(2)}h_1^{(1)}j_1 - j_1h_1^{(1)}j_2^{(2)}) \\
& +8(-j_2^{(3)}h_2j_2^{(2)} + j_2^{(2)}h_2j_2^{(3)}) + 2(-j_2^{(1)}h_2j_2^{(4)} + j_2^{(4)}h_2j_2^{(1)}) + 8(j_2^{(1)}h_2^{(1)}j_2^{(3)} - j_2^{(3)}h_2^{(1)}j_2^{(1)}) \\
& +2(-j_2h_2^{(1)}j_2^{(4)} + j_2^{(4)}h_2^{(1)}j_2) + 12(j_2^{(1)}h_2^{(2)}j_2^{(2)} - j_2^{(2)}h_2^{(2)}j_2^{(1)}) \\
& +4(j_2h_2^{(3)}j_2^{(2)} - j_2^{(2)}h_2^{(3)}j_2) + 2(j_2h_2^{(4)}j_2^{(1)} - j_2^{(1)}h_2^{(4)}j_2) \\
& +5j_2^{(2)}h_1j_2^{(2)} + 8j_2^{(1)}h_1^{(2)}j_2^{(1)} + j_2h_1^{(4)}j_2 + 2(-j_2^{(1)}h_1j_2^{(3)} - j_2^{(3)}h_1j_2^{(1)}) \\
& +4(j_2^{(1)}h_1^{(1)}j_2^{(2)} + j_2^{(2)}h_1^{(1)}j_2^{(1)}) + 2(-j_2h_1^{(1)}j_2^{(3)} - j_2^{(3)}h_1^{(1)}j_2) \\
& -j_2h_1^{(2)}j_2^{(2)} - j_2^{(2)}h_1^{(2)}j_2 + 2(j_2h_1^{(3)}j_2^{(1)} + j_2^{(1)}h_1^{(3)}j_2) \\
& +j_2h_2j_1^{(4)} + j_1^{(4)}h_2j_2 + 6(-j_2^{(1)}h_2j_1^{(3)} - j_1^{(3)}h_2j_2^{(1)}) + 7(j_2^{(2)}h_2j_1^{(2)} + j_1^{(2)}h_2j_2^{(2)}) \\
& +2(-j_2^{(3)}h_2j_1^{(1)} - j_1^{(1)}h_2j_2^{(3)}) + 2(-j_2h_2^{(1)}j_1^{(3)} - j_1^{(3)}h_2^{(1)}j_2) + 2(-j_2^{(3)}h_2^{(1)}j_1 - j_1h_2^{(1)}j_2^{(3)}) \\
& +8(j_2^{(2)}h_2^{(1)}j_1^{(1)} + j_1^{(1)}h_2^{(1)}j_2^{(2)}) + 4(-j_2^{(1)}h_2^{(1)}j_1^{(2)} - j_1^{(2)}h_2^{(1)}j_2^{(1)}) \\
& +4(j_2^{(1)}h_2^{(2)}j_1^{(1)} + j_1^{(1)}h_2^{(2)}j_2^{(1)}) + 5(-j_2h_2^{(2)}j_1^{(2)} - j_1^{(2)}h_2^{(2)}j_2) \\
& +j_2^{(2)}h_2^{(2)}j_1 + j_1h_2^{(2)}j_2^{(2)} + 2(-j_2h_2^{(3)}j_1^{(1)} - j_1^{(1)}h_2^{(3)}j_2) \\
& +2(j_2^{(1)}h_2^{(3)}j_1 + j_1h_2^{(3)}j_2^{(1)})
\end{aligned}
\tag{M.21}
$$

To conclude, we express the inertia tensor B:

$$
\begin{aligned}
B = {} & j_0 h_2 j_0 + j_0 h_0 j_2 + j_2 h_0 j_0 + j_1 h_0 j_1 + j_0 h_1 j_1 + j_1 h_1 j_0 + j_2 h_0^{(1)} j_1 - j_1 h_0^{(1)} j_2 \\
& - j_2^{(1)} h_0 j_1 + j_1 h_0 j_2^{(1)} + 2(j_2 h_0 j_1^{(1)} - j_1^{(1)} h_0 j_2) \\
& + 3(-j_0^{(1)} h_1 j_2 + j_2 h_1 j_0^{(1)}) + j_0 h_1 j_2^{(1)} - j_2^{(1)} h_1 j_0 + 2(-j_0 h_1^{(1)} j_2 + j_2 h_1^{(1)} j_0) \\
& + 3(-j_0^{(1)} h_2 j_1 + j_1 h_2 j_0^{(1)}) + 2(j_0 h_2 j_1^{(1)} - j_1^{(1)} h_2 j_0) - j_0 h_2^{(1)} j_1 + j_1 h_2^{(1)} j_0 \\
& + j_2^{(2)} h_0 j_2 + j_2 h_0 j_2^{(2)} + 2(-j_2 h_0^{(1)} j_2^{(1)} - j_2^{(1)} h_0^{(1)} j_2) - 4 j_2^{(1)} h_0 j_2^{(1)} - 2 j_2 h_0^{(2)} j_2 \\
& + 6(j_0^{(2)} h_2 j_2 + j_2 h_2 j_0^{(2)}) + j_0 h_2 j_2^{(2)} + j_2^{(2)} h_2 j_0 + 6(-j_0^{(1)} h_2 j_2^{(1)} - j_2^{(1)} h_2 j_0^{(1)}) \\
& + 6(j_0^{(1)} h_2^{(1)} j_2 + j_2 h_2^{(1)} j_0^{(1)}) + 4(-j_0 h_2^{(1)} j_2^{(1)} - j_2^{(1)} h_2^{(1)} j_0) + j_0 h_2^{(2)} j_2 + j_2 h_2^{(2)} j_0 \\
& + 2(j_1 h_1 j_1^{(1)} - j_1^{(1)} h_1 j_1) + 3(j_1 h_2 j_1^{(2)} + j_1^{(2)} h_2 j_1) - j_1 h_2^{(1)} j_1^{(1)} - j_1^{(1)} h_2^{(1)} j_1 - 7 j_1^{(1)} h_2 j_1^{(1)} \\
& - j_1 h_2^{(2)} j_1 + j_2 h_1^{(1)} j_1^{(1)} + j_1^{(1)} h_1^{(1)} j_2 + 5(-j_2^{(1)} h_1 j_1^{(1)} - j_1^{(1)} h_1 j_2^{(1)}) + 3(j_2 h_1 j_1^{(2)} + j_1^{(2)} h_1 j_2) \\
& + 3(-j_2^{(1)} h_1^{(1)} j_1 - j_1 h_1^{(1)} j_2^{(1)}) - j_2 h_1^{(2)} j_1 - j_1 h_1^{(2)} j_2 + j_2^{(2)} h_1 j_1 + j_1 h_1 j_2^{(2)} \\
& + 19 j_2^{(2)} h_2 j_2^{(2)} + 16 j_2^{(1)} h_2^{(2)} j_2^{(1)} + j_2 h_2^{(4)} j_2 + j_2 h_2 j_2^{(4)} + j_2^{(4)} h_2 j_2 \\
& + 10(-j_2^{(1)} h_2 j_2^{(3)} - j_2^{(3)} h_2 j_2^{(1)}) + 8(j_2^{(1)} h_2^{(1)} j_2^{(2)} + j_2^{(2)} h_2^{(1)} j_2^{(1)}) \\
& + 6(-j_2 h_2^{(1)} j_2^{(3)} - j_2^{(3)} h_2^{(1)} j_2) + 5(-j_2 h_2^{(2)} j_2^{(2)} - j_2^{(2)} h_2^{(2)} j_2) \\
& + 2(j_2 h_2^{(3)} j_2^{(1)} + j_2^{(1)} h_2^{(3)} j_2) + 7(j_2^{(2)} h_1 j_2^{(1)} - j_2^{(1)} h_1 j_2^{(2)}) + j_2 h_1 j_2^{(3)} - j_2^{(3)} h_1 j_2 \\
& + 4(-j_2 h_1^{(1)} j_2^{(2)} + j_2^{(2)} h_1^{(1)} j_2) + 4(-j_2 h_1^{(2)} j_2^{(1)} + j_2^{(1)} h_1^{(2)} j_2) \\
& + 4(j_2 h_2 j_1^{(3)} - j_1^{(3)} h_2 j_2) - j_2^{(3)} h_2 j_1 + j_1 h_2 j_2^{(3)} + 12(-j_2^{(1)} h_2 j_1^{(2)} + j_1^{(2)} h_2 j_2^{(1)}) \\
& + 8(j_2^{(2)} h_2 j_1^{(1)} - j_1^{(1)} h_2 j_2^{(2)}) + 5(j_2^{(2)} h_2^{(1)} j_1 - j_1 h_2^{(1)} j_2^{(2)}) + 8(-j_2^{(1)} h_2^{(1)} j_1^{(1)} + j_1^{(1)} h_2^{(1)} j_2^{(1)}) \\
& + 4(-j_2 h_2^{(2)} j_1^{(1)} + j_1^{(1)} h_2^{(2)} j_2) + j_2^{(1)} h_2^{(2)} j_1 - j_1 h_2^{(2)} j_2^{(1)} - j_2 h_2^{(3)} j_1 + j_1 h_2^{(3)} j_2
\end{aligned}
\tag{M.22}
$$

Here also, the SCIM Hamiltonian expression is truncated at the second order in SOPO, in coherence with the assumptions of the formalism.

Appendix N

Quadratures

In this appendix, we discuss the numerical approximation of integrals of the following kind:

$$I = \int_a^b g(x)dx \qquad (a,b) \in \mathbb{R}^2 \tag{N.1}$$

Naively, we could try the rectangle or the trapezium rule. However, for an important class of functions, these methods are far from being the most efficient. The goal of this appendix is to present a numerical effective integration method which is called the quadrature method. We first present the Lagrange interpolation method. We then demonstrate an important result about polynomial integration that naturally leads to the definition of the quadratures. Finally, we present an exemple.

N.1 Lagrange interpolation

We consider $(x_1, ..., x_n)$ and $(y_1, ..., y_n) \in \mathbb{R}^n$, such that $\forall i \neq j,\ x_i \neq x_j$. There exists a unique L polynomial of degree n such that $\forall i \in [\![1, n]\!],\ L(x_i) = y_i$. This polynomial is the Lagrange polynomial:

$$L(X) = \sum_{j=1}^{n} y_j \prod_{i=1 i\neq j}^{n} \frac{(X - x_i)}{(x_j - x_i)} \tag{N.2}$$

We call Lagrange associated polynomials the following ones:

$$l_j(X) = \prod_{i=1 i\neq j}^{n} \frac{(X - x_i)}{(x_j - x_i)} \tag{N.3}$$

It is straightforward that $\forall i,\ \forall j \in [\![1, n]\!],\ l(x_j) = \delta_{ij}$. We write:

$$L(X) = \sum_{j=1}^{n} y_j l_j(X) \tag{N.4}$$

It is now clear that the Lagrange polynomial verifies the property announced in the begining of this part.

The Lagrange interpolation of order n of a function f is now very straightforward to present. We start choosing a set $(x_1, ..., x_n)$ of n points. Then, we consider the set $(y_1, ..., y_n) = (f(x_1), ..., f(x_n))$ and find the associated Lagrange poylnomial:

$$\boxed{L_f(X) = \sum_{j=1}^{n} f(x_j) \prod_{i=1 i \neq j}^{n} \frac{(X - x_i)}{(x_j - x_i)}} \tag{N.5}$$

N.2 An important polynomial integration result

We consider a space E of $\mathbb{R} \to \mathbb{R}$ functions. Let $(a, b) \in \bar{\mathbb{R}}^2$ and ω be a $\mathbb{R} \to \mathbb{R}$ function such that:

$$(.|.) : \begin{cases} E^2 \to \mathbb{R} \\ (f|g) \to \int_a^b \omega(x) f(x) g(x) \end{cases} \qquad \text{defines a dot product.} \tag{N.6}$$

We want to show that $\exists!\ (x_1, ..., x_n), (\omega_1, ..., \omega_n) \in \mathbb{R}^n\ ;\ \forall P \in \mathbb{R}_{2n-1}[X]$:

$$\int_a^b \omega(x) P(x) dx = \sum_{i=1}^{n} w_i P(x_i) \qquad w_i \in \mathbb{R} \tag{N.7}$$

We assume that $(x_1, ..., x_n)$ exists. We start by building the polynomial P_n:

$$P_n(X) = \prod_{i=1}^{n} (X - x_i) \tag{N.8}$$

Then, $\forall k \in [\![1, n-1]\!]$, we consider the polynomials $X^k P_n \in \mathbb{R}_{2n-1}[X]$. Eq.$(N.7)$ holds for each of these polynomials:

$$\forall k \in [\![1, n-1]\!]\ \int_a^b \omega(x) x^k P_n(x) dx = (P_n | x_k) = \sum_{i=1}^{n} w_i x_i^k P_n(x_i) = 0 \tag{N.9}$$

Eq.(N.9) shows that the polynomial P_n is orthogonal to the vector subspace $\mathbb{R}_{n-1}[X]$ with respect to the dot product ω. Moreover the degree of P_n is n and it is unitary. It is therefore unique. The points $(x_1, ..., x_n)$ are thus defined to be the n roots of the unitary polynomial whose degree is n and which is orthogonal to the vectorial subspace $\mathbb{R}_{n-1}[X]$ with respect to ω.

We have shown that if $(x_1, ..., x_n)$ exists, it has to verify some conditions. We now demonstrate that under these conditions Eq.$(N.7)$ holds. Let $P \in \mathbb{R}_{2n-1}[X]$. Dividing P by P_n, we obtain:

$$\begin{cases} P(X) = P_n(X) Q(X) + R(X) \\ deg(Q) < n \\ deg(R) < n \end{cases} \tag{N.10}$$

Injecting Eq.(N.10) in Eq.(N.7) leads to:

$$\int_a^b \omega(x)P(x)dx = \int_a^b \omega(x)P_n(x)Q(x)dx + \int_a^b \omega(x)R(x)dx = (P_n|Q) + \int_a^b \omega(x)R(x)dx \tag{N.11}$$

$$\int_a^b \omega(x)P(x)dx = (P_n|Q) + \int_a^b \omega(x)R(x)dx \tag{N.12}$$

As $Q \in \mathbb{R}_{n-1}[X]$, it is clear that $(P_n|Q) = 0$. Thus, we have:

$$\int_a^b \omega(x)P(x)dx = \int_a^b \omega(x)R(x)dx \tag{N.13}$$

Since the degree of R is equal or lower than $n-1$, it is exactly described by a Lagrange interpolation of order n. It reads:

$$R(x) = \sum_{i=1}^{n} l_i(x)R(x_i) \tag{N.14}$$

Then, we inject Eq.(N.14) in Eq.(N.13):

$$\boxed{\int_a^b \omega(x)P(x)dx = \sum_{i=1}^{n} w_i R(x_i) = \sum_{i=1}^{n} w_i R(x_i) + w_i P_n(x_i)Q(x_i) = \sum_{i=1}^{n} w_i P(x_i)} \tag{N.15}$$

It concludes the demonstration and shows the explicit form of the coefficients w_i:

$$\boxed{w_i = \int_a^b \omega(x)l_i(x)dx} \tag{N.16}$$

Note that neither the $\{x_i\}$ nor the $\{w_i\}$ depend on the choice of the polynomial P.

N.3 Quadrature method

Now we present the quadrature method. Let's start with the following integral I:

$$I = \int_a^b g(x)dx \qquad (a,b) \in \mathbb{R}^2 \qquad g \in E \tag{N.17}$$

If this integral is well defined, g can be separated into a product ωf where ω defines a dot product:

$$I = \int_a^b \omega(x)f(x)dx \qquad \text{with} \qquad (a,b) \in \mathbb{R}^2 \qquad \text{and} \qquad g \in E \tag{N.18}$$

We then search for an approximation of this integral using a Lagrange interpolation of order n of the function f. It reads as follows:

$$f(x) \approx \sum_{i=1}^{n} l_i(x) f(x_i) \Rightarrow I \approx \sum_{i=1}^{n} f(x_i) \int_a^b \omega(x) l_i(x) dx = \sum_{i=1}^{n} w_i f(x_i) \tag{N.19}$$

The reader may ask the following question: "*How do we define the points x_i for this approximation to be good ?*". It is indeed a good question, and the quadrature method is an answer to it. We can choose the x_i defined as the n roots of the unitary polynomial which is of degree n and orthogonal to the subspace $\mathbb{R}_{n-1}[X]$ with respect to ω. Doing so, we get a good description of the integral if the behaviour of f is not too far from the one of a polynomial of degree $2n-1$.

N.4 An exemple

In this part, we present an example which is close to the cases useful in the PhD thesis. We consider the following integral:

$$I = \int_{-\infty}^{+\infty} e^{-x^2} P(X) \rho(x) \tag{N.20}$$

Here, P is a polynomial of degree p and ρ is a rather smooth bounded function. Moreover, in this case:

$$(.|.) : \begin{cases} E^2 \to \mathbb{R} \\ (f|g) \to \int_{-\infty}^{+\infty} e^{-x^2} f(x) g(x) dx \end{cases} \quad \text{defines a dot product.} \tag{N.21}$$

For this dot product, the Hermite polynomials are an orthogonal family. To perform a quadrature of degree n, we first need to find the n roots of the Hermite polynomial of degree n. It gives the set $(x_1, ..., x_i)$. We then have access to the l_i, the associated Lagrange polynomials:

$$l_i(x) = \prod_{j=1 j \neq i}^{n} \frac{(X - x_j)}{(x_i - x_j)} \tag{N.22}$$

With that, it is easy to evaluate the w_i coefficients:

$$w_i = \prod_{j=1 j \neq i}^{n} \frac{1}{(x_i - x_j)} \int_{-\infty}^{+\infty} e^{-x^2} \prod_{j=1 j \neq i}^{n} (X - x_j) \tag{N.23}$$

This equation can indeed be solved analytically using integrations by parts. The last required step is to evluate the values of P and ρ at the points $(x_1, ..., x_i)$. Finally, we obtain:

$$\boxed{I \approx \sum_{i=1}^{n} w_i P(x_i) \rho(x_i)} \tag{N.24}$$

Appendix O

Time-reversal symmetry

The time reversal symmetry [85], or T-symmetry, corresponds to the following transformation:

$$\hat{T} : t \to -t \tag{O.1}$$

The operator $\hat{T}$ is called the time-reversal operator. More concretely, this symmetry consists in considering the motion of a physical system in reverse. Therefore, in classical mechanics, the operator $\hat{T}$ is expected to leave positions invariant and reverse velocities. In addition, in the context of quantum mechanics, a similar intrinsic spin inversion is expected.
These requirements can be translated in more precise terms. Noting $|\Phi\rangle$ an arbitrary state, we can write:

$$\begin{cases} \langle\Phi|\hat{T}^+\hat{R}\hat{T}|\Phi\rangle = \langle\Phi|\hat{R}|\Phi\rangle & \Rightarrow \quad [\hat{T},\hat{R}] = 0 \\ \langle\Phi|\hat{T}^+\hat{P}\hat{T}|\Phi\rangle = -\langle\Phi|\hat{P}|\Phi\rangle & \Rightarrow \quad [\hat{T},\hat{P}]_+ = 0 \\ \langle\Phi|\hat{T}^+\hat{J}\hat{T}|\Phi\rangle = -\langle\Phi|\hat{J}|\Phi\rangle & \Rightarrow \quad [\hat{T},\hat{J}]_+ = 0 \end{cases} \tag{O.2}$$

In [85], it is shown that the conditions given in Eq.(O.2) can only be fulfilled defining $\hat{T}$ as an anti-unitary operator. These operators are defined by their fundamental properties. Firstly, they are unitary:

$$\hat{T}^+\hat{T} = \hat{T}\hat{T}^+ = 1 \tag{O.3}$$

Then, considering two arbitrary states $|\Phi_0\rangle$ and $|\Phi_1\rangle$ and two arbitrary complex numbers λ_0 and λ_1, the operator $\hat{T}$ is anti-linear:

$$\hat{T}[\lambda_0|\Phi_0\rangle + \lambda_1|\Phi_1\rangle] = \lambda_0^*\hat{T}|\Phi_0\rangle + \lambda_1^*\hat{T}|\Phi_1\rangle \tag{O.4}$$

Finally, these properties lead to the definition of how $\hat{T}$ operates inside a bra-ket:

$$\langle\Phi_0|(\hat{T}|\Phi_1\rangle) = [(\langle\Phi_0|\hat{T})|\Phi\rangle]^* \tag{O.5}$$

O.1 Action on creation and annihilation operators

Considering a particle wave function $\psi_\alpha(m_\alpha, s_\alpha)$ characterized by m_α, its angular momentum projection along the z-axis and s_α, its intrinsic spin projection along the z-axis, the definition of the operator $\hat{T}$ leads to the following relations:

$$\begin{cases} \hat{T}^+ c_\alpha \hat{T} = \sigma_\alpha c_{\bar{\alpha}} = \bar{c}_\alpha \\ \hat{T}^+ c_\alpha^+ \hat{T} = \sigma_\alpha c_{\bar{\alpha}}^+ = \bar{c}_\alpha^+ \end{cases} \tag{O.6}$$

In Eq.(O.6), the particle creation and annihilation operators c_α^+ and c_α are obviously the ones related to the wave function ψ_α. The notation σ_α stands for an intrinsic spin phasis ($\sigma_\alpha = 1$ if $s_\alpha = 1/2$ and σ_α = -1 if $s_\alpha = -1/2$). In addition, the creation and annihilation particle operators $c_{\bar{\alpha}}^+$ and $c_{\bar{\alpha}}$ correspond to the wave function $\psi_\alpha(-m_\alpha, -s_\alpha)$. Finally, it is clear in Eq.(O.6) that the notation $\bar{c}_\alpha$ corresponds to $c_{\bar{\alpha}}$ multiplied by the intrinsic spin phasis. This convention is very useful in the time-even HFB derivations [47].

The action of $\hat{T}$ on the particle operators directly defines its action on the quasiparticle ones. For instance, if we consider the following annihilation quasiparticle operator ξ_i, relevant within the time-even HFB formalism:

$$\xi_i = \sum_j U_{ki} c_k + V_{ki} \bar{c}_k \tag{O.7}$$

It is clear that the action of $\hat{T}$ on ξ_i reads as follows:

$$\hat{T}^+ \xi_i \hat{T} = \bar{\xi}_i = \sum_j U_{ki} \bar{c}_k + \sigma_k \bar{\sigma}_k V_{ki} c_k = \sum_j U_{ki} \bar{c}_k - V_{ki} c_k \tag{O.8}$$

Finally, if we apply the operator $\hat{T}$ a second time, we find the expected result:

$$\hat{T}^+ \bar{\xi}_i \hat{T} = \sum_j -U_{ki} c_k - V_{ki} \bar{c}_k = -\xi_i \tag{O.9}$$

O.2 Examples

In the following, we illustrate the properties of the time reversal operator $\hat{T}$ by demonstrating two useful results within the time-even HFB formalism.

First of all, we start by considering the time-even density matrix ρ:

$$\rho_{\alpha\beta} = \langle \Phi | c_\beta^+ c_\alpha | \Phi \rangle \tag{O.10}$$

Inserting the operator $\hat{T}$ in Eq.(O.10) leads to:

$$\rho_{\alpha\beta} = (\langle \Phi | \hat{T}^+) c_\beta^+ (\hat{T} \hat{T}^+ c_\alpha \hat{T} | \Phi \rangle) \tag{O.11}$$

Then, we use the anti-linearity of the operator $\hat{T}$ to write:

$$\rho_{\alpha\beta} = [\langle\Phi|(\hat{T}^{+}c_{\beta}^{+}\hat{T}\hat{T}^{+}c_{\alpha}\hat{T}|\Phi\rangle)]^{*} = [\langle\Phi|\bar{c}_{\beta}^{+}\bar{c}_{\alpha}|\Phi\rangle)]^{*} \tag{O.12}$$

As the time-even density matrix ρ is real, we obtain:

$$\boxed{\rho_{\alpha\beta} = \langle\Phi|\bar{c}_{\beta}^{+}\bar{c}_{\alpha}|\Phi\rangle = \sigma_{\alpha}\sigma_{\beta}\langle\Phi|c_{\bar{\beta}}^{+}c_{\bar{\alpha}}|\Phi\rangle = (-1)^{s_{\beta}-s_{\alpha}}\langle\Phi|c_{\bar{\beta}}^{+}c_{\bar{\alpha}}|\Phi\rangle} \tag{O.13}$$

Then, we demonstrate that the time-even pairing tensor κ used in this PhD thesis work is symmetric. The latter reads as follows:

$$\kappa_{\alpha\bar{\beta}} = \langle\Phi|c_{\alpha}\bar{c}_{\beta}|\Phi\rangle \tag{O.14}$$

We start by inserting the operator $\hat{T}$ in Eq.(O.14):

$$\kappa_{\alpha\bar{\beta}} = (\langle\Phi|\hat{T}^{+})c_{\alpha}(\hat{T}\hat{T}^{+}\bar{c}_{\beta}\hat{T}|\Phi\rangle) \tag{O.15}$$

Then, we use the anti-linearity of the operator $\hat{T}$:

$$\kappa_{\alpha\bar{\beta}} = [\langle\Phi|(\hat{T}^{+}c_{\alpha}\hat{T}\hat{T}^{+}\bar{c}_{\beta}\hat{T}|\Phi\rangle)]^{*} = \sigma_{\beta}\sigma_{\bar{\beta}}[\langle\Phi|\bar{c}_{\alpha}c_{\beta}|\Phi\rangle]^{*} = [\langle\Phi|c_{\beta}\bar{c}_{\alpha}|\Phi\rangle]^{*} \tag{O.16}$$

As the time-even pairing tensor κ is real, we finally obtain:

$$\boxed{\kappa_{\alpha\bar{\beta}} = \langle\Phi|c_{\beta}\bar{c}_{\alpha}|\Phi\rangle = \kappa_{\beta\bar{\alpha}}} \tag{O.17}$$

Bibliography

[1] J. Copeland, C. Myers, et al. Cosmic F- and D-strings. *JHEP06 013*, 2004.

[2] E. Martín-Martínez and T. Rick Perche. What gravity mediated entanglement can really tell us about quantum gravity. *Phys. Rev. D 108, L101702*, 2023.

[3] L. Meitner and O. Frisch. *Nature 143*, 1939.

[4] O. Hahn and F. Strassmann. *Naturwissenshaften 26 755*, 1938.

[5] O. Hahn and F. Strassmann. *Naturwissenshaften 27 11*, 1938.

[6] N. Bohr. Neutron capture and nuclear constitution. *Nature 137*, 1936.

[7] N. Bohr and A. Wheeler. The mechanism of nuclear fission. *Phys. Rev. 56, 426*, 1939.

[8] M. G. Mayer and J. H. D. Jensen. Elementary theory of nuclear shell structure. *Wiley, New York.*, 1955.

[9] V. M. Strutinsky. Shell effects in nuclear masses and deformation energies. *Yad.Fiz. 3. 614*, 1966.

[10] M. Bender et al. Future of nuclear fission theory. *J. Phys. G: Nucl. Part. Phys. 47 113002*, 2020.

[11] T. H. R. Skyrme. Cvii. the nuclear surface. *Philosophical Magazine 11*, 1956.

[12] T. H. R. Skyrme. The effective nuclear potential. *Nuclear Physics, 9, 4*, 1958.

[13] D. Vautherin and D. M. Brink. Hartree-Fock calculations with Skyrme's interaction. I. spherical nuclei. *Phys. Rev. C, 5*, 1972.

[14] D. Vautherin. Hartree-Fock calculations with Skyrme's interaction. II. axially deformed nuclei. *Phys. Rev. C, 7*, 1973.

[15] D. Gogny. Proceeding of the international conference on nuclear physics. *J. De Boer and H. J. Mang, (North-Holland, Amsterdam), Vol.1, p. 48*, 1973.

[16] D. Gogny. Nuclear self-consistent fields, trieste. *G. Ripka and M. Porneuf (North-Holland, Amsterdam), p. 333.*, 1975.

[17] J. Dechargé and D. Gogny. *Phys. Rev. C 21, 1568*, 1980.

[18] J.F. Berger, M. Girod, et al. Constrained Hartree-Fock and beyond. *Nucl. Phys. A 502, 85*, 1989.

[19] F. Chapert, N. Pillet, et al. Gogny force with a finite-range density dependence. *Phys. Rev. C 91, 034312*, 2015.

[20] C. Simenel. Nuclear quantum many-body dynamics. *Eur. Phys. J. A 48 152*, 2012.

[21] K. Sekizawa. *Frontiers Phys. 7 20*, 2019.

[22] J. Zhao, Tamara Nikšić, et al. Time-dependent generator coordinate method study of fission: dissipation effects. *Phys. Rev. C 105, 054604*, 2022.

[23] Scamps, C. Simenel, et al. *Phys. Rev. C 92 011602*, 2015.

[24] DL. Hill and J.A. Wheeler. Nuclear constitution and the interpretation of fission phenomena. *Phys. Rev. 89, 1102*, 1953.

[25] J.J. Griffin and J.A. Wheeler. Collective motions in nuclei by the method of generator coordinate. *Phys. Rev. 108, 311*, 1957.

[26] J.F. Berger, M. Girod, et al. Time-dependent quantum collective dynamics applied to nuclear fission. *Comput. Phys. Commun. 63, 365*, 1991.

[27] H. Goutte, J.F. Berger, et al. *Phys. Rev. C 71, 024316*, 2005.

[28] D. Regnier, N. Dubray, et al. *Phys. Rev. C 93, 054611*, 2016.

[29] F. Vives et al. *Nucl. Phys. A 662, 63*, 2000.

[30] S. Pomme et al. *Nucl. Phys. A 560, 689*, 1993.

[31] B. Li, D. Vretenar, et al. *arXiv:2406.11124v1*, 2024.

[32] G. F. Bertsch and K. Hagino. Modeling fission dynamics at the barrier in a discrete-basis formalism. *Phys. Rev. C 107, 044615*, 2023.

[33] R. Bernard. Couplages modes collectifs-excitations intrinsèques dans le processus de fission. *Thèse de doctorat Paris VI*, 2011.

[34] R. Bernard, H. Goutte, et al. Microscopic and nonadiabatic Schrödinger equation derived from the generator coordinate method based on zero- and two-quasiparticle states. *Phys. Rev. C 84, 044308*, 2011.

[35] W. Younes and D. Gogny. Nuclear scission and quantum localization. *Phys. Rev. Lett. 107, 132501*, 2011.

[36] Frosini Mikael, T. Duguet, et al. Multi-reference many-body perturbation theory for nuclei: II. ab initio study of neon isotopes via PGCM and IM-NCSM calculations. *Eur. Phys. J. A*, 2022.

[37] N. Schunck and L.M. Robledo. Microscopic theory of nuclear fission: a review. *Rep. Progr. Phys. 79*, 2016.

[38] M. Baranger and M. Veneroni. An adiabatic time-dependent Hartree-Fock theory of collective motion in finite systems. *Ann. Phys. 114, 123*, 1978.

[39] R. Navarro Perez, N. Schunck, et al. Axially deformed solution of the Skyrme–Hartree–Fock–Bogolyubov equations using the transformed harmonic oscillator basis (iii) hfbtho (v3.00): A new version of the program. *Comput. Phys. Commun. 220, 363*, 2017.

[40] N. Dubray and D. Regnier. Numerical search of discontinuities in self-consistent potential energy surfaces. *Comput. Phys. Commun. 183, 2035–2041*, 2012.

[41] N. N. Bogoliubov. A new method in the theory of superconductivity. *Sov. Phys. JETP7 41. 245*, 1958.

[42] N. N. Bogoliubov. The compensation principle and the self-consistent field method. *Sov. Phys. Usp. 2. 236. 245*, 1959.

[43] N. N. Bogoliubov and V. G. Soloviev. On a variational principle in the many-body problem. *Sov. Phys. Doklady 4. 143. 245, 254*, 1959.

[44] J. G. Valatin. Generalized hartree-fock method. *Phys. Rev. 122 1012. 245, 252*, 1961.

[45] P. Ring and P. Schuck. The nuclear many-body problem. *Springer-Verlag, New-York*, 1980.

[46] W.Younes, D.M. Gogny, et al. Microscopic theory of fission dynamics based on the Generator Coordinate Method. *Series of Lecture Notes in Physics, Springer International Publishing*, 2019.

[47] J.-F. Berger. Approche microscopique auto-consistante des processus nucléaires collectifs de grande amplitude à basse énergie. application à la diffusion d'ions lourds et à la fission. *Thèse de doctorat Paris XI*, 1985.

[48] G. Zietek. Towards a generalized effective nuclear Gogny interaction extended to finite-range spin—orbit and tensor forces. *Thèse de doctorat Université Paris-Saclay*, 2023.

[49] J. C. Slater. A simplification of the Hartree-Fock method. *Phys. Rev. 81, 385*, 1951.

[50] J.L. Egido, J. Lessing, et al. On the solution of the Hartree-Fock-Bogoliubov equations by the conjugate gradient method. *Nucl. Phys. A Volume 594, Pages 70-86*, 1995.

[51] L. M. Robledo and G. F. Bertsch. Application of the gradient method to Hartree-Fock-Bogoliubov theory. *Phys. Rev. C 84, 014312*, 2011.

[52] B. Recht. Lyapunov analysis and the heavy ball method. *Course notes, University of Wisconsin-Madison*, 2012.

[53] N. Dubray et al. Soon to be submitted for publication.

[54] M. Anguiano, J.L. Egido, et al. Particle number projection with effective force. *Nucl. Phys. A 696, 467–493*, 2001.

[55] N-W.T.Lau, R. Bernard, et al. Smoothing of one- and two-dimensional discontinuities in potential energy surfaces. *Phys. Rev. C 105, 034617*, 2022.

[56] W. Younes and D. Gogny. *Phys. Rev. C 80, 054313*, 2009.

[57] R. Han, M. Warda, et al. Scission configuration in self-consistent calculations with neck constraints. *Phys. Rev. C 104, 064602*, 2021.

[58] Y. Beaujeault-Taudière and D. Lacroix. Solving the Lipkin model using quantum computers with two qubits only with a hybrid quantum-classical technique based on the Generator Coordinate Method. *Phys. Rev.C 109, 024327*, 2024.

[59] O. Higgott, D. Wang, et al. Variational quantum computation of excited states. *Quantum 3, 156*, 2019.

[60] P. Carpentier, N. Pillet, et al. Construction of continuous collective energy landscapes for large amplitude nuclear many-body problems. *Phys. Rev. Lett. 133, 152501*, 2024.

[61] N. Boucheneb, M. Asghar, et al. *Nucl. Phys. A535 (1991) 77-93*, 1991.

[62] O. Litaize and O. Serot. *Phys. Rev. C 82, 054616*, 2010.

[63] C. Simenel. Particle transfer reactions with the Time-Dependent Hartree-Fock theory using a particle number projection technique. *Phys. Rev. Lett. 105, 192701*, 2010.

[64] M. Verrière, N. Schunck, et al. Number of particles in fission fragments. *Phys. Rev. C 100, 024612*, 2019.

[65] M. Verrière, N. Schunck, et al. Microscopic calculation of fission product yields with particle number projection. *Phys. Rev. C 103, 054602*, 2021.

[66] A. Bernard, D. Regnier, et al. Soon to be submitted for publication.

[67] L. M. Robledo. Sign of the overlap of Hartree-Fock-Bogoliubov wave functions. *Phys. Rev. C 79, 021302(R)*, 2009.

[68] N. Onishi and S. Yoshida. Generator coordinate method applied to nuclei in the transition region. *Nucl. Phys. Volume 80, Issue 2, Pages 367-376*, 1966.

[69] L. M. Robledo. Formulation of the generator coordinate method with arbitrary bases. *Phys. Rev. C 105, 2*, 2022.

[70] Q. Haider and D. Gogny. Microscopic approach to the generator coordinate method with pairing correlations and density-dependent forces. *J. Phys. G. Nucl. Part. Phys. 18, 993*, 1992.

[71] W. Satula and J. Dobaczewski. Simple regularization scheme for multireference density functional theories. *Phys. Rev. C 90, 054303*, 2014.

[72] A. Savitzky and M. J. E. Golay. Smoothing and differentiation of data by simplified least squares procedures. *Analytical Chemistry. 36 (8): 1627–39*, 1964.

[73] W.H. Press, A. Teukolsky, et al. Numerical recipes: The art of scientific computing. *Cambridge University Press, Cambridge*, 1986.

[74] N. Carjan, M. Rizea, et al. *Rom. J. Phys. 47, 221*, 2002.

[75] P. Marini, J. Taieb, et al. *Phys. Lett. B 835 137513*, 2022.

[76] M. Caamaño and F. Farget. *Phys. Lett. B 770 72-76*, 2017.

[77] Y. Tanimura, D. Lacroix, et al. *Phys. Rev. L 118, 152501*, 2017.

[78] D. Lacroix. Private communcation.

[79] D.J. Thouless. Stability conditions and nuclear rotations in the Hartree-Fock theory. *Nucl. Phys. 21. 225. 310, 615*, 1960.

[80] C. Bloch and A. Messiah. The canonical form of an antisymmetric tensor and its application to the theory of superconductivity. *Nucl. Phys. Volume 39, p. 95-106*, 1962.

[81] H. G. Becker. On the transformation of a complex skew-symmetric matrix into a real normal form and its application to a direct proof of the Bloch-Messiah theorem. *Lett. Nuovo Cimento 8, 185–188*, 1973.

[82] P. Bonche, J. Dobaczewski, et al. *J 1990 Nucl. Phys. A 510 466*, 1990.

[83] C. Cohen-Tanoudji, B. Diu, et al. Mécanique quantique. *CNRS éditions*, 1973.

[84] M. Combescure and D. Robert. Fermionic coherent states. *J. Phys. A: Math. Theor. 45 244005*, 2012.

[85] F. Laloë. Symétries continues. *CNRS éditions*, 2021.